EXPLORATION OF THE SWEET CHERRY MICROBIOME AND POTENTIAL BIOLOGICAL CONTROLS OF *PSEUDOMONAS SYRINGAE* PV. *SYRINGAE*

By

Tammy K. Wilkinson

A DISSERTATION

Submitted to
Michigan State University
in partial fulfillment of the requirements
for the degree of

Horticulture – Doctor of Philosophy

2023

ABSTRACT

Bacterial canker, a disease caused by the bacteria *Pseudomonas syringae pv. syringae* (*Pss*), remains a critical economic hurdle for sweet cherry production. Young trees are most susceptible, while older trees with bacterial canker are sources of inoculum. *Pss* can be found throughout the environment and living on all plant surfaces. Infections can occur through multiple avenues including blossoms, wounds, and various natural openings including leaf scars. *Pss* at low population numbers does not cause pathogenesis but becomes an issue as populations build during periods of cool, wet weather that are typical of spring and fall in Michigan. The *Pss* isolated from Michigan sweet cherry flowers was found to be phylogenetically diverse, with 20 strains belonging to 3 out of the 7 clades in phylogroup (PG) 2 (PG2b, PG2c, PG2d). Virulence tests with the 20 strains on green fruit and sweet cherry wood from two sweet cherry cultivars, 'Sweetheart' and 'Coral Champagne', demonstrated a range of virulence: strains in PG2d were the most virulent, PG2b strains were moderate to avirulent, and PG2c strains were avirulent (PG2d>PG2b>PG2c). The variability of the *Pss* strains also was reflected in their ice nucleation activity (INA) with strains having INA^{+}, INA^{-}, and $INA^{+/-}$ phenotypes, $GATTa^{+\,+\,-\,-}$ and $GATTa^{+\,+\,+\,-}$ profiles, and amplification of the genes encoding for the production and secretion of the phytotoxin syringomycin being $syrB^{+}/syrD^{+}$ and $syrB^{-}/syrD^{+}$. Though much of its epiphytic lifestyle, biology, and ability to live in mixed populations with varying levels of virulence has been elucidated for *Pss*, very little was known about the other bacteria that exist with *Pss* within the sweet cherry leaf microbiome. A survey of the sweet cherry leaf microbiome of three cultivars, 'Benton', 'Gold', and 'Sweetheart' was conducted from Fall 2017- Fall 2019 in two regions of Michigan. There were no regional or cultivar differences in the sweet cherry leaf microbiome. The clear drivers of microbiome stability were season and *Pseudomonas*, as the

microbiome was variable in spring and became more stable in the summer and fall. The microbiome was dominated by the Phylum Proteobacteria (67 to 100% relative abundance) and the genera *Pseudomonas* (26 to 95% relative abundance). The core microbiome was composed of *Pseudomonas* and *Sphingomonas* OTUs. All top taxa have the potential to be beneficial to the sweet cherry tree. As control options for the management of *Pss* populations are limited there is keen fruit grower interest in the potential for biological control agents. Current commercial biological controls (BCAs) moderate to avirulent Michigan *Pss.* The moderately virulent and avirulent Michigan *Pss* were surveyed via in-vitro co-inoculations for their potential to decrease growth of the virulent to moderately virulent *Pss* using the same method. In-vitro co-inoculations were an acceptable way to initially assess potential BCAs. All commercially available BCAs were able to reduce the mean total area of *Pss* growth compared to when they were next to water, with up to 50% suppression in some cases. No single commercial BCA stood out as the premier choice for *Pss* growth suppression. None of the Michigan *Pss* were found to be ideal candidates for the potential biological control of virulent *Pss*, with no statistical differences in growth compared to when inoculated next to water.

This dissertation is dedicated to my children, Gregory & Grant

ACKNOWLEDGEMENTS

I would like to thank Greg Lang, George Sundin, Todd Einhorn, and Quan Zeng for their guidance and patience as I worked towards my Doctor of Philosophy degree at Michigan State University. Thank you to Feiran Li for all of the hours that she put in as my assistant on all of the various experiments and for all the picture wrangling, you are a wizard. Thank you to Erin Lauwers and Audrey Sebolt who gave me a crash course in MLST, phenotype assays and DNA extraction respectively. I also thank Sakib Hasan, and Guanqi Lu for your statistical consulting support. Thanks to Sarah Westcott for answering millions of my Mothur questions. I thank Kurt, Tom, and Scott Wells for allowing me to use their orchard. Thank you to the staff at the Clarksville Research Center, the Horticulture Teaching and Research Center, the Southwest Michigan Research Center, and the Research Technology Support Facility Genomics core. Thank you to Bob Van Buren, Pat Edger, Gou-Qing Song and Amy Iezzoni for the use of their labs and equipment. I would also like to thank the Michigan Cherry Committee for partial funding of this work. I give special thanks to my husband, Fred, and my children, Gregory and Grant, for all of their support, understanding and patience. I would also like to thank my parents and the rest of my family and friends for the never wavering encouragement on my long trek as a career student.

TABLE OF CONTENTS

CHAPTER 1 *PSEUDOMONAS SYRINGAE* PV. *SYRINGAE* AND 55 YEARS OF BACTERIAL CANKER EPIDEMICS IN MICHIGAN: A LITERATURE REVIEW 1
1.1: Michigan Cherry Production and *Pseudomonas syringae* pv. *syringae* 1
1.2: *Pseudomonas syringae* pv. *syringae* 3
1.3: *Pss* Management 8
1.4: *Pss* Epiphytic Living and the Leaf Microbiome 11
1.5: Biological Control 16
1.6: Objectives of Study 21
REFERENCES 23

CHAPTER 2 VIRULENCE AND PHYLOGENY OF MICHIGAN *PSEUDOMONAS SYRINGAE* PV. *SYRINGAE* ISOLATES FROM SWEET CHERRY FLOWERS HIGHLIGHT VARIABILITY, THE NEED FOR CAUTION, AND AREAS OF FUTURE RESEARCH 38
2.1: Abstract 38
2.2: Introduction 39
2.3: Methods 46
2.4: Results 58
2.5: Discussion 63
2.6: Conclusions 70
REFERENCES 94

CHAPTER 3 EXPLORATION OF THE SWEET CHERRY LEAF MICROBIOME REVEALS DOMINATION BY *PSEUDOMONAS* AND SEASONAL COMMUNITY DIRECTIONALITY 104
3.1: Abstract 104
3.2: Introduction 105
3.3: Methods 113
3.4: Results 119
3.5: Discussion 127
3.6: Conclusions 136
REFERENCES 167

CHAPTER 4 *IN VITRO* CO-INOCULATIONS FOR ASSESSMENT OF POTENTIAL *PSEUDOMONAS SYRINGAE* PV. *SYRINGAE* BIOLOGICAL CONTROL AGENTS 177
4.1: Abstract 177
4.2: Introduction 177
4.3: Methods 182
4.4: Results 185
4.5: Discussion 190
4.6: Conclusions 195
REFERENCES 219

APPENDIX A: *PSS* CHARACTERIZATION 224
APPENDIX B: SWEET CHERRY MICROBIOME 359

APPENDIX C: *PSS* VS. BIOLOGICAL CONTROL AGENTS 443

CHAPTER 1

PSEUDOMONAS SYRINGAE PV. *SYRINGAE* AND 55 YEARS OF BACTERIAL CANKER EPIDEMICS IN MICHIGAN: A LITERATURE REVIEW

1.1: Michigan Cherry Production and *Pseudomonas syringae* pv. *syringae*

Michigan is an agriculturally diverse state, with 46,000 farms and 300 agricultural commodities (MDARD, 2023; USDA-Nass, 2021). This agricultural diversity is due to the protection of the Laurentian Great Lakes and fertile soils from glacial deposits (Brown, 1941; Warren and Vermette, 2022). Though orchards are scattered throughout the state, the "fruit belt" region along Lake Michigan is where the majority of fruit production occurs (Brown, 1941; Warren and Vermette, 2022). Michigan is fourth in sweet cherry (*Prunus avium*) production with 7,807 total acres and remains the nation's top tart cherry (*Prunus cerasus*) producer (70% of the nation's supply) with 33,381 total acres (Lang, 2019a; MDARD, 2018; USDA-Nass, 2019). The United States of America (USA) produced 275,000 tons of cherries in 2022, just behind Turkey for the top spot in global cherry production (Lang, 2019a; Bujdosó and Hrotkó, 2017; USDA-Nass, 2022). Global cherry production and consumer demand has increased dramatically over the past 20 years, driven by several factors, including marketing that touts cherries as flavorful "super fruits" that confer a wide range of health benefits (Lang, 2019a).

According to an early census, cultivated cherries were established in Michigan sometime in the 1870s (Brown, 1941). The modern sweet cherry orchard (150+ years later) looks markedly different, moving away from orchards of trees reminiscent of their forested counterparts to high-density plantings grafted on dwarfing to semi-vigorous precocious rootstocks, such as the 'Gisela' series (Gi.6; Gi.5, and Gi3) supported by trellis (Lang et al., 2019). Michigan State University researchers and progressive cherry growers have led the charge toward the adoption

of the high-density “pedestrian orchards” featuring “two-dimensional/planar” production systems like that of the UFO (Upright Fruiting Offshoots) that are trained to form a “fruiting wall” and are easily picked from one side of the tree (i.e., less labor intensive) compared to the traditional “three-dimensional” canopy architectures (Lang et al., 2022). Various covering systems (e.g., row covers, high tunnels, and retractable roofed greenhouses) are also being explored to reduce rain-induced fruit cracking and disease pressure, and promote earlier fruit harvest potential (Lang et al., 2016; Lang, 2019a). These innovative approaches address grower concerns over production challenges due to labor issues (lack of workers and costs) and climatic events (frosts and rain) (Lang, 2019a).

Another major limitation for sweet cherry production is significant disease pressures (e.g., bacterial canker, brown rot, and cherry leaf spot) linked to Michigan’s climate. Cool, wet springs and late falls are typical, and are ideal for the proliferation and infection of the bacterial phytopathogen *Pseudomonas syringae* pv. *syringae* van Hall (*Pss*), the causal agent of bacterial canker disease (Hirano and Upper, 1990; Hirano and Upper, 2000; Jones and Sutton, 1996; Kennelly et al. 2008). Management of this bacterial disease remains difficult and can be devastating to the sweet cherry industry, as young trees are highly susceptible (Spotts, 2010). Historically, Michigan had a lengthy spring with cool temperatures that delay bud break, and warmer falls that avoid late and early “killing frosts,” respectively, as a climatic influence of the Great Lakes (Warren and Vermette, 2022). Due to global climate change and the warming of the lake waters (including decreased ice cover), the occurrence of these previous protections has become quite volatile (Warren and Vermette, 2022). Lang (2019a) summarized climatic data (from J. Andresen, personal communication) from the Traverse City growing region that compared pre- to post-1940, indicating that bud development (side green) is now ~ 10 days

earlier, the number of potential frost events at side green has increased significantly from 5 events to ≥ 20, and annual rainfall has increased 10%. These statistics are particularly alarming when considering the biology of the *Pss* pathogen: in addition to the increase in population size and subsequent infection of cherry during cool, wet weather events, the pathogen is closely linked to the water cycle, being rain splash dispersed and capable of facilitating frost damage via ice nucleation which enables its entry into the plant (Hirano and Upper, 1990; Hirano and Upper, 2000; Jones and Sutton, 1996; Morris et al., 2008; Morris et al., 2013). Growers maintain high-density orchard systems with intensive pruning to promote appropriate leaf area-to-fruit ratios (LA: F), and increase canopy light penetration, yet such pruning can increase the risk of infection by *Pss* (Ayala and Lang, 2017; Whiting and Lang 2004). Dormant, early spring and late spring pruning often occurs concurrently with prime environmental conditions for *Pss* population increases and opportunistic infections via the pruning wounds (Kennelly et al, 2008; Jones and Sutton, 1996; Lang, 2019b; Spotts et al. 2010).

1.2: *Pseudomonas syringae* pv. *syringae*

Jones (1971) reported *Pss* to be present in sweet cherry in Michigan for the first time following a 1968 epidemic (ca. 55 years ago). Most recently, three significant outbreaks have occurred (2002, 2012, and 2021), all occurring after unusually early warm spring weather that induced early bloom followed by intense frost events (Kennelly et al., 2007; Lauwers, 2022; Renick et al., 2008; Sundin and Rothwell, 2012). These large-scale events resulted in significant current and future year crop losses from frost damage as well as infection by *Pss*, leading to blossom blast followed by systemic disease and subsequent spur, shoot, limb, and young tree death (Kennelly et al., 2007; Lauwers, 2022; Renick et al., 2008; Sundin and Rothwell, 2012). Other *Pss* infection symptoms include sunken cankers, gumming, lesions on fruit, and “shot

holes" in leaves (Jones and Sutton, 1996; Kennelly et al., 2007). In addition to *Pss*, Jones (1971) isolated *Pseudomonas syringae* pv. *morsprunorum* (*Psm*) from sweet cherry. This pathogen has since been determined to be two different pathogens, *P. amygdali* pv. *morsprunorum* (race 1) and *P. avellanae* pv. *morsprunorum* (race 2); it is recovered more often on tart cherry and is less virulent than *Pss* in Michigan (Gomila et al., 2017; Hulin et al., 2020; Jones, 1971; Jones and Sutton, 1996; Renick et al., 2008). *Pss* can be differentiated from *Psm* via the biochemical assays GATTa (Gelatin liquefaction, Aesculin hydrolysis, Tyrosinase activity, and Tartrate utilization) and the amplification of the *syrB* or *syrD* gene (syringomycin phytotoxin); *Pss* is generally $G^+ A^+ T^- Ta^-$ while *Psm* is $G^- A^- T^+ Ta^+$, and *Psm* does not produce syringomycin (Bultreys and Gheysen, 1999; Latorre and Jones, 1979b; Lelliot et al., 1966; Renick et al., 2008; Sorensen et al., 1998). *Psm* produces the phytotoxin coronatine (detected through amplification of the *cfl* gene) which *Pss* does not; this toxin is able to interfere with stomatal closure, allowing bacteria to enter the host plant (Bultreys and Gheysen, 1999; Renick et al., 2008; Xin et al., 2018).

Pss is a generalist phytopathogen and the causal agent for bacterial canker, blister bark, and blossom blast in stone fruit (all economically important *Prunus* spp.) and pome fruit (apple and pear) and is pathogenic to over 180 plant species globally (Kennely et al., 2007). *Pseudomonas syringae* (*P.s.*) has been found to have broad overlapping host ranges with phylogroup 2 (the *Pss* clade) having a greater extent of host ranges compared to other *P.s.* (Morris et al., 2019). *Pss* is also an opportunistic pathogen that can infect through wounds (pruning cuts and trellis wire rubs) and natural openings (leaf scars and stomates), but only when populations are high; otherwise, it is well-documented to live benignly on host and non-host plants (Hirano and Upper, 1990; Hirano and Upper, 2000; Kennelly et al., 2007; Latorre and Jones, 1979a; Lillrose et al., 2017).

Pss belong to the same phylogenetic lineage as *Pseudomonas fluorescens* and will fluoresce under UV light when grown on iron-deficient media; this is due to the production of iron (Fe) chelating molecules or siderophores (e.g., pyoverdines) and is often used in the initial steps toward the identification of *Pss* (Cornelis, 2010; Gomila et al., 2017; Latorre and Jones, 1979b; Lelliot et al., 1966). The ability to produce these siderophores confers epiphytic fitness to *Pss* as Fe is limited in the phyllosphere and Wensing et al. (2010) demonstrated that the strain 22d/93, a strong siderophore producer, was able to outcompete/out-colonize *P.s* pv. *glycinea* which produces a lesser amount of the same siderophores. *Pss* is a gram-negative bacterium in the class Gammaproteobacteria, that is phylogenetically placed within genomospecies 1, phylogroup 2, which is part of a much larger species complex composed of 13 phylogroups (Berge et al., 2014; Gardan et al., 1999; Gomila et al., 2017; Gutiérrez-Barranquero et al., 2019; Kennelly et al., 2007; Pulawska et al., 2017). Phylogroup (PG) 2 is composed of 7 clades (2a, 2b, 2c, 2d, 2e, 2f, and 2g) that contain pathogenic *Pss* (PG2b and PG2d), non-pathogenic *Pss* (PG2c) and *Pss* isolated from water and snow (PG2a and PG2e) (Abdellatif et al., 2020; Berge et al., 2014; Hall et al., 2019). The phylogroups 2f and 2g from characterizations of *Pss* strains isolated from grapes (*Vitis vinifera*) and oranges (*Citrus sinensis*) respectively are new additions to the clades originally described in Berge et al. (2014) (Abdellatif et al., 2020; Hall et al., 2019). The *Pss* in PG2c are all non-pathogens and have an atypical type III secretion system (T3SS), an important virulence component (Clarke et al., 2010; Mohr et al. 2008). As inferred by the former, Lauwers (2022) and Renick et al. (2008) classified Michigan *Pss* in PG2a, PG2b, and PG2d. These phylogroups were determined by Lauwers (2022) using multilocus sequence typing/analysis (MLSA/MLST) comparing 4 “housekeeping” genes to those of reference sequences. Current phylogenomic classifications of *Pss* are popularly being constructed utilizing

this method, using from 1-7 “housekeeping” genes (Abdellatif et al., 2019; Almeida et al., 2010; Berge et al., 2014; Bophela et al., 2020; Hall et al., 2019; Hulin et al., 2018a; Hwang et al., 2005; Iličić et al., 2021; Ivanović et al., 2022; Lauwers, 2022; Oksel, 2022; Popović et al., 2021; Sarkar and Guttman, 2004; Vasebi et al., 2020; Visnovsky et al., 2019).

The ability of *Pss* to ice nucleate in plant tissues facilitates frost injury in the spring (Kennely et al., 2007). *Pss* cells are able to ice nucleate due to proteins embedded in their outer membrane and can do so at 0 to -5°C causing frost damage to plants at a higher temperature than would occur in the plant with no INA bacteria (i.e., in cherry, during bud break 50% of buds are killed at -6°C and 90% at -7°C with prolonged temperatures) (Hirano and Upper, 2000; Lindow et al., 1983a; Lindow et al., 1983b; Lukas et al. 2022; Salazar-Gutiérrez et al., 2004). The ice nucleation genes (*ina* genes) encode for outer membrane proteins (e.g., *inaZ*) which form as aggregates with aggregate size correlating to ice nucleus efficiency (Hirano and Upper 2000). The INA-induced frost injury allows *Pss* to enter and infect the plant causing initial blossom blast symptoms, which was a major contributor to a critical state-wide bacterial canker epidemic in Michigan in 2012 (Sundin and Rothwell, 2012). Renick et al. (2008) and Lauwers (2022) found a high level of INA strains in their surveys of Michigan *Pss* collected from cherry flowers with 94% INA and 100% INA respectively. Ice nucleation frequency of *P.s* cells in Pacific Northwest orchards was found to be variable, and strains with an INA phenotype may not be active all at the same time, thereby populations are composed of a combination of $INA^{+/-}$ phenotypes (Hirano and Upper, 2000; Gross et al., 1983; Renick et al., 2008). This is one of the reasons why the creation of recombinant Ice^{-} strains did not persist as a viable biological control option as Ice^{-} strains could not eliminate the mixed $Ice^{+/-}$ wild populations and control by the recombinant strain was based on prior colonization and density of the recombinant strains

(Hirano and Upper, 2000). It has been suggested that ancestrally the ability to ice nucleate may have been a mechanism for preventing cell injury during freezing in aquatic environments and appears to have been a part of the *P.s.* genome for a much longer time than the Type Three Secretion System (T3SS) (Morris et al., 2008; Morris et al. 2010; Morris et al. 2013).

Pss overwinters in flower buds, cankers, bark, and systemically within the plant (Sundin et al., 1988; Jones and Sutton, 1996). Once *Pss* enters the plant, it inhabits the apoplast, where the bacteria can produce virulence factors through the Type Three Secretion System (T3SS), allowing the bacteria to inject effector proteins into plant cells (Alfano and Collmer, 2004). Evidence through whole genome comparisons points to shared genes/proteins in common among strains that have led to the adaptation for pathogenicity on woody hosts, cherry specifically, and proposed co-evolution with *Prunus* spp. (Hulin et al., 2018b; Hulin et al., 2020; Nowell et al., 2016; Ruinelli et al., 2022). These shared genes and proteins are part of the T3SS repertoire; the T3SS consists of an apparatus made by *Pss* (once inside the plant apoplast) that injects effector proteins into the plant cells, releasing nutrients to promote the proliferation of *Pss* and thwart the plants basal immune response (i.e., plant triggered immunity or PTI) (Alfano and Collmer, 2004; Hulin et al., 2018b; Hulin et al., 2020; Nowell et al., 2016; Ruinelli et al., 2022; Ruiz-Bedoya et al., 2023). These effector proteins also are considered “double agents” as they have the potential to elicit an additional plant immune response, or effector-triggered immunity (ETI), which adds another level of infection complexity dependent on both pathogen and plant host genetics (Alfano and Collmer, 2004; Hulin et al., 2018b; Hulin et al., 2020; Nowell et al., 2016; Ruinelli et al., 2022; Ruiz-Bedoya et al., 2023). Effectors are thought to be acquired through horizontal gene transfer, and pathogenicity is a result of the convergent gain and loss of these genes (Hulin et al., 2018b). In the simplest terms, genes encoding for T3SS are the *hrp* and *hrc* genes (part of

a pathogenicity island) while the genes encoding for the effector proteins are the *avr* and *hop* genes (Alfano and Collmer, 2004; Hulin et al., 2018; Kennelly et al., 2007). *Pss* has fewer effector proteins but more phytotoxin gene clusters coding from one to all three toxins (syringomycin, syringolin, and syringopeptin) (Hulin et al., 2018b; Ruinelli et al., 2019). These phytotoxins cause necrosis in plant tissues, and evidence points to a "trade-off" between bacteria phytotoxin production and effector proteins (Hulin et al., 2018b; Kennelly, 2007). The syringomycin phytotoxin is considered to be a significant virulence factor in *Pss* in addition to causing the release of plant nutrients it contributes to symptom development and aids in bacteria movement, and the genes for the production and delivery of the syringomycin phytotoxin, *syrB* and *syrD,* respectively are used as rapid identifiers of *Pss* via polymerase chain reaction (PCR) (Bultreys and Gheysen, 1999; Hulin et al., 2020; Sorensen et al., 1998; Xin et al., 2018).

1.3: *Pss* Management

Management practices for bacterial canker have been limited to copper (Cu) spray applications and cultural practices. Copper-resistant *Pss* populations have been detected throughout Michigan cherry orchards for over 3 decades [89% of strains (137/154) in 1987, 31.7% of strains (100/315) in 2003-2004, and 13.8% of strains (9/65) in 2021] (Lauwers, 2022; Sundin et al., 1989; Renick et al., 2008). Thus, copper is not a long-term sustainable option for bacterial canker management in Michigan. Copper resistance of *Pss* on cherry is due to a 61-kb plasmid that can facilitate the spread of Cu resistance via conjugation (Sundin et al., 1989). Copper resistance genes (*copABCDRS*) are a four-gene operon (copA, copB, copC, and copD) that encode outer membrane and periplasmic space proteins that can sequester Cu molecules, regulated by the genes *copS* (signals) and *copR* (expresses) (Puig et al., 2002). While Cu in trace amounts can be beneficial to plants, long-term use in agriculture has led to excessive Cu

accumulation in soils and can have deleterious effects on earthworms and other beneficial invertebrates, dependent on soil PH and the sensitivity of species (Duque et al., 2023; Karimi et al., 2021).

Other antibiotics such as oxytetracycline, streptomycin, and kasugamycin have been unavailable to Michigan growers for management of *Pss* on sweet cherry, with use restricted to apple (*Malus* x *domestica*) only, for control of the aggressive fire blight bacterial pathogen, *Erwinia amylovora,* due to resistance fears of resistance development (McGhee and Sundin, 2011; Slack et al., 2021; Sundin and Wang, 2018). However, as of 2020, kasugamycin became available for use in cherry, and no resistance has been detected yet in Michigan (Lauwers, 2022). Resistance to streptomycin is prevalent in Michigan, especially in *E. amylovora* populations, but could be acquired easily by *Pss* populations as well (via spontaneous mutation, or via plasmid conjugation or horizontal transfer) since streptomycin resistance has been detected in *Pseudomonas syringae pv. papulans* (Jones et al., 1991; McGhee et al., 2011; McGhee and Sundin, 2011; Slack et al., 2021; Sundin and Bender, 1996; Sundin and Wang, 2018).

The cultural practices used by growers to reduce potential *Pss* infection consist of weed control (to reduce host plant reservoirs), avoidance of overhead irrigation (to reduce dissemination of the bacteria), planting less susceptible cultivars and rootstocks, and pruning during warm, dry weather (Lattore and Jones, 1979; Spotts et al., 2010; Carroll et al., 2010). Currently, there are no sweet cherry cultivars commercially available that are known to be resistant to *Pss*; however, wild, ornamental, and hybrid *Prunus* are being tested for their ability to hinder *Pss* establishment/proliferation, and results are promising (Hulin et al., 2022).

Adherence to cultural control methods does not guarantee disease avoidance. Spotts et al. (2010) found that heading cuts were susceptible to *Pss* infection under field conditions for <1

week in the summer and for 2-3 weeks in the winter. Law (2017) found that sweet cherry trees could be susceptible to infection 17-24 days after pruning with no statistical differences in temperature effect (10°C v. 20°C) in growth chamber experiments. Spotts et al. (2010) found that heading cuts had a high rate of severe *Pss* infections, while Carroll et al. (2010) found that leaving a stub during pruning could lower the risk of infections that eventually spread into the main trunk; both studies recommended summer pruning during warm dry weather. Infection by *Pss* often is observed in Michigan orchards following summer pruning even during "dry" periods. Summer pruning can help to partition photosynthetic carbon towards fruit during pre-harvest, reduce shading, and increase light penetration into the canopy after harvest for improved flower bud formation (Lang, 2019b). Michigan, especially the lower peninsula, frequently experiences periods of high relative humidity (≥ 60%) and extreme high relative humidity (≥ 85%), with the probability of an extended event (≥36 h) being 70% to > 90% (within 14 days) regardless of the time of year (Komoto et al., 2021). Monier and Lindow (2003) showed that *Pss* strain B728a formed more and larger aggregates of cells on leaves in high relative humidity. Lindemann and Upper (1985) also reported that more significant upward fluxes of bacteria into aerosols occurred during warm sunny days (wind speeds >1 m/s) at midday when bean (*Phaseolus vulgaris*) leaves were dry, but not when leaves were wet with dew. They also reported instances in which a significant downward flux of bacteria occurred in the evening during temperature inversions (Lindemann and Upper, 1985). As cherry leaves are sources of inoculant and heavy dew could facilitate dispersal via drip into pruning wounds, further research needs to be conducted in relation to summer infection following pruning, relative to the high humidity and dew points typical in Michigan. Recommendations to Michigan growers may need to include avoiding pruning during periods with high humidity and heavy dew formation.

The quest to find alternative methods for *Pss* management (other than antibiotics) that would complement cultural practices is on the rise. A current hot research initiative is the use of bacteriophage as a possible *Pss* management approach (Akbaba and Ozaktan, 2021; Lauwers, 2022; Luo et al., 2022; Oueslati et al., 2022; Pinheiro et al., 2019; Rabiey et al., 2020). While previously available commercial biological control agents have not been tested as thoroughly for sweet cherry bacterial canker as for fire blight management in apples, in general, biological control of bacterial diseases has had some variable success and is worthy of further investigation (Kennely et al., 2007; Sundin et al., 2009). The sweet cherry microbiome is an additional untapped and extremely valuable area of research for sustainable *Pss* management tactics.

1.4: *Pss* Epiphytic Living and the Leaf Microbiome

Epiphytic populations of bacteria are subject to extreme microclimate shifts; are susceptible to desiccation, UV degradation, and fluctuations in nutrient availability; and are vulnerable to plant immune responses (Vorholt, 2012). *Pss*, however, is successful at living epiphytically due to several complex adaptations such as motility, biosurfactant production, quorum sensing, UV damage repair, siderophore production, and aggregate formations (Burch et al., 2014; Gunasekera and Sundin, 2006; Haefele and Lindow, 1987; Hirano and Upper, 2000; Lindow and Brandl, 2003; Monier and Lindow, 2003; Quiñones et al., 2005; Vorholt, 2012; Wensing et al., 2010). Thirty-one genes significant for epiphytic colonization and fitness have been identified in *Pss* strain B728a, most of which are also important for the occupation of the apoplast, and which encode for amino acid and polysaccharide production (Helmann et al., 2019).

Epiphytic bacteria colonize protected regions of leaf surfaces, such as stomatal openings and the base of trichomes, to escape desiccation and access possible nutrient sources (Beattie and

Lindow, 1999; Mansvelt and Hattingh, 1987; Mansvelt and Hattingh, 1989; Monier and Lindow, 2004; Roos and Hattingh, 1983). *Pss* strain B728a inoculated on bean plants had a greater survival rate when colonized in larger aggregates than solitary cells, and resident populations facilitated the survival of immigrating cells, while aggregates of mixed bacteria populations (*Pss* with *Pantoea agglomerans*) varied in size and appeared to spatially segregate (Beattie and Lindow, 1999; Monier and Lindow, 2004; Monier and Lindow, 2005a; Monier and Lindow, 2005b).

Images from scanning electron microscopy of apple and sweet cherry leaves have shown *Pss* and *Psm* respectively, to aggregate near and within stomata, propagating within the "substomatal chambers" and expelling back out onto the leaf surface, while *Pss* on pear (*Pyrus communis*) was found near stomata and propagation appeared to occur at the base of trichomes and in cuticle depressions (Mansvelt and Hattingh, 1987; Mansvelt and Hattingh, 1989; Roos and Hattingh, 1983). Evapotranspiration from open stomata can cool leaves when temperatures are high, and *Pss* likely aggregates near them to escape desiccating conditions (increased temperature and dryness) (Monier and Lindow, 2004; Gommers, 2020; Kostaki et al., 2020). Bacteria carrying capacity corresponds to nutrient availability on leaves, and while the majority of sugars are depleted during bacteria growth, residual amounts remain, likely in regions of the leaf not occupied by bacteria (Mercier and Lindow, 2000). Mercier and Lindow (2000) found that sugar availability on leaves was species-specific and not evenly distributed across the leaf surface. While sweet cherry leaves have visibly apparent extrafloral nectary glands (which exude sugars) on the junction between the petiole and leaf, there is no mention in the literature of these being a source of nutrients or an infection point for *Pss*. Yee and Chapman (2008) assessed the influx of leaf nutrients available to a *Rhagoletis* sp. on cherry leaves from the extrafloral

nectaries and juice from bird-pecked fruit and Escalante-Péreza et al. (2012) have shown that the sugars from the extrafloral nectaries in Poplar (*Populus* spp.) have antimicrobial properties. It would be prudent to assess these influences on *Pss* population dynamics, especially considering *Pss* populations reportedly are low in the summer (Spotts et al., 2010).

Leaf bacterial populations vary according to plant host species, season, leaf age, location within the canopy, and leaf surface, but they are primarily dependent on "immigration, emigration, growth, and death," with the upper leaf surface communities mainly being influenced by dispersal (Hirano and Upper, 2000; Kinkel, 1997; Lindow and Brandl, 2003; Smets et al., 2022; Vorholt, 2012). Interactions of epiphytic bacteria are complex and can be positive with the production of "common goods" or negative with the production of antibiotic metabolites, as is true with the plant host's experience as well with bacteria causing disease or promoting plant growth (Bashir et al., 2022; Glick and Gamalero, 2021; Mina et al., 2019; Pattnaik et al., 2021; Vortholt, 2012; Xin et al., 2018). Synergisms between *Pseudomonas* spp. pathogens and non-pathogens are apparent. *Pss* and *P. viridiflava* frequently are isolated with the kiwi (*Actinidia* spp.) bacterial canker pathogen *P. syringae* pv. *actinidiae* (*Psa*), which has been reported to enhance *Psa* infections (Purahong et al., 2018). Colonization and infection by *Pseudomonas savastanoi* pv. *savastanoi* (*Psv*), the olive knot pathogen, is enhanced by the presence of the non-pathogens, *Erwinia toletana*, *E. oleae*, and *Pantoea agglomerans* (Buonaurio et al., 2015; Marchi et al., 2006). Michigan *Pss* is phylogenetically diverse (Lauwers 2022; Rennick et al., 2008). However, it is unclear how they interact with one another, if they co-occur on multiple plant organs (they were isolated from flowers), and if they can influence bacterial canker disease severity in certain combinations. Other bacteria occupants of the sweet cherry leaf microbiome are unknown, as are their potential functions or their relationship to *Pss*.

Although bacterial communities on leaves vary, a few species are commonly found (Hirano and Upper 2000; Lindow and Brandl, 2003; Vorholt, 2012). Common and consistent bacteria shared across habitats are known as the core microbiome (Neu et al., 2021; Shade and Handelsman, 2012; Vandenkoornhuyse et al., 2015; Laforest-Lapointe et al., 2016). Laforest-Lapointe et al. (2016) defined a core microbiome for temperate forest tree species as "OTUs (Operational Taxonomic Units) present on 99% or more of all trees sampled". Core microbiomes, however, can be selected via occurrence, relative abundance, or occurrence-abundance with each method having various caveats, neatly described by Neu et al. (2021). Defined core microbiomes can be used as a marker of plant health and are a way to simplify the complex array of bacteria inhabiting the leaf and can be useful to measure responses to various manipulations (Shade and Handelsmann, 2012.) Currently microbiomes are being surveyed at a greater and more thorough rate via culture-independent methods specifically by next-generation sequencing (NGS) technologies and sequencing of the 16S rDNA variable regions of bacteria (Knief, 2014; Kozich et al., 2013). Knowledge of the Michigan sweet cherry epiphytic bacteria that are present with *Pss* could be used to monitor how the community changes along with *Pss* population fluctuations/infections, and conceivably could be manipulated to assess how the community influences *Pss* as well as the potential for biological control of *Pss*.

Evidence of plant "recruitment" of bacteria and the drivers of bacterial community composition on leaves [season/time, host plant species/genotype, plant age, location/region, and neighbors (i.e., environment)] have been elucidated by research in forest/urban trees, grasses (pertinent to biofuels), wild perennials, and cultivated annuals and perennials (Grady et al., 2019; Jackson and Denney, 2011; Kembel et al., 2014; Kim et al., 2012; Laforest-Lapointe et al., 2016a; Laforest-Lapointe et al., 2016b; Laforest-Lapointe et al., 2017; Lajoie and Kembel,

2021a; Lajoie and Kembel, 2021b; Meyer et al., 2022; Noble et al., 2020; Redford et al., 2010; Redford and Fierer, 2009; Stone and Jackson, 2021; Wagner et al., 2015). The apple phyllosphere (bark to flower) microbiome, which harbors the fire blight bacterial disease pathogen, *Erwinia amylovora*, has been explored for community assemblages, responses to antimicrobials (streptomycin, kasugamycin, and copper), responses to microbial inoculations, and differing orchard management styles (organic vs. conventional) (Aleklett et al., 2014; Arrigoni et al., 2018; Cui et al., 2021; Glenn et al., 2015; He et al., 2021; He et al., 2012; Shade et al., 2013; Steven et al., 2018; Tancos and Cox, 2017; Wallis et al., 2021; Yashiro and McManus, 2012). The leaf microbiomes of tea (*Camellia sinensis*), citrus, and grapes have also been analyzed (Carvalho et al., 2020; Cernava et al., 2019; Gobbi et al., 2020; Mina et al., 2020; Miura et al., 2019; Singh et al. 2019; Wu et al. 2020). Ares et al. (2021), assessed the kiwi epiphytic microbiome in male and female plants to determine if the communities varied by sex and how the communities changed with the presence of the kiwi bacterial canker (*Psa*). The leaf microbiomes of the four *Prunus* spp. (apricot, tart cherry, peach, and plum) have also been surveyed and compared in bulk leaf samples (Jo et al., 2015). O'Gorman et al. (2023) recently studied the microbiome communities of sweet cherry fruit and flowers in relation to the cherry slip-skin-maceration disorder (cherry-SSMD), and Zhang et al. (2021) assessed post-harvest sweet cherry fruit microbiomes at room temperature and under cold storage conditions. No surveys of the sweet cherry, *Prunus avium* L., leaf microbiome have been conducted. There is very little understanding of how other bacteria on the leaf surface impact *Pss* virulence or trigger plant immune responses. Xin et al. (2018) discusses this as the 4th vertex of the disease triangle comprised of host, environment, and pathogen. Characterization of the sweet cherry leaf microbiome would further add to the body of knowledge of *Pss* and orchard ecology and create a

foundation for further exploration into community interactions with *Pss*, possibly aiding in the future management of *Pss* populations and perhaps suggesting potential biological control options. There is increasing interest by fruit growers and the crop protection industry in the use and production of biological controls or biopesticides for plant diseases is increasing, as part of the desire to "take a more environmentally friendly approach" (Herrick 2018).

1.5: Biological Control

The key to biocontrol success in managing plant pathogens will likely be an amalgamation of synergistic factors. One important aspect is to choose and isolate the best biocontrol agent for the environment and habitat in which the pathogen resides. For *Pss*, which is ubiquitous in the environment, it is important for biological control to maintain pathogen populations at a level too low for infection to occur. It is possible that through a survey of the bacterial populations that reside epiphytically alongside *Pss*, one could find bacteria that either facilitate or hinder the population growth of *Pss*. Kotan and Sahin (2006) assessed 206 bacteria strains as potential *Pss* biocontrol agents that were recovered from pome fruits in Turkey, using *in vitro*, *in vivo* (on 'Golden Delicious' apple), and carbon utilization assays. Their efforts yielded 10 strains that were most effective in reducing the severity of *Pss* infection in various combinations (Kotan and Sahin 2006). Kotan and Sahin (2006) found that there was an 83% similarity in carbon utilization between the stronger potential biocontrols and *Pss*, as opposed to a 66% similarity in carbon utilization between weaker potential biocontrols and *Pss*. Arrigoni et al. (2018) found that bark of apple and pear is a reservoir of potential biological control agents as bacteria genera from their microbiome analysis are known for their production of secondary metabolites as well as growth promotion and resistance induction capabilities. Bacteria previously isolated from the apple flower microbiome were found to reduce the level of the fire

blight caused by Erwinia amylovora dependent on the strains in the inoculum which were altering the community structure of the flower (Cui et al., 2021). Exploration of the sweet cherry microbiome via characterization of *Pss* strains as well as determining the community constituents alongside *Pss,* could possibly lead to the same potential biological control options for the management of *Pss* populations and, by extension, reduce the incidence of bacterial canker.

Biological controls of plant pathogens are thought to function in two major ways: 1) competitive exclusion of the pathogen from niche or nutrient resources, and 2) through antibiosis (Lindow and Brandl, 2003). Wilson and Lindow (1994) found that the ice nucleating strain *Pss* Ice^+ and the non-ice nucleating strain *Pss* Ice^- share the same niche, compete for the same nutrient resources, and can replace each other. Wilson and Lindow (1993) found that *Pseudomonas fluorescens* A506, which colonizes flower pistils, was able to reduce the amount of infection in pear by *Erwinia amylovora*; 17% of the blossoms were infected when *P. fluorescens* was inoculated 72 h prior to *E. amylovora*, while 50% of blossoms were infected when *E. amylovora* and *P. fluorescens* were co-inoculated, and 71% of blossoms were infected when *E. amylovora* was inoculated alone. *Pseudomonas fluorescens* A506 is in the commercial formulation of BlightBan® A506 (Nufarm, Alsip, Illinois), registered as a biological control of *Erwinia amylovora*, in apples (Stockwell and Stack, 2007). Vanneste et al. (1992) showed that the biocontrol *Erwinia herbicola* Eh252 (*Pantoea agglomerans*) was able to inhibit infection by *Erwinia amylovora* in pear fruit due to antibiotic production. Burr et al. (1996) showed that the isolate *Pseudomonas syringae* 508 was able to prevent conidia of the apple scab pathogen *Venturia inequalis* from germinating in *in vitro* experiments. Wickasono et al. (2017) found that endophytic *Pseudomonas* spp. isolated from the medicinal plant, Mānuka (*Leptospermum*

scoparium), were able to reduce colonization of *Psa* and subsequently kiwi bacterial canker severity through the production of antibiotic compounds. Current research has expanded biocontrol options to include compounds or non-pathogenic bacteria that can induce natural plant defense systems and/or promote plant growth (Lillrose et al. 2017, O'Brien, 2017; Stroud et al. 2022, Syed-Ab-Rahman et al., 2018). Actigard™, is one such product that can induce the plant's immune response as it mimics the defense hormone salicylic acid and is actively used for the management of *Psa* in kiwi (Stroud et al., 2022).

Though biocontrols have been shown experimentally to have the potential for managing plant pathogens, their overall success in the field has been largely inconsistent. Broniarek-Niemiec et al. (2023) tested several biological control/biopesticide products and found that those containing copper were still the most effective at managing bacterial canker in stone fruit. Lillrose et al. (2017) tested two plant-resistant inducers as well as three antibiotics and four biological controls applied to sweet cherry blossoms prior to wounding and inoculation with *Pss* and found that the antibiotic kasugamycin had the best result with 90% reduction in infection followed by the other two antibiotics (copper and oxytetracycline) and the biocontrol Blossom Protect (*Aureobasidium pullulans*) with 45-49% infection reduction. Sundin et al. (2009) showed that biocontrols currently available for fire blight control were not highly effective when tested in Michigan, Virginia, and New York, though success was better when the biocontrols were used with streptomycin. Braun-Kiewnick et al. (2000) had success controlling *Pss*, the basal kernel blight pathogen of barley (*Hordeum vulgare*), in the field when the biocontrol, *Pantoea agglomerans* (*Erwinia herbicola*) was applied before *Pss* infection, reducing the amount of blight 36-74% compared with the standard controls. Though biocontrols currently available for *Erwinia amylovora* have been assessed for blossom infection in apple and sweet cherry, no such

assessments have been documented for the management of epiphytic populations of *Pss* in Michigan cherry orchards (Sundin et al., 2009; Lillrose et al., 2017).

The variability of biological agents to control plant pathogens could be due to the unsuitability of the biocontrol for the environment or climatic conditions in which they are applied (Cook, 1993; Guetsky et al., 2001; Sundin et al., 2009). Guetsky et al. (2001) studied mixing of different types of biocontrols to improve the consistency of control of the fungal pathogen, *Botrytis cinerea*, in strawberry (*Fragaria ananassa*). They found that the yeast, *Pichia guikermondii,* and the bacteria, *Bacillus mycoides*, had different temperature and humidity requirements for optimal growth. When used together, they were able to better control *B. cinerea* under varying conditions (Guetsky et al., 2001). Stockwell et al. (2011) found that mixing biocontrol agents improved control of *Erwinia amylovora* only when the biocontrols did not interfere with one another or were "mechanistically compatible" with each other. The biocontrol *Pseudomonas fluorescens* A506 produces a protease that degrades the antibiotics that are produced by the biocontrols *Pantoea vagans* C9-1 and *Pantoea agglomerans* Eh252, and when applied in combination, did not improve the variation of control of *E. amylovora* (Stockwell et al., 2011). However, when the mutant of *P. fluorescens* A506 (A506 aprX::Tn5) that lacked the enzyme was used with the *Pantoea* sp., fire blight was reduced by 86-78%.

Another likely reason for the variable success of biological control agents in the field could be due to the native pathogen or non-pathogens populations already present on the plants at unknown concentrations that could confound the results of the inoculated pathogen population and the assessment of their possible biological controls. *Pss* and *Pseudomonas*, in general, are a diverse group of organisms with pathogenic and non-pathogenic strains that are able to cohabitate commensally and synergistically with other bacteria (Hulin et al., 2020; Lauwers,

2022; Melnyk et al., 2019; Purahong et al., 2018; Shalev et al., 2021; Shalev et al., 2022; Xin et al. 2018). With this in mind and given the fact that *Pss* is like a wolf in sheep's clothing in that even pathogenic strains can live epiphytically without causing pathogenesis, it could be hypothesized that *Pss* populations would be difficult to manage with biological controls because they are able to adapt to co-existence with a broad range of other bacteria.

Even with the inconsistent nature of available biological controls, grower and industry interest in the use and production of these products (biological controls or biopesticides) for plant diseases is increasing as part of the desire to "take a more environmentally friendly approach", and many companies that produce biocontrols are part of the Biological Products Industry Alliance (Herrick, 2018). Lytic bacteriophage is currently garnering a lot of research attention as a biological control of *Pss* (single phage and cocktails) along with the commercially available AgriPhage™ (Akbaba and Ozaktan, 2021; Lauwers, 2022; Luo et al., 2022; Oueslati et al., 2022; Pinheiro et al., 2019; Rabiey et al., 2020). Rabiey et al. (2020) isolated 70 phages from soil and tested them (singly and in cocktails) against *Pss* populations on bean and cherry leaves and found reductions of ~20-100% in *Pss* populations at specific time points throughout the course of the experiments. Studies in this area are already underway in Michigan (Lauwers, 2022). A thorough understanding of the *Pss* that inhabits the sweet cherry microbiome, along with the elucidation of the other sweet cherry microbiome *Pseudomonas*, could lead to a broader range of possible hosts for use in bacteriophage research in Michigan.

Stroud et al. (2022) highlight the difficulties in making assessments of biological products in field settings and the importance of small-scale laboratory-type studies, such as using tissue culture to better understand how Actigard™ affects *Psa* populations. As field studies and even growth chamber studies with live plants are often time-consuming, resource-intensive, and

often yield inconclusive results, simpler in vitro studies would be ideal to initially screen an organism's potential as a biological control. Dual culture or co-inoculation Petri dish assays are frequently used to assess the potential biological control activity of a bacteria versus a pathogenic fungus (Chaouachi et al., 2021; Cirvilleri et al., 2005, Derikvan et al., 2023; Hammami et al., 2022, Lu et al., 2022; Niem et al., 2020, Nysanth et al. 2022). Mina et al. (2020b) have also demonstrated that this assay type was a viable way to assess the effect of a bacterial biological control agent against the olive knot pathogen *Pseudomonas savastanoi* pv. *savastanoi*. This would also be useful to survey potential biological control agents for *Pss* as well as study how two *Pss* strains that had been isolated from sweet cherry may interact with each other in co-culture.

1.6: Objectives of Study

The objectives of this research dissertation are to: 1) phenotypically and phylogenomically characterize *Pss* strains isolated from cherry flowers via biochemical, virulence assays, and Multilocus sequence analysis (MLST); 2) characterize the sweet cherry leaf microbiome over time (seasons), and across cultivars, in two regions of Michigan to determine a) if there are regional and seasonal differences in the sweet cherry microbiome, b) if the leaf microbiome varies across sweet cherry cultivars, and c) what bacterial species are consistently present with *Pss;* and 3) to evaluate commercially available biological control agents a) for their ability to decrease *Pss* growth *in vitro*, b) determine if avirulent/moderately virulent *Pss* recovered from Michigan sweet cherry orchards can decrease virulent/moderately virulent *Pss* growth *in vitro*, and c) determine whether *in vitro* co-inoculations are a viable, easily employed option for the initial assessment of biological controls for *Pss*. The results of this research will contribute to, and can be integrated with, the current sweet cherry bacterial canker

body of knowledge, thereby advancing the potential success of identifying and utilizing innovative management strategies for *Pss*.

REFERENCES

Abdellatif, E., Kałużna, M., Ferrante, P., Scortichini, M., Bahri, B., Janse, J.D., van Vaerenberg, J., Baeyen, S., Sobiczewski, P., and Rhouma, A. 2020. Phylogenetic, genetic, and phenotypic diversity of Pseudomonas syringae pv. syringae strains isolated from citrus blast and black pit in Tunisia. Plant Pathol. 69: 1414– 1425.

Akbaba, M., Ozaktan, H. 2021. Evaluation of bacteriophages in the biocontrol of Pseudomonas syringae pv. syringae isolated from cankers on sweet cherry (Prunus avium L.) in Turkey. Egypt. J. Biol. Pest Control 31: 35. https://doi.org/10.1186/s41938-021-00385-7

Aleklett, K., Hart, M., and Shade, A. 2014. The microbial ecology of flowers: an emerging frontier in phyllosphere research. Botany 92(4): 253-266.

Alfano, J.R., and Collmer, A. 2004. Type III secretion system effector proteins: double agents in bacterial disease and plant defense. Annu. Rev. Phytopathol. 42: 385-414.

Almeida N.F., Yan S., Cai R., Clarke C.R., Morris C.E., Schaad N.W., Schuenzel E.L., Lacy G.H., Sun X., Jones J.B., Castillo J.A., Bull C.T., Leman S., Guttman D.S., Setubal J.C., and Vinatzer B.A. 2010. PAMDB, a multilocus sequence typing and analysis database and website for plant-associated microbes. Phytopathology 100(3):208-215.

Ares, A., Pereira, J., Garcia, E., Costa, J., and Tiago, I. 2021. The leaf bacterial microbiota of female and male kiwifruit plants in distinct seasons: Assessing the impact of Pseudomonas syringae pv. actinidiae. Phytobiomes J. 5:275-287.

Arrigoni, E., Antonielli, L., Pindo, M., Pertoto, I., and Perazzolli, M. 2018. Tissue age and plant genotype affect the microbiota of apple and pear bark. Microbiological Research 211: 57-58.

Ayala, M., and Lang, G.A. 2017. Morphology, cropping physiology and canopy training. In Quero-Garcia, J., Iezzoni, A., Pulawska, J., and Lang, G. (Eds.), Cherries: botany, production, and uses (pp. 269-304). CAB International.

Bashir, I., War, A.F., Rafiq, I., Reshi, Z.A., Rashid, I., and Shouche, Y.S. 2022. Phyllosphere microbiome: diversity and functions. Microb. Research 254: 126888.

Beattie, G.A. and Lindow, S.E. (1999), Bacterial colonization of leaves: a spectrum of strategies. Phytopathology 89: 353-359.

Berge, O., Monteil C.L., Bartoli, C., Chandeysson, C., Guilbaud, C., Sands, D.C., and Morris, C.E. 2014. A user's guide to a data base of the diversity of pseudomonas syringae and its application to classifying strains in this phylogenetic complex. PLoS ONE 9(9): e105547. doi:10.1371/journal.pone.0105547.

Bophela, K.N., Peterson, Y., Bull, C.T., and Coutinho, T.A. 2020. Identification of Pseudomonas isolates associated with bacterial canker of stone fruit trees in the western cape, South Africa. Plant Disease 104: 882-892.

Braun-Kiewnick, A., Jacobsen, B.J., and Sands, D.C. 2000. Biological control of Pseudomonas syringae pv. syringae, the causal agent of basal kernel blight of barley, by antagonistic Pantoea agglomerans. Phytopathology 90: 368-375.

Brown, E. L. 1941. A study of the cherry industry of the Michigan fruit belt. Master's thesis, Wayne State University, ProQuest Dissertations and Theses Global.

Bujdosó, G., and Hrotkó, K. 2017. Cherry production. In Quero-Garcia, J., Iezzoni, A., Pulawska, J., and Lang, G. (Eds.), Cherries: botany, production, and uses (pp. 1-13). CAB International.

Buonaurio, R., Moretti, C., Passos da Silva, D., Cortese, C., Ramos, C., and Venturi, V. 2015. The olive knot disease as a model to study the role of interspecies bacterial communities in plant disease. Front. Plant Sci. 6 (434): 1-12.

Burch, A.Y., Zeisler, V., Yakota, K., Schreiber, L., and Lindow, S.E. 2014. The hygroscopic biosurfactant syringafactin produced by Pseudomonas syringae enhances fitness on leaf surfaces during fluctuating humidity. Env. Mircrobiol. 16(7): 2086-2098.

Burr, T.J. Matteson, M.C., Smith, C.A., Corral-Garcia, M.R., and Huang, T. 1996. Effectiveness of bacteria and yeasts from apple orchards as biological control agents of apple scab. Biological Control 6:151-157.

Carroll, J., Robinson, T., Burr, T., Hoying, S., and Cox, K. 2010. Evaluation of pruning techniques and bactericides to manage bacterial canker of sweet cherry. New York Fruit Quarterly 18(1): 9-15.

Carvalho, C.R., Dias, A.C., Homma, S.K., and Cardoso, E.J. 2020. Phyllosphere bacterial assembly in citrus crop under conventional and ecological management. PeerJ 8:e9152.

Cernava, T., Chen, X., Krug, L., Li, H., Yang, M., and Berg, G. 2019. The tea leaf microbiome shows specific responses to chemical pesticides and biocontrol applications. The Science of the total environment 667: 33-40.

Chaouachi M., Marzouk, T., Jallouli, S., Elkahoui, S., Gentzbittel, L., Ben, C., and Djébali, N. 2021. Activity assessment of tomato endophytic bacteria bioactive compounds for the postharvest biocontrol of Botrytis cinerea. Postharvest Biol. Tech. 172:111389.

Cirvilleri, G., Bonaccorsi, A., Scuderi, G., and Scortichini, M. 2005. Potential biological control activity and genetic diversity of Pseudomonas syringae pv. syringae strains. J. Phytopathol. 153: 654-666.

Clarke, C.R., Cai, R., Studholme, D.J., Guttman, D.S., and Vinatzer, B.A. 2010. Pseudomonas syringae strains naturally lacking the classical P. syringae hrp/hrc locus are common leaf colonizers equipped with an atypical type III secretion system. Molecular Plant-Microbe Interactions® 23(2): 198-210.

Cook, R.J. 1993. Making greater use of introduced microorganisms for biological control of plant pathogens. Ann. Rev. Phytopathol. 31: 53-80.

Cornelis, P. 2010. Iron uptake and metabolism in pseudomonads. Appl. Microbiol. Biotech. 86(6):1637–1645.

Cui, Z., Huntley, R.B., Schultes, N.P., Steven, B., and Zeng, Q. 2021. Inoculation of stigma-colonizing microbes to apple stigmas alters microbiome structure and reduces the occurrence of Fire Blight disease. Phytobiomes J. 5: 156-165

Derikvan, F., Bazgir, E., El Jarroudi, M., Darvishnia, M., Najafgholi, H.M., Laasli, S-E., and Lahlali, R. 2023. Unleashing the potential of bacterial isolates from apple tree rhizosphere for biocontrol of Monilinia laxa: A promising approach for combatting brown rot disease. J. Fungi 9:828.

Duque, T., Nuriyev, R., Römbke, J., Schäfer, R.B. and Entling, M.H. 2023. Variation in the chemical sensitivity of earthworms from field populations to imidacloprid and copper. Environ Toxicol Chem. https://doi.org/10.1002/etc.5589

Escalante-Péreza, M., Jaborsky, M., Reindersb, J., Kurzaic, O., Hedricha, R., and Achea, P. 2012. Poplar extrafloral nectar is protected against plant and human pathogenic fungus. Molec. Plant 5(5): 1157-1159.

Gardan, L., Shafik, H., Belouin, S., Broch, R., Grimont, F., and Grimont, P.A.D. 1999. DNA relatedness among the pathovars of Pseudomonas syringae and description of Pseudomonas tremae sp. nov. and Pseudomonas cannabina sp. nov. (ex Sutic and Dowson 1959). Int. J. Sys. Bact. 49: 469-478.

Glenn, D.M., Basset, C., and Dowd, S.E. 2015. Effect of pest management system on ‘Empire’ apple leaf phyllosphere populations. Sci. Hort. 183: 58-65.

Glick, B.R., and Gamalero, E. 2021. Recent developments in the study of plant microbiomes. Microorganisms 9(7):1533.

Gobbi, A., Kyrkou, I., Filippi, E., Ellegaard-Jensen, L., and Hansen, L.H. 2020. Seasonal epiphytic microbial dynamics on grapevine leaves under biocontrol and copper fungicide treatments. Scientific Reports 10(1): 681.

Gomila, M., Busquets, A., Mulet, M., García-Valdés, E., and Lalucat, J. 2017. Clarification of taxonomic status within the Pseudomonas syringae species group based on a phylogenomic analysis. Frontiers Microbiol. 8: 2422.

Gommers, C. 2020. Keep cool and open up: temperature-induced stomatal opening. *Plant Physiol.* 182(3):1188–1189.

Grady, K.L., Sorensen, J.W., Stopnisek, N., Guittar, J., and Shade, A. 2019. Assembly and seasonality of core phyllosphere microbiota on perennial biofuel crops. Nat. Commun. 10:4135.

Gunasekera, T.S., and Sundin, G.W. 2006. Role of nucleotide excision repair and photoreactivation in the solar UVB radiation survival of Pseudomonas syringae pv. syringae B728a. J. Appl. Microbiol. 100: 1073-1083.

Guetsky, R., Shtienberg, D., Elad, Y., and Dinoor, A. 2001. Combining biocontrol agents to reduce variability of biological control. Phytopathology 91: 621-627.

Gutiérrez-Barranquero J. A., Cazorla, F. M., de Vicente, A. 2019. Pseudomonas syringae pv. syringae associated with mango trees, a particular pathogen within the “hodgepodge” of the Pseudomonas syringae Complex. Frontiers Plant Sci. 10: 570.

Haefele, D.M. and Lindow S.E. 1987. Flagellar motility confers epiphytic fitness advantages upon pseudomonas syringae. Appl Environ Microbiol 53: 2528-2533.

Hall, S.J., Dry, I.B., Gopurenko, D. and Whitelaw-Weckert, M.A. 2019. Pseudomonas syringae pv. syringae from cool climate Australian grapevine vineyards: new phylogroup PG02f associated with bacterial inflorescence rot. Plant Pathol. 68: 312-322.

Hammami, R., Oueslati, M., Smiri, M., Nefzi, S., Ruissi, M., Comitini, F., Romanazzi, G., Cacciola S.O., and Zouaoui, N.S. 2022. Epiphytic yeast and bacteria as candidate biocontrol agents of green and blue molds of citrus fruits. J. Fungi 8:818.

He, Y-H., Adkar-Purushothama, C.R., Ito, T., Shirakawa, A., Yamamoto, H., Kashiwagi, A., Tatewaki, A., Fujibayashi, M., Sugiyama, S., Yaginuma, K., Akahira, T., Yamamoto, S., Tsushima, S., Matsushita, Y., and Sano, T. 2021. Microbial diversity in the phyllosphere and rhizosphere of an apple orchard managed under prolonged “natural farming” practices. Microorganisms 9: 2056.

He, Y-H., Isono, S., Shibuya, M., Tsuji, M., Adkar-Purushothama, C.R., Tanaka, K., and Sano, T. 2012. Oligo-DNA custom microarray for monitoring major pathogenic and non-pathogenic fungi and bacteria in the phyllosphere of apple trees. PLoS ONE 7(3):e34249.

Helmann, T.C., Deutschbauer, A.M., and Lindow, S.E. 2019. Genome-wide identification of Pseudomonas syringae genes required for fitness during colonization of the leaf surface and apoplast. Proc. Natl. Acad. Sci. 116(38): 18900-18910.

Herrick, C. 2018. Biological controls have a place in fruit production. American Fruit Grower 138(12):10-11.

Hirano, S.S., and Upper, C.D. 1990. Population biology and epidemiology of Pseudomonas syringae. Annu. Rev. Phytopathol. 28:155-177.

Hirano, S.S., and Upper, C.D. 2000. Bacteria in the leaf ecosystem with emphasis on Pseudomonas syringae – a pathogen, ice nucleus, and epiphyte. Microbiol. Mol. Biol. Rev. 64(3): 624-653.

Hulin, M.T., Mansfield, J.W., Brain, P., Xu, X., Jackson, R.W., and Harrison, R.J. 2018a. Characterization of the pathogenicity of strains of Pseudomonas syringae towards cherry and plum. Plant Pathol. 67: 1177-1193.

Hulin, M.T., Armitage, A.D., Vicente, J.G., Holub, E.B., Baxter, L., Bates, H.J., Mansfield, J.W., Jackson, R.W. and Harrison, R.J. 2018b. Comparative genomics of Pseudomonas syringae reveals convergent gene gain and loss associated with specialization onto cherry (Prunus avium). New Phytol. 219: 672-696.

Hulin, M.T., Jackson, R.W., Harrison, R.J., and Mansfield, J.W. 2020. Cherry picking by pseudomonads: After a century of research on canker, genomics provides insights into the evolution of pathogenicity towards stone fruits. Plant Pathol. 69: 962– 978.

Hulin M.T., Vadillo Dieguez A., Cossu F., Lynn S., Russell K., Neale H.C., Jackson R.W., Arnold D.L., Mansfield J.W., and Harrison R.J. 2022. Identifying resistance in wild and ornamental cherry towards bacterial canker caused by Pseudomonas syringae. Plant Pathol. 71(4):949-965.

Hwang, M.S., Morgan, R.L., Sarkar, S.F., Wang, P.W., and Guttman, D.S. 2005. Phylogenetic characterization of virulence and resistance phenotypes of Pseudomonas syringae. Appl Environ Microbiol. 71(9):5182-91.

Iličić, R., Jelušić, A., Marković, S., Barać, G., Bagi, F., and Popović, T. 2021. Pseudomonas cerasi, the new wild cherry pathogen in Serbia and the potential use of recG helicase in bacterial identification. Ann. Appl. Biol. 180: 140-150.

Ivanović, M., Prokić, A., Gašić, K., Menković, J., Kuzmanovic, N., Zlatkovic, N., and Obradović, A. 2022. Characterization of Pseudomonas syringae strains associated with shoot blight of raspberry and blackberry in Serbia. Plant Dis. 10.1094/PDIS-06-22-1425-RE. Advance online publication. https://doi.org/10.1094/PDIS-06-22-1425-RE

Jackson, C.R., and Denney, W.C. 2011. Annual and seasonal variation in the phyllosphere bacterial community associated with leaves of the southern magnolia (Magnolia grandiflora). Microb. Ecol. 61: 113-122.

Jones, A.L. 1971. Bacterial canker of sweet cherry in Michigan. Plant Disease Reporter 55(11): 961-965.

Jones, A.L., Norelli, J.L., and Ehret, G.R. 1991. Detection of streptomycin-resistant Pseudomonas syringae pv. papulans in Michigan apple orchards. Plant Dis. 75: 529-531.

Jones, A.L., and Sutton, T.A. 1996. Diseases of tree fruits in the east. Michigan State University Extension NCR 45 p. 71-72.

Karimi, B., Masson, V., Guilland, C., Leroy, E., Pellegrinelli, S., Giboulot, E., Maron, P., and Ranjard, L. 2021. Ecotoxicity of copper input and accumulation for soil biodiversity in vineyards. Environ. Chem. Lett. 19: 2013–2030. https://doi.org/10.1007/s10311-020-01155-x

Kembel, S.W., O'Connor, T.K., Arnold, H.K., Hubbell, S.P., Wright, S.J., and Green, J.L. 2014. Relationships between phyllosphere bacterial communities and plant functional traits in a neotropical forest. Proc. Nat. Acad. Sci. 111(38):13715–13720.

Kim, M., Singh, D., Lai-Hoe, A., Go, R., Rahim, R.A., A.N., A., Chun, J., and Adams, J.M. 2012. Distinctive phyllosphere bacterial communities in tropical trees. Microb. Ecol. 63:674-681.

Kinkel, L.L. 1997. Microbial population dynamics on leaves. Ann. Rev. Phytopathol. 35(1): 327-347.

Knief, C. 2014. Analysis of plant microbe interactions in the era of next generation sequencing technologies. Front. Plant Sci. 5:1-23

Komoto, K., Soldo, L., Tang, Y., Chivers, M. I., Dahlin, K., Guentchev, G., Rill, L., and Winkler, J.A. 2021. Climatology of persistent high relative humidity: An example of the lower peninsula of Michigan, USA. Int. J. Climatol. 41(Suppl.1): E2517– E2536. https://doi.org/10.1002/joc.6861

Kostaki, K. I., Coupel-Ledru, A., Bonnell, V. C., Gustavsson, M., Sun, P., McLaughlin, F. J., Fraser, D. P., McLachlan, D. H., Hetherington, A. M., Dodd, A. N., and Franklin, K. A. 2020. Guard cells integrate light and temperature signals to control stomatal aperture. Plant Physiol. 182(3): 1404–1419.

Kotan, R., and Sahin, F. 2006. Biological control of Pseudomonas syringae pv. syringae and nutritional similarity in carbon source utilization of pathogen and its potential biocontrol agents. J. Turk. Phytopath. 35 (1-3): 1-13.

Kozich, J.J., Westcott, S.L., Baxter, N.T., Highlande,r S.K., and Schloss P.D. 2013. Development of a dual-index sequencing strategy and curation pipeline for analyzing amplicon sequence data on the MiSeq Illumina sequencing platform. Appl. Environ. Microbiol. 79(17): 5112-5120.

Kennelly, M.M., Carzola, F.M., de Vicente, A., Ramos, C., and Sundin, G.W. 2007. Pseudomonas syringae diseases of fruit trees: progress to understanding and control. Plant Disease 91(1): 4-17.

Laforest-Lapointe, I., Messier, C., and Kembel, S.W. 2016a. Host species identity, site and time drive temperate tree phyllosphere bacterial community structure. Microbiome 4:27.

Laforest-Lapointe, I., Messier, C., and Kembel, S.W. 2016b. Tree phyllosphere bacterial communities: exploring the magnitude of intra- and inter-individual variation among host species. PeerJ 4:e2367

Laforest-Lapointe, I., Messier, C., and Kembel, S.W. 2017. Tree leaf bacterial community structure and diversity differ along a gradient of urban intensity. mSystems 2:e00087-17.

Lajoie, G., and Kembel, S.W. 2021a. Plant-bacteria associations are phylogenetically structures in the phyllosphere. Molec. Ecol. 30: 5572– 5587.

Lajoie, G., and Kembel, S.W. 2021b. Host neighborhood shapes bacterial community assembly and specialization on tree species across a latitudinal gradient. Ecol. Monographs 91(2):e01443.

Lang, G.A. 2019a. The cherry industries in the USA: current trends and future perspectives. Acta Hort. 1235: 119-132.

Lang, G.A. 2019b. Sustainable sweet cherry cultivation: a case study for designing optimized orchard production systems. In Lang, G.A. (Ed.), Achieving sustainable cultivation of temperate zone tree fruits and berries: Volume 2 case studies (pp. 89-123). Burleigh Dodds Science Publishing.

Lang, G.A., Blatt, S., Neilsen, D., Robinson, T.L., and Xu, H. 2022. Ten-year conclusions from the NC-140 sweet cherry canopy architecture-rootstock trials in North America. Acta Hort. 1346: 661-668.

Lang, G.A., Sage, L., and Wilkinson, T. 2016. Ten years of studies on systems to modify sweet cherry production environments: retractable roofs, high tunnels, and rain shelters. Acta Hort. 1130: 83-89.

Lang, G.A., Wilkinson, T., and Larson, J.E. 2019. Insights for orchard design and management using intensive sweet cherry canopy architectures on dwarfing to semi-vigorous rootstocks. Acta Hort. 1235: 161-167.

Latorre, B.A., and Jones, A.L. 1979a. Evaluation of weeds and plant refuse as potential sources of inoculum of *Pseudomonas syringae* in bacterial canker of cherry. Phytopathology 69: 1122-1125.

Latorre, B.A., and Jones, A.L. 1979b. Pseudomonas morsprunorum, the cause of bacterial canker of sour cherry in Michigan, and its epiphytic association with P. syringae. Phytopathology 69:335-339.

Latorre, B.A., González, J.A., Cox, J.A., and Vial, F. 1985. Isolation of Pseudomonas syringae pv. syringae from cankers and effect of free moisture on its epiphytic populations on sweet cherry trees. Plant Disease 69: 409-412.

Latorre, B.A., Lillo, C., and Rioja, M.E. 2002. Effects of temperature, free moisture duration and inoculum concentration on infection of sweet cherry by Pseudomonas syringae pv. syringae. Phytoparasitica 30(4): 410-419.

Lauwers, E. 2022. investigation of bacteriophage as a biological control for bacterial canker of sweet cherry. Master's thesis, Michigan State University, ProQuest Dissertations and Theses Global.

Law, T. 2017. Optimizing trellised canopy architecture for sweet cherry: tree establishment and protection from bacterial canker infection. Master's thesis, Michigan State University, ProQuest Dissertations and Theses Global.

Lelliot, R.A., Billing, E., and Hayward, A.C. 1966. A determinative scheme for the fluorescent plant pathogenic Pseudomonads. J. Appl. Bact. 29(3):470-489.

Lillrose, T., Lang, G.A. and Sundin, G.W. (2017). Strategies to minimize bacterial canker in high density sweet cherry orchards. Acta Hortic. 1161, 457-162
doi:10.176601/ActaHortic.2017.1161.73

Lindemann, J., and Upper, C.D. 1985. Aerial dispersal of epiphytic bacteria over bean plants. Appl. Env. Microbiol. 50(5): 1229-1232.

Lindow, S.E., and Brandl, M.T. 2003. Microbiology of the phyllosphere. Appl. Environ. Microbiol. 69(4): 1875-1883.

Lu, L., Karunatathna, S.C., Hyde, K.D., Suwannarach, N., Elgorban, A.M., Stephenson, S.L., Al-Rejaie, S., Jayawardena, R.S., and Tibpromma, S. 2022. Endophytic fungi associated with coffee leaves in China exhibited in vitro antagonism against fungal and bacterial pathogens. J. Fungi 8:698.

Luo, J., Dai, D., Lv, L., Ahmed, T., Chen, L., Wang, Y., An, Q., Sun, G., and Li, B. 2022. Advancements in the use of bacteriophages to combat the kiwifruit canker phytopathogen Pseudomonas syringae pv. actinidiae. *Viruses* 14(12):2704. https://doi.org/10.3390/v14122704

Mansvelt, E.L., and Hattingh, M.J. 1987. Scanning electron microscopy of colonization of pear leaves by Pseudomonas syringae pv. syringae. Can. J. Bot. 65:2517-2522.

Mansvelt, E.L., and Hattingh, M.J. 1989. Scanning electron microscopy of invasion of apple leaves and blossoms by Pseudomonas syringae pv. syringae. Appl. Env. Microbiol. 55(2): 533-538.

Marchi, G., Sisto, A., Cimmino, A., Andolfi, A., Cipriani, M.G., Evidente, A. and Surico, G. 2006. Interaction between Pseudomonas savastanoi pv. savastanoi and Pantoea agglomerans in olive knots. Plant Pathol. 55: 614-624.

McGhee, G. C., Guasco, J., Bellomo, L. M., Blumer-Schuette, S. E., Shane, W. W., Irish-Brown, A., and Sundin, G. W. 2011. Genetic analysis of streptomycin-resistant (SmR) strains of Erwinia amylovora suggests that dissemination of two genotypes is responsible for the current distribution of SmRE. amylovora in Michigan. Phytopathology 101:182-191.

McGhee, G.C., Sundin, G.W. 2011. Evaluation of kasugamycin for fire blight management, effect on nontarget bacteria, and assessment of kasugamycin resistance potential in Erwinia amylovora. Phytopathology. 101(2): 192-204.

MDARD 2018. Michigan agricultural facts and figures. Retrieved from https://www.michigan.gov/-/media/Project/Websites/mdard/documents/business-development/mi_ag_facts_figures.pdf?rev=9ca97e867d0d40b392470b02a2694e50

MDARD 2023. Michigan agricultural resources: Facts about Michigan agriculture. Retrieved from https://www.michigan.gov/mdard/about/mi-agriculture/michigan-agriculture-resources

Melynyk, R.A., Hossain, S.S., and Haney, C.H. 2019. Convergent gain and loss of genomic islands drive lifestyle changes in plant-associated Pseudomonas. ISME J. 13:1575-1588.

Mercier, J., and Lindow, SE. 2000. Role of leaf surface sugars in colonization of plants by bacterial epiphytes. Appl. Environ. Microbiol. 66(1):369-74.

Meyer, K.M., Porch, R., Muscettola, I.E., Vasconcelos, A.S., Sherman, J.K., Metcalf, C.J.E., Lindow, S.E., and Koskella, B. 2022. Plant neighborhood shapes diversity and reduces interspecific variation of the phyllosphere microbiome. ISME J**.** 16:1376–1387.

Mina, D., Pereira, J.A., Lino-Neto, T., and Baptista, P. 2019. Exploring the phyllosphere bacterial community for improving tree crop protection. In Kumar, V., Prasad, R., Kumar, M., and Choudhary, D.K. (Eds.), Microbiome in plant health and disease (pp. 35-52). Springer, Singapore.

Mina, D., Pereira, J.A., Lino-Neto, T., and Baptista, P. 2020a. Epiphytic and endophytic bacteria on olive tree phyllosphere: Exploring tissue and cultivar effect. Microb. Ecol. 80:145-157.

Mina, D., Pereira, J.A., Lino-Neta, T., and Baptista, P. 2020b. Screening the olive tree phyllosphere: search and find potential antagonists against Pseudomonas savalstanoi pv. savastanoi. Frontiers Microbiol. 11: 2051

Miura, T., Sánchez, R., Castañeda, L.E., Godoy, K., and Barbosa, O. 2019. Shared and unique features of bacterial communities in native forest and vineyard phyllosphere. Ecol. Evol. 9(6): 3295-3305.

Mohr, T. J., Liu, H., Yan, S., Morris, C. E., Castillo, J. A., Jelenska, J., and Vinatzer, B. A. 2008. Naturally occurring nonpathogenic isolates of the plant pathogen Pseudomonas syringae lack a type III secretion system and effector gene orthologues. J. Bacteriol. 190:2858-2870.

Monier, J.M., and Lindow, S.E. 2003. Differential survival of solitary and aggregated bacterial cells promotes aggregate formation on leaf surfaces. PNAS 100(26): 15977-15982.

Monier, J.M. and Lindow, S.E. 2004. Frequency, size, and localization of bacterial aggregates on bean leaf surfaces. Appl. Env. Microbiol. 70: 346-355.

Monier, J.M, and Lindow, S.E. 2005a. Aggregates of resident bacteria facilitate survival of immigrant bacteria on leaf surfaces. Microb. Ecol. 49(3): 343–352.

Monier, J.M, and Lindow, S.E. 2005b. Spatial organization of dual-species bacterial aggregates on leaf surfaces. Appl. Env. Microbiol. 70(9): 5484-5493.

Morris, C.E., Lamichhane, J.R., Nikolić, I., Stanković, S., and Moury, B. 2019. The overlapping continuum of host range among strains in the Pseudomonas syringae complex. Phytopathol. Res. 1:4.

Morris, C.E., Monteil, C.L., and Berge, O. 2013. The life history of Pseudomonas syringae: linking agriculture to earth system processes. Annu. Rev. Phytopathol. 51: 85-104.

Morris, C.E.**,** Sands, D.C.**,** Vanneste, J.L.**,** Montarry, J.**,** Oakley, B**.**, Guilbaud, C., and Glaux, C. 2010**.** Inferring the evolutionary history of the plant pathogen Pseudomonas syringae from its biogeography in headwaters of rivers in North America, Europe and New Zealand. mBio 1(3):e00107–10.

Morris, C., Sands, D., Vinatzer, B., Glaux, C., Guilbaud, C., Buffière, A., Yan, S., Dominguez, H., and Thompson, B.M. 2008. The life history of the plant pathogen *Pseudomonas syringae* is linked to the water cycle. ISME J. 2: 321–334.

Neu, A.T., Allen, E.E., and Roy, K. 2021. Defining and quantifying the core microbiome: Challenges and prospects. Proc. Natl. Acad. Sci. 118(51):e2104429118.

Niem J.M., Billones-Baaijens, R., Stodart, B., and Savocchia, S. 2020. Diversity profiling of grapevine microbial endosphere and antagonistic potential of endophytic Pseudomonas against grapevine trunk disease. Frontiers Microbiol. 11:477.

Noble, A.S., Noe, S., Clearwater, M.J., and Lee, C.K. 2020. A core phyllosphere microbiome exists across distant populations of a tree species indigenous to New Zealand. PLoS ONE 15(8):e0237079.

Nysanth N.S., Sivapriya, S.L., Natarajan, C., and Anith, K.N. 2022. Novel in vitro methods for simultananeous screening of two antagonistic bacteria against multiple fungal phytopathogens in a single agar plate. 3 Biotech 12:140.

O'Brien, P.A. 2017. Biological control of plant diseases. Australasian Plant Pathol. 46:293–304 (2017). https://doi.org/10.1007/s13313-017-0481-4

O'Gorman, D.T., Haag, P., Boulé, J., Healy, G., Fraser, J., Walker, M., and Úrbez-Torres, J.R. 2023. Microbial communities of sweet cherry (Prunus avium L.) and assessment of their association with cherry slip-skip-maceration disorder. Can. J. Plant Pathol. 45(1): 57-69.

Oksel, C., Avin, F.A., Mirik, M., and Baysal-Gurel, F. 2022. Identification and genetic characterization of Pseudomonas syringae pv. syringae from sweet cherry in Turkey. Plant Disease 106: 1253-1261.

Oueslati, M., Holtappels, D., Fortuna, K., Hajlaoui, M. R., Lavigne, R., Sadfi-Zouaoui, N., and Wagemans, J. 2022. Biological and molecular characterization of the lytic bacteriophage SoKa against Pseudomonas syringae pv. syringae, causal agent of citrus blast and black pit in Tunisia. Viruses 14(9): 1949. https://doi.org/10.3390/v14091949

Pattnaik, S.S., Paramanantham, P., and Busi, S. 2021. Agricultural importance of phyllosphere microbiome: recent trends and future perspectives. In Srivastava, A.K., Kashyap, P.L., and Srivastava, M. (Eds.), The plant microbiome and sustainable agriculture (pp. 119-139). Wiley and Sons Ltd.

Pinheiro, L.A.M., Pereira, C., Frazão, C., Balcão, V.M., and Almeida, A. 2019. Efficiency of phage φ6 for biocontrol of Pseudomonas syringae pv. syringae: An in vitro preliminary study. Microorganisms 7(9): 286. doi: 10.3390/microorganisms7090286. PMID: 31450735; PMCID: PMC6780397.

Popović, T., Menković, J., Prokić, A., Zlatković, N., and Obradović, A. 2021. Isolation and characterization of Pseudomonas syringae isolates affecting stone fruits and almond in Montenegro. J. Plant Dis. Prot. 128: 391–405.

Puig, S., Rees, E.M., and Thiele, D.J. 2002. The ABCDs of periplasmic copper trafficking. Structure 10(10): 1292-1295.

Puławska, J., Gétaz, M., Kałużna, M., Kuzmanovic, N., Obradovic, A., Pothier, J., Ruinelli, M., Boscia, D., Saponari, M., Végh, A., and Palkovics, L. 2017. Bacterial diseases. In Quero-Garcia, J., Iezzoni, A., Pulawska, J., and Lang, G. (Eds*.),* Cherries: botany, production, and uses (pp. 365-385). CAB International.

Purahong, W., Orrù, L., Donati, I., Perpetuini, G., Cellini, A., Lamontanara, A., Michelotti, V., Tacconi, G., and Spinelli, F. 2018. Plant microbiome and its link to plant health: Host species, organs and Pseudomonas syringae pv. actinidiae infection shaping bacterial phyllosphere communities of kiwifruit plants. Front. Plant Sci. 9:1563.

Quiñones, B., Dulla, G., and Lindow, S. E. 2005. Quorum sensing regulates exopolysaccharide production, motility, and virulence in Pseudomonas syringae. Molecular plant-microbe interactions 18(7): 682–693.

Rabiey, M., Roy, S.R., Holtappels, D., Franceschetti, L., Quilty, B.J., Creeth, R., Sundin, G.W., Wagemans, J., Lavigne, R., and Jackson, R.W. 2020. Phage biocontrol to combat Pseudomonas

syringae pathogens causing disease in cherry. Microbial Biotechnology 0 (0): 1– 18 https://doi.org/10.1111/1751-7915.13585

Redford, A.J., Bowers, R.M., Knight, R., Linhart, Y., and Fierer, N. 2010. The ecology of the phyllosphere: geographical and phylogenetic variability in the distribution of bacteria on tree leaves. Env. Microbiol. 12(11): 2885-2893.

Redford, A.J., and Fierer, N. 2009. Bacterial succession on the leaf surface: A novel system for studying successional dynamics. Microb. Ecol. 58:189-198.

Renick, L.J., Cogal, A.G., and Sundin, G.W. 2008. Phenotypic and genetic analysis of epiphytic pseudomonas syringae populations from sweet cherry in Michigan. Plant Disease 92(3): 372-378.

Roos, I. M. M. and Hattingh, M. J. 1983, Scanning electron microscopy of Pseudomonas syringae pv, morsprunorum on sweet cherry leaves. Journal of Phytopathology, 108: 18–25.

Sakar, S.F., and Guttman, D.S. 2004. Evolution of the core genome of Pseudomonas syringae, a highly clonal, endemic plant pathogen. Amer. Soc. Microbiol. 70(4): 1999-2012.

Salazar-Gutiérrez, M.R., Chaves, B., Anothai, J., Whiting, M., and Hoogenboom, G. 2014. Variation in cold hardiness of sweet cherry flower buds through different phenological stages. Scientia Horticulturae 172: 161-167.

Shade, A., and Handelsman, J. 2012. Beyond the venn diagram: the hunt for a core microbiome. Env. Microbiol. 14 (1): 4-12.

Shade, A., McManus, P., and Handelsman, H. 2013. Unexpected diversity during community succession in the apple flower microbiome. mBio 4(2):e00602-12.doi:10.1128/mBio.00602-12

Shalev, O., Ashkenazy, H., Neumann, M., and Weigel, D. 2021. Commensal Pseudomonas protect Arabidopsis thaliana from a coexisting pathogen via multiple lineage-dependent mechanisms. ISME J. 16(5):1235-1244. doi: 10.1038/s41396-021-01168-6.

Shalev, O., Karasov, T.L., Lundberg, D.S., Ashkenazy, H., Na Ayutthata, P.P, and Weigel, D. 2022. Commensal *Pseudomonas* strains facilitate protective response against pathogens in the host plant. Nat. Ecol. Evol. 6: 383–396. https://doi.org/10.1038/s41559-022-01673-7

Singh, P., Santoni, S., Weber, A., This, P., and Péros, J-P. 2019. Understanding the phyllosphere microbiome assemblage in grape species (Vitaceae) with amplicon sequence data structures. Scientific Reports 9:14294.

Slack S.M., Walters K.J., Outwater C.A., and Sundin G.W. 2021. Effect of kasugamycin, oxytetracycline, and streptomycin on in-orchard population dynamics of *Erwinia amylovora* on apple flower stigmas. Plant Dis. 105(6):1843-1850.

Smets, W., Chock, M.K., Walsh, C.M., Vanderburgh, C.Q., Kau, E., Lindow, S.E., Fierer, N., and Koskella, B. 2022. Leaf side determines the relative importance of dispersal versus host filtering in the phyllosphere microbiome. Preprint. bioRxiv https://doi.org/10.1101/2022.08.16.504148

Spotts, R.A., Wallis, K.M., Serdani, M., and Azarenko, A.N. 2010. Bacterial Canker of Sweet cherry in Oregon – infection of horticultural and natural woods, and resistance of cultivar and rootstock combinations. Plant Disease 94: 345-350.

Steven, B., Huntley R.B., and Zeng, Q. 2018. The influence of flower anatomy and apple cultivar on the apple flower phytobiome. Phytobiomes 2(3): 171-279

Stockwell, V.O., and Stack, J.P. 2007. Using Pseudomonas spp. for integral biological control. Phytopathology 97: 244-249.

Stockwell, V.O., Johnson, K.B., Sugar, D., and Loper, J.E. 2011. Mechanistically compatible mixtures of bacterial antagonists improve biological control of fire blight of pear. Phytopathology 101: 113-123.

Stone, B.W.G., and Jackson, C.R. 2021. Seasonal patterns contribute more towards phyllosphere bacterial community structure than short-term perturbations. Microb. Ecol. 81:146-156.

Stroud, E.A., Rikkerink, E.H.A., Jayaraman, J., and Templeton, M.D. 2022. Actigard™ induces a defense response to limit Pseudomonas syringae pv. actinidiae in Actinidia chinensis var. chinensis 'Hort16A' tissue culture plants. Scientia Hort. 295: 110806.

Sundin, G.W., and Bender, C.L. 1993. Ecological and genetic analysis of copper and streptomycin resistance in Pseudomonas syringae pv. syringae. Appl. Environ. Microbiol. 59(4): 1018-1024.

Sundin, G.W., Jones, A.L., and Olson, B.D. 1988. Overwintering and population dynamics of Pseudomonas syringae pv. syringae and P.s. pv. morsprunorum on sweet and sour cherry trees. Can. J. Plant Pathol. 10: 281-288.

Sundin, G.W., Jones, A.L., and Fulbright, D.W. 1989. Copper resistance in Pseudomonas syringae pv. syringae from cherry orchards and its associated transfer in vitro and in planta with a plasmid. Phytopathology 79: 861-865.

Sundin, G.W., and Wang, N. 2018. Antibiotic resistance in plant-pathogenic bacteria. Ann. Rev. Phytopathol. 56: 161-180.

Sundin, G.W., Werner, N.A., Yoder, K.S., and Aldwinkle, H.S. 2009. Field evaluations of biological control of fire blight in the eastern united states. Plant Disease 93: 386-394.

Sundin, G., and Rothwell, N. (2012). Managing bacterial canker in sweet cherries: What are the options? Retrieved from

http://msue.anr.msu.edu/news/managing_bacterial_canker_in_sweet_cherries_what_are_the_options

Syed Ab Rahman, S.F., Singh, E., Pieterse, C.M.J, and Schenk, P.M. 2018. Emerging biocontrol strategies for plant pathogens. Plant Sci. 267: 102-111.

Tancos, K.A., and Cox, K.D. 2017. Effects of consecutive streptomycin and kasugamycin applications on epiphytic bacteria in the apple phyllosphere. Plant Disease 101: 158-164.

USDA-Nass 2019. 2017 Census of agriculture: Michigan state and county data. Retrieved from https://www.nass.usda.gov/Publications/AgCensus/2017/Full_Report/Volume_1,_Chapter_1_State_Level/Michigan/miv1.pdf

USDA-Nass 2021. Michigan agricultural overview. Retrieved from https://www.nass.usda.gov/Quick_Stats/Ag_Overview/stateOverview.php?state=MICHIGAN

USDA-Nass 2022. www.nass.usda.gov/Statistics_by_Subject/index.php.

Vandenkoornhuyse, P., Quaiser, A., Duhamel, M., Le Van, A., and Dufresne, A. 2015. The importance of the microbiome of the plant holobiont. New Phytologist 206: 1196-1206.

Vanneste, J.L., Yu, J., and Beer, S.V. 1992. Role of antibiotic production by Erwinia herbicola Eh252 in biological control of Erwinia amylovora. J. Bacteriol. 174(9): 2785-2796.

Vasebi, Y., Khakvar, R., Tian, L., Moubarak, P., Valentini, F., Weisberg, A.J., and Vinatzer, B.A. 2020. Phenotypic characterization and phylogenetic analysis of Pseudomonas syringae strains associated with canker disease on apricot in Iran within the context of the global genetic diversity of the P. syringae complex. Eur. J. Plant Pathol. 158:545-560.

Visnovsky, S.B., Marroni, M.V., Pushparajah, S., Everett, K.R., Taylor, R.K., Vintazer, B.A., and Pitman, A.R. 2019. Using multilocus sequence analysis to distinguish pathogenic from saprotrophic strains of Pseudomonas from stone fruit and kiwifruit. Eur. J. Plant Pathol. 155: 643-658.

Vorholt, J.A. 2012. Microbial life in the phyllosphere. Nature Reviews Microbiol. 10: 828-840 doi:10.1038/nrmicro2910.

Wagner, M.R., Lundberg, D.S., del Rio, T.G., T5ringe, S.G., Dangl, J.L., and Mitchell-Olds, T. 2016. Host genotype and age shape the leaf and root microbiomes of a wild perennial plant. Nature Comms. 7: 12151, doi:10.1038/ncomms12151.

Wallis, A., Gu, G., Ramachandran, P., Reed, E., Ottesen, A., Nou, X., and Cox, K.D. Endophytic bacterial communities in apple leaves are minimally impacted by streptomycin use in fire blight management. Phytobiomes J. 5:350-361.

Warren, R.J., and Vermette, S. 2022. Laurentian great lakes warming threatens northern fruit belt refugia. Int. J. Biometeorol. 66: 669–677.

Wensing, A., Braun, S. D., Büttner, P., Expert, D., Völksch, B., Ullrich, M. S., and Weingart, H. (2010). Impact of siderophore production by Pseudomonas syringae pv. syringae 22d/93 on epiphytic fitness and biocontrol activity against Pseudomonas syringae pv. glycinea 1a/96. Appl. Environ. Microbiol. 76(9): 2704–2711.

Whiting, M.D., and Lang, G.A. 2004. 'Bing' sweet cherry on dwarfing rootstock 'Gisela 5': thinning affects fruit quality and vegetative growth but not net CO_2 exchange. J. Amer. Hort. Sci. 129(3): 407-415.

Wicaksono, W., Jones, E. ,Casonato, S., ,Monk, J, and Ridgway, H. 2017. Biological control of Pseudomonas syringae pv. actinidiae (Psa), the causal agent of bacterial canker of kiwifruit, using endophytic bacteria recovered from a medicinal plant. Bio. Control. 116. 10.1016/j.biocontrol.2017.03.003.

Wilson, M., and Lindow, S.E. 1993. Interactions between the biological control agent Pseudomonas fluorescens A506 and Erwinia amylovora in pear blossom. Phytopathology 83: 117-123.

Wilson, M., and Lindow, S.E. 1994. Ecological similarity and coexistence of epiphytic ice-nucleating (Ice+) Pseudomonas syringae strains and a non-ice-nucleating (Ice-) biological control agent. Appl. Environ. Microbiol. 60(9): 3128-3137.

Wu, Y., Qu, M., Pu, X., Lin, J., and Shu, B. 2020. Distinct microbial communities among different tissues of citrus tree Citrus reticulata cv. chachiensis. Scientific Reports 10: 6068.

Xin, X-F., Kvitko, B., and He, S.Y. 2018. Pseudomonas syringae: what it takes to be a pathogen. Nat. Rev. Microbiol. 16: 316–328.
Yashiro, E., and McManus, P.S. 2012. Effect of streptomycin treatment on bacterial community structure in the apple phyllosphere. PLoS ONE 7(5):e37131.

Yee, W.L., and Chapman, P.S. 2008. Seasonal amounts of nutrients in Western Cherry Fruit Fly (Diptera: Tephritidae) and their relation to nutrient availability on cherry plant surfaces. *Env. Entomol.* 37(5):1086–1098.

Zhang, Q., Shi, W., Zhou, B., Du, H., Xi, L., Zou, M., Zou, H., Xin, L., Gao, Z., and Chen, Y. 2021. Variable characteristics of microbial communities on the surface of sweet cherries under different storage conditions. Postharvest Biol. Tech. 173: 111408.

CHAPTER 2

VIRULENCE AND PHYLOGENY OF MICHIGAN *PSEUDOMONAS SYRINGAE* PV. *SYRINGAE* ISOLATES FROM SWEET CHERRY FLOWERS HIGHLIGHT VARIABILITY, THE NEED FOR CAUTION, AND AREAS OF FUTURE RESEARCH

2.1: Abstract

Michigan's sweet cherry industry is seriously impacted by the susceptibility of young sweet cherry trees to *Pseudomonas syringae* pv. *syringae* (*Pss*), the causal agent of the disease bacterial canker. Characterization of *Pss* strains by biochemical, phenotypical, and molecular analyses is critical for understanding the variation that exists within Michigan orchards and monitoring for emergent pathogens. *Pss* strains isolated from cherry flowers were found to be phylogenomically diverse, determined by multilocus sequence analysis (MLSA) using four housekeeping genes (*gap1*, *gltA*, *gyrB*, and *rpoD*) with 20 strains belonging to three different phylogroups (PG2b, PG2c, and PG2d). Only a single *Pss* strain was resistant to copper and no strains were resistant to streptomycin. *Pss* strains were variable in their GATTa profiles, in their ice nucleation activity (INA), and amplification of the syringomycin gene *syrB*. Notably, the *Pss* strains also exhibited a range of virulence levels determined by measurement of lesion area on green cherry fruit and virulence rating on sweet cherry wood. No new *P.s* pathogens were detected. The strains that were moderate to non-virulent require further investigation of their possible virulence in other *Prunus* spp. and how they impact or interact with the more virulent *Pss*. Without thorough virulence testing, the inadvertent use of moderate to avirulent strains could impact future research where virulence level could influence treatment responses.

2.2: Introduction

Michigan's temperate climate (afforded by the protection of the Great Lakes) and fertile glacial soils is home to a diverse array of crops (Brown, 1941; Warren and Vermette, 2022). Fruit production is largely concentrated in the "fruit belt" region, located along the western coast nearer to Lake Michigan (Brown, 1941; Warren and Vermette, 2022). However, orchards can be found scattered throughout the state. Michigan is one of the most agriculturally diverse states in the U.S., with 46,000 farms and 300 different agrarian commodities (MDARD, 2023; USDA-Nass, 2021). Michigan is the nation's top tart cherry (*Prunus cerasus*) producer (70% of U.S. supply) with 33,381 acres and is ranked fourth in sweet cherry (*Prunus avium*) production with 7,807 acres (Lang, 2019; MDARD, 2018; USDA-Nass, 2019).

According to early census data, cultivated cherries were established in Michigan in the 1870s (Brown, 1941). More than 150 years later, the modern sweet cherry orchard looks markedly different from those early orchards of large trees that mirrored their forest counterparts, replaced with high-density plantings of small trees on dwarfing to semi-vigorous precocious rootstocks, such as the 'Gisela' series (Gi.6, Gi.5, and Gi3), often supported by trellising (Lang et al., 2019). Michigan State University researchers have led the push for progressive cherry growers to adopt high-density "pedestrian orchards" featuring "two-dimensional/planar" training systems like that of the UFO (Upright Fruiting Offshoots, Lillrose et al., 2017) that are trained to form a "fruiting wall" that can be mechanically hedged and easily picked from one side of the tree, thereby requiring less labor compared to the traditional "three-dimensional" tree architectures (Lang et al., 2022). Various covering systems (e.g., row covers, high tunnels and retractable roofed greenhouses) are also have been shown to reduce fruit cracking and disease pressure, and promote earlier fruit harvest potential (Lang et al., 2016; Lang, 2019). These

innovative approaches are grower-driven due to rising concerns over labor issues (lack of workers and costs) and climatic events (frosts and rain) (Lang, 2019).

A major limitation for sweet cherry growers is disease pressures (e.g., bacterial canker, brown rot, and cherry leaf spot) linked to Michigan's climate. The cool, wet spring and late fall weather typical in Michigan are ideal for the proliferation and infection of the bacterial phytopathogen *Pseudomonas syringae* pv. *syringae* van Hall (*Pss*), the causal agent of bacterial canker that can devastate young trees that are highly susceptible (Hirano and Upper, 1990; Hirano and Upper, 2000; Jones and Sutton, 1996; Spotts, 2010). Historically, Michigan had a lengthy spring with cool temperatures that delay bud break and warm falls due to the moderating influence of the Great Lakes, avoiding late and early "killing frosts," respectively, as an influence of the Great Lakes (Warren and Vermette, 2022). Due to global climate change and the warming of the lake waters (including decreased winter ice cover), these previous protections have become quite volatile. Lang (2019) summarized comparisons of pre- to post-1940 climate data from the Michigan state climatologist (J. Andresen) that was recorded near Traverse City, a major cherry-growing region, noting that bud development (side green) is now ~ 10 days earlier, the number of potential frost events (at side green or later) has increased from 5 to over 20, and annual rainfall has increased 10% since 1940. These statistics are particularly alarming considering the biology of *Pss*; in addition to the increase in population size and subsequent potential for infection of cherry during cool, wet weather events, the pathogen is closely linked to the water cycle via rain splash dispersal, and is capable of facilitating frost damage via ice nucleation which enables its entry into the plant tissues (Hirano and Upper, 1990; Hirano and Upper, 2000; Jones and Sutton, 1996; Morris et al., 2008; Morris et al., 2013). *Pss* is also an opportunistic pathogen that can infect through wounds (pruning cuts and rubbing of bark on

trellis wires) and natural openings (leaf scars and stomates), but only when populations are high; otherwise, it is well-documented to live benignly on host and non-host plants (Hirano and Upper, 1990; Hirano and Upper, 2000; Kennelly et al., 2007; Latorre and Jones, 1979a; Lillrose et al., 2017). In the fall, when cool, wet weather persists and leaves drop, higher *Pss* populations can infect trees through leaf scars and subsequently can overwinter in cankers, buds, bark, and systemically (Jones and Sutton, 1996; Sundin et al., 1988).

Jones (1971) was the first to report *Pss* to be present in sweet cherry in Michigan following a 1968 epidemic. Since then, three significant outbreaks have occurred (2002, 2012, and 2021), all occurring after unusually warm early spring weather that induced early bloom followed by numerous frost events (Kennelly et al., 2007; Lauwers, 2022; Renick et al., 2008; Sundin and Rothwell, 2012). These state-wide events resulted in significant current and future year crop losses from frost damage as well as infection by *Pss*, resulting in blossom blast followed by systemic disease and subsequent spur, shoot, limb, and young tree death (Kennelly et al., 2007; Lauwers, 2022; Renick et al., 2008; Sundin and Rothwell, 2012). Other symptoms of *Pss* infection include sunken cankers, gumming, lesions on fruit, and "shot holes" in leaves (Jones and Sutton, 1996; Kennelly et al., 2007). In addition to *Pss*, Jones (1971) isolated *Pseudomonas syringae* pv. *morsprunorum* (*Psm*) from sweet cherry. This pathogen has since been determined to be two different pathogens, *P. amygdali* pv. *morsprunorum* (race 1) and *P. avellanae* pv. *morsprunorum* (race 2) and is recovered more often on tart cherry and is less virulent than *Pss* in Michigan (Gomila et al., 2017; Hulin et al., 2020; Jones, 1971; Jones and Sutton, 1996; Renick et al., 2008).

Pss is a generalist phytopathogen that infects more than 180 plant species, and phylogenetically belongs to genomospecies 1, phylogroup 2, and is part of a large species

complex composed of 13 phylogroups (Berge et al., 2014; Gardan et al., 1999; Gomila et al., 2017; Gutiérrez-Barranquero et al., 2019; Kennelly et al., 2007; Pulawska et al., 2017). Phylogroup (PG) 2 is composed of 7 clades (2a, 2b, 2c, 2d, 2e, 2f, and 2g) that contain non-pathogenic *Pss* (PG2c) and *Pss* isolated from water and snow (Abdellatif et al., 2020; Berge et al., 2014; Hall et al., 2019). In Michigan, *Pss* and *Prunus* spp. are found together in many sweet cherry orchards, and it can be difficult to find a symptomless tree. On a global scale, *Pss* infects all economically important *Prunus* spp. Evidence through whole genome comparisons points to shared genes/proteins in common among strains that have led to the adaptation for pathogenicity on woody hosts, cherry specifically, and proposed co-evolution with *Prunus* spp. (Hulin et al., 2018b; Hulin et al., 2020; Nowell et al., 2016; Ruinelli et al., 2022). These shared genes and proteins are part of the type III secretion system (T3SS) repertoire; the T3SS consists of an apparatus made by *Pss* (once inside the plant apoplast) that injects effector proteins into the plant cells, releasing nutrients to promote the proliferation of *Pss* and to thwart the plant's basal immune response (i.e., PAMP-triggered immunity or PTI) (Alfano and Collmer, 2004; Hulin et al., 2018b; Hulin et al., 2020; Nowell et al., 2016; Ruinelli et al., 2022; Ruiz-Bedoya et al., 2023). These effector proteins also are considered "double agents" as they have the potential to elicit an additional plant immune response, or effector triggered immunity (ETI), which adds another level of infection complexity dependent on both pathogen and plant host genetics (Alfano and Collmer, 2004; Hulin et al., 2018b; Hulin et al., 2020; Nowell et al., 2016; Ruinelli et al., 2022; Ruiz-Bedoya et al., 2023). Effectors are thought to be acquired through horizontal gene transfer, and pathogenicity is a result of the convergent gain and loss of these genes (Hulin et al., 2018b). *Pss* has fewer effector proteins but more phytotoxin gene clusters coding from one to all three toxins (syringomycin, syringolin, and syringopeptin) (Hulin et al., 2018b;

Ruinelli et al., 2019). These phytotoxins cause necrosis in plant tissues, and evidence points to a "trade-off" between bacteria phytotoxin production and effector proteins (Hulin et al., 2018b; Kennelly, 2007). The genes for the production and delivery of the syringomycin phytotoxin, *syrB*, and *syrD*, respectively, are part of the rapid characterization/identification of *Pss* strains using polymerase chain reaction (PCR) (Bultreys and Gheysen, 1999; Sorensen et al., 1998).

Management of Pss in Michigan orchards in problematic, as nothing can be done once the bacteria enter the plant. Strategies for reducing epiphytic *Pss* populations have been limited to cultural practice adjustments and unsustainable copper sprays. *Pss* resistance to copper is prevalent, and use is limited to applications during plant dormancy due to phytotoxicity in cherry (Lamichhane et al., 2018; Lauwers, 2022; Renick et al., 2008; Sundin et al., 1989). However, recent developments have started expanding the *Pss* population management arsenal. Though no bacterial canker-resistant cultivars are currently available, rapid screening protocols are being utilized to assess wild, ornamental, and hybrid *Prunus* for their ability to reduced bacterial multiplication after inoculation with promising results (Hulin et al., 2022). Use of antibiotics such as streptomycin, oxytetracycline, and kasugamycin had previously been restricted for use only in apples to manage the extremely aggressive fire blight pathogen *Erwinia amylovora* (McGhee and Sundin, 2011; Slack et al., 2021; Sundin and Wang, 2018). However, kasugamycin is now available to use in cherry for *Pss* population management, and resistance has yet to be detected in Michigan (Lauwers, 2022). Screening for streptomycin resistance in *Pss* should be done, as *E. amylovora* resistance is prevalent in Michigan and could be transferred to *Pss* via horizontal gene transfer (McGhee and Sundin, 2011; Slack et al., 2021; Sundin and Wang, 2018). Most of the biological control agents developed for *E. amylovora* management have had no definitive success and require more testing for possible management of *Pss* populations

(Kennely et al., 2007; Sundin et al., 2009). However, research using bacteriophage shows some potential, but research is still ongoing (Lauwers, 2022; Rabiey et al., 2020).

Monitoring of *P. syringae* (*P.s*) in sweet cherry orchards is critical for detecting emergent pathogens and understanding the diversity within resident *Pss* populations. Characterization of *Pss* strains entails a combination of biochemical, phenotypical, and molecular tests/analyses. Fluorescence and oxidase enzyme activity often are used in the initial screening of *Pss* since 1) it belongs to the same phylogenetic lineage as *Pseudomonas fluorescens*, 2) will fluoresce under UV light, and 3) lacks the oxidase enzyme thereby eliciting no reaction with Kovacs' oxidase reagent (Gomila et al., 2017; Kovacs, 1956; Latorre and Jones, 1979b; Lelliot et al., 1966). *Pss* is differentiated from *Psm* via the GATTa (Gelatin liquefaction, Aesculin hydrolysis, Tyrosinase activity, and Tartrate utilization) biochemical assays and the amplification of the *syrB* or *syrD* gene (syringomycin phytotoxin); *Pss* is generally $G^+ A^+ T^- Ta^-$ while *Psm* is $G^- A^- T^+ Ta^+$, and *Psm* does not produce syringomycin (Bultreys and Gheysen, 1999; Latorre and Jones, 1979b; Lelliot et al., 1966; Renick et al., 2008; Sorensen et al., 1998). These initial tests also may be followed up with INA, pathogenicity (on immature fruit), and antibiotic resistance assays (Renick et al. 2008; Lauwers 2022). Phylogenomic trees for genomic characterization of *Pss* are popularly being constructed utilizing multilocus sequence analysis/typing (MLSA/MLST) (Abdellatif et al., 2019; Almeida et al., 2010; Berge et al., 2014; Bophela et al., 2020; Hall et al., 2019; Hulin et al., 2018a; Hwang et al., 2005; Iličić et al., 2021; Ivanović et al., 2022; Lauwers, 2022; Oksel, 2022; Popović et al., 2021; Sarkar and Guttman, 2004; Vasebi et al., 2020; Visnovsky et al., 2019). Both MLST and MLSA compare 1 to 7 different "housekeeping" genes (conserved genes necessary for life) of novel strains with reference strains to group them according to similarity and construct phylogenies; MLST does this by assigning the alleles a

number (sequence type) while MLSA (utilized in this study) uses the actual DNA sequences (Almeida et al., 2010; Berge et al., 2014; Hwang et al., 2005; Iličić et al., 2021; Sarkar and Guttman 2004). Sakar and Guttman (2004) began using MLST for characterizing *P.s* spp. with 7 "housekeeping" genes, then Hwang et al. (2005) found that 4 genes [*gapA* (syn. *gap1*), *gltA* (syn. *cts*), *gyrB*, and *rpoD*] were sufficient, while Berge et al. (2014) and Iličić et al. (2021) make the case for using the single genes *cts* (syn. *gltA*) and *recG* respectively, for more rapid classifications. The genes (used in this paper's study), *gap1*, and *gltA* (used in this study) are important for glycolysis and the citric acid cycle encoding for glyceraldehyde-3-phosphate dehydrogenase and citrate synthase respectively, while *gyrB* and *rpoD* are genes encoding for DNA gyrase B, and sigma factor 70, respectively, important for replication and transcription respectively (Hwang et al., 2005; Lauwers, 2022; Vasebi et al. 2020).

Previously, Lauwers (2022), did not find any non-pathogenic *Pss*, while Rennick et al. (2008) mentioned finding non-pathogenic isolates that were not included in the DNA fingerprinting. Rennick et al. (2008) also found four isolates that were pathogenic but clustered outside of the other *Pss* groupings; *P.s.* outgroups were not included in the analysis. Pathogenicity in both studies was determined by the presence or absence of lesion formation on inoculated green fruit but differences in virulence level were not measured, nor was the pathogenicity or virulence level of strains inoculated on cherry wood evaluated (Lauwers, 2022; Rennick et al., 2008). Hulin et al. (2018a, 2022) highlight the importance of determining differences in strain virulence as being critical for use in and interpretation of future research, especially in the screening for resistant cherry cultivars. Both Lauwers (2022) and Renick et al. (2008) studied strains that were resistant to copper (13.8% and 31.7% respectively) and had a high number with INA (100% and 94% respectively). The focus of this paper's study was to

evaluate the phylogenetic, biochemical, and phenotypic variability of *Pss* strains collected from sweet cherry flowers in Michigan and to characterize the range of virulence when inoculated on sweet cherry green fruit and wood.

2.3: Methods

Bacteria Isolation

Bacteria were isolated from sweet cherry flowers collected in May 2019 from orchards located in three regions of Michigan: Site 1, Wells Orchards, (Grand Rapids, Ottawa Co.); Site 2, Michigan State University (MSU) Clarksville Research Center (Clarksville, Ionia Co.); and Site 3, MSU Horticulture Teaching and Research Center (Holt, Ingham Co.) (Figure 2.1). A fourth site, MSU Southwest Michigan Research and Extension Center (Benton Harbor, Berrien Co.) was used for virulence testing. Ten flowers/tree were collected by clipping the pedicel with scissors and sanitized with 10% sodium hypochlorite and 75% ethanol into sterile Whirl-Pak® bags (Nasco, Madison WI). Flowers were selected from 8, 4, and 4 sweet cherry trees at site 1, site 2, and site 3 respectively. Flowers were held on ice in a cooler for transport to the laboratory.

In the laboratory, flowers were transferred into 20 ml cold sterile 0.5x phosphate buffered saline (PBS) in 50 ml conical tubes (8 tubes/site1, 4 tubes/site 2, 4 tubes/site3). Which were then shaken at 200 rpm for 10 min. in a G24 Environmental Incubator Shaker (New Brunswick Scientific Co. Inc., Edison, NJ) and sonicated for 7 min. in an ultrasonic bath (Cole Parmer, Chicago, IL). A 100µl portion of the flower microbiome PBS wash stored at -70°C in 15% glycerin. The remaining flower wash was vortexed, serially diluted to 0, 10^{-1}, 10^{-2}, and 10^{-3}, and plated onto King's B (KB) media amended with 50 µg/ml cycloheximide (3 plates/sample) in four 25 µl drops/dilution (Figure 2.2). Plates were allowed to dry overnight at room temperature and were then placed into a 28°C incubator (Precision Scientific Model 805, Chicago IL) until

the following day when colonies were assessed visually for their likeness to *Pss* (i.e., cream-colored and circular in shape). Single colonies that were considered to be potential *Pss* were selected and re-streaked onto KB media amended with 50 µg/ml cycloheximide and were allowed to grow at 28°C for 2 days. Single colonies were selected from these streak plates for oxidase reaction testing.

Colonies that had oxidase$^-$ reactions (characteristic of *Pss*) were stored from lawns at -70°C in 15% glycerol. Bacteria strains were labeled according to site number (1, 2, or 3), cultivar name abbreviated (e.g., Gold= G, Black York=BY, Black Pearl=BP, Ulster=U, Van=V, Brooks=Br, R=Rainier), and isolate number, so that the final strain name, for example, would be 1-U-9 (site 1, Ulster, isolate 9).

Oxidase Reaction

To test for the presence of the enzyme cytochrome oxidase, a droplet of a 1% solution of N, N, N´, N´-tetra-methyl-p-phenylenediamine dihydrochloride was placed onto Whatman® filter paper (no. 1), then a single colony from a streak plate was picked up with a sterile toothpick and smeared onto the filter paper (Kovacs, 1956; Shields and Cathcart, 2010). Reactions were recorded as + (purple color = enzyme detected), or – (no color change = no enzyme detected) (Figure 2.3). Only the oxidase$^-$ bacteria were used for further characterization, as *Pss* is oxidase$^-$ (Janse, 2010; Latorre and Jones, 1979).

syrD and *syrB* Gene Amplification

Oxidase$^-$ strains were streaked onto KB media amended with 50 µg/ml cycloheximide using a sterile toothpick. Strains were allowed to grow for two days at 28°C. From a single colony for each strain, a small number of cells were scooped up using a sterile toothpick and washed into 20 µl sterile distilled water in polymerase chain reaction (PCR) tubes and vortexed.

The PCR tubes were inserted into a Bio Rad T100™ Thermal Cycler (Bio-Rad Laboratories, Hercules, CA) and incubated at 95°C for 10 min., causing lysis of the bacteria cells (ergo DNA extraction) via boiling.

The extracted DNA was used for PCR amplification of the *syrD* gene that encodes for export/secretion of the phytotoxin syringomycin in *Pss* (Bultreys and Gheysen, 1999; Sorensen et al., 1998). Known *Pss* strains (13-7, 6-9, 26-3, 19-6, FF5-1, 6491, 1680, and 847) from the collection of Dr. George Sundin were also included, as was a sterile water control. The PCR reaction consisted of 2 µl of DNA, 1 µl each of *syrD* forward and reverse primer, 25 µl of One *Taq*® Hot Start 2X Master Mix with Standard Buffer (New England BioLabs®, Ipswich, MA), and Invitrogen™ UltraPure™ distilled water (ThermoFisher Scientific) up to a total volume of 50 µl. The primers used are the same as those in Bultreys and Gheysen (1999) as cited by Renick et al. (2008) (Table 2.1). PCR amplification occurred in the Bio Rad T100™ Thermal Cycler (Bio-Rad Laboratories Inc., Hercules, CA) under the thermal conditions described in Renick et al. (2008) (Table 2.1). Gel electrophoresis of the PCR product was done using a 1% Invitrogen™ UltraPure™ Agarose gel (ThermoFisher Scientific), stained with 1µl Ethidium Bromide (EtBr) (Bio-Rad Laboratories, Hercules, CA), in 1x Tris-Acetate-EDTA buffer (TAE). A 6x ficoll-based loading dye (10 µl) was added to the PCR product before gel loading. A 100 bp DNA ladder (New England BioLabs®) was included. The gel was submerged in 1X TAE and electrophoresis was run in a Horizontal System for Submerged Gel Electrophoresis series 1087, model H5 (Bethesda Research Laboratories, Life Technologies, Gaithersburg MD) at ~60 volts for ~80 min. Gel imaging was done using a Bio Rad Gel Doc™ EZ Imager. Only the strains that had amplification of the *syrD* gene (*syrD*$^{+}$) were used in further classification, as the presence of

syrD is typical of *Pss* (Bultreys and Gheysen, 1999; Janse, 2010; Renick et al., 2008; Sorensen et al., 1998).

Only oxidase$^-$ and *syrD*$^+$ strains were used for the PCR amplification of the *syrB* gene that encodes the synthesis of the phytotoxin syringomycin in *Pss* (Bultreys and Gheysen, 1999; Sorensen et al.,1998). Stored DNA from a -20°C freezer was used; DNA was extracted as described in the *syrD* gene amplification; however, cell lysis occurred in sterile 0.5x sterile PBS via boiling. No additional known *Pss* reference strains were included as two of this study's strains (1-U-9 and 3-BY-37) that were included were verified as *Pss* via whole genome sequencing (Dr. Michelle Hulin, East Malling, U.K., unpublished). The *Psm* strain 627 was included (from Dr. George Sundin's collection) and a sterile water control was included. The PCR reaction volumes were the same as in the *syrD* amplification, the forward and reverse *syrB* primers used were those developed by Sorensen et al. 1998 as cited in Vasebi et al. (2020), using the same thermal profile used was the same as Vasebi et al. (2020) (Table 2.1). Gel electrophoresis and imaging were as described in the *syrD* amplification; however, the gel electrophoresis was run at ~116 V for 20 min., and a 100 bp GoldBio® DNA ladder (Gold Biotechnology, St. Louis, MO) was included.

GATTa Profile and Fluorescence

To separate putative *Pss* from *Psm* the GATTa biochemical profile was determined using 3 day old oxidase$^-$ and *syrD*$^+$ strains and a *Psm* strain 627 control (Figure 2.4). Results were reported as positive (+) or negative (−). Gelatin liquefaction (G) was tested via stabbing cells into 1ml refrigerated (i.e., solid) 12% gelatin media with a sterile toothpick (Latorre and Jones, 1979). Cells were incubated for 7 days at 28°C and then placed in a refrigerator (~4°C) for 15 min before the assessment for liquefaction. All remaining tests involved streaking cells onto the

appropriate media types. Aesculin hydrolysis (A) was evaluated on media containing 0.1% aesculin and 0.5% ferric citrate where a color change (brown color or none) occurred after incubation at 28°C for 24h (Latorre and Jones, 1979; Sneath, 1956). Media containing 0.1% L-tyrosine (0.1%) was used to determine tyrosinase activity (T) consisting of a reddish-brown color change or none after 24h (Lelliot, 1966; Latorre and Jones, 1979). Tartrate utilization (Ta) was tested on Simmons media with 0.2% sodium tartrate, wherein a blue color change after 24 h at 28°C is a – result and no change is a + result (Holding and Collee, 1971; Latorre and Jones, 1979) (Figure 2.4).

Fluorescence was evaluated for two day old oxidase$^-$ and *syrD*$^+$ strains on KB media amended with 50 μg/ml cycloheximide. Plates were then placed in an ultraviolet (UV) light box, where fluorescence was observed through the oculars and recorded as + or – (Figure 2.4). Included were *Pseudomonas fluorescens* (strain GSPB1714), *Erwinia Amylovora* (strain Ca11-7 SmR), and *Psm* strain 627 were included as controls.

Ice Nucleation Activity

The capacity for ice nucleation activity (INA) was assayed by methods similar to Lindow et al. (1982b). The oxidase$^-$ and *syrD*$^+$ strains (4 days old), including *Psm* strain 627 were washed into 900μl sterile PBS and vortexed. The bacteria in PBS (~10^9 to 10^{10} cfu/ml) were pipetted as ten 10μl drops/strain onto two floats that were made from aluminum foil coated with a thin layer of paraffin wax. A row of 10 μl PBS-only drops were also included. The floats were set in a refrigerated circulating water bath (Brinkmann MGW Lauda RMS, Delran, NJ) containing 50:50 ethylene glycol and distilled water (Figure 2.5). The initial bath temperature was set at -3°C, the temperature was then dropped by 0.5°C until reaching -5°C; each temperature was held for 15 min, and the number of frozen drops was recorded. Strains at -5°C

were observed at 15 min and 30 min. Strains were reported to be INA +, –, or +/– depending on the final observations at -5°C.

Copper and Streptomycin Resistance

To evaluate copper (Cu) resistance, a small number of cells of a single colony of two day-old oxidase^{-}/*syrD*$^{+}$ strains growing on KB amended with 50 µg/ml cycloheximide were streaked with a sterile toothpick onto mannitol-glutamate (MG) media with and without 250 µg/ml copper sulphate ($CuSO_4$) (Renick et al., 2008). A known Cu resistant *Pss* strain (BC 43(390) CuR) and Cu susceptible *Pss* strain (26-3) were included (from Dr. George Sundin's collection). The putative *Pss* strains were tested simultaneously alongside the resistant and susceptible *Pss* (Figure 2.6). Plates were assessed after two days of growing at 28°C, recorded as + (growth = resistant) or – (no growth = susceptible). This was repeated for strain 1-U-9 (Appendix A).

Strains resistance to streptomycin were evaluated similarly to the Cu resistance assay, except that cells were streaked onto KB media amended with and without 50µg/ml streptomycin (Sundin and Bender, 1993). A known streptomycin resistant *Erwinia amylovora* strain (Ca11-7 SmR) and a streptomycin susceptible *Pantoea agglomerans* strain (UMAF3067) were included (from Dr. George Sundin's collection). Plates were evaluated and reported as with the Cu resistance assay plates (Figure 2.6).

Multilocus Sequence Analysis (MLSA)

To further characterize the oxidase^{-}/*syrD*$^{+}$ strains and further verify that they are *Pss* a phylogeny was created based on MLSA using 4 housekeeping genes (*gap1*, *gltA*, *gyrB*, *rpoD*). The DNA of two day-old putative *Pss* strains was extracted via where cells were washed into 20µl of sterile 0.5x PBS and incubated at 95°C for 10 min in a Bio Rad T100™ Thermal Cycler.

The DNA was stored temporarily at 4°C for use in the following steps, as well as permanently stored long term at -20°C for later use.

The genes *gap1*, *gltA*, *gyrB*, and *rpoD* were amplified for each strain in a total 25µl PCR reaction with 12.5 µl One *Taq*® Hot Start 2x Master Mix with Standard Buffer (New England BioLabs®), 0.5 µl each of forward and reverse primer, 2 µl DNA, and 9.5 µl Invitrogen™ UltraPure™ distilled water. The PCR primers were the same as those modified by Hwang et al. (2005) as cited by Vasebi et al. (2020) (Table 2.2). PCR amplification occurred in the Bio Rad T100™ Thermal Cycler under thermal conditions that were modified by Vasebi et al. (2020) (Table 2.2). Amplification of each gene was verified with gel electrophoresis using 5 µl of PCR product and 1 µl 6x ficoll-based loading dye on a 1% Agarose gel stained with 1µl Ethidium Bromide (EtBr) in 1x TAE run for 20 min at ~120 V. A 100 bp GoldBio® DNA ladder was included. Gel imaging was done using a Bio Rad Gel Doc™ EZ Imager. The remaining 20 µl of PCR product was cleaned using a QIAquick® PCR Purification Kit (Qiagen, Germantown, MD) following the steps provided in the kit instructions.

The purified PCR product (9µl) was combined with 3 µl forward or reverse sequencing primer for each gene and strain in their own respective wells of a 96 well PCR plate (or strip of 8 PCR tubes in one instance). Sequencing primers were those cited in Vasebi et al. (2020) that had been modified by Hwang et al. (2005) (Table 2.2). A total of 160 gene x strain x primer combinations were submitted to the Genomics Core at the MSU Research Technology Support Facility (RTSF) (East Lansing, MI) for Sanger sequencing using the Applied Biosystems 3730xl DNA Analyzer (ThermoFisher Scientific).

Returned sequences were viewed as chromatograms for sequence quality assessment (no gaps/missing bases and single, clear peaks) using FinchTV v.1.4.0 (Geospiza Inc., 2004-2006).

The forward and reverse sequences of each gene x strain were aligned using NCBI (National Center for Biotechnology Information) BLAST® (Basic local alignment search tool) (Altschul et al., 1990). BLAST® aligned sequences were trimmed to include base pairs (bp) only present in both reads. The trimmed forward reads for each gene x strain were used in all subsequent analyses. Sequences for each strain were aligned together by gene in MEGA11: Molecular Evolutionary Genetics Analysis version 11 (MEGA11) using the MUSCLE algorithm (Tamura et al., 2021; Edgar, 2004).

Reference sequences were downloaded from NCBI GenBank® or the Plant Associated and Environmental Microbes Database (PAMDB.org) for each of the 4 genes from 40 *Pss* and *P.s* pathovars as well as *P. fluorescens* (strain A506), the type strain of *P. viridiflava* (CFBP2107^{T}), *P. savastanoi glycinea* R4, and *P. cersi* (strain H346-S) (Almeida et al. 2010; Clark et al., 2016) (Table 2.3). Genes of reference strains that were gleaned from the whole genome were trimmed to the forward and reverse primers used by Vasebi et al. (2020). Reference strains were aligned by gene alone and then combined into a FASTA file with this study's sequences using Linux command line and were aligned using MUSCLE in MEGA11. All strains were trimmed to be the same length, 473 bp, 501 bp, 507 bp, and 501 bp for the genes *gap1, gltA, gyrB,* and *rpoD,* respectively. The 4 genes were concatenated by strain using Linux command line, all the strains (reference and this study's) which were then aligned a final time using MUSCLE in MEGA11.

This final alignment with the 4 concatenated genes for each strain (reference and this study's) was used to create a Maximum Likelihood (ML) phylogenetic tree in MEGA11. The best fit model for the ML tree was determined by selecting the "Find Best DNA/Protein Models (ML)" option in MEGA11 (Hall 2018). The ML tree was then constructed under the conditions

of the TN93+G+I model, with 1000 bootstrap replications, partial deletion, 95% site cut off, and the default tree inference options (Hall, 2018). The tree was rooted on *P. fluorescens* A506, bootstraps <75% were hidden, the tree was widened and expanded for better viewing in MEGA11 and FigTree v.1.4.4 (2006-2018, Andrew Rambaut, Institute of Evolutionary Biology, University of Edinburgh). The final aesthetics of the tree (Font color, brackets, phylogroup designations, and bootstrap values determined by MEGA11 added manually) were done using InkScape v.1.2 (InkScape.org).

Green Fruit Virulence Assay

Virulence of the oxidase^{-}/*syrD*$^{+}$ strains on sweet cherry fruit harvested with stems on from site 1 were tested in 2019 (3 fruit/strain) and in 2021 (5 fruit/strain). Bacteria suspensions (10µl of 10^{7} cfu/ml) were inoculated into wounds of green to straw colored fruit made via a sterile dissecting probe following surface sterilization with 0.5% sodium hypochlorite for 5 min, then rinsed in sterile distilled water followed by a swab with a sterile pad saturated with 70% isopropyl alcohol (Covidien™ Webcol™, Cardinal Healthcare, Dublin, OH).

Bacteria suspensions in 2019 were from cells grown on KB media washed into 900 µl sterile PBS while in 2021 they were from cells grown overnight in KB broth (3 tubes/strain) that were washed 2x in equal volume of sterile PBS then serially diluted to the desired cfu/ml. Fruit stems were placed through a hole in the lid of a 14 ml round bottom test tubes (Falcon®, Corning, Corning, NY) held in test tube racks so that the stem was submerged in distilled water and the fruit sat on top of the lid (Figure 2.7). The bacteria controls in 2019 consisted of *Pantoea agglomerans* (strain UMAF3067), *Escherichia coli* dh5α, and *Psm* strain 627, as well as PBS only while in 2021 only *Psm* 627 and PBS were included.

The racks of inoculated fruit were placed inside a plastic tub (with lid) containing wet paper towels to keep humidity high. The tub with fruit was placed into a growth chamber with a 16:8 light:dark photoperiod at 24°C. Each fruit was photographed 4 days after inoculation (DAI) next to a U.S. quarter coin (as a known reference size) to measure the area of any lesions formed on the fruit using the ImageJ software (Schneider et al. 2012).

In 2019 to obtain the best threshold contrasts and measurements in ImageJ the background was changed to white using Adobe® Photoshop (Elements 14 Photo Editor, Adobe®, San Jose, CA) so that only the fruit and quarter are the main focus of the image, and in some instances, the lesion color was darkened (without altering lesion size). In 2021 it was unnecessary to remove the background as the contrast was sufficient.

In ImageJ, the image type was set to 8-bit, and the quarter reference was measured by, setting the known distance to 24.6 mm (coin diameter), and checking the Global box. The bottom threshold was then adjusted and recorded for each image so that the lesion on the fruit was prominent (the top threshold remained 0), and a selection tool was then used to select the lesion outline. The Analyze-analyze particles option was selected with size (mm^2) set as 0, circularity set as 0.00-1.00, and show outlines, display results, and include holes were selected to measure the area of the lesion (mm^2) via the software (Figure 2.7). All images used for data analysis for 2019 and 2021 can be found in Appendix A.

Wood Virulence Assessment

Strain virulence on sweet cherry wood was assessed in the field using methods similar to Hulin et al. (2018). In November 2019, six ‘Sweetheart’ trees and seven ‘Coral Champagne’ trees located at site 1 were wounded (~1-1.5 cm in size) via sterile razor blade (sanitized with 10% sodium hypochlorite and 75% ethanol between wounds) and inoculated with the oxidase$^-$

/*syrD*$^+$ strains (5 reps/strain) on two-to-three-year-old wood (Figure 2.8). All trees were trained as tall spindle axe (TSA) (Figure 2.9). The wood at the inoculation site was thoroughly swabbed with a 70% isopropyl alcohol pad before wounding. The inoculant was from strains (stored at ~-70°C) grown overnight in 3 ml KB broth in 15 ml conical tubes (3 tubes/strain) shaken at 200 rpm and 28°C. Cells from the three tubes were combined and washed 2x in 9 ml sterile PBS and then serially diluted to 10^7 cfu/ml (determined by spectrophotometer at 600nm OD) and verified by plate counts. Due to the limited of the number of trees available and tree size, the strains inoculated on the trees were split between the 2 cultivars, 10 strains on 'Sweetheart' (i.e., 1-U-9, 1-V-13, 1-V-14, 1-V-15, 1-G-16, 1-G-17, 1-G-18, 1-R-21, 1-Br-22, and 1-Br-23) and 10 strains on 'Coral Champagne' (i.e., 2-BP-25, 2-BP-26, 2-BP-27, 2-BP-29, 2-BP-30, 2-BP-32, 2-BP-33, 2-BP-34, 3-BY-37, 3-BY-38). Strains were assigned randomly to 4 branches/tree and 3 site locations/branch (basal, mid, and distal) with at least 4 nodes between wounds (Appendix A). Inoculum and PBS only control (3 reps/tree) were applied via pipette in 20µl drops and were covered promptly with parafilm and duct tape for a total of 139 inoculations. Inoculated wood was left wrapped until May 2020 (~ 6 months) when they were unwrapped and assessed for lesion formation. Lesions were rated on the same 4 point scale (4=strong brown/black lesion, spread from inoculation site, gumming; 3= brown/black lesion, gumming; 2=some brown coloration; 1=no lesion) as in Hulin et al. (2018) (Figure 2.10).

This study was repeated in 2021 with some modifications. In March 2021, all strains (5 reps/strain) and PBS only controls (3/tree) were inoculated on 2-to-3-year-old wood of 12 'Sweetheart' trees trained as bi-axis espalier located at site 2 (Ionia Co.) and 20 'Coral Champagne' trees (trained as upright fruiting offshoots [UFO]) at site 4 (Berrien Co.) (Figure 2.1 and Figure 2.9). As with the 2019/2020 study, the strains and reps were assigned to trees

randomly (Appendix A). The trees at site 2 were stronger and had more branching than at site 4 trees, ergo more trees were used at site 4. A total of 296 inoculations (136 at site 2, and 160 at site 4) were made using the same methods as described for 2019, except at site 4, inoculations were in four locations/branch (basal, mid, mid, distal) as only two branches/tree were available (Figure 2.9; Appendix A). Lesion formation was assessed after only 3 months, in June 2021, using the same scale described previously. All images documenting the inoculation and lesion rating assessments for both years can be found in Appendix A.

Statistical Analysis of Virulence Studies

Green fruit lesion area and wood lesion rating data were analyzed in the statistical program R v4.2.2 (R core team 2022). Data were collapsed by phylogenetic groupings (phylogroup) of strains (determined by MLSA) for both experiments due to like values. For analysis of the green fruit lesion area data the two years (2019 and 2021) were combined to improve the robustness of the model and the R code used was modified from Mangiafico (2016). A non-parametric Kruskal-Wallis test was used, followed by pairwise multiple comparisons using Dunn's all pairs test with Bonferroni adjusted p-values (Mangiafico, 2023; Pohlert, 2022). The wood lesion rating data were analyzed using a cumulative links model (clm) for ordinal regression (Christensen, 2022). Model fitness was tested using McFadden's pseudo-R-squared values (Andri et al., 2022; Venables and Ripley, 2002). Post hoc analysis was done with pairwise comparisons of strains using the lsmeans function with Tukey adjusted p-values (Graves et al., 2019; Lenth, 2023,). All graphical representations of data from both experiments were created using 'ggplot2' and 'ggpubr' (Kassambara, 2022; Wickham, 2016). Fonts, colors, and brackets were added or adjusted to the graphs using InkScape v.1.2 (InkScape.org).

2.4: Results

Isolation, Oxidase Reaction, and *syrD*/*syrB* Amplification

A total of 48 plates were used for the flower microbiome dilutions, 47 plates contained dilutions with single colonies (only one was overgrown at all dilutions). Forty-three produced colonies visually similar to *Pss* (i.e., cream-colored and circular in shape). A single colony from each of these 43 plates was selected for streaking to obtain pure cultures for further characterization of strains. Of the 43 pure cultures four were found to be oxidase^{+} and were discarded, having turned purple when exposed to Kovac's oxidase reagent and therefore were not *Pss*. The remaining 39 putative *Pss* strains were oxidase^{-} (no color change) and were stored and used for further analysis.

The remaining 39 strains were then used in the PCR reaction for determining the presence of the *syrD* gene (gene encoding the export of syringomycin) (Appendix A). Of these, 20 strains had amplification of the *syrD* gene (*syrD*$^{+}$), (strain nos. 9, 13, 14, 16, 17, 18, 21, 22, 23, 25, 26, 27, 29, 30, 32, 33, 34, 37, and 38) and were considered possible *Pss* strains (Table 2.4). These 20 oxidase^{-}/*syrD*$^{+}$ strains were named and used in all further experiments. Although the strains were given unique identifiers according to the location and cultivar from which they were collected (helpful for strain and data sharing/comparisons), in most cases only the strain number will be reported for simplicity in this paper.

The 20 oxidase^{-}/*syrD*$^{+}$ strains were also screened for amplification of the *syrB* gene, with varied results (Appendix A). Eleven had amplification of the *syrB* gene (*syrB*$^{+}$) (nos. 9, 22, 23, 25, 26, 27, 32, 33, 34, 37, and 38) while 9 failed to amplify (strain nos. 13, 14, 15, 16, 17, 18, 21, 29, 30) (Table 2.4).

GATTa, Fluorescence, INA, and Cu/Streptomycin Resistance

The 20 oxidase^{-}/*syrD*$^{+}$ strains differed in their GATTa profiles. Fourteen (nos. 9, 25, 26, 27, 37, 38, 22, 23, 32, 33, 34, 16, 17, and 18) had the typical *Pss* GATTa profile of + + − − (Table 2.4). These strains (excluding 16, 17, and 18) were also *syrB*$^{+}$. Strains 16, 17, and 18 were unique in that they exhibited the standard *Pss* GATTa profile but are *syrB*$^{-}$. Six strains (13, 14, 15, 21, 29, and 30) had an atypical GATTa profile of + + + − and were all *syrB*$^{-}$. The control strain of *Psm* 627 had the usual GATTa profile of *Psm* (− − + +), and thus none of the 20 strains were *Psm*. All 20 of the oxidase^{-}/*syrD*$^{+}$ strains fluoresced under UV light when grown on iron (Fe) deficient KB media.

Strains were also variable for ice nucleation activity (INA). All strains that had the typical GATTa$^{+\,+\,-\,-}$ profile were INA^{+}, except for 22, 23, and 18. Strains 22 and 23 were INA^{-}, while strain 18 was INA$^{+/-}$ (i.e., 30% were INA^{+} (n=10)) (Table 2.4). For the atypical GATTa$^{+\,+\,+\,-}$ strains, three were INA^{-} (13, 29, 30), two were INA$^{+/-}$ (14, 15; 10% were INA^{+} (n=10)), and one was INA^{+} (strain 21).

A single strain, 1-U-9, had resistance to Cu while the other 19 oxidase^{-}/*syrD*$^{+}$ strains were susceptible to Cu at 250 μg/ml (Table 2.4). Strain 9 is GATTa$^{+\,+\,-\,-}$, *syrB*$^{+}$/*syrD*$^{+}$, and INA^{+}. No strains were found to be resistant to the antibiotic streptomycin at 50 μg/ml. All images of the Cu and streptomycin media plates can be found in Appendix A.

MLSA

The ML phylogenetic tree produced as a result of the MLSA consisted of 3 main phylogroups (PG) 2, 3, and 1, rooted at *P. fluorescens* A506 (Figure 2.11). The best fit model for the ML tree was the Tamura-Nei (TN93) model with Gamma distributed (5 categories, parameter = 0.2623) invariant sites (37.27%) (G+I), (TN93+G+I) (Tamura and Nei, 1993). The PG2 in this tree are further sub-divided into 5 additional clades (2a, 2b, 2c, 2d, and 2f). All 20 strains are in

PG2, and are found within clades 2b, 2c, and 2d. None of this study's strains were found in PG2a, PG2f, PG1, or PG3, nor did any cluster near *P. viridiflava*.

Of the 20 strains, six are in PG2d (strains 37, 38, 9, 26, 27, and 25) with the well-known virulent *Pss* strain B728a, five are in PG2b (strains 33, 34, 32, 22, and 23) with the well-known virulent Pss strain FF5, and nine are in PG2c (strains 21, 17, 18, 16, 29, 30, 13, and 15) with the atypical, non-virulent *Pss* strain 642 (Figure 2.11). Those in PG2d are GATTa$^{+\,+\,-\,-}$, *syrB*$^{+}$/*syrD*$^{+}$, and INA^{+} (Table 2.4). The PG2d strains 37 and 38 clustered together (95% bootstrap certainty) nearest to a Hungarian (HUN) *Pss* strain 2340, while strain 9 was nearest to a Montenegro (MNE) *Pss* strain K3 (99% bootstrap certainty), and strains 26, 27, and 25 clustered together (96% bootstrap certainty) nearest to a Great Britain (GBR) *Pss* strain HRI-W7924 (98% bootstrap certainty) (Figure 2.11 and Table 2.3). The PG2b strains were also GATTa$^{+\,+\,-\,-}$ and *syrB*$^{+}$/*syrD*$^{+}$, but varied in INA (i.e., 33, 34, and 32 are INA^{+}, while 22, 23 are INA^{-}). The PG2b strains 33, 34, and 32 clustered together with 100% bootstrap certainty, arising from the same branch as the *Pss* type strain CFBP4702 (98% bootstrap certainty). Strains 22 and 23 grouped together with 99% bootstrap certainty nearest to the *Pss* strain FF5-1 (99% bootstrap certainty). Strains in PG2c were variable in their GATTa profiles (67% GATTa$^{+\,+\,+\,-}$, 33% GATTa $^{+\,+\,-\,-}$) and INA (equal no. strains in the INA^{+}, INA^{-}, and INA$^{+/-}$ categories); however, they were all *syrB*$^{-}$/syrD^{+}. The strains 16, 17, and 18 clustered together (99% bootstrap certainty) in PG2c between strain 21 (from this study) and the atypical *Pss* strain 642 with 100% and <75% bootstrap certainty, respectively (Figure 2.11, Table 2.3). Strains 29 and 30 (from this study) clustered together in PG2c with 100% bootstrap support nearest to the atypical *Pss* strain 508 (76% bootstrap certainty), while the strains 13, 14, and 15 clustered together with 100%

bootstrap certainty nearest to the Australian (AUS) *Pss* strain DAR82450 with less than 75% bootstrap support.

Virulence on Green Fruit and Cherry Wood

The lesion area data for strain virulence on green fruit was not normally distributed (Shapiro-Wilk normality test p=3.52e-16), with unequal variances (Levene's test p=0.0003). The Kruskal-Wallis test for non-parametric data showed that the green fruit lesion area was statistically different for strains in the 3 PGs (χ^2=152.98, df=4, p< 2.20e-16). There was a clear trend in the virulence level of the strains inoculated on green fruit (Figure 2.12). The strains 9, 37, 27, 38, 25, and 26 in PG2d were the most virulent strains on green fruit, with median lesion area ranging between 76.6 to 14.2 mm^2. Strains 23, 22, 32, 33, and 34 in PG2b were moderately virulent, with median lesion area ranging from 11.5 to 5.8 mm^2, and strains (13, 14, 15, 16, 17, 18, 21, 29, and 30) in phylogroup 2c are avirulent (0 mm^2). The pairwise analysis of the phylogroups for lesion area supported the graphical interpretations, in which the strain lesion area or virulence in PG2d was statistically different ($p<0.05$) (i.e., more virulent) than strains in PG2b and PG2c, while strains in PG2b were more virulent than strains in PG2c (Appendix A). Strains in PG2c were avirulent, with no statistical difference from PBS (control).

This gradation of virulence is also mirrored in the virulence ratings from strains wound-inoculated on sweet cherry wood (Figure 2.13). Where strains in PG2d (9, 37, 27, 38, 25, and 26) were the most virulent with median virulence ratings that ranged from 4 to 3 for both 'Coral Champagne' (2020 and 2021) and 'Sweetheart' (2020), and from 4 to 1 for 'Sweetheart' in 2021. The strains in PG2b (23, 22, 32, 33, and 34) were moderate to avirulent, with median virulence ratings of 2 to1 for 'Coral Champagne' (2020 and 2021) and 3 to1 for 'Sweetheart' (2020 and 2021). As in the green fruit assay, the strains in PG2c were avirulent, with a median virulence

rating of 1 for both ‘Coral Champagne’ and ‘Sweetheart’ (2020 and 2021), the same as the PBS controls. A proportionally low level of wild *Pss* contamination did occur in PBS control wounds for both cultivars and years, accounting for the single points when the virulence rating was >1. These graphical interpretations of the virulence rating data were further supported by cumulative link model (clm) ordinal regression analysis and post hoc pairwise comparisons of estimated marginal means. The best-fit model for the ordinal regression of the virulence rating data for the 20 *Pss* strains inoculated on sweet cherry wood is presented in Appendix A.

There was a statistical effect of wood virulence rating overall for strains within the 3 phylogroups: PG2d virulence ratings were higher than those in PG2b while the PG2c and PBS control virulence ratings were less than those in PG2b based on the estimate coefficient (Table 2.5). The PG2b strains were variable in virulence and thereby are considered moderately virulent to avirulent. There were instances when PG2b strains were not statistically different from the avirulent 2c strains (on ‘Coral Champagne’ in 2020 and on ‘Sweetheart’ in 2021) and instances where they were statistically different from the PG2c strains (on ‘Sweetheart’ in 2020 and ‘Coral Champagne’ in 2021). There was a singular instance where PG2b strains were not statistically different than the more virulent PG2d strains (on ‘Sweetheart’ in 2020). The PG2c inoculations never differed statistically from the PBS controls for either cultivar or year, and therefore were avirulent. Pairwise comparisons of the marginal estimated means (lsmeans) of the virulence ratings of strains on wood by phylogroups again show virulence from most virulent to least virulent as PG2d > PG2b > PG2c (Appendix A).

2.5: Discussion

syrB and *syrD* Amplification

All 20 oxidase$^-$ strains amplified for the *syrD* gene (*syrD*$^+$) however, there was pronounced variation in the strains that amplified for *syrB* (11 *syrB*$^+$ and 9 *syrB*$^-$ strains) (Table 2.4). The amplification of *syrB* and *syrD* is standard for differentiating *Pss* from *Psm* and is included as part of the positive identification of *P.s* spp. (Bultreys and Gheysen, 1999; Renick et al. 2008; Sorensen et al., 1998; Quigley and Gross 1993). Many studies to characterize *Pss* have only used the amplification of the *syrB* gene to show the presence of the syringomycin phytotoxin (Hall et al. 2019; Ivanović et al., 2022; Lauwers, 2022; Olsel et al., 2022; Popović et al., 2021; Vasebi et al. 2020). This is likely due to the results of research from Sorensen et al. (1998), in which amplification of *syrD* did not always correlate with the presence of the gene in southern blot analyses. However, Bultreys and Gheysen (1999) used a separate set of primers and did not have specificity issues. Consequently those *syrD* primers were used in this study (as well as in Renick et al., 2008) and if only the *syrB* primers had been used then the 9 atypical *Pss* strains may have been discarded. For the 9 *syrB*$^-$ strains (strain nos. 13, 14, 15, 16, 17, 18, 21, 29, 30) there are two possible explanations that should be explored further: 1) these strains lack *syrB*, or 2) the *syrB* gene was not detected with the Sorensen et al. (1998) primers. The latter is entirely plausible given that the *syrB* gene region has been found to be quite diverse in addition to evidence showing variable results with the different *syrD* primers. However, given that the 9 *syrB*$^-$ strains were all found to be non-pathogenic (on cherry) and belong to the same phylogroup (PG2c), it is more likely that they lack *syrB*, as confirmed *Pss* strains lacking the *syrB* gene have been reported previously (Bultreys and Kaluzna, 2010; Hall et al., 2019; Popović et al., 2020; Quigley and Gross 1993; Scortichini et al., 2003). The production of syringomycin can be

verified in the Petri dish bioassay described in Latorre and Jones (1979) or the syrB^{-} strains 16S rDNA sequences could be compared to other globally known *syrB*$^{-}$ strains (Popović et al., 2021). Lauwers (2022) did not find any *syrB*$^{-}$ strains in their characterization of Michigan *Pss* and considered syrB^{+} strains as verified *Pss* (and did not check for *syrD*), while Renick et al. (2008) only amplified *syrD* and considered syrD^{+} strains as verified *Pss*. The syringomycin phytotoxin is considered to be a significant virulence factor in *Pss*; in addition to causing the release of plant nutrients, it contributes to symptom development and aids in bacteria movement (Hulin et al., 2020; Xin et al., 2018). All 20 strains in this study contained syringomycin genes, either *syrB*$^{+}$/*syrD*$^{+}$ or *syrB*$^{-}$/*syrD*$^{+}$, and therefore have the potential to be virulent either on cherry or another *Prunus* species.

GATTa, INA, and Cu/Streptomycin resistance

The 20 oxidase^{-}/syrB$^{+/-}$/*syrD*$^{+}$ strains isolated in this study also had diverse GATTa profiles and INA. The majority were GATTa^{++--} (strain nos. 9, 25, 26, 27, 37, 38, 22, 32, 33, 34, 16, 17, and 18) or GATTa $^{+++-}$ (strain nos. 13, 14, 15, 21, 29, and 30) (Table 2.4). The standard GATTa profile for *Pss* is GATTa^{++--}, GATTa $^{+++-}$ is atypical, and *Psm* is GATTa^{--} $^{++}$ (Latorre and Jones 1979). While GATTa is a good test to differentiate between *Pss* and *Psm*, it is not a good test to use alone for *Pss* identification since tyrosinase activity and tartrate utilization by strains often is variable (Bultreys and Kaluzna, 2010; Hall et al., 2019; Latorre and Jones 1979). In this study six atypical GATTa $^{+++-}$ strains (13, 14, 15, 21, 29, and 30) were *syrB*$^{-}$ non-pathogens (on cherry), and in PG2c, three strains (16, 17, 18) were typical GATTa^{++-} $^{-}$, *syrB*$^{-}$, non-pathogens (on cherry), in PG2c, and 14 strains were typical GATTa^{++--} strains (9, 25, 26, 27, 37, 38, 22, 23, 32, 33, 34, 16, 17, and 18), syrB^{+} that ranged in pathogenicity in PG2b and PG2d (Table 2.4). Hall et al. (2019) reported *Pss* isolated from grapes (*Vitis vinifera*) in

Australian had atypical GATTa profiles that were both pathogenic and non-pathogenic. Lauwers (2022) did not find any *Pss* from Michigan sweet cherries with atypical GATTa profiles, and Renick et al. (2008) did not include GATTa tests in their characterizations of Michigan *Pss*.

Pss strains isolated from sweet cherry flowers in Michigan have been shown to have a high degree of INA. Renick et al. (2008) had 94% INA in their Michigan *Pss* strains while Lauwers (2022) had 100% INA. The 20 strains in the current study were a mix of INA^{+} (60%), INA^{-} (25%), and $INA^{+/-}$ (15%) (Table 2.4). *Pss* strains with a variable INA phenotype may not be active all at the same time, thereby populations are composed of a combination of $INA^{+,-}$, and $^{+/-}$ (Hirano and Upper, 2000; Gross et al. 1983, Renick et al. 2008). *Pss* cells are able to ice nucleate due to proteins embedded in their outer membrane and can do so at 0 to -5°C, causing frost damage to plants at a higher temperature than would occur in the plant with no INA bacteria (i.e., in cherry, during bud break 50% of buds are killed at -6°C and 90% at -7°C with prolonged temperatures) (Hirano and Upper, 2000; Lindow et al., 1983a; Lindow et al., 1983b; Lukas et al. 2022; Salazar-Gutiérrez et al., 2004). This injury allows *Pss* to enter and infect the plant, causing initial blossom blast symptoms, which was a major contributor to a critical state-wide bacterial canker epidemic in Michigan in 2012 (Sundin and Rothwell, 2012).

In this study, only a single strain, 1-U-9 (9), was found to be copper resistant (CuR); this strain was also $GATTa^{++--}$, $syrB^{+}/syrD^{+}$, INA^{+}, and pathogenic (PG2d) (Table 2.4). It was surprising to find such a low incidence of CuR since Cu has been the most widely used and primary control measure for bacterial diseases since the mid-1800s as well as being the primary control option for bacterial canker disease (Lamichhane et al., 2018; Lauwers, 2022; Renick et al., 2008; Sundin et al., 1989). Lauwers (2022) and Renick et al. (2008) had *Pss* strains that were 13.8% and 31.7% CuR respectively. Sundin et al. (1989) found that CuR *Pss* strains from

Michigan cherry orchards contained a 61kb plasmid that was transferrable along with resistance to copper-susceptible (CuS) strains. None of the strains in the current study had resistance to the antibiotic streptomycin (streptomycin susceptible [SmS]) (Table 2.4). This is also a surprise since streptomycin is widely used in Michigan apple orchards, Michigan is ranked 3rd nationally for apple production, and streptomycin resistance (SmR) is prevalent in the fire blight pathogen *E. amylovora* (McGhee and Sundin, 2011; MDARD, 2018; Slack et al., 2021; Sundin and Wang, 2018). Jones et al. (1991) also isolated SmR *P. syringae* pv. *papulans* from Michigan apple orchards.

MLSA and Virulence on Green Fruit and Cherry Wood

Michigan's *Pss* are also phylogenetically diverse. The ML tree in this study showed that Michigan *Pss* belonged to 3 out of the 7 PG2 clades (PG2b, PG2c, and PG2d) (Figure 2.11). Previous MLSA phylogenomic analyses of Michigan *Pss* had placed strains isolated from cherry flowers in phylogroups 2a, 2b, and 2d (Lauwers, 2022). Though both studies had *Pss* strains that belong to PG2b and PG2d, only this study found strains belonging to PG2c, and Lauwers (2022) found strains that belonged to PG2a.

The strains 9, 25, 26, 27, 37, and 38 were in PG2d, and strains 9 and 37 had been confirmed previously as *Pss* from whole genome sequences (Dr. Michelle Hulin, East Malling, U.K., unpublished). These PG2d strains were also virulent on green sweet cherry fruit and wood (Figures 2.12, 2.13) and would be excellent for future experiments for which differences in infection vs. treatment need to be demonstrated. The strains in PG2b (22, 23, 32, 33, and 34) also can be considered to be verified *Pss* isolates since they were also GATTa $^{++--}$, syrB^{+}/syrD^{+}, and INA^{+}/INA^{-} (Table 2.4). They were, however, moderately to avirulent on green sweet cherry fruit and wood, their pathogenicity on other *Prunus* spp., such as plum, apricot, or peach, has yet to be

assayed. Hulin et al. (2018a) showed reduced aggressiveness of some strains when looking at pathogenicity on plum and cherry wood. Since the current study utilized more thorough virulence tests, it is now known that the use of some of these strains in experiments could result in inconsistent infections and make treatments differences harder to discern.

The strains in PG2c (13, 14, 15, 16, 17, 18, 21, 29, 30) were all *syrB*$^{-}$/*syrD*$^{+}$ but had variable GATTa profiles and INA and were avirulent on both the green sweet cherry fruit and sweet cherry wood. Phylogroup 2c is known as a non-pathogenic clade (Berge et al., 2014; Clarke et al., 2010). The strains *Pss* 642 and *P.s* 508, two reference strains included in this MLSA are in PG2c, are capable of INA and phytotoxin production, but have an atypical T3SS (Clarke et al., 2010; Mohr et al. 2008). All of the strains in this phylogroup were syrB^{-}/syrD^{+} and varied in INA (Table 2.4). Strains 21, 17, 18, and 16 are closely related to *Pss* 642, while strains 29 and 30 are closely related to *P.s* 508, so these strains could be considered to be atypical *Pss*. Further sequencing and genome comparisons need to be made to examine the T3SS of these strains. The strains 13, 14, and 15, however, clustered together away from the atypical T3SS strains nearest to the avirulent Australian *Pss* strain DAR82450 (which was also GATTa^{+++-}), but with <75% bootstrap certainty (Figure 2.11) (Hall et al., 2019). Strain 14 had been sequenced previously via the whole genome and was found to belong to a *P.s* outgroup (Dr. Michelle Hulin, East Malling, U.K., unpublished). These three strains should be labeled conservatively as *P.s.* strains rather than *Pss*. It is interesting that they did not classify with any of the *P.s* outgroups included in this MLSA with the 4 "housekeeping" genes (*gap1*, *gltA*, *gyrB*, and *rpoD*) used. While tools like PCR amplification and MLSA with a select subset of genes can give a more "rapid" picture of what *Pss* populations look like, the use of whole genome comparisons (e.g., Hulin et al., 2018b; Ruinelli et al., 2020) would give a more accurate insight into such a diverse

clade of organisms. Gomila et al. (2017) implemented the reorganization of some of the spp. within the *P.s* spp. complex with whole genome sequence comparisons. Baltrus and Orth (2018) discuss this concept in their review of Hulin et al. (2018b) and highlight how changes in technology and affordability will provide for more sophisticated experimental results. This MLSA also showed how Michigan strains are closely related to *Pss* strains from around the world. A prime example is the Michigan *Pss* strain 9 and the K3 *Pss* strain from Montenegro that grouped together in PG2d (Figure 2.11). Both strains are GATTa $^{++--}$, INA^{+}, syrB^{+}, SmS, and CuR, and it would be interesting to compare them further at the genomic level, especially their copper resistance (this studies Table 2.4; Popović et al. 2021).

Strains consistent virulence level on both the green fruit and cherry wood, seem to correspond to phylogroup, since PG2d was the most virulent overall while PG2b had moderate to avirulent strains and PG2c had avirulent strains (Tables 2.5, Figures 2.12-2.13). Hulin et al. (2018a), did not report this putative relationship, whose methodology guided this study's approach. The gradient of virulence for the strains within the 3 phylogroups is also clear. Further virulence assays would be required, especially on wood, to confirm a correlation between phylogroup and virulence, since in 2019, this study split the 20 strains between two cherry cultivars. The use of rapid pathogenicity tests for new pathogen identification only reports a +/– response, so the nuance in virulence levels can be missed, requiring more in-depth characterizations. Virulence gradients may not be of interest to researchers focused on the most virulent *Pss* isolates. For research applicable to Michigan cherry growers, the range demonstrated by these 20 strains should definitely be considered since they all have virulence genes (i.e., *syrD*$^{+}$, and several were INA^{+} or INA$^{+/–}$).

Further research should look at the T3SS/effectors that these strains may possess (especially the PG2b and 2c strains) in addition to looking at those of the most virulent strains. Recently Ruiz-Bedoya et al. (2023) demonstrated that mutant *P.s* strains with a single effector alone are non-virulent but when strains are combined, they can be just as virulent as wild-type pathogens with multiple effectors. *Pss* is known to have few T3SS effectors, and a diverse array of strains can be isolated from the same niche as seen in this study. It is entirely possible that these moderate to avirulent strains could produce some factor that bolsters the more virulent strains and enhances their effectiveness as pathogens (Hulin et al., 2018b; Ruinelli et al., 2019; Ruiz-Bedoya et al., 2023). This concept was also noted by Barrett et al. (2011), who considered pathogen "cooperators" vs. non-pathogen "cheats" in which the fitness of the non- pathogen is improved by the "goods" produced by the pathogen. They also suggested that non-pathogens have a "fitness advantage in non-host environments". *Pss* is a generalist and requires a diverse set of genes to function in the multiple environments in which it is known to exist (Bell and Bell, 2021; Morris et al., 2019). The evidence of "synergisms" between strains in *P.s* populations (albeit in pathogen-pathogen interactions) is also mounting. Petriccione et al. (2017) isolated *Pss* with *P.s.* pv. *actinidiae* and found that co-inoculations enhanced kiwi canker infections. Bophela et al. (2020) isolated *P. viridiflava* with *Ps*s on plum, and Lipps and Samac (2021) noted several more "synergisms" involving *P. viridiflava*. Co-inoculation studies could be done in tandem with further virulence-level studies on cherry wood and other *Prunus* species. These moderate to avirulent strains should be assessed as possible biological control agents, perhaps as compatible vectors for dissemination of bacteriophage, or perhaps they could compete for resources.

This study has provided an initial foundation for the sweet cherry flower microbiome with respect to *Pss* diversity. Elucidation of the cherry microbiome certainly will require

extensive, long-term study. Xin et al. (2018) discussed the importance of the microbiome as part of the classic disease triangle, ostensibly as a "4th vertex" considering that the interactions in the microbiome can "influence plant immunity and/or pathogen virulence", so further study of what are the potential impacts of these moderate to avirulent *Pss* strains in Michigan cherry orchards is warranted. It also would be interesting to see if these moderate to avirulent strains could be recovered from cherry flowers at other locations throughout Michigan and other cherry growing regions to determine the geographic and/or ecological limits of their resident populations.

2.6: Conclusions

This characterization of the *Pss* strains isolated from sweet cherry flowers has highlights the variability in Michigan orchards. The 20 *Pss* strains in this study belong to 3 phylogenomic groups (PG2d, PG2b, and PG2c), exhibited a gradient of virulence on green cherry fruit and wood, had variable GATTa profiles, amplified the syringomycin production gene (syrB), and showed INA. This study also demonstrated the importance of not forgoing thorough virulence tests, as *Pss* researchers could inadvertently select strains with reduced virulence capabilities. Caution also should be used when interpreting MLSA phylogenomic trees and PCR amplification results, since primer/gene sequence selection may bias results. This was evident from the MLSA placement of strain 14 in the atypical *Pss* PG2c, but upon whole genome sequencing it was found to belong in a *P.s* outgroup (Dr. Michelle Hulin, East Malling, U.K., unpublished). Future research questions that should be addressed with these 20 *Pss* strains include: Do the *syrB*$^{-}$ strains produce syringomycin or other phytotoxins? What virulence genes or T3SS/effectors do these Michigan *Pss* strains possess (typical/atypical)? What does the phylogenetic tree look like with whole genome analyses? Are the *Pss* strains in PG2b or PG2c virulent or more virulent on other *Prunus* spp.? How do the strains with varying degrees of

virulence interact with each other on cherry: cheaters, producers, mutualism/synergisms? Can co-inoculations increase virulence in cherry wood or on other *Prunus*? Can these moderate to avirulent strains be isolated from orchards throughout Michigan and from tissues other than flowers? Can they be useful as biological control agents? Answers to these questions may help facilitate the development of future *Pss* population management strategies and tools.



Figure 2.1. Michigan orchards where bacteria strains were isolated from cherry flowers (sites 1, 2, and 3) and where strains were tested for their virulence on wood (sites 1, 2, and 4). Site 1 is Wells Orchards (Grand Rapids, Ottawa Co.), site 2 is Michigan State University (MSU) Clarksville Research Center (Clarksville, Ionia Co.), site 3 is MSU Horticulture Teaching and Research Center (Holt, Ingham Co.), and site 4 is MSU Southwest Michigan Research and Extension Center (Benton Harbor, Berrien Co.).

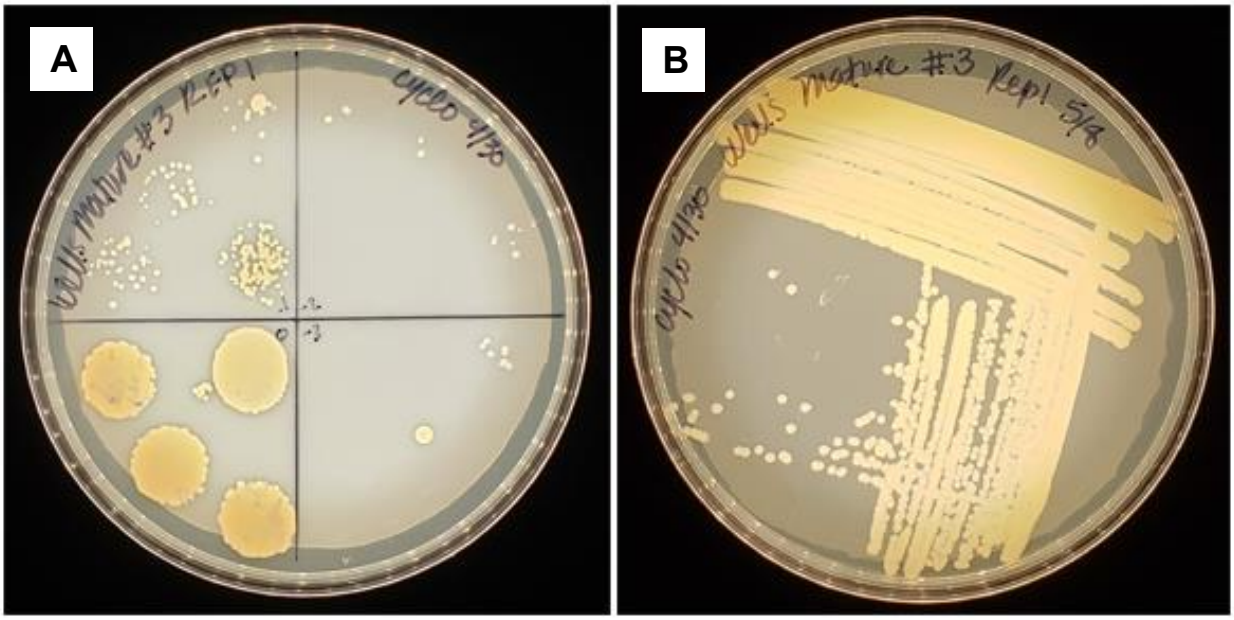


Figure 2.2. Isolation of putative *Pseudomonas syringae* pv. *syringae* (*Pss*) strains from sweet cherry flowers: **A)** an example of the drop plates made from the serial dilutions (0, 10^{-1}, 10^{-2}, 10^{-3}) of the flower wash, and **B)** an example of the streak plates made from the selection of a single colony from the drop plate. Single colonies of this pure culture were then used for oxidase testing and making bacterial lawns for storing strains for further use.

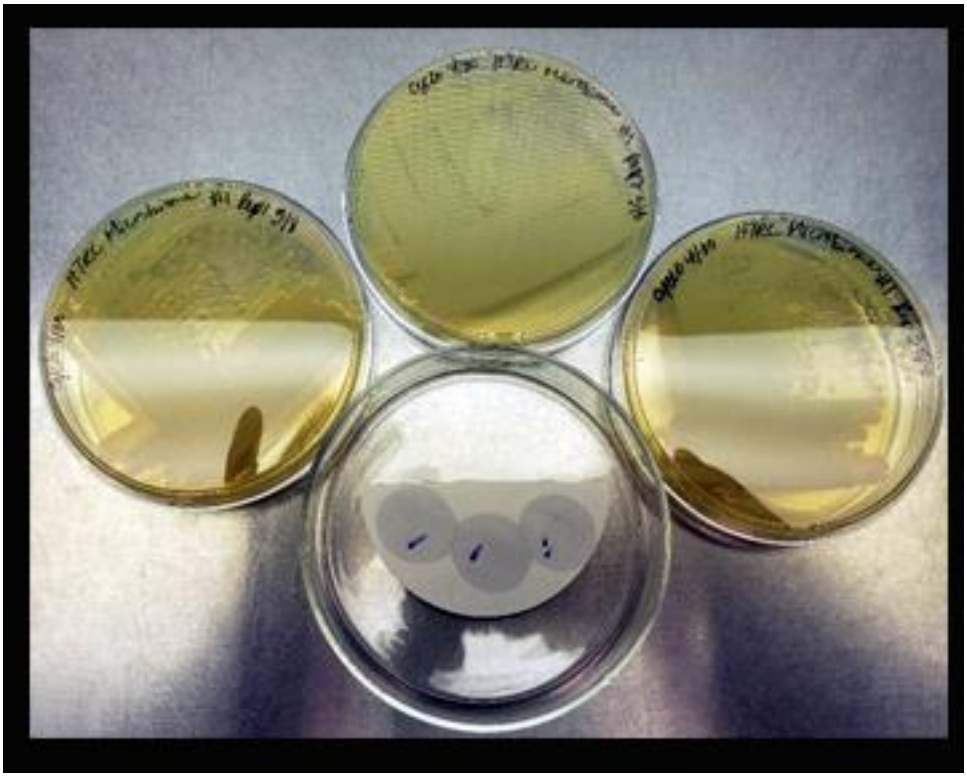


Figure 2.3. Bacterial strains that were positive for the cytochrome oxidase enzyme (oxidase^{+}) turned purple when smeared onto filter paper with Kovacs' oxidase reagent. These strains were not characterized any further since *Pseudomonas syringae* pv. *syringae* (*Pss*) is oxidase^{-} (no reaction/color change).

Table 2.1. Primers and thermal cycler parameters used to amplify the genes syrD and syrB involved in the export and synthesis of the phytotoxin syringomycin in *Pseudomonas syringae*.

Gene	Primer	Thermal profile	Product size (bp)	Reference
syrD	Forward 5′-CAGCGGCGTTGCGTCCATTGC-3′ Reverse 5′-TGCCGCCGACGATGTAGACCAGC-3′	95 °C 2 min. 35 cycles: 94 °C 1 min. 60 °C 1 min. 72 °C 1:30 min. 72 °C 5 min. 12 °C ∞	1,040	Bultreys and Gheysen (1999), Renick et al. (2008)
syrB	Forward 5′-CTTTCCGTGGTCTTGATGAGG-3′ Reverse 5′-TCGATTTTGCCGTGATGAGTC-3′	94 °C 4 min. 35 cycles: 94 °C 1:30 min. 60 °C 1:30 min. 72 °C 3 min. 72 °C 10 min. 12 °C ∞	752	Sorensen et al. (1998), Vasebi et al. (2020)

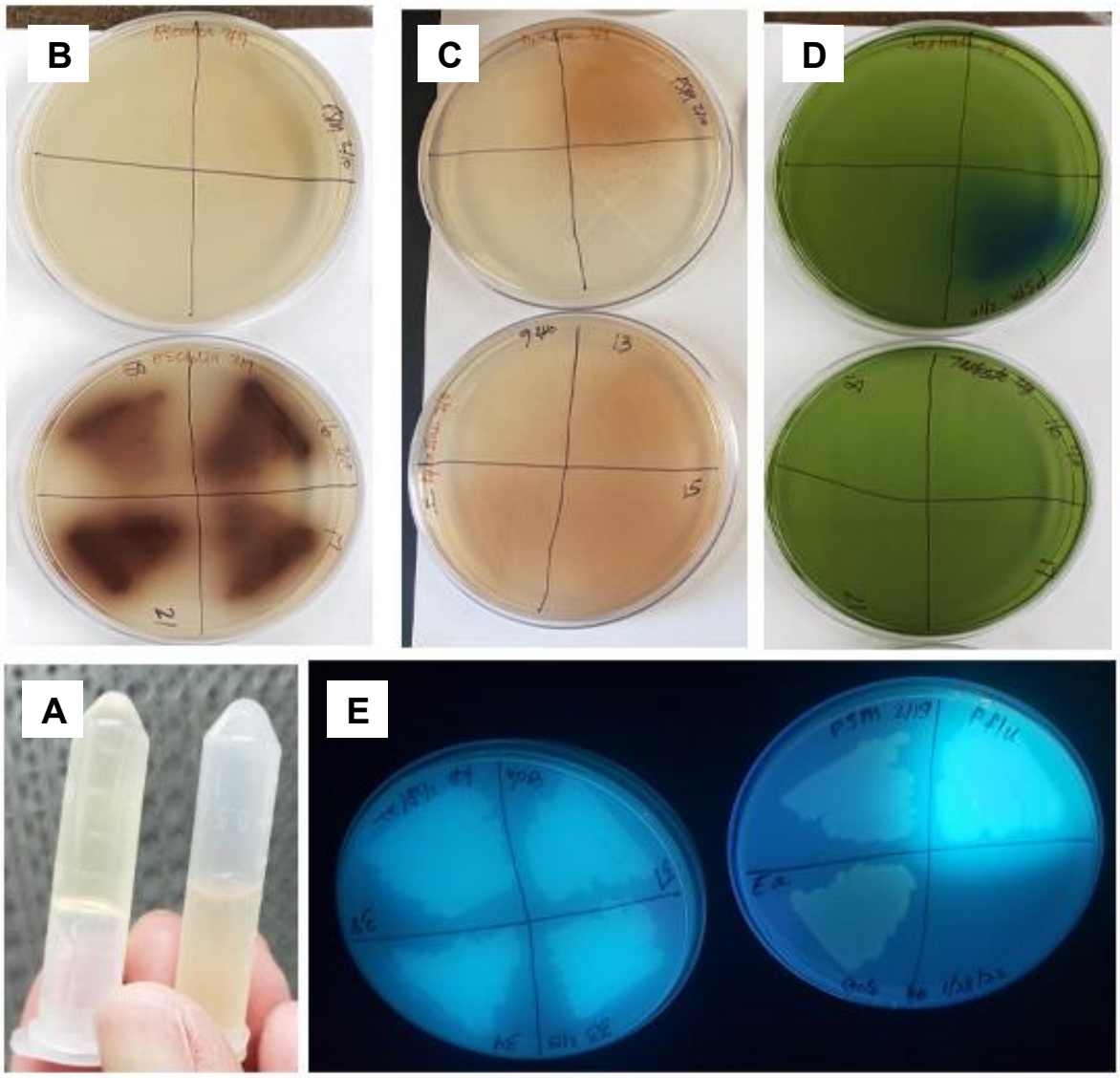


Figure 2.4. Examples of how oxidase^{-}/*syrD*$^{+}$ strains were tested biochemically using various media types for their GATTa profile and the phenological expression of fluorescence commonly used to determine *Pseudomonas syringae* pv. *syringae* (*Pss*) strains. **A)** Gelatin liquefaction [G] tubes, **B)** Aesculin hydrolysis plates [A], **C)** L-tyrosinase activity [T] plates, **D)** Tartrate Utilization [Ta] plates, and **E)** strains tested for fluorescence on KB plates in a UV light box.



Figure 2.5. Floats coated with a thin layer of paraffin wax with 10 replicates of each bacterial strain in a 50% ethylene glycol refrigerated water bath used for testing ice nucleation activity (INA).

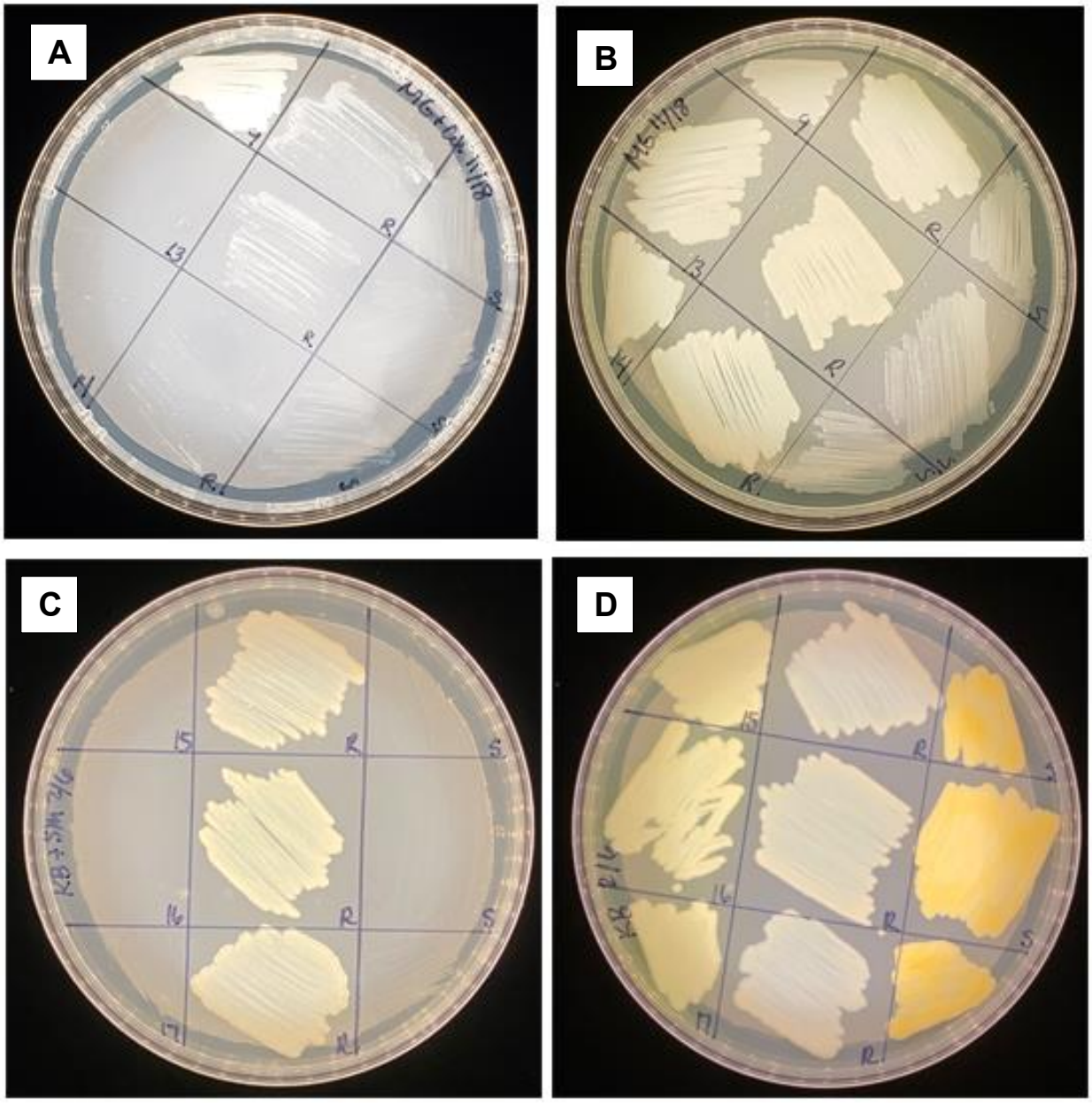


Figure 2.6. Examples of *Pseudomonas syringae* pv. *syringae* (*Pss*) copper (Cu) and streptomycin (Sm) resistance assay plates. **A)** mannitol-glutamate (MG) media amended with 250 µg/ml copper sulphate ($CuSO_4$) with this study's strains streaked in the left side of the plate, the Cu resistant *Pss* BC 43(390) CuR strain in the center, and the susceptible Pss 26-3 on the right side of the plate, **B)** an MG plate without Cu, **C)** King's B (KB) media amended with 50 µg/ml streptomycin with this study's strains streaked on the left side of the plate, the Sm resistant *Erwinia amylovora* strain (Ca11-7 SmR) in the center, and the susceptible *Pantoea agglomerans* strain (UMAF3067) on the right side of the plate. **D)** KB media without streptomycin.

Table 2.2. The PCR primers, sequencing primers, and thermal cycler parameters for the amplification and sequencing of the four housekeeping genes (*gap1*, *gltA*, *gyrB*, and rpoD), using DNA extracted from the oxidase^{-}/*syrD*$^{+}$ bacterial strains isolated in this study from sweet cherry flowers to be used in multilocus sequencing typing analysis (MLSA) and construction of a phylogenetic tree.

Application	**Gene**	**Primer**	The**rmal profile**	**Product size (bp)**	**Reference**
PCR	gap1	Forward 5′-CCGGCSGARCTGCCSTGG-3′ Reverse 5′-GTGTGRTTGGCRTCGAARATCGA-3′	94 °C 3 min. 35 cycles: 94 °C 2 min. 63 °C 1 min. 72 °C 1min. 72 °C 5 min. 12 °C ∞	606	Hwang et al. (2005), Vasebi et al. (2020)
	gltA	Forward 5′-CCTCBTGCGAGTCGAAGATCACC-3′ Reverse 5′-CTTGTAVGGRCYGGAGAGCATTTC-3′		664	
	gyrB	Forward 5′-CBGCRGCVGARGTSATCATGAC-3′ Reverse 5′-TTGTCYTTGGTCTGSGAGCTGAA-3′		748	
	rpoD	Forward 5′-AGGTGGAAGACATCATCCGCATG-3′ Reverse 5′-CCGATGTTGCCTTCCTGGATCAG-3′		894	
Sanger Sequencing	gap1	Forward 5′-CGARTGCACSGGBCTSTTCACC-3′ Reverse 5′-GTGTGRTTGGCRTCGAARATCGA-3′			
	gltA	Forward 5′-CTGRTCGCCAAGATGCCGAC-3′ Reverse 5′-CGAAGATCACGGTGAACATGCTGG-3′			
	gyrB	Forward 5′-CBGCRGCVGARGTSATCATGAC-3′ Reverse 5′-TTGTCYTTGGTCTGSGAGCTGAA-3′			
	rpoD	Forward 5′-YGAAGGCGARATYGRAATCG-3′ Reverse 5′-CCGATGTTGCCTTCCTGGATCAG-3′			

Table 2.3. The reference *Pseudomonas* strains used for multilocus sequence analysis (MLSA), with the four housekeeping genes (*gap1*, *gltA*, *gyrB*, *rpoD*), including the NCBI GenBank accession numbers.

Strain	**Host**	**Country**	**Accession no. x gene** *gap1, gltA* *gyrB, rpoD*	**Sequence Reference**	**Sequence Location**
P.s Cit7	*Citrus* (Orange)	USA[1]	CP073636	Baltrus et al. (2011)	NCBI
P.s tomato DC3000	*Solanum lycopersicum* (Tomato)	GBR[2]	AE016853	Buell et al. (2003)	NCBI
P.s syringae 642	Unknown weed	USA	NZ_ADGB01000062, NZ_ADGB01000077 NZ_ADGB01000027, NZ_ADGB01000033	Clarke et al. (2010)	NCBI
P.s actinidiae CFBP4909^{PT}	*Actinidia deliciosa* (Kiwi)	JPN[3]	KF937408, KF937504 KF937601, KF937698	Cunty et al. (2014)	NCBI
P.s syringae CFBP4702^{T}	*Syringa vulgaris* (Lilac)	GBR	KF937407, KF937504 KF937601, KF937698	Cunty et al. (2014)	NCBI
P. viridiflava CFBP2107^{T}	*Phaseolus* (Bean)	CHE[4]	KF937401, KF937498 KF937595, KF937692	Cunty et al. (2014)	NCBI
P. cerasi H346-S	*Corylus avellana* (Hazelnut)	CAN[5]	NZ_JACSZQ010000001, NZ_JACSZQ010000002 NZ_JACSZQ010000004, NZ_JACSZQ010000016	Ellouze et al. (2020)	NCBI
P.s syringae B728a	*Phaseolus* (Bean)	USA	CP000075	Feil et al. (2005)	NCBI
P.s syringae DAR82441	*Vitis vinifera* (Grape)	AUS[6]	KP127645, KP136850 KP192349, KP229318	Hall et al. (2019)	NCBI

Table 2.3. (cont'd)

P.s syringae DAR82442	*Vitis vinifera* (Grape)	AUS	KP127646, KP136851 KP192350, KP229319	Hall et al. (2019)	NCBI
P.s syringae DAR82446	*Vitis vinifera* (Grape)	AUS	KP127655, KP136860 KP192359, KP229328	Hall et al. (2019)	NCBI
P.s syringae DAR82447	*Vitis vinifera* (Grape)	AUS	KP127656, KP136861 KP192360, KP229329	Hall et al. (2019)	NCBI
P.s syringae DAR82450	*Vitis vinifera* (Grape)	AUS	KP127659, KP136864 KP192363, KP229332	Hall et al. (2019)	NCBI
P.s syringae DAR82452	*Vitis vinifera* (Grape)	AUS	KP127661, KP136866 KP192365, KP229334	Hall et al. (2019)	NCBI
P.s 9643	*Prunus domestica* (Plum)	GBR	NZ_MLET01000002, NZ_MLET01000001 NZ_MLET01000018, NZ_MLET01000007	Hulin et al. (2018)	NCBI
P.s syringae 9654	*Prunus domestica* (Plum)	GBR	NZ_MLES01000019, NZ_MLES01000005 NZ_MLES01000010, NZ_MLES01000016	Hulin et al. (2018)	NCBI
P.s syringae 9656	*Prunus avium* (Sweet cherry)	GBR	NZ_MLEM01000003, NZ_MLEM01000001 NZ_MLEM01000006, NZ_MLEM01000010	Hulin et al. (2018)	NCBI
P.s 508	*Malus* (Apple)	USA	NA	Hwang Schema	PAMDB.org
P.s papulans LMG5076^{PT}	*Malus* (Apple)	CAN	NA	Hwang Schema	PAMDB.org
P.s syringae FF5	*Pyrus calleryana* (Ornamental Pear)	USA	NA	Hwang Schema	PAMDB.org

Table 2.3. (cont'd)

P.s TLP2	*Solanum tuberosum* (Potato)	USA	NA	Hwang Schema	PAMDB.org
P.s syringae KBI222	*Rubus idaeus* (Raspberry)	SRB[7]	MW407117, MW407127 MW407137, MW407147	Ivanović et al. (2022)	NCBI
P.s syringae KFB422	*Rubus fruticosus* (Blackberry)	SRB	MW407115, MW407125 MW407135, MW407145	Ivanović et al. (2022)	NCBI
P. fluorescens A506	*Pyrus* (Pear)	USA	NC_017911	Loper et al. (2012)	NCBI
P.a morsprunorum HRI-W5261R2	*Prunus avium* (Sweet cherry)	GBR	LIIA01000145, NZ_LIIA01000028 NZ_LIIA01000152, NZ_LIIA01000135	Nowell et al. (2016)	NCBI
P.a morsprunorum HRI-W5269R1	*Prunus cerasus* (Tart cherry)	GBR	LIHZ01000103, NZ_LIHZ01000100 NZ_LIHZ01000082, NZ_LIHZ01000058	Nowell et al. (2016)	NCBI
P.s avii CFBP3846^{PT}	*Prunus avium* (Wild cherry)	FRA	LIIJ01000007, NZ_LIIJ01000301 NZ_LIIJ01000227, NZ_LIIJ01000241	Nowell et al. (2016)	NCBI
P.s syringae 2339	*Prunus avium* (Sweet cherry)	HUN[8]	LIHU01000032, NZ_LIHU01000030 NZ_LIHU01000033, NZ_LIHU01000021	Nowell et al. (2016)	NCBI
P.s syringae 2340	*Pyrus* (Pear)	HUN	LIHT01000059, NZ_LIHT01000069 NZ_LIHT01000055, NZ_LIHT01000078	Nowell et al. (2016)	NCBI
P.s syringae HRI-W7872	*Prunus domestica* (Plum)	GBR	LIHS01000009, NZ_LIHS01000071 NZ_LIHS01000040, NZ_LIHS01000028	Nowell et al. (2016)	NCBI

Table 2.3. (cont'd)

P.s syringae HRI-W7924	*Prunus cerasus* (Tart cherry)	GBR	LIHR01000002, NZ_LIHR01000107 NZ_LIHR01000053, NZ_LIHR01000025	Nowell et al. (2016)	NCBI
P.s B7	*Prunus dulcis* (Almond)	MNE[9]	MT295211, MT345293 MT265357, MT240941	Popović et al. (2021)	NCBI
P.s BR1	*Prunus persica* (Peach)	MNE	MT295229, MT345311 MT265375, MT250597	Popović et al. (2021)	NCBI
P.s BR2	*Prunus persica* (Peach)	MNE	MT295230, MT345312 MT265376, MT250598	Popović et al. (2021)	NCBI
P.s JS1	*Prunus salicina* (Japanese plum)	MNE	MT295232, MT345314 MT265378, MT250600	Popović et al. (2021)	NCBI
P.s K3	*Prunus armeniaca* (Apricot)	MNE	MT295221, MT345303 MT265367, MT250589	Popović et al. (2021)	NCBI
P.s N1	*Prunus persica* (Nectarine)	MNE	MT295231, MT345313 MT265377, MT250599	Popović et al. (2021)	NCBI
P.s T1	*Prunus avium* (Sweet cherry)	MNE	MT295228, MT345310 MT265374, MT250596	Popović et al. (2021)	NCBI
P. savastanoi glycinea R4	*Glycine max* (Soybean)	USA	AEGH01000053, AEGH01000062 AEGH01000036, AEGH01000001	Qi et al. (2007)	NCBI
P.s persicae NCPPB2254	*Prunus persica* (Peach)	FRA[10]	LAZV01000005, NZ_LAZV01000082 NZ_LAZV01000085, NZ_LAZV01000167	Zhoa et al. (2015)	NCBI

[1]United States of America (USA), [2]Great Britain (GBR), [3]Japan (JPN), [4]Switzerland (CHE), [5]Canada(CAN), [6]Australia (AUS), [7]Serbia (SRB), [8]Hungary (HUN), [9]Montenegro (MNE), [10]France (FRA)

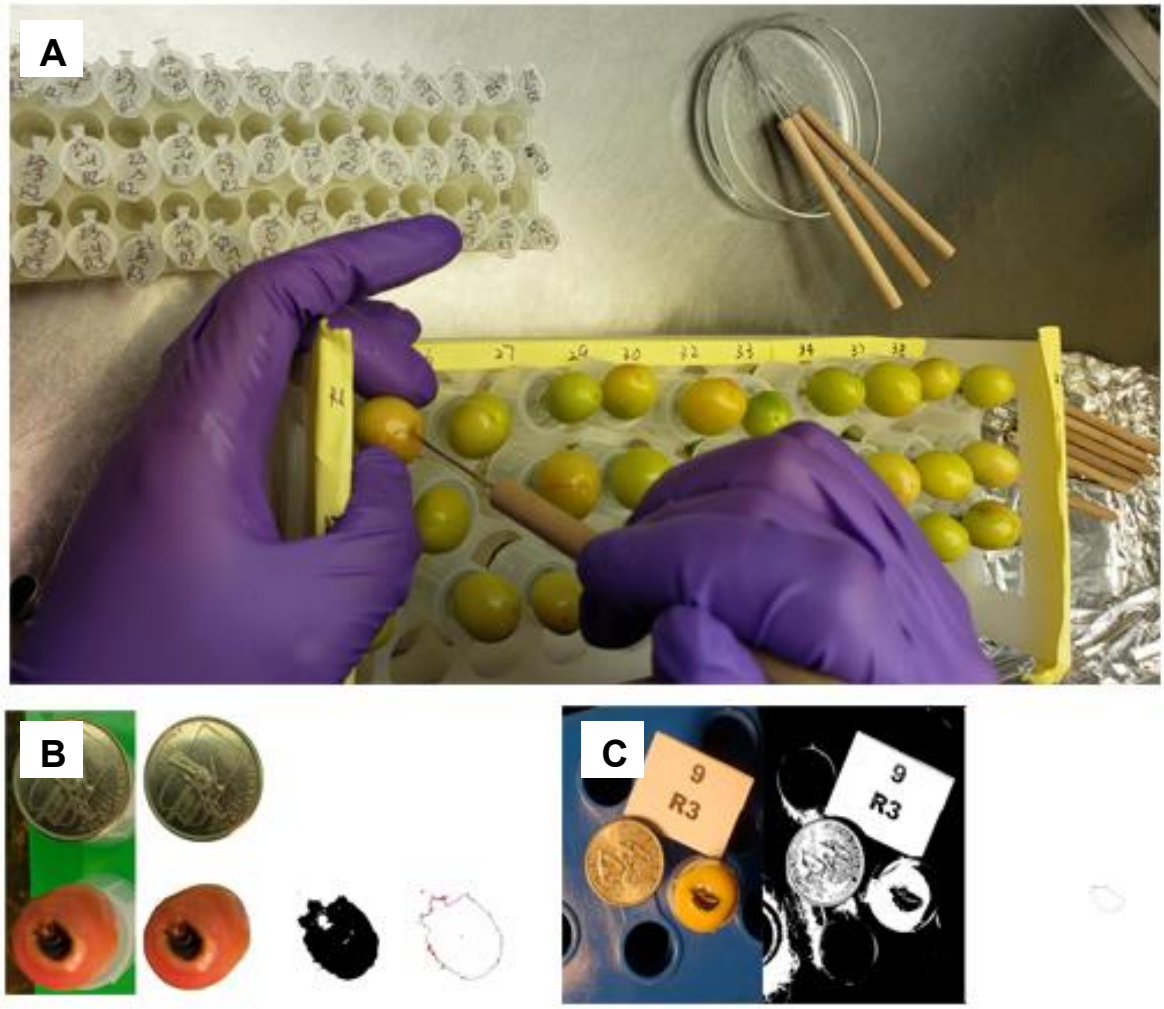


Figure 2.7. Assay to test the virulence of the oxidase^{-}/*syrD*$^{+}$ putative *Pseudomonas syringae* pv. *syringae* (*Pss*) strains on green cherry fruit. **A)** cherries were wounded via stabbing with a sterile dissecting probe before inoculation, **B)** how lesions area was measured in 2019 via ImageJ, and **C)** how lesion area was measured in 2021.

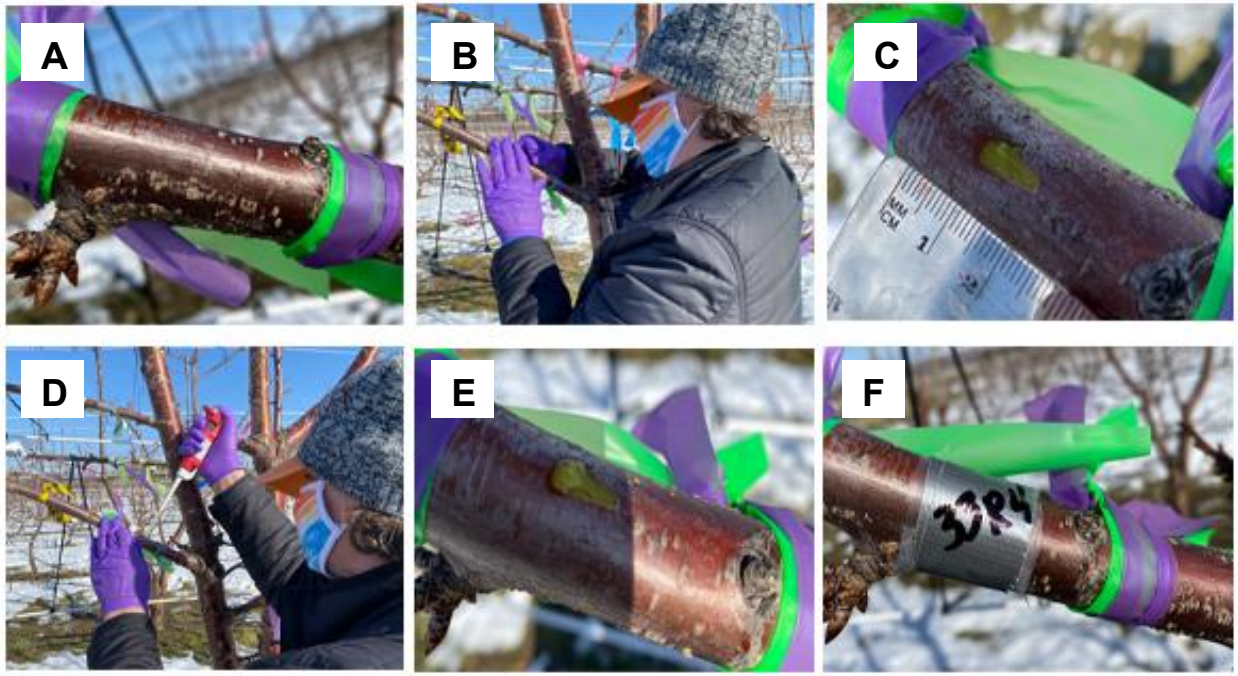


Figure 2.8. The inoculation of sweet cherry wood with oxidase^{-}/*syrD*$^{+}$ putative *Pseudomonas syringae* pv. *syringae* (*Pss*) strains. **A)** wood following sanitizing with a 70% isopropyl alcohol, **B)** wounding with a sterile razor blade, **C)** the wound, **D)** inoculations with 10^{7} cfu/ml of bacteria in 20µl drops, **E)** wound following inoculation, and **F)** the wound covered by parafilm and duct tape with the strain number and rep written on it.

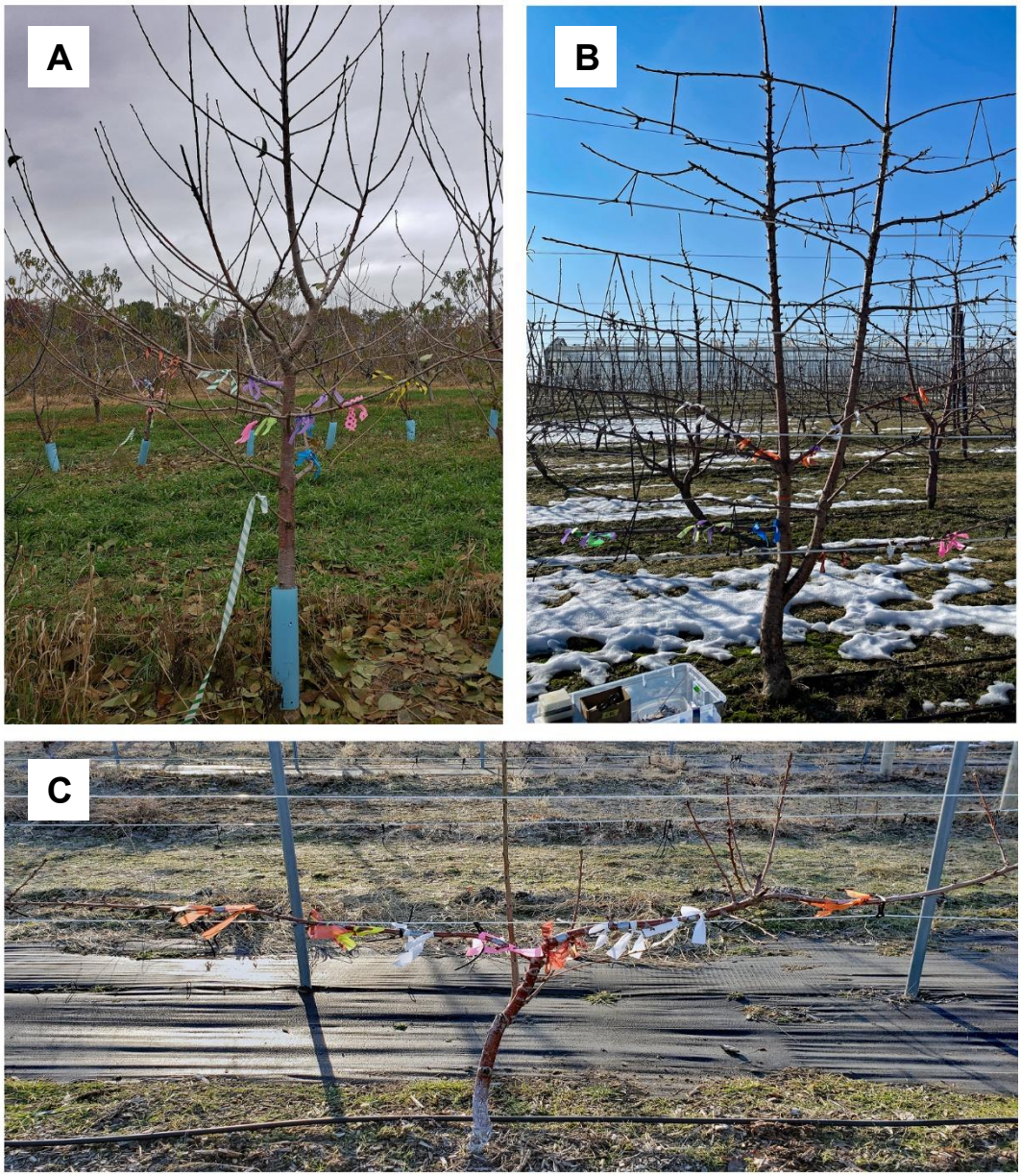


Figure 2.9. Examples of the trees that were used to test for oxidase^{-}/*syrD*$^{+}$ putative *Pseudomonas syringae* pv. *syringae* strain virulence on the sweet cherry cultivars Sweetheart and Coral Champagne. **A)** a TSA tree located at site 1 (Ottawa Co., MI), used for inoculations in 2019, **B)** a Bi-Espalier tree (cv. Sweetheart) located at site 2 (Ionia Co. MI) used for inoculations in 2021, and **C)** a Bi-UFO tree (cv. Coral Champagne) located at site 4 (Berrien Co., MI) in 2021.



Figure 2.10. The lesion rating scale as in Hulin et al. (2018) used to assess oxidase^{-}/*syrD*$^{+}$ putative *Pseudomonas syringae* pv. *syringae* (*Pss*) strain virulence on sweet cherry wood (cv. Sweetheart and Coral Champagne), with 4= black/brown lesion, spread away from the inoculation site, gumming; 3= black/brown lesion, gumming; 2= browning; and 1=no lesion.

Table 2.4. Results of the biochemical tests GATTa (Gelatin liquefaction, Aesculin hydrolysis, Tyrosinase activity, Tartrate utilization) and oxidase enzyme reaction, and the phenotype tests for INA (Ice nucleation activity), fluorescence, copper resistance (Cu R) at 250 µg/ml, and streptomycin resistance (Sm R) at 50 µg/ml. The amplification of the syringomycin-related genes *syrB*/s*yrD*, and phylogroup designation was determined by MLSA for the identification of 20 possible *Pseudomonas syringae* pv. *syringae* (*Pss*) strains (labeled according to isolation collection information: location [site 1, 2, or 3] – sweet cherry cultivar (U=Ulster, V=Van, G=Gold, R=Rainier, Br=Brooks, BP=Black Pearl, BY=Black York) - strain no.). Controls include PBS and the bacteria strains: *P.s morsprunorum* (*Psm 627*), *P. fluorescens* (*P.flu* GSPB 1714), *Erwinia amylovora* (*E.a* Ca11-7 SmR), *Pss* (BC43(390) CuR, 26-3, 19-6, 13-7, 6-9, 847, 6491, 1680, and FF5-1), and *Pantoea agglomerans* (*P.ag* UMAF3067).

Phylogroup	Strain	GATTa	INA	Fluorescence	*syrB*	*syrD*	Oxidase	Cu R	Sm R
2d	1-U-9	+ + − −	+	+	+	+	−	+	−
	2-BP-25	+ + − −	+	+	+	+	−	−	−
	2-BP-26	+ + − −	+	+	+	+	−	−	−
	2-BP-27	+ + − −	+	+	+	+	−	−	−
	3-BY-37	+ + − −	+	+	+	+	−	−	−
	3-BY-38	+ + − −	+	+	+	+	−	−	−
2b	1-Br-22	+ + − −	−	+	+	+	−	−	−
	1-Br-23	+ + − −	−	+	+	+	−	−	−
	2-BP-32	+ + − −	+	+	+	+	−	−	−
	2-BP-33	+ + − −	+	+	+	+	−	−	−
	2-BP-34	+ + − −	+	+	+	+	−	−	−
2c	1-G-16	+ + − −	+	+	−	+	−	−	−
	1-G-17	+ + − −	+	+	−	+	−	−	−
	1-G-18	+ + − −	+/−	+	−	+	−	−	−
	1-V-13	+ + + −	−	+	−	+	−	−	−
	1-V-14	+ + + −	+/−	+	−	+	−	−	−
	1-V-15	+ + + −	+/−	+	−	+	−	−	−
	1-R-21	+ + + −	+	+	−	+	−	−	−
	2-BP-29	+ + + −	−	+	−	+	−	−	−
	2-BP-30	+ + + −	−	+	−	+	−	−	−
ctrl	PBS	NA	−	NA	NA	NA	NA	NA	NA

Table 2.4. (cont'd)

Psm 627	− − + +	−	−	NA	NA	NA	NA	NA
P.flu GSPB 1714	NA	NA	+	NA	NA	NA	NA	NA
E.a Ca11-7 SmR	NA	NA	−	NA	NA	NA	NA	+
Pss BC43(390) CuR	NA	NA	NA	NA	NA	NA	+	NA
Pss 26-3	NA	NA	NA	NA	NA	NA	−	NA
Pss 19-6	NA	NA	NA	NA	+	NA	NA	NA
Pss 13-7	NA	NA	NA	NA	+	NA	NA	NA
Pss 6-9	NA	NA	NA	NA	−	NA	NA	NA
Pss 847	NA	NA	NA	NA	+	NA	NA	NA
Pss 6491	NA	NA	NA	NA	+	NA	NA	NA
Pss 1680	NA	NA	NA	NA	+	NA	NA	NA
Pss FF5-1	NA	NA	NA	NA	+	NA	NA	NA
P.ag UMAF3067	NA	NA	NA	NA	NA	NA	NA	−

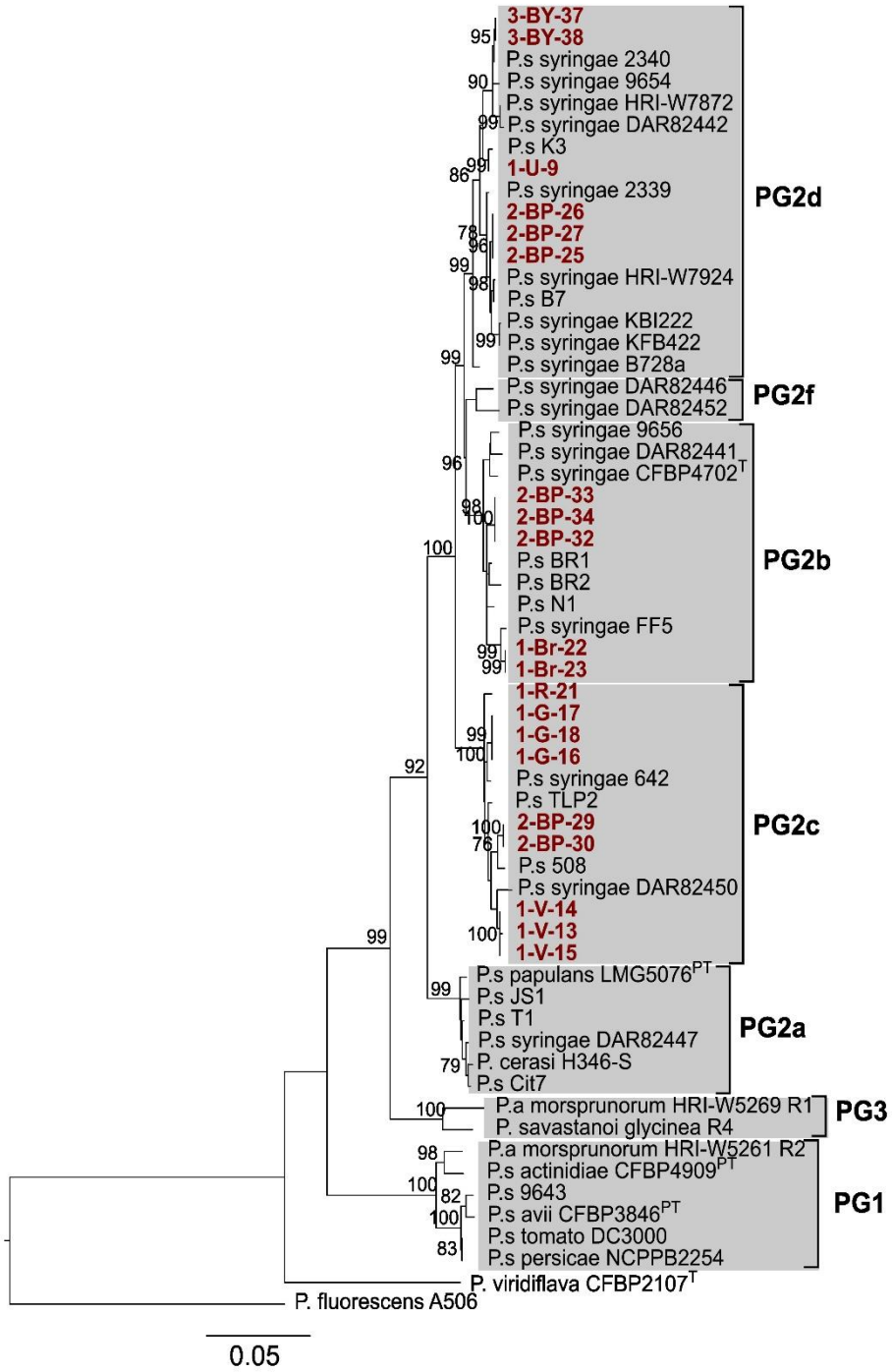


Figure 2.11. A maximum likelihood (ML) phylogenetic tree using the Tamura-Nei model (1000 bootstraps) for MLSA of 4 concatenated housekeeping genes (*gap1*, *gltA*, *gyrB*, and *rpoD*) of 20 possible *Pseudomonas syringae* pv. *syringae* (*Pss*) strains (in red) rooted by *P. fluorescens*, including reference strains from 7 *P.s* phylogroups (PG), PG2 (2a, 2b, 2c, 2d, and 2f), PG1, PG3, and *P. viridiflava*. A distance scale with the number of bp substitutions/site and bootstrap values >75% are shown.

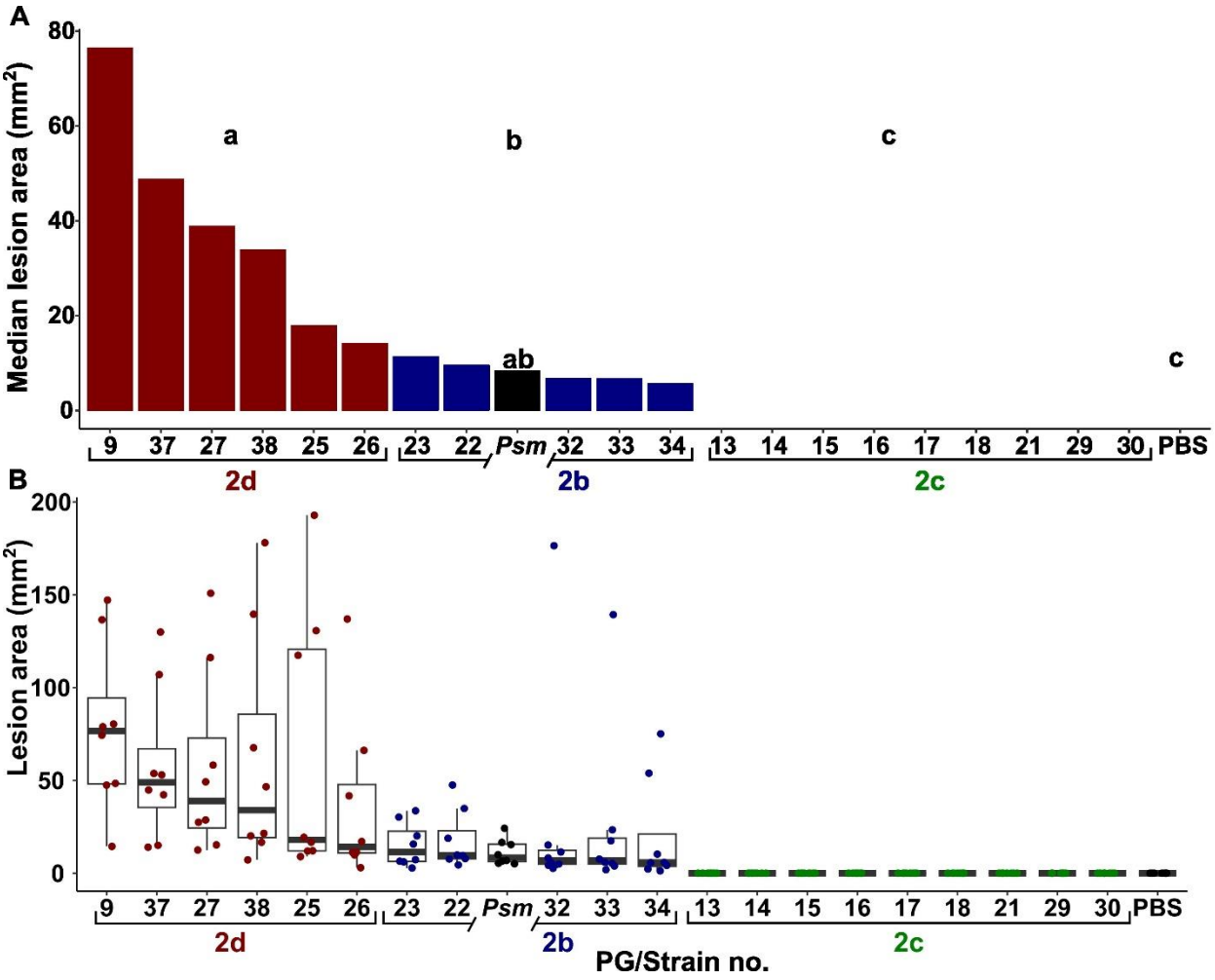


Figure 2.12. Graphs for the green fruit assay for virulence of the 20 *Pseudomonas syringae* strains on immature sweet cherry fruit, including strain *Psm* 627 (*Psm*) and PBS as controls. **A)** Bar graph of the median lesion area (mm^2) for each strain number (Strain no.) within the phylogroup (PG) 2d, 2b, and 2c, letters (a, b, and c) above the bars indicate statistical differences of phylogroup for lesion area or virulence ($p<0.05$) determined by Dunn's all pairs test (Bonferroni adjusted p-values). **B)** Box plot showing the distribution of the lesion areas (mm^2) produced on the individual fruit for each strain (colored points (n=8)) within the 3 phylogroups, and the horizontal black bar within the box signifies the median lesion area (mm^2).

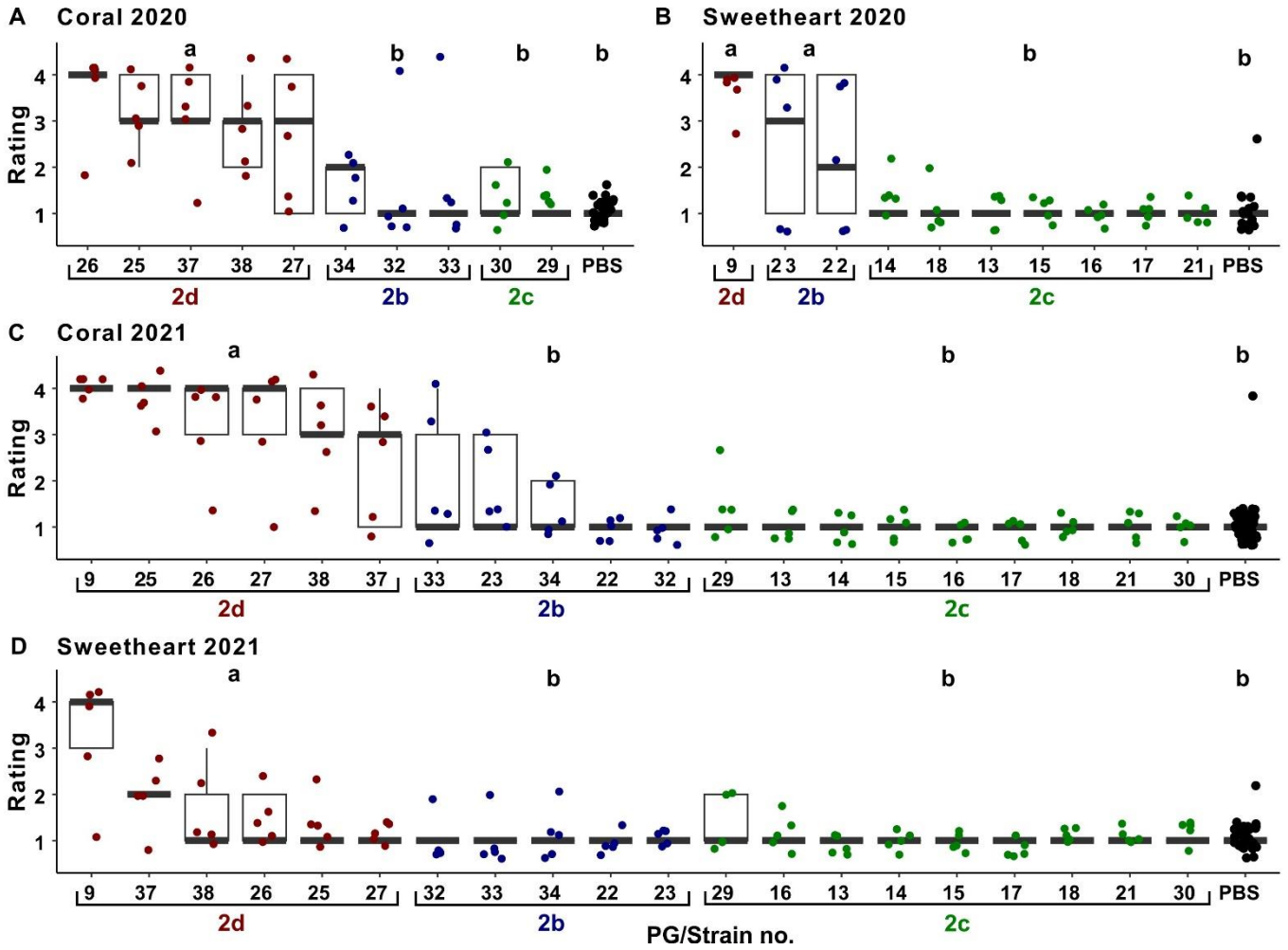


Figure 2.13. Box plots showing the distribution of the virulence rating for *Pseudomonas syringae* strains (strain no.) and the trend of most to least virulent in the phylogroups (PG), 2d, 2b, and 2c, inoculated on sweet cherry wood of the cultivars **A)** Coral Champagne (Coral) in 2020, **B)** Sweetheart in 2020, **C)** Coral in 2021, and **D)** Sweetheart in 2021, with PBS controls. Black horizontal bars are the median rating value for each strain, colored points are the rating value for each rep (n=5). Letters (a, and b) indicate statistical differences of phylogroup for virulence ($p<0.05$) from pairwise comparisons of estimated marginal means (Tukey adjusted p-values).

Table 2.5. Summary statistics from the clm ordinal regression (rating~phylogroup), in which the estimate value indicates an increase (↑, + estimate value) or decrease (↓, − estimate value) in virulence (rating) for phylogroups 2c, 2d, and ctrl (PBS control) in relation to the phylogroup 2b, with standard error (SE), z-value, and the p-value indicating significance when $p<0.05$, for the *Pseudomonas syringae* strains that were rated for virulence on the sweet cherry cultivars Coral Champagne and Sweetheart in 2020 and 2021.

Year	Cultivar	Phylogroup (vs. 2b)	Virulence	Estimate	SE	z-value	p-value
2020	Coral Champagne	2c	↓	-0.35	0.86	-0.41	0.6832
		2d	↑	2.78	0.75	3.70	**0.0002**
		ctrl	↓	-2.39	1.16	-2.06	**0.0396**
	Sweetheart	2c	↓	-3.56	0.99	-3.61	**0.0003**
		2d	↑	2.26	1.29	1.76	0.0787
		ctrl	↓	-3.55	1.22	-2.90	**0.0038**
2021	Coral Champagne	2c	↓	-2.56	1.11	-2.30	**0.0213**
		2d	↑	3.01	0.64	4.67	**3.03e-6**
		ctrl	↓	-2.84	1.11	-2.56	**0.0105**
	Sweetheart	2c	↓	-0.63	0.86	-0.74	0.4612
		2d	↑	1.86	0.72	2.59	**0.0095**
		ctrl	↓	-1.54	1.19	-1.30	0.1946

REFERENCES

Abdellatif, E., Kałużna, M., Ferrante, P., Scortichini, M., Bahri, B., Janse, J.D., van Vaerenberg, J., Baeyen, S., Sobiczewski, P., and Rhouma, A. 2020. Phylogenetic, genetic, and phenotypic diversity of Pseudomonas syringae pv. syringae strains isolated from citrus blast and black pit in Tunisia. Plant Pathol. 69: 1414– 1425.

Alfano, J.R., and Collmer, A. 2004. Type III secretion system effector proteins: double agents in bacterial disease and plant defense. Annu. Rev. Phytopathol. 42: 385-414.

Almeida N.F., Yan S., Cai R., Clarke C.R., Morris C.E., Schaad N.W., Schuenzel E.L., Lacy G.H., Sun X., Jones J.B., Castillo J.A., Bull C.T., Leman S., Guttman D.S., Setubal J.C., and Vinatzer B.A. 2010. PAMDB, a multilocus sequence typing and analysis database and website for plant-associated microbes. Phytopathology 100(3):208-215.

Altschul, S.F., Gish, W., Miller, W., Myers, E.W. and Lipman, D.J. 1990. Basic local alignment search tool. J. Mol. Biol. 215:403-410.

Andri, S. et al. 2017. DescTools: Tools for descriptive statistics. R package version 0.99.23.

Baltrus, D.A., Nishimura, M.T., Romanchuk, A., Chang, J.H., Mukhtar, M.S., Cherkis, K., Roach, J., Grant, S.R., and Jones, C.D. 2011. Dynamic evolution of pathogenicity revealed by sequencing and comparative genomics of 19 Pseudomonas syringae isolates. PLOS Pathogens 7(7): e1002132. https://doi.org/10.1371/journal.ppat.1002132

Baltrus, D.A., and Orth, K.N. 2018. Understanding genomic diversity in Pseudomonas syringae throughout the forest and the trees. New Phytol. 219: 672-696.

Berge, O., Monteil C.L., Bartoli, C., Chandeysson, C., Guilbaud, C., Sands, D.C., and Morris, C.E. 2014. A user's guide to a database of the diversity of pseudomonas syringae and its application to classifying strains in this phylogenetic complex. PLoS ONE 9(9): e105547. doi:10.1371/journal.pone.0105547

Bophela, K.N., Peterson, Y., Bull, C.T., and Coutinho, T.A. 2020. Identification of Pseudomonas isolates associated with bacterial canker of stone fruit trees in the western cape, South Africa. Plant Disease 104: 882-892.

Brown, E. L. 1941. A study of the cherry industry of the Michigan fruit belt. Master's thesis, Wayne State University, ProQuest Dissertations and Theses Global.

Buell, C.R., Joardar, V., Lindeberg, M., Selengut, J., Paulsen, I.T., Gwinn, M.L., Dodson, R.J., Deboy, R.T., Durkin, A.S., Kolonay, J.F., Madupu, R., Daugherty, S., Brinkac, L., Beanan, M.J., Haft, D.H., Nelson, W.C., Davidsen, T., Zafar, N., Zhou, L., Liu, J., Yuan, Q., Khouri, H., Fedorova, N., Tran, B., Russell, D., Berry, K., Utterback, T., Van Aken, S.E., Feldblyum, T.V., D'Ascenzo, M., Deng, W.L., Ramos, A.R., Alfano, J.R., Cartinhour, S., Chatterjee, A.K., Delaney, T.P., Lazarowitz, S.G., Martin, G.B., Schneider, D.J., Tang, X., Bender, C.L., White,

O., Fraser, C.M., and Collmer, A. 2003. The complete genome sequence of the Arabidopsis and tomato pathogen Pseudomonas syringae pv. tomato DC3000. Proc. Natl. Acad. Sci. U. S. A. 100(18):10181-10186. doi:10.1073/pnas.1731982100.

Bultreys, A., and Gheysen, I. 1999. Biological and molecular detection of toxic lipodepsipeptide-producing Pseudomonas syringae strains and PCR identification in plants. Appl. Environ. Microbiol. 65(5):1904-9.

Bultreys, A, and Kaluzna, M. 2010. Bacterial cankers caused by Pseudomonas syringae on stone fruit species with special emphasis on the pathovars syringae and morsprunorum race 1 and race 2. J. Plant Pathol. 92: S21–S33.

Christensen, R.H.B. n.d. Cumulative link models for ordinal regression with the R package ordinal. cran.r-project.org/web/packages/ordinal/vignettes/clm_article.pdf.

Christensen, R.H.B. n.d. 2022. ordinal-Regression models for ordinal data. R package version 2022.11-16. https://CRAN.R-project.org/package=ordinal.

Clark K., Karsch-Mizrachi, I., Lipman, D.J., Ostell J., and Sayers, E.W. 2016. GenBank. Nucleic Acids Res. 44(D1):D67-D72.

Clarke, C.R., Cai, R., Studholme, D.J., Guttman, D.S., and Vinatzer, B.A. 2010. Pseudomonas syringae strains naturally lacking the classical p. syringae hrp/hrc locus are common leaf colonizers equipped with an atypical type III secretion system. Molecular Plant-Microbe Interactions® 23(2): 198-210.

Cunty, A., Poliakoff, F., Rivoal, C., Cesbron, S., Fischer-Le Saux, M., Lemaire, C., Jacques, M.A., Manceau, C. and Vanneste, J.L. 2015. Characterization of Pseudomonas syringae pv. actinidiae (Psa) isolated from France and assignment of Psa biovar 4 to a de novo pathovar: Pseudomonas syringae pv. actinidifoliorum pv. nov. Plant Pathol. 64: 582-596.

Edgar, R.C. 2004. MUSCLE: multiple sequence alignment with high accuracy and high throughput. Nucleic Acids Res. 32(5):1792-1797.

Ellouze, W., Nesbitt, D., Parcey, M., Gayder, S., Marchand, G., Svircev, A.M., Tambong, J.T. 2020. Draft genome sequences of hazelnut-associated Pseudomonas strains isolated in Ontario, Canada. Microbiol. Resour. Announc. 9(45):e01021-20. doi: 10.1128/MRA.01021-20.

Feil, H., Feil, W.S., Chain, P., Larimer, F., DiBartolo, G., Copeland, A., Lykidis, A., Trong, S., Nolan, M., Goltsman, E., Thiel, J., Malfatti, S., Loper, J.E., Lapidus, A., Detter, J.C., Land, M., Richardson, P.M., Kyrpides, N.C., Ivanova, N., Lindow, S.E. 2005. Comparison of the complete genome sequences of Pseudomonas syringae pv. syringae B728a and pv. tomato DC3000. Proc. Natl. Acad. Sci. U.S.A. 102(31):11064-11069. doi: 10.1073/pnas.0504930102.

Gardan, L., Shafik, H., Belouin, S., Broch, R., Grimont, F., and Grimont, P.A.D. 1999. DNA relatedness among the pathovars of Pseudomonas syringae and description of Pseudomonas

tremae sp. nov. and Pseudomonas cannabina sp. nov. (ex Sutic and Dowson 1959). Int. J. Sys. Bact. 49: 469-478.

Gomila, M., Busquets, A., Mulet, M., García-Valdés, E., and Lalucat, J. 2017. Clarification of taxonomic status within the Pseudomonas syringae species group based on a phylogenomic analysis. Frontiers Microbiol. 8: 2422.

Graves, S., Piepho, H., Selzer, L., and Dorai-Raj, S. 2019. multcompView: Visualizations of paired comparisons. R package version 0.1-8. https://CRAN.R-project.org/package=multcomView.

Gross, D. C., Cody, Y. S., Proebsting, E. L., Radamaker, G. K., and Spotts, R. A. 1983. Distribution, population dynamics, and characteristics of ice nucleation-active bacteria in deciduous fruit tree orchards. Appl. Env. Microbiol. 46(6): 1370–1379.

Gutiérrez-Barranquero J. A., Cazorla, F. M., de Vicente, A. 2019. Pseudomonas syringae pv. syringae associated with mango trees, a particular pathogen within the "hodgepodge" of the Pseudomonas syringae complex. Frontiers Plant Sci. 10: 570.

Hall, B.G. 2018. Chapter 9: Maximum likelihood, in phylogenetic trees made easy: A how-to manual (5th ed., pp. 141-149). Oxford University Press.

Hall, S.J., Dry, I.B., Gopurenko, D. and Whitelaw-Weckert, M.A. 2019. Pseudomonas syringae pv. syringae from cool climate Australian grapevine vineyards: new phylogroup PG02f associated with bacterial inflorescence rot. Plant Pathol. 68: 312-322.

Hirano, S.S., and Upper, C.D. 1990. Population biology and epidemiology of Pseudomonas syringae. Annu. Rev. Phytopathol. 28:155-177.

Hirano, S.S., and Upper, C.D. 2000. Bacteria in the leaf ecosystem with emphasis on Pseudomonas syringae – a pathogen, ice nucleus, and epiphyte. Microbiol. Mol. Biol. Rev. 64(3): 624-653.

Holding, A.J., and Collee, J.G. 1971. Chapter 1: Routine biochemical tests, In J.R. Norris and D.W. Ribbons (eds.), Methods in Microbiology, 6:1-32. Academic Press.

Hulin, M.T., Mansfield, J.W., Brain, P., Xu, X., Jackson, R.W., and Harrison, R.J. 2018a. Characterization of the pathogenicity of strains of Pseudomonas syringae towards cherry and plum. Plant Pathol. 67: 1177-1193.

Hulin, M.T., Armitage, A.D., Vicente, J.G., Holub, E.B., Baxter, L., Bates, H.J., Mansfield, J.W., Jackson, R.W. and Harrison, R.J. 2018b. Comparative genomics of Pseudomonas syringae reveals convergent gene gain and loss associated with specialization onto cherry (Prunus avium). New Phytol. 219: 672-696.

Hulin, M.T., Jackson, R.W., Harrison, R.J., and Mansfield, J.W. 2020. Cherry picking by pseudomonads: After a century of research on canker, genomics provides insights into the evolution of pathogenicity towards stone fruits. Plant Pathol. 69: 962– 978.

Hulin M.T., Vadillo Dieguez A., Cossu F., Lynn S., Russell K., Neale H.C., Jackson R.W., Arnold D.L., Mansfield J.W., and Harrison R.J. 2022. Identifying resistance in wild and ornamental cherry towards bacterial canker caused by Pseudomonas syringae. Plant Pathol. 71(4):949-965.

Hwang, M.S., Morgan, R.L., Sarkar, S.F., Wang, P.W., and Guttman, D.S. 2005. Phylogenetic characterization of virulence and resistance phenotypes of Pseudomonas syringae. Appl Environ Microbiol. 71(9):5182-91.

Iličić, R., Jelušić, A., Marković, S., Barać, G., Bagi, F., and Popović, T. 2021. Pseudomonas cerasi, the new wild cherry pathogen in Serbia and the potential use of recG helicase in bacterial identification. Ann. Appl. Biol. 180: 140-150.

Ivanović, M., Prokić, A., Gašić, K., Menković, J., Kuzmanovic, N., Zlatkovic, N., and Obradović, A. 2022. Characterization of Pseudomonas syringae strains associated with shoot blight of raspberry and blackberry in Serbia. Plant Dis. 10.1094/PDIS-06-22-1425-RE. Advance online publication. https://doi.org/10.1094/PDIS-06-22-1425-RE

Janse, J.D. 2010. Diagnostic methods for phytopathogenic bacteria of stone fruits and nuts in COST 873. EPPO Bulletin, 40: 68-85.

Jones, A.L. 1971. Bacterial canker of sweet cherry in Michigan. Plant Disease Reporter 55(11): 961-965.

Jones, A.L., Norelli, J.L., and Ehret, G.R. 1991. Detection of streptomycin-resistant Pseudomonas syringae pv. papulans in Michigan apple orchards. Plant Dis. 75: 529-531.

Jones, A.L., and Sutton, T.A. 1996. Diseases of tree fruits in the east. Michigan State University Extension NCR 45 p. 71-72.

Kassambara, A. 2022. ggpubr: 'ggplot2' based publication ready plots. R package version 0.5.0. https://CRAN.R-project.org/package=ggpubr.

Kennelly, M.M., Carzola, F.M., de Vicente, A., Ramos, C., and Sundin, G.W. 2007. Pseudomonas syringae diseases of fruit trees: progress to understanding and control. Plant Disease 91(1): 4-17.

Kovacs, N. 1956. Identification of Pseudomonas pyocyanea by the oxidase reaction. Nature 178: 703.

Lamichhane, J.R., Osdaghi, E., Behlau, F., Köhl, J., Jones, J.B., and Aubertot, J. 2018 . Thirteen decades of antimicrobial copper compounds applied in agriculture. A review. Agron. Sustain. Dev. 38: 28

Lang, G.A., Sage, L., and Wilkinson, T. 2016. Ten years of studies on systems to modify sweet cherry production environments: retractable roofs, high tunnels, and rain shelters. Acta Hort. 1130: 83-89.

Lang, G.A. 2019. The cherry industries in the USA: current trends and future perspectives. Acta Hort. 1235: 119-132.

Lang, G.A., Wilkinson, T., and Larson, J.E. 2019. Insights for orchard design and management using intensive sweet cherry canopy architectures on dwarfing to semi-vigorous rootstocks. Acta Hort. 1235: 161-167.

Lang, G.A., Blatt, S., Neilsen, D., Robinson, T.L., and Xu, H. 2022. Ten-year conclusions from the NC-140 sweet cherry canopy architecture-rootstock trials in North America. Acta Hort. 1346: 661-668.

Latorre, B.A., and Jones, A.L. 1979a. Evaluation of weeds and plant refuse as potential sources of inoculum of *Pseudomonas syringae* in bacterial canker of cherry. Phytopathology 69: 1122-1125.

Latorre, B.A., and Jones, A.L. 1979b. Pseudomonas morsprunorum, the cause of bacterial canker of sour cherry in Michigan, and its epiphytic association with P. syringae. Phytopathology 69:335-339.

Lauwers, E. 2022. investigation of bacteriophage as a biological control for bacterial canker of sweet cherry. Master's thesis, Michigan State University, ProQuest Dissertations and Theses Global.

Lelliot, R.A., Billing, E., and Hayward, A.C. 1966. A determinative scheme for the fluorescent plant pathogenic Pseudomonads. J. Appl. Bact. 29(3):470-489.

Lenth, R. 2023. emmeans: Estimated marginal means, aka least-squared means. R package version 1.8.4-1. https://CRAN.R-project.org/package=emmeans.

Lillrose, T., Lang, G.A. and Sundin, G.W. (2017). Strategies to minimize bacterial canker in high density sweet cherry orchards. Acta Hortic. 1161, 457-162

Lindow, S.E., Arny, D.C., Upper, C.D. 1982a. Bacterial ice nucleation: a factor in frost injury to plants. Plant Physiol. 70(4):1084-1089.

Lindow, S.E., Hirano, S.S., Barchet, W.R., Arny, D.C, and Upper, C.D. 1982b. Relationship between ice nucleation frequency of bacteria and frost injury. Plant Physiol. 70(4): 1090-1093.

Lipps SM, Samac DA. 2022. Pseudomonas viridiflava: An internal outsider of the Pseudomonas syringae species complex. Mol Plant Pathol. 23(1): 3-15.

Loper, J.E., Hassan, K.A., Mavrodi, D.V. , Davis, E. W.II , Lim, C.K. , Shaffer, B.T., Elbourne, L.D.H. , Stockwell, V.O. , Hartney, S. L. , Breakwell, K., Henkels, M. D. , Tetu, S. G. , Rangel, L. I. , Kidarsa, T. A. , Wilson, N. L. , van de Mortel, J. E. , Song, C. , Blumhagen, R. , Radune, D. , Hostetler, J. B. , Brinkac, L.M. , Durkin, A. S. , Kluepfel, D. A. , Wechter, W. P. , Anderson, A. J. , Kim, Y.C., Pierson, L. S. III , Pierson, E.A. , Lindow, S. E. , Kobayashi, D. Y., Raaijmakers, J. M. , Weller, D. M. , Thomashow, L. S. , Allen, A. E. , and Paulsen, I. T. 2012. Comparative genomics of plant-associated Pseudomonas spp.: Insights into diversity and inheritance of traits involved in multitrophic interactions. PLoS Genet. 8(7): e1002784. doi:10.1371/journal.pgen.1002784

Lukas, M., Schwidetzky, R., Eufemio, R. J., Bonn, M., and Meister, K. 2022. Toward Understanding Bacterial Ice Nucleation. Journal of Physical Chemistry B. 126:1861–1867.

Mangiafico, S.S. 2016. Summary and analysis of extension program evaluation in R, version 1.20.01. rcompanion.org/handbook/.

Mangiafico, S. 2023. rcompanion: Functions to support extension education program evaluation. R package version 2,4,21. https://CRAN.R-project.org/package=rcompanion.

McGhee, G. C., Guasco, J., Bellomo, L. M., Blumer-Schuette, S. E., Shane, W. W., Irish-Brown, A., and Sundin, G. W. 2011. Genetic analysis of streptomycin-resistant (SmR) strains of Erwinia amylovora suggests that dissemination of two genotypes is responsible for the current distribution of SmRE. amylovora in Michigan. Phytopathology 101:182-191.

McGhee, G.C., Sundin, G.W. 2011. Evaluation of kasugamycin for fire blight management, effect on nontarget bacteria, and assessment of kasugamycin resistance potential in Erwinia amylovora. Phytopathology. 101(2): 192-204.

MDARD 2018. Michigan agricultural facts and figures. Retrieved from https://www.michigan.gov/-/media/Project/Websites/mdard/documents/business-development/mi_ag_facts_figures.pdf?rev=9ca97e867d0d40b392470b02a2694e50

MDARD 2023. Michigan agricultural resources: Facts about Michigan agriculture. Retrieved from https://www.michigan.gov/mdard/about/mi-agriculture/michigan-agriculture-resources

Morris, C.E., Lamichhane, J.R., Nikolić, I., Stanković, S., and Moury, B. 2019.The overlapping continuum of host range among strains in the *Pseudomonas syringae* complex. Phytopathol. Res. 1:4 (2019). https://doi.org/10.1186/s42483-018-0010-6

Morris, C.E., Monteil, C.L., and Berge, O. 2013. The life history of *Pseudomonas syringae*: linking agriculture to earth system processes. Annu. Rev. Phytopathol. 51: 85-104.

Morris, C., Sands, D., Vinatzer, B., Glaux, C., Guilbaud, C., Buffière, A., Yan, S., Dominguez, H., and Thompson, B.M. 2008. The life history of the plant pathogen *Pseudomonas syringae* is linked to the water cycle. ISME J. 2: 321–334.

Mohr, T. J., Liu, H., Yan, S., Morris, C. E., Castillo, J. A., Jelenska, J., and Vinatzer, B. A. 2008. Naturally occurring nonpathogenic isolates of the plant pathogen Pseudomonas syringae lack a type III secretion system and effector gene orthologues. J. Bacteriol. 190:2858-2870.

Nowell, R.W., Laue, B.E., Sharp, P.M. and Green, S. 2016. Comparative genomics reveals genes significantly associated with woody hosts in the plant pathogen Pseudomonas syringae. Molec. Plant Pathol. 17: 1409-1424.

Oksel, C., Avin, F.A., Mirik, M., and Baysal-Gurel, F. 2022. Identification and genetic characterization of Pseudomonas syringae pv. syringae from sweet cherry in Turkey. Plant Disease 106: 1253-1261.

Petriccione, M., Zampella, L., Mastrobuoni, F., and Scortichini, M. 2017. Occurrence of copper-resistant Pseudomonas syringae pv. syringae strains isolated from rain and kiwifruit orchards also infected by P. s. pv. actinidiae. Eur. J. Plant Pathol. 149: 953–968

Pohlert, T. 2022. PMCMRplus: Calculate pairwise multiple comparisons of mean rank extended. R package version 1.9.6. https://CRAN.R-project.org/package=PMCMRplus.

Popović, T., Menković, J., Prokić, A., Zlatković, N., and Obradović, A. 2021. Isolation and characterization of Pseudomonas syringae isolates affecting stone fruits and almond in Montenegro. J. Plant Dis. Prot. 128: 391–405.

Puławska, J., Gétaz, M., Kałużna, M., Kuzmanovic, N., Obradovic, A., Pothier, J., Ruinelli, M., Boscia, D., Saponari, M., Végh, A., and Palkovics, L. 2017. Bacterial diseases. In Quero-Garcia, J., Iezzoni, A., Pulawska, J., and Lang, G. (Eds.), Cherries: botany, production, and uses (pp. 365-385). CAB International.

Qi, M., Wang, D., Bradley, C.A., and Zhao, Y. 2011. Genome sequence analyses of Pseudomonas savastanoi pv. glycinea and subtractive hybridization-based comparative genomics with nine pseudomonads. PLoS One 6(1):e16451. doi: 10.1371/journal.pone.0016451.

Quigley, N. B., and Gross, D. C. 1994. Syringomycin production among strains of Pseudomonas syringae pv. syringae: conservation of the syrB and syrD genes and activation of phytotoxin production by plant signal molecules. *Molecular plant-microbe interactions : MPMI 7*(1):78–90.

Rabiey, M., Roy, S.R., Holtappels, D., Franceschetti, L., Quilty, B.J., Creeth, R., Sundin, G.W., Wagemans, J., Lavigne, R., and Jackson, R.W. 2020. Phage biocontrol to combat Pseudomonas syringae pathogens causing disease in cherry. Microb. Biotech. 13(5):1428-1445.

R Core Team. 2022. R: A language and environment for statistical computing. R Foundation for Statistical Computing, Vienna, Austria. URL https://www.R-project.org/.

Renick, L.J., Cogal, A.G., and Sundin, G.W. 2008. Phenotypic and genetic analysis of epiphytic *Pseudomonas syringae* populations from sweet cherry in Michigan. Plant Disease 92(3):372-378.

Ruinelli, M., Blom, J., Smits, T.H.M., and Pothier, J.F. 2019. Comparative genomics and pathogenicity potential of members of the Pseudomonas syringae species complex on Prunus spp. BMC Genomics 20: 172

Ruinelli, M., Blom, J., Smits, T.H.M., Pothier, J.F. 2022. Comparative genomics of *Prunus*-associated members of the *Pseudomonas syringae* species complex reveals traits supporting co-evolution and host adaptation. Front Microbiol. 13: 804681.

Ruiz-Bedoya, T., Wang, P. W., Desveaux, D., and Guttman, D. S. (2023). Cooperative virulence via the collective action of secreted pathogen effectors. *Nature microbiology*, 10.1038/s41564-023-01328-8. Advance online publication. https://doi.org/10.1038/s41564-023-01328-8

Sakar, S.F., and Guttman, D.S. 2004. Evolution of the core genome of Pseudomonas syringae, a highly clonal, endemic plant pathogen. Amer. Soc. Microbiol. 70(4): 1999-2012.

Salazar-Gutiérrez, M.R., Chaves, B., Anothai, J., Whiting, M., and Hoogenboom, G. 2014. Variation in cold hardiness of sweet cherry flower buds through different phenological stages. Scientia Horticulturae 172: 161-167.

Schneider, C., Rasband, W. and Eliceiri, K. 2012. NIH Image to ImageJ: 25 years of image analysis. Nat. Methods 9: 671–675. https://doi.org/10.1038/nmeth.2089

Scortichini, M., Marchesi, U., Dettori, M. . and Rossi, M. . (2003), Genetic diversity, presence of the syrB gene, host preference and virulence of Pseudomonas syringae pv. syringae strains from woody and herbaceous host plants. Plant Pathology, 52: 277-286.

Sheilds, P., and Cathcart, L. 2010. Oxidase test protocol. American Society for Microbiology. https://www.asmscience.org/content/education/protocol/protocol.3229

Slack S.M., Walters K.J., Outwater C.A., and Sundin G.W. 2021. Effect of kasugamycin, oxytetracycline, and streptomycin on in-orchard population dynamics of *Erwinia amylovora* on apple flower stigmas. Plant Dis. 105(6):1843-1850.

Sneath, P.H.A. 1956. Cultural and biochemical characteristics of the genus Chromobacterium. J. Gen. Microbiol. 15:70-98.

Sorensen, K.N., Kim, K.H., and Takemoto, J.Y. 1998. PCR detection of cyclic lipodepsinonapeptide-producing Pseudomonas syringae pv. syringae and similarity of strains. Appl. Environ. Microbiol. 64(1):226-230.

Spotts, R.A., Wallis, K.M., Serdani, M., and Azarenko, A.N. 2010. Bacterial canker of sweet cherry in Oregon – infection of horticultural and natural woods, and resistance of cultivar and rootstock combinations. Plant Disease 94: 345-350.

Sundin, G.W., and Bender, C.L. 1993. Ecological and genetic analysis of copper and streptomycin resistance in Pseudomonas syringae pv. syringae. Appl. Environ. Microbiol. 59(4): 1018-1024.

Sundin, G. W., and Bender, C. L. 1996. Molecular analysis of closely related copper- and streptomycin-resistance plasmids in Pseudomonas syringae pv. syringae. Plasmid *35*(2): 98–107.

Sundin, G.W., Jones, A.L., and Olson, B.D. 1988. Overwintering and population dynamics of Pseudomonas syringae pv. syringae and P.s. pv. morsprunorum on sweet and sour cherry trees. Can. J. Plant Pathol. 10: 281-288.

Sundin, G.W., Jones, A.L., and Fulbright, D.W. 1989. Copper resistance in *Pseudomonas syringae* pv. *syringae* from cherry orchards and its associated transfer in vitro and in planta with a plasmid. Phytopathology 79: 861-865.

Sundin, G.W., and Wang, N. 2018. Antibiotic resistance in plant-pathogenic bacteria. Ann. Rev. Phytopathol. 56: 161-180.

Sundin, G.W., Werner, N.A., Yoder, K.S., and Aldwinkle, H.S. 2009. Field evaluations of biological control of fire blight in the eastern united states. Plant Disease 93: 386-394.

Sundin, G., and Rothwell, N. (2012). Managing bacterial canker in sweet cherries: What are the options? Retrieved from https://www.canr.msu.edu/news/managing_bacterial_canker_in_sweet_cherries_what_are_the_options

Tamura, K. and Nei, M. 1993. Estimation of the number of nucleotide substitutions in the control region of mitochondrial DNA in humans and chimpanzees. Molec. Biol. Evol. 10:512-526.

Tamura K., Stecher G., and Kumar S. 2021. MEGA 11: Molecular Evolutionary Genetics Analysis Version 11. Molec. Biol. Evol. 38(7):3022-3027.

USDA-Nass 2021. Michigan agricultural overview. Retrieved from https://www.nass.usda.gov/Quick_Stats/Ag_Overview/stateOverview.php?state=MICHIGAN

USDA-Nass 2019. 2017 Census of agriculture: Michigan state and county data. Retrieved from https://www.nass.usda.gov/Publications/AgCensus/2017/Full_Report/Volume_1,_Chapter_1_State_Level/Michigan/miv1.pdf

Vasebi, Y., Khakvar, R., Tian, L., Moubarak, P., Valentini, F., Weisberg, A.J., and Vinatzer, B.A. 2020. Phenotypic characterization and phylogenetic analysis of Pseudomonas syringae strains associated with canker disease on apricot in Iran within the context of the global genetic diversity of the P. syringae complex. Eur. J. Plant Pathol. 158:545-560.

Venables, W.N., and Ripley, B.D. 2002. Modern applied statistics with S. 4th edition, Springer, New York. ISBN 0-387-95457-0.

Visnovsky, S.B., Marroni, M.V., Pushparajah, S., Everett, K.R., Taylor, R.K., Vintazer, B.A., and Pitman, A.R. 2019. Using multilocus sequence analysis to distinguish pathogenic from saprotrophic strains of Pseudomonas from stone fruit and kiwifruit. Eur. J. Plant Pathol. 155: 643-658.

Warren, R.J., and Vermette, S. 2022. Laurentian Great Lakes warming threatens northern fruit belt refugia. Int. J. Biometeorol. 66: 669–677.

Wickham, H. 2016. ggplot2: Elegant graphics for data analysis. Springer-Verlag, New York.

Xin, X-F., Kvitko, B., and He, S.Y. 2018. Pseudomonas syringae: what it takes to be a pathogen. Nat. Rev. Microbiol. 16: 316–328.

Zhao, W., Jiang, H., Tian, Q., and Hu, J. 2015. Draft genome sequence of Pseudomonas syringae pv. persicae NCPPB 2254. Genome Announc. 3(3):e00555-15. doi: 10.1128/genomeA.00555-15.

CHAPTER 3

EXPLORATION OF THE SWEET CHERRY LEAF MICROBIOME REVEALS DOMINATION BY *PSEUDOMONAS* AND SEASONAL COMMUNITY DIRECTIONALITY

3.1: Abstract

The pathogen *Pseudomonas syringae* pv. *syringae* (*Pss*), causal agent of a major cherry disease, bacterial canker, is a well-known and much-studied epiphyte. Little is known, however, about the other bacteria that also are present in the leaf microbiome. Knowledge of these other bacteria potentially could lend some insight into how to manage *Pss* populations in the future. The sweet cherry leaf microbiome was surveyed in two regions of Michigan (Ottawa Co. and Ingham Co.) from three cultivars of sweet cherry ('Benton', 'Gold', and 'Sweetheart') over three seasons (Fall 2017 to Fall 2019). The microbiome was dominated by the Phylum Proteobacteria (67% − 100% relative abundance) and the genera *Pseudomonas* (26% − 96% relative abundance). The core microbiome was composed of *Pseudomonas* (OTUs 00001, 00002, 00003, 0001, and 0002) and *Sphingomonas* (OTUs 00004, 0003, and 0007). Season and *Pseudomonas* are the most important drivers of the Michigan sweet cherry leaf microbiome in Michigan, where springs were quite variable, and summer and fall had the most stable communities. Bacterial populations are lowest in the spring and increase during the summer and fall. There were no regional or cultivar differences in the bacterial communities of this study's leaf microbiome. Many of the top bacteria taxa have the potential to be growth-promoting bacteria, and *Sphingomonas* was the second most consistently present taxa in all seasons. This study can serve as the foundation for expanding research of the sweet cherry leaf microbiome with respect to the relationship between *Pss* and its microbiome denizens.

3.2: Introduction

Sweet cherry (*Prunus avium* L.) leaves are well-studied organs imperative for gas exchange/photosynthesis and transpiration, essential for fruit tree growth and development, but they also harbor previously underappreciated microbial communities that are fundamental components of tree health or disease (Bashir et al., 2022; Glick and Gamalero, 2021; Leveau, 2019; Lindow and Brandl, 2003; Mina et al., 2019; Pattnaik et al., 2021; Vorholt, 2012). In Michigan, the primary microbial focus in sweet cherry orchards has been on individual disease-causing organisms like the bacterial canker causal agent *Pseudomonas syringae* pv. *syringae* (*Pss*) (Kennelly et al., 2008; Jones, 1971; Jones and Sutton, 1996; Latorre and Jones, 1979b; Sundin et al., 1988).

Pss is a well-known entity within the plant phyllosphere (aerial portions of the plant), a well-adapted epiphyte on leaf surfaces, and can live as non-pathogens at low population levels (Hirano and Upper, 1990; Hirano and Upper, 2000; Jones and Sutton, 1996; Kennelly et al., 2008; Latorre and Jones, 1979b; Lindow and Brandl, 2003; Sundin et al., 1988; Vorholt, 2012). *Pss* is ubiquitous in Michigan cherry orchards, isolated from weeds, grasses, plant detritus, cherry leaves, flowers, buds, and bark, and is linked to the water cycle, rain splash dispersed, and genetically adapted to *Prunus* spp. (Hirano and Upper, 1990; Hirano and Upper, 2000; Hulin et al., 2018; Hulin et al., 2020; Kennelly et al., 2008; Latorre and Jones, 1979a; Lattore and Jones, 1979b; Nowell et al., 2016; Sundin et al., 1988; Morris et al., 2008; Morris et al., 2013; Ruinelli et al., 2022). Morris et al. (2019) found that *Pseudomonas syringae* (*P.s.*), in general, have broad and overlapping host ranges and that phylogroup 2 (PG2), the clade to which *Pss* belongs, has a greater host range compared to other *P.s.* This is not surprising, considering that *Pss* is a known pathogen in over 180 plant species and can infect through wounds (e.g., pruning, trellis rubs) and

natural openings (e.g., stomata and leaf scars) (Jones and Sutton, 1996; Kennelly et al., 2008; Lillrose et al., 2017). Michigan cherry growers must consider the potential economic benefits of high-density orchard systems and the potential risks of infection by the opportunistic *Pss* pathogen.

In the late 1990s, as sweet cherry growers began the initial move toward converting acreage to dwarfing rootstocks and high-density plantings, a conundrum arose in which fruit size and quality, critical market parameters, appeared to be limited in parallel with tree vigor, prompting extensive investigations into source/sink dynamics (Ayala and Lang 2017). These studies not only elucidated the movement of carbon through the tree from shoots, flowers, and fruits throughout the growing season (bud break to dormancy) but also highlighted the importance of the leaf area to fruit ratio (LA:F) for optimizing marketable fruit production (Ayala and Lang, 2017; Whiting and Lang, 2004). This entails achieving a favorable balance between the amount of leaf area that provides photosynthetic assimilates (carbon) and the number of fruit (crop load) that utilizes those assimilates during development, and optimization is influenced by the combination of scion, rootstock, and environment (Ayala and Lang, 2017; Whiting and Lang, 2004). Precision in training and pruning promotes the balance through the manipulation of leaf area (removal or promotion of growth), the thinning of fruiting sites (reduced flowers per spur), and increasing light distribution to leaves and fruit within the canopy architecture (Ayala and Lang, 2017).

Pruning, however, comes with a cost as dormant, early spring, and late spring pruning that is meant to direct and stimulate growth, improve LA: F, and reduce tree vigor, respectively, occurs concurrently with Michigan's cool wet (rain/snow) weather conditions that are ideal for *Pss* population growth and subsequent infection via the pruning wounds (Kennelly et al., 2008;

Jones and Sutton, 1996; Lang, 2019; Spotts et al., 2010;). Local populations of *Pss* are already present in the spring at and before bud break, as the bacteria overwinter in buds, and as leaf expansion takes place, deposition of *Pss* can occur from adjacent vegetation and rain/snow/air (Hirano and Upper, 2000; Latorre and Jones, 1979a; Lindemann and Upper, 1985; Sundin et al., 1988; Morris et al., 2008). Current pruning recommendations are to wait for periods of dry weather with warmer air temperatures, with summer being ideal, as *Pss* infections can cause necrosis even at temperatures as low as -10 °C (Carroll et al., 2010; Spotts et al., 2010; Sobiczewski and Jones, 1995).

Summer pruning via hedging (pre-harvest and post-harvest) can reduce shade and increase light penetration into the tree canopy while reducing tree vigor and partitioning carbon toward fruits (Lang, 2019). Summer infections by *Pss* still may occur and pruning wounds can be susceptible to *Pss* infections ranging from < 1 week to 24 days (Law, 2017; Spotts et al., 2010). Michigan is subjected to frequent periods of high (≥ 60%) and extremely high (≥ 85%) relative humidity; regardless of the time of year, the probability of an extended (>36 h) humidity event within any 14 day period is 70-90% (Komoto et al., 2021). Monier and Lindow (2003) found that bacterial aggregates of *Pss* strain B728a were more extensive and more numerous at high relative humidity (100%) than at low relative humidity (<50%). In Michigan, even during a "dry" period in the summer, it is possible that *Pss* on leaves covered in heavy dew could be dispersed to pruning wounds via drip and subsequently cause infection. Lindemann and Upper (1985) also reported that more significant upward fluxes of bacteria into aerosols occurred during warm sunny days (wind speeds >1 m/s) at midday when leaves (*Phaseolus vulgaris*) were dry, but not when leaves were wet with dew. While deposition occurred throughout the day, there were instances in which a significant downward flux of bacteria occurred in the evening

during temperature inversions. In a cherry orchard, it could be possible that following one of these events, a higher concentration of *Pss* trapped in dew on leaf surfaces could lead to a higher incidence of infection through pruning wounds. Recommendations to Michigan growers may need to include avoidance of pruning whenever there is high humidity and heavy dew formation (though this hypothesis requires testing).

Bacteria on leaf surfaces aggregate in protected sites and near possible areas of increased nutrient availability, near or within stomata, along leaf veins, trichomes/glandular trichomes, and cuticular fissures (Beattie and Lindow, 1999; Mansvelt and Hattingh, 1987; Mansvelt and Hattingh, 1989; Monier and Lindow, 2004; Roos and Hattingh, 1983). Bacterial aggregates can be mixed populations of varying sizes that have been observed to segregate spatially, and resident populations seem to facilitate the survival of immigrant cells (Beattie and Lindow, 1999; Monier and Lindow, 2004; Monier and Lindow, 2005a; Monier and Lindow, 2005b). On apple and sweet cherry leaves, *Pss* and *Pseudomonas syringae* pv. *morsprunorum* (*Psm*), respectively, were observed to aggregate near and within stomata, propagating within the substomatal chambers and expelling back out onto the leaf surface, while *Pss* on pear was found near stomata and multiplication appeared to occur at the base of trichomes and in cuticle depressions (Mansvelt and Hattingh, 1987; Mansvelt and Hattingh, 1989; Roos and Hattingh, 1983). *Pss* likely aggregate near stomata to escape desiccating conditions (increased temperature and dryness) on the leaf surface, as stomata can cool leaves during high temperatures (Monier and Lindow, 2003; Gommers, 2020; Kostaki et al., 2020). Mercier and Lindow (2000) found that nutrient availability on leaves corresponded to bacteria carrying capacity, and while the majority of sugars were depleted during bacteria growth, residual amounts remained, likely on regions of the leaf not occupied by bacteria, while sugar availability on leaves was species-specific and not

evenly distributed across the leaf surface. Bacterial leaf populations vary according to leaf age, location within the canopy, and leaf side, but they are dependent primarily on "immigration, emigration, growth, and death," with the upper leaf surface communities influenced mainly by dispersal (Kinkel, 1997; Smets et al., 2023). Curiously, there is never any mention in the literature of the visibly apparent extrafloral nectary glands (which exude sugars) on sweet cherry leaves at the junction between the petiole and leaf, which could be a source of nutrients, or an infection point for *Pss*. Perhaps the nectar has antimicrobial properties as described for Poplar (Escalante-Péreza et al., 2012), and it would be prudent to assess these in sweet cherries. Nectar could also be a potential *Pss* population regulator on leaves during summer months when populations reportedly are low. Yee and Chapman (2008) assessed the influx of cherry leaf nutrients available to fruit flies (*Rhagoletis* sp.) from the extrafloral nectaries and juice from bird-pecked fruit. It would also be worthwhile to do the same for *Pss* population dynamics.

Though bacteria on leaf surfaces are subjected to wild fluctuations in microclimate and nutrient availability, they have an arsenal of adaptations to ensure survival, such as motility, biosurfactant production, quorum sensing, UV damage repair, siderophore production, as well as aggregate formations (Burch et al., 2014; Gunasekera and Sundin, 2006; Haefele and Lindow, 1987; Hirano and Upper, 2000; Lindow and Brandl, 2003; Monier and Lindow, 2003; Quiñones et al., 2005; Vorholt, 2012; Wensing et al., 2010). Helmann et al. (2019) have identified 31 genes significant to epiphytic colonization and fitness in *Pss* strain B728a, which included genes encoding for amino acid and polysaccharide production. Most of these genes were also important for occupying the leaf apoplast.

Bacterial interactions on leaf surfaces are complex and can be positive (e.g., the production of "common goods") and negative (e.g., the production of antibiotic metabolites),

which is also true for the plant since bacteria could cause disease (negative) or promote growth (positive) (Bashir et al. 2022; Glick and Gamalero, 2021; Mina et al. 2019; Pattnaik et al. 2021; Vorholt, 2012; Xin et al. 2018). *Pseudomonas* spp. have been found to have close associations with other bacteria (pathogens and nonpathogens) that enhance disease severity and colonization, such as the olive knot pathogen *Pseudomonas savastanoi* pv. *savastanoi* (*Psv*) and the non-pathogens *Erwinia toletana*, *E. oleae*, and *Pantoea agglomerans* (Buonaurio et al. 2015; Marchi et al. 2006). *P. syringae* pv. *actinidiae* (*Psa*), the causal agent of bacterial canker in kiwi, has been frequently isolated with the pathogens *Pss* and *P. viridiflava*, which seem to have a synergistic relationship that boosts *Psa* infections (Purahong et al., 2018). *Pss* isolated from flowers in Michigan cherry orchards is a phylogenetically diverse mix of strains with varying degrees of pathogenicity on green cherry fruit and wood (Wilkinson, Chapter 2). However, it is unclear what type of interactions these strains may have with one another, how they may influence the severity of canker disease, and whether or not this same mix of strains occurs on other plant organs. Michigan sweet cherry orchards are susceptible to bacterial canker infections as the three vertices of the traditional disease triangle (host, environment, and pathogen) converge throughout the year. At the same time, other bacterial occupants of the sweet cherry microbiome, their function, and their relationship to *Pss* remain unknown. Xin et al. (2018) highlighted the microbiome as a fourth critical component of the disease triangle since members can trigger plant immune responses and impact pathogen virulence. Management of *Pss* populations on sweet cherry is problematic, and elucidation of microbiome community members will add to the body of knowledge of *Pss* orchard ecology and may aid the development of future management strategies.

Next-generation sequencing (NGS) technologies and sequencing of the 16S rDNA variable regions for bacteria have stimulated thorough culture-independent exploration of plant microbiomes (Knief, 2014; Kozich et al., 2013). Members of leaf communities have recurring genera (likely due to adaptation to the epiphytic lifestyle) but can vary in community composition (Hirano and Upper, 2000; Lindow and Brandl, 2003; Vorholt, 2012). Often, core microbiomes are determined. They are defined as being common and consistently occurring members of like habitats and are a way to simplify a complex array of organisms that can be used as a marker for plant health and how they respond to various manipulations (Neu et al., 2021; Shade and Handelsman, 2012). Core microbiomes can be determined in several ways, via occurrence, relative abundance, or occurrence-abundance, each method with its own set of caveats, the largest being the arbitrary cut-offs assigned by individual researchers (Custer et al., 2023; Neu et al., 2021). Information about the core bacteria living epiphytically with *Pss* on sweet cherry leaves in Michigan could be a possible way to monitor how the community changes with *Pss* population fluctuations/infections and opens the door for strategic manipulation of the bacteria community (how the community influences *Pss*) and potential biological management of *Pss* populations in the future.

Research on the leaf microbial communities of forest/urban trees, grasses (pertinent to biofuels), wild perennials, and cultivated annuals and perennials have revealed the essential drivers of community composition to be season (time), host plant species (genotype), plant age, and environment (location/ region and neighbors), with some evidence of plant recruitment (Grady et al., 2019; Jackson and Denney, 2011; Kembel et al., 2014; Kim et al., 2012; Laforest-Lapointe et al., 2016a; Laforest-Lapointe et al., 2016b; Laforest-Lapointe et al., 2017; Lajoie and Kembel, 2021a; Lajoie and Kembel, 2021b; Meyer et al., 2022; Noble et al., 2020; Redford et

al., 2010; Redford and Fierer, 2009; Stone and Jackson, 2021; Wagner et al., 2015). Recent studies of fruit crop phyllosphere microbiomes have been driven by associated disease pressures, the quest for alternative management strategies, and a better understanding of pathogen/non-pathogen ecology.

The apple phyllosphere has been surveyed from bark to blossom since the fire blight disease causal agent, *Erwinia amylovora*, can devastate orchards, and research efforts have ranged from community characterization to how the communities respond to antibiotic treatments (streptomycin, kasugamycin and copper), microbial inoculations, and orchard management styles (organic vs. conventional) (Aleklett et al., 2014; Arrigoni et al., 2018; Cui et al., 2021; Glenn et al., 2015; He et al., 2021; He et al., 2012; Shade et al., 2013; Steven et al., 2018; Tancos and Cox, 2017; Wallis et al., 2021; Yashiro and McManus, 2012). Microbiomes of other crops, including tea leaves, citrus, and grapes, have been assessed similarly to apples (Carvalho et al., 2020; Cernava et al., 2019; Gobbi et al., 2020; Mina et al., 2020; Miura et al., 2019; Singh et al., 2019; Wu et al., 2020). Kiwi leaf microbial communities have been analyzed according to plant sex and the presence of the pandemic causal agent of kiwi bacterial canker, *Psa* (Ares et al., 2021). Jo et al. (2015) examined the epiphytic microbiomes of several *Prunus* spp. (apricot, tart cherry, peach, and plum). While Zhang et al. (2021) analyzed sweet cherry fruit microbiomes post-harvest, and O'Gorman et al. (2023) surveyed the microbiomes of sweet cherry fruit and flowers in relation to the emergent disease, cherry slip-skin-maceration disorder (cherry-SSMD), to the author's knowledge no surveys have included the sweet cherry epiphytic bacteria populations. The objectives of this paper are to survey the sweet cherry leaf microbiome bacterial community across three cultivars, three seasons, and in two regions of Michigan to determine: a) if there are seasonal and regional differences in the sweet cherry leaf microbiome,

b) if the leaf microbiome varies across sweet cherry cultivars, and c) the core members of the microbiome. This work will provide a foundation for future microbiome research (e.g., soil/roots, bark, flower) in sweet cherry. It will identify the bacteria that reside epiphytically with *Pss* in Michigan orchards, information that is needed for future work on community interactions with *Pss* and the potential management of *Pss* populations.

3.3: Methods

Orchard Plantings and Sample Collection

In May 2017, three-year-old sweet cherry trees previously grown in pots were planted in two regions in Michigan: Wells Orchards, Grand Rapids, Ottawa Co. (site 1), and at the Michigan State University (MSU) Horticulture Teaching and Research Center, Holt, Ingham Co. (site 2) (Figure 3.1). The sweet cherry cultivars, 'Gold', 'Sweetheart', and 'Benton' on Mazzard rootstock were interplanted with 23 other cultivars in a completely randomized design (Appendix B). The three cultivars were selected based on their susceptibility to *Pss* infection: 'Benton' and 'Sweetheart' are susceptible, while 'Gold' is reported to have an "observable level of tolerance" (Hulin et al., 2022; Spotts et al., 2010; Sundin and Rothwell, 2012). Orchards in both locations were managed using traditional integrative pest management (IPM) strategies for commercial orchards in Michigan. Sites varied in planting orientation, soil composition, and cropping history (Appendix B). Site 1 had sandy clay loam soil and had been planted with peaches for ten years before their removal in 2016. Site 2 had fine sandy loam soil and had been on a corn/soybean crop rotation with soybeans present in 2016.

At both sites, 4 trees of 'Benton' and 'Sweetheart' were sampled, while 3 trees of cultivar 'Gold' were sampled (Fall 2017). The same 11 trees were sampled at site 1 throughout the duration of the experiment (2017- 2019), this was not the case at site 2 due to tree mortality over

the course of the experiment (Appendix B). Leaves (4/tree) were sampled for microbiome analysis in October (Fall) 2017, 2018, and 2019 at 10-25% leaf drop, in May (Spring) 2018 and 2019 when new leaves were fully expanded, and in August (Summer) 2018 and 2019, corresponding with summer pruning timing. A total of 44 leaves/site were harvested Fall 2017 and Spring 2018, 44 leaves at site 1 and 40 leaves at site 2 in Summer and Fall 2018, as well as Spring, Summer, and Fall 2019. Individual leaves with petioles were harvested while wearing gloves sprayed with 75% ethanol, collected from the terminal end of branches and placed into sterile Whirl-Pak® bags (Nasco, Madison, WI) (Figure 3.2). Leaf width and length were measured according to Demirsoy and Lang (2010) to calculate leaf area and then placed into a cooler for transport to the lab. Leaves were collected on the same day for both sites, excluding Spring 2019 when they were collected a day apart due to the safe re-entry period following a spray application at site 2. Each leaf sample was assigned a number for labeling simplicity in all subsequent sample processing steps (Appendix B).

Sample Processing and Metadata Collection

In the laboratory, individual leaves were placed into a 50 ml conical tube with 45 ml sterile 0.5x phosphate-buffered saline (PBS) and were then shaken at 200 rpm for 10 min in a G24 Environmental Incubator Shaker (New Brunswick Scientific, Edison NJ) and sonicated for 7 min in an ultrasonic bath (Cole Parmer, Chicago, IL). For long-term storage, a 100 µl portion of the leaf microbiome wash from each leaf sample was pipetted into sterile 15% glycerol in a cryovial and stored at -70°C.

For counting culturable bacteria, an additional 100 µl portion of the leaf wash for each leaf sample was serially diluted in 900 µl sterile PBS to 0, 10^{-1}, and 10^{-2} for samples collected in 2017 and 2018 and plated onto King's B (KB) media amended with 50 µg/ml cycloheximide

with 2 leaf samples/plate (Figure 3.3). In Spring 2019, serial dilutions were expanded to 0, 10^{-1}, 10^{-2}, and 10^{-3} with one plate/leaf sample. Summer and Fall 2019 serial dilutions were expanded even further to 0, 10^{-1}, 10^{-2}, 10^{-3}, 10^{-4}, 10^{-5}, 10^{-6}, 10^{-7} (2 plates/sample). All plates were allowed to dry overnight at room temperature and then were then placed into a 28°C incubator (Precision Scientific Model 805, Chicago, IL) until the following day when pictures were taken of plates for colony counting. Colony forming units (cfu)/leaf area (cm^2) are reported for each sample.

Weather data was collected from the MSU Enviro-weather system (https://mawn.geo.msu.edu/) for the two weeks prior to each sampling date, including mean daily temperature (°C), mean daily relative humidity (%), and precipitation (mm). For site 1, data were obtained from the nearest weather station located at Kraft Orchards, Sparta, MI. (Kent Co.), ~ 24 km north (Figure 3.1). The data for site 2 was obtained from the on-farm weather station. Spray records were also obtained for each site for the two-week period prior to each leaf sampling date. In Fall 2019, trees used for microbiome sampling were rated for bacterial canker lesions as follows: For trunks, 3=healthy, 2=minor infection (sunken/gumming lesion ≤ 2.5 cm), 1=major infection (multiple sunken/gumming lesions > 2.5 cm), 0=dead; for shoots or branches, 3=healthy, 2=isolated infections, 1=many infections, 0=dead.

DNA Extraction and Sequencing

For each leaf sample, 3 ml of the leaf wash was pipetted into 15 ml conical tubes for DNA extraction. For 2017-2018 no technical replications were made. However, in 2019 technical replications (3 reps) were included with three 15 ml conical tubes of 3 ml leaf wash/leaf sample. All tubes with leaf wash were kept at 4 °C until the time of DNA extraction. Extraction of DNA was accomplished via the E.Z.N.A® Bacterial DNA Kit (OMEGA Bio-tek, Norcross, GA) following the manufacturer's protocol. Samples that were combined or spilled

during the DNA extraction process were omitted from further analysis (6 combined samples in Spring 2018, 1 spilled sample in Fall 2018, and 2 combined samples in Rep 1 and 2 samples in Rep 3 Spring 2019). A "mock" community (+ control) was included consisting of four *Pss* strains (6-9.3, 13-7, 19-6, and 26-3) (from G. Sundin's collection) and a negative control (−was included containing no DNA. The extracted DNA samples were stored at -20°C. The quality of DNA was assessed using the Qubit™ 3.0 fluorometer, polymerase chain reaction (PCR), and gel electrophoresis. The Qubit™ fluorometer assays were conducted in 2017 using the Qubit™ dsDNA BR Assay Kit (Invitrogen, ThermoFisher Scientific, Waltham, MA) and in 2018-2019 using the Qubit™ 1x dsDNA HS Assay Kit following the manufacturer's protocols.

The 16S V4 rDNA conserved region of the bacterial DNA was amplified using PCR in a Bio Rad T100™ Thermal Cycler (Bio-Rad Laboratories, Hercules, CA), with the following reaction components; 4 µl of sample DNA, 12.5 µl of One *Taq*® Hot Start 2x Master Mix with Standard Buffer (New England BioLabs® , Ipswich, MA), 0.5 µl forward and reverse primer, brought up to a 25 µl total reaction volume with Invitrogen™ UltraPure™ distilled water. The 16S V4 primers, forward: GTGCCAGCMGCCGCGGTAA and reverse: GGACTACHVGGGTWTCTAAT and the modified thermal conditions, 94 °C for 3 min., 35 cycles of 94°C for 45 s, 50°C for 60 s, 72°C for 90 s, final 72 °C for 10 min and 4°C infinite, were from Kozich et al. (2013). The PCR product was run on a 1% Invitrogen™ UltraPure™ Agarose gel, stained with 1µl Ethidium Bromide (EtBr) (Bio-Rad Laboratories), in 1x Tris-Acetate-EDTA buffer (TAE) at ~60 V for ~80 min. A 100bp DNA ladder (New England BioLabs®) was included. Gel imaging was done using a Bio Rad Gel Doc™ EZ Imager.

The DNA samples that produced bands were sent to the MSU Research Technology Support Facility Genomics Core (RTSF) for sequencing (Appendix B). Sequencing occurred on

the Illumina MiSeq platform using the 16S V4 rDNA primers (515f/806r) as in Kozich et al. (2013), following the normalization of samples. Sequencing resulted in two 250 bp paired-end reads returned for sequence analysis.

Sequence and Statistical Analysis

Sequences were processed using Mothur software version 1.44.2 following the "MiSeq SOP" (https://mothur.org/wiki/miseq_sop/) with modifications pertinent to this specific data set (Kozich et al., 2013; Schloss et al., 2009). Mothur v.1.44.2 was accessed through the MSU Institute of Cyber-Enabled Research (ICER) High-Performance Computing Center (HPCC) and ran in "batch mode" and in "interactive mode". Sequences from 2017, 2018, and 2019 (Rep 3 only) were processed together, as 2017 and 2018 did not include technical replications. Sequences from 2019 (all reps) were then processed together without 2017 and 2018. All sequences were aligned, and operational taxonomic units (OTUs) were classified with 97% sequence identity against the SILVA database release 132 (Quast et al. 2013; Yilmaz et al. 2014). Chloroplasts, mitochondria, unknowns, Archaea, and Eukaryota were removed from the sequence analysis following the "Miseq SOP" (Schloss et al., 2009). The sequence error rate was determined with the known sequences of *P. syringae* pv. *syringae* strain FF5 (GenBank accession ACXZ00000000.1) set as the reference (Lindeberg, 2011; Sohn et al., 2012). The 2017-2019 and the 2019 sequence data sets were rarefied and subsampled to the same number of sequences (1162); Goods coverage, Alpha diversity (number of OTUs, Shannon Diversity Index, and Shannon Evenness Index), and Beta diversity (Bray-Curtis Index) were calculated via Mothur (Schloss et al., 2009). Relative abundance was calculated (no. OTUs/1162 sequences) using R version 4.3.1 (R core team, 2023). The core microbiome was determined via the Mothur,

with parameters set for relative abundance (≥ 0.01) and the number of samples (at least 50%) (Schloss et al., 2009).

In order to include Fall 2017 in the statistical analysis, year and season were combined in a single parameter time for the 2017-2019 data set. Data was analyzed using R version 4.3.1 (R core team, 2023). Distributions of the data are in Appendix B. These statistics were fit to a robust linear mixed model with site, cultivar, and time (2017-2019 data) or season (for 2019 data) as fixed effects and site, row, and tree as nested random effects (for 2017-2019 data) or site, row, tree, and leaf as nested random effects (for the 2019 data) (Bates et al., 2015). This was followed by analysis of variance (ANOVA) table as well as pairwise comparisons of the estimated marginal means (Lenth, 2023). The Bray-Curtis dissimilarity index was tested for the homogeneity of variances (dispersions) followed by a permutational multivariate analysis of variance (PERMANOVA) with 999 permutations (Oksanen et al., 2022). Nonmetric multidimensional scaling (NMDS) was also performed on the Bray-Curtis dissimilarity for graphical visualization of distances between samples (Oksanen, 2022). Weather data, excluding precipitation, was analyzed using a simple linear model with site and time as fixed effects followed with ANOVA and pairwise comparisons of the estimated marginal means (Lenth, 2023; R core team, 2023). The precipitation data was analyzed via Kruskal-Wallis test (data were not normally distributed), followed by pairwise multiple comparisons using Dunn's test with Bonferroni adjusted p-values (Mangiafico, 2023; Ogle et al., 2023). All graphs were made in R v. 4.3.1 using a combination of base R and ggplot2 and ggpubr (Kassambara, 2023; R core team, 2023; Wickham, 2015). Graphic fonts were edited, and the letters indicating statistical differences were added to graphs via InkScape v.1.2 (InkScape.org).

3.4: Results

Sequencing

A total of 596 leaves were sampled from both orchard sites combined from 2017-2019, 74% (n=443) were sent for sequencing following DNA extraction. For 2019 alone, 252 leaves were collected from both sites with 3 technical DNA extraction replications for a total of 756 samples, of these, 62% (n=471) were sent for sequencing. Only samples that had amplification of the 16S rDNA region following DNA extraction were sent for sequencing (Appendix B). For Spring 2018, only samples from site 1 were sequenced as site 2 did not have PCR amplification of the 16S rDNA region following DNA extraction. Following the processing of sequences at the 97% sequencing identity through the Mothur v. 1.44.2 pipeline for 2017-2019 leaf samples, a total of 17,795,034 sequences were returned ranging from 17 to 135,128 sequences/sample, 61 samples contained < 1,000 sequences (potentially mis-assembled sequences). For 2019 a total of 6,757,926 sequences were returned ranging from 17 to 58,818 sequences/sample, and 151 samples contained <1,000 sequences. Samples that contained <1, 000 sequences/sample were filtered out via subsampling. Both data sets were subsampled to 1162 sequences as it was the smallest number of sequences for the 2017-2019 data set and only excluded two additional samples from the 2019 data set. Sampling effort for both the 2017-2019 and 2019 data sets was very good, with Good's coverage values ranging from 96 to 100% and 98 to 100%, respectively for all the samples with >1000 sequences. Rarefaction curves also demonstrate good sampling effort many are nearing or have reached their species richness asymptotes (Figure 3.4). Following subsampling, a total of 384 and 325 samples remained for the 2017-2019 and 2019 datasets, respectively. The negative control samples did contain sequences however they consisted of <1% of the total sequences for both data sets, therefore, no OTUs were removed

from the data and the negative control samples were used only as a reference and not included in further statistical analysis. Both datasets were rarefied (1000 iterations) via Mothur v. 1.44.2 when calculating the alpha and beta diversity statistics.

Alpha-Diversity

The alpha diversity statistics for 2017-2019, bacteria plate counts (log cfu/cm^2 leaf area), number of OTUs, Shannon diversity index, and the Shannon evenness index ANOVA's revealed that neither site nor cultivar was significant for any of these metrics and could be combined, while time was significant for all four metrics (Table 3.1). For the 2017-2019 plate counts for estimating the number of bacteria in the sweet cherry microbiome of the 596 samples 23% (n=140) of the plates contained too many to count (TMTC), 21% (n=123) of plates had no growth, and 55% (n=333) of plates had countable bacterial growth. The plates that had TMTC were omitted from the analysis, 456 total samples remained in the analysis (n=61, 2017 fall; n=77, 2018 spring; n=53, 2018 summer; n=14, 2018 fall; n=84, 2019 spring; n=83, 2019 summer; n=84, 2019 fall). The mean number of bacteria present on the leaf microbiome was lowest in the spring (2018 and 2019) and continued to increase from summer into fall (2018 and 2019) (Figure 3.5).

Species richness or number of OTUs/sample (n=84, 2017 fall; n=36, 2018 spring (only site 1); n=65 2018 summer; n=54, 2018 fall; n=35, 2019 spring; n=64, 2019 summer; n=46, 2019 fall) had a more variable trend over time where spring, summer, and fall 2018 were not statistically different from each other (Figure 3.5). While a trend similar to that seen for the plate counts occurred where the mean number of OTUs increased from spring to fall for 2019. Overall the spring was the most variable where spring 2018 had the greatest number of OTUs while

spring 2019 had the lowest number of OTUs and was statistically different from all other time points. The summer and fall had more statistically similar numbers of OTUs over time.

The species diversity (Shannon Diversity index) in the sweet cherry leaf microbiome is relatively stable over time, excluding Springtime points, where Spring 2018 had the greatest amount of diversity and Spring 2019 had the least amount of diversity and they were statistically different (Figure 3.5). The Springtime points were also statistically different from all other Summer and Fall time points. The Summer and Fall time points had a species diversity that ranged from a mean of 1.4 to 1.8 and were not statistically different from each other.

The sweet cherry leaf microbiome has approximately the same Shannon evenness values at all summer and fall time points (0.4 to 0.5) and are not statistically different (Figure 3.5). While Spring is variable where 2018 has the greatest evenness value and was statistically different from all other time points excluding fall 2019, while spring 2019 had the lowest species evenness and was statistically different from all other time points.

Beta Diversity

The Bray-Curtis dissimilarity index was used to determine if there are clear differences in the community composition in the sweet cherry leaf microbiome. The ANOVA tables for the test for beta-dispersion or homogeneity of variances for each model parameter show that cultivar has homogeneous variances, while site, and time are heterogeneous (Table 3.2). The PERMANOVA table shows that site is not significant Bray-Curtis dissimilarity, however cultivar, and time was significant. Time (season) however, has greatest explanatory value as it is significant on its own and in interactions and accounts for 19.6% of the variability (R^2=0.196). The NMDS ordination of the Bray-Curtis dissimilarities support this as there were no clear dissimilarities for either site or cultivar (Figure 3.6). While the NMDS ordination of the Bray-Curtis dissimilarities clearly

show differences in time where springtime has the greatest amount of dispersion (furthest distance from the centroid) and has the most dissimilar communities, while summer becomes less dissimilar, and fall communities are the most similar (least distance to the centroid) (Figure 3.7).

Relative Abundances

The ANOVAs for the relative abundances of the Top four Phyla and "other" and the relative abundances of *Pseudomonas* and all "other" taxa were not significant for site, cultivar or time, but were significant for Phylum, time*Phylum and genus, time*genus respectively (Table 3.3). Thereby the site and cultivars were combined and means separations were for only Phylum, time*Phylum and genus, time*genus (n=84, 2017 Fall; n=36, 2018 Spring (only site 1); n=65 2018 Summer; n=54, 2018 Fall; n=35, 2019 Spring; n=64, 2019 Summer; n=46, 2019 Fall) (Appendix B). The sweet cherry leaf microbiome is dominated by the Phylum Proteobacteria at all time points ranging in mean relative abundance of 0.67 (67%) to 1.00 (100%) (Figure 3.8). The other Phyla were present at much lower levels at all time points and included Actinobacteria, Bacteroidetes, Firmicutes, and "other". Within each time point Proteobacteria was statistically different than all of the other Phyla. Across time points the relative abundance of the Proteobacteria in spring is the most variable and is statistically different from all Proteobacteria at the other time points while there again appears to be similarities in summer and fall relative abundance of Proteobacteria. All other Phyla (Actinobacteria, Bacteroidetes, Firmicutes and "other") are considerably lower in relative abundance compared to Proteobacteria with overall little statistical difference from each other within and across time and no consistency in their positions as the next most abundant phylum.

When focusing on the relative abundances of *Pseudomonas* and all "other" taxa, *Pseudomonas* has a clearly defined presence within the sweet cherry leaf microbiome and a seasonal trend in dominance (Figures 3.9, 3.10). The relative abundance of *Pseudomonas* is more variable in the Spring, where "other" taxa was dominate in 2018 while *Pseudomonas* dominated in 2019 (i.e., the greatest differential occurred between the "other" taxa and Pseudomonas in spring). During the summer the differential decreases and *Pseudomonas* becomes more dominate while the most stability occurs during the fall where *Pseudomonas* and the "other" taxa are close to equal in relative abundance.

Within each time point for 2017-2019 the relative abundances at the deepest taxonomic level (genus or family) were examined further i.e., picking apart the "other" taxon present in the leaf microbiome where the top taxa were selected via their mean values and combined into "other" if they had a relative abundance <0.03. The core microbiome that was selected by the occurrence of OTUs in at least 50% of the samples at relative abundance of ≥0.01 and returned four core taxa (*Pseudomonas* OTU00001, *Pseudomonas* OTU00002, *Pseudomonas* OTU00003, *Sphingomonas* OTU00004) (Schloss et al., 2009). Under more stringent parameters such as occurrence in 97% of the samples no core microbiome was returned. The ANOVA table for the top deepest taxonomic level at each time revealed no significance of site or cultivar but was significant for taxa while the core microbiome was not significant for site, cultivar, or time but was significant for genus and time*genus (Table 3.4).

The relative abundances at the top deepest taxonomic levels taxa show *Pseudomonas* to be strikingly dominant at all time points (Fall 2017 to Fall 2019), excluding Spring 2018 when the "other" taxa had a greater relative abundance and *Pseudomonas* had the 2nd highest relative abundance, followed by the rest of the taxa which were not statistically different that one another

(Figure 3.11). Besides *Pseudomonas* the only other taxa that makes the top relative abundances consistently at all time points is *Sphingomonas*, excluding Spring 2019 where it was not included in the top taxa.

The 2017-2019 core microbiome (*Pseudomonas* OTU00001, *Pseudomonas* OTU00002, *Pseudomonas* OTU00003, *Sphingomonas* OTU00004) relative abundance were compared to the relative abundances of the rest of the combined *Pseudomonas* and *Sphingomonas* with the remaining taxa combined into "other" (Figure 3.12). The core *Pseudomonas* OTU00001 has relative abundances that range from 0.50 (50%) to 0.08 (8%), *Pseudomonas* OTU00002 ranged from 0.30 to 0.02 and *Pseudomonas* OTU00003 ranged from 0.21 to 0.1, while *Sphingomonas* OTU00004 ranged from 0.18 to 0.0. These taxa by themselves have relatively low relative abundances but when the *Pseudomonas* core OTUs are combined they make up the majority of the *Pseudomonas* at each time. While the Sphingomonas OTU00004 is often statistically the same as all other Sphingomonas with a few exceptions at all time points.

2019 Alpha-Diversity

The ANOVA table for the 2019 plate counts (log cfu/cm^2), number of OTUs, Shannon diversity index, and the Shannon evenness index show no significant effect of cultivar and while there is some variability with site and site*season effects, there is a significant effect of season for all four alpha-diversity metrics (Table 3.5). All four alpha diversity metrics follow a trend of having lower values in the Spring and then increase into the Summer and Fall (Figure 3.13).

2019 Beta Diversity

The ANOVA for the beta-dispersion for the Bray-Curtis dissimilarity index for 2019 shows that cultivar has homogeneity of variance while site, and season have heterogenous variances (Table 3.6). The PERMANOVA of the Bray-Curtis dissimilarity index is not

significant for site but is for cultivar, and season. Season like 2017-2019 seems to have the most influence over community composition accounting for 15.6% of the variability (R^2=0.156). The NMDS ordination of the Bray-Curtis index for 2019 does not distinguish dissimilarity between communities for sites or cultivars while there is a clear clustering of points by season with summer and fall having less dissimilar community compositions than spring which has more dispersion than the other two seasons. Fall is much more similar in composition (least mean distance to the centroid) than that of summer and spring (which has the furthest mean distance to the centroid) indicating stabilization of community in the Fall (Figure 3.14).

2019 Relative Abundance

As with the 2017-2019 data set the ANOVA for the relative abundances (n=88, spring; n=130, summer; n=107, fall) of the 2019 top Phylum and *Pseudomonas* and "other" was not significant for site, cultivar, or season but was significant for Phylum, season*Phylum, genus, and season*genus respectively (Table 3.7).

As with the 2017-2019 data the 2019 top Phylum is dominated by the Proteobacteria with the other top Phyla being the Actinobacteria, Bacteroidetes, Firmicutes and "other" (Figure 3.15). Bacteroidetes was the second most abundant in the fall and summer, but spring was almost entirely composed of Proteobacteria. The relative abundance of *Pseudomonas* dominated in the spring with the greatest differential from the "other" taxa, while still dominate in Summer the differential was much reduced between it and the "other" taxa (Figure 3.16). The fall *Pseudomonas* was about equal to the "other" bacteria as with the 2017-2019 data set indicating stabilization by the fall season.

The 2019 ANOVA tables for both the deepest taxonomic level (genus or family) and the core microbiome did not have site or cultivar (nor season for the latter) as significant effects

while genus was significant (Table 3.8). At the deepest taxonomic level for 2019 the taxa were similar to that of those in 2017-2019 (Figure 3.17). All three seasons were dominated by *Pseudomonas* while *Sphingomonas* was the next most abundant. As with the 2019-2017 data set the *Sphingomonas* were also consistently in the top taxa present in summer and fall but included in the "other" taxa for spring.

The 2019 core microbiome (*Pseudomonas* OTU0001, *Pseudomonas* OTU0002, *Sphingomonas* OTU00003, *Sphingomonas* OTU00007) relative abundance were compared to the relative abundances of the rest of the combined *Pseudomonas* and *Sphingomonas* with the remaining taxa combined into "other" (Figure 3.18). As with the 2017-2019 data set the core microbiome was selected via the same parameters of occurrence in 50% of the samples and at relative abundance of ≥0.01 and when more stringent parameters were used (97% occurrence) no taxa were returned. The *Pseudomonas* OTU0001 was the most abundant taxa in all three seasons while *Pseudomonas* OTU0002 was the next most abundant in the spring and summer but was 4th in the fall. As with the core *Pseudomonas* in the 2017-2019 data the 2019 core *Pseudomonas* OTUs appear to make up most of the total *Pseudomonas* relative abundance. This is true for the 2019 core microbiome *Sphingomonas* OTUs when compared to the other *Sphingomonas* combined as well.

Weather, Spray Frequency, and Canker Ratings

Precipitation, it was analyzed using the Kruskal-Wallis test and was not significant for site (χ^2=0.356, df=1, p=0.5506) but was significant for time (season) (χ^2=22.877, df=6, p=0.0008). The ANOVA tables for the relative humidity and mean daily temperature also show that site was not significant, while they were both significant for time (season) (Table 3.9). Overall, the amount of precipitation was low, with median values ranging from 0.0 to 2.3 mm,

with little statistical difference (Figure 3.19) The mean relative humidity for the two-week periods was high, ranging from 72.8%-80.6%. Only Fall 2018 was statistically different from Spring and Summer 2018, and Summer 2019, while all other times were not statistically different for relative humidity. The Spring and Fall mean daily temperatures ranged from 12.6-15.4 °C and were not statistically different from one another, excluding Fall 2017 and Spring 2019. Spring and Fall mean daily temperatures were statistically different from all Summer temperatures, which ranged between 21.2-22.6 °C. The Summer temperatures were not statistically different from each other.

The spray records were examined for the two-week periods leading up to each leaf sampling date, spray frequency was quite low at both sites, with site 1 having more spray events when compared to site 2 (Appendix B). By Fall 2019, two years after planting, all trees that were part of the microbiome leaf sampling had bacterial canker (Appendix B).

3.5: Discussion

It is well understood that the leaf microbiome is a harsh environment and generally bears a low amount of biomass, with the microbiome being variable from leaf to leaf, in canopy location, and in tissue age, as well as abaxial and adaxial surfaces (Hirano and Upper, 2000; Kinkel, 1997; Lindow and Brandl, 2003; Smets et al., 2023; Vorholt, 2012). It was not surprising that not all of the leaves sampled in this study yielded DNA or countable bacteria. This is one caveat of single-leaf sampling versus bulk-leaf sampling. However, bulk-leaf sampling could overinflate the mean population size (Donegan et al., 1991; Hirano and Upper, 2000; Kinkle et al., 1995). Sampling coverage via the culture-independent methods was excellent, as indicated by the rarefaction curves and the Good's coverage values (96-100%, 2017-2019; 98-100%, 2019), even with using 3 ml of the leaf wash for the DNA extractions, these results should be an

accurate estimate of the sweet cherry leaf microbiome diversity. There were no striking differences between the 2017-2019 data set and the 2019 alone data set when looking at the alpha and beta diversity as well as relative abundances, as they were reflective of each other. The technical replications of 2019 did ensure that DNA data was available for each site for all seasons, whereas during the Spring of 2018, there was only DNA recovered from site 1 and no DNA recovered from site 2 leaves. It was determined that though some the data distributions were not entirely normal, the structure of the experimental design should be upheld, which contained of multiple fixed effects and random effects, therefore the data was analyzed with a robust linear mixed model. While the use of non-parametric tests would ignore the experimental design, the random effects in particular. Schielzeth et al. (2020) showed that linear mixed models are robust and capable of handling even severe violations of normality.

There were no regional differences (site1 v. site 2) or cultivar differences ('Benton', 'Gold', 'Sweetheart) in the Michigan sweet cherry leaf microbiomes for the 2017-2019 data set when looking at both alpha and beta diversity as well as the relative abundances of Phyla, and *Pseudomonas*. When looking at a single year (2019), some differences in region (sites) were apparent for some alpha diversity metrics but not all. However, the cultivars in 2019 were not statistically different for all metrics, and neither site nor cultivar was different for the Bray-Curtis dissimilarity index (beta diversity). Steven et al. (2018) found no differences in apple flower communities between cultivars (Braeburn, McIntosh, and Sunrise), while host-specific bacterial communities were found in the Olive cultivars (Cobrançosa and Verdeal Transmontana) (Mina et al. 2020). Work in temperate and tropical forests indicates that bacterial community differences are tree species-driven (Kim et al., 2012; Laforest-Lapointe et al. 2016a; Redford et al., 2010). While Singh et al. (2019) found bacterial community differences between species of grapes, they

found that the effect of season was stronger. Researchers have found sites (environment) or nearest neighbors to influence bacterial populations as well (Noble et al. 2020; Laforest-Lapointe et al. 2017; Lajoie and Kemble, 2021b). Muira et al. (2018) found that leaves sampled from surrounding forest tree species shared common OTUs with vineyard grape leaves. It would be interesting to determine if cultivated sweet cherries in Michigan share common bacterial communities with their forested counterparts. Lajoie and Kemble (2021a) found both the phylogenies of the tree host and the leaf bacteria influence associations with each other. Jo et al. (2015), however, found that *Prunus* spp. (*P. armeniaca, P. cerasus*, *P. persica,* and *P. domestica*) from bulk leaf samples harbored unique bacterial diversities with only 23 shared genera.

When looking at the weather data for the two sites, there were also no differences in the mean daily temperatures, precipitation, or humidity as well which was surprising as site 1 is ~34 miles from Lake Michigan while site 2 is ~109 miles from Lake Michigan. Stone and Jackson (2021) found that rainfall did not influence the communities on a limited time scale for the broadleaf cattail (*Typha latifolia*) while "long-term seasonal patterns" did. As both these sites share similar weather when looking at the two-week period leading up to the sampling dates, and both were managed as commercial orchards, though site 1 had more springtime spray events, these sites appear to be identical at this scale and lack explanatory value. Perhaps looking at the sweet cherry trees grown in the more southern or northern regions of Michigan would exhibit site differences in their bacteria communities, which would need to be investigated further. Research has been done in apple and citrus to determine if orchard management strategy (conventional v. organic or ecologically managed) influences bacterial communities with mixed results where citrus bacteria were highly variable between strategies while apple had greater

differences in communities over time than over management practices (Carvalho et al., 2020; Glenn et al., 2015). Wallis et al. (2021) and Yashiro and McManus (2012) looked at the effect of Streptomycin treatments in apples on endophytic and epiphytic bacterial communities, respectively, and both found treatment had little effect, while farm location had greater effect for the former and time and location had more effect for the latter. Sweet cherries in Michigan, however, are not grown organically, nor are antibiotics currently being used.

There are markedly clear trends in the Michigan sweet cherry leaf microbiome driven by time (season). The plate counts of the culturable bacteria (log cfu/cm^2) indicate that bacteria populations are low in the spring and increase through Summer and into Fall. The lack of statistical differences between Summer and Fall for alpha diversity suggests that the population numbers stabilize between Summer and Fall, and the trend appears to be consistent over time points. Summer and Fall also have a similar number of species (OTUs), species diversity (Shannon Diversity Index), and evenness (Shannon evenness index), while the number of OTUs and Shannon diversity and evenness index for spring can vary from being its highest (40.6 OTUs, 2.4 Shannon, and 0.6 evenness) in 2018 to the lowest (6.0 OTUs and 0.3 Shannon, and 0.2 evenness) in 2019. The non-metric dimensional scaling (NMDS) also demonstrates the decrease in dissimilarity of the bacteria community from Spring through Fall, where communities are the most similar/stable. Spring 2019's Shannon diversity index indicates that it was nearing zero (0.3, 2017-2019; 0.2 to 0.5, 2019) where an H′ value=0 would be comprised of a single species, Shannon values typically range between 1.5 to 3.5 (Magurran, 2004). The relative abundance data show that the sweet cherry leaf samples of Spring 2019 consist almost entirely of *Pseudomonas* with a mean of 0.96 (96%), and 0.97 (97%) in the 2017-2019 and 2019 data sets, respectively.

It is not surprising that Spring has the most variability as leaves are newly emergent, have less surface area, nutrient availability, and bacteria populations are just becoming established (Kinkel, 1997). Smets et al. (2022) sampled London plane tree leaves (*Platanus acerifolia*) weekly over a six-week period covering the span of leaf emergence and found clear successional patterns of early, mid, and late communities that shared the greatest dissimilarity and high rate of change right after leaf emergence and stabilized as they neared the end of the sampling period. Though outside the scope of this experiment (i.e., not measured), it should be noted that Spring is also the prime season for *Pss* population increases and subsequent disease pressure, which could influence population variability. *Pss* is known to overwinter in buds and is likely one of the earliest colonizers of the sweet cherry microbiome (Sundin et al., 1988). Perhaps the variability of the springtime microbiome could also be related to the sweet cherry trees' carbon (C) and nitrogen (N) availability to the newly emergent leaves, as these nutrients are just mobilizing from storage tissues, and there is strong competition for these resources, and there is evidence that bacterial communities can be influenced by plant C-N status (Ayala and Lang, 2017; Bringel and Couée, 2015). This could also be included in the future microbiome and *Pss* population work in sweet cherry.

Excluding the variability of Spring, the Michigan sweet cherry leaf microbiome shows stability and predictability over the Summer and Fall time points where the Shannon evenness index shows no statistical differences indicating the relative abundances of the bacteria community are unchanged between time points Summer and Fall 2018 and Summer and Fall 2019 as well as the species richness (no. OTUs and the Shannon diversity index) (Magurran, 2004). The leaf microbiomes of perennial grasses, common bean, soybean, and canola also had microbiomes influences by time where earlier communities were similar to the soil microbiomes

while later communities were distinct leaf communities that were similar among all plants (Copeland et al. 2015; Grady et al. 2019). Grady et al. (2019) bacterial communities could be defined as early, mid, and late with "directional assembly" over the growing season in perennial grasses. While Redford and Fierer (2009) showed that Cottonwood leaves also had early, mid, and late communities, the early and late communities were more similar to one another. Both studies demonstrated predictability from season to season (Grady et al., 2019; Redford and Fierer, 2009). For Magnolia leaf microbiomes, while they were found to have distinct seasonal communities, they were not consistent (predictable) from year to year (Jackson and Denney, 2011).

The Michigan sweet cherry leaf microbiome is dominated by Proteobacteria, the phylum in which *Pseudomonas* belongs, ranging from 67 to100% relative abundance across all time points, the lowest value being Spring 2018 and the maximum value being Spring 2019, a continuing theme of Springtime variability followed by the more stable Summer and Fall relative abundance values for the Proteobacteria. The additional top Phyla present in the sweet cherry leaf microbiome consists of low relative abundances of Actinobacteria (0 to11%), Bacteroidetes(0 to 8%), and Firmicutes (0 to 16%). These phyla are typical of leaf microbiomes (Vorholt, 2012). Jo et al. (2015) also recovered the same 4 phyla from the bulk leaf samples from four *Prunus* spp. where Proteobacteria was also dominant (93%), followed by Bacteroidetes (4%), Actinobacteria (2%), and Firmicutes (1%). Proteobacteria was also dominant in the leaves of olive (60.8%) and kiwi (76.9%) and in apple flowers (>90% total sequences) (Ares et al., 2021; Mine et al., 2020; Steven et al., 2018).

The most dominant of all of the taxa are *Pseudomonas* in the Michigan sweet cherry leaf microbiome. When looking at only *Pseudomonas* again, there appears to be a trend of variability

in the Spring (26% in Spring 2018 vs. 96% in Spring 2019) and more stability in the Summer and Fall as there is no statistical difference between the *Pseudomonas* relative abundances at those time points. *Pseudomonas* is a clear driving force of modulation of the relative abundances of all "other" taxa, as *Pseudomonas* relative abundance increases the relative abundance of the "other" taxa is driven down while, when the relative abundance of Pseudomonas nears 50% it seems to have a "neutralizing" effect as the "other" taxa also approach 50% relative abundance which coincides with the Fall time points only to further lend strength to the evidence pointing to the stabilization of the bacterial community by the Fall season. The only time where the "other" taxa exceed *Pseudomonas* was in Spring 2018 when *Pseudomonas* dropped to 26% relative abundance, however, there was not a single taxa that took its place as the top genus at that time. Grady et al. (2019) found that *Pseudomonas* was replaced over time by *Methylobacterium* as part of a "compensatory relationship". Ares et al. (2021) also saw a decrease in *Pseudomonas* and an increase in *Methylobacterium* in the Fall. In this study, *Methylobacterium* (3% relative abundance) was in the top taxa for Spring 2018 but did not replace *Pseudomonas*. Steven et al. (2018) found that *Pseudomonas* and Enterobacteriaceae were dominant in the apple flower microbiome and had a negative correlation as one increased, the other decreased. Though Enterobacteriaceae was present in the top taxa in Fall 2017 (16%), Summer 2018 (5%), Spring 2019 (3%), and Summer 2019 (8%), a relationship between the two is not evident (Figure 3.30 and Table 3.14). Steven et al. (2018) also emphasized that the ability of *Pseudomonas* spp. to produce antimicrobial compounds could be a likely explanation as to how *Pseudomonas* is regulating the microbiome. *Pseudomonas* is also capable of living commensally in the microbiome, has been isolated from sweet cherry previously with other virulent and avirulent *Pseudomonas*, is ubiquitous in the environment, with a broad host range, and in the case of *Pss*, a

strong evolutionary connection to agriculture and cherry, in particular, which could also potentially explain the large presence of this bacteria in the sweet cherry leaf microbiome (Hulin et al., 2018; Hulin et al., 2020; Morris et al., 2013; Morris et al., 2019; Nowell et al., 2016; Shalev et al., 2022; Ruinelli et al., 2022; Wilkinson, Chapter 2; Xin et al., 2018). An important next step would be to determine how many of these *Pseudomonas* recovered from the sweet cherry leaf microbiome are actually *Pss*, which could be determined via qPCR quantification of the *syr*B1 gene specific to *Pss* (Petriccione et al., 2017). Further "Omics" studies should also be undertaken in the future, as well as co-inoculations, as looking into the function of these bacteria and how they interact with each other could indicate how these bacteria are able to cohabitate or dominate in the phyllosphere as well (Vilanova and Porcar, 2016). Ares et al. (2021), found that inoculations of the pathogen *Pseudomonas syringae* pv. *actinidiae* on Kiwi leaves altered the microbiome community structure and relative abundances. While Cui et al. (2021) inoculations with known stigma colonizing bacteria in apple flowers could alter disease pressure by *Erwinia amylovora*. Cernava et al. (2019) also showed that biological control treatments increased tea leaf microbiome diversity.

Jo et al. (2015), curiously did not find *Pseudomonas* to be the most dominant genera, while *Sphingomonas* and *Methylobacterium* were in the four *Prunus* spp. leaf microbiomes they analyzed. In their tart cherry leaf analysis, *Pseudomonas* was third amongst the top four bacterial genera recovered with 258 sequences, proceeded by *Methylobacterium* (865 sequences) and *Sphingomonas* (399 sequences) and followed by *Mucilaginibacter* (120 sequences). In this study analysis of the sweet cherry leaf microbiome, *Sphingomonas* was consistently present in the top taxa (ranging from 4% to 23% relative abundance) at all time points excluding the Spring 2019 (Figure 3.30 and Table 3.14).

The core microbiome of the Michigan sweet cherry leaf was also composed of *Pseudomonas* and *Sphingomonas* OTUs, with the *Pseudomonas* OTUs being dominant and, when combined, make up the lion's share of all the *Pseudomonas*. The Mothur method for determining the core microbiome was opted for based on convenience and ease of use as well as the methods that it applies, which used the number of samples the bacteria are present in (or occupancy/occurrence), as well as the relative abundances (Schloss et al., 2009). Custer et al. (2023) compared four methods that can be used for defining core microbiomes and found that occurrence and abundance used together were the most accurate and that hard cutoff values caused over-inflated core memberships. In this study, analysis of the core microbiome hard cutoff values, such as 97% occurrence (present in 97% of samples), failed to yield a core microbiome, while the less stringent parameter of 50% present in samples did return a core microbiome. In addition to quantifying the number of *Pss*, via qPCR, in the sweet cherry leaf microbiome, it should also be ascertained if any of the core microbiome *Pseudomonas* OTUs (OTU 00001, OTU 00002, OTU 00003 from 2017-2019, and OTU 0001, OTU 0002 from 2019) are possibly *Pss* via phylogenetic comparisons with known *Pss* 16S sequences. The *Sphingomonas* core microbiome OTUs (OTU 00004 from 2017-2019 and OTU 0003, OTU 0007 from 2019) should also be investigated further compared to known 16S sequenced *Sphingomonas* in regard to their potential to be beneficial to sweet cherry itself or as potential biological control agents of *Pss*. *Sphingomonas* recovered from the plant *Arabidopsis thaliana* have been found to promote plant growth, boost plant defense, suppress pathogen growth and disease progression, and grow more slowly than *Pseudomonas* (Innerebner et al., 2011; Lundberg et al., 2022). In terms of hunting additional biological control agents for *Pss*,

microbiome work should be expanded to other sweet cherry tree tissues, as Arrigono et al. (2018) found bark to be a potential reservoir for biological control agents in apple and pear.

Several of the other top taxa found in the sweet cherry leaf microbiome are possible plant growth promoters, such as *Acinetobacter*, *Chryseobacterium,* and *Bradyrhizobium,* which are also found on the rhizosphere (Kuor et al., 2019). While *Xanthomonas,* a known *Prunus* pathogen, and *Curtobacterium*, a bacteria wilt pathogen, also in the top taxa, could be plant growth promoters or possible pathogens on other plants (Chase et al., 2016; Jones and Sutton, 1996). It is likely that many of these top taxa have multiple possible functional roles in the sweet cherry phyllosphere, many of which could likely be beneficial. In addition to being a plant growth promoter, *Methylobacterium* is able to utilize methanol, a volatile organic compound emitted by plants, *Curtobacterium* can degrade organic compounds, while *Pseudomonas* can promote plant growth and suppress bacterial growth (Chase et al., 2016; Bringel and Couée, 2015; Preston, 2004; Sah et al., 2021).

3.6: Conclusions

This is the first time the sweet cherry leaf microbiome has been surveyed to identify the bacteria present in the Michigan sweet cherry orchards, likely living alongside *Pss* as it is a well-known epiphyte. In addition to adding to the previously unknown body of knowledge for the sweet cherry leaf microbiome and ecology, the results of this study provide a foundation for further detailed studies of the sweet cherry microbiome in relation to *Pss*.

There were no regional or cultivar differences in the sweet cherry leaf microbiomes, while season exerted a strong influence on the microbiome. Bacteria populations were low in the spring and increased during summer and fall, whereas the spring communities were quite variable; they began to stabilize during summer and were most stable by fall. Proteobacteria was

the most prevalent phylum in all seasons. The genera *Pseudomonas* was consistent and a dominant presence within the microbiome, serving as an additional driver along with season in directing the stabilization of the microbiome into fall. While all other top taxa present were variable, *Sphingomonas* was consistently present in the top taxa in all seasons, excluding the Spring of 2019, when *Pseudomonas* was nearing 100% relative abundance.

The Michigan sweet cherry leaf microbiome had a core microbiome (present in 50% of samples with at least 1% relative abundance) that also consisted of *Pseudomonas* and *Sphingomonas* OTUs. These OTUs should be studied further to determine if any of the *Pseudomonas* OTUs are *Pss* by phylogenetic comparisons with known *Pss* 16S sequences (100% bootstrap certainty). The *Sphingomonas* OTUs also should be studied to determine if they share any phylogenetic relationships with known beneficial *Sphingomonas* spp. as possible biological control agents for *Pss* or as plant beneficials. Further analysis of the microbiome DNA from this study could also quantify the number of the *Pss* present in the samples via qPCR.

Continuing research into the sweet cherry microbiome could expand to other tissues (flowers, bark, buds, roots) to determine if *Pseudomonas* is strongly present in all organs of the tree across seasons. Leaf microbiomes from Michigan's southern and northern fruit belt regions could be assessed for regional differences. Future work should determine how the microbiome shifts with the inoculation of virulent *Pss* (and vice versa), and how the microbiome changes with the addition of biological control agents. The spring microbiome should be examined for C-N movement within the leaves in correlation to the microbiome (or core microbiome) and the presence of *Pss* and disease pressure, alone and relative to the harshness of winter or frost events. This could explain the variability in spring populations more definitively. Other "omics" type studies and co-inoculation experiments could determine the function or role that these bacteria

play within the leaf microbiome, as many could potentially be beneficial to the sweet cherry tree. This could also shed light on how they are all able to live together in the same environment, especially with *Pseudomonas* as the strongest presence.

This research is the first documentation of the sweet cherry leaf microbiome bacterial community that Xin et al. (2018) considers to be the 4th vertex of the disease triangle. Much has yet to be ascertained as to how these bacteria could be manipulated in order to manage *Pss* populations and subsequently reduce disease incidence.

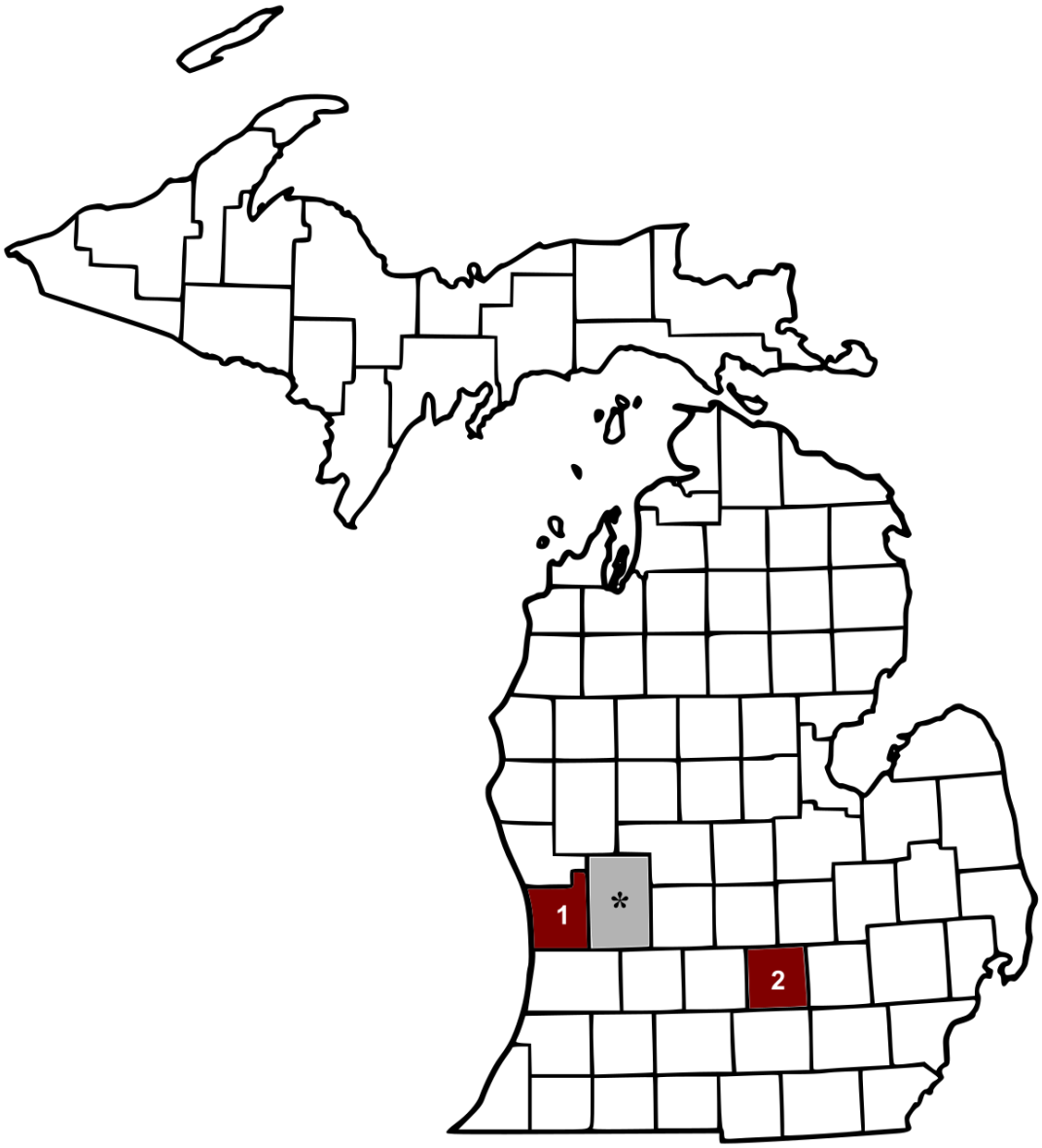


Figure 3.1. Michigan orchards where the sweet cherry cultivars were planted for surveying the sweet cherry leaf microbiome. Red highlighted counties are where site 1: Wells Orchards, Grand Rapids MI, (Ottawa Co.), and site 2: Michigan State University Horticulture Teaching and Research Center, Holt MI, (Ingham Co.) is located, the gray highlighted county site *: Kraft Orchards, Sparta MI, (Kent Co.) is where the weather station is located used for site 1 weather data (~24 km, North of site 1).



Figure 3.2. Sampling sweet cherry leaves for microbiome analysis, **A)** wearing gloves sanitized with 75% ethanol, leaves were selected individually from the terminal end of branches and placed into sterile Whirl-Pak® bags, and **B)** the length and width of each leaf was measured and then placed into a cooler for transport to the laboratory.

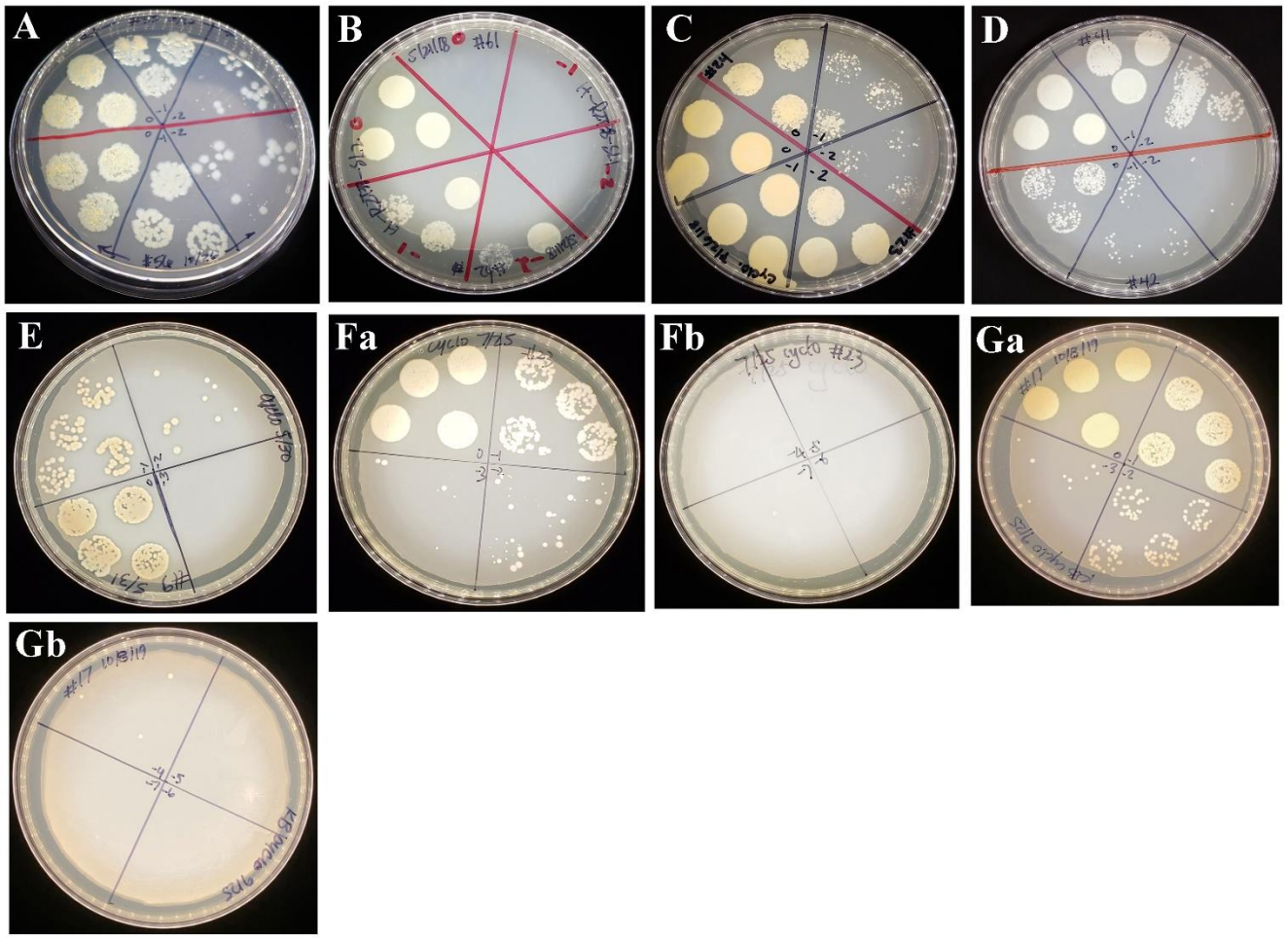


Figure 3.3. Examples of the King's B (KB) media amended with 50 µg/ml cycloheximide used for counting culturable bacteria from the sweet cherry leaf microbiome, **A-D)** colonies from serial dilutions of 0, 10^{-1}, and 10^{-2} with 2 leaf samples/plate in Fall 2017, Spring, Summer, and Fall 2018 respectively, **E)** colonies from serial dilutions of 0, 10^{-1}, 10^{-2}, and 10^{-3} with a single leaf sample/plate in Spring 2019, **Fa-Gb)** colonies from serial dilutions of 0, 10^{-1}, 10^{-2}, and 10^{-3} with a single leaf sample/plate and dilutions of 10^{-4}, 10^{-5}, 10^{-6}, and 10^{-7} from the same single leaf sample in Summer (Fa, Fb) and Fall 2019 (Ga, Gb) respectively.

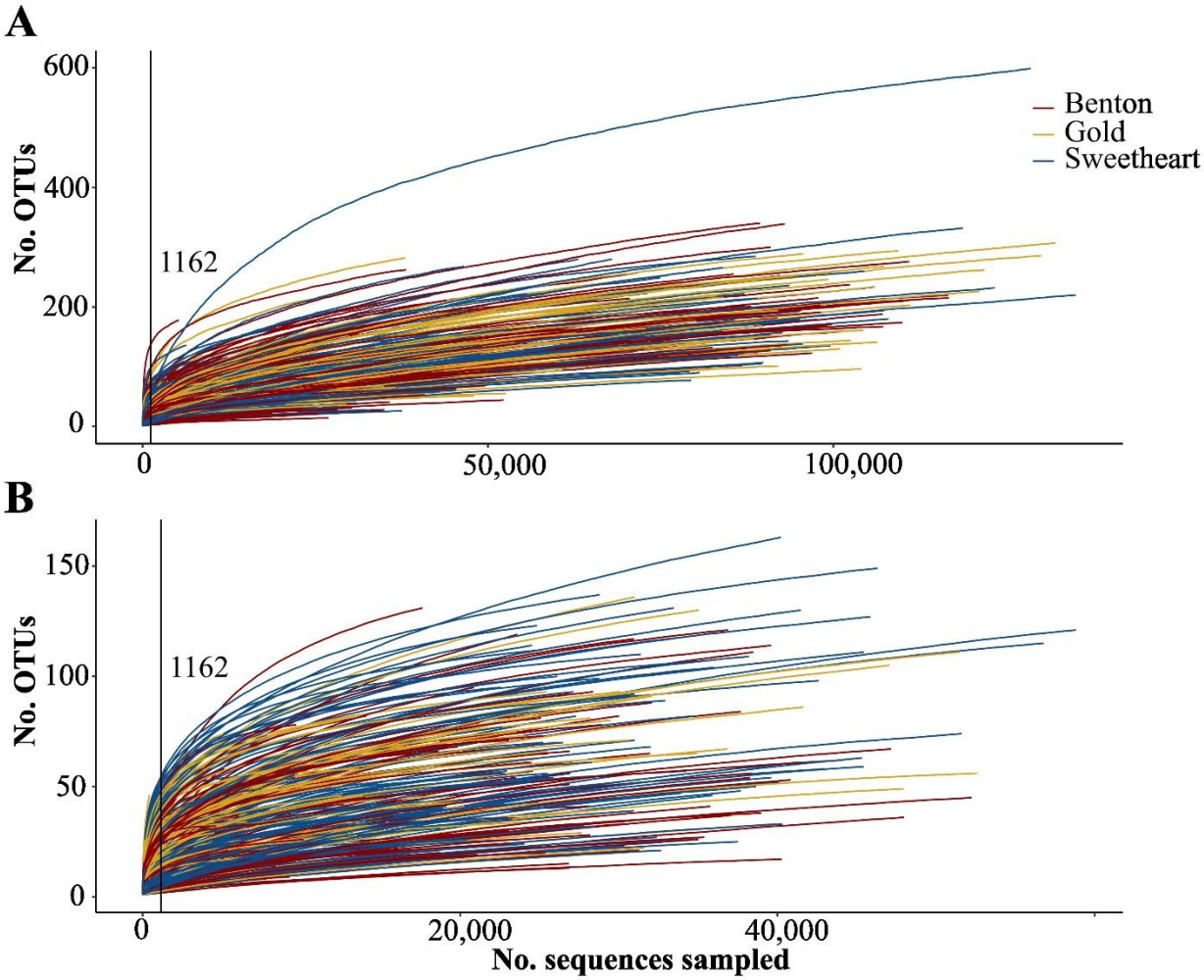


Figure 3.4. The rarefaction curves demonstrate the sampling effort with the number of OTUs and number of sequences per sample from the sweet cherry cultivars 'Benton', 'Gold', and 'Sweetheart' sampled from two sites in Michigan, with OTUs assigned according to 97% sequence identity **A)** includes the curves for the 2017-2019 sampling seasons (Fall 2017, Spring, Summer, Fall 2018, and Spring, Summer, Fall 2019) and **B)** includes the curves for the 2019 sampling season (Spring, Summer, and Fall) which included 3 technical replications/ leaf sample, the vertical line in both graphs denotes subsampling at 1162 sequences.

Table 3.1. The ANOVA tables for the α-diversity statistics, bacteria plate counts (log cfu/cm^2), the number of OTUs (no. OTUs), the Shannon diversity, and Shannon evenness indices. Following the linear mixed model with site, cultivar, and time as fixed effects and nested random effects of (1 | site:row) + (1 | site:row:tree), with significance determined by p-value ≤ 0.05.

α-statistic	Model term	df1	df2	F-ratio	p-value
log cfu/cm^2	site	1	5.63	1.100	0.3373
	cultivar	2	12.43	0.411	0.6714
	time	6	440.50	108.805	**<0.0001**
no. OTUs	site	1	6.28	1.031	0.3475
	cultivar	2	12.68	0.368	0.6993
	time	6	363.55	36.369	**<0.0001**
Shannon diversity index	site	1	6.81	0.156	0.7048
	cultivar	2	11.77	0.846	0.4535
	time	6	364.62	29.206	**<0.0001**
Shannon evenness index	site	1	6.83	0.000	0.9996
	cultivar	2	11.74	1.101	0.3646
	time	6	364.68	24.127	**<0.0001**

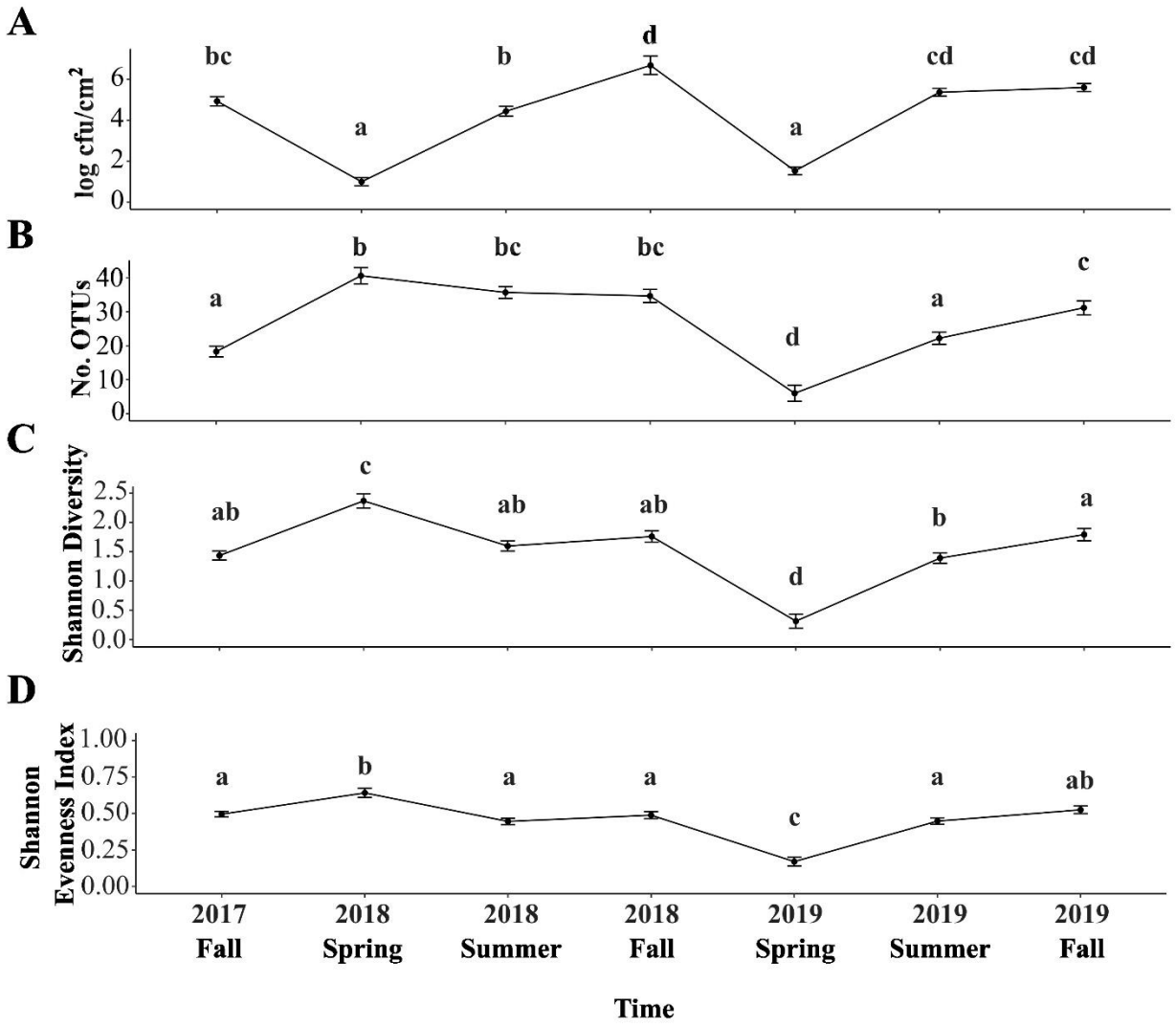


Figure 3.5. Mean alpha diversity metrics ± SE for the sweet cherry leaf microbiome over time with letters indicating statistical differences for each individual statistic: **A)** cultured bacteria colony counts (log cfu/m^2 of leaf area), **B)** the observed number of OTUs (spp. richness), **C)** the Shannon diversity index (spp. richness and evenness) and **D)** the Shannon evenness index (spp. evenness) calculated from 16S rDNA sequenced from 3 ml of leaf wash.

Table 3.2. The ANOVA tables following the test for Beta-dispersion (homogeneity of variances) and the Permutational analysis of variances (PERMANOVA) (999 permutations) of the Bray-Curtis dissimilarity index to determine the differences in community composition in the sweet cherry leaf microbiome sampled at different times (seasons).

Beta-dispersion ANOVA						
Model term		**df**	**Sum of Squares**	**Mean squares**	**F-value**	**p-value**
cultivar	Groups	2	0.009	0.004	0.368	0.6921
	Residuals	381	4.390	0.012		
site	Groups	1	0.1504	0.150	14.203	**0.0002**
	Residuals	382	4.0463	0.011		
time	Groups	6	1.808	0.301	25.442	**< 2.2e-16**
	Residuals	377	4.465	0.012		
row	Groups	3	0.033	0.011	0.995	0.3951
	Residuals	380	4.240	0.011		
tree	Groups	16	0.425	0.027	2.162	**0.0060**
	Residuals	367	4.507	0.012		

PERMANOVA					
Model term	**df**	**Sum of Squares**	**R^2**	**F-value**	**p-value**
cultivar	2	0.984	0.008	2.277	**0.0090**
time	6	23.009	0.196	17.746	**0.0010**
site	1	0.778	0.007	3.598	0.9990
cultivar*time	12	4.568	0.039	1.762	**0.0010**
time*site	5	8.406	0.072	7.779	**0.0010**
site*row	6	1.525	0.013	1.176	0.1820
site*row*tree	15	5.441	0.046	1.679	**0.0010**
Residual	336	72.610	0.619		
Total	383	117.320	1.000		

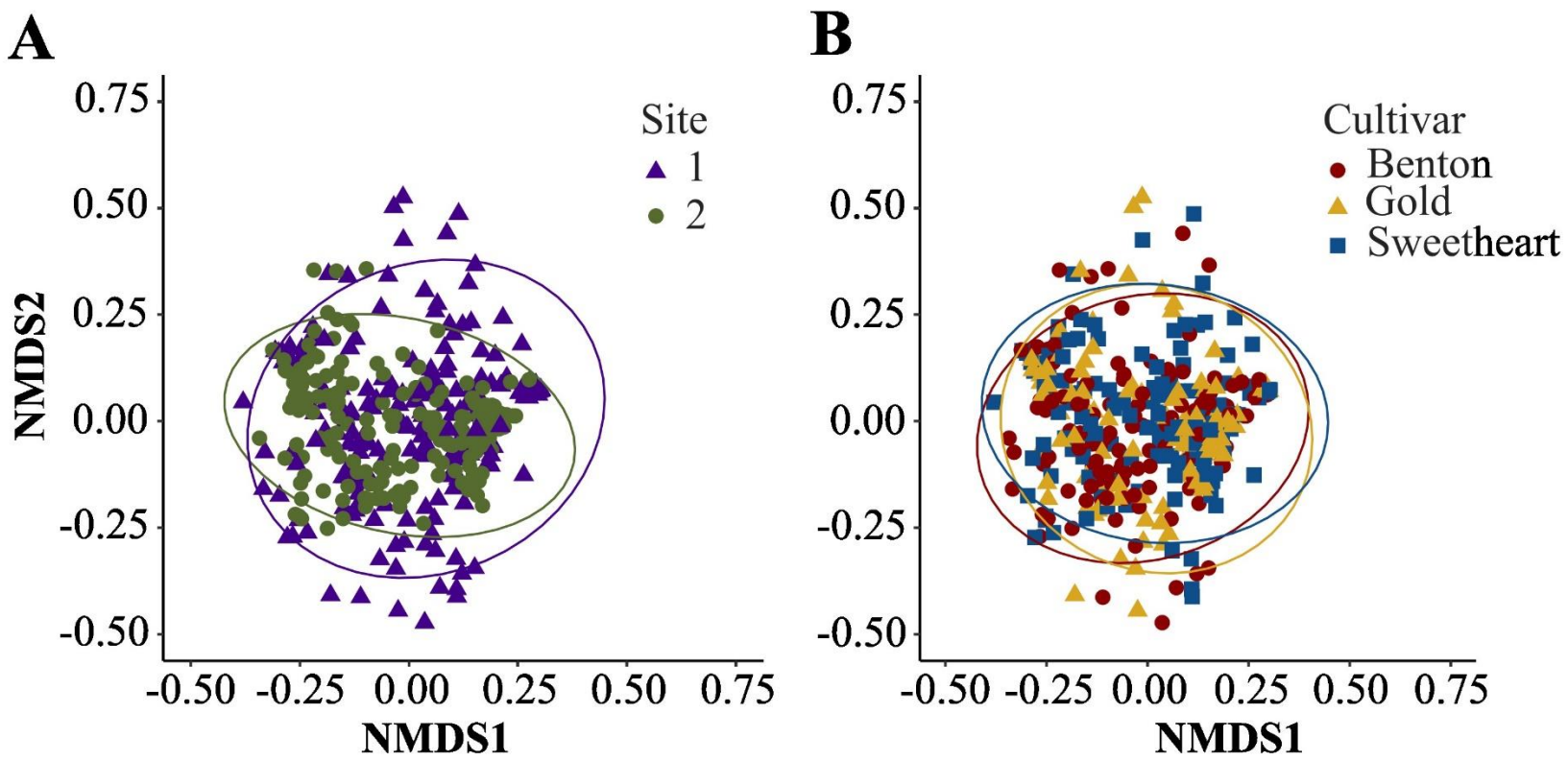


Figure 3.6. The Nonmetric multidimensional scaling (NMDS) ordination of the Bray-Curtis dissimilarities to show the relationship between bacteria community composition of the sweet cherry leaf microbiome from **A)** two sites in Michigan (Ottawa Co. and Ingham Co.) and from **B)** the three sweet cherry cultivars ('Benton', 'Gold', and 'Sweetheart') that the leaves and leaf microbiomes were sampled from over time (Fall 2017, and Spring, Summer, and Fall 2018 and 2019). The ellipses represent the 95% confidence intervals for each parameter (site or cultivar). Stress k=0.216.

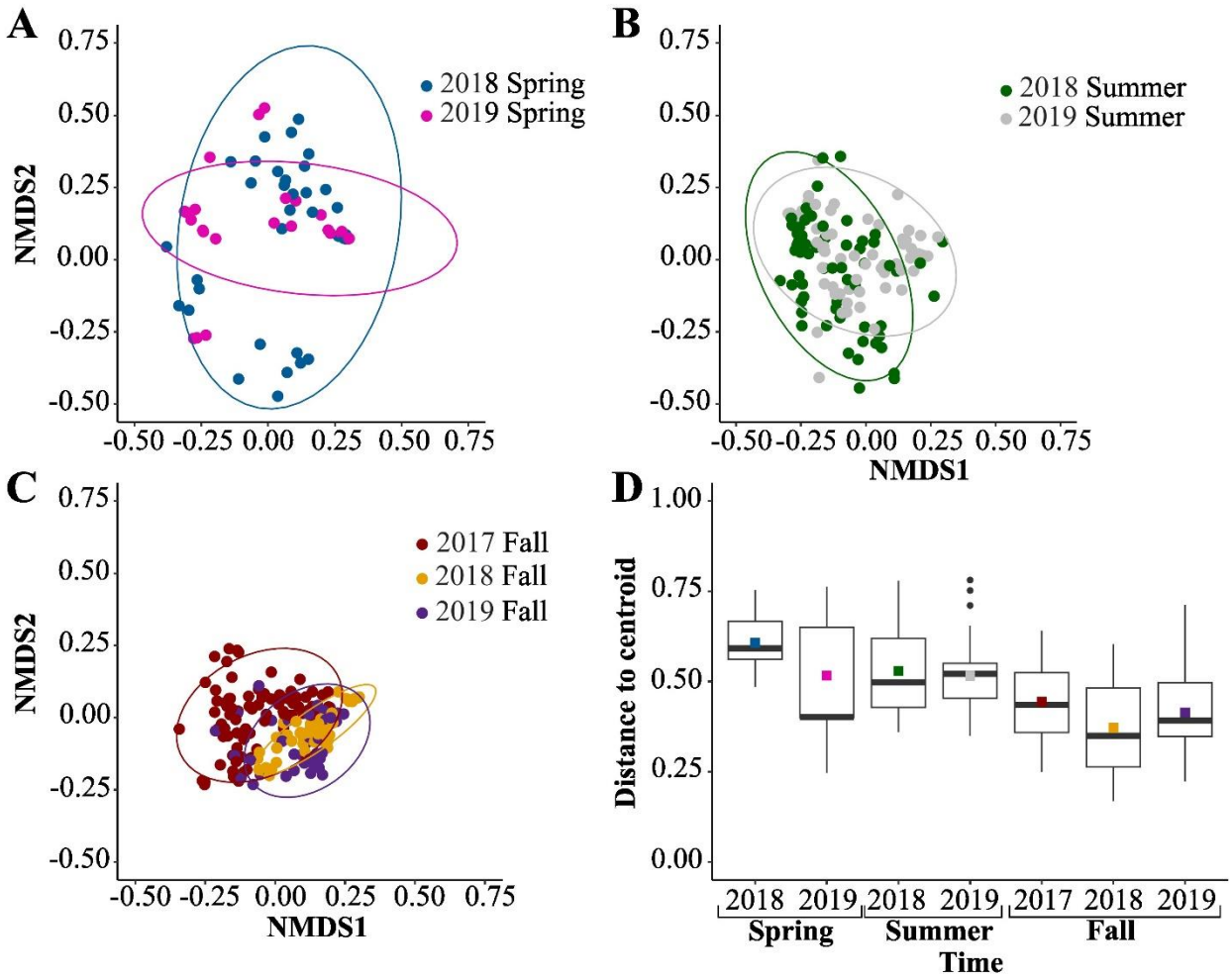


Figure 3.7. The Nonmetric multidimensional scaling (NMDS) ordination of the Bray-Curtis dissimilarities (stress k=0.216) to show the relationship between bacteria community composition of the Michigan sweet cherry leaf microbiome over time for **A)** Spring 2018 and 2019, **B)** Summer 2018 and 2019, **C)** and Fall 2017, 2018, and 2019 where the ellipses represent the 95% confidence intervals for each time, and **D)** is a box plot of the distributions of the distances from the centroid for samples at each time point where the solid black bar is the median, and the colored square points indicate the mean distance from the centroid.

Table 3.3. The ANOVA tables for the relative abundance of the top four Phyla and rarer Phyla combined into "other", and the relative abundance at the deepest taxonomic level (genus) of *Pseudomonas,* and all "other" taxa at the deepest taxonomic level (genus or family) combined. Following the linear mixed model with site, cultivar, time, phylum (or genus), and time*phylum (or time*genus) as fixed effects and nested random effects of (1 | site:row) + (1 | site:row:tree), with significance determined by p-value ≤ 0.05.

α-statistic	Model term	df1	df2	F-ratio	p-value
Relative abundance	site	1	6.97	0.000	1.0000
Top Phyla	cultivar	2	11.58	0.000	1.0000
	time	6	1425.47	0.000	1.0000
	phylum	4	1864.07	8894.394	**<0.0001**
	time*phylum	24	1864.07	31.653	**<0.0001**
Relative abundance	site	1	6.97	0.000	1.0000
Pseudomonas	cultivar	2	11.58	0.000	1.0000
	time	6	694.12	0.000	1.0000
	genus	1	733.07	57.870	**<0.0001**
	time*genus	6	733.07	48.879	**<0.0001**

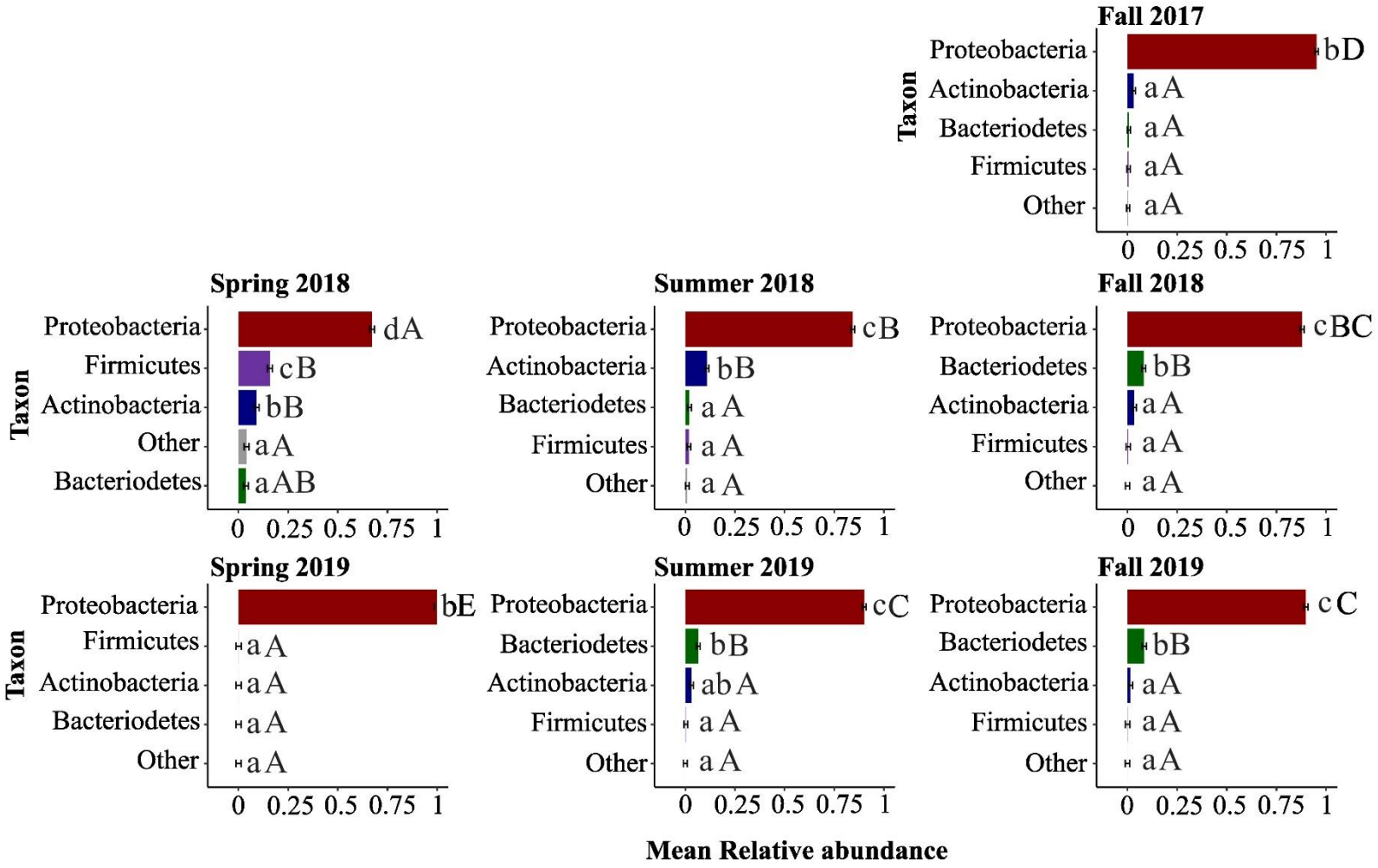


Figure 3.8. The mean relative abundance ± SE of the top 4 Phyla and the rarer Phyla combined into "other" that make up the sweet cherry leaf microbiome for Fall 2017, Spring, Summer, and Fall 2018, and Spring, Summer, and Fall 2019. Lower-case letters indicate statistical differences in Phyla within each time (season), and the upper-case letters indicate statistical differences of each Phyla across each time. With significance determined by p-value ≤0.05

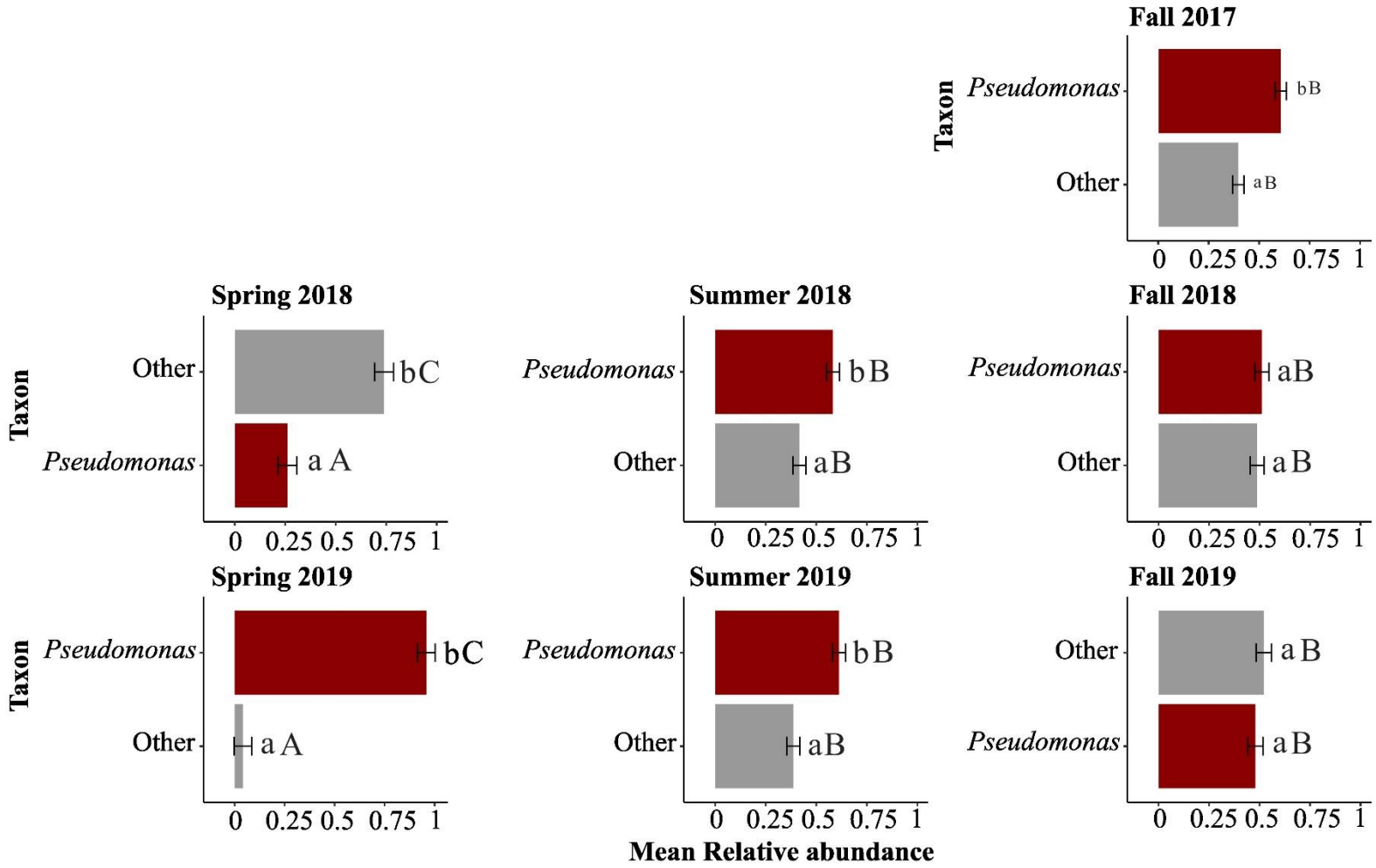


Figure 3.9. The mean relative abundances of *Pseudomonas* and all "other" taxa at the genus/family level ± SE in the sweet cherry leaf microbiome. Letters indicate statistical differences, lower-cased letters indicate statistical differences within each time, while upper-cased letters indicate statistical differences of each *Pseudomonas* or "other" across time, with significance determined by p-value ≤ 0.05.

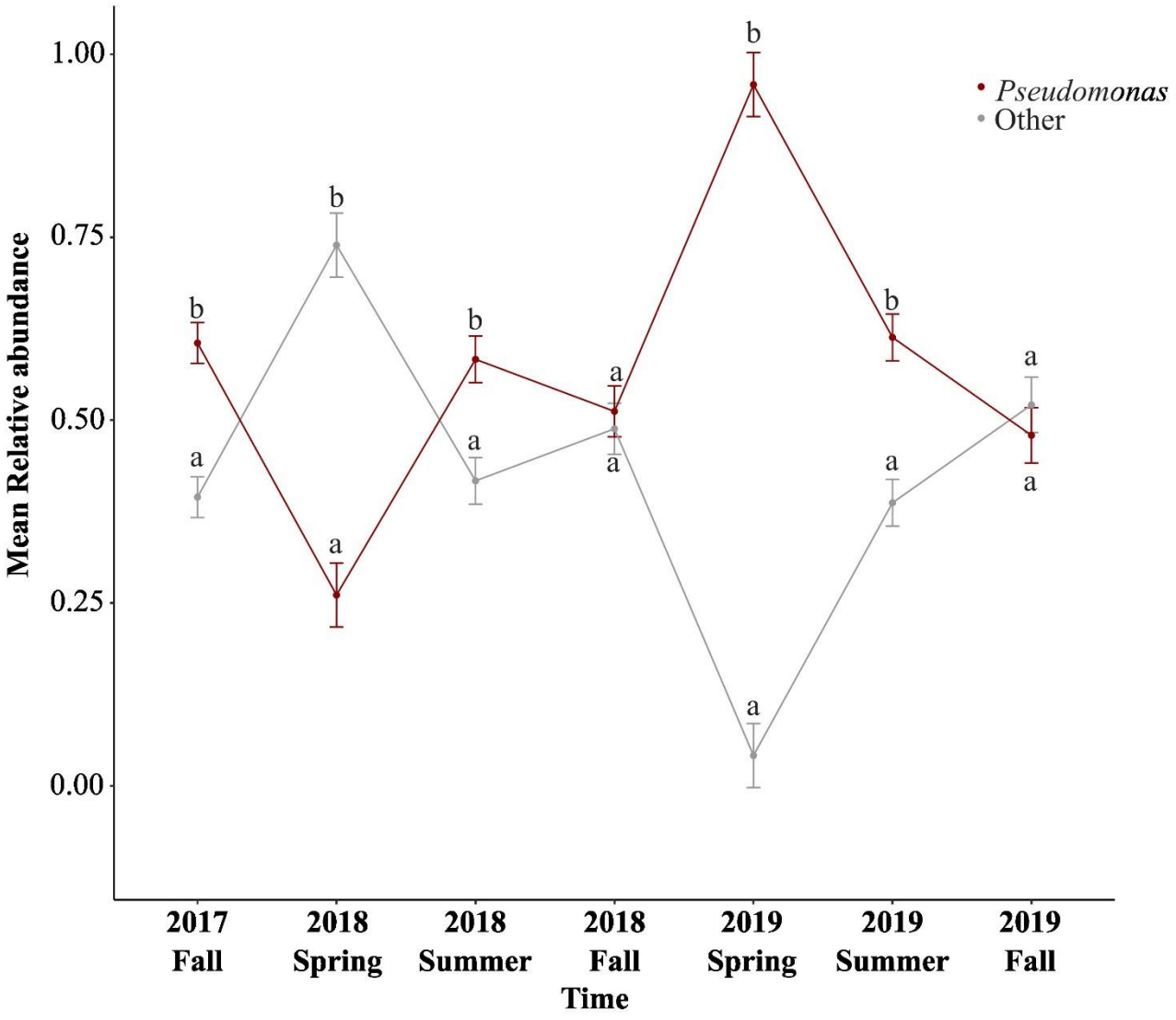


Figure 3.10. Visualization highlighting the modulating influence that *Pseudomonas* appears to have on the "other" taxa in the sweet cherry leaf microbiome with evident community stabilization by Fall. Values are the mean relative abundances of *Pseudomonas* and all "other" taxa at the genus/family level ± SE over each time point (season), lower-cased letters indicate statistical differences within each time, with significance determined by p-value ≤ 0.05.

Table 3.4. The ANOVA tables of the top deepest taxonomic level (genus or family) by time (season) where taxa of relative abundance <0.03 were combined into "other". Following the linear mixed model with site, cultivar, and taxa as fixed effects and nested random effects of (1 | site:row) + (1 | site:row:tree), with significance determined by p-value ≤ 0.05. Spring 2018 is for site 1 only with the linear mixed model sans site. The ANOVA table of the core microbiome relative abundances (genus and OTU identifier), the rest of the combined *Pseudomonas* and combined *Sphingomonas,* and the remaining taxa combined as "other". Following the linear mixed model with site, cultivar, time, genus, and time*genus as fixed effects and nested random effects of (1 | site:row) + (1 | site:row:tree).

α-statistic	Model term	df1	df2	F-ratio	p-value
Relative abundance					
Top deepest taxa by time					
Fall 2017	site	1	5.51	0.000	1.0000
	cultivar	2	12.15	0.000	1.0000
	taxa	4	394.16	179.468	**<0.0001**
Spring 2018	cultivar	2	4.40	0.000	1.0000
	taxa	7	270.28	38.533	**<0.0001**
Summer 2018	site	1	4.72	0.000	1.0000
	cultivar	2	10.26	0.000	1.0000
	taxa	4	302.47	68.751	**<0.0001**
Fall 2018	site	1	4.32	0.000	1.0000
	cultivar	2	8.58	0.000	1.0000
	taxa	4	300.70	119.306	**<0.0001**
Spring 2019	site	1	7.72	0.000	1.0000
	cultivar	2	3.97	0.000	1.0000
	taxa	2	88.95	1438.871	**<0.0001**
Summer 2019	site	1	6.28	0.000	1.0000
	cultivar	2	10.27	0.000	1.0000
	taxa	5	359.74	141.591	**<0.0001**
Fall 2019	site	1	5.17	0.000	1.0000
	cultivar	2	9.26	0.000	1.0000
	taxa	6	300.43	79.168	**<0.0001**
Relative abundance	site	1	6.97	0.000	1.0000
Core Taxa	cultivar	2	11.58	0.000	1.0000
	time	6	1774.48	0.000	1.0000
	genus	6	2618.07	122.153	**<0.0001**
	time*genus	36	2618.07	17.591	**<0.0001**

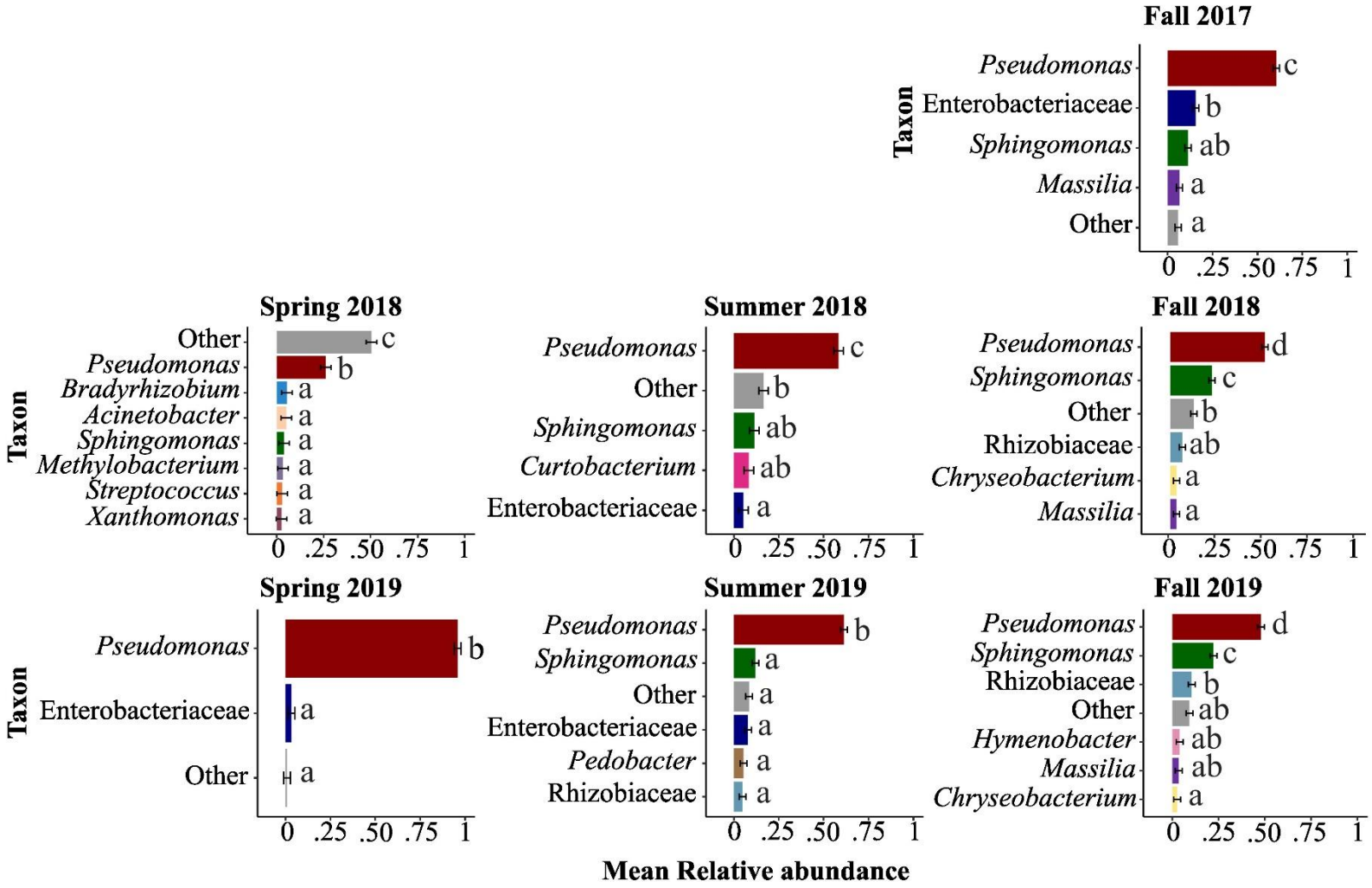


Figure 3.11. The mean relative abundances ± SE of the top deepest taxonomic level (genus or family) for the sweet cherry leaf microbiome by time (season) in which taxa of relative abundance <0.03 were combined into "other". Letters indicate statistical differences, with significance determined by p-value ≤ 0.05.

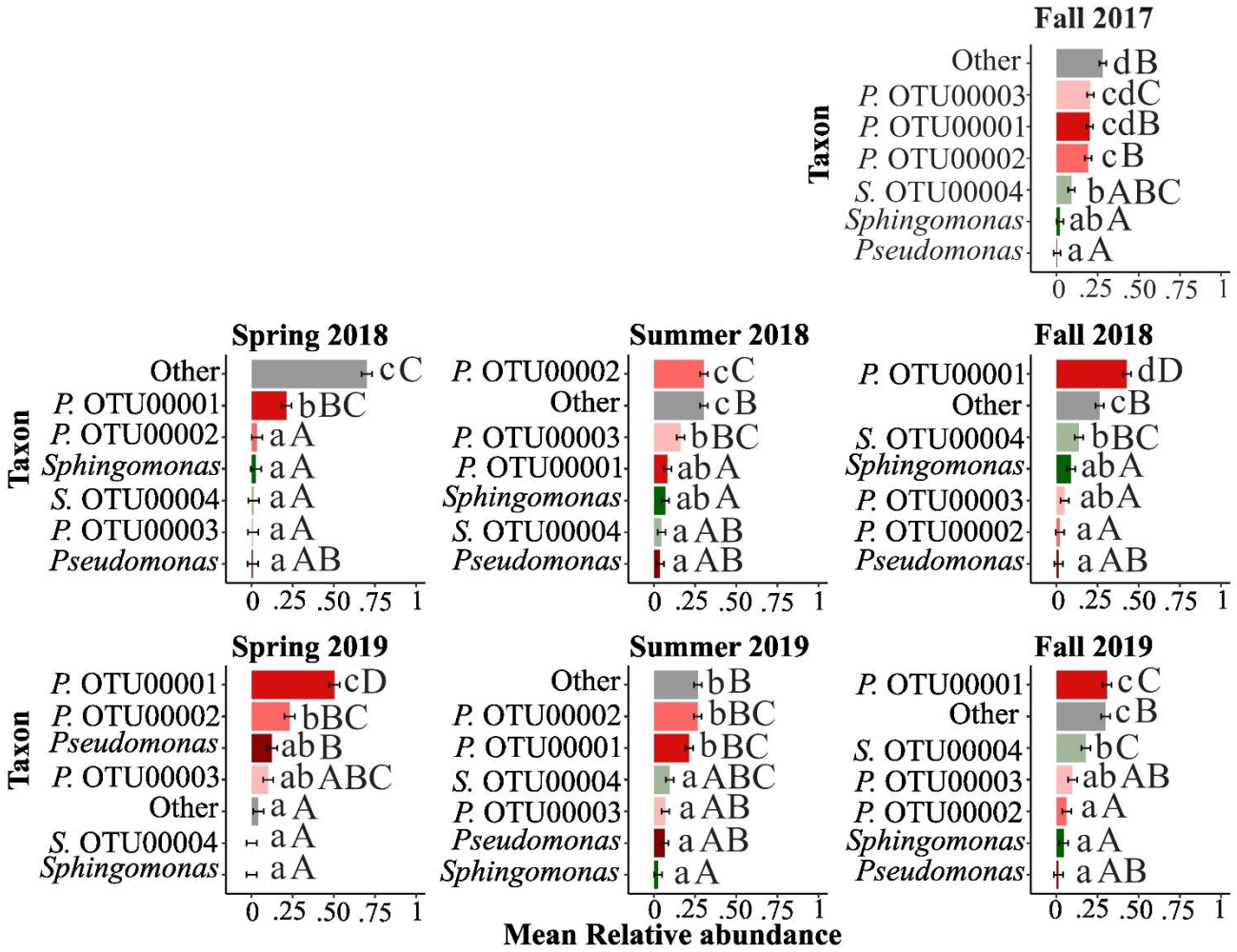


Figure 3.12. The mean relative abundances of the core microbiome taxon (genus [*P.* (*Pseudomonas*) and *S.* (*Sphingomonas*)] and OTU identifier), the rest of the combined *Pseudomonas* and combined *Sphingomonas*, and the remaining combined "other" taxa ± SE over time (season). Letters indicate statistical differences, lower-cased letters are within each time, while upper-cased letters indicate statistical differences of each genus/OTU across time, with significance determined by p-value ≤ 0.05.

Table 3.5. The 2019 ANOVA tables for the α-diversity statistics, bacteria plate counts (log cfu/cm^2), the number of OTUs (no. OTUs), the Shannon diversity, and Shannon evenness indices. Following the linear mixed model with site, cultivar, season, and site*season as fixed effects and nested random effects of (1|site:row)+(1|site:row:tree) for the log cfu/cm^2 and (1 | site:row) + (1 | site:row:tree)+(1|site:row:tree:leaf) for the remaining α-diversity statistics, with significance determined by p-value ≤ 0.05.

α-statistic	Model term	df1	df2	F-ratio	p-value
log cfu/cm^2	site	1	5.54	0.888	0.3854
	cultivar	2	11.75	1.456	0.2722
	season	2	226.00	231.684	**<0.0001**
	site*season	2	226.00	10.968	**<0.0001**
no. OTUs	**site**	1	7.39	27.343	**0.0010**
	cultivar	2	11.22	0.380	0.6921
	season	2	289.16	157.640	**<0.0001**
	site*season	2	289.71	4.985	**0.0074**
Shannon diversity index	**site**	1	7.26	11.215	**0.0116**
	cultivar	2	11.36	0.257	0.7780
	season	2	287.63	125.751	**<0.0001**
	site*season	2	288.10	2.046	0.1312
Shannon evenness index	site	1	7.28	4.226	0.0773
	cultivar	2	11.34	0.077	0.9268
	season	2	287.90	79.149	**<0.0001**
	site*season	2	288.39	4.141	**0.0129**

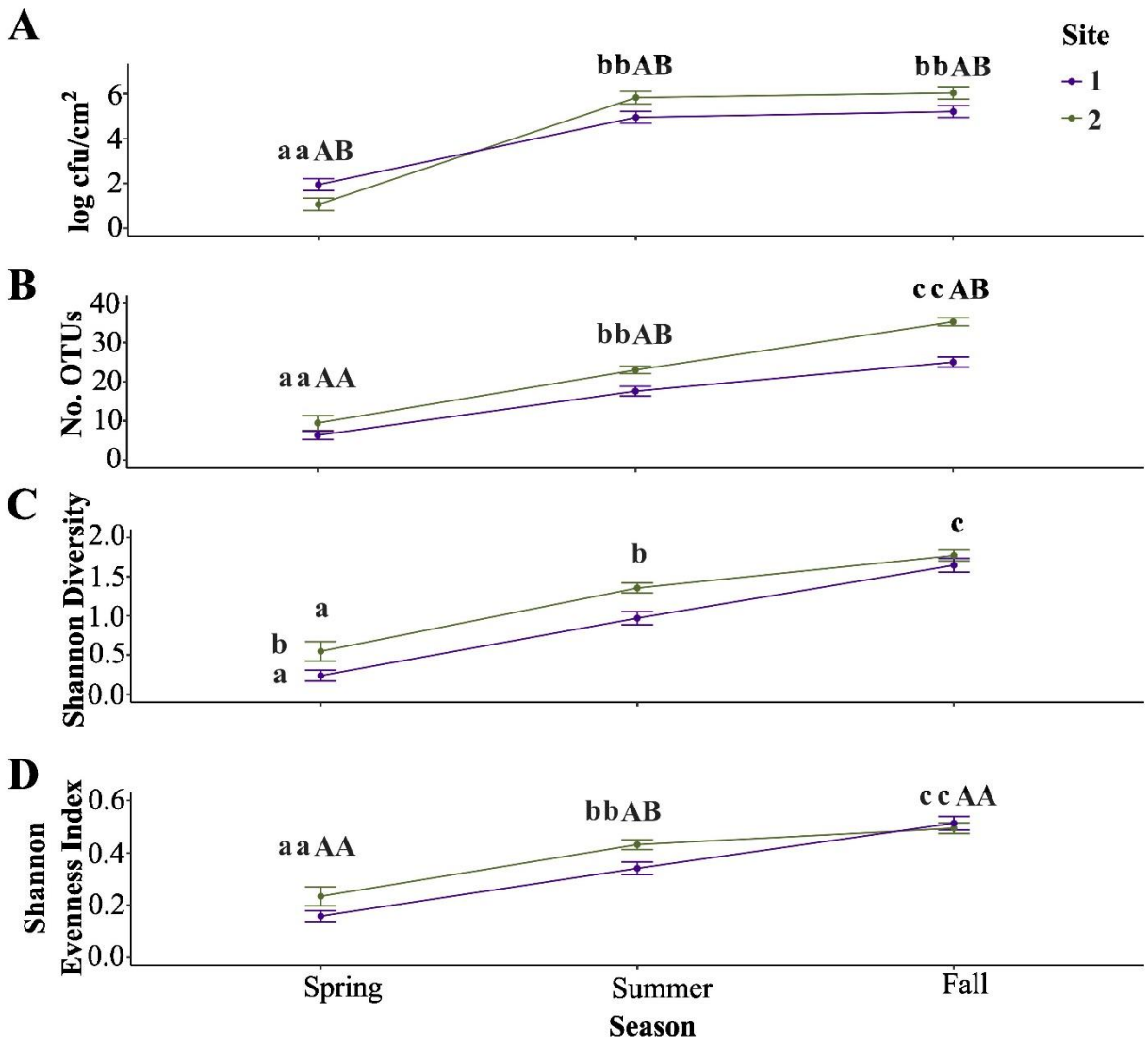


Figure 3.13. Mean alpha diversity metrics ± SE, 2019, for the sweet cherry leaf microbiome for the two sites in Michigan, over three seasons. For each individual statistic the lower-cased letters indicate statistical differences in season within each site and the upper-cased letters indicate statistical differences between the two sites for each season, with an exception for the Shannon diversity index for which the two lower-cased letters at the end of each line graph indicated statistical differences between the two sites and the letter above the line graphs indicate statistical differences between seasons. **A)** cultured bacteria colony counts (log cfu/m^2 of leaf area), **B)** the observed number of OTUs (spp. richness), **C)** the Shannon diversity index (spp. richness and evenness) and **D)** the Shannon evenness index (spp. evenness) calculated from 16S rDNA sequenced from 3 ml of leaf wash.

Table 3.6. The 2019 ANOVA tables following the test for Beta-dispersion (homogeneity of variances) and the Permutational analysis of variances (PERMANOVA) (999 permutations) of the Bray-Curtis dissimilarity index to determine the differences in community composition in the sweet cherry leaf microbiome sampled at different seasons.

Beta-dispersion ANOVA						
Model term		**df**	**Sum of Squares**	**Mean squares**	**F-value**	**p-value**
cultivar	Groups	2	0.041	0.021	1.009	0.3658
	Residuals	322	6.560	0.020		
site	Groups	1	0.336	0.336	17.632	**3.47e-05**
	Residuals	323	6.162	0.019		
season	Groups	2	0.798	0.399	22.095	**1.018e-09**
	Residuals	322	5.813	0.018		
row	Groups	3	0.247	0.082	4.340	**0.0051**
	Residuals	321	6.080	0.019		
tree	Groups	14	0.626	0.045	2.172	**0.0088**
	Residuals	310	6.380	0.021		
leaf	Groups	3	0.021	0.007	0.351	0.7888
	Residuals	321	6.349	0.020		

PERMANOVA					
Model term	**df**	**Sum of Squares**	**R^2**	**F-value**	**p-value**
cultivar	2	1.615	0.022	6.778	**0.0010**
season	2	11.436	0.156	47.979	**0.0010**
site	1	1.034	0.014	8.675	0.3560
cultivar*season	4	3.248	0.044	6.813	**0.0010**
season*site	2	4.578	0.062	19.206	**0.0010**
site*row	6	1.860	0.025	2.601	**0.0010**
site*row*tree	12	4.478	0.061	3.131	**0.0010**
site*row*tree*leaf	60	17.277	0.235	2.416	**0.0010**
Residual	235	28.006	0.381		
Total	324	73.531	1.000		

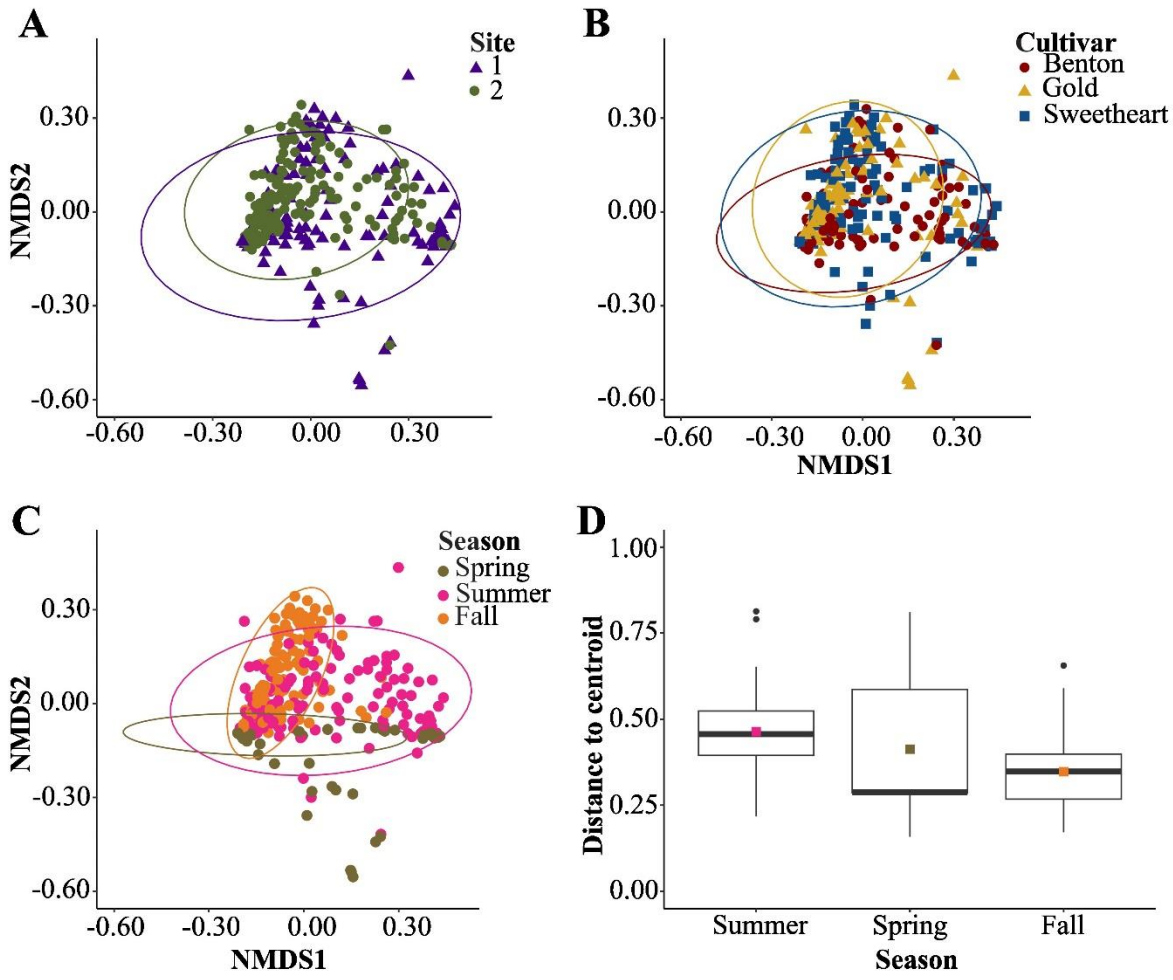


Figure 3.14. The 2019 Nonmetric multidimensional scaling (NMDS) ordination of the Bray-Curtis dissimilarities (stress k=0.136) to show the relationship between bacteria community composition of the Michigan sweet cherry leaf microbiome for **A)** the two sites where leaves were sampled, **B)** the three sweet cherry cultivars ('Benton', 'Gold', and 'Sweetheart') that the leaves and leaf microbiomes were sampled from, and **C)** the three sampling seasons (Spring, Summer, and Fall) for which the ellipses represent the 95% confidence intervals for each time, and **D)** is a box plot of the distributions of the distances from the centroid for samples in each season for which the solid black bar is the median, and the colored square points indicate the mean distance from the centroid.

Table 3.7. The 2019 ANOVA tables for the relative abundance of the top four Phyla and rarer Phyla combined into "other", and the relative abundance at the deepest taxonomic level (genus) of *Pseudomonas*, and all "other" taxa at the deepest taxonomic level (genus or family) combined. Following the linear mixed model with site, cultivar, season, phylum (or genus), and season*phylum (or season*genus) as fixed effects and nested random effects of (1|site:row)+(1|site:row:tree)+(1|site:row:tree:leaf), with significance determined by p-value ≤ 0.05.

α-statistic	Model term	df1	df2	F-ratio	p-value
Relative abundance	site	1	7.17	0.000	1.0000
Top Phyla	cultivar	2	10.08	0.000	1.0000
	season	2	564.66	0.000	1.0000
	phylum	4	1543.34	20916.890	**<0.0001**
	season*phylum	8	1543.34	33.282	**<0.0001**
Relative abundance	site	1	7.17	0.000	1.0000
Pseudomonas	cultivar	2	10.08	0.000	1.0000
	season	2	411.89	0.000	1.0000
	genus	1	577.34	707.545	**<0.0001**
	season*genus	2	577.34	257.777	**<0.0001**

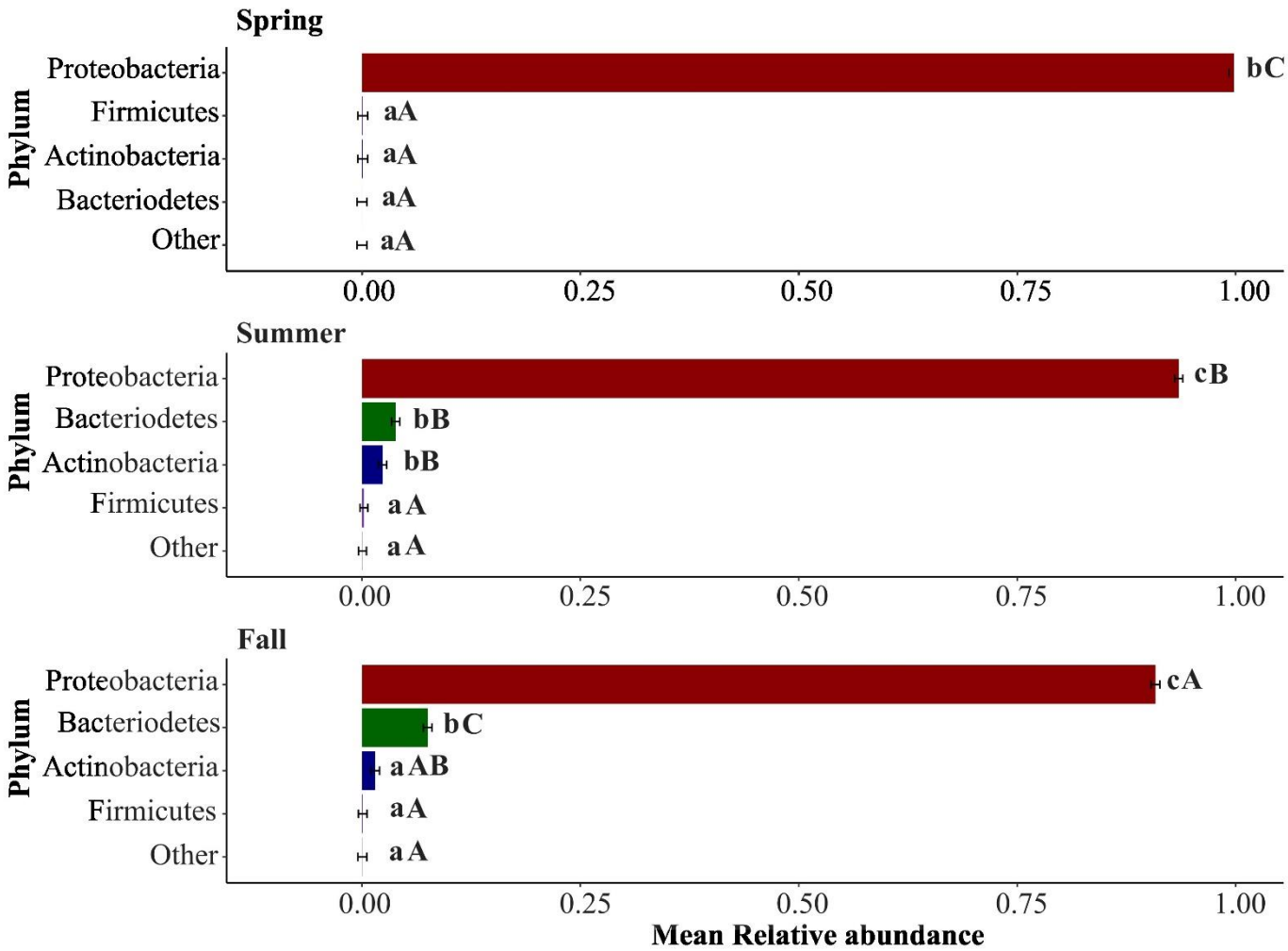


Figure 3.15. The 2019 mean relative abundance ± SE of the top 4 Phyla and the rarer Phyla combined into "other" that make up the sweet cherry leaf microbiome for Spring, Summer, and Fall. Lower-case letters indicate statistical differences in Phyla within each season, and the upper-case letters indicate statistical differences of each Phyla across each season, with significance determined by p-value ≤0.05.

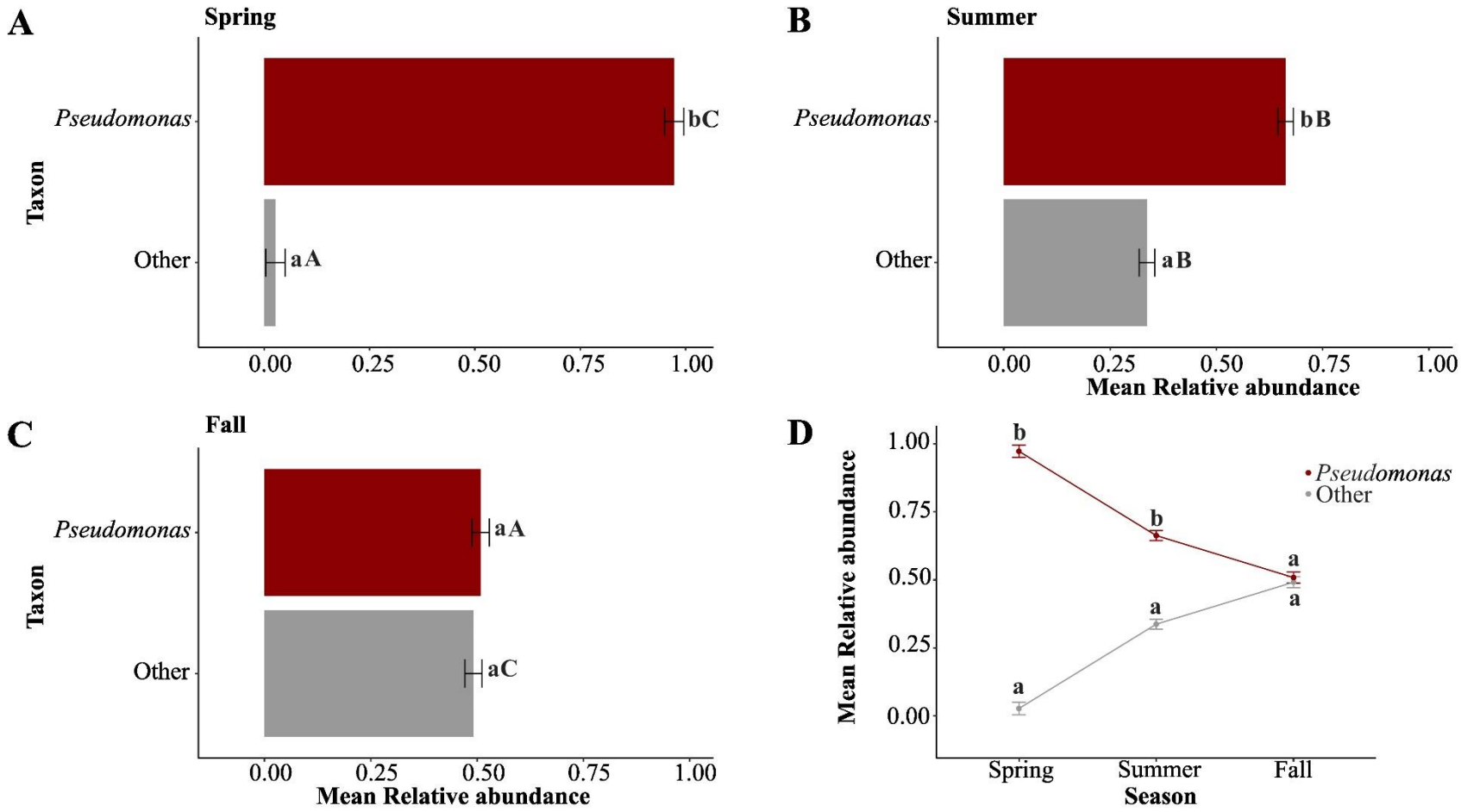


Figure 3.16. The 2019 mean relative abundances of *Pseudomonas* and all "other" taxa at the genus/family level ± SE in the sweet cherry leaf microbiome for **A)** Spring, **B)** Summer, **C)** Fall, and **D)** the visualization highlighting the influence that *Pseudomonas* appears to have on the "other" taxa in the sweet cherry leaf microbiome with evident community stabilization by Fall. Letters indicate statistical differences, lower-cased letters indicate statistical differences within each season, while upper-cased letters indicate statistical differences of each *Pseudomonas* or "other" across seasons, with significance determined by p-value ≤ 0.05.

Table 3.8. The 2019 ANOVA tables of the top deepest taxonomic level (genus or family) by season where taxa of relative abundance <0.03 were combined into "other". Following the linear mixed model with site, cultivar, and genus as fixed effects and nested random effects of (1|site:row)+(1|site:row:tree)+(1|site:row:tree:leaf) with significance determined by p-value ≤ 0.05. The 2019 ANOVA table of the core microbiome relative abundances (genus and OTU identifier), the rest of the combined *Pseudomonas* and combined *Sphingomonas,* and the remaining taxa combined as "other". Following the linear mixed model with site, cultivar, season, genus, and season*genus as fixed effects and nested random effects of (1|site:row)+(1|site:row:tree)+(1|site:row:tree:leaf).

α-statistic	Model term	df1	df2	F-ratio	p-value
Relative abundance Top deepest taxa by season					
Spring	site	1	13.62	0.000	1.0000
	cultivar	2	5.04	0.000	1.0000
	genus	1	137.37	7563.751	**<0.0001**
Summer	site	1	7.49	0.000	1.0000
	cultivar	2	8.96	0.000	1.0000
	genus	6	848.97	410.924	**<0.0001**
Fall	site	1	5.23	0.000	1.0000
	cultivar	2	8.99	0.000	1.0000
	genus	6	692.36	227.867	**<0.0001**
Relative abundance Core Taxa	site	1	7.17	0.000	1.0000
	cultivar	2	10.08	0.000	1.0000
	season	2	604.09	0.000	1.0000
	genus	6	2187.34	245.136	**<0.0001**
	season*genus	12	2187.34	28.563	**<0.0001**

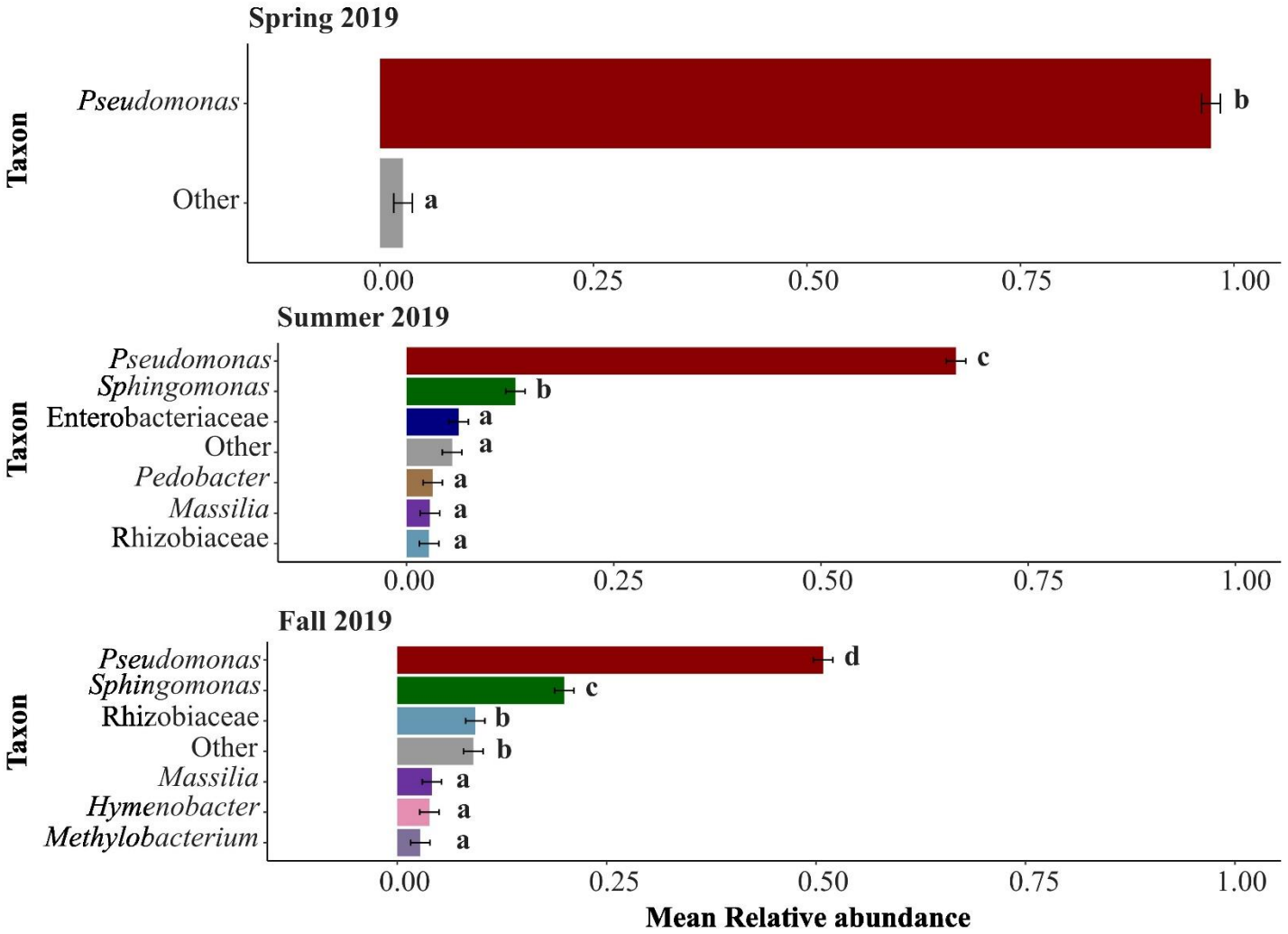


Figure 3.17. The 2019 mean relative abundances ± SE of the top deepest taxonomic level (genus or family) for the sweet cherry leaf microbiome by season in which taxa of relative abundance <0.03 were combined into "other". Letters indicate statistical differences within season, with significance determined by p-value ≤ 0.05.

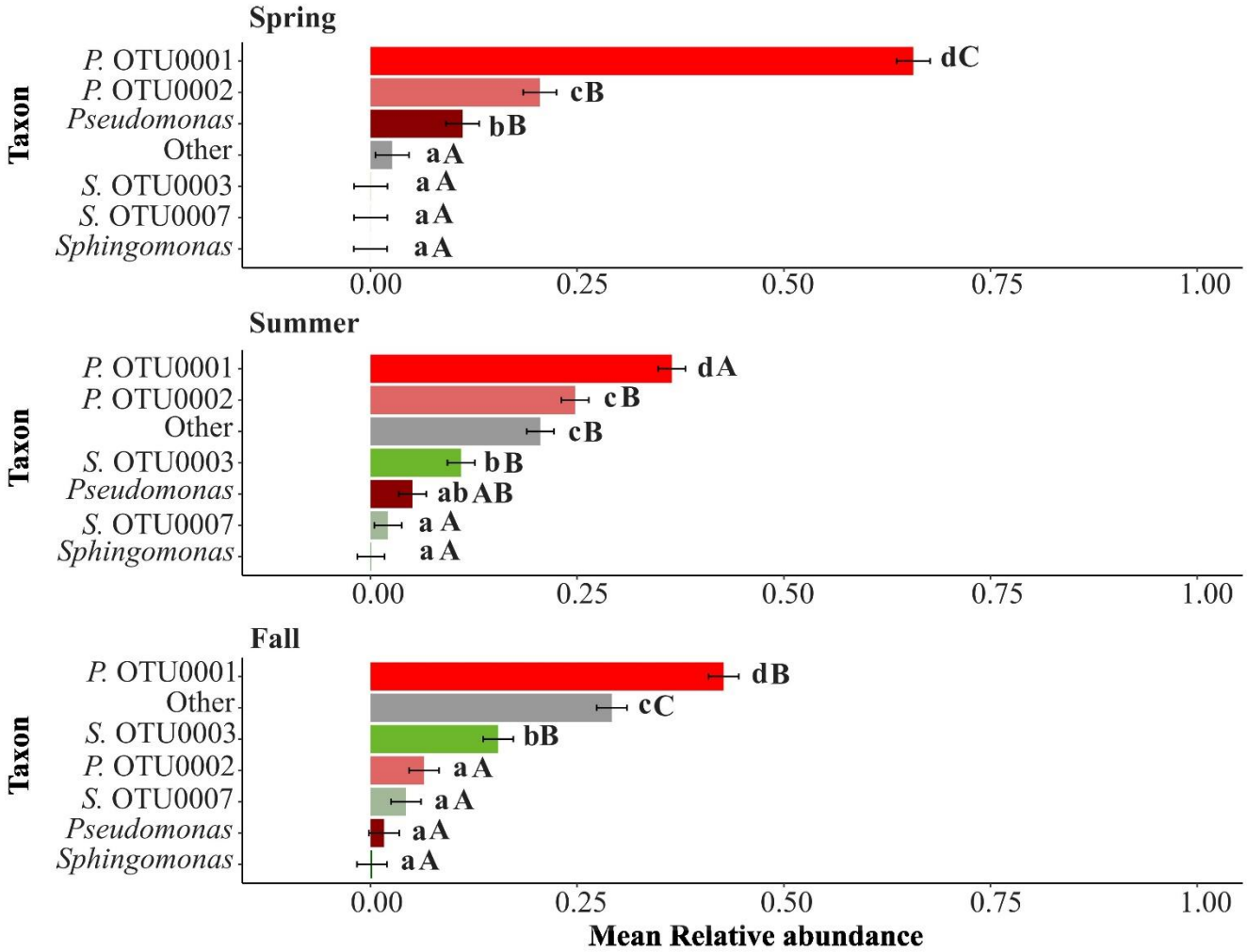


Figure 3.18. The 2019 mean relative abundances of the core microbiome taxon (genus and OTU identifier), the rest of the combined *Pseudomonas* and combined *Sphingomonas*, and the remaining combined "other" taxa ± SE over season. Letters indicate statistical differences, lower-cased letters are within each season, while upper-cased letters indicate statistical differences of each genus/OTU across the seasons, with significance determined by p-value ≤ 0.05. Core taxa were selected via occurrence and relative abundance when they occurred in 50% of all samples and had a relative abundance of ≥ 0.01.

Table 3.9. The ANOVA tables for the relative humidity (%), daily temperature (°C), and the and Kruskal-Wallis test result for the precipitation (mm) compiled from the two-week period leading up to the microbiome leaf sampling dates.

Metric	Model term	df1	df2	F-ratio	p-value
Relative humidity (%)	site	1	188	0.648	0.4220
	time	6	188	3.436	**0.0030**
Daily temperature (°C)	site	1	188	1.265	0.2621
	time	6	188	35.477	**<0.0001**

Metric	Model term	χ^2	df	p-value
Precipitation (mm)	site	0.356	1	0.5506
	time	22.877	6	**0.0008**

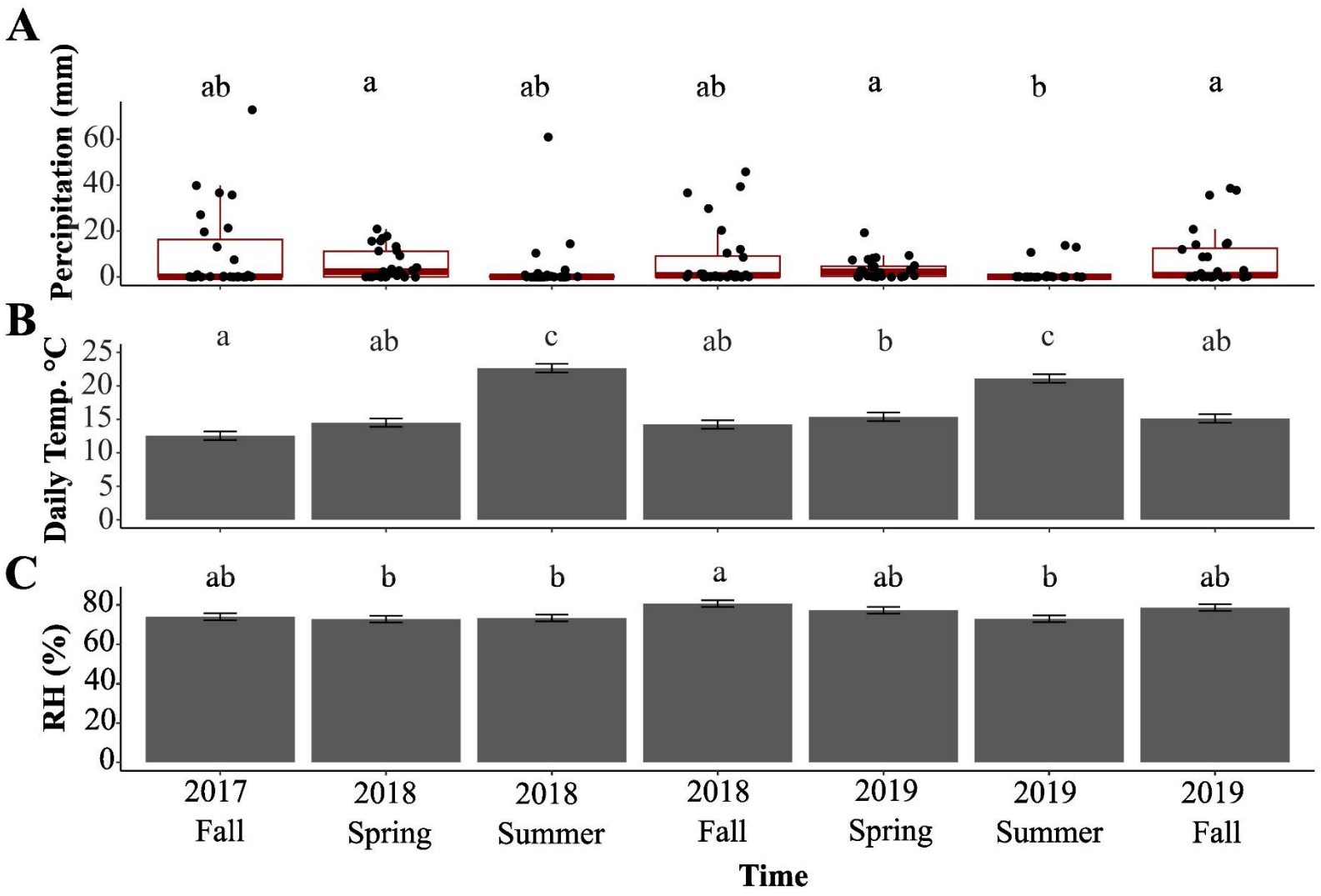


Figure 3.19. The weather data collected from 2017-2019 over a two-week period leading up to each leaf microbiome sampling date, **A)** The distribution of the precipitation (mm) data, **B)** The mean daily temperature (°C), and **C)** the mean relative humidity (%).

REFERENCES

Aleklett, K., Hart, M., and Shade, A. 2014. The microbial ecology of flowers: an emerging frontier in phyllosphere research. Botany 92(4): 253-266.

Ares, A., Pereira, J., Garcia, E., Costa, J., and Tiago, I. 2021. The leaf bacterial microbiota of female and male kiwifruit plants in distinct seasons: assessing the impact of Pseudomonas syringae pv. actinidiae. Phytobiomes J. 5:275-287.

Arrigoni, E., Antonielli, L., Pindo, M., Pertoto, I., and Perazzolli, M. 2018. Tissue age and plant genotype affect the microbiota of apple and pear bark. Microbiological Research 211: 57-58.

Ayala, M., and Lang, G.A. 2017. Morphology, cropping physiology and canopy training. In Quero-Garcia, J., Iezzoni, A., Pulawska, J., and Lang, G. (Eds.), Cherries: botany, production, and uses (pp. 269-304). CAB International.

Bashir, I., War, A.F., Rafiq, I., Reshi, Z.A., Rashid, I., and Shouche, Y.S. 2022. Phyllosphere microbiome: Diversity and functions. Microb. Research 254: 126888.

Bates, D., Maechler, M., Bolker, B., and Walker, S. 2015. Fitting linear mixed-effects models using lme4. J. Statistical Software 67(1):1-48. doi:10.18637/jss.v067.i01.

Beattie, G.A., and Lindow, S.E. 1999. Bacterial colonization of leaves: A spectrum of strategies. Phytopathol. 89: 353-359.

Buonaurio, R., Moretti, C., da Silva, D. P., Cortese, C., Ramos, C., and Venturi, V. 2015. The olive knot disease as a model to study the role of interspecies bacterial communities in plant disease. Front. Plant Sci. 6: 434.

Burch, A.Y., Zeisler, V., Yakota, K., Schreiber, L., and Lindow, S.E. 2014. The hygroscopic biosurfactant syringafactin produced by Pseudomonas syringae enhances fitness on leaf surfaces during fluctuating humidity. Env. Mircrobiol. 16(7): 2086-2098.

Carroll, J., Robinson, T., Hoying, S., and Cox, K. 2010. Evaluation of pruning techniques and bactericides to manage bacterial canker of sweet cherry. New York Fruit Quarterly 18(1): 9-15.

Carvalho, C.R., Dias, A.C., Homma, S.K., and Cardoso, E.J. 2020. Phyllosphere bacterial assembly in citrus crop under conventional and ecological management. PeerJ 8:e9152.

Cernava, T., Chen, X., Krug, L., Li, H., Yang, M., and Berg, G. 2019. The tea leaf microbiome shows specific responses to chemical pesticides and biocontrol applications. The Science of the total environment 667: 33-40.

Cornelis, P. 2010. Iron uptake and metabolism in pseudomonads. Appl. Microbiol. Biotech. 86(6):1637–1645.

Cui, Z., Huntley, R.B., Schultes, N.P., Steven, B., and Zeng, Q. 2021. Inoculation of stigma-colonizing microbes to apple stigmas alters microbiome structure and reduces the occurrence of Fire Blight disease. Phytobiomes J. 5: 156-165.

Custer, G.F, Gans, M., van Diepen, L.T.A., Dini-Andreote, F., and Buerkle, C.A. 2023. Comparative analysis of core microbiome assignments: Implications for ecological studies. mSystems 8(1): e01066-22.

Demirsoy, H., and Lang, G.A. 2010. Short communication: Validation of a leaf area estimation model for sweet cherry. Spanish J. Ag. Res. 8(3): 830-832.

Escalante-Péreza, M., Jaborsky, M., Reindersb, J., Kurzaic, O., Hedricha, R., and Achea, P. 2012. Poplar extrafloral nectar is protected against plant and human pathogenic fungus. Molec. Plant 5(5): 1157-1159.

Glenn, D.M., Basset, C., and Dowd, S.E. 2015. Effect of pest management system on 'Empire' apple leaf phyllosphere populations. Sci. Hort. 183: 58-65.

Glick, B.R., and Gamalero, E. 2021. Recent developments in the study of plant microbiomes. Microorganisms 9(7):1533.

Gobbi, A., Kyrkou, I., Filippi, E., Ellegaard-Jensen, L., and Hansen, L.H. 2020. Seasonal epiphytic microbial dynamics on grapevine leaves under biocontrol and copper fungicide treatments. Scientific Reports 10(1): 681.

Gommers, C. 2020. Keep cool and open up: temperature-induced stomatal opening. Plant Physiol. 182(3):1188–1189.

Grady, K.L., Sorensen, J.W., Stopnisek, N., Guittar, J., and Shade, A. 2019. Assembly and seasonality of core phyllosphere microbiota on perennial biofuel crops. Nat. Commun. 10:4135.

Gunasekera, T.S., and Sundin, G.W. 2006. Role of nucleotide excision repair and photoreactivation in the solar UVB radiation survival of Pseudomonas syringae pv. syringae B728a. J. Appl. Microbiol. 100: 1073-1083.

Haefele, D.M. and Lindow S.E. 1987. Flagellar motility confers epiphytic fitness advantages upon Pseudomonas syringae. Appl Environ Microbiol 53: 2528-2533.

He, Y-H., Adkar-Purushothama, C.R., Ito, T., Shirakawa, A., Yamamoto, H., Kashiwagi, A., Tatewaki, A., Fujibayashi, M., Sugiyama, S., Yaginuma, K., Akahira, T., Yamamoto, S., Tsushima, S., Matsushita, Y., and Sano, T. 2021. Microbial diversity in the phyllosphere and rhizosphere of an apple orchard managed under prolonged "natural farming" practices. Microorganisms 9: 2056.

He, Y-H., Isono, S., Shibuya, M., Tsuji, M., Adkar-Purushothama, C.R., Tanaka, K., and Sano, T. 2012. Oligo-DNA custom microarray for monitoring major pathogenic and non-pathogenic fungi and bacteria in the phyllosphere of apple trees. PLoS ONE 7(3):e34249.

Helmann, T.C., Deutschbauer, A.M., and Lindow, S.E. 2019. Genome-wide identification of Pseudomonas syringae genes required for fitness during colonization of the leaf surface and apoplast. Proc. Natl. Acad. Sci. 116(38): 18900-18910.

Hirano, S.S., and Upper, C.D. 1990. Population biology and epidemiology of Pseudomonas syringae. Annu. Rev. Phytopathol. 28:155-177.

Hirano, S.S., and Upper, C.D. 2000. Bacteria in the leaf ecosystem with emphasis on Pseudomonas syringae – a pathogen, ice nucleus, and epiphyte. Microbiol. Mol. Biol. Rev. 64(3): 624-653.

Hulin, M.T., Armitage, A.D., Vicente, J.G., Holub, E.B., Baxter, L., Bates, H.J., Mansfield, J.W., Jackson, R.W. and Harrison, R.J. 2018. Comparative genomics of Pseudomonas syringae reveals convergent gene gain and loss associated with specialization onto cherry (Prunus avium). New Phytol. 219: 672-696.

Hulin, M.T., Jackson, R.W., Harrison, R.J., and Mansfield, J.W. 2020. Cherry picking by pseudomonads: After a century of research on canker, genomics provides insights into the evolution of pathogenicity towards stone fruits. Plant Pathol. 69: 962– 978.

Hulin, M.T., Vadillo Dieguez, A., Cossu, F., Lynn, S., Russell, K., Neale, H.C., Jackson, R.W., Arnold, D.L., Mansfield, J.W., and Harrison, R.J. 2022. Identifying resistance in wild and ornamental cherry towards bacterial canker caused by Pseudomonas syringae. Plant Pathol. 71: 949-965.

Jackson, C.R., and Denney, W.C. 2011. Annual and seasonal variation in the phyllosphere bacterial community associated with leaves of the southern magnolia (Magnolia grandiflora). Microb. Ecol. 61: 113-122.

Jo, Y., Cho, J.K., Choi, H., Chu, H., Lian, S., and Cho, W.K. 2015. Bacterial communities in the phyllosphere of Prunus species. J. Basic Microbiol. 55:504-508.

Jones, A.L. 1971. Bacterial canker of sweet cherry in Michigan. Plant Disease Reporter 55(11): 961-965.

Jones, A.L., and Sutton, T.A. 1996. Diseases of tree fruits in the east. Michigan State University Extension NCR 45 p. 71-72.

Kembel, S.W., O'Connor, T.K., Arnold, H.K., Hubbell, S.P., Wright, S.J., and Green, J.L. 2014. Relationships between phyllosphere bacterial communities and plant functional traits in a neotropical forest. Proc. Nat. Acad. Sci. 111(38):13715–13720.

Kennelly, M.M., Carzola, F.M., de Vicente, A., Ramos, C., and Sundin, G.W. 2007. Pseudomonas syringae diseases of fruit trees: progress to understanding and control. Plant Disease 91(1): 4-17.

Kim, M., Singh, D., Lai-Hoe, A., Go, R., Rahim, R.A., A.N., A., Chun, J., and Adams, J.M. 2012. Distinctive phyllosphere bacterial communities in tropical trees. Microb. Ecol. 63:674-681.

Kinkel, L.L. 1997. Microbial population dynamics on leaves. Ann. Rev. Phytopathol. 35(1): 327-347.

Knief, C. 2014. Analysis of plant microbe interactions in the era of next generation sequencing technologies. Front. Plant Sci. 5:1-23

Komoto, K., Soldo, L., Tang, Y., Chivers, M. I., Dahlin, K., Guentchev, G., Rill, L., and Winkler, J.A. 2021. Climatology of persistent high relative humidity: An example of the lower peninsula of Michigan, USA. Int. J. Climatol. 41(Suppl.1): E2517– E2536. https://doi.org/10.1002/joc.6861

Kostaki, K. I., Coupel-Ledru, A., Bonnell, V. C., Gustavsson, M., Sun, P., McLaughlin, F. J., Fraser, D. P., McLachlan, D. H., Hetherington, A. M., Dodd, A. N., and Franklin, K. A. 2020. Guard cells integrate light and temperature signals to control stomatal aperture. Plant Physiol. 182(3): 1404–1419.

Kozich, J.J., Westcott, S.L., Baxter, N.T., Highlande,r S.K., and Schloss P.D. 2013. Development of a dual-index sequencing strategy and curation pipeline for analyzing amplicon sequence data on the MiSeq Illumina sequencing platform. Appl. Environ. Microbiol. 79(17): 5112-5120.

Laforest-Lapointe, I., Messier, C., and Kembel, S.W. 2016a. Host species identity, site and time drive temperate tree phyllosphere bacterial community structure. Microbiome 4:27.

Laforest-Lapointe, I., Messier, C., and Kembel, S.W. 2016b. Tree phyllosphere bacterial communities: exploring the magnitude of intra- and inter-individual variation among host species. PeerJ 4:e2367.

Laforest-Lapointe, I., Messier, C., and Kembel, S.W. 2017. Tree leaf bacterial community structure and diversity differ along a gradient of urban intensity. mSystems 2:e00087-17.

Lajoie, G., and Kembel, S.W. 2021a. Plant-bacteria associations are phylogenetically structures in the phyllosphere. Molec. Ecol. 30: 5572– 5587.

Lajoie, G., and Kembel, S.W. 2021b. Host neighborhood shapes bacterial community assembly and specialization on tree species across a latitudinal gradient. Ecol. Monographs 91(2):e01443.

Lang, G.A. 2019. Sustainable sweet cherry cultivation: a case study for designing optimized orchard production systems. In Lang, G.A. (Ed.), Achieving sustainable cultivation of temperate zone tree fruits and berries: Volume 2 case studies (pp. 89-123). Burleigh Dodds Science Publishing.

Latorre, B.A., and Jones, A.L. 1979a. Evaluation of weeds and plant refuse as potential sources of inoculum of *Pseudomonas syringae* in bacterial canker of cherry. Phytopathology 69: 1122-1125.

Latorre, B.A., and Jones, A.L. 1979b. Pseudomonas morsprunorum, the cause of bacterial canker of sour cherry in Michigan, and its epiphytic association with P. syringae. Phytopathology 69:335-339.

Law, T. 2017. Optimizing trellised canopy architecture for sweet cherry: tree establishment and protection from bacterial canker infection. Master's thesis, Michigan State University, ProQuest Dissertations and Theses Global.

Leveau, J. H.J. 2019. A brief from the leaf: latest research to inform our understanding of the phyllosphere microbiome. Current Opinion in Microbiology 49: 41-49.

Lillrose, T., Lang, G.A. and Sundin, G.W. (2017). Strategies to minimize bacterial canker in high density sweet cherry orchards. Acta Hortic. 1161: 457-162.

Lindeberg, M. 2011. Information management of genome enabled data streams for Pseudomonas syringae on the Pseudomonas-Plant Interaction (PPI) Website. Genes 2(4): 841-852. https://doi.org/10.3390/genes2040841

Lindemann, J., and Upper, C.D. 1985. Aerial dispersal of epiphytic bacteria over bean plants. Appl. Env. Microbiol. 50(5): 1229-1232.

Lindow, S.E., and Brandl, M.T. 2003. Microbiology of the phyllosphere. Appl. Env. Microbiol. 69(4): 1875-1883.

Mangiafico, Salvatore S. (2023). rcompanion: Functions to support extension education program evaluation. version 2.4.30. Rutgers Cooperative Extension. New Brunswick, New Jersey. https://CRAN.R-project.org/package=rcompanion

Mansvelt, E.L., and Hattingh, M.J. 1987. Scanning electron microscopy of colonization of pear leaves by Pseudomonas syringae pv. syringae. Can. J. Bot. 65:2517-2522.

Mansvelt, E.L., and Hattingh, M.J. 1989. Scanning electron microscopy of invasion of apple leaves and blossoms by Pseudomonas syringae pv. syringae. Appl. Env. Microbiol. 55(2): 533-538.

Marchi, G., Sisto, A., Cimmino, A., Andolfi, A., Cipriani, M.G., Evidente, A. and Surico, G. 2006. Interaction between Pseudomonas savastanoi pv. savastanoi and Pantoea agglomerans in olive knots. Plant Pathol. 55: 614-624.

Mercier, J., and Lindow, SE. 2000. Role of leaf surface sugars in colonization of plants by bacterial epiphytes. Appl. Environ. Microbiol. 66(1):369-74.

Meyer, K.M., Porch, R., Muscettola, I.E., Vasconcelos, A.S., Sherman, J.K., Metcalf, C.J.E., Lindow, S.E., and Koskella, B. 2022. Plant neighborhood shapes diversity and reduces interspecific variation of the phyllosphere microbiome. ISME J**.** 16:1376–1387.

Mina, D., Pereira, J.A., Lino-Neto, T., and Baptista, P. 2019. Exploring the phyllosphere bacterial community for improving tree crop protection. In Kumar, V., Prasad, R., Kumar, M., and Choudhary, D.K. (Eds.), Microbiome in plant health and disease (pp. 35-52). Springer, Singapore.

Mina, D., Pereira, J.A., Lino-Neto, T., and Baptista, P. 2020. Epiphytic and endophytic bacteria on olive tree phyllosphere: Exploring tissue and cultivar effect. Microb. Ecol. 80:145-157.

Miura, T., Sánchez, R., Castañeda, L.E., Godoy, K., and Barbosa, O. 2019. Shared and unique features of bacterial communities in native forest and vineyard phyllosphere. Ecol. Evol. 9(6): 3295-3305.

Monier, J.M, and Lindow, S.E. 2003. Differential survival of solitary and aggregated bacterial cells promotes aggregate formation on leaf surfaces. Proc. Natl. Acad. Sci. 100(26): 5977–15982.

Monier, J.M, and Lindow, S.E. 2004. Frequency, size, and localization of bacterial aggregates on bean leaf surfaces. Appl. Env. Microbiol. 70(1): 346-355.

Monier, J.M, and Lindow, S.E. 2005a. Aggregates of resident bacteria facilitate survival of immigrant bacteria on leaf surfaces. Microb. Ecol. 49(3): 343–352.

Monier, J.M, and Lindow, S.E. 2005b. Spatial organization of dual-species bacterial aggregates on leaf surfaces. Appl. Env. Microbiol. 70(9): 5484-5493.

Morris, C.E., Monteil, C.L., and Berge, O. 2013. The life history of Pseudomonas syringae: linking agriculture to earth system processes. Annu. Rev. Phytopathol. 51: 85-104.

Morris, C., Sands, D., Vinatzer, B., Glaux, C., Guilbaud, C., Buffière, A., Yan, S., Dominguez, H., and Thompson, B.M. 2008. The life history of the plant pathogen Pseudomonas syringae is linked to the water cycle. ISME J. 2: 321–334.

Noble, A.S., Noe, S., Clearwater, M.J., and Lee, C.K. 2020. A core phyllosphere microbiome exists across distant populations of a tree species indigenous to New Zealand. PLoS ONE 15(8):e0237079.

Nowell, R.W., Laue, B.E., Sharp, P.M. and Green, S. 2016. Comparative genomics reveals genes significantly associated with woody hosts in the plant pathogen Pseudomonas syringae. Molec. Plant Pathol. 17: 1409-1424.

Neu, A.T., Allen, E.E., and Roy, K. 2021. Defining and quantifying the core microbiome: Challenges and prospects. Proc. Natl. Acad. Sci. 118(51):e2104429118.

Ogle, D.H., Doll, J.C., Wheeler, A.P., and Dinno, A. 2023. FSA: Simple fisheries stock assessment methods. R package version 0.9.4. https://CRAN.R-project.org/package=FSA

Oksanen, J., Simpson, G., Blanchet, F., Kindt, R., Legendre, P., Minchin, P., O'Hara, R., Solymos, P., Stevens, M., Szoecs, E., Wagner, H., Barbour, M., Bedward, M., Bolker, B., Borcard, D., Carvalho, G., Chirico, M., De Caceres, M., Durand, S., Evangelista, H., FitzJohn, R., Friendly, M, Furneaux, B., Hannigan, G., Hill, M., Lahti, L., McGlinn, D., Ouellette, M., Ribeiro Cunha, E., Smith, T., Stier, A., Ter Braak, C., and Weedon, J. 2022. vegan: community ecology package. R package version 2.6-4. <https://CRAN.R-project.org/package=vegan>.

O'Gorman, D.T., Haag, P., Boulé, J., Healy, G., Fraser, J., Walker, M., and Úrbez-Torres, J.R. 2023. Microbial communities of sweet cherry (Prunus avium L.) and assessment of their association with cherry slip-skip-maceration disorder. Can. J. Plant Pathol. 45(1): 57-69.

Pattnaik, S.S., Paramanantham, P., and Busi, S. 2021. Agricultural importance of phyllosphere microbiome: recent trends and future perspectives. In Srivastava, A.K., Kashyap, P.L., and Srivastava, M. (Eds.), The plant microbiome and sustainable agriculture (pp. 119-139). Wiley and Sons Ltd.

Purahong, W., Orrù, L., Donati, I., Perpetuini, G., Cellini, A., Lamontanara, A., Michelotti, V., Tacconi, G., and Spinelli, F. 2018. Plant microbiome and its link to plant health: Host species, organs and Pseudomonas syringae pv. actinidiae infection shaping bacterial phyllosphere communities of kiwifruit plants. Front. Plant Sci. 9:1563.

Quast, C., Pruesse, E., Yilmaz, P., Gerken, J., Schweer, T., Yarza, P., Peplies, J., and Glöckner, F.O. 2013. The SILVA ribosomal RNA gene database project: improved data processing and web-based tools. Nucl. Acids Res. 41(D1): D590-D596.

Quiñones, B., Dulla, G., and Lindow, S. E. 2005. Quorum sensing regulates exopolysaccharide production, motility, and virulence in Pseudomonas syringae. Molecular plant-microbe interactions 18(7): 682–693.

R Core Team. 2023. R: A language and environment for statistical computing. R Foundation for Statistical Computing, Vienna, Austria. https://www.R-project.org/.

Redford, A.J., Bowers, R.M., Knight, R., Linhart, Y., and Fierer, N. 2010. The ecology of the phyllosphere: geographical and phylogenetic variability in the distribution of bacteria on tree leaves. Env. Microbiol. 12(11): 2885-2893.

Redford, A.J., and Fierer, N. 2009. Bacterial succession on the leaf surface: A novel system for studying successional dynamics. Microb. Ecol. 58:189-198.

Roos, I.M.M, and Hattingh, M.J. 1983. Scanning electron microscopy of Pseudomonas syringae pv. morsprunorum on sweet cherry leaves. J. Phytopathol. 108: 8-25.

Ruinelli, M., Blom, J., Smits, T.H.M., Pothier, J.F. 2022. Comparative genomics of prunus-associated members of the Pseudomonas syringae species complex reveals traits supporting co-evolution and host adaptation. Front Microbiol. 13: 804681.

Schloss, P.D., Westcott, S.L., Ryabin, T., Hall, J.R., Hartmann, M., Hollister, E.B., Lesniewski, R.A., Oakley, B.B., Parks, D.H., Robinson, C.J., Sahl, J.W, Stres, B., Thallinger, G.G., Van Horn, D.J., and Weber, C.F. 2009. Introducing mothur: Open-source, platform-independent, community-supported software for describing and comparing microbial communities. Appl. Environ. Microbiol. 75(23):7537-7541.

Shade, A., and Handelsman, J. 2012. Beyond the venn diagram: the hunt for a core microbiome. Env. Microbiol. 14(1): 4-12.

Shade, A., McManus, P.S., and Handelsman, J. 2013. Unexpected diversity during community succession in the apple flower microbiome. mBio. 4(2): e00602-12.

Singh, P., Santoni, S., Weber, A., This, P., and Péros, J-P. 2019. Understanding the phyllosphere microbiome assemblage in grape species (Vitaceae) with amplicon sequence data structures. Scientific Reports 9:14294.

Smets, W., Chock, M.K., Walsh, C.M., Vanderburgh, C.Q., Kau, E., Lindow, S.E., Fierer, N., and Koskella, B. 2023. Leaf side determines the relative importance of dispersal versus host filtering in the phyllosphere microbiome. mBio 0(ahead of print): e01111-23. https://doi.org/10.1128/mbio.01111-23.

Sobiczewski, P., and Jones, A.L. 1995. Effect of freezing temperatures on necrosis in sweet cherry shoots inoculated with Pseudomonas syringae pv. syringae or P.s morsprunorum. Plant Dis. 76: 447-451.

Sohn, K.H., Jones, J.D., and Studholme, D.J. 2012. Draft genome sequence of Pseudomonas syringae pathovar syringae strain FF5, causal agent of stem tip dieback disease on ornamental pear. J Bacteriol. 194(14):3733-4. doi: 10.1128/JB.00567-12.

Spotts, R.A., Wallis, K.M., Serdani, M., and Azarenko, A.N. 2010. Bacterial canker of sweet cherry in Oregon- Infection of horticultural and natural wounds, and resistance of cultivar and rootstock combinations. Plant Dis. 94: 345-350.

Steven, B., Huntley, R.B., and Zeng, Q. 2018, The influence of flower anatomy and apple cultivar on the apple flower phytobiome. Phytobiomes J. 2:171-179.

Stone, B.W.G., and Jackson, C.R. 2021. Seasonal patterns contribute more towards phyllosphere bacterial community structure than short-term perturbations. Microb. Ecol. 81:146-156.

Sundin, G.W., Jones, A.L., and Olson, B.D. 1988. Overwintering and population dynamics of Pseudomonas syringae pv. syringae and P.s. pv. morsprunorum on sweet and sour cherry trees. Can. J. Plant Pathol. 10: 281-288.

Sundin, G., and Rothwell, N. (2012). Managing bacterial canker in sweet cherries: What are the options? Retrieved from https://www.canr.msu.edu/news/managing_bacterial_canker_in_sweet_cherries_what_are_the_options

Tancos, K.A., and Cox, K.D. 2017. Effects of consecutive streptomycin and kasugamycin applications on epiphytic bacteria in the apple phyllosphere. Plant Disease 101: 158-164.

Vorholt, J.A. 2012. Microbial life in the phyllosphere. Nat. Rev. Microbiol. 10: 828–840.

Wagner, M.R., Lindberg, D.S., del Rio, T.G., Tringe, S.G., Dangl, J.L., and Mitchell-Olds, T. 2016. Host genotype and age shape leaf and root microbiomes of a wild perennial plant. Nat. Comm. 7:12151.

Wallis, A., Gu, G., Ramachandran, P., Reed, E., Ottesen, A., Nou, X., and Cox, K.D. Endophytic bacterial communities in apple leaves are minimally impacted by streptomycin use in fire blight management. Phytobiomes J. 5:350-361.

Wensing, A., Braun, S. D., Büttner, P., Expert, D., Völksch, B., Ullrich, M. S., and Weingart, H. (2010). Impact of siderophore production by Pseudomonas syringae pv. syringae 22d/93 on epiphytic fitness and biocontrol activity against Pseudomonas syringae pv. glycinea 1a/96. Appl. Environ. Microbiol. 76(9): 2704–2711.

Whiting, M.D., and Lang, G.A. 2004. ‘Bing’ sweet cherry on dwarfing rootstock ‘Gisela 5’: thinning affects fruit quality and vegetative growth but not net CO_2 exchange. J. Amer. Hort. Sci. 129(3): 407-415.

Wu, Y., Qu, M., Pu, X., Lin, J., and Shu, B. 2020. Distinct microbial communities among different tissues of citrus tree Citrus reticulata cv. Chachiensis. Scientific Reports 10: 6068.

Xin, X-F., Kvitko, B., and He, S.Y. 2018. Pseudomonas syringae: what it takes to be a pathogen. Nat. Rev. Microbiol. 16(5): 316-328.

Yashiro, E., and McManus, P.S. 2012. Effect of streptomycin treatment on bacterial community structure in the apple phyllosphere. PLoS ONE 7(5):e37131.

Yee, W.L., and Chapman, P.S. 2008. Seasonal amounts of nutrients in western cherry fruit fly (Diptera: Tephritidae) and their relation to nutrient availability on cherry plant surfaces. Env. Entomol. 37(5):1086–1098.

Yilmaz, P., Parfrey, L.W., Yarza, P., Gerken, J., Pruesse, E., Quast, C., Schweer, T., Peplies, J., Ludwig, W., and Glöckner, F.O. 2014. The SILVA and "All-species Living Tree Project (LTP)" taxonomic frameworks. Nucl. Acids Res. 42: D643-D648.

Zhang, Q., Shi, W., Zhou, B., Du, H., Xi, L., Zou, M., Zou, H., Xin, L., Gao, Z., and Chen, Y. 2021. Variable characteristics of microbial communities on the surface of sweet cherries under different storage conditions. Postharvest Biol. Tech. 173: 111408.

CHAPTER 4

IN VITRO CO-INOCULATIONS FOR ASSESSMENT OF POTENTIAL *PSEUDOMONAS SYRINGAE* PV. *SYRINGAE* BIOLOGICAL CONTROL AGENTS

4.1: Abstract

In vitro co-inoculation experiments can be used to initially assess how putative commercial biological control agents (BCAs) may influence the growth of *Pseudomonas syringae* pv. *syringae* (*Pss*) strains found on flowers in Michigan sweet cherry orchards. Strains of *Pss* that were identified previously for differences in virulence on green fruit and wood also varied in their strength of growth in-vitro. All commercial BCAs tested (Serenade® Opti, Blossom Protect™, BlightBan®A506, Bloomtime™, and Double Nickel55™) decreased the mean total area of growth of *Pss* compared to a water control, with up to a 50% decrease in growth in some cases. When the more virulent *Pss* strains were co-inoculated with the less virulent or avirulent *Pss* strains, there were no significant decreases in their mean total area of growth. This demonstrated their ability to coexist commensally and revealed that these particular less virulent to avirulent strains would not be effective candidates for potential biological control of the more virulent strains.

4.2: Introduction

The bacterial canker disease causal agent, *Pseudomonas syringae* pv. *syringae* (*Pss*), is a globally economically devastating pathogen in the cherry industry, with young trees particularly being susceptible to whole tree death (Marroni et al., 2023; Spotts et al., 2010). Spotts et al. (2010) reported up to 75% loss of trees in Oregon, U.S.A., while Marroni et al. (2023) cited losses of 20-50% in New Zealand orchards. Copper has been the standard for management of *Pss* and new formulations are being tested continually (Broniarek-Niemiec et al., 2023). Broniarek-

Niemiec et al., (2023) field tested various copper formulations along with biological control agents and found the copper-containing products to be the most efficacious for reducing *Pss* on leaves and fruit of *Prunus* spp. The use of copper for *Pss* population management in Michigan orchards, however, is not a sustainable option as the phylogenetically diverse *Pss* strains have been found to be resistant to copper (Lauwers, 2022; Renick et al., 2008; Wilkinson, Chapter 2). Copper accumulations in agricultural soils also has been found to have deleterious effects on beneficial invertebrates (Duque et al., 2023; Karimi et al., 2021).

For many years, antibiotics such as oxytetracycline, streptomycin, and kasugamycin were unavailable to cherry growers for management of *Pss* because use was restricted to control of the highly aggressive fire blight bacterial pathogen, *Erwinia amylovora*, to reduce the potential for development of resistance (Lauwers, 2022; McGhee and Sundin, 2011; Slack et al., 2021; Sundin and Wang, 2018). Recently (2020), however kasugamycin has become available for use in cherry and has been shown to reduce flower infection by *Pss* in sweet cherry by 90% (Lillrose et al., 2017). Although no *Pss* resistance to kasugamycin has been detected in Michigan thus far, resistance development is still a serious concern, so kasugamycin is not used routinely for pre-emptive *Pss* management (Lauwers, 2022; Lillrose et al., 2017; Sundin and Wang, 2018). In addition to the use of copper for *Pss* management, cultural practices are widely used, such as weed control, drip (rather than sprinkler) irrigation, and timing of pruning, none of which are not guaranteed to prevent *Pss* infection (Lattore and Jones, 1979; Spotts et al., 2010; Carroll et al., 2010). There are also no sweet cherry cultivars resistant to *Pss*, although wild, ornamental, and hybrid *Prunus* are being tested to identify sources of genetic resistance (Hulin et al., 2022).

There is a keen fruit grower interest in finding alternatives to antibiotics that are sustainable and “environmentally friendly” and could complement cultural practices for

management of *Pss*. The most recent research trend for management of *Pss* is with lytic bacteriophage (single phage and cocktails) along with the commercially available AgriPhage™ (Akbaba and Ozaktan, 2021; Brown, 2023; Lauwers, 2022; Luo et al., 2022; Oueslati et al., 2022; Pinheiro et al., 2019; Rabiey et al., 2020). In Michigan, bacteriophage cocktails including native bacteriophage isolated from Michigan soils have been tested for efficacy of *Pss* population management and have been found to be limited by UV exposure (Brown, 2023; Lauwers 2022). A boom in the bio-pesticide, bio-protectant, bio-control industry has created confusion as to what is the true definition of biological control is (Lahlali et al., 2022; Stenberg et al., 2021). Stenberg et al. (2021) proposed that products that contain plant growth promoting bacteria and incite systemic acquired resistance (SAR) or induced systemic resistance (ISR) should belonging under the bioprotectant umbrella but remain a separate entity compared to what is traditionally considered a biological control. Actigard™ is a type of SAR, that "primes" the plant's innate immunity, as it mimics the defense hormone salicylic acid, and has been found to be an effective complement to other management strategies for *Pseudomonas syringae* pv. *actinidiae* (*Psa*) in kiwi production, but it was not efficacious on sweet cherry for *Pss* (Lillrose et al., 2017; Stroub et al., 2022). The overlying theme of all of these products is that they are inconsistently effective in the field and in spite of potential demand, they are slowly produced and have not been adopted widely by growers (Lahlali et al., 2022).

The biocontrols currently available for *Erwinia amylovora* have been assessed for blossom infection in apple and sweet cherry however, no such assessments have been documented for the management of epiphytic *Pss* populations of in Michigan cherry orchards (Sundin et al., 2009; Lillrose et al., 2017). As *Pss* is a known epiphyte, the ability to manage populations on leaves may be a key component of successful reduction in disease incidence. The

sweet cherry leaf microbiome could be an untapped source of possible biological control agents (BCAs) since the sweet cherry leaf microbiome has been shown to be heavily dominated by *Pseudomonas* spp. (Wilkinson, Chapter 3), which are capable of plant growth promotion, ISR, the production of secondary metabolites and volatile organic compounds that elicit antibiosis, as well as competitive exclusion (Dimkić et al., 2022). Potential BCAs for *Pss* have been assessed from apple fruits, and the pear and apple bark has been identified as a reservoir for potential BCAs as well (Kotan and Sahin, 2006; Arrigoni et al., 2018). Cui et al. (2021) demonstrated that bacteria isolated from the apple flower microbiome could influence the prevalence of the bacterial canker pathogen when reintroduced to the flower in certain compositions. Vasebi et al. (2023) found 18 strains that had been isolated from the almond and apricot phyllosphere and endosphere that were antagonistic to *Pss* in *in vitro* bioassays. The *Pss* isolated from Michigan cherry flowers are also a phylogenetically diverse group belonging to phylogroups 2a, 2b, 2c, and 2d, and having a range in their level of virulence on green fruit and wood, should also be assessed for their biological control potential (Lauwers, 2022; Renick et al., 2008; Wilkinson, Chapter 2).

Biological controls of plant pathogens are thought to function in two major ways: 1) competitive exclusion of the pathogen from niche or nutrient resources, and 2) through antibiosis (Lindow and Brandl, 2003). Though *in vitro* assays do not necessarily translate into field efficacy, they are suitable for the initial determination of whether potential BCAs are capable of limiting the growth of the pathogen via either competition or antibiosis. Stroud et al. (2022) touted the importance of small-scale *in vitro* assays since the actual way a BCA affects the target pathogen can be lost in the complexity of a field study. As field and growth chamber studies with live plants are time-consuming, resource-intensive, nearly impossible for tree species, and

often yield inconclusive results, simpler *in vitro* studies are valuable for initial screening of potential BCAs. Stroud et al. (2022) used tissue culture to determine how Actigard™ was able to limit *Psa* population sizes. Dual culture or co-inoculation *in vitro* assays, in Petri plates have long been used to assess the biological control potential of bacteria against fungal pathogens (Chaouachi et al., 2021; Cirvilleri et al., 2005, Derikvan et al., 2023; Hammami et al., 2022; Lu et al., 2022; Niem et al., 2020; Nysanth et al. 2022). Often a mycelium plug is co-inoculated with either a pipetted amount of bacteria or a streak of bacteria, and in some cases multiple co-inoculations may be made on the same Petri plate (Chaouachi et al., 2021; Cirvilleri et al., 2005, Derikvan et al., 2023; Hammami et al., 2022; Lu et al., 2022; Niem et al., 2020; Nysanth et al. 2022). Vasebi et al. (2023) made a lawn of *Pss* first, followed by 5µl of each of the bacteria being assessed for their antagonistic properties. In these cases, the zones of inhibition were measured. Mina et al. (2020) showed that this method also worked well for testing the interaction between two bacteria, in which the olive knot bacteria pathogen *Pseudomonas savastanoi* pv. *savastanoi* was co-inoculated next to potential BCAs. *In vitro* dual culture or co-inoculation should be a viable method to assess the currently available commercial biological control agents having potential for managing *Pss* populations, as well as a way to initially determine how the *Pss* strains isolated from sweet cherry flowers may interact with one another. The objectives of this experiment were to a) demonstrate that *in vitro* co-inoculations are a viable, easily employed option for the initial assessment of BCAs for *Pss*, b) evaluate commercially available BCAs for their ability to decrease *Pss* growth *in vitro*, and c) determine if avirulent or moderately virulent *Pss* strains recovered from Michigan sweet cherry orchards can decrease growth of virulent or moderately virulent *Pss* strains *in vitro*.

4.3: Methods

2019 Co-Inoculations *Pss* PG 2d vs. BP, SO, and H_2O

During 2019, *Pss* strains 9, 25, 37, and 38 from phylogroup (PG) 2d, all belonging to the most virulent phylogroup recovered from sweet cherry flowers in Michigan (Wilkinson, Chapter 2) were co-inoculated next to the commercially available biocontrol agents (BCAs) Serenade® Opti (SO), *Bacillus subtilis*, a bacterium (Bayer CropScience LP, St. Louis, MO), and Blossom Protect™ (BP), *Aureobasidium pullulans*, (Westbridge, Chelsea Vista, CA), a yeast-like fungus, or sterile water in Petri dish assays (Table 4.1). Sterile filter paper discs ~34 mm² in area were placed ~32 mm apart onto 100 mm x 15 mm Petri plates (VWR®, Radnor PA) containing sterile King's B media (KB) (Figure 4.1). For each Petri dish (5 replications/strain/treatment [n= 60 plates]), one filter paper disk was inoculated with a 5 µl droplet of 10^8 cfu/ml of one of the virulent *Pss* strains, and the other disk was inoculated with a 5 µl droplet of the biocontrol agent at the maximum recommended field rate or a sterile water control. All co-inoculations occurred on the same day. Inoculations were allowed to dry overnight on the lab bench before the plates were sealed on trays in a plastic bag (to prevent drying out) and were placed into an incubator at 28°C (Precision Scientific Model 805, Chicago IL). Photographs of each plate were taken at 4 days after inoculation (DAI) and the area of growth of the *Pss* next and the co-inoculated biocontrol or water control could be measured using the software ImageJ (Schneider et al. 2012). To obtain the best threshold contrasts and measurements in ImageJ, in certain instances Adobe® Photoshop (Elements 14 Photo Editor, Adobe®, San Jose, CA) was used to highlight the area of bacterial growth (without altering area size). In ImageJ, the image type was set to 8-bit, and the plate diameter (85 mm) was used as a known reference size. The top threshold was then adjusted so that the area of *Pss* vs. biocontrol growth was prominent (the bottom threshold remained

constant, 255), a selection tool was then used to select each growth area outline. Then Analyze-analyze particles option was selected with size (mm^2) set as 20 (and 1 for smaller pipette splatter areas), circularity set as 0.00-1.00, and show outlines, display results, and include holes were selected. Pipette splatter was included as the part of the total area of growth as long as it was distinguishable as being either *Pss* or BCA as it is considered part of the original 5µl of inoculum. The area of *Pss* growth (mm^2) was reported. All images can be viewed in Appendix C.

2021 Co-Inoculations *Pss* PG 2b, 2c, 2d vs. BB, BLT, BP, DN, SO, and H_2O

In 2021 the co-inoculations of *Pss* vs. biocontrols was expanded to include ten *Pss* strains that had been recovered from sweet cherry flowers in Michigan (Wilkinson, Chapter 2) from the moderately virulent PG 2b strains 22, 23, 34, the avirulent PG 2c strain 14, and the virulent PG2d strains 9, 25, 26, 27, 37, 38. The commercially available biological controls were also expanded to include BlightBan®A506 (BB) (a bacterium, *Pseudomonas fluorescens*) (Nufarm Americas Inc., Alsip,, IL), and Bloomtime™ (BLT) (a bacterium, *Pantoea agglomerans*) (Verdesian Life Science, US, LLC, Cary, NC), and Double Nickel55™ (DN) (a bacterium, *Bacillus amyloliquefaciens*) (Certis USA LLC, Columbia, MD), in addition to BP and SO (Table 4.1). All co-inoculations were done as described previously for the 2019 Petri dish assays; however the biological controls were applied at 3 different rates: 1.0x which was the maximum recommend rate, then 0.5x (half the recommended rate) and 1.5x (1.5 times the maximum recommended rate) and plates for *Pss* vs. BP were also co-inoculated on Potato Dextrose Agar (PDA) (BD Difco™, Becton Dickinson, Franklin Lakes, NJ) in addition to KB media. As BP is the only fungus the PDA media may better support BP growth and could result in better *Pss* suppression by BP. A total of 1,200 plates were co-inoculated. Due to space limitations in growth chambers and an effort to control inoculation error or contamination, co-inoculations

occurred in groups according to strain and growth chamber, with strains being randomly assigned to a group (Table 4.2). The area of growth of the *Pss* strains grown next to the challenging BCA was measured as described above using ImageJ (Schneider et al. 2012).

2022 Co-Inoculations *Pss* PG 2b, 2d vs. *Pss* PG 2c, 2b, and H_2O

In 2022 co-inoculation assays were conducted to determine what effect the *Pss* strains collected from Michigan sweet cherry flowers belonging to the phylogroups 2b (strains 23 and 33) and 2c (strains 14 and 18) moderate virulence and avirulent strains respectively may have on the most virulent PG2d (strains 9 and 25) and the moderately virulent PG2b strains when co-inoculated in petri assays. The *Pss* co-inoculations plus sterile water controls were applied to KB plates as described for 2019 (5 reps [150 plates total]). The PG2d (virulent) and PG2b (moderate-virulence) *Pss* strains were inoculated at 10^8, 10^6, and 10^4 cfu/ml (assigned to different days to prevent error/contamination) while the challenging PG2c (avirulent) and PG2b (moderate-virulence) strains were inoculated at a constant rate of 10^8 cfu/ml (Table 4.3). The area of growth for the PG 2b and PG 2d strains were measured as described previously using ImageJ (Schneider et al. 2012).

Statistical Analysis

All data was analyzed using R version 4.3.1 with a linear model with ANOVA and pairwise comparisons of the estimated marginal means (Kuznetsova et al., 2017; Lenth, 2023; R core team, 2023). Distribution of data can be found in Appendix C for all co-inoculation experiments. Data for 2021 was analyzed separately according to group assignment. The 2021 data containing BP was analyzed first with all the other BCAs on KB media separately for each group and then with BP and H_2O treatments only on KB and PDA media. The data for 2022 was also analyzed separately for each group. Plates that were contaminated were omitted from the

analysis. When an effect of treatment was evident the % decrease in the total area of *Pss* growth (mm^2) compared to the growth next H_2O was calculated using the formula: % decrease=[(old value – new value)/(old value)] *100 (i.e. [(mean area *Pss* next to H_2O – mean area *Pss* next to BCA)/(mean area Pss next to H_2O)]*100). All graphs were made in R v. 4.3.1 using a combination of base R and ggplot2 and ggpubr (Kassambara, 2023; R core team, 2023; Wickham, 2015). Graphic fonts were edited, and the letters indicating statistical differences were added to graphs via InkScape v.1.2 (InkScape.org).

4.4: Results

2019 *Pss* PG 2d vs. BP, SO, and H_2O

There were no statistical differences between the virulent PG2d strains (9, 25, 37, and 38) mean total areas of growth when co-inoculated next to the BCAs BP, SO or H_2O. There were statistical treatment effects, where the mean area of growth of the PG2d strains was suppressed by 25% and 27% when co-inoculated next to BP and SO respectively compared to when next to water (Table 4.4 and Figure 4.2). There were no statistical differences between the two BCAs.

2021 *Pss* PG 2b, 2c, 2d vs. BB, BLT, BP, DN, SO, and H_2O

Group1: *Pss* 14 (PG2c), 25 (PG2D), 38 (PG2d)

For the three *Pss* strains 14 (PG2c), 25 (PG2D), and 38 (PG2d**)** grown next to the BCAs BB, BLT, BP, DN, SO, and H_2O there was only an effect of BCA rate on the mean total area of growth (mm^2) of the *Pss* strains (Table 4.5). Where *Pss* strains grown next to BCAs inoculated at a rate of 1.5x had the greatest mean total area of growth followed by *Pss* strains grown next to BCAs inoculated at a rate of 0.5x, while strains grown next to BCAs inoculated at a rate of 1.0x had the least amount of growth (i.e., the most suppression of growth) (Figure 4.3). Only the 1.0x and 1.5x BCA rates were statistically different.

Group2: *Pss* 23 (PG2b), 34 (PG2b)

For the two PG2b strains 23 and 34 when co-inoculated next to the five BCAs or water there were statistically significant effects of treatment, strain, rate*treatment, and treatment*strain (Table 4.5). All BCA treatments were able to suppress the mean total area of growth of *Pss* strain 23 and 34 (23% to 36%) when compared to water-(Figure 4.4). SO was the only BCA that was not statistically different than water. Strain 34 was the strongest of the two strains when grown next to BCAs with a larger mean total area of growth than strain 23. When considering the rate* treatment effect the greatest suppression of *Pss* growth occurred when BCAs were inoculated at the 1.0x rate (27% to 50%) when compared to the *Pss* next to H_2O, however only BP was statistically different from water at this rate. The *Pss* next to BCAs inoculated at 0.5x had a 21% to 50% decrease in growth when compared to those next to water, with only BB and BLT being statistically different than water at that rate. While the *Pss* next to BCAs inoculated at 1.5x had no suppression (SO) to very little suppression of growth (3% to 15%) and no statistical differences from water. For the treatment*strain effect *Pss* strain 34 had a 32% to 49% decrease in the mean total area of growth when co-inoculated next to BCAs compared to when next to water (all statistically different from water) while strain 23 had no suppression (BP) to very little suppression (1% to 12%) in the mean total area of growth when co-inoculated next to BCAs compared to when next to water with no statistical differences from water.

Group3: *Pss* 22 (PG2b), 26 (PG2d), 37 (PG2d)

The *in vitro* co-inoculation of the two PG2d strains 26 and 33 and the PG2b strain next to BCAs or water had an effect of BCA rate, *Pss* strain, and treatment*strain (Table 4.5). The mean total area of growth of the *Pss* next to BCAs at three rates can be ranked as 0.5x<1.0x<1.5x,

where only the 0.5x and 1.5x rates were statistically different (Figure 4.5). While the PG2b strain and the PG2d strains can be ranked according to their mean total area of growth (mm^2) next to BCAs as 22<26<37 with all being statistically different from one another. For the treatment*strain interaction the mean total area of growth of strain 37 was suppressed by 11 to 36% in co-inoculations with BCAs with only SO being statistically different from water. While strain 26 and 22 had no statistical difference from water with suppression of growth (strain 26) and only 1% suppression of growth next to BB and BLT (strain 22).

Group4: *Pss* 9 (PG2d), 27 (PG2d)

The PG2d strains (9 and 27) only had an effect of BCA rate and *Pss* strain (Table 4.5). Where the mean area of *Pss* growth was greatest at the BCA rate of 1.0x, followed by 1.5x and the least at 0.5x with only 0.5x and 1.0x being statistically different (Figure 4.6). Strain 27 had a greater mean area of growth and was statistically different from strain 9 when co-inoculated next to BCAs.

2021 *Pss* PG 2b, 2c, 2d vs. BP and H_2O on KB and PDA Media

Group 1: *Pss* 14 (PG2c), 25 (PG2d), 38 (PG2d)

For the two PG2d strains, 25 and 38, and the PG2c strain 14 co-inoculated with BP or water on KB or PDA media there was an effect of strain and media*rate*treatment(trt)*strain (Table 4.6). Strains can be ranked for their mean total area of growth as 25<38<14 with statistical difference only between PG2c strain 14 and PG2d strain 25 (Figure 4.7). Though there was an effect of media*rate*trt*strain, no statistical differences could be discerned however, unless the interaction of rate*trt*strain was nested within media. Strain 38 (PG2d) had the greatest suppression of growth when co-inoculated next to BP at all rates on KB (16% to 44%) and on PDA at 0.5x and 1.0x (31% and 28%) but there were no statistical differences from water. Strain

25 (PG2d) had suppression of growth when BP was inoculated at 0.5x (19%) and 1.0x (29%) rates on KB and at the rate 0.5x (40%) on PDA however there were no statistical differences when compared to water. Strain 14 (PG2c) had a 66% suppression of growth with BP at 1.5x rate on KB which was statistically different than water, while there was suppression of growth (2% to 18%) of this strain at all BP rates on PDA there were not statistical differences from water.

Group 2: *Pss* 23 (PG2b), 34 (PG2b)

The PG2b strains 23 and 34 had significant effects of media, rate, treatment (trt), media*rate, media*strain, trt*strain, and media*trt*strain (Table 4.6). Overall, these *Pss* strains when co-inoculated next to either BP or H_2O had a statistically greater mean total area of growth on KB media than on PDA (Figure 4.8). The mean total area of growth of the strains when grown next to BP at the three rates can be ranked as 1.5x<0.5x<1.0x where only 1.5x and 1.0x are statistically different. The PG2b strains had a 19% decrease in growth when grown next to BP compared to when next to H_2O. Overall *Pss* grown on KB media had a greater mean total area of growth at all inoculation rates of BP compared to those on PDA, however they were only statistically different at the 0.5x rate (Figure 4.9). Strain 23 and 34 were only statistically different on KB media where 34 had the strongest mean total area of growth. Strain 23 had 4% suppression of growth however only strain 34 was statistically different from water with a 30% suppression of growth next to BP. On KB strain 34 was also statistically different from water with a 44% suppression in growth next to BP, while 23 was decreased by 15% on PDA there was no statistical difference when next to water.

Group 3: *Pss* 22 (PG2b), 26 (PG2d), 37 (PG2d)

For *Pss* strain 22 (PG 2b) and the two PG2d strains 26 and 37 co-inoculated with the BCA BP or water on KB or PDA media there was only an effect of BP inoculation rate and an

effect of *Pss* strain (Table 4.6). Where strains grown next to BP or H_2O at 1.0x and 1.5x had statistical differences in their mean total areas of growth as strains next to BP at 1.0x had the least amount of total area of growth while those next to BP at the rate 1.5x had the greatest mean total area of growth (Figure 4.10). The PG2d strains (26 and 37) had the strongest total mean area of growth while strain 22 was statistically different with the weaker amount of growth.

Group 4: *Pss* 9 (PG2d), 27 (PG2d)

For the PG2d *Pss* strains 9 and 27 there was a significant effect of media*rate, rate*strain, and media*trt (Table 4.6). The strains on KB media had stronger growth than on PDA at the 1.0x and 1.5x BP rates however the only statistical differences between the two medias occurred at the 0.5x BP rate when strains on PDA had stronger growth than when on KB (Figure 4.11). Strain 27 (with the greater mean area of growth) was statistically different from strain 9 only when BP was inoculated at the 1.0x rate. Although there was an effect of media*trt pairwise comparisons of the estimated marginal means did not show any statistical differences unless nested within rate (Appendix C). Even with the nested rate parameter there were no significant differences between media and treatment compared to water though *Pss* growth was suppressed by 4% at 0.5x BP and 15% at 1.0x BP on KB media (Figure 4.12).

2022 Co-Inoculations *Pss* PG 2b, 2d vs. *Pss* PG 2c, 2b, and H_2O

Group 1: *Pss* v. *Pss* at 10^8 cfu/ml

When all strains were co-inoculated at 10^8 cfu/ml there was only a significant effect of strain (Table 4.7). The virulent phylogroup 2d *Pss* strains 9 and 25 had the greater mean area of growth when grown next to a PG 2c/2b *Pss* strains or water compared to the moderately virulent strains PG2b *Pss* strains 23 and 33 when co-inoculated with PG2c. Strain 23 with the weakest

growth was statistically different than all strains, while strain 9 with the strongest mean area of total growth was statistically different from both PG2b strains (23 and 33) (Figure 4.13).

Group 2: *Pss* at 10^6 cfu/ml v. *Pss* at 10^8 cfu/ml

Pss PG2d/2b strains 9, 25, 23 and 33 at the rate 10^6 cfu/ml next to the *Pss* PG2c/PG2b strains 14, 18, 23, 33 at 10^8 cfu/ml had an effect of strain and a weak treatment effect (Table 4.7). The PG2d strains 9 and 25 grew stronger and were statistically different than the PG2b strains 23 and 33 (Figure 4.14). Though no treatments were statistically different than water the PG2d strains 9 and 25 at 10^6 cfu/ml had a 20% and 8% decrease in mean total area of growth when grown next PG2b strain 33 and PG2c strain 14 at 10^8 cfu/ml respectively.

Group 3: *Pss* at 10^4 cfu/ml v. *Pss* at 10^8 cfu/ml

For the *Pss* PG2d/2b strains 9, 25, 23 and 33 at the rate 10^4 cfu/ml next to the *Pss* PG2c/PG2b strains 14,18, 23, 33 at 10^8 cfu/ml there was only an effect of treatment (Table 4.7). Though no treatments were statistically different than water there was suppression of growth of the PG2d and PG2c strains (14% to 33%) when challenged with PG2b and PG2c strains (Figure 4.15).

4.5: Discussion

Though this experiment's methodology was most similar to that employed by Mina et al. (2020) it was simpler, more time efficient, and more precise. While Mina et al. (2020) measured the radial growth (toward the antagonist) daily until the growth stopped this study measured the total area of growth at a single time point (4 DAI). In this study the total area of growth was precisely measured using the ImageJ software while Mina et al. (2020) does not specify exactly how the growth was physically measured, likely via ruler, they estimated the growth/day via the slope from regression analysis. The percent decrease in growth for both this study and Mina et al.

(2020) used the same equation which used the growth of the pathogen next to water or alone and the growth of the pathogen next to the BCA. Mina et al. (2020) also used additional assays to measure siderophore, lipase, and protease production which was not done in this study but should be done in future assays especially with the microbiome or flower isolated *Pss* bacteria strains. A clever assay to prove that the volatiles produced by the BCA was a mode of action that reduced the pathogens growth was employed by removing a strip of the media that was between the co-inoculants (Mina et al., 2020). This type of assay should be used as a follow up experiment for both the commercial BCAs and the *Pss* used in this study's experiment.

The experimental design of this study was not conducive to measuring competitive exclusion and the modes of action of the BCAs were either the production of secondary metabolites or volatiles. The BCAs BB, BLT and BP are thought to function as competitive excluders of the fire blight pathogen, *E. amylovora* (Sundin et al., 2009; Wilson and Lindow 1994; Zeng et al., 2023). However, strains of *Pseudomonas fluorescens*, *Bacillus amyloliquefaciens*, *Bacillus subtilis*, and *Aureobasidium pullulans* which are the bacteria or fungi in the BCAs BB, DN, SO, and BP respectively, have been documented to produce volatile organic compounds as a mode of action for the suppression of plant pathogens (Dimkić et al., 2022; Köhl et al., 2019; Tilocca et al., 2020). While strains of *Pseudomonas fluorescens*, *Bacillus amyloliquefaciens*, *Bacillus subtilis*, and *Pantoea agglomerans* which are the organisms in the BCAs BB, DN, SO, and BLT and are well known producers of secondary metabolites with antibiotic activity (Dimkić et al., 2022; Köhl et al., 2019; Lorenzi et al., 2022; Sundin et al., 2009; Tilocca et al., 2020). Again, it should be emphasized that this type of experiment is very simplistic and only can give an initial glimpse into what may occur between the pathogen and the BCA, and it excludes the nuances of additional benefits or interactions the BCA may provide in-

planta. For example, BP is also thought to induce host resistance of the plant to *E. amylovora* due to the apparent pathogenesis of *A*. *pullulans* itself, which could only be deduced from in-planta experiments (Zeng et al., 2023). Additionally, a major caveat in the execution of this specific experiment was the way in which the co-inoculated plates were stored within the growth chamber. The individual Petri plates were not sealed but were stacked on trays and then sealed en masse within a plastic bag with the intention of preventing drying of the media which may have resulted in the unintended gassing, via volatiles, of the entire experiment which may have influenced results. As mentioned above *Pseudomonas* spp. themselves are capable of producing volatiles and the *Pss* strains in these experiments also contributed to the malodorous malady (Dimkić et al., 2022; Tilocca et al., 2020). Seiber et al. (2020) found that a volatile is likely the signal to induce the production of mangotoxin in the *Pss* causal agent of bacterial apical necrosis in Mango.

This experiment was successful in demonstrating that the commercially available biological controls can affect the mean total area of growth of *Pss* at all experimental time points (2019-2021). Where in 2019, there was an overall 25 to 27% decrease for *Pss* PG2d next to BP and SO, in 2021, there was an overall decrease for the PG2b strains *Pss* 23 and 34 next to BB, BLT, BP, DN, and SO, while strain 34 on its own had a 32 to 49% decrease in growth. This was inconsistent across the strains where strains 14 (PG2c), 25 (PG2d), and 38 (PG2d) did not have a treatment effect only rate, and the PG2d strains 9 and 27 also had no effect of treatment only strain and BCA rate. No BCA stood out from all the others as a better contender for decreasing *Pss* growth as they were not statistically different from one another and equally capable of suppressing growth or not.

The effect of strain only demonstrates that certain strains are stronger when in-vitro next to BCAs or water but does not indicate any clear level of suppression. For example, strain 34 grew stronger than strain 23, however strain 34 had a greater level of suppression (32 to 49%) than strain 23 which had a range of no suppression to 12% suppression compared to when next to water. This was also true for strain 37 (PG2d) which was a stronger strain compared to strains 26 (PG2d) and 22 (PG2b) but it had a higher level of suppression when grown next to all BCAs ranging from 11to 36% while strain 26 and 22 did not have any suppression of growth and in some instances had a greater mean area of growth the next to the BCA than when next to water. These strain differences in their responses to BCAs also highlights the importance of understanding the types of strains that are present in an orchard. Where if strains like 22, 23, and 26 that were resistant to the influence of BCAs were to be dominate in the sweet cherry microbiome then the use of BCAs for population management would be and exercise in futility while if the microbiome were dominated by the strains 34 and 37 that had suppression of growth when challenged with BCAs there could be a stronger possibility for successful usage of BCAs for population management. *Pss* and *Pseudomonas*, in general, are a diverse group of organisms with pathogenic and non-pathogenic strains and are able to cohabitate commensally and synergistically with other bacteria it could be that some of these strains are better at co-existing with a broader range of other bacteria genera and that is why there are differences in effects of the BCAs (Hulin et al., 2020; Lauwers, 2022; Melnyk et al., 2019; Purahong et al., 2018; Shalev et al., 2021; Shalev et al., 2022; Xin et al. 2018). These strains should be analyzed further at the molecular to determine if differences exist genetically between strains as it has been determined that some *Pseudomonas* have had genetic gains and losses in relation to pathogenicity, their

ability to live commensally, as well as their ability induce plant protection (Melnyk et al., 2019; Shalev et al., 2022).

Overall, the 1.5x rate did not give any advantage to those treatments where the lowest mean total area of growth was at 0.5x and 1.0x with no statistical differences between them. For strains 9 and 27, however, the 1.5x and 0.5x rates had a lower mean total area of growth but then there was no statistical difference between 1x and 1.5x rates. The 1x rate is a suitable rate for this type of experiment. There was no advantage conferred to the lone fungal BCA, Blossom Protect™ (BP), by including assay on the PDA media as overall there were no differences between strains grown next to water than when grown next to BP. It was demonstrated that the strains grew stronger on KB and the effect of the BCAs on KB were more pronounced which indicates that KB is a more suitable media for this experiment, and the assays on KB were more informative.

For the 2022 in-vitro experiments were the virulent to moderately virulent *Pss* strains were co-inoculated next to the moderate to avirulent *Pss* strains that were isolated from the sweet cherry flower there were no effects of treatment when the virulent to moderate strains were inoculated at 10^8, 10^6, or 10^4 cfu/ml next to the moderate to avirulent *Pss* inoculated at 10^8 cfu/ml. Strain differences in their mean total area of growth demonstrated that the more virulent PG2d strains (9, 25) had stronger mean area of growth than the PG2b strains (23, 33), with strain 23 being the weakest. When the virulent to moderately virulent strains were inoculated at 10^4 cfu/ml next to the moderate to avirulent *Pss* inoculated at 10^8 though not statistically different, the strains 33 and 23 caused a 33% decrease in growth of the strains 9 and 25, while the treatment strains 18 and 14 had a 14% to 28% decrease in the growth of the strains PG2d/2b strains (9, 25, 33, 23) when compared to those co-inoculated with water. Considering that these

strains were already capable of living side by side on the sweet cherry flower in the field it may again be a demonstration of their ability to co-exist with one another it is curious that they do so while having different levels of virulence. Again, these strains should be analyzed at the genetic level to determine what genes they have in common.

4.6: Conclusions

This experiment demonstrated that in-vitro co-inoculations assays are a good initial way to look at the potential interactions between *Pss* and BCAs. All the BCAs tested had the ability to decrease the mean total area of growth of *Pss* likely via secondary metabolite or volatiles while no one particular BCA excelled over the other. None of the avirulent to moderately virulent *Pss* were able to significantly decrease the mean total area of growth of the virulent to moderately virulent *Pss,* but they were closer to achieving an effect when the virulent to moderately virulent *Pss* were inoculated at a lower rate (10^4 cfu/ml) while the virulent to moderately virulent strains were at the higher rate (10^8 cfu/ml). However, it is clear that these avirulent to moderately virulent strains are also not good candidates as potential biological control agent of pathogenic *Pss*. Further experiments done using this method should include the assays for volatiles, enzymes and secondary metabolites like those used in Mina et al. (2020), and all plates should be individually sealed. The *Pss* strains should be investigated further on the genetic level comparing virulence genes and the genes necessary for commensal living.

Table 4.1. The rates of the commercial biological control agents (BCA) with the abbreviations used in tables and figures (per 100 gallons of water), organism, and manufacturer used in all of the co-inoculation experiments in which *Pss* was grown next to a BCA or next to H_2O, including the year (Exp. year) when the experiment took place or in which the BCA was used, where 1x is the maximum recommended label rate (in **bold**), 0.5x is half that, and 1.5x is that above the maximum recommended.

BCA	Organism/Manufacturer	Type	Rate/100 gal.		Exp. Year
BlightBan®A506	*Pseudomonas fluorescens* A506	Bacteria	2.65 oz	0.5x	2021
(BB)	Nufarm Americas Inc., Alsip,, IL		**5.30 oz**	**1.0x**	2021
			7.95 oz	1.5x	2021
Bloomtime™	*Pantoea agglomerans* E325, NRRL B-21586	Bacteria	75.0 g	0.5x	2021
(BLT)	Verdesian Life Science, US, LLC, Cary, NC		**150.0 g**	**1.0x**	2021
			225.0 g	1.5x	2021
Blossom Protect™ :	*Aureobasidium pullulans* DSM 14940, DSM 14941	Fungus	0.63 : 4.38 lb	0.5x	2021
Buffer Protect	Westbridge, Chelsea Vista, CA		**1.25 : 8.75 lb**	**1.0x**	2019, 2021
(BP)			1.88 : 13.13 lb	1.5x	2021
Double Nickel55™	*Bacillus amyloliquefaciens* D747	Bacteria	1.5 lb	0.5x	2021
(DN)	Certis USA LLC, Columbia, MD		**3.0 lb**	**1.0x**	2021
			4.5 lb	1.5x	2021
Serenade®Opti	*Bacillus subtilis* QST 713	Bacteria	10.0 oz	0.5x	2021
(SO)	Bayer CropScience LP, St. Louis, MO		**20.0 oz**	**1.0x**	2019, 2021
			30.0 oz	1.5x	2021

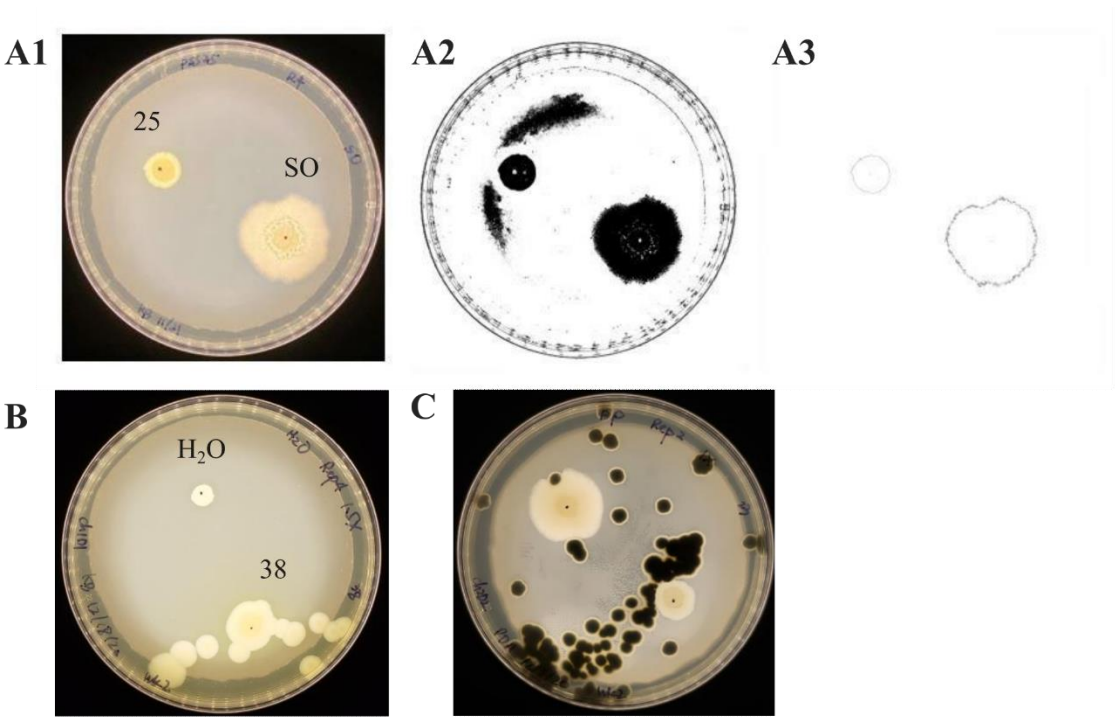


Figure 4.1. An example of co-inoculated plates: **A1)** *Pss* strain 25 next to the biological control agent (BCA) Serenade®Opti (SO), **A2)** the threshold image produced by ImageJ that is used for defining the area to be measured, **A3)** is the outline of the measured area of growth (mm^2) for the *Pss* strain 25 used in the analysis and SO (area not included in the statistical analysis), **B)** the filter paper alone (no growth) that was inoculated with H_2O and an example of pipette splatter during inoculation of strain 38 for which the total area of growth (mm^2) was measured, and **C)** an example of a plate that was contaminated with an unknown fungus and was excluded from the statistical analysis.

Table 4.2. The 2021 grouping of *Pss* strains that were co-inoculated next to the biological control agents BlightBan®A506 (BB), Bloomtime™ (BLT), Blossom Protect™ (BP), Double Nickel55™ (DN), Serenade® Opti (SO), or H_2O, their phylogroup (PG), inoculation timing and growth chamber assignment.

Year	Group	*Pss* strains	PG	Week	Day	Growth chamber
2021	**1**	14	2c	A	1	1
		25	2d			
		38	2d			
	2	23	2b		2	2
		34	2b			
	3	22	2b	B	1	1
		26	2d			
		37	2d			
	4	9	2d		2	2
		27	2d			

Table 4.3. The 2022 group assignment of *Pss* strains 9, 25, 23, 33 (the virulent to moderately virulent strains) that were co-inoculated next to the avirulent and moderately virulent (strains 14, 18, 23, 33), their phylogroups, the rates at which they were inoculated, and day of inoculation. Water (ctrl) was co-inoculated next to strains 9 , 25, 23, 33 for each group.

Group	Day	*Pss* strain	PG	Rate (cfu/ml)		*Pss* strain	PG	Rate (cfu/ml)	virulence
1	1	9	2d	**10^8**	v.	33	2b	10^8	virulent v. moderate
					v.	18	2c	10^8	virulent v. avirulent
					v.	H_2O			ctrl
		25	2d	**10^8**	v.	23	2b	10^8	virulent v. moderate
					v.	14	2c	10^8	virulent v. avirulent
					v.	H_2O			ctrl
		33	2b	**10^8**	v.	18	2c	10^8	moderate v. avirulent
					v.	H_2O			ctrl
		23	2b	**10^8**	v.	14	2c	10^8	moderate v. avirulent
					v.	H_2O			ctrl
2	2	9	2d	**10^6**	v.	33	2b	10^8	virulent v. moderate
					v.	18	2c	10^8	virulent v. avirulent
					v.	H_2O			ctrl
		25	2d	**10^6**	v.	23	2b	10^8	virulent v. moderate
					v.	14	2c	10^8	virulent v. avirulent
					v.	H_2O			ctrl
		33	2b	**10^6**	v.	18	2c	10^8	moderate v. avirulent
					v.	H_2O			ctrl
		23	2b	**10^6**	v.	14	2c	10^8	moderate v. avirulent
					v.	H_2O			ctrl
3	3	9	2d	**10^4**	v.	33	2b	10^8	virulent v. moderate
					v.	18	2c	10^8	virulent v. avirulent
					v.	H_2O			ctrl
		25	2d	**10^4**	v.	23	2b	10^8	virulent v. moderate
					v.	14	2c	10^8	virulent v. avirulent
					v.	H_2O			ctrl
		33	2b	**10^4**	v.	18	2c	10^8	moderate v. avirulent
					v.	H_2O			ctrl
		23	2b	**10^4**	v.	14	2c	10^8	moderate v. avirulent
						H_2O			ctrl

Table 4.4. The 2019 ANOVA for co-inoculations of the virulent *Pss* phylogroup (PG) 2d strains 9, 25, 37, and 38 grown next to the commercial biological controls Serenade® Opti (SO), Blossom Protect™ (BP) or water (H_2O) in Petri plates with KB media.

Year	Model term	df 1	df 2	F-ratio	p-value
2019	**trt**	2	48	6.246	**0.0039**
	strain	3	48	0.458	0.7132
	trt * strain	6	48	0.680	0.6663

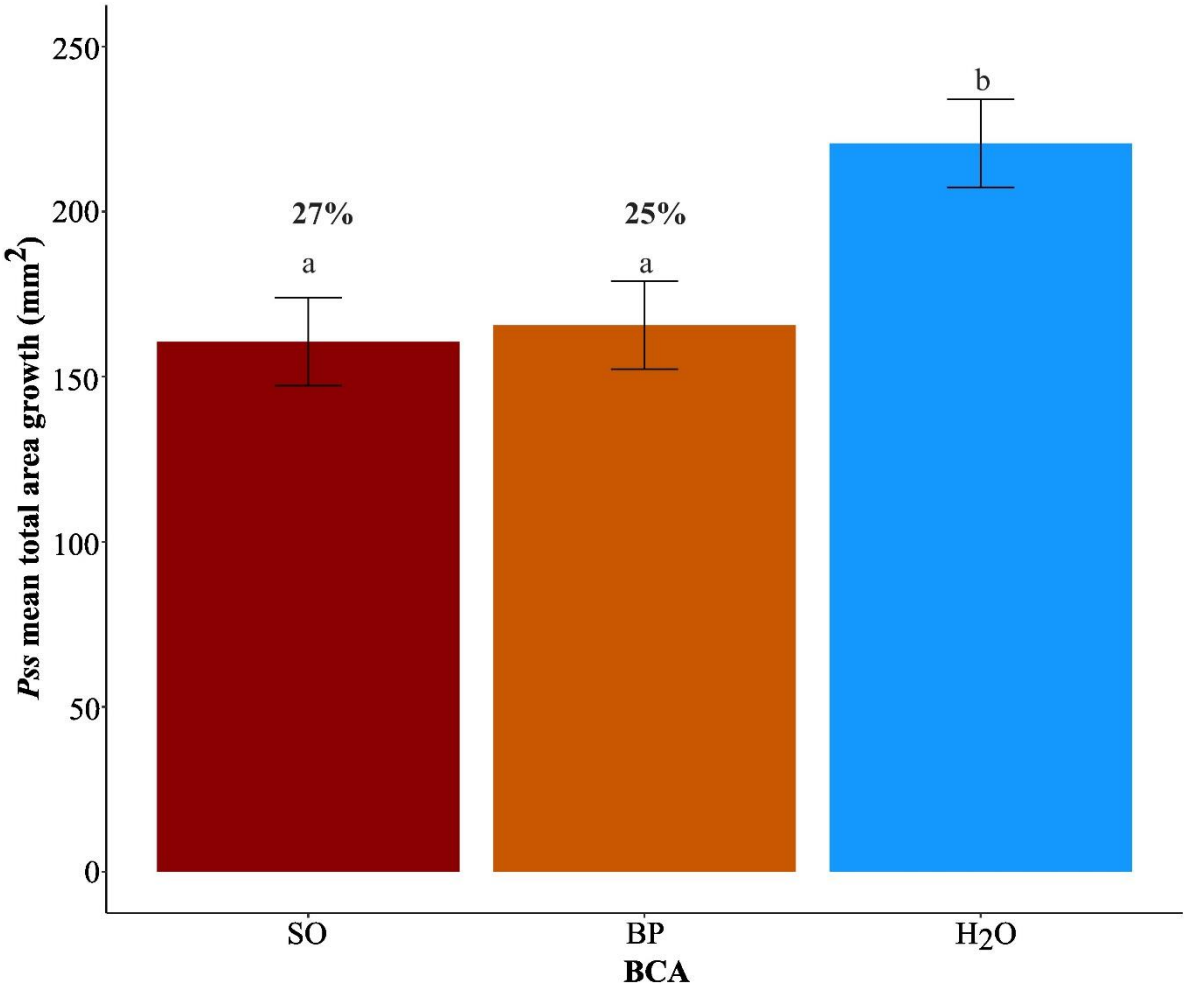


Figure 4.2. The mean total area of growth (mm^2) ± SE of virulent *Pss* phylogroup (PG) 2d strains 9, 25, 37, and 38 at 10^8 cfu/ml grown next to the commercial biological control agents (BCAs) Serenade® Opti (SO), Blossom Protect™ (BP) or water (H_2O). The % decrease in growth for the strains in co-inoculated with the BCAs vs. H_2O is shown. The letters indicate statistical differences of the treatments with significance determined by p-value ≤0.05.

Table 4.5. The 2021 ANOVA tables for co-inoculations of ten *Pss* strains (9, 14, 22, 23, 25, 26, 27, 34, 37, 38) from three phylogroups (PG) ranging in virulence level (PG 2d virulent, PG 2b moderate virulence, 2c avirulent) grown next to the commercial biological control agents (BCAs) BlightBan®A506 (BB), Bloomtime™ (BLT), Blossom Protect™ (BP), Double Nickel55™ (DN), Serenade® Opti (SO), or water (H_2O) in Petri plates with KB media; "group" corresponds to the *Pss* strains that were inoculated next to each BCA or H_2O as the 3 to 2 strains for each group were challenged by the BCA on separate occasions.

Year	group	strains/PG	Model term	df 1	df 2	F-ratio	p-value
2021	1	14 2c	**rate**	2	199	3.995	**0.0199**
		25 2d	trt	5	199	1.066	0.3802
		38 2d	strain	2	199	2.006	0.1372
			rate*trt	10	199	1.074	0.3841
			rate*strain	4	199	1.688	0.1543
			trt*strain	10	199	0.675	0.7467
			rate*trt*strain	20	199	1.031	0.4270
	2	23 2b	rate	2	119	1.123	0.3288
		34 2b	**trt**	5	119	5.353	**0.0002**
			strain	1	119	6.557	**0.0117**
			rate*trt	10	119	1.914	**0.0496**
			rate*strain	2	119	0.813	0.4459
			trt*strain	5	119	4.204	**0.0015**
			rate*trt*strain	10	119	1.12	0.3533
	3	22 2b	**rate**	2	189	5.103	**0.0069**
		26 2d	trt	5	189	1.210	0.3058
		37 2d	**strain**	2	189	15.802	**<0.0001**
			rate*trt	10	189	1.273	0.2483
			rate*strain	4	189	0.928	0.4490
			trt*strain	10	189	2.060	**0.0297**
			rate*trt*strain	20	189	1.032	0.4265
	4	9 2d	**rate**	2	144	4.022	**0.0200**
		27 2d	trt	5	144	2.003	0.0816
			strain	1	144	19.039	**<0.0001**
			trt*strain	5	144	0.898	0.4845

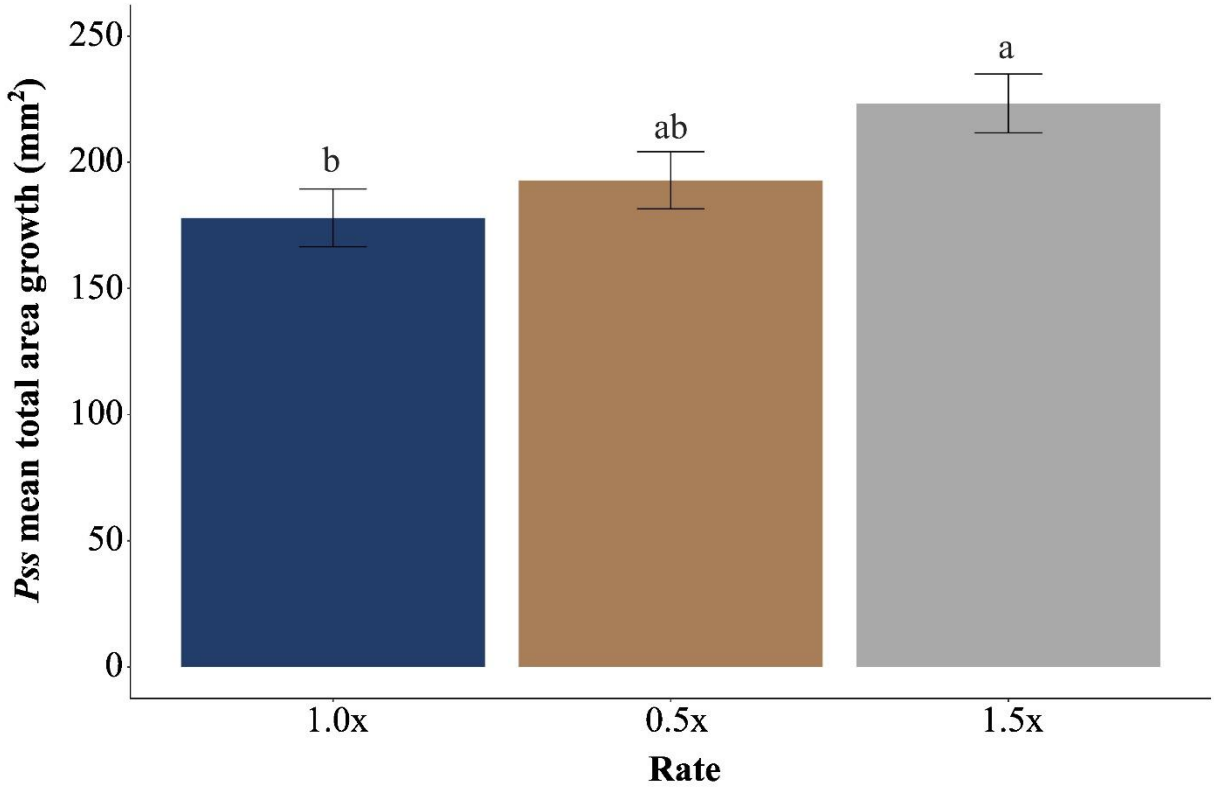


Figure 4.3. Group 1 2021, mean total area of growth ($mm^2 \pm$ SE) of *Pss* strains 14, 25, and 38, belonging to phylogroup (PG) 2c, 2d, and 2d, respectively, co-inoculated at 10^8 cfu/ml next to the five biological control agents (BCAs; BlightBan®A506, Bloomtime™, Blossom Protect™, Double Nickel55™, Serenade® Opti) or H_2O at the rates 0.5x, 1.0x, and 1.5x. Letters indicate statistical differences in *Pss* growth by BCA rate with significance determined by p-value ≤0.05.

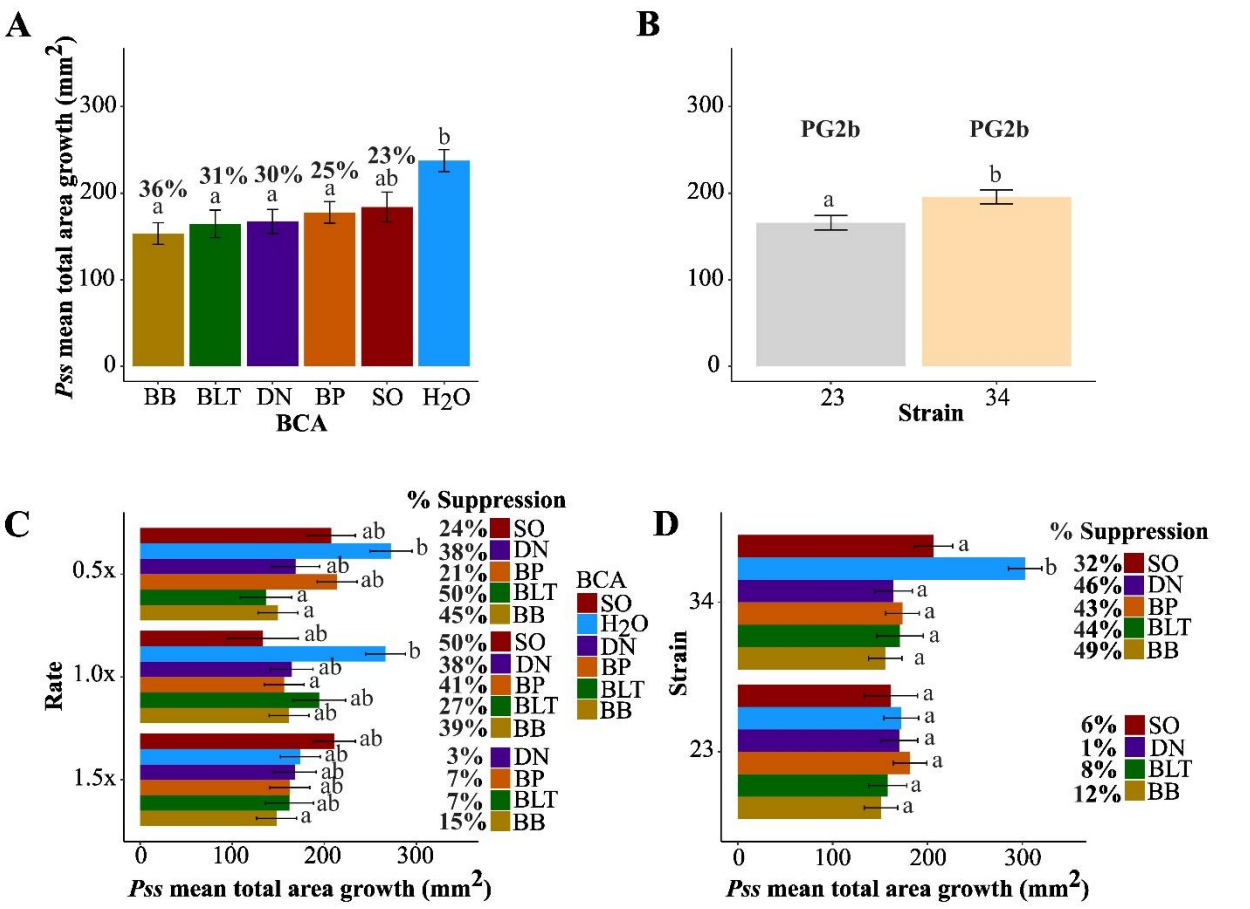


Figure 4.4. Group 2 (2021) *Pss* strains 23 and 34, belonging to phylogroup (PG) 2b ± SE co-inoculated at 10^8 cfu/ml next to the five biological control agents [BCAs; BlightBan®A506 (BB), Bloomtime™ (BLT), Blossom Protect™ (BP), Double Nickel55™ (DN), Serenade® Opti (SO)] or H_2O at the rates 0.5x, 1.0x, and 1.5x. **A)** mean total area of growth (mm^2 ± SE) of *Pss* by BCA (trt), **B)** mean total area of growth (mm^2 ± SE) by *Pss* strain overall when next to each BCA or H_2O, **C)** mean total area of growth (mm^2 ± SE) of *Pss* by BCA(trt) and BCA rate (0.5x, 1.0x, 1.5x) (rate*trt)and **D)** mean total area of growth (mm^2) of *Pss* next to each BCA (trt*strain). Letters indicate statistical differences in *Pss* growth, with significance determined by p-value ≤0.05 and the % decrease in growth of *Pss* next to each BCA vs. H_2O for trt (BCA), rate*trt, and trt*strain.

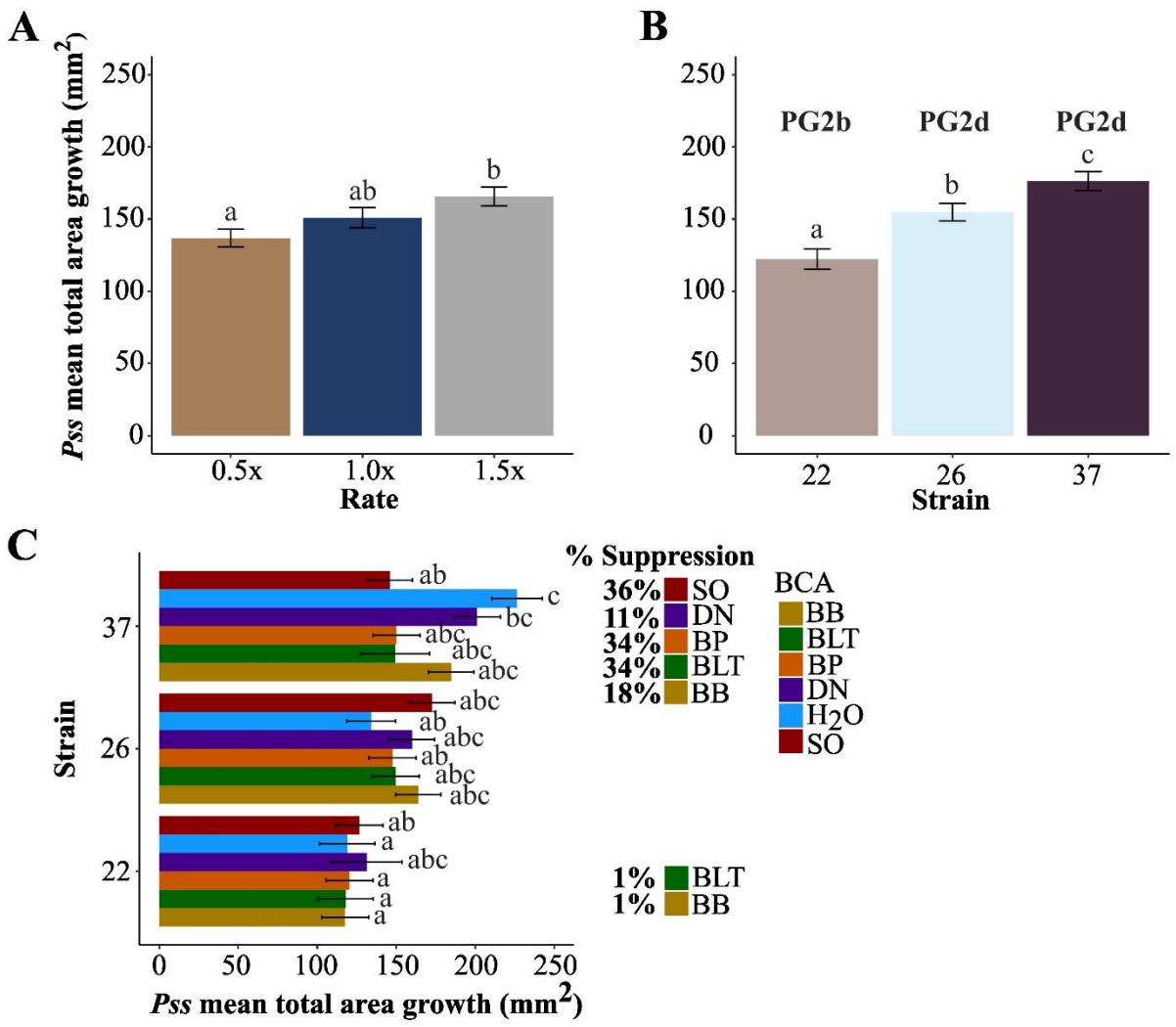


Figure 4.5. Group 3 (2021) *Pss* strains 22, 26, and 37, belonging to phylogroup (PG) 2b, 2d, and 2d, respectively, co-inoculated at 10^8 cfu/ml next to the five biological control agents [BCAs; BlightBan®A506 (BB), Bloomtime™ (BLT), Blossom Protect™ (BP), Double Nickel55™ (DN), Serenade® Opti (SO)] or H_2O at the rates 0.5x, 1.0x, and 1.5x. **A)** mean total area of growth ($mm^2 \pm$ SE) of *Pss* by BCA rate, **B)** mean total area of growth ($mm^2 \pm$ SE) by *Pss* strain overall when next to each BCA or H_2O, and **C)** mean total area of growth ($mm^2 \pm$ SE) of each *Pss* strain next to each BCA(trt) (trt*strain). Letters indicate statistical differences in *Pss* growth, with significance determined by p-value ≤0.05 and the % decrease in growth of *Pss* next to each BCA vs. H_2O for trt*strain.

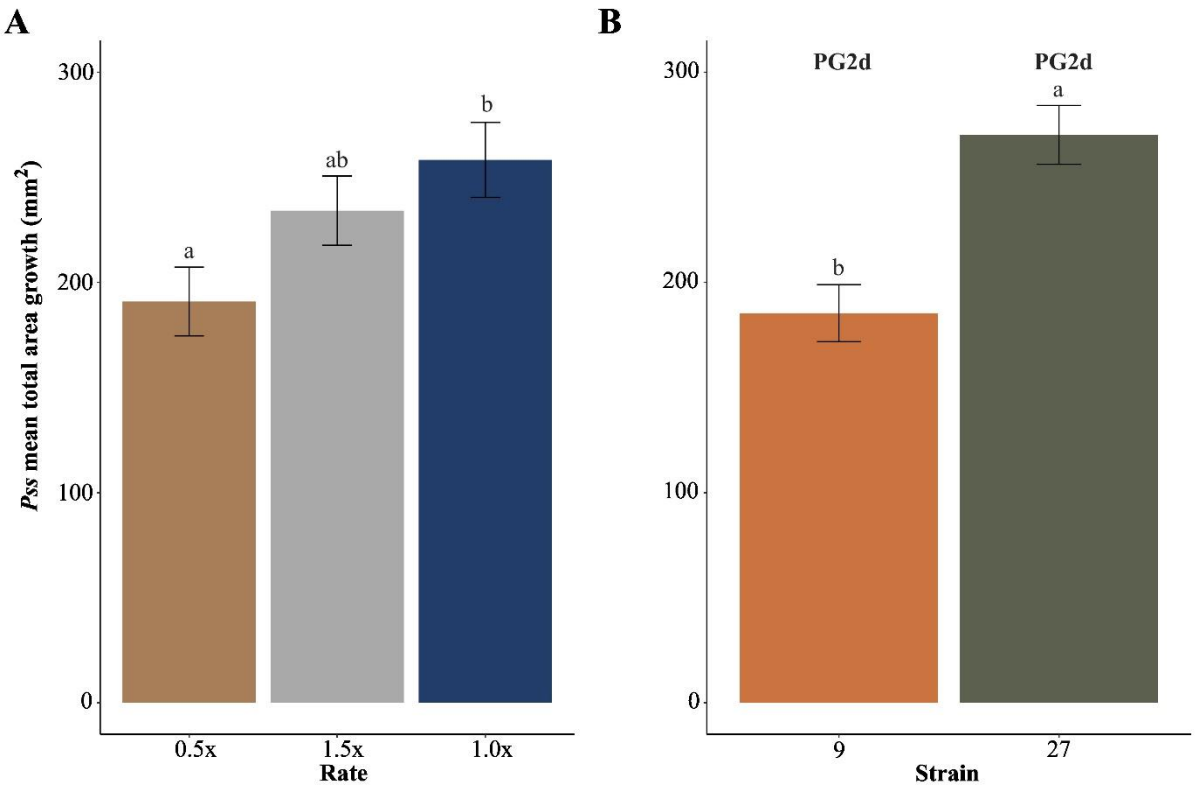


Figure 4.6. Group 4 (2021) *Pss* strains 9 and 27, belonging to phylogroup (PG) 2d ± SE co-inoculated at 10^8 cfu/ml next to the five biological control agents [BCAs; BlightBan®A506, Bloomtime™, Blossom Protect™, Double Nickel55™, Serenade® Opti] or H_2O at the rates 0.5x, 1.0x, and 1.5x. **A)** mean total area of growth (mm^2 ± SE) of *Pss* by BCA rate, and **B)** mean total area of growth (mm^2 ± SE) by *Pss* strains overall when next to each BCA or H_2O. Letters indicate statistical differences in *Pss* growth with significance determined by p-value ≤0.05.

Table 4.6. The 2021 ANOVA tables for co-inoculations of ten *Pss* strains (9, 14, 22, 23, 25, 26, 27, 34, 37, 38) from three phylogroups (PG) ranging in virulence level (PG 2d virulent, PG 2b moderate virulence, 2c avirulent) grown next to the commercial biological control agent (BCA), Blossom Protect™ (BP) or water (H_2O) in Petri plates with KB or PDA media; "group" corresponds to the *Pss* strains that were inoculated next to each BCA or H2O as the 3 to 2 strains for each group were challenged by the BCA on separate occasions.

Year	group	strains/PG	Model term	df 1	df 2	F-ratio	p-value
2021	1	14 2c	media	1	139	1.134	0.2888
		25 2d	rate	2	139	3.025	0.0518
		38 2d	trt	1	139	3.522	0.0627
			strain	2	139	3.104	0.0480
			media*rate	2	139	0.152	0.8591
			media*trt	1	139	1.263	0.2631
			media*strain	2	139	0.183	0.8333
			rate*trt	2	139	0.854	0.4280
			rate*strain	4	139	1.291	0.2767
			trt*strain	2	139	0.597	0.5518
			media*rate*trt	2	139	2.991	0.0535
			media*rate*strain	4	139	1.077	0.3703
			media*trt*strain	2	139	0.808	0.4477
			rate*trt*strain	4	139	0.485	0.7466
			media*rate*trt*strain	4	139	3.302	**0.0128**
	2	23 2b	**media**	1	93	36.438	**<0.0001**
		34 2b	**rate**	2	93	4.079	**0.0200**
			trt	1	93	6.728	**0.0110**
			strain	1	93	2.578	0.1117
			media*rate	2	93	3.755	**0.0270**
			media*trt	1	93	3.701	0.0574
			media*strain	1	93	9.064	**0.0034**
			rate*trt	2	93	1.264	0.2872
			rate*strain	2	93	1.381	0.2565
			trt*strain	1	93	4.560	**0.0354**
			media*rate*trt	2	93	1.071	0.3468
			media*rate*strain	2	93	1.735	0.1821
			media*trt*strain	1	93	9.518	**0.0027**
			rate*trt*strain	2	93	0.140	0.8693
			media*rate*trt*strain	2	93	1.815	0.1686
	3	22 2b	media	1	126	0.183	0.6693
		26 2d	**rate**	2	126	7.021	**0.0013**
		37 2d	trt	1	126	0.708	0.4016
			strain	2	126	9.185	**0.0002**
			media*rate	2	126	0.249	0.7802

Table 4.6. (cont'd)

			media*trt	1	126	1.127	0.2904
			media*strain	2	126	1.841	0.1630
			rate*trt	2	126	1.497	0.2277
			rate*strain	4	126	1.037	0.3909
			trt*strain	2	126	2.232	0.1116
			media*rate*trt	2	126	0.896	0.4108
			media*rate*strain	4	126	1.460	0.2182
			media*trt*strain	2	126	1.396	0.2513
			rate*trt*strain	4	126	1.228	0.3022
			media*rate*trt*strain	4	126	0.152	0.9616
4	9 2d		media	1	94	0.455	0.5015
	27 2d		rate	2	94	1.626	0.2021
			trt	1	94	1.428	0.2351
			strain	1	94	2.746	0.1009
			media*rate	2	94	9.652	**0.0002**
			media*trt	1	94	4.282	**0.0413**
			media*strain	1	94	3.641	0.0594
			rate*trt	2	94	0.272	0.7621
			rate*strain	2	94	6.877	**0.0016**
			trt*strain	1	94	0.015	0.9043
			media*rate*trt	2	94	1.198	0.3063
			media*rate*strain	2	94	1.223	0.2991
			media*trt*strain	1	94	0.102	0.7501
			rate*trt*strain	2	94	1.656	0.1965
			media*rate*trt*strain	2	94	0.614	0.5434

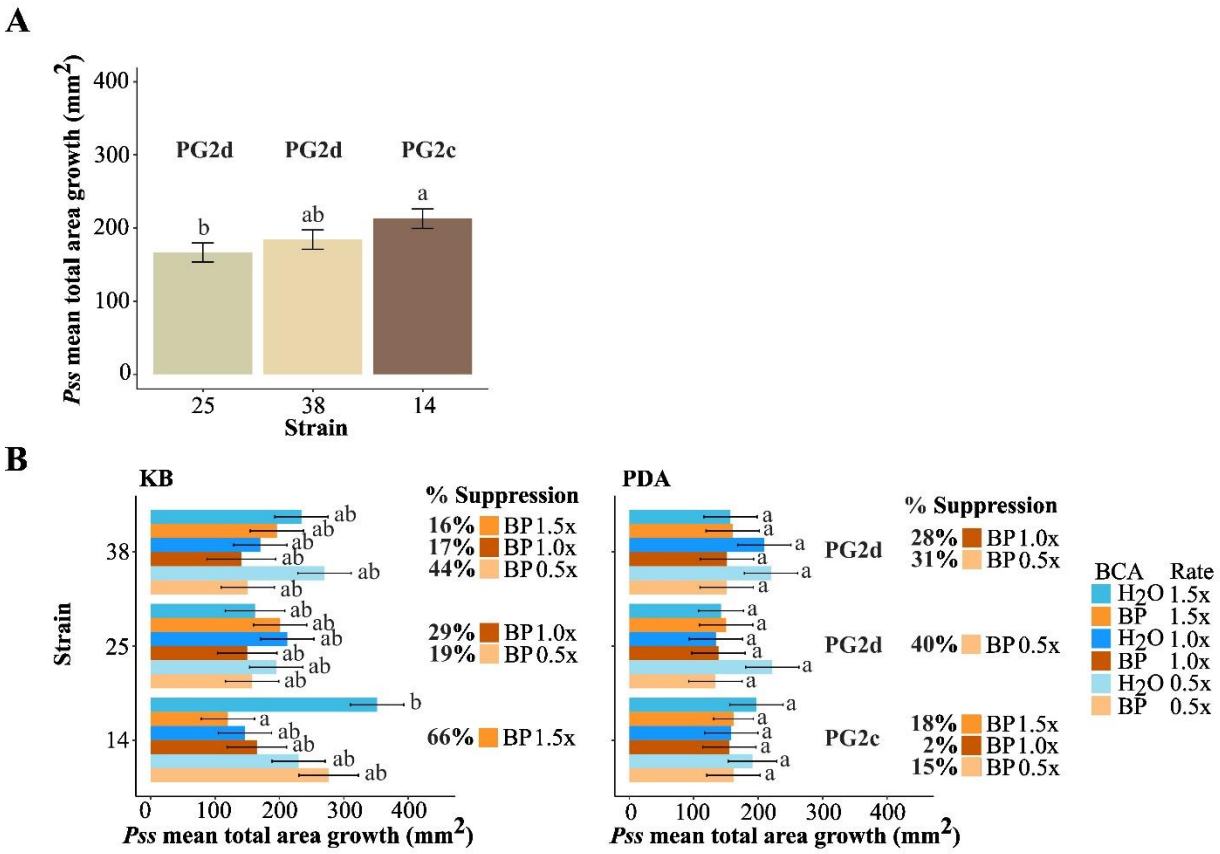


Figure 4.7. Group 1 (2021) *Pss* strains 14, 25, and 38 belonging to phylogroup (PG) 2c, 2d, and 2d, respectively, co-inoculated at 10^8 cfu/ml next to Blossom Protect™ (BP) or H_2O on KB or PDA media at the rates 0.5x, 1.0x, and 1.5x. **A)** mean total area of growth ($mm^2 \pm$ SE) of *Pss* strains overall, **B)** the mean total area of growth ($mm^2 \pm$ SE) of each *Pss* strain next to each BCA(trt) and rate nested within media (rate*trt*strain|media). Letters indicate statistical differences in *Pss* growth, with significance determined by p-value ≤0.05 and the % decrease in growth of *Pss* next to each BP vs. H_2O for rate*trt*strain|media.

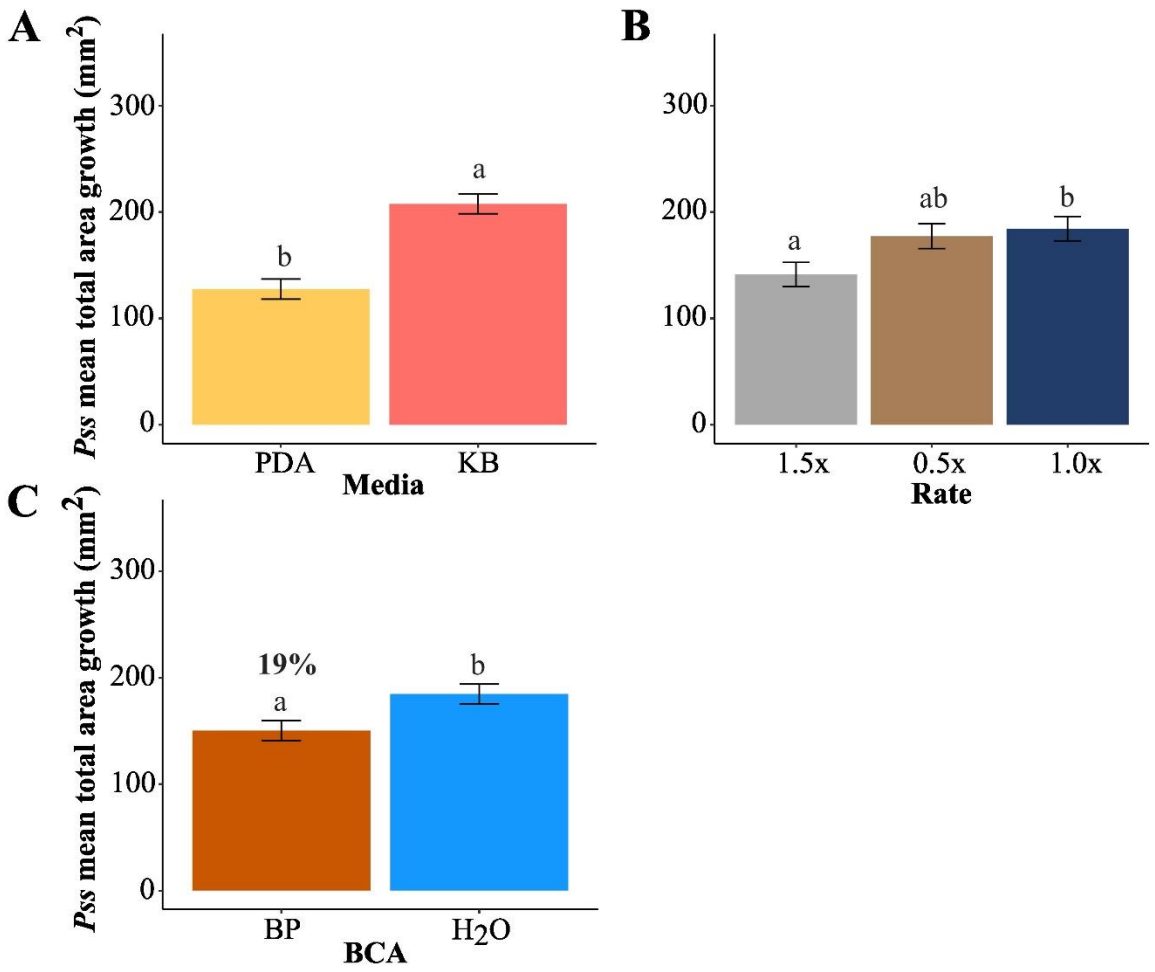


Figure 4.8. Group 2 (2021) *Pss* strains 23 and 34, belonging to phylogroup (PG) 2b co-inoculated at 10^8 cfu/ml next to the biological control agent (BCA) Blossom Protect™ (BP) or H_2O at the rates 0.5x, 1.0x, and 1.5x on KB or PDA media. **A)** mean total area of growth ($mm^2 \pm$ SE) of *Pss* when grown next to BP or H_2O on KB or PDA media, **B)** mean total area of growth ($mm^2 \pm$ SE) of *Pss* by BP rate (0.5x, 1.0x, 1.5x), and **C)** mean total area of growth ($mm^2 \pm$ SE) by *Pss* strain next to BP or H_2O. Letters indicate statistical differences in *Pss* growth with significance determined by p-value ≤0.05 and the % decrease in growth of *Pss* next to BP vs. H_2O.

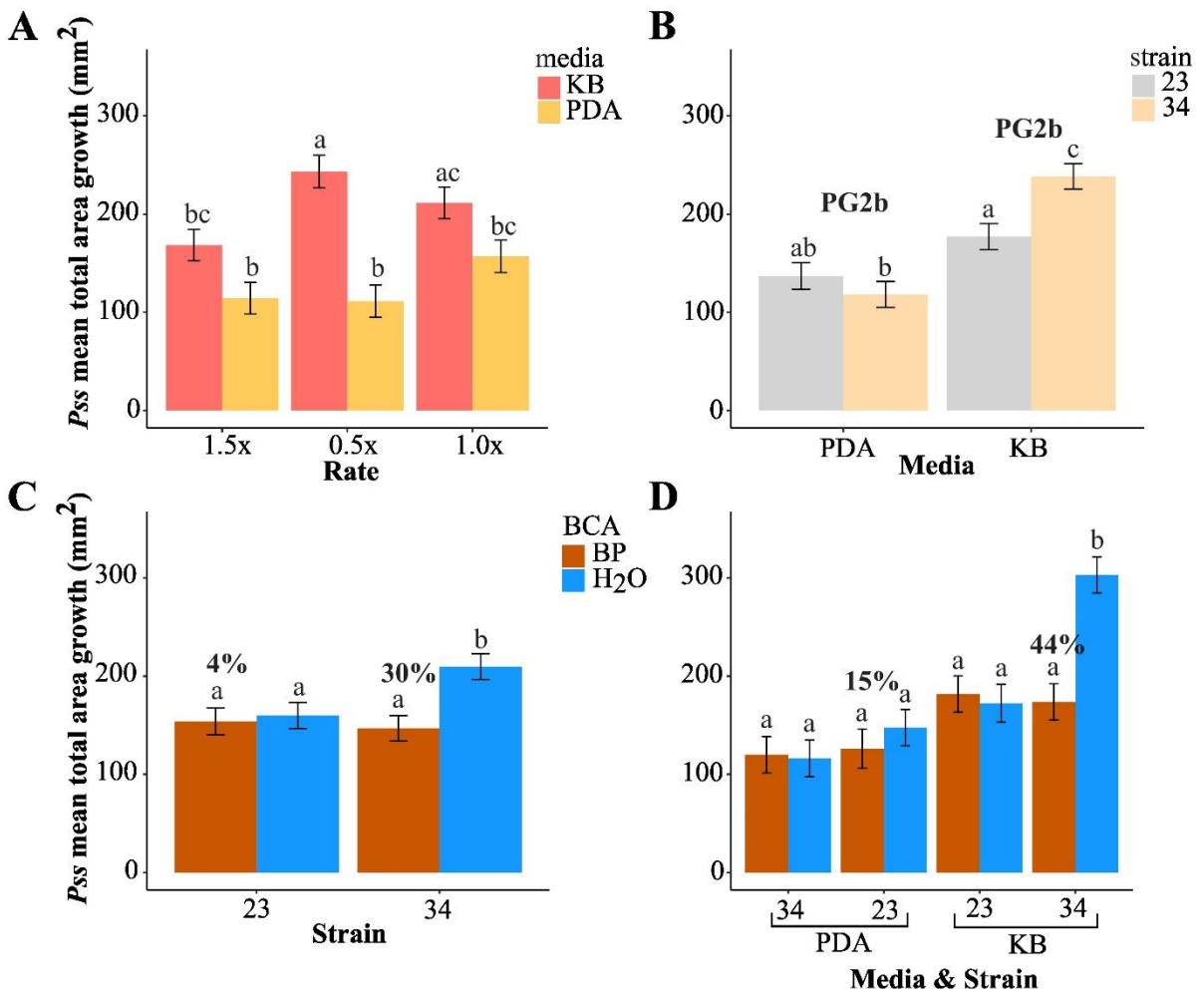


Figure 4.9. Group 2 (2021) *Pss* strains 23 and 34, belonging to phylogroup (PG) 2b co-inoculated at 10^8 cfu/ml next to the biological control agent (BCA) Blossom Protect™ (BP) or H_2O at the rates 0.5x, 1.0x, and 1.5x on KB or PDA media. **A)** mean total area of growth ($mm^2 \pm$ SE) of *Pss* when grown next to BP or H_2O at the various rates on each media (media*rate), **B)** mean total area of growth ($mm^2 \pm$ SE) of each *Pss* strain on each media (media*strain), **C)** mean total area of growth ($mm^2 \pm$ SE) by *Pss* strain next to BP or H_2O (trt*strain), and **D)** mean total area of growth ($mm^2 \pm$ SE) by *Pss* strain and media type next to BP or H_2O (media*trt*strain). Letters indicate statistical differences in *Pss* growth, with significance determined by p-value ≤0.05 and the % decrease in growth of *Pss* next to BP vs. H_2O for trt*strain and (media*trt*strain).

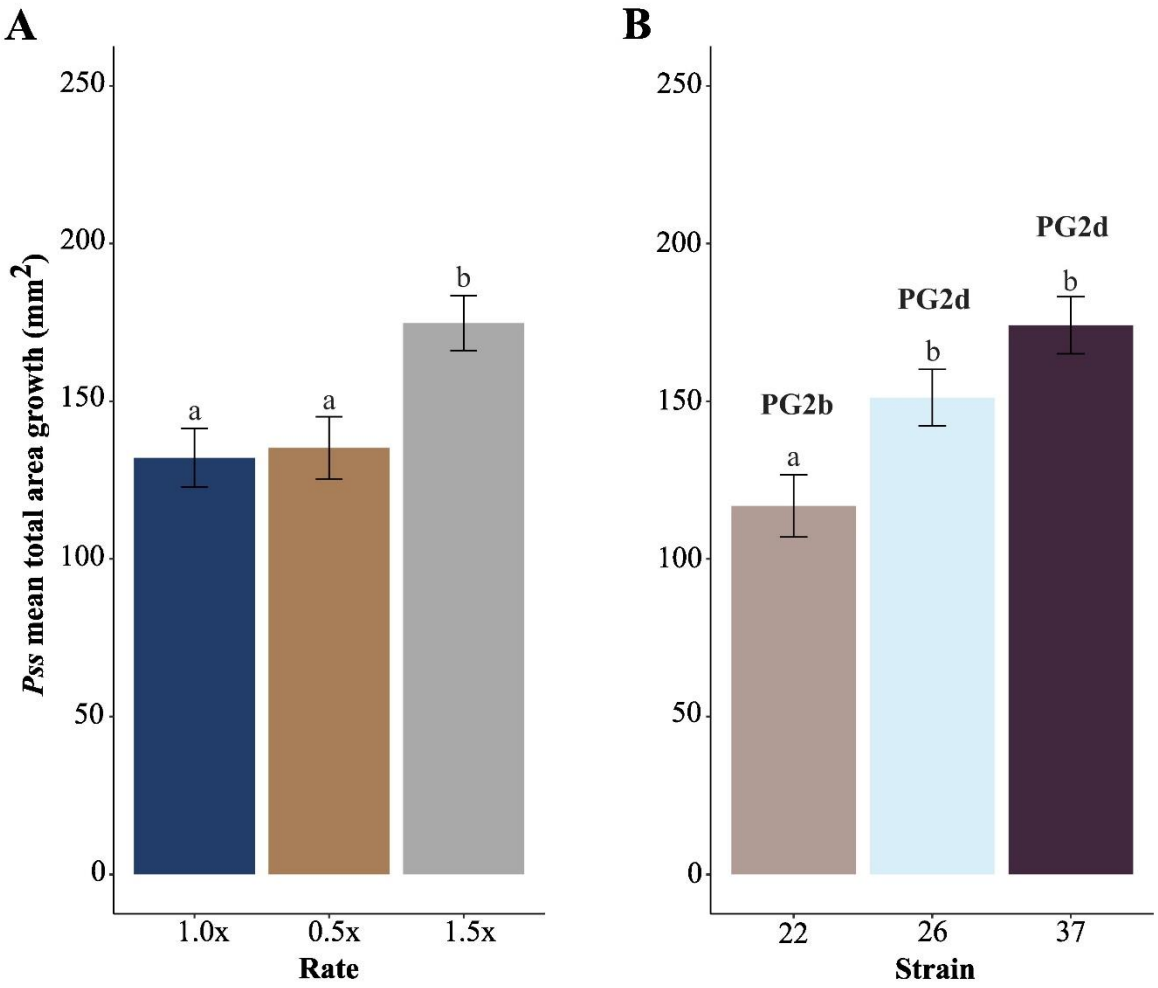


Figure 4.10. Group 3 (2021) *Pss* strains 22, 26, and 37, belonging to phylogroup (PG) 2b, 2d, and 2d, respectively, co-inoculated at 10^8 cfu/ml next to Blossom Protect™ (BP) or H_2O at the rates 0.5x, 1.0x, and 1.5x on KB and PDA media. **A)** mean total area of growth ($mm^2 \pm$ SE) of *Pss* by BP rate, **B)** mean total area of growth ($mm^2 \pm$ SE) by *Pss* strain overall when next to BP or H_2O. Letters indicate statistical differences in *Pss* growth, with significance determined by p-value ≤ 0.05.

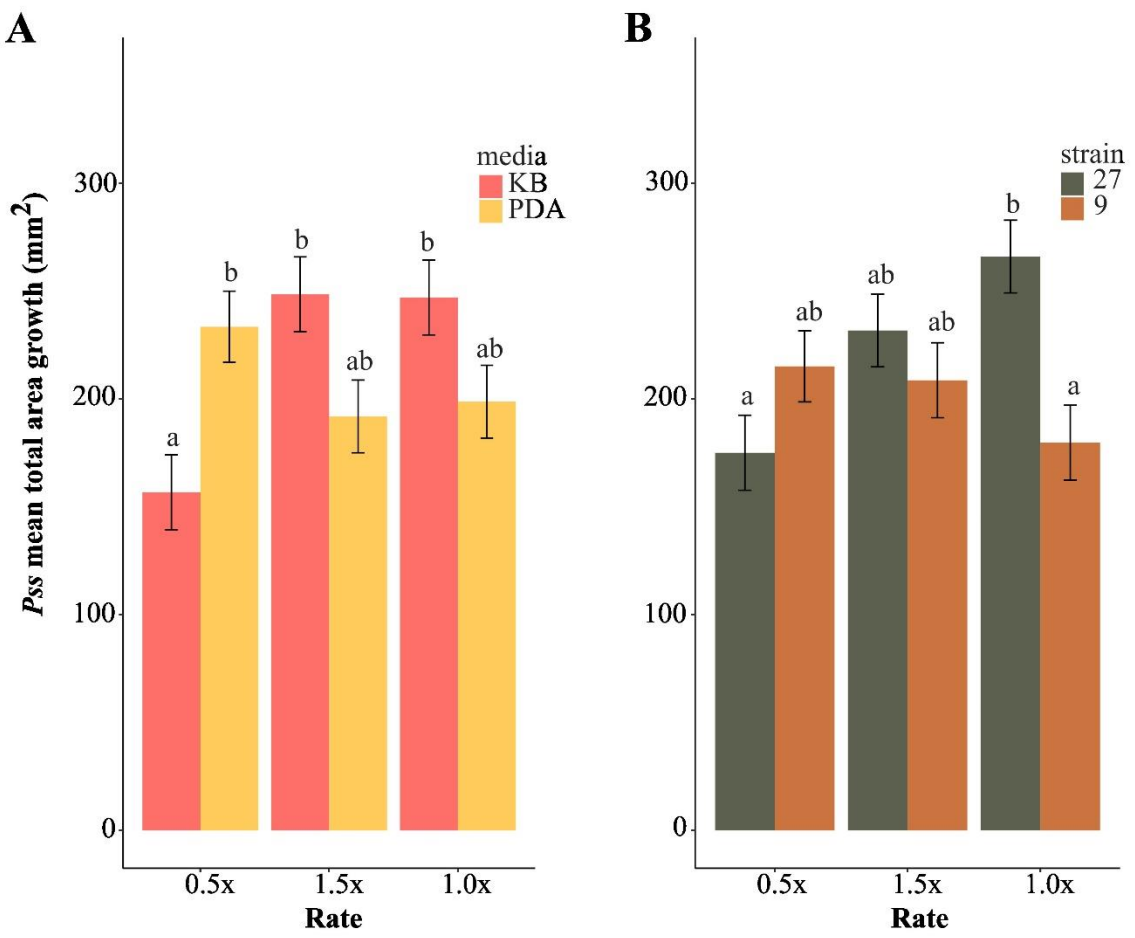


Figure 4.11. Group 4 (2021) *Pss* strains 9 and 27, belonging to phylogroup (PG) 2d co-inoculated at 10^8 cfu/ml next to Blossom Protect™ (BP) or H_2O at the rates 0.5x, 1.0x, and 1.5x on KB and PDA media. **A)** mean total area of growth ($mm^2 \pm$ SE) of *Pss* for each media by BP rate (media*rate), and **B)** mean total area of growth ($mm^2 \pm$ SE) by *Pss* strains overall at each BP rate (rate*strain). Letters indicate statistical differences in *Pss* growth, with significance determined by p-value ≤0.05.

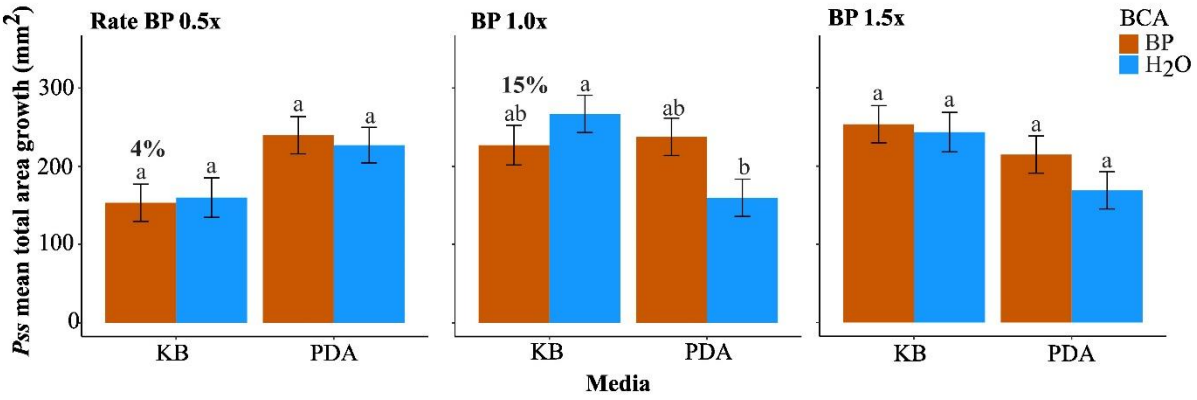


Figure 4.12. Group 4 (2021) *Pss* strains 9 and 27, belonging to phylogroup (PG) 2d co-inoculated at 10^8 cfu/ml next to Blossom Protect™ (BP) or H_2O at the rates 0.5x, 1.0x, and 1.5x on KB and PDA media: mean total area of growth ($mm^2 \pm$ SE) of *Pss* next to BP or H_2O for each media by BP rate (media*trt|rate). Letters indicate statistical differences in *Pss* growth, with significance determined by p-value ≤0.05 and the % decrease in growth of *Pss* strains next to BP vs. H_2O.

Table 4.7. The 2022 ANOVA tables for co-inoculations of *Pss* strains 9, 25 (PG 2d virulent) and 23, 33 (PG2b moderate virulence) grown next to the strains 14, 18 (PG 2c avirulent), and 23,33 (PG2b moderate virulence) or water (H_2O) in Petri plates with KB media; "group" corresponds to the rate combination at which the PG2d and PG2b strains were inoculated next to the PG2c and PG2b strains or H_2O, for which group 1 strains were inoculated at 10^8 cfu/ml, group 2 strains at 10^6 v. 10^8 cfu/ml, and group 3 strains at 10^4 v. 10^8 cfu/ml.

Year	group	strains/PG	Rate (cfu/ml)	Model term	df 1	df 2	F-ratio	p-value
2022	1	9 (2d) v. 33 (2b) /18 (2c) or H_2O 25 (2d) v. 23 (2b) /14 (2c) or H_2O 23 (2b) v. 14 (2c) or H_2O 33 (2b) v. 18 (2c) or H_2O	10^8 v. 10^8	**strain** trt	3 4	41 41	20.525 0.689	**<0.0001** 0.6038
	2	9 (2d) v. 33 (2b) /18 (2c) or H2O 25 (2d) v. 23 (2b) /14 (2c) or H2O 23 (2b) v. 14 (2c) or H2O 33 (2b) v. 18 (2c) or H2O	10^6 v. 10^8	**strain** **trt**	3 4	42 42	22.128 2.584	**<0.0001** **0.0507**
	3	9 (2d) v. 33 (2b) /18 (2c) or H2O 25 (2d) v. 23 (2b) /14 (2c) or H2O 23 (2b) v. 14 (2c) or H2O 33 (2b) v. 18 (2c) or H2O	10^4 v. 10^8	strain **trt**	3 4	42 42	2.467 2.669	0.0753 **0.0452**

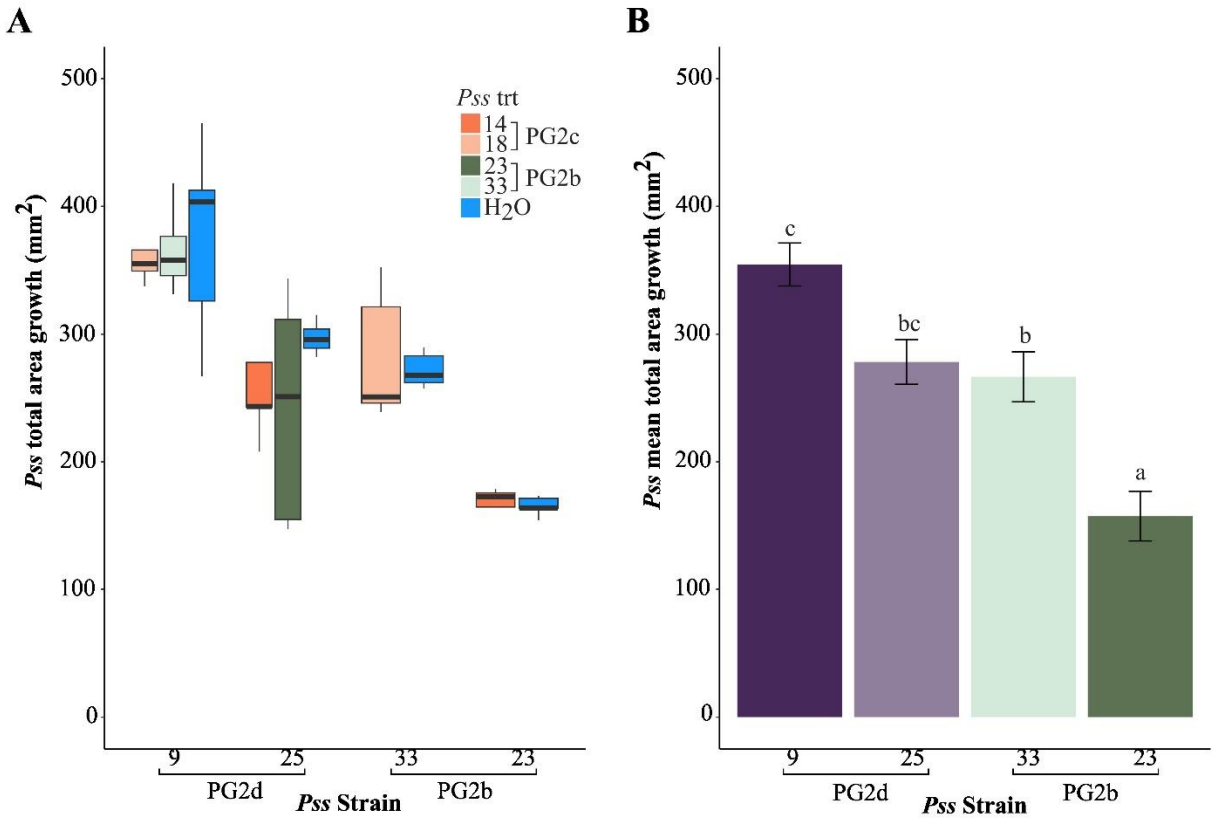


Figure 4.13. Group 1 (2022) co-inoculations of *Pss* strains 9, 25 (PG 2d virulent) or 23, 33 (PG2b moderate virulence) grown next to the treatment strains 14, 18 (PG 2c avirulent), or 23,33 (PG2b moderate virulence) or water (H_2O) in Petri plates with KB media, in which all strains were inoculated at 10^8 cfu/ml. **A)** distribution of the total area of growth ($mm^2 \pm$ SE) for each strain next to each treatment *Pss* (*Pss* trt), and **B)** mean total area of growth ($mm^2 \pm$ SE) for the strains overall. Letters indicate statistical differences, with significance determined by p-value ≤ 0.05.

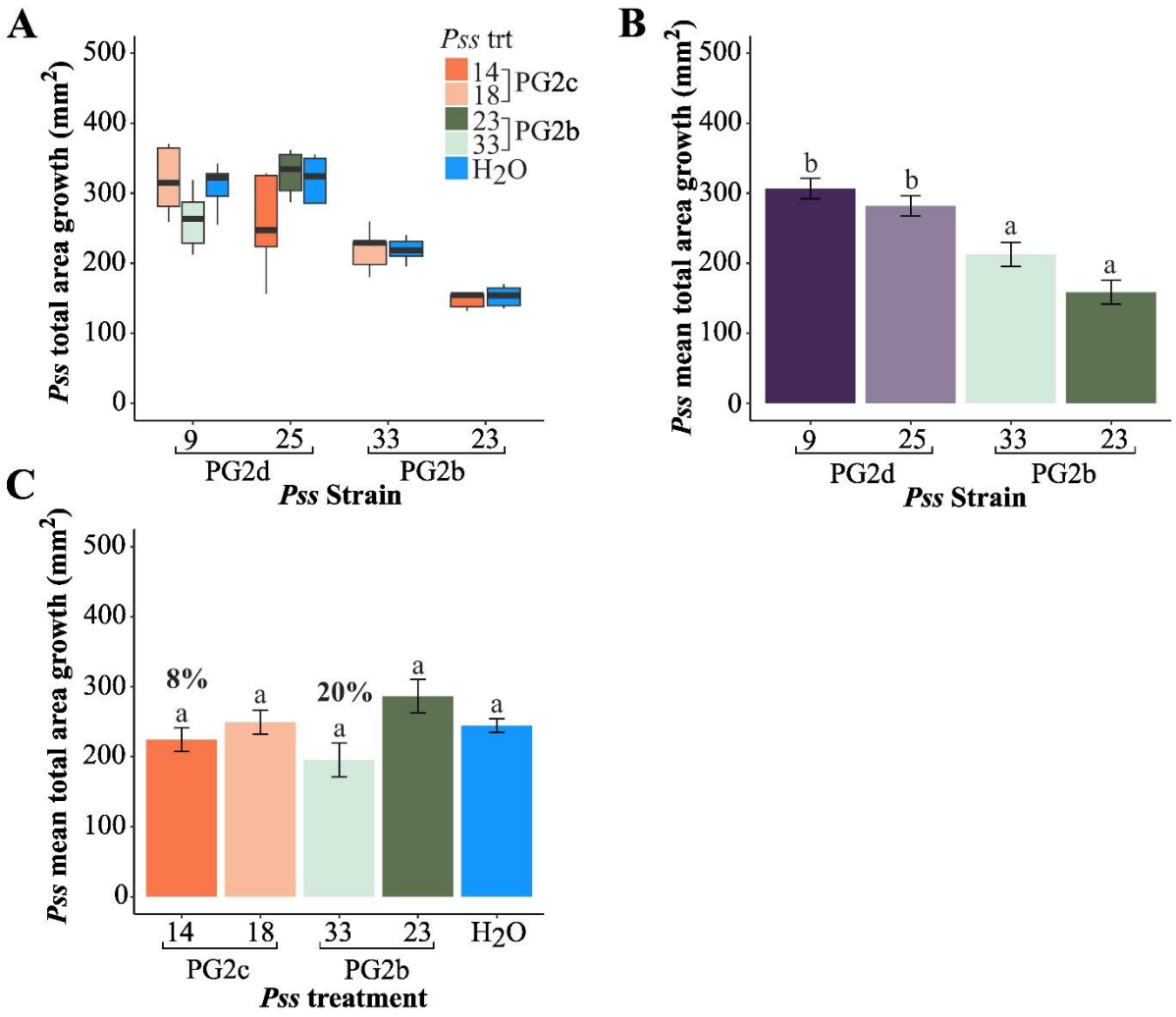


Figure 4.14. Group 2 (2022) co-inoculations of *Pss* strains 9, 25 (PG 2d virulent) or 23, 33 (PG2b moderate virulence) at 10^6 cfu/ml that are grown next to the treatment strains 14, 18 (PG 2c avirulent), or 23, 33 (PG2b moderate virulence) at 10^8 cfu/ml, or water (H_2O) in Petri plates with KB media. **A)** distribution of the total area of growth ($mm^2 \pm$ SE) for each strain next to each treatment *Pss* (*Pss* trt), and **B)** mean total area of growth ($mm^2 \pm$ SE) for the strains overall, and **C)** mean total area of growth ($mm^2 \pm$ SE) of the *Pss* strains 9, 25, or 23, 33 according to the treatment *Pss*. Letters indicate statistical differences, with significance determined by p-value ≤0.05 and the % decrease in growth of *Pss* strains grown next to the treatment *Pss* vs. water.

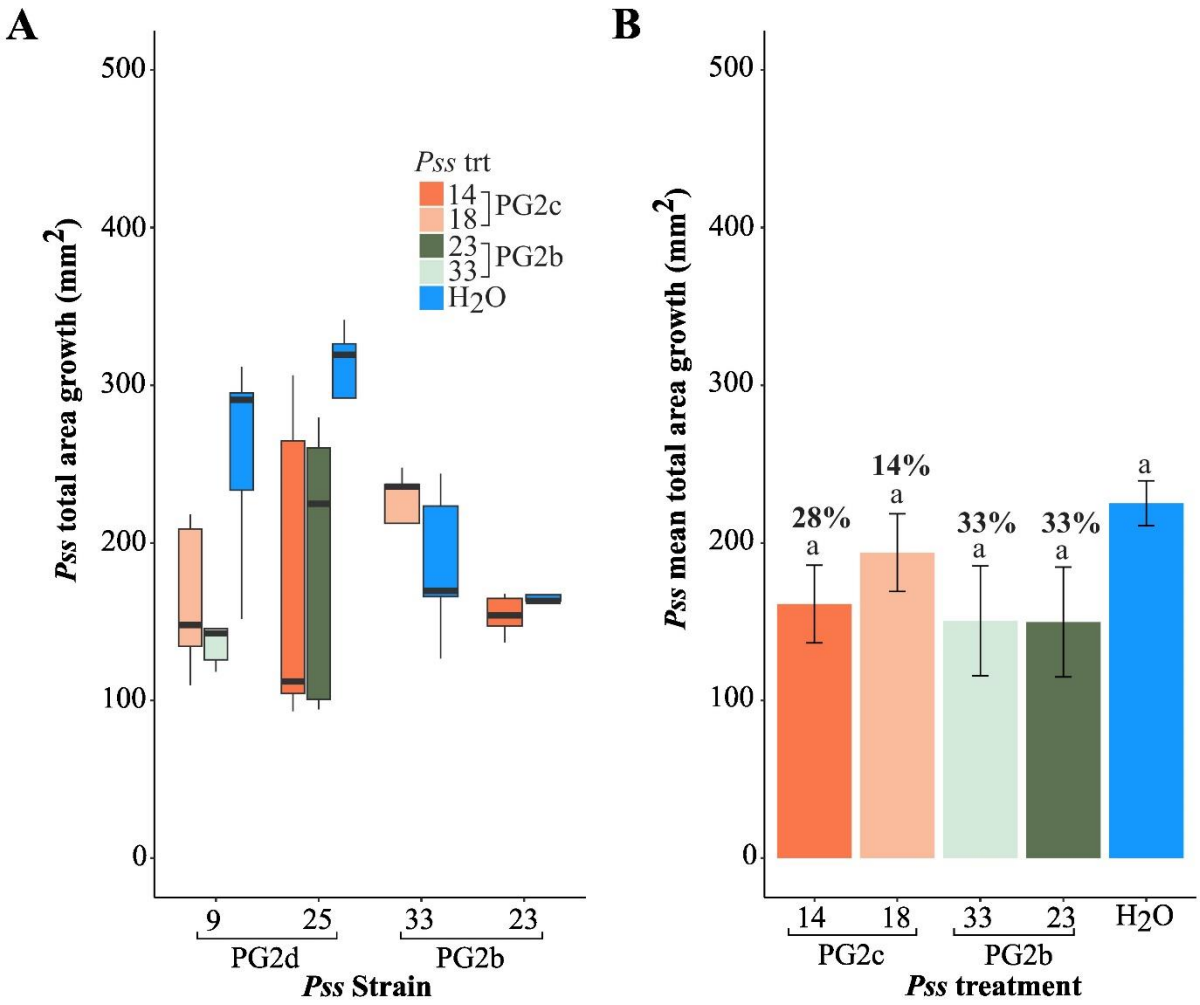


Figure 4.15. Group 3 (2022) co-inoculations of *Pss* strains 9, 25 (PG 2d virulent) or 23, 33 (PG2b moderate virulence) at 10^4 cfu/ml that are grown next to the treatment strains 14, 18 (PG 2c avirulent), or 23, 33 (PG2b moderate virulence) at 10^8 cfu/ml, or water (H_2O) in Petri plates with KB media. **A)** distribution of the total area of growth ($mm^2 \pm$ SE)) for each strain next to each treatment *Pss* (*Pss* trt), and **B)** mean total area of growth ($mm^2 \pm$ SE) of the *Pss* strains 9, 25, or 23, 33 according to the treatment *Pss*. Letters indicate statistical differences, with significance determined by p-value ≤0.05 and the % decrease in growth of *Pss* strains grown next to the treatment *Pss* vs. water.

REFERENCES

Akbaba, M., Ozaktan, H. 2021. Evaluation of bacteriophages in the biocontrol of Pseudomonas syringae pv. syringae isolated from cankers on sweet cherry (Prunus avium L.) in Turkey. Egypt. J. Biol. Pest Control 31: 35. https://doi.org/10.1186/s41938-021-00385-7

Arrigoni, E., Antonielli, L., Pindo, M., Pertoto, I., and Perazzolli, M. 2018. Tissue age and plant genotype affect the microbiota of apple and pear bark. Microbiological Research 211: 57-58.

Broniarek-Niemiec, A., Børve, J., and Puławska, J. 2023. Control of bacterial canker in stone fruit trees by chemical and biological products. *Agronomy* 13(4): 1166. https://doi.org/10.3390/agronomy13041166

Brown, L.E. 2023. Bacteriophage as a potential biological control for bacterial canker of sweet cherry. Master's thesis, Michigan State University, ProQuest Dissertations and Theses Global.

Carroll, J., Robinson, T., Burr, T., Hoying, S., and Cox, K. 2010. Evaluation of pruning techniques and bactericides to manage bacterial canker of sweet cherry. New York Fruit Quarterly 18(1): 9-15.

Chaouachi M., Marzouk, T., Jallouli, S., Elkahoui, S., Gentzbittel, L., Ben, C., and Djébali, N. 2021. Activity assessment of tomato endophytic bacteria bioactive compounds for the postharvest biocontrol of Botrytis cinerea. Postharvest Biol. Tech. 172:111389.

Cirvilleri, G., Bonaccorsi, A., Scuderi, G., and Scortichini, M. 2005. Potential biological control activity and genetic diversity of Pseudomonas syringae pv. syringae strains. J. Phytopathol. 153: 654-666.

Cui, Z., Huntley, R.B., Schultes, N.P., Steven, B., and Zeng, Q. 2021. Inoculation of stigma-colonizing microbes to apple stigmas alters microbiome structure and reduces the occurrence of Fire Blight disease. Phytobiomes J. 5: 156-165

Derikvan, F., Bazgir, E., El Jarroudi, M., Darvishnia, M., Najafgholi, H.M., Laasli, S-E., and Lahlali, R. 2023. Unleashing the potential of bacterial isolates from apple tree rhizosphere for biocontrol of Monilinia laxa: A promising approach for combatting brown rot disease. J. Fungi 9:828.

Dimkić, I., Janakiev, T., Petrović, M., Degrassi, G., and Fira, D. 2022. Plant-associated Bacillus and Pseudomonas antimicrobial activities in plant disease suppression via biological control mechanisms- A review. Physiol. Molec. Plant Pathol. 117:101754.

Duque, T., Nuriyev, R., Römbke, J., Schäfer, R.B. and Entling, M.H. 2023. Variation in the chemical sensitivity of earthworms from field populations to imidacloprid and copper. Environ Toxicol Chem. https://doi.org/10.1002/etc.5589

Hammami, R., Oueslati, M., Smiri, M., Nefzi, S., Ruissi, M., Comitini, F., Romanazzi, G., Cacciola S.O., and Zouaoui, N.S. 2022. Epiphytic yeast and bacteria as candidate biocontrol agents of green and blue molds of citrus fruits. J. Fungi 8:818.

Hulin M.T., Vadillo Dieguez A., Cossu F., Lynn S., Russell K., Neale H.C., Jackson R.W., Arnold D.L., Mansfield J.W., and Harrison R.J. 2022. Identifying resistance in wild and ornamental cherry towards bacterial canker caused by Pseudomonas syringae. Plant Pathol. 71(4):949-965.

Karimi, B., Masson, V., Guilland, C., Leroy, E., Pellegrinelli, S., Giboulot, E., Maron, P., and Ranjard, L. 2021. Ecotoxicity of copper input and accumulation for soil biodiversity in vineyards. Environ. Chem. Lett. 19: 2013–2030. https://doi.org/10.1007/s10311-020-01155-x

Kassambara A (2023). ggpubr: 'ggplot2' based publication ready plots. R package version 0.6.0 https://CRAN.R-project.org/package=ggpubr

Köhl, J., Kolnaar, R., and Ravensberg, W.J. 2019. Mode of action of microbial biological control agents against plant diseases: Relevance beyond efficacy. Frontiers Plant Sci. 10: 845. doi:10.3389/fpls.2019.00845.

Kotan, R., and Sahin, F. 2006. Biological control of Pseudomonas syringae pv. syringae and nutritional similarity in carbon source utilization of pathogen and its potential biocontrol agents. J. Turk. Phytopath. 35 (1-3): 1-13.

Kuznetsova, A., Brockhoff, P.B., and Christensen, R.H.B. 2017 . lmerTest package: tests in linear mixed effects models. J. Stat. Software 82(13): 1-26. https://doi.org/10.18637/jss.v082.i13

Lahlali, R., Ezrari, S., Radouane, N., Kenfaoui, J., Esmaeel, Q., El Hamss, H., Belabess, Z., and Barka, E.A. 2022. Biological control of plant pathogens: A global perspective. Microorganisms 10(3):596. doi:10.3390/microorganisms10030596

Latorre, B.A., and Jones, A.L. 1979. Evaluation of weeds and plant refuse as potential sources of inoculum of Pseudomonas syringae in bacterial canker of cherry. Phytopathology 69: 1122-1125.

Lauwers, E. 2022. Investigation of bacteriophage as a biological control for bacterial canker of sweet cherry. Master's thesis, Michigan State University, ProQuest Dissertations and Theses Global.

Lenth, R. 2023. emmeans: Estimated marginal means, aka least-squares means. R package version 1.8.7 https://CRAN.R-project.org/package=emmeans

Lillrose, T., Lang, G.A. and Sundin, G.W. (2017). Strategies to minimize bacterial canker in high density sweet cherry orchards. Acta Hortic. 1161, 457-162 doi:10.176601/ActaHortic.2017.1161.73

Lindow, S.E., and Brandl, M.T. 2003. Microbiology of the phyllosphere. Appl. Environ. Microbiol. 69(4): 1875-1883.

Lorenzi, A.S., Bonatelli, M.L., Chia, M.A., Peressim, L., and Quecine, M.C. 2022. Opposite sides of *Pantoea agglomerans* and its associated commercial outlook. Microorganisms 10(10):2072. doi: 10.3390/microorganisms10102072.

Lu, L., Karunatathna, S.C., Hyde, K.D., Suwannarach, N., Elgorban, A.M., Stephenson, S.L., Al-Rejaie, S., Jayawardena, R.S., and Tibpromma, S. 2022. Endophytic fungi associated with coffee leaves in China exhibited in vitro antagonism against fungal and bacterial pathogens. J. Fungi 8:698.

Marroni, M.V., Casonato, S., Pitman, A.R., Visnovsky, S.B., Beresford, R.M., and Jones, E.E. 2023. Review of Pseudomonas species causing bacterial canker of Prunus species with emphasis on sweet cherry (Prunus avium) in New Zealand. Eur. J. Plant Pathol. https://doi.org/10.1007/s10658-023-02755-3

McGhee, G.C., Sundin, G.W. 2011. Evaluation of kasugamycin for fire blight management, effect on nontarget bacteria, and assessment of kasugamycin resistance potential in Erwinia amylovora. Phytopathology. 101(2): 192-204.

Niem J.M., Billones-Baaijens, R., Stodart, B., and Savocchia, S. 2020. Diversity profiling of grapevine microbial endosphere and antagonistic potential of endophytic Pseudomonas against grapevine trunk disease. Frontiers Microbiol. 11:477.

Nysanth N.S., Sivapriya, S.L., Natarajan, C., and Anith, K.N. 2022. Novel in vitro methods for simultananeous screening of two antagonistic bacteria against multiple fungal phytopathogens in a single agar plate. 3 Biotech 12:140.

Oueslati, M., Holtappels, D., Fortuna, K., Hajlaoui, M. R., Lavigne, R., Sadfi-Zouaoui, N., and Wagemans, J. 2022. Biological and molecular characterization of the lytic bacteriophage SoKa against Pseudomonas syringae pv. syringae, causal agent of citrus blast and black pit in Tunisia. *Viruses* 14(9): 1949. https://doi.org/10.3390/v14091949

Pinheiro, L.A.M., Pereira, C., Frazão, C., Balcão, V.M., and Almeida, A. 2019. Efficiency of phage φ6 for biocontrol of Pseudomonas syringae pv. syringae: An in vitro preliminary study. Microorganisms 7(9): 286. doi: 10.3390/microorganisms7090286. PMID: 31450735; PMCID: PMC6780397.

R Core Team. 2023. R: A language and environment for statistical computing. R Foundation for Statistical Computing, Vienna, Austria. URL https://www.R-project.org/.

Rabiey, M., Roy, S.R., Holtappels, D., Franceschetti, L., Quilty, B.J., Creeth, R., Sundin, G.W., Wagemans, J., Lavigne, R., and Jackson, R.W. 2020. Phage biocontrol to combat Pseudomonas syringae pathogens causing disease in cherry. Microbial Biotechnology 0 (0): 1– 18 https://doi.org/10.1111/1751-7915.13585

Renick, L.J., Cogal, A.G., and Sundin, G.W. 2008. Phenotypic and genetic analysis of epiphytic pseudomonas syringae populations from sweet cherry in Michigan. Plant Disease 92(3): 372-378.

Schneider, C., Rasband, W. and Eliceiri, K. 2012. NIH Image to ImageJ: 25 years of image analysis. Nat. Methods 9: 671–675. https://doi.org/10.1038/nmeth.2089

Slack S.M., Walters K.J., Outwater C.A., and Sundin G.W. 2021. Effect of kasugamycin, oxytetracycline, and streptomycin on in-orchard population dynamics of *Erwinia amylovora* on apple flower stigmas. Plant Dis. 105(6):1843-1850.

Spotts, R.A., Wallis, K.M., Serdani, M., and Azarenko, A.N. 2010. Bacterial canker of sweet cherry in Oregon – infection of horticultural and natural woods, and resistance of cultivar and rootstock combinations. Plant Disease 94: 345-350.

Stenberg, J.A., Sundh, I., Becher, P.G., Björkman, C., Dubey, M., Egan, P.A., Friberg, H., Gil, J.F., Jensen, D.F., Jonsson, M., Karlsson, M., Khalil, S., Ninkovic, V., Rehermann, G., Vetukuri, R.R., and Viketoft, M. 2021. When is it biological control? A framework for definitions, mechanisms, and classifications. J. Pest Sci. 94:665-676. https://doi.org?10.1007/s10340-021-01354-7.

Stroud, E.A., Rikkerink, E.H.A., Jayaraman, J., and Templeton, M.D. 2022. Actigard™ induces a defense response to limit Pseudomonas syringae pv. actinidiae in Actinidia chinensis var. chinensis 'Hort16A' tissue culture plants. Scientia Hort. 295: 110806.

Sundin, G.W., and Wang, N. 2018. Antibiotic resistance in plant-pathogenic bacteria. Ann. Rev. Phytopathol. 56: 161-180.

Sundin, G.W., Werner, N.A., Yoder, K.S., and Aldwinkle, H.S. 2009. Field evaluations of biological control of fire blight in the eastern united states. Plant Disease 93: 386-394.

Tilocca, B., Cao, A., and Migheli, Q. 2020. Scent of a killer: Microbial volatilome and its role in the biological control of plant pathogens. Frontiers Microbiol. 11:41. doi: 10.3389/fmicb.2020.00041.

Vasebi, Y., Khakvar, R., and Vinatzer, B.A. 2023. Characterization of culturable epiphytic and endophytic bacteria of Prunus spp. and their potential for plant growth promotion and antagonistic activity against bacterial canker disease. J. Plant Pathol. 105:749-766.

Wickham, H. 2016. ggplot2: Elegant Graphics for Data Analysis. Springer-Verlag, New York.

Wilson, M., and Lindow, S.E. 1994. Ecological similarity and coexistence of epiphytic ice-nucleating (ice) pseudomonas syringae strains and a non-ice-nucleating (ice) biological control agent. Appl. Environ. Microbiol. 60(9):3128-37. doi: 10.1128/aem.60.9.3128-3137.1994.

Zeng, Q., Johnson, K.B., Mukhtar, S., Nason, S., Huntley, R., Millet, F., Yang, C.H., Hassani, M.A., Zuverza-Mena, N., and Sundin, G.W. 2023. Aureobasidium pullulans from the fire blight biocontrol product, Blossom Protect, induces host resistance in apple flowers. Phytopathol. 113(7):1192-1201. doi: 10.1094/PHYTO-12-22-0452-R.

Table A1. Inoculations of oxidase^{-}/*syrD*$^{+}$ putative *Pseudomonas syringae* pv. *syringae* strains were randomly applied at each orchard site (1, 2, and 4) on the sweet cherry cultivars Sweetheart and Coral Champagne, in 2019/2020 and 2021. Strain number and replication (e.g., 22/3 is strain 22 rep 3) is shown for each branch (1, 2, 3, and 4) and location on the branch (basal, middle, or distal) along with each cultivar's row and tree number.

		Branch	**1**			**2**			**3**			**4**		
		no./location	**bas.**	**mid.**	**dist.**	**bas.**	**mid.**	**dist.**	**bas.**	**mid.**	**dist.**	**bas.**	**mid.**	**dist.**
Site	**cv./Year**	**Row/Tree**	**Strain no./Rep**											
1	**Sweetheart 2019/2020**	**1/16**	23/1	ctrl	13/1	ctrl	22/2	14/3	9/4	22/4	ctrl	9/5	18/1	
		1/40	17/1	23/2	ctrl	15/3	13/4	ctrl	13/5	23/5	23/3	ctrl	18/2	23/4
		2/18	ctrl	22/1	21/1	ctrl	9/2	13/3	14/4	14/5	ctrl	17/3	15/2	
		2/48	15/1	ctrl	13/2	21/3	22/3	ctrl	15/4	15/5	ctrl	17/4	16/3	
		3/14	14/1	ctrl	14/2	9/3	ctrl	16/4	ctrl	16/5	22/5	17/5	21/4	
		4/28	16/1	21/2	ctrl	ctrl	16/2	18/3	18/4	18/5	ctrl	9/1	17/2	21/5
	Coral Champagne 2019/2020	**1/18**	30/1	26/2	27/2	ctrl	26/3	25/4	33/5	ctrl	37/5	34/1	ctrl	
		1/36	25/1	ctrl	34/2	30/2	ctrl	37/3	26/4	25/5	32/5	ctrl	27/5	
		2/14	ctrl	27/1	33/2		30/3	27/3	ctrl	27/4	38/5	ctrl		
		2/30	37/1	38/2	ctrl	25/2	32/3	ctrl	38/4	34/4	26/5	33/3	ctrl	
		3/16	29/1		37/2	34/3	ctrl	30/4	37/4	ctrl	30/5	ctrl	29/4	
		3/30	32/1	38/1	ctrl		32/2	25/3	38/3	33/4	ctrl	34/5	ctrl	
		4/3	33/1	26/1	ctrl	ctrl	29/2	29/3	ctrl	32/4	29/5			
2	**Sweetheart 2021**	**3/4**	ctrl	37/1	26/1	38/3	18/2	9/5	ctrl	18/3	21/4	37/4	ctrl	13/5
		4/4	26/5	ctrl	ctrl	30/3	33/3	27/2	15/4	18/1	ctrl	29/5	33/2	25/2
		5/24	34/4	32/5	ctrl	ctrl	29/2	34/1	15/2	ctrl	13/3	25/1	25/3	23/4
		6/23	38/1	22/2	ctrl	23/2	29/3	ctrl	25/4	13/4	23/5	ctrl	17/3	18/5
		7/9	21/1	27/1	37/2	ctrl	ctrl	15/5	34/3	29/4	23/3	15/3	ctrl	
		8/10	9/4	27/3	34/2	27/5	9/1	29/1	38/4	ctrl	ctrl	14/3	ctrl	
		9/4	33/5	37/5	ctrl	32/4	ctrl	38/2	ctrl	22/1		17/4	9/3	
		10/4	14/5	32/2	ctrl	33/4	21/3	ctrl	22/4	9/2	15/1	34/5	32/1	ctrl
		12/23	13/2	ctrl	22/5	30/1	ctrl	16/5	14/2	32/3	33/1	16/4	ctrl	
		12/24	ctrl	16/2	ctrl	14/4	25/5	22/3	16/1	13/1	26/4	ctrl	17/5	

Table A1. (cont'd)

		13/10	21/2	38/5	23/1	27/4	ctrl	ctrl	17/2	16/3			26/3	ctrl
		14/8	17/1	30/2	14/1	ctrl	37/3	21/5	30/5	26/2	ctrl	18/4	ctrl	30/4
		Branch	**1 (North)**					**2 (South)**						
		no./location	**bas.**	**mid.**	**mid.**	**dist.**		**bas.**	**mid.**	**mid.**	**dist.**			
Site	**cv./Year**	**Row/Tree**	**Strain no./Rep**											
4	**Coral Champagne 2021**	**1/5**	32/3	26/4	ctrl	17/2		23/1	ctrl	33/5	ctrl			
		1/6	ctrl	26/5	ctrl	18/4		23/2	22/1	ctrl	13/3			
		1/7	ctrl	29/5	18/3	34/2		22/4	ctrl	ctrl	33/1			
		1/16	34/4	33/3	9/1	ctrl		18/5	25/2	ctrl	ctrl			
		1/17	27/1	15/5	16/4	ctrl		ctrl	29/3	ctrl	9/2			
		1/25	ctrl	ctrl	27/2	37/1		27/3	14/4	22/5	ctrl			
		1/26	38/3	ctrl	29/2	25/1		23/4	34/5	ctrl	ctrl			
		1/27	17/1	9/5	ctrl	37/3		15/4	ctrl	21/2	ctrl			
		2/2	ctrl	26/3	21/5	38/2		ctrl	38/4	29/1	ctrl			
		2/3	15/1	ctrl	16/3	ctrl		ctrl	37/2	37/5	30/4			
		2/16	30/5	17/3	ctrl	13/2		ctrl	ctrl	37/4	13/1			
		2/17	30/1	14/3	27/4	22/2		27/5	ctrl	ctrl	ctrl			
		2/24	14/2	9/3	17/4	18/1		ctrl	ctrl	14/5	ctrl			
		3/8	ctrl	26/1	25/4	38/5		21/3	ctrl	15/2	ctrl			
		3/9	26/2	ctrl	ctrl	16/1		22/3	ctrl	32/4	16/5			
		3/10	18/2	ctrl	34/1	34/3		23/5	ctrl	ctrl	33/4			
		3/18	ctrl	30/3	ctrl	21/4		ctrl	32/1	32/5	16/2			
		3/19	17/5	21/1	ctrl	33/2		ctrl	ctrl	25/3	9/4			
		3/29	ctrl	38/1	ctrl	30/2		25/5	23/3	ctrl	29/4			
		3/30	ctrl	13/4	32/2	ctrl		ctrl	13/5	14/1	15/3			

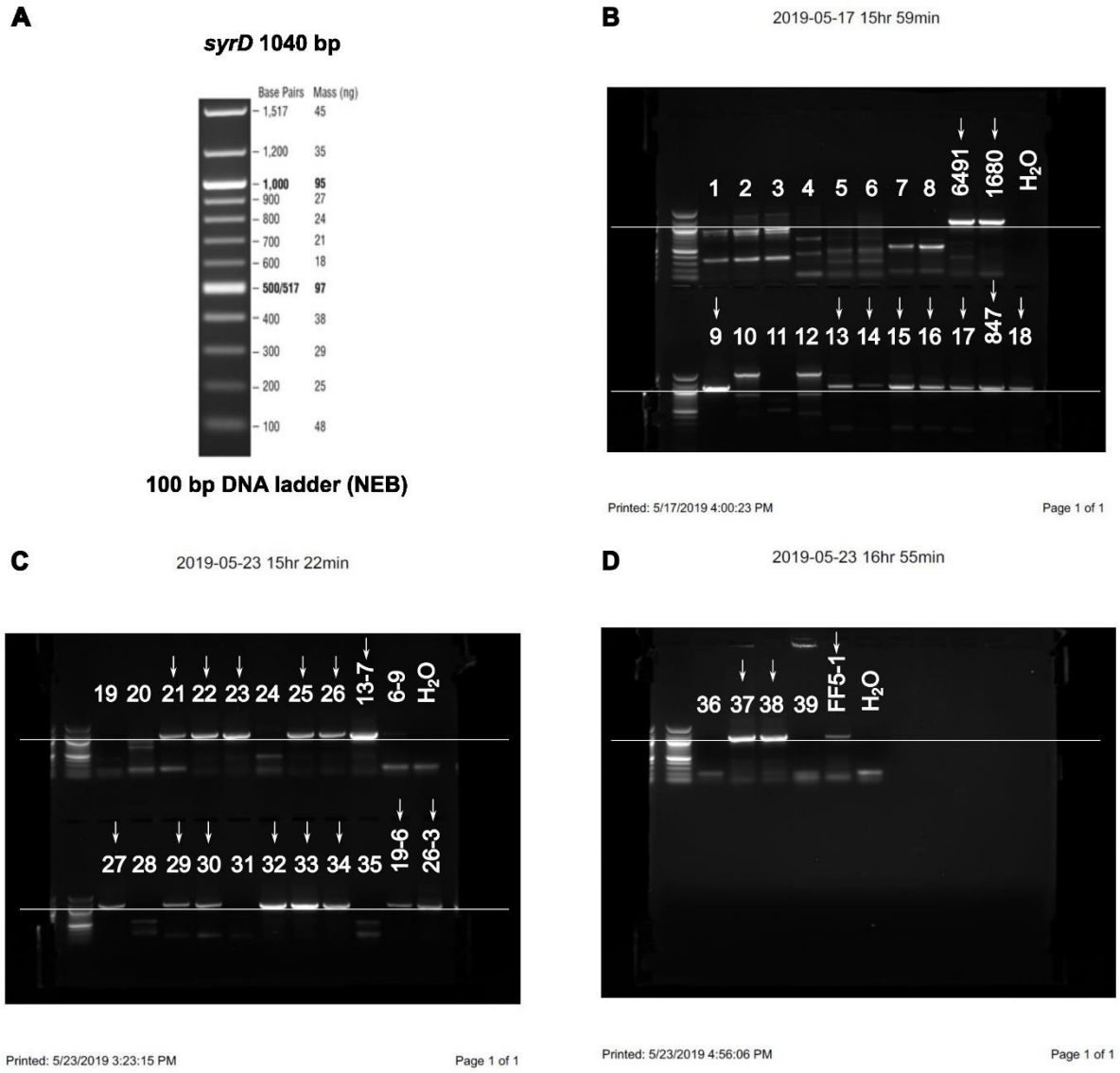


Figure A1. Gel images showing bands for the amplified *syrD* gene (present in *P.s* spp.) for the 39 oxidase⁻ putative *Pseudomonas syringae* pv. *syringae* (*Pss*) strains that were isolated from sweet cherry flowers. Strains with the *syrD* gene and possible *Pss* are highlighted by arrows; water controls and known *Pss* isolates are included (B-D). **A)** the New England BioLabs® (NEB) 100 bp DNA ladder included in the gel electrophoresis runs, denoting that the DNA fragment amplified for *syrD* is 1040 bp, as indicated by the white lines on the gel images (B-D); **B)** the oxidase⁻ strains no.1-18 along with the known *Pss* strains 6491, 1680, and 847; **C)** the oxidase⁻ strains 19-35 along with known *Pss* strains 13-7, 6-9, 19-6, and 26-3; **D)** the oxidase⁻ strains 36-39 along with the known *Pss* strain FF5-1.

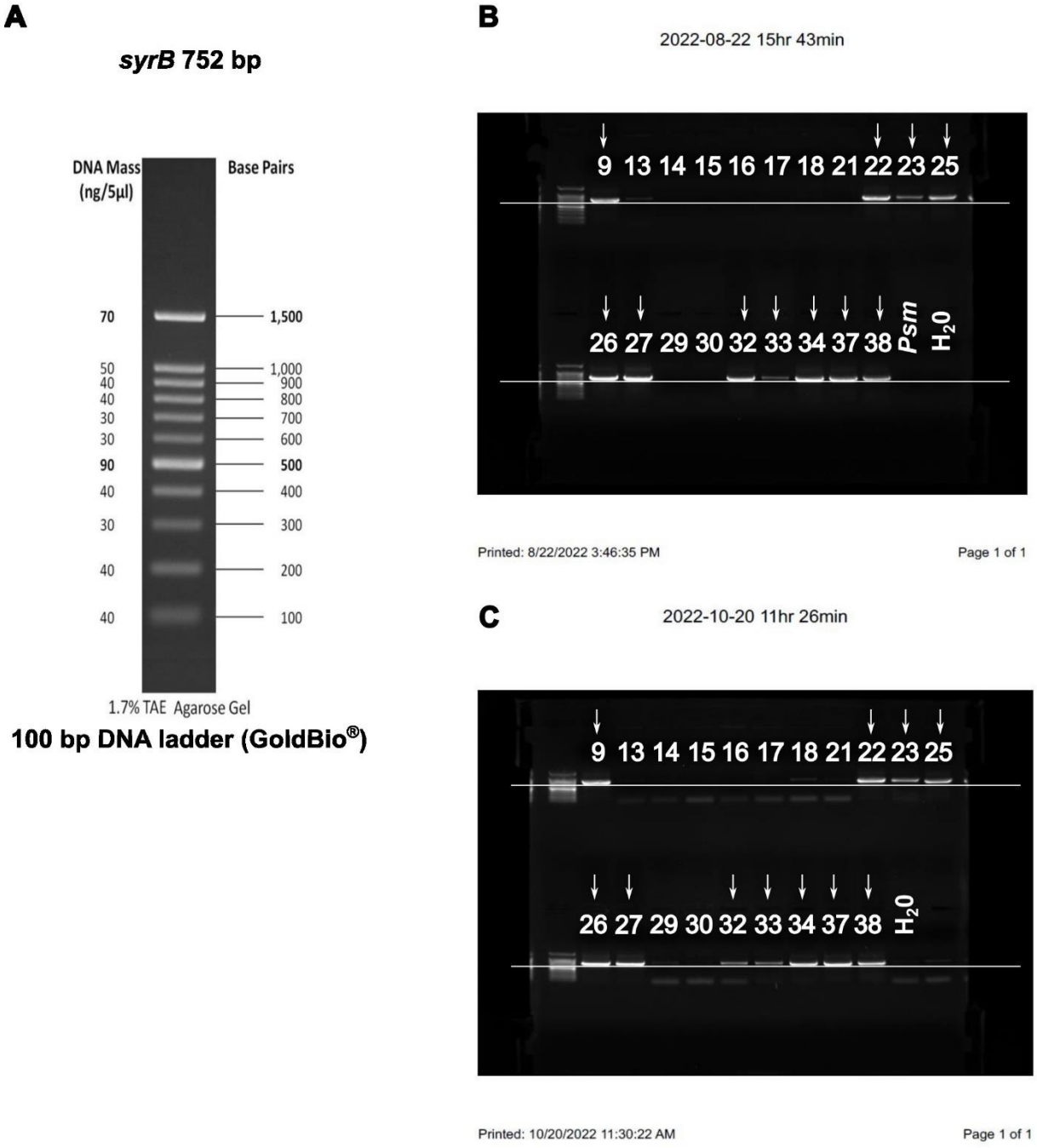


Figure A2. Gel images showing bands for the amplified *syrB* gene (present in *P.s* spp.) for the 20 oxidase^{-}/*syrD*$^{+}$ strains. Strains with the *syrB* gene are highlighted by arrows; water controls are included (B-C). **A)** The GoldBio® 100 bp DNA ladder included in the gel electrophoresis runs, denoting that the DNA fragment amplified for *syrB* is 752 bp, as indicated by the white lines on the gel images (B-C); **B)** the 20 oxidase^{-}/*syrD*$^{+}$ strains no. 9-38; **C)** the gel from the repeated PCR reaction of strains 9-38 to verify weaker gel bands seen in image B.

Table A2. Results of the Dunn's all pairs test for the green fruit lesion area data for the combined years 2019 and 2021, where *Pseudomonas syringae* strains were collapsed by phylogroup and *Psm* 627 and PBS are included as controls. Letters a, b, and c indicate overall significant differences ($p<0.05$) in virulence based on Bonferroni adjusted p-values.

Test	comparison	p-value	phylogroup	letter
Dunn's all pairs	2b - 2d	**0.0398**	**2d**	**a**
	2c - 2b	**1.96e-13**	**2b**	**b**
	2c - 2d	**3.79e-29**	**2c**	**c**
	Psm - 2b	1.0000	***Psm*627**	**ab**
	Psm - 2c	**0.0008**	**PBS**	**c**
	Psm - 2d	0.8670		
	PBS - 2b	**0.0010**		
	PBS - 2c	1.0000		
	PBS - 2d	**2.59e-07**		
	PBS - Psm	**0.0325**		

Table A3. Model fitting for the cumulative links model (clm) ordinal regression for the virulence ratings of *Pseudomonas syringae* strains (collapsed by phylogroup) that were inoculated on sweet cherry wood of cultivars Coral Champagne (Coral) and Sweetheart, assessed in 2020 and 2021, where the lower AIC and p-values are the best-fit models used in further analysis.

Year				**2020**			
Model	**Cultivar**	**no. par**	**AIC**	**Log Likelihood**	**Log Ratio**	**df**	**p-value**
*rating ~ 1	Coral	3	169.51	-81.75			
	Sweetheart		102.59	-48.29			
rating ~ phylogroup	**Coral**	6	**128.54**	-58.27	46.97	3	**3.53e-10**
	Sweetheart		**71.94**	-29.97	36.65		**5.45e-8**
rating ~ phylogroup + time	Coral	7	130.14	-58.07	0.39	1	0.5298
	Sweetheart		73.25	-29.63	0.69		0.4075
rating ~ phylogroup + branchloc	Coral	8	131.01	-57.51	1.13	1	0.2882
	Sweetheart		75.45	-29.72	-0.20		1.0000
rating ~ phylogroup + branchno	Coral	9	132.16	-57.08	0.85	1	0.3556
	Sweetheart		74.94	-28.47	2.51		0.1135
rating ~ phylogroup + time + branchno	Coral	10	133.82	-56.91	0.34	1	0.5585
	Sweetheart		76.28	-28.14	0.66		0.4161
rating ~ phylogroup + time + branchno + branchloc	Coral	12	136.89	-56.44	0.93	2	0.6270
	Sweetheart		79.33	-27.67	0.95		0.6218
				2021			
***rating ~ 1	Coral	3	224.28	-109.14			
	Sweetheart		152.33	-73.17			
rating ~ phylogroup	**Coral**	6	**135.24**	-61.62	95.04	3	**<2.00e-16**
	Sweetheart		**133.46**	-60.73	24.87		**1.64e-5**
rating ~ phylogroup + branchloc	Coral	7	137.18	-61.59	0.06	1	0.7998
	Sweetheart	8	135.89	-59.95	1.57	2	0.4563

Table A3. (cont'd)

rating ~ phylogroup + branchno	Coral	8	138.17	-61.09	1.00	1	0.3163
	Sweetheart	9	139.18	-60.59	-1.28		1.0000
rating ~ phylogroup + branchloc + branchno	Coral	9	140.09	-61.05	0.08	1	0.7732
	Sweetheart	11	141.68	-59.84	1.50	2	0.4732

*Null model

Table A4. Pairwise comparisons (contrast) of virulence ratings for the *Pseudomonas syringae* strains collapsed by phylogroups (2b, 2d, 2c) and the control (ctrl), that were inoculated on the cultivars Coral Champagne and Sweetheart in 2020 and 2021, using estimated marginal means (lsmeans) analysis, following clm ordinal regression (rating ~ phylogroup). The group letters a and b indicate overall significant differences ($p<0.05$) in virulence based on adjusted Tukey p-values.

Cultivar/Year					**Coral Champagne 2020**						
Contrast	**estimate**	**SE**	**df**	**z-ratio**	**p-value**	**phylogroup**	**lsmean**	**SE**	**df**	**Asymp. LCL**	**Asymp. UCL**	**group**
2b-2c	0.35	0.86	Inf	0.41	0.9771	**2d**	0.92	0.39	Inf	0.16	1.67	**a**
2b-2d	-2.78	0.75		-3.70	**0.0012**	**2b**	-1.86	0.60		-3.03	-0.70	**b**
2b-ctrl	2.39	1.16		2.06	0.1671	**2c**	-2.22	0.72		-3.62	-0.81	**b**
2c-2d	-3.13	0.85		-3.68	**0.0013**	**ctrl**	-4.25	1.06		-6.34	-2.17	**b**
2c-ctrl	2.04	1.23		1.66	0.3434							
2d-ctrl	5.17	1.16		4.45	**0.0001**							
					Sweetheart 2020							
2b-2c	3.56	0.99	Inf	3.61	**0.0017**	**2d**	2.27	1.14	Inf	0.05	4.50	**a**
2b-2d	-2.26	1.29		-1.76	0.2937	**2b**	0.01	0.61		-1.19	1.21	**a**
2b-ctrl	3.55	1.22		2.90	**0.0197**	**2c**	-3.55	0.78		-5.07	-2.03	**b**
2c-2d	-5.82	1.42		-4.10	**0.0002**	**ctrl**	-3.53	1.06		-5.61	-1.45	**b**
2c-ctrl	-0.02	1.26		-0.01	1.0000							
2d-ctrl	5.81	1.59		3.65	**0.0015**							
					Coral Champagne 2021							
2b-2c	2.56	1.11	Inf	2.30	0.0975	**2d**	1.25	0.40	Inf	0.48	2.03	**a**
2b-2d	-3.01	0.65		-4.67	**<0.0001**	**2b**	-1.76	0.47		-2.69	-0.83	**b**
2b-ctrl	2.84	1.11		2.56	0.0514	**2c**	-4.32	1.02		-6.32	-2.32	**b**
2c-2d	-5.57	1.11		-5.00	**<0.0001**	**ctrl**	-4.60	1.02		-6.59	-2.60	**b**
2c-ctrl	0.28	1.43		0.20	0.9974							
2d-ctrl	5.85	1.11		5.26	**<0.0001**							

Table A4. (cont'd)

Sweetheart 2021											
2b-2c	0.63	0.86		0.74	0.8822	**2d**	-1.45	0.42		-2.27	-0.63	**a**
2b-2d	-1.86	0.72		-2.59	**0.0470**	**2b**	-3.31	0.68	Inf	-4.63	-1.98	**b**
2b-ctrl	1.54	1.19	Inf	1.30	0.5648	**2c**	-3.94	0.66		-5.24	-2.64	**b**
2c-2d	-2.49	0.70		-3.54	**0.0023**	**ctrl**	-4.84	1.06		-6.91	-2.77	**b**
2c-ctrl	0.91	1.18		0.77	0.8679							
2d-ctrl	3.39	1.08		3.14	**0.0091**							

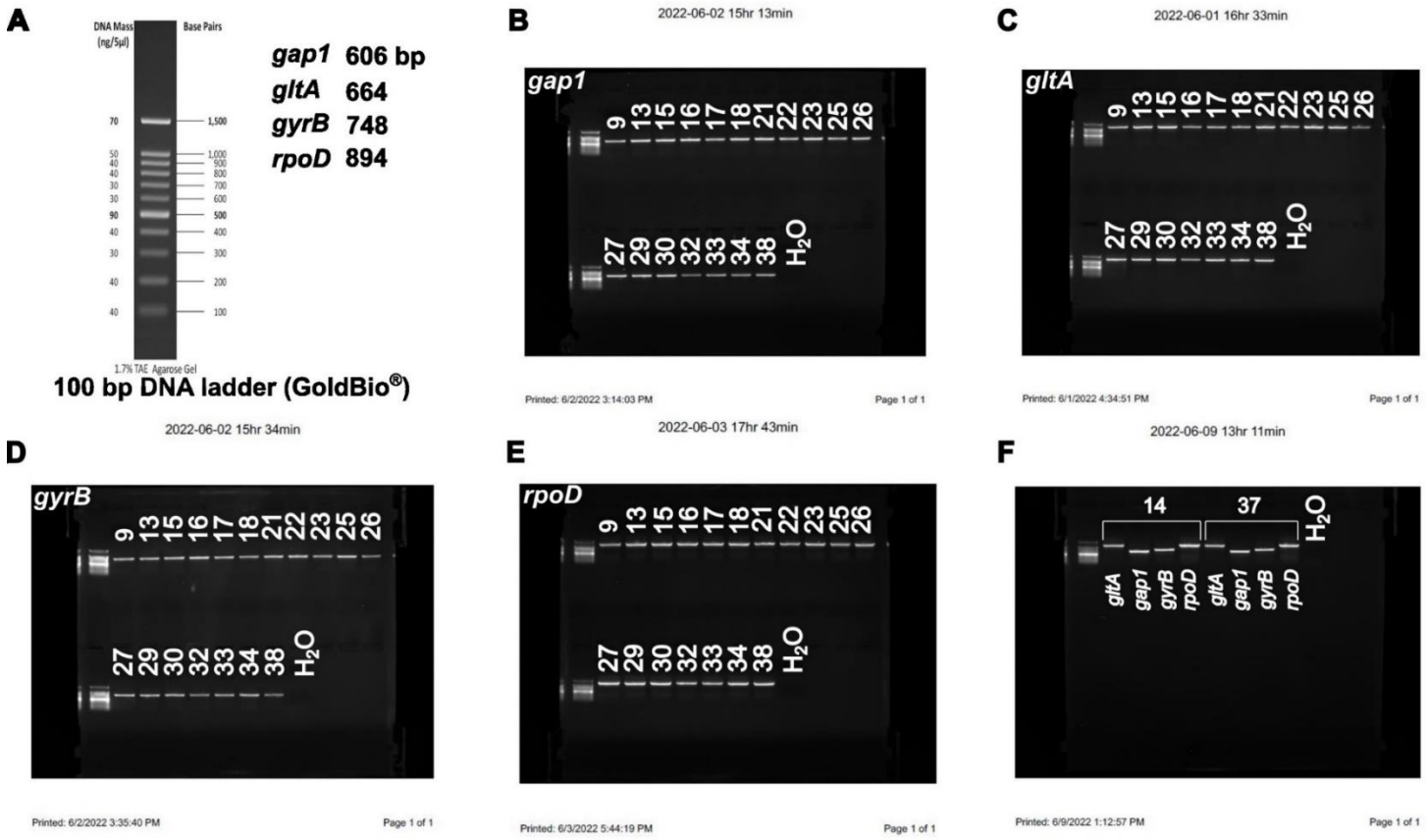


Figure A3. Gel images showing the amplified DNA bands of four housekeeping genes used in the Multilocus sequence analysis (MLSA) with **A)** the GoldBio® 100 base pair (bp) DNA ladder with gene fragment size of each gene indicated, **B)** *gap*1 gene encoding for glyceraldehyde-3-phosphate dehydrogenase in glycolysis, **C)** *glt*A gene encoding for citrate synthase in the citric acid cycle, **D)** *gyr*B gene encoding for DNA gyrase B in replication, **E)** *rpo*D encoding for sigma factor 70 in transcription, and **F)** all four genes.

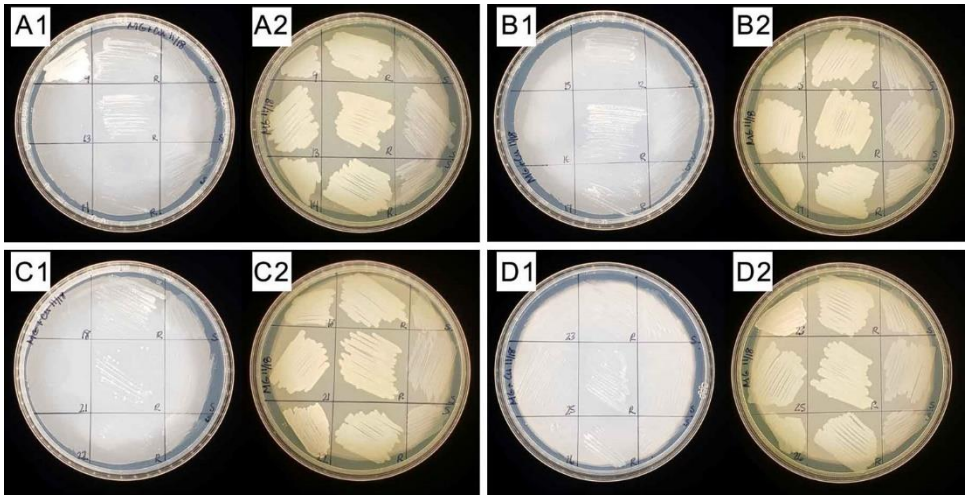


Figure A4. 2019 copper resistance assay plates two days after inoculation. **A1)** *Pss* 9, *Pss* 13 and *Pss*14 (left), Cu resistant *Pss* strain (middle), and Cu susceptible *Pss* strain (right) on MG media amended with 250 µg/ml $CuSO_4$. **A2)** *Pss* 9, *Pss* 13 and *Pss*14 (left), Cu resistant *Pss* strain (middle), and Cu susceptible *Pss* strain (right) on MG media alone. **B1)** *Pss* 15, *Pss* 16 and *Pss*17 (left), Cu resistant *Pss* strain (middle), and Cu susceptible *Pss* strain (right) on MG media amended with 250 µg/ml $CuSO_4$. **B2)** *Pss* 15, *Pss* 16 and *Pss*17 (left), Cu resistant *Pss* strain (middle), and Cu susceptible *Pss* strain (right) on MG media alone. **C1)** *Pss* 18, *Pss* 21 and *Pss*22 (left), Cu resistant *Pss* strain (middle), and Cu susceptible *Pss* strain (right) on MG media amended with 250 µg/ml $CuSO_4$. **C2)** *Pss* 18, *Pss* 21 and *Pss* 22 (left), Cu resistant *Pss* strain (middle), and Cu susceptible *Pss* strain (right) on MG media alone. **D1)** *Pss* 23, *Pss* 25 and *Pss* 26 (left), Cu resistant *Pss* strain (middle), and Cu susceptible *Pss* strain (right) on MG media amended with 250 µg/ml $CuSO_4$. **D2)** *Pss* 23, *Pss* 25 and *Pss* 26 (left), Cu resistant *Pss* strain (middle), and Cu susceptible *Pss* strain (right) on MG media alone.

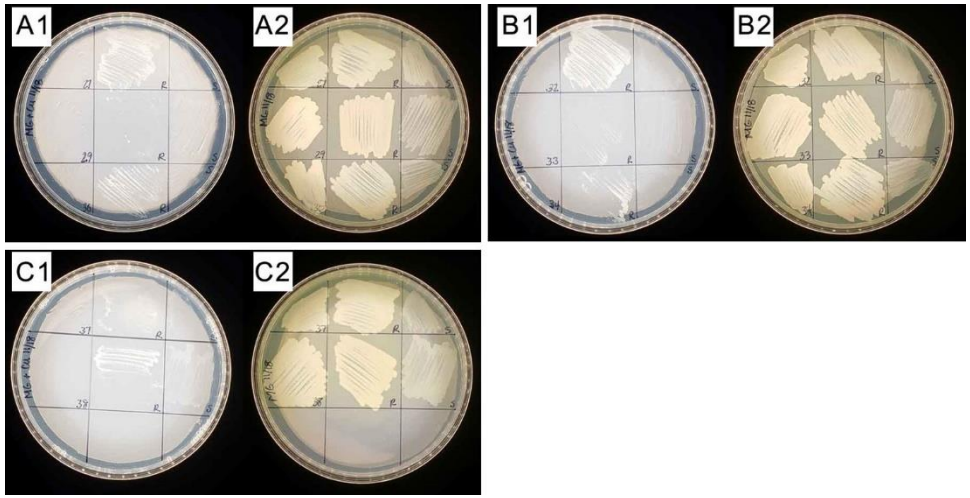


Figure A5. 2019 copper resistance assay plates two days after inoculation. **A1)** *Pss* 27, *Pss* 29 and *Pss* 30 (left), Cu resistant *Pss* strain (middle), and Cu susceptible *Pss* strain (right) on MG media amended with 250 µg/ml $CuSO_4$. A2: *Pss* 27, *Pss* 29 and *Pss* 30 (left), Cu resistant *Pss* strain (middle), and Cu susceptible *Pss* strain (right) on MG media alone. **B1)** *Pss* 32, *Pss* 33 and *Pss*34 (left), Cu resistant *Pss* strain (middle), and Cu susceptible *Pss* strain (right) on MG media amended with 250 µg/ml $CuSO_4$. **B2)** *Pss* 32, *Pss* 33 and *Pss*34 (left), Cu resistant *Pss* strain (middle), and Cu susceptible *Pss* strain (right) on MG media alone. **C1)** *Pss* 37, *Pss* 38 (left), Cu resistant *Pss* strain (middle), and Cu susceptible *Pss* strain (right) on MG media amended with 250 µg/ml $CuSO_4$. **C2)** *Pss* 37, *Pss* 38 (left), Cu resistant *Pss* strain (middle), and Cu susceptible *Pss* strain (right) on MG media alone.

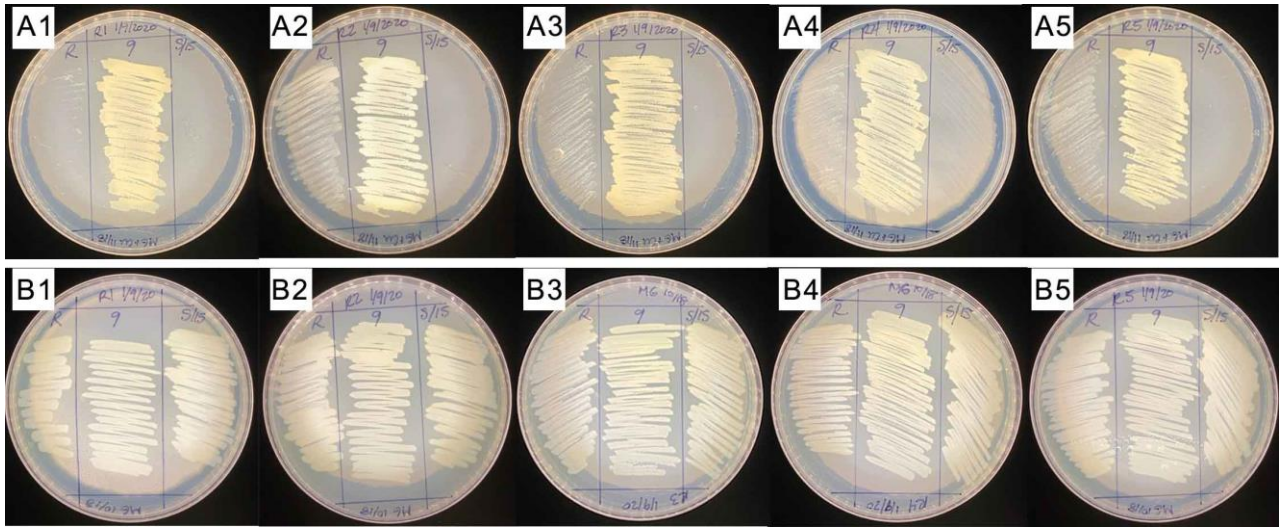


Figure A6. 2020 copper resistance assay plates two days after inoculation. **A1-A5**) Cu resistant *Pss* strain (left), *Pss* 9 (middle) and Cu susceptible *Pss* strain (right) on MG media amended with 250 µg/ml $CuSO_4$. **B1-B5)** Cu resistant *Pss* strain (left), *Pss* 9 (middle) and Cu susceptible *Pss* strain (right) on MG media without $CuSO_4$.

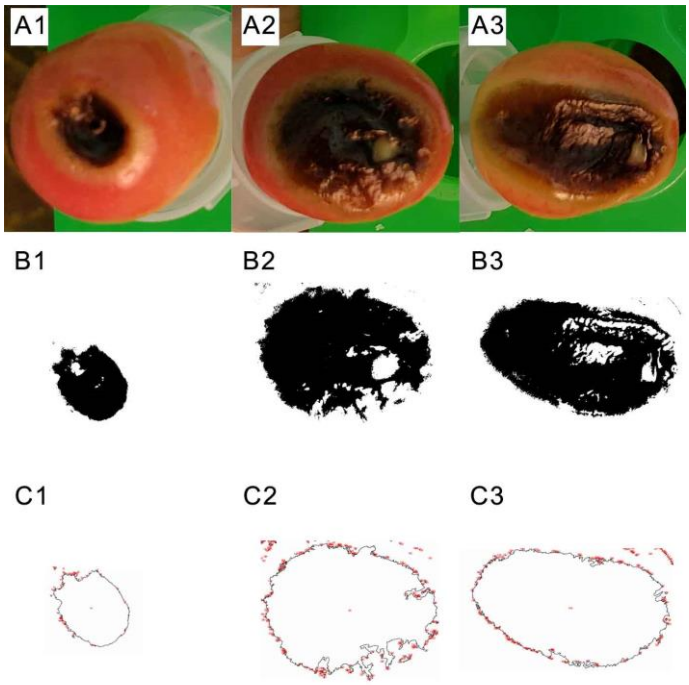


Figure A7. 2019 green cherry fruit ('Hedelfinger') lesions four days after inoculation. **A1-A3)** *Pss* 9 inoculated in stab wound. **B1-B3)** Images after threshold adjustment in ImageJ. **C1-C3)** Image of measured area. A1, B1, C1: Replication 1; A2, B2, C2: Replication 2; A3, B3, C3: Replication 3.



Figure A8. 2019 green cherry fruit (‘Hedelfinger’) lesion four days after inoculation. **A1-A3)** *Pss* 13 inoculated in stab wound, with no lesions for measuring in ImageJ.

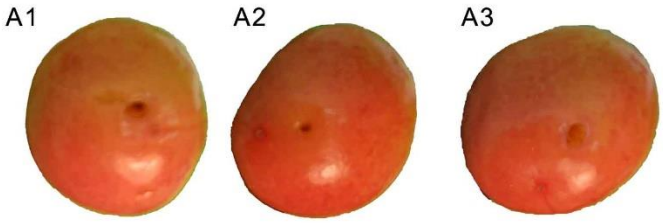


Figure A9. 2019 green cherry fruit ('Hedelfinger') lesion four days after inoculation. **A1-A3)** *Pss* 14 inoculated in stab wound, with no lesions for measuring in ImageJ.

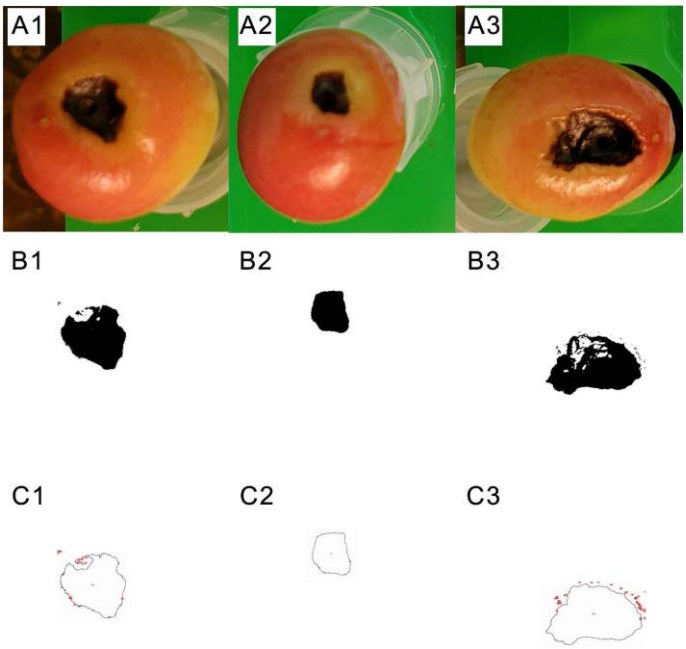


Figure A10. 2019 green cherry fruit ('Hedelfinger') lesion four days after inoculation. **A1-A3)** *Pss* 22 inoculated in stab wound. **B1-B3)**Images after threshold adjustment in ImageJ. **C1-C3)** Image of measured area. A1, B1, C1: Replication 1; A2, B2, C2: Replication 2; A3, B3, C3: Replication 3.

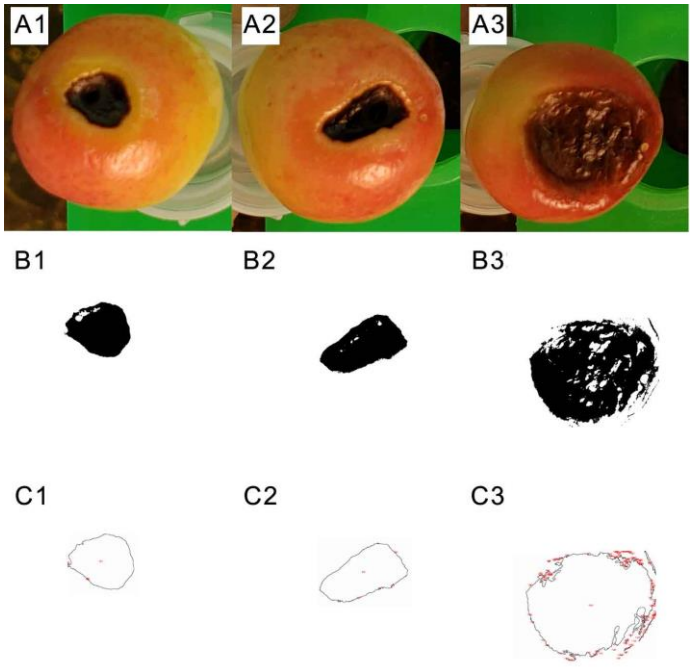


Figure A11. 2019 green cherry fruit (‘Hedelfinger’) lesion four days after inoculation. **A1-A3)** *Pss* 23 inoculated in stab wound. **B1-B3)**Images after threshold adjustment in ImageJ. **C1-C3)** Image of measured area. A1, B1, C1: Replication 1; A2, B2, C2: Replication 2; A3, B3, C3: Replication 3.

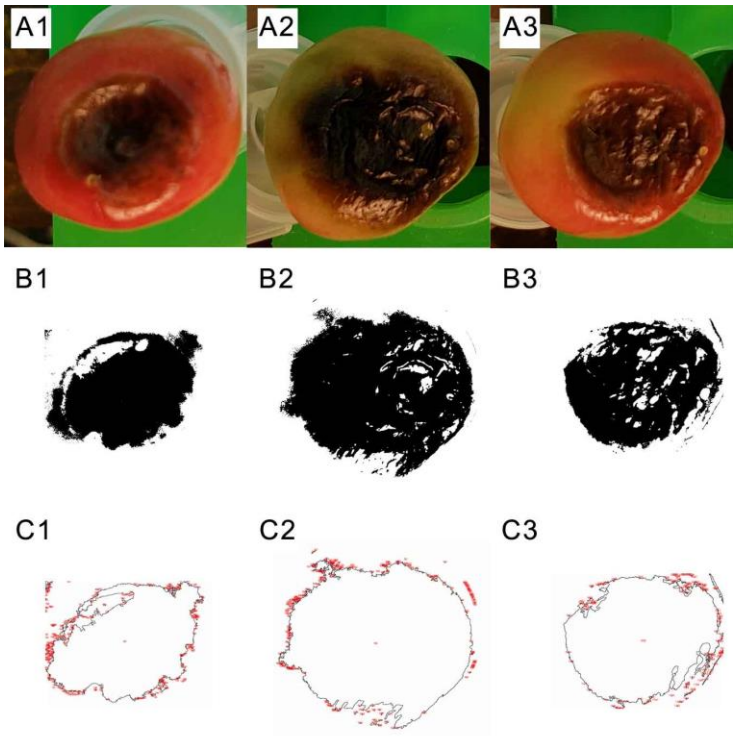


Figure A12. 2019 green cherry fruit ('Hedelfinger') lesion four days after inoculation. **A1-A3)** *Pss* 25 inoculated in stab wound. **B1-B3)**Images after threshold adjustment in ImageJ. **C1-C3)** Image of measured area. A1, B1, C1: Replication 1; A2, B2, C2: Replication 2; A3, B3, C3: Replication 3.

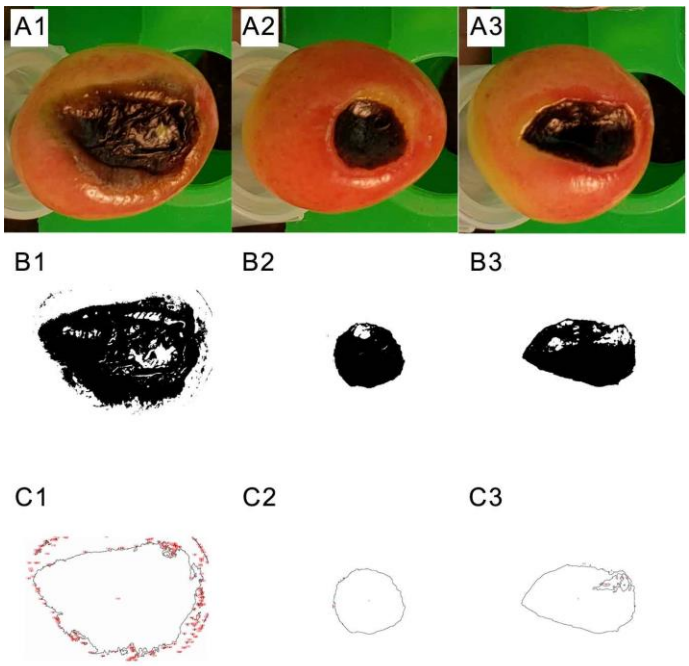


Figure A13. 2019 green cherry fruit ('Hedelfinger') lesion four days after inoculation. **A1-A3)** *Pss* 26 inoculated in stab wound. **B1-B3)**Images after threshold adjustment in ImageJ. **C1-C3)** Image of measured area. A1, B1, C1: Replication 1; A2, B2, C2: Replication 2; A3, B3, C3: Replication 3.

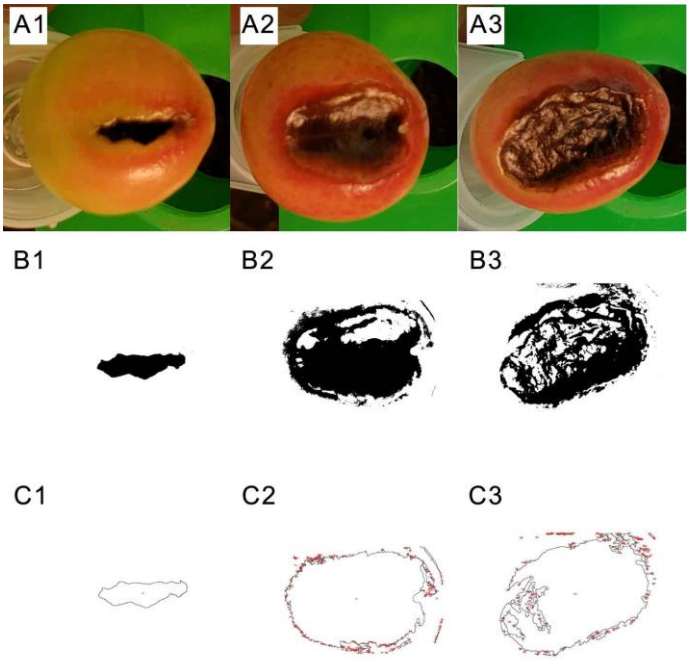


Figure A14. 2019 green cherry fruit ('Hedelfinger') lesion four days after inoculation. **A1-A3)** *Pss* 27 inoculated in stab wound. **B1-B3)**Images after threshold adjustment in ImageJ. **C1-C3)** Image of measured area. A1, B1, C1: Replication 1; A2, B2, C2: Replication 2; A3, B3, C3: Replication 3.

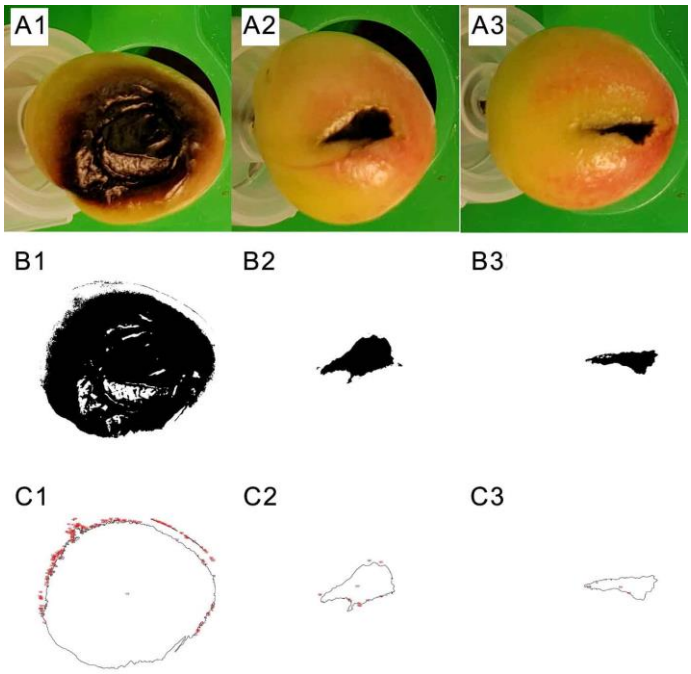


Figure A15. 2019 green cherry fruit ('Hedelfinger') lesion four days after inoculation. **A1-A3)** *Pss* 32 inoculated in stab wound. **B1-B3)**Images after threshold adjustment in ImageJ. **C1-C3)** Image of measured area. A1, B1, C1: Replication 1; A2, B2, C2: Replication 2; A3, B3, C3: Replication 3.

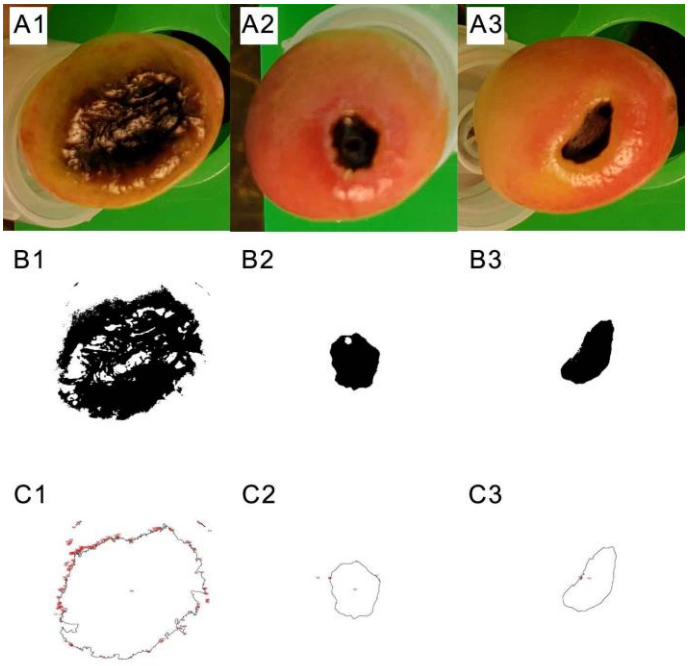


Figure A16. 2019 green cherry fruit ('Hedelfinger') lesion four days after inoculation. **A1-A3)** *Pss* 33 inoculated in stab wound. **B1-B3)**Images after threshold adjustment in ImageJ. **C1-C3)** Image of measured area. A1, B1, C1: Replication 1; A2, B2, C2: Replication 2; A3, B3, C3: Replication 3.

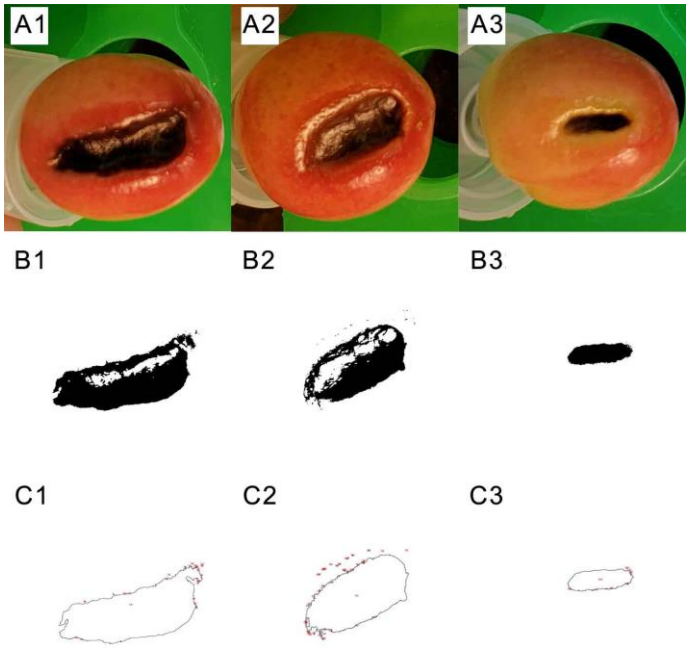


Figure A17. 2019 green cherry fruit ('Hedelfinger') lesion four days after inoculation. **A1-A3)** *Pss* 34 inoculated in stab wound. **B1-B3)**Images after threshold adjustment in ImageJ. **C1-C3)** Image of measured area. A1, B1, C1: Replication 1; A2, B2, C2: Replication 2; A3, B3, C3: Replication 3.

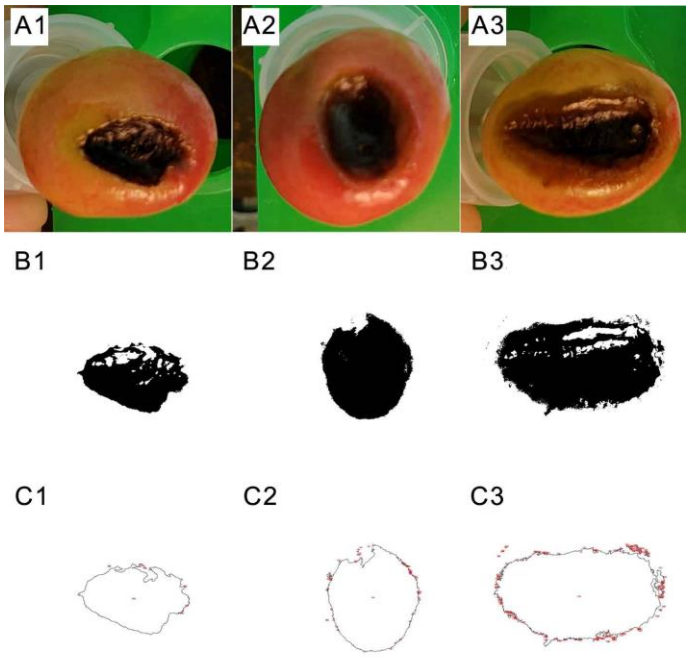


Figure A18. 2019 green cherry fruit ('Hedelfinger') lesion four days after inoculation. **A1-A3)** *Pss* 37 inoculated in stab wound. **B1-B3)**Images after threshold adjustment in ImageJ. **C1-C3)** Image of measured area. A1, B1, C1: Replication 1; A2, B2, C2: Replication 2; A3, B3, C3: Replication 3.

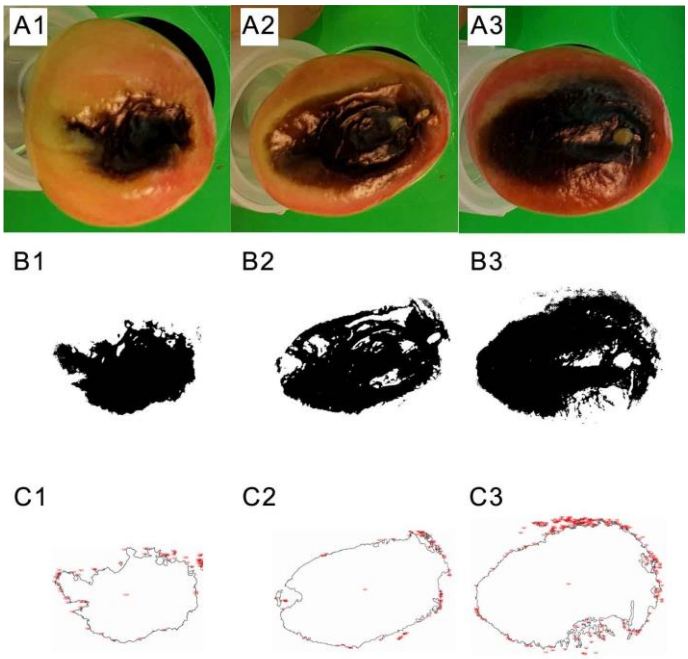


Figure A19. 2019 green cherry fruit ('Hedelfinger') lesion four days after inoculation. **A1-A3)** *Pss* 38 inoculated in stab wound. **B1-B3)** Images after threshold adjustment in ImageJ. **C1-C3)** Image of measured area. A1, B1, C1: Replication 1; A2, B2, C2: Replication 2; A3, B3, C3: Replication 3.

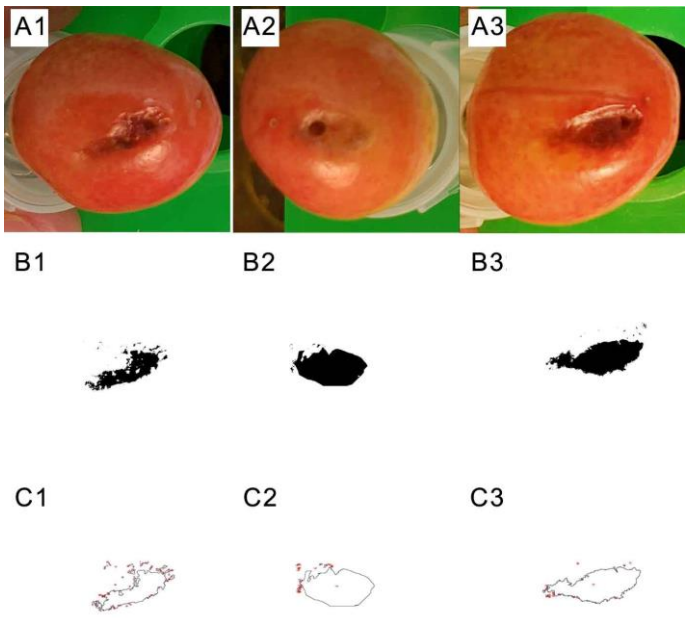


Figure A20. 2019 green cherry fruit ('Hedelfinger') lesion four days after inoculation. **A1-A3***Psm* inoculated stab wound. **B1-B3)** Images after threshold adjustment in ImageJ. **C1-C3)** Image of measured area. A1, B1, C1. Replication 1; A2, B2, C2: Replication 2; A3, B3, C3: Replication 3.

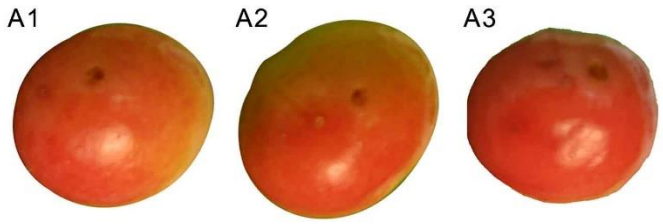


Figure A21. 2019 green cherry fruit (‘Hedelfinger’) lesion four days after inoculation. **A1-A3)** PBS (control) inoculated stab wound, with no lesions for measuring in ImageJ.

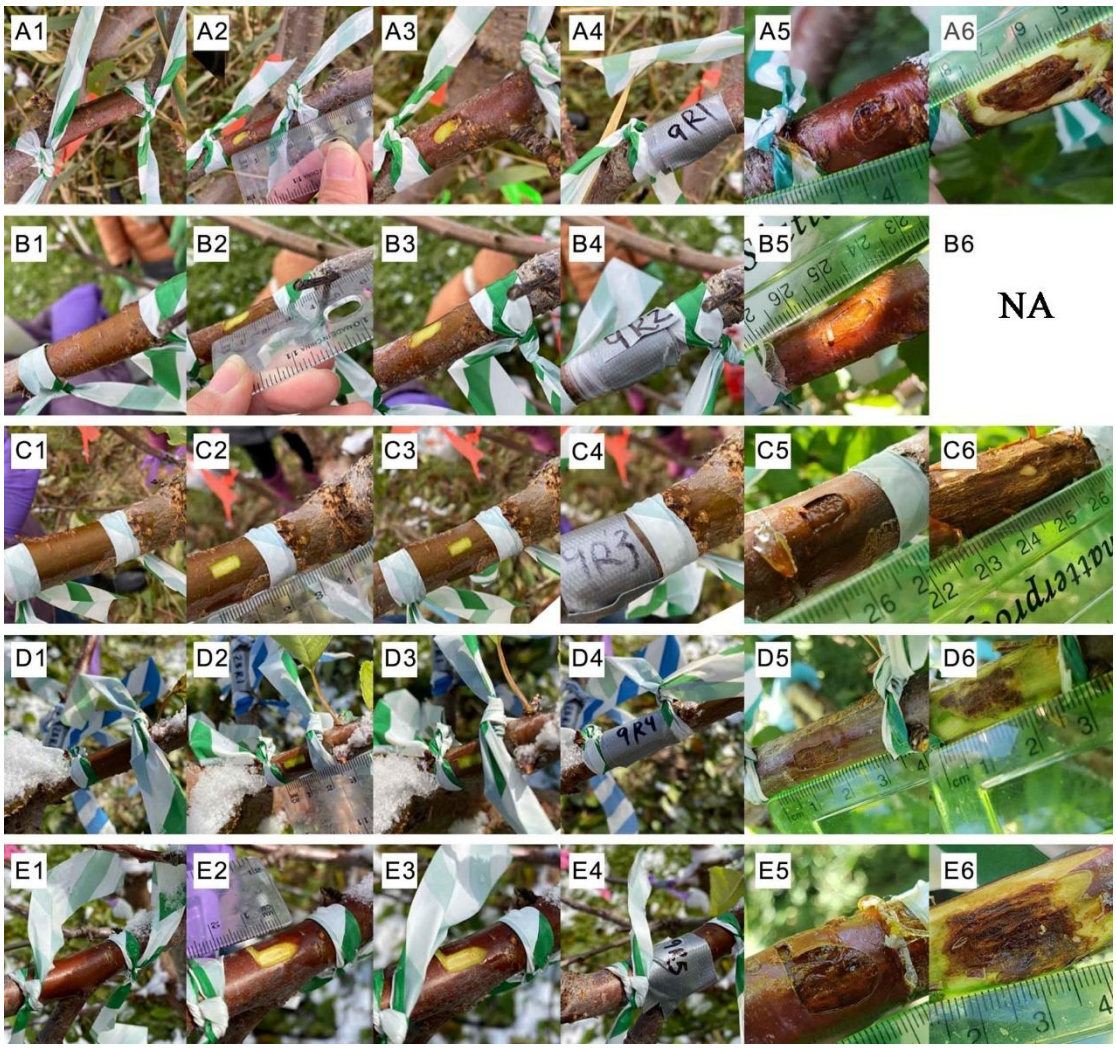


Figure A22. 2019 wound inoculations on 'Sweetheart' cherry wood with *Pss* 9. **A1-E1)** The inoculation site before wounding. **A2-E2)** The inoculation site after wounding by razor blade. **A3-E3)** The inoculation site after pipetting inoculum into the wound. **A4-E4)** The inoculation site after being covered with Parafilm and tape. **A5-E5)** The inoculation site exterior assessment in the summer. **A6-E6)** The inoculation site interior assessment in the spring of 2020. A1-A6. Replication 1. B1-B6. Replication 2. C1-C6. Replication 3. D1-D6. Replication 4. E1-E6. Replication 5. Images with NA are not available.



Figure A23. 2019 wound inoculations on 'Sweetheart' cherry wood with *Pss* 13. **A1-E1)** The inoculation site before wounding. **A2-E2)** The inoculation site after wounding by razor blade. **A3-E3)** The inoculation site after pipetting inoculum into the wound. **A4-E4)** The inoculation site after being covered with Parafilm and tape. **A5-E5)** The inoculation site exterior assessment in the summer. **A6-E6)** The inoculation site interior assessment in the spring of 2020. A1-A6. Replication 1. B1-B6. Replication 2. C1-C6. Replication 3. D1-D6. Replication 4. E1-E6. Replication 5.

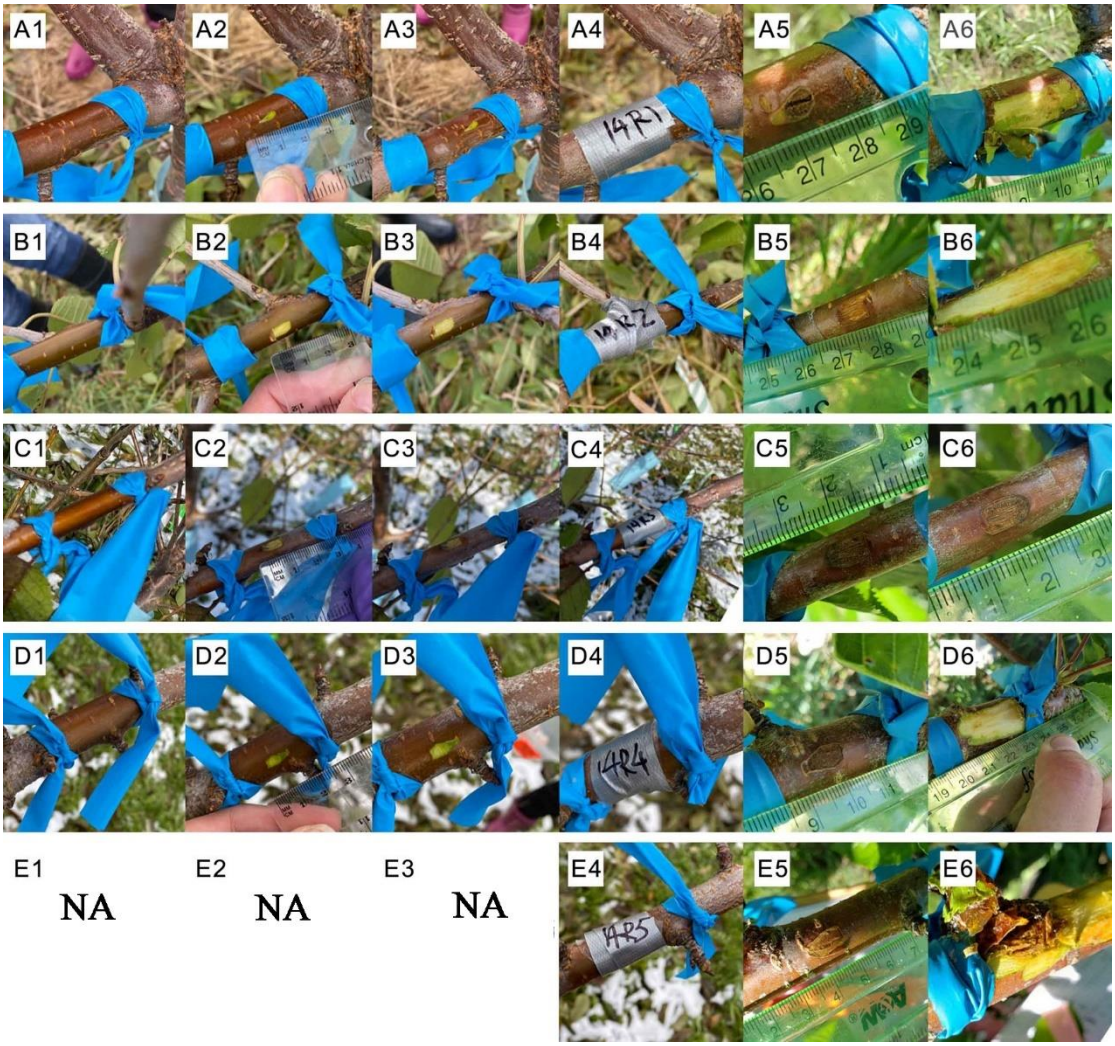


Figure A24. 2019 wound inoculations on 'Sweetheart' cherry wood with *Pss* 14. **A1-E1)** The inoculation site before wounding. **A2-E2)** The inoculation site after wounding by razor blade. **A3-E3)** The inoculation site after pipetting inoculum into the wound. **A4-E4)** The inoculation site after being covered with Parafilm and tape. **A5-E5)** The inoculation site exterior assessment in the summer. **A6-E6)** The inoculation site interior assessment in the spring of 2020. A1-A6. Replication 1. B1-B6. Replication 2. C1-C6. Replication 3. D1-D6. Replication 4. E1-E6. Replication 5. Images with NA are not available.



Figure A25. 2019 wound inoculations on 'Sweetheart' cherry wood with *Pss* 15. **A1-E1)** The inoculation site before wounding. **A2-E2)** The inoculation site after wounding by razor blade. **A3-E3)** The inoculation site after pipetting inoculum into the wound. **A4-E4)** The inoculation site after being covered with Parafilm and tape. **A5-E5)** The inoculation site exterior assessment in the summer. **A6-E6)** The inoculation site interior assessment in the spring of 2020. A1-A6. Replication 1. B1-B6. Replication 2. C1-C6. Replication 3. D1-D6. Replication 4. E1-E6. Replication 5.

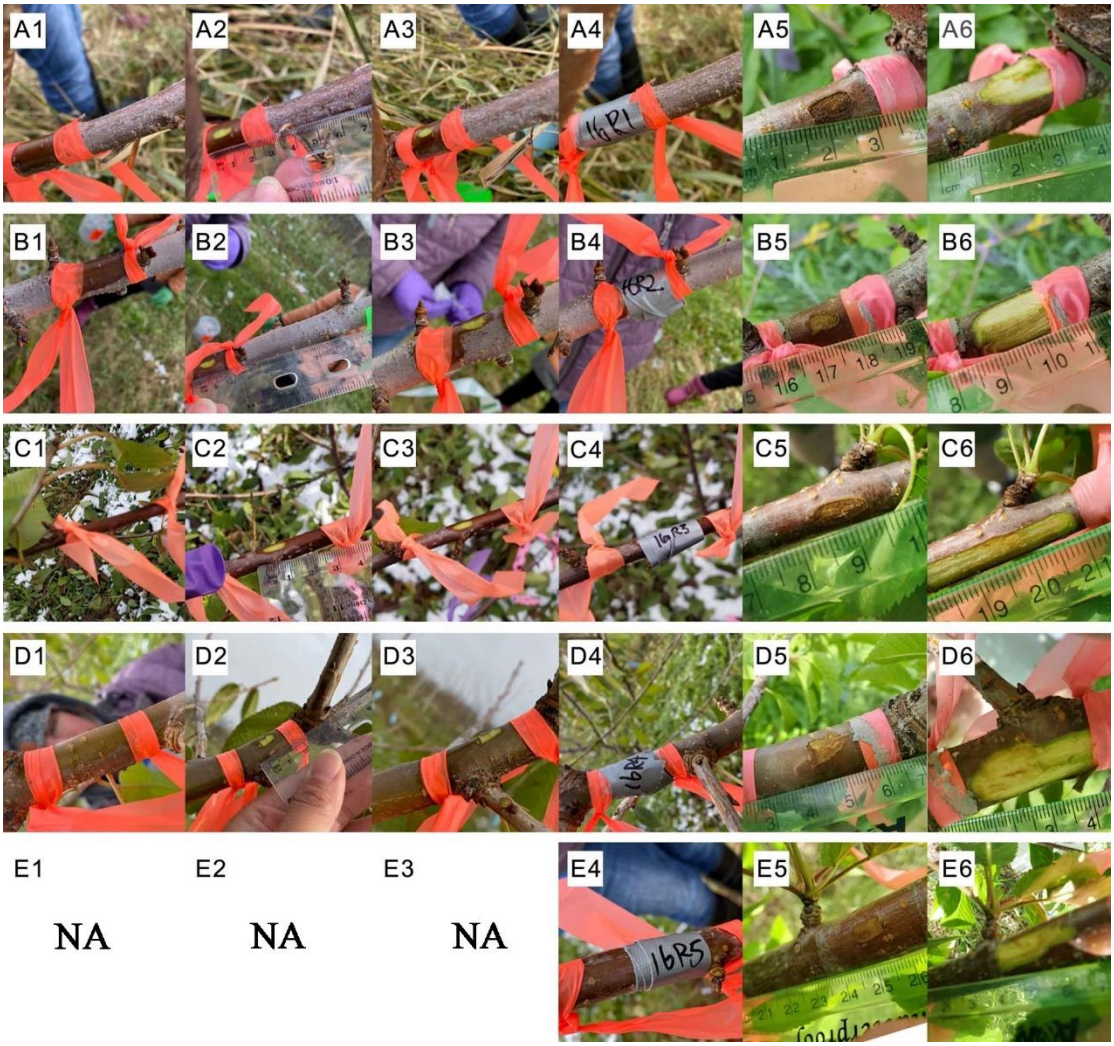


Figure A26. 2019 wound inoculations on 'Sweetheart' cherry wood with *Pss* 16. **A1-E1)** The inoculation site before wounding. **A2-E2)** The inoculation site after wounding by razor blade. **A3-E3)** The inoculation site after pipetting inoculum into the wound. **A4-E4)** The inoculation site after being covered with Parafilm and tape. **A5-E5)** The inoculation site exterior assessment in the summer. **A6-E6)** The inoculation site interior assessment in the spring of 2020. A1-A6. Replication 1. B1-B6. Replication 2. C1-C6. Replication 3. D1-D6. Replication 4. E1-E6. Replication 5. Images with NA are not available.

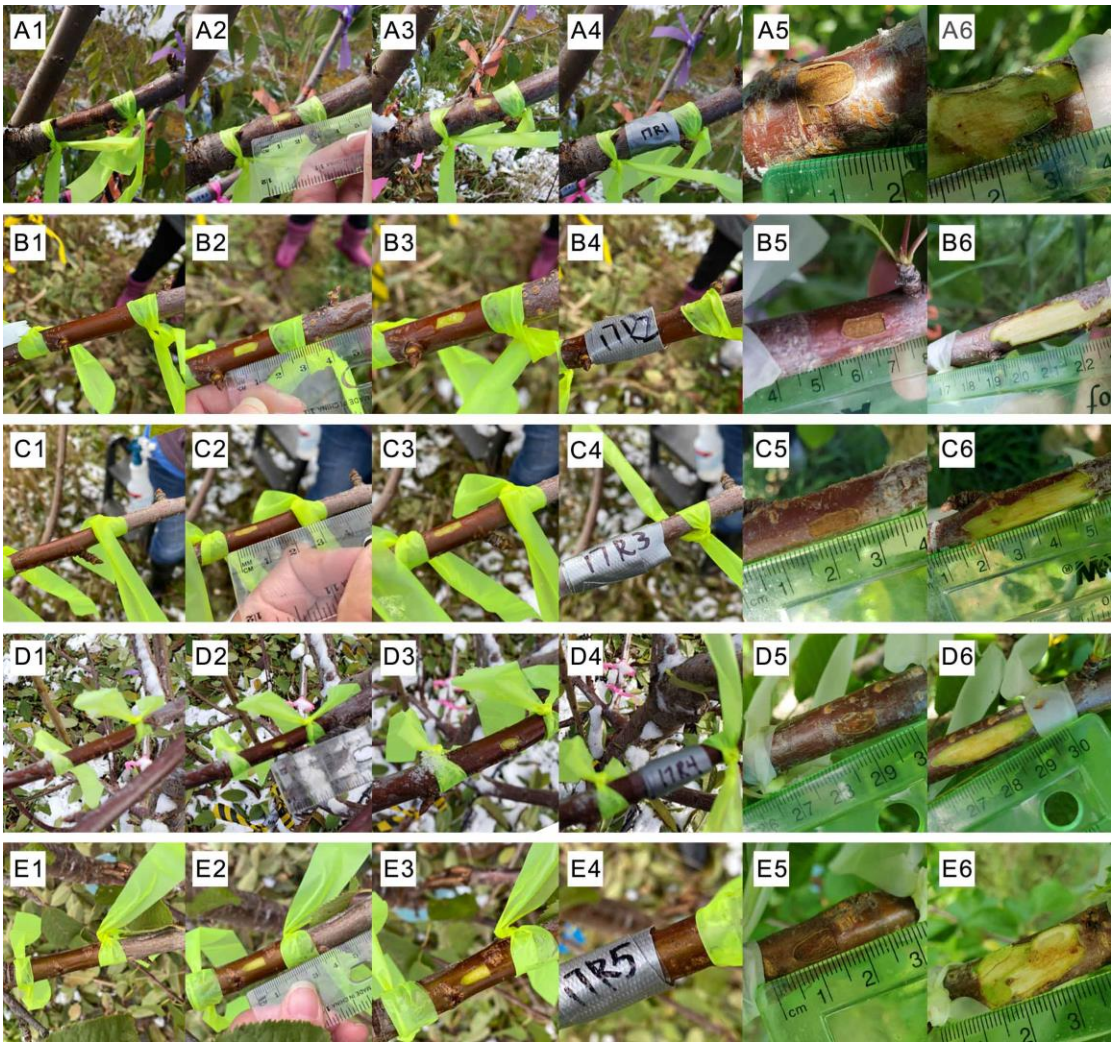


Figure A27. 2019 wound inoculations on 'Sweetheart' cherry wood with *Pss* 17. **A1-E1)** The inoculation site before wounding. **A2-E2)** The inoculation site after wounding by razor blade. **A3-E3)** The inoculation site after pipetting inoculum into the wound. **A4-E4)** The inoculation site after being covered with Parafilm and tape. **A5-E5)** The inoculation site exterior assessment in the summer. **A6-E6)** The inoculation site interior assessment in the spring of 2020. A1-A6. Replication 1. B1-B6. Replication 2. C1-C6. Replication 3. D1-D6. Replication 4. E1-E6. Replication 5.

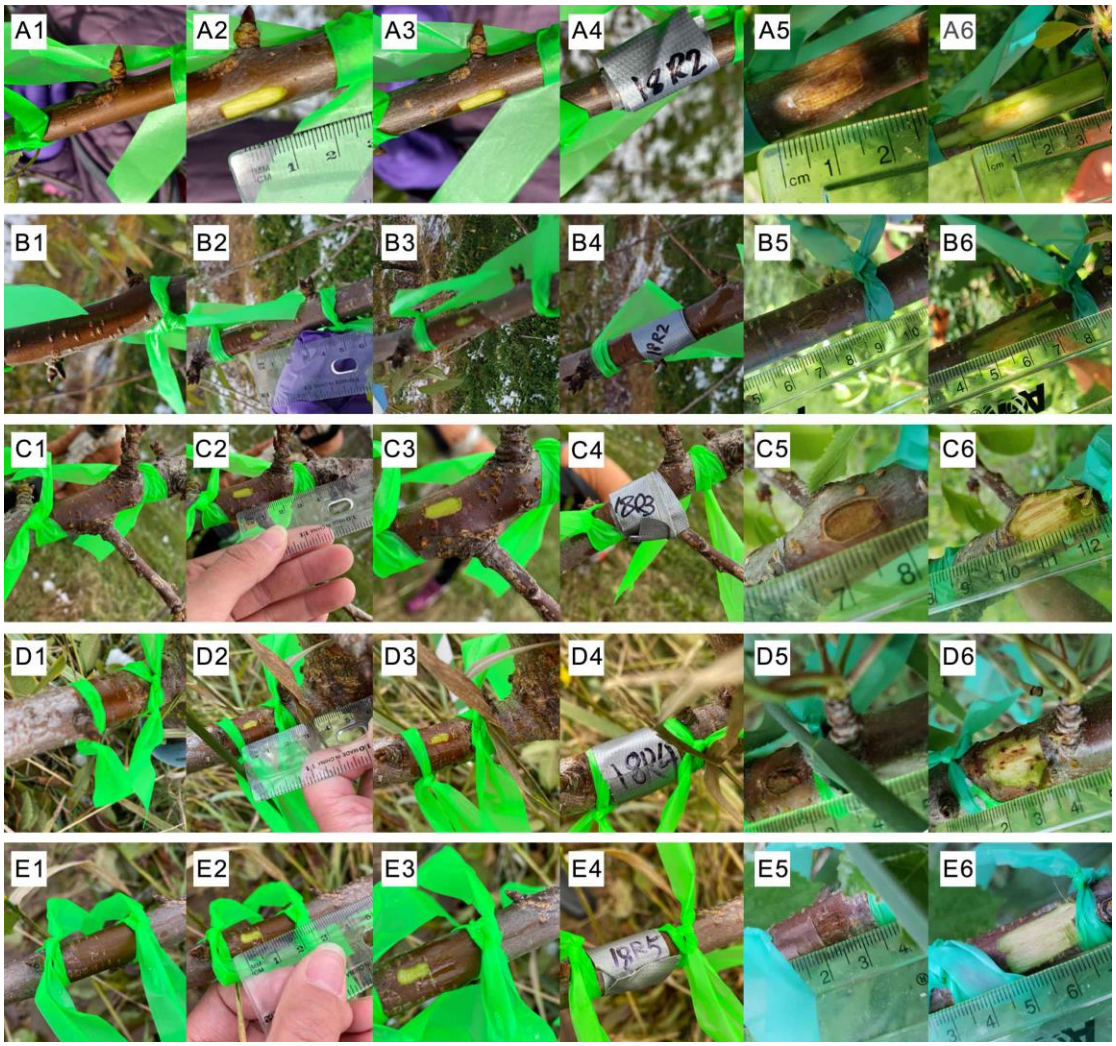


Figure A28. 2019 wound inoculations on 'Sweetheart' cherry wood with *Pss* 18. **A1-E1)** The inoculation site before wounding. **A2-E2)** The inoculation site after wounding by razor blade. **A3-E3)** The inoculation site after pipetting inoculum into the wound. **A4-E4)** The inoculation site after being covered with Parafilm and tape. **A5-E5)** The inoculation site exterior assessment in the summer. **A6-E6)** The inoculation site interior assessment in the spring of 2020. A1-A6. Replication 1. B1-B6. Replication 2. C1-C6. Replication 3. D1-D6. Replication 4. E1-E6. Replication 5.



Figure A29. 2019 wound inoculations on 'Sweetheart' cherry wood with *Pss* 21. **A1-E1)** The inoculation site before wounding. **A2-E2)** The inoculation site after wounding by razor blade. **A3-E3)** The inoculation site after pipetting inoculum into the wound. **A4-E4)** The inoculation site after being covered with Parafilm and tape. **A5-E5)** The inoculation site exterior assessment in the summer. **A6-E6)** The inoculation site interior assessment in the spring of 2020. A1-A6. Replication 1. B1-B6. Replication 2. C1-C6. Replication 3. D1-D6. Replication 4. E1-E6. Replication 5.

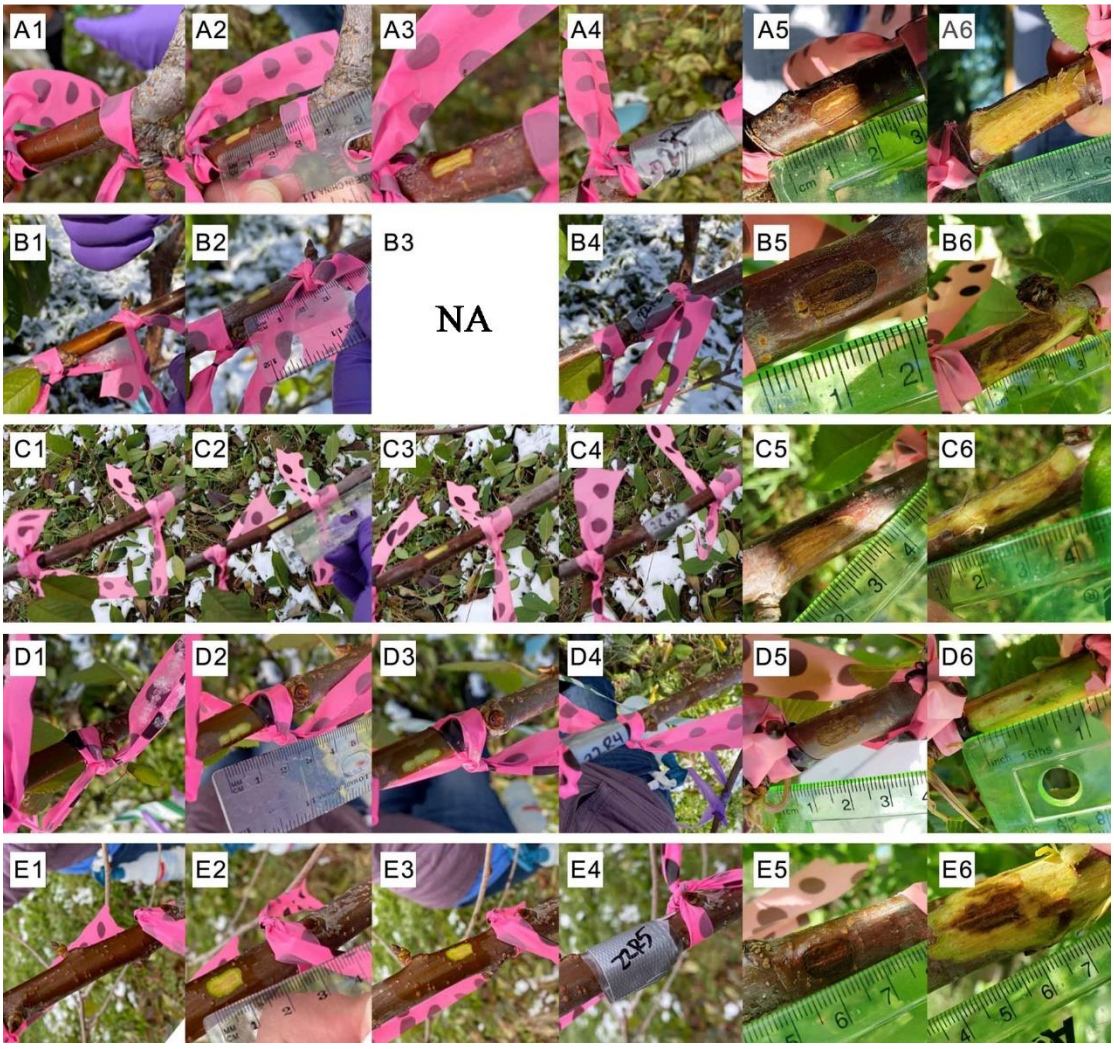


Figure A30. 2019 wound inoculations on 'Sweetheart' cherry wood with *Pss* 22. **A1-E1)** The inoculation site before wounding. **A2-E2)** The inoculation site after wounding by razor blade. **A3-E3)** The inoculation site after pipetting inoculum into the wound. **A4-E4)** The inoculation site after being covered with Parafilm and tape. **A5-E5)** The inoculation site exterior assessment in the summer. **A6-E6)** The inoculation site interior assessment in the spring of 2020. A1-A6. Replication 1. B1-B6. Replication 2. C1-C6. Replication 3. D1-D6. Replication 4. E1-E6. Replication 5. Images with NA are not available.

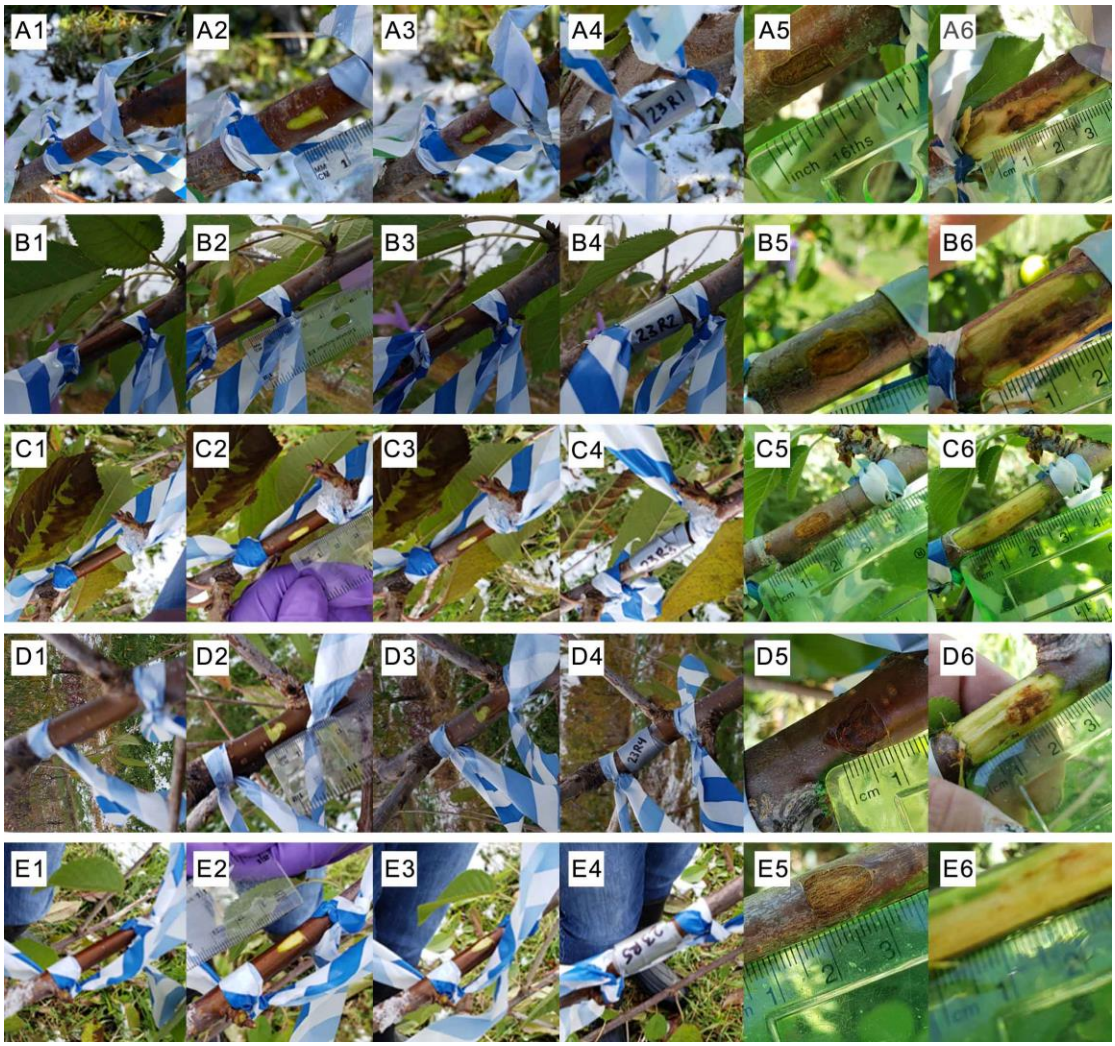


Figure A31. 2019 wound inoculations on 'Sweetheart' cherry wood with *Pss* 23. **A1-E1)** The inoculation site before wounding. **A2-E2)** The inoculation site after wounding by razor blade. **A3-E3)** The inoculation site after pipetting inoculum into the wound. **A4-E4)** The inoculation site after being covered with Parafilm and tape. **A5-E5)** The inoculation site exterior assessment in the summer. **A6-E6)** The inoculation site interior assessment in the spring of 2020. A1-A6. Replication 1. B1-B6. Replication 2. C1-C6. Replication 3. D1-D6. Replication 4. E1-E6. Replication 5.

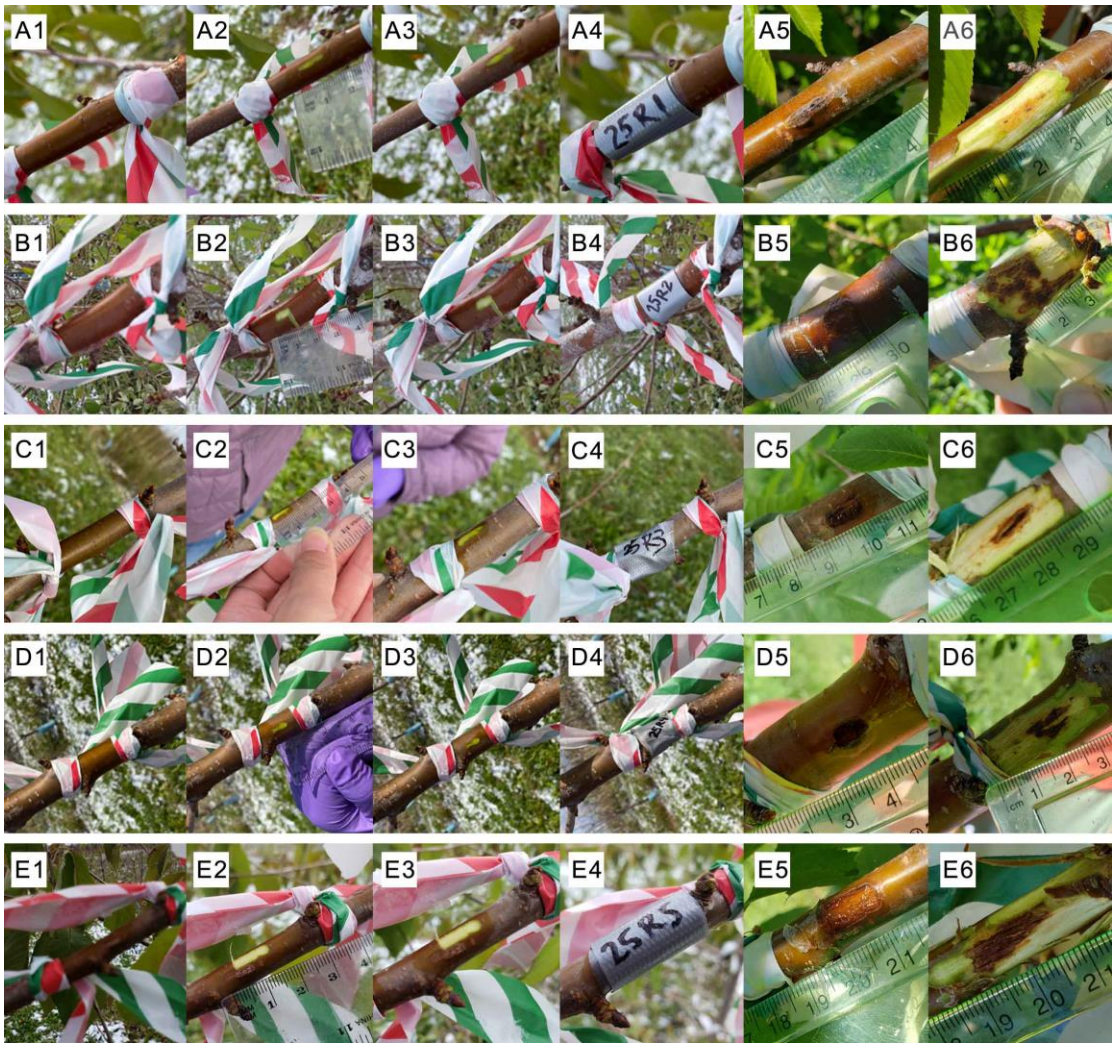


Figure A32. 2019 wound inoculations on 'Coral' cherry wood with *Pss* 25. **A1-E1)** The inoculation site before wounding. **A2-E2)** The inoculation site after wounding by razor blade. **A3-E3)** The inoculation site after pipetting inoculum into the wound. **A4-E4)** The inoculation site after being covered with Parafilm and tape. **A5-E5)** The inoculation site exterior assessment in the summer. **A6-E6)** The inoculation site interior assessment in the spring of 2020. A1-A6. Replication 1. B1-B6. Replication 2. C1-C6. Replication 3. D1-D6. Replication 4. E1-E6. Replication 5.

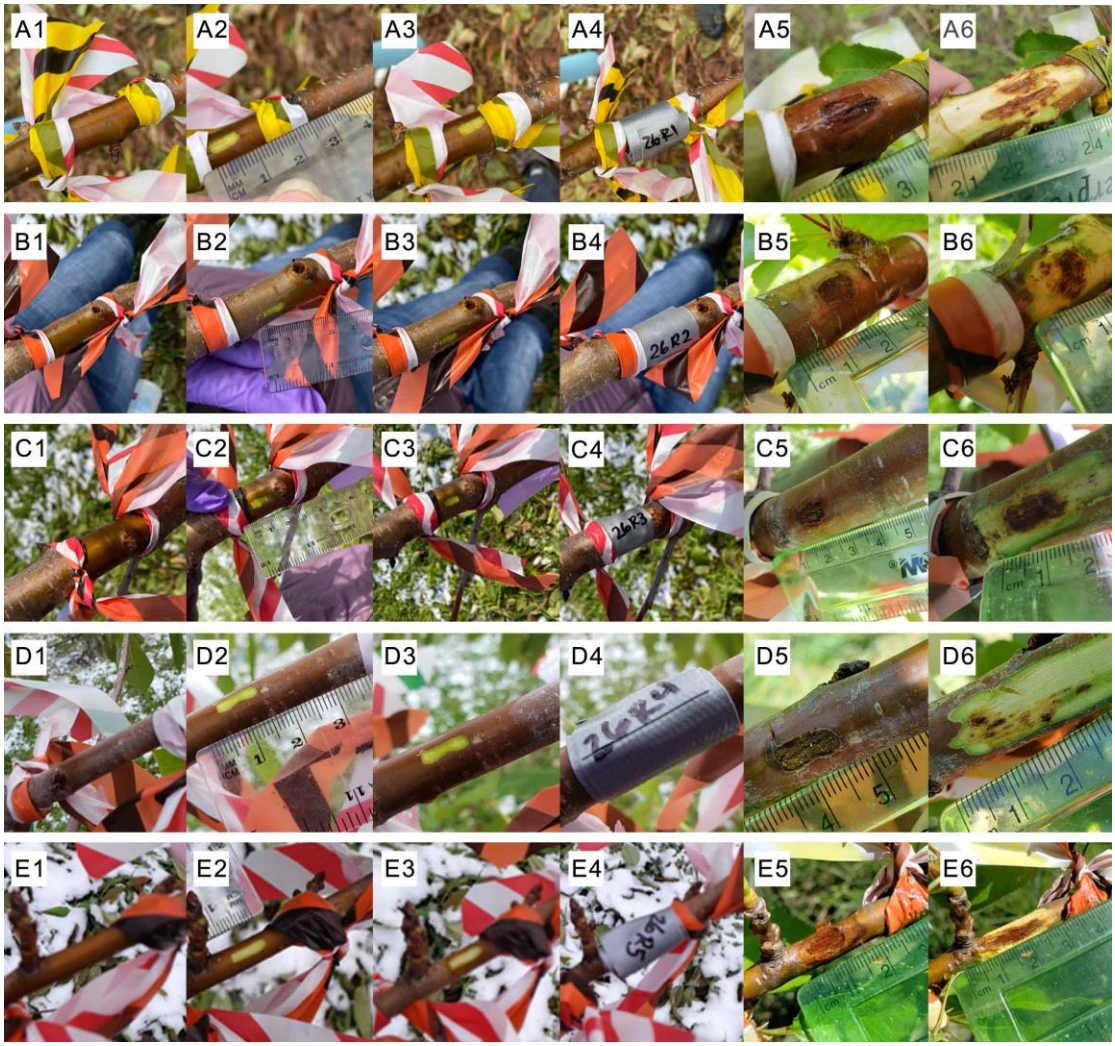


Figure A33. 2019 wound inoculations on 'Coral' cherry wood with *Pss* 26. **A1-E1)** The inoculation site before wounding. **A2-E2)** The inoculation site after wounding by razor blade. **A3-E3)** The inoculation site after pipetting inoculum into the wound. **A4-E4)** The inoculation site after being covered with Parafilm and tape. **A5-E5)** The inoculation site exterior assessment in the summer. **A6-E6)** The inoculation site interior assessment in the spring of 2020. A1-A6. Replication 1. B1-B6. Replication 2. C1-C6. Replication 3. D1-D6. Replication 4. E1-E6. Replication 5.

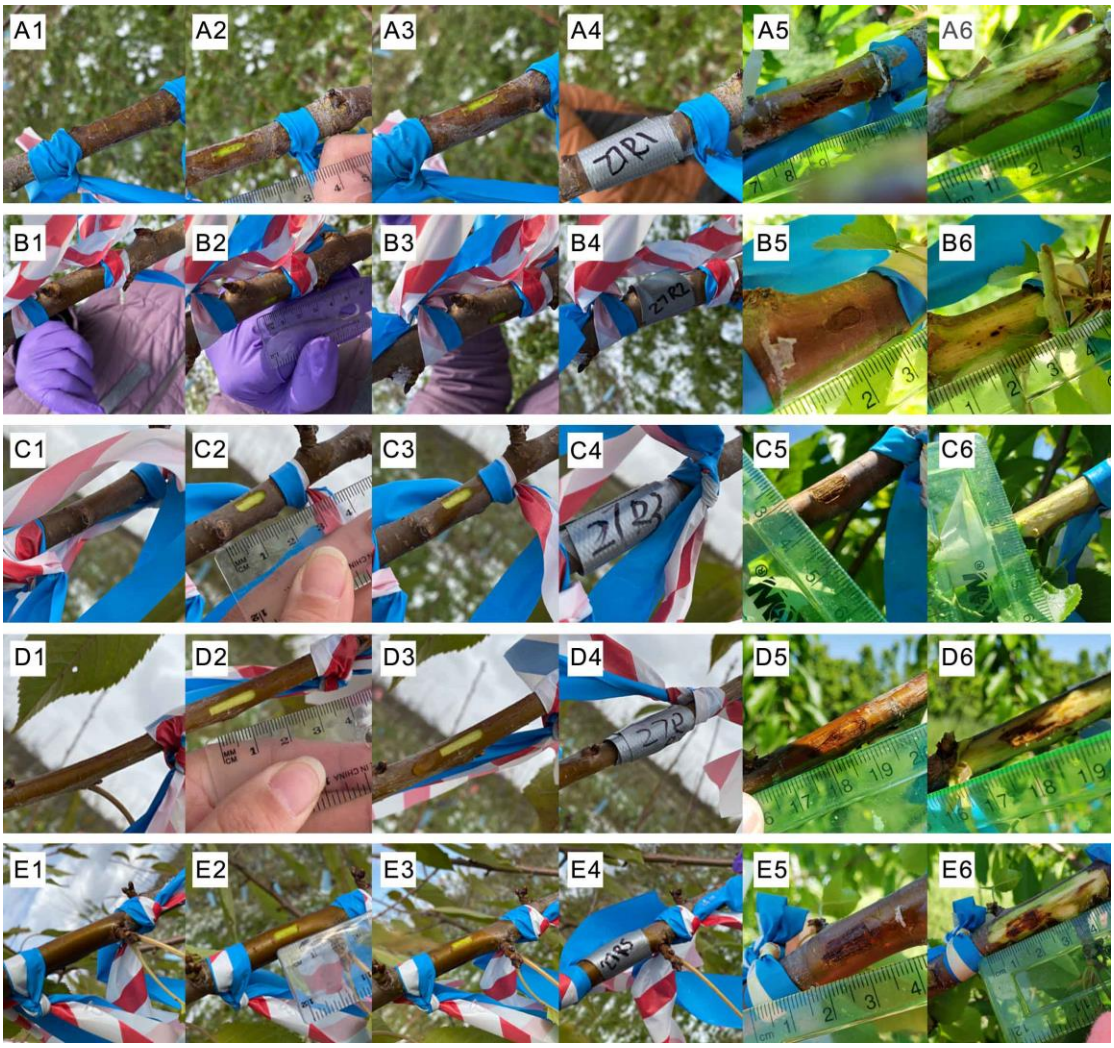


Figure A34. 2019 wound inoculations on 'Coral' cherry wood with *Pss* 27. **A1-E1)** The inoculation site before wounding. **A2-E2)** The inoculation site after wounding by razor blade. **A3-E3)** The inoculation site after pipetting inoculum into the wound. **A4-E4)** The inoculation site after being covered with Parafilm and tape. **A5-E5)** The inoculation site exterior assessment in the summer. **A6-E6)** The inoculation site interior assessment in the spring of 2020. A1-A6. Replication 1. B1-B6. Replication 2. C1-C6. Replication 3. D1-D6. Replication 4. E1-E6. Replication 5.

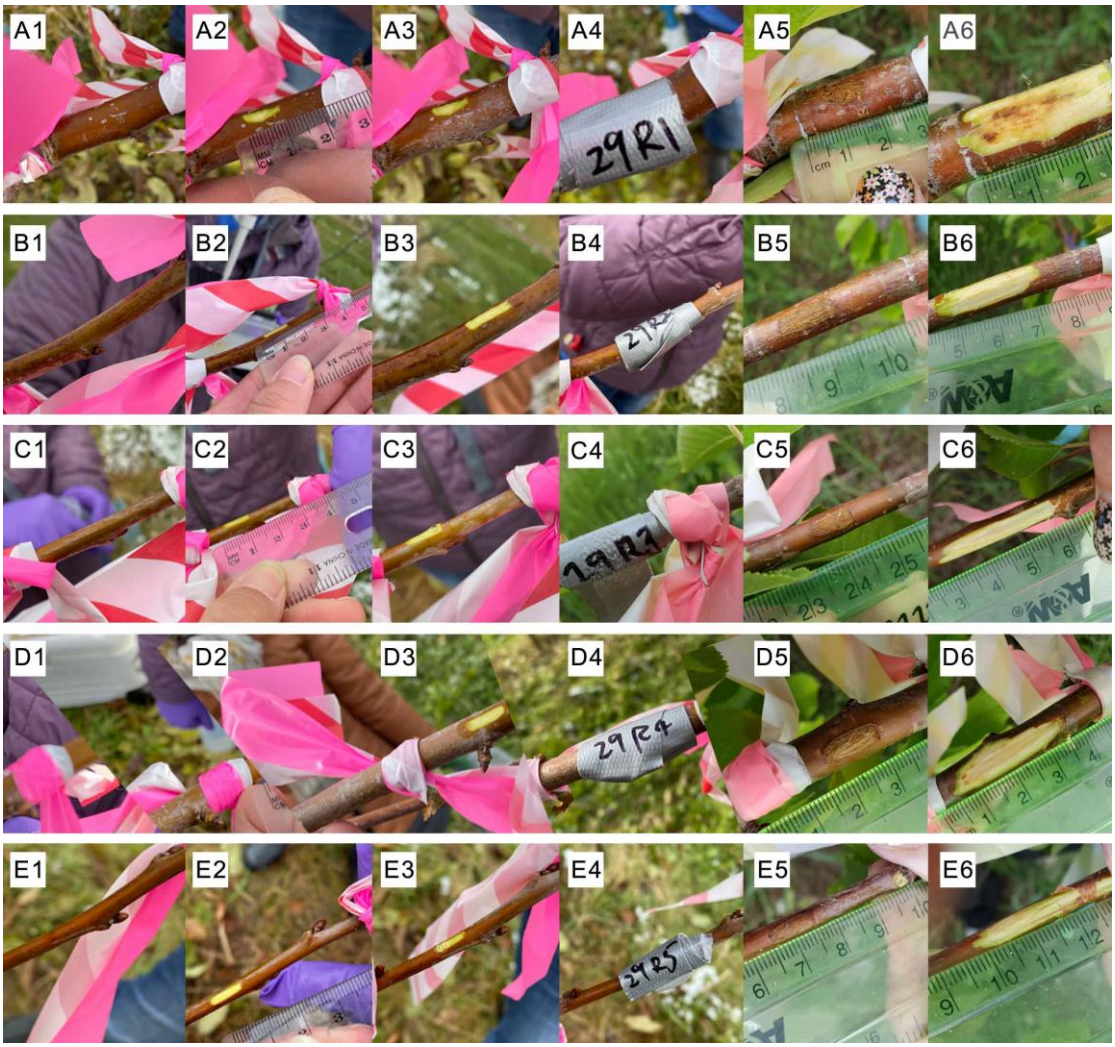


Figure A35. 2019 wound inoculations on 'Coral' cherry wood with *Pss* 29. **A1-E1)** The inoculation site before wounding. **A2-E2)** The inoculation site after wounding by razor blade. **A3-E3)** The inoculation site after pipetting inoculum into the wound. **A4-E4)** The inoculation site after being covered with Parafilm and tape. **A5-E5)** The inoculation site exterior assessment in the summer. **A6-E6)** The inoculation site interior assessment in the spring of 2020. A1-A6. Replication 1. B1-B6. Replication 2. C1-C6. Replication 3. D1-D6. Replication 4. E1-E6. Replication 5.

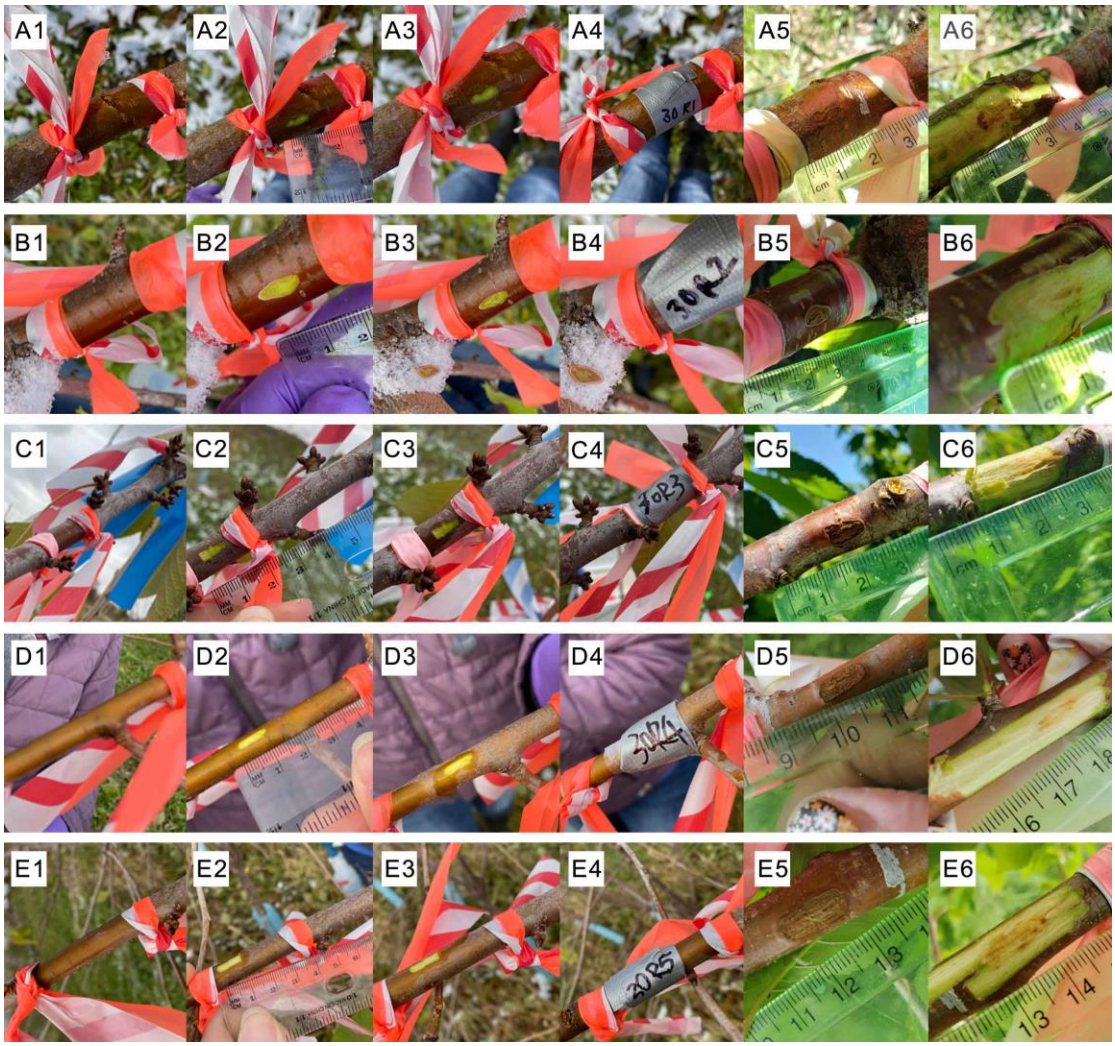


Figure A36. 2019 wound inoculations on 'Coral' cherry wood with *Pss* 30. **A1-E1)** The inoculation site before wounding. **A2-E2)** The inoculation site after wounding by razor blade. **A3-E3)** The inoculation site after pipetting inoculum into the wound. **A4-E4)** The inoculation site after being covered with Parafilm and tape. **A5-E5)** The inoculation site exterior assessment in the summer. **A6-E6)** The inoculation site interior assessment in the spring of 2020. A1-A6. Replication 1. B1-B6. Replication 2. C1-C6. Replication 3. D1-D6. Replication 4. E1-E6. Replication 5.

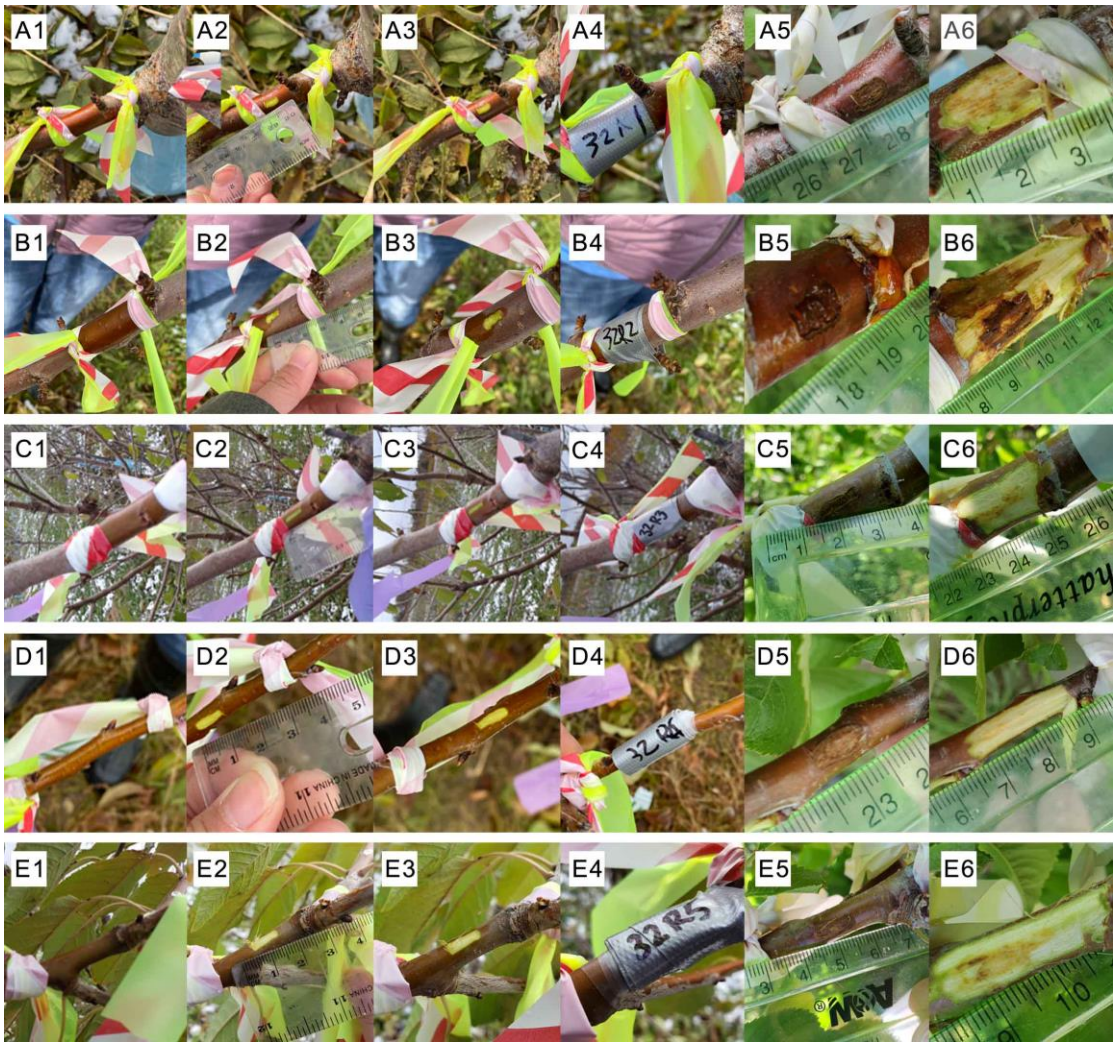


Figure A37. 2019 wound inoculations on 'Coral' cherry wood with *Pss* 32. **A1-E1)** The inoculation site before wounding. **A2-E2)** The inoculation site after wounding by razor blade. **A3-E3)** The inoculation site after pipetting inoculum into the wound. **A4-E4)** The inoculation site after being covered with Parafilm and tape. **A5-E5)** The inoculation site exterior assessment in the summer. **A6-E6)** The inoculation site interior assessment in the spring of 2020. A1-A6. Replication 1. B1-B6. Replication 2. C1-C6. Replication 3. D1-D6. Replication 4. E1-E6. Replication 5.

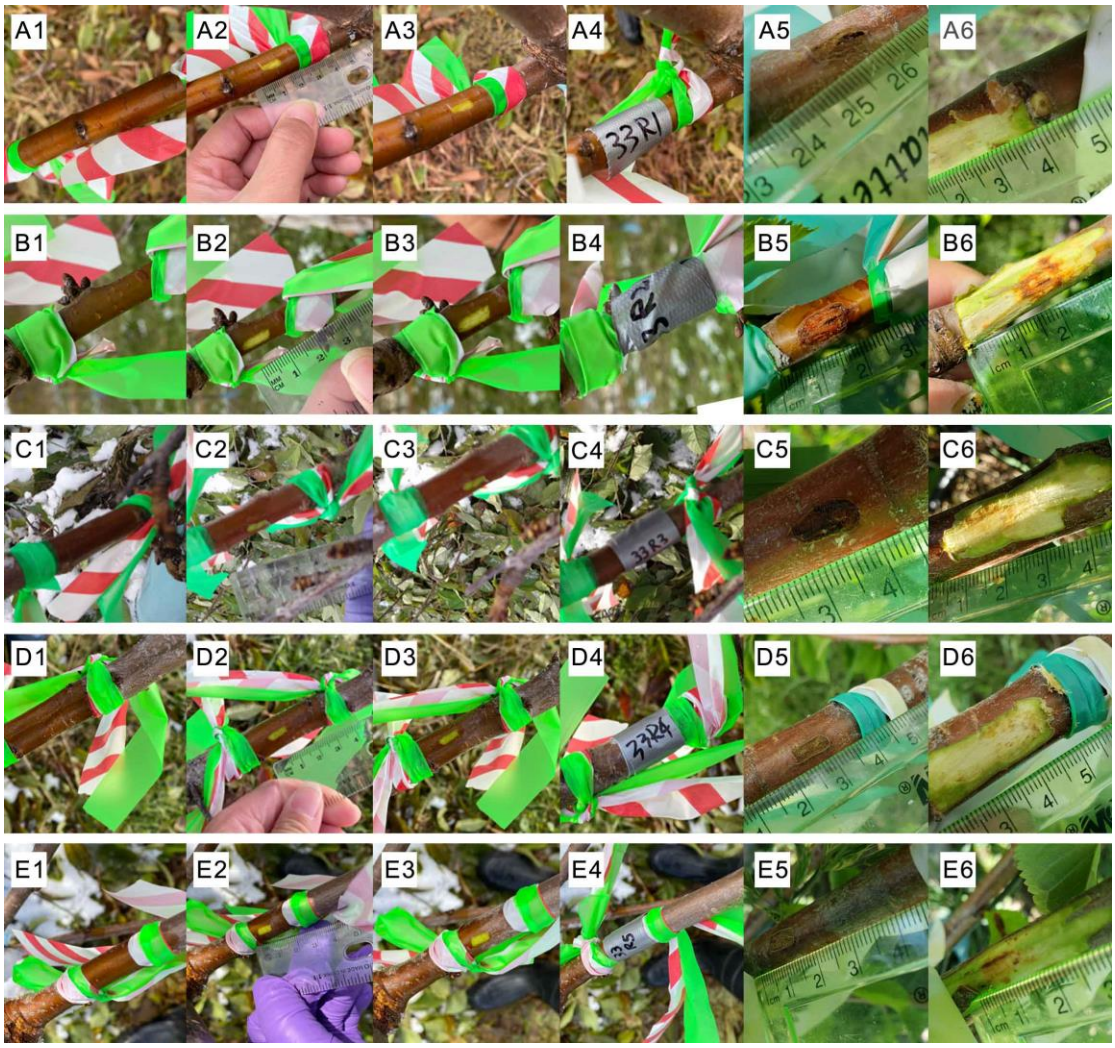


Figure A38. 2019 wound inoculations on 'Coral' cherry wood with *Pss* 33. **A1-E1)** The inoculation site before wounding. **A2-E2)** The inoculation site after wounding by razor blade. **A3-E3)** The inoculation site after pipetting inoculum into the wound. **A4-E4)** The inoculation site after being covered with Parafilm and tape. **A5-E5)** The inoculation site exterior assessment in the summer. **A6-E6)** The inoculation site interior assessment in the spring of 2020. A1-A6. Replication 1. B1-B6. Replication 2. C1-C6. Replication 3. D1-D6. Replication 4. E1-E6. Replication 5.

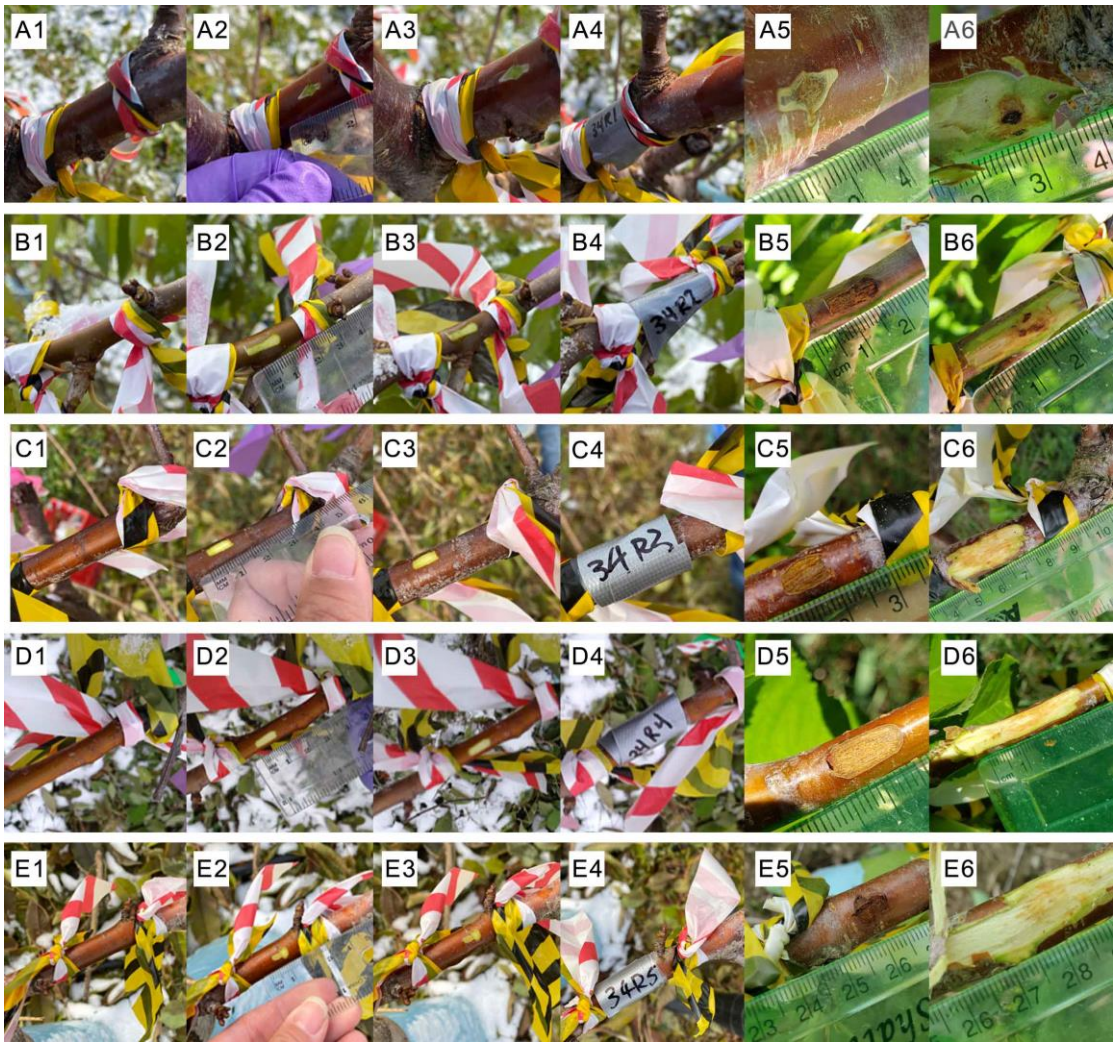


Figure A39. 2019 wound inoculations on 'Coral' cherry wood with *Pss* 34. **A1-E1)** The inoculation site before wounding. **A2-E2)** The inoculation site after wounding by razor blade. **A3-E3)** The inoculation site after pipetting inoculum into the wound. **A4-E4)** The inoculation site after being covered with Parafilm and tape. **A5-E5)** The inoculation site exterior assessment in the summer. **A6-E6)** The inoculation site interior assessment in the spring of 2020. A1-A6. Replication 1. B1-B6. Replication 2. C1-C6. Replication 3. D1-D6. Replication 4. E1-E6. Replication 5.

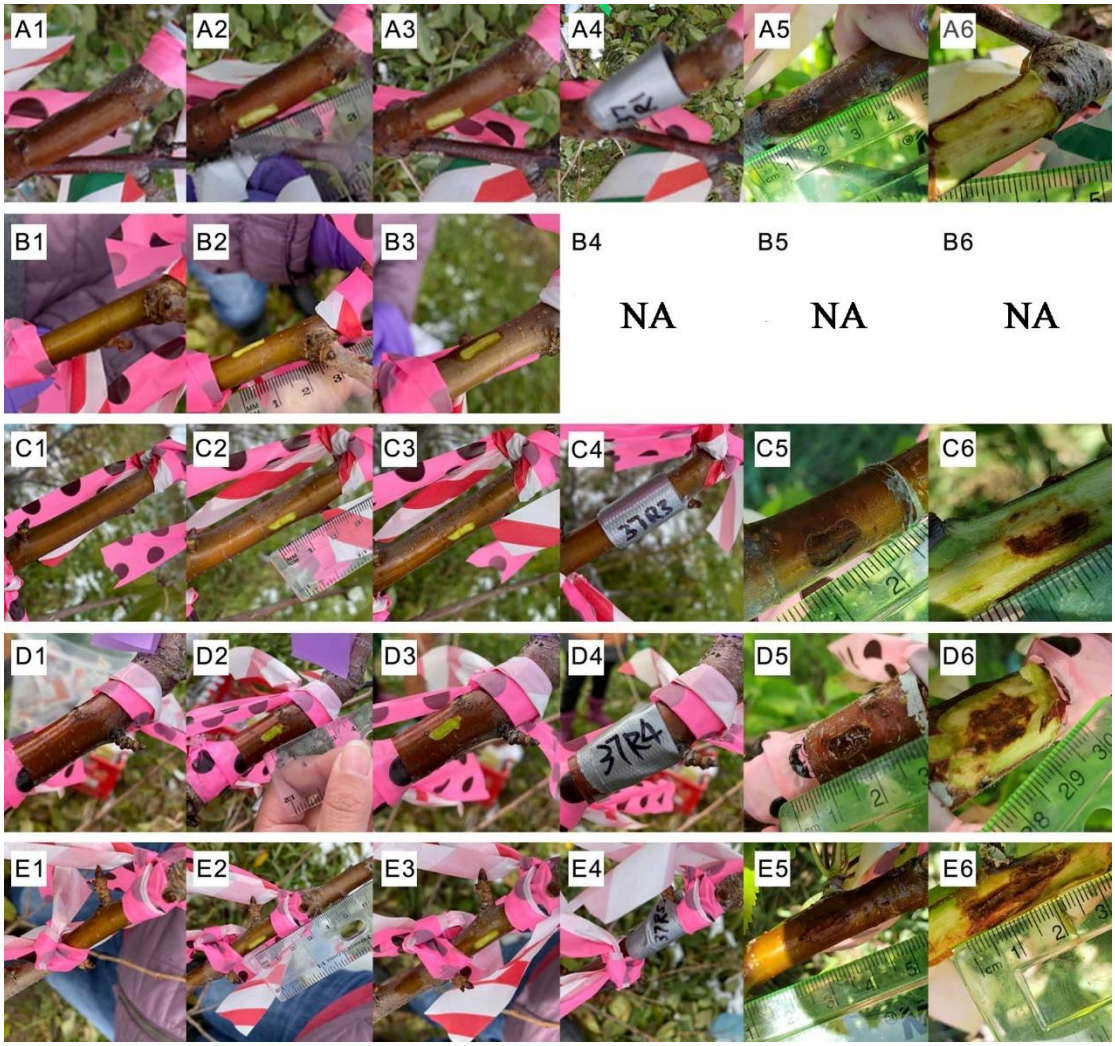


Figure A40. 2019 wound inoculations on 'Coral' cherry wood with *Pss* 37. **A1-E1)** The inoculation site before wounding. **A2-E2)** The inoculation site after wounding by razor blade. **A3-E3)** The inoculation site after pipetting inoculum into the wound. **A4-E4)** The inoculation site after being covered with Parafilm and tape. **A5-E5)** The inoculation site exterior assessment in the summer. **A6-E6)** The inoculation site interior assessment in the spring of 2020. A1-A6. Replication 1. B1-B6. Replication 2. C1-C6. Replication 3. D1-D6. Replication 4. E1-E6. Replication 5. Images with NA are not available.

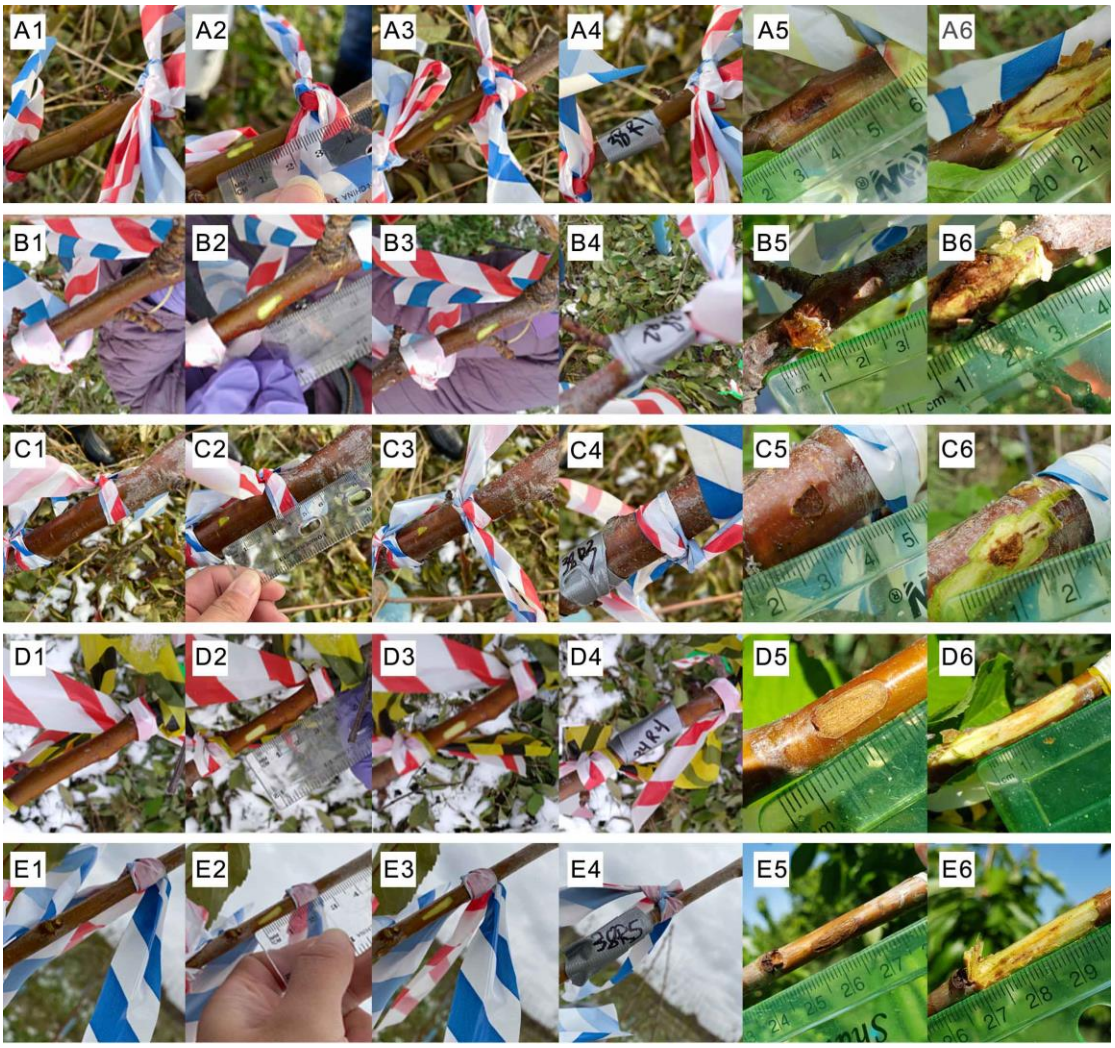


Figure A41. 2019 wound inoculations on 'Coral' cherry wood with *Pss* 38. **A1-E1)** The inoculation site before wounding. **A2-E2)** The inoculation site after wounding by razor blade. **A3-E3)** The inoculation site after pipetting inoculum into the wound. **A4-E4)** The inoculation site after being covered with Parafilm and tape. **A5-E5)** The inoculation site exterior assessment in the summer. **A6-E6)** The inoculation site interior assessment in the spring of 2020. A1-A6. Replication 1. B1-B6. Replication 2. C1-C6. Replication 3. D1-D6. Replication 4. E1-E6. Replication 5.

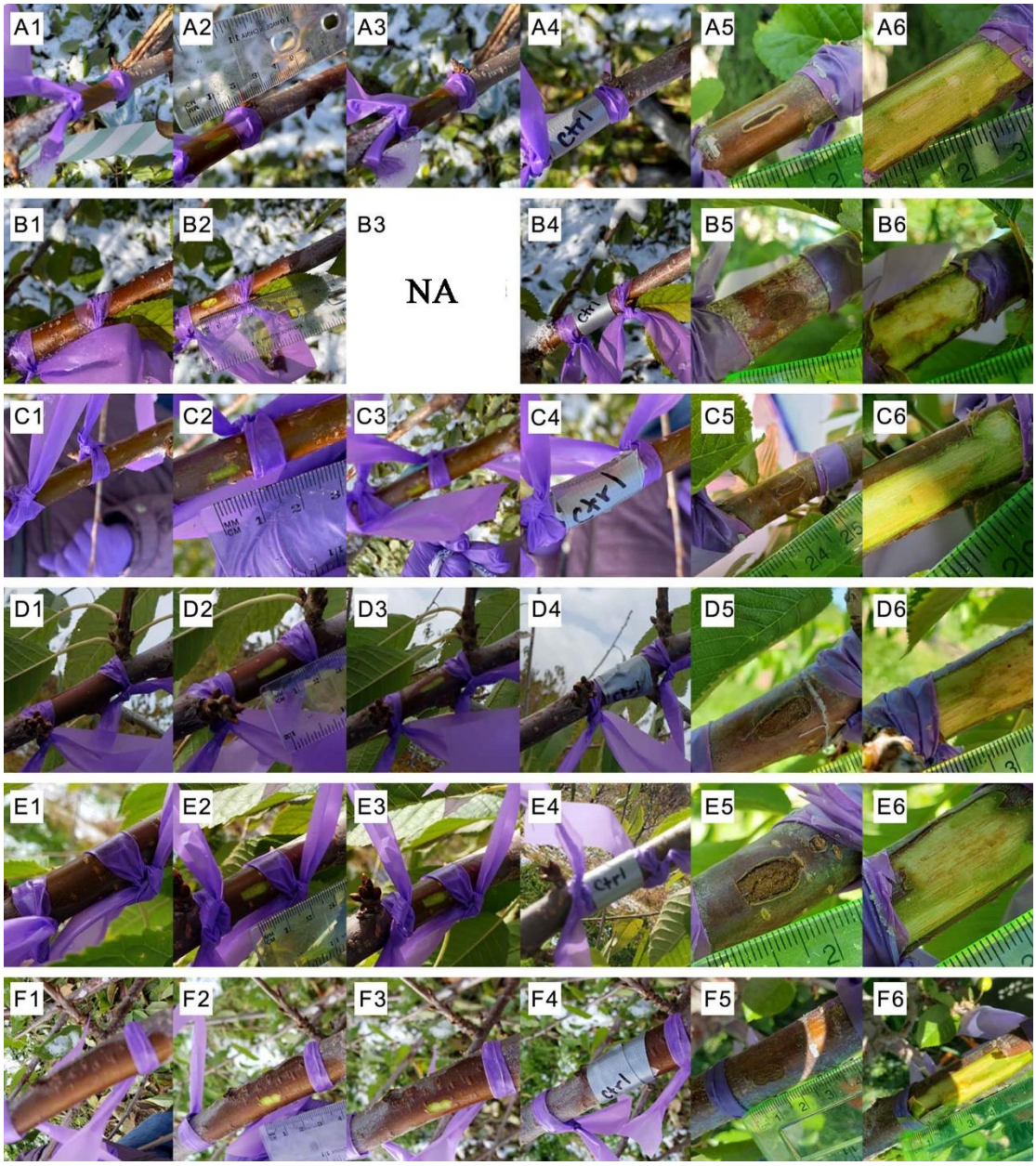


Figure A42. 2019 wound inoculations on 'Sweetheart' cherry wood with PBS. **A1-F1)** The inoculation site before wounding. **A2-F2)** The inoculation site after wounding by razor blade. **A3-F3)** The inoculation site after pipetting inoculum into the wound. **A4-F4)** The inoculation site after being covered with Parafilm and tape. **A5-F5)** The inoculation site exterior assessment in the summer. **A6-F6)** The inoculation site interior assessment in the spring of 2020. Images with NA are not available.

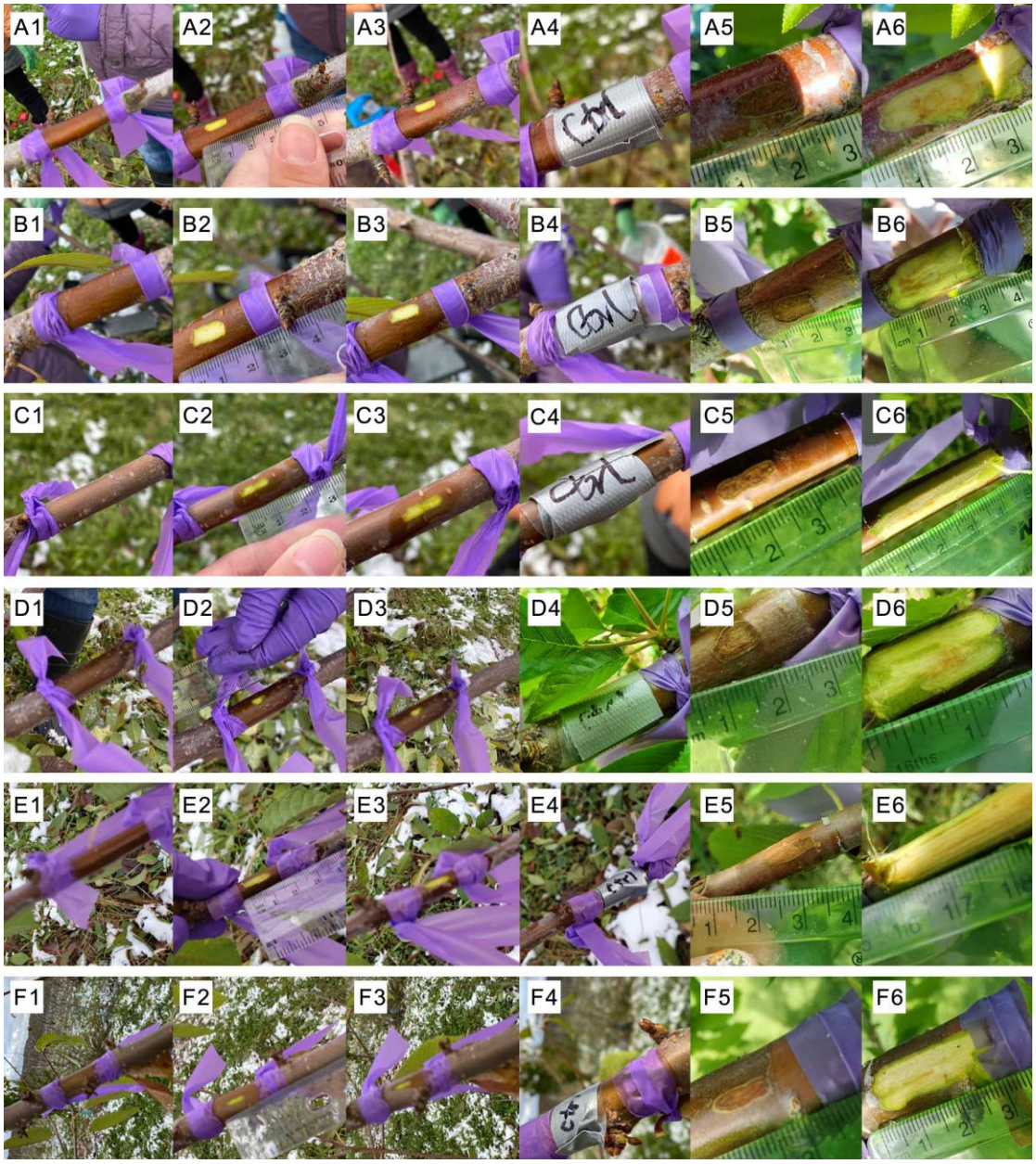


Figure A43. 2019 wound inoculations on 'Sweetheart' cherry wood with PBS. **A1-F1)** The inoculation site before wounding. **A2-F2)** The inoculation site after wounding by razor blade. **A3-F3)** The inoculation site after pipetting inoculum into the wound. **A4-F4)** The inoculation site after being covered with Parafilm and tape. **A5-F5)** The inoculation site exterior assessment in the summer. **A6-F6)** The inoculation site interior assessment in the spring of 2020.

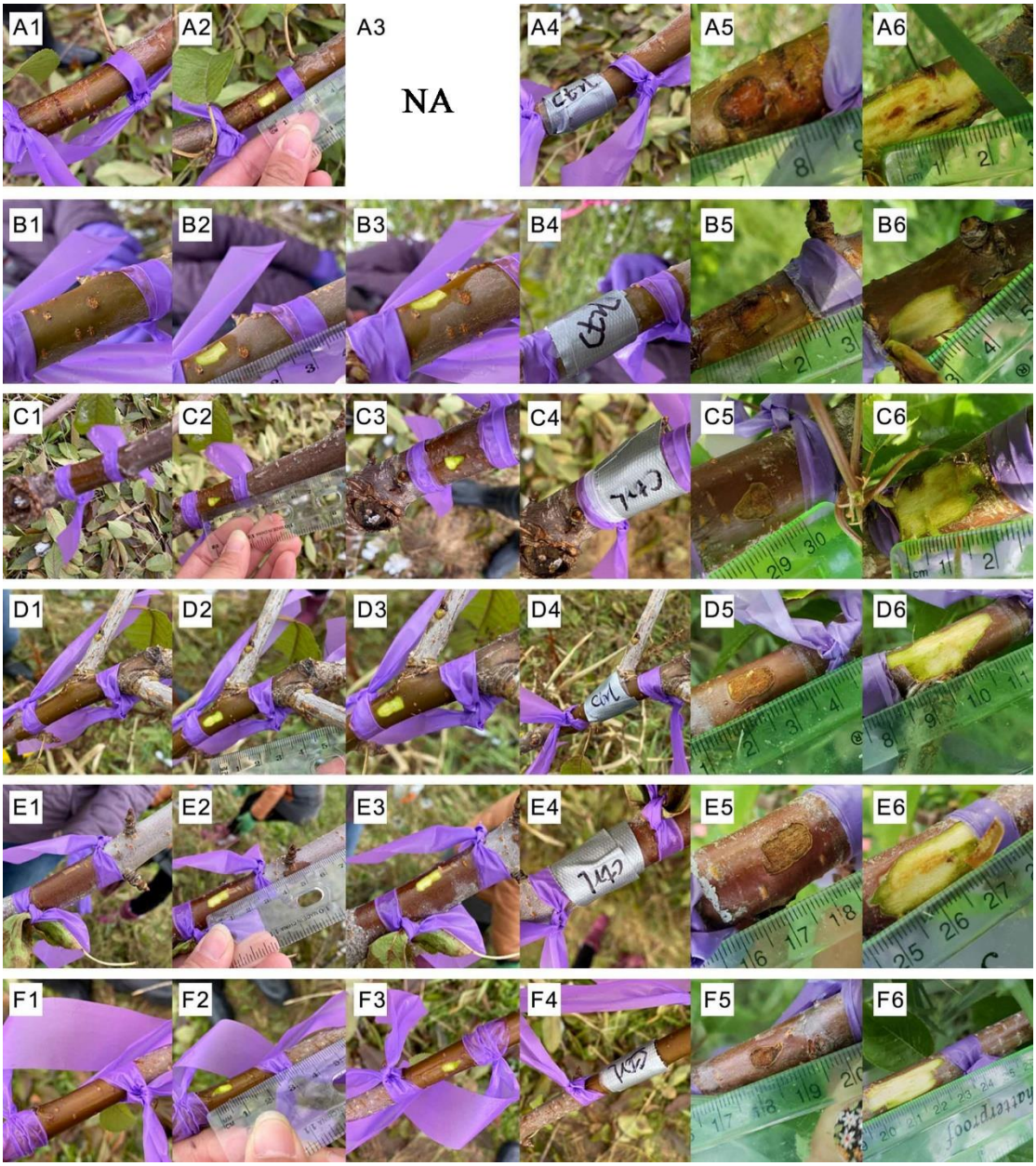


Figure A44. 2019 wound inoculations on 'Sweetheart' cherry wood with PBS. **A1-F1)** The inoculation site before wounding. **A2-F2)** The inoculation site after wounding by razor blade. **A3-F3)** The inoculation site after pipetting inoculum into the wound. **A4-F4)** The inoculation site after being covered with Parafilm and tape. **A5-F5)** The inoculation site exterior assessment in the summer. **A6-F6)** The inoculation site interior assessment in the spring of 2020. Images with NA are not available.

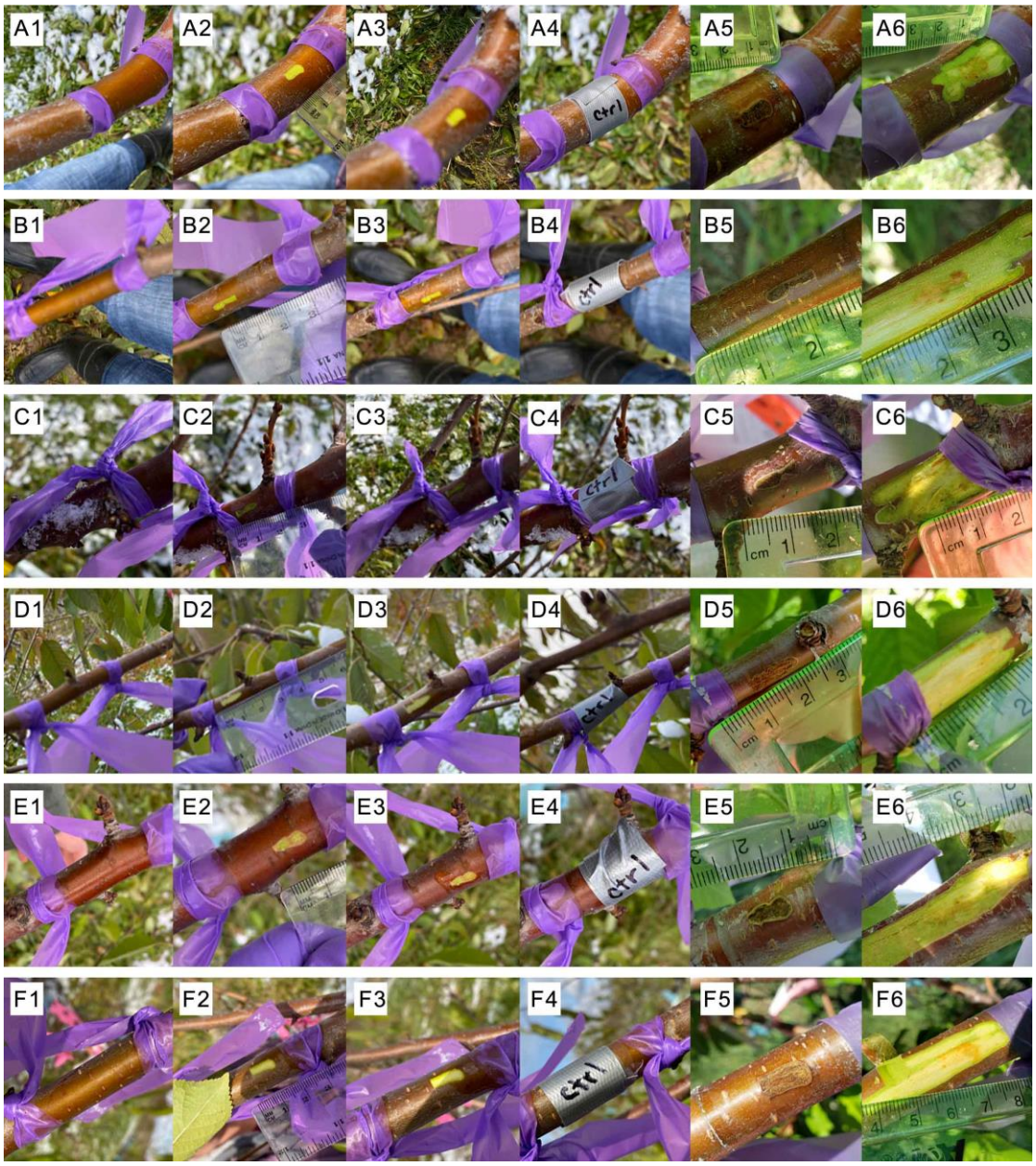


Figure A45. 2019 wound inoculations on 'Coral' cherry wood with PBS. **A1-F1)** The inoculation site before wounding. **A2-F2)** The inoculation site after wounding by razor blade. **A3-F3)** The inoculation site after pipetting inoculum into the wound. **A4-F4)** The inoculation site after being covered with Parafilm and tape. **A5-F5)** The inoculation site exterior assessment in the summer. **A6-F6)** The inoculation site interior assessment in the spring of 2020.

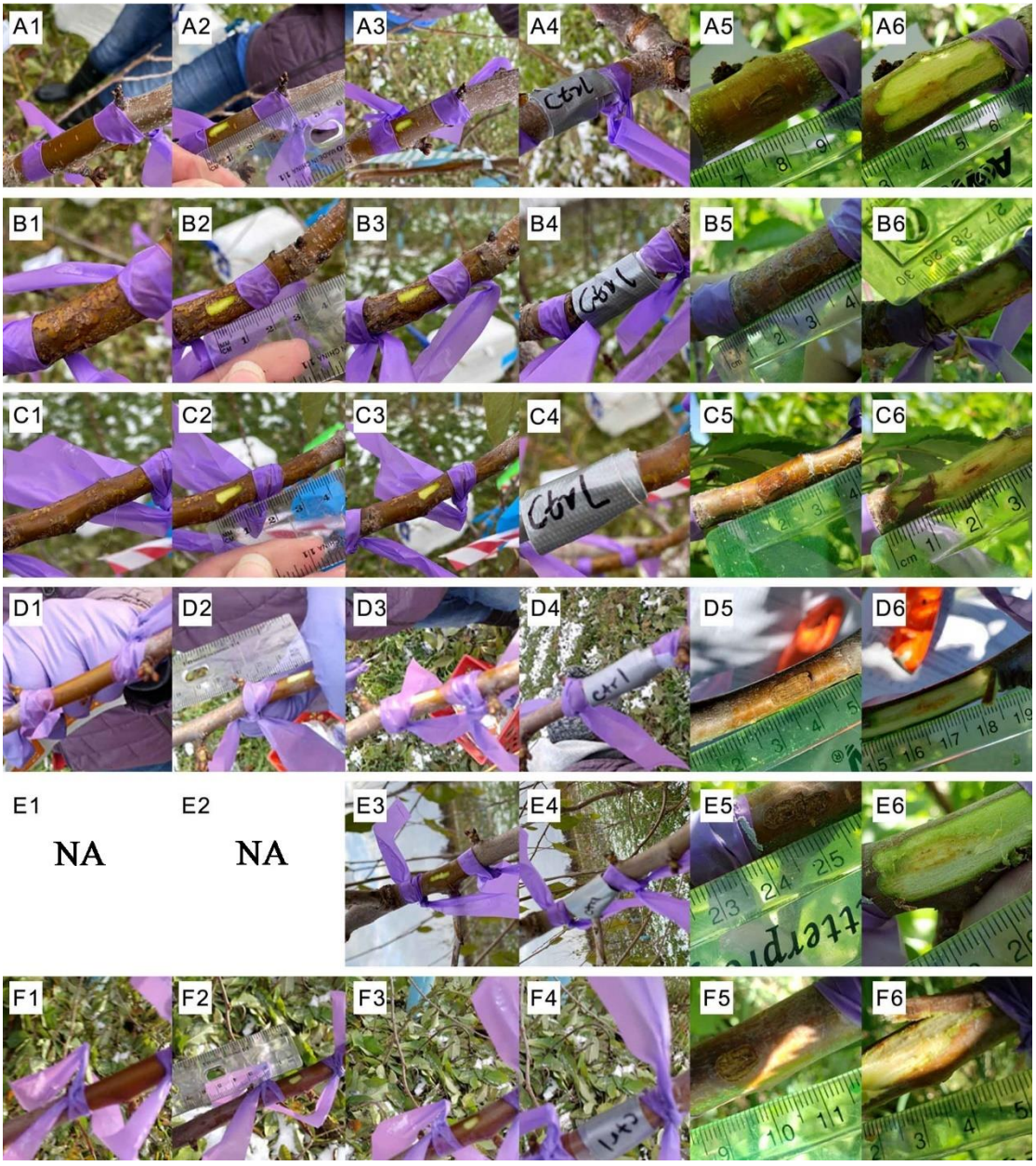


Figure A46. 2019 wound inoculations on 'Coral' cherry wood with PBS.**A1-F1)** The inoculation site before wounding. **A2-F2)** The inoculation site after wounding by razor blade. **A3-F3)** The inoculation site after pipetting inoculum into the wound. **A4-F4)** The inoculation site after being covered with Parafilm and tape. **A5-F5)** The inoculation site exterior assessment in the summer. **A6-F6)** The inoculation site interior assessment in the spring of 2020. Images with NA are not available.



Figure A47. 2019 wound inoculations on 'Coral' cherry wood with PBS. **A1-F1)** The inoculation site before wounding. **A2-F2)** The inoculation site after wounding by razor blade. **A3-F3)** The inoculation site after pipetting inoculum into the wound. **A4-F4)** The inoculation site after being covered with Parafilm and tape. **A5-F5)** The inoculation site exterior assessment in the summer. **A6-F6)** The inoculation site interior assessment in the spring of 2020.

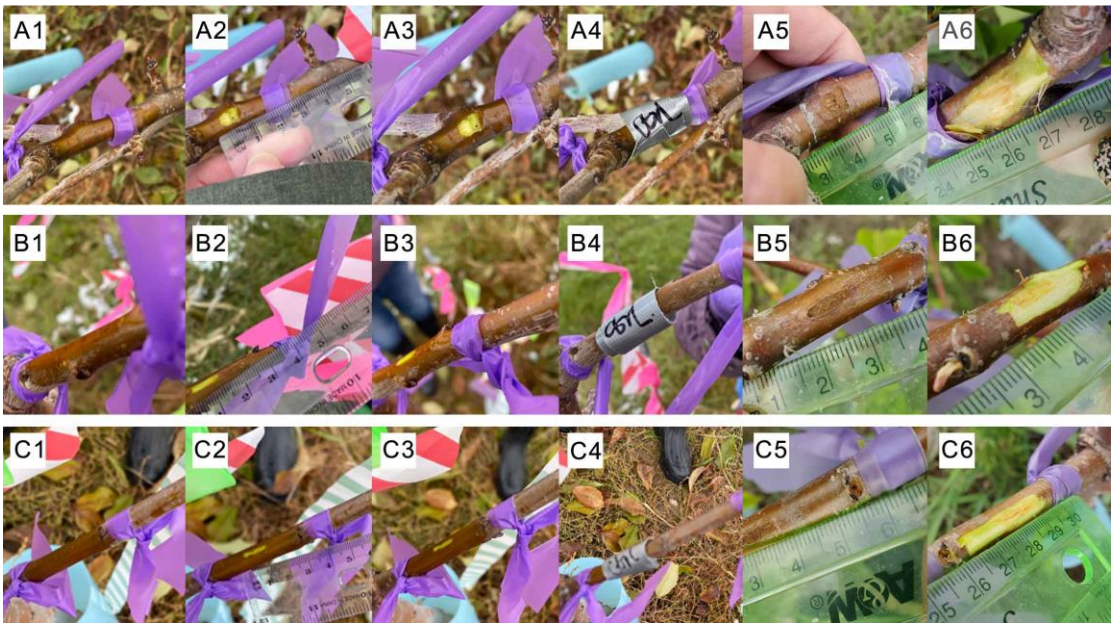


Figure A48. 2019 wound inoculations on 'Coral' cherry wood with PBS. **A1-C1)** The inoculation site before wounding. **A2-C2)** The inoculation site after wounding by razor blade. **A3-C3)** The inoculation site after pipetting inoculum into the wound. **A4-C4)** The inoculation site after being covered with Parafilm and tape. **A5-C5)** The inoculation site exterior assessment in the summer. **A6-C6)** The inoculation site interior assessment in the spring of 2020.

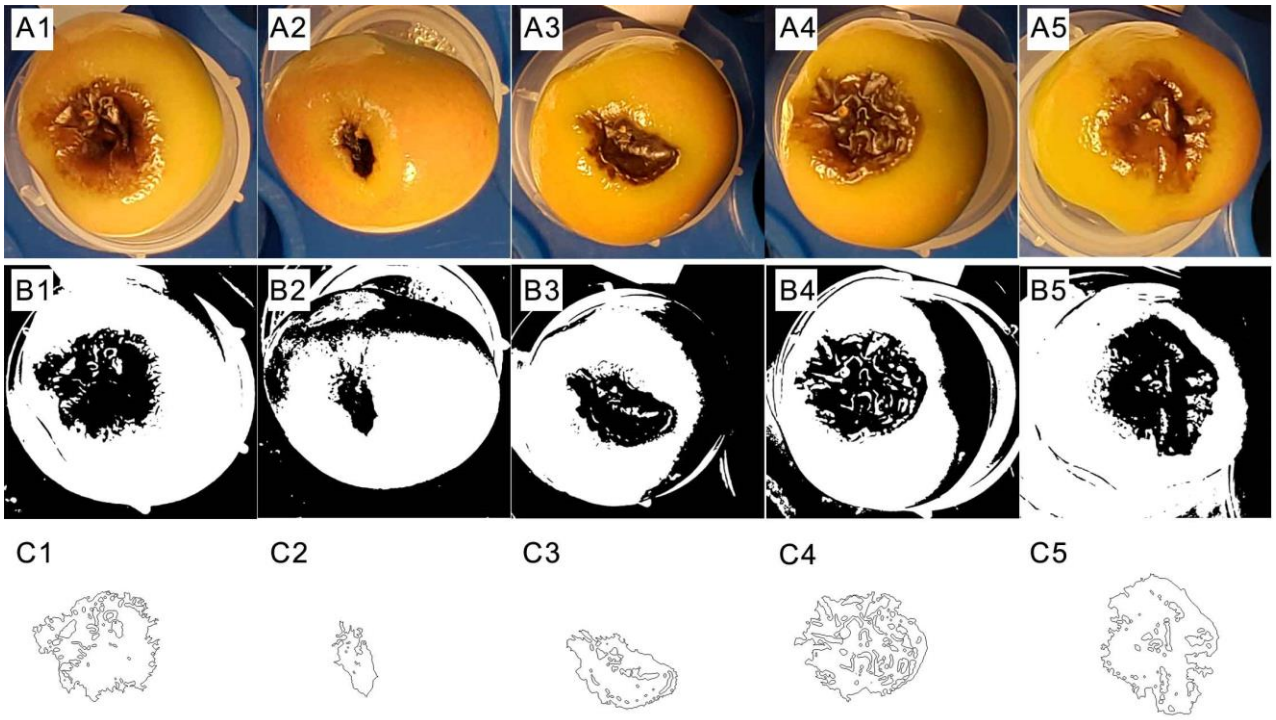


Figure A49. 2021 green cherry fruit ('Hedelfinger') lesion four days after inoculation. **A1-A5)** *Pss* 9 inoculated in stab wound. **B1-B5)** Images after threshold adjustment in ImageJ. **C1-C5)** Image of measured area. A1, B1, C1: Replication 1; A2, B2, C2: Replication 2; A3, B3, C3: Replication 3; A4, B4, C4: Replication4; A5, B5, C5: Replication 5.

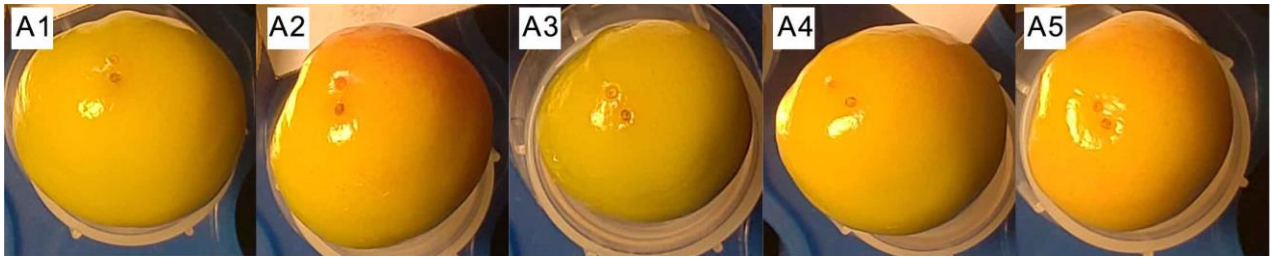


Figure A50. 2021 green cherry fruit ('Hedelfinger') lesion four days after inoculation. **A1-A5)** *Pss* 13 inoculated in stab wound, with no lesions for measuring in ImageJ.

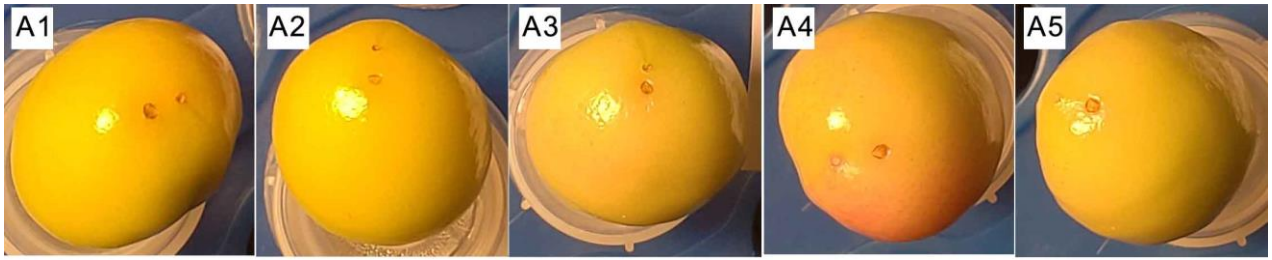


Figure A51. 2021 green cherry fruit (‘Hedelfinger’) lesion four days after inoculation. **A1-A5)** *Pss* 14 inoculated in stab wound, with no lesions for measuring in ImageJ.

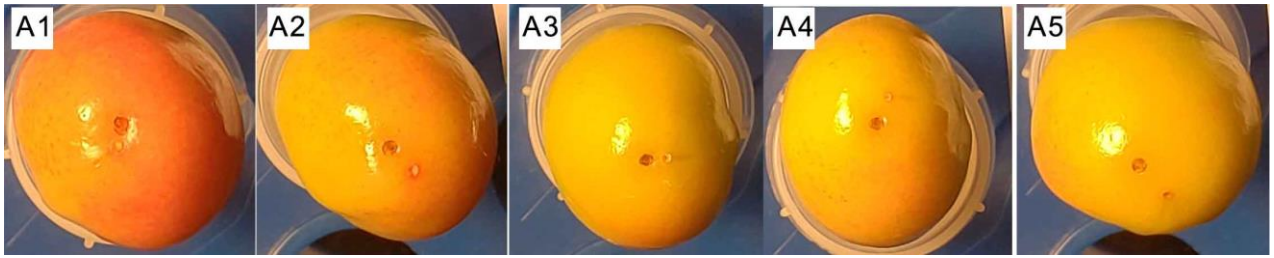


Figure A52. 2021 green cherry fruit ('Hedelfinger') lesion four days after inoculation. **A1-A5)** *Pss* 15 inoculated in stab wound, with no lesions for measuring in ImageJ.

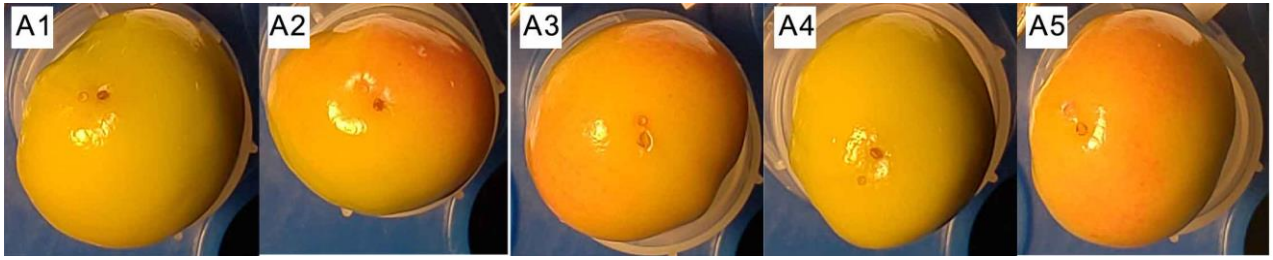


Figure A53. 2021 green cherry fruit ('Hedelfinger') lesion four days after inoculation. **A1-A5)** *Pss* 16 inoculated in stab wound, with no lesions for measuring in ImageJ.

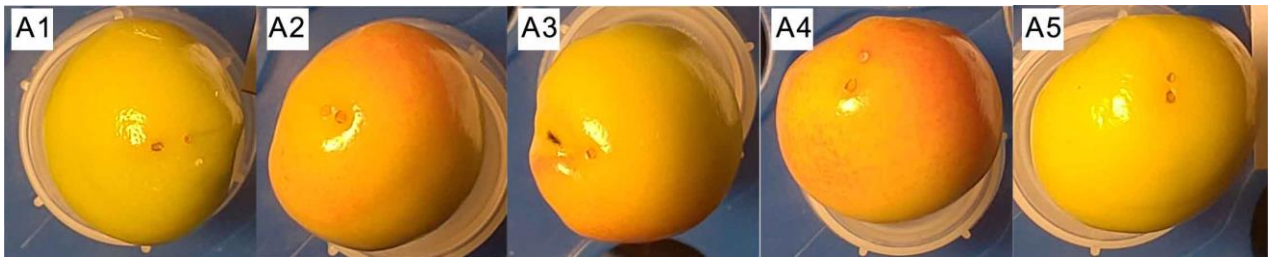


Figure A54. 2021 green cherry fruit ('Hedelfinger') lesion four days after inoculation. **A1-A5)** *Pss* 17 inoculated in stab wound, with no lesions for measuring in ImageJ.

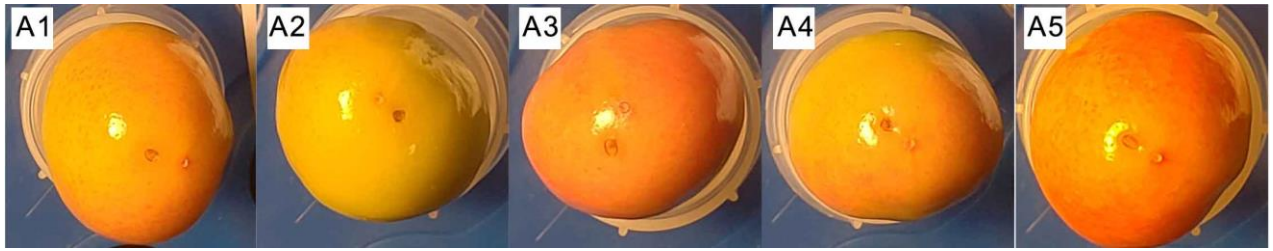


Figure A55. 2021 green cherry fruit ('Hedelfinger') lesion four days after inoculation. **A1-A5)** *Pss* 18 inoculated in stab wound, with no lesions for measuring in ImageJ.

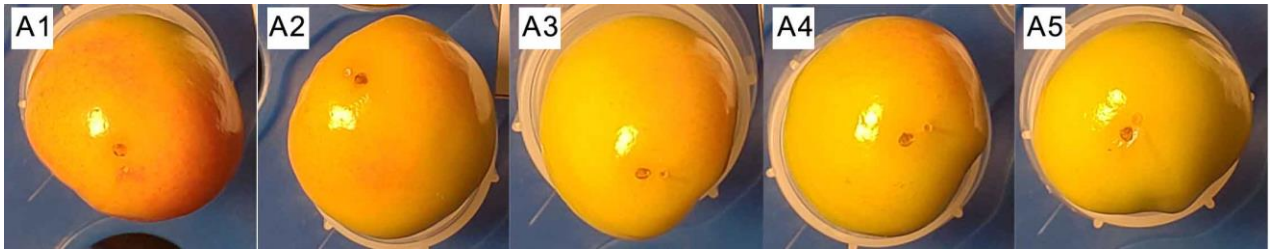


Figure A56. 2021 green cherry fruit ('Hedelfinger') lesion four days after inoculation. **A1-A5)** *Pss* 21 inoculated in stab wound, with no lesions for measuring in ImageJ.

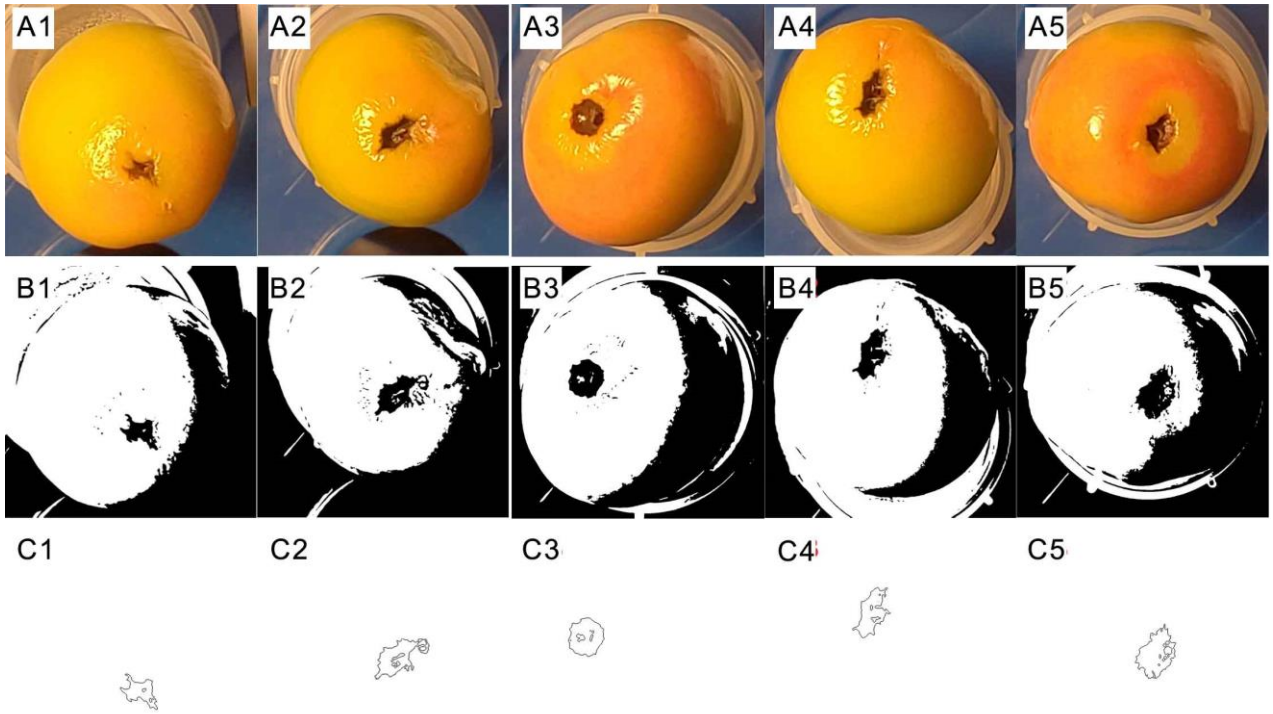


Figure A57. 2021 green cherry fruit ('Hedelfinger') lesion four days after inoculation. **A1-A5)** *Pss* 22 inoculated in stab wound. **B1-B5)** Images after threshold adjustment in ImageJ. **C1-C5)** Image of measured area. A1, B1, C1: Replication 1; A2, B2, C2: Replication 2; A3, B3, C3: Replication 3; A4, B4, C4: Replication4; A5, B5, C5: Replication 5.

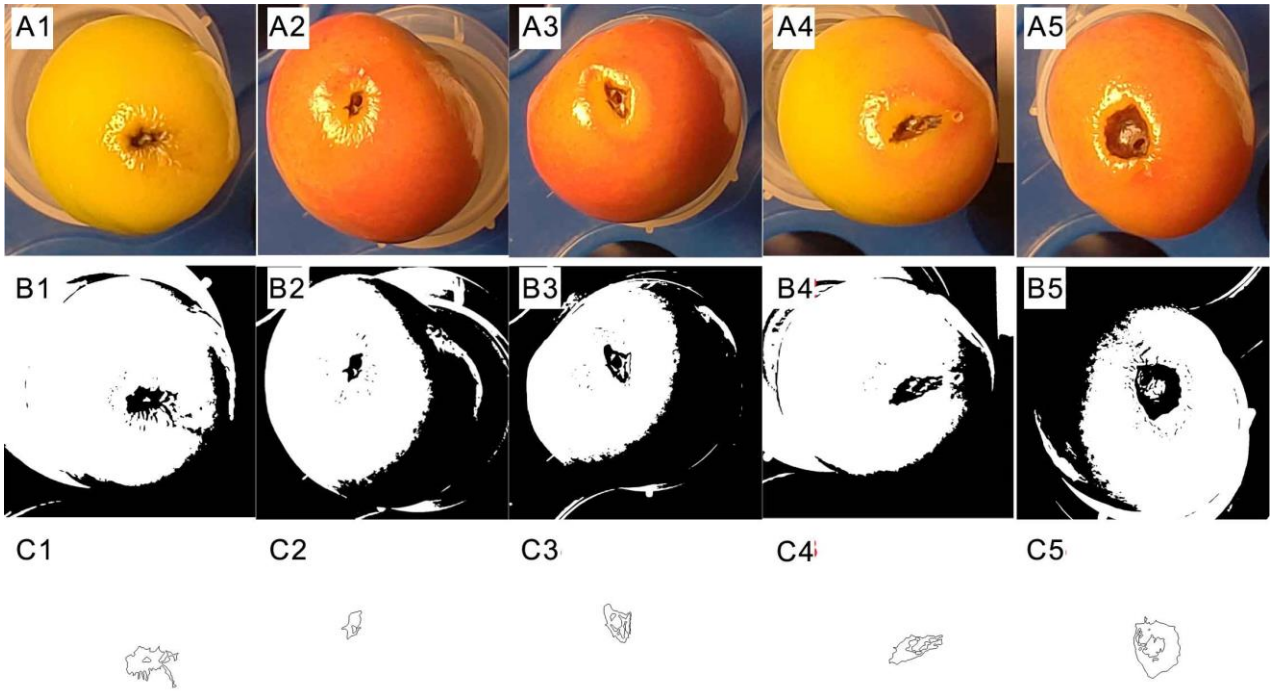


Figure A58. 2021 green cherry fruit (‘Hedelfinger’) lesion four days after inoculation. **A1-A5)** *Pss* 23 inoculated in stab wound. **B1-B5)** Images after threshold adjustment in ImageJ. **C1-C5)** Image of measured area. A1, B1, C1: Replication 1; A2, B2, C2: Replication 2; A3, B3, C3: Replication 3; A4, B4, C4: Replication4; A5, B5, C5: Replication 5.

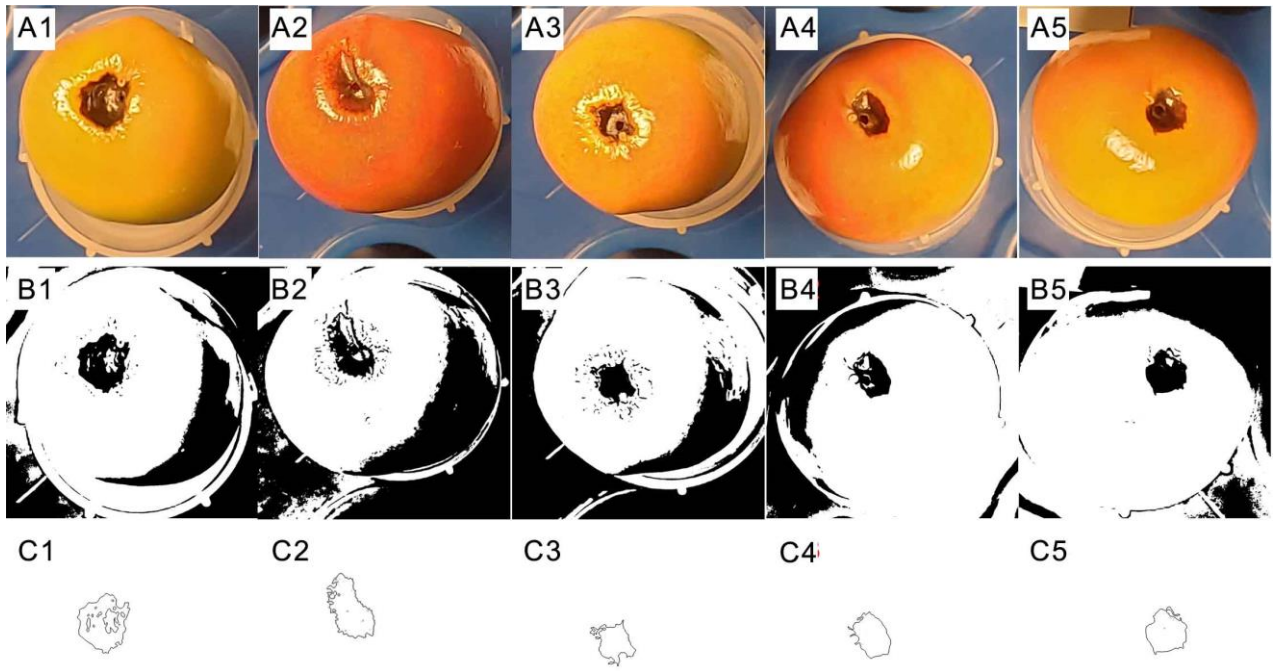


Figure A59. 2021 green cherry fruit ('Hedelfinger') lesion four days after inoculation. **A1-A5)** *Pss* 25 inoculated in stab wound. **B1-B5)** Images after threshold adjustment in ImageJ. **C1-C5)** Image of measured area. A1, B1, C1: Replication 1; A2, B2, C2: Replication 2; A3, B3, C3: Replication 3; A4, B4, C4: Replication4; A5, B5, C5: Replication 5.

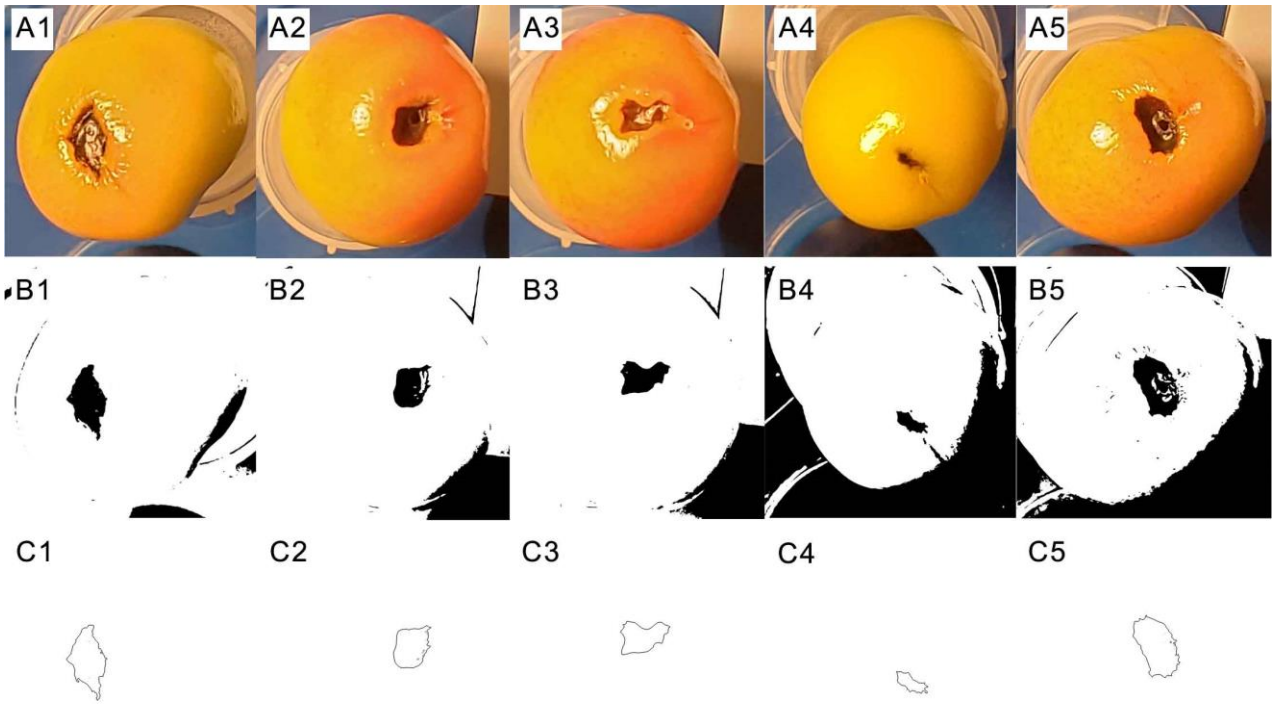


Figure A60. 2021 green cherry fruit ('Hedelfinger') lesion four days after inoculation. **A1-A5)** *Pss* 26 inoculated in stab wound. **B1-B5)** Images after threshold adjustment in ImageJ. **C1-C5)** Image of measured area. A1, B1, C1: Replication 1; A2, B2, C2: Replication 2; A3, B3, C3: Replication 3; A4, B4, C4: Replication4; A5, B5, C5: Replication 5.

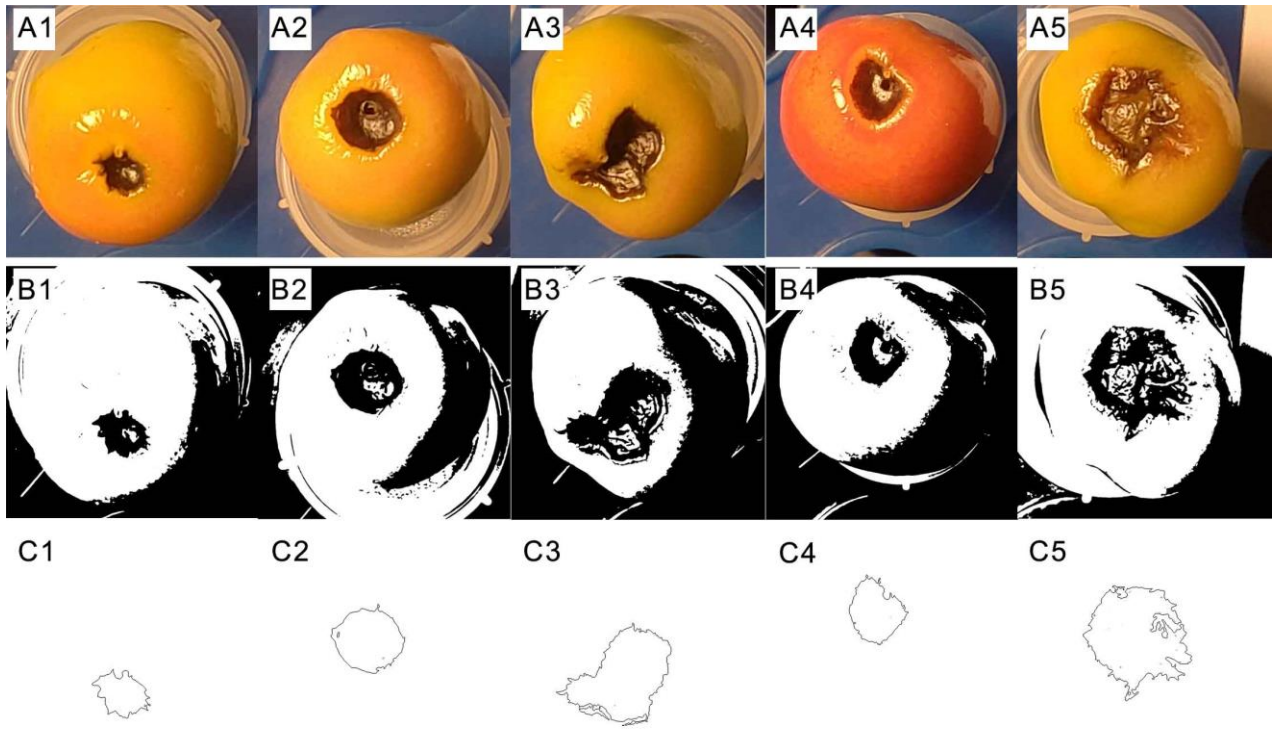


Figure A61. 2021 green cherry fruit ('Hedelfinger') lesion four days after inoculation. **A1-A5)** *Pss* 27 inoculated in stab wound. **B1-B5)** Images after threshold adjustment in ImageJ. **C1-C5)** Image of measured area. A1, B1, C1: Replication 1; A2, B2, C2: Replication 2; A3, B3, C3: Replication 3; A4, B4, C4: Replication4; A5, B5, C5: Replication 5.

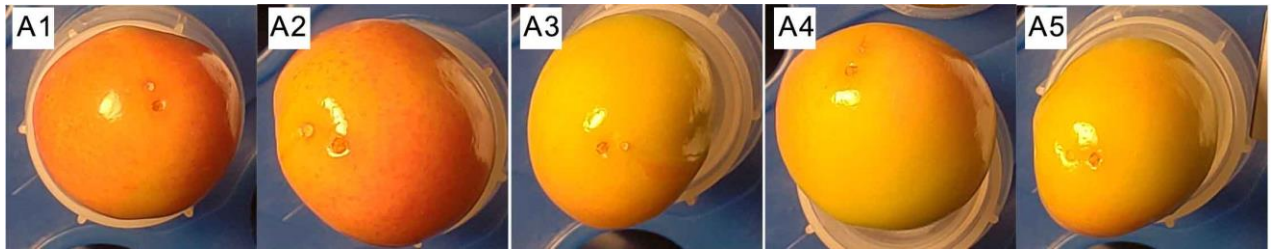


Figure A62. 2021 green cherry fruit ('Hedelfinger') lesion four days after inoculation. **A1-A5)** *Pss* 29 inoculated in stab wound, with no lesions for measuring in ImageJ.

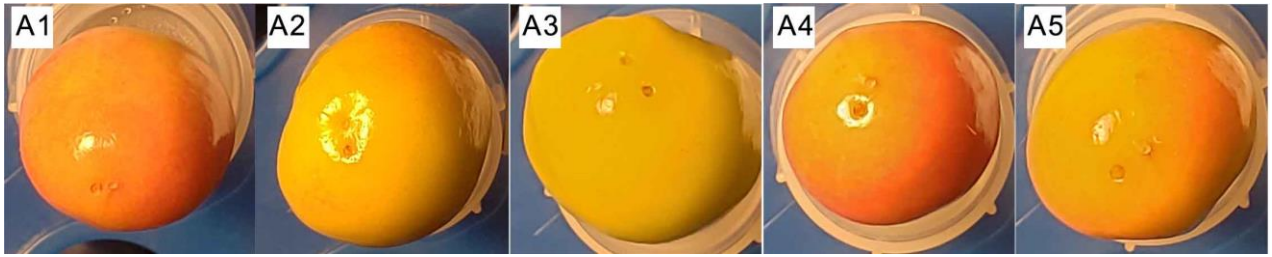


Figure A63. 2021 green cherry fruit ('Hedelfinger') lesion four days after inoculation. **A1-A5)** *Pss* 30 inoculated in stab wound, with no lesions for measuring in ImageJ.

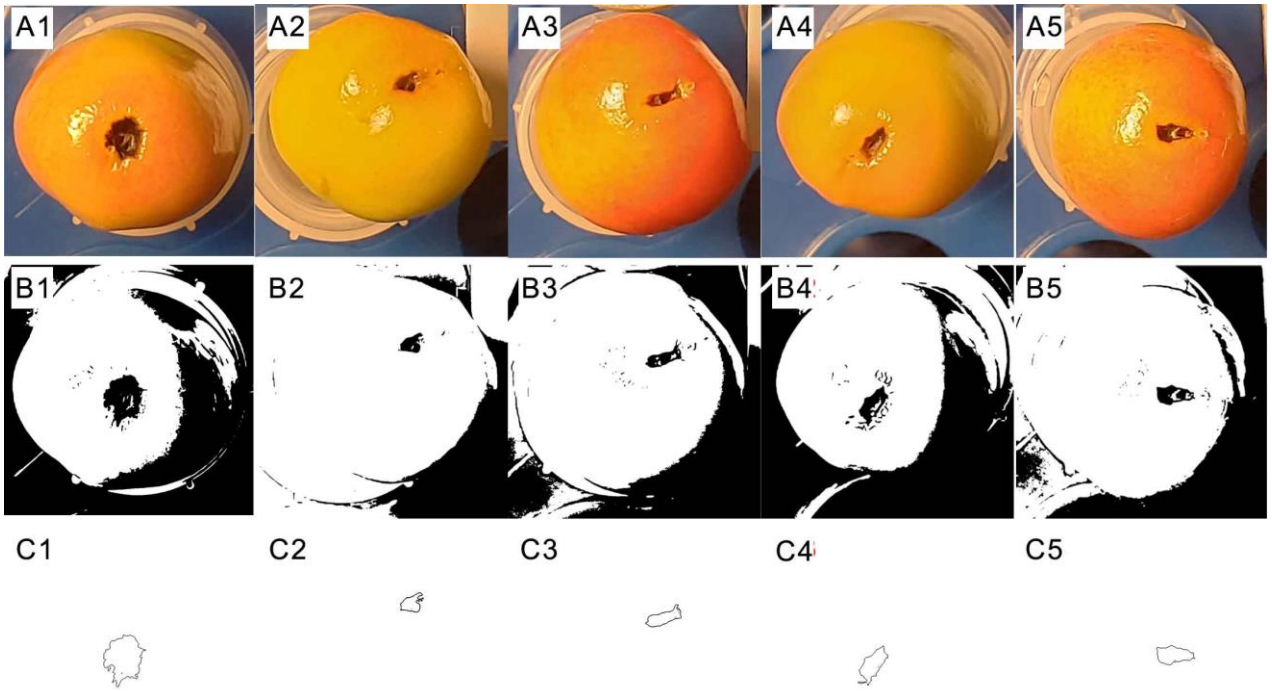


Figure A64. 2021 green cherry fruit ('Hedelfinger') lesion four days after inoculation. **A1-A5)** *Pss* 32 inoculated in stab wound. **B1-B5)** Images after threshold adjustment in ImageJ. **C1-C5)** Image of measured area. A1, B1, C1: Replication 1; A2, B2, C2: Replication 2; A3, B3, C3: Replication 3; A4, B4, C4: Replication4; A5, B5, C5: Replication 5.

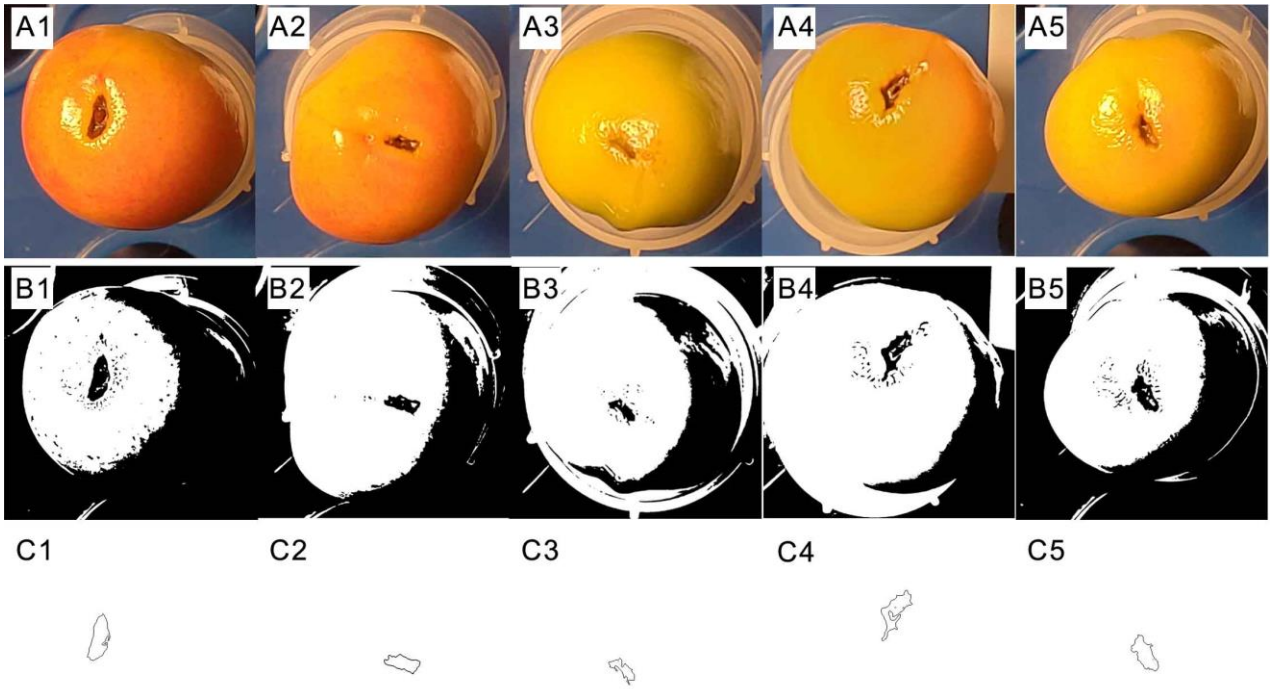


Figure A65. 2021 green cherry fruit ('Hedelfinger') lesion four days after inoculation. **A1-A5)** *Pss* 33 inoculated in stab wound. **B1-B5)** Images after threshold adjustment in ImageJ. **C1-C5)** Image of measured area. A1, B1, C1: Replication 1; A2, B2, C2: Replication 2; A3, B3, C3: Replication 3; A4, B4, C4: Replication4; A5, B5, C5: Replication 5.

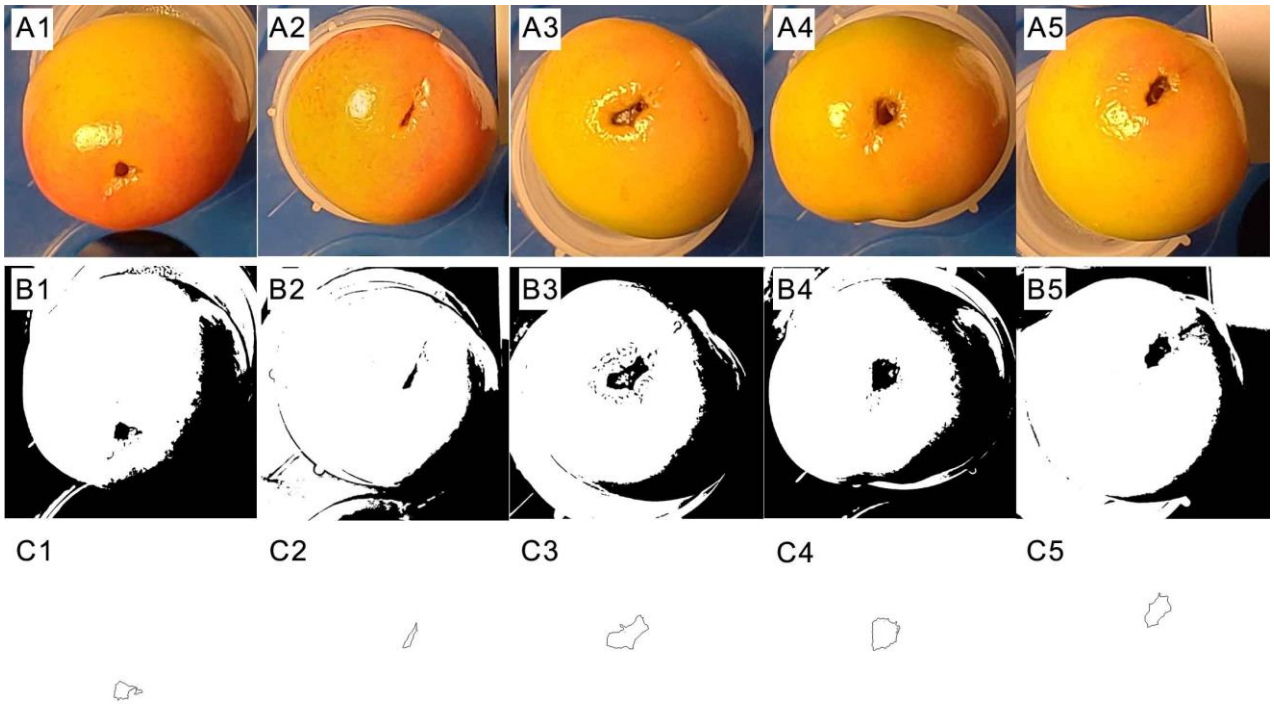


Figure A66. 2021 green cherry fruit ('Hedelfinger') lesion four days after inoculation. **A1-A5)** *Pss* 34 inoculated in stab wound. **B1-B5)** Images after threshold adjustment in ImageJ. **C1-C5)** Image of measured area. A1, B1, C1: Replication 1; A2, B2, C2: Replication 2; A3, B3, C3: Replication 3; A4, B4, C4: Replication4; A5, B5, C5: Replication 5.

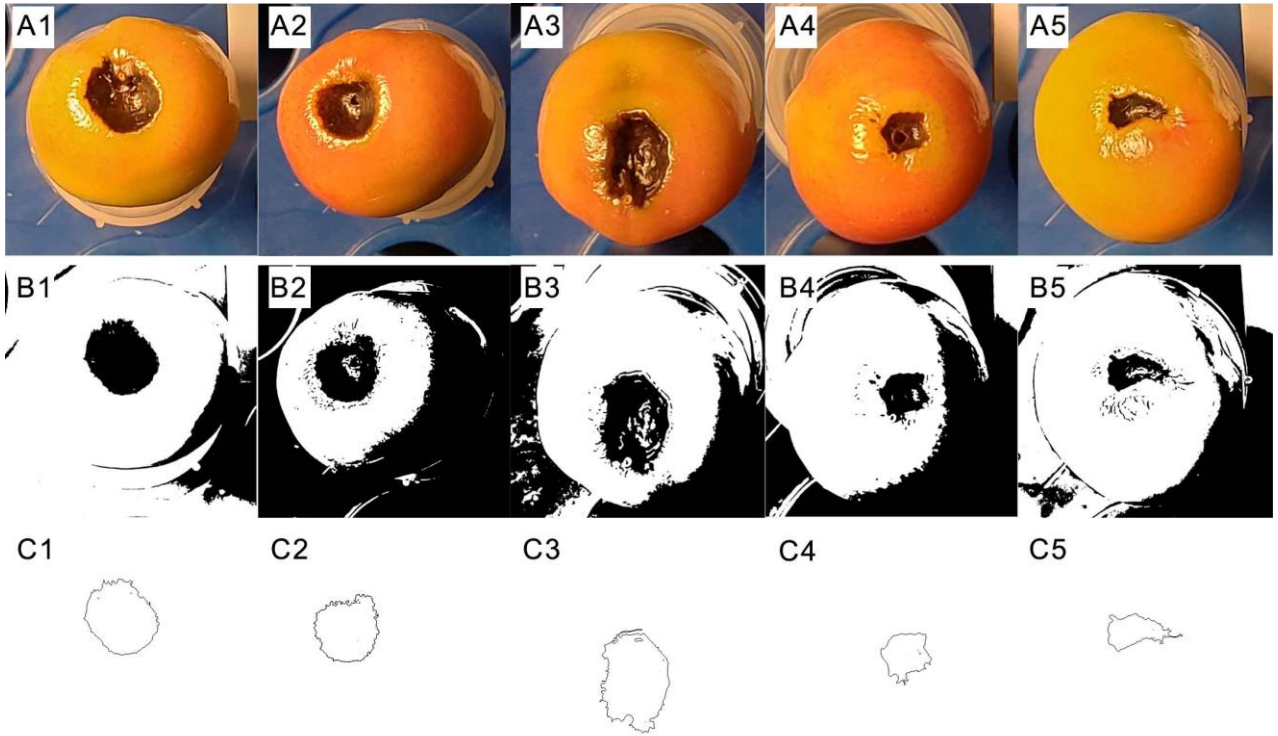


Figure A67. 2021 green cherry fruit ('Hedelfinger') lesion four days after inoculation. **A1-A5)** *Pss* 37 inoculated in stab wound. **B1-B5)** Images after threshold adjustment in ImageJ. **C1-C5)** Image of measured area. A1, B1, C1: Replication 1; A2, B2, C2: Replication 2; A3, B3, C3: Replication 3; A4, B4, C4: Replication4; A5, B5, C5: Replication 5.

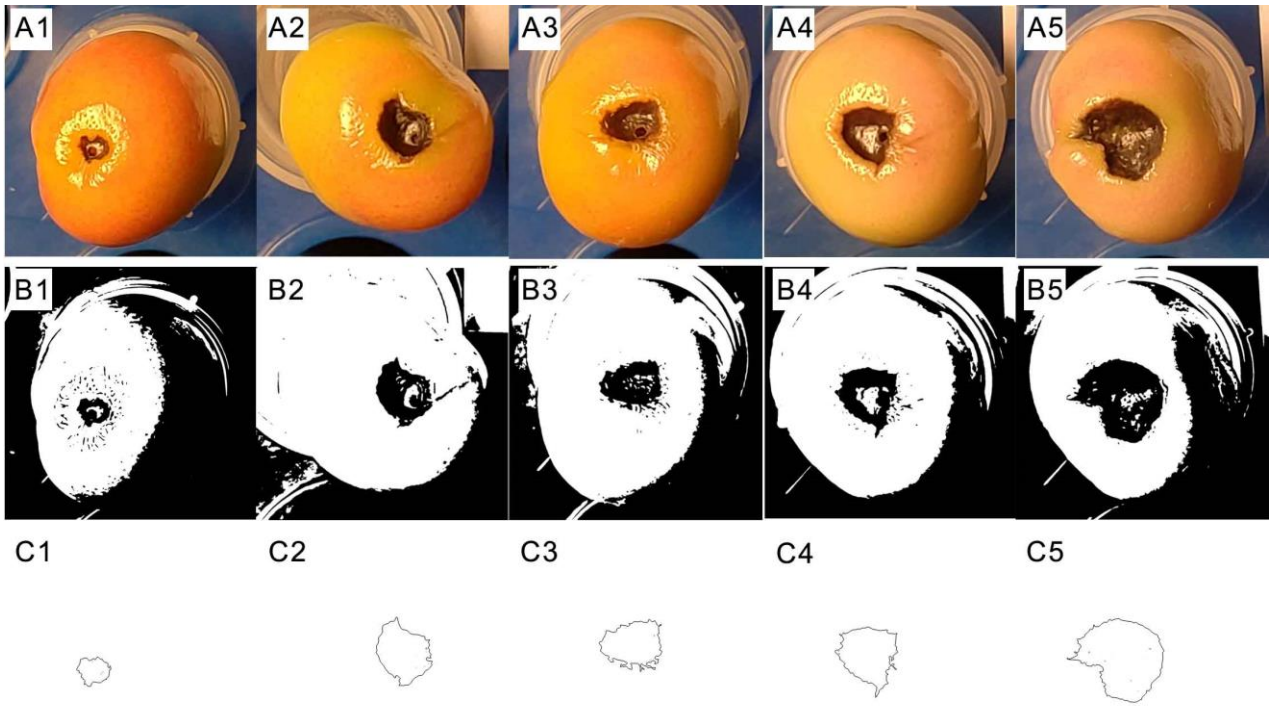


Figure A68. 2021 green cherry fruit ('Hedelfinger') lesion four days after inoculation. **A1-A5)** *Pss* 38 inoculated in stab wound. **B1-B5)** Images after threshold adjustment in ImageJ. **C1-C5)** Image of measured area. A1, B1, C1: Replication 1; A2, B2, C2: Replication 2; A3, B3, C3: Replication 3; A4, B4, C4: Replication4; A5, B5, C5: Replication 5.

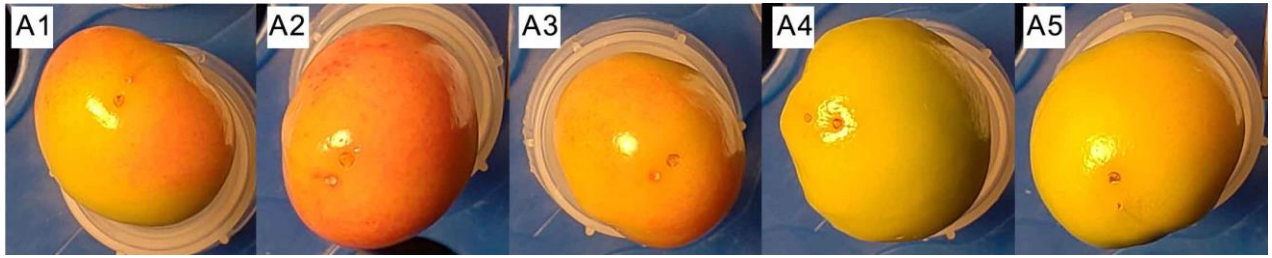


Figure A69. 2021 green cherry fruit (‘Hedelfinger’) lesion four days after inoculation. **A1-A5)** PBS inoculated in stab wound, with no lesions for measuring in ImageJ.

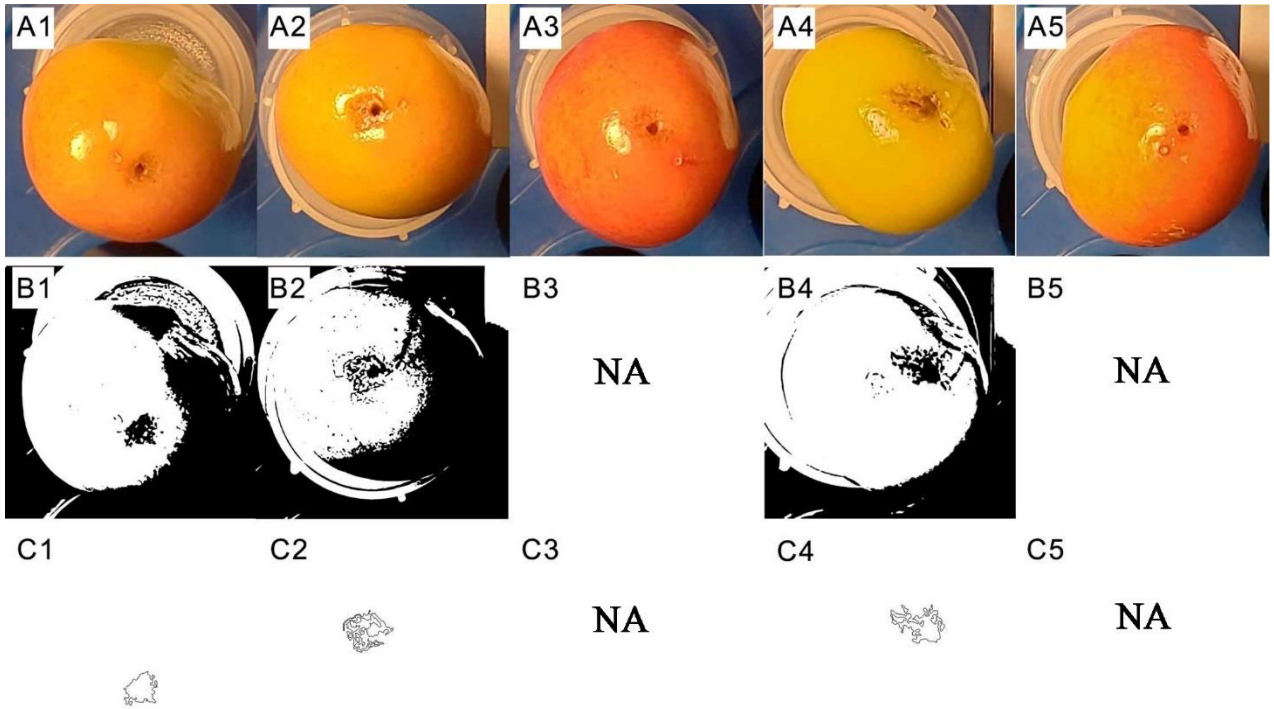


Figure A70. 2021 green cherry fruit ('Hedelfinger') lesion four days after inoculation. **A1-A5)** *Psm* inoculated in stab wound. **B1-B5)** Images after threshold adjustment in ImageJ. **C1-C5)** Image of measured area. A1, B1, C1: Replication 1; A2, B2, C2: Replication 2; A3, B3, C3: Replication 3; A4, B4, C4: Replication4; A5, B5, C5: Replication 5. Images with NA are not available.

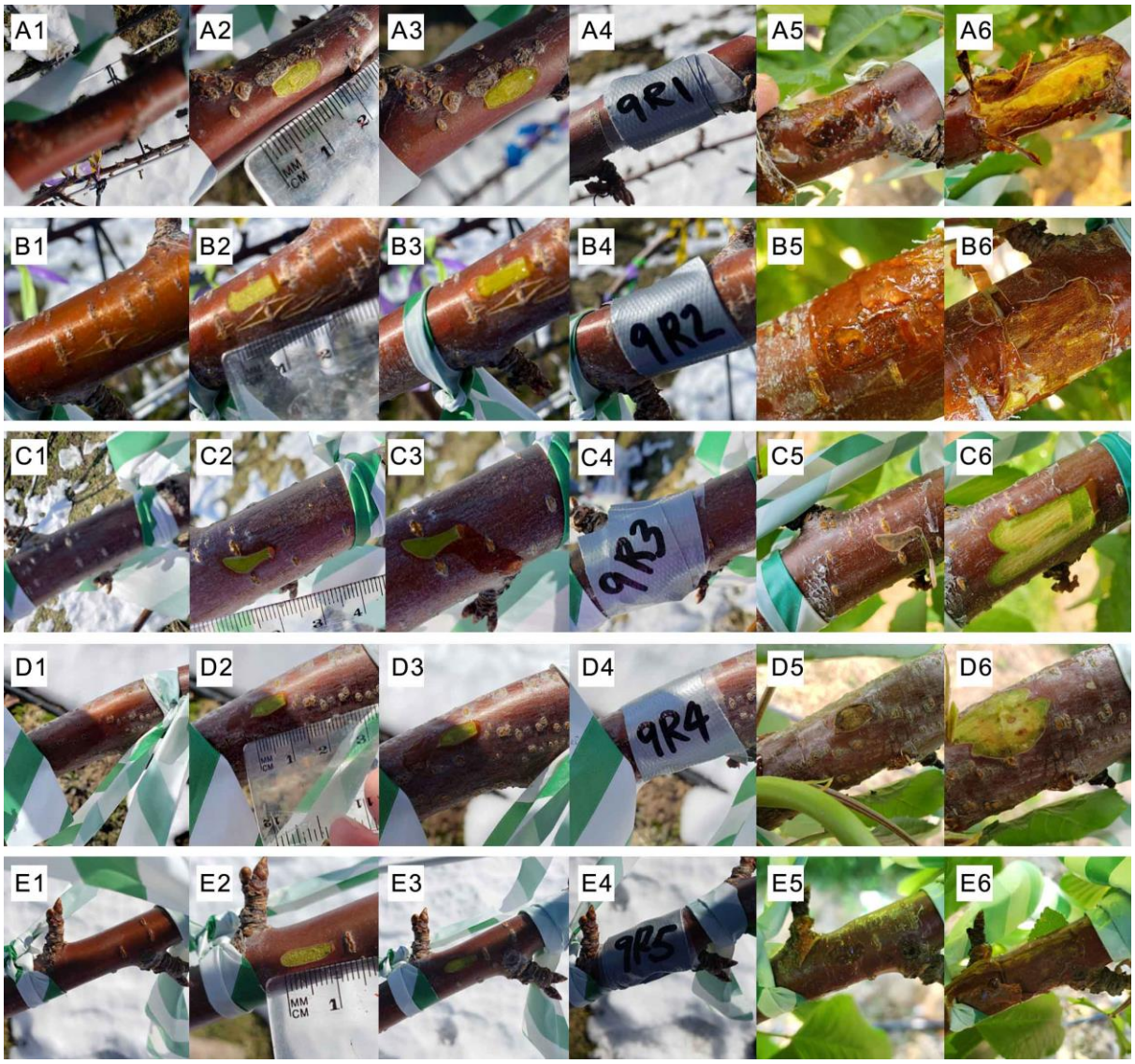


Figure A71. 2021 wound inoculation on 'Sweetheart' cherry wood with *Pss* 9. **A1-E1)** The inoculation site before wounding. **A2-E2)** The inoculation site after wounding by sterile razor blade **A3-E3)** The inoculation site after pipetting inoculum into the wound. **A4-E4)** The inoculation site after covering with Parafilm and tape. **A5-E5)** The inoculation site exterior assessment in the spring. **A6-E6)** The inoculation site interior assessment in the spring. A1-A6: Replication 1. B1-B6: Replication 2. C1-C6: Replication 3. D1-D6: Replication 4. E1-E6: Replication 5.

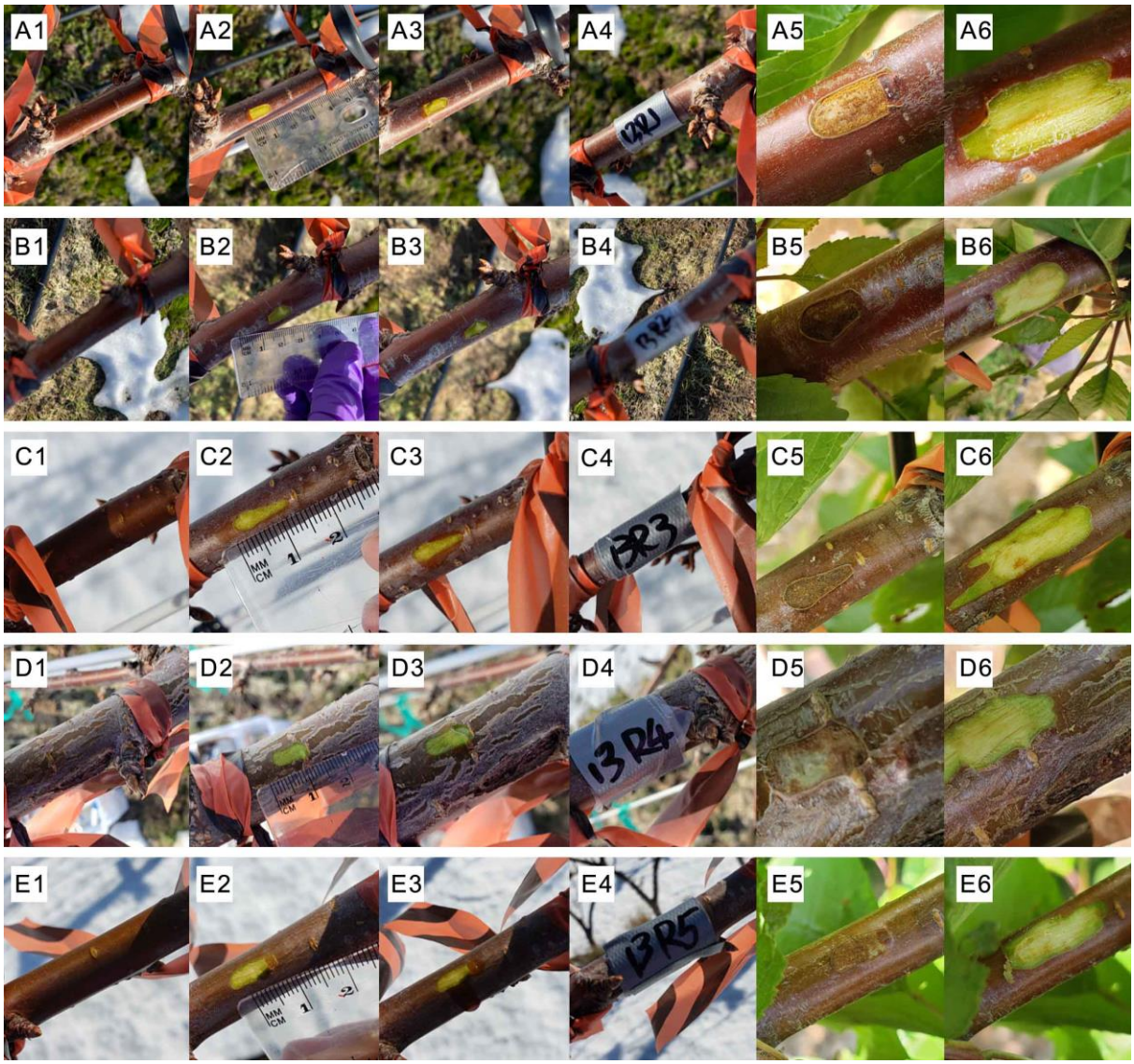


Figure A72. 2021 wound inoculation on 'Sweetheart' cherry wood with *Pss* 13. **A1-E1)** The inoculation site before wounding. **A2-E2)** The inoculation site after wounding by sterile razor blade **A3-E3)** The inoculation site after pipetting inoculum into the wound. **A4-E4)** The inoculation site after covering with Parafilm and tape. **A5-E5)** The inoculation site exterior assessment in the spring. **A6-E6)** The inoculation site interior assessment in the spring. A1-A6: Replication 1. B1-B6: Replication 2. C1-C6: Replication 3. D1-D6: Replication 4. E1-E6: Replication 5.

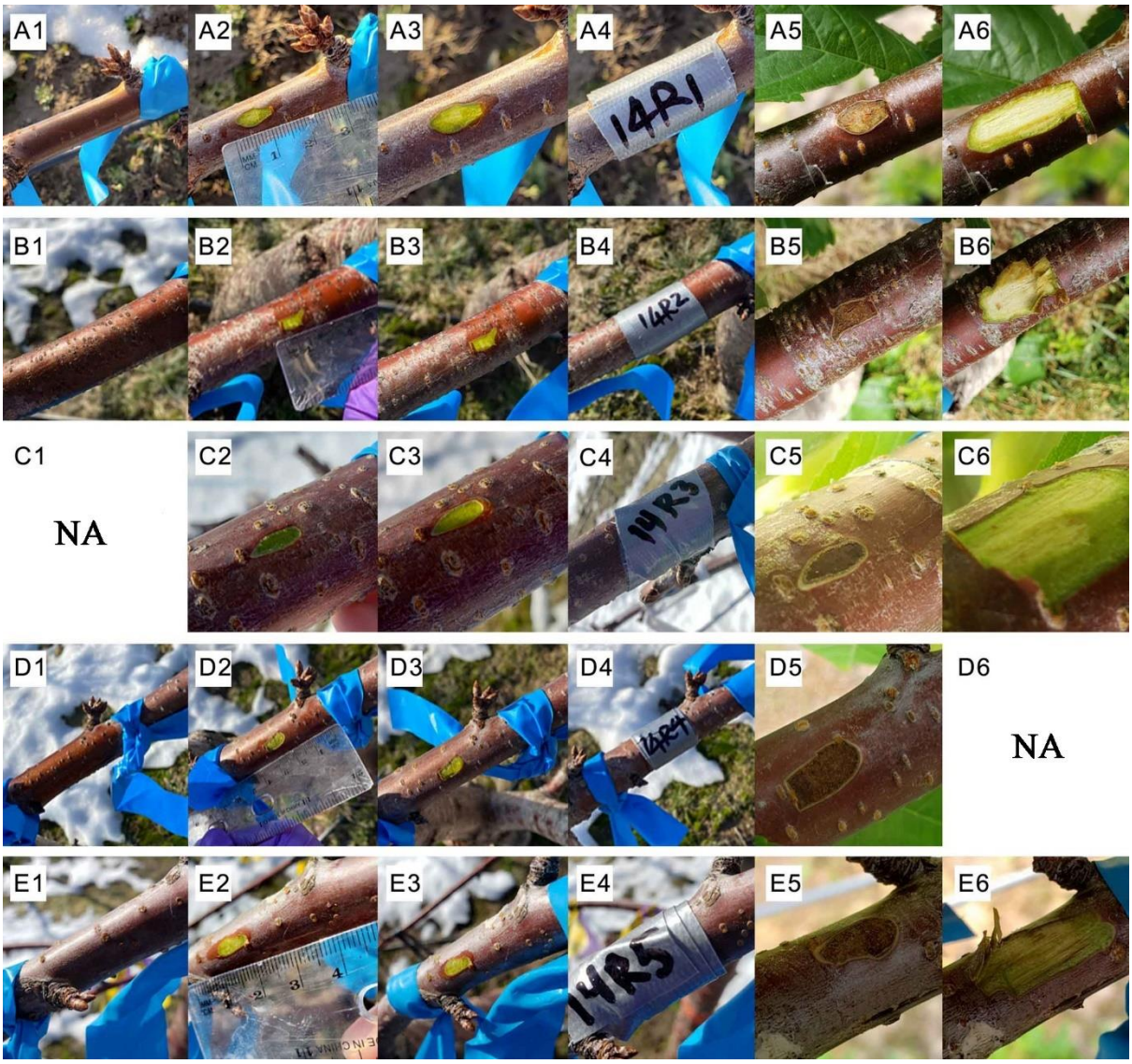


Figure A73. 2021 wound inoculation on 'Sweetheart' cherry wood with *Pss* 14. **A1-E1)** The inoculation site before wounding. **A2-E2)** The inoculation site after wounding by sterile razor blade **A3-E3)** The inoculation site after pipetting inoculum into the wound. **A4-E4)** The inoculation site after covering with Parafilm and tape. **A5-E5)** The inoculation site exterior assessment in the spring. **A6-E6)** The inoculation site interior assessment in the spring. A1-A6: Replication 1. B1-B6: Replication 2. C1-C6: Replication 3. D1-D6: Replication 4. E1-E6: Replication 5. Images with NA are not available.



Figure A74. 2021 wound inoculation on 'Sweetheart' cherry wood with *Pss* 15. **A1-E1)** The inoculation site before wounding. **A2-E2)** The inoculation site after wounding by sterile razor blade **A3-E3)** The inoculation site after pipetting inoculum into the wound. **A4-E4)** The inoculation site after covering with Parafilm and tape. **A5-E5)** The inoculation site exterior assessment in the spring. **A6-E6)** The inoculation site interior assessment in the spring. A1-A6: Replication 1. B1-B6: Replication 2. C1-C6: Replication 3. D1-D6: Replication 4. E1-E6: Replication 5.



Figure A75. 2021 wound inoculation on 'Sweetheart' cherry wood with *Pss* 16. **A1-E1)** The inoculation site before wounding. **A2-E2)** The inoculation site after wounding by sterile razor blade **A3-E3)** The inoculation site after pipetting inoculum into the wound. **A4-E4)** The inoculation site after covering with Parafilm and tape. **A5-E5)** The inoculation site exterior assessment in the spring. **A6-E6)** The inoculation site interior assessment in the spring. A1-A6: Replication 1. B1-B6: Replication 2. C1-C6: Replication 3. D1-D6: Replication 4. E1-E6: Replication 5.

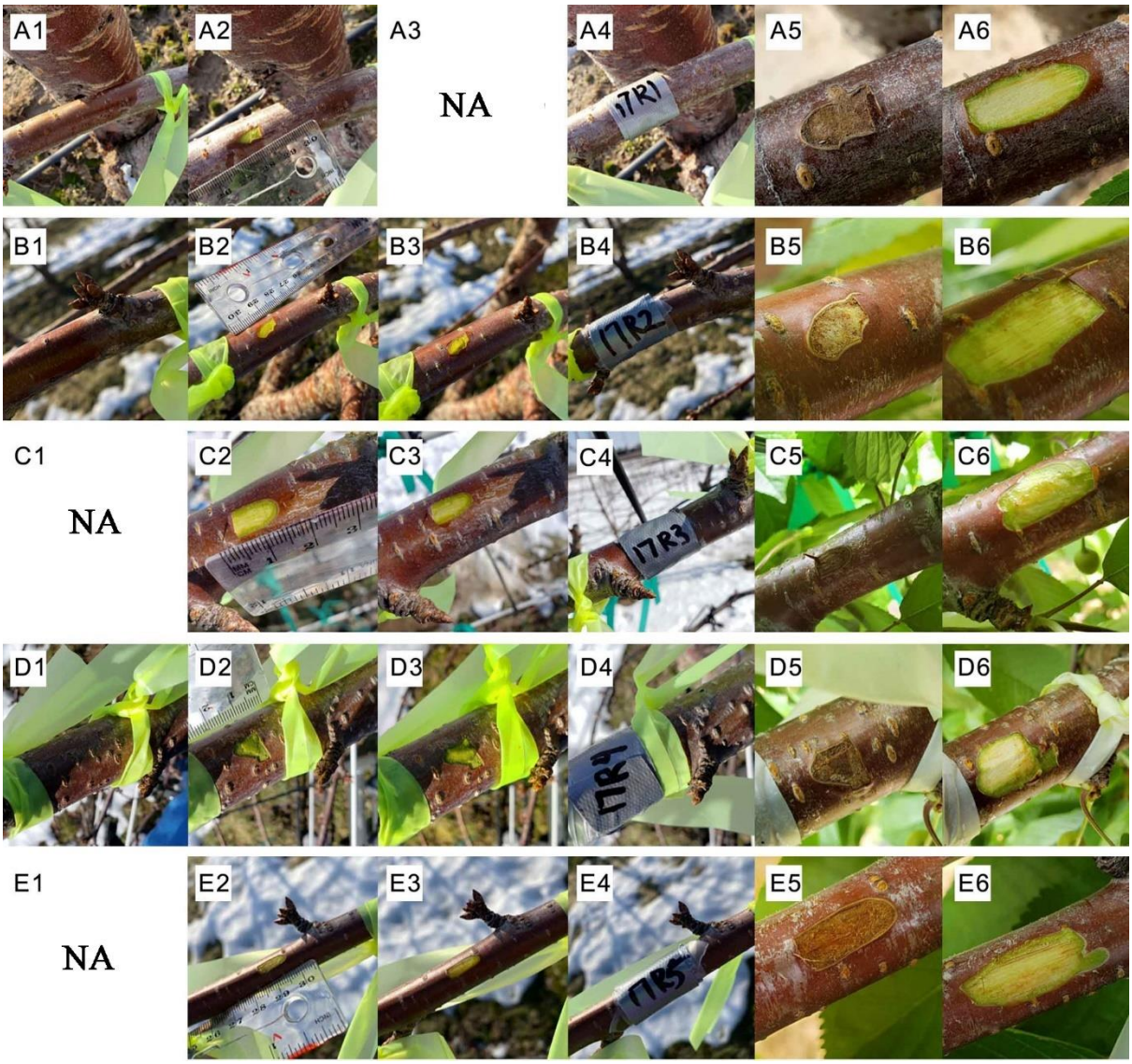


Figure A76. 2021 wound inoculation on 'Sweetheart' cherry wood with *Pss* 17. **A1-E1)** The inoculation site before wounding. **A2-E2)** The inoculation site after wounding by sterile razor blade **A3-E3)** The inoculation site after pipetting inoculum into the wound. **A4-E4)** The inoculation site after covering with Parafilm and tape. **A5-E5)** The inoculation site exterior assessment in the spring. **A6-E6)** The inoculation site interior assessment in the spring. A1-A6: Replication 1. B1-B6: Replication 2. C1-C6: Replication 3. D1-D6: Replication 4. E1-E6: Replication 5. Images with NA are not available.

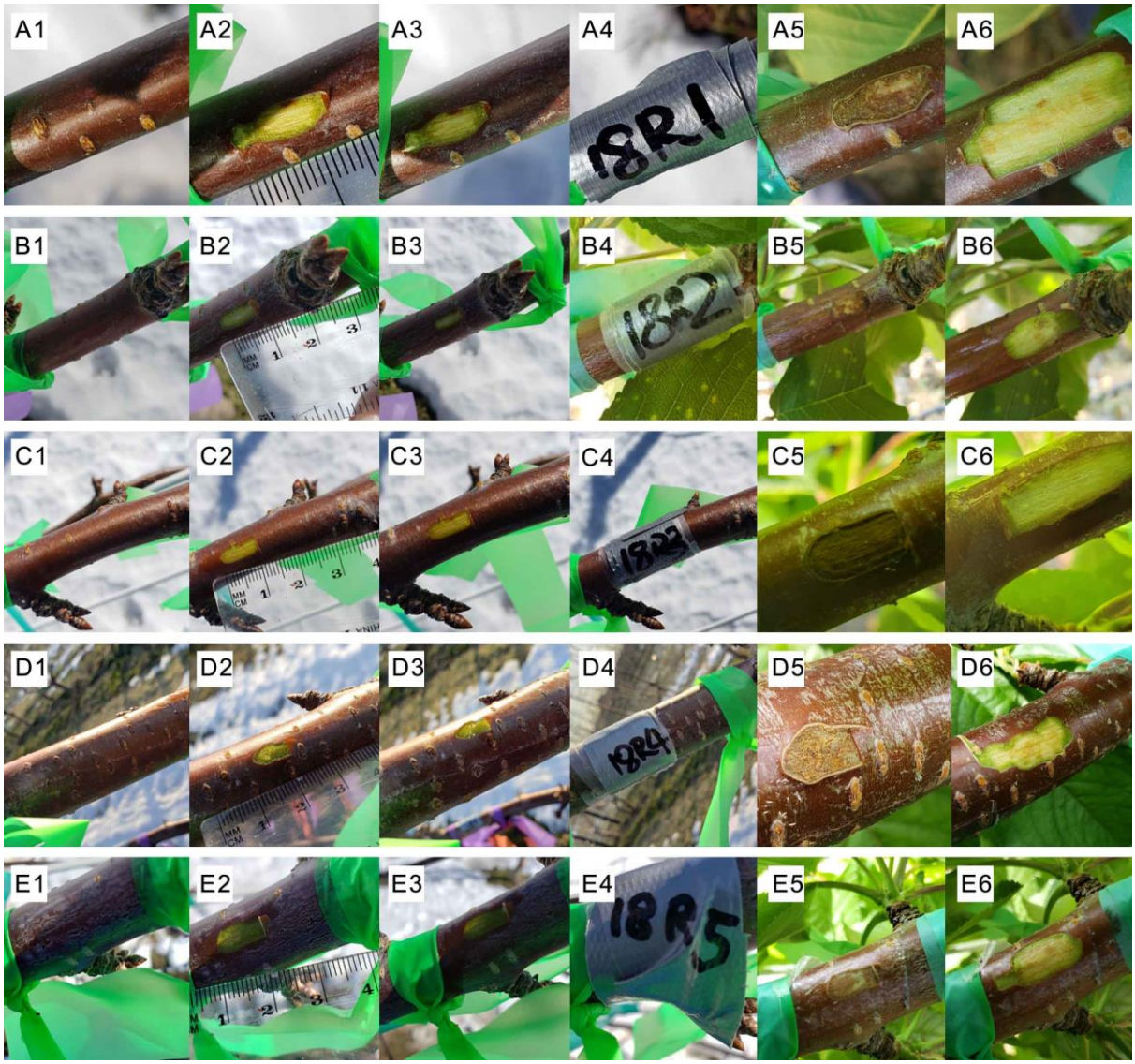


Figure A77. 2021 wound inoculation on 'Sweetheart' cherry wood with *Pss* 18. **A1-E1)** The inoculation site before wounding. **A2-E2)** The inoculation site after wounding by sterile razor blade **A3-E3)** The inoculation site after pipetting inoculum into the wound. **A4-E4)** The inoculation site after covering with Parafilm and tape. **A5-E5)** The inoculation site exterior assessment in the spring. **A6-E6)** The inoculation site interior assessment in the spring. A1-A6: Replication 1. B1-B6: Replication 2. C1-C6: Replication 3. D1-D6: Replication 4. E1-E6: Replication 5.

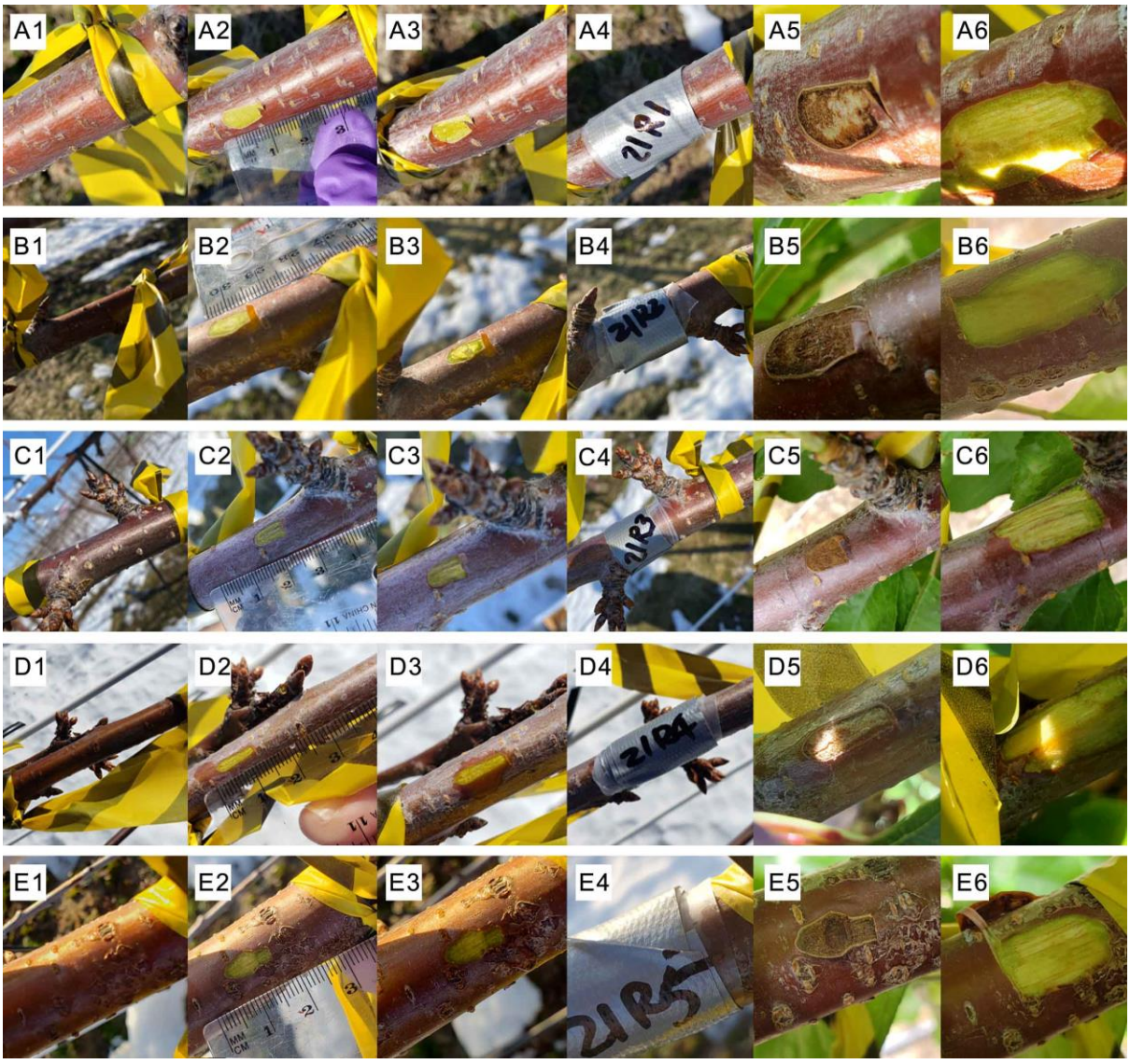


Figure A78. 2021 wound inoculation on 'Sweetheart' cherry wood with *Pss* 21. **A1-E1)** The inoculation site before wounding. **A2-E2)** The inoculation site after wounding by sterile razor blade **A3-E3)** The inoculation site after pipetting inoculum into the wound. **A4-E4)** The inoculation site after covering with Parafilm and tape. **A5-E5)** The inoculation site exterior assessment in the spring. **A6-E6)** The inoculation site interior assessment in the spring. A1-A6: Replication 1. B1-B6: Replication 2. C1-C6: Replication 3. D1-D6: Replication 4. E1-E6: Replication 5.



Figure A79. 2021 wound inoculation on 'Sweetheart' cherry wood with *Pss* 22. **A1-E1)** The inoculation site before wounding. **A2-E2)** The inoculation site after wounding by sterile razor blade **A3-E3)** The inoculation site after pipetting inoculum into the wound. **A4-E4)** The inoculation site after covering with Parafilm and tape. **A5-E5)** The inoculation site exterior assessment in the spring. **A6-E6)** The inoculation site interior assessment in the spring. A1-A6: Replication 1. B1-B6: Replication 2. C1-C6: Replication 3. D1-D6: Replication 4. E1-E6: Replication 5.

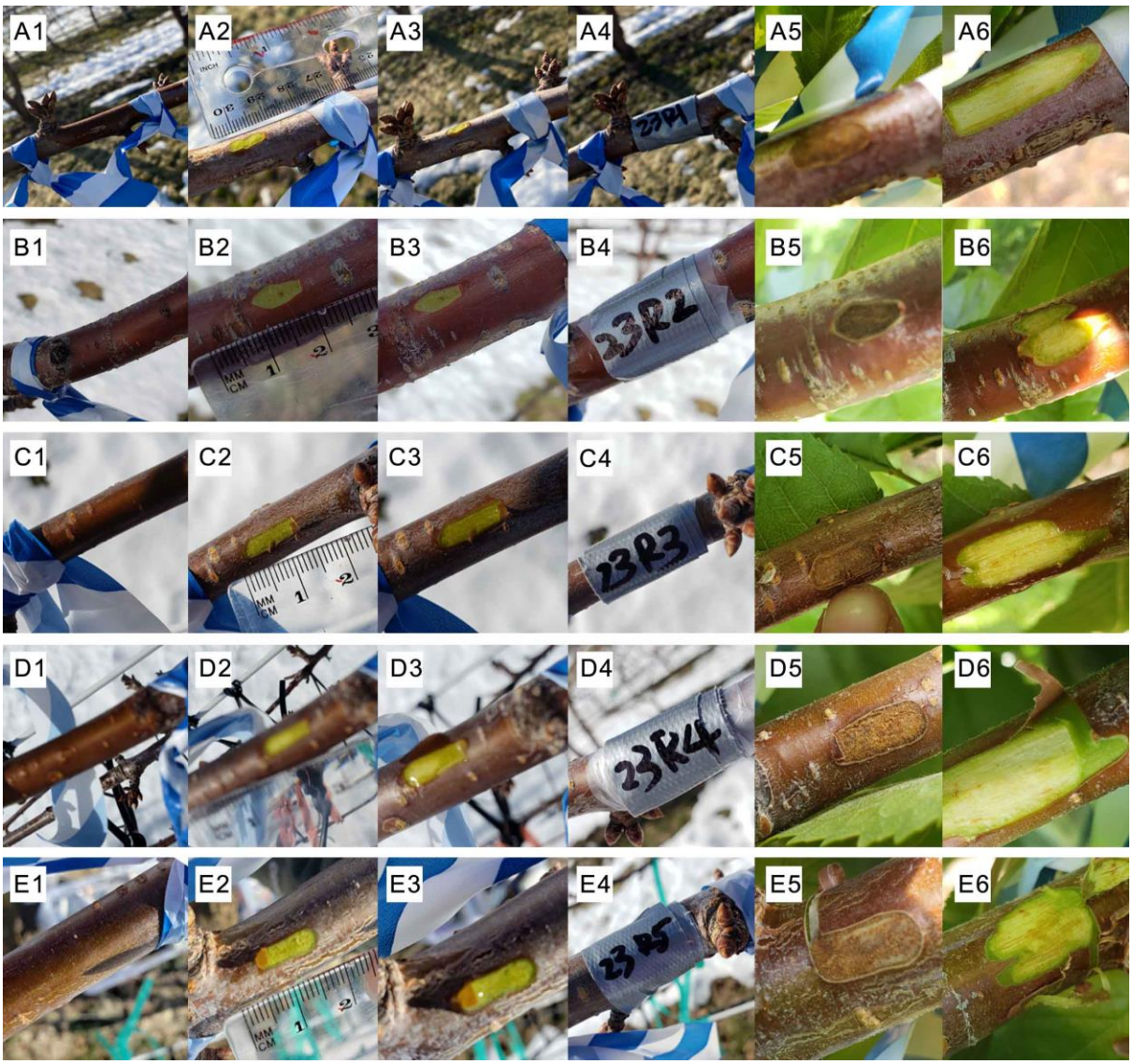


Figure A80. 2021 wound inoculation on 'Sweetheart' cherry wood with *Pss* 23. **A1-E1)** The inoculation site before wounding. **A2-E2)** The inoculation site after wounding by sterile razor blade **A3-E3)** The inoculation site after pipetting inoculum into the wound. **A4-E4)** The inoculation site after covering with Parafilm and tape. **A5-E5)** The inoculation site exterior assessment in the spring. **A6-E6)** The inoculation site interior assessment in the spring. A1-A6: Replication 1. B1-B6: Replication 2. C1-C6: Replication 3. D1-D6: Replication 4. E1-E6: Replication 5.

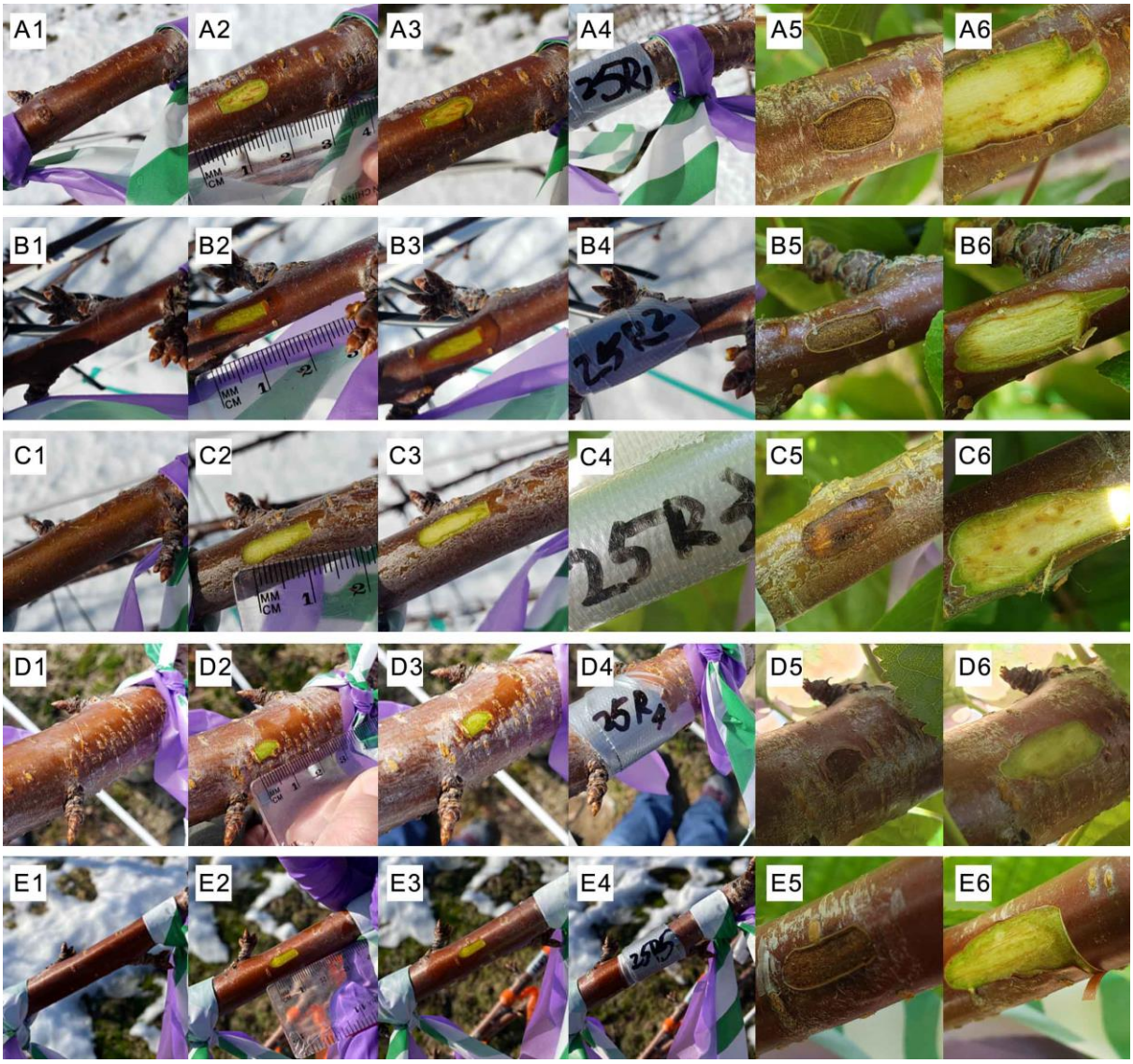


Figure A81. 2021 wound inoculation on 'Sweetheart' cherry wood with *Pss* 25. **A1-E1)** The inoculation site before wounding. **A2-E2)** The inoculation site after wounding by sterile razor blade **A3-E3)** The inoculation site after pipetting inoculum into the wound. **A4-E4)** The inoculation site after covering with Parafilm and tape. **A5-E5)** The inoculation site exterior assessment in the spring. **A6-E6)** The inoculation site interior assessment in the spring. A1-A6: Replication 1. B1-B6: Replication 2. C1-C6: Replication 3. D1-D6: Replication 4. E1-E6: Replication 5.

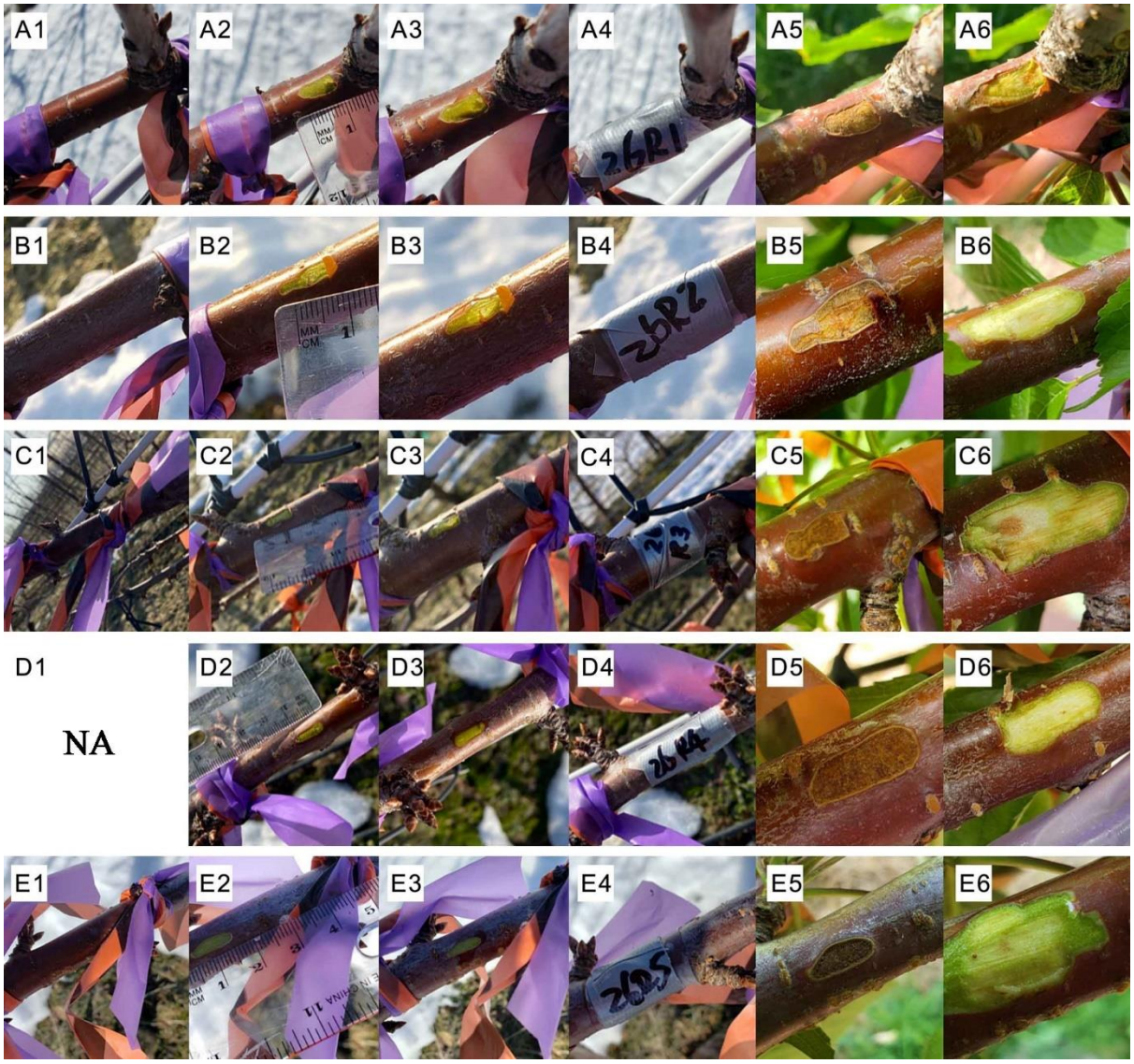


Figure A82. 2021 wound inoculation on 'Sweetheart' cherry wood with *Pss* 26. **A1-E1)** The inoculation site before wounding. **A2-E2)** The inoculation site after wounding by sterile razor blade **A3-E3)** The inoculation site after pipetting inoculum into the wound. **A4-E4)** The inoculation site after covering with Parafilm and tape. **A5-E5)** The inoculation site exterior assessment in the spring. **A6-E6)** The inoculation site interior assessment in the spring. A1-A6: Replication 1. B1-B6: Replication 2. C1-C6: Replication 3. D1-D6: Replication 4. E1-E6: Replication 5. Images with NA are not available.



Figure A83. 2021 wound inoculation on 'Sweetheart' cherry wood with *Pss* 27. **A1-E1)** The inoculation site before wounding. **A2-E2)** The inoculation site after wounding by sterile razor blade **A3-E3)** The inoculation site after pipetting inoculum into the wound. **A4-E4)** The inoculation site after covering with Parafilm and tape. **A5-E5)** The inoculation site exterior assessment in the spring. **A6-E6)** The inoculation site interior assessment in the spring. A1-A6: Replication 1. B1-B6: Replication 2. C1-C6: Replication 3. D1-D6: Replication 4. E1-E6: Replication 5.

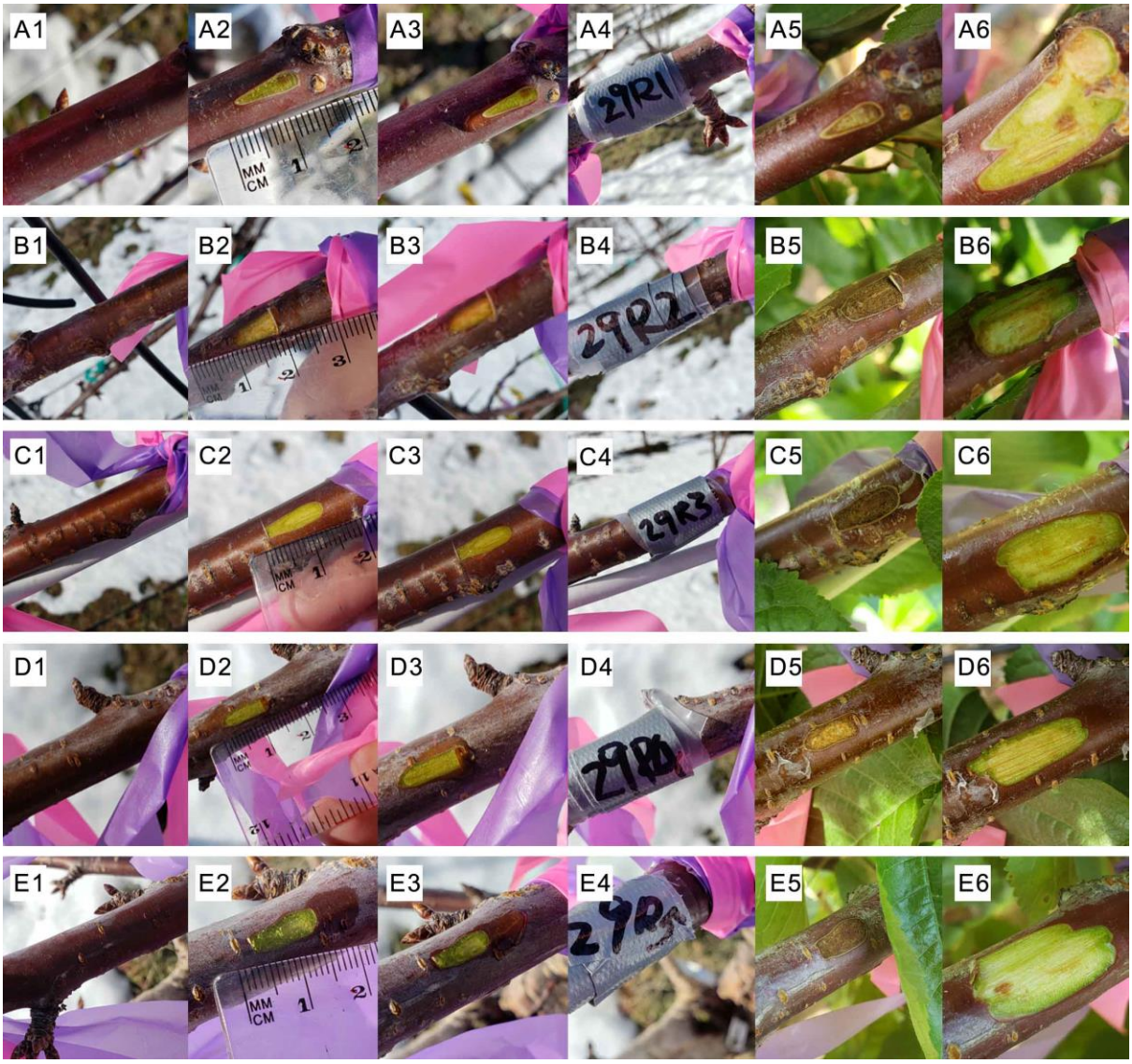


Figure A84. 2021 wound inoculation on 'Sweetheart' cherry wood with *Pss* 29. **A1-E1)** The inoculation site before wounding. **A2-E2)** The inoculation site after wounding by sterile razor blade **A3-E3)** The inoculation site after pipetting inoculum into the wound. **A4-E4)** The inoculation site after covering with Parafilm and tape. **A5-E5)** The inoculation site exterior assessment in the spring. **A6-E6)** The inoculation site interior assessment in the spring. A1-A6: Replication 1. B1-B6: Replication 2. C1-C6: Replication 3. D1-D6: Replication 4. E1-E6: Replication 5.

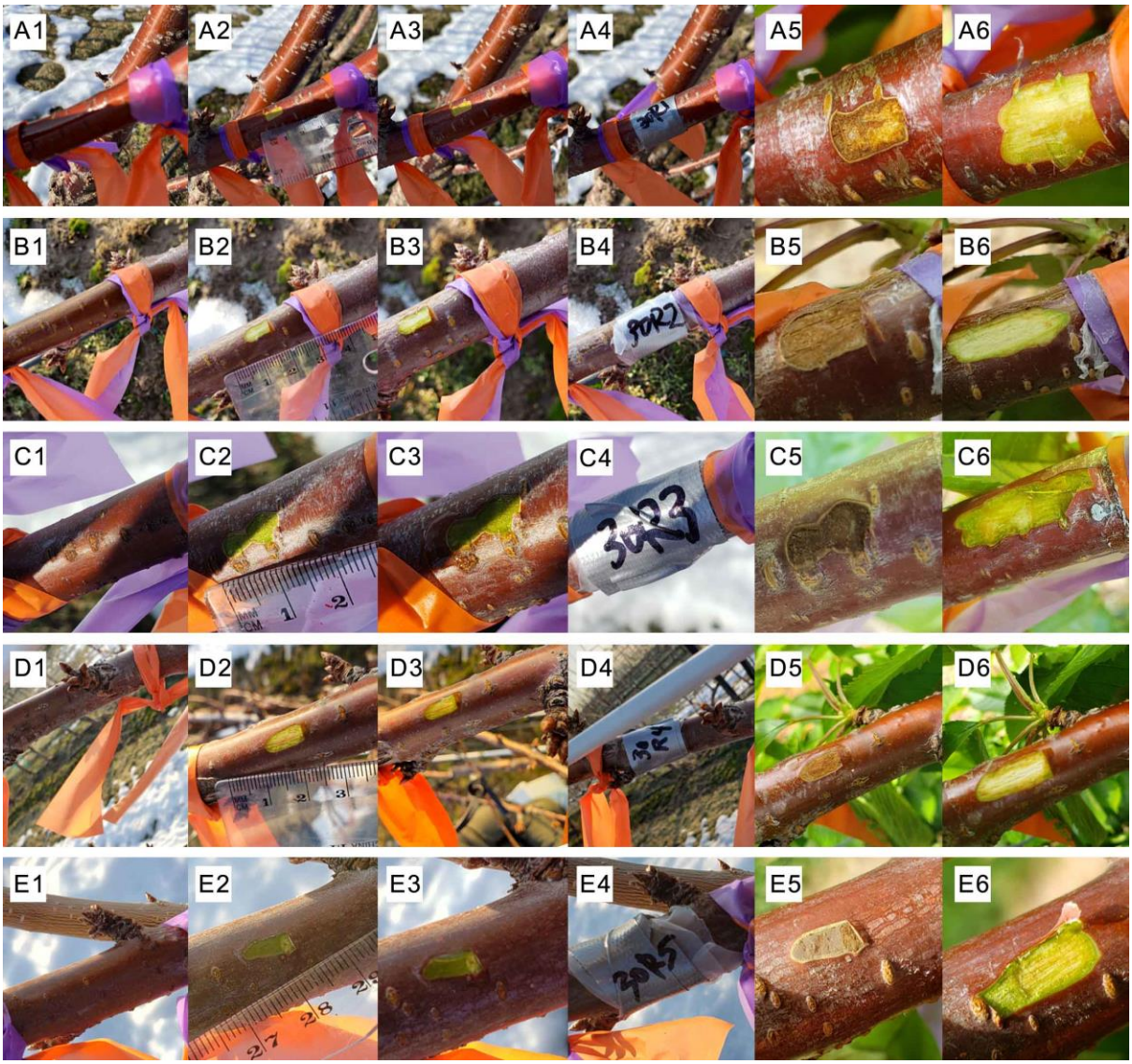


Figure A85. 2021 wound inoculation on 'Sweetheart' cherry wood with *Pss* 30. **A1-E1)** The inoculation site before wounding. **A2-E2)** The inoculation site after wounding by sterile razor blade **A3-E3)** The inoculation site after pipetting inoculum into the wound. **A4-E4)** The inoculation site after covering with Parafilm and tape. **A5-E5)** The inoculation site exterior assessment in the spring. **A6-E6)** The inoculation site interior assessment in the spring. A1-A6: Replication 1. B1-B6: Replication 2. C1-C6: Replication 3. D1-D6: Replication 4. E1-E6: Replication 5.

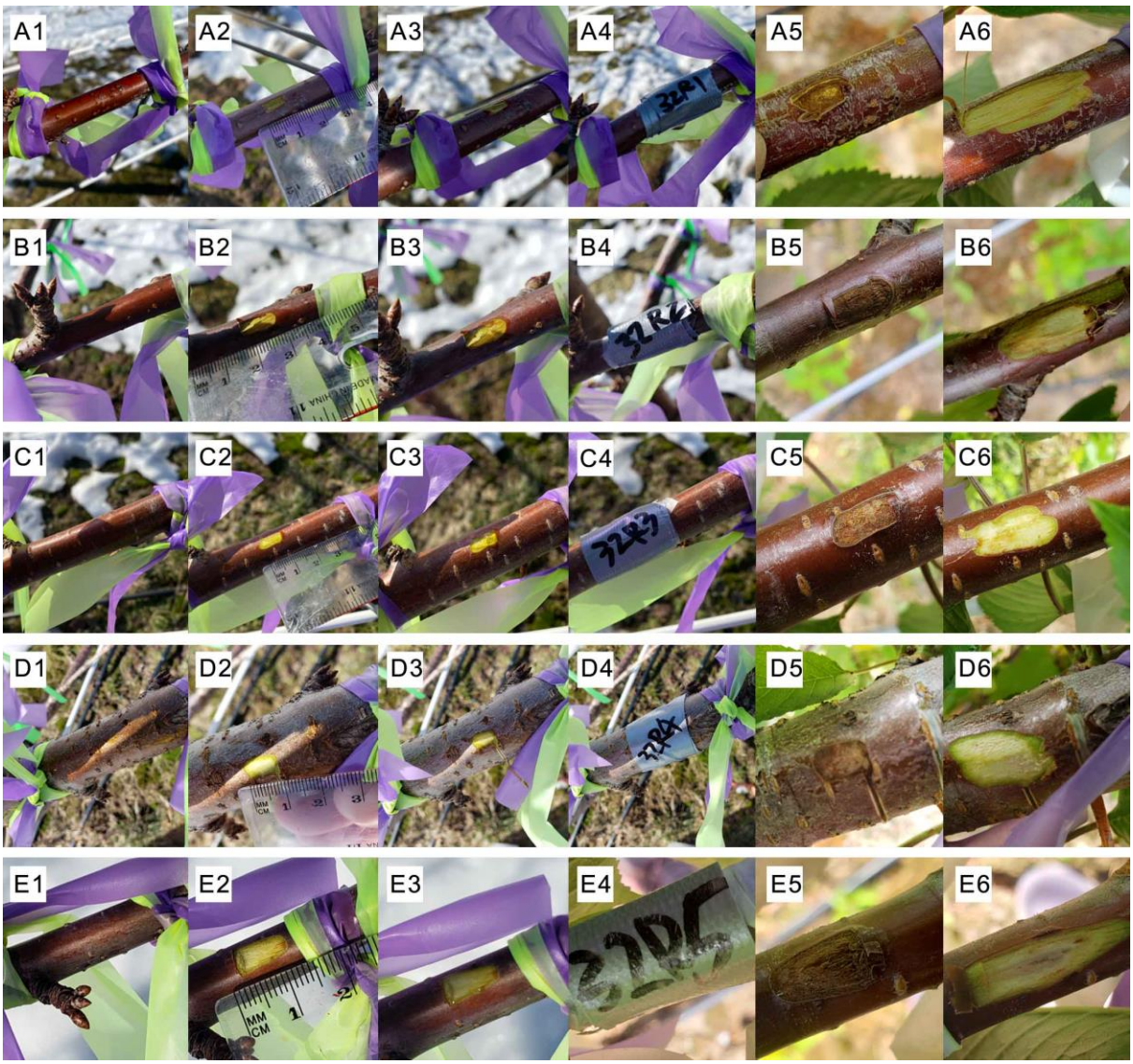


Figure A86. 2021 wound inoculation on 'Sweetheart' cherry wood with *Pss* 32. **A1-E1)** The inoculation site before wounding. **A2-E2)** The inoculation site after wounding by sterile razor blade **A3-E3)** The inoculation site after pipetting inoculum into the wound. **A4-E4)** The inoculation site after covering with Parafilm and tape. **A5-E5)** The inoculation site exterior assessment in the spring. **A6-E6)** The inoculation site interior assessment in the spring. A1-A6: Replication 1. B1-B6: Replication 2. C1-C6: Replication 3. D1-D6: Replication 4. E1-E6: Replication 5.

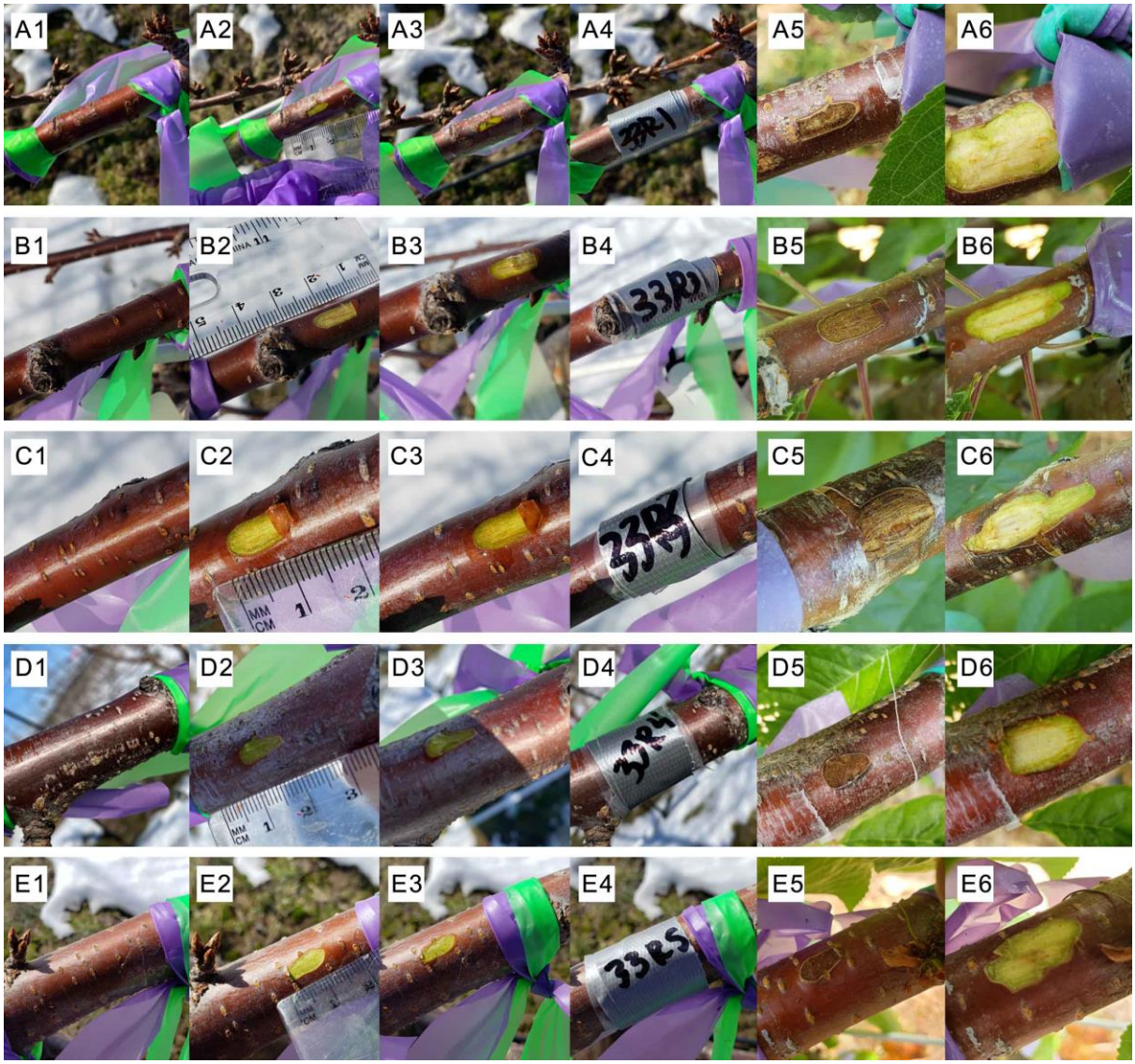


Figure A87. 2021 wound inoculation on 'Sweetheart' cherry wood with *Pss* 33. **A1-E1)** The inoculation site before wounding. **A2-E2)** The inoculation site after wounding by sterile razor blade **A3-E3)** The inoculation site after pipetting inoculum into the wound. **A4-E4)** The inoculation site after covering with Parafilm and tape. **A5-E5)** The inoculation site exterior assessment in the spring. **A6-E6)** The inoculation site interior assessment in the spring. A1-A6: Replication 1. B1-B6: Replication 2. C1-C6: Replication 3. D1-D6: Replication 4. E1-E6: Replication 5.

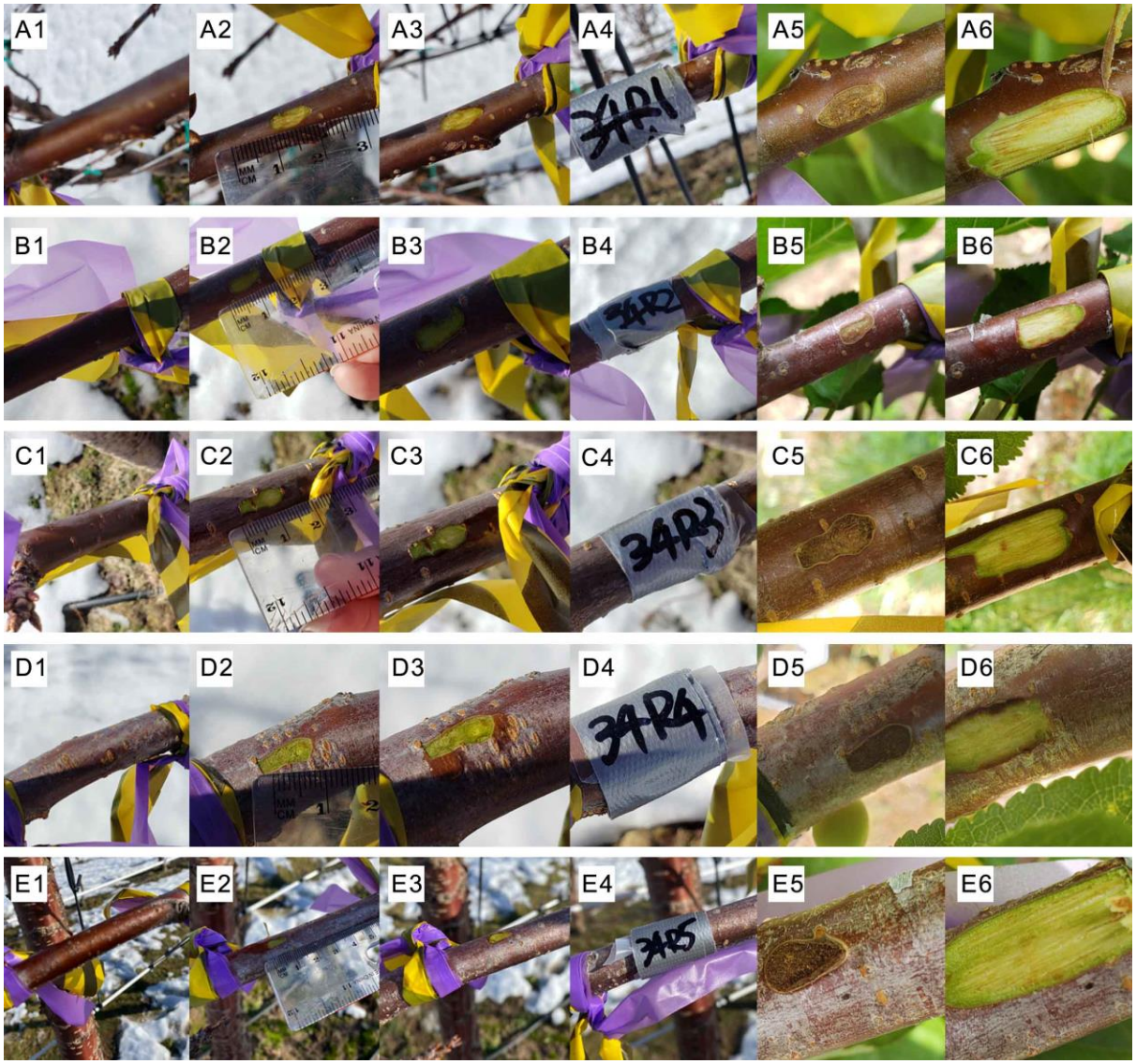


Figure A88. 2021 wound inoculation on 'Sweetheart' cherry wood with *Pss* 34. **A1-E1)** The inoculation site before wounding. **A2-E2)** The inoculation site after wounding by sterile razor blade **A3-E3)** The inoculation site after pipetting inoculum into the wound. **A4-E4)** The inoculation site after covering with Parafilm and tape. **A5-E5)** The inoculation site exterior assessment in the spring. **A6-E6)** The inoculation site interior assessment in the spring. A1-A6: Replication 1. B1-B6: Replication 2. C1-C6: Replication 3. D1-D6: Replication 4. E1-E6: Replication 5.



Figure A89. 2021 wound inoculation on 'Sweetheart' cherry wood with *Pss* 37. **A1-E1)** The inoculation site before wounding. **A2-E2)** The inoculation site after wounding by sterile razor blade **A3-E3)** The inoculation site after pipetting inoculum into the wound. **A4-E4)** The inoculation site after covering with Parafilm and tape. **A5-E5)** The inoculation site exterior assessment in the spring. **A6-E6)** The inoculation site interior assessment in the spring. A1-A6: Replication 1. B1-B6: Replication 2. C1-C6: Replication 3. D1-D6: Replication 4. E1-E6: Replication 5.

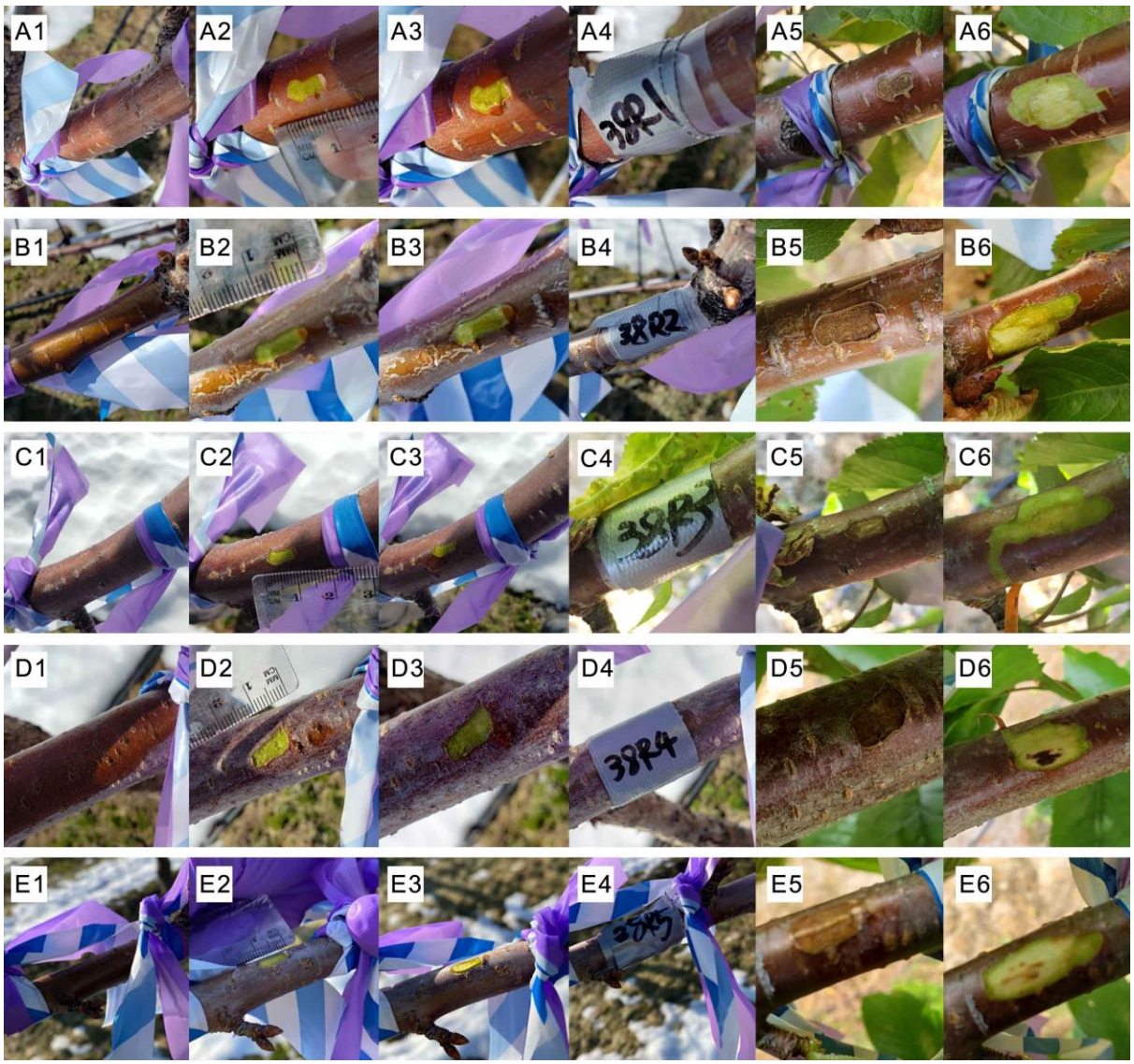


Figure A90. 2021 wound inoculation on 'Sweetheart' cherry wood with *Pss* 38. **A1-E1)** The inoculation site before wounding. **A2-E2)** The inoculation site after wounding by sterile razor blade **A3-E3)** The inoculation site after pipetting inoculum into the wound. **A4-E4)** The inoculation site after covering with Parafilm and tape. **A5-E5)** The inoculation site exterior assessment in the spring. **A6-E6)** The inoculation site interior assessment in the spring. A1-A6: Replication 1. B1-B6: Replication 2. C1-C6: Replication 3. D1-D6: Replication 4. E1-E6: Replication 5.



Figure A91. 2021 wound inoculation on 'Sweetheart' cherry wood with PBS. **A1-F1)** The inoculation site before wounding. **A2-F2)** The inoculation site after wounding by sterile razor blade **A3-F3)** The inoculation site after pipetting inoculum into the wound. **A4-F4)** The inoculation site after covering with Parafilm and tape. **A5-F5)** The inoculation site exterior assessment in the spring. **A6-F6)** The inoculation site interior assessment in the spring.

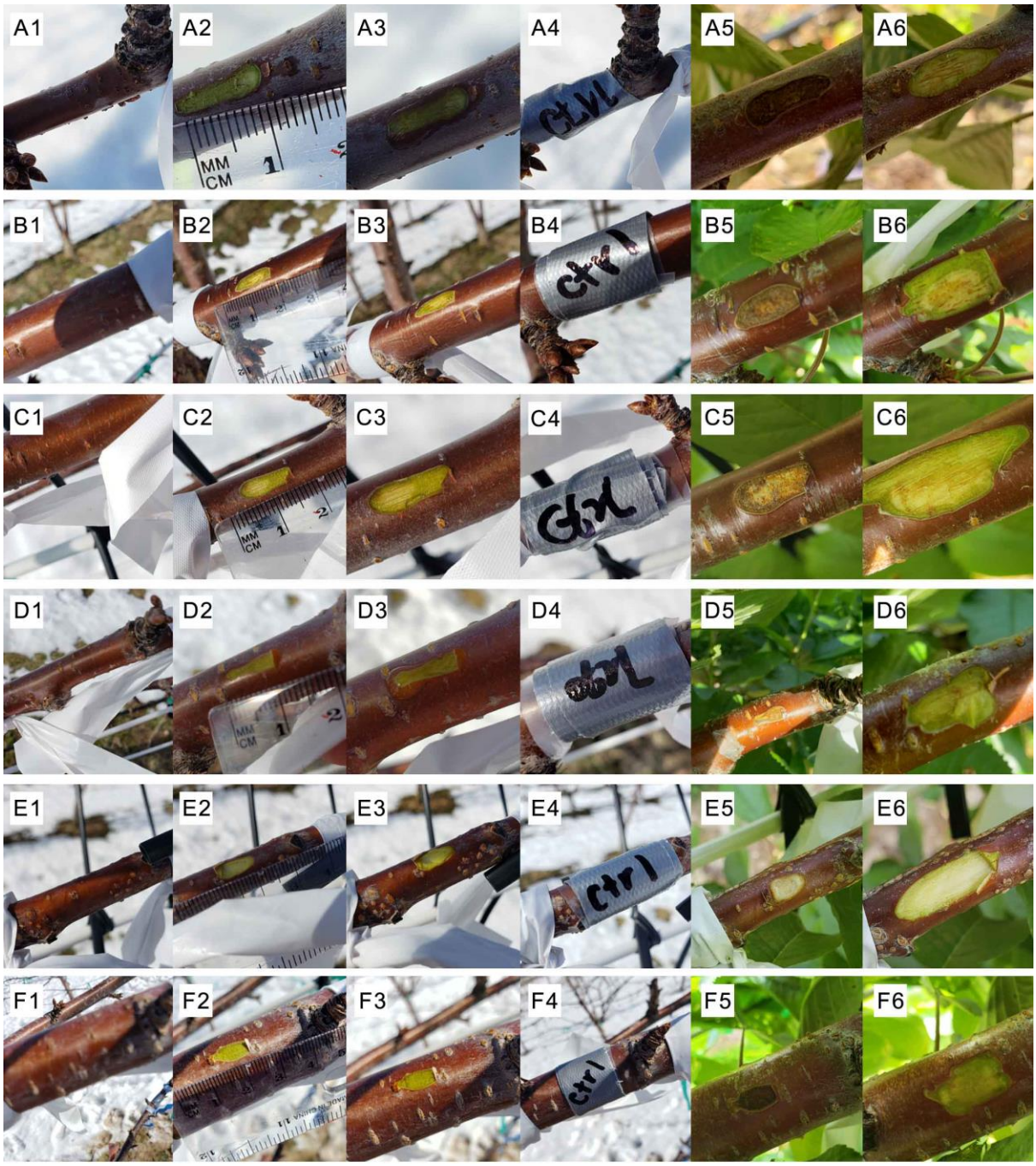


Figure A92. 2021 wound inoculation on 'Sweetheart' cherry wood with PBS. **A1-F1)** The inoculation site before wounding. **A2-F2)** The inoculation site after wounding by sterile razor blade **A3-F3)** The inoculation site after pipetting inoculum into the wound. **A4-F4)** The inoculation site after covering with Parafilm and tape. **A5-F5)** The inoculation site exterior assessment in the spring. **A6-F6)** The inoculation site interior assessment in the spring.

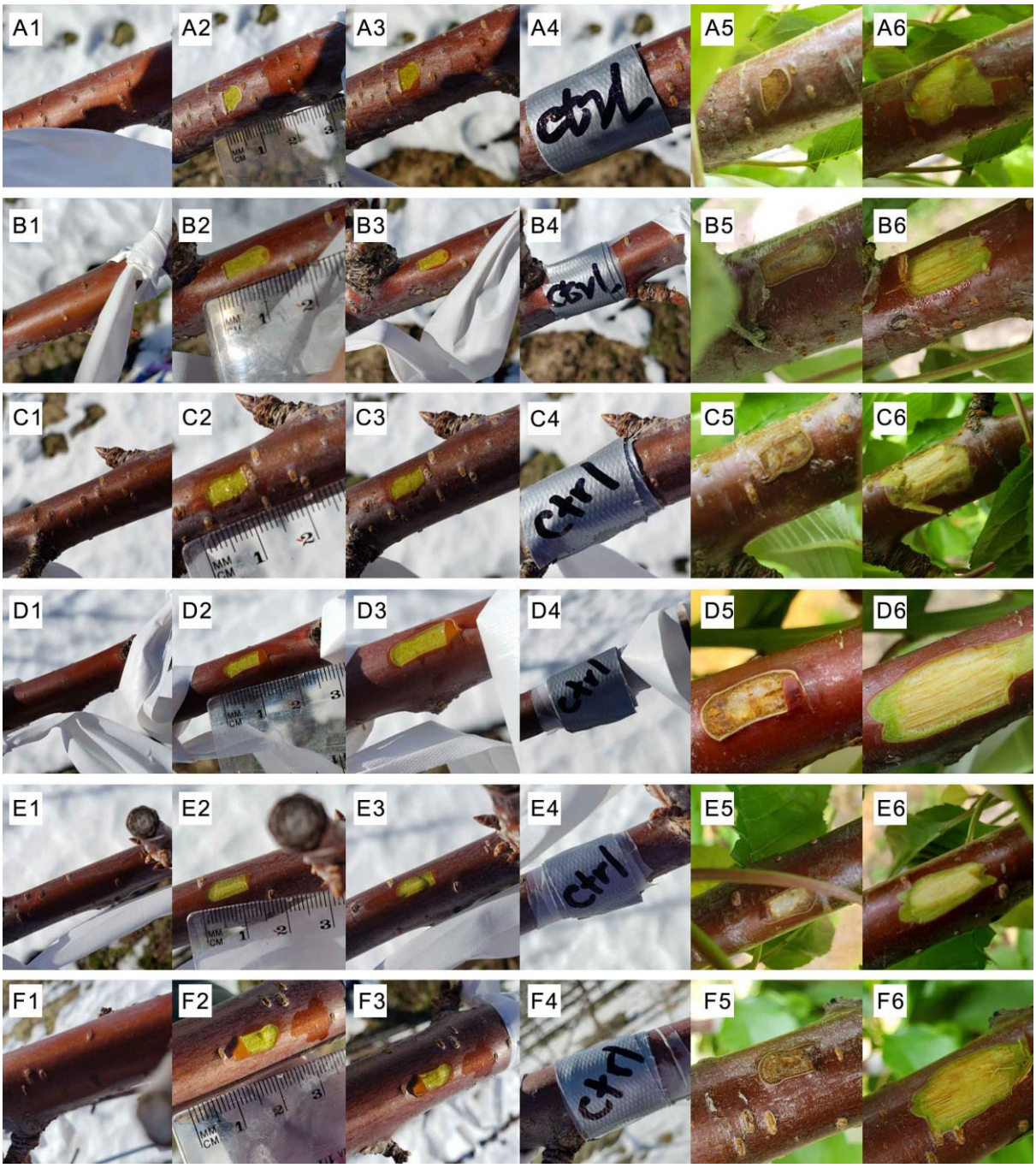


Figure A93. 2021 wound inoculation on 'Sweetheart' cherry wood with PBS. **A1-F1)** The inoculation site before wounding. **A2-F2)** The inoculation site after wounding by sterile razor blade **A3-F3)** The inoculation site after pipetting inoculum into the wound. **A4-F4)** The inoculation site after covering with Parafilm and tape. **A5-F5)** The inoculation site exterior assessment in the spring. **A6-F6)** The inoculation site interior assessment in the spring.



Figure A94. 2021 wound inoculation on 'Sweetheart' cherry wood with PBS. **A1-F1)** The inoculation site before wounding. **A2-F2)** The inoculation site after wounding by sterile razor blade **A3-F3)** The inoculation site after pipetting inoculum into the wound. **A4-F4)** The inoculation site after covering with Parafilm and tape. **A5-F5)** The inoculation site exterior assessment in the spring. **A6-F6)** The inoculation site interior assessment in the spring.

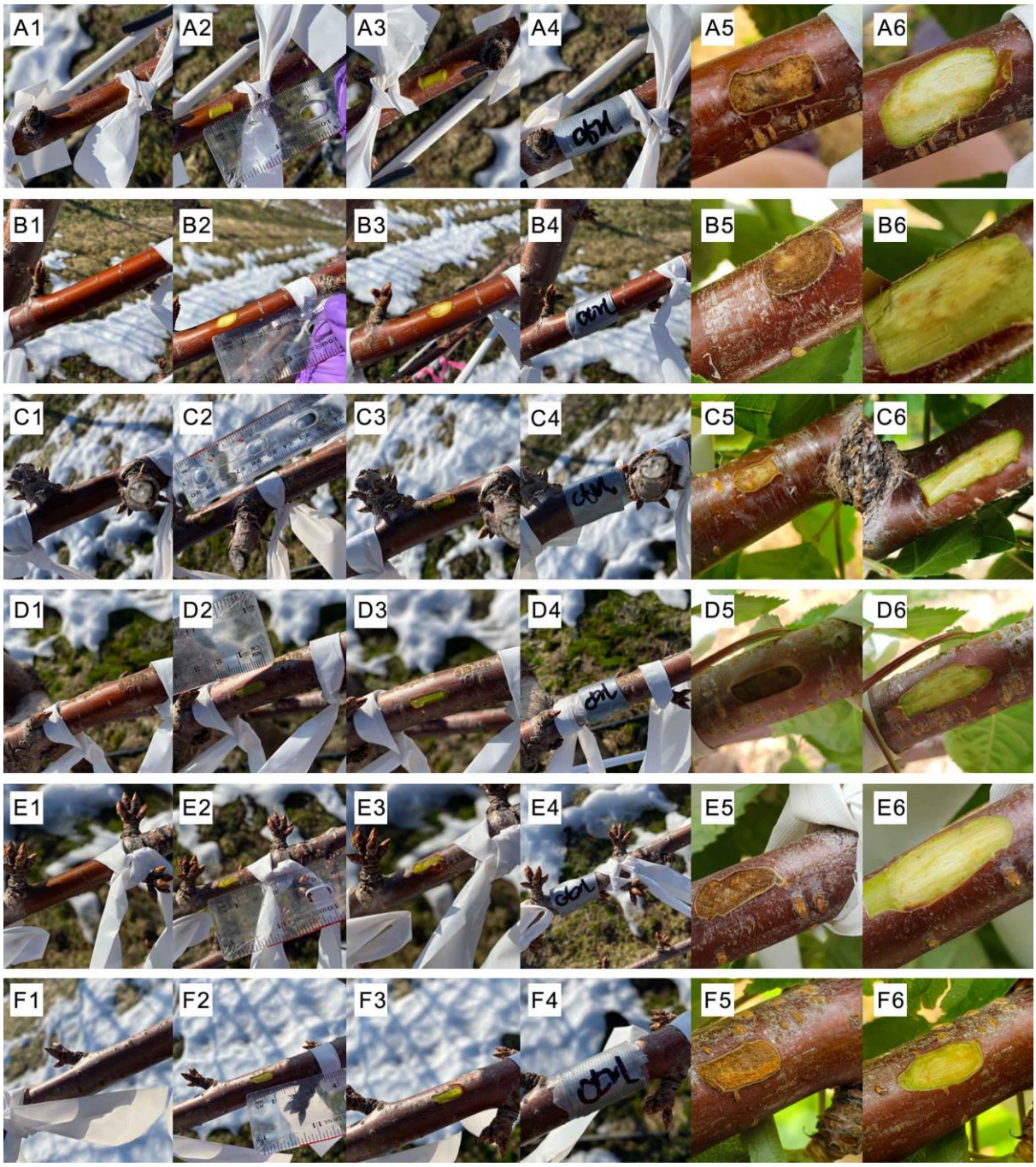


Figure A95. 2021 wound inoculation on 'Sweetheart' cherry wood with PBS. **A1-F1)** The inoculation site before wounding. **A2-F2)** The inoculation site after wounding by sterile razor blade **A3-F3)** The inoculation site after pipetting inoculum into the wound. **A4-F4)** The inoculation site after covering with Parafilm and tape. **A5-F5)** The inoculation site exterior assessment in the spring. **A6-F6)** The inoculation site interior assessment in the spring.



Figure A96. 2021 wound inoculation on 'Sweetheart' cherry wood with PBS. **A1-F1)** The inoculation site before wounding. **A2-F2)** The inoculation site after wounding by sterile razor blade **A3-F3)** The inoculation site after pipetting inoculum into the wound. **A4-F4)** The inoculation site after covering with Parafilm and tape. **A5-F5)** The inoculation site exterior assessment in the spring. **A6-F6)** The inoculation site interior assessment in the spring.

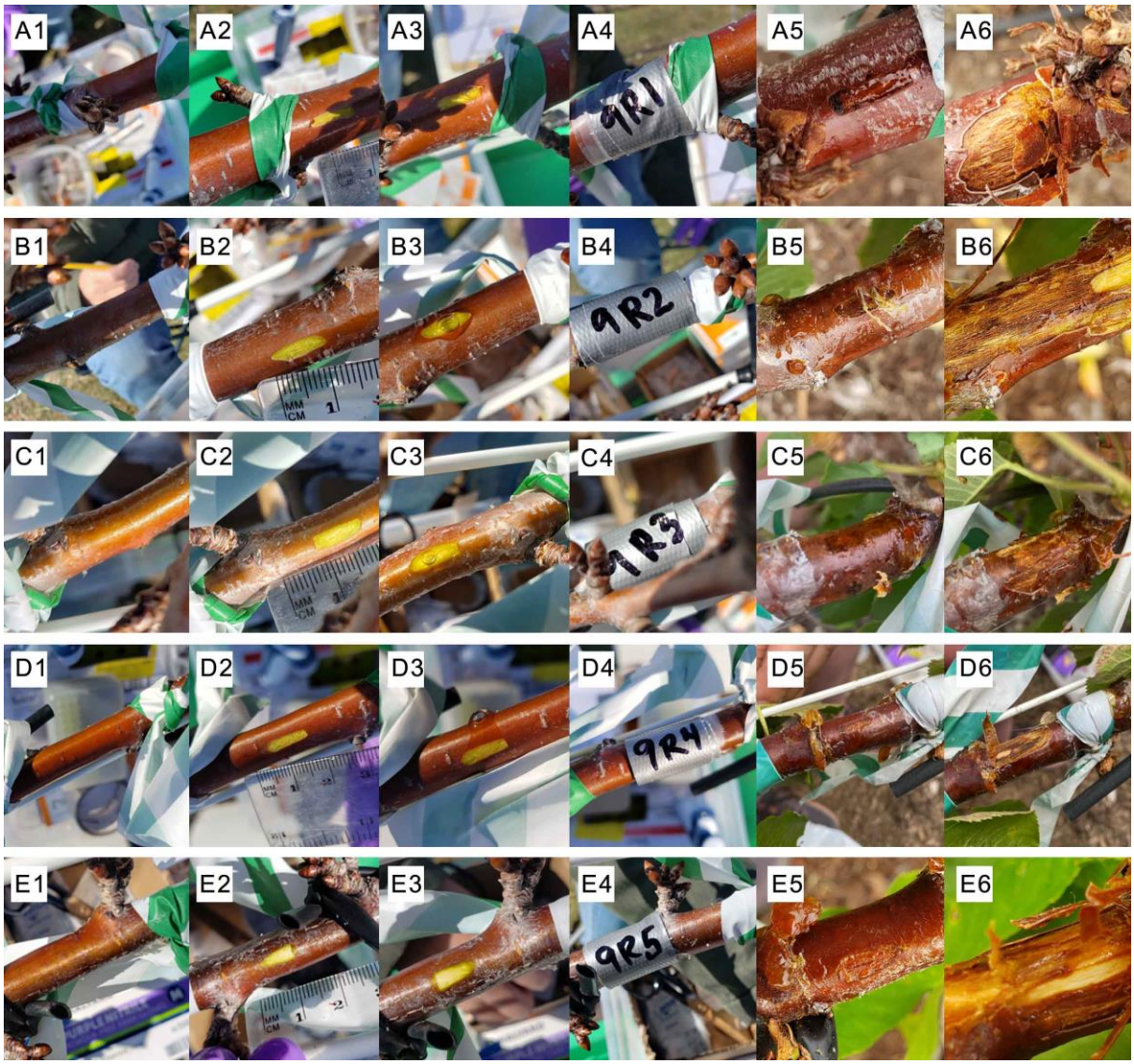


Figure A97. 2021 wound inoculation on 'Coral' cherry wood with *Pss* 9. **A1-E1)** The inoculation site before wounding. **A2-E2)** The inoculation site after wounding by sterile razor blade **A3-E3)** The inoculation site after pipetting inoculum into the wound. **A4-E4)** The inoculation site after covering with Parafilm and tape. **A5-E5)** The inoculation site exterior assessment in the spring. **A6-E6)** The inoculation site interior assessment in the spring. A1-A6: Replication 1. B1-B6: Replication 2. C1-C6: Replication 3. D1-D6: Replication 4. E1-E6: Replication 5.

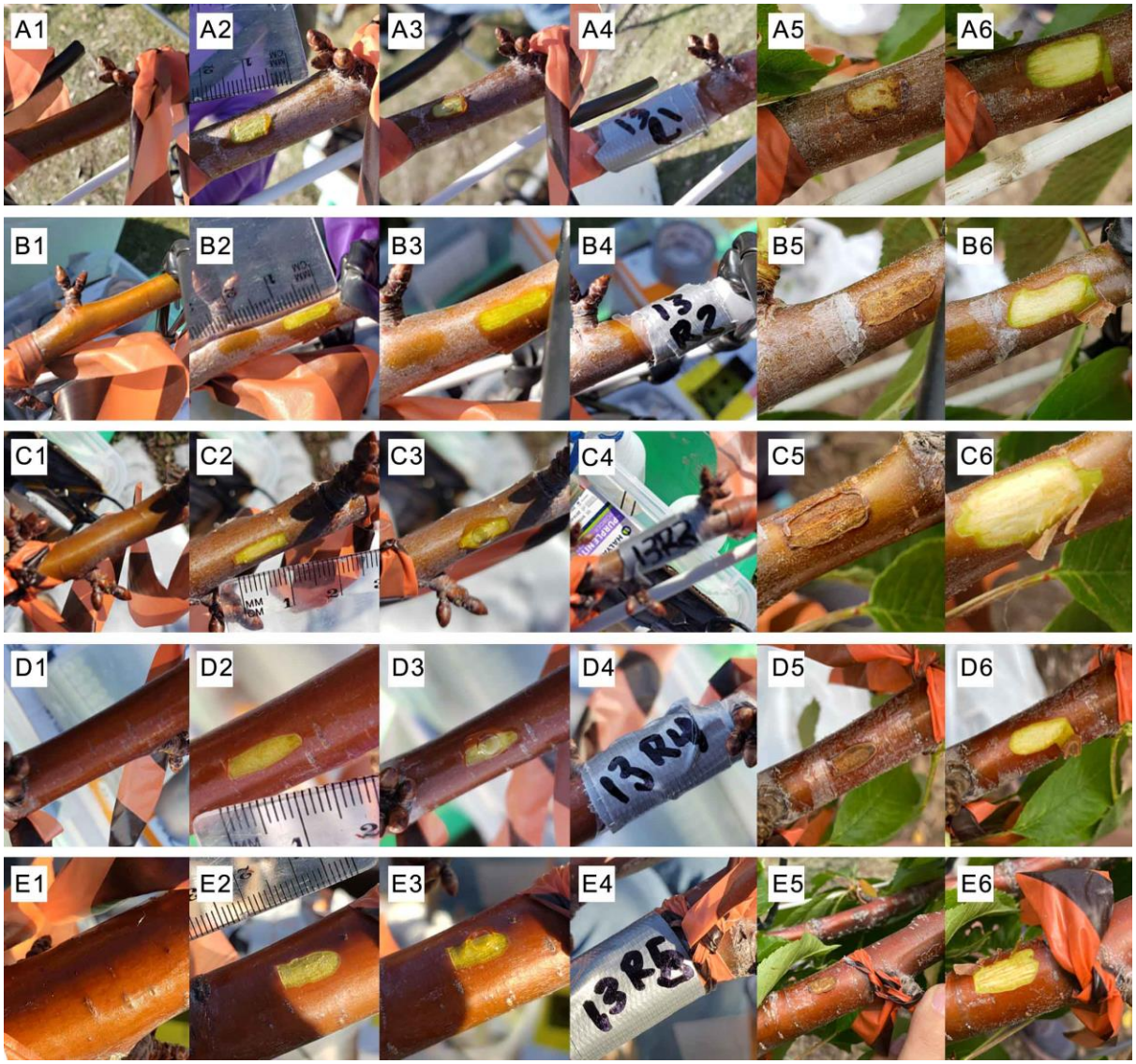


Figure A98. 2021 wound inoculation on 'Coral' cherry wood with *Pss* 13. **A1-E1)** The inoculation site before wounding. **A2-E2)** The inoculation site after wounding by sterile razor blade **A3-E3)** The inoculation site after pipetting inoculum into the wound. **A4-E4)** The inoculation site after covering with Parafilm and tape. **A5-E5)** The inoculation site exterior assessment in the spring. **A6-E6)** The inoculation site interior assessment in the spring. A1-A6: Replication 1. B1-B6: Replication 2. C1-C6: Replication 3. D1-D6: Replication 4. E1-E6: Replication 5.

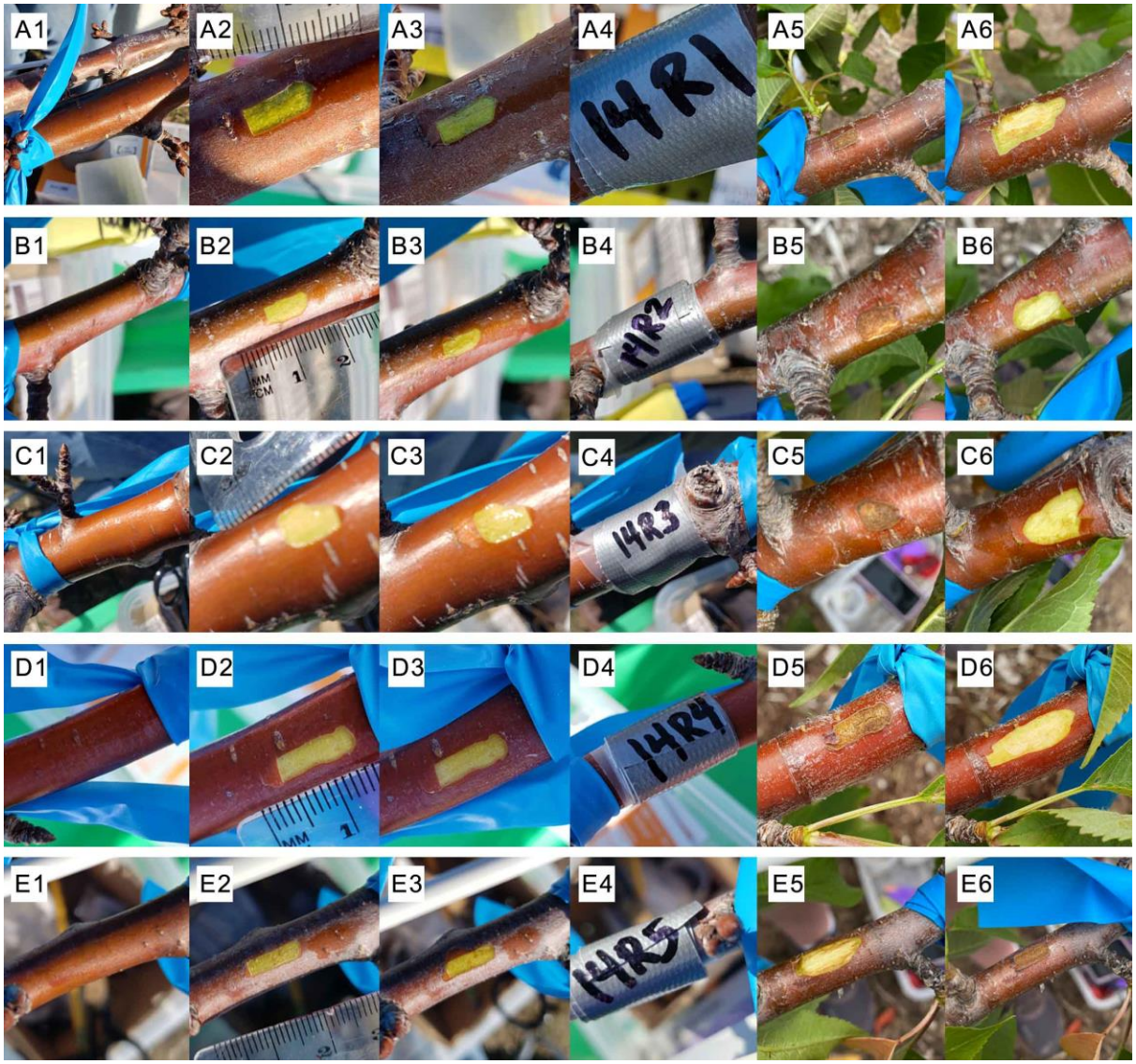


Figure A99. 2021 wound inoculation on 'Coral' cherry wood with *Pss* 14. **A1-E1)** The inoculation site before wounding. **A2-E2)** The inoculation site after wounding by sterile razor blade **A3-E3)** The inoculation site after pipetting inoculum into the wound. **A4-E4)** The inoculation site after covering with Parafilm and tape. **A5-E5)** The inoculation site exterior assessment in the spring. **A6-E6)** The inoculation site interior assessment in the spring. A1-A6: Replication 1. B1-B6: Replication 2. C1-C6: Replication 3. D1-D6: Replication 4. E1-E6: Replication 5.



Figure A100. 2021 wound inoculation on 'Coral' cherry wood with *Pss* 15. **A1-E1)** The inoculation site before wounding. **A2-E2)** The inoculation site after wounding by sterile razor blade **A3-E3)** The inoculation site after pipetting inoculum into the wound. **A4-E4)** The inoculation site after covering with Parafilm and tape. **A5-E5)** The inoculation site exterior assessment in the spring. **A6-E6)** The inoculation site interior assessment in the spring. A1-A6: Replication 1. B1-B6: Replication 2. C1-C6: Replication 3. D1-D6: Replication 4. E1-E6: Replication 5.



Figure A101. 2021 wound inoculation on 'Coral' cherry wood with *Pss* 16. **A1-E1)** The inoculation site before wounding. **A2-E2)** The inoculation site after wounding by sterile razor blade **A3-E3)** The inoculation site after pipetting inoculum into the wound. **A4-E4)** The inoculation site after covering with Parafilm and tape. **A5-E5)** The inoculation site exterior assessment in the spring. **A6-E6)** The inoculation site interior assessment in the spring. A1-A6: Replication 1. B1-B6: Replication 2. C1-C6: Replication 3. D1-D6: Replication 4. E1-E6: Replication 5.

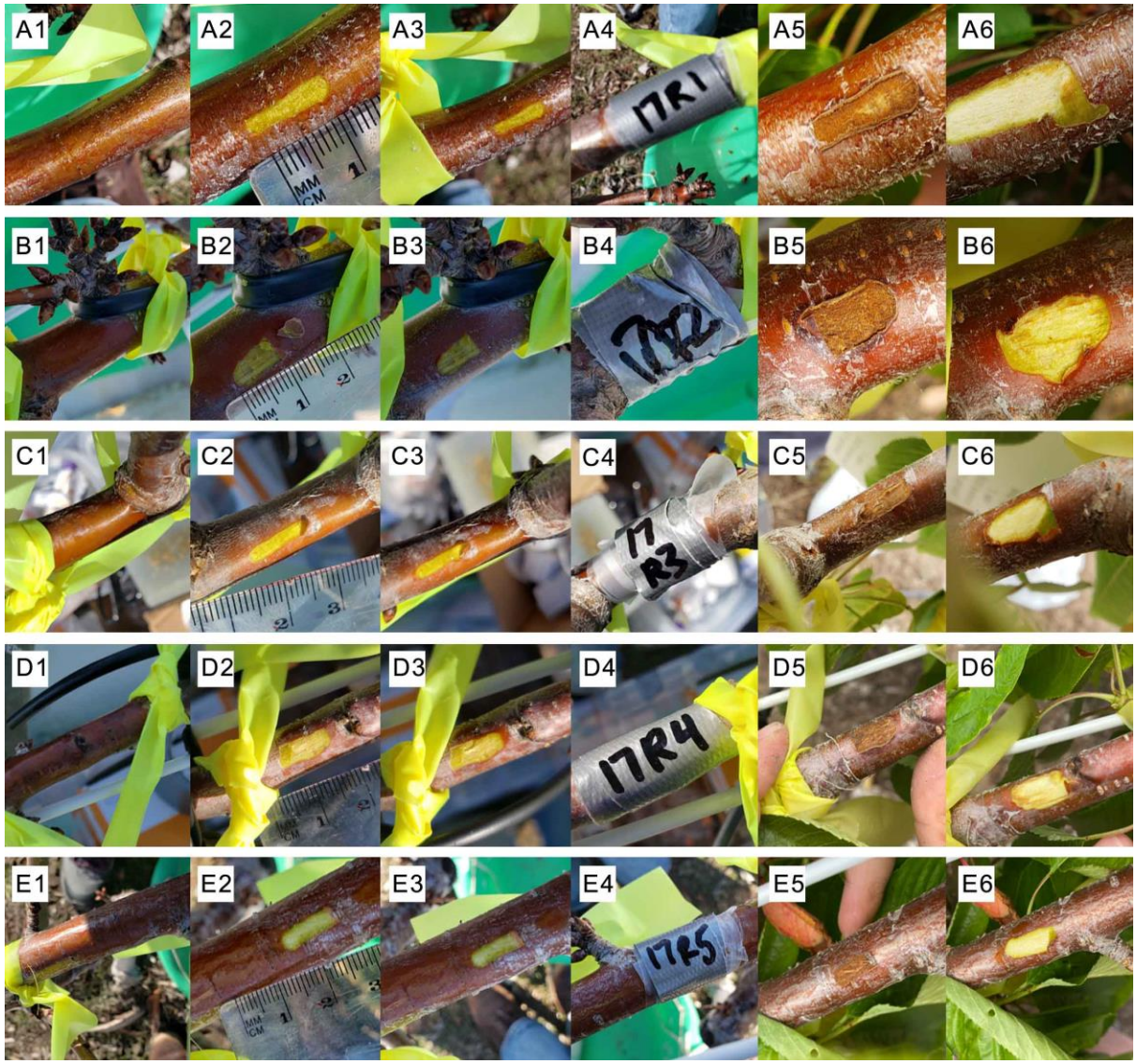


Figure A102. 2021 wound inoculation on 'Coral' cherry wood with *Pss* 17. **A1-E1)** The inoculation site before wounding. **A2-E2)** The inoculation site after wounding by sterile razor blade **A3-E3)** The inoculation site after pipetting inoculum into the wound. **A4-E4)** The inoculation site after covering with Parafilm and tape. **A5-E5)** The inoculation site exterior assessment in the spring. **A6-E6)** The inoculation site interior assessment in the spring. A1-A6: Replication 1. B1-B6: Replication 2. C1-C6: Replication 3. D1-D6: Replication 4. E1-E6: Replication 5.

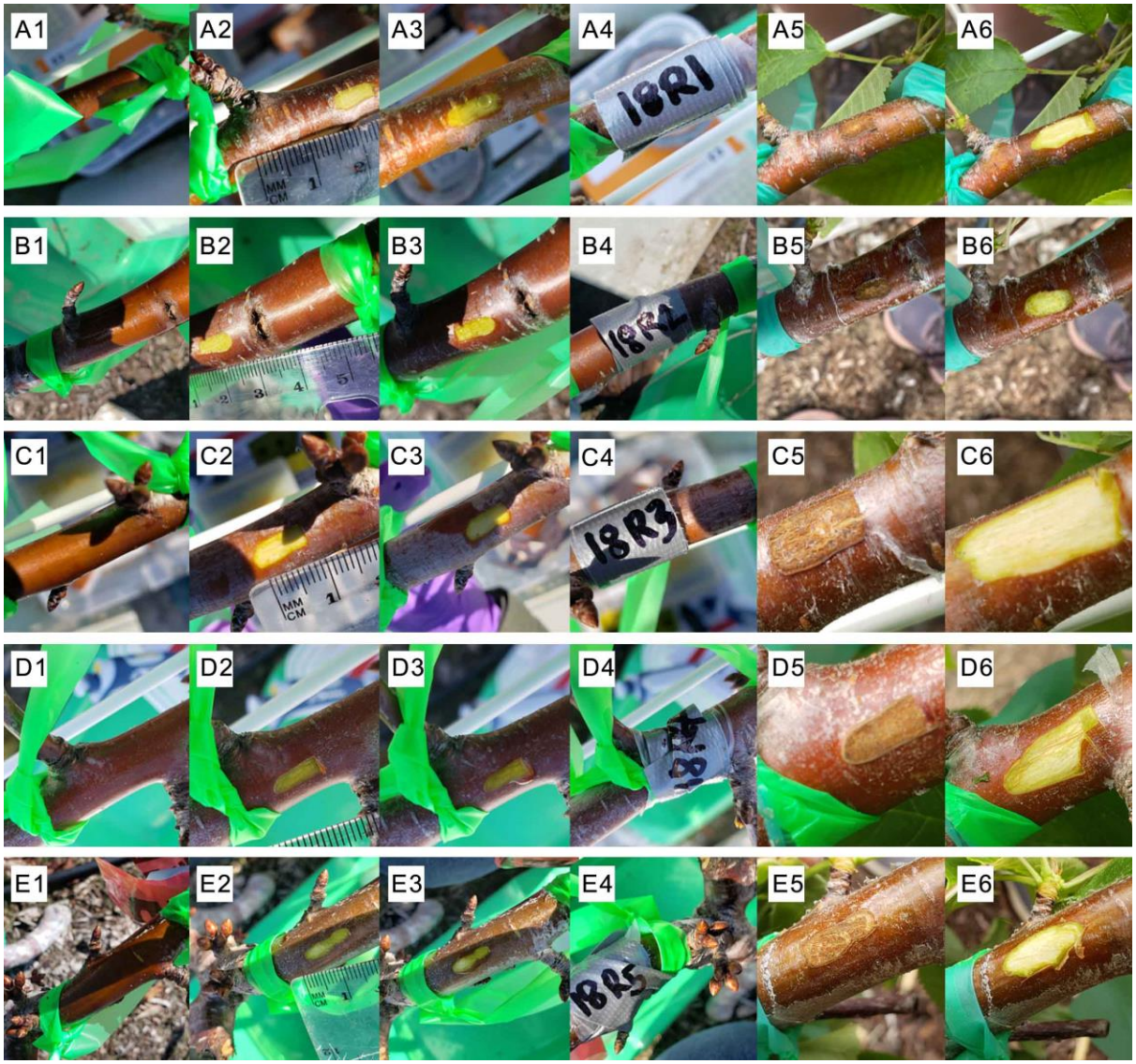


Figure A103. 2021 wound inoculation on 'Coral' cherry wood with *Pss* 18. **A1-E1)** The inoculation site before wounding. **A2-E2)** The inoculation site after wounding by sterile razor blade **A3-E3)** The inoculation site after pipetting inoculum into the wound. **A4-E4)** The inoculation site after covering with Parafilm and tape. **A5-E5)** The inoculation site exterior assessment in the spring. **A6-E6)** The inoculation site interior assessment in the spring. A1-A6: Replication 1. B1-B6: Replication 2. C1-C6: Replication 3. D1-D6: Replication 4. E1-E6: Replication 5.

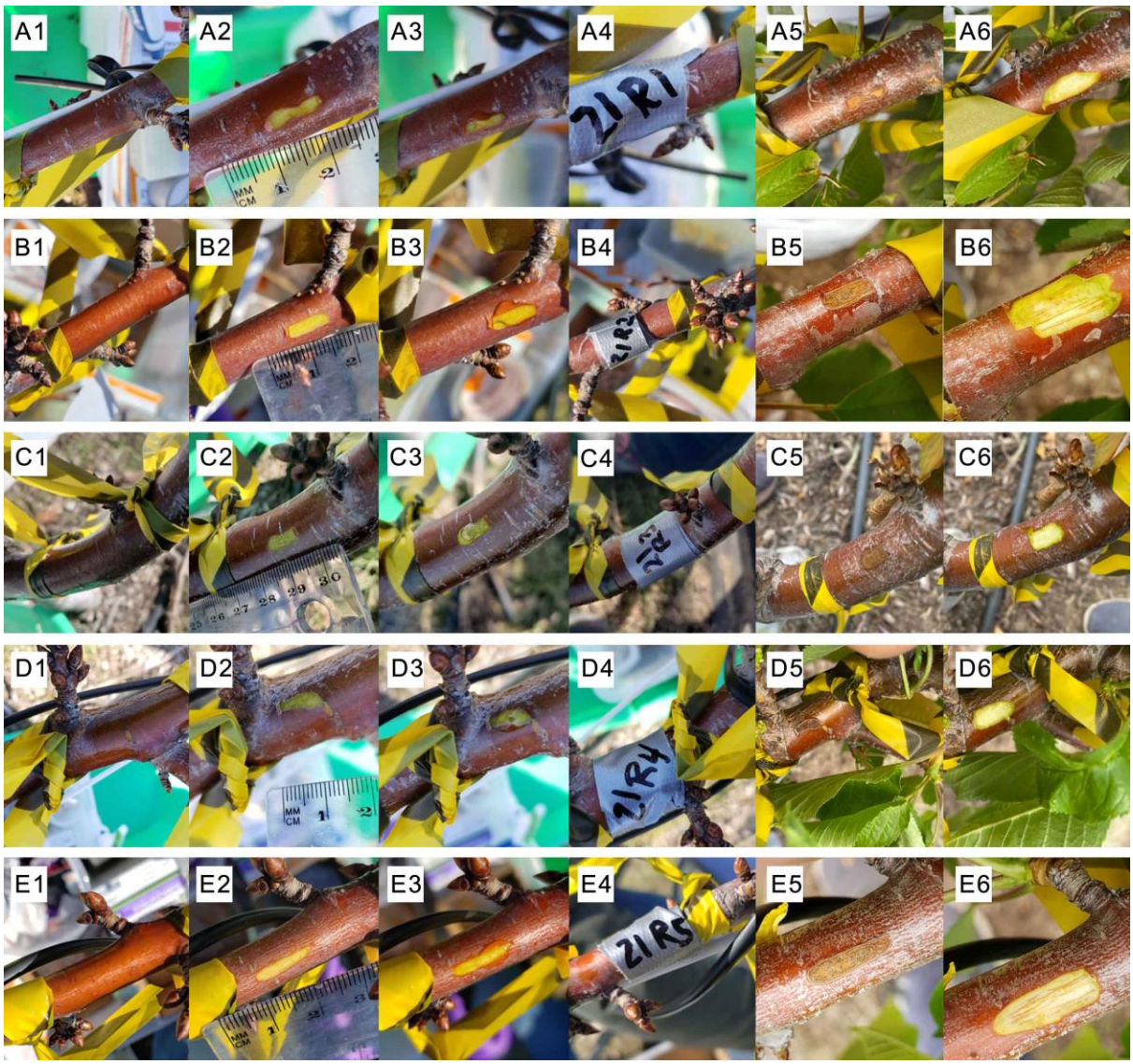


Figure A104. 2021 wound inoculation on 'Coral' cherry wood with *Pss* 21. **A1-E1)** The inoculation site before wounding. **A2-E2)** The inoculation site after wounding by sterile razor blade **A3-E3)** The inoculation site after pipetting inoculum into the wound. **A4-E4)** The inoculation site after covering with Parafilm and tape. **A5-E5)** The inoculation site exterior assessment in the spring. **A6-E6)** The inoculation site interior assessment in the spring. A1-A6: Replication 1. B1-B6: Replication 2. C1-C6: Replication 3. D1-D6: Replication 4. E1-E6: Replication 5.



Figure A105. 2021 wound inoculation on 'Coral' cherry wood with *Pss* 22. **A1-E1)** The inoculation site before wounding. **A2-E2)** The inoculation site after wounding by sterile razor blade **A3-E3)** The inoculation site after pipetting inoculum into the wound. **A4-E4)** The inoculation site after covering with Parafilm and tape. **A5-E5)** The inoculation site exterior assessment in the spring. **A6-E6)** The inoculation site interior assessment in the spring. A1-A6: Replication 1. B1-B6: Replication 2. C1-C6: Replication 3. D1-D6: Replication 4. E1-E6: Replication 5.

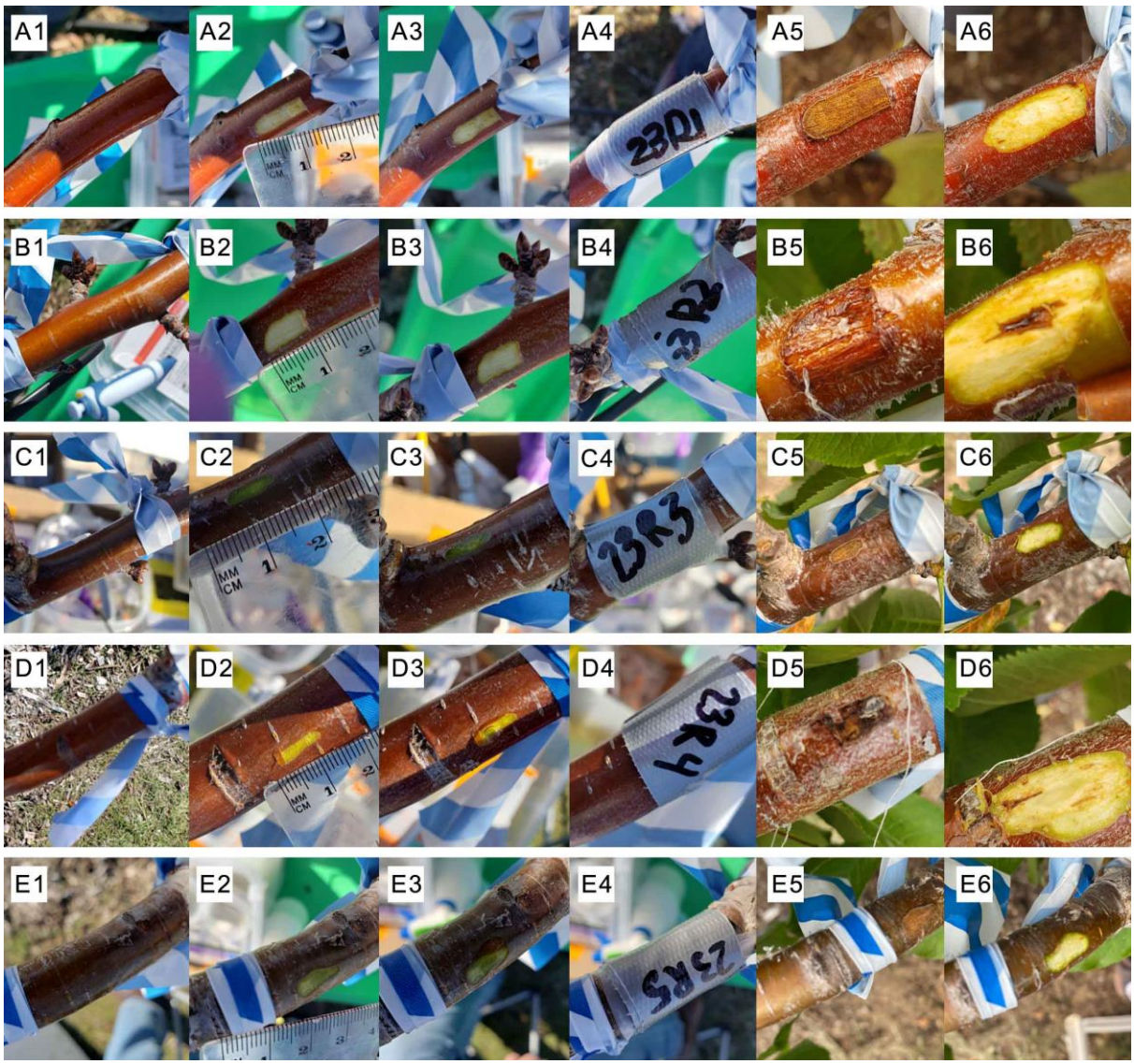


Figure A106. 2021 wound inoculation on 'Coral' cherry wood with *Pss* 23. **A1-E1)** The inoculation site before wounding. **A2-E2)** The inoculation site after wounding by sterile razor blade **A3-E3)** The inoculation site after pipetting inoculum into the wound. **A4-E4)** The inoculation site after covering with Parafilm and tape. **A5-E5)** The inoculation site exterior assessment in the spring. **A6-E6)** The inoculation site interior assessment in the spring. A1-A6: Replication 1. B1-B6: Replication 2. C1-C6: Replication 3. D1-D6: Replication 4. E1-E6: Replication 5.

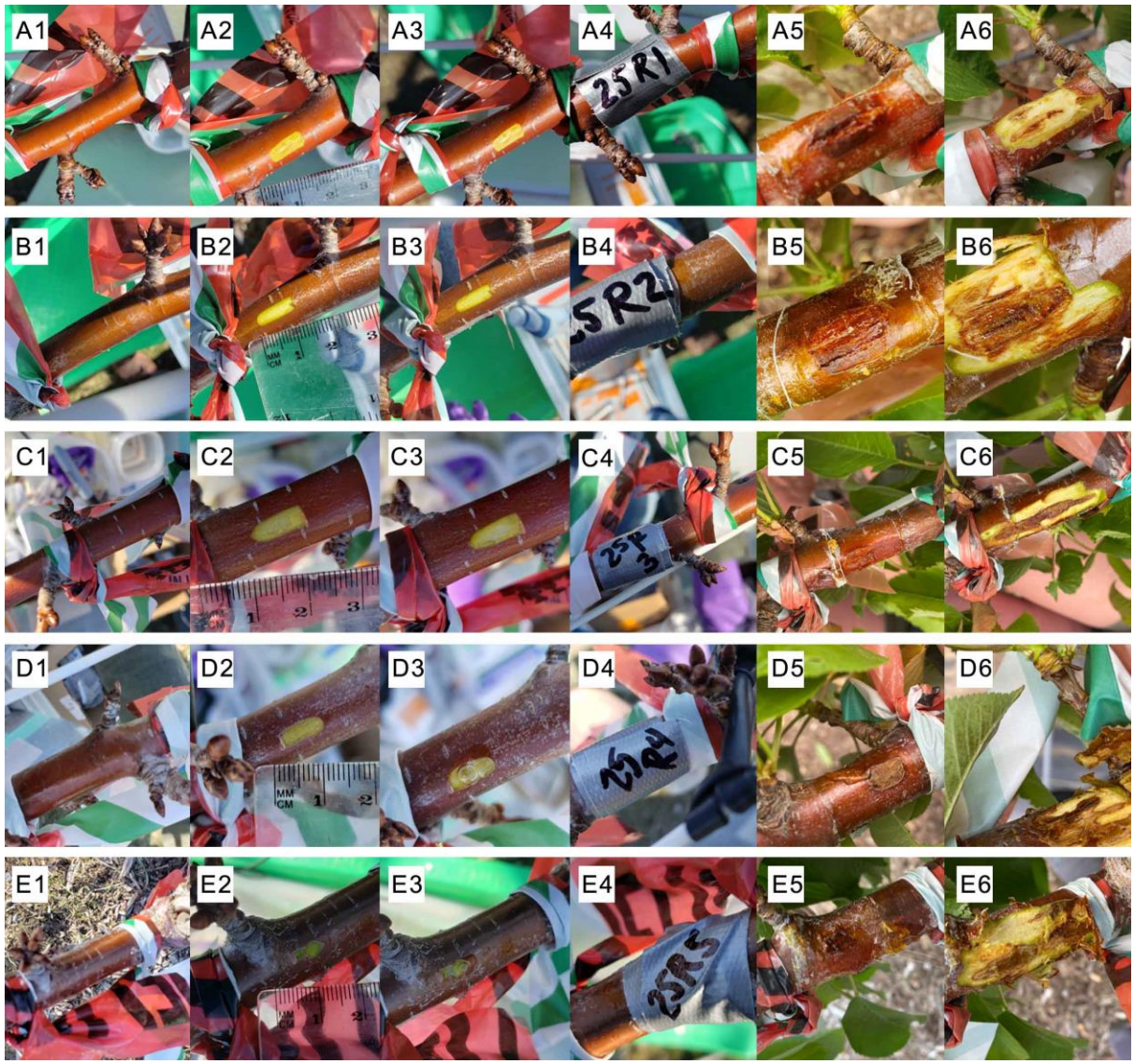


Figure A107. 2021 wound inoculation on 'Coral' cherry wood with *Pss* 25. **A1-E1)** The inoculation site before wounding. **A2-E2)** The inoculation site after wounding by sterile razor blade **A3-E3)** The inoculation site after pipetting inoculum into the wound. **A4-E4)** The inoculation site after covering with Parafilm and tape. **A5-E5)** The inoculation site exterior assessment in the spring. **A6-E6)** The inoculation site interior assessment in the spring. A1-A6: Replication 1. B1-B6: Replication 2. C1-C6: Replication 3. D1-D6: Replication 4. E1-E6: Replication 5.

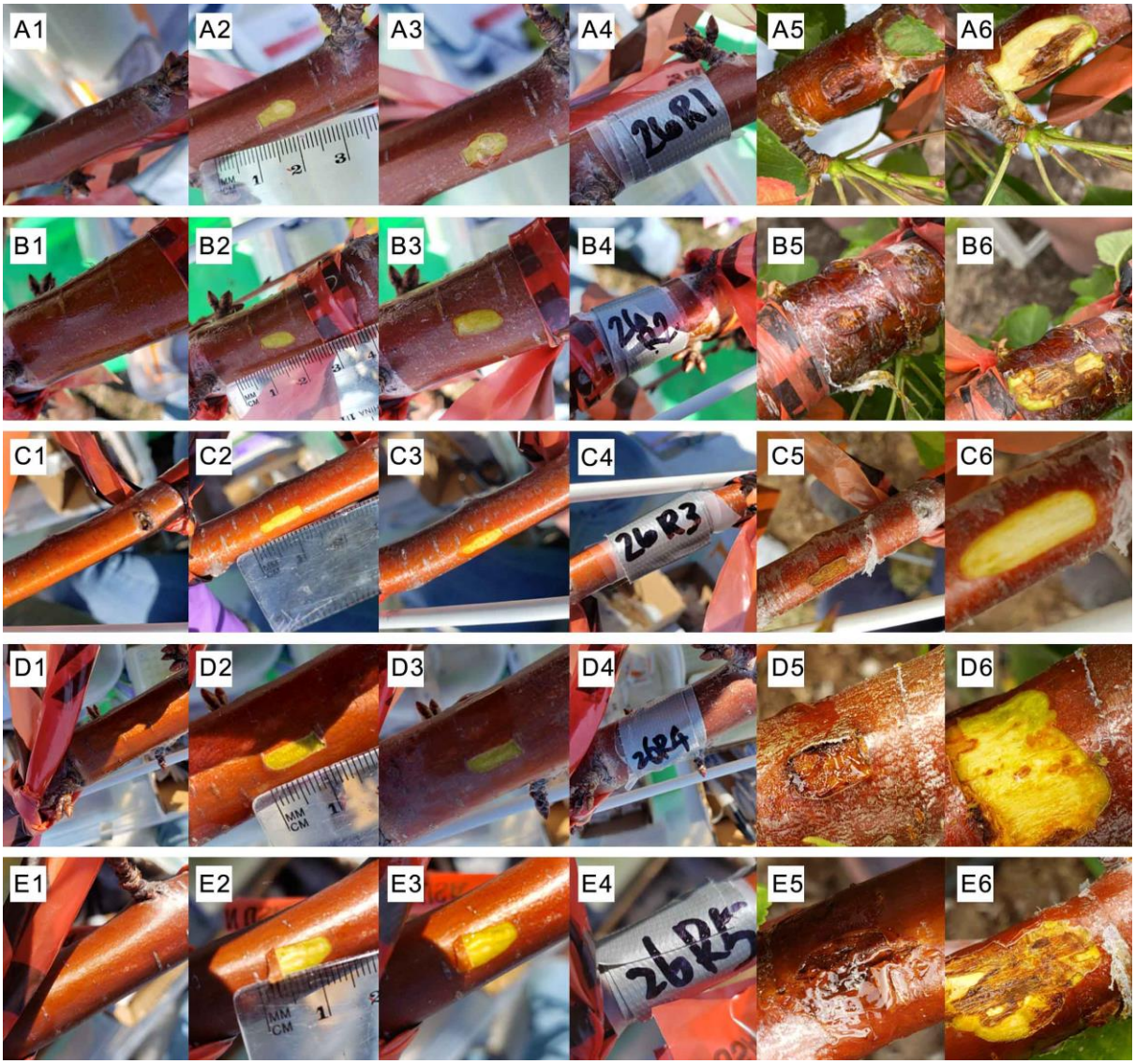


Figure A108. 2021 wound inoculation on 'Coral' cherry wood with *Pss* 26. **A1-E1)** The inoculation site before wounding. **A2-E2)** The inoculation site after wounding by sterile razor blade **A3-E3)** The inoculation site after pipetting inoculum into the wound. **A4-E4)** The inoculation site after covering with Parafilm and tape. **A5-E5)** The inoculation site exterior assessment in the spring. **A6-E6)** The inoculation site interior assessment in the spring. A1-A6: Replication 1. B1-B6: Replication 2. C1-C6: Replication 3. D1-D6: Replication 4. E1-E6: Replication 5.



Figure A109. 2021 wound inoculation on 'Coral' cherry wood with *Pss* 27. **A1-E1)** The inoculation site before wounding. **A2-E2)** The inoculation site after wounding by sterile razor blade **A3-E3)** The inoculation site after pipetting inoculum into the wound. **A4-E4)** The inoculation site after covering with Parafilm and tape. **A5-E5)** The inoculation site exterior assessment in the spring. **A6-E6)** The inoculation site interior assessment in the spring. A1-A6: Replication 1. B1-B6: Replication 2. C1-C6: Replication 3. D1-D6: Replication 4. E1-E6: Replication 5.

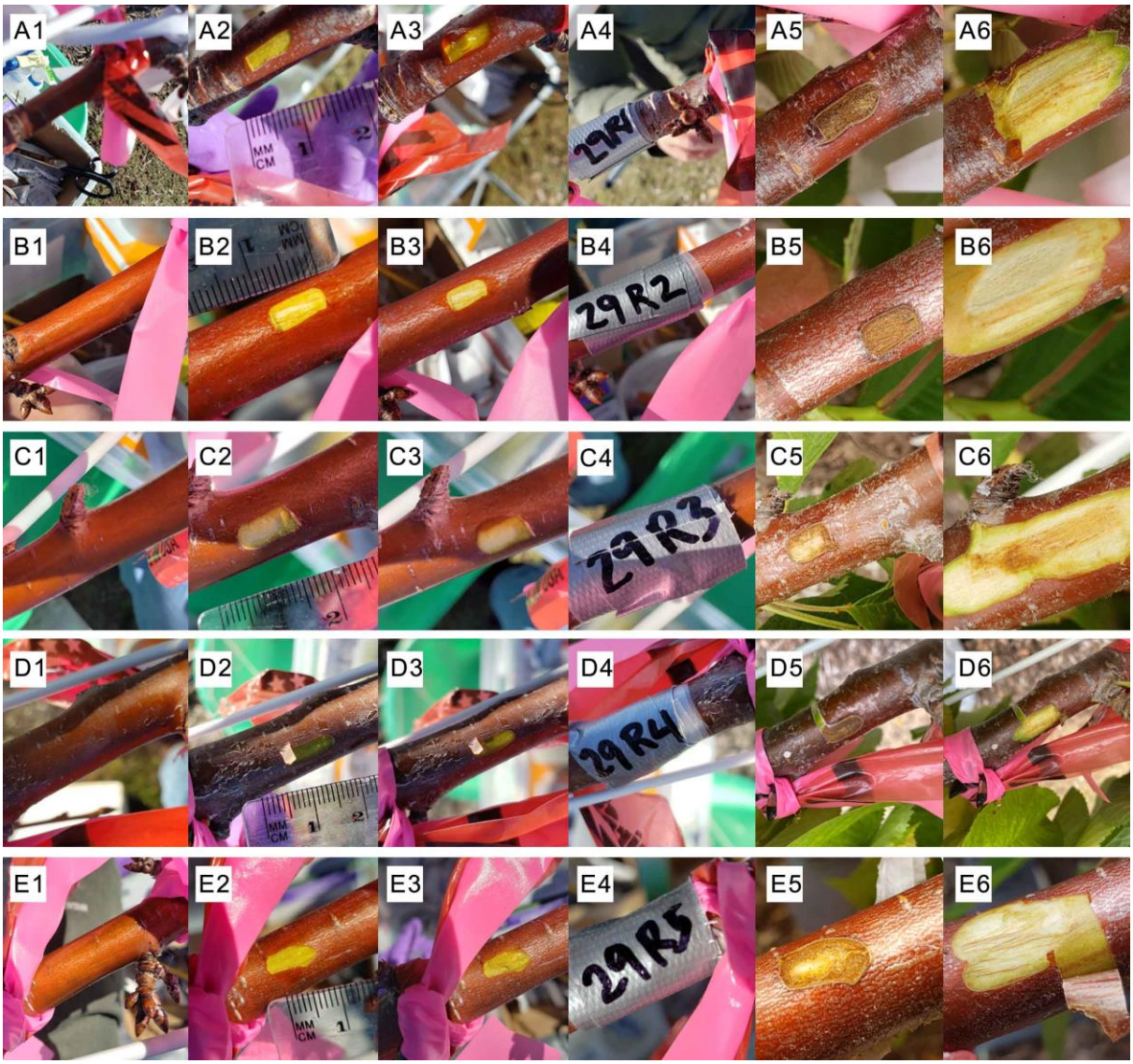


Figure A110. 2021 wound inoculation on 'Coral' cherry wood with *Pss* 29. **A1-E1)** The inoculation site before wounding. **A2-E2)** The inoculation site after wounding by sterile razor blade **A3-E3)** The inoculation site after pipetting inoculum into the wound. **A4-E4)** The inoculation site after covering with Parafilm and tape. **A5-E5)** The inoculation site exterior assessment in the spring. **A6-E6)** The inoculation site interior assessment in the spring. A1-A6: Replication 1. B1-B6: Replication 2. C1-C6: Replication 3. D1-D6: Replication 4. E1-E6: Replication 5.

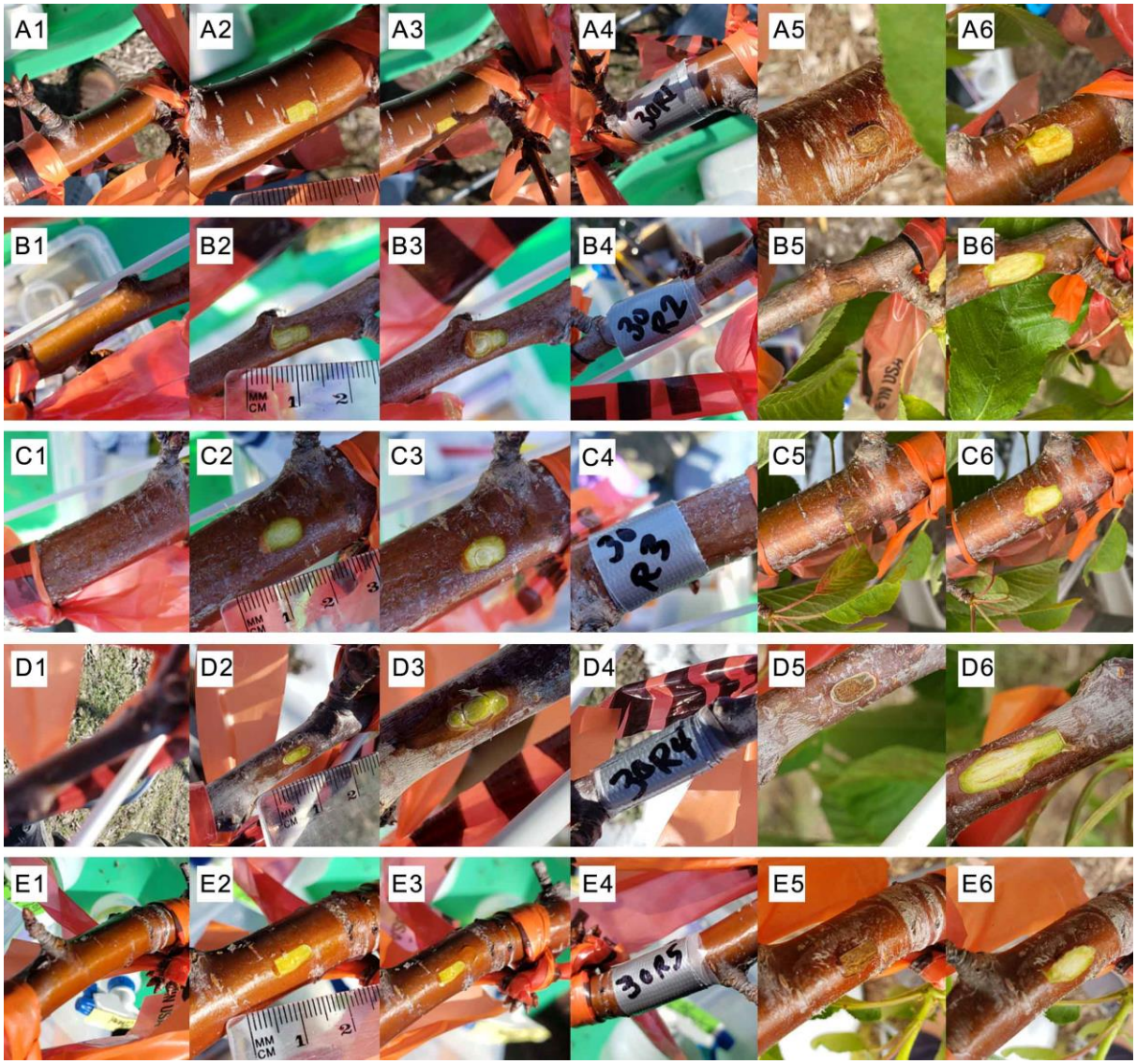


Figure A111. 2021 wound inoculation on 'Coral' cherry wood with *Pss* 30. **A1-E1)** The inoculation site before wounding. **A2-E2)** The inoculation site after wounding by sterile razor blade **A3-E3)** The inoculation site after pipetting inoculum into the wound. **A4-E4)** The inoculation site after covering with Parafilm and tape. **A5-E5)** The inoculation site exterior assessment in the spring. **A6-E6)** The inoculation site interior assessment in the spring. A1-A6: Replication 1. B1-B6: Replication 2. C1-C6: Replication 3. D1-D6: Replication 4. E1-E6: Replication 5.

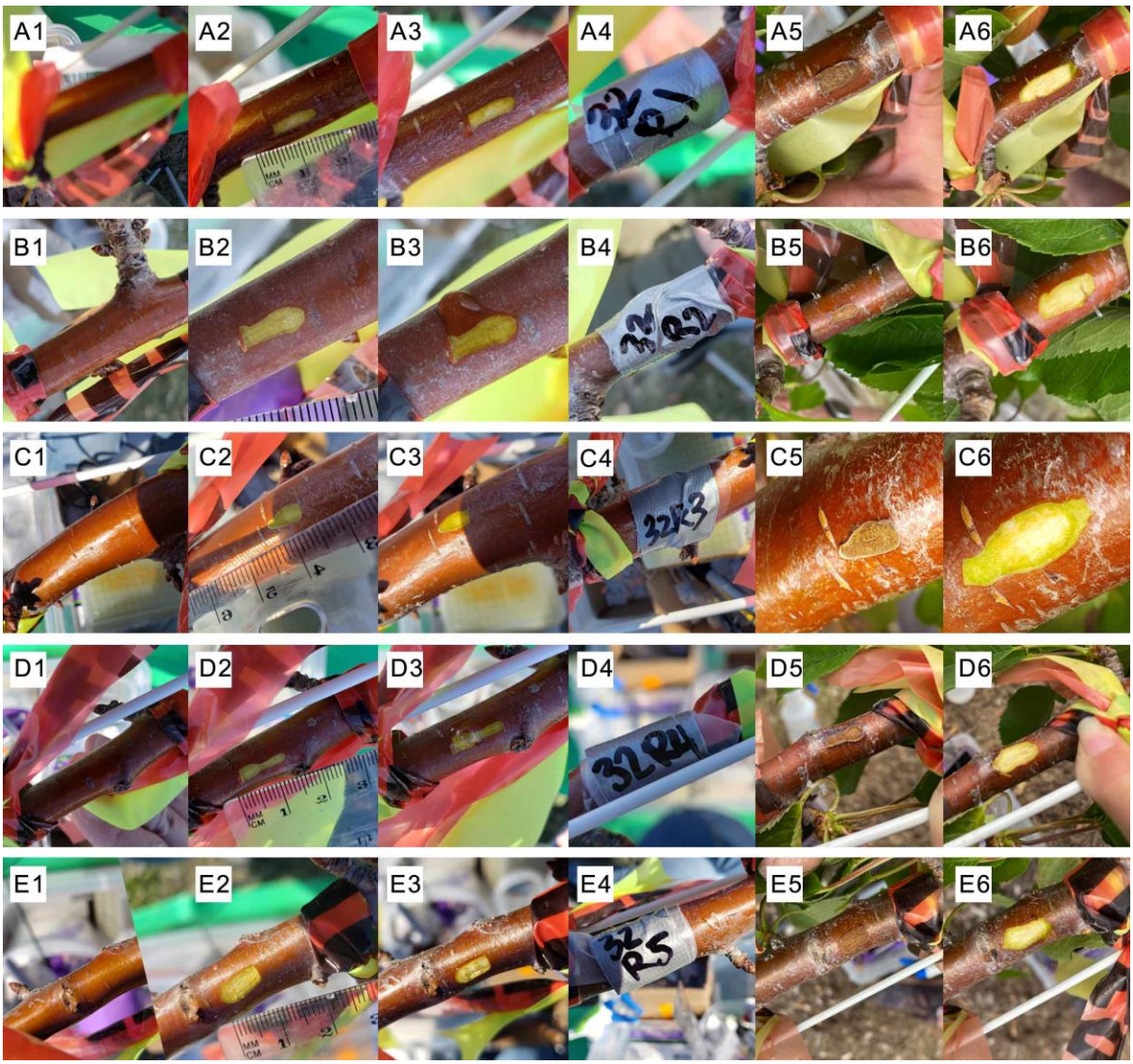


Figure A112. 2021 wound inoculation on 'Coral' cherry wood with *Pss* 32. **A1-E1)** The inoculation site before wounding. **A2-E2)** The inoculation site after wounding by sterile razor blade **A3-E3)** The inoculation site after pipetting inoculum into the wound. **A4-E4)** The inoculation site after covering with Parafilm and tape. **A5-E5)** The inoculation site exterior assessment in the spring. **A6-E6)** The inoculation site interior assessment in the spring. A1-A6: Replication 1. B1-B6: Replication 2. C1-C6: Replication 3. D1-D6: Replication 4. E1-E6: Replication 5.

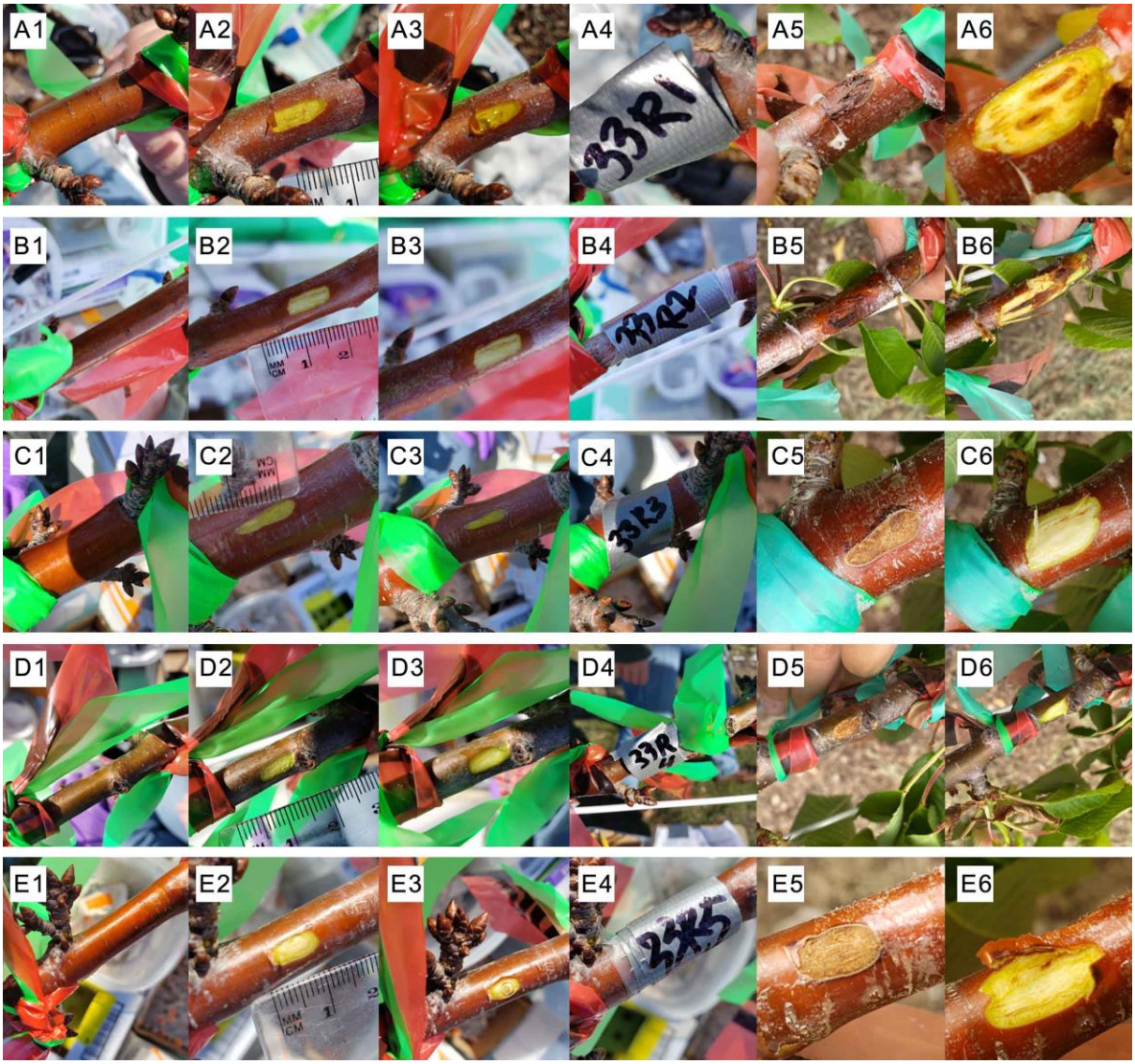


Figure A113. 2021 wound inoculation on 'Coral' cherry wood with *Pss* 33. **A1-E1)** The inoculation site before wounding. **A2-E2)** The inoculation site after wounding by sterile razor blade **A3-E3)** The inoculation site after pipetting inoculum into the wound. **A4-E4)** The inoculation site after covering with Parafilm and tape. **A5-E5)** The inoculation site exterior assessment in the spring. **A6-E6)** The inoculation site interior assessment in the spring. A1-A6: Replication 1. B1-B6: Replication 2. C1-C6: Replication 3. D1-D6: Replication 4. E1-E6: Replication 5.

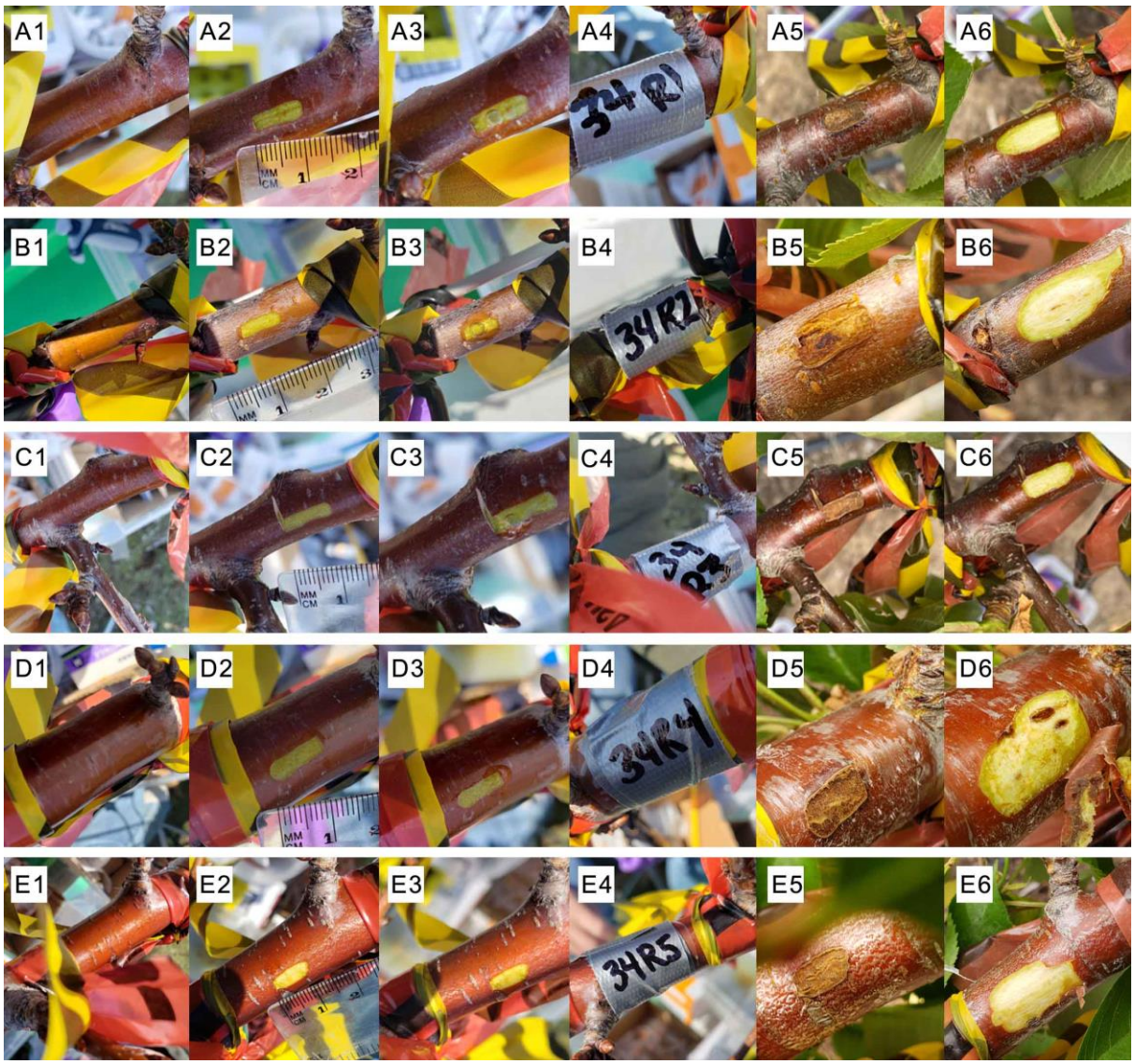


Figure A114. 2021 wound inoculation on 'Coral' cherry wood with *Pss* 34. **A1-E1)** The inoculation site before wounding. **A2-E2)** The inoculation site after wounding by sterile razor blade **A3-E3)** The inoculation site after pipetting inoculum into the wound. **A4-E4)** The inoculation site after covering with Parafilm and tape. **A5-E5)** The inoculation site exterior assessment in the spring. **A6-E6)** The inoculation site interior assessment in the spring. A1-A6: Replication 1. B1-B6: Replication 2. C1-C6: Replication 3. D1-D6: Replication 4. E1-E6: Replication 5.

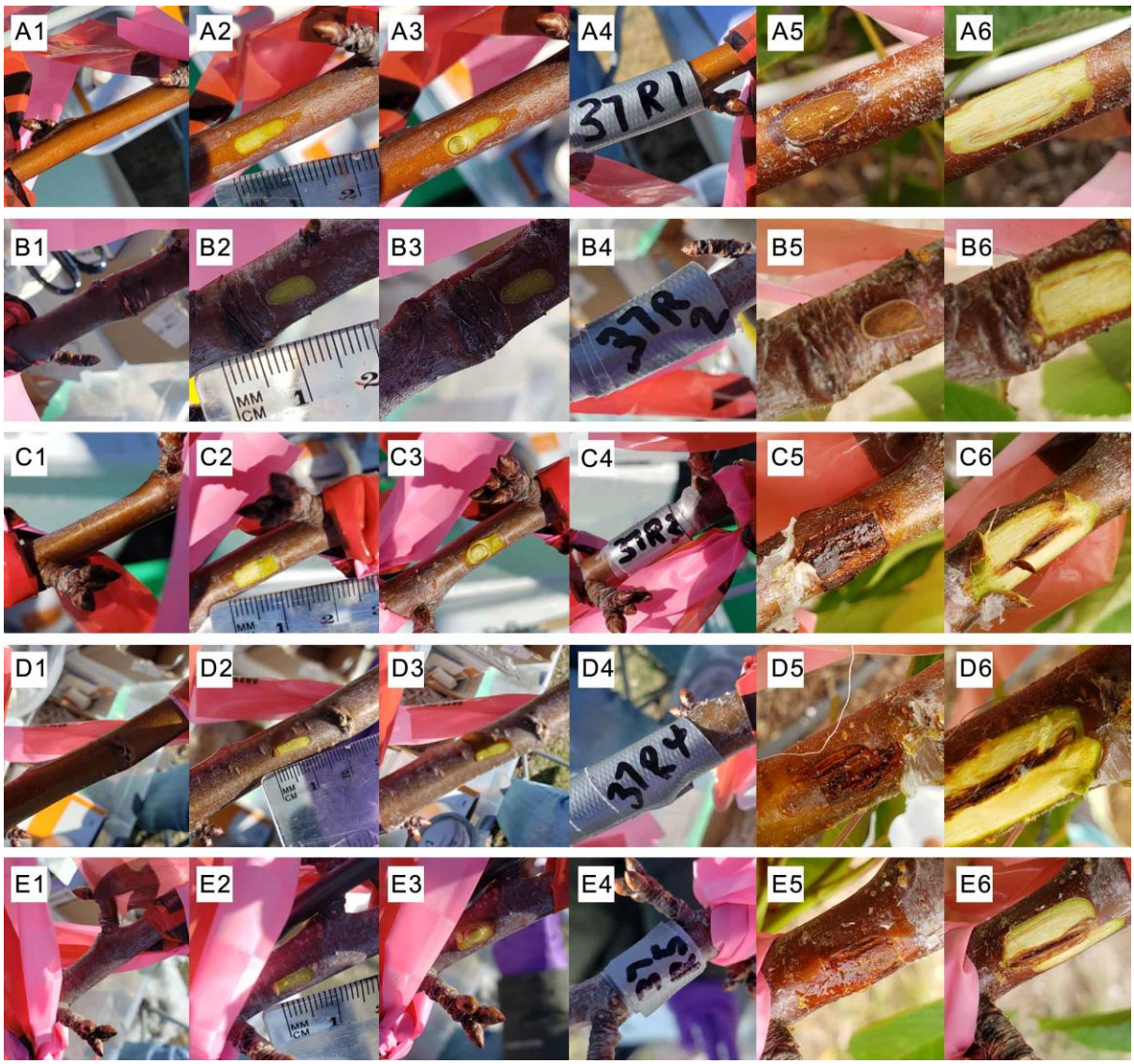


Figure A115. 2021 wound inoculation on 'Coral' cherry wood with *Pss* 37. **A1-E1)** The inoculation site before wounding. **A2-E2)** The inoculation site after wounding by sterile razor blade **A3-E3)** The inoculation site after pipetting inoculum into the wound. **A4-E4)** The inoculation site after covering with Parafilm and tape. **A5-E5)** The inoculation site exterior assessment in the spring. **A6-E6)** The inoculation site interior assessment in the spring. A1-A6: Replication 1. B1-B6: Replication 2. C1-C6: Replication 3. D1-D6: Replication 4. E1-E6: Replication 5.

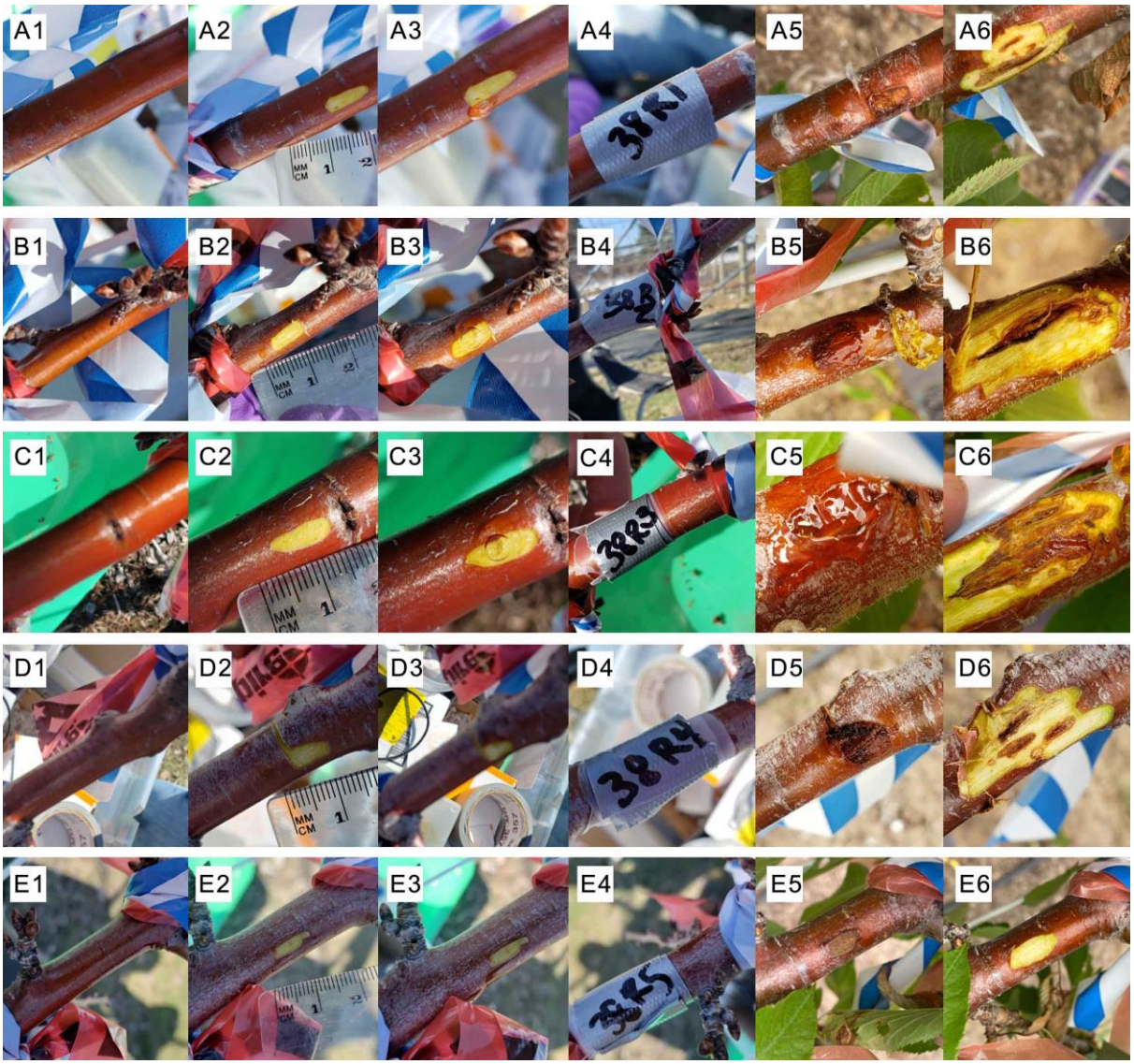


Figure A116. 2021 wound inoculation on 'Coral' cherry wood with *Pss* 38. **A1-E1)** The inoculation site before wounding. **A2-E2)** The inoculation site after wounding by sterile razor blade **A3-E3)** The inoculation site after pipetting inoculum into the wound. **A4-E4)** The inoculation site after covering with Parafilm and tape. **A5-E5)** The inoculation site exterior assessment in the spring. **A6-E6)** The inoculation site interior assessment in the spring. A1-A6: Replication 1. B1-B6: Replication 2. C1-C6: Replication 3. D1-D6: Replication 4. E1-E6: Replication 5.

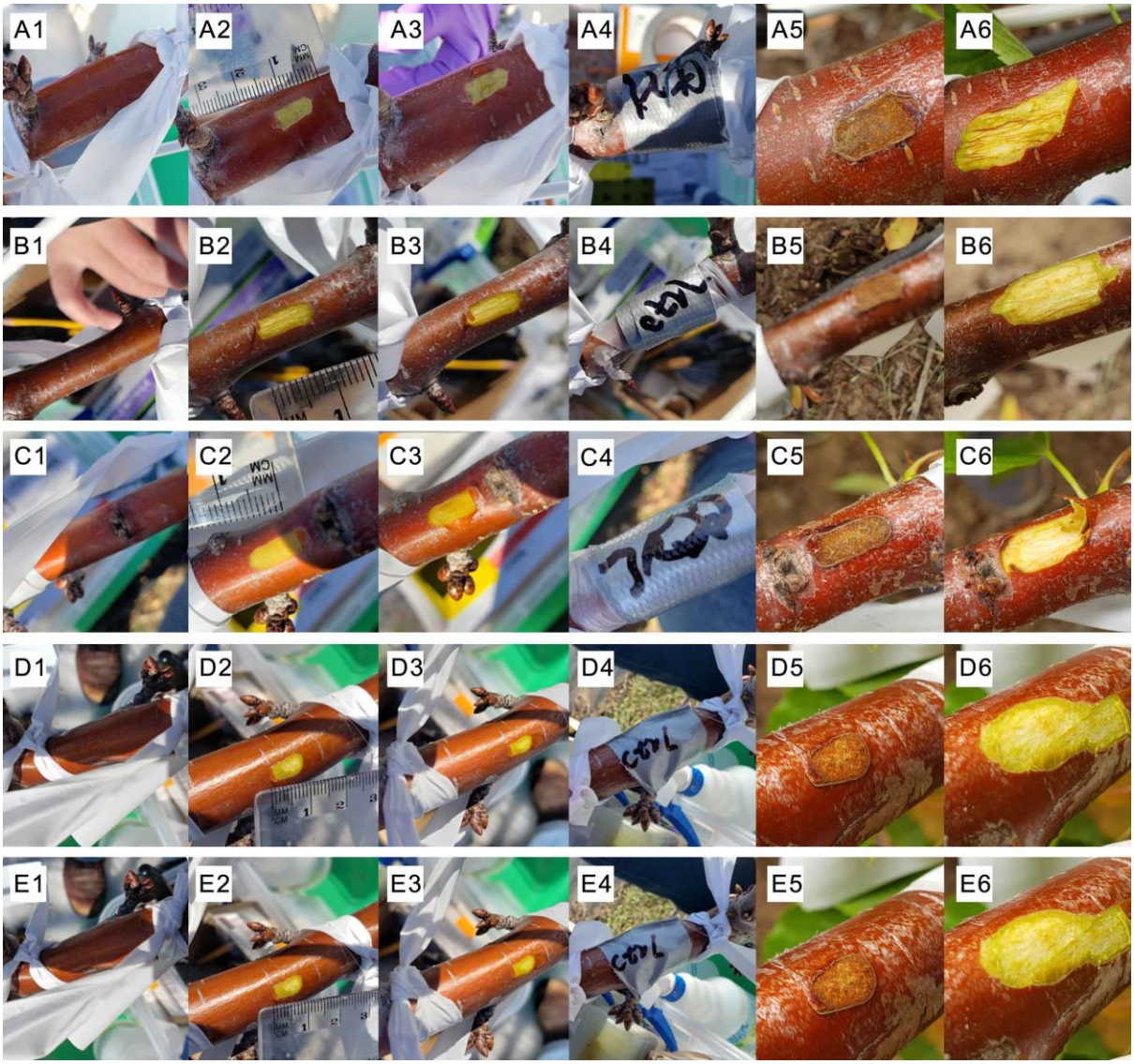


Figure A117. 2021 wound inoculation on 'Coral' cherry wood with PBS. **A1-E1)** The inoculation site before wounding. **A2-E2)** The inoculation site after wounding by sterile razor blade **A3-E3)** The inoculation site after pipetting inoculum into the wound. **A4-E4)** The inoculation site after covering with Parafilm and tape. **A5-E5)** The inoculation site exterior assessment in the spring. **A6-E6)** The inoculation site interior assessment in the spring.

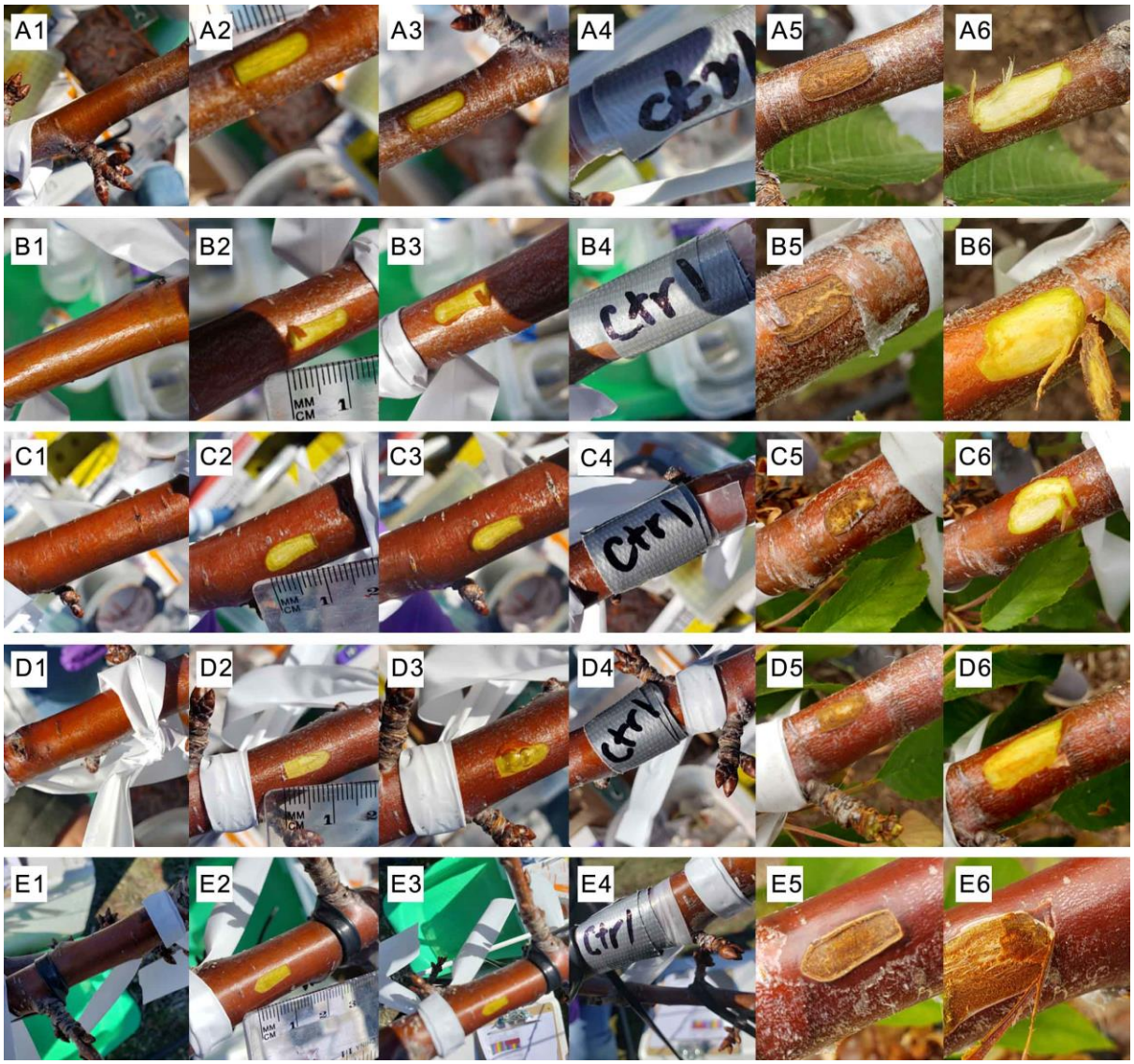


Figure A118. 2021 wound inoculation on 'Coral' cherry wood with PBS. **A1-E1)** The inoculation site before wounding. **A2-E2)** The inoculation site after wounding by sterile razor blade **A3-E3)** The inoculation site after pipetting inoculum into the wound. **A4-E4)** The inoculation site after covering with Parafilm and tape. **A5-E5)** The inoculation site exterior assessment in the spring. **A6-E6)** The inoculation site interior assessment in the spring.

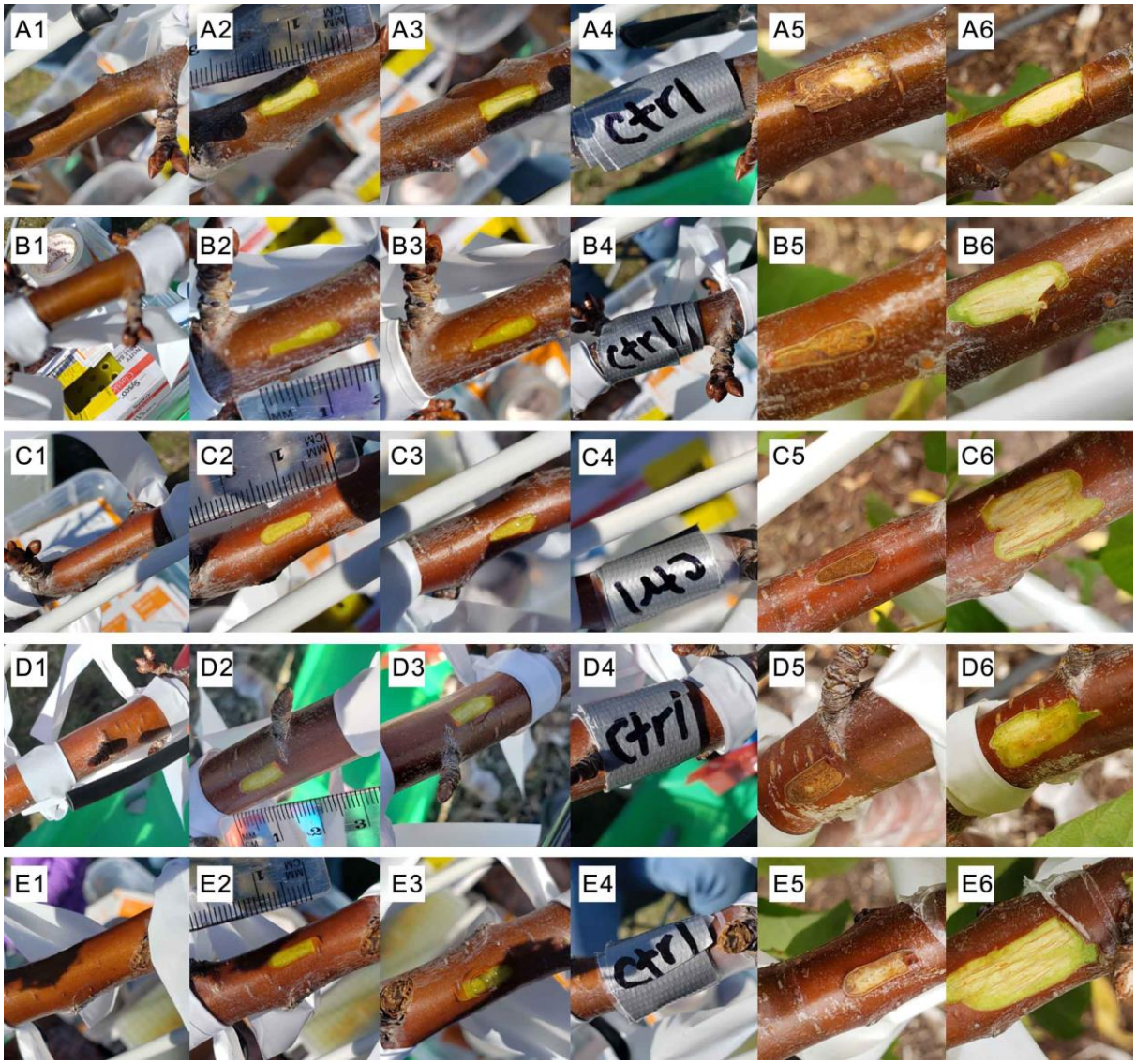


Figure A119. 2021 wound inoculation on 'Coral' cherry wood with PBS. **A1-E1)** The inoculation site before wounding. **A2-E2)** The inoculation site after wounding by sterile razor blade **A3-E3)** The inoculation site after pipetting inoculum into the wound. **A4-E4)** The inoculation site after covering with Parafilm and tape. **A5-E5)** The inoculation site exterior assessment in the spring. **A6-E6)** The inoculation site interior assessment in the spring.

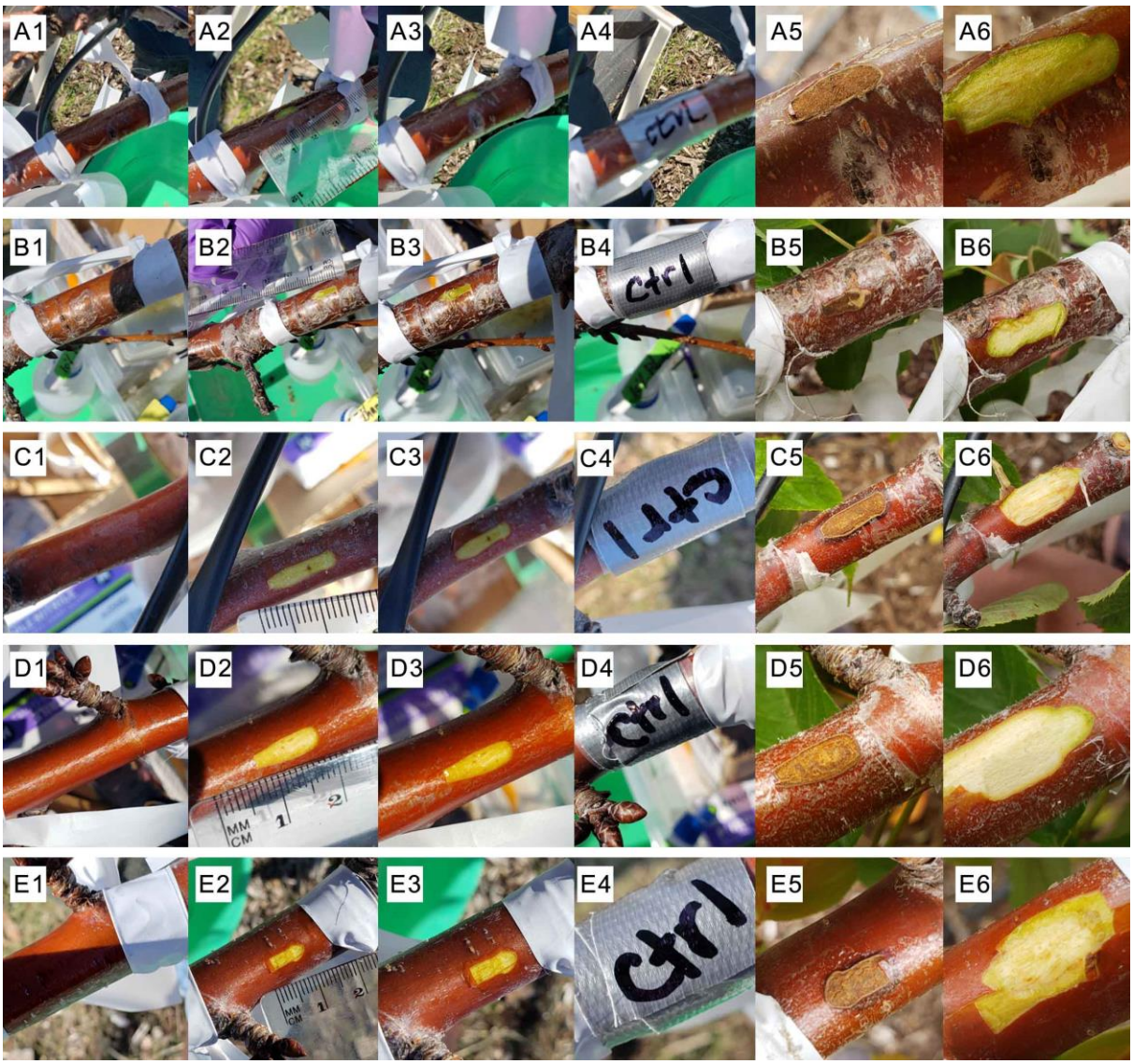


Figure A120. 2021 wound inoculation on 'Coral' cherry wood with PBS. **A1-E1)** The inoculation site before wounding. **A2-E2)** The inoculation site after wounding by sterile razor blade **A3-E3)** The inoculation site after pipetting inoculum into the wound. **A4-E4)** The inoculation site after covering with Parafilm and tape. **A5-E5)** The inoculation site exterior assessment in the spring. **A6-E6)** The inoculation site interior assessment in the spring.

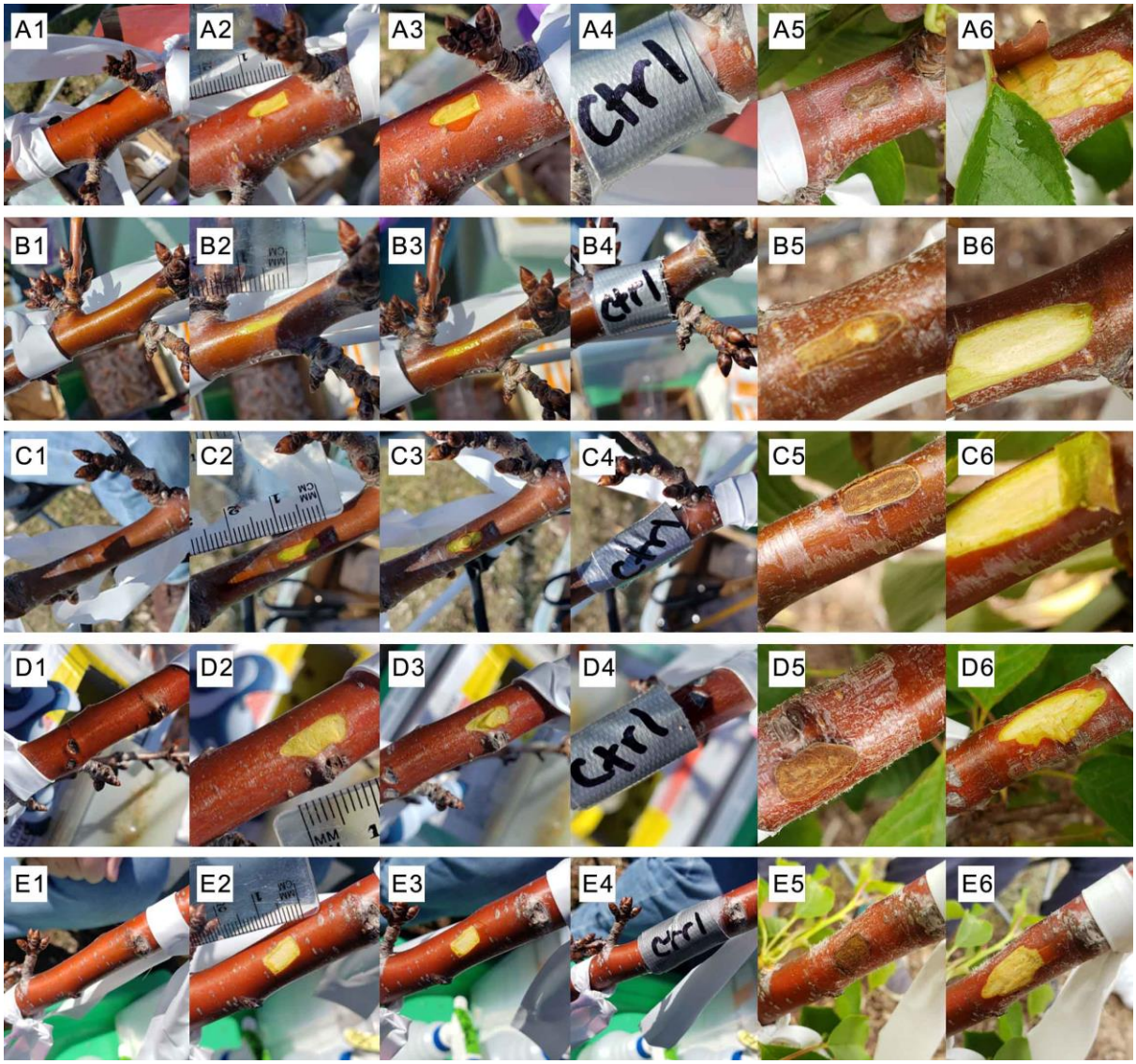


Figure A121. 2021 wound inoculation on 'Coral' cherry wood with PBS. **A1-E1)** The inoculation site before wounding. **A2-E2)** The inoculation site after wounding by sterile razor blade **A3-E3)** The inoculation site after pipetting inoculum into the wound. **A4-E4)** The inoculation site after covering with Parafilm and tape. **A5-E5)** The inoculation site exterior assessment in the spring. **A6-E6)** The inoculation site interior assessment in the spring.



Figure A122. 2021 wound inoculation on 'Coral' cherry wood with PBS. **A1-E1)** The inoculation site before wounding. **A2-E2)** The inoculation site after wounding by sterile razor blade **A3-E3)** The inoculation site after pipetting inoculum into the wound. **A4-E4)** The inoculation site after covering with Parafilm and tape. **A5-E5)** The inoculation site exterior assessment in the spring. **A6-E6)** The inoculation site interior assessment in the spring.



Figure A123. 2021 wound inoculation on 'Coral' cherry wood with PBS. **A1-E1)** The inoculation site before wounding. **A2-E2)** The inoculation site after wounding by sterile razor blade **A3-E3)** The inoculation site after pipetting inoculum into the wound. **A4-E4)** The inoculation site after covering with Parafilm and tape. **A5-E5)** The inoculation site exterior assessment in the spring. **A6-E6)** The inoculation site interior assessment in the spring.

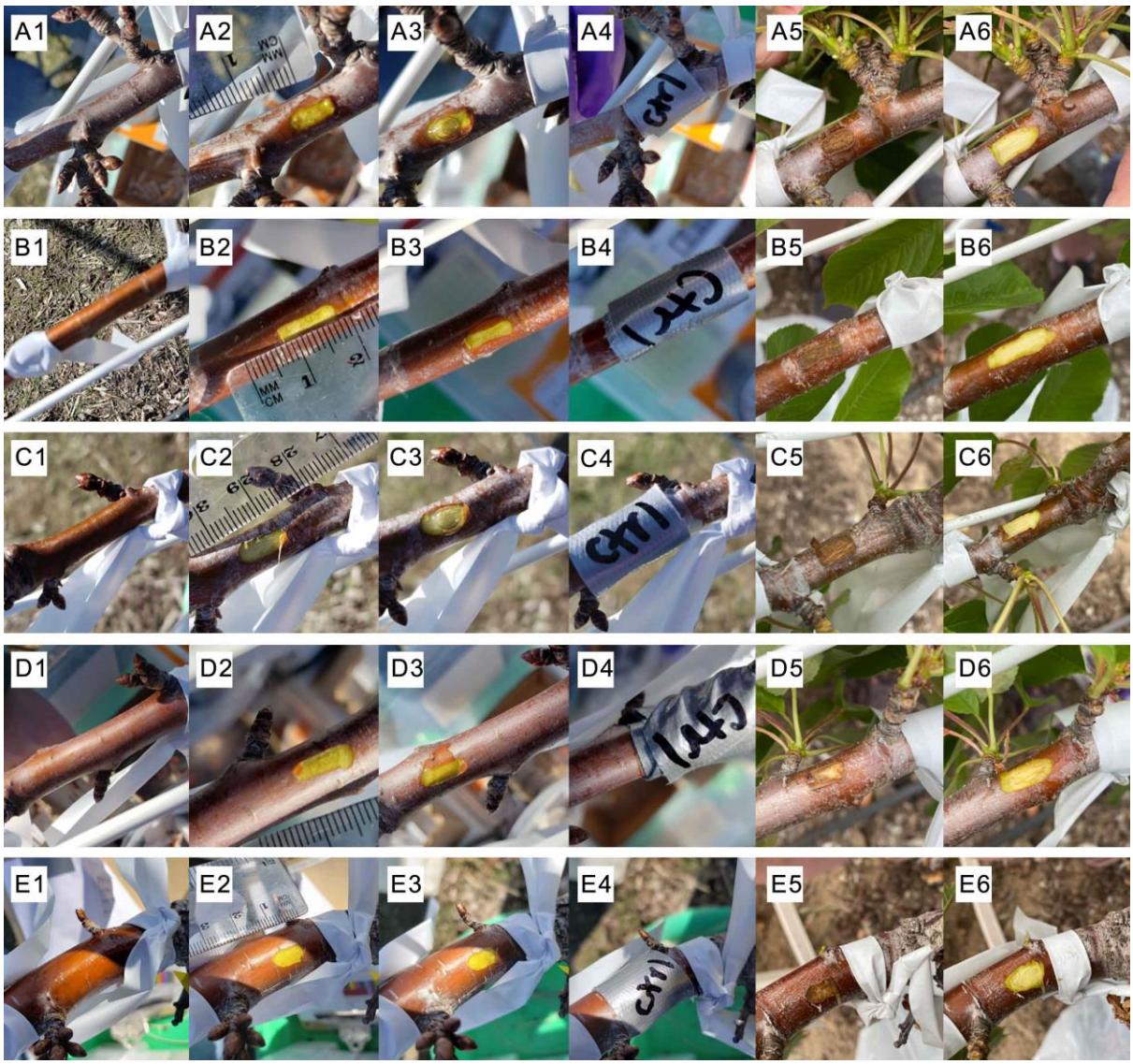


Figure A124. 2021 wound inoculation on 'Coral' cherry wood with PBS. **A1-E1)** The inoculation site before wounding. **A2-E2)** The inoculation site after wounding by sterile razor blade **A3-E3)** The inoculation site after pipetting inoculum into the wound. **A4-E4)** The inoculation site after covering with Parafilm and tape. **A5-E5)** The inoculation site exterior assessment in the spring. **A6-E6)** The inoculation site interior assessment in the spring.

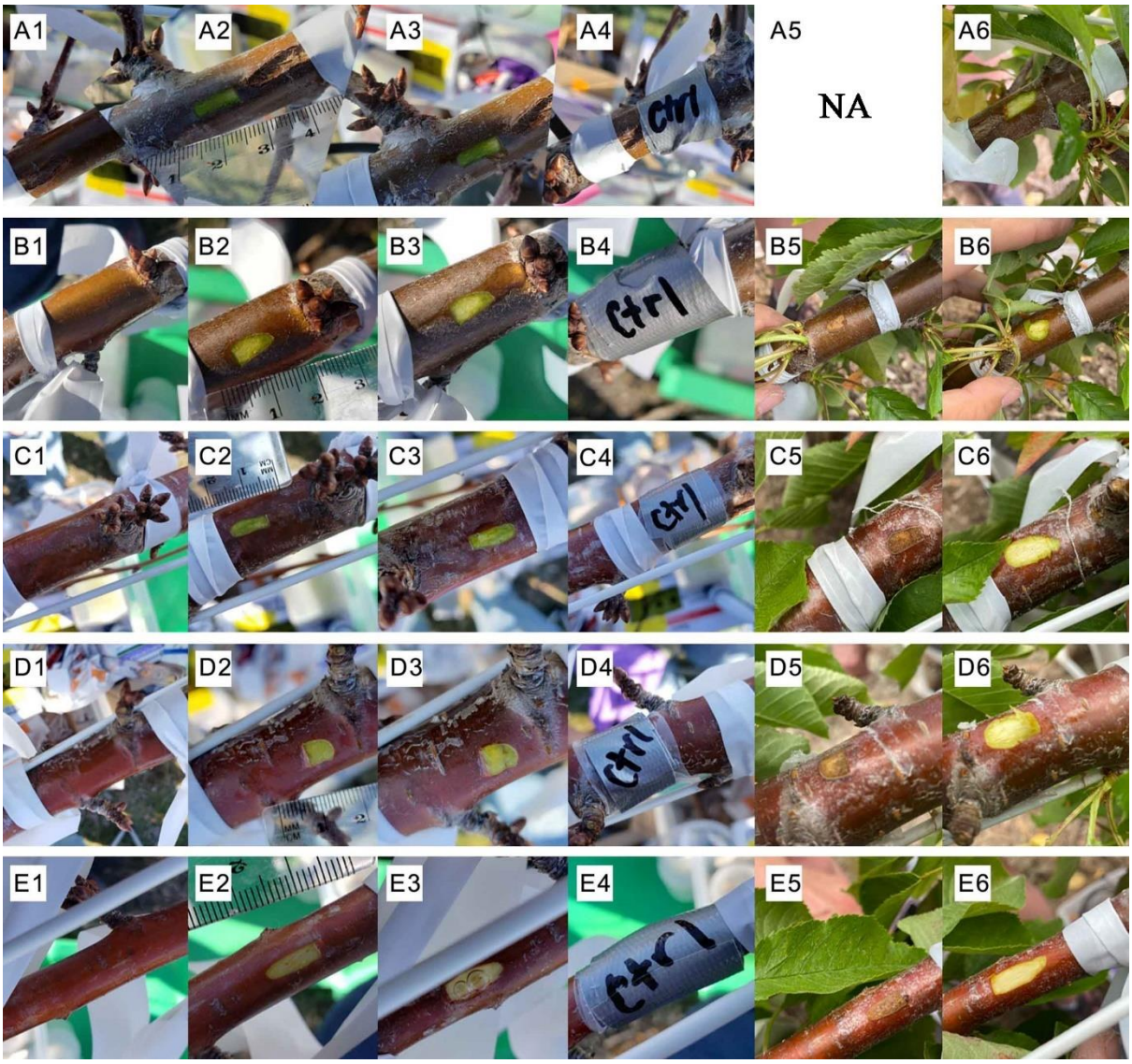


Figure A125. 2021 wound inoculation on 'Coral' cherry wood with PBS. **A1-E1)** The inoculation site before wounding. **A2-E2)** The inoculation site after wounding by sterile razor blade **A3-E3)** The inoculation site after pipetting inoculum into the wound. **A4-E4)** The inoculation site after covering with Parafilm and tape. **A5-E5)** The inoculation site exterior assessment in the spring. **A6-E6)** The inoculation site interior assessment in the spring. Images with NA are not available.

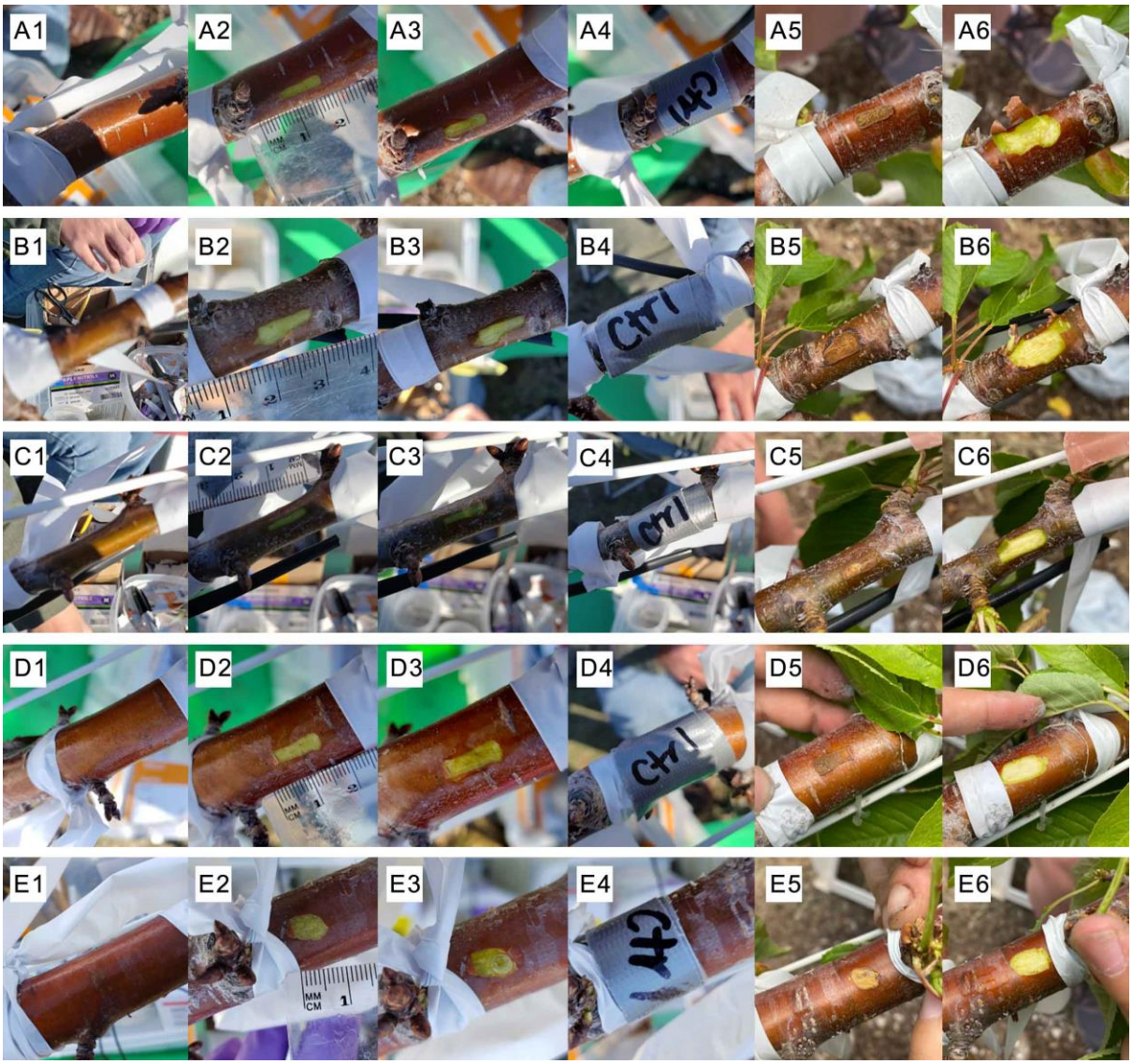


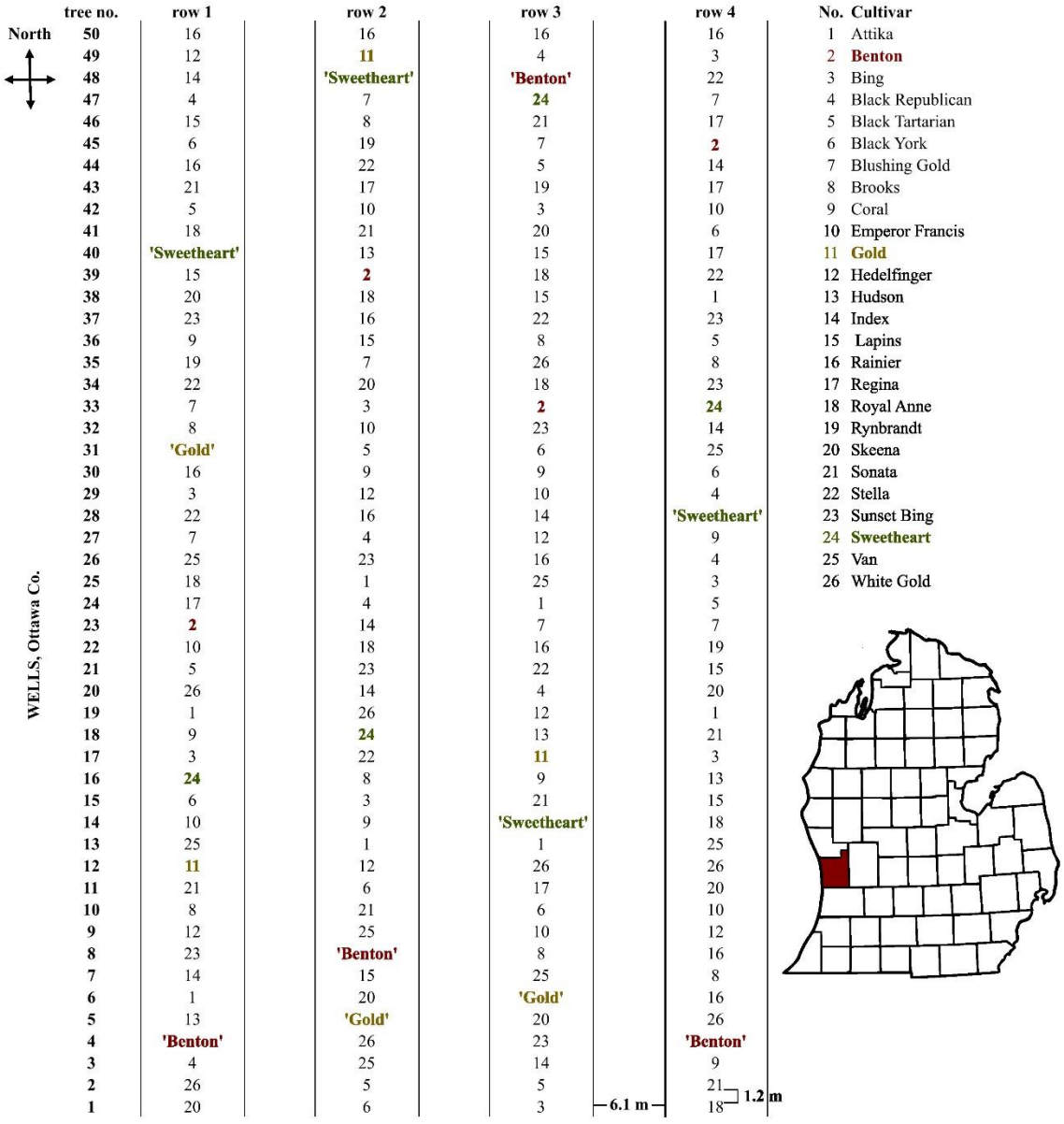
Figure A126. 2021 wound inoculation on 'Coral' cherry wood with PBS. **A1-E1)** The inoculation site before wounding. **A2-E2)** The inoculation site after wounding by sterile razor blade **A3-E3)** The inoculation site after pipetting inoculum into the wound. **A4-E4)** The inoculation site after covering with Parafilm and tape. **A5-E5)** The inoculation site exterior assessment in the spring. **A6-E6)** The inoculation site interior assessment in the spring.



Figure A127. 2021 wound inoculation on 'Coral' cherry wood with PBS. **A1-E1)** The inoculation site before wounding. **A2-E2)** The inoculation site after wounding by sterile razor blade **A3-E3)** The inoculation site after pipetting inoculum into the wound. **A4-E4)** The inoculation site after covering with Parafilm and tape. **A5-E5)** The inoculation site exterior assessment in the spring. **A6-E6)** The inoculation site interior assessment in the spring.



Figure A128. 2021 wound inoculation on 'Coral' cherry wood with PBS. **A1-E1)** The inoculation site before wounding. **A2-E2)** The inoculation site after wounding by sterile razor blade **A3-E3)** The inoculation site after pipetting inoculum into the wound. **A4-E4)** The inoculation site after covering with Parafilm and tape. **A5-E5)** The inoculation site exterior assessment in the spring. **A6-E6)** The inoculation site interior assessment in the spring.



tree no.	row 1	row 2	row 3	row 4
50	16	16	16	16
49	12	11	4	3
48	14	'Sweetheart'	'Benton'	22
47	4	7	24	7
46	15	8	21	17
45	6	19	7	2
44	16	22	5	14
43	21	17	19	17
42	5	10	3	10
41	18	21	20	6
40	'Sweetheart'	13	15	17
39	15	2	18	22
38	20	18	15	1
37	23	16	22	23
36	9	15	8	5
35	19	7	26	8
34	22	20	18	23
33	7	3	2	24
32	8	10	23	14
31	'Gold'	5	6	25
30	16	9	9	6
29	3	12	10	4
28	22	16	14	'Sweetheart'
27	7	4	12	9
26	25	23	16	4
25	18	1	25	3
24	17	4	1	5
23	2	14	7	7
22	10	18	16	19
21	5	23	22	15
20	26	14	4	20
19	1	26	12	1
18	9	24	13	21
17	3	22	11	3
16	24	8	9	13
15	6	3	21	15
14	10	9	'Sweetheart'	18
13	25	1	1	25
12	11	12	26	26
11	21	6	17	20
10	8	21	6	10
9	12	25	10	12
8	23	'Benton'	8	16
7	14	15	25	8
6	1	20	'Gold'	16
5	13	'Gold'	20	26
4	'Benton'	26	23	'Benton'
3	4	25	14	9
2	26	5	5	21
1	20	6	3	18

Figure B1. Map of the sweet cherries ‘Benton’ (4 trees), ‘Gold’ (3 trees), and ‘Sweetheart’ (4 trees), sampled for leaf microbiome analysis. Interplanted with 23 other cultivars (see key) in a completely randomized design in 4 rows, 50 trees/row, 1.2 m between trees, and 6.1 m alleywaysat site 1, Wells Orchards, Grand Rapids, MI (Ottawa county).

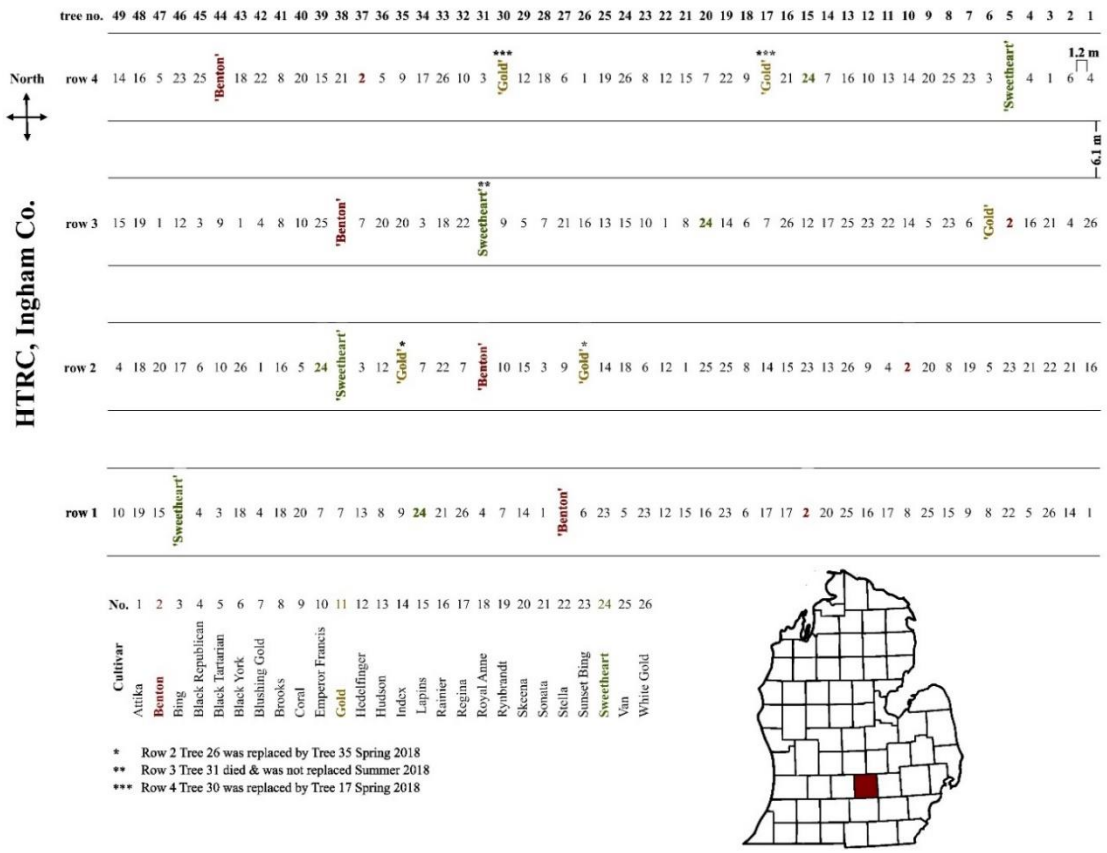


Figure B2. Map of the sweet cherries ‘Benton’ (4 trees), ‘Gold’ (3 trees), and ‘Sweetheart’ (4 trees), sampled for leaf microbiome analysis. Interplanted with 23 other cultivars (see key) in a completely randomized design in 4 rows, 49 trees/row, with 1.2 m between trees and 6.1 m alleyways at site 2, Michigan State University Horticulture Teaching and Research Center, Holt, MI, (Ingham county.), with asterisks indicating trees replaced due to mortality (see key).

Table B1. The sample numbers assigned to each leaf collected from the three sweet cherry cultivars (Benton, Gold, and Sweetheart) and controls (+ and −) for microbiome determination at the orchards in two regions of Michigan (site 1 and 2) with the corresponding row and tree number, in each season/year (Fall 2017, Spring 2018, Summer 2018, Fall 2018, Spring 2019, Summer 2019, and Fall 2019).

Season/Year	Site	Row	Tree	Leaf sample nos.	Cultivar	Site	Row	Tree	Sample nos.	Cultivar
Fall 2017	**1**	1	4	**1 - 4**	Benton	**2**	1	27	**45-48**	Benton
		1	31	**5 - 8**	Gold		1	46	**49-52**	Sweetheart
		1	40	**9 - 12**	Sweetheart		2	26	**53-56**	Gold
		2	5	**13 -16**	Gold		2	31	**57-60**	Benton
		2	8	**17-20**	Benton		2	38	**61-64**	Sweetheart
		2	48	**21-24**	Sweetheart		3	6	**65-68**	Gold
		3	6	**25-28**	Gold		3	31	**69-72**	Sweetheart
		3	14	**29-32**	Sweetheart		3	38	**73-76**	Benton
		3	48	**33-36**	Benton		4	5	**77-80**	Sweetheart
		4	4	**37-40**	Benton		4	30	**81-84**	Gold
		4	28	**41-44**	Sweetheart		4	44	**85-88**	Benton
									89	+ Ctrl “mock”
									90	− Ctrl
Spring 2018		1	4	**1 - 4**	Benton		1	27	**45-48**	Benton
		1	31	**5 - 8**	Gold		1	46	**49-52**	Sweetheart
		1	40	**9 - 12**	Sweetheart		2	31	**53-56**	Benton
		2	5	**13 -16**	Gold		2	35	**57-60**	Gold
		2	8	**17-20**	Benton		2	38	**61-64**	Sweetheart
		2	48	**21-24**	Sweetheart		3	6	**65-68**	Gold
		3	6	**25-28**	Gold		3	31	**69-72**	Sweetheart
		3	14	**29-32**	Sweetheart		3	38	**73-76**	Benton
		3	48	**33-36**	Benton		4	5	**77-80**	Sweetheart
		4	4	**37-40**	Benton		4	17	**81-84**	Gold
		4	28	**41-44**	Sweetheart		4	44	**85-88**	Benton

Table B1. (cont'd)

									89	+ Ctrl "mock"
									90	− Ctrl
Summer 2018	**1**	1	4	**1 - 4**	Benton	**2**	1	27	**45-48**	Benton
		1	31	**5 - 8**	Gold		1	46	**49-52**	Sweetheart
		1	40	**9 - 12**	Sweetheart		2	31	**53-56**	Benton
		2	5	**13 -16**	Gold		2	35	**57-60**	Gold
		2	8	**17-20**	Benton		2	38	**61-64**	Sweetheart
		2	48	**21-24**	Sweetheart		3	6	**65-68**	Gold
		3	6	**25-28**	Gold		3	38	**69-72**	Benton
		3	14	**29-32**	Sweetheart		4	5	**73-76**	Sweetheart
		3	48	**33-36**	Benton		4	17	**77-80**	Gold
		4	4	**37-40**	Benton		4	44	**81-84**	Benton
		4	28	**41-44**	Sweetheart				**85**	− Ctrl
									86	+ Ctrl "mock"
Fall 2018		1	4	**1-4**	Benton		1	27	**45-48**	Benton
		1	31	**5 - 8**	Gold		1	46	**49-52**	Sweetheart
		1	40	**9 - 12**	Sweetheart		2	31	**53-56**	Benton
		2	5	**13 -16**	Gold		2	35	**57-60**	Gold
		2	8	**17-20**	Benton		2	38	**61-64**	Sweetheart
		2	48	**21-24**	Sweetheart		3	6	**65-68**	Gold
		3	6	**25-28**	Gold		3	38	**69-72**	Benton
		3	14	**29-32**	Sweetheart		4	5	**73-76**	Sweetheart
		3	48	**33-36**	Benton		4	17	**77-80**	Gold
		4	4	**37-40**	Benton		4	44	**81-84**	Benton
		4	28	**41-44**	Sweetheart				**85**	+ Ctrl "mock"
									86	− Ctrl

Table B1. (cont'd)

Spring 2019	**1**	1	4	**1-4**	Benton	**2**	1	27	**45-48**	Benton
		1	31	**5 - 8**	Gold		1	46	**49-52**	Sweetheart
		1	40	**9 - 12**	Sweetheart		2	31	**53-56**	Benton
		2	5	**13 -16**	Gold		2	35	**57-60**	Gold
		2	8	**17-20**	Benton		2	38	**61-64**	Sweetheart
		2	48	**21-24**	Sweetheart		3	6	**65-68**	Gold
		3	6	**25-28**	Gold		3	38	**69-72**	Benton
		3	14	**29-32**	Sweetheart		4	5	**73-76**	Sweetheart
		3	48	**33-36**	Benton		4	17	**77-80**	Gold
		4	4	**37-40**	Benton		4	44	**81-84**	Benton
		4	28	**41-44**	Sweetheart				**85**	+ Ctrl "mock"
									86	− Ctrl
Summer 2019		1	4	**1-4**	Benton		1	27	**45-48**	Benton
		1	31	**5 - 8**	Gold		1	46	**49-52**	Sweetheart
		1	40	**9 - 12**	Sweetheart		2	31	**53-56**	Benton
		2	5	**13 -16**	Gold		2	35	**57-60**	Gold
		2	8	**17-20**	Benton		2	38	**61-64**	Sweetheart
		2	48	**21-24**	Sweetheart		3	6	**65-68**	Gold
		3	6	**25-28**	Gold		3	38	**69-72**	Benton
		3	14	**29-32**	Sweetheart		4	5	**73-76**	Sweetheart
		3	48	**33-36**	Benton		4	17	**77-80**	Gold
		4	4	**37-40**	Benton		4	44	**81-84**	Benton
		4	28	**41-44**	Sweetheart				**85**	+ Ctrl "mock"
									86	− Ctrl

Table B1. (cont'd)

Fall 2019	**1**	1	4	**1-4**	Benton	**2**	1	27	**45-48**	Benton
		1	31	**5 - 8**	Gold		1	46	**49-52**	Sweetheart
		1	40	**9 - 12**	Sweetheart		2	31	**53-56**	Benton
		2	5	**13 -16**	Gold		2	35	**57-60**	Gold
		2	8	**17-20**	Benton		2	38	**61-64**	Sweetheart
		2	48	**21-24**	Sweetheart		3	6	**65-68**	Gold
		3	6	**25-28**	Gold		3	38	**69-72**	Benton
		3	14	**29-32**	Sweetheart		4	5	**73-76**	Sweetheart
		3	48	**33-36**	Benton		4	17	**77-80**	Gold
		4	4	**37-40**	Benton		4	44	**81-84**	Benton
		4	28	**41-44**	Sweetheart				**85**	+ Ctrl "mock"
									86	− Ctrl

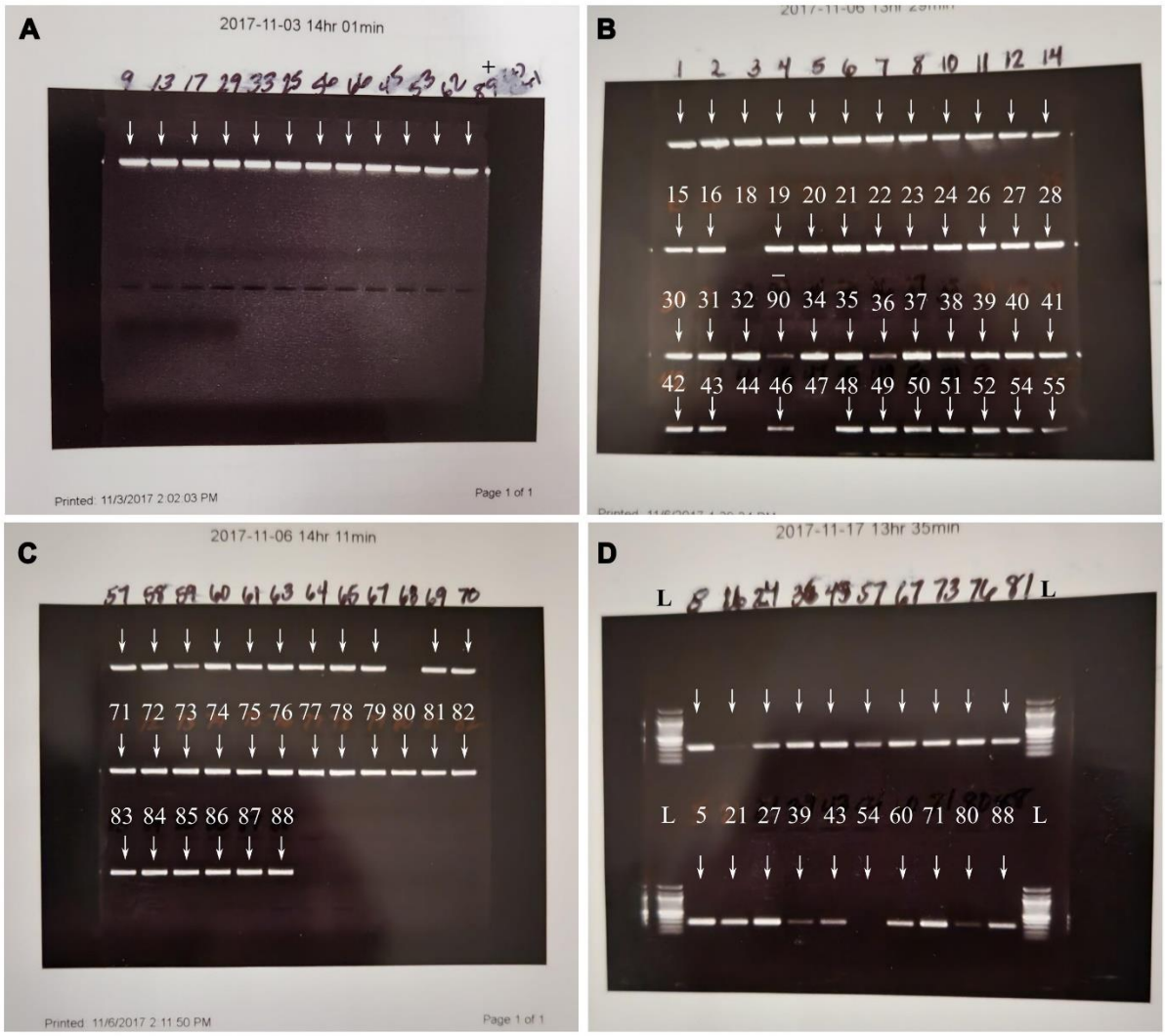


Figure B3. Gel images showing the amplification of the bacteria 16 S rDNA from the leaf samples collected in Fall 2017 from sweet cherry orchards in two regions of Michigan, **A-C)** where the arrows (↓) indicate the DNA samples that were sent for sequencing. The leaf sample numbers (above the bands) 1-44 are from orchard site one, numbers 45-88 are from orchard site two, and the controls (samples 89 and 90) are indicated with a + or – sign indicating the positive/"mock" control and negative/sans DNA control, respectively. The tree and cultivar identities of each sample no. are defined in Table B1, **D)** are some repeated amplifications of leaf sample DNA with the 100 bp DNA ladder (L) present.

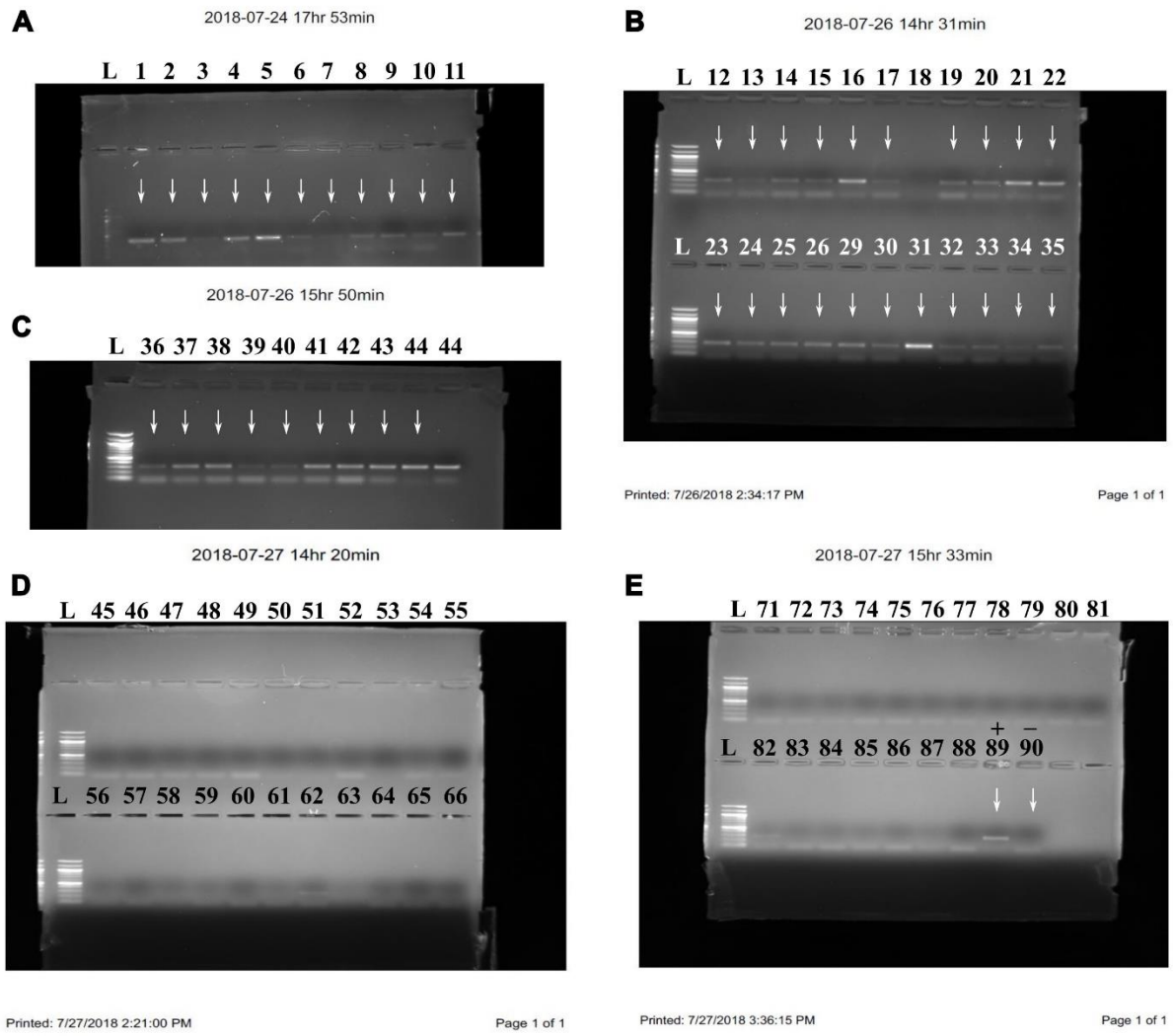


Figure B4. Gel images showing the amplification of the bacteria 16 S rDNA from the leaf samples collected in Spring 2018 from sweet cherry orchards in two regions of Michigan, where the arrows (↓) indicate the DNA samples that were sent for sequencing, **A-C)** are from orchard site one with the DNA sample nos. (above the bands) 1-44 (missing combined samples 27 and 28) with the 100 bp DNA ladder (L) present in the first lane of each gel, and **D-E)** are from orchard site two with the DNA sample nos. 45-88 (missing combined samples 67, 68, 69, and 70), the 100 bp DNA ladder (L) present in the first lane of each gel, and the controls (samples 89 and 90) are indicated with a + or – sign indicating the positive/"mock" control and negative/sans DNA control, respectively. The tree and cultivar identities of each sample no. are defined in Table B1.

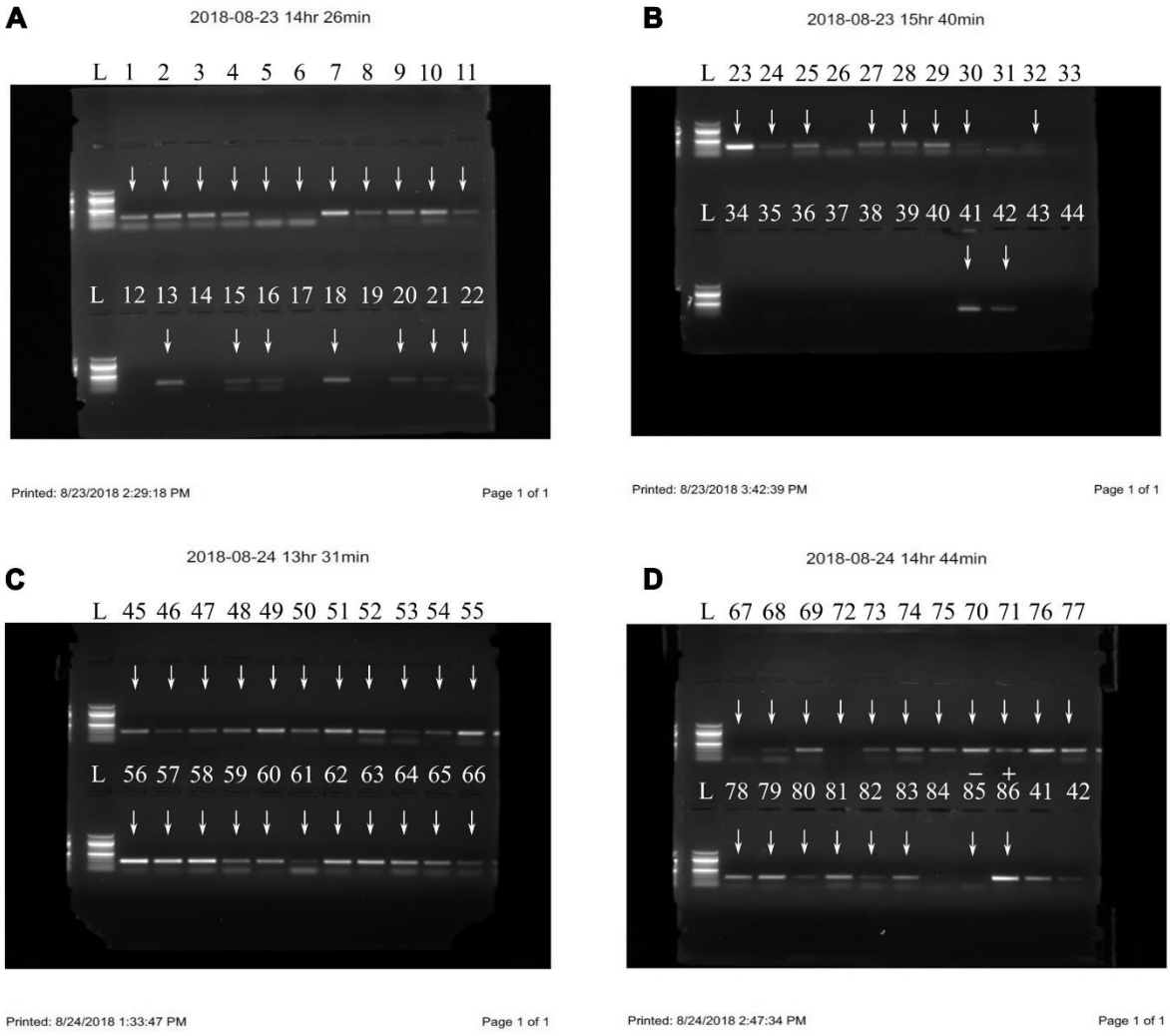


Figure B5. Gel images showing the amplification of the bacteria 16 S rDNA from the leaf samples collected in Summer 2018 from sweet cherry orchards in two regions of Michigan, where the arrows (↓) indicate the DNA samples that were sent for sequencing, **A-B)** are from orchard site one with the DNA sample nos. (above the bands) 1-44 with the 100 bp DNA ladder (L) present in the first lane of each gel, and **C-D)** are from orchard site two with the DNA sample nos. 45-84, the 100 bp DNA ladder (L) present in the first lane of each gel, and the controls (samples 86 and 85) are indicated with a + or – sign indicating the positive/"mock" control and negative/sans DNA control, respectively. The tree and cultivar identities of each sample no. are defined in Table B1.

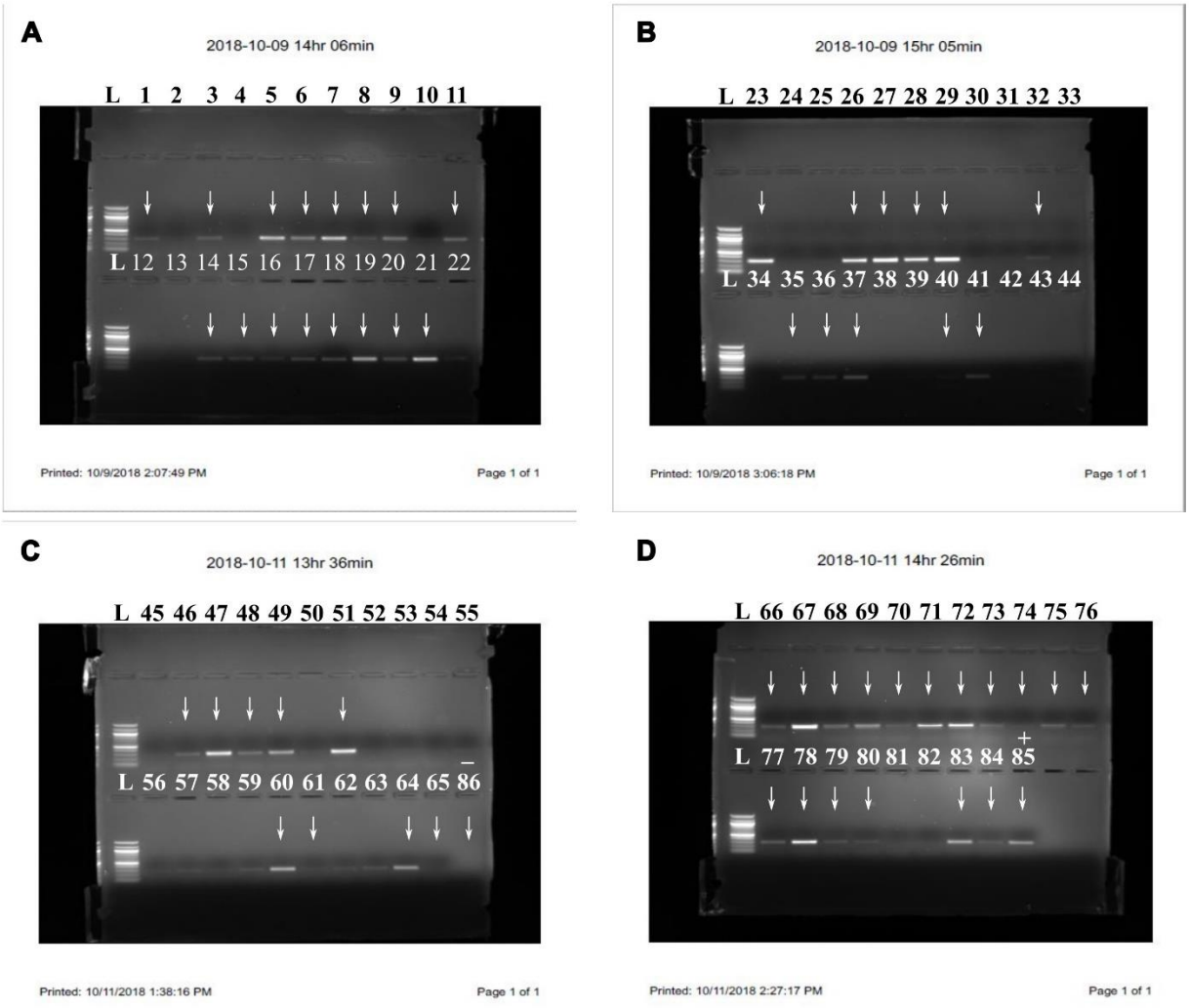


Figure B6. Gel images showing the amplification of the bacteria 16 S rDNA from the leaf samples collected in Fall 2018 from sweet cherry orchards in two regions of Michigan, where the arrows (↓) indicate the DNA samples that were sent for sequencing, **A-B)** are from orchard site one with the DNA sample nos. (above the bands) 1-44 with the 100 bp DNA ladder (L) present in the first lane of each gel, and **C-D)** are from orchard site two with the DNA sample nos. 45-84 (missing spilled sample 58), the 100 bp DNA ladder (L) present in the first lane of each gel, and the controls (samples 85 and 86) are indicated with a + or – sign indicating the positive/"mock" control and negative/sans DNA control, respectively. The tree and cultivar identities of each sample no. are defined in Table B1.

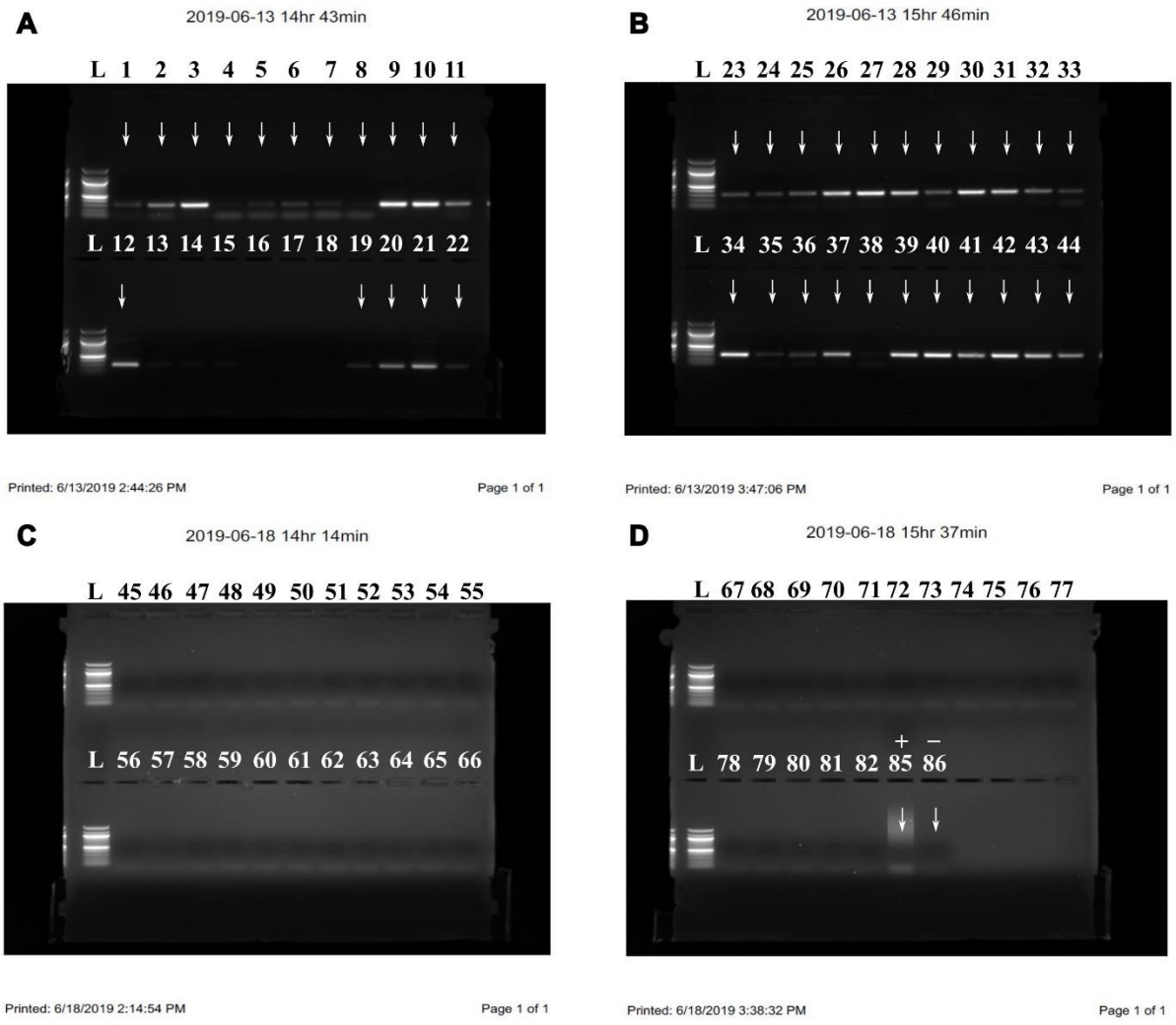


Figure B7. Gel images showing the amplification of the bacteria 16 S rDNA from the leaf samples collected in Spring 2019 (technical Rep 1) from sweet cherry orchards in two regions of Michigan, where the arrows (↓) indicate the DNA samples that were sent for sequencing, **A-B)** are from orchard site one with the DNA sample nos. (above the bands) 1-44 with the 100 bp DNA ladder (L) present in the first lane of each gel, and **C-D)** are from orchard site two with the DNA sample nos. 45-84 (missing combined samples 83 and 84), the 100 bp DNA ladder (L) present in the first lane of each gel, and the controls (samples 85 and 86) are indicated with a + or – sign indicating the positive/"mock" control and negative/sans DNA control, respectively. The tree and cultivar identities of each sample no. are defined in Table B1.

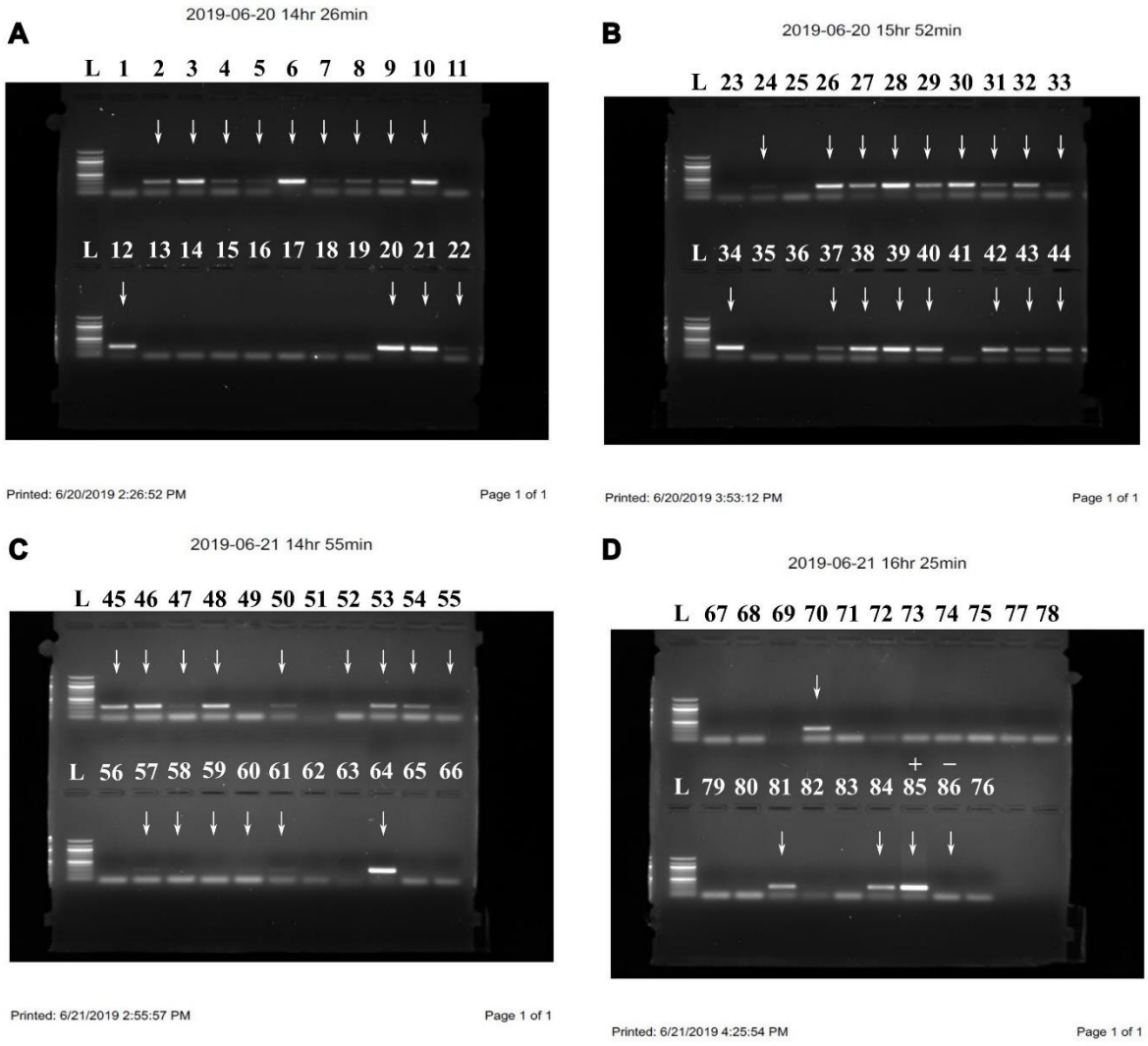


Figure B8. Gel images showing the amplification of the bacteria 16 S rDNA from the leaf samples collected in Spring 2019 (technical Rep 2) from sweet cherry orchards in two regions of Michigan, where the arrows (↓) indicate the DNA samples that were sent for sequencing, **A-B)** are from orchard site one with the DNA sample nos. (above the bands) 1-44 with the 100 bp DNA ladder (L) present in the first lane of each gel, and **C-D)** are from orchard site two with the DNA sample nos. 45-84, the 100 bp DNA ladder (L) present in the first lane of each gel, and the controls (samples 85 and 86) are indicated with a + or – sign indicating the positive/"mock" control and negative/sans DNA control, respectively. The tree and cultivar identities of each sample no. are defined in Table B1.

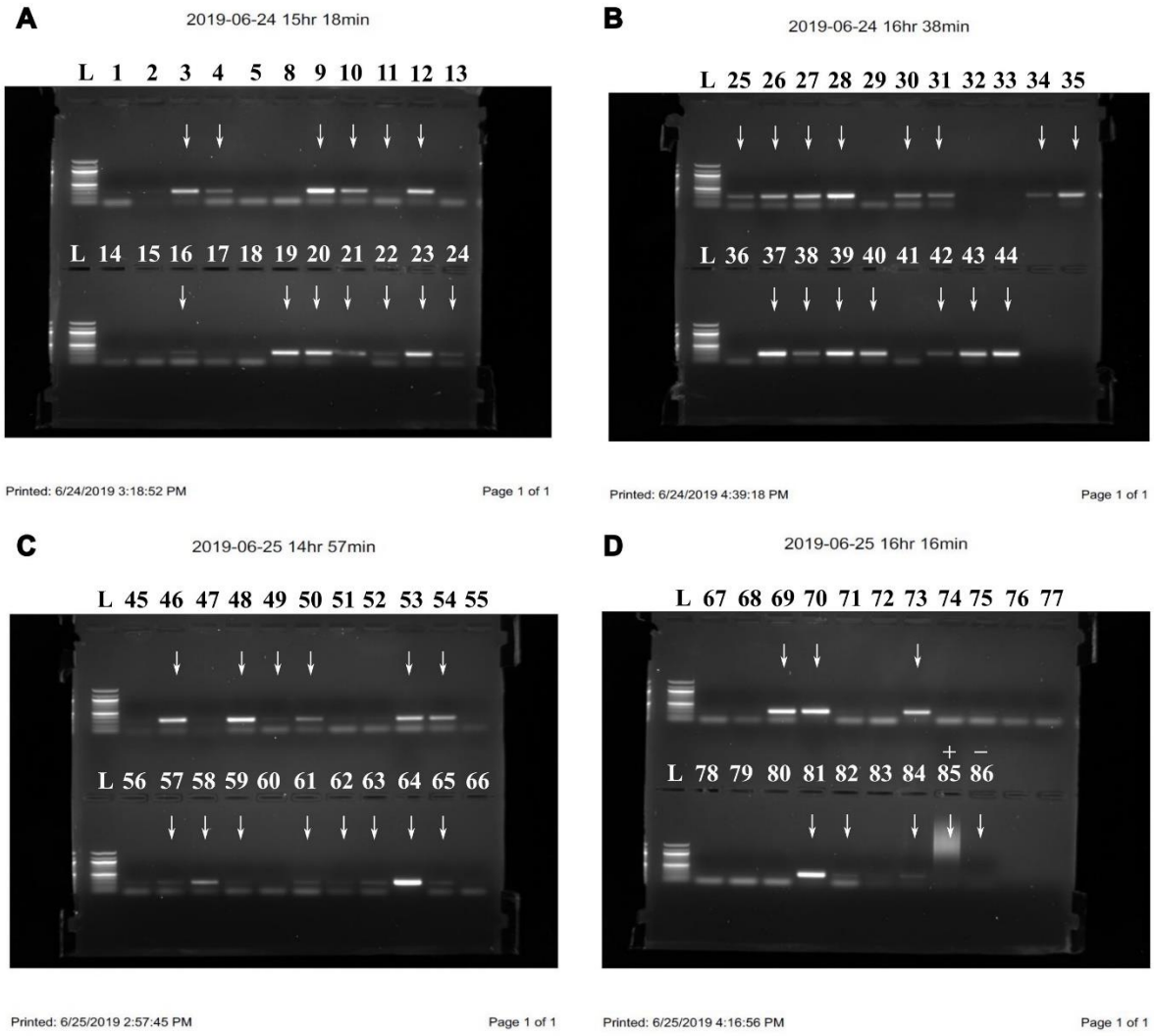


Figure B9. Gel images showing the amplification of the bacteria 16 S rDNA from the leaf samples collected in Spring 2019 (technical Rep 3) from sweet cherry orchards in two regions of Michigan, where the arrows (↓) indicate the DNA samples that were sent for sequencing, **A-B)** are from orchard site one with the DNA sample nos. (above the bands) 1-44 (missing combined samples 6 and 7) with the 100 bp DNA ladder (L) present in the first lane of each gel, and **C-D)** are from orchard site two with the DNA sample nos. 45-84, the 100 bp DNA ladder (L) present in the first lane of each gel, and the controls (samples 85 and 86) are indicated with a + or – sign indicating the positive/"mock" control and negative/sans DNA control, respectively. The tree and cultivar identities of each sample no. are defined in Table B1.

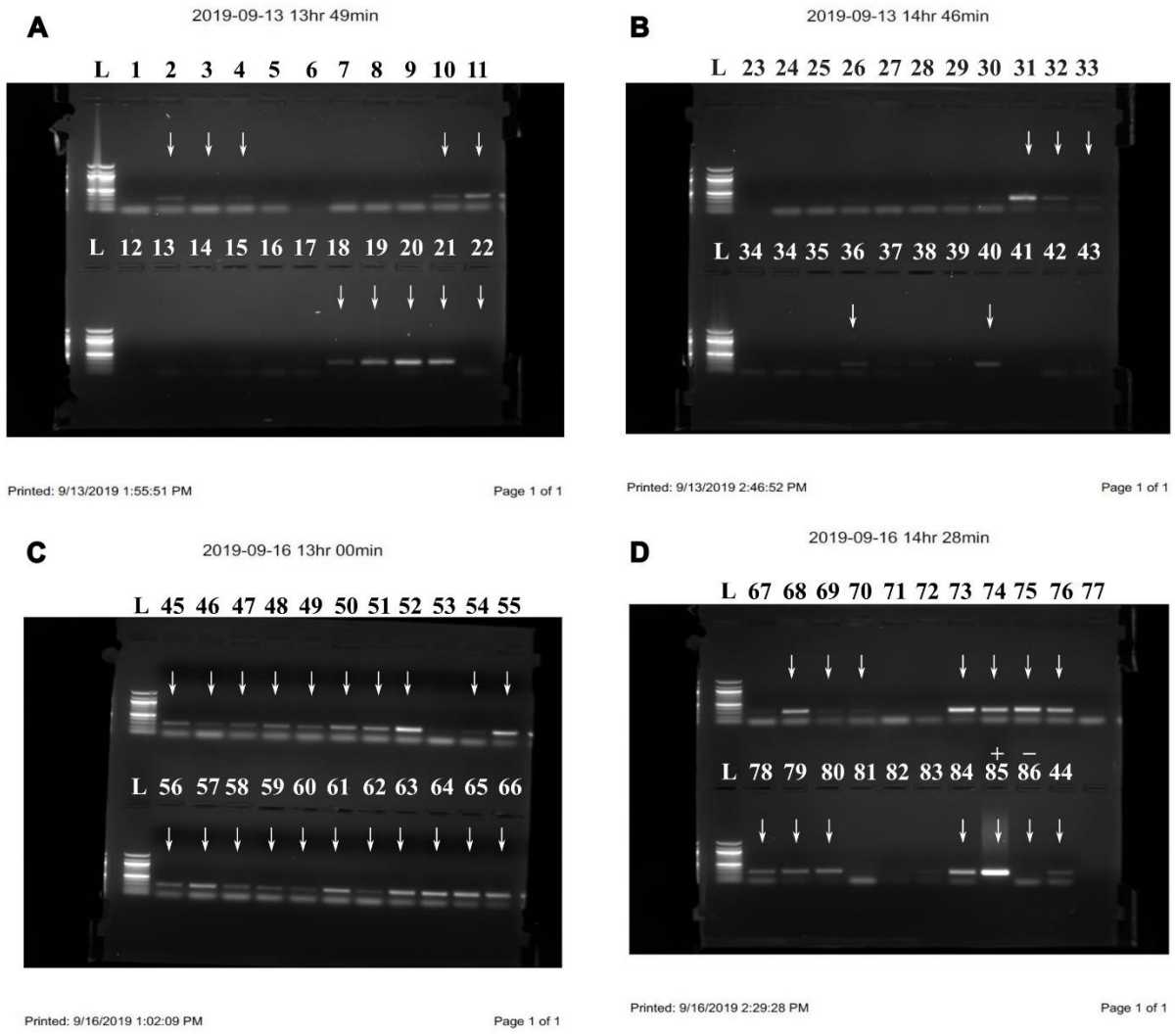


Figure B10. Gel images showing the amplification of the bacteria 16 S rDNA from the leaf samples collected in Summer 2019 (technical Rep 1) from sweet cherry orchards in two regions of Michigan, where the arrows (↓) indicate the DNA samples that were sent for sequencing, **A-B)** are from orchard site one with the DNA sample nos. (above the bands) 1-44 with the 100 bp DNA ladder (L) present in the first lane of each gel, and **C-D)** are from orchard site two with the DNA sample nos. 45-84, the 100 bp DNA ladder (L) present in the first lane of each gel, and the controls (samples 85 and 86) are indicated with a + or – sign indicating the positive/"mock" control and negative/sans DNA control, respectively. The tree and cultivar identities of each sample no. are defined in Table B1.

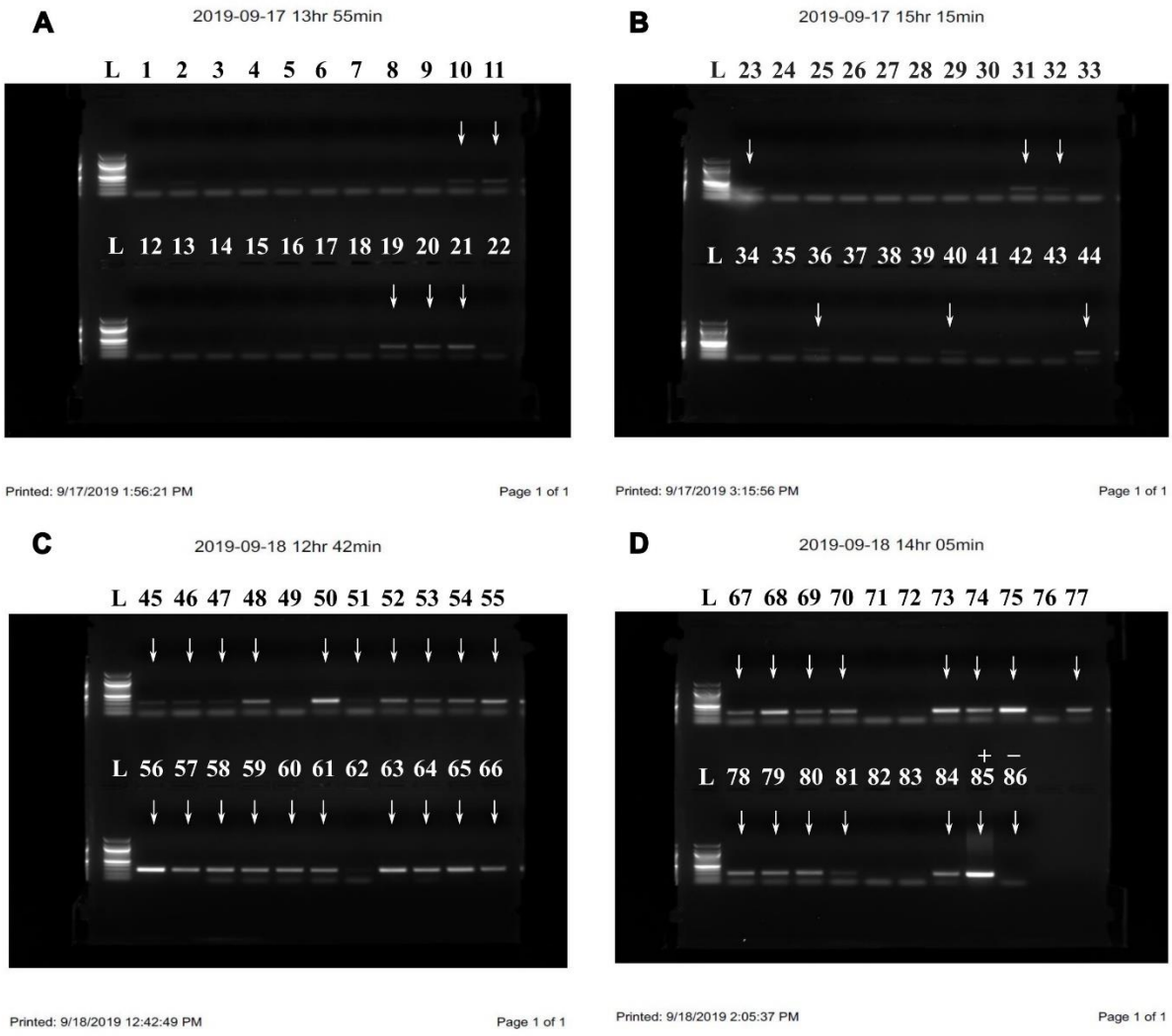


Figure B11. Gel images showing the amplification of the bacteria 16 S rDNA from the leaf samples collected in Summer 2019 (technical Rep 2) from sweet cherry orchards in two regions of Michigan, where the arrows (↓) indicate the DNA samples that were sent for sequencing, **A-B)** are from orchard site one with the DNA sample nos. (above the bands) 1-44 with the 100 bp DNA ladder (L) present in the first lane of each gel, and **C-D)** are from orchard site two with the DNA sample nos. 45-84, the 100 bp DNA ladder (L) present in the first lane of each gel, and the controls (samples 85 and 86) are indicated with a + or – sign indicating the positive/"mock" control and negative/sans DNA control, respectively. The tree and cultivar identities of each sample no. are defined in Table B1.

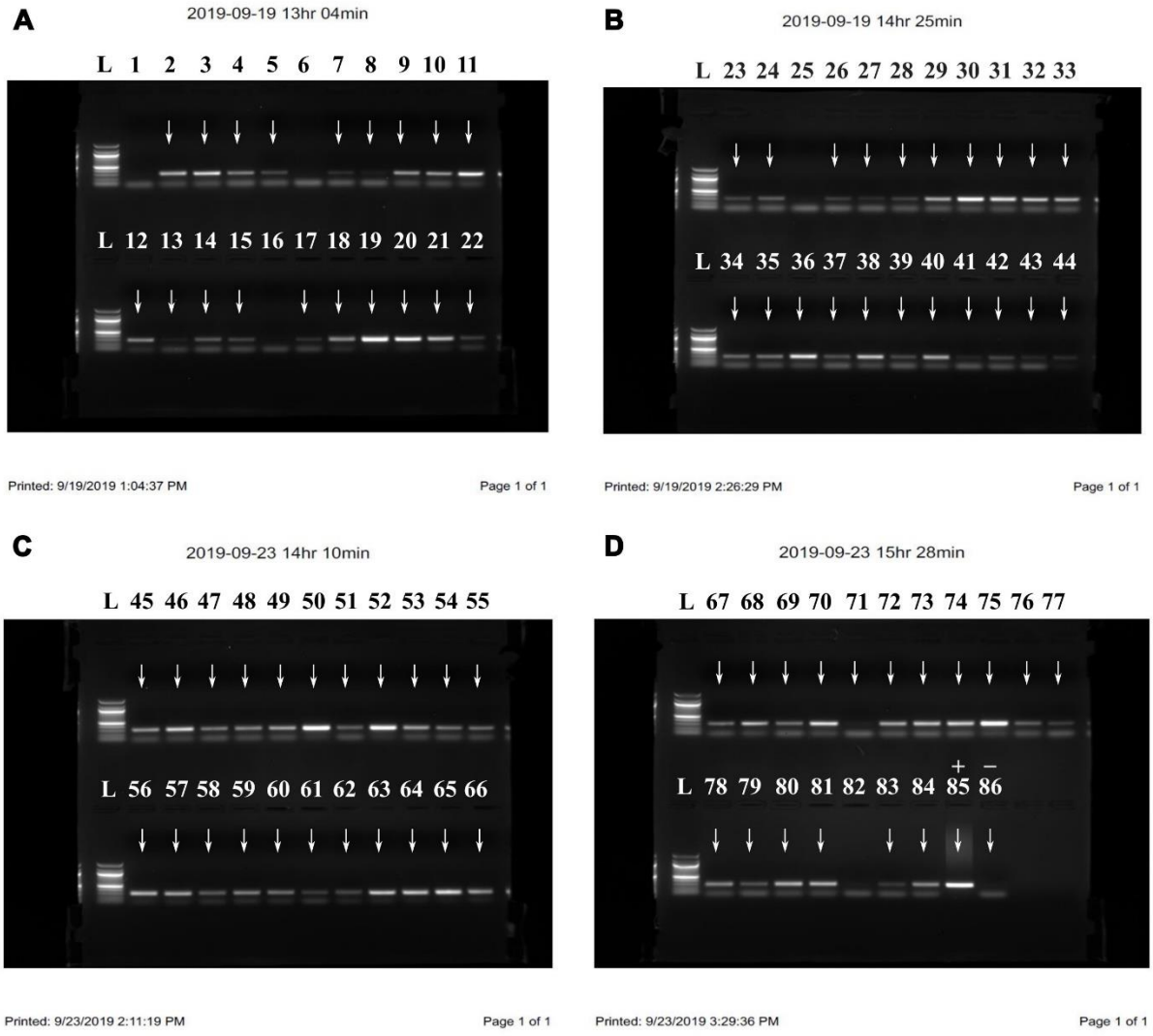


Figure B12. Gel images showing the amplification of the bacteria 16 S rDNA from the leaf samples collected in Summer 2019 (technical Rep 3) from sweet cherry orchards in two regions of Michigan, where the arrows (↓) indicate the DNA samples that were sent for sequencing, **A-B)** are from orchard site one with the DNA sample nos. (above the bands) 1-44 with the 100 bp DNA ladder (L) present in the first lane of each gel, and **C-D)** are from orchard site two with the DNA sample nos. 45-84, the 100 bp DNA ladder (L) present in the first lane of each gel, and the controls (samples 85 and 86) are indicated with a + or – sign indicating the positive/"mock" control and negative/sans DNA control, respectively. The tree and cultivar identities of each sample no. are defined in Table B1.

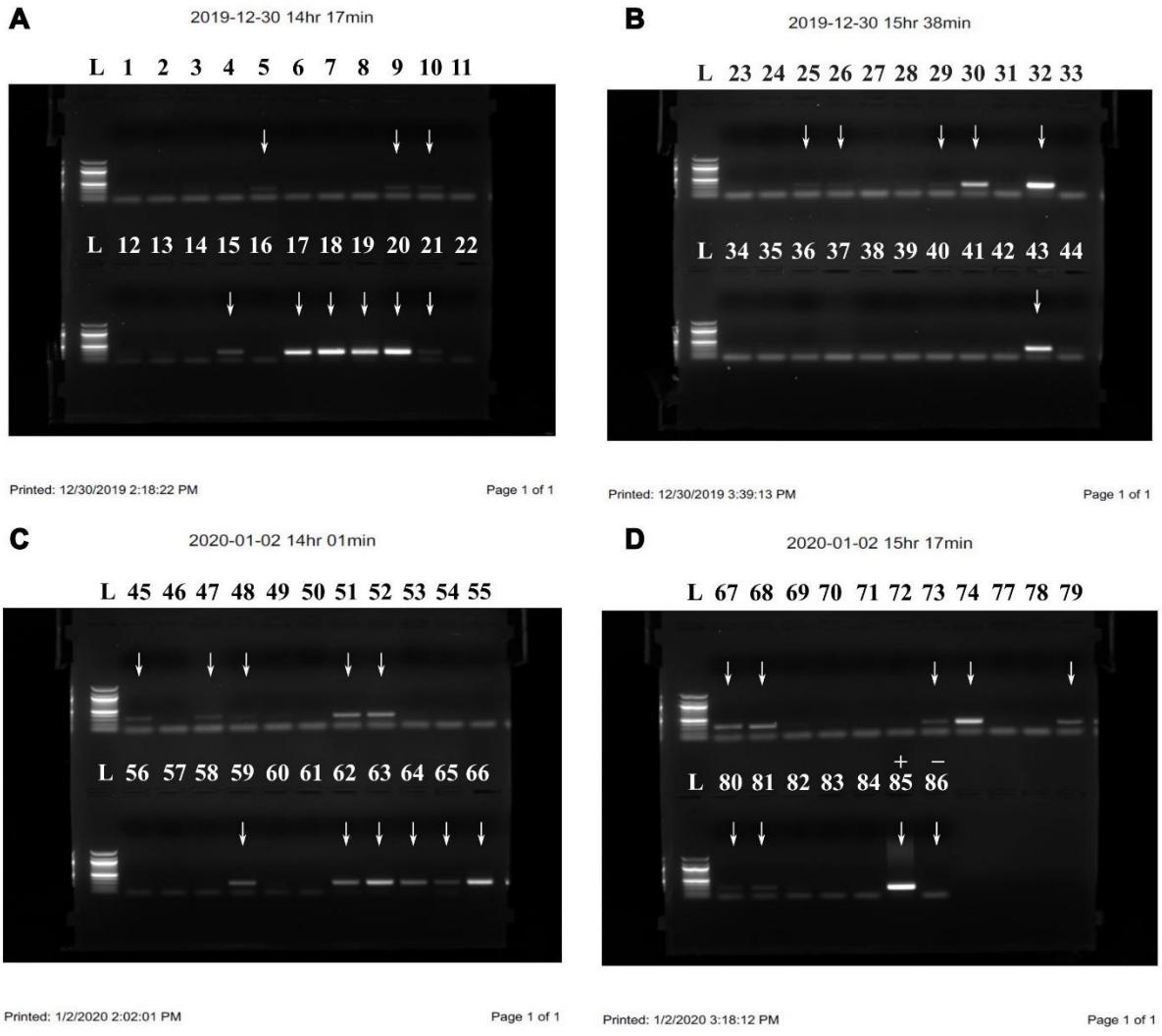


Figure B13. Gel images showing the amplification of the bacteria 16 S rDNA from the leaf samples collected in Fall 2019 (technical Rep 1) from sweet cherry orchards in two regions of Michigan, where the arrows (↓) indicate the DNA samples that were sent for sequencing, **A-B)** are from orchard site one with the DNA sample nos. (above the bands) 1-44 with the 100 bp DNA ladder (L) present in the first lane of each gel, and **C-D)** are from orchard site two with the DNA sample nos. 45-84 (missing combined samples 75 and 76), the 100 bp DNA ladder (L) present in the first lane of each gel, and the controls (samples 85 and 86) are indicated with a + or – sign indicating the positive/"mock" control and negative/sans DNA control, respectively. The tree and cultivar identities of each sample no. are defined in Table B1.

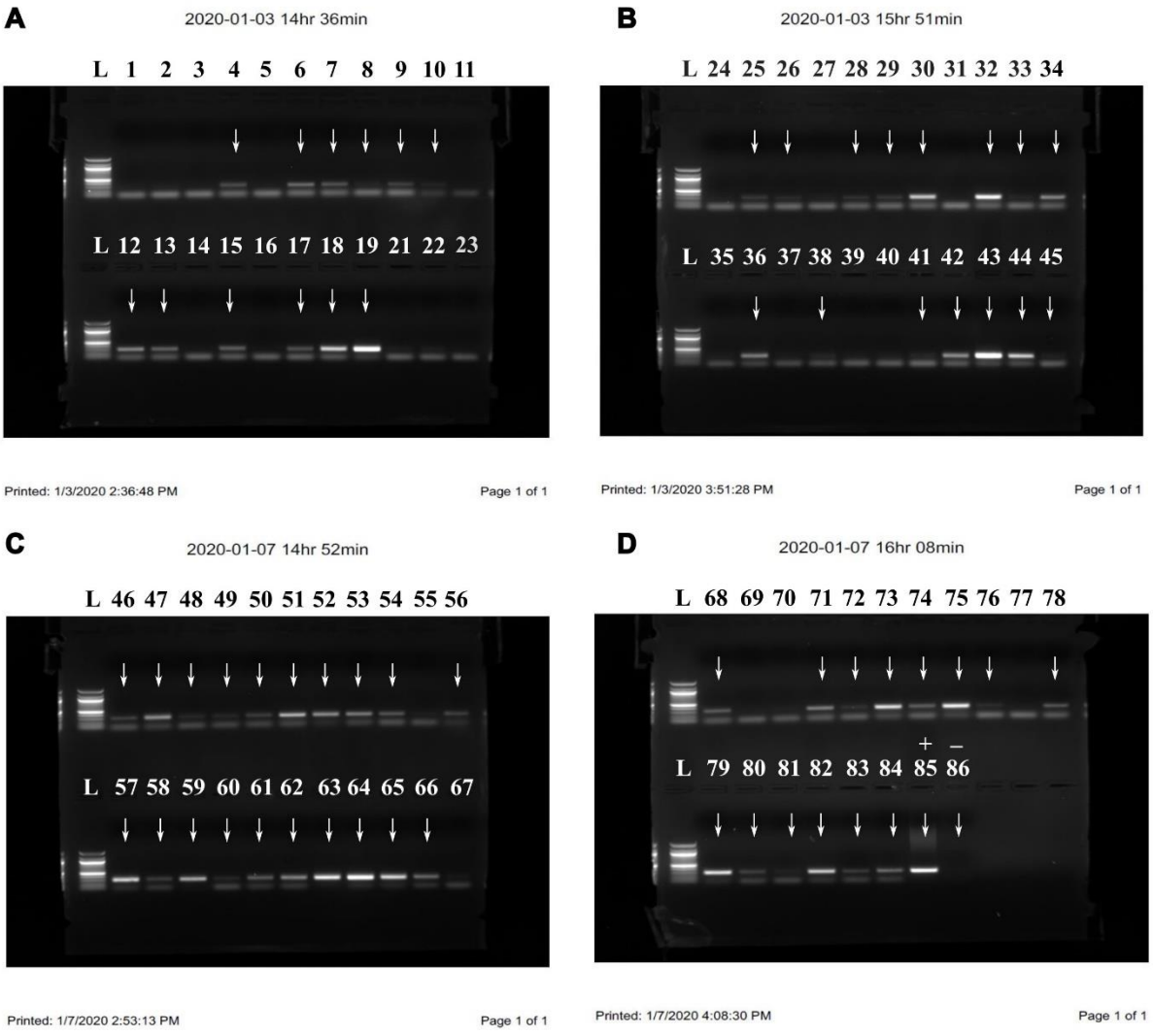


Figure B14. Gel images showing the amplification of the bacteria 16 S rDNA from the leaf samples collected in Fall 2019 (technical Rep 2) from sweet cherry orchards in two regions of Michigan, where the arrows (↓) indicate the DNA samples that were sent for sequencing, **A-B)** are from orchard site one with the DNA sample nos. (above the bands) 1-44 (missing spilled sample 20) with the 100 bp DNA ladder (L) present in the first lane of each gel, and **C-D)** are from orchard site two with the DNA sample nos. 45-84, the 100 bp DNA ladder (L) present in the first lane of each gel, and the controls (samples 85 and 86) are indicated with a + or – sign indicating the positive/"mock" control and negative/sans DNA control, respectively. The tree and cultivar identities of each sample no. are defined in Table B1.

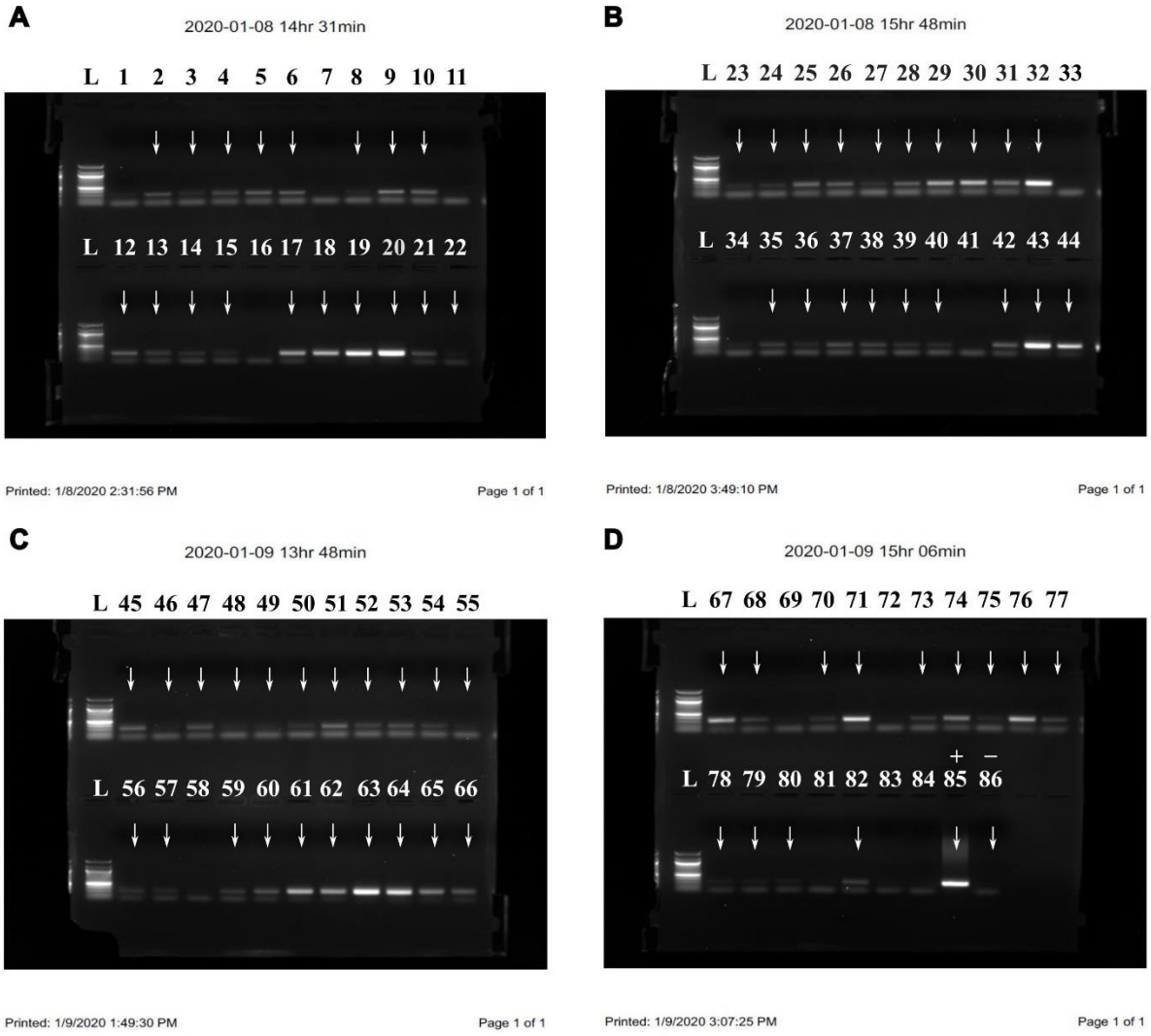


Figure B15. Gel images showing the amplification of the bacteria 16 S rDNA from the leaf samples collected in Fall 2019 (technical Rep 3) from sweet cherry orchards in two regions of Michigan, where the arrows (↓) indicate the DNA samples that were sent for sequencing, **A-B)** are from orchard site one with the DNA sample nos. (above the bands) 1-44 with the 100 bp DNA ladder (L) present in the first lane of each gel, and **C-D)** are from orchard site two with the DNA sample nos. 45-84, the 100 bp DNA ladder (L) present in the first lane of each gel, and the controls (samples 85 and 86) are indicated with a + or – sign indicating the positive/"mock" control and negative/sans DNA control, respectively. The tree and cultivar identities of each sample no. are defined in Table B1.

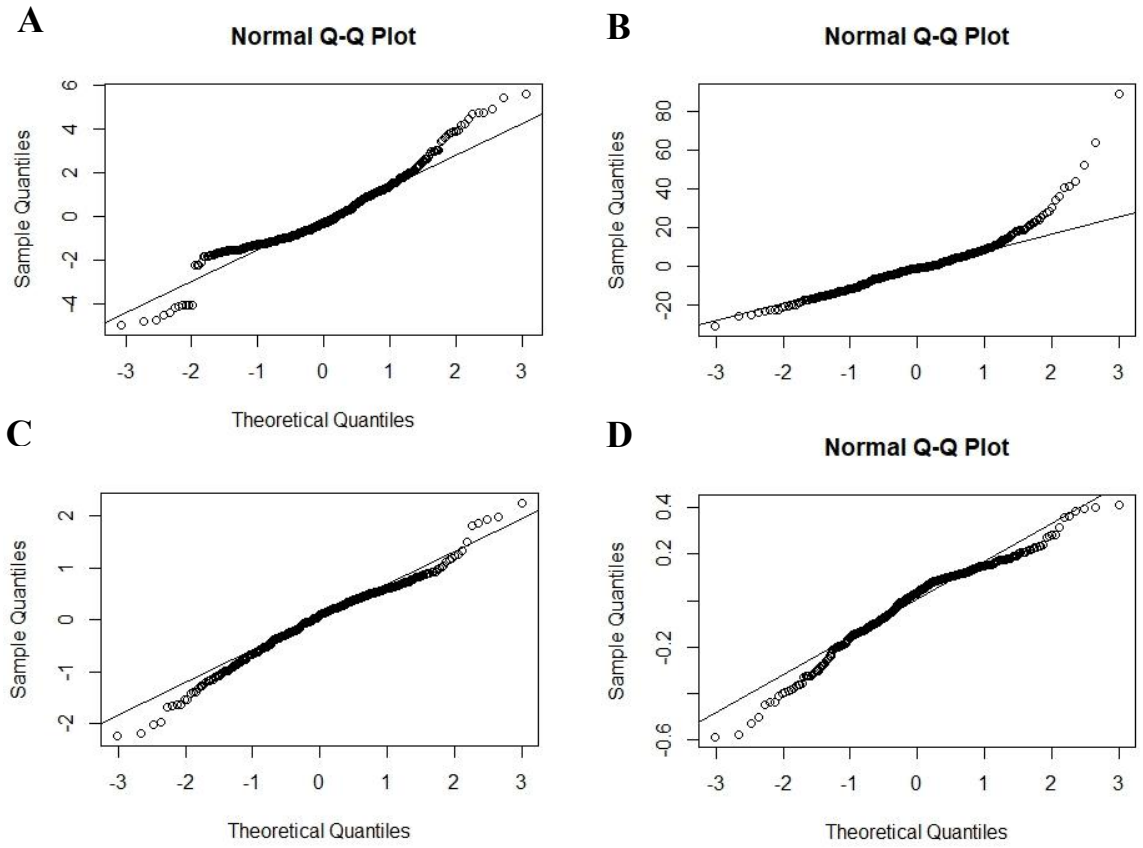


Figure B16. The quantile-quantile plots (qqplot) of the residuals for graphical visualization of the distribution of the alpha diversity statistics data, **A)** bacteria plate counts (log cfu/cm^2), **B)** the number of otus (no. otus), **C)** the Shannon diversity, and **D)** Shannon evenness indices.

Table B2. The mean log cfu/cm^2 of leaf area ± SE of bacteria plate counts for each sampling time point, including the pairwise comparisons of the estimated marginal means with the confidence limits (lower and upper C.L.) and the p-value. Letters indicate statistical differences, with significance determined by p-value ≤ 0.05.

Time	Mean log cfu/cm^2	SE	df	lower C.L.	upper C.L.	
2017 Fall	4.9	0.2	84	4.5	5.4	bc
2018 Spring	1.0	0.2	60	0.6	1.4	a
2018 Summer	4.4	0.2	105	4.0	4.9	b
2018 Fall	6.7	0.5	371	5.8	7.6	d
2019 Spring	1.5	0.2	53	1.1	1.9	a
2019 Summer	5.4	0.2	53	5.0	5.8	cd
2019 Fall	5.6	0.2	53	5.2	6.0	cd

Contrast	estimate	SE	df	t-ratio	p-value
2017 Fall v. 2018 Fall	-1.8	0.5	444	-3.576	0.0071
2017 Fall v. 2018 Spring	3.9	0.3	443	13.989	<0.0001
2017 Fall v. 2018 Summer	0.5	0.3	441	1.591	0.6881
2017 Fall v. 2019 Fall	-0.7	0.3	440	-2.424	0.1910
2017 Fall v. 2019 Spring	3.4	0.3	440	12.346	<0.0001
2017 Fall v. 2019 Summer	-0.4	0.3	441	-1.588	0.6901
2018 Fall v. 2018 Spring	5.7	0.5	444	11.803	<0.0001
2018 Fall v. 2018 Summer	2.2	0.5	444	4.502	0.0002
2018 Fall v. 2019 Fall	1.1	0.5	443	2.267	0.2627
2018 Fall v. 2019 Spring	5.2	0.5	443	10.795	<0.0001
2018 Fall v. 2019 Summer	1.3	0.5	443	2.743	0.0902
2018 Spring v. 2018 Summer	-3.4	0.3	436	-11.819	<0.0001
2018 Spring v. 2019 Fall	-4.6	0.3	434	-17.927	<0.0001
2018 Spring v. 2019 Spring	-0.5	0.3	434	-2.066	0.3751
2018 Spring v. 2019 Summer	-4.4	0.3	435	-16.985	<0.0001
2018 Summer v. 2019 Fall	-1.2	0.3	432	-4.054	0.0012
2018 Summer v. 2019 Spring	2.9	0.3	432	10.194	<0.0001
2018 Summer v. 2019 Summer	-0.9	0.3	432	-3.244	0.0215
2019 Fall v. 2019 Spring	4.1	0.3	427	16.310	<0.0001
2019 Fall v. 2019 Summer	0.2	0.3	427	0.915	0.9701
2019 Spring v. 2019 Summer	-3.8	0.3	427	-15.344	<0.0001

Table B3. The mean number of OTUs ± SE at each sampling time point including the pairwise comparisons of the estimated marginal means with the confidence limits (lower and upper C.L.) and the p-value. Letters indicate statistical differences, with significance determined by p-value ≤ 0.05.

Time	Mean no. OTUs	SE	df	lower C.L.	upper C.L.	
2017 Fall	18.3	1.6	43	15.1	21.4	a
2018 Spring	40.6	2.4	167	35.9	45.3	b
2018 Summer	35.7	1.8	63	32.2	39.2	bc
2018 Fall	34.7	1.9	84	30.9	38.5	bc
2019 Spring	6.0	2.4	162	1.3	10.7	d
2019 Summer	22.2	1.8	69	18.7	25.8	a
2019 Fall	31.2	2.1	111	27.1	35.3	c

contrast	estimate	SE	df	t-ratio	p-value
2017 Fall v. 2018 Fall	-16.4	2.3	371	-7.075	<0.0001
2017 Fall v. 2018 Spring	-22.4	2.7	364	-8.234	<0.0001
2017 Fall v. 2018 Summer	-17.4	2.2	371	-7.933	<0.0001
2017 Fall v. 2019 Fall	-12.9	2.5	369	-5.273	<0.0001
2017 Fall v. 2019 Spring	12.3	2.7	368	4.568	0.0001
2017 Fall v. 2019 Summer	-3.9	2.2	370	-1.788	0.5573
2018 Fall v. 2018 Spring	-6.0	2.9	360	-2.042	0.3901
2018 Fall v. 2018 Summer	-1.0	2.4	363	-0.425	0.9995
2018 Fall v. 2019 Fall	3.5	2.7	365	1.309	0.8475
2018 Fall v. 2019 Spring	28.7	2.9	366	9.877	<0.0001
2018 Fall v. 2019 Summer	12.5	2.5	363	5.094	<0.0001
2018 Spring v. 2018 Summer	4.9	2.9	360	1.726	0.5988
2018 Spring v. 2019 Fall	9.4	3.0	363	3.101	0.0337
2018 Spring v. 2019 Spring	34.6	3.2	363	10.970	<0.0001
2018 Spring v. 2019 Summer	18.4	2.9	359	6.450	<0.0001
2018 Summer v. 2019 Fall	4.5	2.5	364	1.778	0.5637
2018 Summer v. 2019 Spring	29.7	2.8	367	10.523	<0.0001
2018 Summer v. 2019 Summer	13.5	2.3	362	5.822	<0.0001
2019 Fall v. 2019 Spring	25.2	3.0	371	8.318	<0.0001
2019 Fall v. 2019 Summer	9.0	2.6	364	3.518	0.0088
2019 Spring v. 2019 Summer	-16.2	2.8	365	-5.769	<0.0001

Table B4. The mean Shannon diversity index ± SE at each sampling time point, including the pairwise comparisons of the estimated marginal means with the confidence limits (lower and upper C.L.) and the p-value. Letters indicate statistical differences, with significance determined by p-value ≤ 0.05.

Time	Mean Shannon diversity index	SE	df	lower C.L.	upper C.L.	
2017 Fall	1.4	0.1	81	1.3	1.6	ab
2018 Spring	2.4	0.1	255	2.1	2.6	c
2018 Summer	1.6	0.1	111	1.4	1.8	ab
2018 Fall	1.8	0.1	143	1.6	1.9	ab
2019 Spring	0.3	0.1	246	0.1	0.6	d
2019 Summer	1.4	0.1	127	1.2	1.6	b
2019 Fall	1.8	0.1	187	1.6	2.0	a

contrast	estimate	SE	df	t-ratio	p-value
2017 Fall v. 2018 Fall	-0.3	0.1	372	-2.691	0.1033
2017 Fall v. 2018 Spring	-0.9	0.1	365	-6.565	<0.0001
2017 Fall v. 2018 Summer	-0.2	0.1	372	-1.423	0.7892
2017 Fall v. 2019 Fall	-0.4	0.1	367	-2.807	0.0768
2017 Fall v. 2019 Spring	1.1	0.1	371	7.955	<0.0001
2017 Fall v. 2019 Summer	0.0	0.1	370	0.373	0.9998
2018 Fall v. 2018 Spring	-0.6	0.2	363	-3.975	0.0016
2018 Fall v. 2018 Summer	0.2	0.1	366	1.273	0.8638
2018 Fall v. 2019 Fall	0.0	0.1	370	-0.234	1.0000
2018 Fall v. 2019 Spring	1.4	0.2	370	9.485	<0.0001
2018 Fall v. 2019 Summer	0.4	0.1	367	2.869	0.0651
2018 Spring v. 2018 Summer	0.8	0.2	363	5.156	<0.0001
2018 Spring v. 2019 Fall	0.6	0.2	367	3.609	0.0064
2018 Spring v. 2019 Spring	2.1	0.2	368	12.394	<0.0001
2018 Spring v. 2019 Summer	1.0	0.2	362	6.515	<0.0001
2018 Summer v. 2019 Fall	-0.2	0.1	369	-1.464	0.7658
2018 Summer v. 2019 Spring	1.3	0.1	371	8.661	<0.0001
2018 Summer v. 2019 Summer	0.2	0.1	366	1.691	0.6227
2019 Fall v. 2019 Spring	1.5	0.2	372	9.321	<0.0001
2019 Fall v. 2019 Summer	0.4	0.1	369	2.996	0.0457
2019 Spring v. 2019 Summer	-1.1	0.1	369	-7.297	<0.0001

Table B5. The mean Shannon evenness index ± SE at each sampling time point, including the pairwise comparisons of the estimated marginal means with the confidence limits (lower and upper C.L.) and the p-value. Letters indicate statistical differences, with significance determined by p-value ≤ 0.05.

Time	Mean Shannon evenness index	SE	df	lower C.L.	upper C.L.	
2017 Fall	0.5	0.02	83	0.5	0.5	a
2018 Spring	0.6	0.03	257	0.6	0.7	b
2018 Summer	0.4	0.02	112	0.4	0.5	a
2018 Fall	0.5	0.02	145	0.4	0.5	a
2019 Spring	0.2	0.03	248	0.1	0.2	c
2019 Summer	0.4	0.02	130	0.4	0.5	a
2019 Fall	0.5	0.03	190	0.5	0.6	ab

contrast	estimate	SE	df	t-ratio	p-value
2017 Fall v. 2018 Fall	0.01	0.03	372	0.236	1.0000
2017 Fall v. 2018 Spring	-0.15	0.04	365	-4.044	0.0012
2017 Fall v. 2018 Summer	0.05	0.03	372	1.724	0.6006
2017 Fall v. 2019 Fall	-0.03	0.03	367	-0.912	0.9706
2017 Fall v. 2019 Spring	0.33	0.04	371	9.156	<0.0001
2017 Fall v. 2019 Summer	0.05	0.03	370	1.647	0.6515
2018 Fall v. 2018 Spring	-0.15	0.04	363	-3.944	0.0018
2018 Fall v. 2018 Summer	0.04	0.03	367	1.322	0.8413
2018 Fall v. 2019 Fall	-0.04	0.04	370	-1.038	0.9449
2018 Fall v. 2019 Spring	0.32	0.04	370	8.270	<0.0001
2018 Fall v. 2019 Summer	0.04	0.03	367	1.252	0.8729
2018 Spring v. 2018 Summer	0.20	0.04	363	5.166	<0.0001
2018 Spring v. 2019 Fall	0.12	0.04	367	2.877	0.0638
2018 Spring v. 2019 Spring	0.47	0.04	368	11.248	<0.0001
2018 Spring v. 2019 Summer	0.19	0.04	362	5.100	<0.0001
2018 Summer v. 2019 Fall	-0.08	0.03	369	-2.353	0.2220
2018 Summer v. 2019 Spring	0.28	0.04	371	7.369	<0.0001
2018 Summer v. 2019 Summer	0.00	0.03	366	-0.066	1.0000
2019 Fall v. 2019 Spring	0.35	0.04	372	8.862	<0.0001
2019 Fall v. 2019 Summer	0.08	0.03	369	2.283	0.2549
2019 Spring v. 2019 Summer	-0.28	0.04	369	-7.449	<0.0001

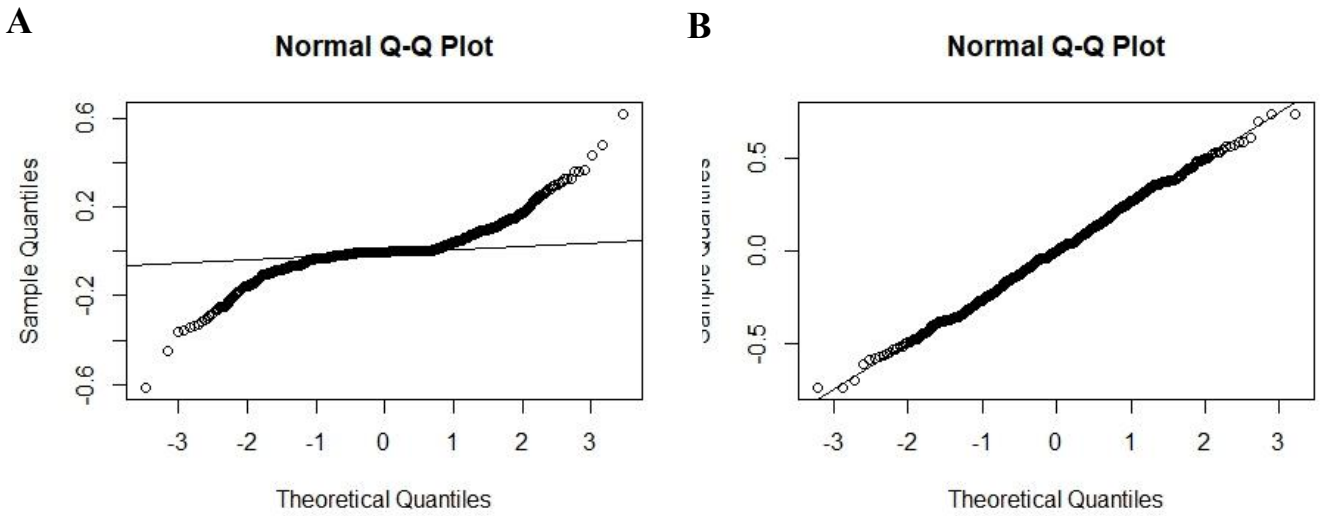


Figure B17. The quantile-quantile plots (qqplot) of the residuals for graphical visualization of the distribution of the relative abundance data for: **A)** the top 4 Phyla and the rare Phyla combined into "other" relative abundance, and **B)** the *Pseudomonas* and all "other" taxa relative abundances.

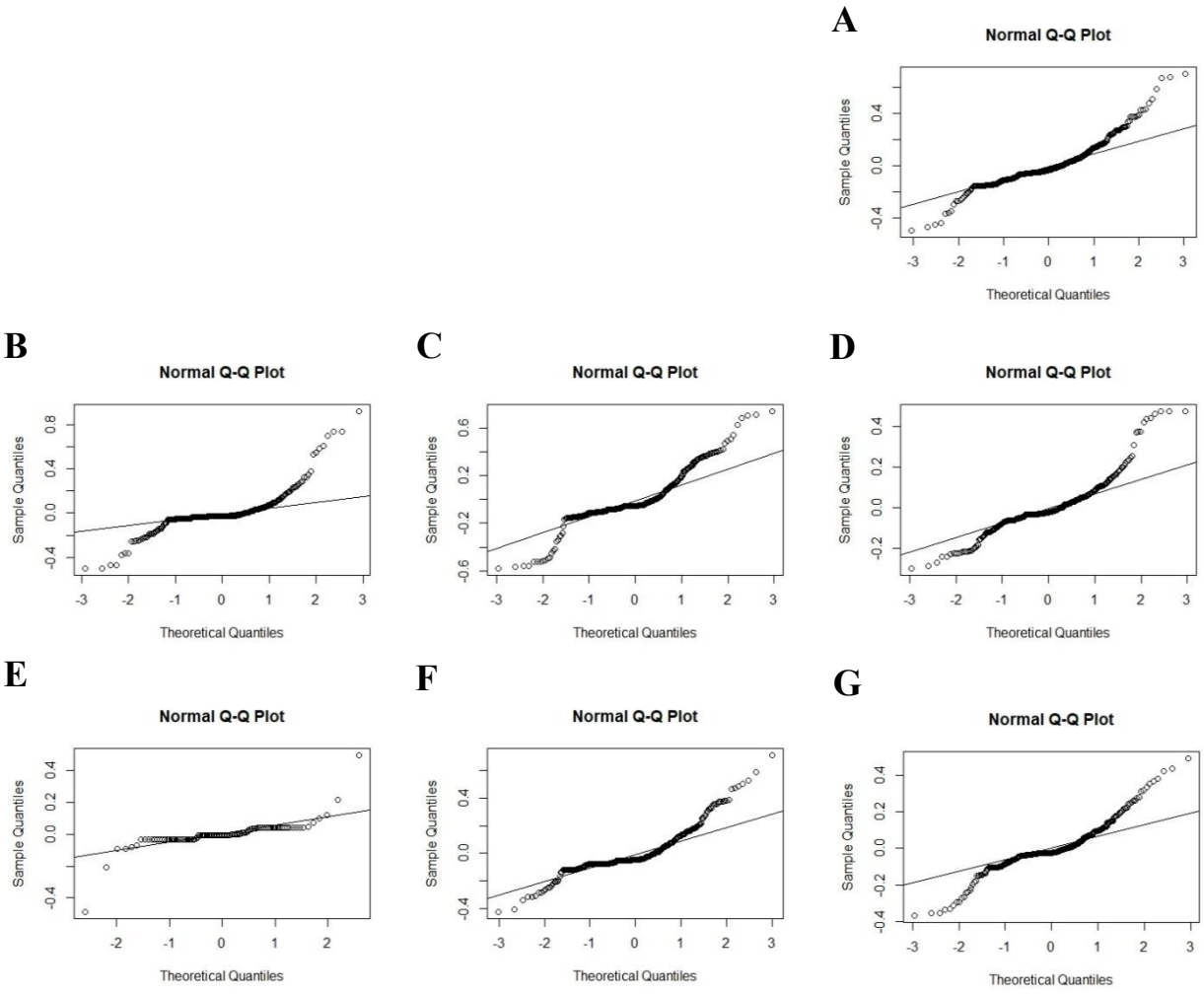


Figure B18. The quantile-quantile plots (qqplot) of the residuals for graphical visualization of the distribution of the relative abundance data at the deepest taxonomic level (genus or family), in which taxa that had a relative abundance <0.03 were combined into "other". For each time (season) **A)** Fall 2017, **B)** Spring 2018, **C)** Summer 2018, **D)** Fall 2018, **E)** Spring 2019, **F)** Summer 2019, and **G)** Fall 2019.

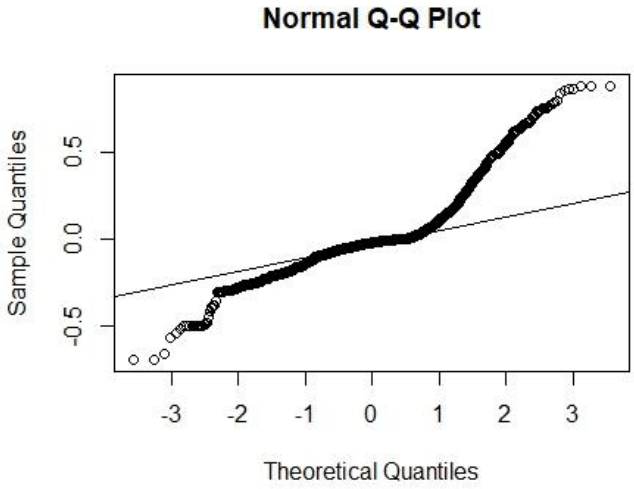


Figure B19. The quantile-quantile plot (qqplot) of the residuals for graphical visualization of the distribution of the relative abundance data of the core microbiome (genus and OTU). Includes the four core genera *Pseudomonas* Otu00001, *Pseudomonas* Otu00002, *Pseudomonas* Otu00003 and *Sphingomonas* Otu00004, with the other *Pseudomonas* combined and *Sphingomonas* combined and remaining additional taxa combined into "other". Core taxa were selected via occurrence and relative abundance when they occurred in 50% of all samples and had a relative abundance of ≥ 0.01.

Table B6. The mean relative abundances of the top 4 Phyla and "other" rarer Phyla combined ± SE, with the confidence limits (lower and upper C.L.) and the p-value. Letters indicate statistical differences, superscripted letters following Phyla indicate significance within each time while upper-cased letters indicate statistical differences of each Phyla across time, with significance determined by p-value ≤ 0.05.

Time	Phylum	Mean	SE	df	lower C.L.	upper C.L.	
2017 Fall	Proteobacteria [b]	0.95	0.01	1167	0.94	0.97	D
	Actinobacteria [a]	0.03	0.01	1167	0.02	0.05	A
	Bacteroidetes [a]	0.01	0.01	1167	-0.01	0.02	A
	Firmicutes [a]	0.01	0.01	1167	-0.01	0.02	A
	Other [a]	0.00	0.01	1167	-0.01	0.02	A
2018 Spring	Proteobacteria [d]	0.67	0.01	1725	0.65	0.70	A
	Firmicutes [c]	0.16	0.01	1725	0.13	0.18	B
	Actinobacteria [b]	0.09	0.01	1725	0.07	0.12	B
	Other [a]	0.04	0.01	1725	0.02	0.07	A
	Bacteroidetes [a]	0.04	0.01	1725	0.01	0.06	AB
2018 Summer	Proteobacteria [c]	0.84	0.01	1334	0.82	0.86	B
	Actinobacteria [b]	0.11	0.01	1334	0.09	0.13	B
	Bacteroidetes [a]	0.02	0.01	1334	0.00	0.04	A
	Firmicutes [a]	0.02	0.01	1334	0.00	0.04	A
	Other [a]	0.01	0.01	1334	-0.01	0.03	A
2018 Fall	Proteobacteria [c]	0.88	0.01	1475	0.86	0.90	BC
	Bacteroidetes [b]	0.08	0.01	1475	0.06	0.10	B
	Actinobacteria [a]	0.03	0.01	1475	0.01	0.05	A
	Firmicutes [a]	0.00	0.01	1475	-0.02	0.02	A
	Other [a]	0.00	0.01	1475	-0.02	0.02	A
2019 Spring	Proteobacteria [b]	1.00	0.01	1723	0.97	1.02	E
	Firmicutes [a]	0.00	0.01	1723	-0.02	0.03	A
	Actinobacteria [a]	0.00	0.01	1723	-0.02	0.03	A
	Bacteroidetes [a]	0.00	0.01	1723	-0.03	0.03	A
	Other [a]	0.00	0.01	1723	-0.03	0.03	A
2019 Summer	Proteobacteria [c]	0.90	0.01	1418	0.88	0.92	C
	Bacteroidetes [b]	0.07	0.01	1418	0.05	0.08	B
	Actinobacteria [ab]	0.03	0.01	1418	0.01	0.05	A
	Firmicutes [a]	0.00	0.01	1418	-0.02	0.02	A
	Other [a]	0.00	0.01	1418	-0.02	0.02	A
2019 Fall	Proteobacteria [c]	0.90	0.01	1613	0.88	0.92	C
	Bacteroidetes [b]	0.08	0.01	1613	0.06	0.11	B
	Actinobacteria [a]	0.01	0.01	1613	-0.01	0.04	A
	Firmicutes [a]	0.00	0.01	1613	-0.02	0.02	A
	Other [a]	0.00	0.01	1613	-0.02	0.02	A

Table B7. The pairwise comparison of the estimated marginal means of relative abundances of the top 4 Phyla and "other" Phyla for each time point and for each Phyla across each time point with the p-values, with significance determined by p-value ≤ 0.05.

Time	Contrast	Estimate	SE	df	t-ratio	p-value
2017 Fall	Actinobacteria v. Bacteroidetes	0.02	0.01	1864	2.116	0.2135
	Actinobacteria v. Firmicutes	0.03	0.01	1864	2.255	0.1602
	Actinobacteria v. Other	0.03	0.01	1864	2.458	0.1009
	Actinobacteria v. Proteobacteria	-0.92	0.01	1864	-79.182	<0.0001
	Bacteroidetes v. Firmicutes	0.00	0.01	1864	0.139	0.9999
	Bacteroidetes v. Other	0.00	0.01	1864	0.342	0.9971
	Bacteroidetes v. Proteobacteria	-0.95	0.01	1864	-81.298	<0.0001
	Firmicutes v. Other	0.00	0.01	1864	0.203	0.9996
	Firmicutes v. Proteobacteria	-0.95	0.01	1864	-81.437	<0.0001
	Other v. Proteobacteria	-0.95	0.01	1864	-81.639	<0.0001
2018 Spring	Actinobacteria v. Bacteroidetes	0.05	0.02	1864	3.012	0.0221
	Actinobacteria v. Firmicutes	-0.07	0.02	1864	-3.803	0.0014
	Actinobacteria v. Other	0.05	0.02	1864	2.837	0.0371
	Actinobacteria v. Proteobacteria	-0.58	0.02	1864	-32.718	<0.0001
	Bacteroidetes v. Firmicutes	-0.12	0.02	1864	-6.814	<0.0001
	Bacteroidetes v. Other	0.00	0.02	1864	-0.175	0.9998
	Bacteroidetes v. Proteobacteria	-0.63	0.02	1864	-35.730	<0.0001
	Firmicutes v. Other	0.12	0.02	1864	6.640	<0.0001
	Firmicutes v. Proteobacteria	-0.51	0.02	1864	-28.915	<0.0001
	Other v. Proteobacteria	-0.63	0.02	1864	-35.555	<0.0001
2018 Summer	Actinobacteria v. Bacteroidetes	0.09	0.01	1864	6.695	<0.0001
	Actinobacteria v. Firmicutes	0.09	0.01	1864	6.866	<0.0001
	Actinobacteria v. Other	0.10	0.01	1864	7.537	<0.0001
	Actinobacteria v. Proteobacteria	-0.73	0.01	1864	-55.520	<0.0001
	Bacteroidetes v. Firmicutes	0.00	0.01	1864	0.171	0.9998
	Bacteroidetes v. Other	0.01	0.01	1864	0.842	0.9175
	Bacteroidetes v. Proteobacteria	-0.82	0.01	1864	-62.215	<0.0001
	Firmicutes v. Other	0.01	0.01	1864	0.671	0.9627

Table B7. (cont'd)

	Firmicutes v. Proteobacteria	-0.83	0.01	1864	-62.386	<0.0001
	Other v. Proteobacteria	-0.83	0.01	1864	-63.057	<0.0001
2018 Fall	Actinobacteria v. Bacteroidetes	-0.05	0.01	1864	-3.316	0.0083
	Actinobacteria v. Firmicutes	0.03	0.01	1864	2.072	0.2325
	Actinobacteria v. Other	0.03	0.01	1864	2.317	0.1397
	Actinobacteria v. Proteobacteria	-0.85	0.01	1864	-58.304	<0.0001
	Bacteroidetes v. Firmicutes	0.08	0.01	1864	5.388	<0.0001
	Bacteroidetes v. Other	0.08	0.01	1864	5.633	<0.0001
	Bacteroidetes v. Proteobacteria	-0.80	0.01	1864	-54.989	<0.0001
	Firmicutes v. Other	0.00	0.01	1864	0.245	0.9992
	Firmicutes v. Proteobacteria	-0.88	0.01	1864	-60.377	<0.0001
	Other v. Proteobacteria	-0.88	0.01	1864	-60.622	<0.0001
2019 Spring	Actinobacteria v. Bacteroidetes	0.00	0.02	1864	0.015	1.0000
	Actinobacteria v. Firmicutes	0.00	0.02	1864	-0.016	1.0000
	Actinobacteria v. Other	0.00	0.02	1864	0.019	1.0000
	Actinobacteria v. Proteobacteria	-1.00	0.02	1864	-55.405	<0.0001
	Bacteroidetes v. Firmicutes	0.00	0.02	1864	-0.031	1.0000
	Bacteroidetes v. Other	0.00	0.02	1864	0.004	1.0000
	Bacteroidetes v. Proteobacteria	-1.00	0.02	1864	-55.420	<0.0001
	Firmicutes v. Other	0.00	0.02	1864	0.035	1.0000
	Firmicutes v. Proteobacteria	-1.00	0.02	1864	-55.389	<0.0001
	Other v. Proteobacteria	-1.00	0.02	1864	-55.424	<0.0001
2019 Summer	Actinobacteria v. Bacteroidetes	-0.03	0.01	1864	-2.546	0.0811
	Actinobacteria v. Firmicutes	0.03	0.01	1864	2.171	0.1912
	Actinobacteria v. Other	0.03	0.01	1864	2.312	0.1413
	Actinobacteria v. Proteobacteria	-0.87	0.01	1864	-65.306	<0.0001
	Bacteroidetes v. Firmicutes	0.06	0.01	1864	4.717	<0.0001
	Bacteroidetes v. Other	0.06	0.01	1864	4.859	<0.0001
	Bacteroidetes v. Proteobacteria	-0.84	0.01	1864	-62.760	<0.0001

Table B7. (cont'd)

	Firmicutes v. Other	0.00	0.01	1864	0.141	0.9999
	Firmicutes v. Proteobacteria	-0.90	0.01	1864	-67.477	<0.0001
	Other v. Proteobacteria	-0.90	0.01	1864	-67.618	<0.0001
2019 Fall	Actinobacteria v. Bacteroidetes	-0.07	0.02	1864	-4.442	0.0001
	Actinobacteria v. Firmicutes	0.01	0.02	1864	0.884	0.9028
	Actinobacteria v. Other	0.01	0.02	1864	0.915	0.8912
	Actinobacteria v. Proteobacteria	-0.88	0.02	1864	-56.222	<0.0001
	Bacteroidetes v. Firmicutes	0.08	0.02	1864	5.326	<0.0001
	Bacteroidetes v. Other	0.08	0.02	1864	5.357	<0.0001
	Bacteroidetes v. Proteobacteria	-0.81	0.02	1864	-51.780	<0.0001
	Firmicutes v. Other	0.00	0.02	1864	0.031	1.0000
	Firmicutes v. Proteobacteria	-0.90	0.02	1864	-57.106	<0.0001
	Other v. Proteobacteria	-0.90	0.02	1864	-57.137	<0.0001
Phylum	**Contrast**	**Estimate**	**SE**	**df**	**t-ratio**	**p-value**
Actinobacteria	2017 Fall v. 2018 Fall	0.00	0.01	1881	-0.172	1.0000
	2017 Fall v. 2018 Spring	-0.06	0.02	1874	-3.920	0.0018
	2017 Fall v. 2018 Summer	-0.08	0.01	1881	-6.198	<0.0001
	2017 Fall v. 2019 Fall	0.02	0.01	1874	1.208	0.8913
	2017 Fall v. 2019 Spring	0.03	0.02	1880	2.057	0.3792
	2017 Fall v. 2019 Summer	0.00	0.01	1879	0.046	1.0000
	2018 Fall v. 2018 Spring	-0.06	0.02	1872	-3.493	0.0088
	2018 Fall v. 2018 Summer	-0.08	0.01	1875	-5.396	<0.0001
	2018 Fall v. 2019 Fall	0.02	0.02	1879	1.253	0.8728
	2018 Fall v. 2019 Spring	0.03	0.02	1879	2.043	0.3876
	2018 Fall v. 2019 Summer	0.00	0.01	1876	0.203	1.0000
	2018 Spring v. 2018 Summer	-0.02	0.02	1872	-1.136	0.9170
	2018 Spring v. 2019 Fall	0.08	0.02	1876	4.494	0.0002
	2018 Spring v. 2019 Spring	0.09	0.02	1877	5.049	<0.0001
	2018 Spring v. 2019 Summer	0.06	0.02	1871	3.778	0.0031
	2018 Summer v. 2019 Fall	0.09	0.01	1878	6.466	<0.0001

Table B7. (cont'd)

	2018 Summer v. 2019 Spring	0.11	0.02	1880	6.834	<0.0001
	2018 Summer v. 2019 Summer	0.08	0.01	1875	5.859	<0.0001
	2019 Fall v. 2019 Spring	0.01	0.02	1879	0.857	0.9787
	2019 Fall v. 2019 Summer	-0.02	0.01	1878	-1.108	0.9259
	2019 Spring v. 2019 Summer	-0.03	0.02	1878	-1.931	0.4599
Bacteroidetes	2017 Fall v. 2018 Fall	-0.07	0.01	1881	-5.695	<0.0001
	2017 Fall v. 2018 Spring	-0.03	0.02	1874	-2.010	0.4084
	2017 Fall v. 2018 Summer	-0.01	0.01	1881	-1.072	0.9362
	2017 Fall v. 2019 Fall	-0.08	0.01	1874	-5.609	<0.0001
	2017 Fall v. 2019 Spring	0.01	0.02	1880	0.457	0.9993
	2017 Fall v. 2019 Summer	-0.06	0.01	1879	-4.630	0.0001
	2018 Fall v. 2018 Spring	0.04	0.02	1872	2.728	0.0920
	2018 Fall v. 2018 Summer	0.06	0.01	1875	4.431	0.0002
	2018 Fall v. 2019 Fall	0.00	0.02	1879	-0.180	1.0000
	2018 Fall v. 2019 Spring	0.08	0.02	1879	4.988	<0.0001
	2018 Fall v. 2019 Summer	0.02	0.01	1876	1.219	0.8871
	2018 Spring v. 2018 Summer	0.02	0.02	1872	1.078	0.9345
	2018 Spring v. 2019 Fall	-0.05	0.02	1876	-2.794	0.0773
	2018 Spring v. 2019 Spring	0.04	0.02	1877	2.083	0.3634
	2018 Spring v. 2019 Summer	-0.03	0.02	1871	-1.738	0.5907
	2018 Summer v. 2019 Fall	-0.06	0.01	1878	-4.424	0.0002
	2018 Summer v. 2019 Spring	0.02	0.02	1880	1.279	0.8616
	2018 Summer v. 2019 Summer	-0.04	0.01	1875	-3.357	0.0141
	2019 Fall v. 2019 Spring	0.08	0.02	1879	4.980	<0.0001
	2019 Fall v. 2019 Summer	0.02	0.01	1878	1.352	0.8268
	2019 Spring v. 2019 Summer	-0.06	0.02	1878	-4.080	0.0009
Firmicutes	2017 Fall v. 2018 Fall	0.00	0.01	1881	0.119	1.0000
	2017 Fall v. 2018 Spring	-0.15	0.02	1874	-10.117	<0.0001
	2017 Fall v. 2018 Summer	-0.01	0.01	1881	-1.021	0.9494
	2017 Fall v. 2019 Fall	0.00	0.01	1874	0.317	0.9999

Table B7. (cont'd)

	2017 Fall v. 2019 Spring	0.00	0.02	1880	0.313	0.9999
	2017 Fall v. 2019 Summer	0.00	0.01	1879	0.261	1.0000
	2018 Fall v. 2018 Spring	-0.15	0.02	1872	-9.469	<0.0001
	2018 Fall v. 2018 Summer	-0.01	0.01	1875	-1.028	0.9476
	2018 Fall v. 2019 Fall	0.00	0.02	1879	0.187	1.0000
	2018 Fall v. 2019 Spring	0.00	0.02	1879	0.195	1.0000
	2018 Fall v. 2019 Summer	0.00	0.01	1876	0.122	1.0000
	2018 Spring v. 2018 Summer	0.14	0.02	1872	8.879	<0.0001
	2018 Spring v. 2019 Fall	0.16	0.02	1876	9.308	<0.0001
	2018 Spring v. 2019 Spring	0.16	0.02	1877	8.797	<0.0001
	2018 Spring v. 2019 Summer	0.16	0.02	1871	9.864	<0.0001
	2018 Summer v. 2019 Fall	0.02	0.01	1878	1.178	0.9026
	2018 Summer v. 2019 Spring	0.02	0.02	1880	1.101	0.9279
	2018 Summer v. 2019 Summer	0.02	0.01	1875	1.204	0.8929
	2019 Fall v. 2019 Spring	0.00	0.02	1879	0.022	1.0000
	2019 Fall v. 2019 Summer	0.00	0.01	1878	-0.077	1.0000
	2019 Spring v. 2019 Summer	0.00	0.02	1878	-0.094	1.0000
Other	2017 Fall v. 2018 Fall	0.00	0.01	1881	0.210	1.0000
	2017 Fall v. 2018 Spring	-0.04	0.02	1874	-2.478	0.1678
	2017 Fall v. 2018 Summer	-0.01	0.01	1881	-0.498	0.9989
	2017 Fall v. 2019 Fall	0.00	0.01	1874	0.183	1.0000
	2017 Fall v. 2019 Spring	0.00	0.02	1880	0.201	1.0000
	2017 Fall v. 2019 Summer	0.00	0.01	1879	0.223	1.0000
	2018 Fall v. 2018 Spring	-0.04	0.02	1872	-2.465	0.1727
	2018 Fall v. 2018 Summer	-0.01	0.01	1875	-0.646	0.9952
	2018 Fall v. 2019 Fall	0.00	0.02	1879	-0.016	1.0000
	2018 Fall v. 2019 Spring	0.00	0.02	1879	0.017	1.0000
	2018 Fall v. 2019 Summer	0.00	0.01	1876	0.002	1.0000
	2018 Spring v. 2018 Summer	0.03	0.02	1872	1.979	0.4284
	2018 Spring v. 2019 Fall	0.04	0.02	1876	2.366	0.2138

Table B7. (cont'd)

	2018 Spring v. 2019 Spring	0.04	0.02	1877	2.260	0.2644
	2018 Spring v. 2019 Summer	0.04	0.02	1871	2.542	0.1451
	2018 Summer v. 2019 Fall	0.01	0.01	1878	0.601	0.9968
	2018 Summer v. 2019 Spring	0.01	0.02	1880	0.583	0.9973
	2018 Summer v. 2019 Summer	0.01	0.01	1875	0.678	0.9938
	2019 Fall v. 2019 Spring	0.00	0.02	1879	0.031	1.0000
	2019 Fall v. 2019 Summer	0.00	0.01	1878	0.018	1.0000
	2019 Spring v. 2019 Summer	0.00	0.02	1878	-0.016	1.0000
Proteobacteria	2017 Fall v. 2018 Fall	0.07	0.01	1881	5.537	<0.0001
	2017 Fall v. 2018 Spring	0.28	0.02	1874	18.525	<0.0001
	2017 Fall v. 2018 Summer	0.11	0.01	1881	8.789	<0.0001
	2017 Fall v. 2019 Fall	0.05	0.01	1874	3.901	0.0019
	2017 Fall v. 2019 Spring	-0.05	0.02	1880	-3.028	0.0400
	2017 Fall v. 2019 Summer	0.05	0.01	1879	4.100	0.0008
	2018 Fall v. 2018 Spring	0.21	0.02	1872	12.700	<0.0001
	2018 Fall v. 2018 Summer	0.04	0.01	1875	2.638	0.1152
	2018 Fall v. 2019 Fall	-0.02	0.02	1879	-1.245	0.8764
	2018 Fall v. 2019 Spring	-0.12	0.02	1879	-7.244	<0.0001
	2018 Fall v. 2019 Summer	-0.02	0.01	1876	-1.546	0.7167
	2018 Spring v. 2018 Summer	-0.17	0.02	1872	-10.800	<0.0001
	2018 Spring v. 2019 Fall	-0.23	0.02	1876	-13.375	<0.0001
	2018 Spring v. 2019 Spring	-0.33	0.02	1877	-18.188	<0.0001
	2018 Spring v. 2019 Summer	-0.23	0.02	1871	-14.446	<0.0001
	2018 Summer v. 2019 Fall	-0.06	0.01	1878	-3.820	0.0026
	2018 Summer v. 2019 Spring	-0.16	0.02	1880	-9.797	<0.0001
	2018 Summer v. 2019 Summer	-0.06	0.01	1875	-4.385	0.0002
	2019 Fall v. 2019 Spring	-0.10	0.02	1879	-5.890	<0.0001
	2019 Fall v. 2019 Summer	0.00	0.01	1878	-0.186	1.0000
	2019 Spring v. 2019 Summer	0.10	0.02	1878	6.121	<0.0001

Table B8. The mean relative abundances of *Pseudomonas* and all "other" taxa at the genus/family level ± SE, with the confidence limits (lower and upper C.L.). Superscripted letters following *Pseudomonas* or "other" indicate statistical differences within each time while upper-cased letters indicate statistical differences of each *Pseudomonas* or "other" across time, with significance determined by p-value ≤ 0.05.

Time	Genera	Mean	SE	df	lower C.L.	upper C.L.	
2017 Fall	*Pseudomonas* [b]	0.61	0.03	297	0.55	0.66	B
	Other [a]	0.39	0.03	297	0.34	0.45	B
2018 Spring	Other [b]	0.74	0.04	620	0.65	0.83	C
	Pseudomonas [a]	0.26	0.04	620	0.18	0.35	A
2018 Summer	*Pseudomonas* [b]	0.58	0.03	371	0.52	0.65	B
	Other [a]	0.42	0.03	371	0.35	0.48	B
2018 Fall	*Pseudomonas* [a]	0.51	0.03	444	0.44	0.58	B
	Other [a]	0.49	0.03	444	0.42	0.56	B
2019 Spring	*Pseudomonas* [b]	0.96	0.04	613	0.87	1.04	C
	Other [a]	0.04	0.04	613	-0.04	0.13	A
2019 Summer	*Pseudomonas* [b]	0.61	0.03	414	0.55	0.68	B
	Other [a]	0.39	0.03	414	0.32	0.45	B
2019 Fall	Other [a]	0.52	0.04	530	0.45	0.60	B
	Pseudomonas [a]	0.48	0.04	530	0.40	0.55	B

Table B9. The pairwise comparison of the estimated marginal means of relative abundances of *Pseudomonas* and "other" taxa at the genus or family level for each time point and for each taxon across each time point with the p-values, with significance determined by p-value ≤ 0.05.

Time	Contrast	Estimate	SE	df	t-ratio	p-value
2017 Fall	Other v. *Pseudomonas*	-0.21	0.04	733	-5.359	<0.0001
2018 Spring	Other v. *Pseudomonas*	0.48	0.06	733	7.967	<0.0001
2018 Summer	Other v. *Pseudomonas*	-0.17	0.04	733	-3.717	0.0002
2018 Fall	Other v. *Pseudomonas*	-0.02	0.05	733	-0.485	0.6282
2019 Spring	Other v. *Pseudomonas*	-0.92	0.06	733	-15.062	<0.0001
2019 Summer	Other v. *Pseudomonas*	-0.23	0.05	733	-5.022	<0.0001
2019 Fall	Other v. *Pseudomonas*	0.04	0.05	733	0.786	0.4323

Genus	Contrast	Estimate	SE	df	t-ratio	p-value
Other	2017 Fall v. 2018 Fall	-0.09	0.04	750	-2.095	0.3564
	2017 Fall v. 2018 Spring	-0.34	0.05	742	-6.659	<0.0001
	2017 Fall v. 2018 Summer	-0.02	0.04	750	-0.528	0.9984
	2017 Fall v. 2019 Fall	-0.13	0.05	743	-2.688	0.1028
	2017 Fall v. 2019 Spring	0.35	0.05	749	6.837	<0.0001
	2017 Fall v. 2019 Summer	0.01	0.04	748	0.183	1.0000
	2018 Fall v. 2018 Spring	-0.25	0.06	741	-4.500	0.0002
	2018 Fall v. 2018 Summer	0.07	0.05	744	1.511	0.7384
	2018 Fall v. 2019 Fall	-0.03	0.05	748	-0.637	0.9956
	2018 Fall v. 2019 Spring	0.45	0.06	748	7.998	<0.0001
	2018 Fall v. 2019 Summer	0.10	0.05	745	2.139	0.3307
	2018 Spring v. 2018 Summer	0.32	0.05	741	5.946	<0.0001
	2018 Spring v. 2019 Fall	0.22	0.06	745	3.769	0.0033
	2018 Spring v. 2019 Spring	0.70	0.06	746	11.453	<0.0001
	2018 Spring v. 2019 Summer	0.35	0.05	740	6.483	<0.0001

Table B9. (cont'd)

	2018 Summer v. 2019 Fall	-0.10	0.05	747	-2.111	0.3473
	2018 Summer v. 2019 Spring	0.38	0.05	749	6.939	<0.0001
	2018 Summer v. 2019 Summer	0.03	0.05	744	0.668	0.9943
	2019 Fall v. 2019 Spring	0.48	0.06	748	8.280	<0.0001
	2019 Fall v. 2019 Summer	0.13	0.05	747	2.712	0.0967
	2019 Spring v. 2019 Summer	-0.35	0.05	747	-6.386	<0.0001
Pseudomonas	2017 Fall v. 2018 Fall	0.09	0.04	750	2.095	0.3564
	2017 Fall v. 2018 Spring	0.34	0.05	742	6.659	<0.0001
	2017 Fall v. 2018 Summer	0.02	0.04	750	0.528	0.9984
	2017 Fall v. 2019 Fall	0.13	0.05	743	2.688	0.1028
	2017 Fall v. 2019 Spring	-0.35	0.05	749	-6.837	<0.0001
	2017 Fall v. 2019 Summer	-0.01	0.04	748	-0.183	1.0000
	2018 Fall v. 2018 Spring	0.25	0.06	741	4.500	0.0002
	2018 Fall v. 2018 Summer	-0.07	0.05	744	-1.511	0.7384
	2018 Fall v. 2019 Fall	0.03	0.05	748	0.637	0.9956
	2018 Fall v. 2019 Spring	-0.45	0.06	748	-7.998	<0.0001
	2018 Fall v. 2019 Summer	-0.10	0.05	745	-2.139	0.3307
	2018 Spring v. 2018 Summer	-0.32	0.05	741	-5.946	<0.0001
	2018 Spring v. 2019 Fall	-0.22	0.06	745	-3.769	0.0033
	2018 Spring v. 2019 Spring	-0.70	0.06	746	-11.453	<0.0001
	2018 Spring v. 2019 Summer	-0.35	0.05	740	-6.483	<0.0001
	2018 Summer v. 2019 Fall	0.10	0.05	747	2.111	0.3473
	2018 Summer v. 2019 Spring	-0.38	0.05	749	-6.939	<0.0001
	2018 Summer v. 2019 Summer	-0.03	0.05	744	-0.668	0.9943
	2019 Fall v. 2019 Spring	-0.48	0.06	748	-8.280	<0.0001
	2019 Fall v. 2019 Summer	-0.13	0.05	747	-2.712	0.0967
	2019 Spring v. 2019 Summer	0.35	0.05	747	6.386	<0.0001

Table B10. The mean relative abundances of the top deepest taxonomic level (genus or family) by time (season) where taxa of relative abundance <0.03 were combined into "other" ± SE, with the confidence limits (lower and upper C.L.). Letters indicate statistical differences, with significance determined by p-value ≤ 0.05.

Time	Genera	Mean	SE	df	lower C.L.	upper C.L.	
2017 Fall	*Pseudomonas*	0.61	0.02	111	0.57	0.64	c
	Enterobacteriaceae	0.16	0.02	111	0.12	0.19	b
	Sphingomonas	0.11	0.02	111	0.08	0.15	ab
	Massilia	0.07	0.02	111	0.03	0.10	a
	Other	0.06	0.02	111	0.02	0.09	a
2018 Spring	Other	0.50	0.03	112	0.45	0.56	c
	Pseudomonas	0.26	0.03	112	0.21	0.32	b
	Bradyrhizobium	0.05	0.03	112	0.00	0.11	a
	Acinetobacter	0.05	0.03	112	0.00	0.11	a
	Sphingomonas	0.04	0.03	112	-0.02	0.09	a
	Methylobacterium	0.03	0.03	112	-0.02	0.09	a
	Streptococcus	0.03	0.03	112	-0.03	0.08	a
	Xanthomonas	0.03	0.03	112	-0.03	0.08	a
2018 Summer	*Pseudomonas*	0.58	0.03	91	0.53	0.64	c
	Other	0.17	0.03	91	0.11	0.22	b
	Sphingomonas	0.11	0.03	91	0.06	0.17	ab
	Curtobacterium	0.08	0.03	91	0.03	0.14	ab
	Enterobacteriaceae	0.05	0.03	91	0.00	0.11	a
2018 Fall	*Pseudomonas*	0.51	0.02	116	0.48	0.55	d
	Sphingomonas	0.23	0.02	116	0.19	0.26	c
	Other	0.13	0.02	116	0.09	0.16	b
	Rhizobiaceae	0.07	0.02	116	0.03	0.10	ab
	Chryseobacterium	0.03	0.02	116	0.00	0.07	a
	Massilia	0.03	0.02	116	0.00	0.07	a
2019 Spring	*Pseudomonas*	0.96	0.02	23	0.92	1.00	b
	Enterobacteriaceae	0.03	0.02	23	-0.01	0.07	a
	Other	0.01	0.02	23	-0.03	0.05	a
2019 Summer	*Pseudomonas*	0.61	0.02	143	0.58	0.65	b
	Sphingomonas	0.12	0.02	143	0.08	0.16	a
	Other	0.09	0.02	143	0.05	0.12	a
	Enterobacteriaceae	0.08	0.02	143	0.04	0.12	a
	Pedobacter	0.05	0.02	143	0.02	0.09	a
	Rhizobiaceae	0.05	0.02	143	0.01	0.09	a
2019 Fall	*Pseudomonas*	0.48	0.02	144	0.44	0.52	d
	Sphingomonas	0.22	0.02	144	0.19	0.26	c
	Rhizobiaceae	0.10	0.02	144	0.07	0.14	b

Table B10. (cont'd)

Other	0.09	0.02	144	0.06	0.13	ab
Hymenobacter	0.04	0.02	144	0.00	0.08	ab
Massilia	0.03	0.02	144	0.00	0.07	ab
Chryseobacterium	0.03	0.02	144	-0.01	0.06	a

Table B11. The pairwise comparison of the estimated marginal means of relative abundances of the deepest taxonomic level (genus or family) by time (season) where taxa of relative abundance <0.03 were combined into "other" with significance determined by p-value ≤ 0.05.

Time	Contrast	Estimate	SE	df	t-ratio	p-value
2017 Fall	Enterobacteriaceae v. Massilia	0.09	0.02	394	3.702	0.0023
	Enterobacteriaceae v. Other	0.10	0.02	394	4.014	0.0007
	Enterobacteriaceae v. Pseudomonas	-0.45	0.02	394	-18.506	<0.0001
	Enterobacteriaceae v. Sphingomonas	0.04	0.02	394	1.742	0.4093
	Massilia v. Other	0.01	0.02	394	0.312	0.9979
	Massilia v. Pseudomonas	-0.54	0.02	394	-22.208	<0.0001
	Massilia v. Sphingomonas	-0.05	0.02	394	-1.960	0.2879
	Other v. Pseudomonas	-0.55	0.02	394	-22.519	<0.0001
	Other v. Sphingomonas	-0.06	0.02	394	-2.271	0.1564
	Pseudomonas v. Sphingomonas	0.49	0.02	394	20.248	<0.0001
2018 Spring	Acinetobacter v. Bradyrhizobium	0.00	0.04	270	-0.094	1.0000
	Acinetobacter v. Methylobacterium	0.02	0.04	270	0.455	0.9998
	Acinetobacter v. Other	-0.45	0.04	270	-11.557	<0.0001
	Acinetobacter v. Pseudomonas	-0.21	0.04	270	-5.343	<0.0001
	Acinetobacter v. Sphingomonas	0.01	0.04	270	0.306	1.0000
	Acinetobacter v. Streptococcus	0.02	0.04	270	0.561	0.9993
	Acinetobacter v. Xanthomonas	0.02	0.04	270	0.634	0.9984
	Bradyrhizobium v. Methylobacterium	0.02	0.04	270	0.549	0.9994
	Bradyrhizobium v. Other	-0.45	0.04	270	-11.463	<0.0001
	Bradyrhizobium v. Pseudomonas	-0.21	0.04	270	-5.249	<0.0001
	Bradyrhizobium v. Sphingomonas	0.02	0.04	270	0.400	0.9999
	Bradyrhizobium v. Streptococcus	0.03	0.04	270	0.655	0.9980
	Bradyrhizobium v. Xanthomonas	0.03	0.04	270	0.728	0.9961
	Methylobacterium v. Other	-0.47	0.04	270	-12.012	<0.0001
	Methylobacterium v. Pseudomonas	-0.23	0.04	270	-5.798	<0.0001
	Methylobacterium v. Sphingomonas	-0.01	0.04	270	-0.149	1.0000

Table B11. (cont'd)

	Methylobacterium v. Streptococcus	0.00	0.04	270	0.106	1.0000
	Methylobacterium v. Xanthomonas	0.01	0.04	270	0.179	1.0000
	Other v. Pseudomonas	0.24	0.04	270	6.214	<0.0001
	Other v. Sphingomonas	0.47	0.04	270	11.863	<0.0001
	Other v. Streptococcus	0.48	0.04	270	12.118	<0.0001
	Other v. Xanthomonas	0.48	0.04	270	12.191	<0.0001
	Pseudomonas v. Sphingomonas	0.22	0.04	270	5.649	<0.0001
	Pseudomonas v. Streptococcus	0.23	0.04	270	5.904	<0.0001
	Pseudomonas v. Xanthomonas	0.23	0.04	270	5.977	<0.0001
	Sphingomonas v. Streptococcus	0.01	0.04	270	0.255	1.0000
	Sphingomonas v. Xanthomonas	0.01	0.04	270	0.328	1.0000
	Streptococcus v. Xanthomonas	0.00	0.04	270	0.073	1.0000
2018 Summer	Curtobacterium v. Enterobacteriaceae	0.03	0.04	302	0.807	0.9284
	Curtobacterium v. Other	-0.08	0.04	302	-2.207	0.1801
	Curtobacterium v. Pseudomonas	-0.50	0.04	302	-13.427	<0.0001
	Curtobacterium v. Sphingomonas	-0.03	0.04	302	-0.824	0.9231
	Enterobacteriaceae v. Other	-0.11	0.04	302	-3.013	0.0233
	Enterobacteriaceae v. Pseudomonas	-0.53	0.04	302	-14.234	<0.0001
	Enterobacteriaceae v. Sphingomonas	-0.06	0.04	302	-1.631	0.4788
	Other v. Pseudomonas	-0.42	0.04	302	-11.221	<0.0001
	Other v. Sphingomonas	0.05	0.04	302	1.382	0.6394
	Pseudomonas v. Sphingomonas	0.47	0.04	302	12.603	<0.0001
2018 Fall	Chryseobacterium v. Massilia	0.00	0.02	301	0.018	1.0000
	Chryseobacterium v. Other	-0.09	0.02	301	-3.920	0.0015
	Chryseobacterium v. Pseudomonas	-0.48	0.02	301	-20.028	<0.0001
	Chryseobacterium v. Rhizobiaceae	-0.03	0.02	301	-1.299	0.7856
	Chryseobacterium v. Sphingomonas	-0.19	0.02	301	-8.023	<0.0001
	Massilia v. Other	-0.09	0.02	301	-3.938	0.0014
	Massilia v. Pseudomonas	-0.48	0.02	301	-20.046	<0.0001
	Massilia v. Rhizobiaceae	-0.03	0.02	301	-1.317	0.7756

Table B11. (cont'd)

	Massilia v. Sphingomonas	-0.19	0.02	301	-8.041	<0.0001
	Other v. Pseudomonas	-0.38	0.02	301	-16.108	<0.0001
	Other v. Rhizobiaceae	0.06	0.02	301	2.622	0.0952
	Other v. Sphingomonas	-0.10	0.02	301	-4.103	0.0007
	Pseudomonas v. Rhizobiaceae	0.45	0.02	301	18.729	<0.0001
	Pseudomonas v. Sphingomonas	0.29	0.02	301	12.005	<0.0001
	Rhizobiaceae v. Sphingomonas	-0.16	0.02	301	-6.724	<0.0001
2019 Spring	Enterobacteriaceae v. Other	0.02	0.02	89	1.228	0.4401
	Enterobacteriaceae v. Pseudomonas	-0.93	0.02	89	-45.832	<0.0001
	Other v. Pseudomonas	-0.95	0.02	89	-47.059	<0.0001
2019 Summer	Enterobacteriaceae v. Other	-0.01	0.03	360	-0.234	0.9999
	Enterobacteriaceae v. Pedobacter	0.03	0.03	360	0.961	0.9297
	Enterobacteriaceae v. Pseudomonas	-0.53	0.03	360	-20.407	<0.0001
	Enterobacteriaceae v. Rhizobiaceae	0.03	0.03	360	1.163	0.8541
	Enterobacteriaceae v. Sphingomonas	-0.04	0.03	360	-1.573	0.6170
	Other v. Pedobacter	0.03	0.03	360	1.195	0.8390
	Other v. Pseudomonas	-0.53	0.03	360	-20.173	<0.0001
	Other v. Rhizobiaceae	0.04	0.03	360	1.397	0.7291
	Other v. Sphingomonas	-0.04	0.03	360	-1.339	0.7630
	Pedobacter v. Pseudomonas	-0.56	0.03	360	-21.368	<0.0001
	Pedobacter v. Rhizobiaceae	0.01	0.03	360	0.201	1.0000
	Pedobacter v. Sphingomonas	-0.07	0.03	360	-2.534	0.1170
	Pseudomonas v. Rhizobiaceae	0.56	0.03	360	21.570	<0.0001
	Pseudomonas v. Sphingomonas	0.49	0.03	360	18.834	<0.0001
	Rhizobiaceae v. Sphingomonas	-0.07	0.03	360	-2.736	0.0708
2019 Fall	Chryseobacterium v. Hymenobacter	-0.01	0.03	300	-0.503	0.9988
	Chryseobacterium v. Massilia	-0.01	0.03	300	-0.320	0.9999
	Chryseobacterium v. Other	-0.07	0.03	300	-2.565	0.1407
	Chryseobacterium v. Pseudomonas	-0.45	0.03	300	-17.479	<0.0001

Table B11. (cont'd)

Chryseobacterium v. Rhizobiaceae	-0.08	0.03	300	-3.027	0.0424
Chryseobacterium v. Sphingomonas	-0.20	0.03	300	-7.572	<0.0001
Hymenobacter v. Massilia	0.00	0.03	300	0.183	1.0000
Hymenobacter v. Other	-0.05	0.03	300	-2.062	0.3780
Hymenobacter v. Pseudomonas	-0.44	0.03	300	-16.976	<0.0001
Hymenobacter v. Rhizobiaceae	-0.07	0.03	300	-2.524	0.1545
Hymenobacter v. Sphingomonas	-0.18	0.03	300	-7.069	<0.0001
Massilia v. Other	-0.06	0.03	300	-2.245	0.2748
Massilia v. Pseudomonas	-0.44	0.03	300	-17.159	<0.0001
Massilia v. Rhizobiaceae	-0.07	0.03	300	-2.707	0.1001
Massilia v. Sphingomonas	-0.19	0.03	300	-7.252	<0.0001
Other v. Pseudomonas	-0.39	0.03	300	-14.914	<0.0001
Other v. Rhizobiaceae	-0.01	0.03	300	-0.462	0.9993
Other v. Sphingomonas	-0.13	0.03	300	-5.007	<0.0001
Pseudomonas v. Rhizobiaceae	0.37	0.03	300	14.452	<0.0001
Pseudomonas v. Sphingomonas	0.26	0.03	300	9.907	<0.0001
Rhizobiaceae v. Sphingomonas	-0.12	0.03	300	-4.546	0.0002

Table B12. The mean relative abundances of the core microbiome taxon (genus and OTU identifier), the rest of the combined *Pseudomonas* and combined *Sphingomonas,* and the remaining combined "other" taxa ± SE over time (season), with the confidence limits (lower and upper C.L.). Superscripted letters following genus/OTUs indicate statistical differences within each time, while upper-cased letters indicate statistical differences of each genus/OTU across time, with significance determined by p-value ≤ 0.05.

Time	Genera	Mean	SE	df	lower C.L.	upper C.L.	
2017 Fall	Other [d]	0.28	0.02	1834	0.241	0.3211	B
	Pseudomonas Otu00003 [cd]	0.21	0.02	1834	0.165	0.2458	C
	Pseudomonas Otu00001 [cd]	0.20	0.02	1834	0.163	0.2432	B
	Pseudomonas Otu00002 [c]	0.19	0.02	1834	0.153	0.2335	B
	Sphingomonas Otu00004 [b]	0.09	0.02	1834	0.052	0.1321	ABC
	Sphingomonas [ab]	0.02	0.02	1834	-0.018	0.0621	A
	Pseudomonas [a]	0.00	0.02	1834	-0.037	0.0436	A
2018 Spring	Other [c]	0.70	0.03	2472	0.638	0.7617	C
	Pseudomonas Otu00001 [b]	0.21	0.03	2472	0.150	0.2736	BC
	Pseudomonas Otu00002 [a]	0.03	0.03	2472	-0.029	0.0947	A
	Sphingomonas [a]	0.03	0.03	2472	-0.035	0.0885	A
	Sphingomonas Otu00004 [a]	0.01	0.03	2472	-0.049	0.0744	A
	Pseudomonas Otu00003 [a]	0.01	0.03	2472	-0.053	0.0705	A
	Pseudomonas [a]	0.01	0.03	2472	-0.054	0.0695	AB
2018 Summer	*Pseudomonas* Otu00002 [c]	0.30	0.02	2038	0.257	0.3486	C
	Other [c]	0.30	0.02	2038	0.257	0.3485	B
	Pseudomonas Otu00003 [b]	0.16	0.02	2038	0.116	0.2070	BC
	Pseudomonas Otu00001 [ab]	0.08	0.02	2038	0.037	0.1281	A
	Sphingomonas [ab]	0.07	0.02	2038	0.023	0.1144	A
	Sphingomonas Otu00004 [a]	0.05	0.02	2038	0.000	0.0913	AB
	Pseudomonas [a]	0.04	0.02	2038	-0.009	0.0822	AB

Table B12. (cont'd)

2018 Fall	*Pseudomonas* Otu00001 [d]	0.43	0.03	2202	0.377	0.4775	D
	Other [c]	0.26	0.03	2202	0.212	0.3125	B
	Sphingomonas Otu00004 [b]	0.14	0.03	2202	0.087	0.1876	BC
	Sphingomonas [ab]	0.09	0.03	2202	0.038	0.1385	A
	Pseudomonas Otu00003 [ab]	0.05	0.03	2202	0.000	0.1001	A
	Pseudomonas Otu00002 [a]	0.02	0.03	2202	-0.029	0.0718	A
	Pseudomonas [a]	0.01	0.03	2202	-0.037	0.0631	AB
2019 Spring	*Pseudomonas* Otu00001 [c]	0.50	0.03	2472	0.441	0.5659	D
	Pseudomonas Otu00002 [b]	0.23	0.03	2472	0.169	0.2936	BC
	Pseudomonas [ab]	0.12	0.03	2472	0.061	0.1857	B
	Pseudomonas Otu00003 [ab]	0.10	0.03	2472	0.038	0.1631	ABC
	Other [a]	0.04	0.03	2472	-0.021	0.1038	A
	Sphingomonas Otu00004 [a]	0.00	0.03	2472	-0.062	0.0627	A
	Sphingomonas [a]	0.00	0.03	2472	-0.062	0.0625	A
2019 Summer	Other [b]	0.27	0.02	2136	0.221	0.3128	B
	Pseudomonas Otu00002 [b]	0.27	0.02	2136	0.219	0.3116	BC
	Pseudomonas Otu00001 [b]	0.21	0.02	2136	0.168	0.2600	BC
	Sphingomonas Otu00004 [a]	0.10	0.02	2136	0.050	0.1417	ABC
	Pseudomonas Otu00003 [a]	0.07	0.02	2136	0.023	0.1156	AB
	Pseudomonas [a]	0.06	0.02	2136	0.018	0.1101	AB
	Sphingomonas [a]	0.02	0.02	2136	-0.021	0.0707	A
2019 Fall	*Pseudomonas* Otu00001 [c]	0.31	0.03	2355	0.253	0.3618	C
	Other [c]	0.30	0.03	2355	0.244	0.3527	B
	Sphingomonas Otu00004 [b]	0.18	0.03	2355	0.124	0.2329	C
	Pseudomonas Otu00003 [ab]	0.10	0.03	2355	0.043	0.1520	AB
	Pseudomonas Otu00002 [a]	0.06	0.03	2355	0.008	0.1164	A
	Sphingomonas [a]	0.04	0.03	2355	-0.010	0.0984	A
	Pseudomonas [a]	0.01	0.03	2355	-0.042	0.0664	AB

Table B13. The pairwise comparison of the estimated marginal means of relative abundances of core microbiome taxon (genus and OTU identifier) the rest of the combined *Pseudomonas* and combined *Sphingomonas* and the remaining combined "other" taxa for each time point and for each taxon across each time point with significance determined by p-value ≤ 0.05.

Time	Contrast	Estimate	SE	df	t-ratio	p-value
2017 Fall	Other v. *Pseudomonas*	0.28	0.03	2618	9.584	<0.0001
	Other v. *Pseudomonas* Otu00001	0.08	0.03	2618	2.691	0.1009
	Other v. *Pseudomonas* Otu00002	0.09	0.03	2618	3.025	0.0402
	Other v. *Pseudomonas* Otu00003	0.08	0.03	2618	2.603	0.1253
	Other v. *Sphingomonas*	0.26	0.03	2618	8.946	<0.0001
	Other v. *Sphingomonas* Otu00004	0.19	0.03	2618	6.528	<0.0001
	Pseudomonas v. *Pseudomonas* Otu00001	-0.20	0.03	2618	-6.893	<0.0001
	Pseudomonas v. *Pseudomonas* Otu00002	-0.19	0.03	2618	-6.558	<0.0001
	Pseudomonas v. *Pseudomonas* Otu00003	-0.20	0.03	2618	-6.980	<0.0001
	Pseudomonas v. *Sphingomonas*	-0.02	0.03	2618	-0.638	0.9956
	Pseudomonas v. *Sphingomonas* Otu00004	-0.09	0.03	2618	-3.056	0.0367
	Pseudomonas Otu00001 v. *Pseudomonas* Otu00002	0.01	0.03	2618	0.334	0.9999
	Pseudomonas Otu00001 v. *Pseudomonas* Otu00003	0.00	0.03	2618	-0.088	1.0000
	Pseudomonas Otu00001 v. *Sphingomonas*	0.18	0.03	2618	6.255	<0.0001
	Pseudomonas Otu00001 v. *Sphingomonas* Otu00004	0.11	0.03	2618	3.837	0.0024
	Pseudomonas Otu00002 v. *Pseudomonas* Otu00003	-0.01	0.03	2618	-0.422	0.9996
	Pseudomonas Otu00002 v. *Sphingomonas*	0.17	0.03	2618	5.920	<0.0001
	Pseudomonas Otu00002 v. *Sphingomonas* Otu00004	0.10	0.03	2618	3.503	0.0085
	Pseudomonas Otu00003 v. *Sphingomonas*	0.18	0.03	2618	6.342	<0.0001
	Pseudomonas Otu00003 v. *Sphingomonas* Otu00004	0.11	0.03	2618	3.925	0.0017
	Sphingomonas v. *Sphingomonas* Otu00004	-0.07	0.03	2618	-2.418	0.1914

Table B13. (cont'd)

2018 Spring	Other v. *Pseudomonas*	0.69	0.04	2618	15.650	<0.0001
	Other v. *Pseudomonas* Otu00001	0.49	0.04	2618	11.034	<0.0001
	Other v. *Pseudomonas* Otu00002	0.67	0.04	2618	15.080	<0.0001
	Other v. *Pseudomonas* Otu00003	0.69	0.04	2618	15.626	<0.0001
	Other v. *Sphingomonas*	0.67	0.04	2618	15.220	<0.0001
	Other v. *Sphingomonas* Otu00004	0.69	0.04	2618	15.537	<0.0001
	Pseudomonas v. *Pseudomonas* Otu00001	-0.20	0.04	2618	-4.615	0.0001
	Pseudomonas v. *Pseudomonas* Otu00002	-0.03	0.04	2618	-0.570	0.9976
	Pseudomonas v. *Pseudomonas* Otu00003	0.00	0.04	2618	-0.023	1.0000
	Pseudomonas v. *Sphingomonas*	-0.02	0.04	2618	-0.430	0.9995
	Pseudomonas v. *Sphingomonas* Otu00004	0.00	0.04	2618	-0.112	1.0000
	Pseudomonas Otu00001 v. *Pseudomonas* Otu00002	0.18	0.04	2618	4.046	0.0011
	Pseudomonas Otu00001 v. *Pseudomonas* Otu00003	0.20	0.04	2618	4.592	0.0001
	Pseudomonas Otu00001 v. *Sphingomonas*	0.19	0.04	2618	4.185	0.0006
	Pseudomonas Otu00001 v. *Sphingomonas* Otu00004	0.20	0.04	2618	4.503	0.0001
	Pseudomonas Otu00002 v. *Pseudomonas* Otu00003	0.02	0.04	2618	0.546	0.9981
	Pseudomonas Otu00002 v. *Sphingomonas*	0.01	0.04	2618	0.139	1.0000
	Pseudomonas Otu00002 v. *Sphingomonas* Otu00004	0.02	0.04	2618	0.457	0.9993
	Pseudomonas Otu00003 v. *Sphingomonas*	-0.02	0.04	2618	-0.407	0.9997
	Pseudomonas Otu00003 v. *Sphingomonas* Otu00004	0.00	0.04	2618	-0.089	1.0000
	Sphingomonas v. *Sphingomonas* Otu00004	0.01	0.04	2618	0.318	0.9999
2018 Summer	Other v. *Pseudomonas*	0.27	0.03	2618	8.088	<0.0001
	Other v. *Pseudomonas* Otu00001	0.22	0.03	2618	6.696	<0.0001

Table B13. (cont'd)

	Other v. *Pseudomonas* Otu00002	0.00	0.03	2618	-0.003	1.0000
	Other v. *Pseudomonas* Otu00003	0.14	0.03	2618	4.298	0.0004
	Other v. *Sphingomonas*	0.23	0.03	2618	7.110	<0.0001
	Other v. *Sphingomonas* Otu00004	0.26	0.03	2618	7.815	<0.0001
	Pseudomonas v. *Pseudomonas* Otu00001	-0.05	0.03	2618	-1.393	0.8059
	Pseudomonas v. *Pseudomonas* Otu00002	-0.27	0.03	2618	-8.092	<0.0001
	Pseudomonas v. *Pseudomonas* Otu00003	-0.12	0.03	2618	-3.791	0.0029
	Pseudomonas v. *Sphingomonas*	-0.03	0.03	2618	-0.978	0.9588
	Pseudomonas v. *Sphingomonas* Otu00004	-0.01	0.03	2618	-0.274	1.0000
	Pseudomonas Otu00001 v. *Pseudomonas* Otu00002	-0.22	0.03	2618	-6.699	<0.0001
	Pseudomonas Otu00001 v. *Pseudomonas* Otu00003	-0.08	0.03	2618	-2.398	0.1997
	Pseudomonas Otu00001 v. *Sphingomonas*	0.01	0.03	2618	0.415	0.9996
	Pseudomonas Otu00001 v. *Sphingomonas* Otu00004	0.04	0.03	2618	1.119	0.9225
	Pseudomonas Otu00002 v. *Pseudomonas* Otu00003	0.14	0.03	2618	4.301	0.0004
	Pseudomonas Otu00002 v. *Sphingomonas*	0.23	0.03	2618	7.114	<0.0001
	Pseudomonas Otu00002 v. *Sphingomonas* Otu00004	0.26	0.03	2618	7.818	<0.0001
	Pseudomonas Otu00003 v. *Sphingomonas*	0.09	0.03	2618	2.813	0.0734
	Pseudomonas Otu00003 v. *Sphingomonas* Otu00004	0.12	0.03	2618	3.517	0.0081
	Sphingomonas v. *Sphingomonas* Otu00004	0.02	0.03	2618	0.704	0.9924
2018 Fall	Other v. *Pseudomonas*	0.25	0.04	2618	6.905	<0.0001
	Other v. *Pseudomonas* Otu00001	-0.17	0.04	2618	-4.569	0.0001
	Other v. *Pseudomonas* Otu00002	0.24	0.04	2618	6.664	<0.0001
	Other v. *Pseudomonas* Otu00003	0.21	0.04	2618	5.881	<0.0001
	Other v. *Sphingomonas*	0.17	0.04	2618	4.817	<0.0001

Table B13. (cont'd)

	Other v. *Sphingomonas* Otu00004	0.12	0.04	2618	3.458	0.0099
	Pseudomonas v. *Pseudomonas* Otu00001	-0.41	0.04	2618	-11.474	<0.0001
	Pseudomonas v. *Pseudomonas* Otu00002	-0.01	0.04	2618	-0.240	1.0000
	Pseudomonas v. *Pseudomonas* Otu00003	-0.04	0.04	2618	-1.024	0.9487
	Pseudomonas v. *Sphingomonas*	-0.08	0.04	2618	-2.088	0.3603
	Pseudomonas v. *Sphingomonas* Otu00004	-0.12	0.04	2618	-3.447	0.0103
	Pseudomonas Otu00001 v. *Pseudomonas* Otu00002	0.41	0.04	2618	11.233	<0.0001
	Pseudomonas Otu00001 v. *Pseudomonas* Otu00003	0.38	0.04	2618	10.450	<0.0001
	Pseudomonas Otu00001 v. *Sphingomonas*	0.34	0.04	2618	9.386	<0.0001
	Pseudomonas Otu00001 v. *Sphingomonas* Otu00004	0.29	0.04	2618	8.027	<0.0001
	Pseudomonas Otu00002 v. *Pseudomonas* Otu00003	-0.03	0.04	2618	-0.783	0.9866
	Pseudomonas Otu00002 v. *Sphingomonas*	-0.07	0.04	2618	-1.847	0.5161
	Pseudomonas Otu00002 v. *Sphingomonas* Otu00004	-0.12	0.04	2618	-3.206	0.0230
	Pseudomonas Otu00003 v. *Sphingomonas*	-0.04	0.04	2618	-1.064	0.9385
	Pseudomonas Otu00003 v. *Sphingomonas* Otu00004	-0.09	0.04	2618	-2.423	0.1893
	Sphingomonas v. *Sphingomonas* Otu00004	-0.05	0.04	2618	-1.359	0.8235
2019 Spring	Other v. *Pseudomonas*	-0.08	0.04	2618	-1.827	0.5299
	Other v. *Pseudomonas* Otu00001	-0.46	0.04	2618	-10.300	<0.0001
	Other v. *Pseudomonas* Otu00002	-0.19	0.04	2618	-4.230	0.0005
	Other v. *Pseudomonas* Otu00003	-0.06	0.04	2618	-1.322	0.8418
	Other v. *Sphingomonas*	0.04	0.04	2618	0.921	0.9693
	Other v. *Sphingomonas* Otu00004	0.04	0.04	2618	0.917	0.9700

Table B13. (cont'd)

	Pseudomonas v. *Pseudomonas* Otu00001	-0.38	0.04	2618	-8.474	<0.0001
	Pseudomonas v. *Pseudomonas* Otu00002	-0.11	0.04	2618	-2.403	0.1974
	Pseudomonas v. *Pseudomonas* Otu00003	0.02	0.04	2618	0.505	0.9988
	Pseudomonas v. *Sphingomonas*	0.12	0.04	2618	2.748	0.0872
	Pseudomonas v. *Sphingomonas* Otu00004	0.12	0.04	2618	2.744	0.0881
	Pseudomonas Otu00001 v. *Pseudomonas* Otu00002	0.27	0.04	2618	6.070	<0.0001
	Pseudomonas Otu00001 v. *Pseudomonas* Otu00003	0.40	0.04	2618	8.978	<0.0001
	Pseudomonas Otu00001 v. *Sphingomonas*	0.50	0.04	2618	11.221	<0.0001
	Pseudomonas Otu00001 v. *Sphingomonas* Otu00004	0.50	0.04	2618	11.217	<0.0001
	Pseudomonas Otu00002 v. *Pseudomonas* Otu00003	0.13	0.04	2618	2.908	0.0564
	Pseudomonas Otu00002 v. *Sphingomonas*	0.23	0.04	2618	5.151	<0.0001
	Pseudomonas Otu00002 v. *Sphingomonas* Otu00004	0.23	0.04	2618	5.147	<0.0001
	Pseudomonas Otu00003 v. *Sphingomonas*	0.10	0.04	2618	2.243	0.2729
	Pseudomonas Otu00003 v. *Sphingomonas* Otu00004	0.10	0.04	2618	2.239	0.2749
	Sphingomonas v. *Sphingomonas* Otu00004	0.00	0.04	2618	-0.004	1.0000
2019 Summer	Other v. *Pseudomonas*	0.20	0.03	2618	6.110	<0.0001
	Other v. *Pseudomonas* Otu00001	0.05	0.03	2618	1.592	0.6878
	Other v. *Pseudomonas* Otu00002	0.00	0.03	2618	0.037	1.0000
	Other v. *Pseudomonas* Otu00003	0.20	0.03	2618	5.944	<0.0001
	Other v. *Sphingomonas*	0.24	0.03	2618	7.298	<0.0001
	Other v. *Sphingomonas* Otu00004	0.17	0.03	2618	5.159	<0.0001
	Pseudomonas v. *Pseudomonas* Otu00001	-0.15	0.03	2618	-4.518	0.0001

Table B13. (cont'd)

	Pseudomonas v. *Pseudomonas* Otu00002	-0.20	0.03	2618	-6.073	<0.0001
	Pseudomonas v. *Pseudomonas* Otu00003	-0.01	0.03	2618	-0.166	1.0000
	Pseudomonas v. *Sphingomonas*	0.04	0.03	2618	1.188	0.8989
	Pseudomonas v. *Sphingomonas* Otu00004	-0.03	0.03	2618	-0.950	0.9641
	Pseudomonas Otu00001 v. *Pseudomonas* Otu00002	-0.05	0.03	2618	-1.555	0.7113
	Pseudomonas Otu00001 v. *Pseudomonas* Otu00003	0.14	0.03	2618	4.352	0.0003
	Pseudomonas Otu00001 v. *Sphingomonas*	0.19	0.03	2618	5.706	<0.0001
	Pseudomonas Otu00001 v. *Sphingomonas* Otu00004	0.12	0.03	2618	3.568	0.0067
	Pseudomonas Otu00002 v. *Pseudomonas* Otu00003	0.20	0.03	2618	5.907	<0.0001
	Pseudomonas Otu00002 v. *Sphingomonas*	0.24	0.03	2618	7.261	<0.0001
	Pseudomonas Otu00002 v. *Sphingomonas* Otu00004	0.17	0.03	2618	5.122	<0.0001
	Pseudomonas Otu00003 v. *Sphingomonas*	0.04	0.03	2618	1.354	0.8262
	Pseudomonas Otu00003 v. *Sphingomonas* Otu00004	-0.03	0.03	2618	-0.785	0.9865
	Sphingomonas v. *Sphingomonas* Otu00004	-0.07	0.03	2618	-2.138	0.3302
2019 Fall	Other v. *Pseudomonas*	0.29	0.04	2618	7.315	<0.0001
	Other v. *Pseudomonas* Otu00001	-0.01	0.04	2618	-0.233	1.0000
	Other v. *Pseudomonas* Otu00002	0.24	0.04	2618	6.037	<0.0001
	Other v. *Pseudomonas* Otu00003	0.20	0.04	2618	5.129	<0.0001
	Other v. *Sphingomonas*	0.25	0.04	2618	6.498	<0.0001
	Other v. *Sphingomonas* Otu00004	0.12	0.04	2618	3.061	0.0361
	Pseudomonas v. *Pseudomonas* Otu00001	-0.30	0.04	2618	-7.549	<0.0001
	Pseudomonas v. *Pseudomonas* Otu00002	-0.05	0.04	2618	-1.278	0.8622
	Pseudomonas v. *Pseudomonas* Otu00003	-0.09	0.04	2618	-2.186	0.3032
	Pseudomonas v. *Sphingomonas*	-0.03	0.04	2618	-0.818	0.9832

Table B13. (cont'd)

	Pseudomonas v. *Sphingomonas* Otu00004	-0.17	0.04	2618	-4.254	0.0004
	Pseudomonas Otu00001 v. *Pseudomonas* Otu00002	0.25	0.04	2618	6.271	<0.0001
	Pseudomonas Otu00001 v. *Pseudomonas* Otu00003	0.21	0.04	2618	5.362	<0.0001
	Pseudomonas Otu00001 v. *Sphingomonas*	0.26	0.04	2618	6.731	<0.0001
	Pseudomonas Otu00001 v. *Sphingomonas* Otu00004	0.13	0.04	2618	3.295	0.0173
	Pseudomonas Otu00002 v. *Pseudomonas* Otu00003	-0.04	0.04	2618	-0.908	0.9713
	Pseudomonas Otu00002 v. *Sphingomonas*	0.02	0.04	2618	0.460	0.9993
	Pseudomonas Otu00002 v. *Sphingomonas* Otu00004	-0.12	0.04	2618	-2.976	0.0465
	Pseudomonas Otu00003 v. *Sphingomonas*	0.05	0.04	2618	1.369	0.8185
	Pseudomonas Otu00003 v. *Sphingomonas* Otu00004	-0.08	0.04	2618	-2.068	0.3723
	Sphingomonas v. *Sphingomonas* Otu00004	-0.13	0.04	2618	-3.437	0.0107
Genus/OTU	**Contrast**	**Estimate**	**SE**	**df**	**t-ratio**	**p-value**
Other	2017 Fall v. 2018 Fall	0.02	0.03	2635	0.567	0.9977
	2017 Fall v. 2018 Spring	-0.42	0.04	2628	-11.144	<0.0001
	2017 Fall v. 2018 Summer	-0.02	0.03	2635	-0.704	0.9924
	2017 Fall v. 2019 Fall	-0.02	0.03	2628	-0.504	0.9988
	2017 Fall v. 2019 Spring	0.24	0.04	2634	6.331	<0.0001
	2017 Fall v. 2019 Summer	0.01	0.03	2633	0.455	0.9993
	2018 Fall v. 2018 Spring	-0.44	0.04	2626	-10.780	<0.0001
	2018 Fall v. 2018 Summer	-0.04	0.03	2629	-1.169	0.9059
	2018 Fall v. 2019 Fall	-0.04	0.04	2633	-0.954	0.9635
	2018 Fall v. 2019 Spring	0.22	0.04	2633	5.411	<0.0001
	2018 Fall v. 2019 Summer	0.00	0.03	2630	-0.127	1.0000

Table B13. (cont'd)

	2018 Spring v. 2018 Summer	0.40	0.04	2626	10.115	<0.0001
	2018 Spring v. 2019 Fall	0.40	0.04	2630	9.556	<0.0001
	2018 Spring v. 2019 Spring	0.66	0.04	2631	14.751	<0.0001
	2018 Spring v. 2019 Summer	0.43	0.04	2625	11.003	<0.0001
	2018 Summer v. 2019 Fall	0.00	0.04	2632	0.123	1.0000
	2018 Summer v. 2019 Spring	0.26	0.04	2634	6.619	<0.0001
	2018 Summer v. 2019 Summer	0.04	0.03	2629	1.089	0.9314
	2019 Fall v. 2019 Spring	0.26	0.04	2633	6.082	<0.0001
	2019 Fall v. 2019 Summer	0.03	0.04	2632	0.869	0.9770
	2019 Spring v. 2019 Summer	-0.23	0.04	2632	-5.697	<0.0001
Pseudomonas	2017 Fall v. 2018 Fall	-0.01	0.03	2635	-0.291	1.0000
	2017 Fall v. 2018 Spring	0.00	0.04	2628	-0.112	1.0000
	2017 Fall v. 2018 Summer	-0.03	0.03	2635	-1.066	0.9378
	2017 Fall v. 2019 Fall	-0.01	0.03	2628	-0.251	1.0000
	2017 Fall v. 2019 Spring	-0.12	0.04	2634	-3.167	0.0260
	2017 Fall v. 2019 Summer	-0.06	0.03	2633	-1.946	0.4501
	2018 Fall v. 2018 Spring	0.01	0.04	2626	0.131	1.0000
	2018 Fall v. 2018 Summer	-0.02	0.03	2629	-0.681	0.9937
	2018 Fall v. 2019 Fall	0.00	0.04	2633	0.024	1.0000
	2018 Fall v. 2019 Spring	-0.11	0.04	2633	-2.701	0.0983
	2018 Fall v. 2019 Summer	-0.05	0.03	2630	-1.471	0.7621
	2018 Spring v. 2018 Summer	-0.03	0.04	2626	-0.736	0.9904
	2018 Spring v. 2019 Fall	0.00	0.04	2630	-0.105	1.0000
	2018 Spring v. 2019 Spring	-0.12	0.04	2631	-2.591	0.1291
	2018 Spring v. 2019 Summer	-0.06	0.04	2625	-1.433	0.7838
	2018 Summer v. 2019 Fall	0.02	0.04	2632	0.676	0.9939
	2018 Summer v. 2019 Spring	-0.09	0.04	2634	-2.197	0.2972
	2018 Summer v. 2019 Summer	-0.03	0.03	2629	-0.833	0.9816
	2019 Fall v. 2019 Spring	-0.11	0.04	2633	-2.633	0.1167
	2019 Fall v. 2019 Summer	-0.05	0.04	2632	-1.432	0.7844

Table B13. (cont'd)

	2019 Spring v. 2019 Summer	0.06	0.04	2632	1.497	0.7467
Pseudomonas Otu00001	2017 Fall v. 2018 Fall	-0.22	0.03	2635	-6.846	<0.0001
	2017 Fall v. 2018 Spring	-0.01	0.04	2628	-0.233	1.0000
	2017 Fall v. 2018 Summer	0.12	0.03	2635	3.888	0.0020
	2017 Fall v. 2019 Fall	-0.10	0.03	2628	-3.030	0.0397
	2017 Fall v. 2019 Spring	-0.30	0.04	2634	-7.938	<0.0001
	2017 Fall v. 2019 Summer	-0.01	0.03	2633	-0.351	0.9999
	2018 Fall v. 2018 Spring	0.22	0.04	2626	5.311	<0.0001
	2018 Fall v. 2018 Summer	0.34	0.03	2629	9.972	<0.0001
	2018 Fall v. 2019 Fall	0.12	0.04	2633	3.180	0.0251
	2018 Fall v. 2019 Spring	-0.08	0.04	2633	-1.862	0.5057
	2018 Fall v. 2019 Summer	0.21	0.03	2630	6.145	<0.0001
	2018 Spring v. 2018 Summer	0.13	0.04	2626	3.297	0.0172
	2018 Spring v. 2019 Fall	-0.10	0.04	2630	-2.276	0.2559
	2018 Spring v. 2019 Spring	-0.29	0.04	2631	-6.533	<0.0001
	2018 Spring v. 2019 Summer	0.00	0.04	2625	-0.055	1.0000
	2018 Summer v. 2019 Fall	-0.23	0.04	2632	-6.220	<0.0001
	2018 Summer v. 2019 Spring	-0.42	0.04	2634	-10.661	<0.0001
	2018 Summer v. 2019 Summer	-0.13	0.03	2629	-3.979	0.0014
	2019 Fall v. 2019 Spring	-0.20	0.04	2633	-4.638	0.0001
	2019 Fall v. 2019 Summer	0.09	0.04	2632	2.575	0.1340
	2019 Spring v. 2019 Summer	0.29	0.04	2632	7.316	<0.0001
Pseudomonas Otu00002	2017 Fall v. 2018 Fall	0.17	0.03	2635	5.239	<0.0001
	2017 Fall v. 2018 Spring	0.16	0.04	2628	4.269	0.0004
	2017 Fall v. 2018 Summer	-0.11	0.03	2635	-3.530	0.0077
	2017 Fall v. 2019 Fall	0.13	0.03	2628	3.808	0.0027
	2017 Fall v. 2019 Spring	-0.04	0.04	2634	-0.998	0.9545
	2017 Fall v. 2019 Summer	-0.07	0.03	2633	-2.317	0.2363
	2018 Fall v. 2018 Spring	-0.01	0.04	2626	-0.275	1.0000

Table B13. (cont'd)

	2018 Fall v. 2018 Summer	-0.28	0.03	2629	-8.129	<0.0001
	2018 Fall v. 2019 Fall	-0.04	0.04	2633	-1.072	0.9364
	2018 Fall v. 2019 Spring	-0.21	0.04	2633	-5.128	<0.0001
	2018 Fall v. 2019 Summer	-0.24	0.03	2630	-7.023	<0.0001
	2018 Spring v. 2018 Summer	-0.27	0.04	2626	-6.879	<0.0001
	2018 Spring v. 2019 Fall	-0.03	0.04	2630	-0.696	0.9929
	2018 Spring v. 2019 Spring	-0.20	0.04	2631	-4.441	0.0002
	2018 Spring v. 2019 Summer	-0.23	0.04	2625	-5.911	<0.0001
	2018 Summer v. 2019 Fall	0.24	0.04	2632	6.654	<0.0001
	2018 Summer v. 2019 Spring	0.07	0.04	2634	1.817	0.5365
	2018 Summer v. 2019 Summer	0.04	0.03	2629	1.130	0.9191
	2019 Fall v. 2019 Spring	-0.17	0.04	2633	-4.001	0.0013
	2019 Fall v. 2019 Summer	-0.20	0.04	2632	-5.604	<0.0001
	2019 Spring v. 2019 Summer	-0.03	0.04	2632	-0.870	0.9770
Pseudomonas Otu00003	2017 Fall v. 2018 Fall	0.16	0.03	2635	4.749	<0.0001
	2017 Fall v. 2018 Spring	0.20	0.04	2628	5.237	<0.0001
	2017 Fall v. 2018 Summer	0.04	0.03	2635	1.426	0.7877
	2017 Fall v. 2019 Fall	0.11	0.03	2628	3.132	0.0291
	2017 Fall v. 2019 Spring	0.10	0.04	2634	2.772	0.0818
	2017 Fall v. 2019 Summer	0.14	0.03	2633	4.364	0.0003
	2018 Fall v. 2018 Spring	0.04	0.04	2626	1.017	0.9503
	2018 Fall v. 2018 Summer	-0.11	0.03	2629	-3.219	0.0221
	2018 Fall v. 2019 Fall	-0.05	0.04	2633	-1.264	0.8683
	2018 Fall v. 2019 Spring	-0.05	0.04	2633	-1.242	0.8779
	2018 Fall v. 2019 Summer	-0.02	0.03	2630	-0.565	0.9977
	2018 Spring v. 2018 Summer	-0.15	0.04	2626	-3.888	0.0020
	2018 Spring v. 2019 Fall	-0.09	0.04	2630	-2.117	0.3430
	2018 Spring v. 2019 Spring	-0.09	0.04	2631	-2.060	0.3768
	2018 Spring v. 2019 Summer	-0.06	0.04	2625	-1.547	0.7163
	2018 Summer v. 2019 Fall	0.06	0.04	2632	1.760	0.5755

Table B13. (cont'd)

	2018 Summer v. 2019 Spring	0.06	0.04	2634	1.536	0.7233
	2018 Summer v. 2019 Summer	0.09	0.03	2629	2.774	0.0814
	2019 Fall v. 2019 Spring	0.00	0.04	2633	-0.072	1.0000
	2019 Fall v. 2019 Summer	0.03	0.04	2632	0.773	0.9875
	2019 Spring v. 2019 Summer	0.03	0.04	2632	0.786	0.9864
Sphingomonas	2017 Fall v. 2018 Fall	-0.07	0.03	2635	-2.029	0.3967
	2017 Fall v. 2018 Spring	0.00	0.04	2628	-0.127	1.0000
	2017 Fall v. 2018 Summer	-0.05	0.03	2635	-1.509	0.7397
	2017 Fall v. 2019 Fall	-0.02	0.03	2628	-0.643	0.9954
	2017 Fall v. 2019 Spring	0.02	0.04	2634	0.578	0.9974
	2017 Fall v. 2019 Summer	0.00	0.03	2633	-0.088	1.0000
	2018 Fall v. 2018 Spring	0.06	0.04	2626	1.520	0.7327
	2018 Fall v. 2018 Summer	0.02	0.03	2629	0.568	0.9977
	2018 Fall v. 2019 Fall	0.04	0.04	2633	1.175	0.9036
	2018 Fall v. 2019 Spring	0.09	0.04	2633	2.163	0.3165
	2018 Fall v. 2019 Summer	0.06	0.03	2630	1.835	0.5244
	2018 Spring v. 2018 Summer	-0.04	0.04	2626	-1.071	0.9366
	2018 Spring v. 2019 Fall	-0.02	0.04	2630	-0.414	0.9996
	2018 Spring v. 2019 Spring	0.03	0.04	2631	0.596	0.9969
	2018 Spring v. 2019 Summer	0.00	0.04	2625	0.051	1.0000
	2018 Summer v. 2019 Fall	0.02	0.04	2632	0.681	0.9936
	2018 Summer v. 2019 Spring	0.07	0.04	2634	1.739	0.5898
	2018 Summer v. 2019 Summer	0.04	0.03	2629	1.332	0.8367
	2019 Fall v. 2019 Spring	0.04	0.04	2633	1.042	0.9443
	2019 Fall v. 2019 Summer	0.02	0.04	2632	0.534	0.9983
	2019 Spring v. 2019 Summer	-0.02	0.04	2632	-0.622	0.9961
Sphingomonas Otu00004	2017 Fall v. 2018 Fall	-0.05	0.03	2635	-1.390	0.8075
	2017 Fall v. 2018 Spring	0.08	0.04	2628	2.109	0.3473
	2017 Fall v. 2018 Summer	0.05	0.03	2635	1.495	0.7482

Table B13. (cont'd)

2017 Fall v. 2019 Fall	-0.09	0.03	2628	-2.513	0.1549
2017 Fall v. 2019 Spring	0.09	0.04	2634	2.423	0.1892
2017 Fall v. 2019 Summer	0.00	0.03	2633	-0.118	1.0000
2018 Fall v. 2018 Spring	0.12	0.04	2626	3.076	0.0345
2018 Fall v. 2018 Summer	0.09	0.03	2629	2.657	0.1099
2018 Fall v. 2019 Fall	-0.04	0.04	2633	-1.089	0.9314
2018 Fall v. 2019 Spring	0.14	0.04	2633	3.360	0.0139
2018 Fall v. 2019 Summer	0.04	0.03	2630	1.205	0.8923
2018 Spring v. 2018 Summer	-0.03	0.04	2626	-0.839	0.9809
2018 Spring v. 2019 Fall	-0.17	0.04	2630	-3.948	0.0016
2018 Spring v. 2019 Spring	0.01	0.04	2631	0.278	1.0000
2018 Spring v. 2019 Summer	-0.08	0.04	2625	-2.108	0.3481
2018 Summer v. 2019 Fall	-0.13	0.04	2632	-3.675	0.0045
2018 Summer v. 2019 Spring	0.05	0.04	2634	1.147	0.9132
2018 Summer v. 2019 Summer	-0.05	0.03	2629	-1.514	0.7367
2019 Fall v. 2019 Spring	0.18	0.04	2633	4.220	0.0005
2019 Fall v. 2019 Summer	0.08	0.04	2632	2.284	0.2519
2019 Spring v. 2019 Summer	-0.10	0.04	2632	-2.411	0.1940

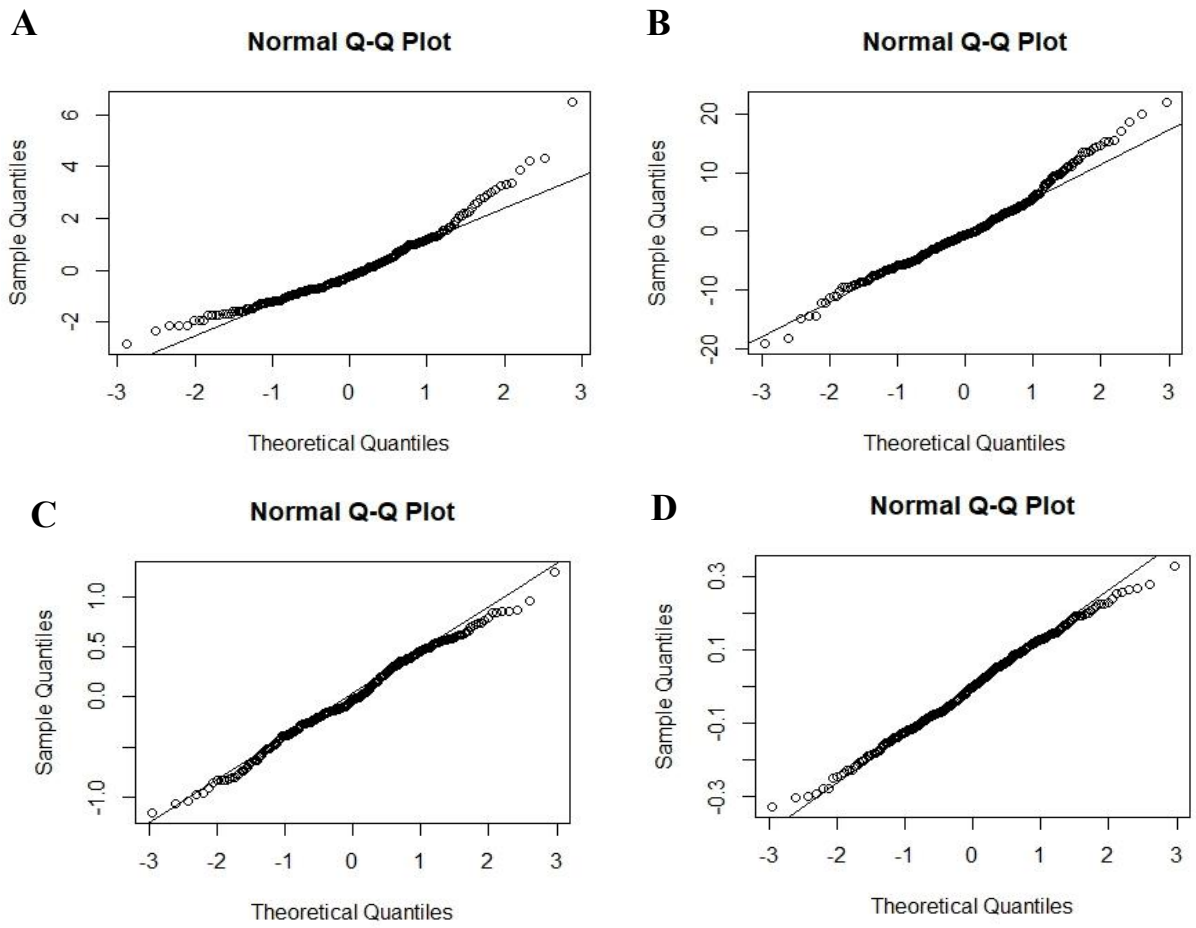


Figure B20. The 2019 quantile-quantile plots (qqplot) of the residuals for graphical visualization of the distribution of the alpha diversity statistics data, **A)** bacteria plate counts (log cfu/cm^2), **B)** the number of OTUs, **C)** the Shannon diversity, and **D)** Shannon evenness indices

Table B14. The mean 2019 log cfu/cm^2 of leaf area ± SE of bacteria plate counts for each site and season, including the pairwise comparisons of the estimated marginal means with the confidence limits (lower and upper C.L.) and the p-value. Superscripted letters following the season indicate statistical differences within each site and upper-case letters indicate statistical differences across sites for each season, with significance determined by p-value ≤ 0.05.

Site	Season	Mean log cfu/cm^2	SE	df	lower C.L.	upper C.L.	
1	Spring [a]	1.9	0.3	15	1.4	2.5	A
	Summer [b]	4.9	0.3	15	4.4	5.5	A
	Fall [b]	5.2	0.3	15	4.6	5.8	A
2	Spring [a]	1.1	0.3	18	0.5	1.6	B
	Summer [b]	5.8	0.3	18	5.2	6.4	B
	Fall [b]	6.0	0.3	18	5.4	6.6	B

Site	Contrast	estimate	SE	df	t-ratio	p-value
1	Fall v. Spring	3.3	0.3	226	11.0	<0.0001
	Fall v. Summer	0.3	0.3	226	0.9	0.6666
	Spring v. Summer	-3.0	0.3	226	-10.1	<0.0001
2	Fall v. Spring	5.0	0.3	226	16.0	<0.0001
	Fall v. Summer	0.2	0.3	226	0.7	0.7868
	Spring v. Summer	-4.8	0.3	226	-15.3	<0.0001

Season	Contrast	estimate	SE	df	t-ratio	p-value
Spring	Site 1 v. 2	-0.9	0.4	16	-2.305	0.0345
Summer	Site 1 v. 2	0.9	0.4	17	2.290	0.0355
Fall	Site 1 v. 2	0.8	0.4	16	2.166	0.0453

Table B15. The 2019 mean number of OTUs ± SE for each site and season including the pairwise comparisons of the estimated marginal means with the confidence limits (lower and upper C.L.) and the p-value. Superscripted letters following the season indicate statistical differences within each site and upper-case letters indicate statistical differences across sites for each season, with significance determined by p-value ≤ 0.05.

Site	Season	Mean no. OTUs	SE	df	lower C.L.	upper C.L.	
1	Spring [a]	6.3	1.0	17	4.1	8.5	A
	Summer [b]	17.6	1.2	33	15.1	20.1	A
	Fall [c]	25.0	1.3	35	22.3	27.6	A
2	Spring [a]	9.5	1.9	130	5.8	13.1	A
	Summer [b]	23.0	0.9	11	20.9	25.0	B
	Fall [c]	35.2	1.0	16	33.1	37.4	B

Site	Contrast	estimate	SE	df	t-ratio	p-value
1	Fall - Spring	18.6	1.5	271	12.397	<0.0001
	Fall - Summer	7.4	1.6	293	4.619	<0.0001
	Spring - Summer	-11.2	1.4	293	-7.987	<0.0001
2	Fall - Spring	25.8	2.0	305	12.811	<0.0001
	Fall - Summer	12.3	1.2	270	10.621	<0.0001
	Spring - Summer	-13.5	2.0	299	-6.939	<0.0001

Season	Contrast	estimate	SE	df	t-ratio	p-value
Spring	Site 1 v. 2	3.1	2.1	66	1.477	0.1444
Summer	Site 1 v. 2	5.4	1.6	21	3.469	0.0023
Fall	Site 1 v. 2	10.3	1.7	25	6.184	<0.0001

Table B16. The 2019 mean Shannon diversity index ± SE for each site and season including the pairwise comparisons of the estimated marginal means with the confidence limits (lower and upper C.L.) and the p-value. Statistical differences by site and season are indicated by superscripted letters following site and season, with significance determined by p-value ≤ 0.05.

Site	Season	Mean Shannon diversity index	SE	df	lower C.L.	upper C.L.
1 [a]	Spring [a]	0.2	0.1	16.1	0.1	0.387
	Summer [b]	1.0	0.1	30.7	0.8	1.139
	Fall [c]	1.6	0.1	32.5	1.5	1.822
2 [b]	Spring [a]	0.5	0.1	120.1	0.3	0.792
	Summer [b]	1.4	0.1	10.5	1.2	1.496
	Fall [c]	1.8	0.1	14.5	1.6	1.917

	Contrast	estimate	SE	df	t-ratio	p-value
	Fall - Spring	1.3	0.1	298	15.800	<0.0001
	Fall - Summer	0.5	0.1	288	8.361	<0.0001
	Spring - Summer	-0.8	0.1	298	-9.733	<0.0001

	Contrast	estimate	SE	df	t-ratio	p-value
	Site 1 v. 2	0.3	0.1	7	3.349	0.0116

Table B17. The 2019 mean Shannon evenness index ± SE for each site and season including the pairwise comparisons of the estimated marginal means with the confidence limits (lower and upper C.L.) and the p-value. Superscripted letters following the season indicate statistical differences within each site and upper-case letters indicate statistical differences across sites for each season, with significance determined by p-value ≤ 0.05.

Site	Season	Mean no. OTUs	SE	df	lower C.L.	upper C.L.	
1	Spring [a]	0.2	0.02	16	0.1	0.2	A
	Summer [b]	0.3	0.02	31	0.3	0.4	A
	Fall [c]	0.5	0.03	33	0.5	0.6	A
2	Spring [a]	0.2	0.04	122	0.2	0.3	A
	Summer [b]	0.4	0.02	11	0.4	0.5	B
	Fall [c]	0.5	0.02	15	0.5	0.5	A

Site	Contrast	estimate	SE	df	t-ratio	p-value
1	Fall - Spring	0.4	0.03	274	12.170	<.0001
	Fall - Summer	0.2	0.03	293	5.552	<.0001
	Spring - Summer	-0.2	0.03	291	-6.697	<.0001
2	Fall - Spring	0.3	0.04	303	6.659	<.0001
	Fall - Summer	0.1	0.02	269	2.797	0.0152
	Spring - Summer	-0.2	0.04	298	-5.231	<.0001

Season	Contrast	estimate	SE	df	t-ratio	p-value
Spring	Site 1 v. 2	0.08	0.04	61.6	1.834	0.0715
Summer	Site 1 v. 2	0.09	0.03	19.5	2.965	0.0078
Fall	Site 1 v. 2	-0.02	0.03	23.2	-0.591	0.5600

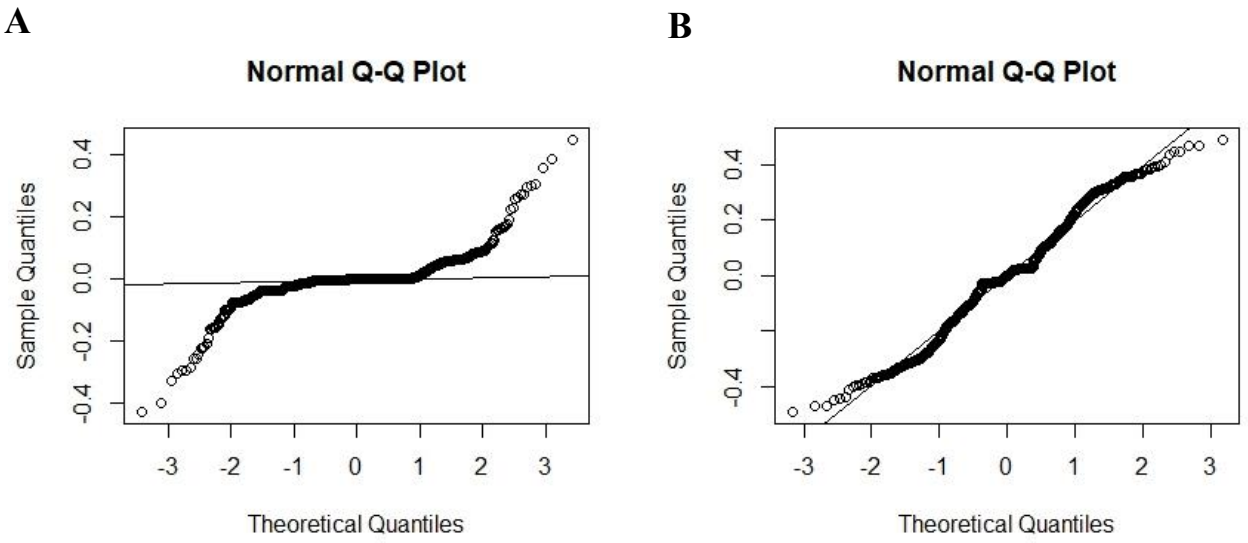


Figure B21. The 2019 quantile-quantile plots (qqplot) of the residuals for graphical visualization of the distribution of the relative abundance data for **A)** the top 4 Phyla and the rare Phyla combined into "other" relative abundance, and **B)** the *Pseudomonas* and all "other" taxa relative abundances.

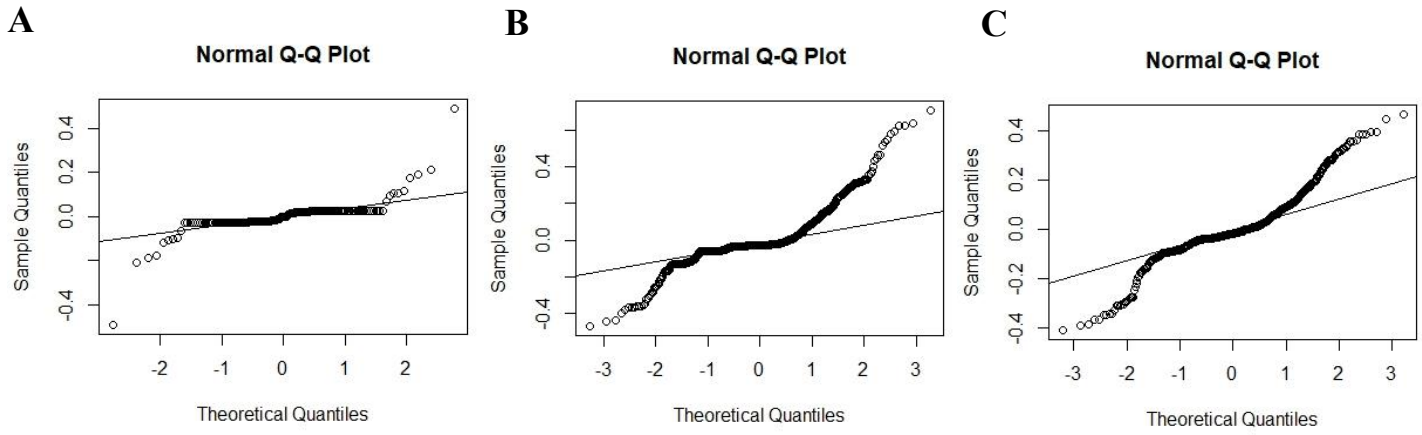


Figure B22. The 2019 quantile-quantile plots (qqplot) of the residuals for graphical visualization of the distribution of the relative abundance data at the deepest taxonomic level (genus or family), where taxa that had a relative abundance <0.03 were combined into "other". For each season **A)** Spring, **B)** Summer, **C)** Fall.

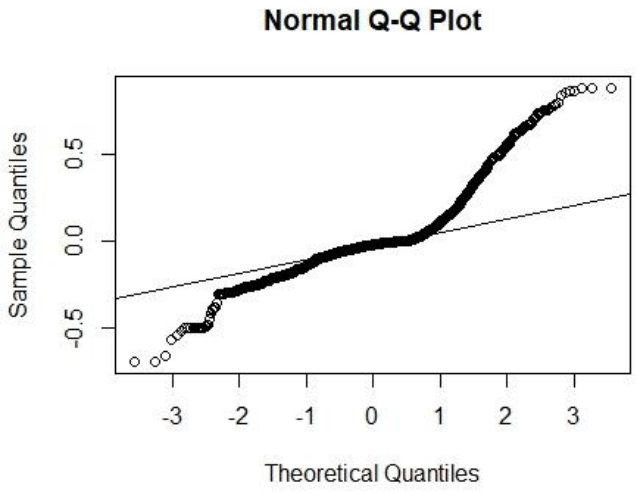


Figure B23. The 2019 quantile-quantile plot (qqplot) of the residuals for graphical visualization of the distribution of the relative abundance data of the core microbiome (genus and OTU). Includes the four core genera *Pseudomonas* Otu0001, *Pseudomonas* Otu0002, *Sphingomonas* Otu0003 and *Sphingomonas* Otu0007, with the other *Pseudomonas* combined and *Sphingomonas* combined and remaining additional taxa combined into "other". Core taxa were selected via occurrence and relative abundance when they occurred in 50% of all samples and had a relative abundance of ≥ 0.01.

Table B18. The 2019 mean relative abundances of the top 4 Phyla and "other" rarer Phyla combined ± SE, with the confidence limits (lower and upper C.L.) and the p-value. Superscripted letters following Phyla indicate statistical differences within each season while upper-cased letters indicate statistical differences of each Phyla across season, with significance determined by p-value ≤ 0.05.

Season	Phylum	Mean	SE	df	lower C.L.	upper C.L.	
Spring	Proteobacteria [b]	1.00	0.01	831	0.99	1.01	C
	Firmicutes [a]	0.00	0.01	831	-0.01	0.01	A
	Actinobacteria [a]	0.00	0.01	831	-0.01	0.01	A
	Bacteroidetes [a]	0.00	0.01	831	-0.01	0.01	A
	Other [a]	0.00	0.01	831	-0.01	0.01	A
Summer	Proteobacteria [c]	0.93	0.005	556	0.93	0.94	B
	Bacteroidetes [b]	0.04	0.005	556	0.03	0.05	B
	Actinobacteria [b]	0.02	0.005	556	0.01	0.03	B
	Firmicutes [a]	0.00	0.005	556	-0.01	0.01	A
	Other [a]	0.00	0.005	556	-0.01	0.01	A
Fall	Proteobacteria [c]	0.91	0.01	662	0.90	0.92	A
	Bacteroidetes [b]	0.08	0.01	662	0.07	0.09	C
	Actinobacteria [a]	0.02	0.01	662	0.01	0.03	AB
	Firmicutes [a]	0.00	0.01	662	-0.01	0.01	A
	Other [a]	0.00	0.01	662	-0.01	0.01	A

Table B19. The 2019 pairwise comparisons of the estimated marginal means of relative abundances of the top 4 Phyla and "other" combined Phyla for each season and for each Phyla across season with p-values, with significance determined by p-value ≤ 0.05.

Season	Contrast	Estimate	SE	df	t-ratio	p-value
Spring	Actinobacteria v. Bacteroidetes	0.001	0.008	1543	0.102	1.0000
	Actinobacteria v. Firmicutes	0.000	0.008	1543	-0.009	1.0000
	Actinobacteria v. Other	0.001	0.008	1543	0.108	1.0000
	Actinobacteria v. Proteobacteria	-0.997	0.008	1543	-128.587	<0.0001
	Bacteroidetes v. Firmicutes	-0.001	0.008	1543	-0.111	1.0000
	Bacteroidetes v. Other	0.000	0.008	1543	0.006	1.0000
	Bacteroidetes v. Proteobacteria	-0.998	0.008	1543	-128.690	<0.0001
	Firmicutes v. Other	0.001	0.008	1543	0.117	1.0000
	Firmicutes v. Proteobacteria	-0.997	0.008	1543	-128.579	<0.0001
	Other v. Proteobacteria	-0.998	0.008	1543	-128.696	<0.0001
Summer	Actinobacteria v. Bacteroidetes	-0.015	0.006	1543	-2.323	0.1380
	Actinobacteria v. Firmicutes	0.021	0.006	1543	3.365	0.0070
	Actinobacteria v. Other	0.023	0.006	1543	3.628	0.0027
	Actinobacteria v. Proteobacteria	-0.911	0.006	1543	-142.818	<0.0001
	Bacteroidetes v. Firmicutes	0.036	0.006	1543	5.688	<0.0001
	Bacteroidetes v. Other	0.038	0.006	1543	5.951	<0.0001
	Bacteroidetes v. Proteobacteria	-0.896	0.006	1543	-140.495	<0.0001
	Firmicutes v. Other	0.002	0.006	1543	0.263	0.9990
	Firmicutes v. Proteobacteria	-0.933	0.006	1543	-146.183	<0.0001
	Other v. Proteobacteria	-0.934	0.006	1543	-146.446	<0.0001
Fall	Actinobacteria v. Bacteroidetes	-0.060	0.007	1543	-8.551	<0.0001
	Actinobacteria v. Firmicutes	0.014	0.007	1543	2.028	0.2530
	Actinobacteria v. Other	0.015	0.007	1543	2.090	0.2250
	Actinobacteria v. Proteobacteria	-0.893	0.007	1543	-127.012	<0.0001
	Bacteroidetes v. Firmicutes	0.074	0.007	1543	10.579	<0.0001
	Bacteroidetes v. Other	0.075	0.007	1543	10.640	<0.0001
	Bacteroidetes v. Proteobacteria	-0.833	0.007	1543	-118.462	<0.0001
	Firmicutes v. Other	0.000	0.007	1543	0.062	1.0000

Table B19. (cont'd)

	Firmicutes v. Proteobacteria	-0.907	0.007	1543	-129.040	<0.0001
	Other v. Proteobacteria	-0.908	0.007	1543	-129.102	<0.0001

Phylum	Contrast	estimate	SE	df	t-ratio	p-value
Actinobacteria	Fall - Spring	0.014	0.008	1530	1.882	0.1442
	Fall - Summer	-0.009	0.007	1587	-1.277	0.4085
	Spring - Summer	-0.023	0.007	1577	-3.145	0.0048
Bacteroidetes	Fall - Spring	0.075	0.008	1530	9.935	<0.0001
	Fall - Summer	0.037	0.007	1587	5.453	<0.0001
	Spring - Summer	-0.038	0.007	1577	-5.296	<0.0001
Firmicutes	Fall - Spring	0.000	0.008	1530	-0.012	0.9999
	Fall - Summer	-0.001	0.007	1587	-0.206	0.9769
	Spring - Summer	-0.001	0.007	1577	-0.178	0.9826
Other	Fall - Spring	0.000	0.008	1530	0.051	0.9986
	Fall - Summer	0.000	0.007	1587	-0.022	0.9997
	Spring - Summer	-0.001	0.007	1577	-0.073	0.9971
Proteobacteria	Fall - Spring	-0.090	0.008	1530	-11.855	<0.0001
	Fall - Summer	-0.027	0.007	1587	-3.949	0.0002
	Spring - Summer	0.063	0.007	1577	8.692	<0.0001

Table B20. The 2019 mean relative abundances of *Pseudomonas* and all "other" taxa at the genus/family level ± SE, including the pairwise comparisons of the estimated marginal means with the confidence limits (lower and upper C.L.). Superscripted letters following *Pseudomonas* or "other" indicate statistical differences within each season, while upper-cased letters indicate statistical differences of each *Pseudomonas* or "other" across seasons, with significance determined by p-value ≤ 0.05.

Season	Genera	Mean	SE	df	lower C.L.	upper C.L.	
Spring	*Pseudomonas* [b]	0.97	0.02	205	0.928	1.0180	C
	Other [a]	0.03	0.02	205	-0.018	0.0719	A
Summer	*Pseudomonas* [b]	0.66	0.02	116	0.627	0.6993	B
	Other [a]	0.34	0.02	116	0.301	0.3734	B
Fall	*Pseudomonas* [a]	0.51	0.02	142	0.469	0.5483	A
	Other [a]	0.49	0.02	142	0.452	0.5313	C

Season	Contrast	estimate	SE	df	t-ratio	p-value
Spring	Other v. *Pseudomonas*	-0.95	0.03	577	-30.864	<0.0001
Summer	Other v. *Pseudomonas*	-0.33	0.03	577	-12.924	<0.0001
Fall	Other v. *Pseudomonas*	-0.02	0.03	577	-0.612	0.5406

Genera	Contrast	estimate	SE	df	t-ratio	p-value
Pseudomonas	Fall - Spring	-0.47	0.03	575	-15.056	<0.0001
	Fall - Summer	-0.15	0.03	621	-5.780	<0.0001
	Spring - Summer	0.31	0.03	614	10.465	<0.0001
Other	Fall - Spring	0.47	0.03	575	15.056	<0.0001
	Fall - Summer	0.15	0.03	621	5.787	<0.0001
	Spring - Summer	-0.31	0.03	614	-10.465	<0.0001

Table B21. The 2019 mean relative abundances of the top deepest taxonomic level (genus or family) by season where taxa of relative abundance <0.03 were combined into "other" ± SE, with the confidence limits (lower and upper C.L.). Letters indicate statistical differences within season, with significance determined by p-value ≤ 0.05.

Season	Genera	Mean	SE	df	lower C.L.	upper C.L.	
Spring	*Pseudomonas*	0.97	0.01	21	0.95	1.00	b
	Other	0.03	0.01	21	0.00	0.05	a
Summer	*Pseudomonas*	0.66	0.01	220	0.64	0.69	c
	Sphingomonas	0.13	0.01	220	0.11	0.15	b
	Enterobacteriaceae	0.06	0.01	220	0.04	0.09	a
	Other	0.06	0.01	220	0.03	0.08	a
	Pedobacter	0.03	0.01	220	0.01	0.05	a
	Massilia	0.03	0.01	220	0.01	0.05	a
	Rhizobiaceae	0.03	0.01	220	0.00	0.05	a
Fall	*Pseudomonas*	0.51	0.01	175	0.49	0.53	d
	Sphingomonas	0.20	0.01	175	0.18	0.22	c
	Rhizobiaceae	0.09	0.01	175	0.07	0.12	b
	Other	0.09	0.01	175	0.07	0.11	b
	Massilia	0.04	0.01	175	0.02	0.06	a
	Hymenobacter	0.04	0.01	175	0.02	0.06	a
	Methylobacterium	0.03	0.01	175	0.00	0.05	a

Season	contrast	estimate	SE	df	t-ratio	p-value
Spring	Other v. *Pseudomonas*	-0.95	0.01	137	-86.970	<0.0001
Summer	Enterobacteriaceae v. *Massilia*	0.03	0.02	849	2.149	0.3251
	Enterobacteriaceae v. Other	0.01	0.02	849	0.492	0.9990
	Enterobacteriaceae v. *Pedobacter*	0.03	0.02	849	1.934	0.4579
	Enterobacteriaceae v. *Pseudomonas*	-0.60	0.02	849	-37.030	<0.0001
	Enterobacteriaceae v. Rhizobiaceae	0.04	0.02	849	2.209	0.2918
	Enterobacteriaceae v. *Sphingomonas*	-0.07	0.02	849	-4.222	0.0005

Table B21. (cont'd)

	Massilia v. Other	-0.03	0.02	849	-1.657	0.6453
	Massilia v. *Pedobacter*	0.00	0.02	849	-0.214	1.0000
	Massilia v. *Pseudomonas*	-0.63	0.02	849	-39.178	<0.0001
	Massilia v. *Rhizobiaceae*	0.00	0.02	849	0.060	1.0000
	Massilia v. *Sphingomonas*	-0.10	0.02	849	-6.371	<0.0001
	Other v. *Pedobacter*	0.02	0.02	849	1.442	0.7785
	Other v. *Pseudomonas*	-0.61	0.02	849	-37.522	<0.0001
	Other v. *Rhizobiaceae*	0.03	0.02	849	1.717	0.6050
	Other v. *Sphingomonas*	-0.08	0.02	849	-4.714	0.0001
	Pedobacter v. *Pseudomonas*	-0.63	0.02	849	-38.964	<0.0001
	Pedobacter v. Rhizobiaceae	0.00	0.02	849	0.274	1.0000
	Pedobacter v. *Sphingomonas*	-0.10	0.02	849	-6.157	<0.0001
	Pseudomonas v. Rhizobiaceae	0.64	0.02	849	39.238	<0.0001
	Pseudomonas v. *Sphingomonas*	0.53	0.02	849	32.807	<0.0001
	Rhizobiaceae v. *Sphingomonas*	-0.10	0.02	849	-6.431	<0.0001
Fall	*Hymenobacter* v. *Massilia*	0.00	0.02	692	-0.184	1.0000
	Hymenobacter v. *Methylobacterium*	0.01	0.02	692	0.680	0.9937
	Hymenobacter v. Other	-0.05	0.02	692	-3.265	0.0196
	Hymenobacter v. *Pseudomonas*	-0.47	0.02	692	-29.249	<0.0001
	Hymenobacter v. Rhizobiaceae	-0.05	0.02	692	-3.405	0.0124
	Hymenobacter v. *Sphingomonas*	-0.16	0.02	692	-10.017	<0.0001
	Massilia v. *Methylobacterium*	0.01	0.02	692	0.864	0.9776
	Massilia v. Other	-0.05	0.02	692	-3.081	0.0348
	Massilia v. *Pseudomonas*	-0.47	0.02	692	-29.064	<0.0001
	Massilia v. *Rhizobiaceae*	-0.05	0.02	692	-3.221	0.0226
	Massilia v. *Sphingomonas*	-0.16	0.02	692	-9.833	<0.0001
	Methylobacterium v. Other	-0.06	0.02	692	-3.945	0.0017
	Methylobacterium v. *Pseudomonas*	-0.48	0.02	692	-29.929	<0.0001
	Methylobacterium v. Rhizobiaceae	-0.07	0.02	692	-4.085	0.0010
	Methylobacterium v. *Sphingomonas*	-0.17	0.02	692	-10.697	<0.0001

Table B21. (cont'd)

Other v. *Pseudomonas*	-0.42	0.02	692	-25.983	<0.0001
Other v. Rhizobiaceae	0.00	0.02	692	-0.140	1.0000
Other v. *Sphingomonas*	-0.11	0.02	692	-6.752	<0.0001
Pseudomonas v. Rhizobiaceae	0.42	0.02	692	25.844	<0.0001
Pseudomonas v. *Sphingomonas*	0.31	0.02	692	19.232	<0.0001
Rhizobiaceae v. *Sphingomonas*	-0.11	0.02	692	-6.612	<0.0001

Table B22. The 2019 mean relative abundances of the core microbiome taxon (genus and OTU identifier), the rest of the combined *Pseudomonas* and combined *Sphingomonas,* and the remaining combined "other" taxa ± SE over season, with the confidence limits (lower and upper C.L.). Superscripted letters following genus/OTUs indicate statistical differences within each season, while upper-cased letters indicate statistical differences of each genus/OTU across time, with significance determined by p-value ≤ 0.05.

Season	Genera	Mean	SE	df	lower C.L.	upper C.L.	
Spring	*Pseudomonas* Otu0001 [d]	0.66	0.02	1340	0.62	0.70	C
	Pseudomonas Otu0002 [c]	0.20	0.02	1340	0.17	0.24	B
	Pseudomonas [b]	0.11	0.02	1340	0.07	0.15	B
	Other [a]	0.03	0.02	1340	-0.01	0.07	A
	Sphingomonas Otu0003 [a]	0.00	0.02	1340	-0.04	0.04	A
	Sphingomonas Otu0007 [a]	0.00	0.02	1340	-0.04	0.04	A
	Sphingomonas [a]	0.00	0.02	1340	-0.04	0.04	A
Summer	*Pseudomonas* Otu0001 [d]	0.36	0.02	953	0.33	0.40	A
	Pseudomonas Otu0002 [c]	0.25	0.02	953	0.22	0.28	B
	Other [c]	0.21	0.02	953	0.17	0.24	B
	Sphingomonas Otu0003 [b]	0.11	0.02	953	0.08	0.14	B
	Pseudomonas [ab]	0.05	0.02	953	0.02	0.08	AB
	Sphingomonas Otu0007 [a]	0.02	0.02	953	-0.01	0.05	A
	Sphingomonas [a]	0.00	0.02	953	-0.03	0.03	A
Fall	*Pseudomonas* Otu0001 [d]	0.43	0.02	1113	0.39	0.46	B
	Other [c]	0.29	0.02	1113	0.26	0.33	C
	Sphingomonas Otu0003 [b]	0.15	0.02	1113	0.12	0.19	B
	Pseudomonas Otu0002 [a]	0.06	0.02	1113	0.03	0.10	A
	Sphingomonas Otu0007 [a]	0.04	0.02	1113	0.01	0.08	A
	Pseudomonas [a]	0.02	0.02	1113	-0.02	0.05	A
	Sphingomonas [a]	0.00	0.02	1113	-0.03	0.04	A

Table B23. The 2019 pairwise comparisons of the estimated marginal means of relative abundances of core microbiome taxon (genus and OTU identifier), the rest of the combined *Pseudomonas* and combined *Sphingomonas* and the remaining combined "other" taxa for each season, and for each taxon across each season with significance determined by p-value ≤ 0.05.

Season	Contrast	Estimate	SE	df	t-ratio	p-value
Spring	Other v. *Pseudomonas*	-0.09	0.03	2187	-3.020	0.0409
	Other v. *Pseudomonas* Otu0001	-0.63	0.03	2187	-22.364	<0.0001
	Other v. *Pseudomonas* Otu0002	-0.18	0.03	2187	-6.337	<0.0001
	Other v. *Sphingomonas*	0.03	0.03	2187	0.932	0.9675
	Other v. *Sphingomonas* Otu0003	0.03	0.03	2187	0.922	0.9691
	Other v. *Sphingomonas* Otu0007	0.03	0.03	2187	0.925	0.9687
	Pseudomonas v. *Pseudomonas* Otu0001	-0.55	0.03	2187	-19.344	<0.0001
	Pseudomonas v. *Pseudomonas* Otu0002	-0.09	0.03	2187	-3.317	0.0161
	Pseudomonas v. *Sphingomonas*	0.11	0.03	2187	3.952	0.0016
	Pseudomonas v. *Sphingomonas* Otu0003	0.11	0.03	2187	3.942	0.0016
	Pseudomonas v. *Sphingomonas* Otu0007	0.11	0.03	2187	3.945	0.0016
	Pseudomonas Otu0001 v. *Pseudomonas* Otu0002	0.45	0.03	2187	16.027	<0.0001
	Pseudomonas Otu0001 v. *Sphingomonas*	0.66	0.03	2187	23.296	<0.0001
	Pseudomonas Otu0001 v. *Sphingomonas* Otu0003	0.66	0.03	2187	23.286	<0.0001
	Pseudomonas Otu0001 v. *Sphingomonas* Otu0007	0.66	0.03	2187	23.289	<0.0001
	Pseudomonas Otu0002 v. *Sphingomonas*	0.20	0.03	2187	7.269	<0.0001
	Pseudomonas Otu0002 v. *Sphingomonas* Otu0003	0.20	0.03	2187	7.259	<0.0001
	Pseudomonas Otu0002 v. *Sphingomonas* Otu0007	0.20	0.03	2187	7.262	<0.0001
	Sphingomonas v. *Sphingomonas* Otu0003	0.00	0.03	2187	-0.010	1.0000
	Sphingomonas v. *Sphingomonas* Otu0007	0.00	0.03	2187	-0.007	1.0000
	Sphingomonas Otu0003 v. *Sphingomonas* Otu0007	0.00	0.03	2187	0.003	1.0000
2019 Summer	Other v. *Pseudomonas*	0.15	0.02	2187	6.669	<0.0001
	Other v. *Pseudomonas* Otu0001	-0.16	0.02	2187	-6.856	<0.0001
	Other v. *Pseudomonas* Otu0002	-0.04	0.02	2187	-1.812	0.5401
	Other v. *Sphingomonas*	0.20	0.02	2187	8.836	<0.0001

Table B23. (cont'd)

	Other v. *Sphingomonas* Otu0003	0.10	0.02	2187	4.135	0.0007
	Other v. *Sphingomonas* Otu0007	0.18	0.02	2187	7.949	<0.0001
	Pseudomonas v. *Pseudomonas* Otu0001	-0.31	0.02	2187	-13.525	<0.0001
	Pseudomonas v. *Pseudomonas* Otu0002	-0.20	0.02	2187	-8.481	<0.0001
	Pseudomonas v. *Sphingomonas*	0.05	0.02	2187	2.167	0.3140
	Pseudomonas v. *Sphingomonas* Otu0003	-0.06	0.02	2187	-2.534	0.1476
	Pseudomonas v. *Sphingomonas* Otu0007	0.03	0.02	2187	1.279	0.8616
	Pseudomonas Otu0001 v. *Pseudomonas* Otu0002	0.12	0.02	2187	5.044	<0.0001
	Pseudomonas Otu0001 v. *Sphingomonas*	0.36	0.02	2187	15.692	<0.0001
	Pseudomonas Otu0001 v. *Sphingomonas* Otu0003	0.25	0.02	2187	10.991	<0.0001
	Pseudomonas Otu0001 v. *Sphingomonas* Otu0007	0.34	0.02	2187	14.805	<0.0001
	Pseudomonas Otu0002 v. *Sphingomonas*	0.25	0.02	2187	10.648	<0.0001
	Pseudomonas Otu0002 v. *Sphingomonas* Otu0003	0.14	0.02	2187	5.947	<0.0001
	Pseudomonas Otu0002 v. *Sphingomonas* Otu0007	0.23	0.02	2187	9.760	<0.0001
	Sphingomonas v. *Sphingomonas* Otu0003	-0.11	0.02	2187	-4.701	0.0001
	Sphingomonas v. *Sphingomonas* Otu0007	-0.02	0.02	2187	-0.888	0.9744
	Sphingomonas Otu0003 v. *Sphingomonas* Otu0007	0.09	0.02	2187	3.813	0.0027
2019 Fall	Other v. *Pseudomonas*	0.28	0.03	2187	10.777	<0.0001
	Other v. *Pseudomonas* Otu0001	-0.14	0.03	2187	-5.288	<0.0001
	Other v. *Pseudomonas* Otu0002	0.23	0.03	2187	8.887	<0.0001
	Other v. *Sphingomonas*	0.29	0.03	2187	11.348	<0.0001
	Other v. *Sphingomonas* Otu0003	0.14	0.03	2187	5.377	<0.0001
	Other v. *Sphingomonas* Otu0007	0.25	0.03	2187	9.741	<0.0001
	Pseudomonas v. *Pseudomonas* Otu0001	-0.41	0.03	2187	-16.065	<0.0001
	Pseudomonas v. *Pseudomonas* Otu0002	-0.05	0.03	2187	-1.890	0.4873
	Pseudomonas v. *Sphingomonas*	0.01	0.03	2187	0.571	0.9976
	Pseudomonas v. *Sphingomonas* Otu0003	-0.14	0.03	2187	-5.400	<0.0001
	Pseudomonas v. *Sphingomonas* Otu0007	-0.03	0.03	2187	-1.036	0.9456
	Pseudomonas Otu0001 v. *Pseudomonas* Otu0002	0.36	0.03	2187	14.176	<0.0001

Table B23. (cont'd)

	Pseudomonas Otu0001 v. *Sphingomonas*	0.43	0.03	2187	16.636	<0.0001
	Pseudomonas Otu0001 v. *Sphingomonas* Otu0003	0.27	0.03	2187	10.665	<0.0001
	Pseudomonas Otu0001 v. *Sphingomonas* Otu0007	0.38	0.03	2187	15.029	<0.0001
	Pseudomonas Otu0002 v. *Sphingomonas*	0.06	0.03	2187	2.461	0.1744
	Pseudomonas Otu0002 v. *Sphingomonas* Otu0003	-0.09	0.03	2187	-3.511	0.0083
	Pseudomonas Otu0002 v. *Sphingomonas* Otu0007	0.02	0.03	2187	0.853	0.9791
	Sphingomonas v. *Sphingomonas* Otu0003	-0.15	0.03	2187	-5.971	<0.0001
	Sphingomonas v. *Sphingomonas* Otu0007	-0.04	0.03	2187	-1.607	0.6777
	Sphingomonas Otu0003 v. *Sphingomonas* Otu0007	0.11	0.03	2187	4.364	0.0003

Genus/OTU	Contrast	Estimate	SE	df	t-ratio	p-value
Other	Fall - Spring	0.27	0.03	2172	9.721	<0.0001
	Fall - Summer	0.09	0.02	2232	3.536	0.0012
	Spring - Summer	-0.18	0.03	2220	-6.834	<0.0001
Pseudomonas	Fall - Spring	-0.09	0.03	2172	-3.473	0.0015
	Fall - Summer	-0.03	0.02	2232	-1.405	0.3383
	Spring - Summer	0.06	0.03	2220	2.309	0.0547
Pseudomonas Otu0001	Fall - Spring	-0.23	0.03	2172	-8.397	<0.0001
	Fall - Summer	0.06	0.02	2232	2.562	0.0283
	Spring - Summer	0.29	0.03	2220	11.139	<0.0001
Pseudomonas Otu0002	Fall - Spring	-0.14	0.03	2172	-5.127	<0.0001
	Fall - Summer	-0.18	0.02	2232	-7.473	<0.0001
	Spring - Summer	-0.04	0.03	2220	-1.625	0.2352
Sphingomonas	Fall - Spring	0.00	0.03	2172	0.068	0.9974
	Fall - Summer	0.00	0.02	2232	0.053	0.9984
	Spring - Summer	0.00	0.03	2220	-0.022	0.9997
Sphingomonas Otu0003	Fall - Spring	0.15	0.03	2172	5.643	<0.0001
	Fall - Summer	0.04	0.02	2232	1.837	0.1578

Table B23. (cont'd)

	Spring - Summer	-0.11	0.03	2220	-4.168	0.0001
Sphingomonas Otu0007	Fall - Spring	0.04	0.03	2172	1.565	0.2613
	Fall - Summer	0.02	0.02	2232	0.891	0.6458
	Spring - Summer	-0.02	0.03	2220	-0.799	0.7035

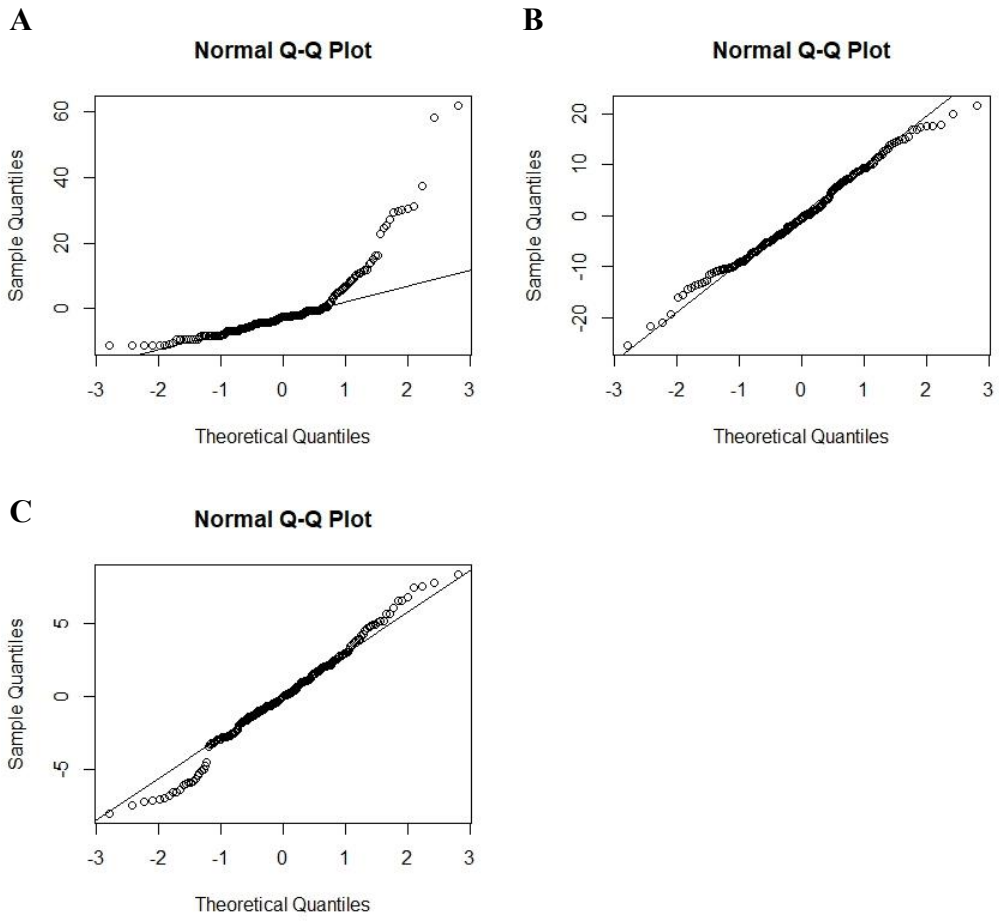


Figure B24. The qqplots for the residuals for **A)** precipitation, **B)** relative humidity, and **C)** temperature, over a two week period leading up to leaf sampling.

Table B24 The means ± SE with the lower and upper confidence limits for the relative humidity (%), daily temperature °C, and the median precipitation (mm) compiled from the two-week period leading up to the microbiome leaf sampling dates.

Metric	Time	Mean	SE	df	Lower C.L.	Upper C.L	
Relative humidity (%)	2017 Fall	74.0	1.8	188	70.5	77.4	ab
	2018 Spring	72.8	1.7	188	69.4	76.1	b
	2018 Summer	73.3	1.7	188	70.0	76.7	b
	2018 Fall	80.6	1.7	188	77.3	84.0	a
	2019 Spring	77.2	1.7	188	73.9	80.6	ab
	2019 Summer	72.9	1.7	188	69.6	76.3	b
	2019 Fall	78.6	1.7	188	75.3	82.0	ab
Daily temperature (°C)	2017 Fall	12.6	0.6	188	11.3	13.8	a
	2018 Spring	14.5	0.6	188	13.3	15.7	ab
	2018 Summer	22.6	0.6	188	21.4	23.9	c
	2018 Fall	14.2	0.6	188	13.0	15.5	ab
	2019 Spring	15.4	0.6	188	14.1	16.6	b
	2019 Summer	21.1	0.6	188	19.8	22.3	c
	2019 Fall	15.1	0.6	188	13.9	16.4	ab

Metric	Time	Median	
Precipitation (mm)	2017 Fall	0.0	ab
	2018 Spring	2.3	a
	2018 Summer	0.0	ab
	2018 Fall	0.6	ab
	2019 Spring	2.2	a
	2019 Summer	0.0	b
	2019 Fall	0.8	a

Table B25. The p-values for the pairwise comparisons of the estimated marginal means of the relative humidity (%), and daily temperature (°C), and the p-values and Bonferroni adjusted p-values for the pairwise comparisons of the distribution (medians) of the precipitation (mm) data following the Dunns Test; all data was assembled from the two-week period leading up to microbiome leaf sampling.

Metric	Contrast	Estimate	SE	df	t-ratio	p-value
Relative humidity (%)	2017 Fall v. 2018 Fall	-6.7	2.5	188	-2.735	0.0953
	2017 Fall v. 2018 Spring	1.2	2.4	188	0.495	0.9989
	2017 Fall v. 2018 Summer	0.6	2.5	188	0.254	1.0000
	2017 Fall v. 2019 Fall	-4.7	2.5	188	-1.913	0.4746
	2017 Fall v. 2019 Spring	-3.3	2.5	188	-1.343	0.8309
	2017 Fall v. 2019 Summer	1.0	2.5	188	0.415	0.9996
	2018 Fall v. 2018 Spring	7.9	2.4	188	3.285	0.0205
	2018 Fall v. 2018 Summer	7.3	2.4	188	3.017	0.0452
	2018 Fall v. 2019 Fall	2.0	2.4	188	0.830	0.9815
	2018 Fall v. 2019 Spring	3.4	2.4	188	1.406	0.7983
	2018 Fall v. 2019 Summer	7.7	2.4	188	3.179	0.0282
	2018 Spring v. 2018 Summer	-0.6	2.4	188	-0.242	1.0000
	2018 Spring v. 2019 Fall	-5.9	2.4	188	-2.447	0.1852
	2018 Spring v. 2019 Spring	-4.5	2.4	188	-1.867	0.5049
	2018 Spring v. 2019 Summer	-0.2	2.4	188	-0.078	1.0000
	2018 Summer v. 2019 Fall	-5.3	2.4	188	-2.186	0.3079
	2018 Summer v. 2019 Spring	-3.9	2.4	188	-1.611	0.6754
	2018 Summer v. 2019 Summer	0.4	2.4	188	0.163	1.0000
	2019 Fall v. 2019 Spring	1.4	2.4	188	0.575	0.9974
	2019 Fall v. 2019 Summer	5.7	2.4	188	2.349	0.2266
	2019 Spring v. 2019 Summer	4.3	2.4	188	1.774	0.5674
Daily Temperature (°C)	2017 Fall v. 2018 Fall	-1.7	0.9	188	-1.840	0.5226
	2017 Fall v. 2018 Spring	-1.9	0.9	188	-2.160	0.3226
	2017 Fall v. 2018 Summer	-10.1	0.9	188	-11.102	<.0001
	2017 Fall v. 2019 Fall	-2.6	0.9	188	-2.825	0.0759

Table B25. (cont'd)

	2017 Fall v. 2019 Spring	-2.8	0.9	188	-3.104	0.0352
	2017 Fall v. 2019 Summer	-8.5	0.9	188	-9.392	<.0001
	2018 Fall v. 2018 Spring	-0.3	0.9	188	-0.307	0.9999
	2018 Fall v. 2018 Summer	-8.4	0.9	188	-9.348	<.0001
	2018 Fall v. 2019 Fall	-0.9	0.9	188	-0.994	0.9548
	2018 Fall v. 2019 Spring	-1.1	0.9	188	-1.276	0.8623
	2018 Fall v. 2019 Summer	-6.9	0.9	188	-7.622	<.0001
	2018 Spring v. 2018 Summer	-8.1	0.9	188	-9.122	<.0001
	2018 Spring v. 2019 Fall	-0.6	0.9	188	-0.696	0.9927
	2018 Spring v. 2019 Spring	-0.9	0.9	188	-0.980	0.9578
	2018 Spring v. 2019 Summer	-6.6	0.9	188	-7.381	<.0001
	2018 Summer v. 2019 Fall	7.5	0.9	188	8.354	<.0001
	2018 Summer v. 2019 Spring	7.3	0.9	188	8.072	<.0001
	2018 Summer v. 2019 Summer	1.6	0.9	188	1.726	0.5996
	2019 Fall v. 2019 Spring	-0.3	0.9	188	-0.282	1.0000
	2019 Fall v. 2019 Summer	-6.0	0.9	188	-6.628	<.0001
	2019 Spring v. 2019 Summer	-5.7	0.9	188	-6.346	<.0001

Precipitation (mm)	**Comparison**	**z-test**	**p-value**	**adj. p-value**
	2017 Fall v. 2018 Fall	-0.385	0.7006	1.0000
	2017 Fall v. 2018 Spring	-1.071	0.2843	1.0000
	2017 Fall v. 2018 Summer	-0.689	0.4906	1.0000
	2017 Fall v. 2019 Fall	1.593	0.1111	1.0000
	2017 Fall v. 2019 Spring	1.996	0.0459	0.9647
	2017 Fall v. 2019 Summer	2.703	0.0069	0.1444
	2018 Fall v. 2018 Spring	-0.912	0.3619	1.0000
	2018 Fall v. 2018 Summer	-0.532	0.5947	1.0000
	2018 Fall v. 2019 Fall	0.153	0.8788	1.0000
	2018 Fall v. 2019 Spring	-2.528	0.0115	0.2409
	2018 Fall v. 2019 Summer	-1.164	0.2443	1.0000

Table B25. (cont'd)

2018 Spring v. 2018 Summer	-0.787	0.4313	1.0000
2018 Spring v. 2019 Fall	-0.104	0.9168	1.0000
2018 Spring v. 2019 Spring	-2.783	0.0054	0.1132
2018 Spring v. 2019 Summer	-0.255	0.7989	1.0000
2018 Summer v. 2019 Fall	2.281	0.0225	0.4731
2018 Summer v. 2019 Spring	2.690	0.0071	0.1499
2018 Summer v. 2019 Summer	3.403	0.0007	0.0140
2019 Fall v. 2019 Spring	0.694	0.4874	1.0000
2019 Fall v. 2019 Summer	3.223	0.0013	0.0267
2019 Spring v. 2019 Summer	3.477	0.0005	0.0106

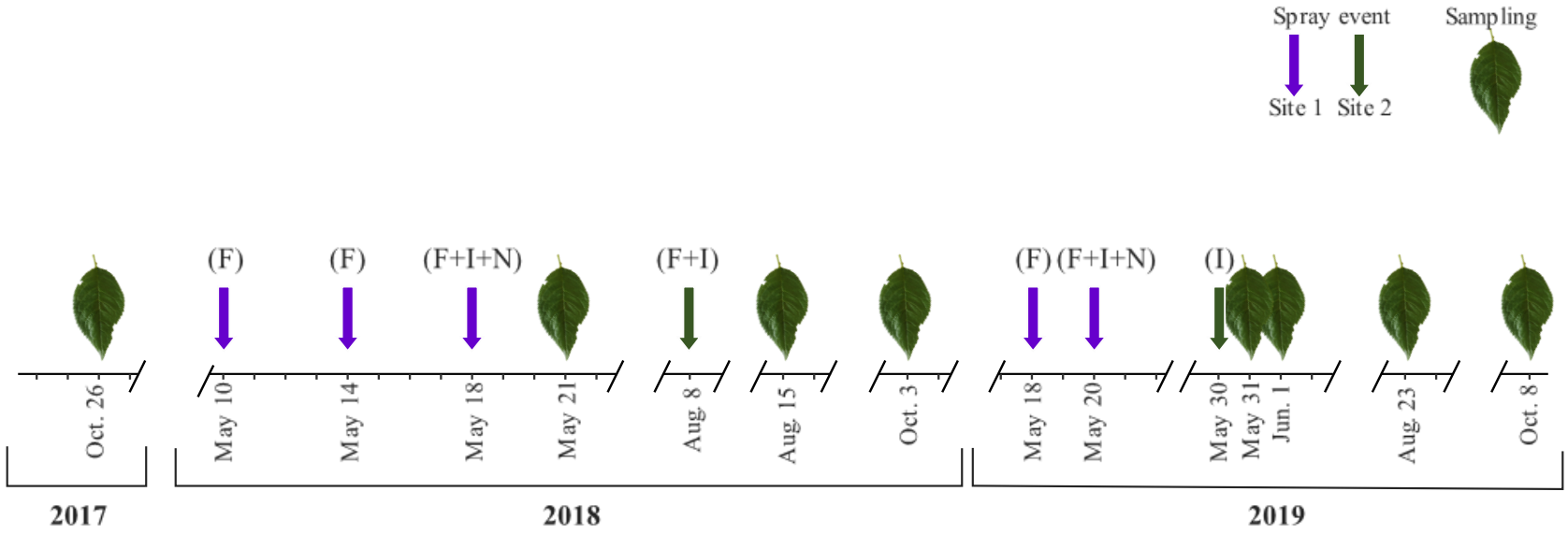


Figure B25. Timeline of the spray events that occurred at the two sites for each two-week period leading up to the leaf sampling date. The leaves indicate the sample date, while purple (site 1) and green (site 2) arrows indicate a spray event for each site. Sprays consisted of insecticides (I), fungicides (F), and foliar nutrients (N) at site 1 and insecticides (I) and fungicides (F) at site 2.

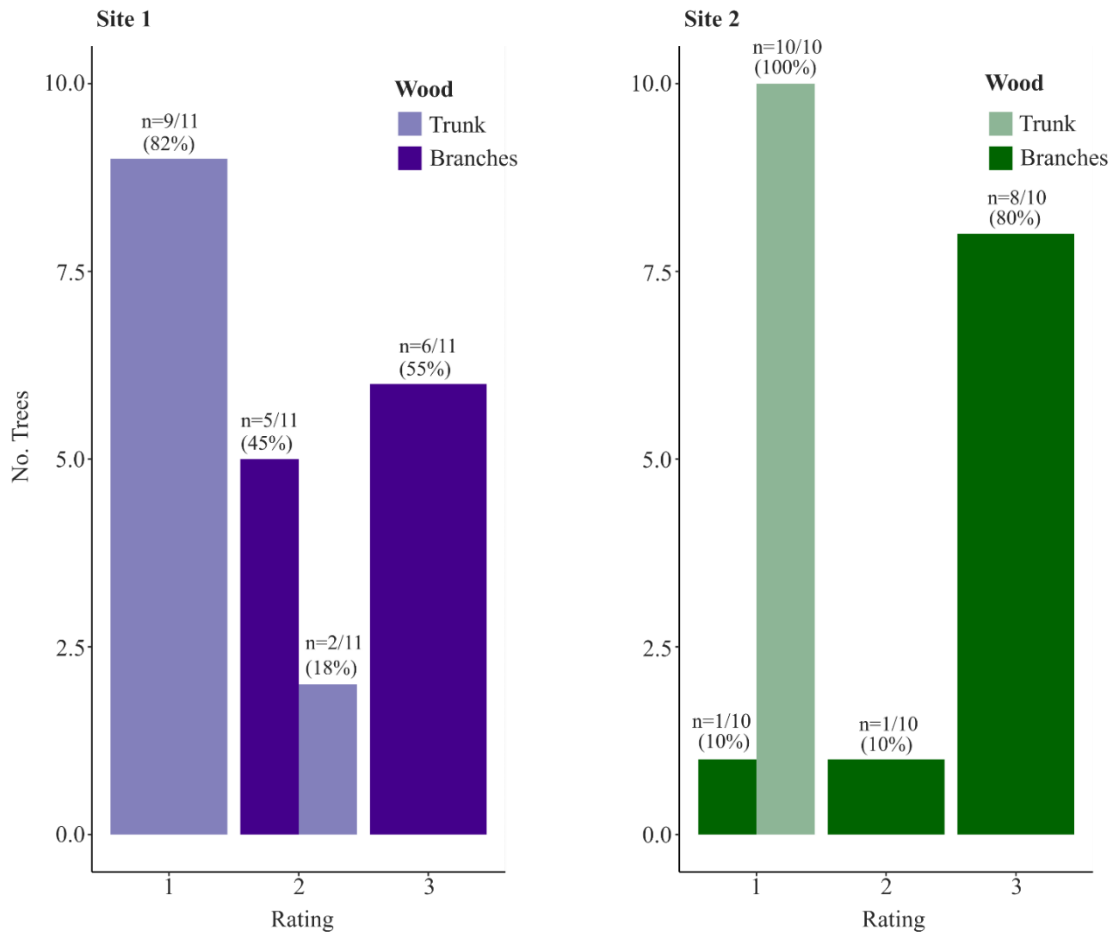


Figure B26. Fall 2019 bacterial canker ratings for trees planted at sites 1 and 2, two years after planting (Spring 2017). Ratings were recorded for structural wood, the trunk, and branches, where canker ratings range from no canker (3=healthy) to moderate infection (2=minor) to severe infection (1=major infection).

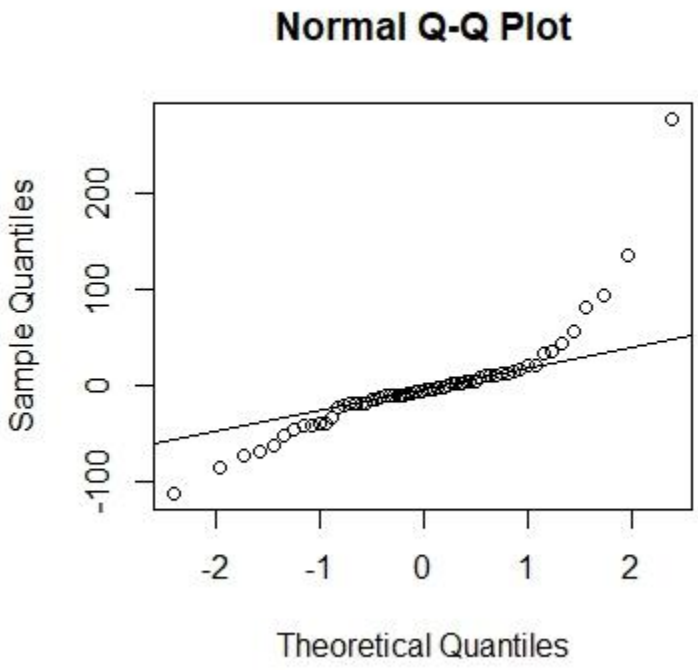


Figure C1. The 2019 quantile-quantile plots (qqplot) of the residuals for graphical visualization of the distribution of the total area of growth (mm^2) of *Pss* phylogroup (PG) 2d strains 9, 25, 37, and 38 at 10^8 cfu/ml co-inoculated next to the commercial biological controls Serenade® Opti (SO), Blossom Protect™ (BP) or water (H_2O).

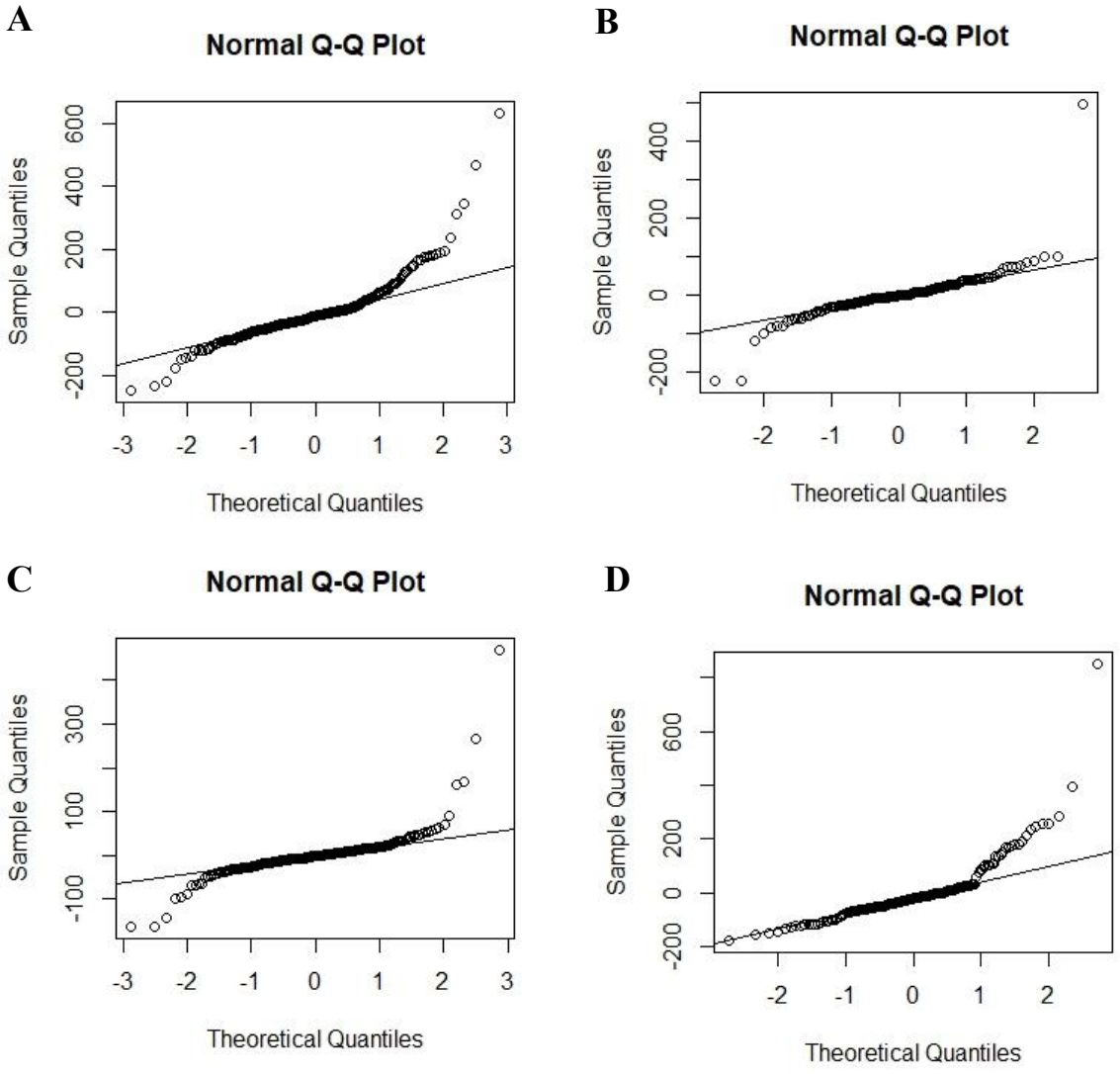


Figure C2. The 2021 quantile-quantile plots (qqplot) of the residuals for graphical visualization of the distribution of the total area of growth (mm^2) of *Pss* strains at 10^8 cfu/ml co-inoculated next to the commercial biological controls BlightBan®A506 (BB), Bloomtime™ (BLT), Blossom Protect™ (BP), Double Nickel55™ (DN), Serenade® Opti (SO), or water (H_2O) at 3 rates (0.5x, 1.0x, 1.5). **A)** Group 1 *Pss* strains 14 (PG 2c), 25 (PG2d), and 38 (PG2d), **B)** Group 2 *Pss* strains 23 and 34 (PG2b), **C)** Group 3 *Pss* strains 22 (PG2b), 26 (PG2d), and 37 (PG2d), and **D)** Group 4 *Pss* strains 9 and 27 (PG2d).

Table C1. The 2019 co-inoculations of the virulent *Pss* phylogroup (PG) 2d strains 9, 25, 37, and 38 grown next to the commercial biological controls Serenade® Opti (SO), Blossom Protect™ (BP) or water (H_2O) in Petri plates with KB media, with the mean total area of growth (mm^2) of the strains ± SE, confidence limits (lower and upper C.L.) and the p-value for the pairwise comparisons of the estimated marginal means for each treatment, with letters indicating statistical differences with significance determined by p-value ≤0.05.

Treatment	Mean total area (mm^2)	SE	df	lower C.L.	upper C.L.	
SO	160.6	13.3	48	133.8	187.4	a
BP	165.6	13.3	48	138.8	192.4	a
H_2O	220.7	13.3	48	193.9	247.5	b

Contrast	Estimate	SE	df	t-ratio	p-value
BP v. H2O	-55.1	18.9	48	-2.920	0.0145
BP v. SO	5.0	18.9	48	0.265	0.9621
H2O v. SO	60.1	18.9	48	3.185	0.0071

Table C2. Group 1 2021, mean total area of growth (mm^2) of *Pss* strains 14, 25, and 38, belonging to phylogroup (PG) 2c, 2d, and 2d, respectively ± SE grown next to the five biological control agents (BCA) or H_2O co-inoculated at the rates 0.5x, 1.0x, and 1.5x. With confidence limits (lower and upper C.L.) and the p-value for the pairwise comparisons of the estimated marginal means at each rate, with letters indicating statistical differences with significance determined by p-value ≤0.05.

Year	Group	Strain/PG	BCA rate	*Pss* Mean total area (mm2)	SE	df	lower C.L.	upper C.L.	
2021	1	14 2c	1.0x	178.0	11.4	199	155.4	200.6	b
		25 2d	0.5x	192.9	11.3	199	170.6	215.2	ab
		38 2d	1.5x	223.4	11.7	199	200.4	246.4	a

Year	Group	Strain/PG	contrast	estimate	SE	df	t-ratio	p-value
2021	1	14 2c	0.5x v. 1.5x	-30.5	16.3	199	-1.875	0.1486
		25 2d	0.5x v. 1.0x	14.9	16.1	199	0.926	0.6247
		38 2d	1.5x v. 1.0x	45.4	16.3	199	2.777	0.0165

Table C3. Group 2 2021, by treatment (trt, i.e., biological control agent, BCA) and by strain, mean total area of growth (mm^2) of *Pss* strains 23 and 34, belonging to phylogroup (PG) 2b ± SE in co-inoculations of BCAs [BlightBan®A506 (BB), Bloomtime™ (BLT), Blossom Protect™ (BP), Double Nickel55™ (DN), Serenade® Opti (SO), or water (H_2O)] at three rates (0.5x, 1.0x, 1.5x), with confidence limits (lower and upper C.L.) and the p-value for the pairwise comparisons of the estimated marginal means for each treatment and strain, with letters indicating statistical differences with significance determined by p-value ≤0.05.

Year	Group	Strain/PG	Treatment (BCA)	*Pss* Mean total area (mm2)	SE	df	lower C.L.	upper C.L.	
2021	2	23 2b	BB	153.3	12.5	119	128.5	178.0	a
		34 2b	BLT	164.5	15.9	119	133.0	196.1	a
			BP	177.7	12.5	119	152.9	202.4	a
			DN	167.3	13.9	119	139.8	194.8	a
			H_2O	237.6	12.8	119	212.4	262.9	b
			SO	184.0	17.2	119	149.8	218.1	ab

Year	Group	Strain/PG	contrast	estimate	SE	df	t-ratio	p-value
2021	2	23 2b	BB v. BLT	-11.2	20.3	119	-0.555	0.9936
		34 2b	BB v. BP	-24.4	17.7	119	-1.382	0.7375
			BB v. DN	-14.0	18.7	119	-0.751	0.9749
			BB v. H_2O	-84.4	17.9	119	-4.725	0.0001
			BB v. SO	-30.7	21.3	119	-1.442	0.7011
			BLT v. BP	-13.2	20.3	119	-0.651	0.9867
			BLT v. DN	-2.8	21.1	119	-0.132	1.0000
			BLT v. H_2O	-73.1	20.4	119	-3.583	0.0064
			BLT v. SO	-19.5	23.5	119	-0.829	0.9615
			BP v. DN	10.4	18.7	119	0.556	0.9935
			BP v. H_2O	-59.9	17.9	119	-3.356	0.0132
			BP v. SO	-6.3	21.3	119	-0.295	0.9997
			DN v. H_2O	-70.3	18.9	119	-3.729	0.0039
			DN v. SO	-16.7	22.1	119	-0.753	0.9746
			H2O v. SO	53.7	21.4	119	2.502	0.1318

Year	Group	Strain	PG	Mean total area (mm2)	SE	df	lower C.L.	upper C.L.	
2021	2	23	2b	165.8	8.4	119	149.2	182.4	a
		34		195.6	8.1	119	179.7	211.6	b

Year	Group	contrast	estimate	SE	df	t-ratio	p-value
2021	2	23 v. 34	-29.8	11.6	119	-2.561	0.0117

Table C4. Group 2 2021 mean total area of growth (mm^2) of *Pss* strains 23 and 34, belonging to phylogroup (PG) 2b ± SE in co-inoculations of biological control agents (BCAs) [BlightBan®A506 (BB), Bloomtime™ (BLT), Blossom Protect™ (BP), Double Nickel55™ (DN), Serenade® Opti (SO), or water (H_2O)] at three rates (0.5x, 1.0x, 1.5x), with confidence limits (lower and upper C.L.) and the p-value for the pairwise comparisons of the estimated marginal means for each rate*treatment, with letters indicating statistical differences with significance determined by p-value ≤0.05.

Year	Group	Strain/PG	Rate	Treatment (BCA)	*Pss* Mean total area (mm2)	SE	df	lower C.L.	upper C.L.	
2021	2	23 2b	0.5x	BB	149.7	21.6	119	106.8	192.6	a
		34 2b	1.5x	BB	148.3	21.6	119	105.4	191.2	a
			1.0x	BB	161.8	21.6	119	118.9	204.7	ab
			0.5x	BLT	136.7	27.9	119	81.4	192.1	a
			1.5x	BLT	162.3	26.1	119	110.5	214.0	ab
			1.0x	BLT	194.5	28.6	119	137.8	251.3	ab
			0.5x	BP	214.0	21.6	119	171.1	256.9	ab
			1.5x	BP	162.6	21.6	119	119.7	205.5	ab
			1.0x	BP	156.5	21.6	119	113.6	199.3	a
			0.5x	DN	168.8	26.1	119	117.1	220.6	ab
			1.5x	DN	168.3	23.0	119	122.8	213.7	ab
			1.0x	DN	164.8	23.0	119	119.3	210.3	ab
			0.5x	H_2O	272.4	23.0	119	226.9	317.8	b
			1.5x	H_2O	174.1	21.6	119	131.2	216.9	ab
			1.0x	H_2O	266.5	21.6	119	223.6	309.4	b
			0.5x	SO	207.6	26.1	119	155.9	259.4	ab
			1.5x	SO	210.8	23.0	119	165.3	256.3	ab
			1.0x	SO	133.5	38.3	119	57.7	209.3	ab

Table C4. (cont'd)

Year	Group	Strain/PG	contrast	estimate	SE	df	t-ratio	p-value
2021	2	23 2b	0.5x BB v. 1.5x BB	1.4	30.6	119	0.046	1.0000
		34 2b	0.5x BB v. 1.0x BB	-12.1	30.6	119	-0.395	1.0000
			0.5x BB v. 0.5x BLT	13.0	35.4	119	0.367	1.0000
			0.5x BB v. 1.5x BLT	-12.6	33.9	119	-0.370	1.0000
			0.5x BB v. 1.0x BLT	-44.8	35.9	119	-1.249	0.9986
			0.5x BB v. 0.5x BP	-64.3	30.6	119	-2.100	0.8104
			0.5x BB v. 1.5x BP	-12.9	30.6	119	-0.421	1.0000
			0.5x BB v. 1.0x BP	-6.8	30.6	119	-0.221	1.0000
			0.5x BB v. 0.5x DN	-19.1	33.9	119	-0.563	1.0000
			0.5x BB v. 1.5x DN	-18.6	31.6	119	-0.588	1.0000
			0.5x BB v. 1.0x DN	-15.1	31.6	119	-0.478	1.0000
			0.5x BB v. 0.5x H_2O	-122.7	31.6	119	-3.887	0.0184
			0.5x BB v. 1.5x H_2O	-24.4	30.6	119	-0.795	1.0000
			0.5x BB v. 1.0x H_2O	-116.8	30.6	119	-3.815	0.0233
			0.5x BB v. 0.5x SO	-57.9	33.9	119	-1.707	0.9616
			0.5x BB v. 1.5x SO	-61.1	31.6	119	-1.936	0.8917
			0.5x BB v. 1.0x SO	16.2	44.0	119	0.369	1.0000
			1.5x BB v. 1.0x BB	-13.5	30.6	119	-0.441	1.0000
			1.5x BB v. 0.5x BLT	11.6	35.4	119	0.327	1.0000
			1.5x BB v. 1.5x BLT	-14.0	33.9	119	-0.411	1.0000
			1.5x BB v. 1.0x BLT	-46.3	35.9	119	-1.288	0.9980
			1.5x BB v. 0.5x BP	-65.7	30.6	119	-2.147	0.7832
			1.5x BB v. 1.5x BP	-14.3	30.6	119	-0.467	1.0000
			1.5x BB v. 1.0x BP	-8.2	30.6	119	-0.267	1.0000
			1.5x BB v. 0.5x DN	-20.5	33.9	119	-0.605	1.0000
			1.5x BB v. 1.5x DN	-20.0	31.6	119	-0.633	1.0000
			1.5x BB v. 1.0x DN	-16.5	31.6	119	-0.523	1.0000
			1.5x BB v. 0.5x H_2O	-124.1	31.6	119	-3.931	0.0159
			1.5x BB v. 1.5x H_2O	-25.8	30.6	119	-0.842	1.0000

Table C4. (cont'd)

1.5x BB v. 1.0x H_2O	-118.2	30.6	119	-3.861	0.0200
1.5x BB v. 0.5x SO	-59.4	33.9	119	-1.749	0.9524
1.5x BB v. 1.5x SO	-62.5	31.6	119	-1.981	0.8722
1.5x BB v. 1.0x SO	14.8	44.0	119	0.337	1.0000
1.0x BB v. 0.5x BLT	25.1	35.4	119	0.709	1.0000
1.0x BB v. 1.5x BLT	-0.5	33.9	119	-0.014	1.0000
1.0x BB v. 1.0x BLT	-32.8	35.9	119	-0.913	1.0000
1.0x BB v. 0.5x BP	-52.2	30.6	119	-1.706	0.9618
1.0x BB v. 1.5x BP	-0.8	30.6	119	-0.026	1.0000
1.0x BB v. 1.0x BP	5.3	30.6	119	0.173	1.0000
1.0x BB v. 0.5x DN	-7.0	33.9	119	-0.208	1.0000
1.0x BB v. 1.5x DN	-6.5	31.6	119	-0.205	1.0000
1.0x BB v. 1.0x DN	-3.0	31.6	119	-0.096	1.0000
1.0x BB v. 0.5x H_2O	-110.6	31.6	119	-3.504	0.0601
1.0x BB v. 1.5x H_2O	-12.3	30.6	119	-0.401	1.0000
1.0x BB v. 1.0x H_2O	-104.7	30.6	119	-3.420	0.0761
1.0x BB v. 0.5x SO	-45.9	33.9	119	-1.351	0.9965
1.0x BB v. 1.5x SO	-49.0	31.6	119	-1.553	0.9844
1.0x BB v. 1.0x SO	28.3	44.0	119	0.644	1.0000
0.5x BLT v. 1.5x BLT	-25.5	38.3	119	-0.667	1.0000
0.5x BLT v. 1.0x BLT	-57.8	40.0	119	-1.445	0.9927
0.5x BLT v. 0.5x BP	-77.3	35.4	119	-2.186	0.7583
0.5x BLT v. 1.5x BP	-25.9	35.4	119	-0.732	1.0000
0.5x BLT v. 1.0x BP	-19.8	35.4	119	-0.559	1.0000
0.5x BLT v. 0.5x DN	-32.1	38.3	119	-0.839	1.0000
0.5x BLT v. 1.5x DN	-31.5	36.2	119	-0.872	1.0000
0.5x BLT v. 1.0x DN	-28.1	36.2	119	-0.776	1.0000
0.5x BLT v. 0.5x H_2O	-135.6	36.2	119	-3.750	0.0286
0.5x BLT v. 1.5x H_2O	-37.3	35.4	119	-1.056	0.9998

Table C4. (cont'd)

0.5x BLT v. 1.0x H_2O	-129.8	35.4	119	-3.671	0.0366
0.5x BLT v. 0.5x SO	-70.9	38.3	119	-1.853	0.9227
0.5x BLT v. 1.5x SO	-74.1	36.2	119	-2.048	0.8390
0.5x BLT v. 1.0x SO	3.2	47.4	119	0.068	1.0000
1.5x BLT v. 1.0x BLT	-32.3	38.8	119	-0.833	1.0000
1.5x BLT v. 0.5x BP	-51.8	33.9	119	-1.525	0.9871
1.5x BLT v. 1.5x BP	-0.3	33.9	119	-0.010	1.0000
1.5x BLT v. 1.0x BP	5.8	33.9	119	0.170	1.0000
1.5x BLT v. 0.5x DN	-6.6	37.0	119	-0.178	1.0000
1.5x BLT v. 1.5x DN	-6.0	34.8	119	-0.172	1.0000
1.5x BLT v. 1.0x DN	-2.5	34.8	119	-0.073	1.0000
1.5x BLT v. 0.5x H_2O	-110.1	34.8	119	-3.164	0.1484
1.5x BLT v. 1.5x H_2O	-11.8	33.9	119	-0.348	1.0000
1.5x BLT v. 1.0x H_2O	-104.2	33.9	119	-3.071	0.1853
1.5x BLT v. 0.5x SO	-45.4	37.0	119	-1.228	0.9989
1.5x BLT v. 1.5x SO	-48.6	34.8	119	-1.395	0.9950
1.5x BLT v. 1.0x SO	28.8	46.3	119	0.621	1.0000
1.0x BLT v. 0.5x BP	-19.5	35.9	119	-0.542	1.0000
1.0x BLT v. 1.5x BP	32.0	35.9	119	0.890	1.0000
1.0x BLT v. 1.0x BP	38.1	35.9	119	1.060	0.9998
1.0x BLT v. 0.5x DN	25.7	38.8	119	0.663	1.0000
1.0x BLT v. 1.5x DN	26.3	36.7	119	0.716	1.0000
1.0x BLT v. 1.0x DN	29.7	36.7	119	0.810	1.0000
1.0x BLT v. 0.5x H_2O	-77.8	36.7	119	-2.120	0.7991
1.0x BLT v. 1.5x H_2O	20.5	35.9	119	0.571	1.0000
1.0x BLT v. 1.0x H_2O	-71.9	35.9	119	-2.004	0.8612
1.0x BLT v. 0.5x SO	-13.1	38.8	119	-0.338	1.0000
1.0x BLT v. 1.5x SO	-16.3	36.7	119	-0.443	1.0000
1.0x BLT v. 1.0x SO	61.1	47.8	119	1.278	0.9982

Table C4. (cont'd)

0.5x BP v. 1.5x BP	51.4	30.6	119	1.679	0.9669
0.5x BP v. 1.0x BP	57.5	30.6	119	1.879	0.9138
0.5x BP v. 0.5x DN	45.2	33.9	119	1.331	0.9971
0.5x BP v. 1.5x DN	45.8	31.6	119	1.450	0.9924
0.5x BP v. 1.0x DN	49.2	31.6	119	1.559	0.9838
0.5x BP v. 0.5x H_2O	-58.4	31.6	119	-1.849	0.9241
0.5x BP v. 1.5x H_2O	40.0	30.6	119	1.305	0.9977
0.5x BP v. 1.0x H_2O	-52.5	30.6	119	-1.714	0.9601
0.5x BP v. 0.5x SO	6.4	33.9	119	0.188	1.0000
0.5x BP v. 1.5x SO	3.2	31.6	119	0.102	1.0000
0.5x BP v. 1.0x SO	80.5	44.0	119	1.832	0.9297
1.5x BP v. 1.0x BP	6.1	30.6	119	0.200	1.0000
1.5x BP v. 0.5x DN	-6.2	33.9	119	-0.184	1.0000
1.5x BP v. 1.5x DN	-5.7	31.6	119	-0.179	1.0000
1.5x BP v. 1.0x DN	-2.2	31.6	119	-0.070	1.0000
1.5x BP v. 0.5x H_2O	-109.8	31.6	119	-3.478	0.0646
1.5x BP v. 1.5x H_2O	-11.5	30.6	119	-0.374	1.0000
1.5x BP v. 1.0x H_2O	-103.9	30.6	119	-3.394	0.0819
1.5x BP v. 0.5x SO	-45.1	33.9	119	-1.327	0.9972
1.5x BP v. 1.5x SO	-48.2	31.6	119	-1.528	0.9868
1.5x BP v. 1.0x SO	29.1	44.0	119	0.662	1.0000
1.0x BP v. 0.5x DN	-12.4	33.9	119	-0.364	1.0000
1.0x BP v. 1.5x DN	-11.8	31.6	119	-0.373	1.0000
1.0x BP v. 1.0x DN	-8.3	31.6	119	-0.264	1.0000
1.0x BP v. 0.5x H_2O	-115.9	31.6	119	-3.672	0.0364
1.0x BP v. 1.5x H_2O	-17.6	30.6	119	-0.574	1.0000
1.0x BP v. 1.0x H_2O	-110.0	30.6	119	-3.593	0.0462
1.0x BP v. 0.5x SO	-51.2	33.9	119	-1.507	0.9885
1.0x BP v. 1.5x SO	-54.3	31.6	119	-1.722	0.9585

Table C4. (cont'd)

1.0x BP v. 1.0x SO	23.0	44.0	119	0.523	1.0000
0.5x DN v. 1.5x DN	0.6	34.8	119	0.017	1.0000
0.5x DN v. 1.0x DN	4.0	34.8	119	0.116	1.0000
0.5x DN v. 0.5x H_2O	-103.5	34.8	119	-2.975	0.2294
0.5x DN v. 1.5x H_2O	-5.2	33.9	119	-0.154	1.0000
0.5x DN v. 1.0x H_2O	-97.7	33.9	119	-2.877	0.2816
0.5x DN v. 0.5x SO	-38.8	37.0	119	-1.050	0.9999
0.5x DN v. 1.5x SO	-42.0	34.8	119	-1.206	0.9991
0.5x DN v. 1.0x SO	35.4	46.3	119	0.763	1.0000
1.5x DN v. 1.0x DN	3.5	32.5	119	0.106	1.0000
1.5x DN v. 0.5x H_2O	-104.1	32.5	119	-3.206	0.1340
1.5x DN v. 1.5x H_2O	-5.8	31.6	119	-0.184	1.0000
1.5x DN v. 1.0x H_2O	-98.2	31.6	119	-3.113	0.1680
1.5x DN v. 0.5x SO	-39.4	34.8	119	-1.132	0.9996
1.5x DN v. 1.5x SO	-42.6	32.5	119	-1.310	0.9976
1.5x DN v. 1.0x SO	34.8	44.6	119	0.779	1.0000
1.0x DN v. 0.5x H_2O	-107.6	32.5	119	-3.312	0.1019
1.0x DN v. 1.5x H_2O	-9.3	31.6	119	-0.293	1.0000
1.0x DN v. 1.0x H_2O	-101.7	31.6	119	-3.222	0.1286
1.0x DN v. 0.5x SO	-42.8	34.8	119	-1.231	0.9989
1.0x DN v. 1.5x SO	-46.0	32.5	119	-1.417	0.9941
1.0x DN v. 1.0x SO	31.3	44.6	119	0.702	1.0000
0.5x H_2O v. 1.5x H_2O	98.3	31.6	119	3.115	0.1671
0.5x H_2O v. 1.0x H_2O	5.9	31.6	119	0.186	1.0000
0.5x H_2O v. 0.5x SO	64.7	34.8	119	1.860	0.9205
0.5x H_2O v. 1.5x SO	61.6	32.5	119	1.896	0.9078
0.5x H_2O v. 1.0x SO	138.9	44.6	119	3.112	0.1683
1.5x H_2O v. 1.0x H2O	-92.4	30.6	119	-3.019	0.2083
1.5x H_2O v. 0.5x SO	-33.6	33.9	119	-0.990	0.9999

Table C4. (cont'd)

1.5x H_2O v. 1.5x SO	-36.8	31.6	119	-1.165	0.9994
1.5x H_2O v. 1.0x SO	40.6	44.0	119	0.923	1.0000
1.0x H_2O v. 0.5x SO	58.8	33.9	119	1.734	0.9559
1.0x H_2O v. 1.5x SO	55.7	31.6	119	1.765	0.9486
1.0x H_2O v. 1.0x SO	133.0	44.0	119	3.025	0.2055
0.5x SO v. 1.5x SO	-3.2	34.8	119	-0.091	1.0000
0.5x SO – 1.0x SO	74.2	46.3	119	1.600	0.9790
1.5x SO – 1.0x SO	77.3	44.6	119	1.733	0.9561

Table C5. Group 2 2021 mean total area of growth (mm^2) of *Pss* strains 23 and 34, belonging to phylogroup (PG) 2b ± SE in co-inoculations of biological control agents (BCAs) [BlightBan®A506 (BB), Bloomtime™ (BLT), Blossom Protect™ (BP), Double Nickel55™ (DN), Serenade® Opti (SO), or water (H_2O)] at three rates (0.5x, 1.0x, 1.5x), with confidence limits (lower and upper C.L.) and the p-value for the pairwise comparisons of the estimated marginal means for each trt*strain, with letters indicating statistical differences with significance determined by p-value ≤0.05.

Year	Group	Strain/PG	Treatment (BCA)	*Pss* Mean total area (mm2)	SE	df	lower C.L.	upper C.L.	
2021	2	23 2b	BB	151.0	17.7	119	116.0	186.0	a
			BLT	158.1	20.2	119	118.1	198.0	a
			BP	181.7	17.7	119	146.7	216.7	a
			DN	170.3	19.5	119	131.6	209.0	a
			H_2O	172.4	18.4	119	136.0	208.8	a
			SO	161.6	27.9	119	106.2	216.9	a
		34 2b	BB	155.5	17.7	119	120.5	190.5	a
			BLT	171.0	24.6	119	122.2	219.8	a
			BP	173.7	17.7	119	138.7	208.7	a
			DN	164.3	19.8	119	125.2	203.5	a
			H_2O	302.9	17.7	119	267.9	337.9	b
			SO	206.4	20.2	119	166.4	246.4	a

Year	Group	Contrast	estimate	SE	df	t-ratio	p-value
2021	2	BB strain 23 v. BLT strain 23	-7.0	26.8	119	-0.263	1.0000
		BB strain 23 v. BP strain 23	-30.7	25.0	119	-1.228	0.9856
		BB strain 23 v. DN strain 23	-19.3	26.3	119	-0.731	0.9999
		BB strain 23 v. H_2O strain 23	-21.4	25.5	119	-0.838	0.9995
		BB strain 23 v. SO strain 23	-10.5	33.1	119	-0.319	1.0000
		BB strain 23 v. BB strain 34	-4.5	25.0	119	-0.180	1.0000
		BB strain 23 v. BLT strain 34	-19.9	30.3	119	-0.658	1.0000

Table C5. (cont'd)

BB strain 23 v. BP strain 34	-22.7	25.0	119	-0.907	0.9989
BB strain 23 v. DN strain 34	-13.3	26.5	119	-0.502	1.0000
BB strain 23 v. H_2O strain 34	-151.9	25.0	119	-6.076	<0.0001
BB strain 23 v. SO strain 34	-55.4	26.8	119	-2.064	0.6490
BLT strain 23 v. BP strain 23	-23.6	26.8	119	-0.881	0.9992
BLT strain 23 v. DN strain 23	-12.2	28.1	119	-0.434	1.0000
BLT strain 23 v. H_2O strain 23	-14.3	27.3	119	-0.524	1.0000
BLT strain 23 v. SO strain 23	-3.5	34.5	119	-0.101	1.0000
BLT strain 23 v. BB strain 34	2.5	26.8	119	0.095	1.0000
BLT strain 23 v. BLT strain 34	-12.9	31.9	119	-0.405	1.0000
BLT strain 23 v. BP strain 34	-15.6	26.8	119	-0.582	1.0000
BLT strain 23 v. DN strain 34	-6.3	28.3	119	-0.222	1.0000
BLT strain 23 v. H_2O strain 34	-144.8	26.8	119	-5.397	<0.0001
BLT strain 23 v. SO strain 34	-48.3	28.6	119	-1.693	0.8681
BP strain 23 v. DN strain 23	11.4	26.3	119	0.434	1.0000
BP strain 23 v. H_2O strain 23	9.3	25.5	119	0.365	1.0000
BP strain 23 v. SO strain 23	20.2	33.1	119	0.609	1.0000
BP strain 23 v. BB strain 34	26.2	25.0	119	1.048	0.9962
BP strain 23 v. BLT strain 34	10.7	30.3	119	0.354	1.0000
BP strain 23 v. BP strain 34	8.0	25.0	119	0.321	1.0000
BP strain 23 v. DN strain 34	17.4	26.5	119	0.655	1.0000
BP strain 23 v. H_2O strain 34	-121.2	25.0	119	-4.848	0.0002
BP strain 23 v. SO strain 34	-24.7	26.8	119	-0.920	0.9988
DN strain 23 v. H_2O strain 23	-2.1	26.8	119	-0.079	1.0000
DN strain 23 v. SO strain 23	8.7	34.1	119	0.255	1.0000
DN strain 23 v. BB strain 34	14.7	26.3	119	0.560	1.0000
DN strain 23 v. BLT strain 34	-0.7	31.5	119	-0.022	1.0000
DN strain 23 v. BP strain 34	-3.4	26.3	119	-0.130	1.0000
DN strain 23 v. DN strain 34	5.9	27.8	119	0.213	1.0000

Table C5. (cont'd)

DN strain 23 v. H_2O strain 34	-132.6	26.3	119	-5.034	0.0001
DN strain 23 v. SO strain 34	-36.1	28.1	119	-1.286	0.9794
H_2O strain 23 v. SO strain 23	10.8	33.5	119	0.324	1.0000
H_2O strain 23 v. BB strain 34	16.9	25.5	119	0.661	1.0000
H_2O strain 23 v. BLT strain 34	1.4	30.8	119	0.046	1.0000
H_2O strain 23 v. BP strain 34	-1.3	25.5	119	-0.051	1.0000
H_2O strain 23 v. DN strain 34	8.0	27.0	119	0.298	1.0000
H_2O strain 23 v. H2O strain 34	-130.5	25.5	119	-5.116	0.0001
H_2O strain 23 v. SO strain 34	-34.0	27.3	119	-1.245	0.9839
SO strain 23 v. BB strain 34	6.0	33.1	119	0.183	1.0000
SO strain 23 v. BLT strain 34	-9.4	37.3	119	-0.252	1.0000
SO strain 23 v. BP strain 34	-12.1	33.1	119	-0.367	1.0000
SO strain 23 v. DN strain 34	-2.8	34.2	119	-0.081	1.0000
SO strain 23 v. H_2O strain 34	-141.3	33.1	119	-4.274	0.0022
SO strain 23 v. SO strain 34	-44.9	34.5	119	-1.301	0.9775
BB strain 34 v. BLT strain 34	-15.4	30.3	119	-0.509	1.0000
BB strain 34 v. BP strain 34	-18.2	25.0	119	-0.727	0.9999
BB strain 34 v. DN strain 34	-8.8	26.5	119	-0.333	1.0000
BB strain 34 v. H_2O strain 34	-147.4	25.0	119	-5.896	<0.0001
BB strain 34 v. SO strain 34	-50.9	26.8	119	-1.896	0.7593
BLT strain 34 v. BP strain 34	-2.7	30.3	119	-0.090	1.0000
BLT strain 34 v. DN strain 34	6.6	31.6	119	0.210	1.0000
BLT strain 34 v. H_2O strain 34	-131.9	30.3	119	-4.350	0.0017
BLT strain 34 v. SO strain 34	-35.4	31.9	119	-1.112	0.9936
BP strain 34 v. DN strain 34	9.4	26.5	119	0.353	1.0000
BP strain 34 v. H_2O strain 34	-129.2	25.0	119	-5.169	0.0001
BP strain 34 v. SO strain 34	-32.7	26.8	119	-1.219	0.9864
DN strain 34 v. H_2O strain 34	-138.6	26.5	119	-5.226	<0.0001
DN strain 34 v. SO strain 34	-42.1	28.3	119	-1.489	0.9409
H2O strain 34 v. SO strain 34	96.5	26.8	119	3.595	0.0229

Table C6. Group 3 2021, by rate and by strain, mean total area of growth (mm^2) of *Pss* strains 22, 26, and 37, belonging to phylogroup (PG) 2b and 2d, ± SE, in co-inoculations of biological control agents (BCAs) [BlightBan®A506 (BB), Bloomtime™ (BLT), Blossom Protect™ (BP), Double Nickel55™ (DN), Serenade® Opti (SO), or water (H_2O)] at three rates (0.5x, 1.0x, 1.5x), with confidence limits (lower and upper C.L.) and the p-value for the pairwise comparisons of the estimated marginal means for each treatment and strain, with letters indicating statistical differences with significance determined by p-value ≤0.05.

Year	Group	Strain/PG	Rate	*Pss* Mean total area (mm2)	SE	df	lower C.L.	upper C.L.	
2021	3	22 2b	0.5x	136.8	6.2	189	124.5	149.0	a
		26 2d	1.5x	165.5	6.5	189	152.6	178.4	b
		37 2d	1.0x	150.9	7.0	189	137.2	164.6	ab

Year	Group	Strain/PG	contrast	estimate	SE	df	t-ratio	p-value
2021	3	22 2b	0.5x v. 1.5x	-28.8	9.0	189	-3.194	0.0047
		26 2d	0.5x v. 1.0x	-14.1	9.3	189	-1.518	0.2849
		37 2d	1.5x v. 1.0x	14.6	9.5	189	1.532	0.2781

Year	Group	Strain	PG	Mean total area (mm2)	SE	df	lower C.L.	upper C.L.	
2021	3	22	2b	122.2	7.0	189	108.3	136.0	a
		26	2d	154.7	6.0	189	142.9	166.6	b
		37	2d	176.3	6.6	189	163.2	189.4	c

Year	Group	contrast	estimate	SE	df	t-ratio	p-value
2021	3	strain 22 v. strain 26	-32.5	9.2	189	-3.520	0.0016
		strain 22 v. strain 37	-54.1	9.7	189	-5.598	<0.0001
		strain 26 v. strain 37	-21.6	9.0	189	-2.411	0.0443

Table C7. Group 3 2021 mean total area of growth (mm^2) of *Pss* strains 22, 26, and 37, belonging to phylogroup (PG) 2b and 2d, ± SE, in co-inoculations of biological control agents (BCAs) [BlightBan®A506 (BB), Bloomtime™ (BLT), Blossom Protect™ (BP), Double Nickel55™ (DN), Serenade® Opti (SO), or water (H_2O)] at three rates (0.5x, 1.0x, 1.5x), with confidence limits (lower and upper C.L.) and the p-value for the pairwise comparisons of the estimated marginal means for each treatment*strain, with letters indicating statistical differences with significance determined by p-value ≤0.05.

Year	Group	Strain/PG	Treatment (BCA)	*Pss* Mean total area (mm2)	SE	df	lower C.L.	upper C.L.	
2021	3	22 2b	BB	117.7	14.9	189	88.3	147.1	a
			BLT	118.0	17.5	189	83.4	152.6	a
			BP	120.5	14.9	189	91.1	149.8	a
			DN	131.4	22.2	189	87.5	175.2	abc
			H_2O	119.0	17.5	189	84.5	153.6	a
			SO	126.7	14.9	189	97.3	156.1	ab
		26 2d	BB	164.0	14.3	189	135.8	192.2	abc
			BLT	149.7	14.9	189	120.3	179.1	abc
			BP	147.7	14.9	189	118.3	177.1	ab
			DN	160.0	14.3	189	131.8	188.2	abc
			H_2O	134.2	15.5	189	103.7	164.7	ab
			SO	172.8	14.3	189	144.5	201.0	abc
		37 2d	BB	184.8	14.3	189	156.6	213.1	abc
			BLT	149.3	21.9	189	106.1	192.4	abc
			BP	150.2	14.9	189	120.8	179.6	abc
			DN	201.1	14.9	189	171.7	230.5	bc
			H_2O	226.4	16.0	189	194.9	258.0	c
			SO	146.0	14.3	189	117.8	174.2	ab

Table C7. (cont'd)

Year	Group	Contrast	estimate	SE	df	t-ratio	p-value
2021	3	BB strain 22 v. BLT strain 22	-0.3	23.0	189	-0.014	1.0000
		BB strain 22 v. BP strain 22	-2.8	21.1	189	-0.132	1.0000
		BB strain 22 v. DN strain 22	-13.7	26.8	189	-0.511	1.0000
		BB strain 22 v. H_2O strain 22	-1.4	23.0	189	-0.060	1.0000
		BB strain 22 v. SO strain 22	-9.0	21.1	189	-0.427	1.0000
		BB strain 22 v. BB strain 26	-46.3	20.7	189	-2.243	0.7224
		BB strain 22 v. BLT strain 26	-32.0	21.1	189	-1.519	0.9883
		BB strain 22 v. BP strain 26	-30.0	21.1	189	-1.425	0.9941
		BB strain 22 v. DN strain 26	-42.3	20.7	189	-2.050	0.8407
		BB strain 22 v. H_2O strain 26	-16.5	21.5	189	-0.769	1.0000
		BB strain 22 v. SO strain 26	-55.1	20.7	189	-2.668	0.4104
		BB strain 22 v. BB strain 37	-67.2	20.7	189	-3.252	0.1133
		BB strain 22 v. BLT strain 37	-31.6	26.5	189	-1.194	0.9993
		BB strain 22 v. BP strain 37	-32.5	21.1	189	-1.543	0.9862
		BB strain 22 v. DN strain 37	-83.4	21.1	189	-3.961	0.0124
		BB strain 22 v. H_2O strain 37	-108.8	21.9	189	-4.975	0.0002
		BB strain 22 v. SO strain 37	-28.3	20.7	189	-1.372	0.9962
		BLT strain 22 v. BP strain 22	-2.5	23.0	189	-0.107	1.0000
		BLT strain 22 v. DN strain 22	-13.4	28.3	189	-0.472	1.0000
		BLT strain 22 v. H_2O strain 22	-1.0	24.8	189	-0.042	1.0000
		BLT strain 22 v. SO strain 22	-8.7	23.0	189	-0.377	1.0000
		BLT strain 22 v. BB strain 26	-46.0	22.6	189	-2.033	0.8493
		BLT strain 22 v. BLT strain 26	-31.7	23.0	189	-1.377	0.9960
		BLT strain 22 v. BP strain 26	-29.7	23.0	189	-1.291	0.9981
		BLT strain 22 v. DN strain 26	-42.0	22.6	189	-1.857	0.9237
		BLT strain 22 v. H_2O strain 26	-16.2	23.4	189	-0.693	1.0000
		BLT strain 22 v. SO strain 26	-54.8	22.6	189	-2.421	0.5930
		BLT strain 22 v. BB strain 37	-66.9	22.6	189	-2.954	0.2339
		BLT strain 22 v. BLT strain 37	-31.3	28.0	189	-1.116	0.9997

Table C7. (cont'd)

BLT strain 22 v. BP strain 37	-32.2	23.0	189	-1.399	0.9952
BLT strain 22 v. DN strain 37	-83.1	23.0	189	-3.613	0.0396
BLT strain 22 v. H_2O strain 37	-108.4	23.7	189	-4.569	0.0012
BLT strain 22 v. SO strain 37	-28.0	22.6	189	-1.238	0.9989
BP strain 22 v. DN strain 22	-10.9	26.8	189	-0.407	1.0000
BP strain 22 v. H_2O strain 22	1.4	23.0	189	0.062	1.0000
BP strain 22 v. SO strain 22	-6.2	21.1	189	-0.295	1.0000
BP strain 22 v. BB strain 26	-43.5	20.7	189	-2.108	0.8084
BP strain 22 v. BLT strain 26	-29.2	21.1	189	-1.387	0.9957
BP strain 22 v. BP strain 26	-27.2	21.1	189	-1.293	0.9981
BP strain 22 v. DN strain 26	-39.6	20.7	189	-1.915	0.9027
BP strain 22 v. H_2O strain 26	-13.7	21.5	189	-0.639	1.0000
BP strain 22 v. SO strain 26	-52.3	20.7	189	-2.533	0.5088
BP strain 22 v. BB strain 37	-64.4	20.7	189	-3.117	0.1600
BP strain 22 v. BLT strain 37	-28.8	26.5	189	-1.089	0.9998
BP strain 22 v. BP strain 37	-29.7	21.1	189	-1.410	0.9948
BP strain 22 v. DN strain 37	-80.7	21.1	189	-3.828	0.0196
BP strain 22 v. H_2O strain 37	-106.0	21.9	189	-4.847	0.0004
BP strain 22 v. SO strain 37	-25.5	20.7	189	-1.237	0.9989
DN strain 22 v. H_2O strain 22	12.3	28.3	189	0.435	1.0000
DN strain 22 v. SO strain 22	4.7	26.8	189	0.175	1.0000
DN strain 22 v. BB strain 26	-32.6	26.5	189	-1.234	0.9989
DN strain 22 v. BLT strain 26	-18.3	26.8	189	-0.684	1.0000
DN strain 22 v. BP strain 26	-16.3	26.8	189	-0.610	1.0000
DN strain 22 v. DN strain 26	-28.7	26.5	189	-1.083	0.9998
DN strain 22 v. H_2O strain 26	-2.8	27.1	189	-0.104	1.0000
DN strain 22 v. SO strain 26	-41.4	26.5	189	-1.566	0.9839
DN strain 22 v. BB strain 37	-53.5	26.5	189	-2.022	0.8548
DN strain 22 v. BLT strain 37	-17.9	31.2	189	-0.574	1.0000

Table C7. (cont'd)

DN strain 22 v. BP strain 37	-18.8	26.8	189	-0.703	1.0000
DN strain 22 v. DN strain 37	-69.8	26.8	189	-2.605	0.4552
DN strain 22 v. H_2O strain 37	-95.1	27.4	189	-3.469	0.0615
DN strain 22 v. SO strain 37	-14.7	26.5	189	-0.554	1.0000
H_2O strain 22 v. SO strain 22	-7.6	23.0	189	-0.332	1.0000
H_2O strain 22 v. BB strain 26	-45.0	22.6	189	-1.987	0.8718
H_2O strain 22 v. BLT strain 26	-30.6	23.0	189	-1.332	0.9973
H_2O strain 22 v. BP strain 26	-28.7	23.0	189	-1.245	0.9988
H_2O strain 22 v. DN strain 26	-41.0	22.6	189	-1.810	0.9381
H_2O strain 22 v. H_2O strain 26	-15.1	23.4	189	-0.648	1.0000
H_2O strain 22 v. SO strain 26	-53.7	22.6	189	-2.375	0.6276
H_2O strain 22 v. BB strain 37	-65.8	22.6	189	-2.908	0.2585
H_2O strain 22 v. BLT strain 37	-30.2	28.0	189	-1.079	0.9998
H_2O strain 22 v. BP strain 37	-31.1	23.0	189	-1.353	0.9967
H_2O strain 22 v. DN strain 37	-82.1	23.0	189	-3.568	0.0456
H_2O strain 22 v. H_2O strain 37	-107.4	23.7	189	-4.525	0.0014
H_2O strain 22 v. SO strain 37	-27.0	22.6	189	-1.192	0.9993
SO strain 22 v. BB strain 26	-37.3	20.7	189	-1.807	0.9391
SO strain 22 v. BLT strain 26	-23.0	21.1	189	-1.091	0.9998
SO strain 22 v. BP strain 26	-21.0	21.1	189	-0.997	0.9999
SO strain 22 v. DN strain 26	-33.3	20.7	189	-1.614	0.9783
SO strain 22 v. H_2O strain 26	-7.5	21.5	189	-0.350	1.0000
SO strain 22 v. SO strain 26	-46.1	20.7	189	-2.232	0.7299
SO strain 22 v. BB strain 37	-58.2	20.7	189	-2.816	0.3122
SO strain 22 v. BLT strain 37	-22.6	26.5	189	-0.854	1.0000
SO strain 22 v. BP strain 37	-23.5	21.1	189	-1.115	0.9997
SO strain 22 v. DN strain 37	-74.4	21.1	189	-3.533	0.0507
SO strain 22 v. H_2O strain 37	-99.8	21.9	189	-4.563	0.0012
SO strain 22 v. SO strain 37	-19.3	20.7	189	-0.936	1.0000

Table C7. (cont'd)

BB strain 26 v. BLT strain 26	14.3	20.7	189	0.694	1.0000
BB strain 26 v. BP strain 26	16.3	20.7	189	0.790	1.0000
BB strain 26 v. DN strain 26	4.0	20.2	189	0.197	1.0000
BB strain 26 v. H_2O strain 26	29.8	21.1	189	1.415	0.9945
BB strain 26 v. SO strain 26	-8.8	20.2	189	-0.434	1.0000
BB strain 26 v. BB strain 37	-20.8	20.2	189	-1.030	0.9999
BB strain 26 v. BLT strain 37	14.7	26.1	189	0.564	1.0000
BB strain 26 v. BP strain 37	13.8	20.7	189	0.670	1.0000
BB strain 26 v. DN strain 37	-37.1	20.7	189	-1.796	0.9420
BB strain 26 v. H_2O strain 37	-62.4	21.5	189	-2.908	0.2586
BB strain 26 v. SO strain 37	18.0	20.2	189	0.889	1.0000
BLT strain 26 v. BP strain 26	2.0	21.1	189	0.094	1.0000
BLT strain 26 v. DN strain 26	-10.3	20.7	189	-0.501	1.0000
BLT strain 26 v. H_2O strain 26	15.5	21.5	189	0.721	1.0000
BLT strain 26 v. SO strain 26	-23.1	20.7	189	-1.119	0.9997
BLT strain 26 v. BB strain 37	-35.2	20.7	189	-1.703	0.9639
BLT strain 26 v. BLT strain 37	0.4	26.5	189	0.015	1.0000
BLT strain 26 v. BP strain 37	-0.5	21.1	189	-0.024	1.0000
BLT strain 26 v. DN strain 37	-51.4	21.1	189	-2.442	0.5774
BLT strain 26 v. H_2O strain 37	-76.8	21.9	189	-3.511	0.0542
BLT strain 26 v. SO strain 37	3.7	20.7	189	0.177	1.0000
BP strain 26 v. DN strain 26	-12.3	20.7	189	-0.596	1.0000
BP strain 26 v. H_2O strain 26	13.5	21.5	189	0.629	1.0000
BP strain 26 v. SO strain 26	-25.1	20.7	189	-1.215	0.9991
BP strain 26 v. BB strain 37	-37.2	20.7	189	-1.799	0.9414
BP strain 26 v. BLT strain 37	-1.6	26.5	189	-0.060	1.0000
BP strain 26 v. BP strain 37	-2.5	21.1	189	-0.118	1.0000
BP strain 26 v. DN strain 37	-53.4	21.1	189	-2.536	0.5066
BP strain 26 v. H_2O strain 37	-78.7	21.9	189	-3.602	0.0411

Table C7. (cont'd)

BP strain 26 v. SO strain 37	1.7	20.7	189	0.081	1.0000
DN strain 26 v. H_2O strain 26	25.8	21.1	189	1.226	0.9990
DN strain 26 v. SO strain 26	-12.8	20.2	189	-0.631	1.0000
DN strain 26 v. BB strain 37	-24.8	20.2	189	-1.227	0.9990
DN strain 26 v. BLT strain 37	10.7	26.1	189	0.411	1.0000
DN strain 26 v. BP strain 37	9.8	20.7	189	0.476	1.0000
DN strain 26 v. DN strain 37	-41.1	20.7	189	-1.989	0.8706
DN strain 26 v. H_2O strain 37	-66.4	21.5	189	-3.094	0.1693
DN strain 26 v. SO strain 37	14.0	20.2	189	0.692	1.0000
H_2O strain 26 v. SO strain 26	-38.6	21.1	189	-1.832	0.9316
H_2O strain 26 v. BB strain 37	-50.7	21.1	189	-2.405	0.6051
H_2O strain 26 v. BLT strain 37	-15.1	26.8	189	-0.563	1.0000
H_2O strain 26 v. BP strain 37	-16.0	21.5	189	-0.745	1.0000
H_2O strain 26 v. DN strain 37	-66.9	21.5	189	-3.117	0.1598
H_2O strain 26 v. H_2O strain 37	-92.2	22.2	189	-4.146	0.0063
H_2O strain 26 v. SO strain 37	-11.8	21.1	189	-0.561	1.0000
SO strain 26 v. BB strain 37	-12.1	20.2	189	-0.596	1.0000
SO strain 26 v. BLT strain 37	23.5	26.1	189	0.900	1.0000
SO strain 26 v. BP strain 37	22.6	20.7	189	1.094	0.9998
SO strain 26 v. DN strain 37	-28.3	20.7	189	-1.371	0.9962
SO strain 26 v. H_2O strain 37	-53.6	21.5	189	-2.499	0.5342
SO strain 26 v. SO strain 37	26.8	20.2	189	1.323	0.9975
BB strain 37 v. BLT strain 37	35.6	26.1	189	1.362	0.9965
BB strain 37 v. BP strain 37	34.7	20.7	189	1.679	0.9684
BB strain 37 v. DN strain 37	-16.3	20.7	189	-0.787	1.0000
BB strain 37 v. H_2O strain 37	-41.6	21.5	189	-1.937	0.8938
BB strain 37 v. SO strain 37	38.8	20.2	189	1.919	0.9010
BLT strain 37 v. BP strain 37	-0.9	26.5	189	-0.034	1.0000
BLT strain 37 v. DN strain 37	-51.8	26.5	189	-1.959	0.8842

Table C7. (cont'd)

BLT strain 37 v. H_2O strain 37	-77.2	27.1	189	-2.848	0.2929
BLT strain 37 v. SO strain 37	3.3	26.1	189	0.125	1.0000
BP strain 37 v. DN strain 37	-50.9	21.1	189	-2.418	0.5953
BP strain 37 v. H_2O strain 37	-76.3	21.9	189	-3.488	0.0581
BP strain 37 v. SO strain 37	4.2	20.7	189	0.202	1.0000
DN strain 37 v. H_2O strain 37	-25.3	21.9	189	-1.158	0.9995
DN strain 37 v. SO strain 37	55.1	20.7	189	2.667	0.4106
H_2O strain 37 v. SO strain 37	80.4	21.5	189	3.746	0.0258

Table C8. Group 4 2021, by rate and by strain, mean total area of growth (mm^2) of *Pss* strains 9 and 27, belonging to phylogroup (PG) 2d, ± SE, in co-inoculations of biological control agents (BCAs) [BlightBan®A506 (BB), Bloomtime™ (BLT), Blossom Protect™ (BP), Double Nickel55™ (DN), Serenade® Opti (SO), or water (H_2O)] at three rates (0.5x, 1.0x, 1.5x), with confidence limits (lower and upper C.L.) and the p-value for the pairwise comparisons of the estimated marginal means for each rate and strain, with letters indicating statistical differences with significance determined by p-value ≤0.05.

Year	Group	Strain/PG	Rate	*Pss* Mean total area (mm2)	SE	df	lower C.L.	upper C.L.	
2021	4	9 2d	0.5x	190.9	16.4	144	158.6	223.3	a
		27 2d	1.5x	234.2	16.5	144	201.6	266.8	ab
			1.0x	258.3	17.9	144	223.0	293.6	b

Year	Group	Strain/PG	contrast	estimate	SE	df	t-ratio	p-value
2021	4	9 2d	0.5x v. 1.5x	-43.2	23.3	144	-1.856	0.1552
		27 2d	0.5x v. 1.0x	-67.4	24.3	144	-2.774	0.0172
			1.5x v. 1.0x	-24.2	24.2	144	-0.997	0.5799

Year	Group	Strain	PG	Mean total area (mm2)	SE	df	lower C.L.	upper C.L.
2021	4	9	2d	185.4	13.6	144	158.5	212.2
		27	2d	270.3	14.0	144	242.6	297.9

Year	Group	contrast	estimate	SE	df	t-ratio	p-value
2021	4	strain 27 v. strain 9	84.9	19.5	144	4.363	<0.0001

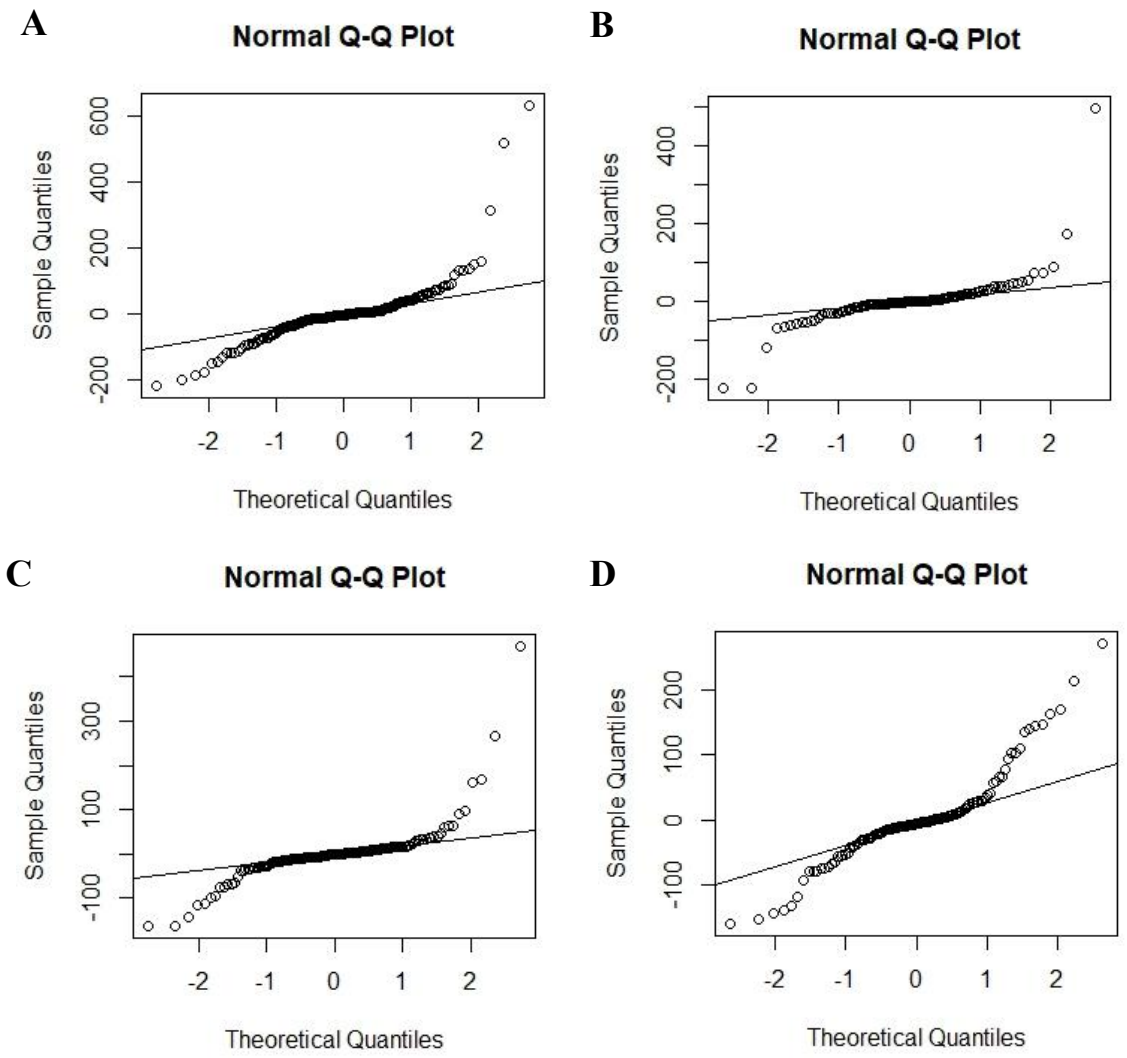


Figure C3. The 2021 quantile-quantile plots (qqplot) of the residuals for graphical visualization of the distribution of the total area of growth (mm^2) of *Pss* strains at 10^8 cfu/ml co-inoculated next to the commercial biological control Blossom Protect™ (BP) or water (H_2O) on KB or PDA media at three rates (0.5x, 1.0x, 1.5x) **A)** Group 1 *Pss* strains 14 (PG 2c), 25 (PG2d), and 38 (PG2d), **B)** Group 2 *Pss* strains 23 and 34 (PG2b), **C)** Group 3 *Pss* strains 22 (PG2b), 26 (PG2d), and 37 (PG2d), and **D)** Group 4 *Pss* strains 9 and 27 (PG2d).

Table C9. The 2021 group 1 *Pss* strains v. Blossom Protect™ (BP) or water (H_2O) in Petri plates with KB or PDA media, mean total area of growth (mm^2) of *Pss* strains 14, 25, and 38, belonging to phylogroup (PG) 2c, 2d, and 2d, respectively ± SE co-inoculated with BP at the rates 0.5x, 1.0x, and 1.5x. With confidence limits (lower and upper C.L.) and the p-value for the pairwise comparisons of the estimated marginal means for each strain, with letters indicating statistical differences with significance determined by p-value ≤0.05.

Year	Group	Strain	PG	*Pss* Mean total area (mm2)	SE	df	lower C.L.	upper C.L.	
2021	1	14	2c	212.9	13.4	139	186.5	239.4	a
		25	2d	166.6	13.1	139	140.7	192.5	b
		38	2d	184.3	13.3	139	158.0	210.7	ab

Year	Group	contrast	estimate	SE	df	t-ratio	p-value
2021	1	14 v. 25	46.3	18.7	139	2.473	0.0386
		14 v. 38	28.6	18.9	139	1.514	0.2876
		25 v. 38	-17.7	18.7	139	-0.947	0.6114

Table C10. The 2021 group 1 *Pss* strains v. Blossom Protect™ (BP) or water (H_2O) in Petri plates with KB or PDA media, mean total area of growth (mm^2) of *Pss* strains 14, 25, and 38, belonging to phylogroup (PG) 2c, 2d, and 2d, respectively ± SE co-inoculated with BP at the rates 0.5x, 1.0x, and 1.5x. With confidence limits (lower and upper C.L.) and the p-value for the pairwise comparisons of the estimated marginal means for media*rate*trt*strain with letters indicating statistical differences with significance determined by p-value ≤0.05.

Year	Group	media	Strain/PG	Treatment	Rate	*Pss* Mean total area (mm2)	SE	df	lower C.L.	upper C.L.	
2021	1	KB	14 2c	BP	0.5x	276.5	50.3	139	177.1	375.9	ab
				BP	1.5x	120.0	45.0	139	31.1	209.0	a
				BP	1.0x	164.9	50.3	139	65.5	264.4	ab
				H_2O	0.5x	229.8	45.0	139	140.9	318.7	ab
				H_2O	1.5x	351.7	45.0	139	262.8	440.6	b
				H_2O	1.0x	146.5	45.0	139	57.6	235.4	ab
			25 2d	BP	0.5x	157.7	45.0	139	68.7	246.6	ab
				BP	1.5x	201.2	45.0	139	112.3	290.1	ab
				BP	1.0x	150.1	50.3	139	50.7	249.5	ab
				H_2O	0.5x	195.1	45.0	139	106.1	284.0	ab
				H_2O	1.5x	162.2	50.3	139	62.7	261.6	ab
				H_2O	1.0x	212.3	45.0	139	123.4	301.2	ab
			38 2d	BP	0.5x	150.9	45.0	139	62.0	239.8	ab
				BP	1.5x	196.1	45.0	139	107.1	285.0	ab
				BP	1.0x	140.9	58.1	139	26.1	255.7	ab
				H_2O	0.5x	270.0	45.0	139	181.1	359.0	ab
				H_2O	1.5x	234.2	45.0	139	145.3	323.1	ab
				H_2O	1.0x	170.4	45.0	139	81.5	259.3	ab

Table C10. (cont'd)

2021	1	PDA	14	BP	0.5x	161.6	45.0	139	72.7	250.5	a
			14	BP	1.5x	363.9	50.3	139	264.5	463.3	a
			14	BP	1.0x	155.3	45.0	139	66.4	244.3	a
			14	H_2O	0.5x	229.4	45.0	139	140.5	318.4	a
			14	H_2O	1.5x	197.3	45.0	139	108.4	286.2	a
			14	H_2O	1.0x	158.3	45.0	139	69.4	247.2	a
			25	BP	0.5x	133.7	45.0	139	44.8	222.7	a
			25	BP	1.5x	150.3	45.0	139	61.4	239.2	a
			25	BP	1.0x	138.4	45.0	139	49.5	227.3	a
			25	H_2O	0.5x	222.0	45.0	139	133.0	310.9	a
			25	H_2O	1.5x	142.4	38.0	139	67.2	217.5	a
			25	H_2O	1.0x	134.4	45.0	139	45.5	223.3	a
			38	BP	0.5x	151.1	45.0	139	62.2	240.1	a
			38	BP	1.5x	160.4	45.0	139	71.5	249.3	a
			38	BP	1.0x	151.5	45.0	139	62.6	240.5	a
			38	H_2O	0.5x	219.9	45.0	139	131.0	308.8	a
			38	H_2O	1.5x	157.0	45.0	139	68.1	246.0	a
			38	H_2O	1.0x	209.6	45.0	139	120.7	298.5	a

Year	Group	Media	Contrast	estimate	SE	df	t-ratio	p-value
2021	1	KB	0.5x BP strain 14 v. 1.5x BP strain 14	156.5	67.5	139	2.319	0.6680
			0.5x BP strain 14 v. 1.0x BP strain 14	111.6	71.1	139	1.569	0.9831
			0.5x BP strain 14 v. 0.5x H_2O strain 14	46.7	67.5	139	0.693	1.0000
			0.5x BP strain 14 v. 1.5x H_2O strain 14	-75.2	67.5	139	-1.115	0.9997
			0.5x BP strain 14 v. 1.0x H_2O strain 14	130.0	67.5	139	1.927	0.8962
			0.5x BP strain 14 v. 0.5x BP strain 25	118.8	67.5	139	1.762	0.9499
			0.5x BP strain 14 v. 1.5x BP strain 25	75.3	67.5	139	1.117	0.9997
			0.5x BP strain 14 v. 1.0x BP strain 25	126.4	71.1	139	1.778	0.9458
			0.5x BP strain 14 v. 0.5x H_2O strain 25	81.4	67.5	139	1.207	0.9991
			0.5x BP strain 14 v. 1.5x H_2O strain 25	114.3	71.1	139	1.608	0.9784
			0.5x BP strain 14 v. 1.0x H_2O strain 25	64.2	67.5	139	0.952	1.0000

Table C10. (cont'd)

0.5x BP strain 14 v. 0.5x BP strain 38	125.6	67.5	139	1.862	0.9206
0.5x BP strain 14 v. 1.5x BP strain 38	80.4	67.5	139	1.192	0.9993
0.5x BP strain 14 v. 1.0x BP strain 38	135.6	76.8	139	1.766	0.9490
0.5x BP strain 14 v. 0.5x H_2O strain 38	6.5	67.5	139	0.096	1.0000
0.5x BP strain 14 v. 1.5x H_2O strain 38	42.3	67.5	139	0.627	1.0000
0.5x BP strain 14 v. 1.0x H_2O strain 38	106.1	67.5	139	1.573	0.9827
1.5x BP strain 14 v. 1.0x BP strain 14	-44.9	67.5	139	-0.666	1.0000
1.5x BP strain 14 v. 0.5x H_2O strain 14	-109.7	63.6	139	-1.725	0.9583
1.5x BP strain 14 v. 1.5x H_2O strain 14	-231.7	63.6	139	-3.643	**0.0384**
1.5x BP strain 14 v. 1.0x H_2O strain 14	-26.4	63.6	139	-0.416	1.0000
1.5x BP strain 14 v. 0.5x BP strain 25	-37.6	63.6	139	-0.591	1.0000
1.5x BP strain 14 v. 1.5x BP strain 25	-81.1	63.6	139	-1.276	0.9983
1.5x BP strain 14 v. 1.0x BP strain 25	-30.0	67.5	139	-0.445	1.0000
1.5x BP strain 14 v. 0.5x H_2O strain 25	-75.0	63.6	139	-1.179	0.9994
1.5x BP strain 14 v. 1.5x H_2O strain 25	-42.1	67.5	139	-0.624	1.0000
1.5x BP strain 14 v. 1.0x H_2O strain 25	-92.2	63.6	139	-1.450	0.9926
1.5x BP strain 14 v. 0.5x BP strain 38	-30.9	63.6	139	-0.485	1.0000
1.5x BP strain 14 v. 1.5x BP strain 38	-76.0	63.6	139	-1.195	0.9992
1.5x BP strain 14 v. 1.0x BP strain 38	-20.9	73.4	139	-0.284	1.0000
1.5x BP strain 14 v. 0.5x H_2O strain 38	-150.0	63.6	139	-2.358	0.6396
1.5x BP strain 14 v. 1.5x H_2O strain 38	-114.2	63.6	139	-1.795	0.9413
1.5x BP strain 14 v. 1.0x H_2O strain 38	-50.4	63.6	139	-0.792	1.0000
1.0x BP strain 14 v. 0.5x H_2O strain 14	-64.8	67.5	139	-0.961	1.0000
1.0x BP strain 14 v. 1.5x H_2O strain 14	-186.8	67.5	139	-2.769	0.3451
1.0x BP strain 14 v. 1.0x H_2O strain 14	18.5	67.5	139	0.274	1.0000
1.0x BP strain 14 v. 0.5x BP strain 25	7.3	67.5	139	0.108	1.0000
1.0x BP strain 14 v. 1.5x BP strain 25	-36.2	67.5	139	-0.537	1.0000
1.0x BP strain 14 v. 1.0x BP strain 25	14.9	71.1	139	0.209	1.0000
1.0x BP strain 14 v. 0.5x H_2O strain 25	-30.1	67.5	139	-0.446	1.0000
1.0x BP strain 14 v. 1.5x H_2O strain 25	2.8	71.1	139	0.039	1.0000

Table C10. (cont'd)

1.0x BP strain 14 v. 1.0x H_2O strain 25	-47.3	67.5	139	-0.702	1.0000
1.0x BP strain 14 v. 0.5x BP strain 38	14.0	67.5	139	0.208	1.0000
1.0x BP strain 14 v. 1.5x BP strain 38	-31.1	67.5	139	-0.461	1.0000
1.0x BP strain 14 v. 1.0x BP strain 38	24.0	76.8	139	0.313	1.0000
1.0x BP strain 14 v. 0.5x H_2O strain 38	-105.1	67.5	139	-1.558	0.9842
1.0x BP strain 14 v. 1.5x H_2O strain 38	-69.3	67.5	139	-1.027	0.9999
1.0x BP strain 14 v. 1.0x H_2O strain 38	-5.5	67.5	139	-0.081	1.0000
0.5x H_2O strain 14 v. 1.5x H_2O strain 14	-121.9	63.6	139	-1.917	0.9004
0.5x H_2O strain 14 v. 1.0x H_2O strain 14	83.3	63.6	139	1.310	0.9977
0.5x H_2O strain 14 v. 0.5x BP strain 25	72.1	63.6	139	1.134	0.9996
0.5x H_2O strain 14 v. 1.5x BP strain 25	28.6	63.6	139	0.450	1.0000
0.5x H_2O strain 14 v. 1.0x BP strain 25	79.7	67.5	139	1.182	0.9993
0.5x H_2O strain 14 v. 0.5x H_2O strain 25	34.7	63.6	139	0.546	1.0000
0.5x H_2O strain 14 v. 1.5x H_2O strain 25	67.6	67.5	139	1.002	0.9999
0.5x H_2O strain 14 v. 1.0x H_2O strain 25	17.5	63.6	139	0.275	1.0000
0.5x H_2O strain 14 v. 0.5x BP strain 38	78.9	63.6	139	1.240	0.9988
0.5x H_2O strain 14 v. 1.5x BP strain 38	33.7	63.6	139	0.530	1.0000
0.5x H_2O strain 14 v. 1.0x BP strain 38	88.9	73.4	139	1.210	0.9991
0.5x H_2O strain 14 v. 0.5x H_2O strain 38	-40.3	63.6	139	-0.633	1.0000
0.5x H_2O strain 14 v. 1.5x H_2O strain 38	-4.4	63.6	139	-0.069	1.0000
0.5x H_2O strain 14 v. 1.0x H_2O strain 38	59.4	63.6	139	0.934	1.0000
1.5x H_2O strain 14 v. 1.0x H_2O strain 14	205.2	63.6	139	3.227	0.1247
1.5x H_2O strain 14 v. 0.5x BP strain 25	194.1	63.6	139	3.051	0.1914
1.5x H_2O strain 14 v. 1.5x BP strain 25	150.5	63.6	139	2.367	0.6335
1.5x H_2O strain 14 v. 1.0x BP strain 25	201.6	67.5	139	2.989	0.2203
1.5x H_2O strain 14 v. 0.5x H_2O strain 25	156.7	63.6	139	2.463	0.5620
1.5x H_2O strain 14 v. 1.5x H_2O strain 25	189.6	67.5	139	2.810	0.3192
1.5x H_2O strain 14 v. 1.0x H_2O strain 25	139.4	63.6	139	2.192	0.7551
1.5x H_2O strain 14 v. 0.5x BP strain 38	200.8	63.6	139	3.157	0.1485
1.5x H_2O strain 14 v. 1.5x BP strain 38	155.6	63.6	139	2.447	0.5739

Table C10. (cont'd)

1.5x H_2O strain 14 v. 1.0x BP strain 38	210.8	73.4	139	2.871	0.2832
1.5x H_2O strain 14 v. 0.5x H_2O strain 38	81.7	63.6	139	1.284	0.9982
1.5x H_2O strain 14 v. 1.5x H_2O strain 38	117.5	63.6	139	1.848	0.9254
1.5x H_2O strain 14 v. 1.0x H_2O strain 38	181.3	63.6	139	2.851	0.2948
1.0x H_2O strain 14 v. 0.5x BP strain 25	-11.2	63.6	139	-0.176	1.0000
1.0x H_2O strain 14 v. 1.5x BP strain 25	-54.7	63.6	139	-0.860	1.0000
1.0x H_2O strain 14 v. 1.0x BP strain 25	-3.6	67.5	139	-0.053	1.0000
1.0x H_2O strain 14 v. 0.5x H_2O strain 25	-48.6	63.6	139	-0.764	1.0000
1.0x H_2O strain 14 v. 1.5x H_2O strain 25	-15.7	67.5	139	-0.232	1.0000
1.0x H_2O strain 14 v. 1.0x H_2O strain 25	-65.8	63.6	139	-1.035	0.9999
1.0x H_2O strain 14 v. 0.5x BP strain 38	-4.4	63.6	139	-0.069	1.0000
1.0x H_2O strain 14 v. 1.5x BP strain 38	-49.6	63.6	139	-0.780	1.0000
1.0x H_2O strain 14 v. 1.0x BP strain 38	5.6	73.4	139	0.076	1.0000
1.0x H_2O strain 14 v. 0.5x H_2O strain 38	-123.6	63.6	139	-1.943	0.8899
1.0x H_2O strain 14 v. 1.5x H_2O strain 38	-87.7	63.6	139	-1.379	0.9957
1.0x H_2O strain 14 v. 1.0x H_2O strain 38	-23.9	63.6	139	-0.376	1.0000
0.5x BP strain 25 v. 1.5x BP strain 25	-43.5	63.6	139	-0.684	1.0000
0.5x BP strain 25 v. 1.0x BP strain 25	7.6	67.5	139	0.112	1.0000
0.5x BP strain 25 v. 0.5x H_2O strain 25	-37.4	63.6	139	-0.588	1.0000
0.5x BP strain 25 v. 1.5x H_2O strain 25	-4.5	67.5	139	-0.067	1.0000
0.5x BP strain 25 v. 1.0x H_2O strain 25	-54.6	63.6	139	-0.859	1.0000
0.5x BP strain 25 v. 0.5x BP strain 38	6.8	63.6	139	0.106	1.0000
0.5x BP strain 25 v. 1.5x BP strain 38	-38.4	63.6	139	-0.604	1.0000
0.5x BP strain 25 v. 1.0x BP strain 38	16.8	73.4	139	0.228	1.0000
0.5x BP strain 25 v. 0.5x H_2O strain 38	-112.4	63.6	139	-1.767	0.9486
0.5x BP strain 25 v. 1.5x H_2O strain 38	-76.5	63.6	139	-1.203	0.9992
0.5x BP strain 25 v. 1.0x H_2O strain 38	-12.8	63.6	139	-0.201	1.0000
1.5x BP strain 25 v. 1.0x BP strain 25	51.1	67.5	139	0.758	1.0000
1.5x BP strain 25 v. 0.5x H_2O strain 25	6.1	63.6	139	0.096	1.0000
1.5x BP strain 25 v. 1.5x H_2O strain 25	39.0	67.5	139	0.578	1.0000

Table C10. (cont'd)

1.5x BP strain 25 v. 1.0x H_2O strain 25	-11.1	63.6	139	-0.174	1.0000
1.5x BP strain 25 v. 0.5x BP strain 38	50.3	63.6	139	0.791	1.0000
1.5x BP strain 25 v. 1.5x BP strain 38	5.1	63.6	139	0.080	1.0000
1.5x BP strain 25 v. 1.0x BP strain 38	60.3	73.4	139	0.821	1.0000
1.5x BP strain 25 v. 0.5x H_2O strain 38	-68.9	63.6	139	-1.083	0.9998
1.5x BP strain 25 v. 1.5x H_2O strain 38	-33.0	63.6	139	-0.519	1.0000
1.5x BP strain 25 v. 1.0x H_2O strain 38	30.8	63.6	139	0.484	1.0000
1.0x BP strain 25 v. 0.5x H_2O strain 25	-45.0	67.5	139	-0.667	1.0000
1.0x BP strain 25 v. 1.5x H_2O strain 25	-12.1	71.1	139	-0.170	1.0000
1.0x BP strain 25 v. 1.0x H_2O strain 25	-62.2	67.5	139	-0.922	1.0000
1.0x BP strain 25 v. 0.5x BP strain 38	-0.8	67.5	139	-0.012	1.0000
1.0x BP strain 25 v. 1.5x BP strain 38	-46.0	67.5	139	-0.682	1.0000
1.0x BP strain 25 v. 1.0x BP strain 38	9.2	76.8	139	0.120	1.0000
1.0x BP strain 25 v. 0.5x H_2O strain 38	-120.0	67.5	139	-1.778	0.9457
1.0x BP strain 25 v. 1.5x H_2O strain 38	-84.1	67.5	139	-1.247	0.9987
1.0x BP strain 25 v. 1.0x H_2O strain 38	-20.3	67.5	139	-0.301	1.0000
0.5x H_2O strain 25 v. 1.5x H_2O strain 25	32.9	67.5	139	0.488	1.0000
0.5x H_2O strain 25 v. 1.0x H_2O strain 25	-17.2	63.6	139	-0.271	1.0000
0.5x H_2O strain 25 v. 0.5x BP strain 38	44.2	63.6	139	0.694	1.0000
0.5x H_2O strain 25 v. 1.5x BP strain 38	-1.0	63.6	139	-0.016	1.0000
0.5x H_2O strain 25 v. 1.0x BP strain 38	54.2	73.4	139	0.737	1.0000
0.5x H_2O strain 25 v. 0.5x H_2O strain 38	-75.0	63.6	139	-1.179	0.9994
0.5x H_2O strain 25 v. 1.5x H_2O strain 38	-39.1	63.6	139	-0.615	1.0000
0.5x H_2O strain 25 v. 1.0x H_2O strain 38	24.6	63.6	139	0.387	1.0000
1.5x H_2O strain 25 v. 1.0x H_2O strain 25	-50.1	67.5	139	-0.743	1.0000
1.5x H_2O strain 25 v. 0.5x BP strain 38	11.3	67.5	139	0.167	1.0000
1.5x H_2O strain 25 v. 1.5x BP strain 38	-33.9	67.5	139	-0.503	1.0000
1.5x H_2O strain 25 v. 1.0x BP strain 38	21.3	76.8	139	0.277	1.0000
1.5x H_2O strain 25 v. 0.5x H_2O strain 38	-107.9	67.5	139	-1.599	0.9796
1.5x H_2O strain 25 v. 1.5x H_2O strain 38	-72.0	67.5	139	-1.068	0.9998

Table C10. (cont'd)

			1.5x H_2O strain 25 v. 1.0x H_2O strain 38	-8.3	67.5	139	-0.122	1.0000
			1.0x H_2O strain 25 v. 0.5x BP strain 38	61.4	63.6	139	0.965	1.0000
			1.0x H_2O strain 25 v. 1.5x BP strain 38	16.2	63.6	139	0.255	1.0000
			1.0x H_2O strain 25 v. 1.0x BP strain 38	71.4	73.4	139	0.972	1.0000
			1.0x H_2O strain 25 v. 0.5x H_2O strain 38	-57.8	63.6	139	-0.908	1.0000
			1.0x H_2O strain 25 v. 1.5x H_2O strain 38	-21.9	63.6	139	-0.345	1.0000
			1.0x H_2O strain 25 v. 1.0x H_2O strain 38	41.9	63.6	139	0.658	1.0000
			0.5x BP strain 38 v. 1.5x BP strain 38	-45.2	63.6	139	-0.710	1.0000
			0.5x BP strain 38 v. 1.0x BP strain 38	10.0	73.4	139	0.136	1.0000
			0.5x BP strain 38 v. 0.5x H_2O strain 38	-119.1	63.6	139	-1.873	0.9167
			0.5x BP strain 38 v. 1.5x H_2O strain 38	-83.3	63.6	139	-1.310	0.9977
			0.5x BP strain 38 v. 1.0x H_2O strain 38	-19.5	63.6	139	-0.307	1.0000
			1.5x BP strain 38 v. 1.0x BP strain 38	55.2	73.4	139	0.751	1.0000
			1.5x BP strain 38 v. 0.5x H_2O strain 38	-74.0	63.6	139	-1.163	0.9995
			1.5x BP strain 38 v. 1.5x H_2O strain 38	-38.1	63.6	139	-0.600	1.0000
			1.5x BP strain 38 v. 1.0x H_2O strain 38	25.7	63.6	139	0.403	1.0000
			1.0x BP strain 38 v. 0.5x H_2O strain 38	-129.1	73.4	139	-1.758	0.9507
			1.0x BP strain 38 v. 1.5x H_2O strain 38	-93.3	73.4	139	-1.270	0.9984
			1.0x BP strain 38 v. 1.0x H_2O strain 38	-29.5	73.4	139	-0.402	1.0000
			0.5x H_2O strain 38 v. 1.5x H_2O strain 38	35.8	63.6	139	0.564	1.0000
			0.5x H_2O strain 38 v. 1.0x H_2O strain 38	99.6	63.6	139	1.566	0.9834
			1.5x H_2O strain 38 v. 1.0x H_2O strain 38	63.8	63.6	139	1.003	0.9999
2021	1	PDA	0.5x BP strain 14 v. 1.5x BP strain 14	-202.4	67.5	139	-3.000	0.2152
			0.5x BP strain 14 v. 1.0x BP strain 14	6.2	63.6	139	0.098	1.0000
			0.5x BP strain 14 v. 0.5x H_2O strain 14	-67.9	63.6	139	-1.067	0.9998
			0.5x BP strain 14 v. 1.5x H_2O strain 14	-35.7	63.6	139	-0.561	1.0000
			0.5x BP strain 14 v. 1.0x H_2O strain 14	3.3	63.6	139	0.052	1.0000
			0.5x BP strain 14 v. 0.5x BP strain 25	27.8	63.6	139	0.438	1.0000
			0.5x BP strain 14 v. 1.5x BP strain 25	11.3	63.6	139	0.178	1.0000
			0.5x BP strain 14 v. 1.0x BP strain 25	23.2	63.6	139	0.364	1.0000

Table C10. (cont'd)

0.5x BP strain 14 v. 0.5x H_2O strain 25	-60.4	63.6	139	-0.949	1.0000
0.5x BP strain 14 v. 1.5x H_2O strain 25	19.2	58.9	139	0.326	1.0000
0.5x BP strain 14 v. 1.0x H_2O strain 25	27.2	63.6	139	0.427	1.0000
0.5x BP strain 14 v. 0.5x BP strain 38	10.4	63.6	139	0.164	1.0000
0.5x BP strain 14 v. 1.5x BP strain 38	1.2	63.6	139	0.019	1.0000
0.5x BP strain 14 v. 1.0x BP strain 38	10.0	63.6	139	0.158	1.0000
0.5x BP strain 14 v. 0.5x H_2O strain 38	-58.3	63.6	139	-0.917	1.0000
0.5x BP strain 14 v. 1.5x H_2O strain 38	4.5	63.6	139	0.071	1.0000
0.5x BP strain 14 v. 1.0x H_2O strain 38	-48.0	63.6	139	-0.755	1.0000
1.5x BP strain 14 v. 1.0x BP strain 14	208.6	67.5	139	3.092	0.1739
1.5x BP strain 14 v. 0.5x H_2O strain 14	134.5	67.5	139	1.994	0.8672
1.5x BP strain 14 v. 1.5x H_2O strain 14	166.7	67.5	139	2.471	0.5565
1.5x BP strain 14 v. 1.0x H_2O strain 14	205.7	67.5	139	3.049	0.1925
1.5x BP strain 14 v. 0.5x BP strain 25	230.2	67.5	139	3.412	0.0758
1.5x BP strain 14 v. 1.5x BP strain 25	213.7	67.5	139	3.167	0.1450
1.5x BP strain 14 v. 1.0x BP strain 25	225.5	67.5	139	3.343	0.0918
1.5x BP strain 14 v. 0.5x H_2O strain 25	142.0	67.5	139	2.105	0.8088
1.5x BP strain 14 v. 1.5x H_2O strain 25	221.6	63.0	139	3.515	0.0563
1.5x BP strain 14 v. 1.0x H_2O strain 25	229.5	67.5	139	3.402	0.0780
1.5x BP strain 14 v. 0.5x BP strain 38	212.8	67.5	139	3.154	0.1496
1.5x BP strain 14 v. 1.5x BP strain 38	203.5	67.5	139	3.017	0.2068
1.5x BP strain 14 v. 1.0x BP strain 38	212.4	67.5	139	3.148	0.1519
1.5x BP strain 14 v. 0.5x H_2O strain 38	144.0	67.5	139	2.135	0.7908
1.5x BP strain 14 v. 1.5x H_2O strain 38	206.9	67.5	139	3.067	0.1846
1.5x BP strain 14 v. 1.0x H_2O strain 38	154.3	67.5	139	2.288	0.6903
1.0x BP strain 14 v. 0.5x H_2O strain 14	-74.1	63.6	139	-1.165	0.9994
1.0x BP strain 14 v. 1.5x H_2O strain 14	-41.9	63.6	139	-0.659	1.0000
1.0x BP strain 14 v. 1.0x H_2O strain 14	-2.9	63.6	139	-0.046	1.0000
1.0x BP strain 14 v. 0.5x BP strain 25	21.6	63.6	139	0.340	1.0000
1.0x BP strain 14 v. 1.5x BP strain 25	5.1	63.6	139	0.080	1.0000

Table C10. (cont'd)

1.0x BP strain 14 v. 1.0x BP strain 25	16.9	63.6	139	0.266	1.0000
1.0x BP strain 14 v. 0.5x H_2O strain 25	-66.6	63.6	139	-1.047	0.9999
1.0x BP strain 14 v. 1.5x H_2O strain 25	13.0	58.9	139	0.221	1.0000
1.0x BP strain 14 v. 1.0x H_2O strain 25	20.9	63.6	139	0.329	1.0000
1.0x BP strain 14 v. 0.5x BP strain 38	4.2	63.6	139	0.066	1.0000
1.0x BP strain 14 v. 1.5x BP strain 38	-5.0	63.6	139	-0.079	1.0000
1.0x BP strain 14 v. 1.0x BP strain 38	3.8	63.6	139	0.060	1.0000
1.0x BP strain 14 v. 0.5x H_2O strain 38	-64.5	63.6	139	-1.015	0.9999
1.0x BP strain 14 v. 1.5x H_2O strain 38	-1.7	63.6	139	-0.027	1.0000
1.0x BP strain 14 v. 1.0x H_2O strain 38	-54.2	63.6	139	-0.853	1.0000
0.5x H_2O strain 14 v. 1.5x H_2O strain 14	32.2	63.6	139	0.506	1.0000
0.5x H_2O strain 14 v. 1.0x H_2O strain 14	71.2	63.6	139	1.119	0.9997
0.5x H_2O strain 14 v. 0.5x BP strain 25	95.7	63.6	139	1.505	0.9890
0.5x H_2O strain 14 v. 1.5x BP strain 25	79.2	63.6	139	1.245	0.9987
0.5x H_2O strain 14 v. 1.0x BP strain 25	91.0	63.6	139	1.431	0.9936
0.5x H_2O strain 14 v. 0.5x H_2O strain 25	7.5	63.6	139	0.118	1.0000
0.5x H_2O strain 14 v. 1.5x H_2O strain 25	87.1	58.9	139	1.479	0.9908
0.5x H_2O strain 14 v. 1.0x H_2O strain 25	95.0	63.6	139	1.494	0.9898
0.5x H_2O strain 14 v. 0.5x BP strain 38	78.3	63.6	139	1.231	0.9989
0.5x H_2O strain 14 v. 1.5x BP strain 38	69.1	63.6	139	1.086	0.9998
0.5x H_2O strain 14 v. 1.0x BP strain 38	77.9	63.6	139	1.225	0.9990
0.5x H_2O strain 14 v. 0.5x H_2O strain 38	9.6	63.6	139	0.150	1.0000
0.5x H_2O strain 14 v. 1.5x H_2O strain 38	72.4	63.6	139	1.138	0.9996
0.5x H_2O strain 14 v. 1.0x H_2O strain 38	19.9	63.6	139	0.312	1.0000
1.5x H_2O strain 14 v. 1.0x H_2O strain 14	39.0	63.6	139	0.613	1.0000
1.5x H_2O strain 14 v. 0.5x BP strain 25	63.5	63.6	139	0.999	0.9999
1.5x H_2O strain 14 v. 1.5x BP strain 25	47.0	63.6	139	0.739	1.0000
1.5x H_2O strain 14 v. 1.0x BP strain 25	58.8	63.6	139	0.925	1.0000
1.5x H_2O strain 14 v. 0.5x H_2O strain 25	-24.7	63.6	139	-0.388	1.0000
1.5x H_2O strain 14 v. 1.5x H_2O strain 25	54.9	58.9	139	0.933	1.0000

Table C10. (cont'd)

1.5x H_2O strain 14 v. 1.0x H_2O strain 25	62.8	63.6	139	0.988	0.9999
1.5x H_2O strain 14 v. 0.5x BP strain 38	46.1	63.6	139	0.725	1.0000
1.5x H_2O strain 14 v. 1.5x BP strain 38	36.9	63.6	139	0.580	1.0000
1.5x H_2O strain 14 v. 1.0x BP strain 38	45.7	63.6	139	0.719	1.0000
1.5x H_2O strain 14 v. 0.5x H_2O strain 38	-22.6	63.6	139	-0.356	1.0000
1.5x H_2O strain 14 v. 1.5x H_2O strain 38	40.2	63.6	139	0.632	1.0000
1.5x H_2O strain 14 v. 1.0x H_2O strain 38	-12.3	63.6	139	-0.194	1.0000
1.0x H_2O strain 14 v. 0.5x BP strain 25	24.5	63.6	139	0.386	1.0000
1.0x H_2O strain 14 v. 1.5x BP strain 25	8.0	63.6	139	0.126	1.0000
1.0x H_2O strain 14 v. 1.0x BP strain 25	19.8	63.6	139	0.312	1.0000
1.0x H_2O strain 14 v. 0.5x H_2O strain 25	-63.7	63.6	139	-1.001	0.9999
1.0x H_2O strain 14 v. 1.5x H_2O strain 25	15.9	58.9	139	0.270	1.0000
1.0x H_2O strain 14 v. 1.0x H_2O strain 25	23.8	63.6	139	0.375	1.0000
1.0x H_2O strain 14 v. 0.5x BP strain 38	7.1	63.6	139	0.112	1.0000
1.0x H_2O strain 14 v. 1.5x BP strain 38	-2.1	63.6	139	-0.033	1.0000
1.0x H_2O strain 14 v. 1.0x BP strain 38	6.7	63.6	139	0.106	1.0000
1.0x H_2O strain 14 v. 0.5x H_2O strain 38	-61.6	63.6	139	-0.969	1.0000
1.0x H_2O strain 14 v. 1.5x H_2O strain 38	1.2	63.6	139	0.019	1.0000
1.0x H_2O strain 14 v. 1.0x H_2O strain 38	-51.3	63.6	139	-0.807	1.0000
0.5x BP strain 25 v. 1.5x BP strain 25	-16.5	63.6	139	-0.260	1.0000
0.5x BP strain 25 v. 1.0x BP strain 25	-4.7	63.6	139	-0.074	1.0000
0.5x BP strain 25 v. 0.5x H_2O strain 25	-88.2	63.6	139	-1.387	0.9955
0.5x BP strain 25 v. 1.5x H_2O strain 25	-8.6	58.9	139	-0.146	1.0000
0.5x BP strain 25 v. 1.0x H_2O strain 25	-0.7	63.6	139	-0.011	1.0000
0.5x BP strain 25 v. 0.5x BP strain 38	-17.4	63.6	139	-0.273	1.0000
0.5x BP strain 25 v. 1.5x BP strain 38	-26.6	63.6	139	-0.419	1.0000
0.5x BP strain 25 v. 1.0x BP strain 38	-17.8	63.6	139	-0.280	1.0000
0.5x BP strain 25 v. 0.5x H_2O strain 38	-86.1	63.6	139	-1.354	0.9965
0.5x BP strain 25 v. 1.5x H_2O strain 38	-23.3	63.6	139	-0.366	1.0000
0.5x BP strain 25 v. 1.0x H_2O strain 38	-75.8	63.6	139	-1.192	0.9993

Table C10. (cont'd)

1.5x BP strain 25 v. 1.0x BP strain 25	11.9	63.6	139	0.186	1.0000
1.5x BP strain 25 v. 0.5x H_2O strain 25	-71.7	63.6	139	-1.127	0.9996
1.5x BP strain 25 v. 1.5x H_2O strain 25	7.9	58.9	139	0.135	1.0000
1.5x BP strain 25 v. 1.0x H_2O strain 25	15.9	63.6	139	0.249	1.0000
1.5x BP strain 25 v. 0.5x BP strain 38	-0.9	63.6	139	-0.013	1.0000
1.5x BP strain 25 v. 1.5x BP strain 38	-10.1	63.6	139	-0.159	1.0000
1.5x BP strain 25 v. 1.0x BP strain 38	-1.3	63.6	139	-0.020	1.0000
1.5x BP strain 25 v. 0.5x H_2O strain 38	-69.6	63.6	139	-1.094	0.9998
1.5x BP strain 25 v. 1.5x H_2O strain 38	-6.8	63.6	139	-0.106	1.0000
1.5x BP strain 25 v. 1.0x H_2O strain 38	-59.3	63.6	139	-0.932	1.0000
1.0x BP strain 25 v. 0.5x H_2O strain 25	-83.5	63.6	139	-1.313	0.9976
1.0x BP strain 25 v. 1.5x H_2O strain 25	-3.9	58.9	139	-0.067	1.0000
1.0x BP strain 25 v. 1.0x H_2O strain 25	4.0	63.6	139	0.063	1.0000
1.0x BP strain 25 v. 0.5x BP strain 38	-12.7	63.6	139	-0.200	1.0000
1.0x BP strain 25 v. 1.5x BP strain 38	-22.0	63.6	139	-0.345	1.0000
1.0x BP strain 25 v. 1.0x BP strain 38	-13.1	63.6	139	-0.206	1.0000
1.0x BP strain 25 v. 0.5x H_2O strain 38	-81.5	63.6	139	-1.281	0.9982
1.0x BP strain 25 v. 1.5x H_2O strain 38	-18.6	63.6	139	-0.293	1.0000
1.0x BP strain 25 v. 1.0x H_2O strain 38	-71.2	63.6	139	-1.119	0.9997
0.5x H_2O strain 25 v. 1.5x H_2O strain 25	79.6	58.9	139	1.352	0.9966
0.5x H_2O strain 25 v. 1.0x H_2O strain 25	87.5	63.6	139	1.376	0.9958
0.5x H_2O strain 25 v. 0.5x BP strain 38	70.8	63.6	139	1.113	0.9997
0.5x H_2O strain 25 v. 1.5x BP strain 38	61.6	63.6	139	0.968	1.0000
0.5x H_2O strain 25 v. 1.0x BP strain 38	70.4	63.6	139	1.107	0.9997
0.5x H_2O strain 25 v. 0.5x H_2O strain 38	2.1	63.6	139	0.032	1.0000
0.5x H_2O strain 25 v. 1.5x H_2O strain 38	64.9	63.6	139	1.021	0.9999
0.5x H_2O strain 25 v. 1.0x H_2O strain 38	12.4	63.6	139	0.194	1.0000
1.5x H_2O strain 25 v. 1.0x H_2O strain 25	7.9	58.9	139	0.135	1.0000
1.5x H_2O strain 25 v. 0.5x BP strain 38	-8.8	58.9	139	-0.149	1.0000
1.5x H_2O strain 25 v. 1.5x BP strain 38	-18.0	58.9	139	-0.306	1.0000

Table C10. (cont'd)

1.5x H_2O strain 25 v. 1.0x BP strain 38	-9.2	58.9	139	-0.156	1.0000
1.5x H_2O strain 25 v. 0.5x H_2O strain 38	-77.5	58.9	139	-1.317	0.9975
1.5x H_2O strain 25 v. 1.5x H_2O strain 38	-14.7	58.9	139	-0.249	1.0000
1.5x H_2O strain 25 v. 1.0x H_2O strain 38	-67.2	58.9	139	-1.142	0.9996
1.0x H_2O strain 25 v. 0.5x BP strain 38	-16.7	63.6	139	-0.263	1.0000
1.0x H_2O strain 25 v. 1.5x BP strain 38	-26.0	63.6	139	-0.408	1.0000
1.0x H_2O strain 25 v. 1.0x BP strain 38	-17.1	63.6	139	-0.269	1.0000
1.0x H_2O strain 25 v. 0.5x H_2O strain 38	-85.5	63.6	139	-1.344	0.9968
1.0x H_2O strain 25 v. 1.5x H_2O strain 38	-22.6	63.6	139	-0.356	1.0000
1.0x H_2O strain 25 v. 1.0x H_2O strain 38	-75.2	63.6	139	-1.182	0.9993
0.5x BP strain 38 v. 1.5x BP strain 38	-9.2	63.6	139	-0.145	1.0000
0.5x BP strain 38 v. 1.0x BP strain 38	-0.4	63.6	139	-0.006	1.0000
0.5x BP strain 38 v. 0.5x H_2O strain 38	-68.8	63.6	139	-1.081	0.9998
0.5x BP strain 38 v. 1.5x H_2O strain 38	-5.9	63.6	139	-0.093	1.0000
0.5x BP strain 38 v. 1.0x H_2O strain 38	-58.4	63.6	139	-0.919	1.0000
1.5x BP strain 38 v. 1.0x BP strain 38	8.8	63.6	139	0.139	1.0000
1.5x BP strain 38 v. 0.5x H_2O strain 38	-59.5	63.6	139	-0.936	1.0000
1.5x BP strain 38 v. 1.5x H_2O strain 38	3.3	63.6	139	0.053	1.0000
1.5x BP strain 38 v. 1.0x H_2O strain 38	-49.2	63.6	139	-0.774	1.0000
1.0x BP strain 38 v. 0.5x H_2O strain 38	-68.3	63.6	139	-1.075	0.9998
1.0x BP strain 38 v. 1.5x H_2O strain 38	-5.5	63.6	139	-0.086	1.0000
1.0x BP strain 38 v. 1.0x H_2O strain 38	-58.0	63.6	139	-0.913	1.0000
0.5x H_2O strain 38 v. 1.5x H_2O strain 38	62.8	63.6	139	0.988	0.9999
0.5x H_2O strain 38 v. 1.0x H_2O strain 38	10.3	63.6	139	0.162	1.0000
1.5x H_2O strain 38 v. 1.0x H_2O strain 38	-52.5	63.6	139	-0.826	1.0000

Table C11. Group 2 2021, by media, rate, and treatment (trt, i.e., biological control agent, BCA), mean total area of growth (mm^2) of *Pss* strains 23 and 34, belonging to phylogroup (PG) 2b ± SE in co-inoculations of Blossom Protect™ (BP) or water (H_2O) at three rates (0.5x, 1.0x, 1.5x) grown on KB or PDA media, with confidence limits (lower and upper C.L.) and the p-value for the pairwise comparisons of the estimated marginal means for each media, rate, and treatment, with letters indicating statistical differences with significance determined by p-value ≤0.05.

Year	Group	Strain/PG	Media	*Pss* Mean total area (mm2)	SE	df	lower C.L.	upper C.L.	
2021	2	23 2b	KB	208.0	9.3	93	189.0	226.0	a
		34 2b	PDA	128.0	9.4	93	109.0	146.0	b
Year	**Group**	**Strain/PG**	**contrast**	**estimate**	**SE**	**df**	**t-ratio**	**p-value**	
2021	2	23 2b 34 2b	KB v. PDA	80.1	13.3	93	6.036	<0.0001	

Year	Group	Strain/PG	Rate	*Pss* Mean total area (mm2)	SE	df	lower C.L.	upper C.L.	
2021	2	23 2b	0.5x	177.0	11.6	93	154.0	200.0	ab
		34 2b	1.5x	141.0	11.4	93	119.0	164.0	a
			1.0x	184.0	11.5	93	162.0	207.0	b
Year	**Group**	**Strain/PG**	**contrast**	**estimate**	**SE**	**df**	**t-ratio**	**p-value**	
2021	2	23 2b	0.5x v. 1.5x	35.9	16.3	93	2.210	0.0748	
		34 2b	0.5x v. 1x	-7.0	16.3	93	-0.430	0.9034	
			1.5x v. 1x	-43.0	16.1	93	-2.662	0.0246	

Year	Group	Strain/PG	Treatment (BCA)	Pss Mean total area (mm2)	SE	df	lower C.L.	upper C.L.	
2021	2	23 2b	BP	150.4	9.4	93	131.7	169.1	a
		34 2b	H_2O	184.8	9.4	93	166.3	203.4	b
Year	**Group**	**Strain/PG**	**contrast**	**estimate**	**SE**	**df**	**t-ratio**	**p-value**	
2021	2	23 2b 34 2b	BP v. H_2O	-34.4	13.3	93	-2.594	0.0110	

Table C12. Group 2 2021 mean total area of growth (mm^2) of *Pss* strains 23 and 34, belonging to phylogroup (PG) 2b ± SE in co-inoculations of biological control agent Blossom Protect™ (BP) or water (H_2O) at three rates (0.5x, 1.0x, 1.5x) grown on KB or PDA media, with confidence limits (lower and upper C.L.) and the p-value for the pairwise comparisons of the estimated marginal means for each media*rate, with letters indicating statistical differences with significance determined by p-value ≤0.05.

Year	Group	Strain/PG	Media	Rate	*Pss* Mean total area (mm2)	SE	df	lower C.L.	upper C.L.	
2021	2	23 2b	KB	0.5x	243.2	16.5	93	210.5	275.9	a
		34 2b	PDA	0.5x	111.3	16.5	93	78.6	144.0	b
			KB	1.5x	168.3	16.0	93	136.6	200.1	bc
			PDA	1.5x	114.3	16.1	93	82.3	146.4	b
			KB	1.0x	211.5	16.0	93	179.8	243.2	ac
			PDA	1.0x	157.1	16.5	93	124.4	189.8	bc

Year	Group	Strain/PG	contrast	estimate	SE	df	t-ratio	p-value
2021	2	23 2b	KB 0.5x v. PDA 0.5x	131.9	23.3	93	5.662	<0.0001
		34 2b	KB 0.5x v. KB 1.5x	74.9	22.9	93	3.263	0.0187
			KB 0.5x v. PDA 1.5x	128.9	23.1	93	5.589	<0.0001
			KB 0.5x v. KB 1.0x	31.7	22.9	93	1.382	0.7378
			KB 0.5x v. PDA 1.0x	86.1	23.3	93	3.698	0.0048
			PDA 0.5x v. KB 1.5x	-57.0	22.9	93	-2.484	0.1395
			PDA 0.5x v. PDA 1.5x	-3.0	23.1	93	-0.129	1.0000
			PDA 0.5x v. KB 1.0x	-100.2	22.9	93	-4.365	0.0005
			PDA 0.5x v. PDA 1.0x	-45.7	23.3	93	-1.964	0.3706
			KB 1.5x v. PDA 1.5x	54.0	22.7	93	2.378	0.1747
			KB 1.5x v. KB 1.0x	-43.2	22.6	93	-1.910	0.4025
			KB 1.5x v. PDA 1.0x	11.3	22.9	93	0.490	0.9964
			PDA 1.5x v. KB 1.0x	-97.2	22.7	93	-4.279	0.0006
			PDA 1.5x v. PDA 1.0x	-42.8	23.1	93	-1.854	0.4367
			KB 1.0x v. PDA 1.0x	54.4	22.9	93	2.372	0.1771

Table C13. Group 2 2021 mean total area of growth (mm^2) of *Pss* strains 23 and 34, belonging to phylogroup (PG) 2b ± SE in co-inoculations of biological control agent Blossom Protect™ (BP) or water (H_2O)) at three rates (0.5x, 1.0x, 1.5x) grown on KB or PDA media, with confidence limits (lower and upper C.L.) and the p-value for the pairwise comparisons of the estimated marginal means for each media*strain and with letters indicating statistical differences with significance determined by p-value ≤0.05.

Year	Group	Strain/PG	Media	Strain	*Pss* Mean total area (mm2)	SE	df	lower C.L.	upper C.L.	
2021	2	23 2b	KB	23	177.0	13.3	93	150.6	203.5	a
		34 2b	PDA	23	136.9	13.6	93	109.9	163.9	ab
			KB	34	238.3	13.0	93	212.4	264.2	c
			PDA	34	118.3	13.1	93	92.2	144.3	b

Year	Group	Strain/PG	contrast	estimate	SE	df	t-ratio	p-value
2021	2	23 2b	KB strain 23 v. PDA strain 23	40.1	19.0	93	2.111	0.1571
		34 2b	KB strain 23 v. KB strain 34	-61.3	18.6	93	-3.286	0.0077
			KB strain 23 v. PDA strain 34	58.8	18.7	93	3.144	0.0118
			PDA strain 23 v. KB strain 34	-101.4	18.8	93	-5.386	<0.0001
			PDA strain 23 v. PDA strain 34	18.6	18.9	93	0.987	0.7572
			KB strain 34 v. PDA strain 34	120.0	18.5	93	6.485	<0.0001

Table C14. Group 2 2021 mean total area of growth (mm^2) of *Pss* strains 23 and 34, belonging to phylogroup (PG) 2b ± SE in co-inoculations of biological control agent Blossom Protect™ (BP) or water (H_2O) at three rates (0.5x, 1.0x, 1.5x) grown on KB or PDA media,, with confidence limits (lower and upper C.L.) and the p-value for the pairwise comparisons of the estimated marginal means for each treatment*strain and with letters indicating statistical differences with significance determined by p-value ≤0.05.

Year	Group	Strain/PG	Treatment (BCA)	Strain	*Pss* Mean total area (mm2)	SE	df	lower C.L.	upper C.L.	
2021	2	23 2b	BP	23	153.9	13.6	93	127.0	180.9	a
		34 2b	H_2O	23	160.0	13.3	93	133.6	186.4	a
			BP	34	146.9	13.0	93	121.0	172.8	a
			H_2O	34	209.6	13.1	93	183.6	235.7	b

Year	Group	Strain/PG	contrast	estimate	SE	df	t-ratio	p-value
2021	2	23 2b	BP strain 23 - H_2O strain 23	-6.1	19.0	93	-0.320	0.9886
		34 2b	BP strain 23 - BP strain 34	7.0	18.8	93	0.373	0.9822
			BP strain 23 - H_2O strain 34	-55.7	18.9	93	-2.950	0.0206
			H_2O strain 23 - BP strain 34	13.1	18.6	93	0.704	0.8955
			H_2O strain 23 - H_2O strain 34	-49.6	18.7	93	-2.654	0.0454
			BP strain 34 - H_2O strain 34	-62.8	18.5	93	-3.390	0.0056

Table C15. Group 2 2021 mean total area of growth (mm^2) of *Pss* strains 23 and 34, belonging to phylogroup (PG) 2b ± SE in co-inoculations of biological control agent Blossom Protect™ (BP) or water (H_2O) at three rates (0.5x, 1.0x, 1.5x) grown on KB or PDA media,, with confidence limits (lower and upper C.L.) and the p-value for the pairwise comparisons of the estimated marginal means for each media*treatment*strain with letters indicating statistical differences with significance determined by p-value ≤0.05.

Year	Group	Media	Treatment (BCA)	Strain	*Pss* Mean total area (mm2)	SE	df	lower C.L.	upper C.L.	
2021	2	KB	BP	23	181.7	18.4	93	145.1	218.3	a
		PDA	BP	23	126.2	19.9	93	86.6	165.7	a
		KB	H_2O	23	172.4	19.2	93	134.3	210.5	a
		PDA	H_2O	23	147.6	18.4	93	111.0	184.3	a
		KB	BP	34	173.7	18.4	93	137.1	210.3	a
		PDA	BP	34	120.1	18.4	93	83.5	156.7	a
		KB	H_2O	34	302.9	18.4	93	266.3	339.5	b
		PDA	H_2O	34	116.4	18.7	93	79.3	153.5	a

Year	Group	contrast	estimate	SE	df	t-ratio	p-value
2021	2	KB BP strain 23 v. PDA BP strain 23	55.6	27.2	93	2.046	0.4574
		KB BP strain 23 v. KB H_2O strain 23	9.3	26.6	93	0.350	1.0000
		KB BP strain 23 v. PDA H_2O strain 23	34.1	26.1	93	1.306	0.8945
		KB BP strain 23 v. KB BP strain34	8.0	26.1	93	0.307	1.0000
		KB BP strain 23 v. PDA BP strain34	61.6	26.1	93	2.361	0.2730
		KB BP strain 23 v. KB H_2O strain34	-121.2	26.1	93	-4.646	0.0003
		KB BP strain 23 v. PDA H_2O strain34	65.3	26.3	93	2.486	0.2144
		PDA BP strain 23 v. KB H_2O strain 23	-46.2	27.7	93	-1.671	0.7058
		PDA BP strain 23 v. PDA H_2O strain 23	-21.5	27.2	93	-0.792	0.9932
		PDA BP strain 23 v. KB BP strain34	-47.5	27.2	93	-1.751	0.6543
		PDA BP strain 23 v. PDA BP strain34	6.0	27.2	93	0.222	1.0000
		PDA BP strain 23 v. KB H_2O strain34	-176.8	27.2	93	-6.509	<0.0001

Table C15.(cont'd)

PDA BP strain 23 v. PDA H_2O strain34	9.8	27.3	93	0.357	1.0000
KB H_2O strain 23 v. PDA H_2O strain 23	24.7	26.6	93	0.929	0.9824
KB H_2O strain 23 v. KB BP strain34	-1.3	26.6	93	-0.049	1.0000
KB H_2O strain 23 v. PDA BP strain34	52.3	26.6	93	1.963	0.5120
KB H_2O strain 23 v. KB H_2O strain34	-130.5	26.6	93	-4.902	0.0001
KB H_2O strain 23 v. PDA H_2O strain34	56.0	26.8	93	2.089	0.4298
PDA H_2O strain 23 v. KB BP strain34	-26.1	26.1	93	-0.998	0.9736
PDA H_2O strain 23 v. PDA BP strain34	27.5	26.1	93	1.055	0.9642
PDA H_2O strain 23 v. KB H_2O strain34	-155.3	26.1	93	-5.951	<0.0001
PDA H_2O strain 23 v. PDA H_2O strain34	31.3	26.3	93	1.189	0.9330
KB BP strain34 v. PDA BP strain34	53.6	26.1	93	2.054	0.4523
KB BP strain34 v. KB H_2O strain34	-129.2	26.1	93	-4.953	0.0001
KB BP strain34 v. PDA H_2O strain34	57.3	26.3	93	2.181	0.3727
PDA BP strain34 v. KB H_2O strain34	-182.8	26.1	93	-7.007	<0.0001
PDA BP strain34 v. PDA H_2O strain34	3.7	26.3	93	0.141	1.0000
KB H_2O strain34 v. PDA H_2O strain34	186.5	26.3	93	7.100	<0.0001

Table C16. Group 3 2021, by rate and by strain, mean total area of growth (mm^2) of *Pss* strains 22, 26, and 37, belonging to phylogroup (PG) 2b and 2d, ± SE, in co-inoculations of biological control agent Blossom Protect™ (BP) or water (H_2O) at three rates (0.5x, 1.0x, 1.5x), with confidence limits (lower and upper C.L.) and the p-value for the pairwise comparisons of the estimated marginal means for each rate and strain, with letters indicating statistical differences with significance determined by p-value ≤0.05.

Year	Group	Strain/PG	Rate	*Pss* Mean total area (mm2)	SE	df	lower C.L.	upper C.L.	
2021	3	22 2b	0.5x	135.2	9.9	126	115.7	154.8	a
		26 2d	1.5x	174.8	8.7	126	157.6	192.0	b
		37 2d	1.0x	132.1	9.3	126	113.7	150.5	a

Year	Group	Strain/PG	contrast	estimate	SE	df	t-ratio	p-value
2021	3	22 2b	0.5x v. 1.5x	-39.6	13.2	126	-3.007	0.0089
		26 2d	0.5x v. 1.0x	3.2	13.6	126	0.233	0.9705
		37 2d	1.5x v. 1.0x	42.7	12.7	126	3.354	0.0030

Year	Group	Strain	PG	Mean total area (mm2)	SE	df	lower C.L.	upper C.L.	
2021	3	22	2b	116.8	9.9	126	97.3	136.4	a
		26	2d	151.1	9.0	126	133.4	168.9	b
		37	2d	174.1	9.1	126	156.2	192.0	b

Year	Group	contrast	estimate	SE	df	t-ratio	p-value
2021	3	strain 22 v. strain 26	-34.3	13.3	126	-2.574	0.0300
		strain 22 v. strain 37	-57.3	13.4	126	-4.276	0.0001
		strain 26 v. strain 37	-22.9	12.7	126	-1.801	0.1733

Table C17. Group 4 2021, mean total area of growth (mm^2) of *Pss* strains 9 and 27, belonging to phylogroup (PG) 2d, ± SE, in co-inoculations of biological control agent Blossom Protect™ (BP) or water (H_2O) at three rates (0.5x, 1.0x, 1.5x), with confidence limits (lower and upper C.L.) and the p-value for the pairwise comparisons of the estimated marginal means for each media*rate, with letters indicating statistical differences with significance determined by p-value ≤0.05.

Year	Group	Strain/PG	media	Rate	*Pss* Mean total area (mm2)	SE	df	lower C.L.	upper C.L.	
2021	4	9 2d	KB	0.5x	156.7	17.4	94	122.3	191.2	a
		27 2d	PDA	0.5x	233.4	16.5	94	200.7	266.2	b
			KB	1.5x	248.5	17.4	94	214.0	283.0	b
			PDA	1.5x	191.9	16.9	94	158.4	225.4	ab
			KB	1.0x	247.0	17.4	94	212.6	281.5	b
			PDA	1.0x	198.7	16.9	94	165.3	232.2	ab

Year	Group	Strain/PG	contrast	estimate	SE	df	t-ratio	p-value
2021	4	9 2d	KB 0.5x - PDA 0.5x	-76.7	24.0	94	-3.202	0.0223
		27 2d	KB 0.5x - KB 1.5x	-91.7	24.6	94	-3.735	0.0042
			KB 0.5x - PDA 1.5x	-35.2	24.2	94	-1.453	0.6946
			KB 0.5x - KB 1x	-90.3	24.6	94	-3.676	0.0051
			KB 0.5x - PDA 1x	-42.0	24.2	94	-1.735	0.5125
			PDA 0.5x - KB 1.5x	-15.0	24.0	94	-0.628	0.9887
			PDA 0.5x - PDA 1.5x	41.5	23.6	94	1.762	0.4953
			PDA 0.5x - KB 1x	-13.6	24.0	94	-0.568	0.9929
			PDA 0.5x - PDA 1x	34.7	23.6	94	1.472	0.6826
			KB 1.5x - PDA 1.5x	56.6	24.2	94	2.338	0.1896
			KB 1.5x - KB 1x	1.4	24.6	94	0.059	1.0000
			KB 1.5X - PDA 1X	49.8	24.2	94	2.056	0.3195
			PDA 1.5x - KB 1x	-55.1	24.2	94	-2.278	0.2133
			PDA 1.5x - PDA 1x	-6.8	23.8	94	-0.286	0.9997
			KB 1X - PDA 1X	48.3	24.2	94	1.996	0.3522

Table C18. Group 4 2021, mean total area of growth (mm^2) of *Pss* strains 9 and 27, belonging to phylogroup (PG) 2d, ± SE, in co-inoculations of biological control agent Blossom Protect™ (BP) or water (H_2O) at three rates (0.5x, 1.0x, 1.5x), with confidence limits (lower and upper C.L.) and the p-value for the pairwise comparisons of the estimated marginal means for each rate*strain, with letters indicating statistical differences with significance determined by p-value ≤0.05.

Year	Group	Rate	strain	*Pss* Mean total area (mm2)	SE	df	lower C.L.	upper C.L.	
2021	4	0.5x	27	175.1	17.4	94	140.6	209.5	a
		1.5x	27	231.7	16.9	94	198.3	265.2	ab
		1.0x	27	266.0	16.9	94	232.5	299.5	b
		0.5x	9	215.1	16.5	94	182.4	247.9	ab
		1.5x	9	208.7	17.4	94	174.2	243.2	ab
		1.0x	9	179.8	17.4	94	145.3	214.3	a
Year	**Group**		**contrast**	**estimate**	**SE**	**df**	**t-ratio**	**p-value**	
2021	4	0.5x strain 27 v. 1.5x strain 27		-56.7	24.2	94	-2.341	0.1884	
		0.5x strain 27 v. 1x strain 27		-90.9	24.2	94	-3.758	0.0039	
		0.5x strain 27 v. 0.5x strain 9		-40.1	24.0	94	-1.672	0.5534	
		0.5x strain 27 v. 1.5x strain 9		-33.6	24.6	94	-1.368	0.7459	
		0.5x strain 27 v. 1x strain 9		-4.7	24.6	94	-0.192	1.0000	
		1.5x strain 27 v. 1x strain 27		-34.3	23.8	94	-1.439	0.7035	
		1.5x strain 27 v. 0.5x strain 9		16.6	23.6	94	0.704	0.9811	
		1.5x strain 27 v. 1.5x strain 9		23.1	24.2	94	0.952	0.9315	
		1.5x strain 27 v. 1x strain 9		51.9	24.2	94	2.146	0.2730	
		1x strain 27 v. 0.5x strain 9		50.9	23.6	94	2.158	0.2676	
		1x strain 27 v. 1.5x strain 9		57.3	24.2	94	2.369	0.1779	
		1x strain 27 v. 1x strain 9		86.2	24.2	94	3.563	0.0074	
		0.5x strain 9 v. 1.5x strain 9		6.5	24.0	94	0.269	0.9998	
		0.5x strain 9 v. 1x strain 9		35.4	24.0	94	1.476	0.6804	
		1.5x strain 9 v. 1x strain 9		28.9	24.6	94	1.176	0.8470	

Table C19. Group 4 2021, mean total area of growth (mm^2) of *Pss* strains 9 and 27, belonging to phylogroup (PG) 2d, ± SE, in co-inoculations of biological control agent Blossom Protect™ (BP) or water (H_2O) at three rates (0.5x, 1.0x, 1.5x), with confidence limits (lower and upper C.L.) and the p-value for the pairwise comparisons of the estimated marginal means for each media*treatment nested within rate, with letters indicating statistical differences with significance determined by p-value ≤0.05.

Year	Group	Strain/PG	Rate	media	treatment	*Pss* Mean total area (mm2)	SE	df	lower C.L.	upper C.L.	
2021	4	9 2d	0.5x	KB	BP	153.4	23.8	94	106.1	200.8	a
		27 2d		PDA	BP	239.8	23.8	94	192.5	287.1	a
				KB	H_2O	160.0	25.3	94	109.9	210.2	a
				PDA	H_2O	227.1	22.8	94	181.8	272.4	a
			1.5x	KB	BP	253.5	23.8	94	206.2	300.8	a
				PDA	BP	214.7	23.8	94	167.4	262.1	a
				KB	H_2O	243.5	25.3	94	193.3	293.6	a
				PDA	H_2O	169.1	23.8	94	121.7	216.4	a
			1.0x	KB	BP	227.1	25.3	94	176.9	277.2	ab
				PDA	BP	237.7	23.8	94	190.4	285.0	ab
				KB	H_2O	267.0	23.8	94	219.7	314.3	a
				PDA	H_2O	159.8	23.8	94	112.4	207.1	b

Year	Group	Strain/PG	Rate	contrast	estimate	SE	df	t-ratio	p-value
2021	4	9 2d	0.5x	KB BP v. PDA BP	-86.4	33.7	94	-2.563	0.0570
		27 2d		KB BP v. KB H_2O	-6.6	34.7	94	-0.190	0.9976
				KB BP v. PDA H_2O	-73.6	33.0	94	-2.232	0.1222
				PDA BP v. KB H_2O	79.8	34.7	94	2.296	0.1062
				PDA BP v. PDA H_2O	12.7	33.0	94	0.386	0.9803
				KB H_2O v. PDA H_2O	-67.0	34.1	94	-1.969	0.2072
			1.5x	KB BP v. PDA BP	38.8	33.7	94	1.150	0.6597

Table C19.(cont'd)

	KB BP v. KB H_2O	10.0	34.7	94	0.289	0.9916
	KB BP v. PDA H_2O	84.4	33.7	94	2.505	0.0656
	PDA BP v. KB H_2O	-28.7	34.7	94	-0.827	0.8416
	PDA BP v. PDA H_2O	45.7	33.7	94	1.355	0.5303
	KB H_2O v. PDA H_2O	74.4	34.7	94	2.142	0.1476
1.0x	KB BP v. PDA BP	-10.6	34.7	94	-0.306	0.9900
	KB BP v. KB H_2O	-40.0	34.7	94	-1.151	0.6593
	KB BP v. PDA H_2O	67.3	34.7	94	1.937	0.2196
	PDA BP v. KB H_2O	-29.3	33.7	94	-0.870	0.8202
	PDA BP v. PDA H_2O	77.9	33.7	94	2.313	0.1024
	KB H_2O v. PDA H_2O	107.3	33.7	94	3.183	0.0105

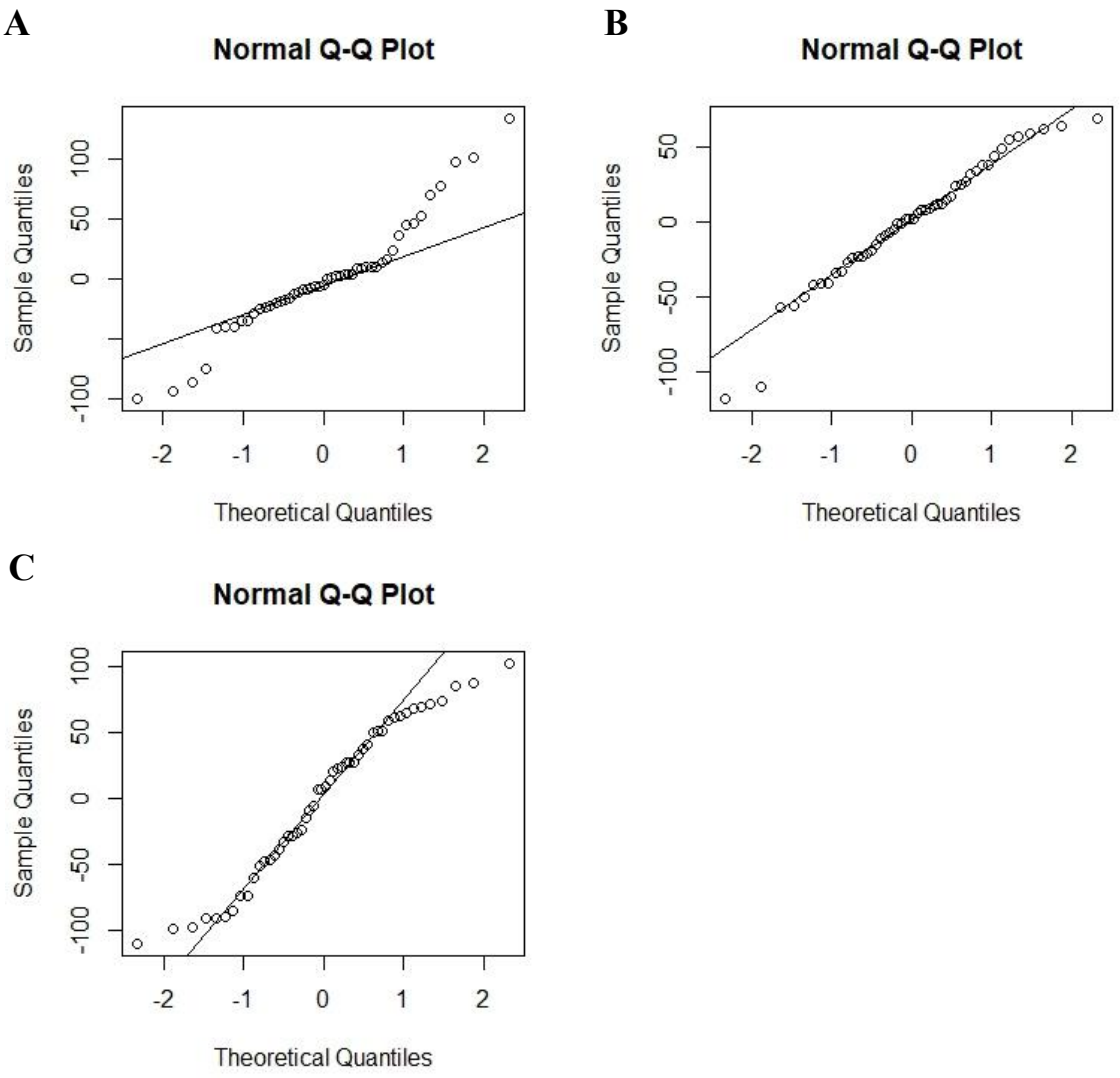


Figure C4. The 2022 quantile-quantile plots (qqplot) of the residuals for graphical visualization of the distribution of the total area of growth (mm^2) of *Pss* strains 9, 25 (PG 2d virulent) and 23,33 (PG2b moderate virulence) grown next to the strains 14, 18 (PG 2c avirulent), and 23,33 (PG2b moderate virulence) or water (H_2O) in Petri plates with KB media, group corresponds to the rate combination at which the PG2d and PG2b strains were inoculated next to the PG2c and PG2b strains or H_2O, where **A)** group 1 all strains were inoculated at 10^8 cfu/ml, **B)** group 2 strains were inoculated at 10^6 v. 10^8 cfu/ml, and **C)** group 3 strains were inoculated at 10^4 v. 10^8 cfu/ml.

Table C20. The 2022 co-inoculations of *Pss* strains 9, 25 (PG 2d virulent) and 23,33 (PG2b moderate virulence) grown next to the strains 14, 18 (PG 2c avirulent), and 23,33 (PG2b moderate virulence) or water (H_2O) in Petri plates with KB media, group corresponds to the rate combination at which the PG2d and PG2b strains were inoculated next to the PG2c and PG2b strains or H_2O, for group 1 all strains were inoculated at 10^8 cfu/ml. With confidence limits (lower and upper C.L.) and the p-value for the pairwise comparisons of the estimated marginal means for each strain, with letters indicating statistical differences with significance determined by p-value ≤0.05.

Year	Group	Strain/PG	*Pss* Mean total area (mm2)	SE	df	lower C.L.	upper C.L.	
2022	1	23 2b	157.4	19.4	41	118.2	196.6	a
		25 2d	278.2	17.5	41	242.9	313.5	bc
		33 2b	266.6	19.6	41	227.0	306.1	b
		9 2d	354.5	16.8	41	320.5	388.5	c

Year	Group	contrast	estimate	SE	df	t-ratio	p-value
2022	1	23 v. 25	-120.8	23.0	41	-5.240	<0.0001
		23 v. 33	-109.2	27.6	41	-3.961	0.0016
		23 v. 9	-197.1	27.6	41	-7.152	<0.0001
		25 v. 33	11.6	28.6	41	0.405	0.9772
		25 v. 9	-76.4	28.6	41	-2.668	0.0511
		33 v. 9	-88.0	22.4	41	-3.927	0.0018

Table C21. The 2022 co-inoculations of *Pss* strains 9, 25 (PG 2d virulent) and 23,33 (PG2b moderate virulence) grown next to the strains 14, 18 (PG 2c avirulent), and 23,33 (PG2b moderate virulence) or water (H_2O) in Petri plates with KB media, group corresponds to the rate combination at which the PG2d and PG2b strains were inoculated next to the PG2c and PG2b strains or H_2O, for group 2 all strains were inoculated at 10^6 v. 10^8 cfu/ml. With confidence limits (lower and upper C.L.) and the p-value for the pairwise comparisons of the estimated marginal means for each strain and treatment, with letters indicating statistical differences with significance determined by p-value ≤0.05.

Year	Group	Strain/PG	*Pss* Mean total area (mm2)	SE	df	lower C.L.	upper C.L.	
2022	2	23	158.5	17.0	42	124.2	192.9	a
		25	282.0	14.6	42	252.6	311.4	b
		33	212.6	17.0	42	178.2	246.9	a
		9	306.7	14.6	42	277.3	336.1	b

Year	Group	contrast	estimate	SE	df	t-ratio	p-value
2022	2	23 v. 25	-123.5	19.7	42	-6.282	<0.0001
		23 v. 33	-54.1	24.1	42	-2.246	0.1277
		23 v. 9	-148.1	24.1	42	-6.154	<0.0001
		25 v. 33	69.4	24.1	42	2.883	0.0303
		25 v. 9	-24.7	24.1	42	-1.025	0.7358
		33 v. 9	-94.1	19.7	42	-4.787	0.0001

Year	Group	Treatment	*Pss* Mean total area (mm2)	SE	df	lower C.L.	upper C.L.	
2022	2	14	224.4	17.0	42	190.0	258.7	a
		18	249.2	17.0	42	214.8	283.5	a
		23	286.5	24.1	42	237.9	335.0	a
		33	195.4	24.1	42	146.8	243.9	a
		H2O	244.3	9.8	42	224.5	264.2	a

Year	Group	contrast	estimate	SE	df	t-ratio	p-value
2022	2	14 v. 18	-24.8	27.8	42	-0.892	0.8981
		14 v. 23	-62.1	26.0	42	-2.388	0.1387
		14 v. 33	29.0	32.6	42	0.890	0.8989
		14 v. H2O	-20.0	19.7	42	-1.015	0.8470

Table C21. (cont'd)

18 v. 23	-37.3	32.6	42	-1.144	0.7825
18 v. 33	53.8	26.0	42	2.070	0.2519
18 v. H2O	4.9	19.7	42	0.247	0.9991
23 v. 33	91.1	36.8	42	2.478	0.1153
23 v. H2O	42.1	26.0	42	1.621	0.4931
33 v. H2O	-49.0	26.0	42	-1.883	0.3418

Table C22. The 2022 co-inoculations of *Pss* strains 9, 25 (PG 2d virulent) and 23,33 (PG2b moderate virulence) grown next to the strains 14, 18 (PG 2c avirulent), and 23,33 (PG2b moderate virulence) or water (H_2O) in Petri plates with KB media, group corresponds to the rate combination at which the PG2d and PG2b strains were inoculated next to the PG2c and PG2b strains or H_2O, for group 3 all strains were inoculated at 10^4 v. 10^8 cfu/ml. With confidence limits (lower and upper C.L.) and the p-value for the pairwise comparisons of the estimated marginal means for each strain and treatment, with letters indicating statistical differences with significance determined by p-value ≤0.05.

Year	Group	Treatment	*Pss* Mean total area (mm2)	SE	df	lower C.L.	upper C.L.	
2022	3	14	161.2	24.6	42	111.5	210.9	a
		18	193.8	24.6	42	144.1	243.5	a
		23	149.8	34.8	42	79.4	220.1	a
		33	150.5	34.8	42	80.1	220.8	a
		H_2O	225.1	14.2	42	196.4	253.8	a
Year	**Group**	**contrast**	**estimate**	**SE**	**df**	**t-ratio**	**p-value**	
2022	3	14 - 18	-32.6	40.2	42	-0.811	0.9258	
		14 - 23	11.4	37.6	42	0.303	0.9981	
		14 - 33	10.7	47.2	42	0.227	0.9994	
		14 - H_2O	-63.9	28.5	42	-2.247	0.1827	
		18 - 23	44.0	47.2	42	0.933	0.8823	
		18 - 33	43.3	37.6	42	1.151	0.7783	
		18 - H_2O	-31.3	28.5	42	-1.100	0.8054	
		23 - 33	-0.7	53.2	42	-0.013	1.0000	
		23 - H_2O	-75.3	37.6	42	-2.002	0.2829	
		33 - H_2O	-74.6	37.6	42	-1.983	0.2918	

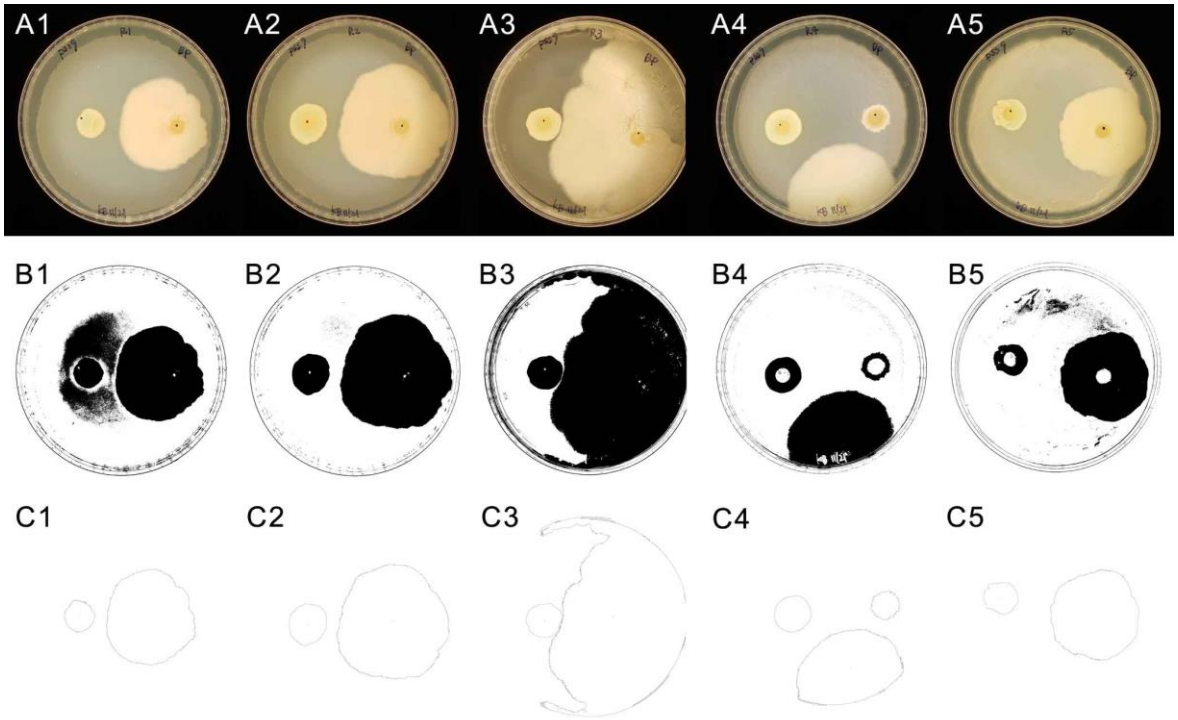


Figure C5. 2019 co-inoculated Petri plates four days after inoculation. **A1-A5)** *Pss* 9 vs. BP on KB media. **B1-B5)** Images after threshold adjustment in ImageJ. **C1-C5)** Image of measured area. A1, B1, C1: Replication 1; A2, B2, C2: Replication 2; A3, B3, C3: Replication 3; A4, B4, C4: Replication 4; A5, B5, C5: Replication 5.

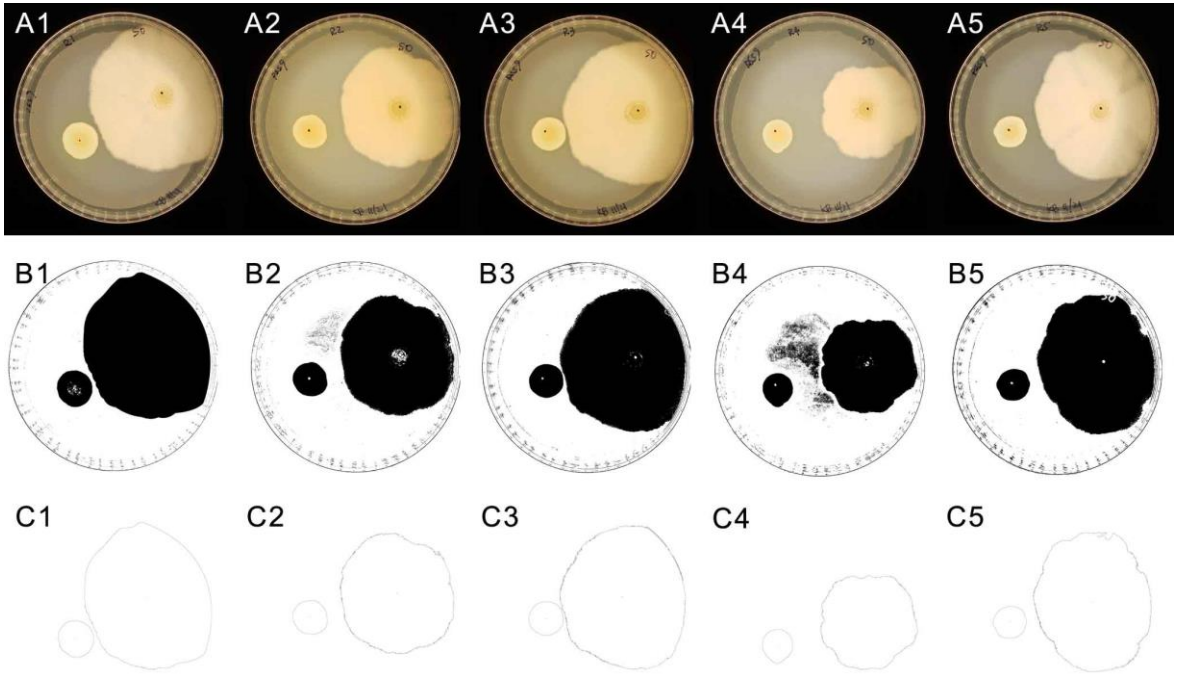


Figure C6. 2019 co-inoculated Petri plates four days after inoculation. **A1-A5)** *Pss* 9 vs. SO on KB media. **B1-B5)** Images after threshold adjustment in ImageJ. **C1-C5)** Image of measured area. A1, B1, C1: Replication 1; A2, B2, C2: Replication 2; A3, B3, C3: Replication 3; A4, B4, C4: Replication 4; A5, B5, C5: Replication 5.

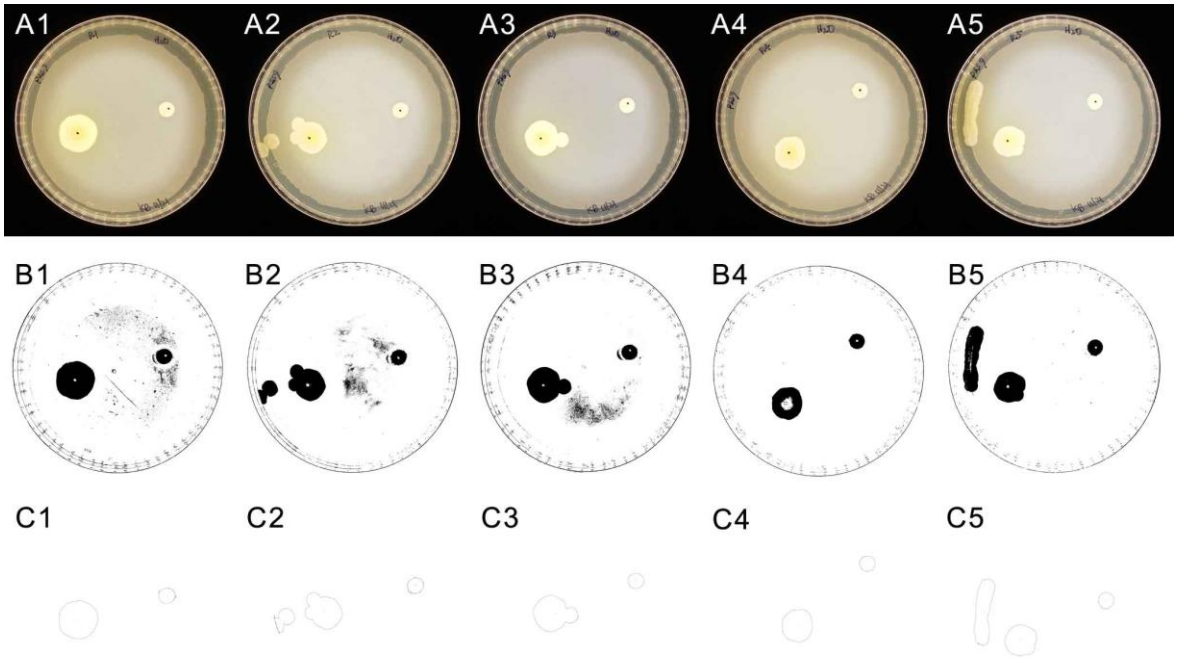


Figure C7. 2019 co-inoculated Petri plates four days after inoculation. **A1-A5)** *Pss* 9 vs. H_2O on KB media. **B1-B5)** Images after threshold adjustment in ImageJ. **C1-C5)** Image of measured area. A1, B1, C1: Replication 1; A2, B2, C2: Replication 2; A3, B3, C3: Replication 3; A4, B4, C4: Replication 4; A5, B5, C5: Replication 5.

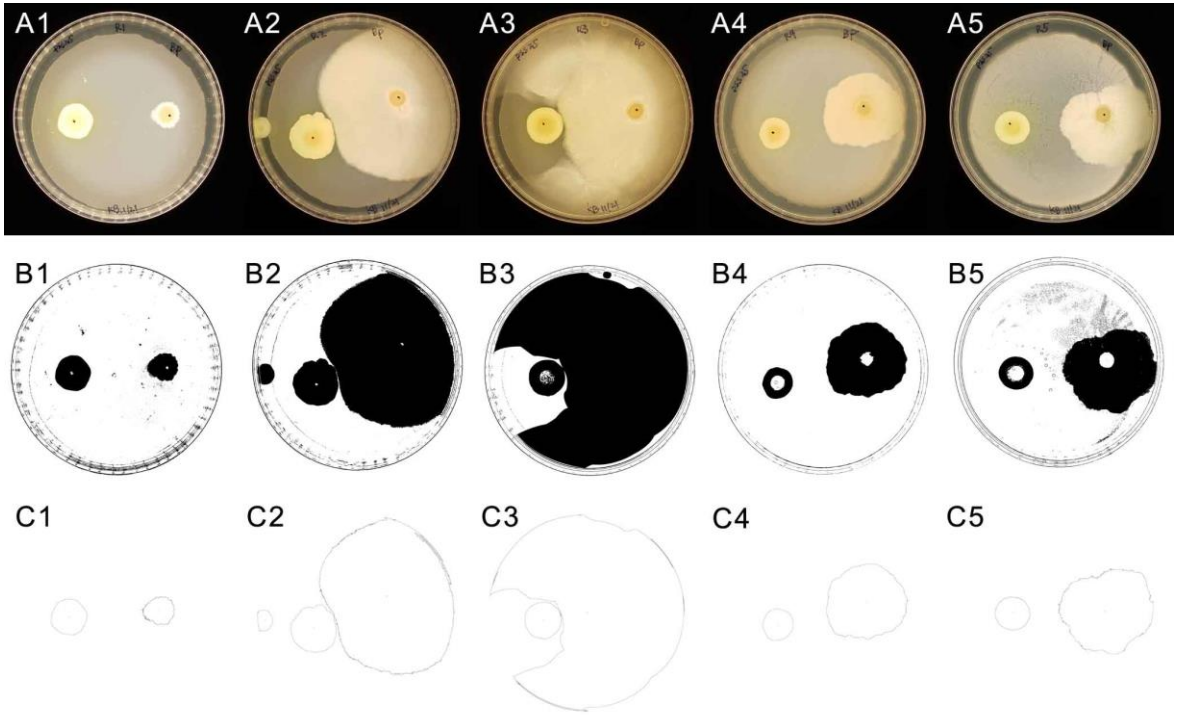


Figure C8. 2019 co-inoculated Petri plates four days after inoculation. **A1-A5)** *Pss* 25 vs. BP on KB media. **B1-B5)** Images after threshold adjustment in ImageJ. **C1-C5)** Image of measured area. A1, B1, C1: Replication 1; A2, B2, C2: Replication 2; A3, B3, C3: Replication 3; A4, B4, C4: Replication 4; A5, B5, C5: Replication 5.

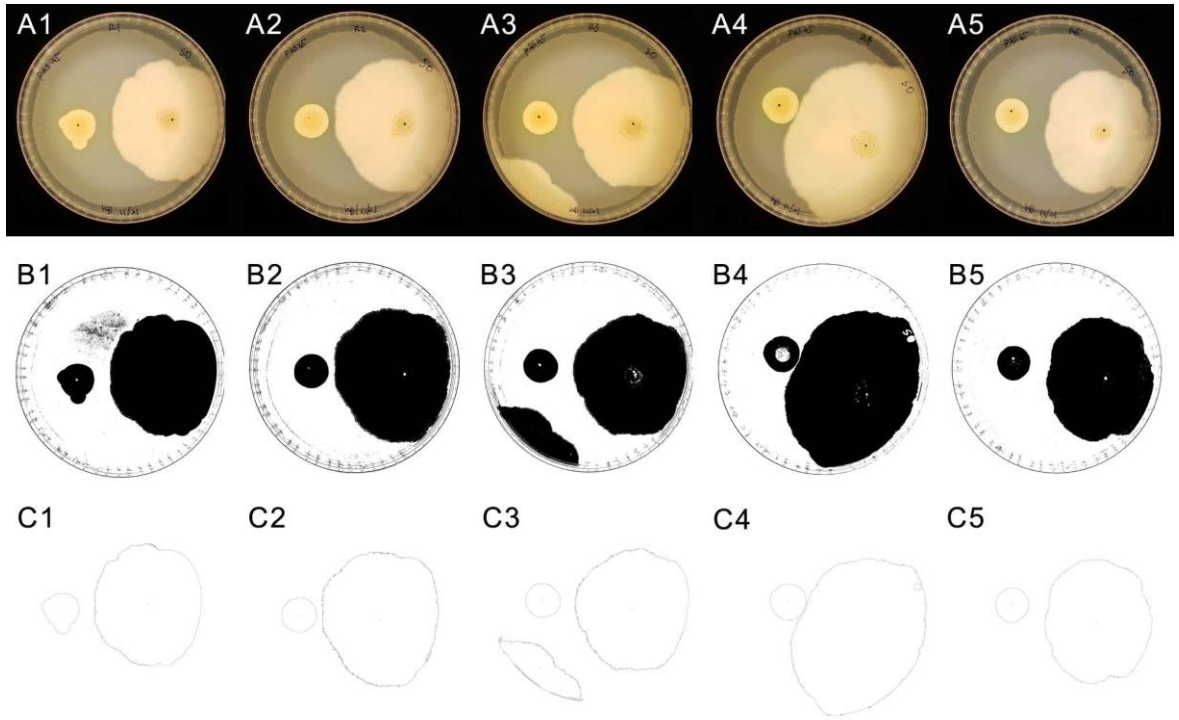


Figure C9. 2019 co-inoculated Petri plates four days after inoculation. **A1-A5)** *Pss* 25 vs. SO on KB media. **B1-B5)** Images after threshold adjustment in ImageJ. **C1-C5)** Image of measured area. A1, B1, C1: Replication 1; A2, B2, C2: Replication 2; A3, B3, C3: Replication 3; A4, B4, C4: Replication 4; A5, B5, C5: Replication 5.

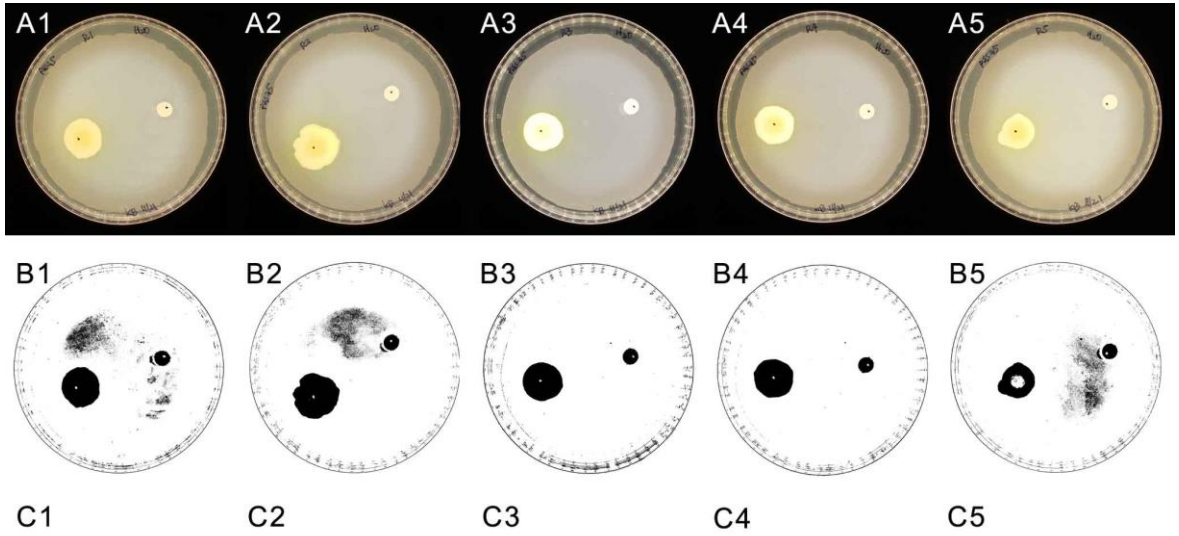


Figure C10. 2019 co-inoculated Petri plates four days after inoculation. **A1-A5)** *Pss* 25 vs. H_2O on KB media. **B1-B5)** Images after threshold adjustment in ImageJ. **C1-C5)** Image of measured area. A1, B1, C1: Replication 1; A2, B2, C2: Replication 2; A3, B3, C3: Replication 3; A4, B4, C4: Replication 4; A5, B5, C5: Replication 5.

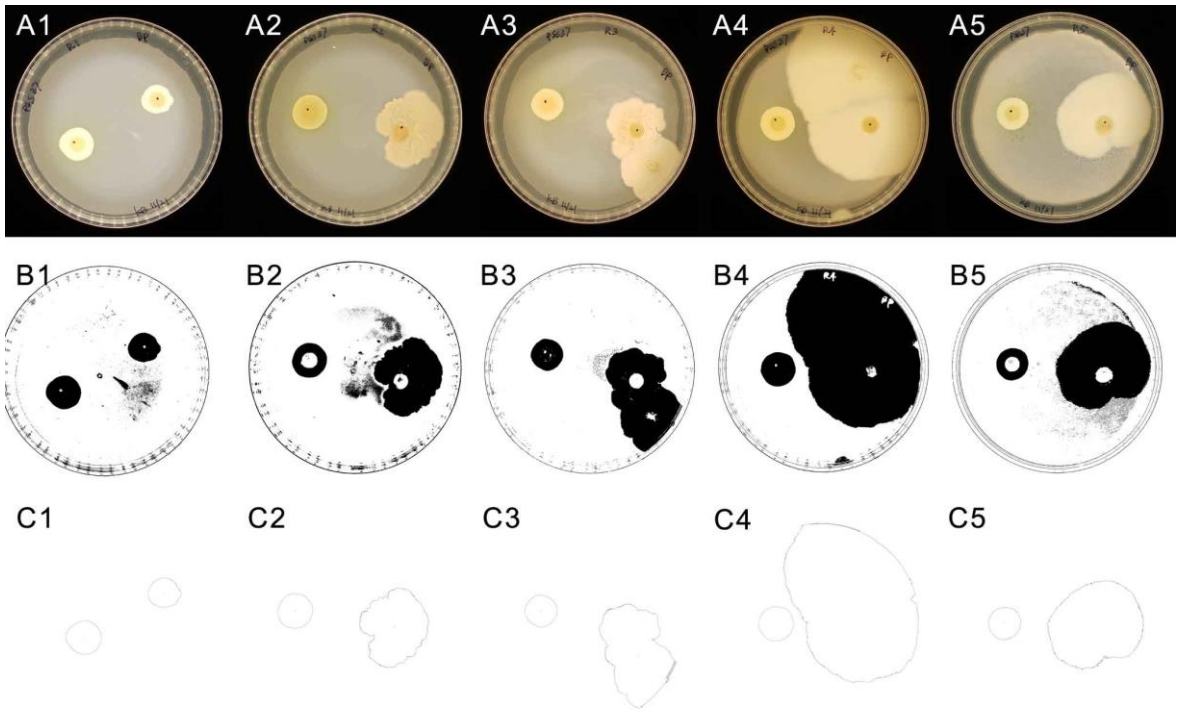


Figure C11. 2019 co-inoculated Petri plates four days after inoculation. **A1-A5)** *Pss* 37 vs. BP on KB media. **B1-B5)** Images after threshold adjustment in ImageJ. **C1-C5)** Image of measured area. A1, B1, C1: Replication 1; A2, B2, C2: Replication 2; A3, B3, C3: Replication 3; A4, B4, C4: Replication 4; A5, B5, C5: Replication 5.

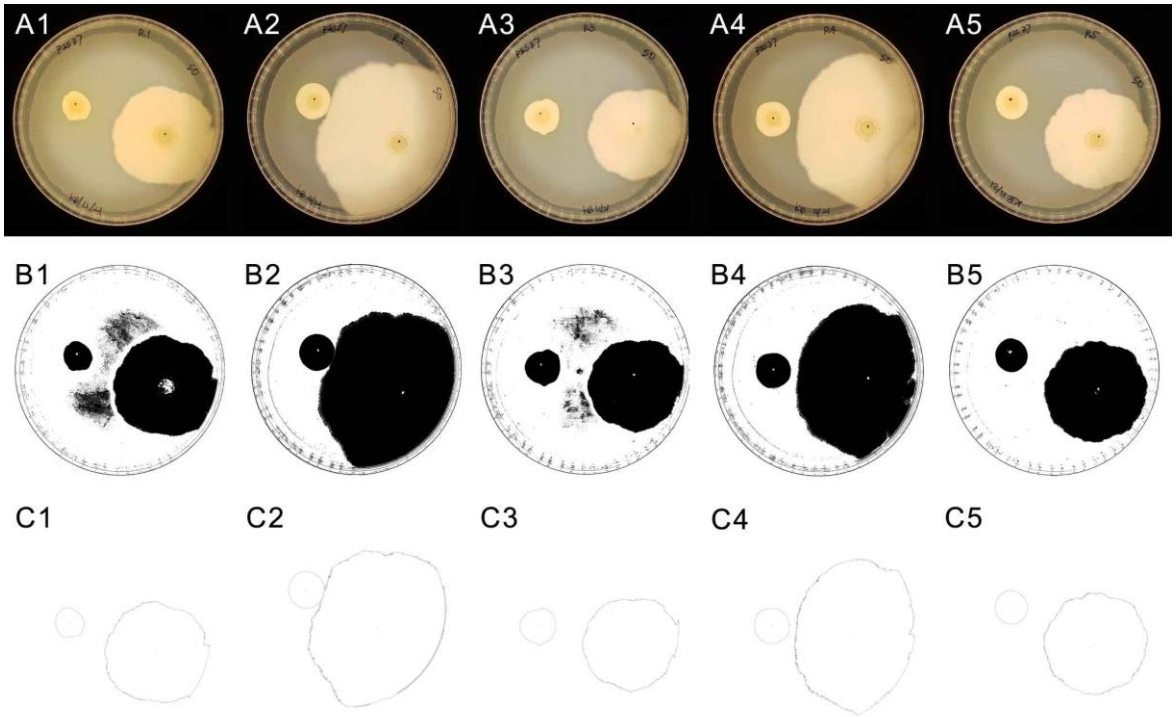


Figure C12. 2019 co-inoculated Petri plates four days after inoculation. **A1-A5)** *Pss* 37 vs. SO on KB media. **B1-B5)** Images after threshold adjustment in ImageJ. **C1-C5)** Image of measured area. A1, B1, C1: Replication 1; A2, B2, C2: Replication 2; A3, B3, C3: Replication 3; A4, B4, C4: Replication 4; A5, B5, C5: Replication 5.

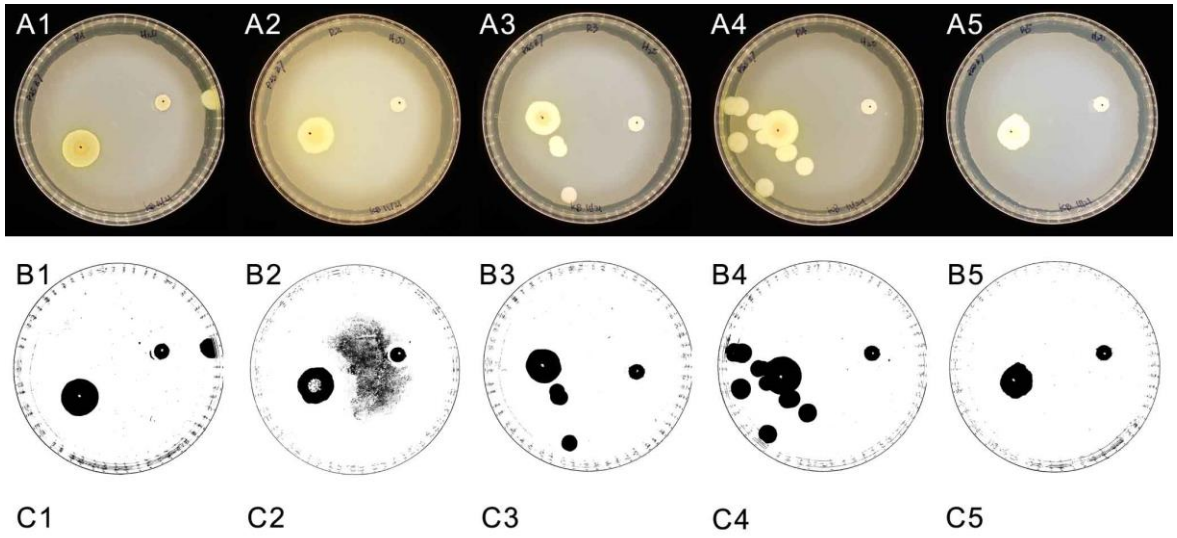


Figure C13. 2019 co-inoculated Petri plates four days after inoculation. **A1-A5)** *Pss* 37 vs. H_2O on KB media. **B1-B5)** Images after threshold adjustment in ImageJ. **C1-C5)** Image of measured area. A1, B1, C1: Replication 1; A2, B2, C2: Replication 2; A3, B3, C3: Replication 3; A4, B4, C4: Replication 4; A5, B5, C5: Replication 5.

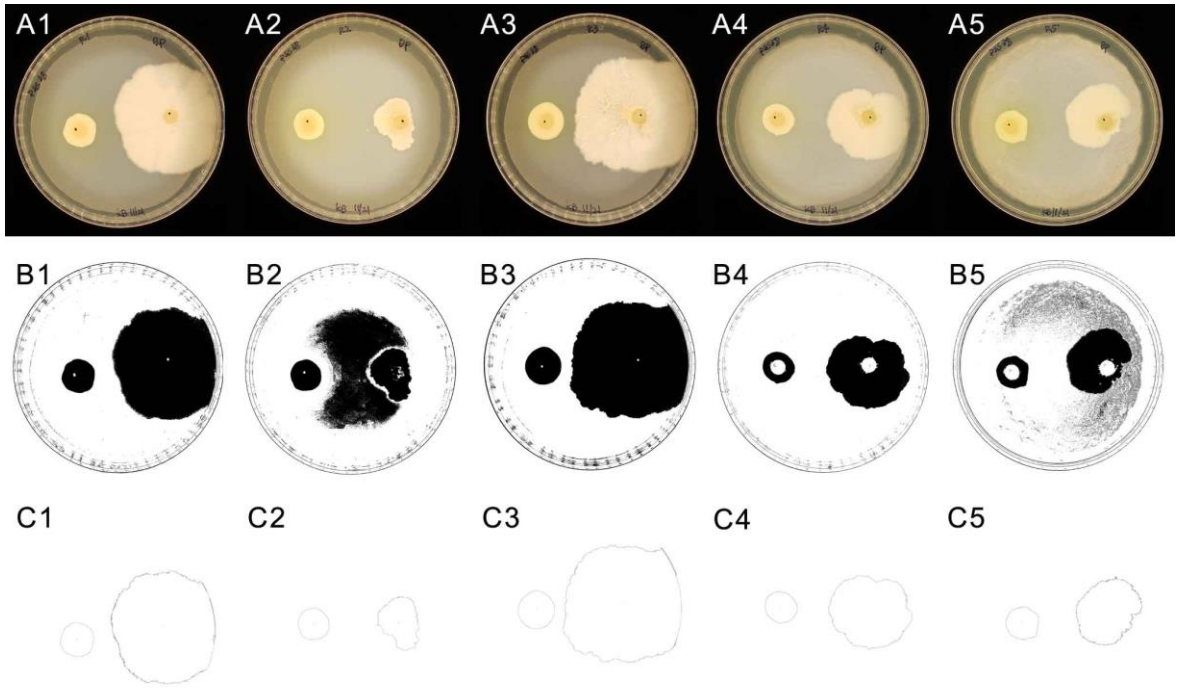


Figure C14. 2019 co-inoculated Petri plates four days after inoculation. **A1-A5)** *Pss* 38 vs. BP on KB media. **B1-B5)** Images after threshold adjustment in ImageJ. **C1-C5)** Image of measured area. A1, B1, C1: Replication 1; A2, B2, C2: Replication 2; A3, B3, C3: Replication 3; A4, B4, C4: Replication 4; A5, B5, C5: Replication 5.

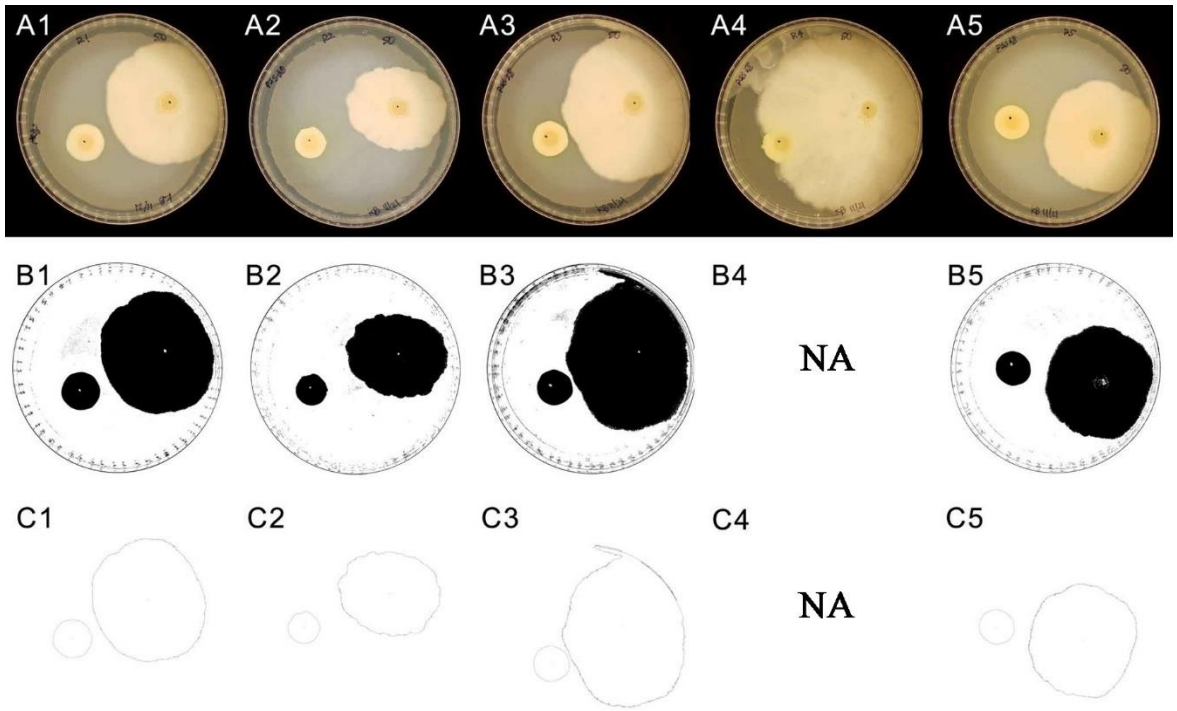


Figure C15. 2019 co-inoculated Petri plates four days after inoculation. **A1-A5)** *Pss* 38 vs. SO on KB media. **B1-B5)** Images after threshold adjustment in ImageJ. **C1-C5)** Image of measured area. A1, B1, C1: Replication 1; A2, B2, C2: Replication 2; A3, B3, C3: Replication 3; A4, B4, C4: Replication 4; A5, B5, C5: Replication 5. Images with NA are not available.

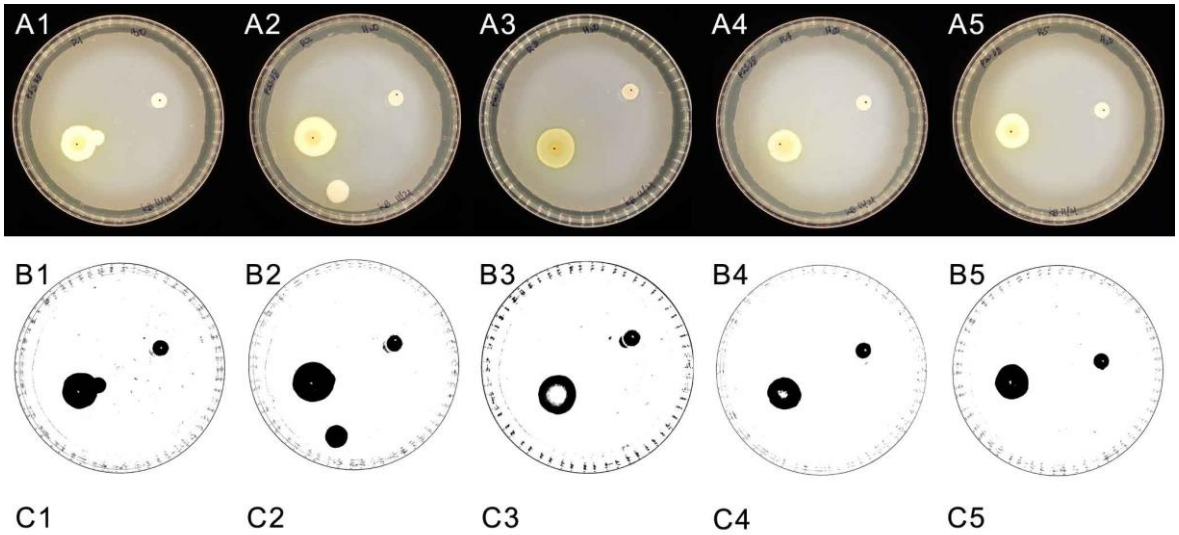


Figure C16. 2019 co-inoculated Petri plates four days after inoculation. **A1-A5)** *Pss* 38 vs. H_2O on KB media. **B1-B5)** Images after threshold adjustment in ImageJ. **C1-C5)** Image of measured area. A1, B1, C1: Replication 1; A2, B2, C2: Replication 2; A3, B3, C3: Replication 3; A4, B4, C4: Replication 4; A5, B5, C5: Replication 5.

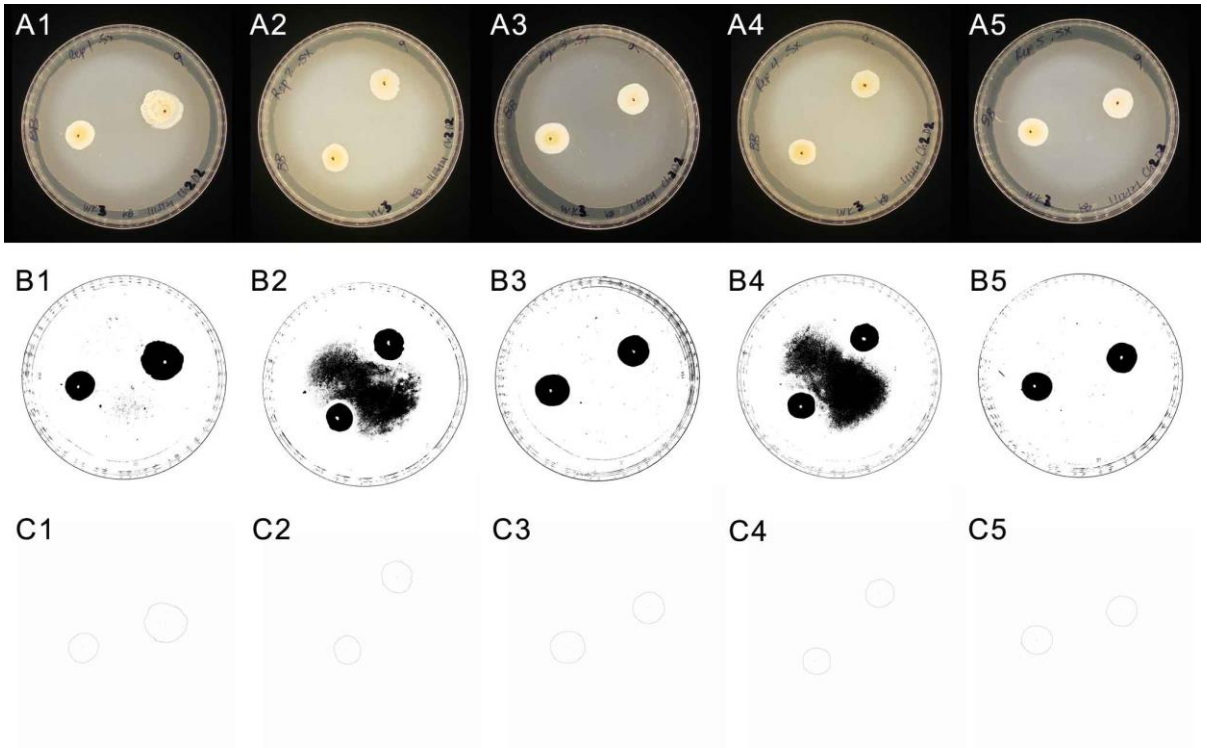


Figure C17. 2021 co-inoculated Petri plates four days after inoculation. **A1-A5)** 0.5x BB vs. *Pss* 9 on KB media. **B1-B5)** Images after threshold adjustment in ImageJ. **C1-C5)** Image of measured area. A1, B1, C1: Replication 1; A2, B2, C2: Replication 2; A3, B3, C3: Replication 3; A4, B4, C4: Replication 4; A5, B5, C5: Replication 5.

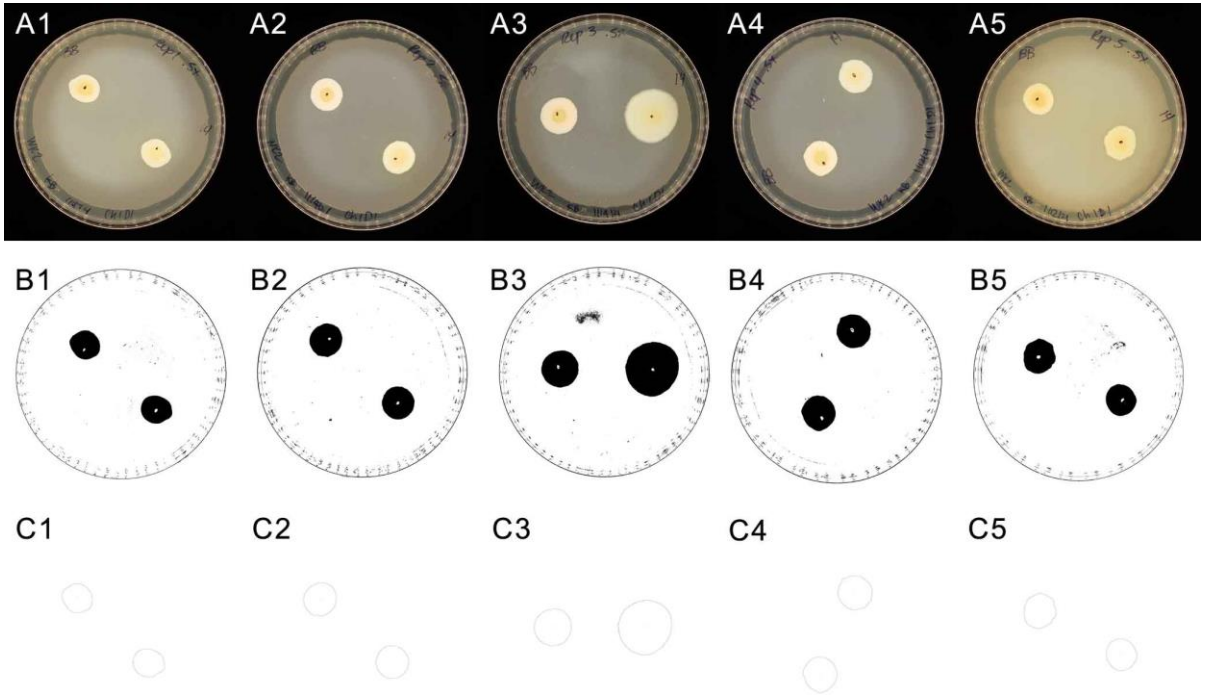


Figure C18. 2021 co-inoculated Petri plates four days after inoculation. **A1-A5)** 0.5x BB vs. *Pss* 14 on KB media. **B1-B5)** Images after threshold adjustment in ImageJ. **C1-C5)** Image of measured area. A1, B1, C1: Replication 1; A2, B2, C2: Replication 2; A3, B3, C3: Replication 3; A4, B4, C4: Replication 4; A5, B5, C5: Replication 5.

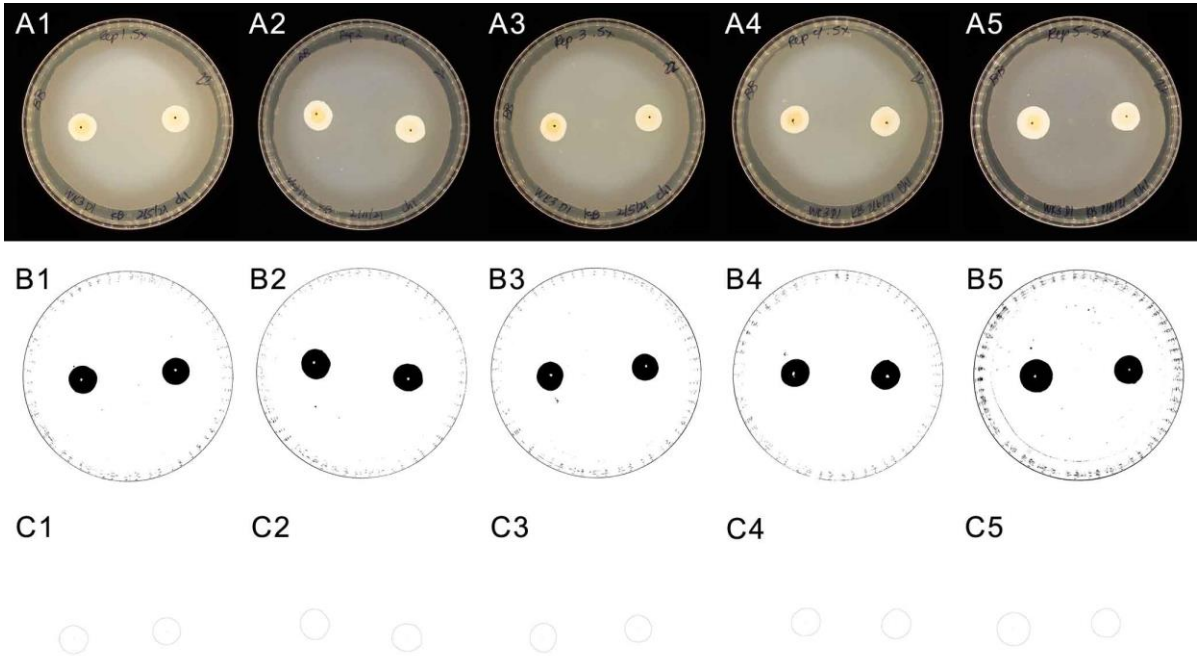


Figure C19. 2021 co-inoculated Petri plates four days after inoculation. **A1-A5)** 0.5x BB vs. *Pss* 22 on KB media. **B1-B5)** Images after threshold adjustment in ImageJ. **C1-C5)** Image of measured area. A1, B1, C1: Replication 1; A2, B2, C2: Replication 2; A3, B3, C3: Replication 3; A4, B4, C4: Replication 4; A5, B5, C5: Replication 5.

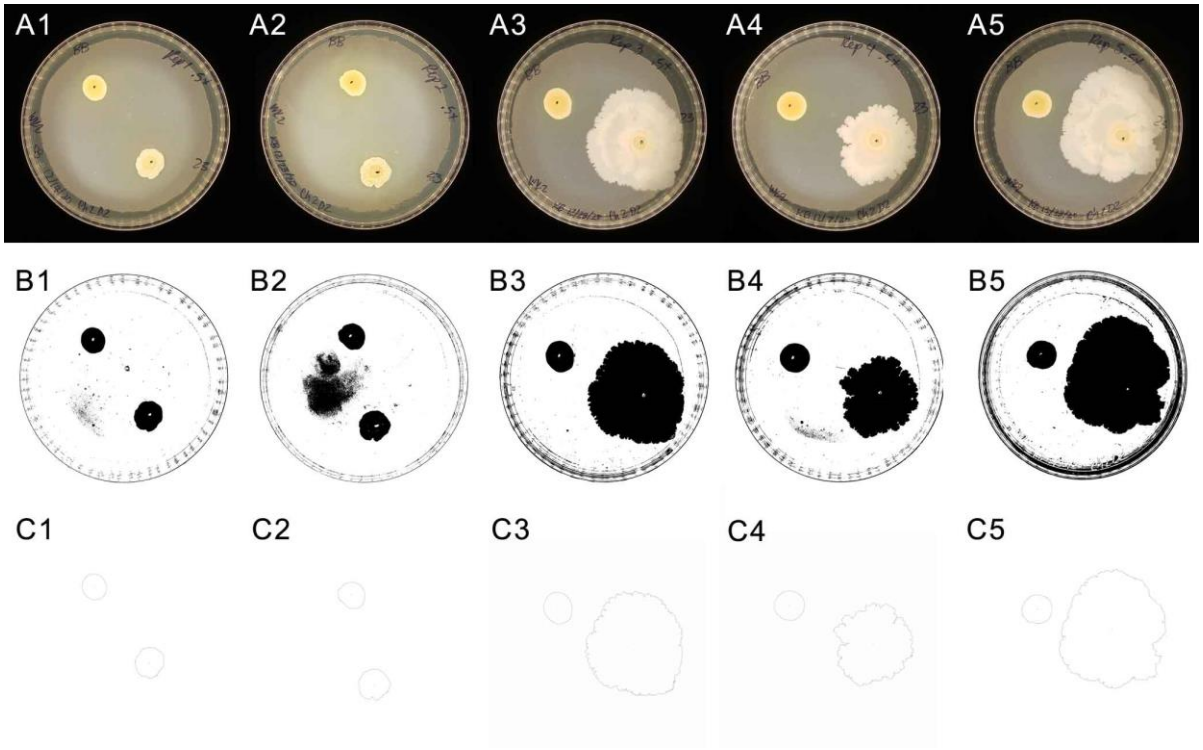


Figure C20. 2021 co-inoculated Petri plates four days after inoculation. **A1-A5)** 0.5x BB vs. *Pss* 23 on KB media. **B1-B5)** Images after threshold adjustment in ImageJ. **C1-C5)** Image of measured area. A1, B1, C1: Replication 1; A2, B2, C2: Replication 2; A3, B3, C3: Replication 3; A4, B4, C4: Replication 4; A5, B5, C5: Replication 5.

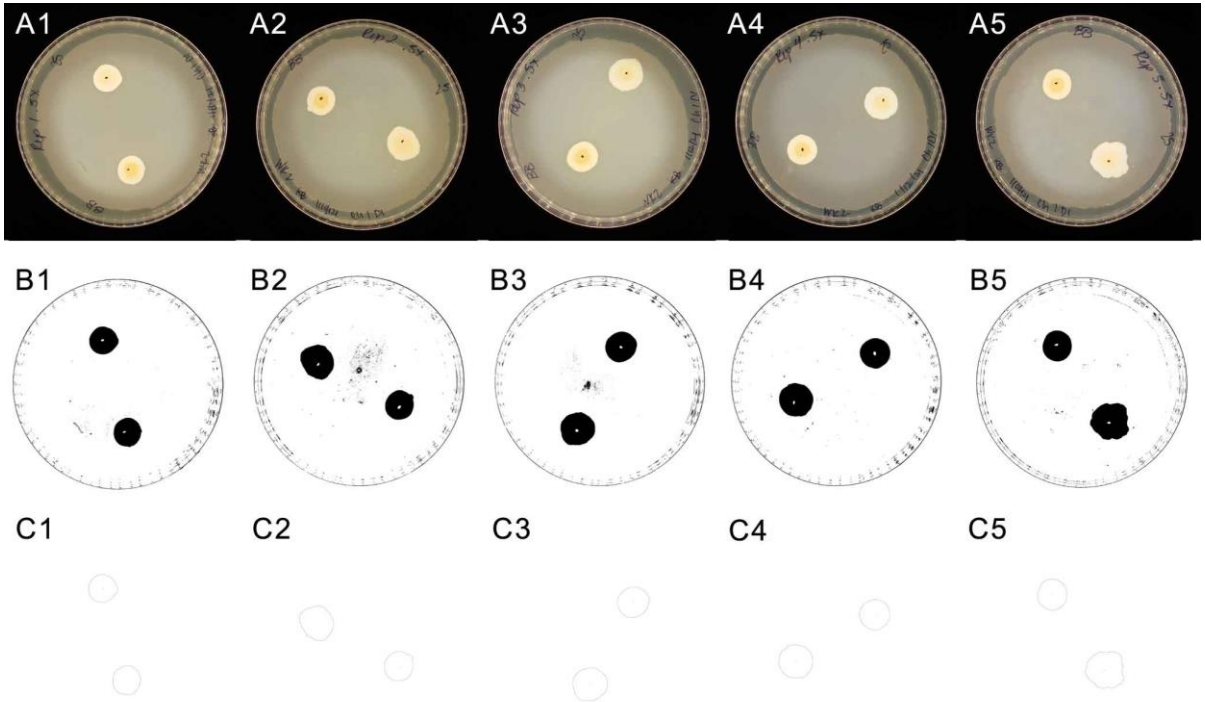


Figure C21. 2021 co-inoculated Petri plates four days after inoculation. **A1-A5)** 0.5x BB vs. *Pss* 25 on KB media. **B1-B5)** Images after threshold adjustment in ImageJ. **C1-C5)** Image of measured area. A1, B1, C1: Replication 1; A2, B2, C2: Replication 2; A3, B3, C3: Replication 3; A4, B4, C4: Replication 4; A5, B5, C5: Replication 5.

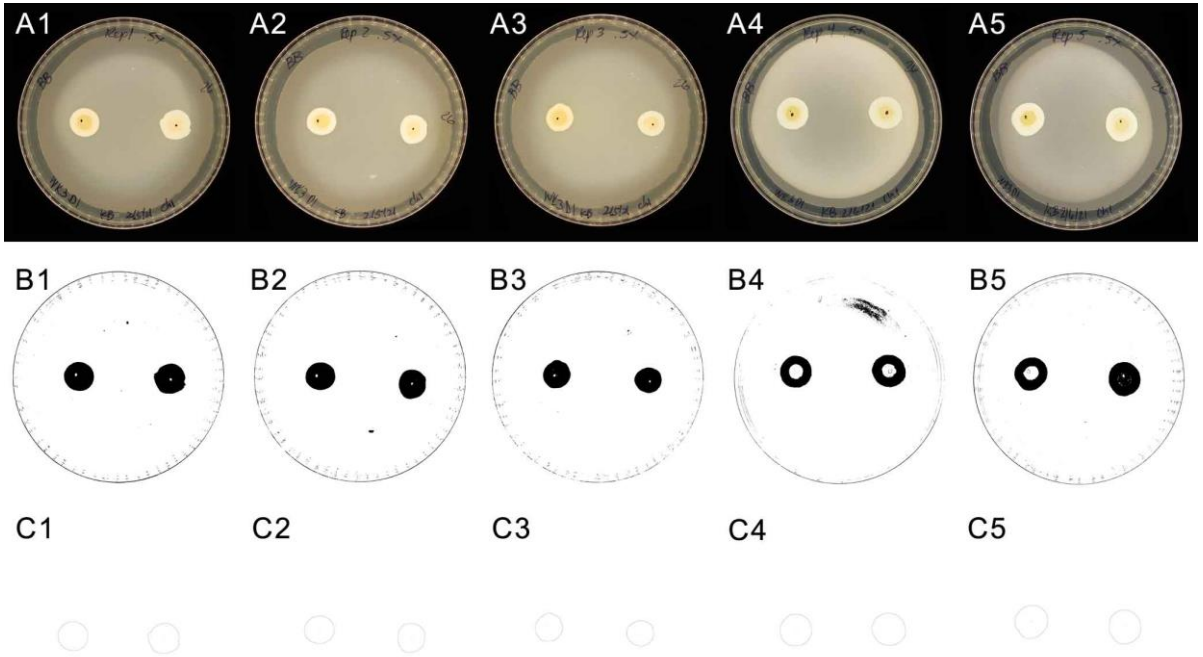


Figure C22. 2021 co-inoculated Petri plates four days after inoculation. **A1-A5)** 0.5x BB vs. *Pss* 26 on KB media. **B1-B5)** Images after threshold adjustment in ImageJ. **C1-C5)** Image of measured area. A1, B1, C1: Replication 1; A2, B2, C2: Replication 2; A3, B3, C3: Replication 3; A4, B4, C4: Replication 4; A5, B5, C5: Replication 5.

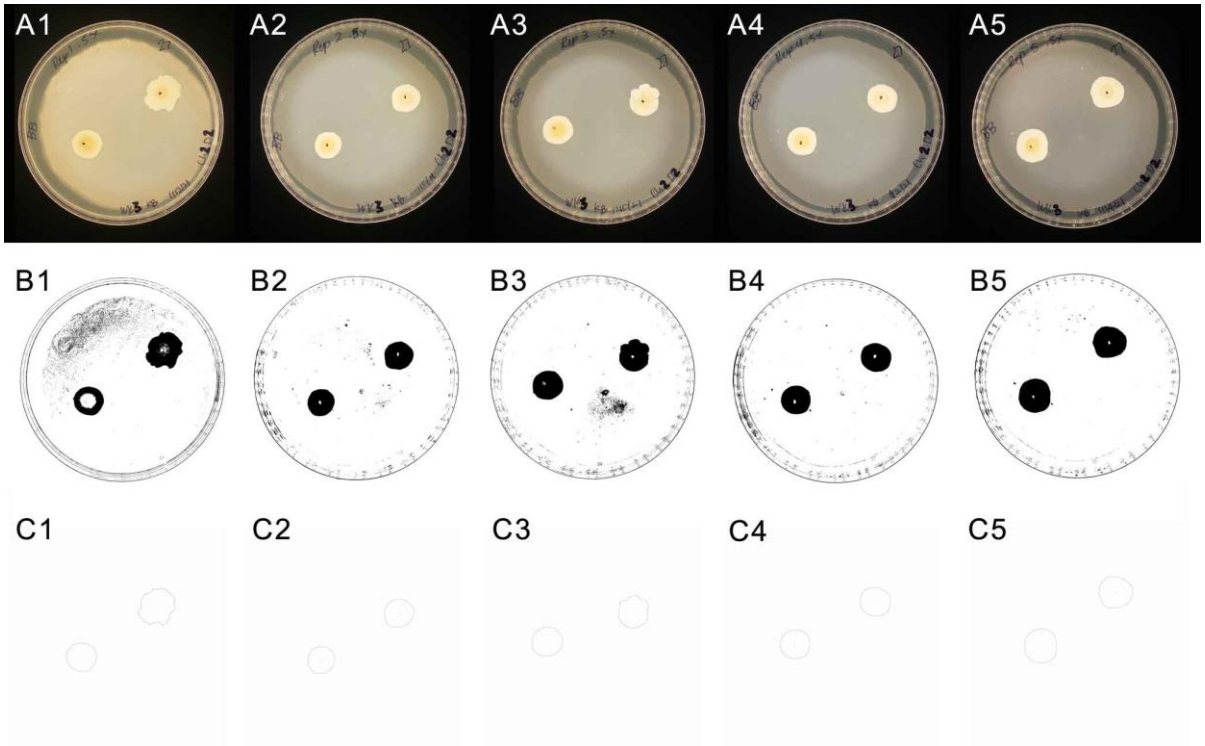


Figure C23. 2021 co-inoculated Petri plates four days after inoculation. **A1-A5)** 0.5x BB vs. *Pss* 27 on KB media. **B1-B5)** Images after threshold adjustment in ImageJ. **C1-C5)** Image of measured area. A1, B1, C1: Replication 1; A2, B2, C2: Replication 2; A3, B3, C3: Replication 3; A4, B4, C4: Replication 4; A5, B5, C5: Replication 5.

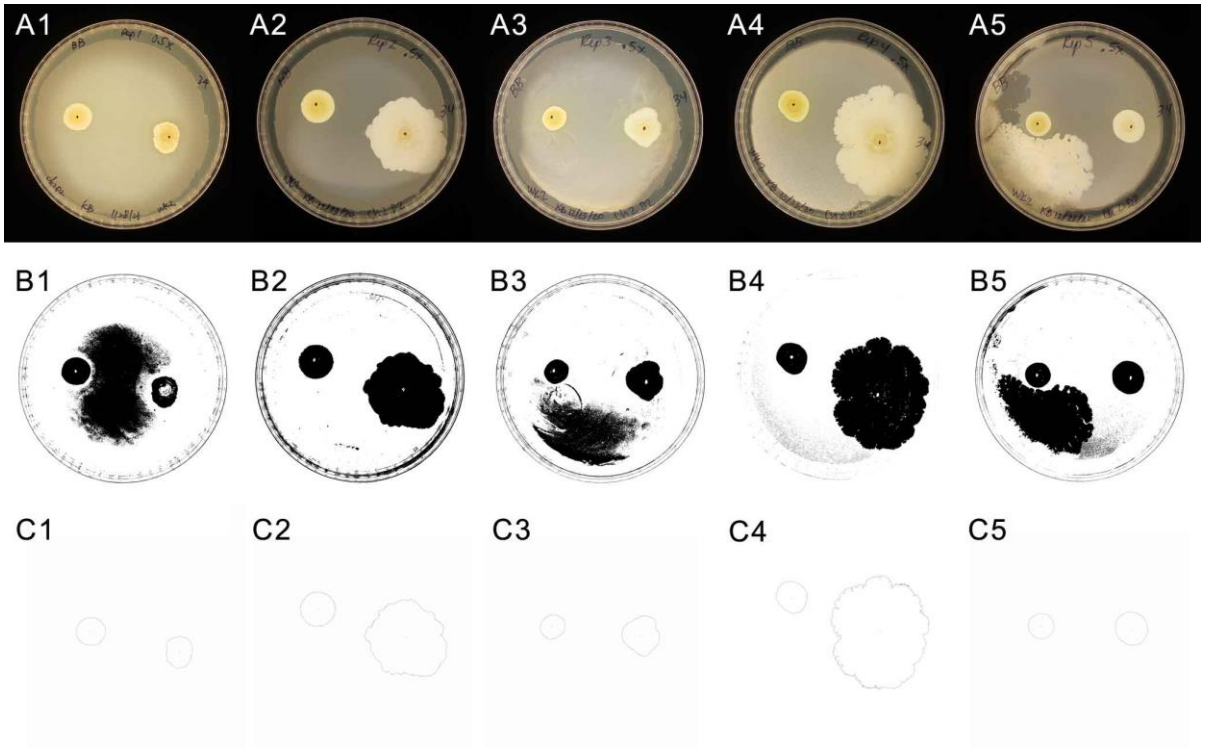


Figure C24. 2021 co-inoculated Petri plates four days after inoculation. **A1-A5)** 0.5x BB vs. *Pss* 34 on KB media. **B1-B5)** Images after threshold adjustment in ImageJ. **C1-C5)** Image of measured area. A1, B1, C1: Replication 1; A2, B2, C2: Replication 2; A3, B3, C3: Replication 3; A4, B4, C4: Replication 4; A5, B5, C5: Replication 5.

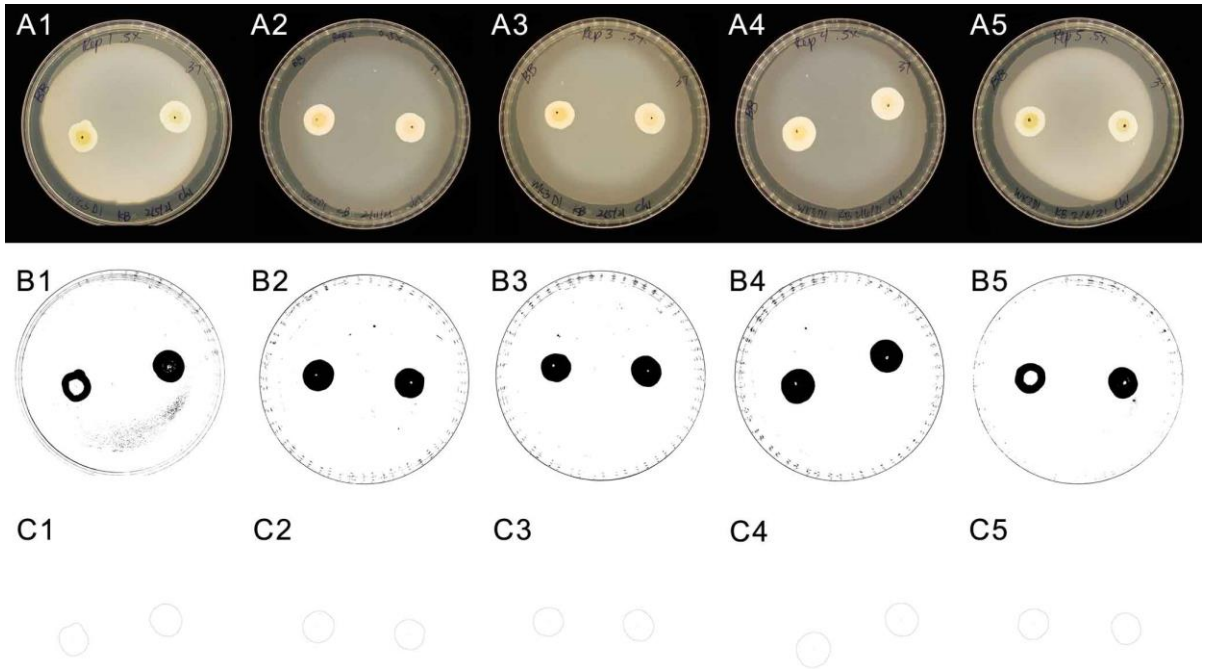


Figure C25. 2021 co-inoculated Petri plates four days after inoculation. **A1-A5)** 0.5x BB vs. *Pss* 37 on KB media. **B1-B5)** Images after threshold adjustment in ImageJ. **C1-C5)** Image of measured area. A1, B1, C1: Replication 1; A2, B2, C2: Replication 2; A3, B3, C3: Replication 3; A4, B4, C4: Replication 4; A5, B5, C5: Replication 5.

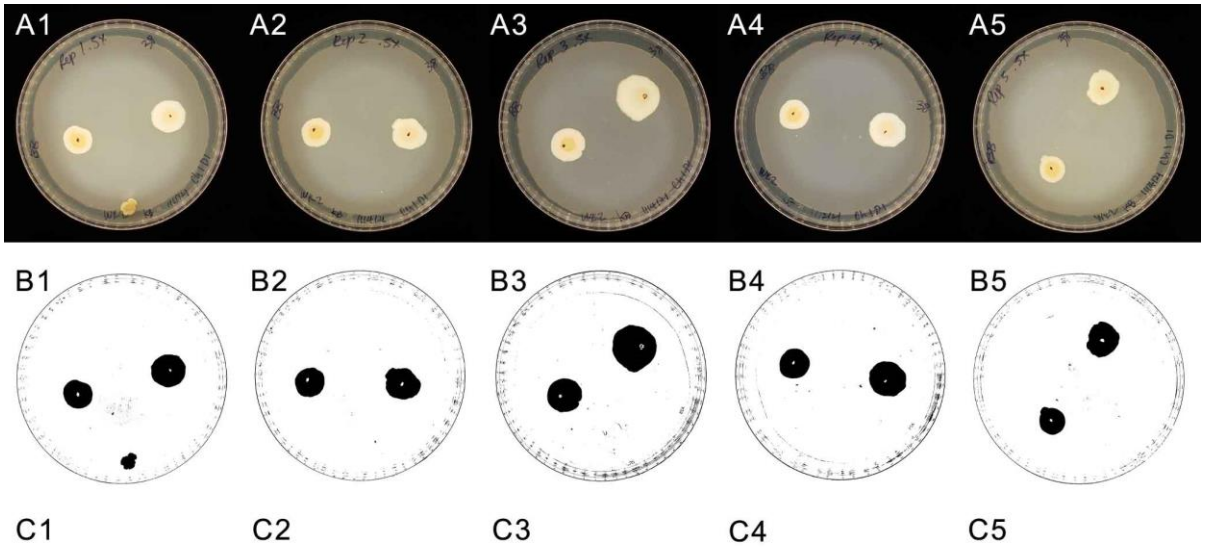


Figure C26. 2021 co-inoculated Petri plates four days after inoculation. **A1-A5)** 0.5x BB vs. *Pss* 38 on KB media. **B1-B5)** Images after threshold adjustment in ImageJ. **C1-C5)** Image of measured area. A1, B1, C1: Replication 1; A2, B2, C2: Replication 2; A3, B3, C3: Replication 3; A4, B4, C4: Replication 4; A5, B5, C5: Replication 5.

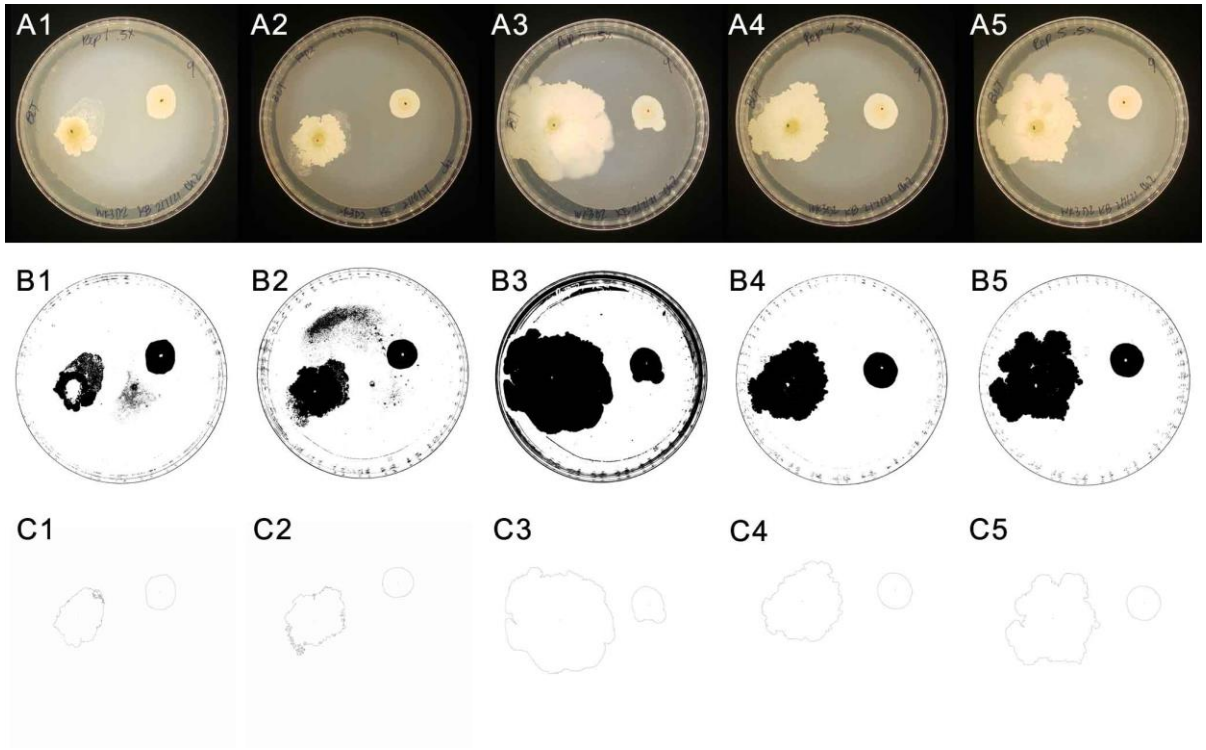


Figure C27. 12021 co-inoculated Petri plates four days after inoculation. **A1-A5)** 0.5x BLT vs. *Pss* 9 on KB media. **B1-B5)** Images after threshold adjustment in ImageJ. **C1-C5)** Image of measured area. A1, B1, C1: Replication 1; A2, B2, C2: Replication 2; A3, B3, C3: Replication 3; A4, B4, C4: Replication 4; A5, B5, C5: Replication 5.

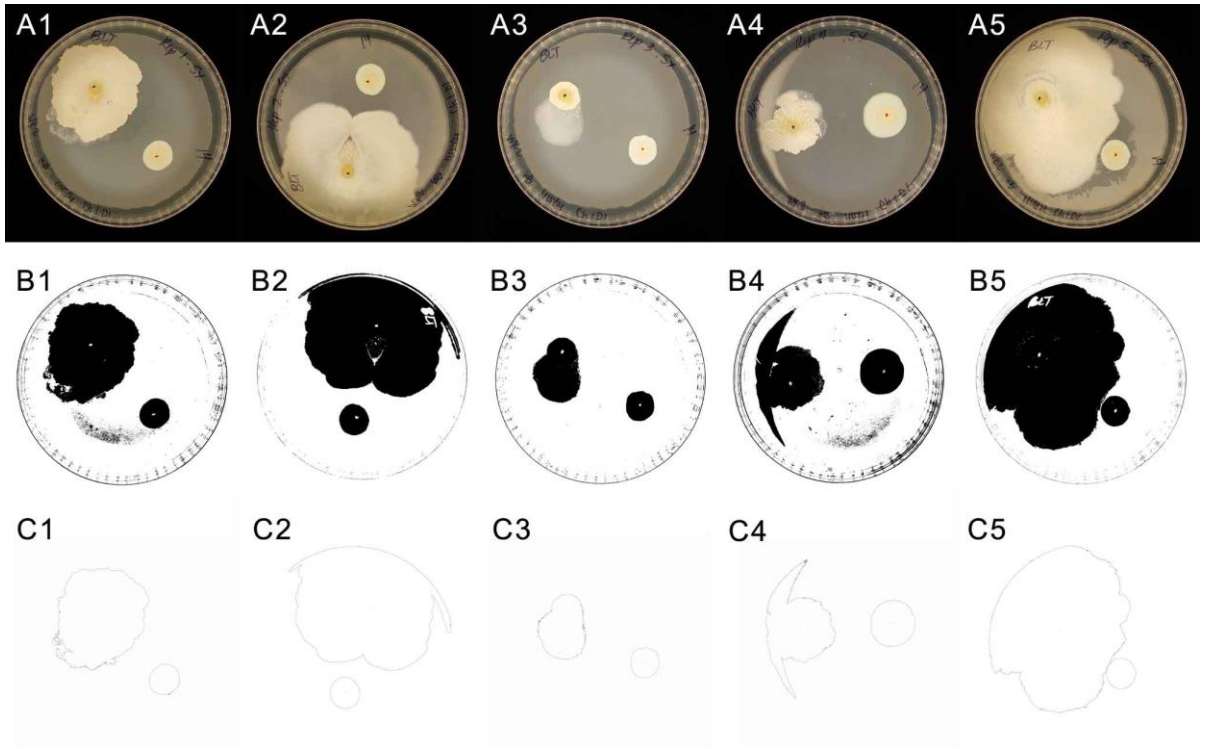


Figure C28. 2021 co-inoculated Petri plates four days after inoculation. **A1-A5)** 0.5x BLT vs. *Pss* 14 on KB media. **B1-B5)** Images after threshold adjustment in ImageJ. **C1-C5)** Image of measured area. A1, B1, C1: Replication 1; A2, B2, C2: Replication 2; A3, B3, C3: Replication 3; A4, B4, C4: Replication 4; A5, B5, C5: Replication 5.

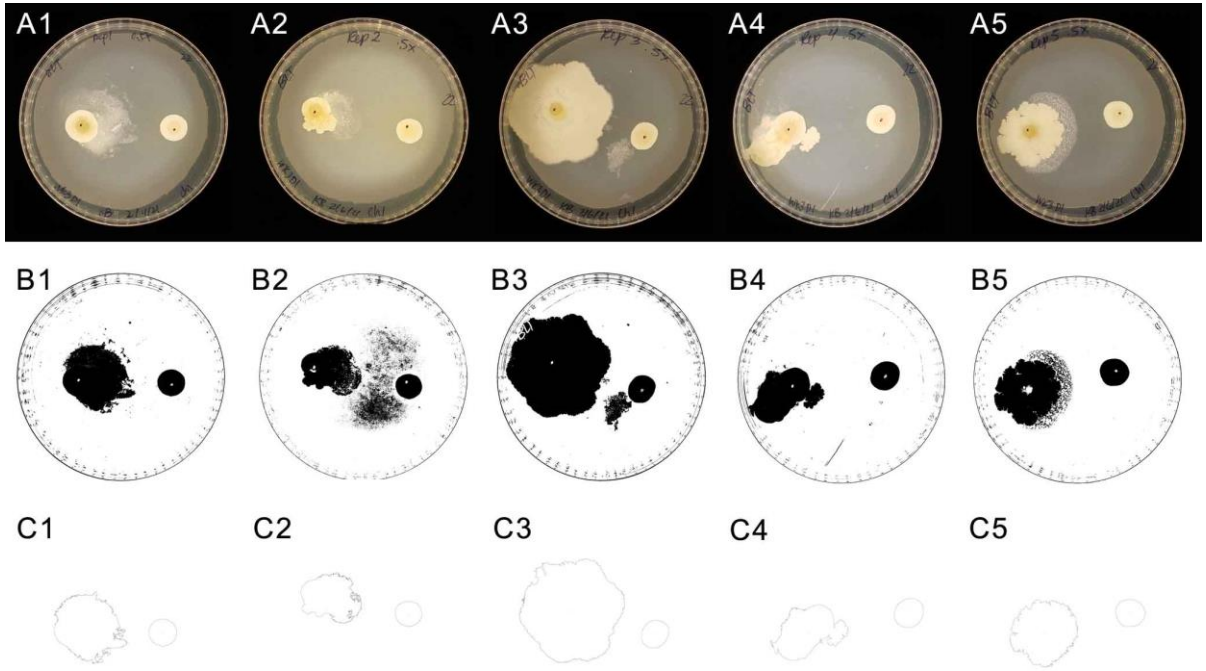


Figure C29. 2021 co-inoculated Petri plates four days after inoculation. **A1-A5)** 0.5x BLT vs. *Pss* 22 on KB media. **B1-B5)** Images after threshold adjustment in ImageJ. **C1-C5)** Image of measured area. A1, B1, C1: Replication 1; A2, B2, C2: Replication 2; A3, B3, C3: Replication 3; A4, B4, C4: Replication 4; A5, B5, C5: Replication 5.

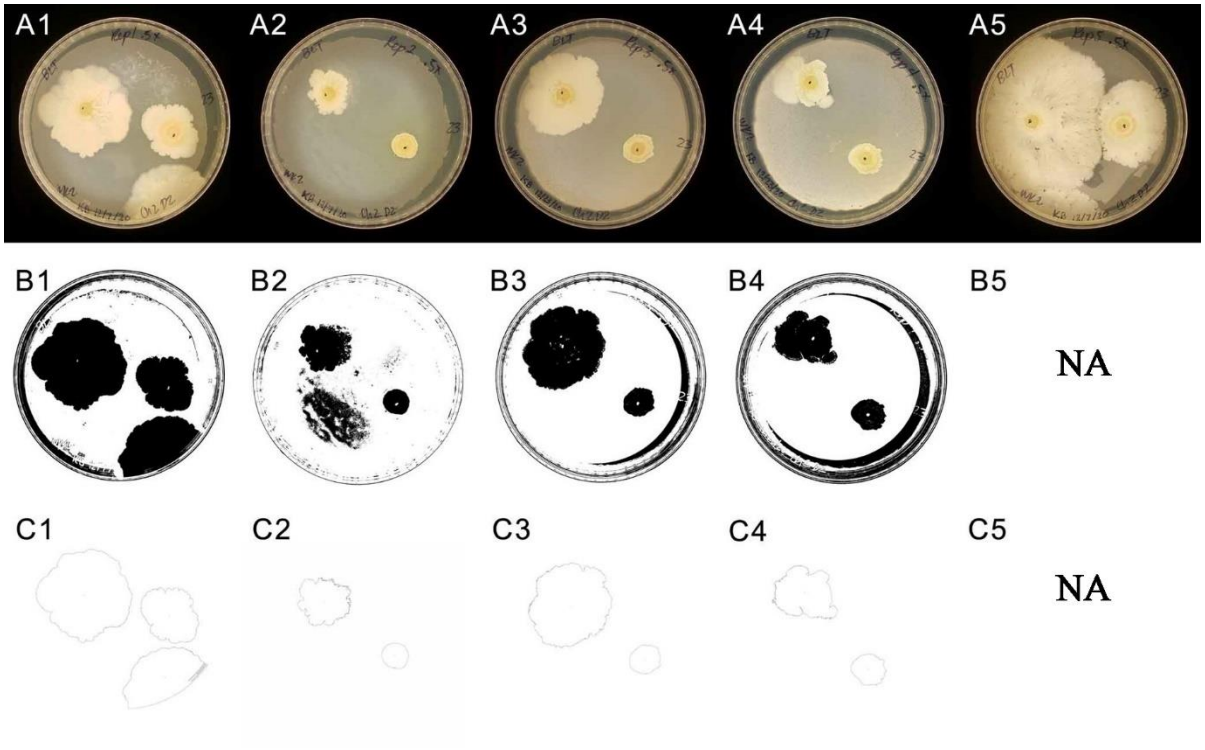


Figure C30. 2021 co-inoculated Petri plates four days after inoculation. **A1-A5)** 0.5x BLT vs. *Pss* 23 on KB media. **B1-B5)** Images after threshold adjustment in ImageJ. **C1-C5)** Image of measured area. A1, B1, C1: Replication 1; A2, B2, C2: Replication 2; A3, B3, C3: Replication 3; A4, B4, C4: Replication 4; A5, B5, C5: Replication 5. Images with NA are not available.

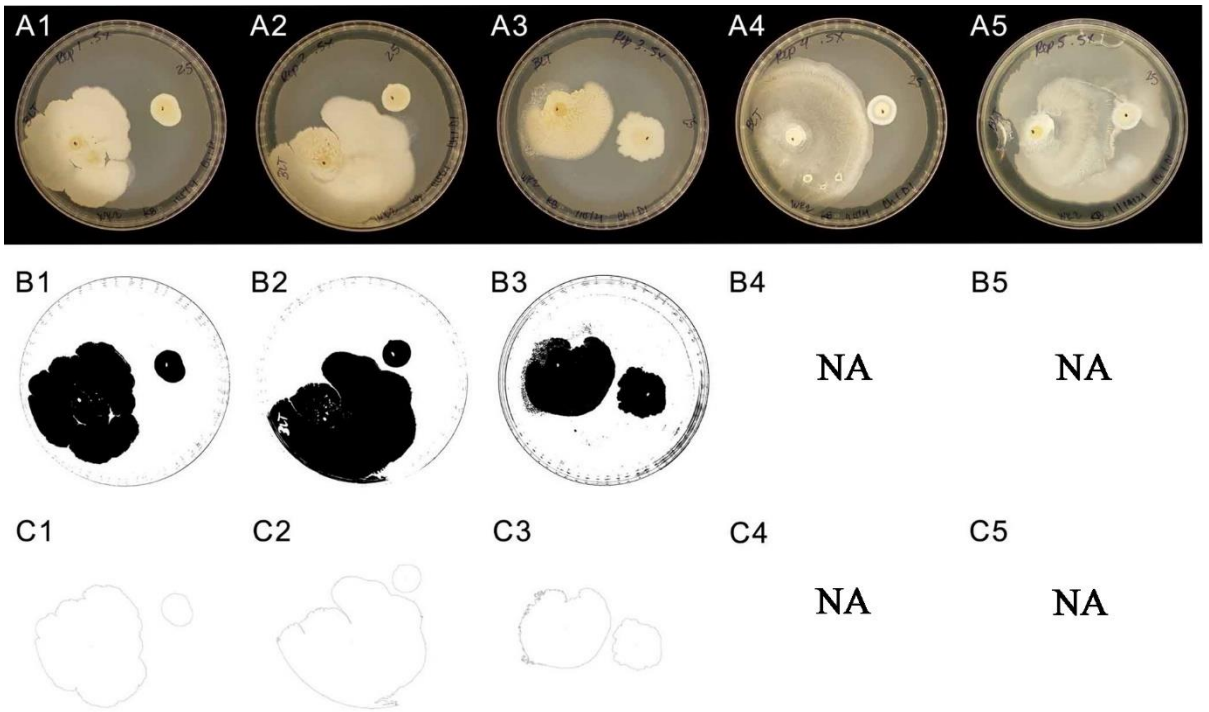


Figure C31. 22021 co-inoculated Petri plates four days after inoculation. **A1-A5)** 0.5x BLT vs. *Pss* 25 on KB media. **B1-B5)** Images after threshold adjustment in ImageJ. **C1-C5)** Image of measured area. A1, B1, C1: Replication 1; A2, B2, C2: Replication 2; A3, B3, C3: Replication 3; A4, B4, C4: Replication 4; A5, B5, C5: Replication 5. Images with NA are not available.

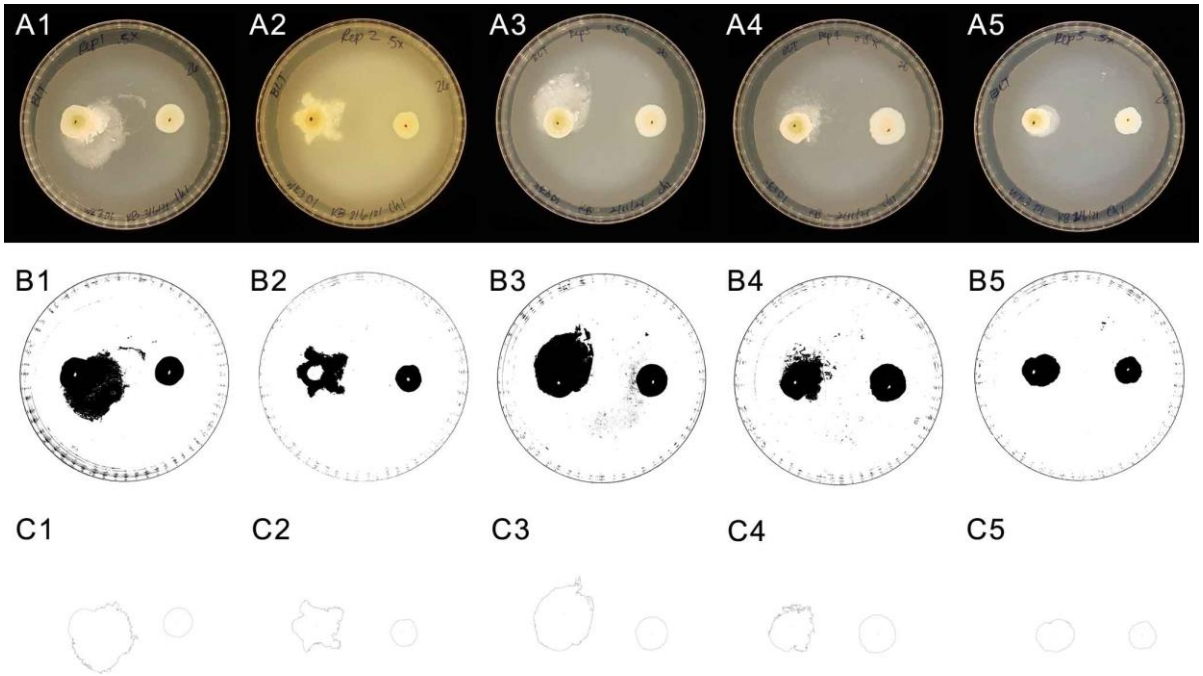


Figure C32. 2021 co-inoculated Petri plates four days after inoculation. **A1-A5)** 0.5x BLT vs. *Pss* 26 on KB media. **B1-B5)** Images after threshold adjustment in ImageJ. **C1-C5)** Image of measured area. A1, B1, C1: Replication 1; A2, B2, C2: Replication 2; A3, B3, C3: Replication 3; A4, B4, C4: Replication 4; A5, B5, C5: Replication 5.

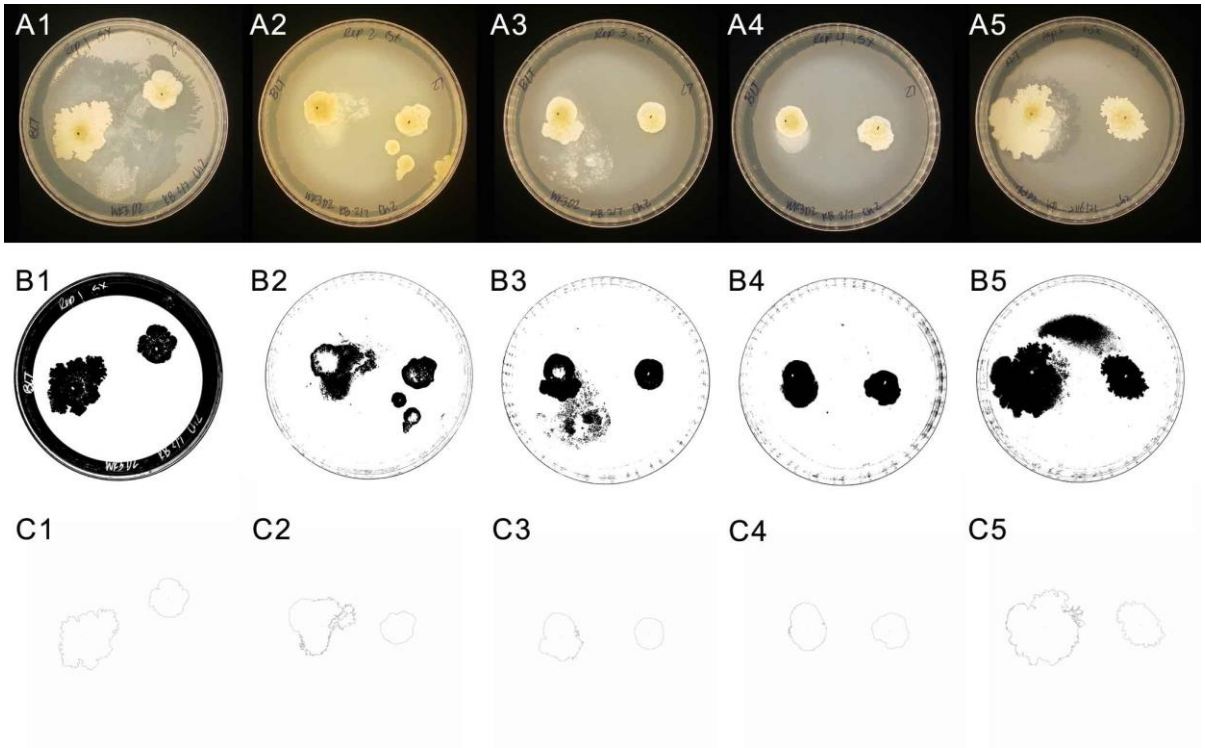


Figure C33. 2021 co-inoculated Petri plates four days after inoculation. **A1-A5)** 0.5x BLT vs. *Pss* 27 on KB media. **B1-B5)** Images after threshold adjustment in ImageJ. **C1-C5)** Image of measured area. A1, B1, C1: Replication 1; A2, B2, C2: Replication 2; A3, B3, C3: Replication 3; A4, B4, C4: Replication 4; A5, B5, C5: Replication 5.

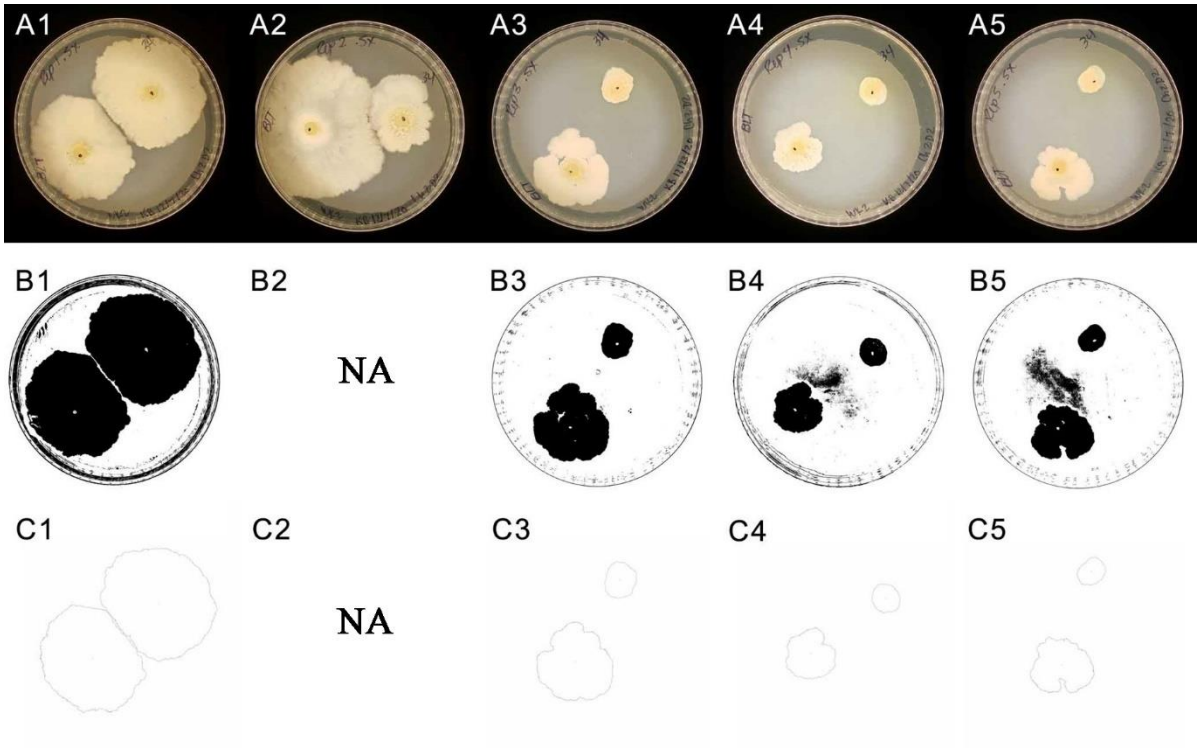


Figure C34. 2021 co-inoculated Petri plates four days after inoculation. **A1-A5)** 0.5x BLT vs. *Pss* 26 on KB media. **B1-B5)** Images after threshold adjustment in ImageJ. **C1-C5)** Image of measured area. A1, B1, C1: Replication 1; A2, B2, C2: Replication 2; A3, B3, C3: Replication 3; A4, B4, C4: Replication 4; A5, B5, C5: Replication 5. Images with NA are not available.

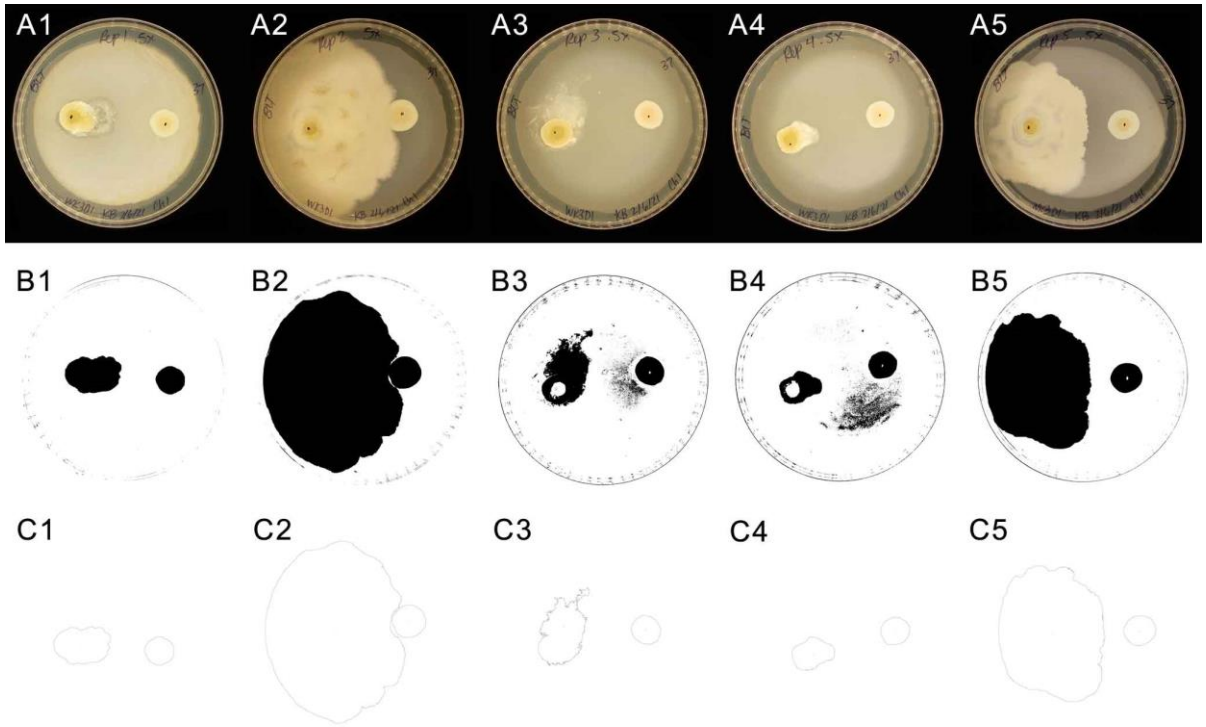


Figure C35. 2021 co-inoculated Petri plates four days after inoculation. **A1-A5)** 0.5x BLT vs. *Pss* 37 on KB media. **B1-B5)** Images after threshold adjustment in ImageJ. **C1-C5)** Image of measured area. A1, B1, C1: Replication 1; A2, B2, C2: Replication 2; A3, B3, C3: Replication 3; A4, B4, C4: Replication 4; A5, B5, C5: Replication 5.

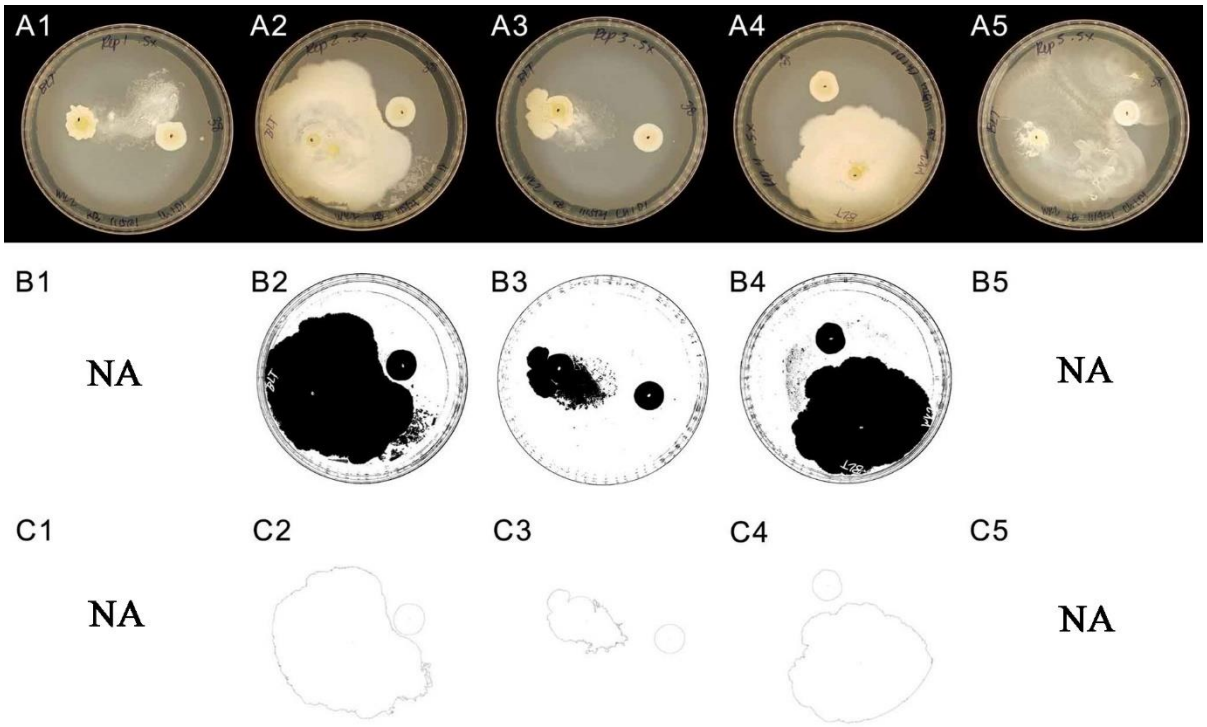


Figure C36. 32021 co-inoculated Petri plates four days after inoculation. **A1-A5)** 0.5x BLT vs. *Pss* 38 on KB media. **B1-B5)** Images after threshold adjustment in ImageJ. **C1-C5)** Image of measured area. A1, B1, C1: Replication 1; A2, B2, C2: Replication 2; A3, B3, C3: Replication 3; A4, B4, C4: Replication 4; A5, B5, C5: Replication 5. Images with NA are not available.

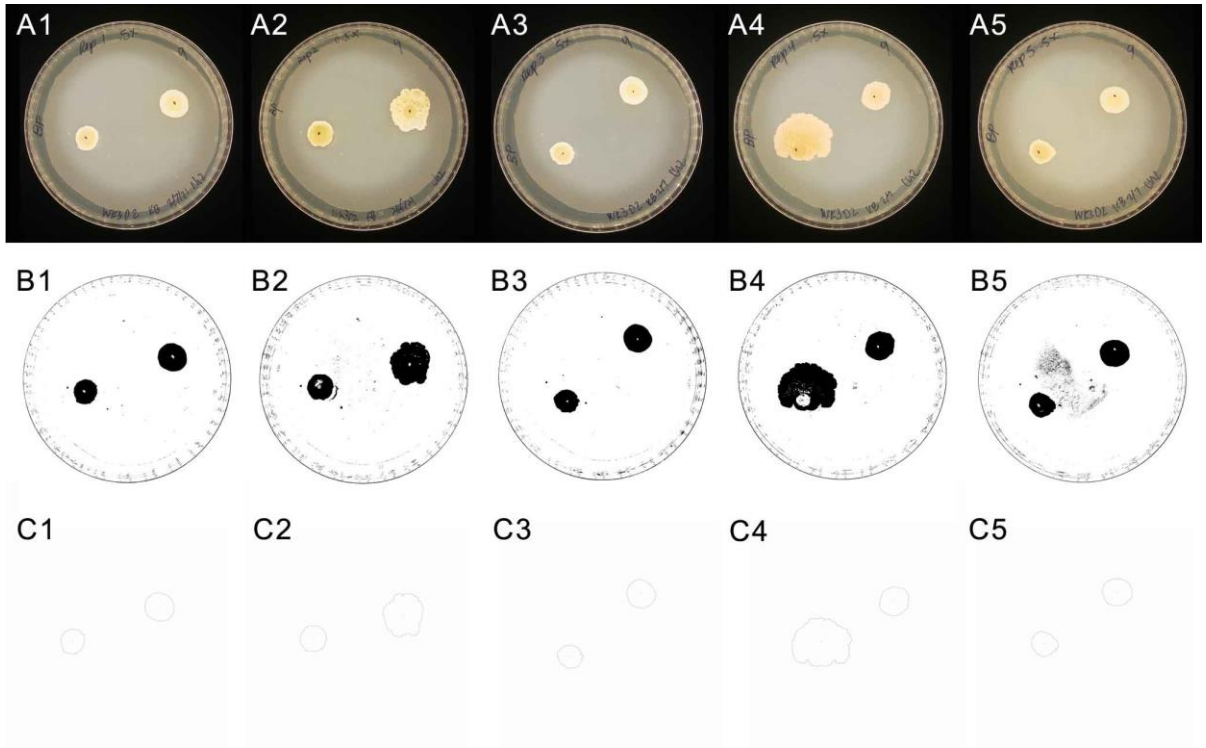


Figure C37. 2021 co-inoculated Petri plates four days after inoculation. **A1-A5)** 0.5x BP vs. *Pss* 9 on KB media. **B1-B5)** Images after threshold adjustment in ImageJ. **C1-C5)** Image of measured area. A1, B1, C1: Replication 1; A2, B2, C2: Replication 2; A3, B3, C3: Replication 3; A4, B4, C4: Replication 4; A5, B5, C5: Replication 5.

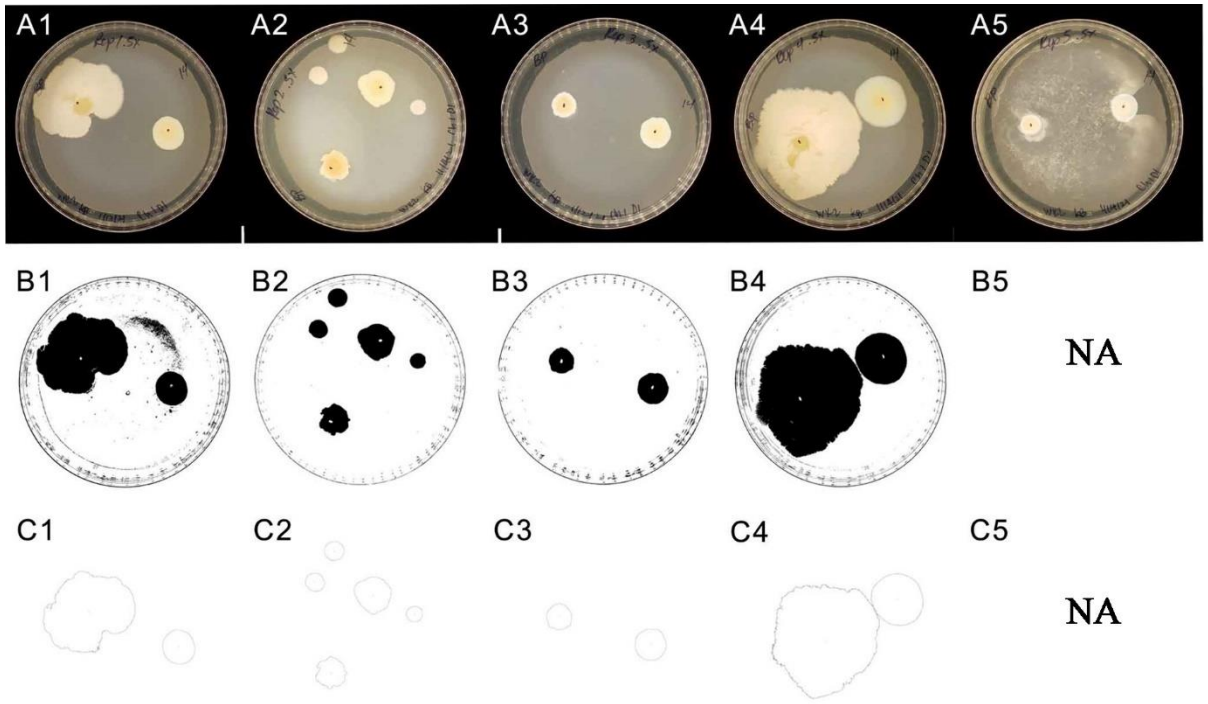


Figure C38. 2021 co-inoculated Petri plates four days after inoculation. **A1-A5)** 0.5x BP vs. *Pss* 14 on KB media. **B1-B5)** Images after threshold adjustment in ImageJ. **C1-C5)** Image of measured area. A1, B1, C1: Replication 1; A2, B2, C2: Replication 2; A3, B3, C3: Replication 3; A4, B4, C4: Replication 4; A5, B5, C5: Replication 5. Images with NA are not available.

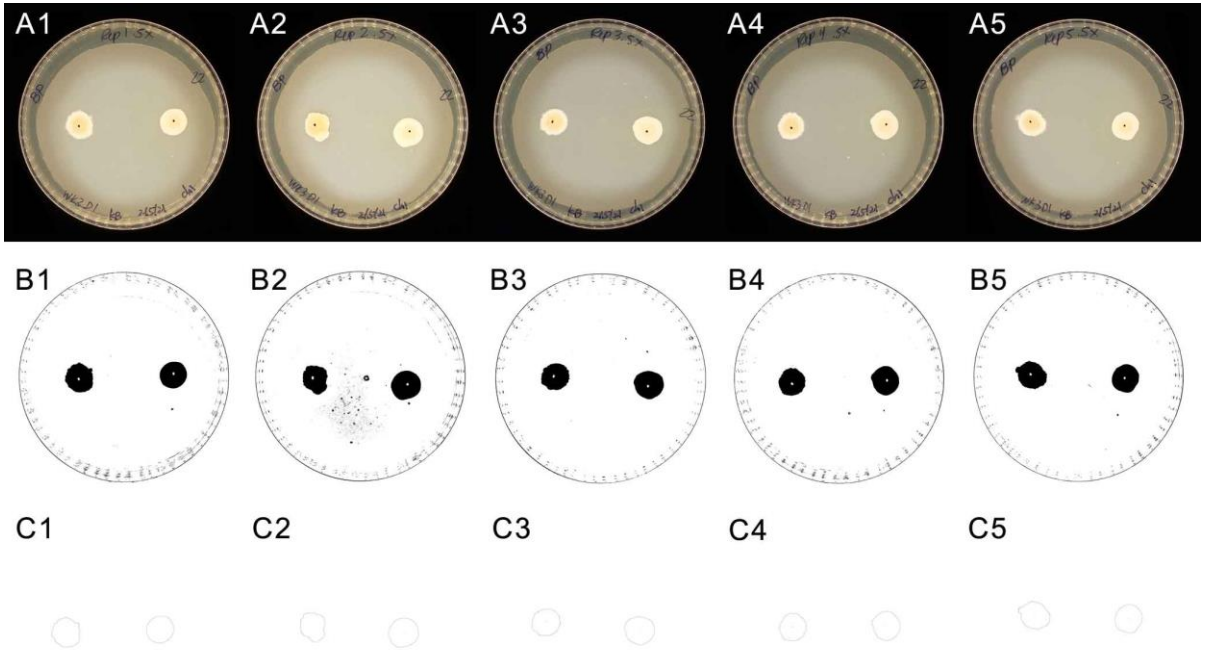


Figure C39. 2021 co-inoculated Petri plates four days after inoculation. **A1-A5)** 0.5x BP vs. *Pss* 22 on KB media. **B1-B5)** Images after threshold adjustment in ImageJ. **C1-C5)** Image of measured area. A1, B1, C1: Replication 1; A2, B2, C2: Replication 2; A3, B3, C3: Replication 3; A4, B4, C4: Replication 4; A5, B5, C5: Replication 5.

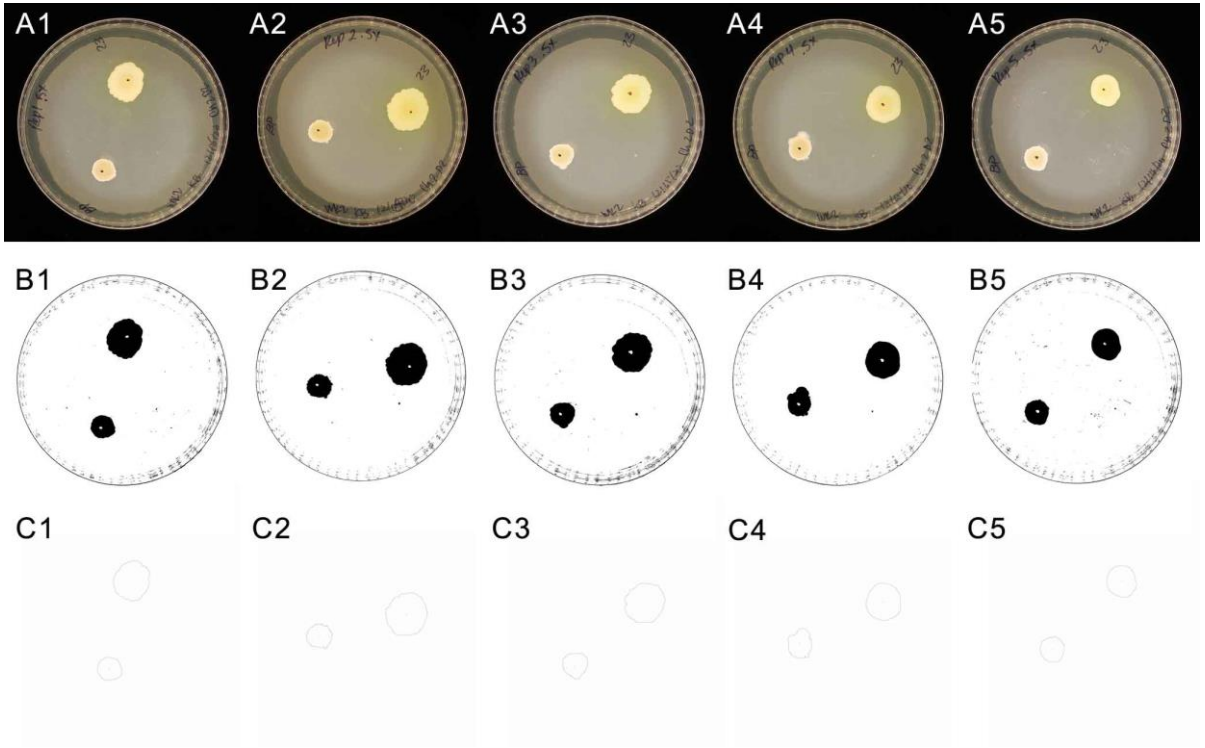


Figure C40. 2021 co-inoculated Petri plates four days after inoculation. **A1-A5)** 0.5x BP vs. *Pss* 23 on KB media. **B1-B5)** Images after threshold adjustment in ImageJ. **C1-C5)** Image of measured area. A1, B1, C1: Replication 1; A2, B2, C2: Replication 2; A3, B3, C3: Replication 3; A4, B4, C4: Replication 4; A5, B5, C5: Replication 5.

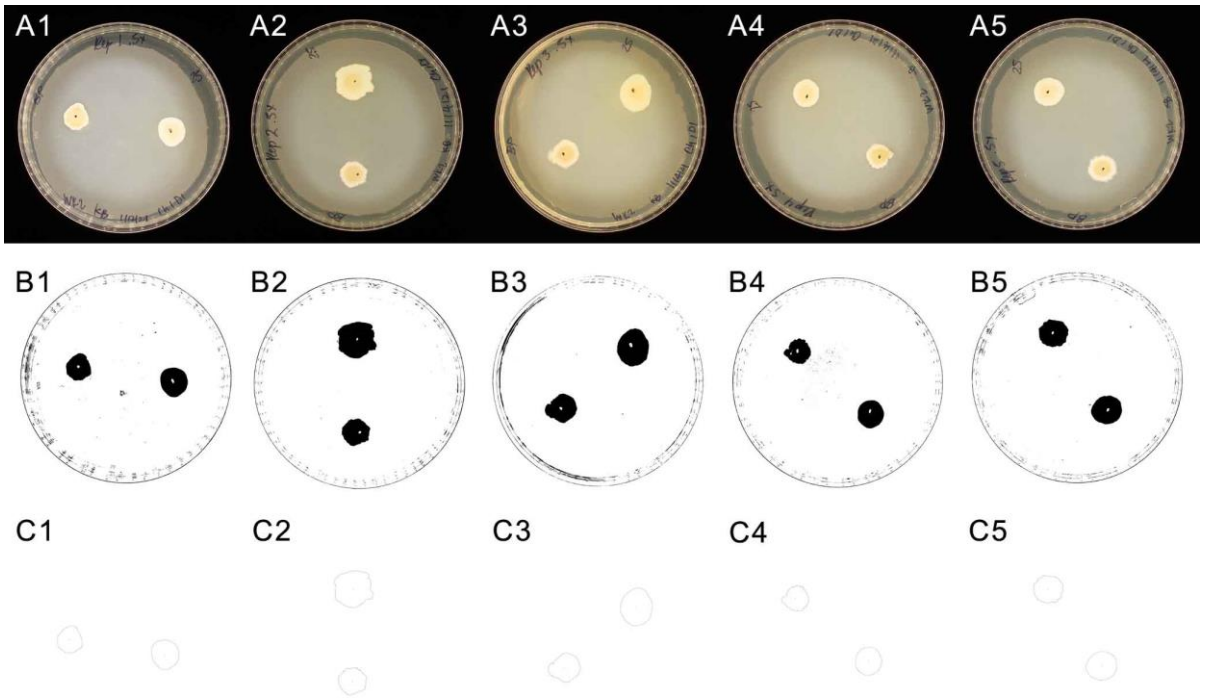


Figure C41. 2021 co-inoculated Petri plates four days after inoculation. **A1-A5)** 0.5x BP vs. *Pss* 25 on KB media. **B1-B5)** Images after threshold adjustment in ImageJ. **C1-C5)** Image of measured area. A1, B1, C1: Replication 1; A2, B2, C2: Replication 2; A3, B3, C3: Replication 3; A4, B4, C4: Replication 4; A5, B5, C5: Replication 5.

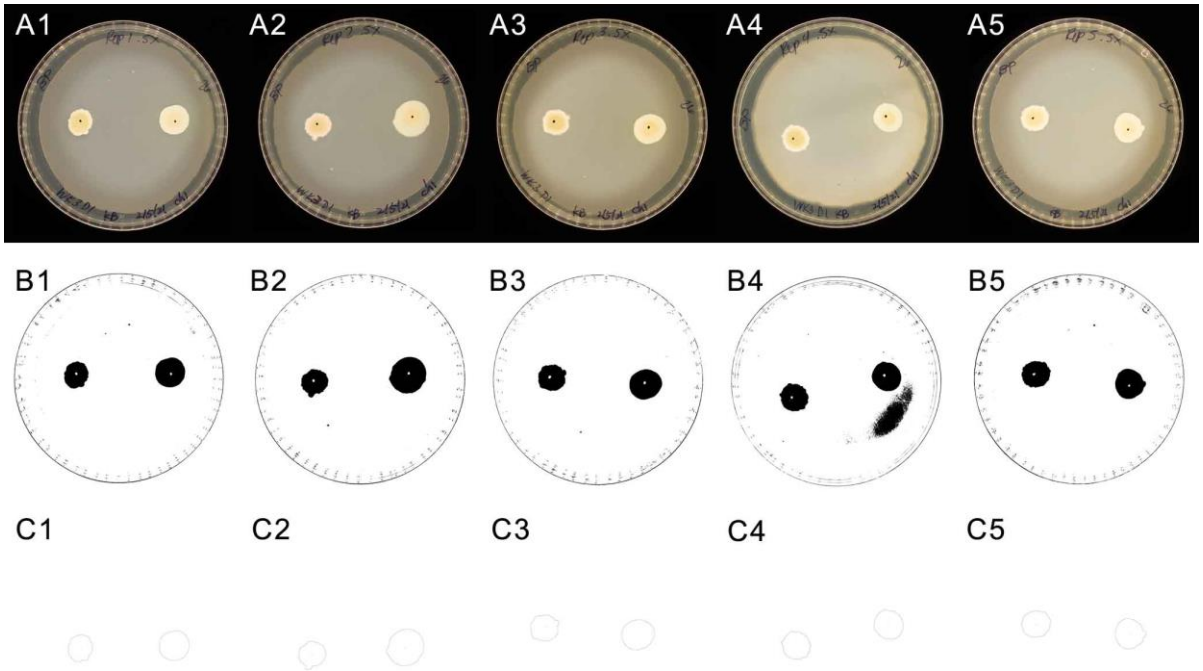


Figure C42. 2021 co-inoculated Petri plates four days after inoculation. **A1-A5)** 0.5x BP vs. *Pss* 26 on KB media. **B1-B5)** Images after threshold adjustment in ImageJ. **C1-C5)** Image of measured area. A1, B1, C1: Replication 1; A2, B2, C2: Replication 2; A3, B3, C3: Replication 3; A4, B4, C4: Replication 4; A5, B5, C5: Replication 5.

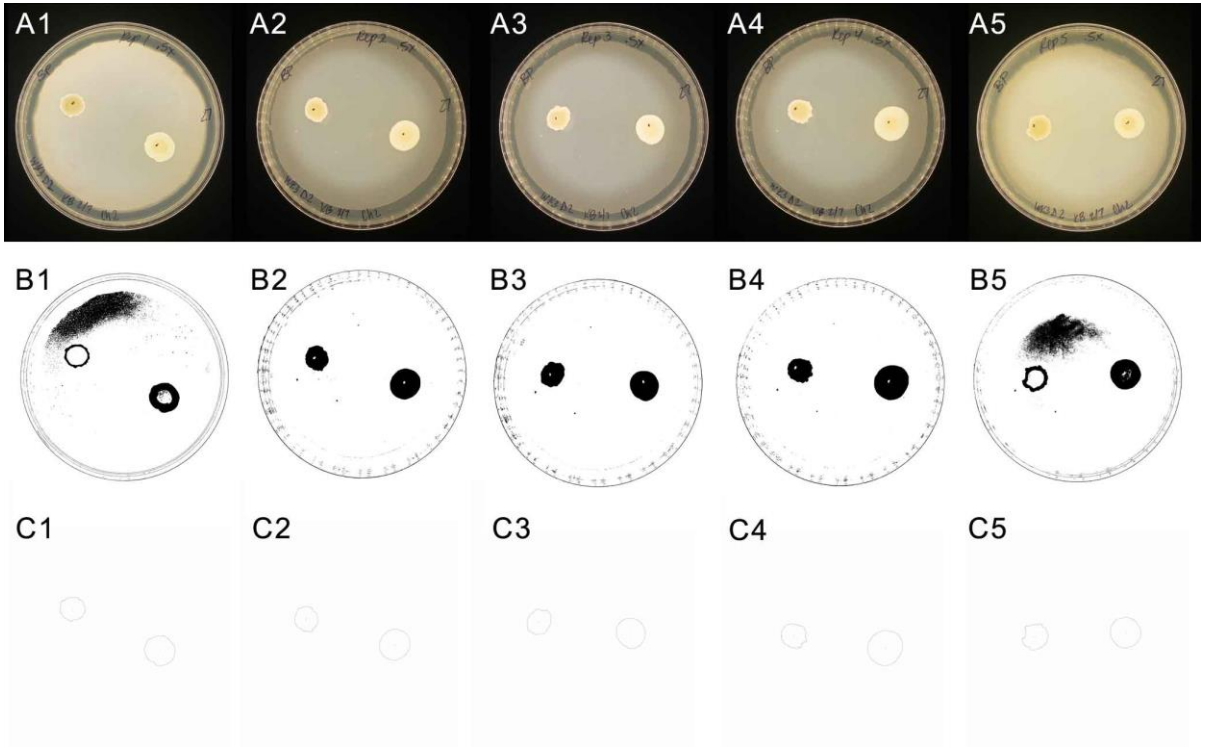


Figure C43. 2021 co-inoculated Petri plates four days after inoculation. **A1-A5)** 0.5x BP vs. *Pss* 27 on KB media. **B1-B5)** Images after threshold adjustment in ImageJ. **C1-C5)** Image of measured area. A1, B1, C1: Replication 1; A2, B2, C2: Replication 2; A3, B3, C3: Replication 3; A4, B4, C4: Replication 4; A5, B5, C5: Replication 5.

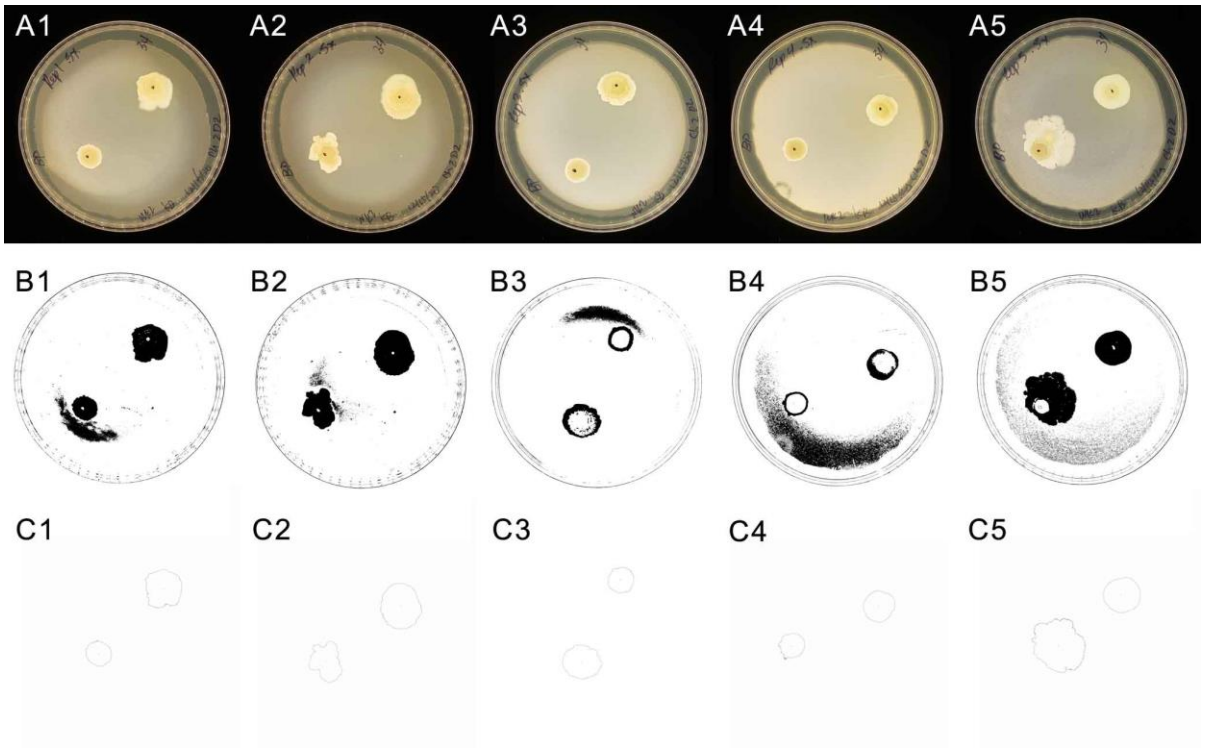


Figure C44. 2021 co-inoculated Petri plates four days after inoculation. **A1-A5)** 0.5x BP vs. *Pss* 34 on KB media. **B1-B5)** Images after threshold adjustment in ImageJ. **C1-C5)** Image of measured area. A1, B1, C1: Replication 1; A2, B2, C2: Replication 2; A3, B3, C3: Replication 3; A4, B4, C4: Replication 4; A5, B5, C5: Replication 5.

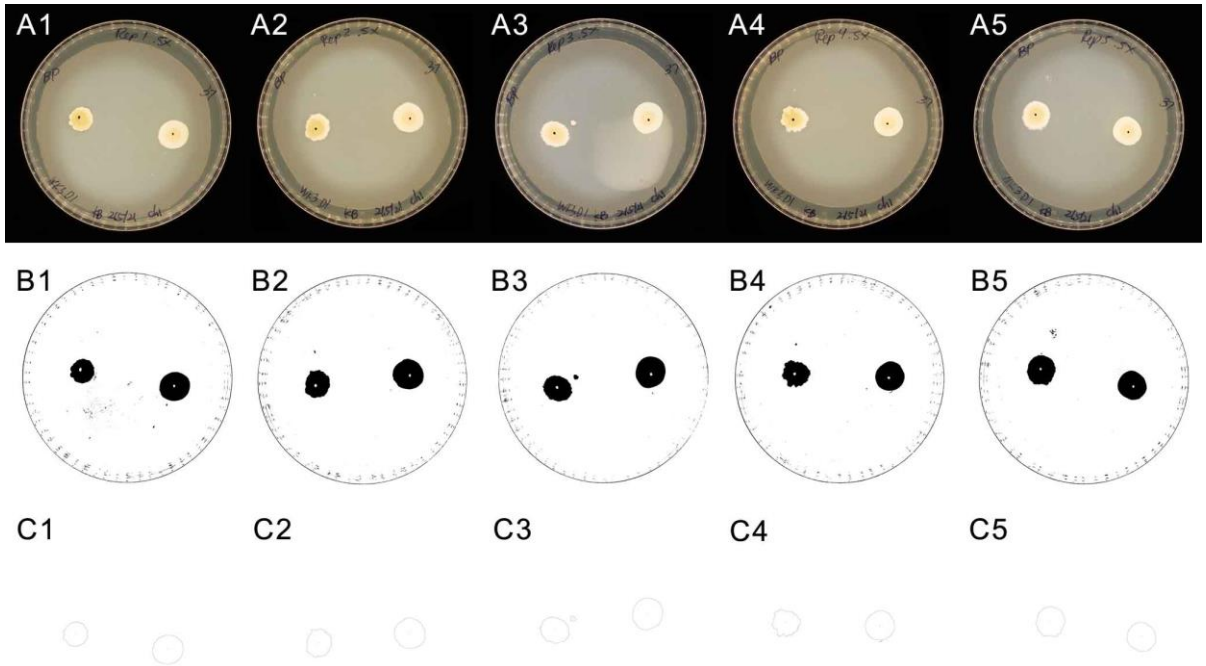


Figure C45. 2021 co-inoculated Petri plates four days after inoculation. **A1-A5)** 0.5x BP vs. *Pss* 37 on KB media. **B1-B5)** Images after threshold adjustment in ImageJ. **C1-C5)** Image of measured area. A1, B1, C1: Replication 1; A2, B2, C2: Replication 2; A3, B3, C3: Replication 3; A4, B4, C4: Replication 4; A5, B5, C5: Replication 5.

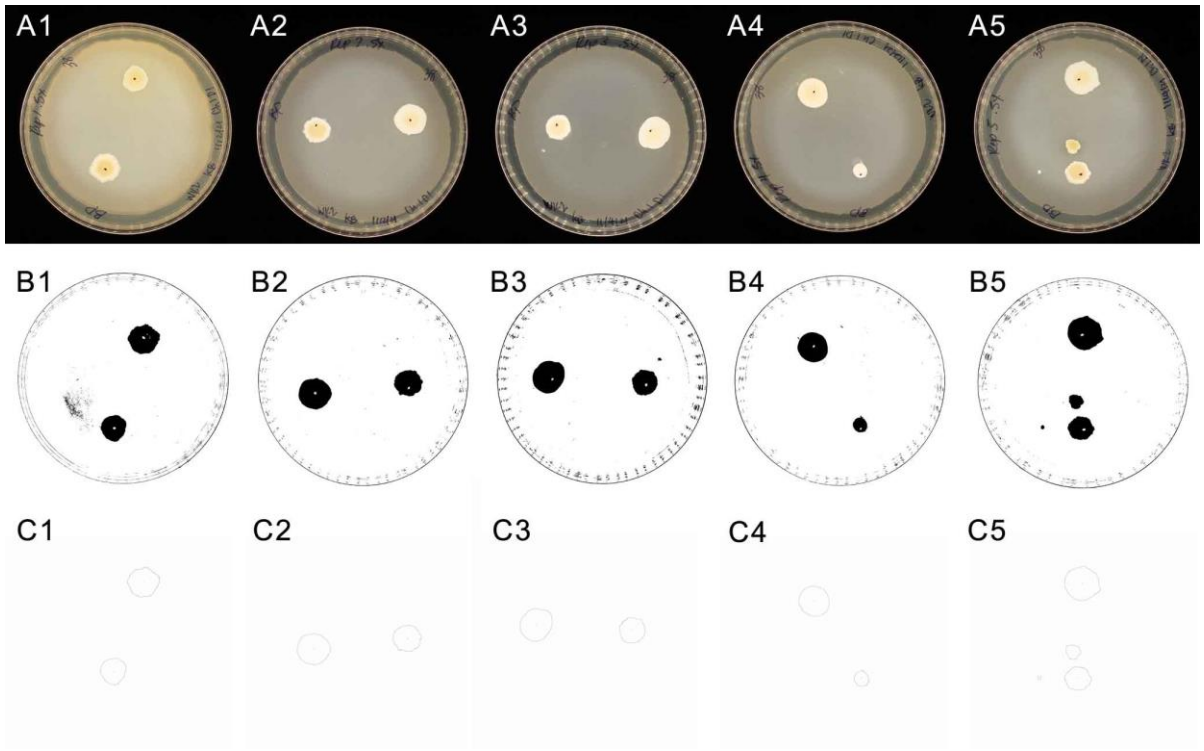


Figure C46. 2021 co-inoculated Petri plates four days after inoculation. **A1-A5)** 0.5x BP vs. *Pss* 38 on KB media. **B1-B5)** Images after threshold adjustment in ImageJ. **C1-C5)** Image of measured area. A1, B1, C1: Replication 1; A2, B2, C2: Replication 2; A3, B3, C3: Replication 3; A4, B4, C4: Replication 4; A5, B5, C5: Replication 5.

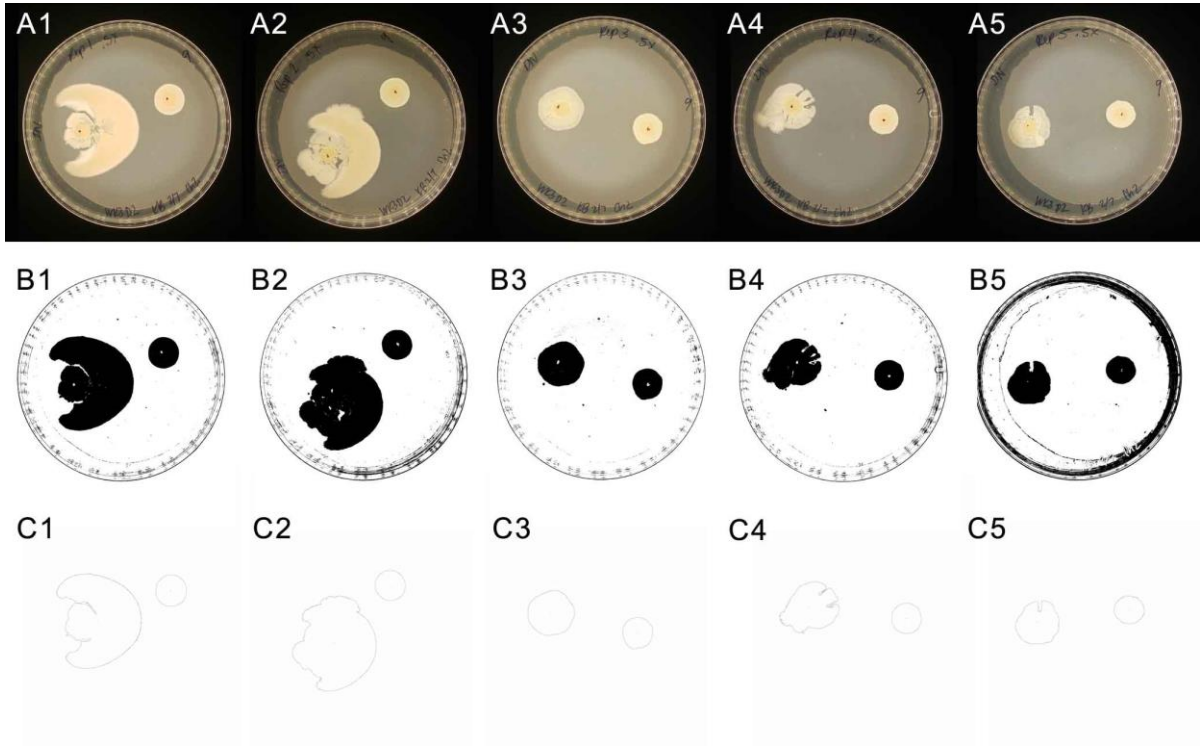


Figure C47. 2021 co-inoculated Petri plates four days after inoculation. **A1-A5)** 0.5x DN vs. *Pss* 9 on KB media. **B1-B5)** Images after threshold adjustment in ImageJ. **C1-C5)** Image of measured area. A1, B1, C1: Replication 1; A2, B2, C2: Replication 2; A3, B3, C3: Replication 3; A4, B4, C4: Replication 4; A5, B5, C5: Replication 5.

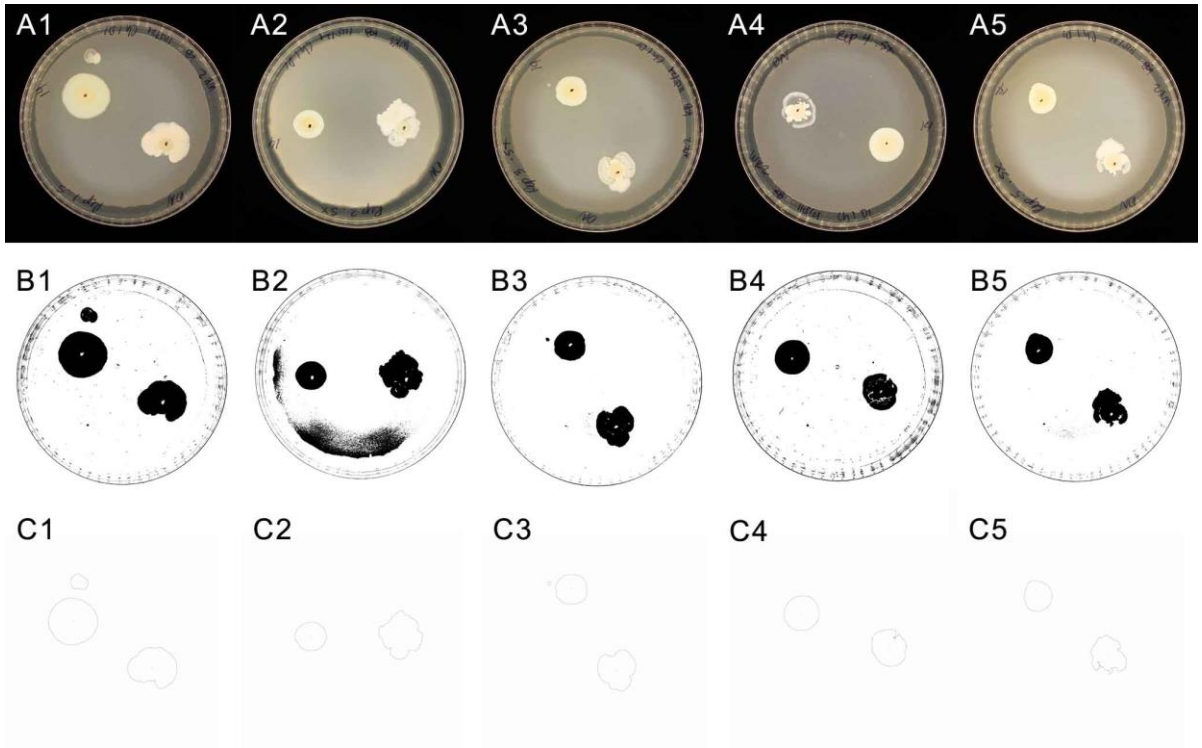


Figure C48. 2021 co-inoculated Petri plates four days after inoculation. **A1-A5)** 0.5x DN vs. *Pss* 14 on KB media. **B1-B5)** Images after threshold adjustment in ImageJ. **C1-C5)** Image of measured area. A1, B1, C1: Replication 1; A2, B2, C2: Replication 2; A3, B3, C3: Replication 3; A4, B4, C4: Replication 4; A5, B5, C5: Replication 5.

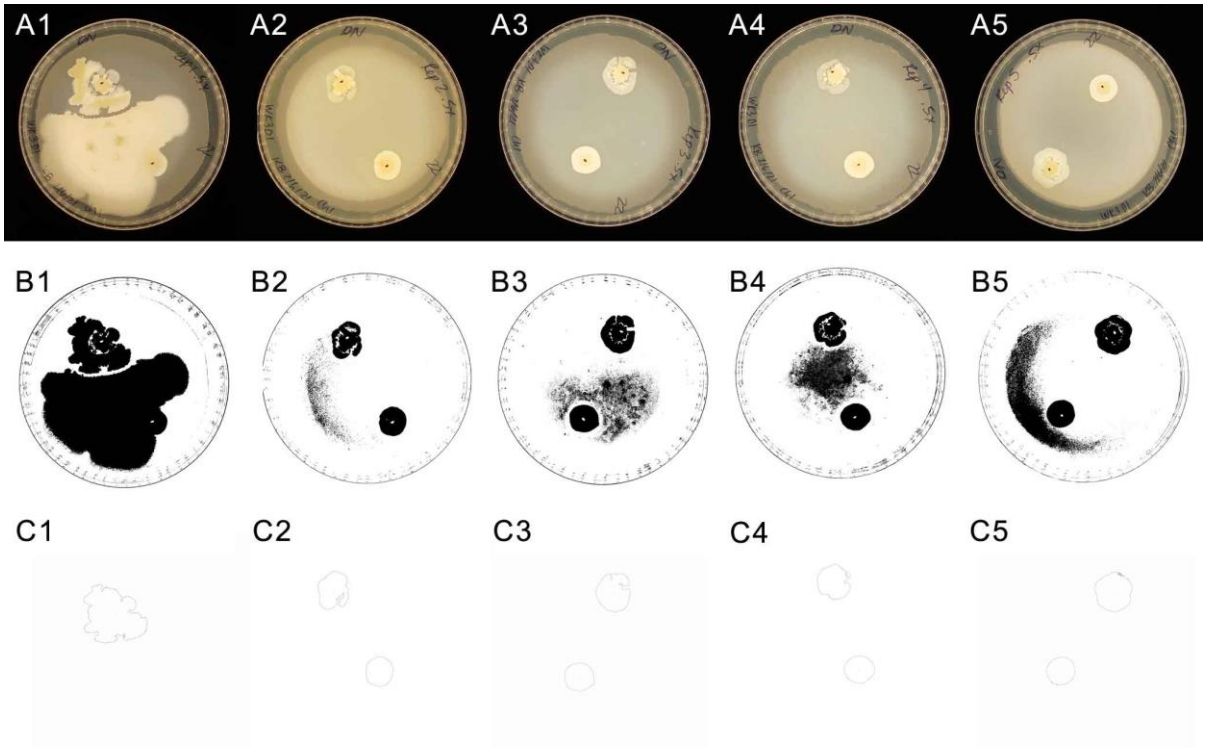


Figure C49. 2021 co-inoculated Petri plates four days after inoculation. **A1-A5)** 0.5x DN vs. *Pss* 22 on KB media. **B1-B5)** Images after threshold adjustment in ImageJ. **C1-C5)** Image of measured area. A1, B1, C1: Replication 1; A2, B2, C2: Replication 2; A3, B3, C3: Replication 3; A4, B4, C4: Replication 4; A5, B5, C5: Replication 5.

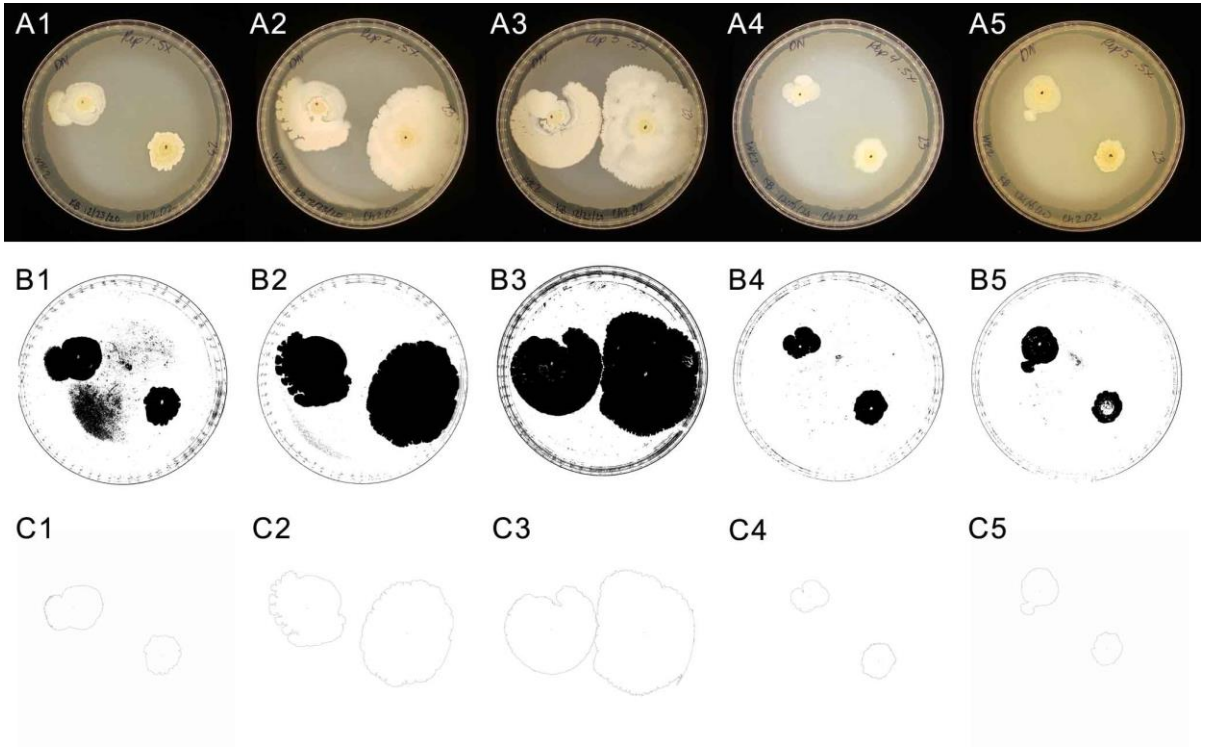


Figure C50. 2021 co-inoculated Petri plates four days after inoculation. **A1-A5)** 0.5x DN vs. *Pss* 23 on KB media. **B1-B5)** Images after threshold adjustment in ImageJ. **C1-C5)** Image of measured area. A1, B1, C1: Replication 1; A2, B2, C2: Replication 2; A3, B3, C3: Replication 3; A4, B4, C4: Replication 4; A5, B5, C5: Replication 5.

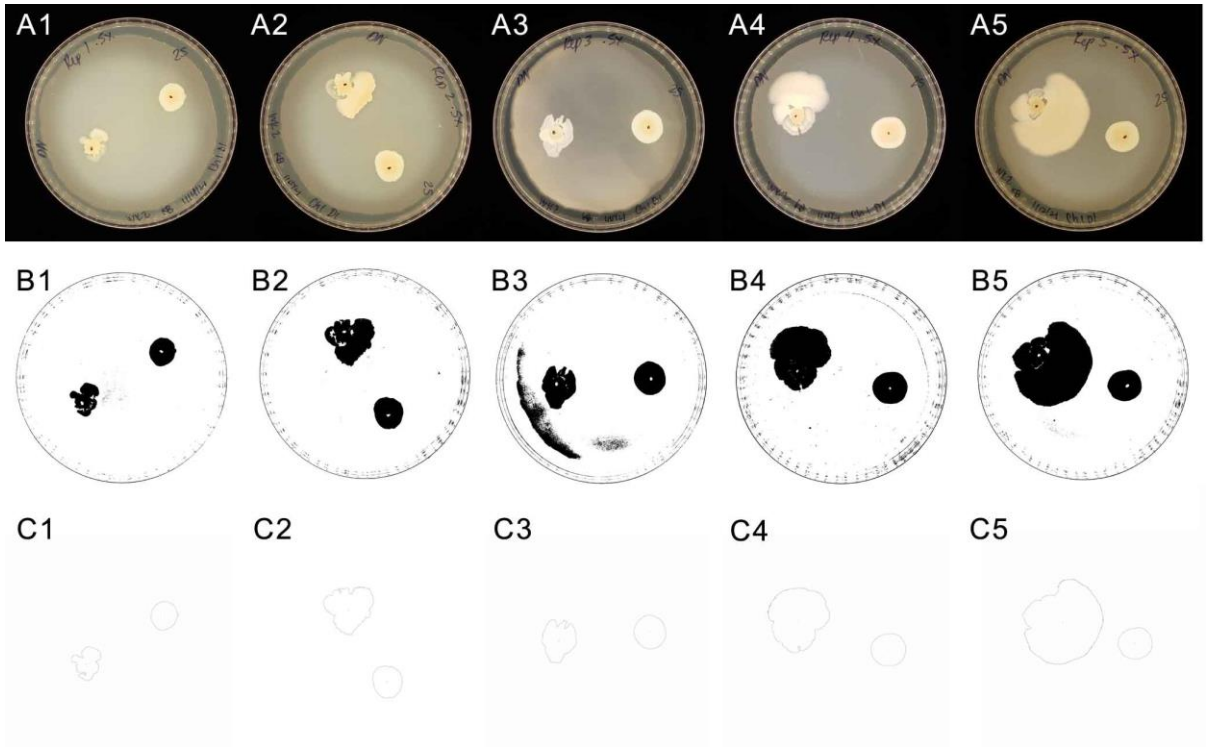


Figure C51. 2021 co-inoculated Petri plates four days after inoculation. **A1-A5)** 0.5x DN vs. *Pss* 25 on KB media. **B1-B5)** Images after threshold adjustment in ImageJ. **C1-C5)** Image of measured area. A1, B1, C1: Replication 1; A2, B2, C2: Replication 2; A3, B3, C3: Replication 3; A4, B4, C4: Replication 4; A5, B5, C5: Replication 5.

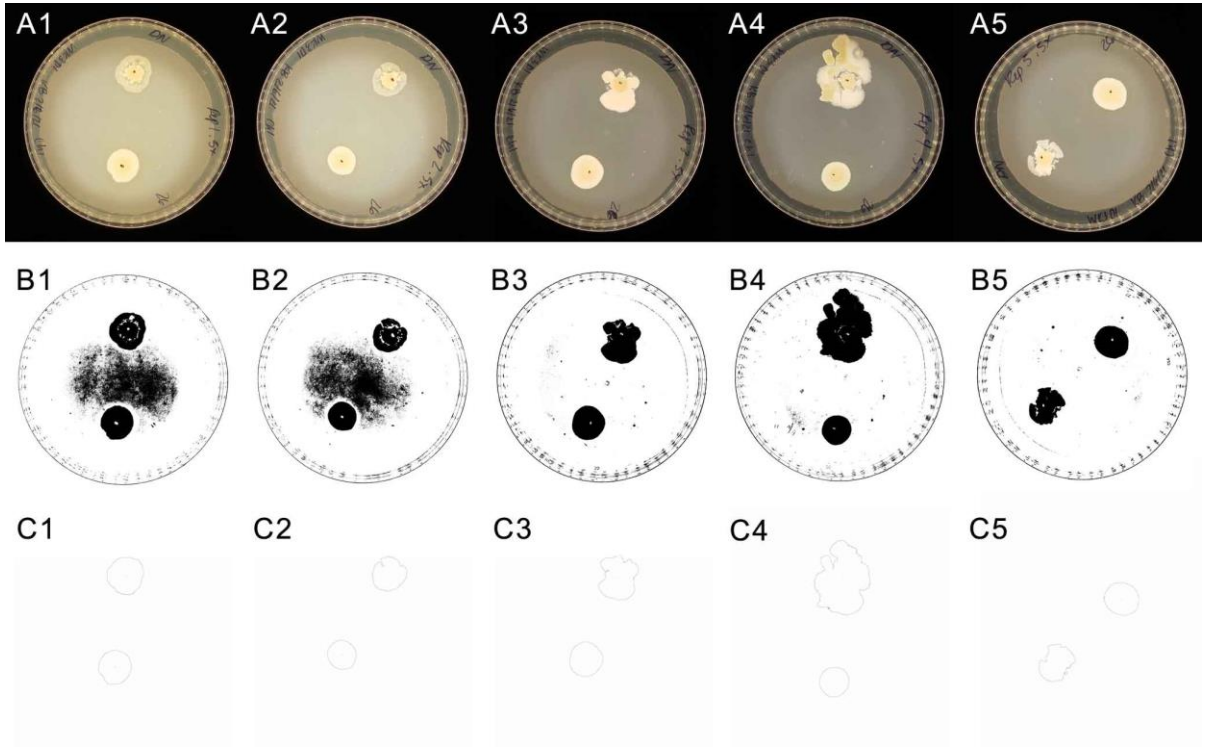


Figure C52. 2021 co-inoculated Petri plates four days after inoculation. **A1-A5)** 0.5x DN vs. *Pss* 26 on KB media. **B1-B5)** Images after threshold adjustment in ImageJ. **C1-C5)** Image of measured area. A1, B1, C1: Replication 1; A2, B2, C2: Replication 2; A3, B3, C3: Replication 3; A4, B4, C4: Replication 4; A5, B5, C5: Replication 5.

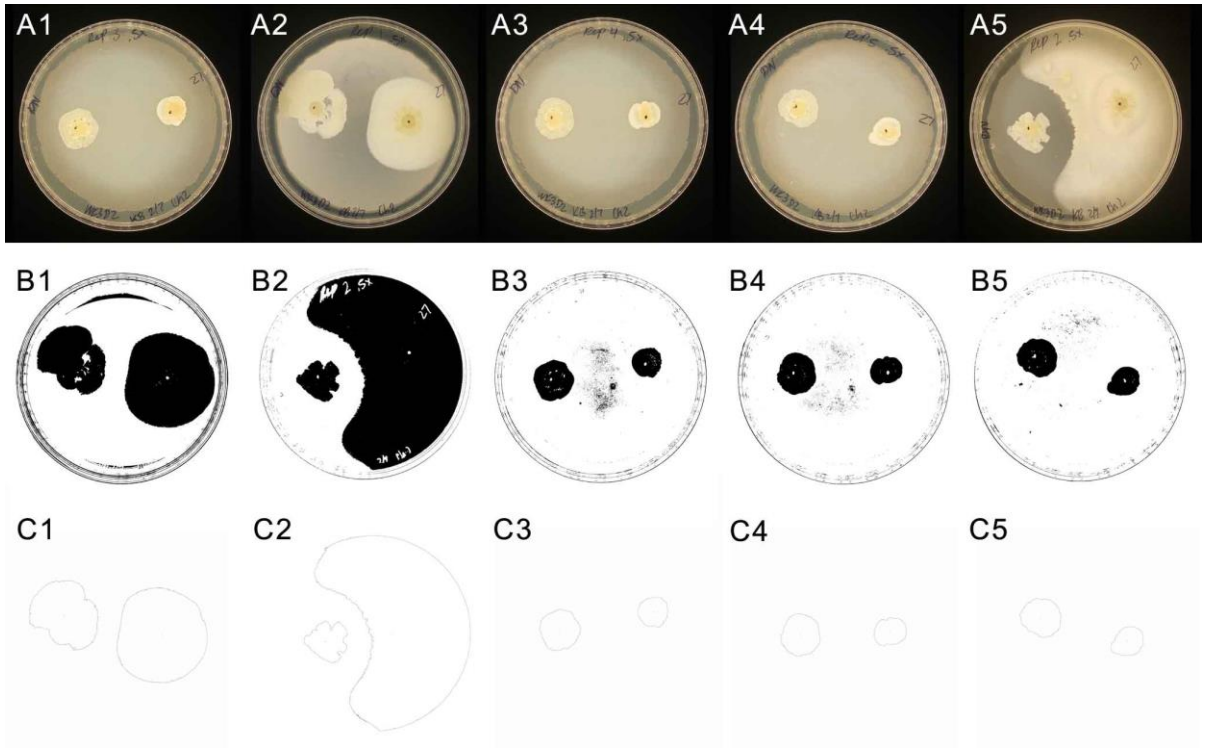


Figure C53. 2021 co-inoculated Petri plates four days after inoculation. **A1-A5)** 0.5x DN vs. *Pss* 27 on KB media. **B1-B5)** Images after threshold adjustment in ImageJ. **C1-C5)** Image of measured area. A1, B1, C1: Replication 1; A2, B2, C2: Replication 2; A3, B3, C3: Replication 3; A4, B4, C4: Replication 4; A5, B5, C5: Replication 5.

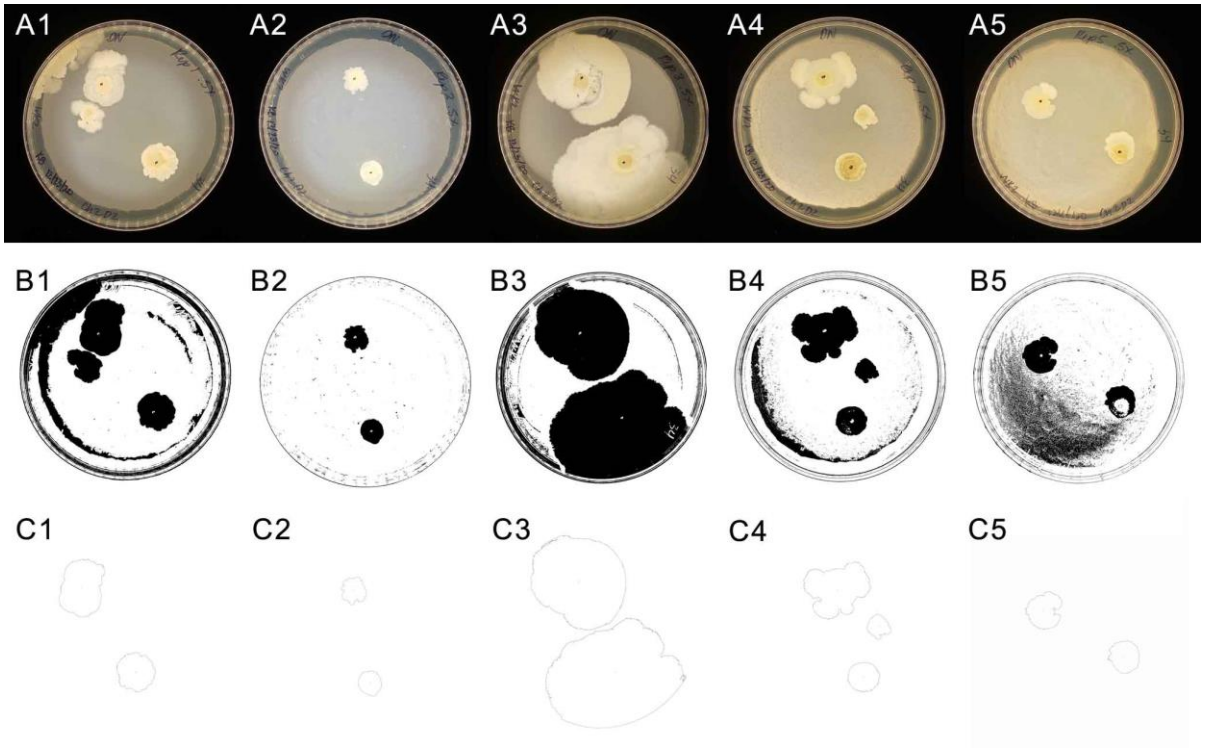


Figure C54. 2021 co-inoculated Petri plates four days after inoculation. **A1-A5)** 0.5x DN vs. *Pss* 34 on KB media. **B1-B5)** Images after threshold adjustment in ImageJ. **C1-C5)** Image of measured area. A1, B1, C1: Replication 1; A2, B2, C2: Replication 2; A3, B3, C3: Replication 3; A4, B4, C4: Replication 4; A5, B5, C5: Replication 5.

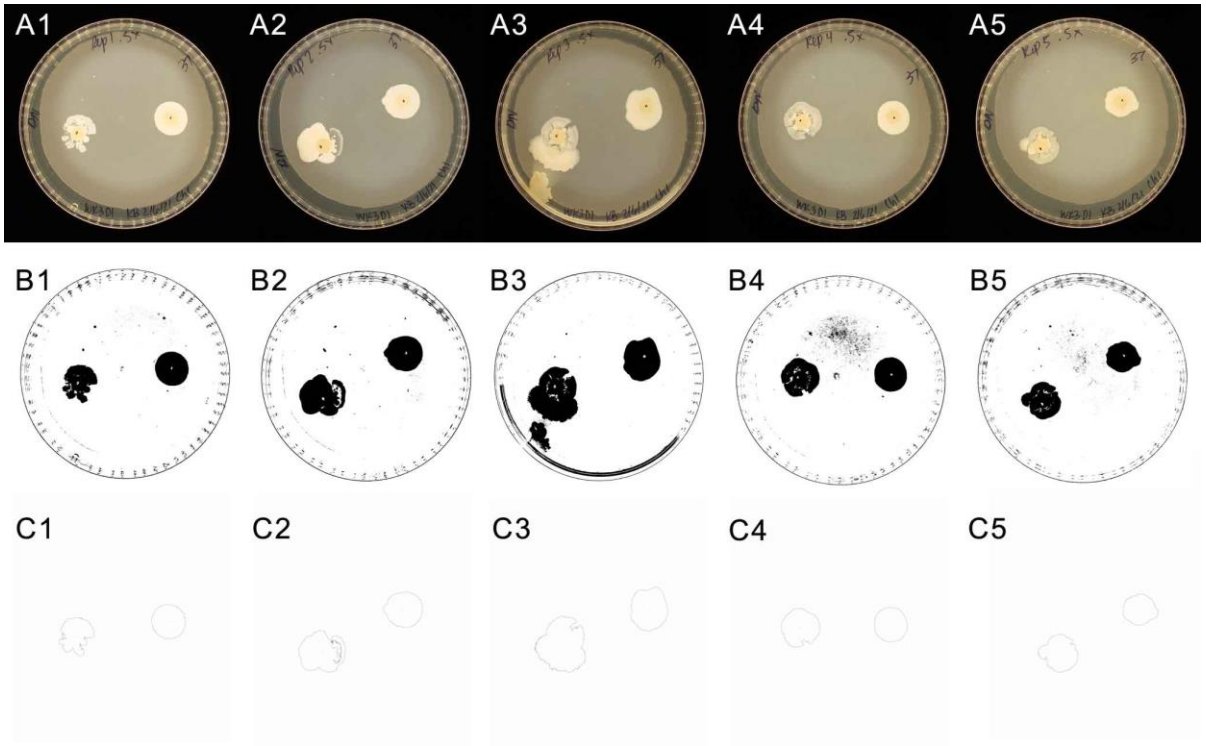


Figure C55. 2021 co-inoculated Petri plates four days after inoculation. **A1-A5)** 0.5x DN vs. *Pss* 37 on KB media. **B1-B5)** Images after threshold adjustment in ImageJ. **C1-C5)** Image of measured area. A1, B1, C1: Replication 1; A2, B2, C2: Replication 2; A3, B3, C3: Replication 3; A4, B4, C4: Replication 4; A5, B5, C5: Replication 5.

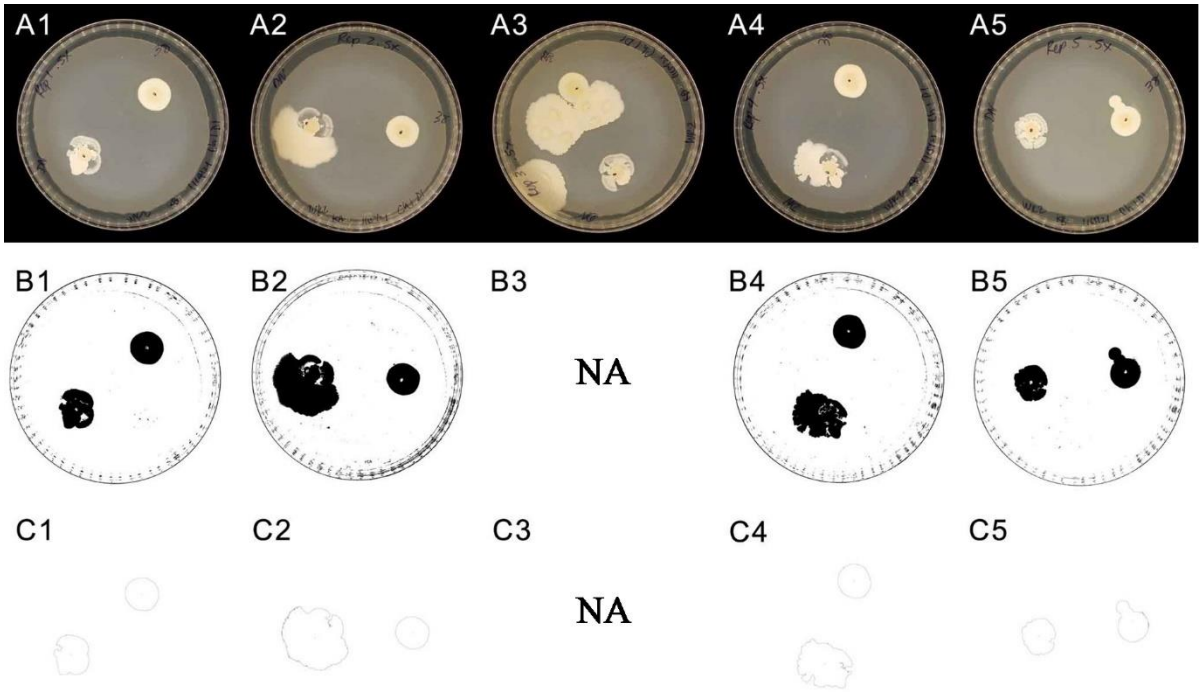


Figure C56. 2021 co-inoculated Petri plates four days after inoculation. **A1-A5)** 0.5x DN vs. *Pss* 38 on KB media. **B1-B5)** Images after threshold adjustment in ImageJ. **C1-C5)** Image of measured area. A1, B1, C1: Replication 1; A2, B2, C2: Replication 2; A3, B3, C3: Replication 3; A4, B4, C4: Replication 4; A5, B5, C5: Replication 5. Images with NA are not available.

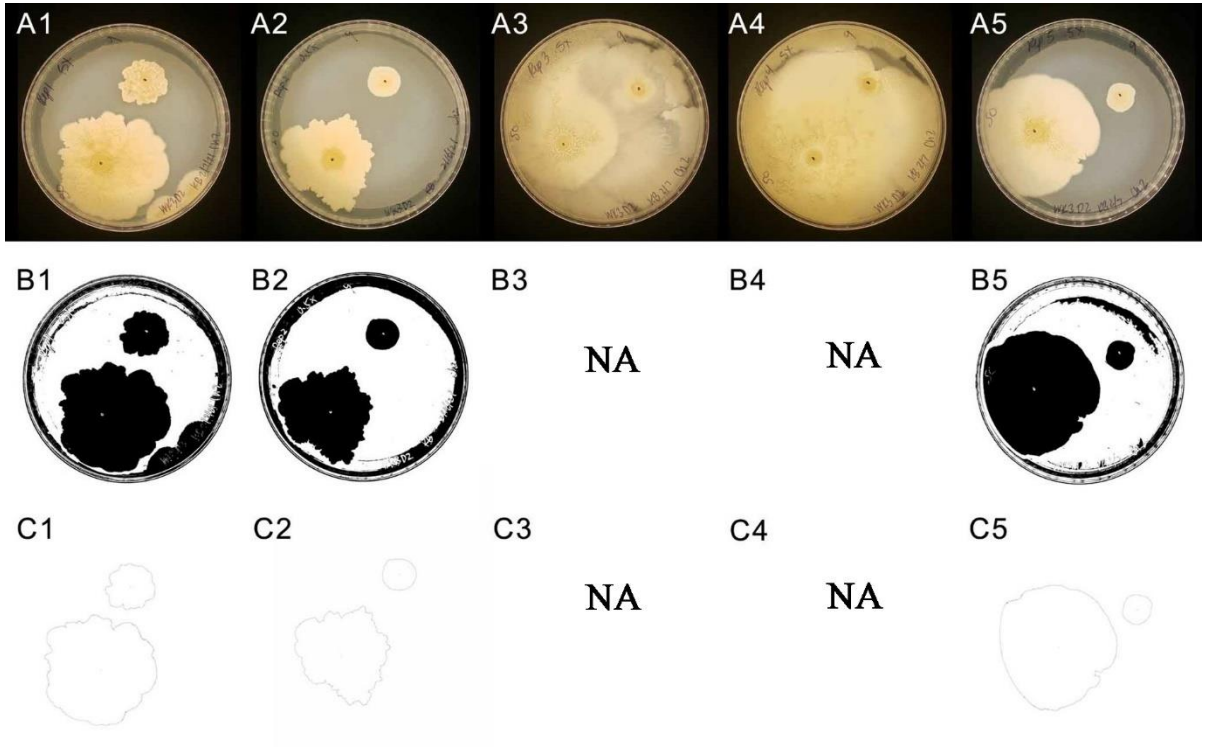


Figure C57. 2021 co-inoculated Petri plates four days after inoculation. **A1-A5)** 0.5x SO vs. *Pss* 9 on KB media. **B1-B5)** Images after threshold adjustment in ImageJ. **C1-C5)** Image of measured area. A1, B1, C1: Replication 1; A2, B2, C2: Replication 2; A3, B3, C3: Replication 3; A4, B4, C4: Replication 4; A5, B5, C5: Replication 5. Images with NA are not available.

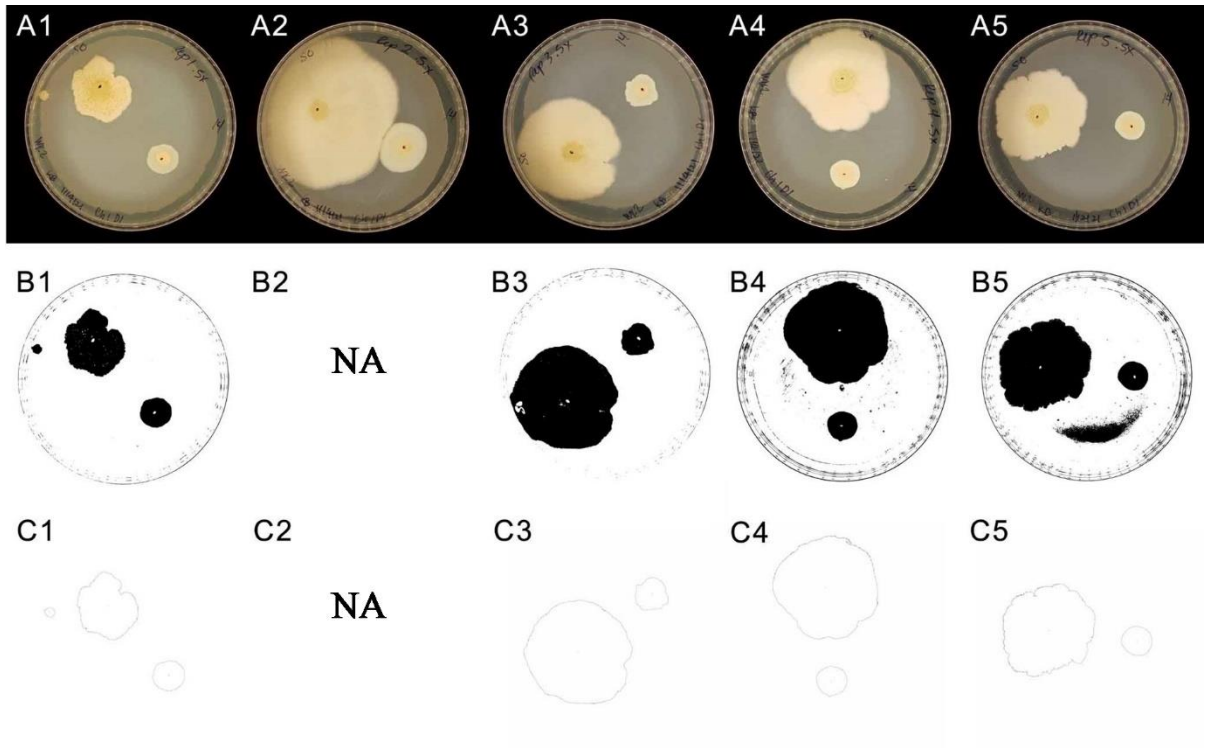


Figure C58. 2021 co-inoculated Petri plates four days after inoculation. **A1-A5)** 0.5x SO vs. *Pss* 14 on KB media. **B1-B5)** Images after threshold adjustment in ImageJ. **C1-C5)** Image of measured area. A1, B1, C1: Replication 1; A2, B2, C2: Replication 2; A3, B3, C3: Replication 3; A4, B4, C4: Replication 4; A5, B5, C5: Replication 5. Images with NA are not available.

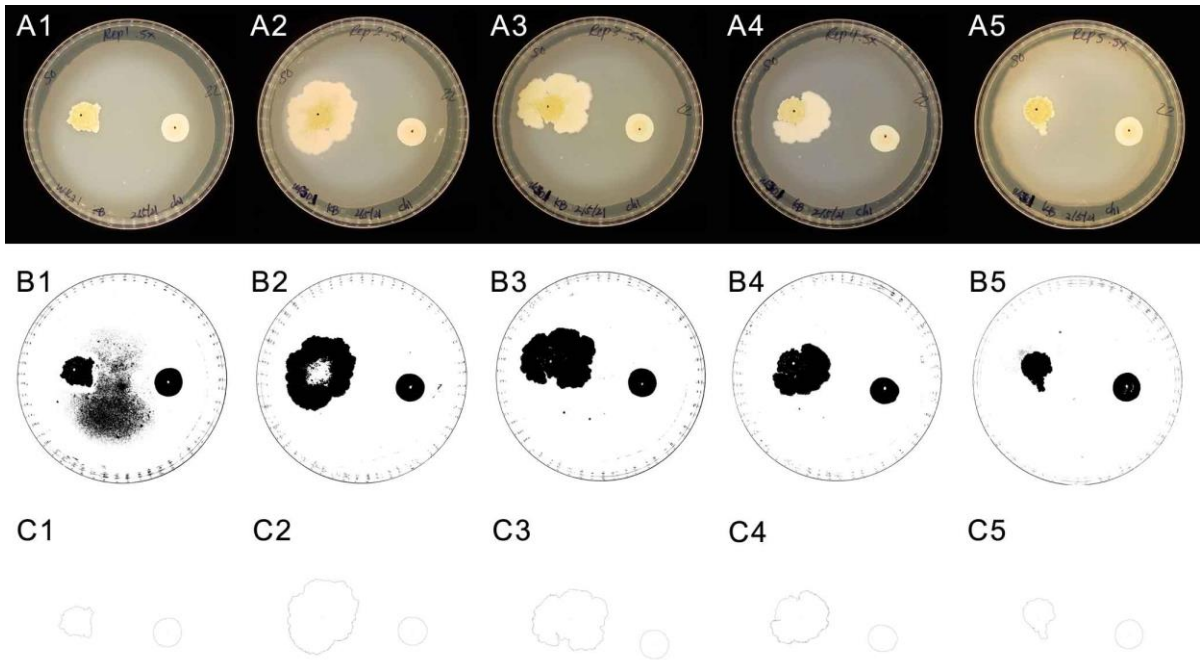


Figure C59. 2021 co-inoculated Petri plates four days after inoculation. **A1-A5)** 0.5x SO vs. *Pss* 22 on KB media. **B1-B5)** Images after threshold adjustment in ImageJ. **C1-C5)** Image of measured area. A1, B1, C1: Replication 1; A2, B2, C2: Replication 2; A3, B3, C3: Replication 3; A4, B4, C4: Replication 4; A5, B5, C5: Replication 5.

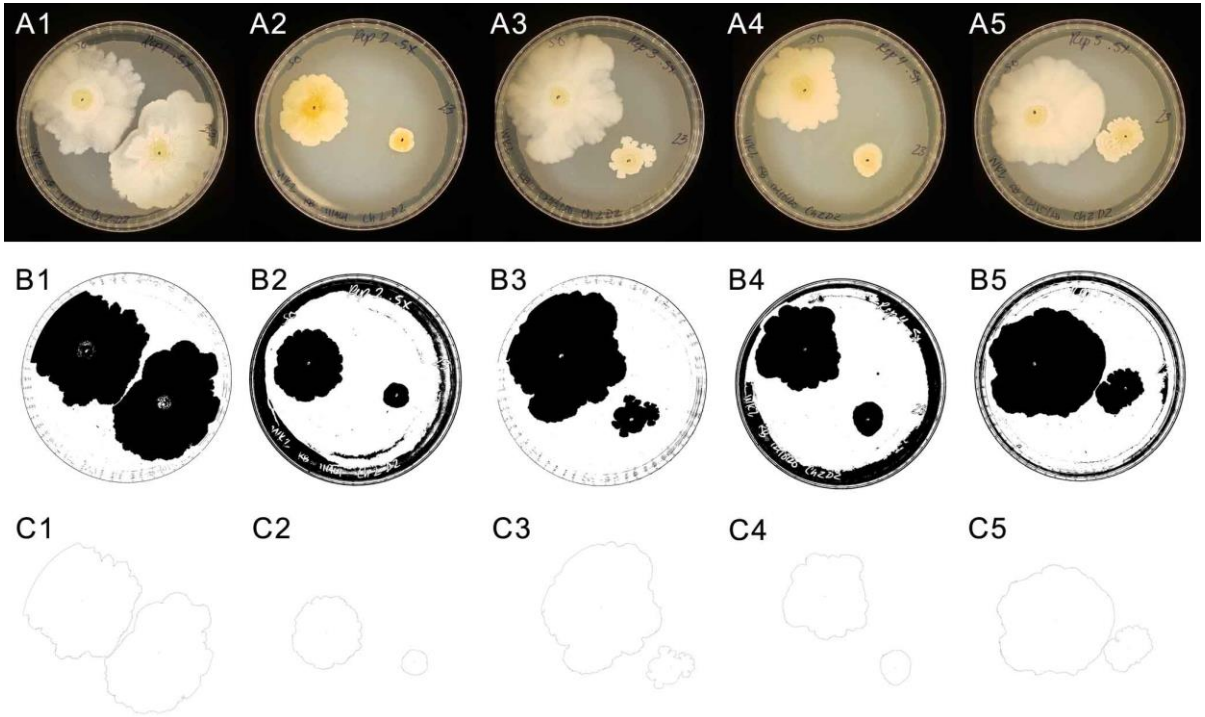


Figure C60. 2021 co-inoculated Petri plates four days after inoculation. **A1-A5)** 0.5x SO vs. *Pss* 9 on KB media. **B1-B5)** Images after threshold adjustment in ImageJ. **C1-C5)** Image of measured area. A1, B1, C1: Replication 1; A2, B2, C2: Replication 2; A3, B3, C3: Replication 3; A4, B4, C4: Replication 4; A5, B5, C5: Replication 5.

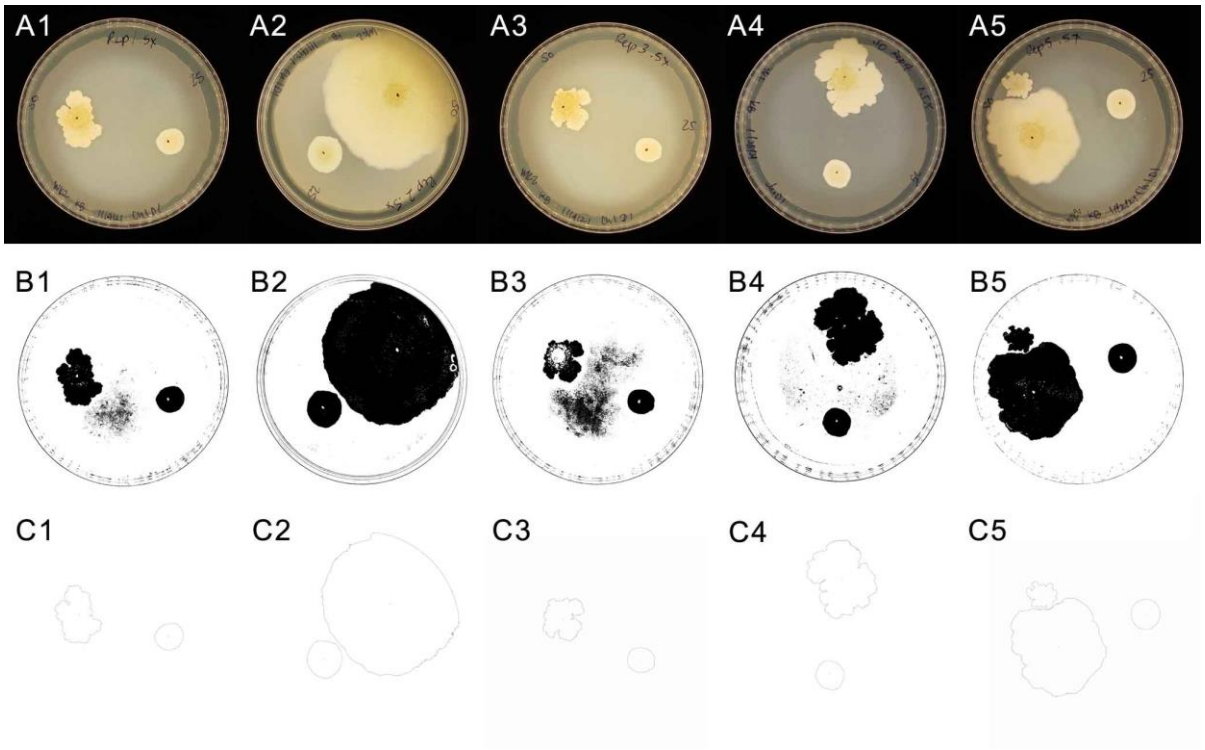


Figure C61. 2021 co-inoculated Petri plates four days after inoculation. **A1-A5)** 0.5x SO vs. *Pss* 25 on KB media. **B1-B5)** Images after threshold adjustment in ImageJ. **C1-C5)** Image of measured area. A1, B1, C1: Replication 1; A2, B2, C2: Replication 2; A3, B3, C3: Replication 3; A4, B4, C4: Replication 4; A5, B5, C5: Replication 5.

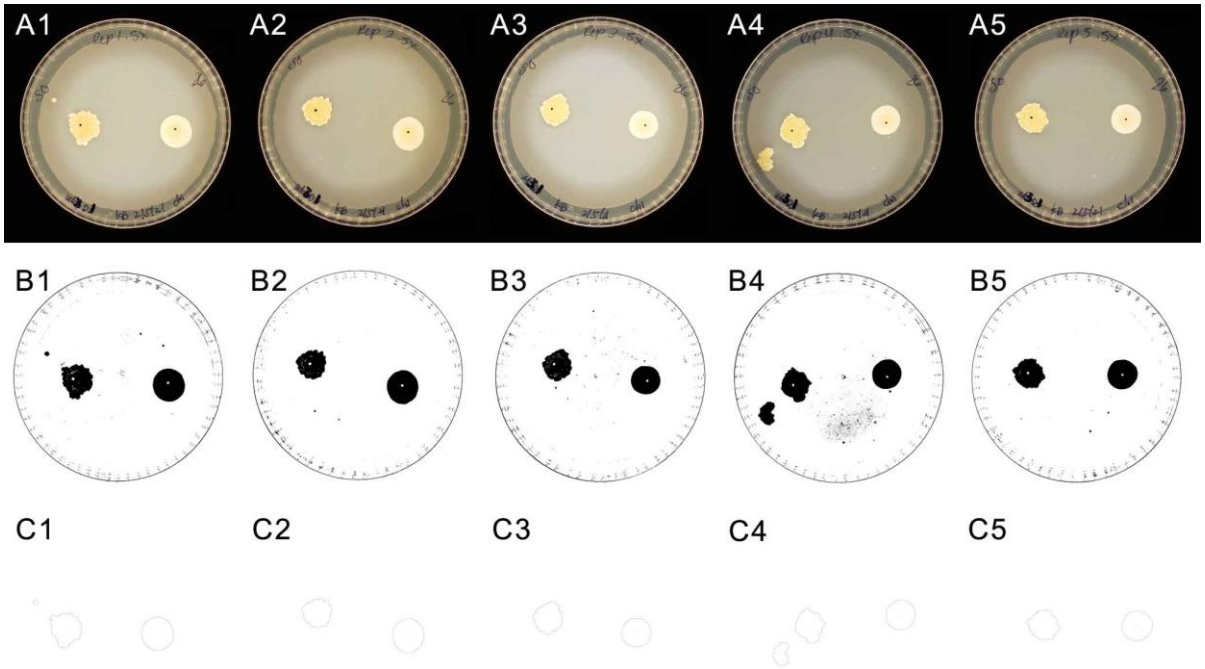


Figure C62. 2021 co-inoculated Petri plates four days after inoculation. **A1-A5)** 0.5x SO vs. *Pss* 26 on KB media. **B1-B5)** Images after threshold adjustment in ImageJ. **C1-C5)** Image of measured area. A1, B1, C1: Replication 1; A2, B2, C2: Replication 2; A3, B3, C3: Replication 3; A4, B4, C4: Replication 4; A5, B5, C5: Replication 5.

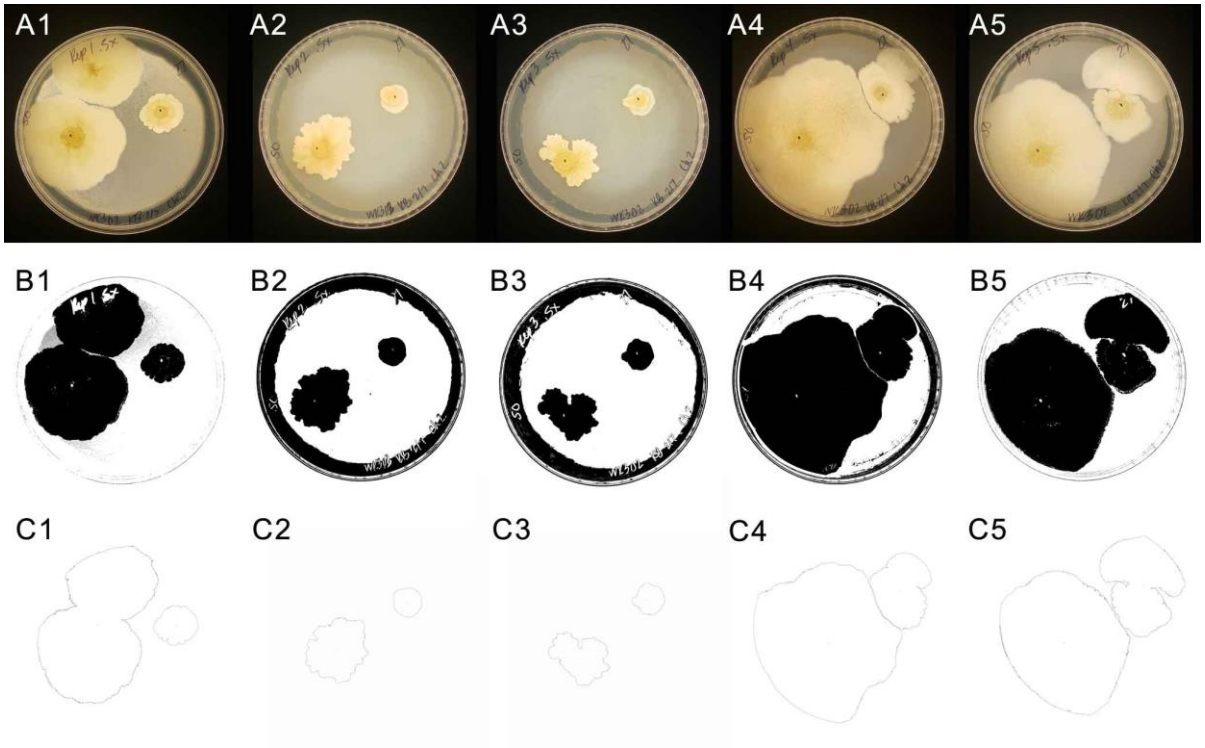


Figure C63. 2021 co-inoculated Petri plates four days after inoculation. **A1-A5)** 0.5x SO vs. *Pss* 27 on KB media. **B1-B5)** Images after threshold adjustment in ImageJ. **C1-C5)** Image of measured area. A1, B1, C1: Replication 1; A2, B2, C2: Replication 2; A3, B3, C3: Replication 3; A4, B4, C4: Replication 4; A5, B5, C5: Replication 5.

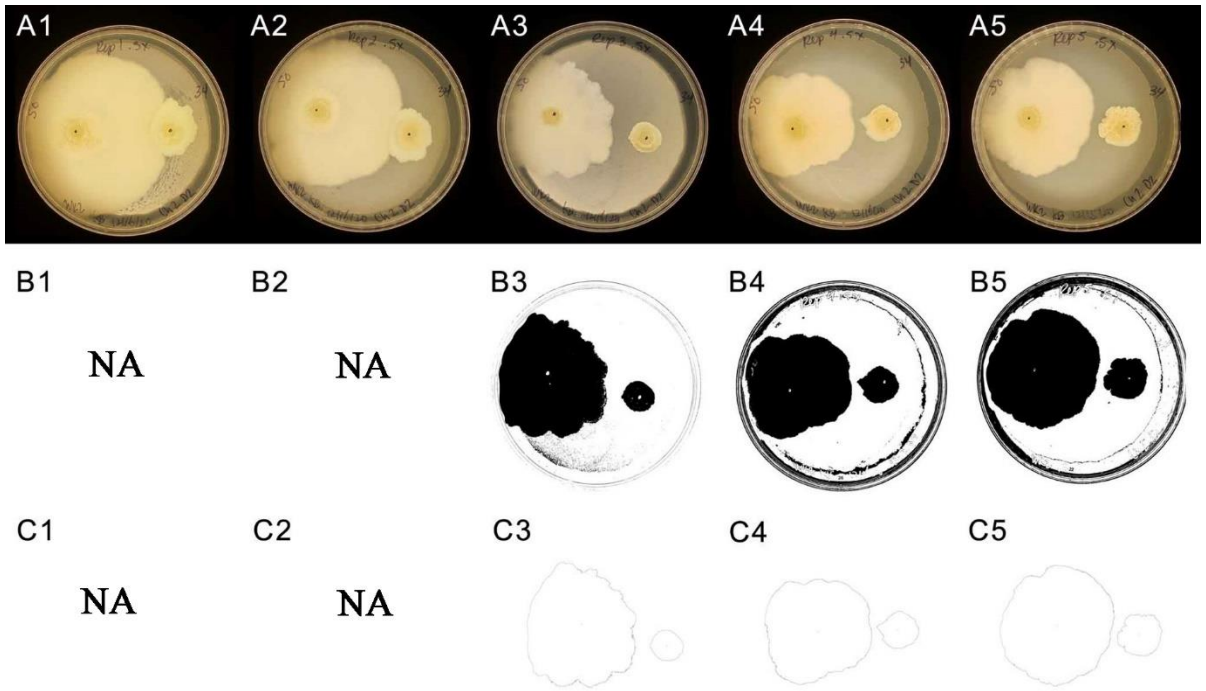


Figure C64. 2021 co-inoculated Petri plates four days after inoculation. **A1-A5)** 0.5x SO vs. *Pss* 34 on KB media. **B1-B5)** Images after threshold adjustment in ImageJ. **C1-C5)** Image of measured area. A1, B1, C1: Replication 1; A2, B2, C2: Replication 2; A3, B3, C3: Replication 3; A4, B4, C4: Replication 4; A5, B5, C5: Replication 5. Images with NA are not available.

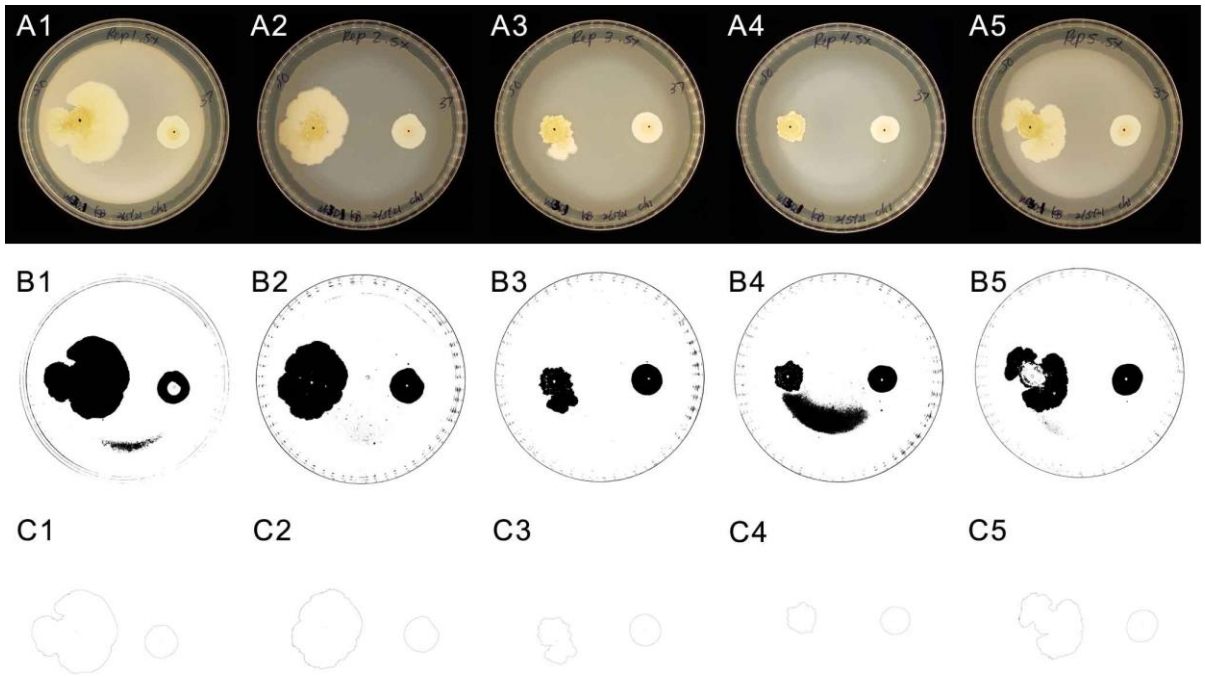


Figure C65. 2021 co-inoculated Petri plates four days after inoculation. **A1-A5)** 0.5x SO vs. *Pss* 37 on KB media. **B1-B5)** Images after threshold adjustment in ImageJ. **C1-C5)** Image of measured area. A1, B1, C1: Replication 1; A2, B2, C2: Replication 2; A3, B3, C3: Replication 3; A4, B4, C4: Replication 4; A5, B5, C5: Replication 5.

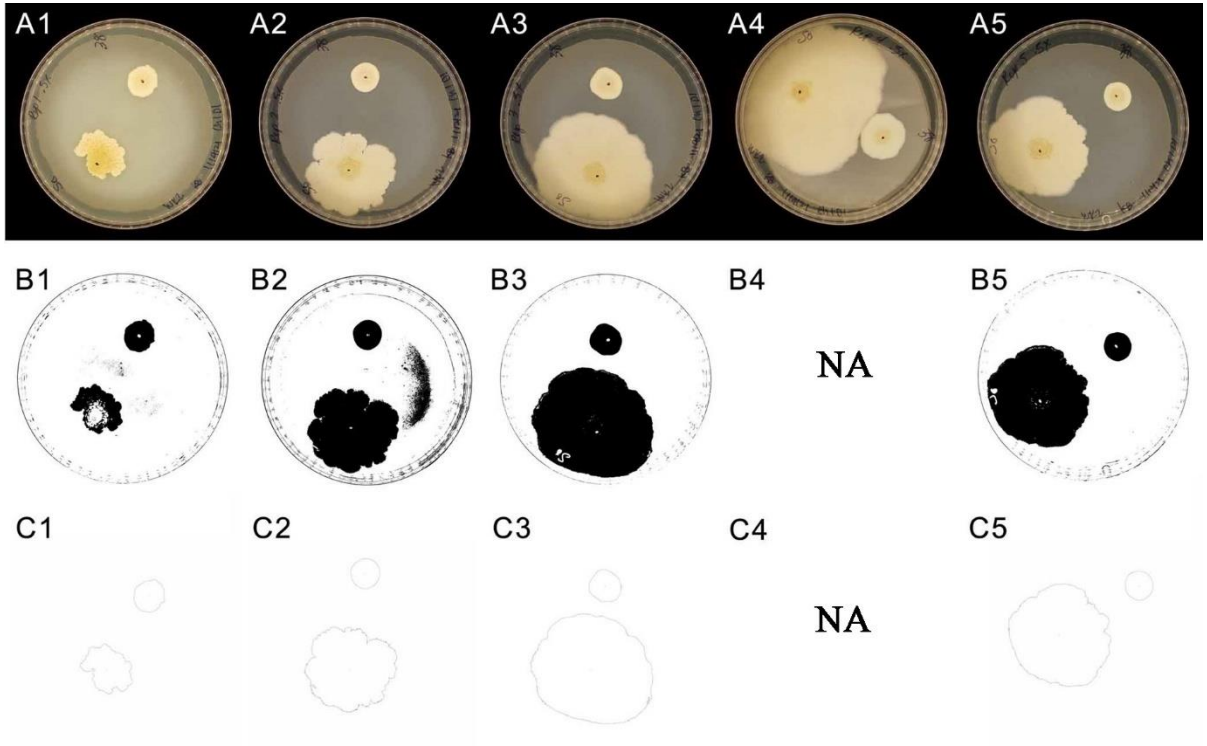


Figure C66. 2021 co-inoculated Petri plates four days after inoculation. **A1-A5)** 0.5x SO vs. *Pss* 38 on KB media. **B1-B5)** Images after threshold adjustment in ImageJ. **C1-C5)** Image of measured area. A1, B1, C1: Replication 1; A2, B2, C2: Replication 2; A3, B3, C3: Replication 3; A4, B4, C4: Replication 4; A5, B5, C5: Replication 5. Images with NA are not available.

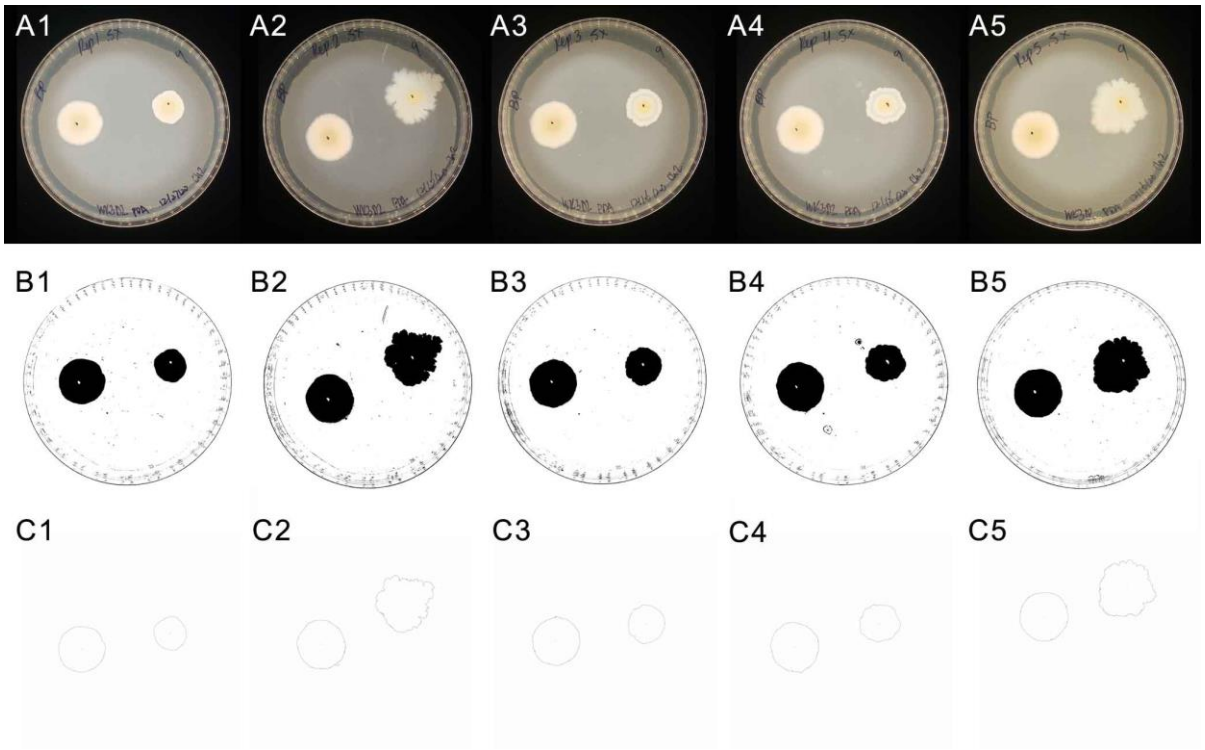


Figure C67. 2021 co-inoculated Petri plates four days after inoculation. **A1-A5)** 0.5x BP vs. *Pss* 9 on PDA media. **B1-B5)** Images after threshold adjustment in ImageJ. **C1-C5)** Image of measured area. A1, B1, C1: Replication 1; A2, B2, C2: Replication 2; A3, B3, C3: Replication 3; A4, B4, C4: Replication 4; A5, B5, C5: Replication 5.

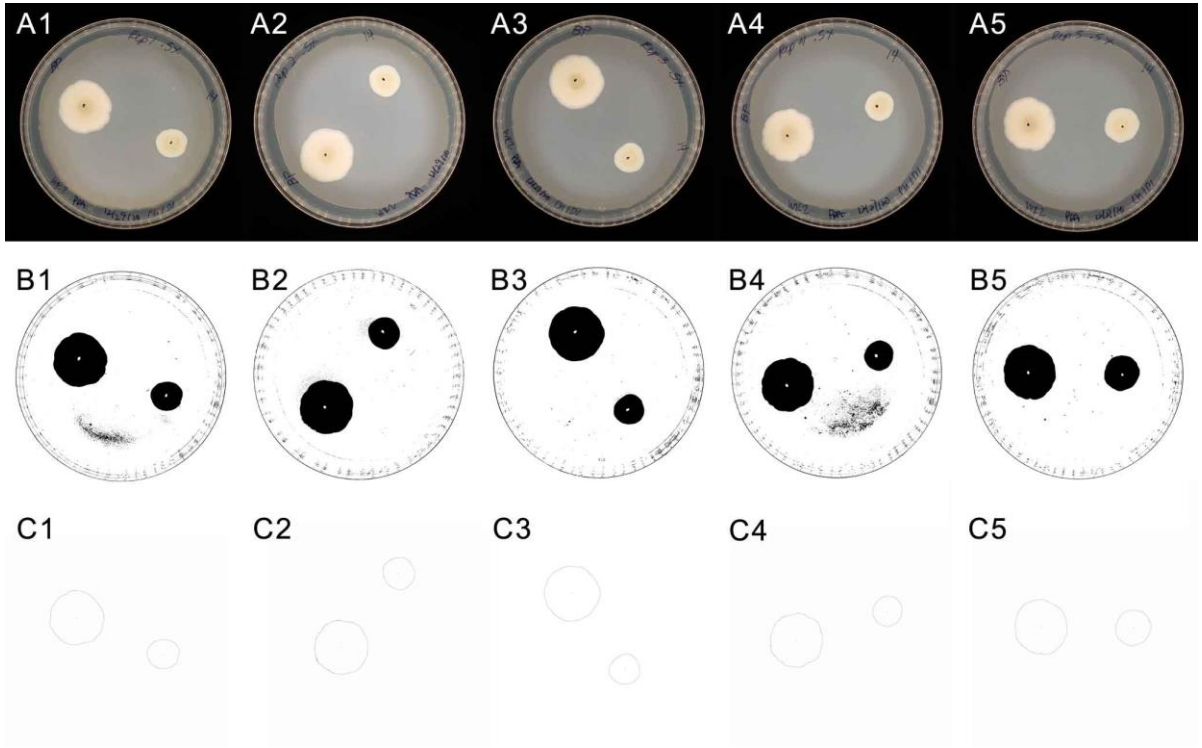


Figure C68. 2021 co-inoculated Petri plates four days after inoculation. **A1-A5)** 0.5x BP vs. *Pss* 14 on PDA media. **B1-B5)** Images after threshold adjustment in ImageJ. **C1-C5)** Image of measured area. A1, B1, C1: Replication 1; A2, B2, C2: Replication 2; A3, B3, C3: Replication 3; A4, B4, C4: Replication 4; A5, B5, C5: Replication 5.

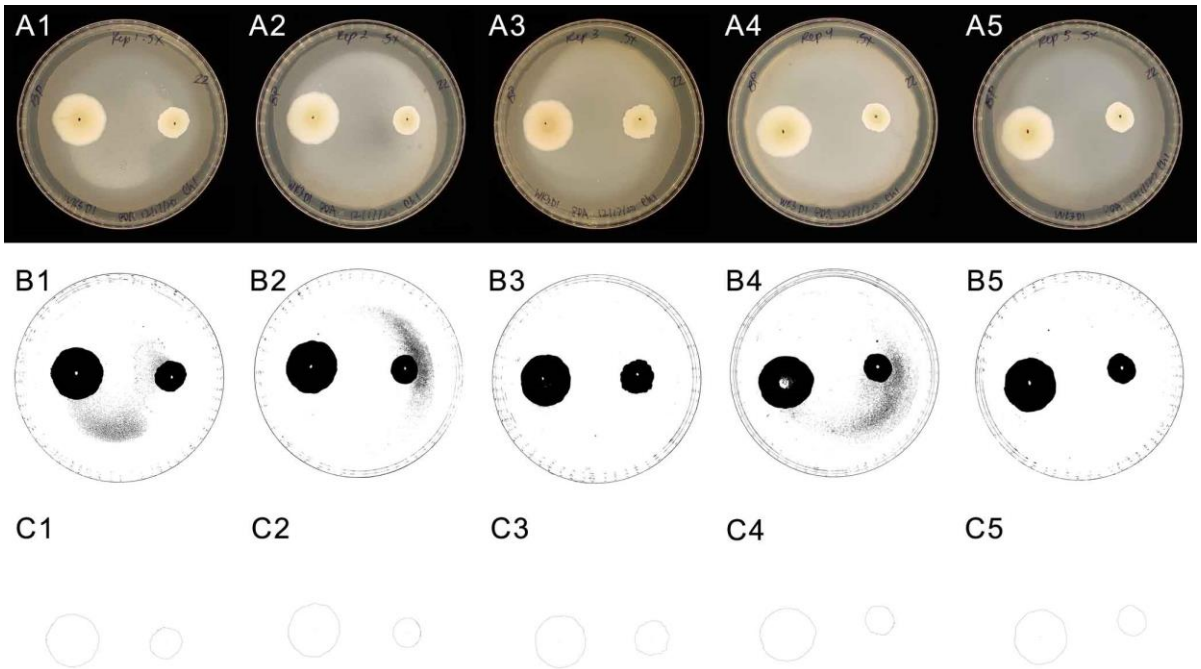


Figure C69. 2021 co-inoculated Petri plates four days after inoculation. **A1-A5)** 0.5x BP vs. *Pss* 22 on PDA media. **B1-B5)** Images after threshold adjustment in ImageJ. **C1-C5)** Image of measured area. A1, B1, C1: Replication 1; A2, B2, C2: Replication 2; A3, B3, C3: Replication 3; A4, B4, C4: Replication 4; A5, B5, C5: Replication 5.

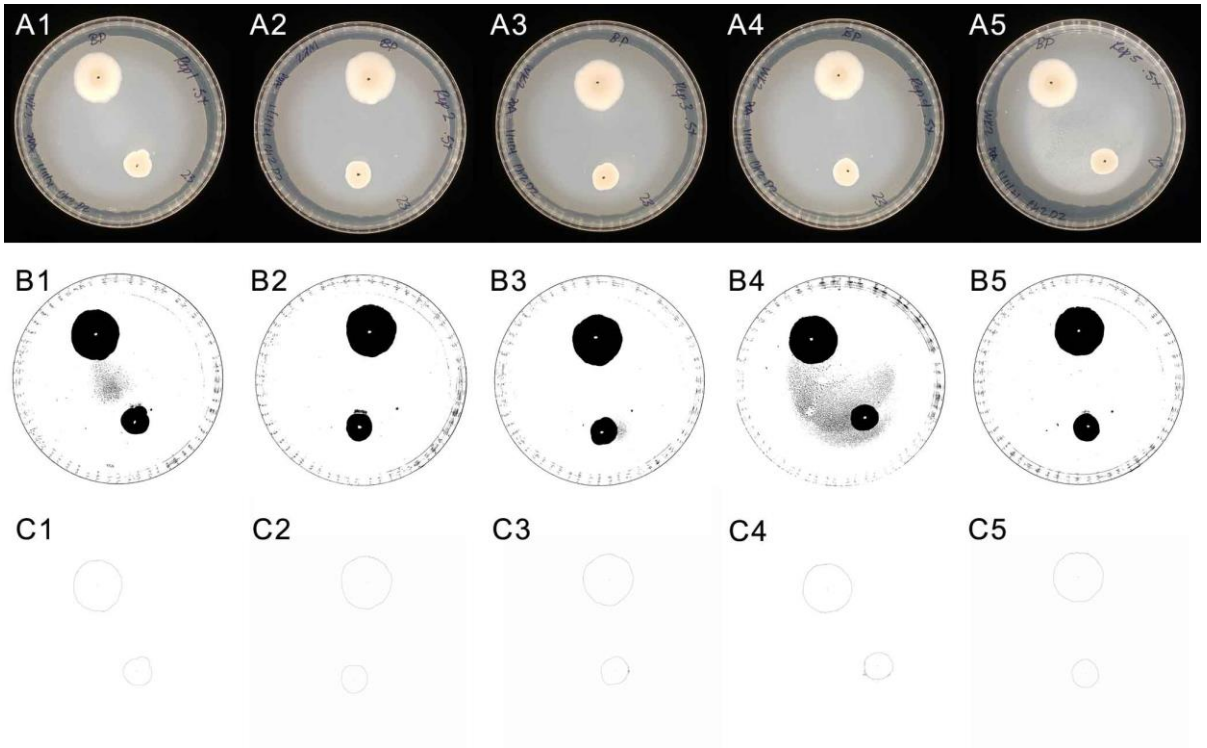


Figure C70. 2021 co-inoculated Petri plates four days after inoculation. **A1-A5)** 0.5x BP vs. *Pss* 23 on PDA media. **B1-B5)** Images after threshold adjustment in ImageJ. **C1-C5)** Image of measured area. A1, B1, C1: Replication 1; A2, B2, C2: Replication 2; A3, B3, C3: Replication 3; A4, B4, C4: Replication 4; A5, B5, C5: Replication 5.

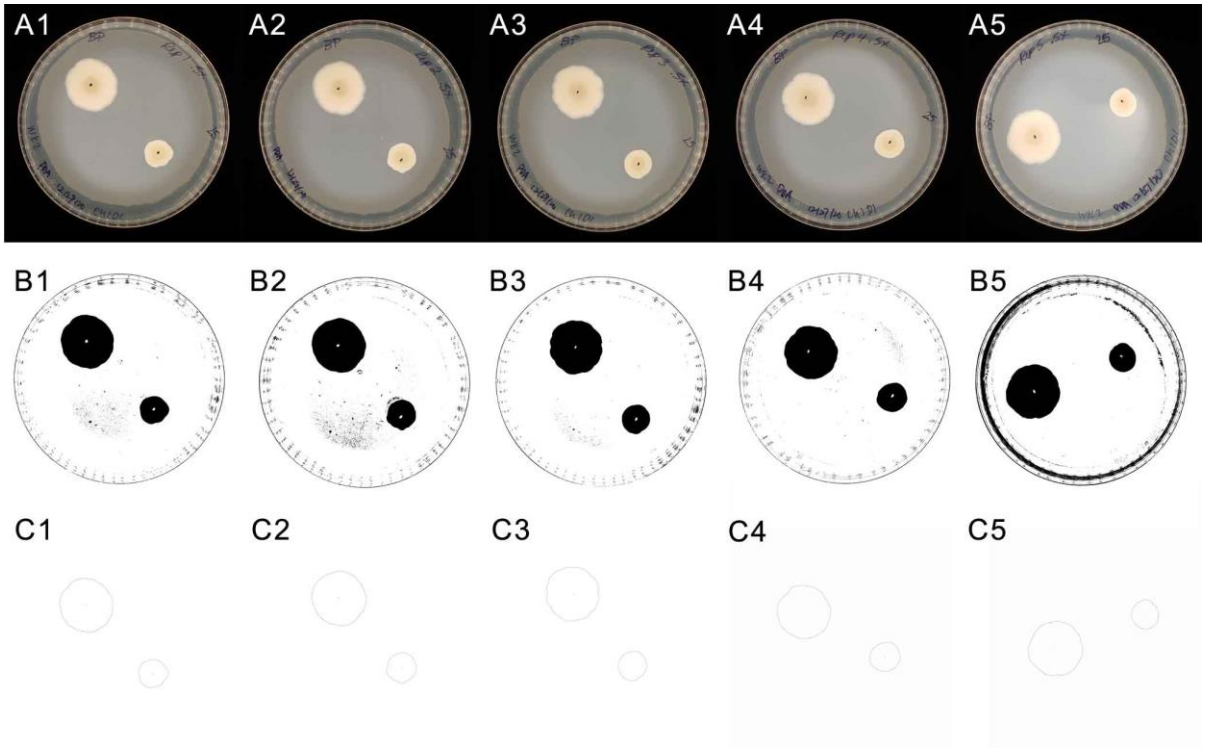


Figure C71. 42021 co-inoculated Petri plates four days after inoculation. **A1-A5)** 0.5x BP vs. *Pss* 25 on PDA media. **B1-B5)** Images after threshold adjustment in ImageJ. **C1-C5)** Image of measured area. A1, B1, C1: Replication 1; A2, B2, C2: Replication 2; A3, B3, C3: Replication 3; A4, B4, C4: Replication 4; A5, B5, C5: Replication 5.

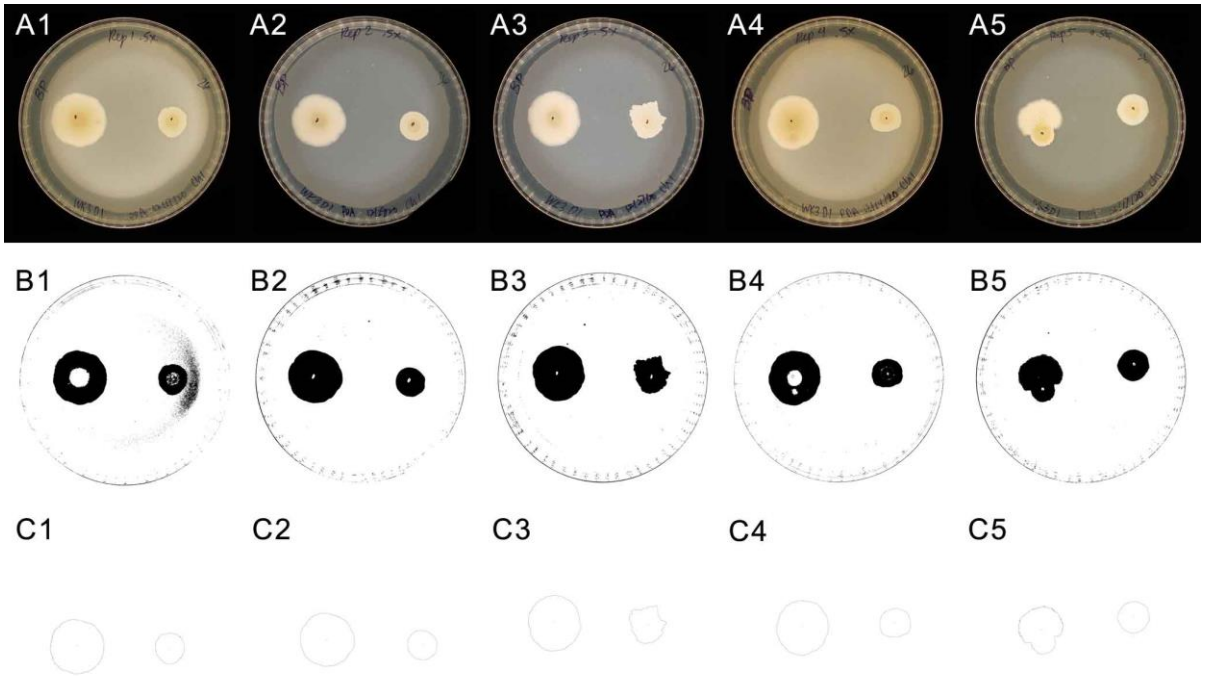


Figure C72. 2021 co-inoculated Petri plates four days after inoculation. **A1-A5)** 0.5x BP vs. *Pss* 26 on PDA media. **B1-B5)** Images after threshold adjustment in ImageJ. **C1-C5)** Image of measured area. A1, B1, C1: Replication 1; A2, B2, C2: Replication 2; A3, B3, C3: Replication 3; A4, B4, C4: Replication 4; A5, B5, C5: Replication 5.

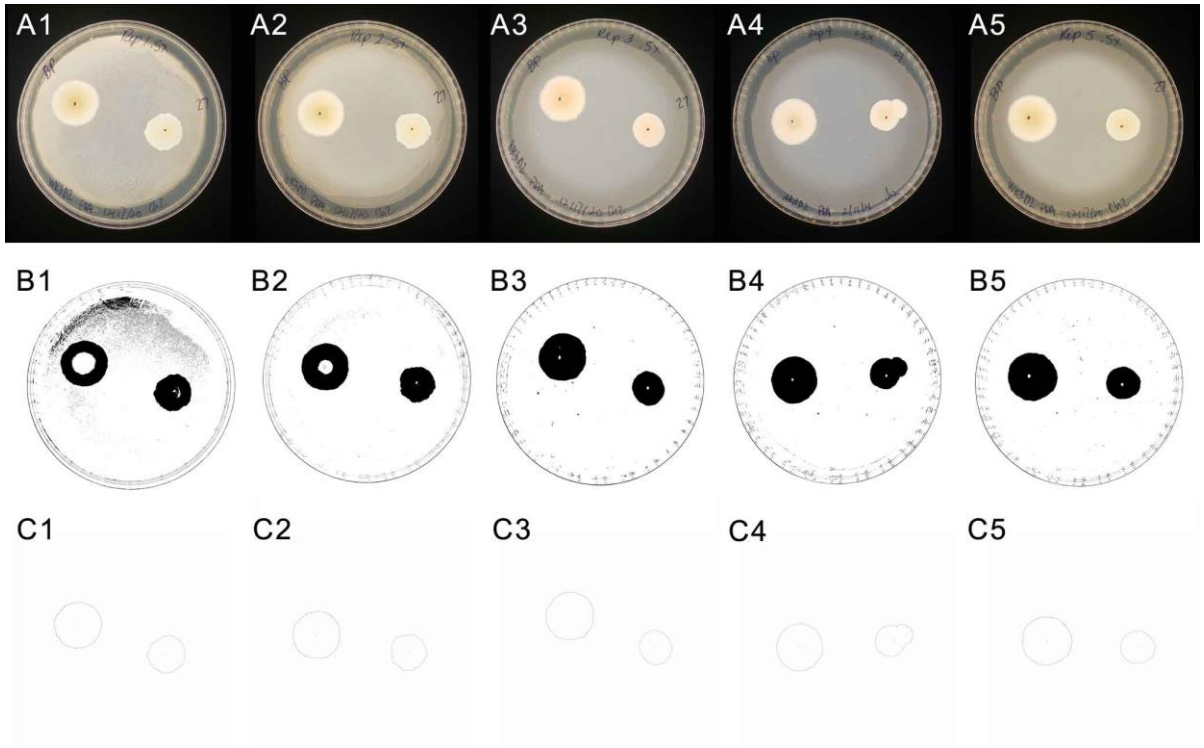


Figure C73. 2021 co-inoculated Petri plates four days after inoculation. **A1-A5)** 0.5x BP vs. *Pss* 27 on PDA media. **B1-B5)** Images after threshold adjustment in ImageJ. **C1-C5)** Image of measured area. A1, B1, C1: Replication 1; A2, B2, C2: Replication 2; A3, B3, C3: Replication 3; A4, B4, C4: Replication 4; A5, B5, C5: Replication 5.

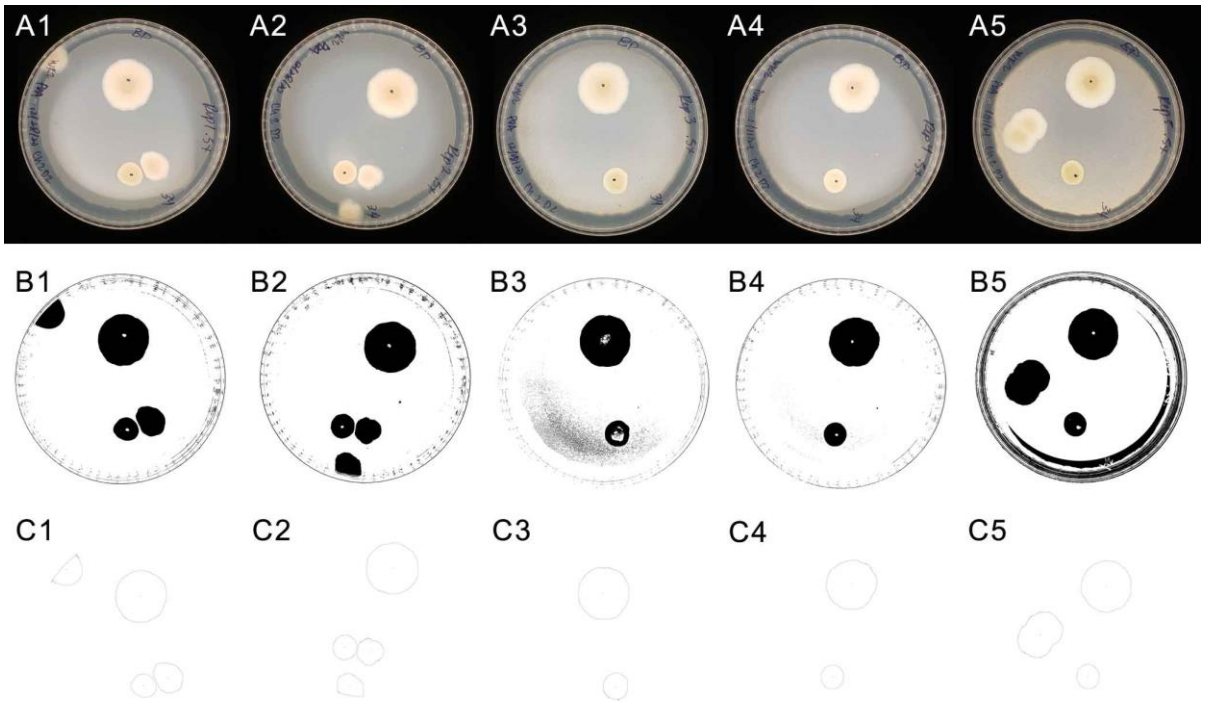


Figure C74. 2021 co-inoculated Petri plates four days after inoculation. **A1-A5)** 0.5x BP vs. *Pss* 34 on PDA media. **B1-B5)** Images after threshold adjustment in ImageJ. **C1-C5)** Image of measured area. A1, B1, C1: Replication 1; A2, B2, C2: Replication 2; A3, B3, C3: Replication 3; A4, B4, C4: Replication 4; A5, B5, C5: Replication 5.

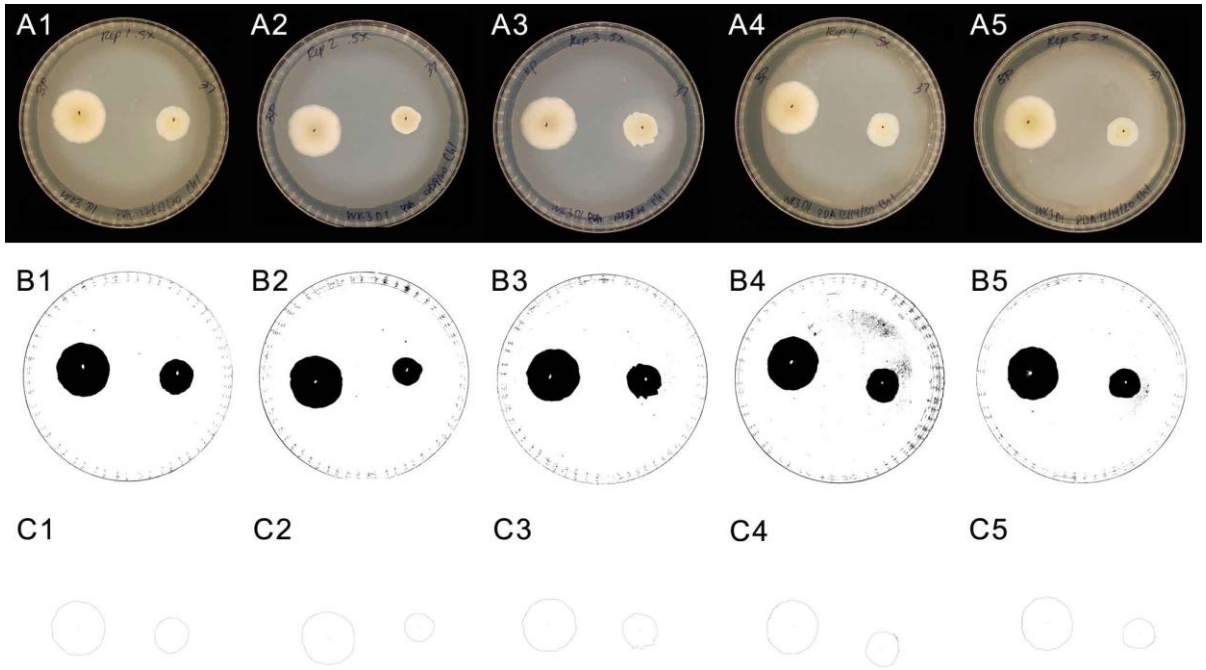


Figure C75. 2021 co-inoculated Petri plates four days after inoculation. **A1-A5)** 0.5x BP vs. *Pss* 37 on PDA media. **B1-B5)** Images after threshold adjustment in ImageJ. **C1-C5)** Image of measured area. A1, B1, C1: Replication 1; A2, B2, C2: Replication 2; A3, B3, C3: Replication 3; A4, B4, C4: Replication 4; A5, B5, C5: Replication 5.

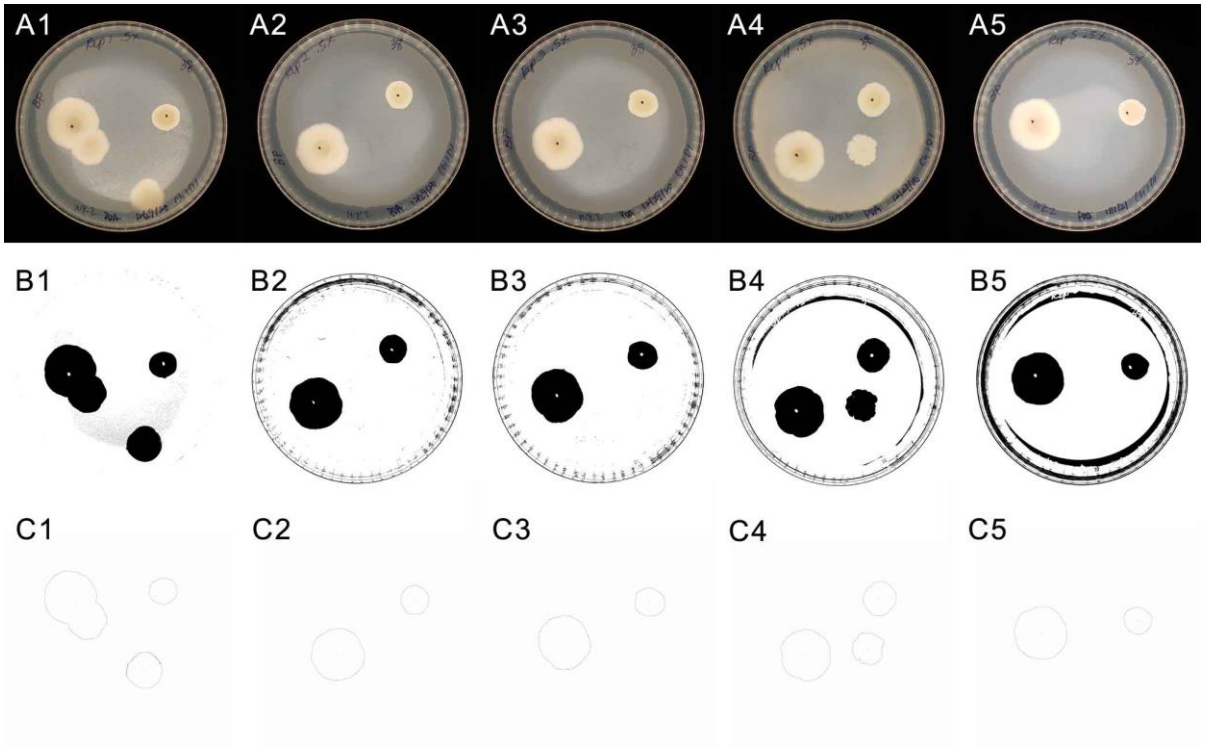


Figure C76. 2021 co-inoculated Petri plates four days after inoculation. **A1-A5)** 0.5x BP vs. *Pss* 38 on PDA media. **B1-B5)** Images after threshold adjustment in ImageJ. **C1-C5)** Image of measured area. A1, B1, C1: Replication 1; A2, B2, C2: Replication 2; A3, B3, C3: Replication 3; A4, B4, C4: Replication 4; A5, B5, C5: Replication 5.

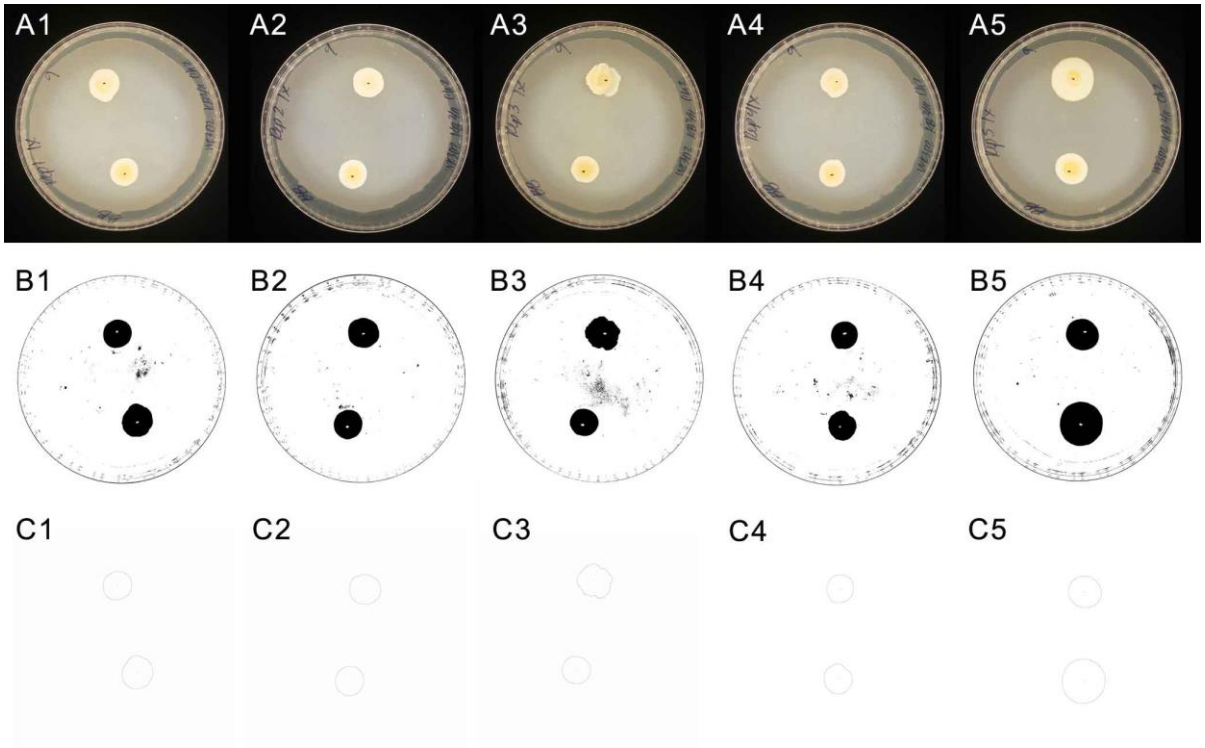


Figure C77. 2021 co-inoculated Petri plates four days after inoculation. **A1-A5)** 1x BB vs. *Pss* 9 on KB media. **B1-B5)** Images after threshold adjustment in ImageJ. **C1-C5)** Image of measured area. A1, B1, C1: Replication 1; A2, B2, C2: Replication 2; A3, B3, C3: Replication 3; A4, B4, C4: Replication 4; A5, B5, C5: Replication 5.

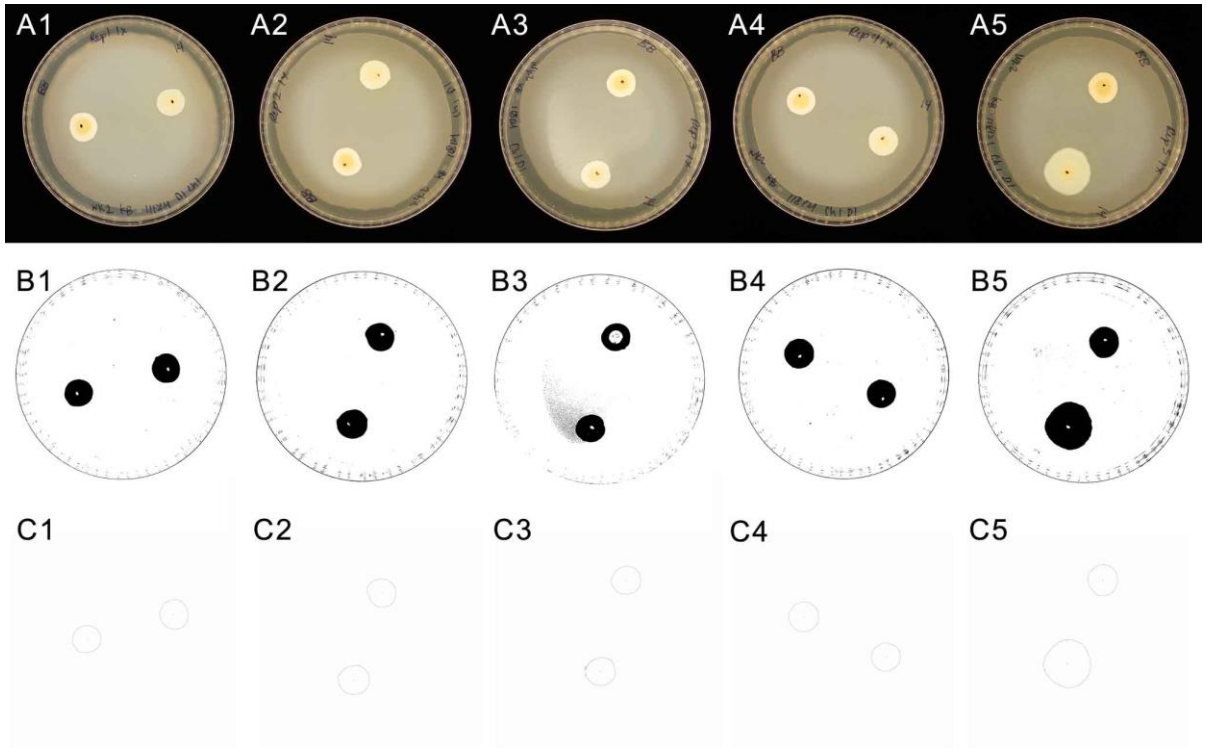


Figure C78. 2021 co-inoculated Petri plates four days after inoculation. **A1-A5)** 1x BB vs. *Pss* 14 on KB media. **B1-B5)** Images after threshold adjustment in ImageJ. **C1-C5)** Image of measured area. A1, B1, C1: Replication 1; A2, B2, C2: Replication 2; A3, B3, C3: Replication 3; A4, B4, C4: Replication 4; A5, B5, C5: Replication 5.

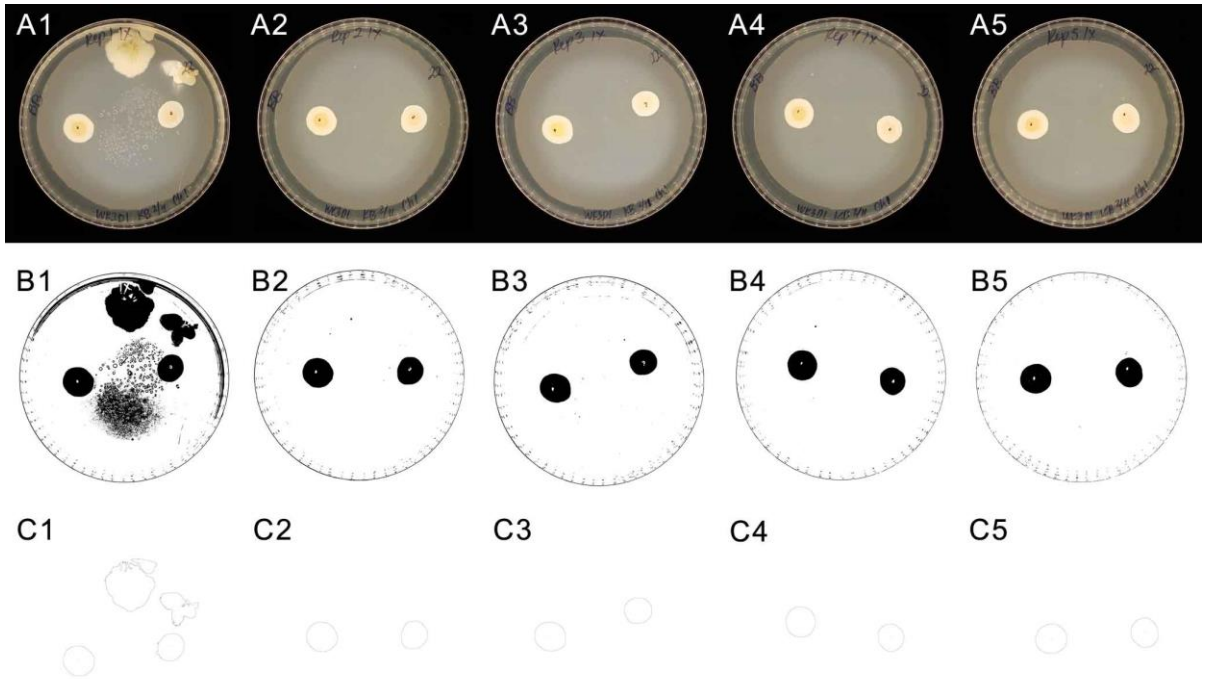


Figure C79. 2021 co-inoculated Petri plates four days after inoculation. **A1-A5)** 1x BB vs. *Pss* 22 on KB media. **B1-B5)** Images after threshold adjustment in ImageJ. **C1-C5)** Image of measured area. A1, B1, C1: Replication 1; A2, B2, C2: Replication 2; A3, B3, C3: Replication 3; A4, B4, C4: Replication 4; A5, B5, C5: Replication 5.

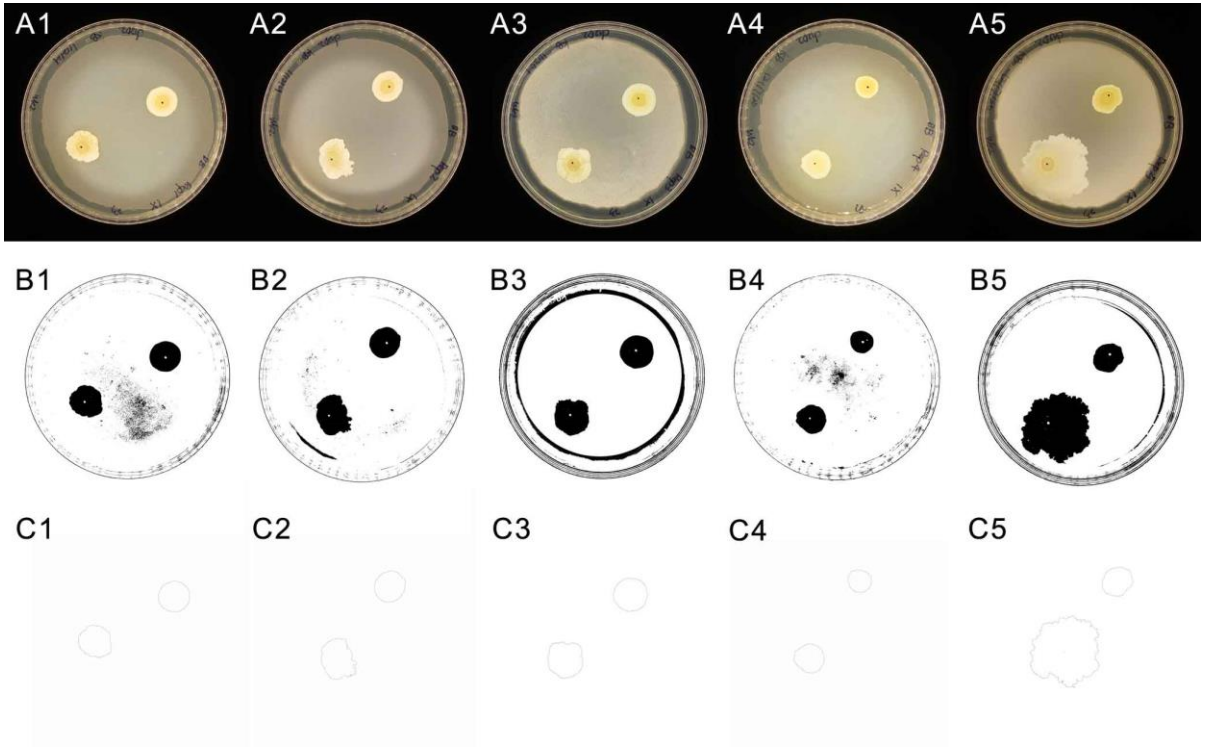


Figure C80. 2021 co-inoculated Petri plates four days after inoculation. **A1-A5)** 1x BB vs. *Pss* 23 on KB media. **B1-B5)** Images after threshold adjustment in ImageJ. **C1-C5)** Image of measured area. A1, B1, C1: Replication 1; A2, B2, C2: Replication 2; A3, B3, C3: Replication 3; A4, B4, C4: Replication 4; A5, B5, C5: Replication 5.

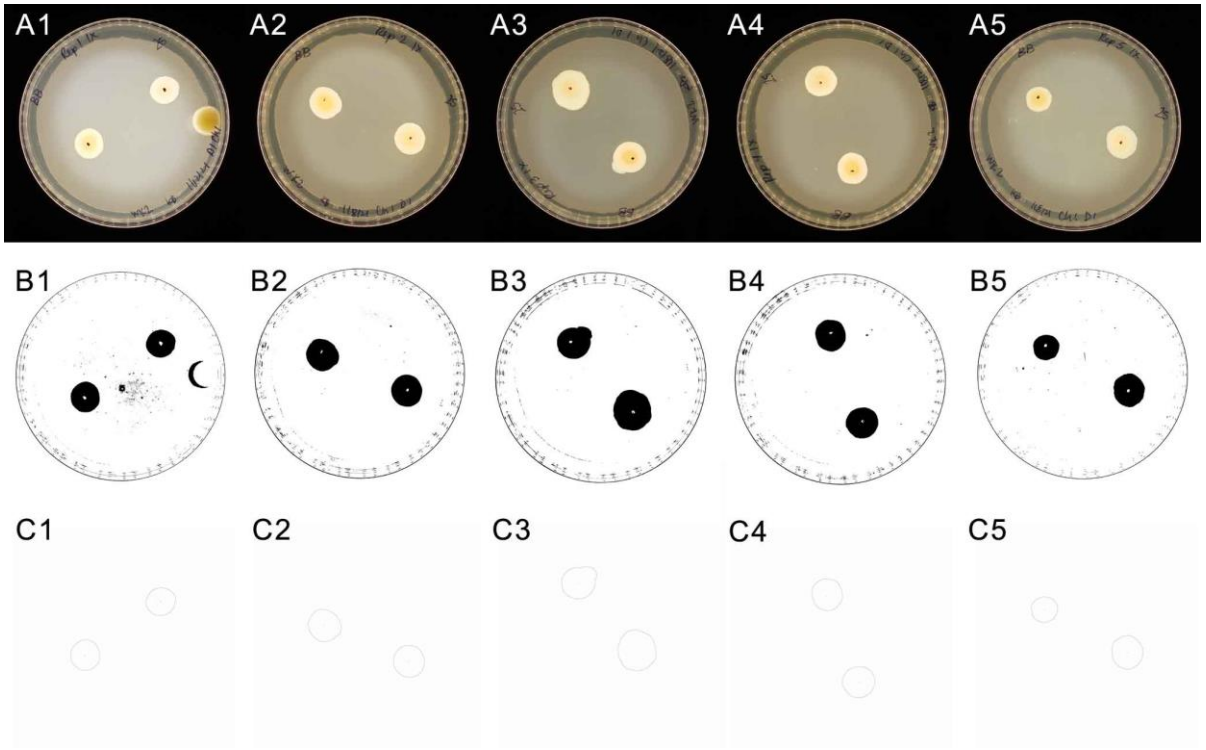


Figure C81. 2021 co-inoculated Petri plates four days after inoculation. **A1-A5)** 1x BB vs. *Pss* 25 on KB media. **B1-B5)** Images after threshold adjustment in ImageJ. **C1-C5)** Image of measured area. A1, B1, C1: Replication 1; A2, B2, C2: Replication 2; A3, B3, C3: Replication 3; A4, B4, C4: Replication 4; A5, B5, C5: Replication 5.

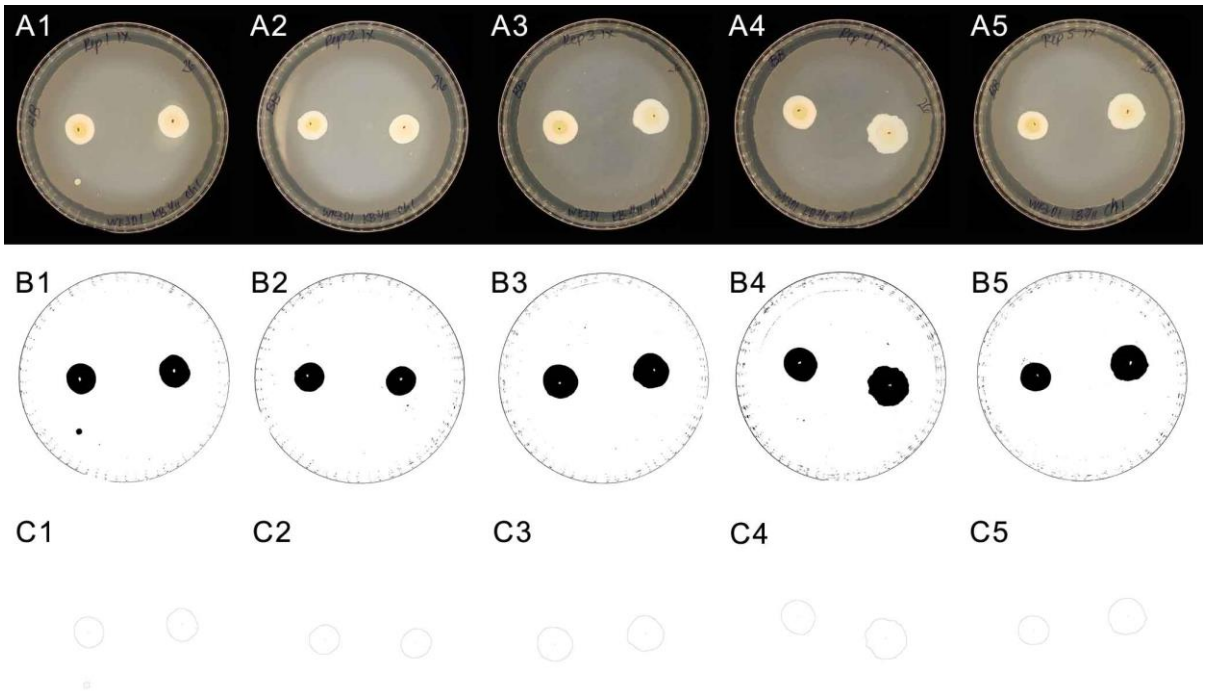


Figure C82. 2021 co-inoculated Petri plates four days after inoculation. **A1-A5)** 1x BB vs. *Pss* 26 on KB media. **B1-B5)** Images after threshold adjustment in ImageJ. **C1-C5)** Image of measured area. A1, B1, C1: Replication 1; A2, B2, C2: Replication 2; A3, B3, C3: Replication 3; A4, B4, C4: Replication 4; A5, B5, C5: Replication 5.

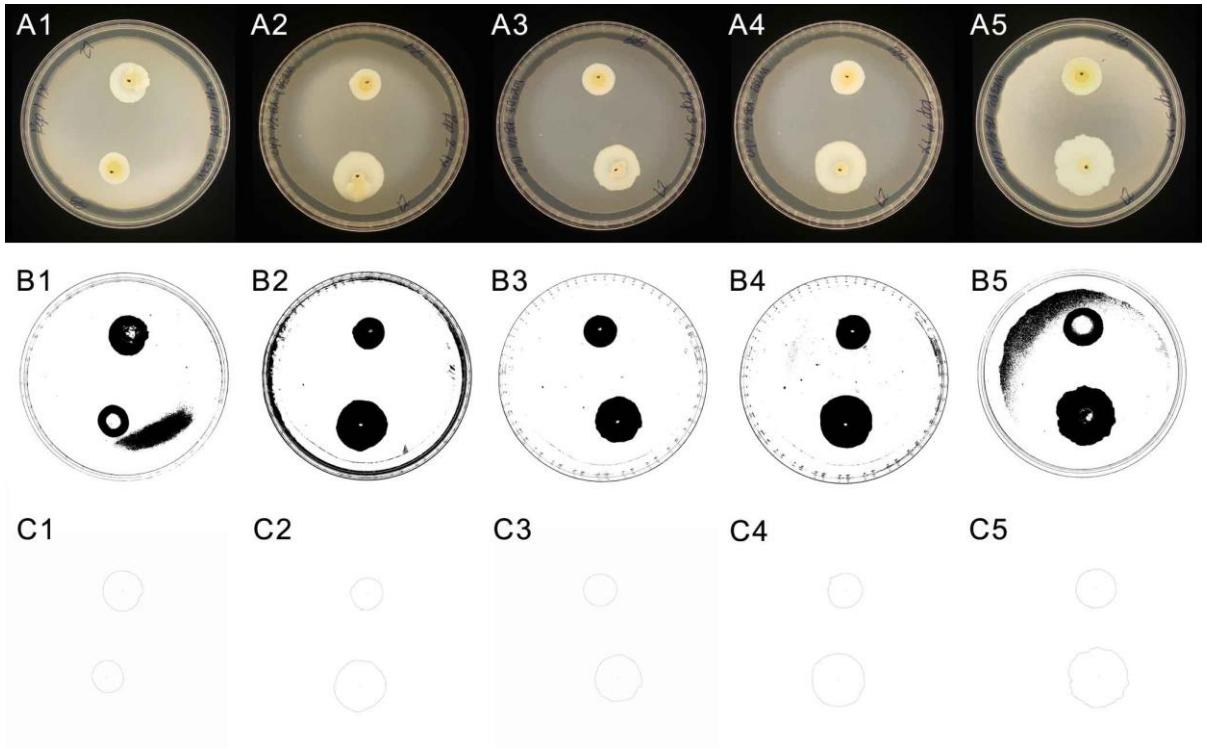


Figure C83. 2021 co-inoculated Petri plates four days after inoculation. **A1-A5)** 1x BB vs. *Pss* 27 on KB media. **B1-B5)** Images after threshold adjustment in ImageJ. **C1-C5)** Image of measured area. A1, B1, C1: Replication 1; A2, B2, C2: Replication 2; A3, B3, C3: Replication 3; A4, B4, C4: Replication 4; A5, B5, C5: Replication 5.

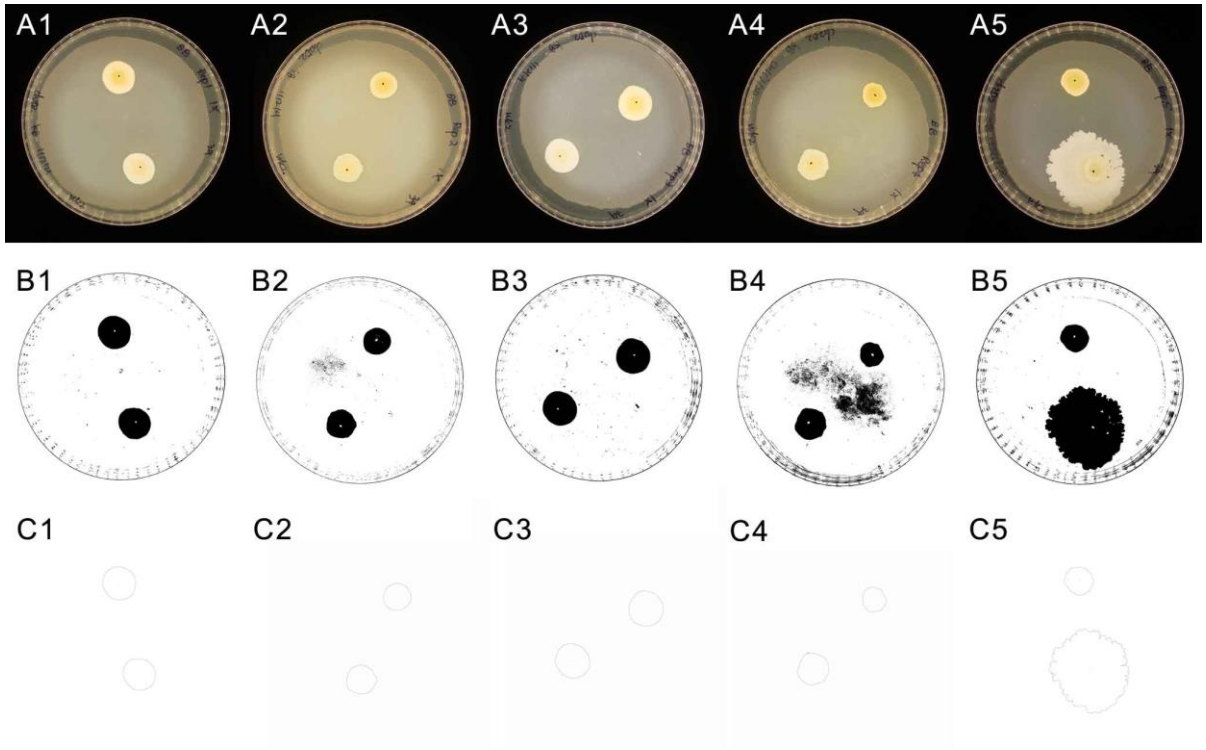


Figure C84. 2021 co-inoculated Petri plates four days after inoculation. **A1-A5)** 1x BB vs. *Pss* 34 on KB media. **B1-B5)** Images after threshold adjustment in ImageJ. **C1-C5)** Image of measured area. A1, B1, C1: Replication 1; A2, B2, C2: Replication 2; A3, B3, C3: Replication 3; A4, B4, C4: Replication 4; A5, B5, C5: Replication 5.

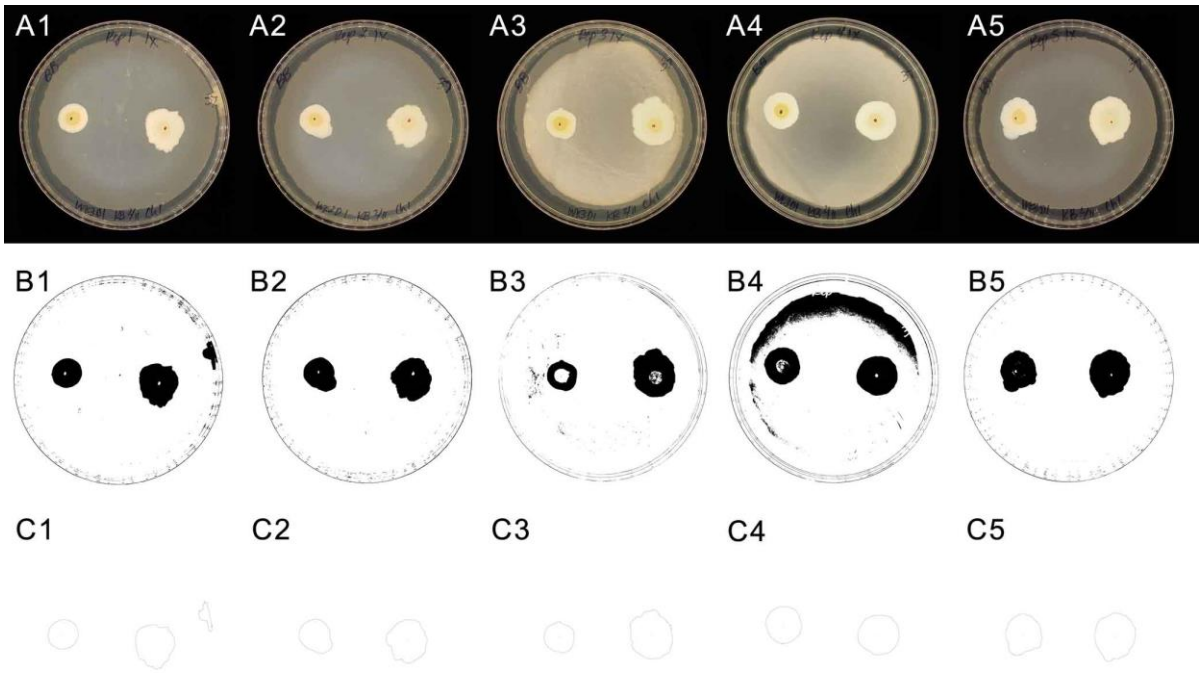


Figure C85. 2021 co-inoculated Petri plates four days after inoculation. **A1-A5)** 1x BB vs. *Pss* 37 on KB media. **B1-B5)** Images after threshold adjustment in ImageJ. **C1-C5)** Image of measured area. A1, B1, C1: Replication 1; A2, B2, C2: Replication 2; A3, B3, C3: Replication 3; A4, B4, C4: Replication 4; A5, B5, C5: Replication 5.

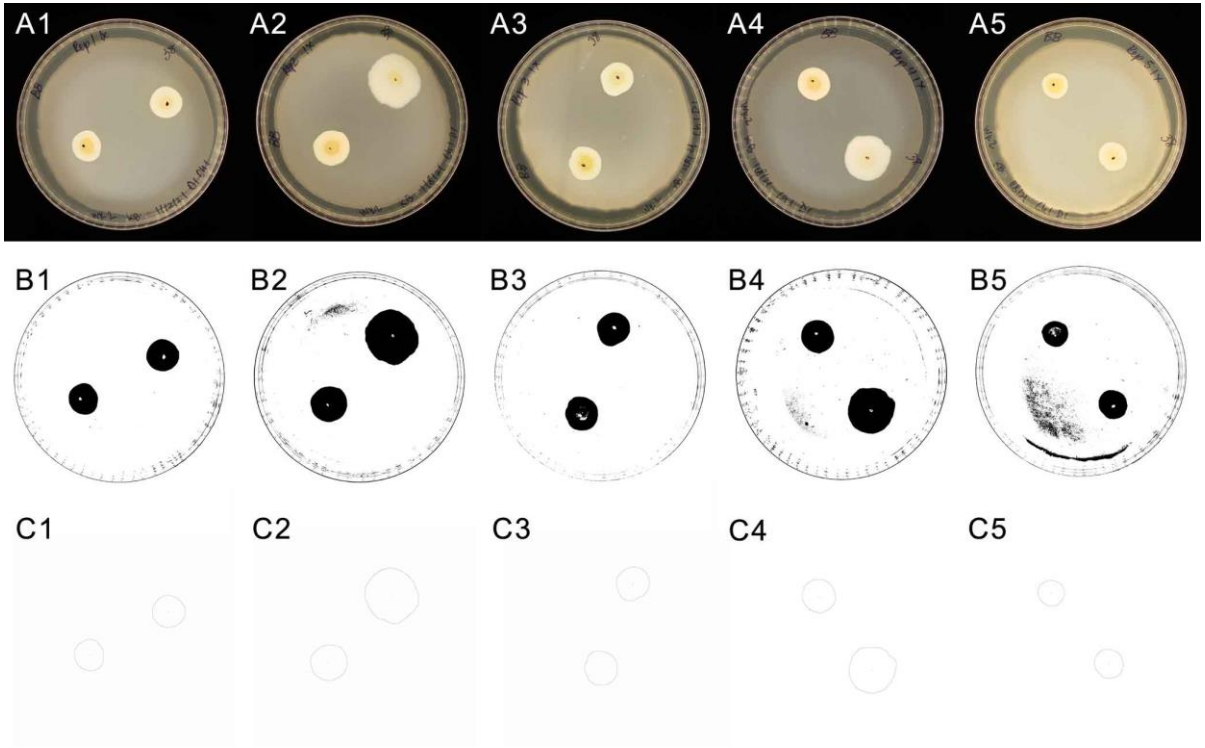


Figure C86. 2021 co-inoculated Petri plates four days after inoculation. **A1-A5)** 1x BB vs. *Pss* 38 on KB media. **B1-B5)** Images after threshold adjustment in ImageJ. **C1-C5)** Image of measured area. A1, B1, C1: Replication 1; A2, B2, C2: Replication 2; A3, B3, C3: Replication 3; A4, B4, C4: Replication 4; A5, B5, C5: Replication 5.

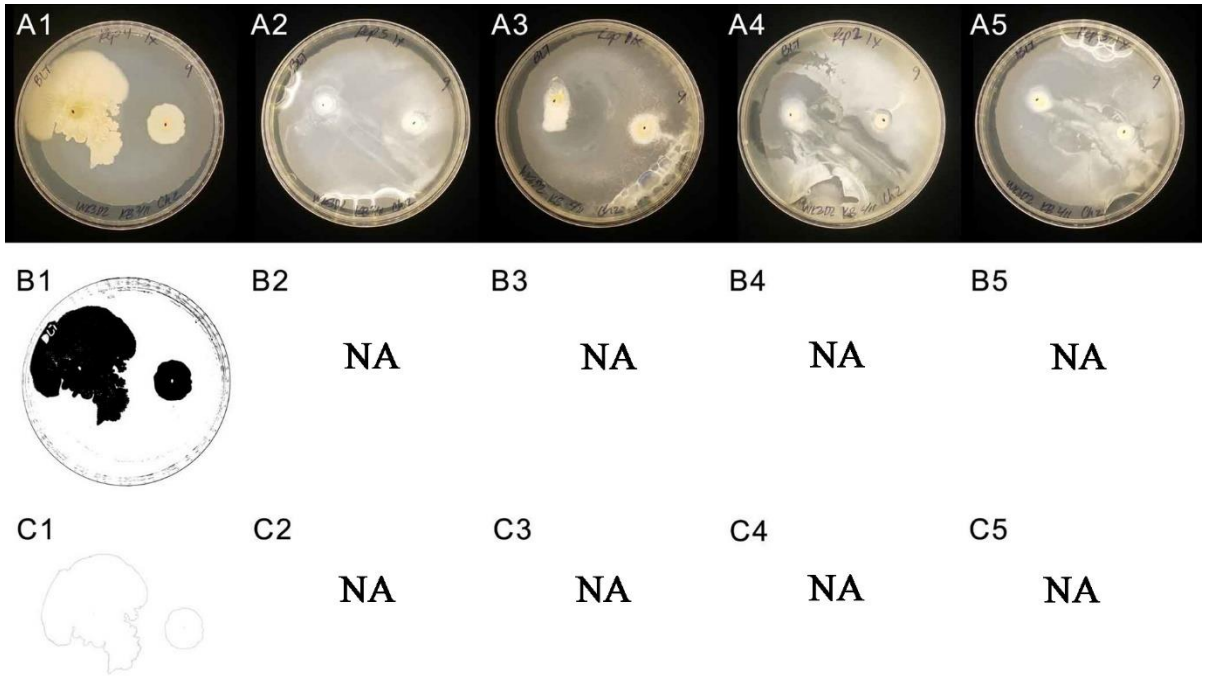


Figure C87. 2021 co-inoculated Petri plates four days after inoculation. **A1-A5)** 1x BLT vs. *Pss* 9 on KB media. **B1-B5)** Images after threshold adjustment in ImageJ. **C1-C5)** Image of measured area. A1, B1, C1: Replication 1; A2, B2, C2: Replication 2; A3, B3, C3: Replication 3; A4, B4, C4: Replication 4; A5, B5, C5: Replication 5. Images with NA are not available.

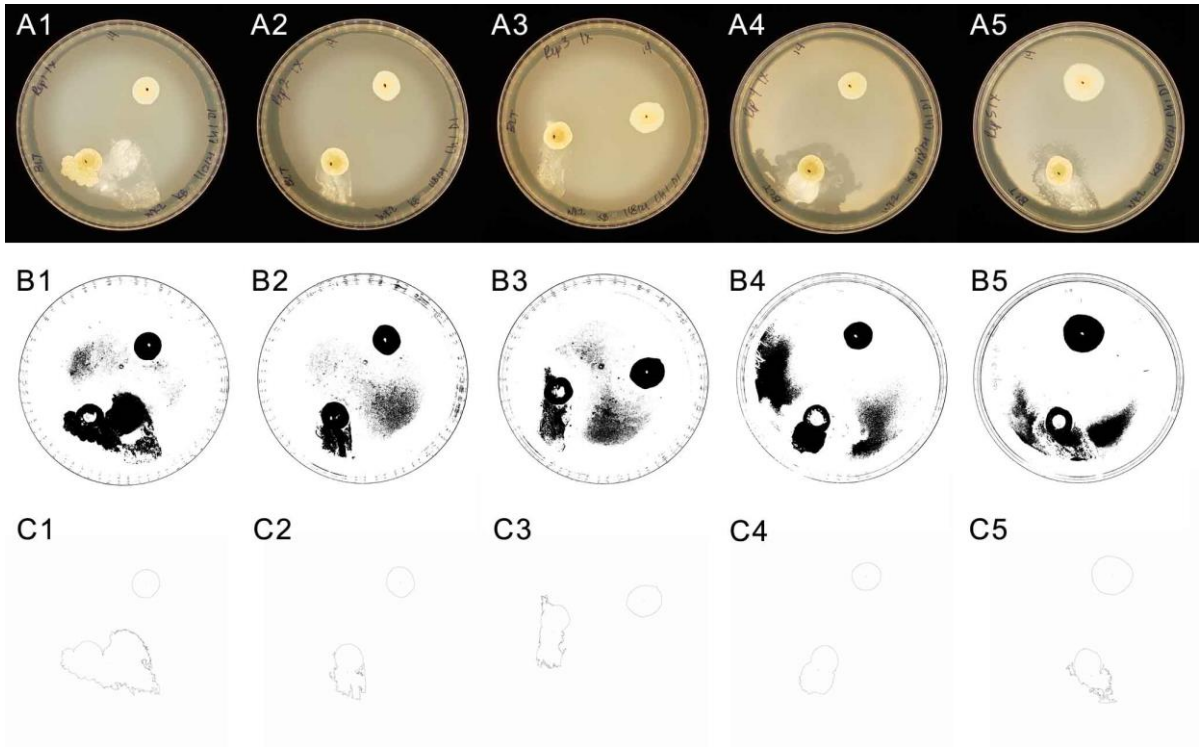


Figure C88. 2021 co-inoculated Petri plates four days after inoculation. **A1-A5)** 1x BLT vs. *Pss* 14 on KB media. **B1-B5)** Images after threshold adjustment in ImageJ. **C1-C5)** Image of measured area. A1, B1, C1: Replication 1; A2, B2, C2: Replication 2; A3, B3, C3: Replication 3; A4, B4, C4: Replication 4; A5, B5, C5: Replication 5.

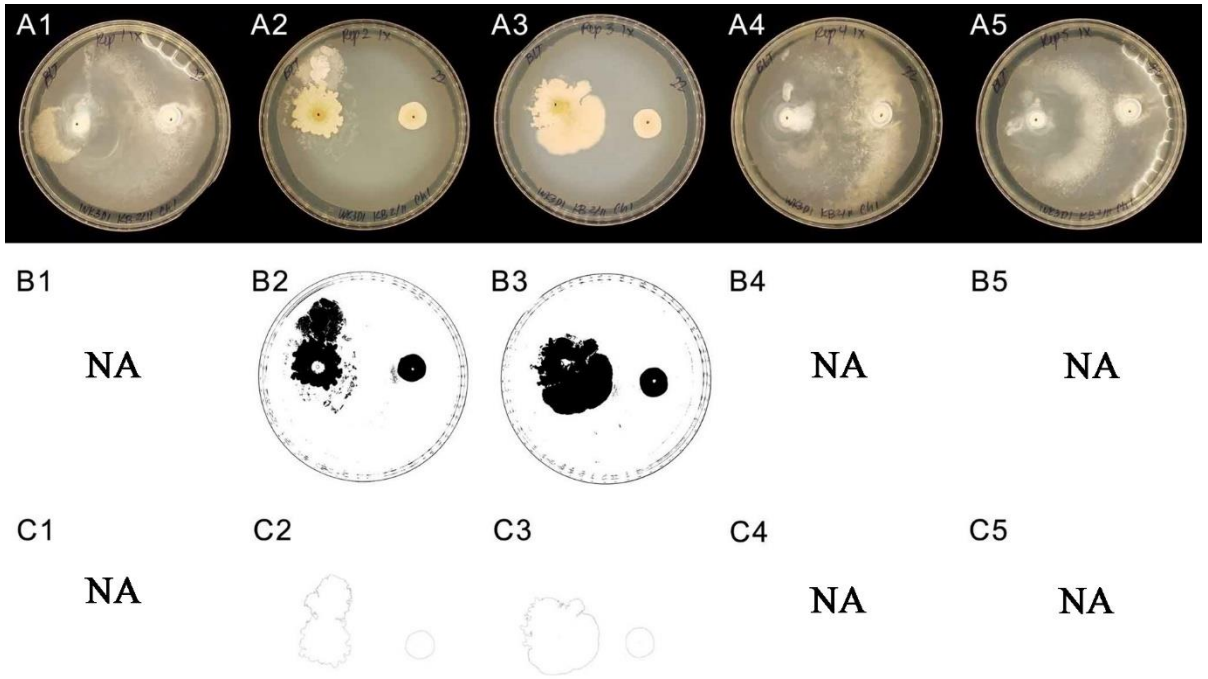


Figure C89. 2021 co-inoculated Petri plates four days after inoculation. **A1-A5)** 1x BLT vs. *Pss* 22 on KB media. **B1-B5)** Images after threshold adjustment in ImageJ. **C1-C5)** Image of measured area. A1, B1, C1: Replication 1; A2, B2, C2: Replication 2; A3, B3, C3: Replication 3; A4, B4, C4: Replication 4; A5, B5, C5: Replication 5. Images with NA are not available.

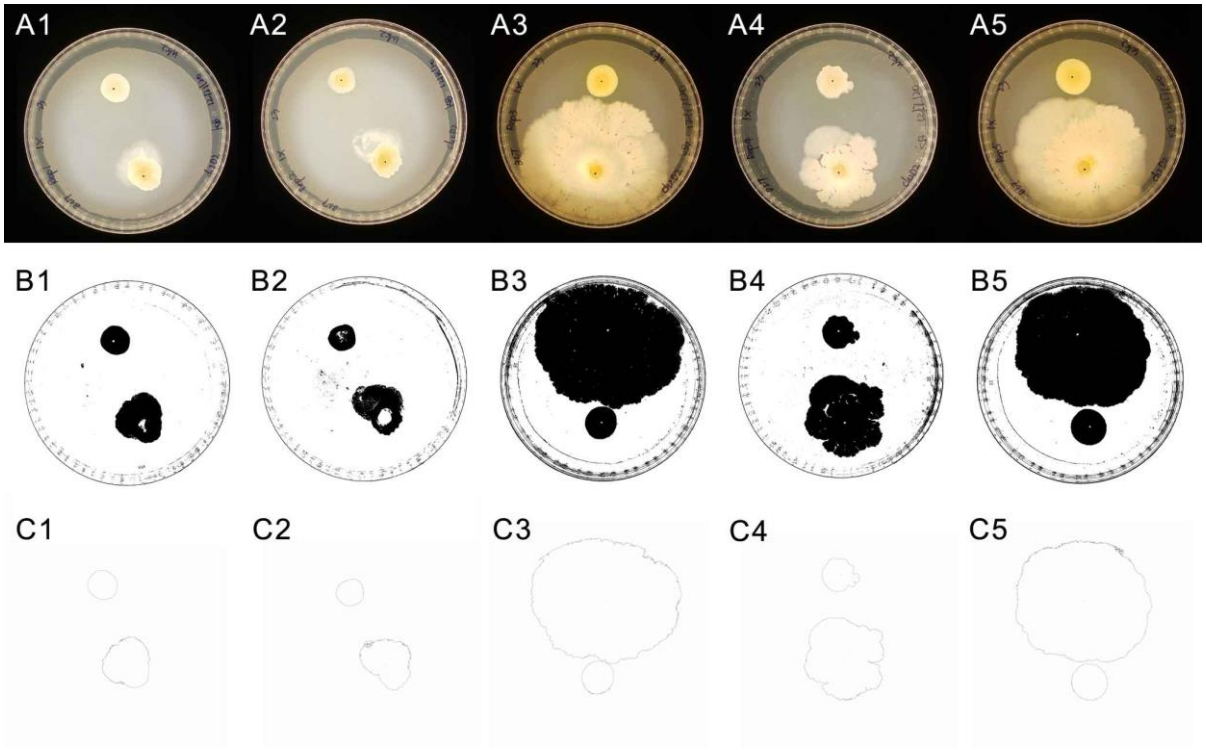


Figure C90. 2021 co-inoculated Petri plates four days after inoculation. **A1-A5)** 1x BLT vs. *Pss* 23 on KB media. **B1-B5)** Images after threshold adjustment in ImageJ. **C1-C5)** Image of measured area. A1, B1, C1: Replication 1; A2, B2, C2: Replication 2; A3, B3, C3: Replication 3; A4, B4, C4: Replication 4; A5, B5, C5: Replication 5.

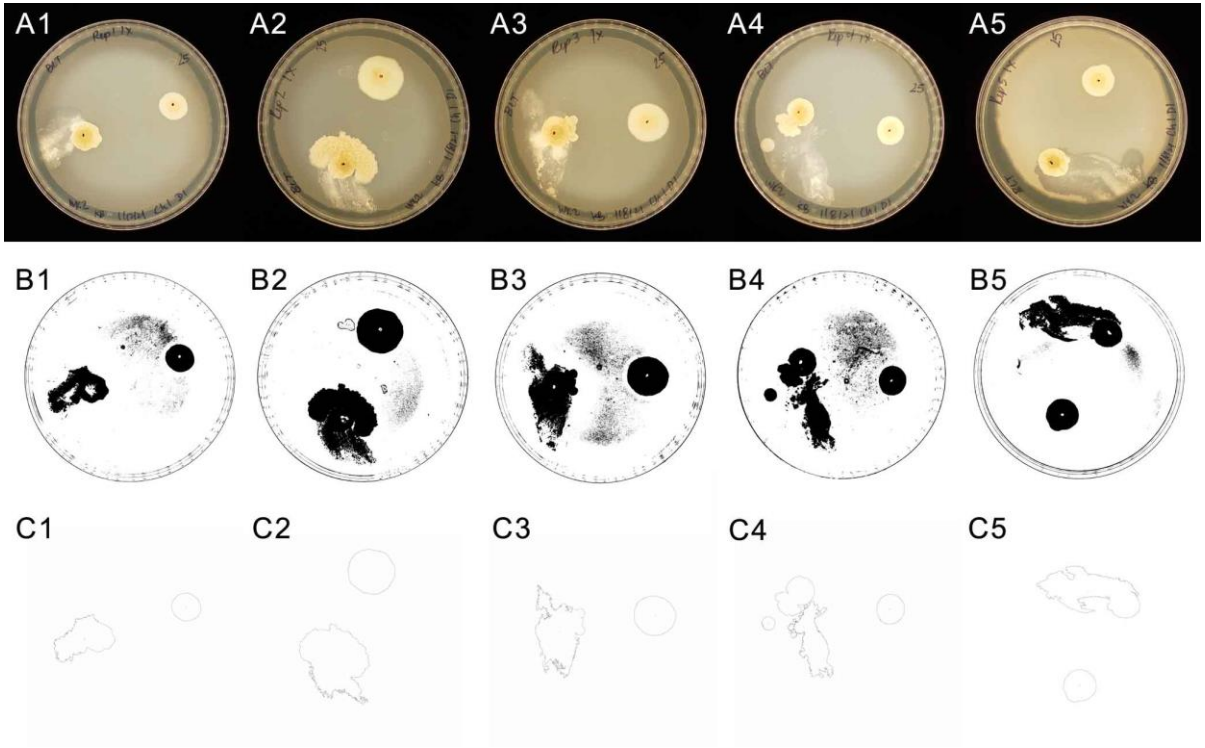


Figure C91. 2021 co-inoculated Petri plates four days after inoculation. **A1-A5)** 1x BLT vs. *Pss* 25 on KB media. **B1-B5)** Images after threshold adjustment in ImageJ. **C1-C5)** Image of measured area. A1, B1, C1: Replication 1; A2, B2, C2: Replication 2; A3, B3, C3: Replication 3; A4, B4, C4: Replication 4; A5, B5, C5: Replication 5.

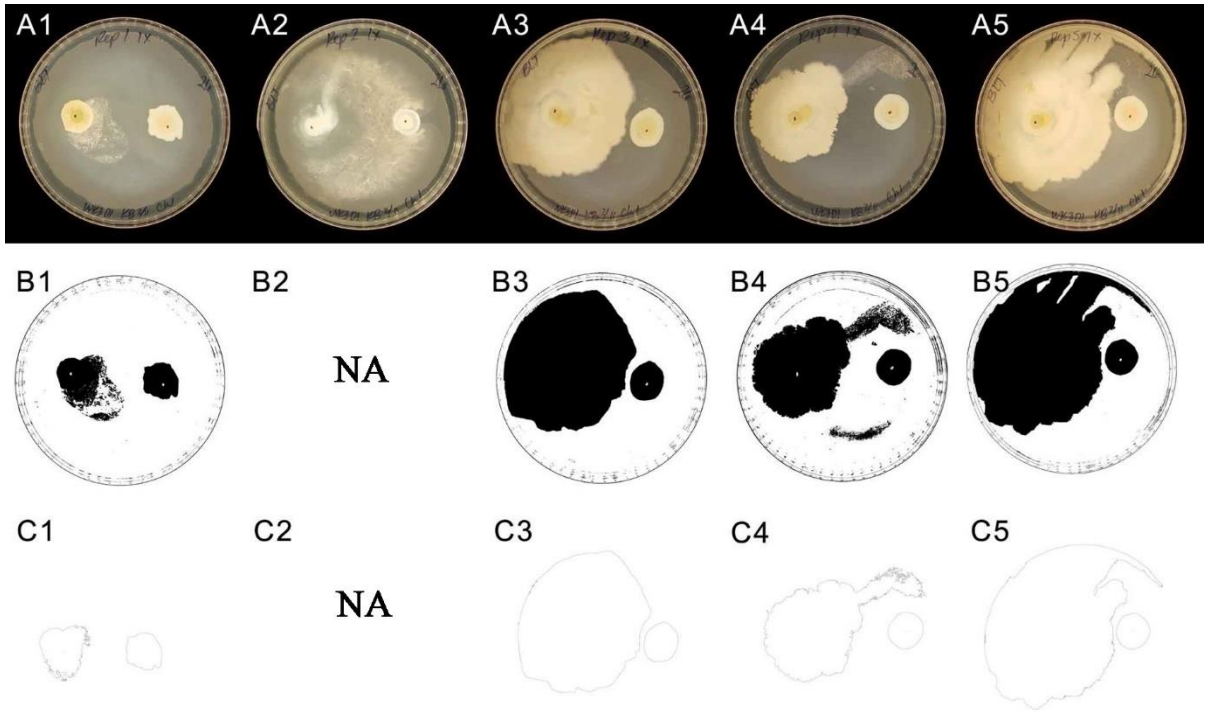


Figure C92. 2021 co-inoculated Petri plates four days after inoculation. **A1-A5)** 1x BLT vs. *Pss* 26 on KB media. **B1-B5)** Images after threshold adjustment in ImageJ. **C1-C5)** Image of measured area. A1, B1, C1: Replication 1; A2, B2, C2: Replication 2; A3, B3, C3: Replication 3; A4, B4, C4: Replication 4; A5, B5, C5: Replication 5. Images with NA are not available.

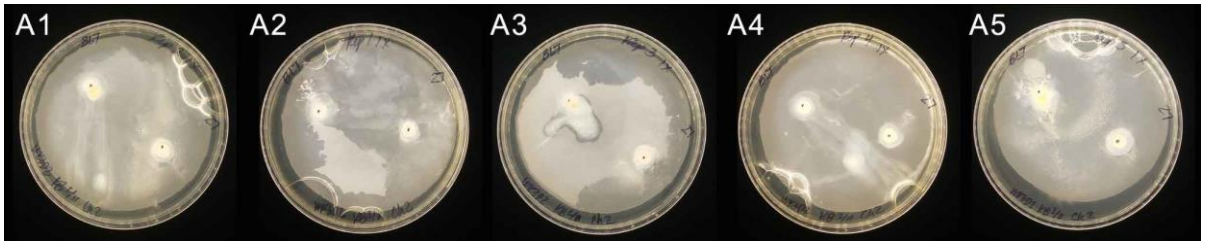


Figure C93. 2021 co-inoculated Petri plates four days after inoculation. **A1-A5)** 1x BLT vs. *Pss* 27 on KB media. Replications 1-5. No measurements were taken as all plates were overgrown.

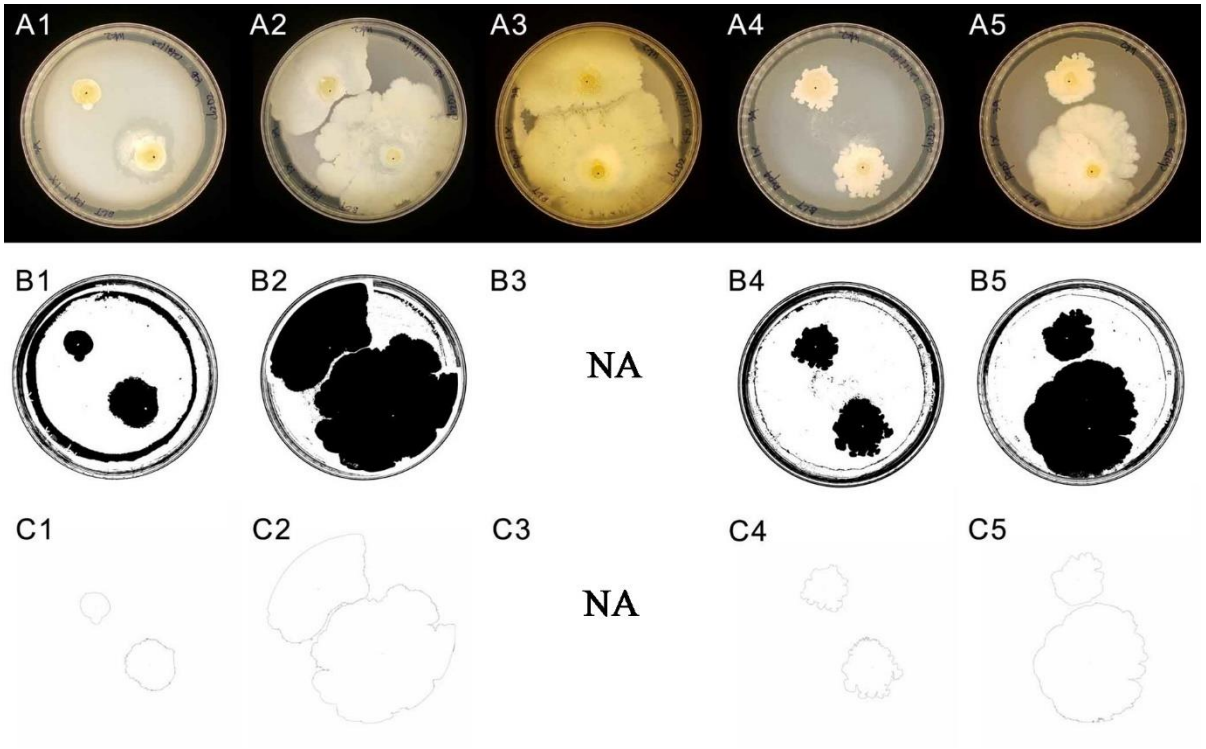


Figure C94. 2021 co-inoculated Petri plates four days after inoculation. **A1-A5)** 1x BLT vs. *Pss* 34 on KB media. **B1-B5)** Images after threshold adjustment in ImageJ. **C1-C5)** Image of measured area. A1, B1, C1: Replication 1; A2, B2, C2: Replication 2; A3, B3, C3: Replication 3; A4, B4, C4: Replication 4; A5, B5, C5: Replication 5. Images with NA are not available.

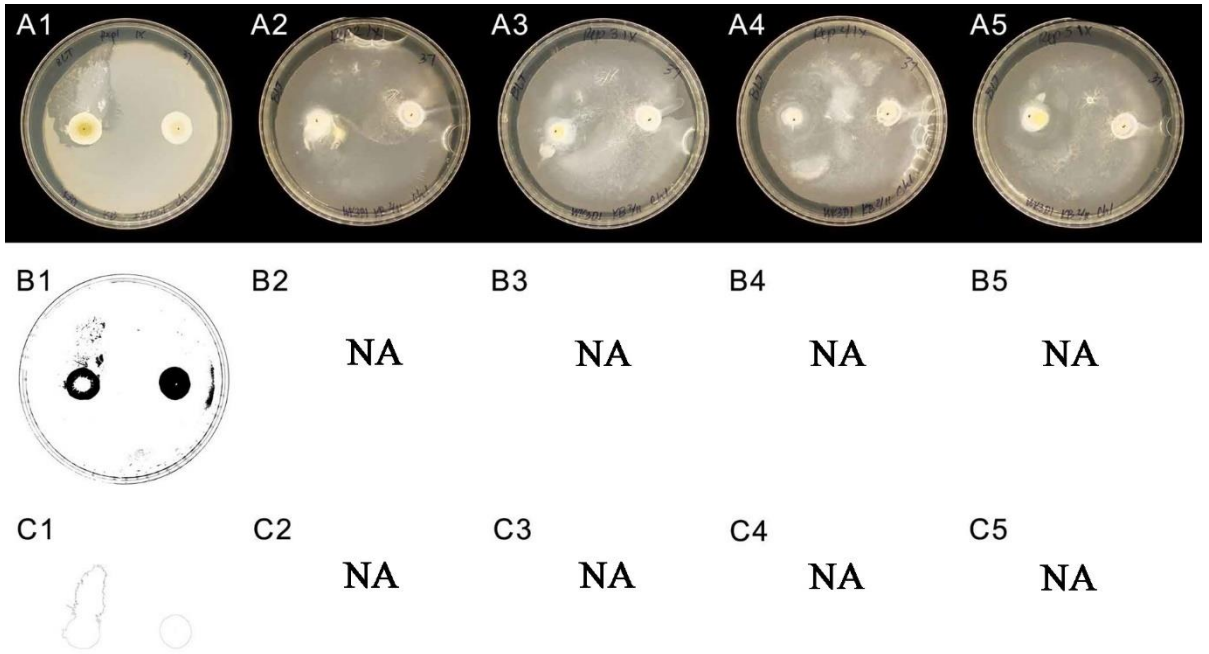


Figure C95. 2021 co-inoculated Petri plates four days after inoculation. **A1-A5)** 1x BLT vs. *Pss* 37 on KB media. **B1-B5)** Images after threshold adjustment in ImageJ. **C1-C5)** Image of measured area. A1, B1, C1: Replication 1; A2, B2, C2: Replication 2; A3, B3, C3: Replication 3; A4, B4, C4: Replication 4; A5, B5, C5: Replication 5. Images with NA are not available.

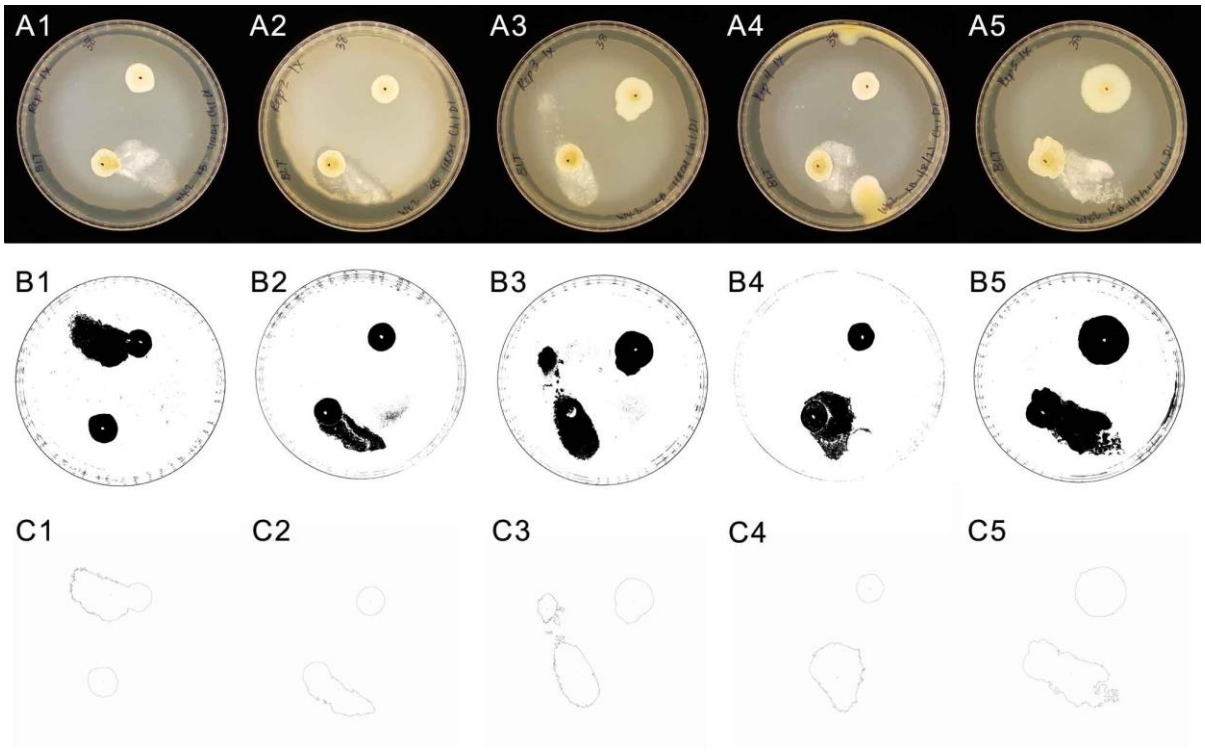


Figure C96. 2021 co-inoculated Petri plates four days after inoculation. **A1-A5)** 1x BLT vs. *Pss* 38 on KB media. **B1-B5)** Images after threshold adjustment in ImageJ. **C1-C5)** Image of measured area. A1, B1, C1: Replication 1; A2, B2, C2: Replication 2; A3, B3, C3: Replication 3; A4, B4, C4: Replication 4; A5, B5, C5: Replication 5.

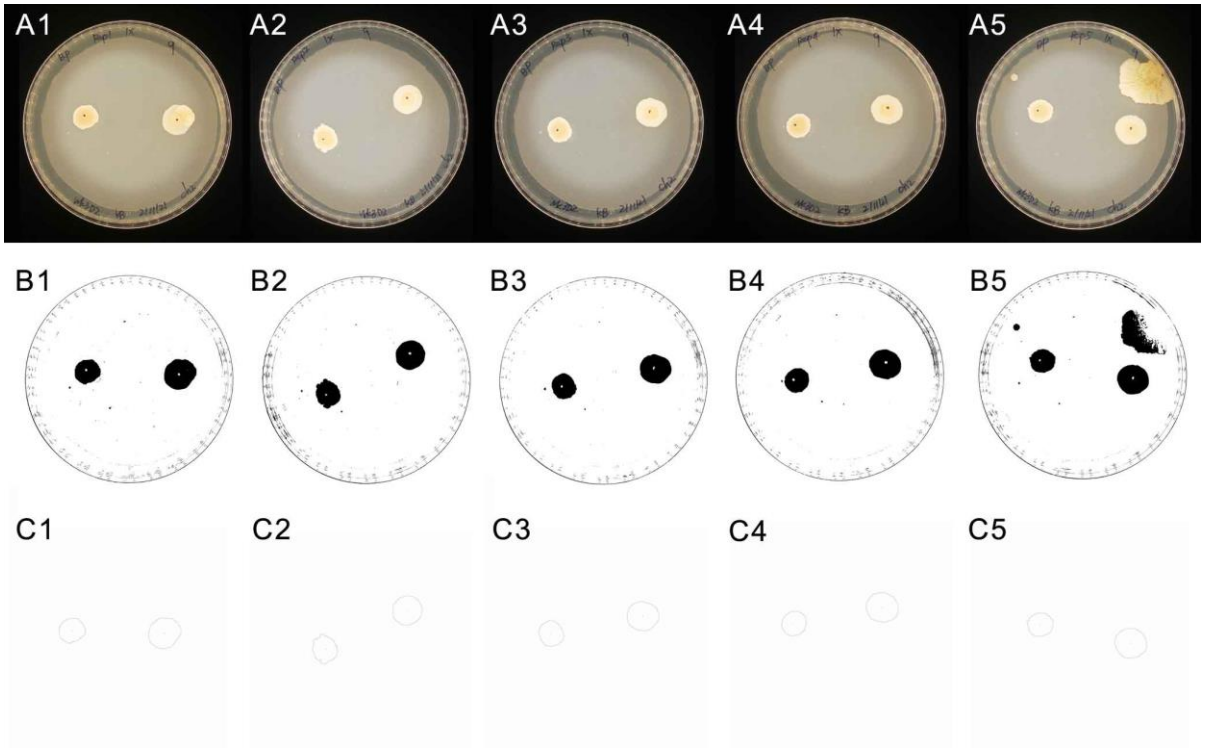


Figure C97. 2021 co-inoculated Petri plates four days after inoculation. **A1-A5)** 1x BP vs. *Pss* 9 on KB media. **B1-B5)** Images after threshold adjustment in ImageJ. **C1-C5)** Image of measured area. A1, B1, C1: Replication 1; A2, B2, C2: Replication 2; A3, B3, C3: Replication 3; A4, B4, C4: Replication 4; A5, B5, C5: Replication 5.

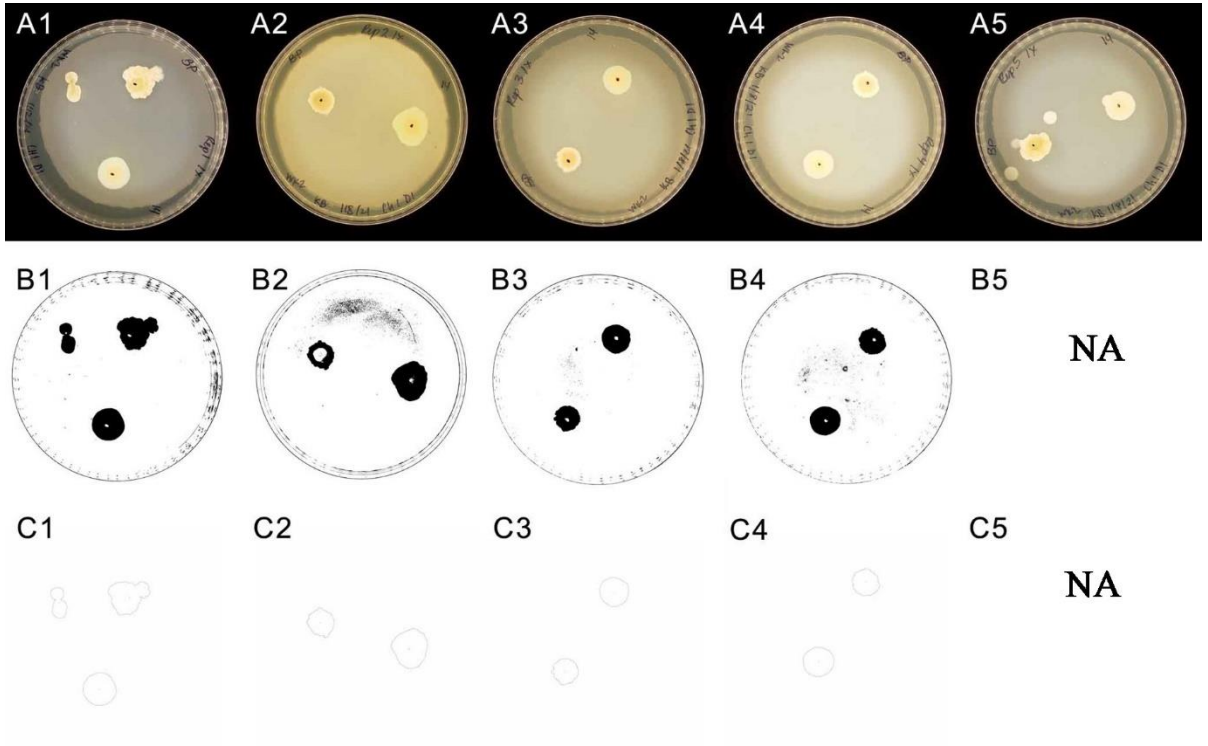


Figure C98. 2021 co-inoculated Petri plates four days after inoculation. **A1-A5)** 1x BP vs. *Pss* 14 on KB media. **B1-B5)** Images after threshold adjustment in ImageJ. **C1-C5)** Image of measured area. A1, B1, C1: Replication 1; A2, B2, C2: Replication 2; A3, B3, C3: Replication 3; A4, B4, C4: Replication 4; A5, B5, C5: Replication 5. Images with NA are not available.

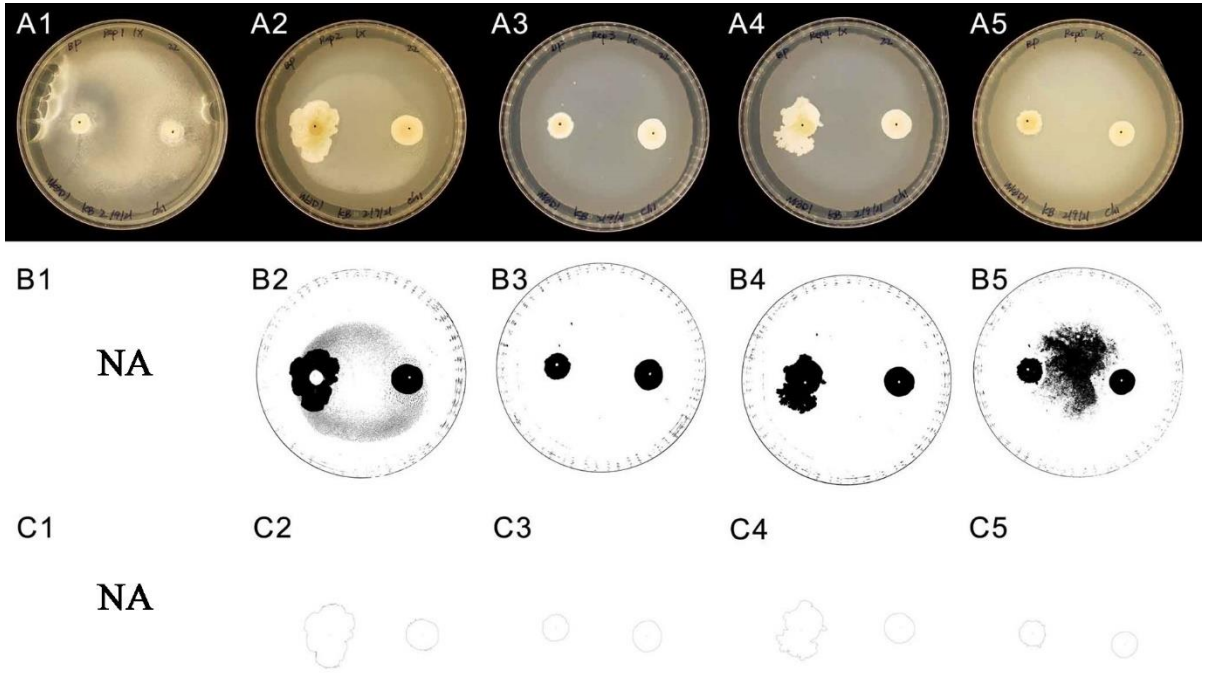


Figure C99. 2021 co-inoculated Petri plates four days after inoculation. **A1-A5)** 1x BP vs. *Pss* 22 on KB media. **B1-B5)** Images after threshold adjustment in ImageJ. **C1-C5)** Image of measured area. A1, B1, C1: Replication 1; A2, B2, C2: Replication 2; A3, B3, C3: Replication 3; A4, B4, C4: Replication 4; A5, B5, C5: Replication 5. Images with NA are not available.

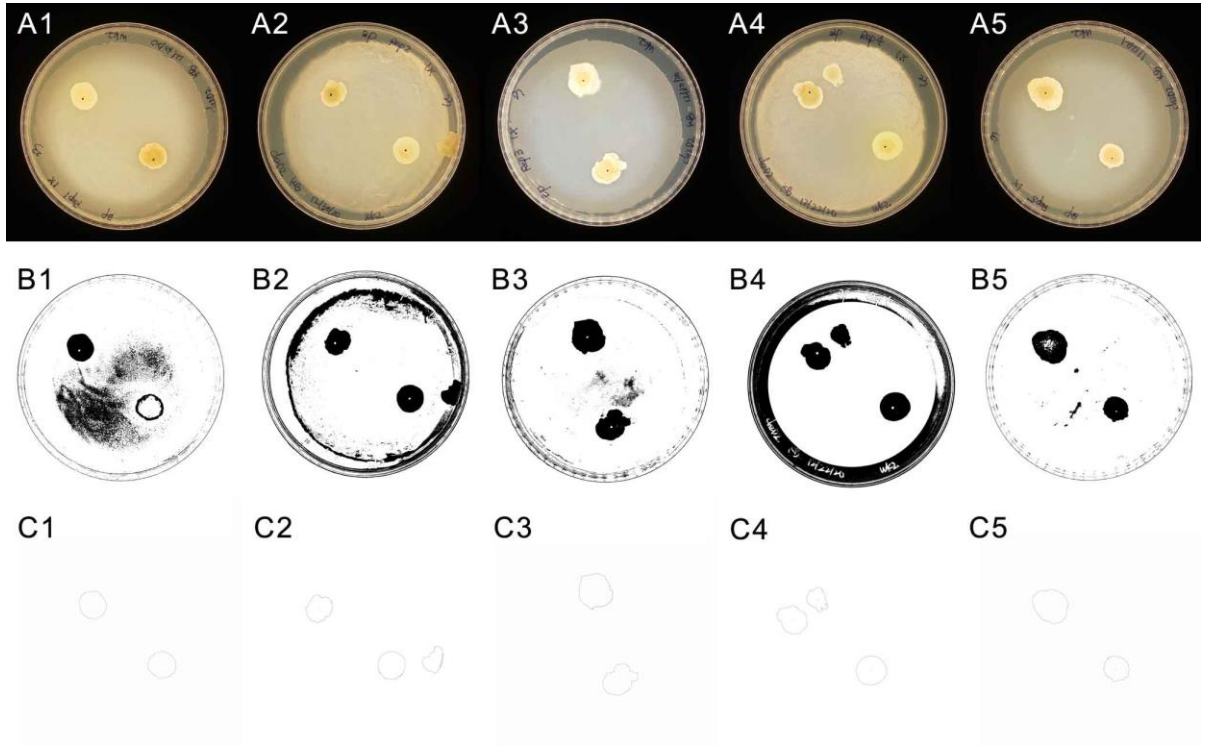


Figure C100. 2021 co-inoculated Petri plates four days after inoculation. **A1-A5)** 1x BP vs. *Pss* 23 on KB media. **B1-B5)** Images after threshold adjustment in ImageJ. **C1-C5)** Image of measured area. A1, B1, C1: Replication 1; A2, B2, C2: Replication 2; A3, B3, C3: Replication 3; A4, B4, C4: Replication 4; A5, B5, C5: Replication 5.

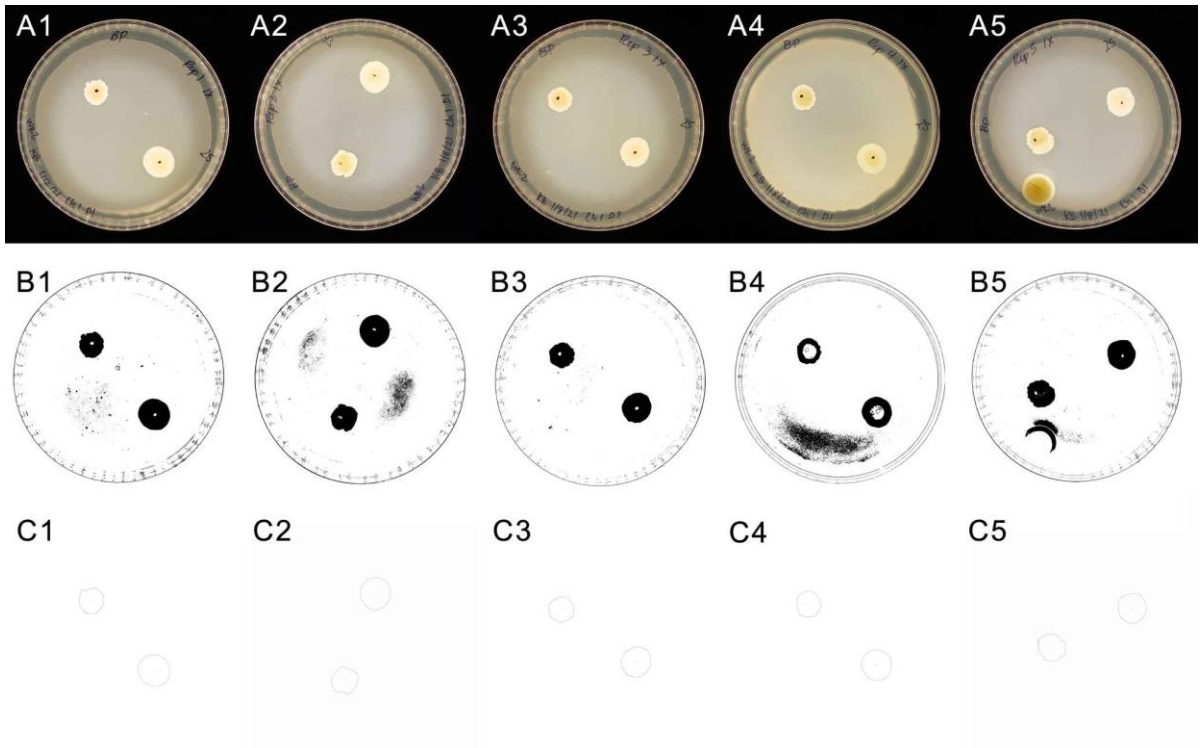


Figure C101. 2021 co-inoculated Petri plates four days after inoculation. **A1-A5)** 1x BP vs. *Pss* 25 on KB media. **B1-B5)** Images after threshold adjustment in ImageJ. **C1-C5)** Image of measured area. A1, B1, C1: Replication 1; A2, B2, C2: Replication 2; A3, B3, C3: Replication 3; A4, B4, C4: Replication 4; A5, B5, C5: Replication 5.

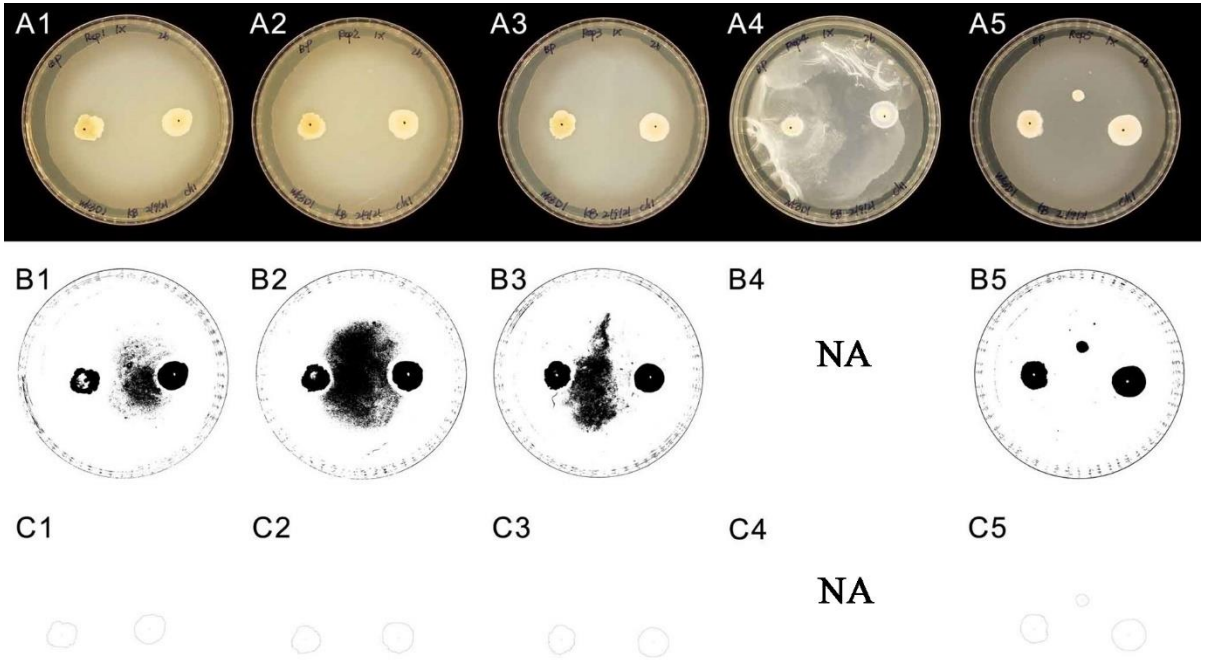


Figure C102. 2021 co-inoculated Petri plates four days after inoculation. **A1-A5)** 1x BP vs. *Pss* 26 on KB media. **B1-B5)** Images after threshold adjustment in ImageJ. **C1-C5)** Image of measured area. A1, B1, C1: Replication 1; A2, B2, C2: Replication 2; A3, B3, C3: Replication 3; A4, B4, C4: Replication 4; A5, B5, C5: Replication 5. Images with NA are not available.

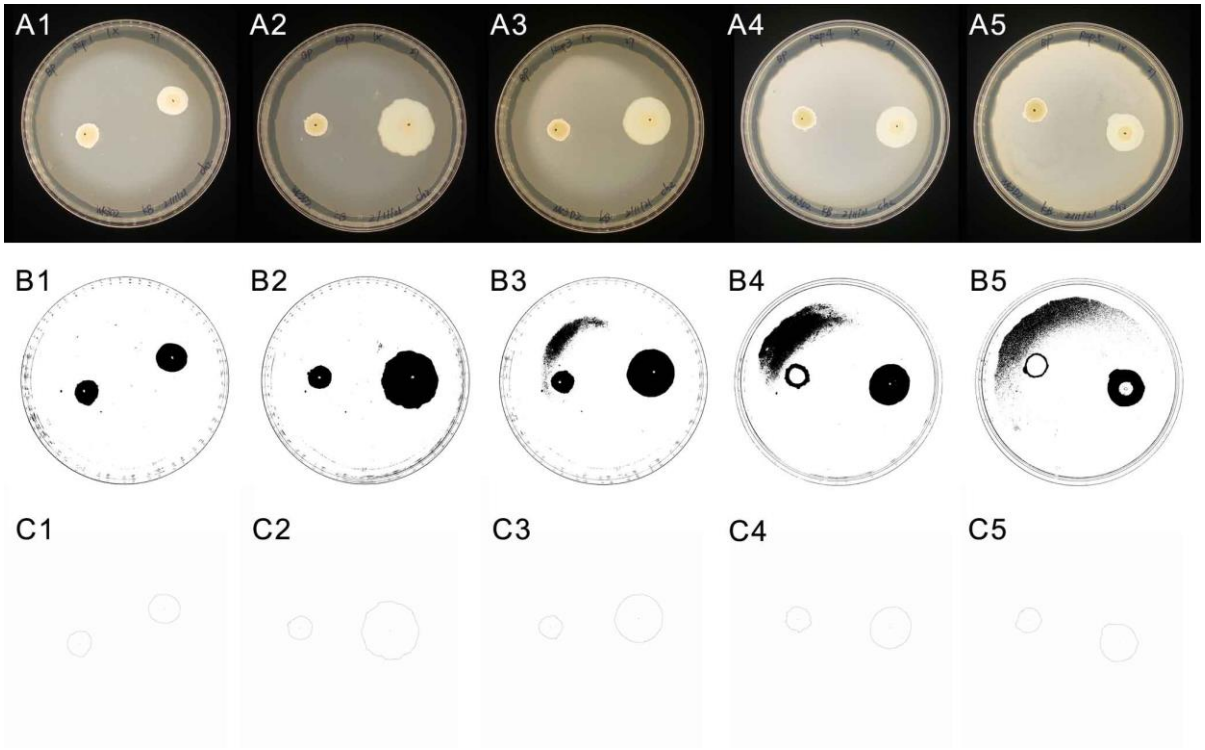


Figure C103. 2021 co-inoculated Petri plates four days after inoculation. **A1-A5)** 1x BP vs. *Pss* 27 on KB media. **B1-B5)** Images after threshold adjustment in ImageJ. **C1-C5)** Image of measured area. A1, B1, C1: Replication 1; A2, B2, C2: Replication 2; A3, B3, C3: Replication 3; A4, B4, C4: Replication 4; A5, B5, C5: Replication 5.

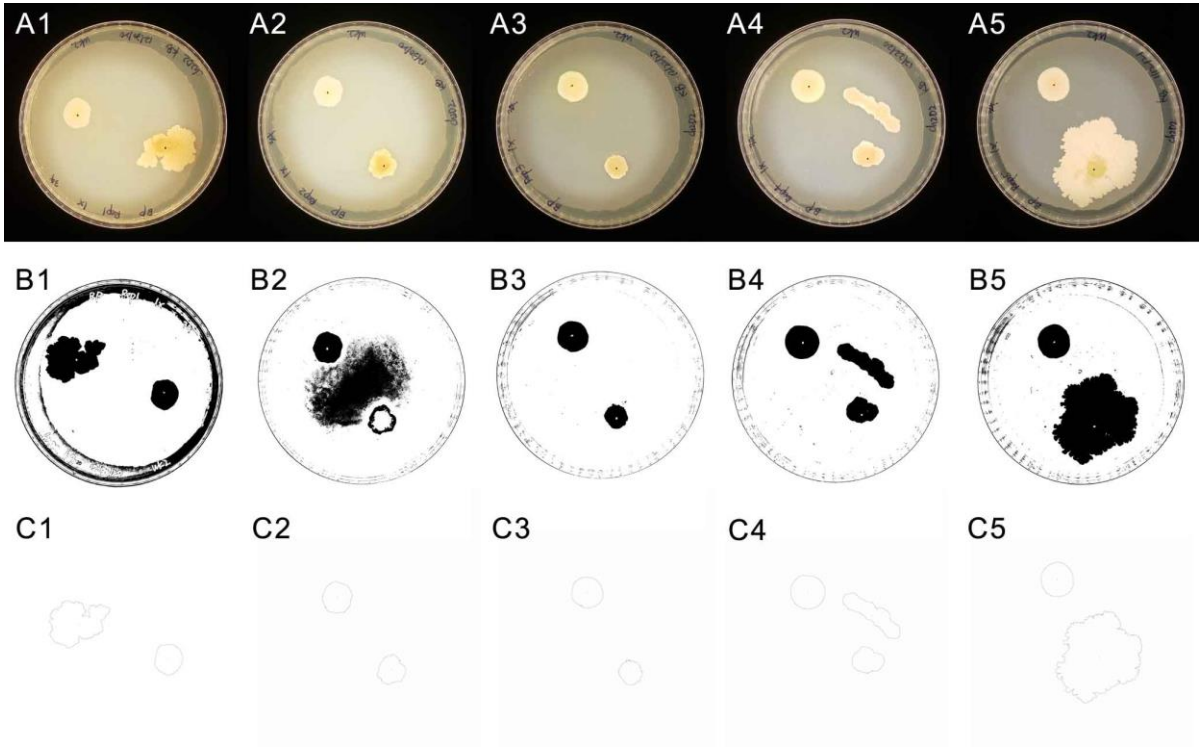


Figure C104. 2021 co-inoculated Petri plates four days after inoculation. **A1-A5)** 1x BP vs. *Pss* 34 on KB media. **B1-B5)** Images after threshold adjustment in ImageJ. **C1-C5)** Image of measured area. A1, B1, C1: Replication 1; A2, B2, C2: Replication 2; A3, B3, C3: Replication 3; A4, B4, C4: Replication 4; A5, B5, C5: Replication 5.

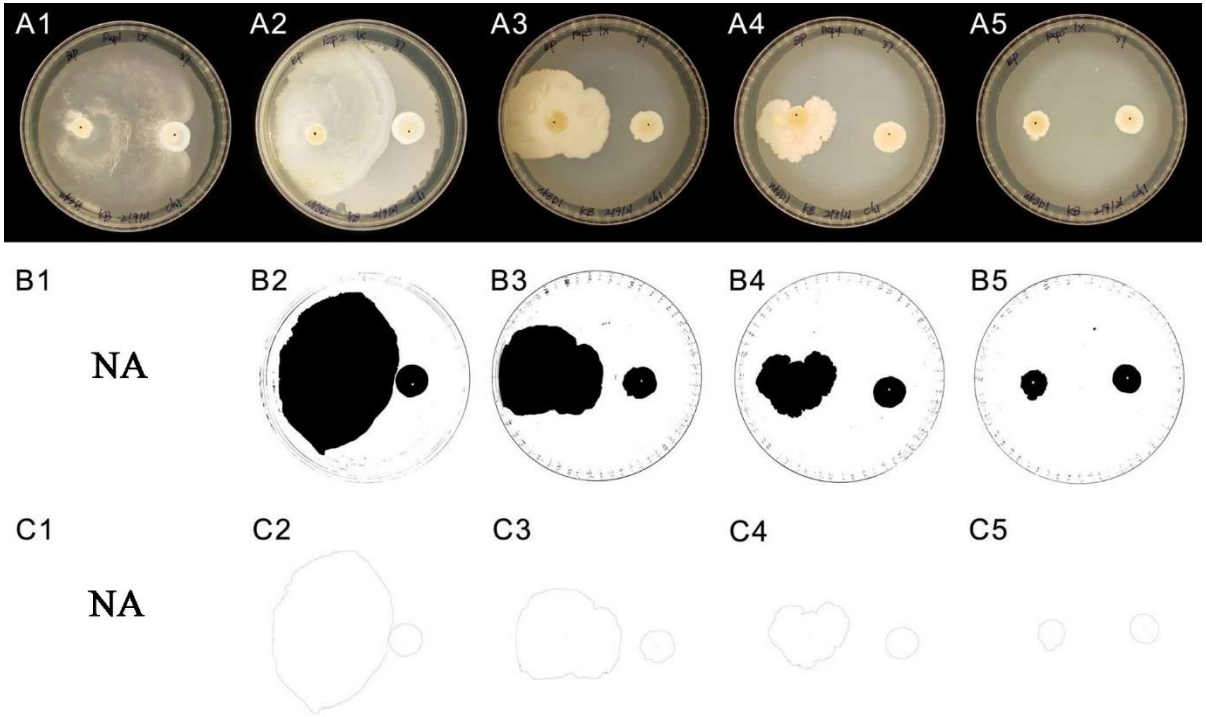


Figure C105. 2021 co-inoculated Petri plates four days after inoculation. **A1-A5)** 1x BP vs. *Pss* 37 on KB media. **B1-B5)** Images after threshold adjustment in ImageJ. **C1-C5)** Image of measured area. A1, B1, C1: Replication 1; A2, B2, C2: Replication 2; A3, B3, C3: Replication 3; A4, B4, C4: Replication 4; A5, B5, C5: Replication 5. Images with NA are not available.

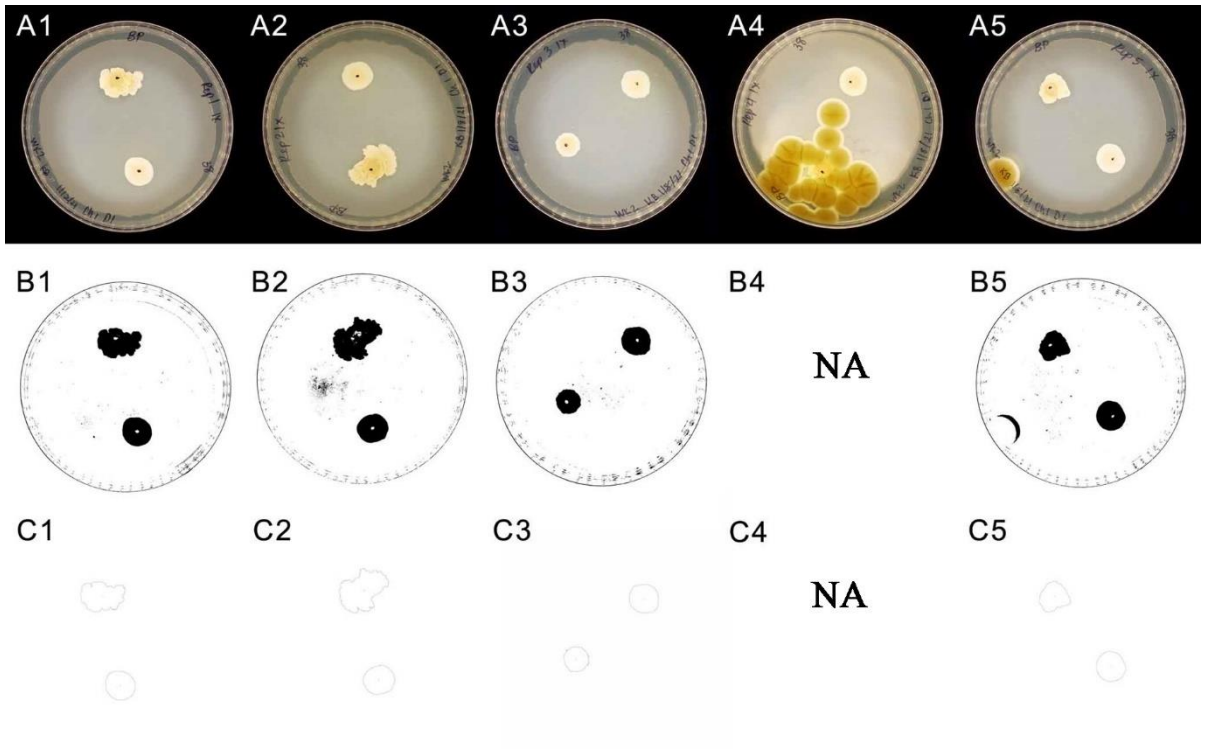


Figure C106. 2021 co-inoculated Petri plates four days after inoculation. **A1-A5)** 1x BP vs. *Pss* 38 on KB media. **B1-B5)** Images after threshold adjustment in ImageJ. **C1-C5)** Image of measured area. A1, B1, C1: Replication 1; A2, B2, C2: Replication 2; A3, B3, C3: Replication 3; A4, B4, C4: Replication 4; A5, B5, C5: Replication 5. Images with NA are not available.

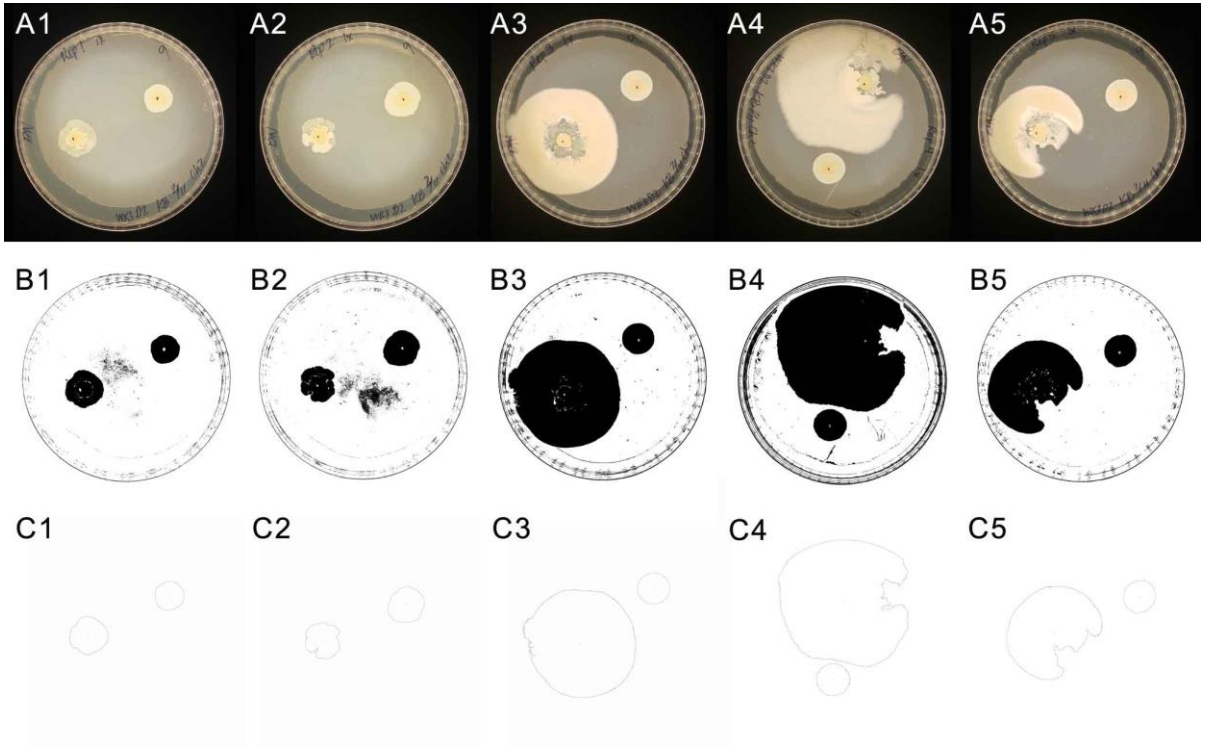


Figure C107. 2021 co-inoculated Petri plates four days after inoculation. **A1-A5)** 1x DN vs. *Pss* 9 on KB media. **B1-B5)** Images after threshold adjustment in ImageJ. **C1-C5)** Image of measured area. A1, B1, C1: Replication 1; A2, B2, C2: Replication 2; A3, B3, C3: Replication 3; A4, B4, C4: Replication 4; A5, B5, C5: Replication 5.

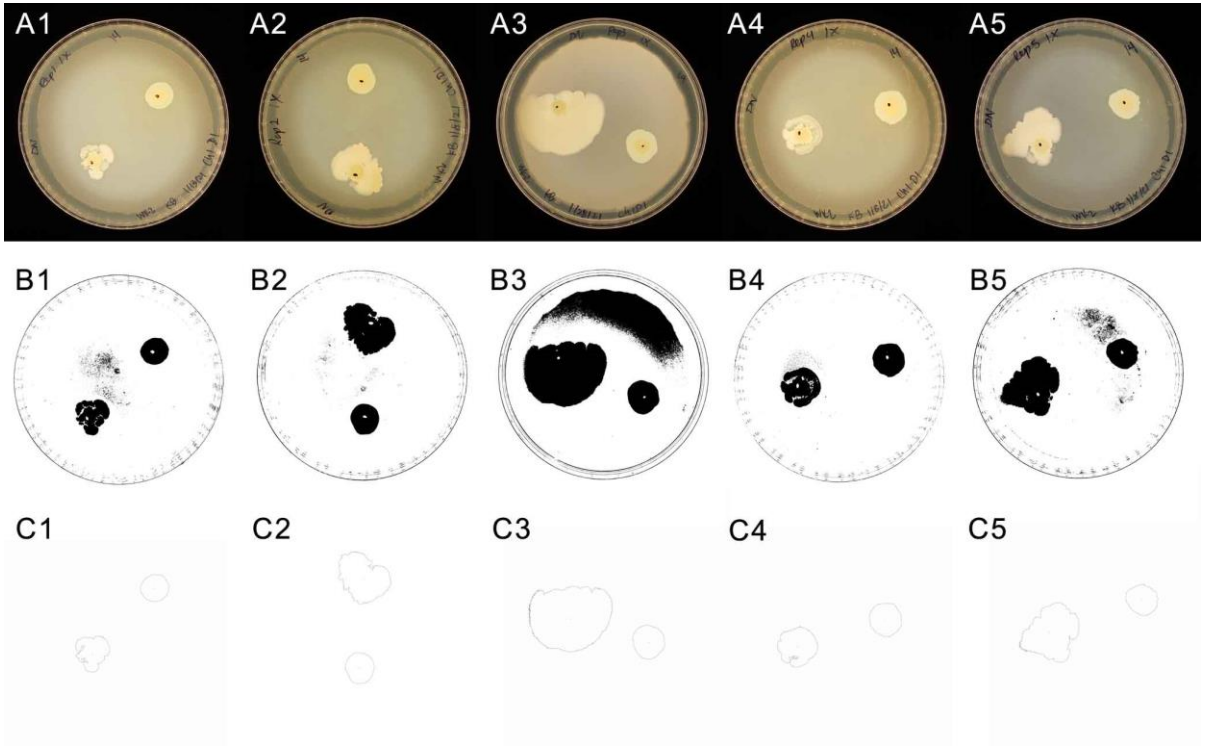


Figure C108. 2021 co-inoculated Petri plates four days after inoculation. **A1-A5)** 1x DN vs. *Pss* 14 on KB media. **B1-B5)** Images after threshold adjustment in ImageJ. **C1-C5)** Image of measured area. A1, B1, C1: Replication 1; A2, B2, C2: Replication 2; A3, B3, C3: Replication 3; A4, B4, C4: Replication 4; A5, B5, C5: Replication 5.

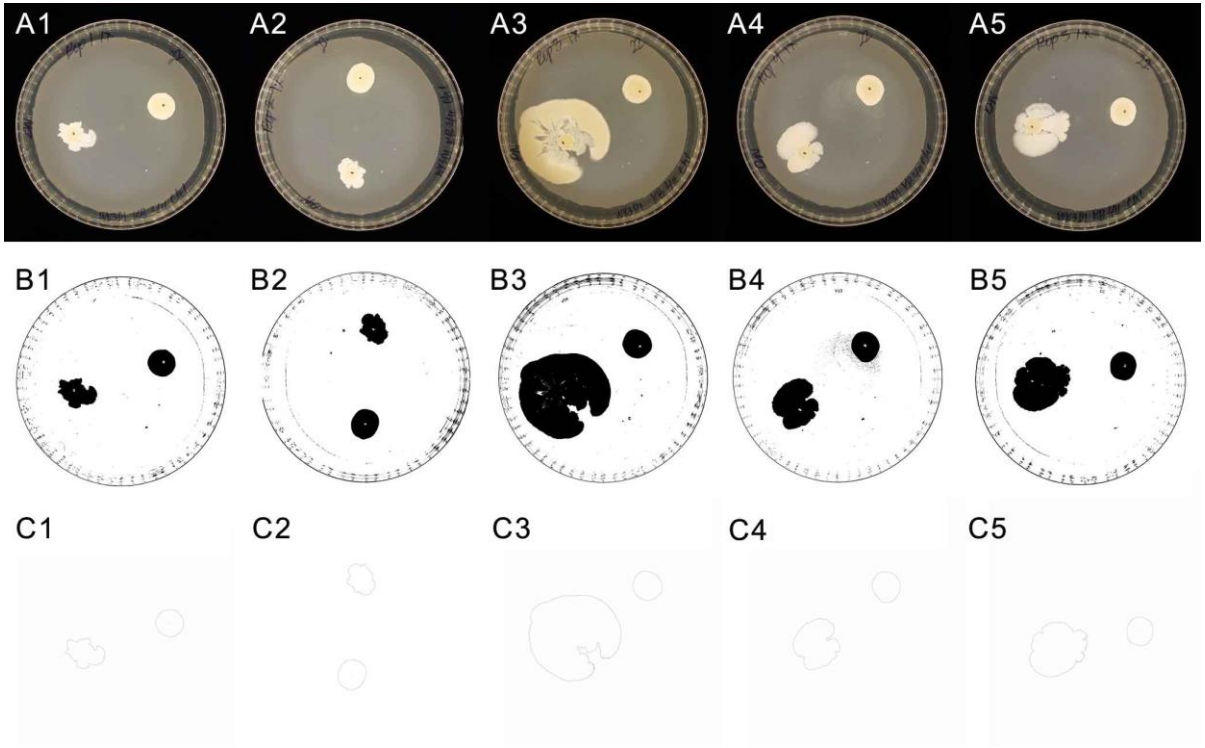


Figure C109. 2021 co-inoculated Petri plates four days after inoculation. **A1-A5)** 1x DN vs. *Pss* 22 on KB media. **B1-B5)** Images after threshold adjustment in ImageJ. **C1-C5)** Image of measured area. A1, B1, C1: Replication 1; A2, B2, C2: Replication 2; A3, B3, C3: Replication 3; A4, B4, C4: Replication 4; A5, B5, C5: Replication 5.

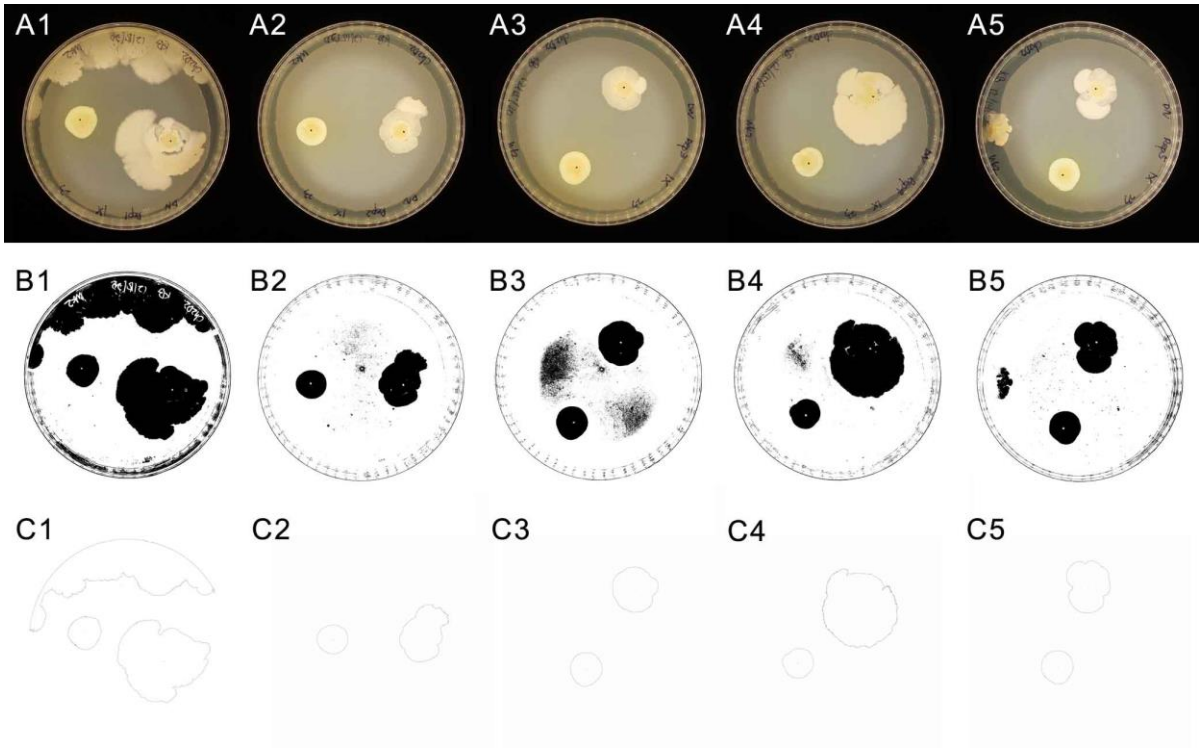


Figure C110. 2021 co-inoculated Petri plates four days after inoculation. **A1-A5)** 1x DN vs. *Pss* 23 on KB media. **B1-B5)** Images after threshold adjustment in ImageJ. **C1-C5)** Image of measured area. A1, B1, C1: Replication 1; A2, B2, C2: Replication 2; A3, B3, C3: Replication 3; A4, B4, C4: Replication 4; A5, B5, C5: Replication 5.

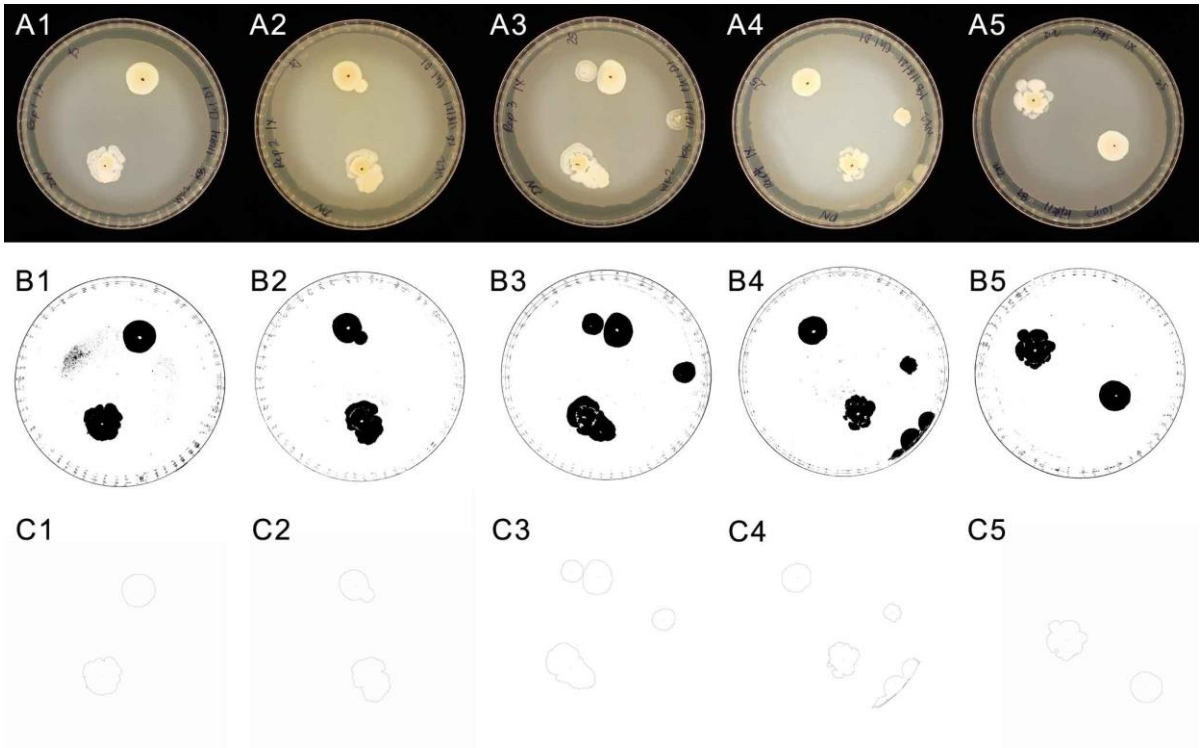


Figure C111. 2021 co-inoculated Petri plates four days after inoculation. **A1-A5)** 1x DN vs. *Pss* 25 on KB media. **B1-B5)** Images after threshold adjustment in ImageJ. **C1-C5)** Image of measured area. A1, B1, C1: Replication 1; A2, B2, C2: Replication 2; A3, B3, C3: Replication 3; A4, B4, C4: Replication 4; A5, B5, C5: Replication 5.

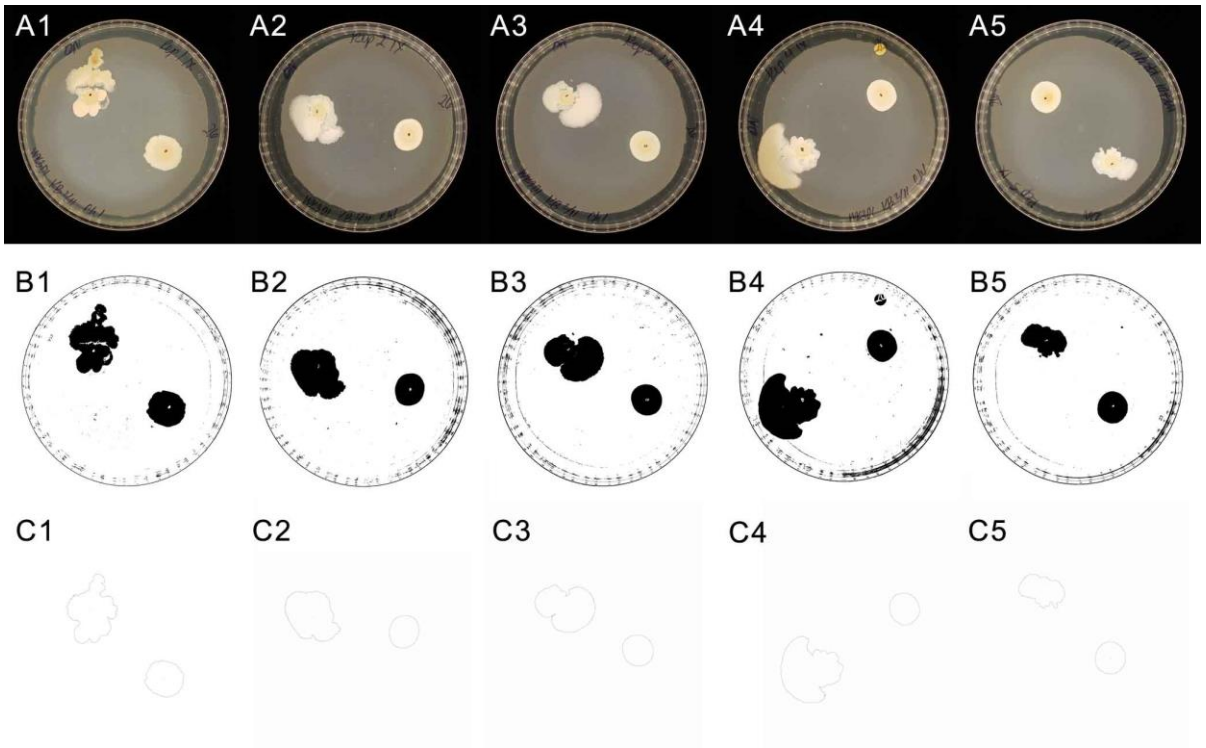


Figure C112. 2021 co-inoculated Petri plates four days after inoculation. **A1-A5)** 1x DN vs. *Pss* 26 on KB media. **B1-B5)** Images after threshold adjustment in ImageJ. **C1-C5)** Image of measured area. A1, B1, C1: Replication 1; A2, B2, C2: Replication 2; A3, B3, C3: Replication 3; A4, B4, C4: Replication 4; A5, B5, C5: Replication 5.

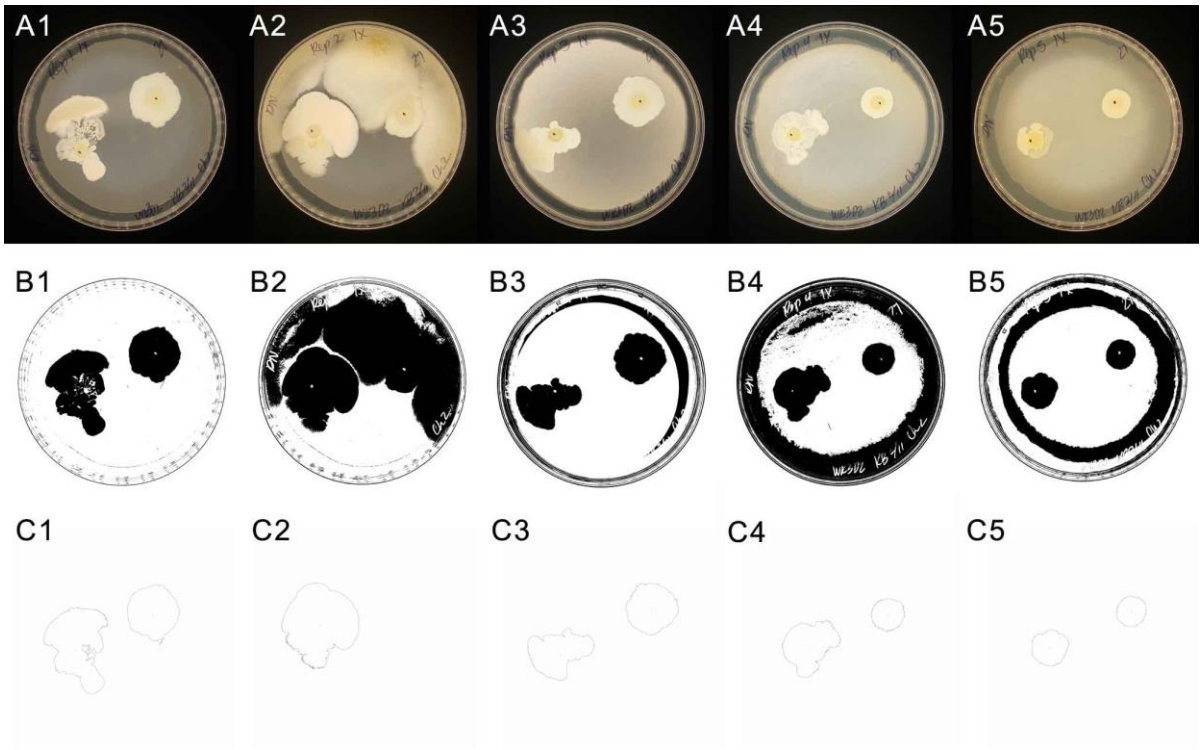


Figure C113. 2021 co-inoculated Petri plates four days after inoculation. **A1-A5)** 1x DN vs. *Pss* 27 on KB media. **B1-B5)** Images after threshold adjustment in ImageJ. **C1-C5)** Image of measured area. A1, B1, C1: Replication 1; A2, B2, C2: Replication 2; A3, B3, C3: Replication 3; A4, B4, C4: Replication 4; A5, B5, C5: Replication 5.

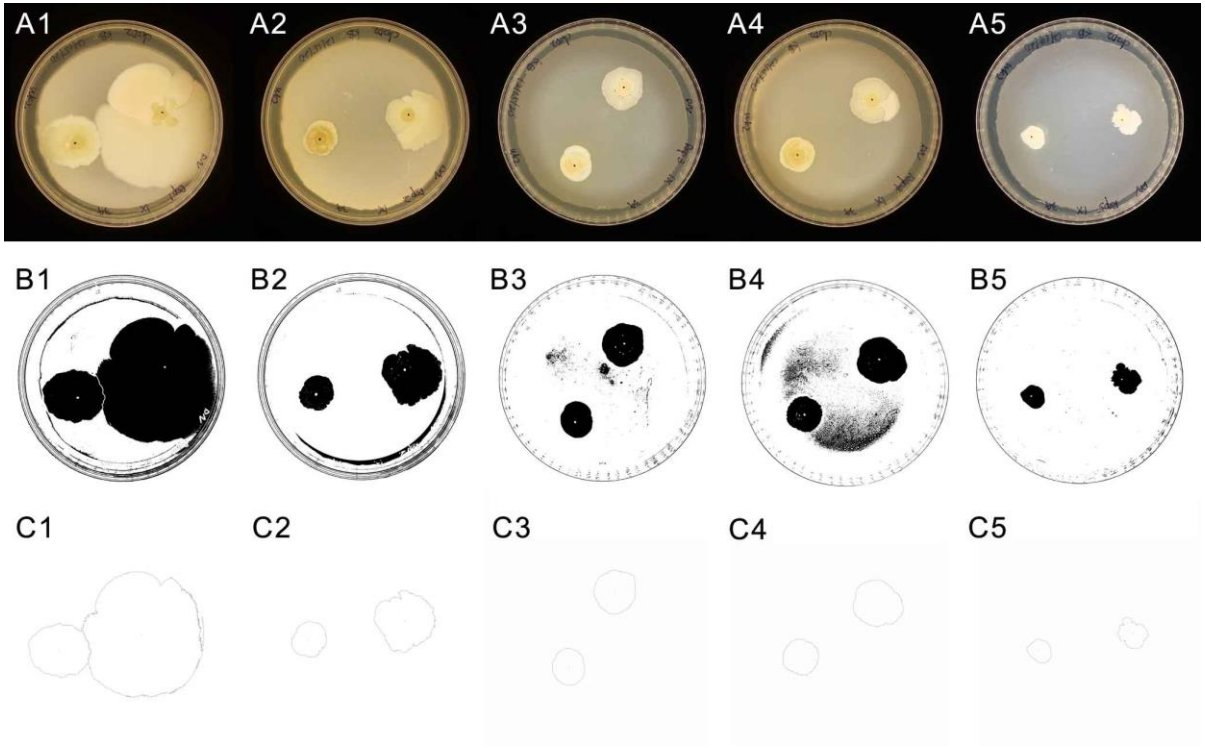


Figure C114. 2021 co-inoculated Petri plates four days after inoculation. **A1-A5)** 1x DN vs. *Pss* 34 on KB media. **B1-B5)** Images after threshold adjustment in ImageJ. **C1-C5)** Image of measured area. A1, B1, C1: Replication 1; A2, B2, C2: Replication 2; A3, B3, C3: Replication 3; A4, B4, C4: Replication 4; A5, B5, C5: Replication 5.

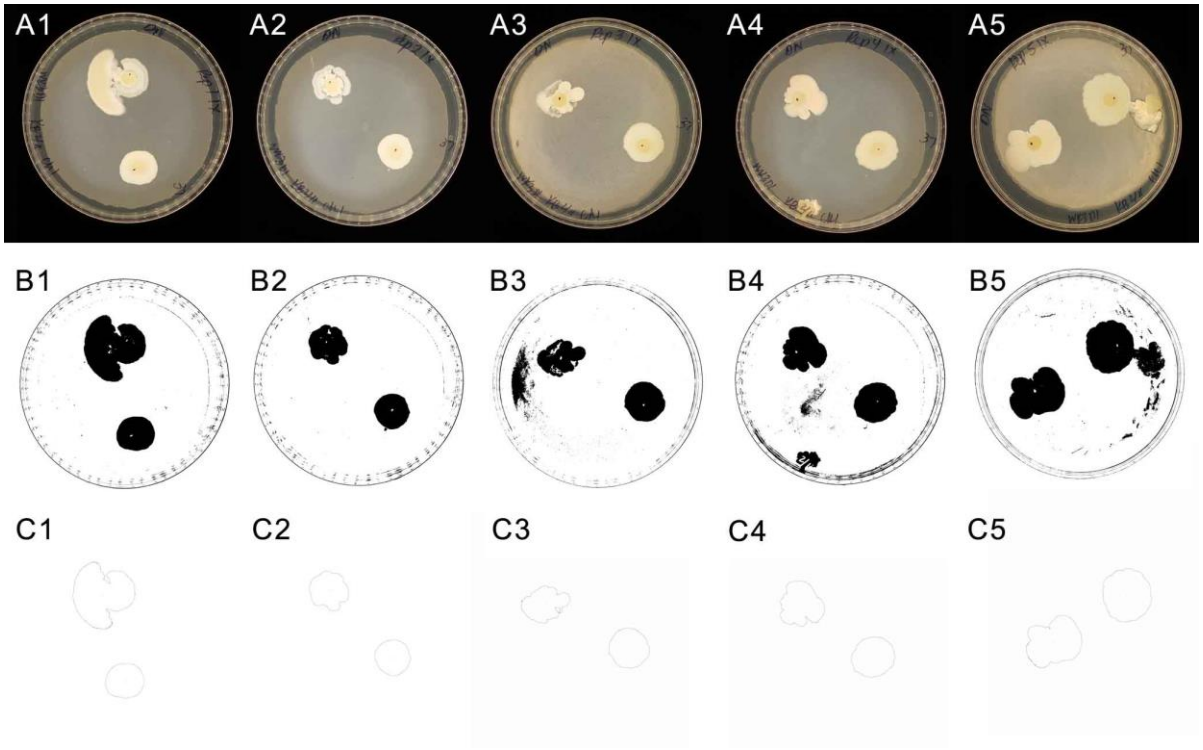


Figure C115. 2021 co-inoculated Petri plates four days after inoculation. **A1-A5)** 1x DN vs. *Pss* 37 on KB media. **B1-B5)** Images after threshold adjustment in ImageJ. **C1-C5)** Image of measured area. A1, B1, C1: Replication 1; A2, B2, C2: Replication 2; A3, B3, C3: Replication 3; A4, B4, C4: Replication 4; A5, B5, C5: Replication 5.

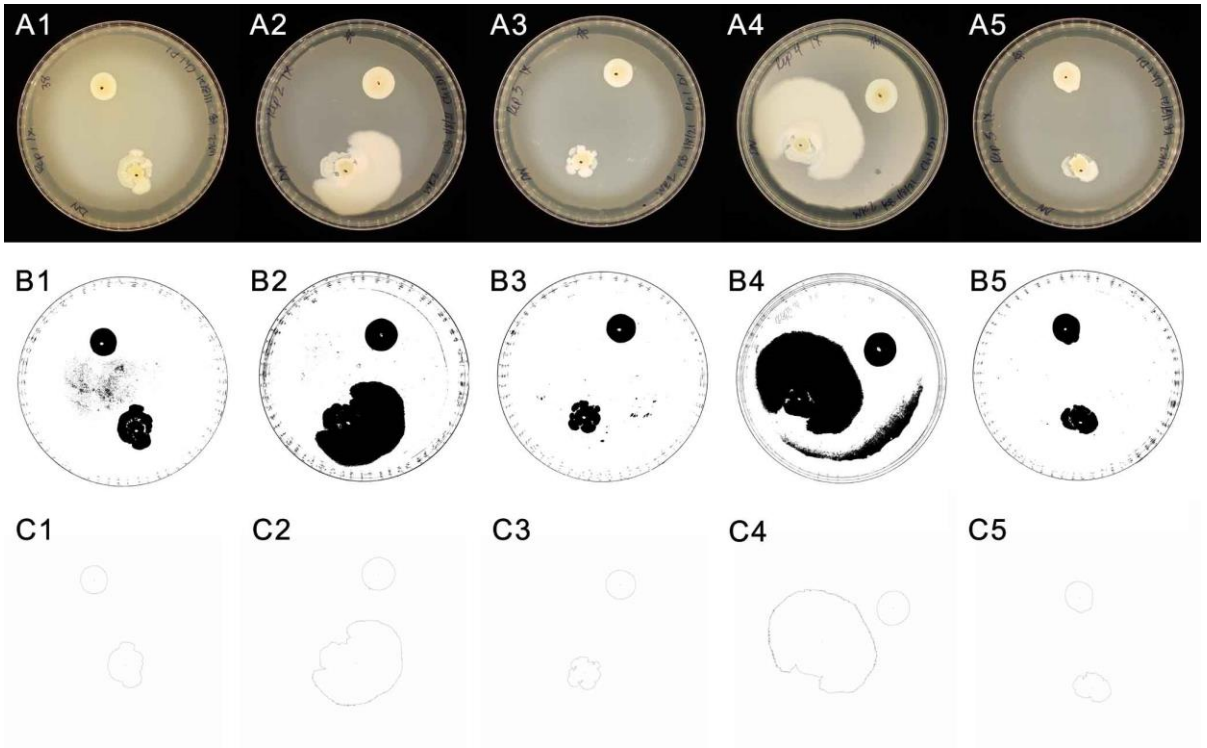


Figure C116. 2021 co-inoculated Petri plates four days after inoculation. **A1-A5)** 1x DN vs. *Pss* 38 on KB media. **B1-B5)** Images after threshold adjustment in ImageJ. **C1-C5)** Image of measured area. A1, B1, C1: Replication 1; A2, B2, C2: Replication 2; A3, B3, C3: Replication 3; A4, B4, C4: Replication 4; A5, B5, C5: Replication 5.

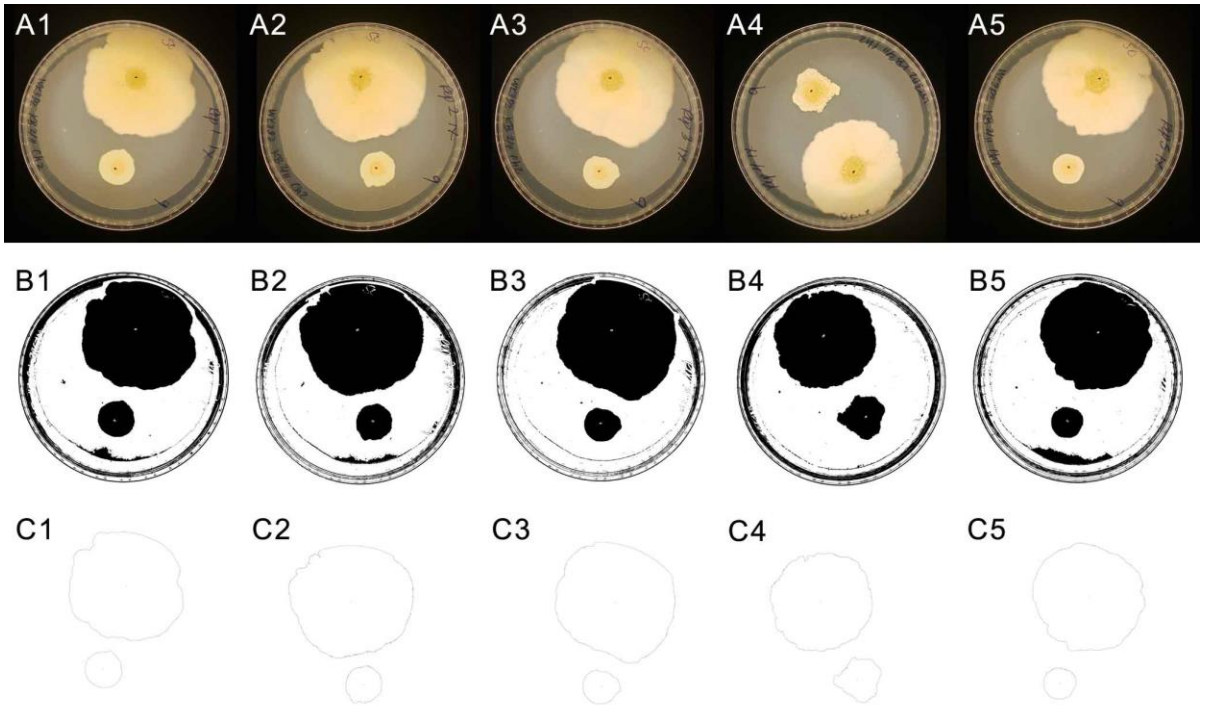


Figure C117. 2021 co-inoculated Petri plates four days after inoculation. **A1-A5)** 1x SO vs. *Pss* 9 on KB media. **B1-B5)** Images after threshold adjustment in ImageJ. **C1-C5)** Image of measured area. A1, B1, C1: Replication 1; A2, B2, C2: Replication 2; A3, B3, C3: Replication 3; A4, B4, C4: Replication 4; A5, B5, C5: Replication 5.

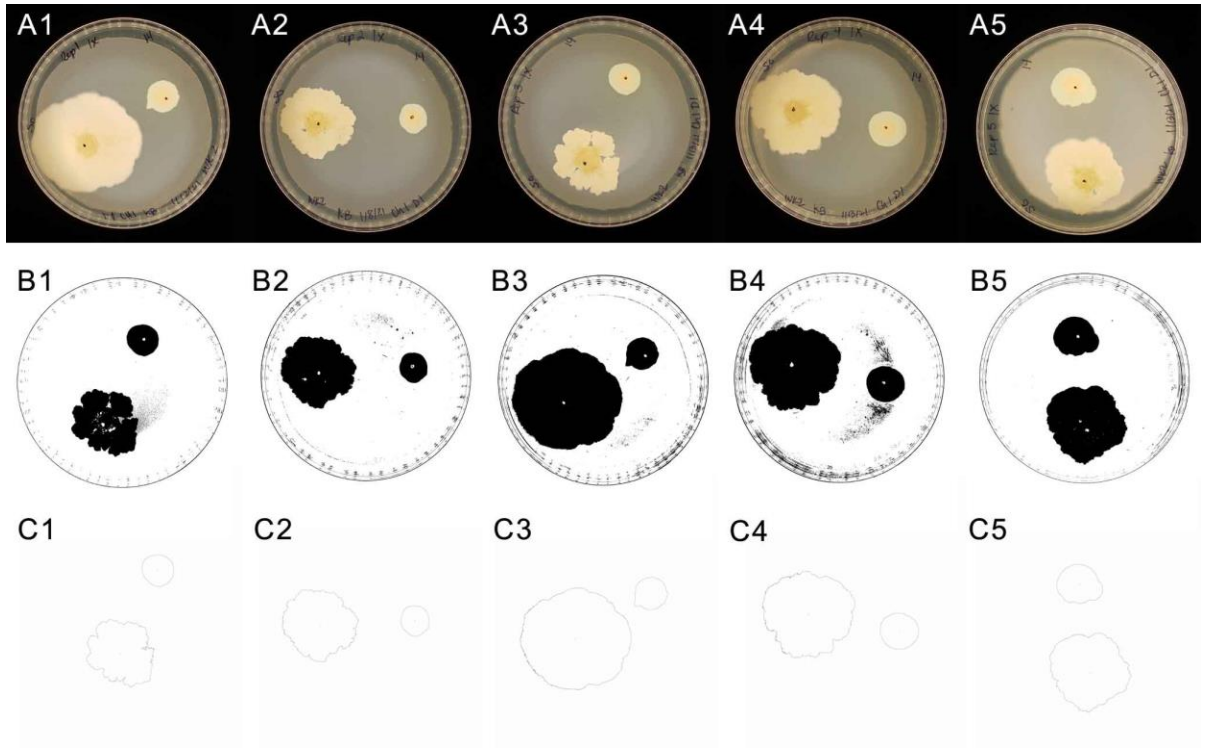


Figure C118. 2021 co-inoculated Petri plates four days after inoculation. **A1-A5)** 1x SO vs. *Pss* 14 on KB media. **B1-B5)** Images after threshold adjustment in ImageJ. **C1-C5)** Image of measured area. A1, B1, C1: Replication 1; A2, B2, C2: Replication 2; A3, B3, C3: Replication 3; A4, B4, C4: Replication 4; A5, B5, C5: Replication 5.

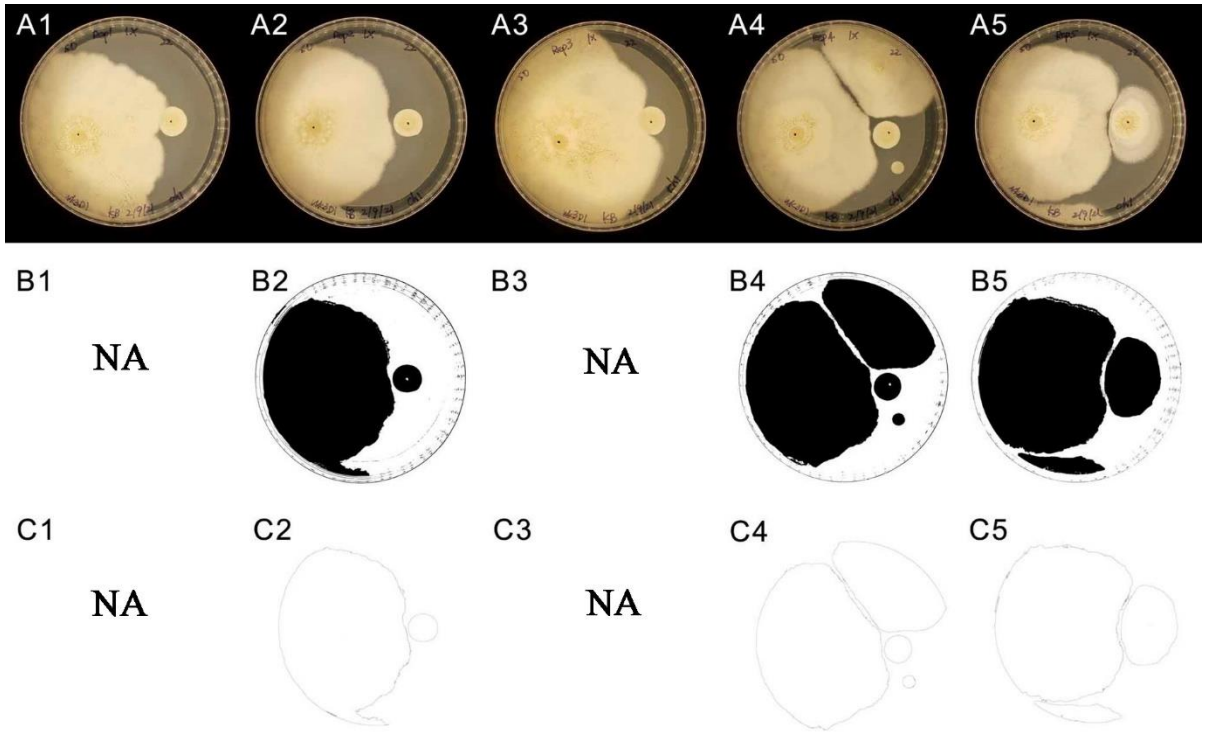


Figure C119. 2021 co-inoculated Petri plates four days after inoculation. **A1-A5)** 1x SO vs. *Pss* 22 on KB media. **B1-B5)** Images after threshold adjustment in ImageJ. **C1-C5)** Image of measured area. A1, B1, C1: Replication 1; A2, B2, C2: Replication 2; A3, B3, C3: Replication 3; A4, B4, C4: Replication 4; A5, B5, C5: Replication 5. Images with NA are not available.

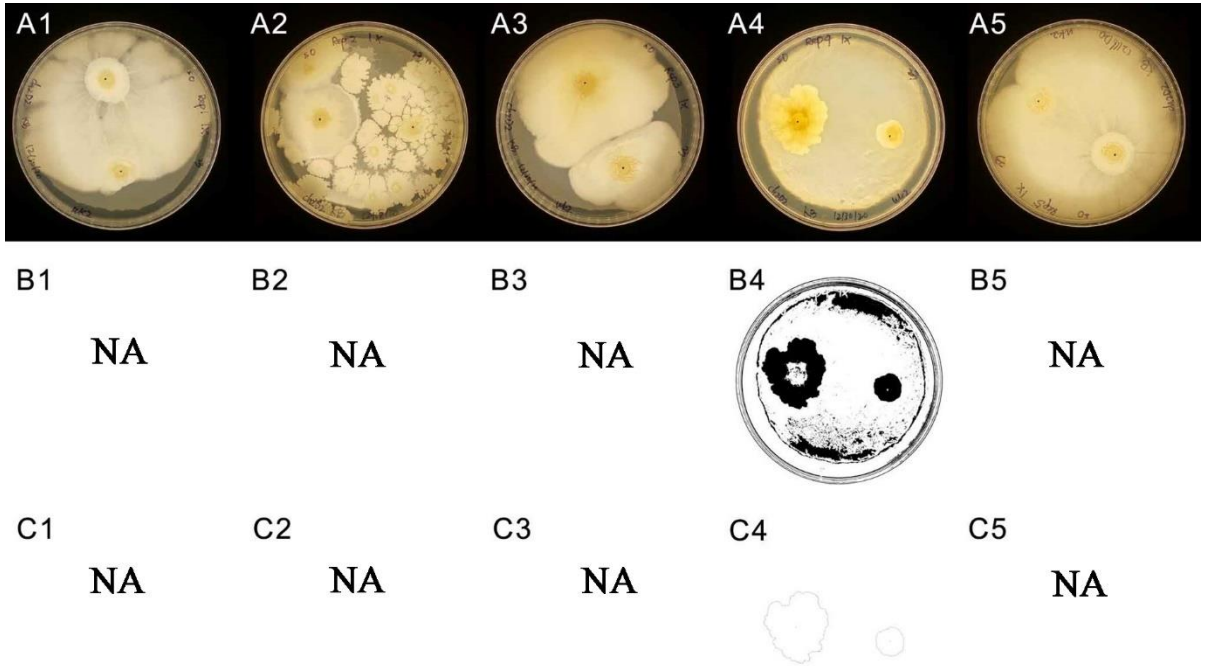


Figure C120. 2021 co-inoculated Petri plates four days after inoculation. **A1-A5)** 1x SO vs. *Pss* 23 on KB media. **B1-B5)** Images after threshold adjustment in ImageJ. **C1-C5)** Image of measured area. A1, B1, C1: Replication 1; A2, B2, C2: Replication 2; A3, B3, C3: Replication 3; A4, B4, C4: Replication 4; A5, B5, C5: Replication 5. Images with NA are not available.

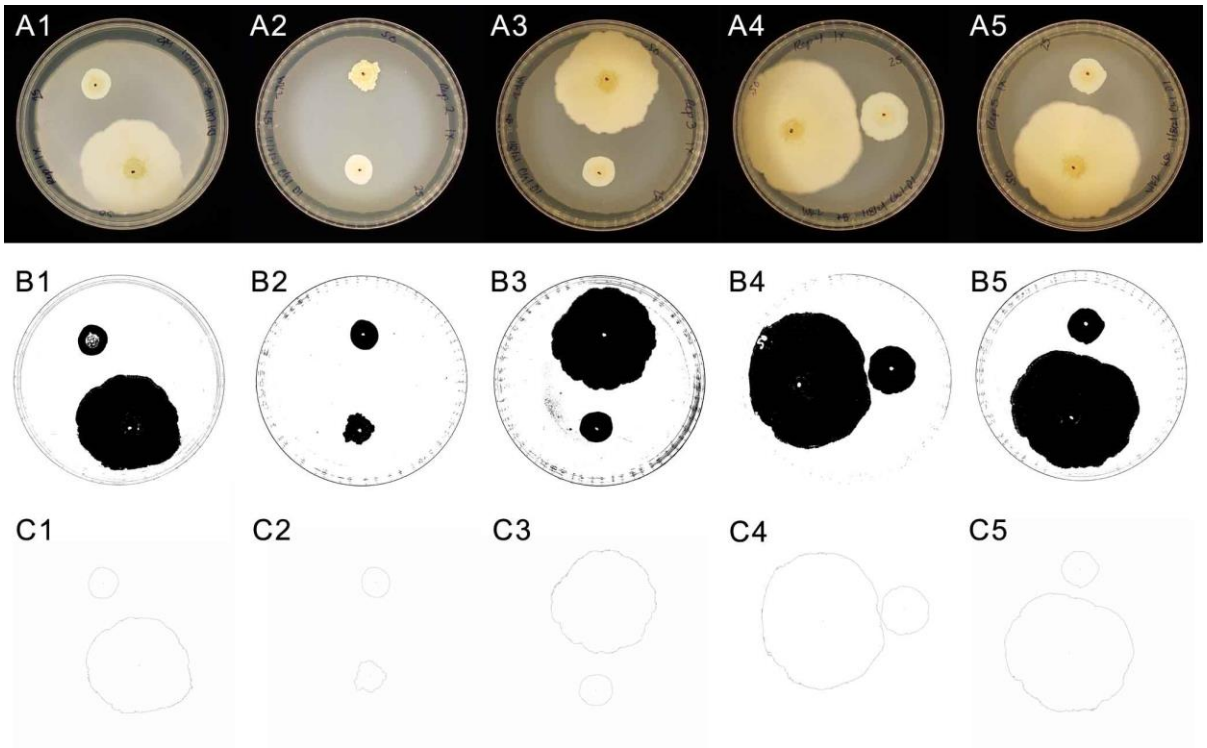


Figure C121. 2021 co-inoculated Petri plates four days after inoculation. **A1-A5)** 1x SO vs. *Pss* 25 on KB media. **B1-B5)** Images after threshold adjustment in ImageJ. **C1-C5)** Image of measured area. A1, B1, C1: Replication 1; A2, B2, C2: Replication 2; A3, B3, C3: Replication 3; A4, B4, C4: Replication 4; A5, B5, C5: Replication 5.

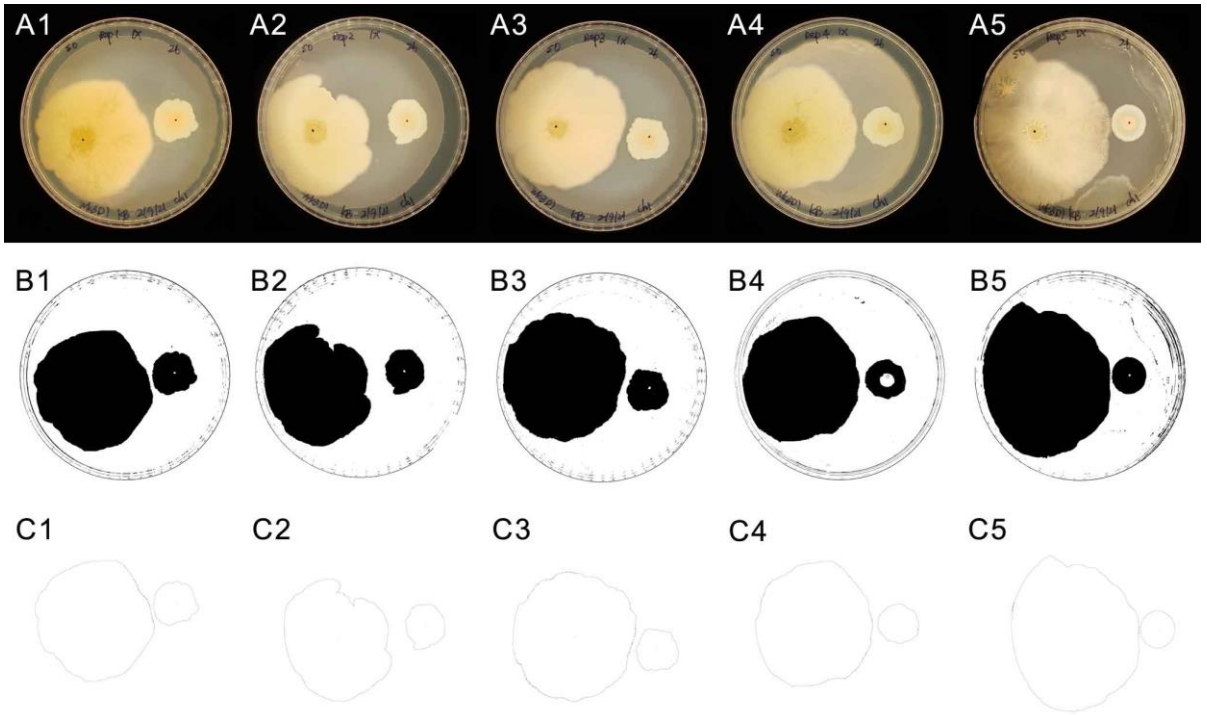


Figure C122. 2021 co-inoculated Petri plates four days after inoculation. **A1-A5)** 1x SO vs. *Pss* 26 on KB media. **B1-B5)** Images after threshold adjustment in ImageJ. **C1-C5)** Image of measured area. A1, B1, C1: Replication 1; A2, B2, C2: Replication 2; A3, B3, C3: Replication 3; A4, B4, C4: Replication 4; A5, B5, C5: Replication 5.

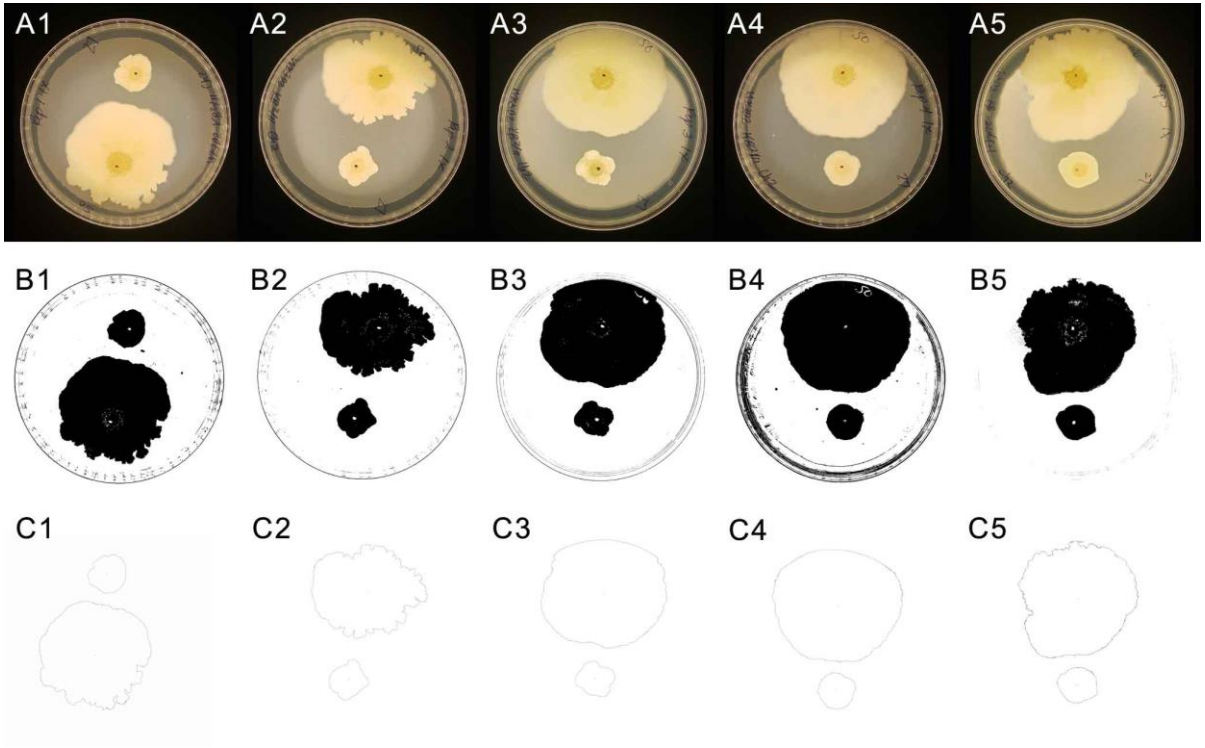


Figure C123. 2021 co-inoculated Petri plates four days after inoculation. **A1-A5)** 1x SO vs. *Pss* 27 on KB media. **B1-B5)** Images after threshold adjustment in ImageJ. **C1-C5)** Image of measured area. A1, B1, C1: Replication 1; A2, B2, C2: Replication 2; A3, B3, C3: Replication 3; A4, B4, C4: Replication 4; A5, B5, C5: Replication 5.

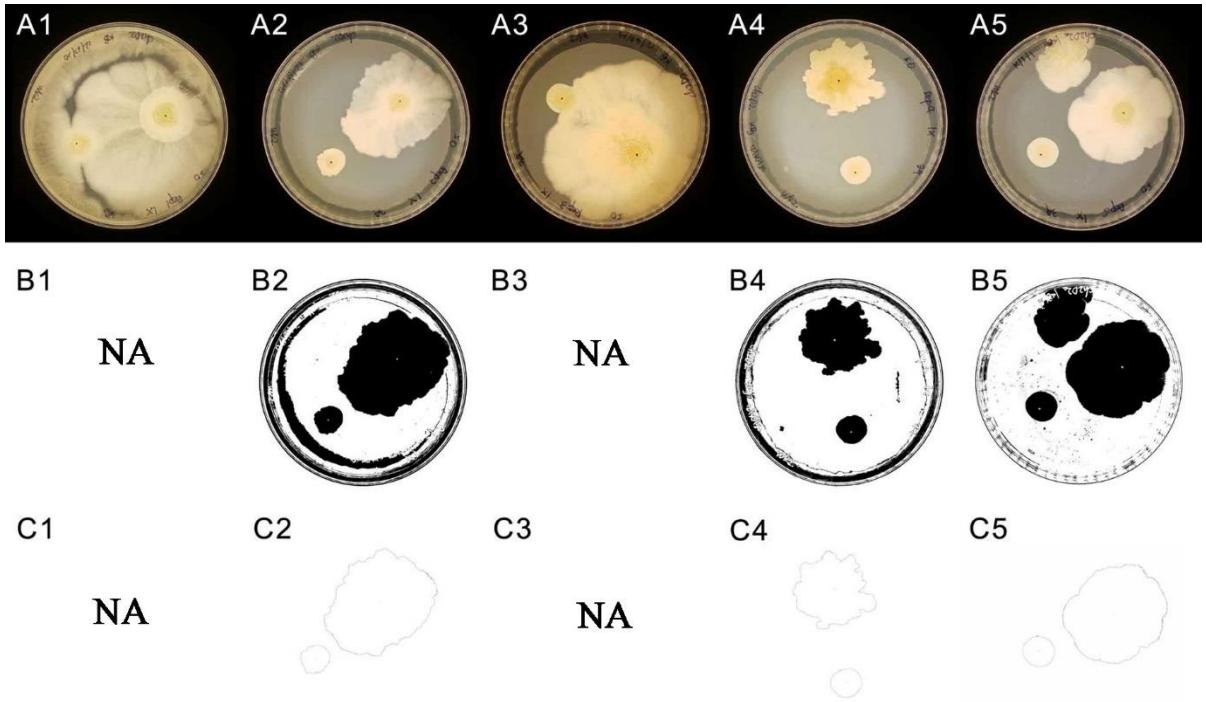


Figure C124. 2021 co-inoculated Petri plates four days after inoculation. **A1-A5)** 1x SO vs. *Pss* 34 on KB media. **B1-B5)** Images after threshold adjustment in ImageJ. **C1-C5)** Image of measured area. A1, B1, C1: Replication 1; A2, B2, C2: Replication 2; A3, B3, C3: Replication 3; A4, B4, C4: Replication 4; A5, B5, C5: Replication 5. Images with NA are not available.

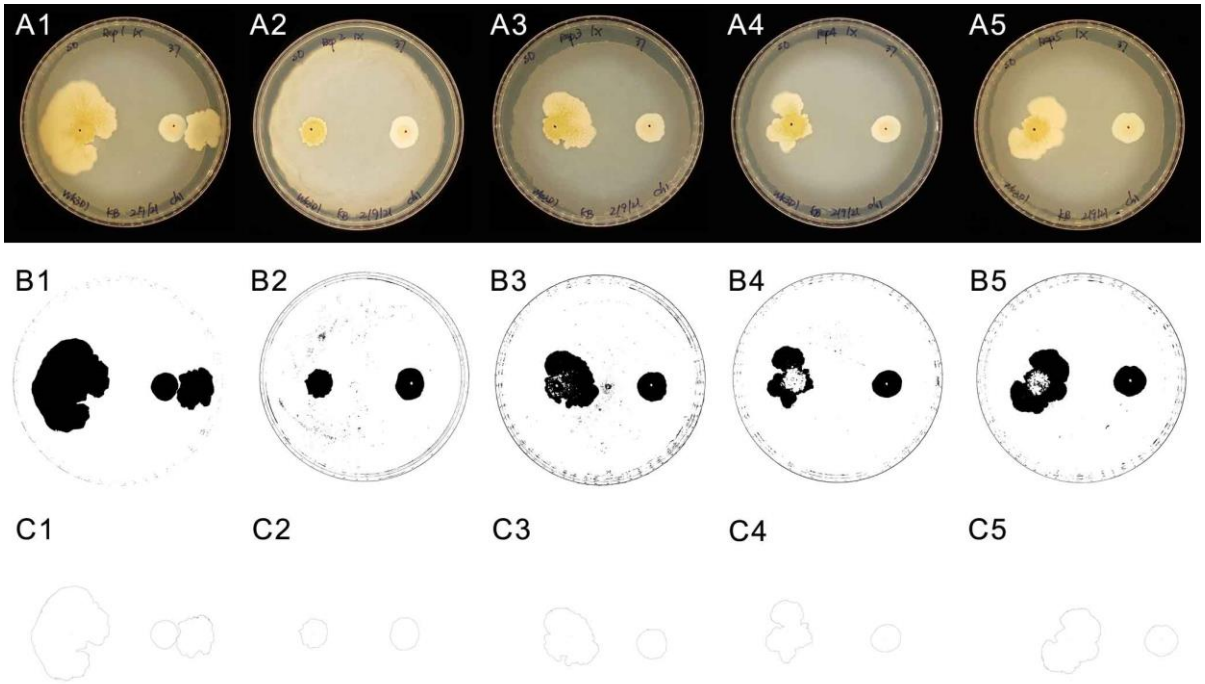


Figure C125. 2021 co-inoculated Petri plates four days after inoculation. **A1-A5)** 1x SO vs. *Pss* 37 on KB media. **B1-B5)** Images after threshold adjustment in ImageJ. **C1-C5)** Image of measured area. A1, B1, C1: Replication 1; A2, B2, C2: Replication 2; A3, B3, C3: Replication 3; A4, B4, C4: Replication 4; A5, B5, C5: Replication 5.

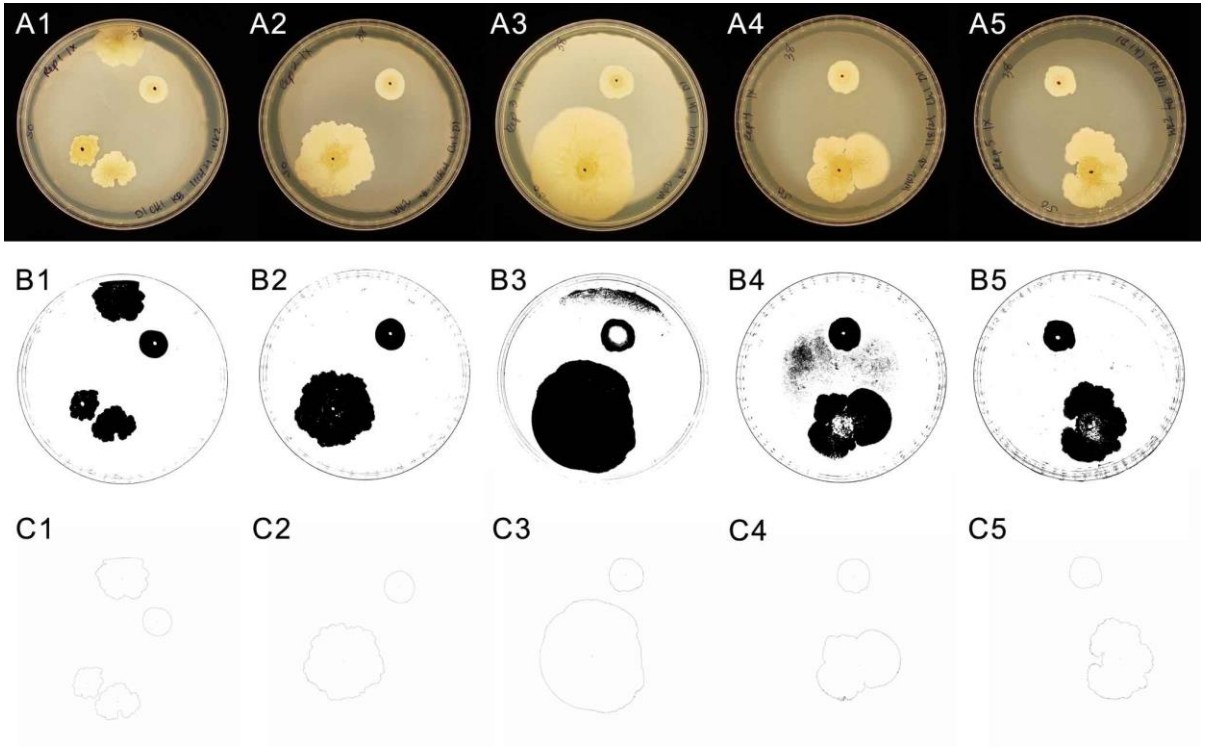


Figure C126. 2021 co-inoculated Petri plates four days after inoculation. **A1-A5)** 1x SO vs. *Pss* 38 on KB media. **B1-B5)** Images after threshold adjustment in ImageJ. **C1-C5)** Image of measured area. A1, B1, C1: Replication 1; A2, B2, C2: Replication 2; A3, B3, C3: Replication 3; A4, B4, C4: Replication 4; A5, B5, C5: Replication 5.

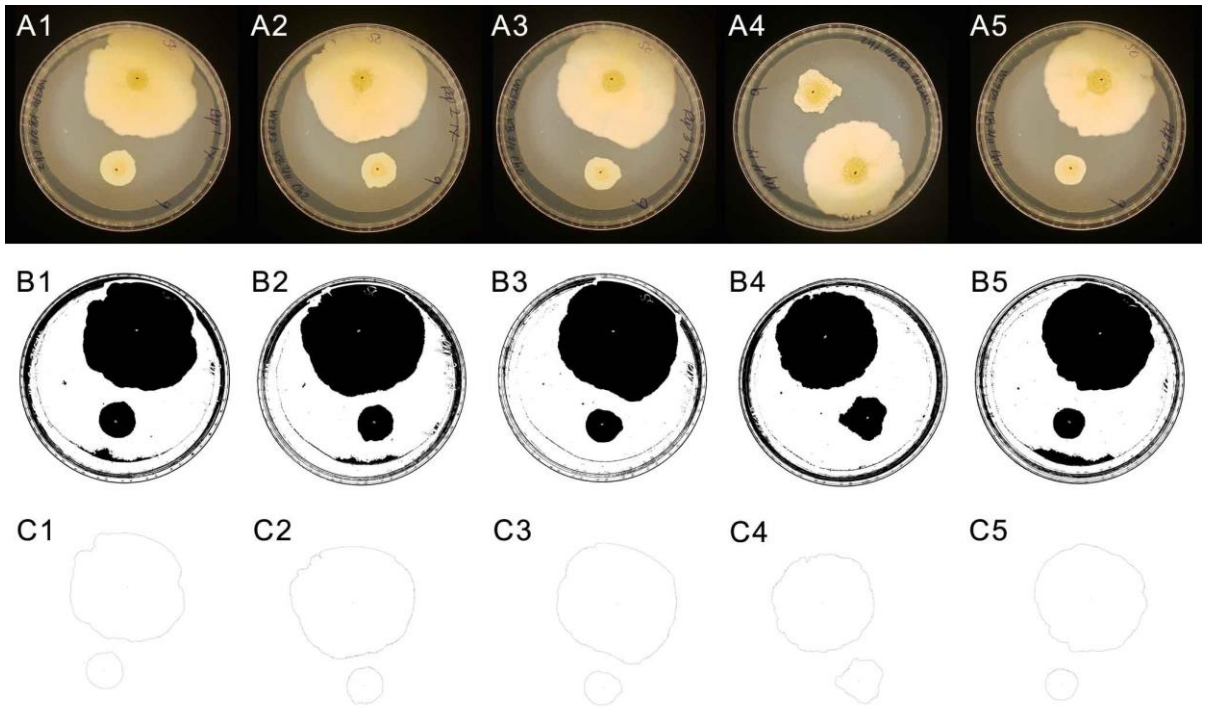


Figure C127. 2021 co-inoculated Petri plates four days after inoculation. **A1-A5)** 1x BP vs. *Pss* 9 on PDA media. **B1-B5)** Images after threshold adjustment in ImageJ. **C1-C5)** Image of measured area. A1, B1, C1: Replication 1; A2, B2, C2: Replication 2; A3, B3, C3: Replication 3; A4, B4, C4: Replication 4; A5, B5, C5: Replication 5.

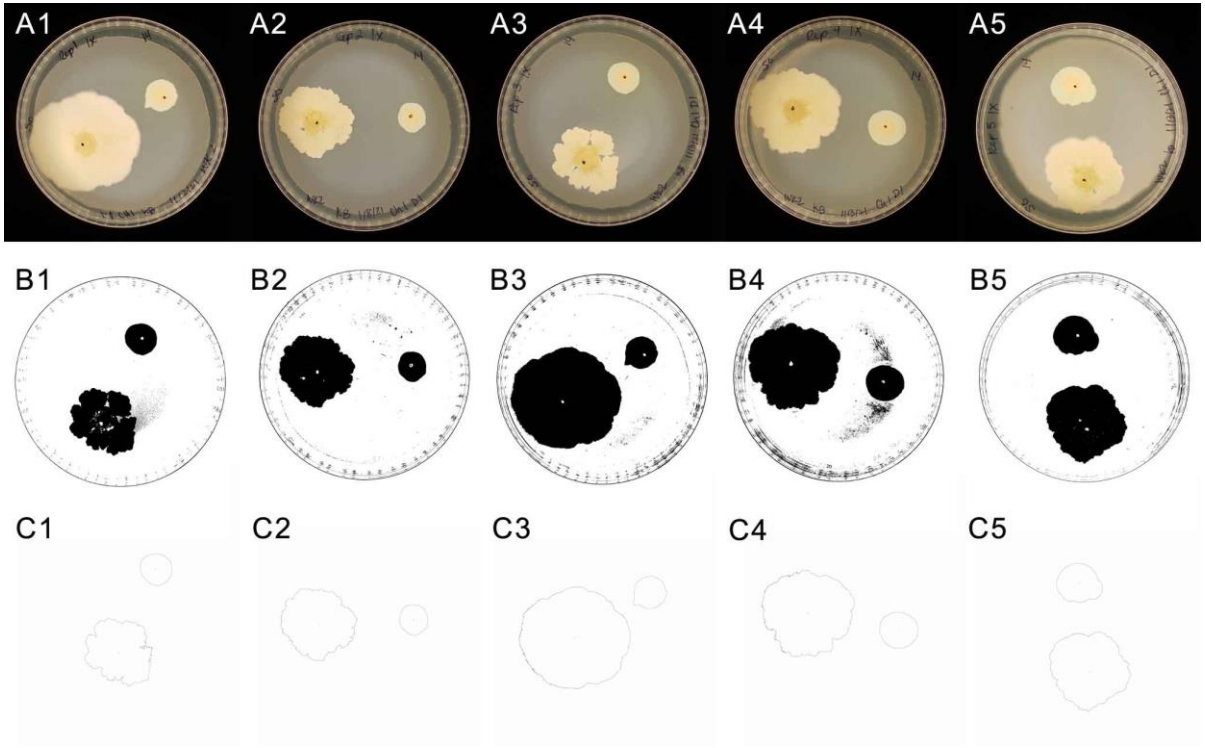


Figure C128. 2021 co-inoculated Petri plates four days after inoculation. **A1-A5)** 1x BP vs. *Pss* 14 on PDA media. **B1-B5)** Images after threshold adjustment in ImageJ. **C1-C5)** Image of measured area. A1, B1, C1: Replication 1; A2, B2, C2: Replication 2; A3, B3, C3: Replication 3; A4, B4, C4: Replication 4; A5, B5, C5: Replication 5.

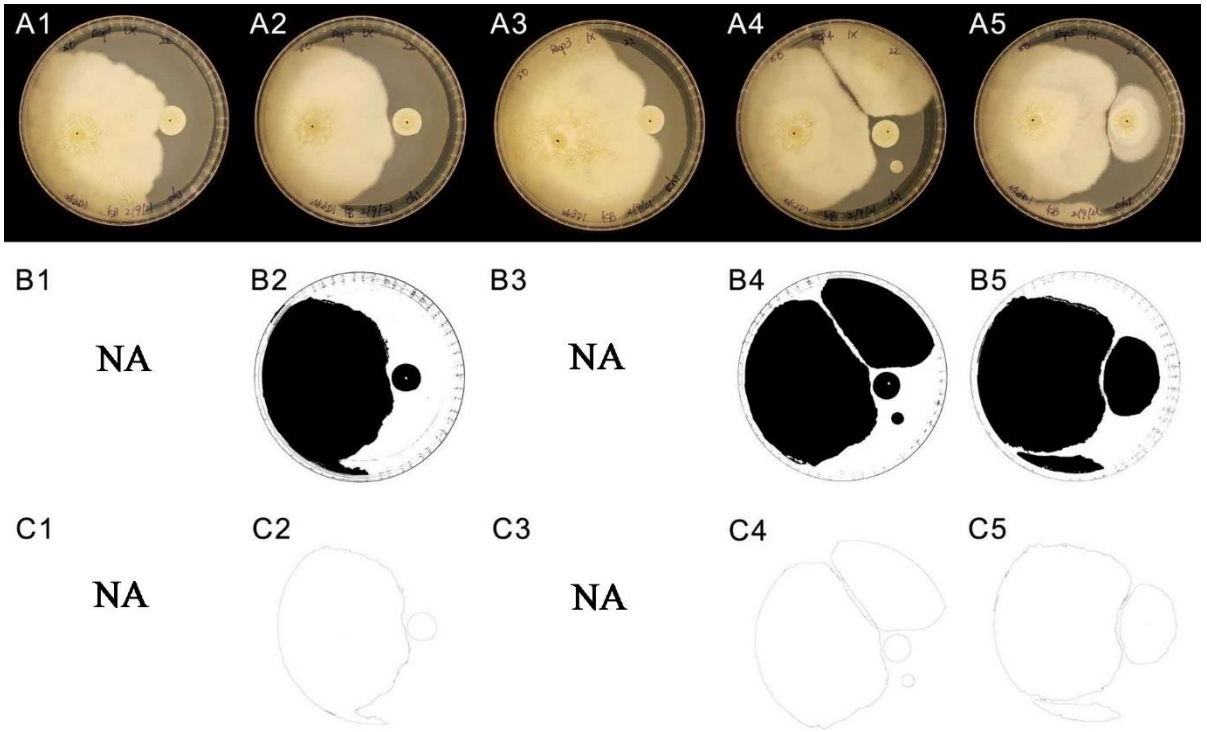


Figure C129. 2021 co-inoculated Petri plates four days after inoculation. **A1-A5)** 1x BP vs. *Pss* 22 on PDA media. **B1-B5)** Images after threshold adjustment in ImageJ. **C1-C5)** Image of measured area. A1, B1, C1: Replication 1; A2, B2, C2: Replication 2; A3, B3, C3: Replication 3; A4, B4, C4: Replication 4; A5, B5, C5: Replication 5. Images with NA are not available.

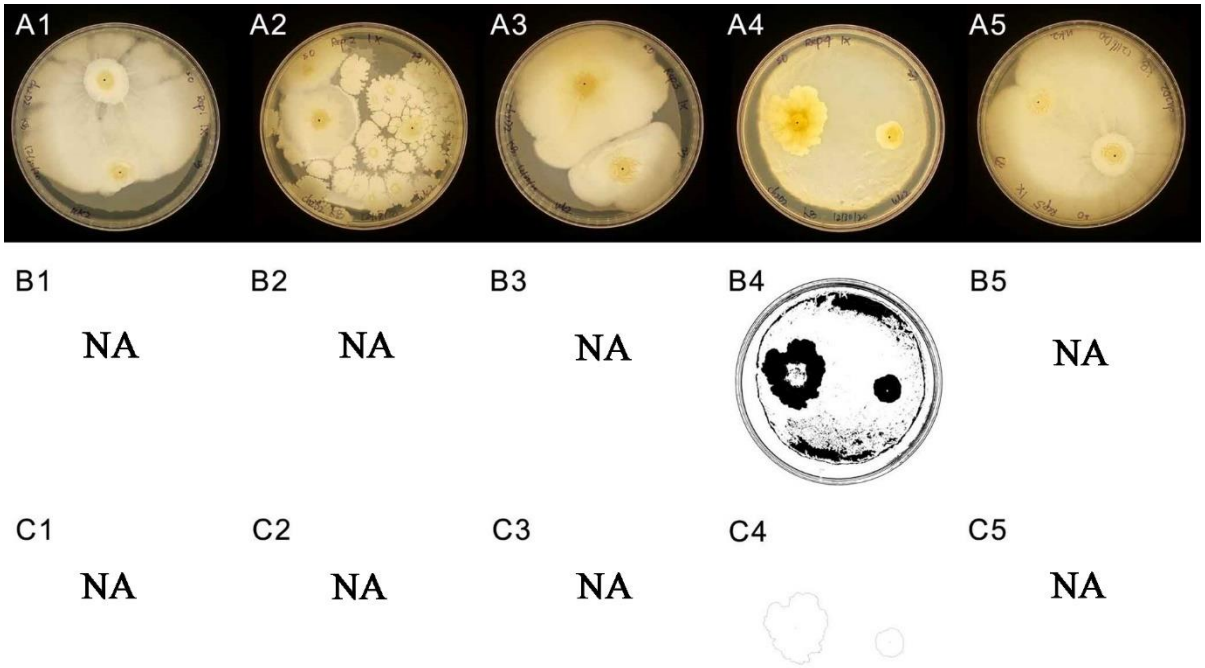


Figure C130. 2021 co-inoculated Petri plates four days after inoculation. **A1-A5)** 1x BP vs. *Pss* 23 on PDA media. **B1-B5)** Images after threshold adjustment in ImageJ. **C1-C5)** Image of measured area. A1, B1, C1: Replication 1; A2, B2, C2: Replication 2; A3, B3, C3: Replication 3; A4, B4, C4: Replication 4; A5, B5, C5: Replication 5. Images with NA are not available.

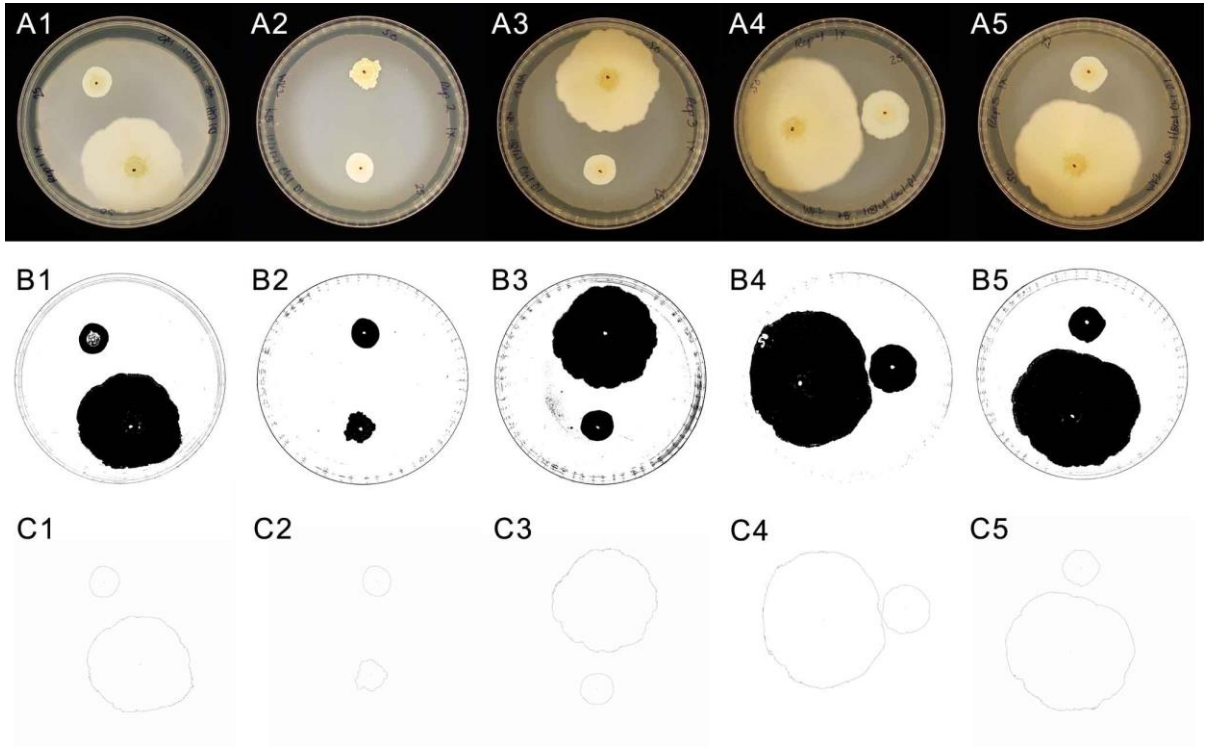


Figure C131. 2021 co-inoculated Petri plates four days after inoculation. **A1-A5)** 1x BP vs. *Pss* 25 on PDA media. **B1-B5)** Images after threshold adjustment in ImageJ. **C1-C5)** Image of measured area. A1, B1, C1: Replication 1; A2, B2, C2: Replication 2; A3, B3, C3: Replication 3; A4, B4, C4: Replication 4; A5, B5, C5: Replication 5.

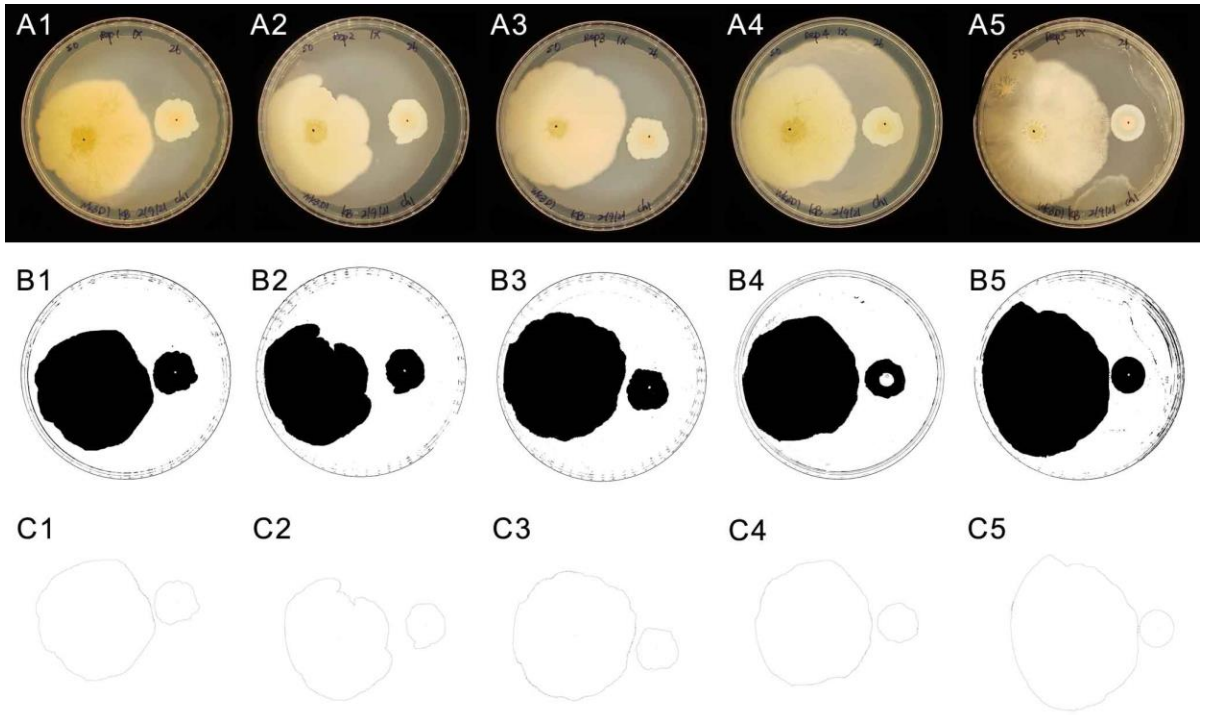


Figure C132. 2021 co-inoculated Petri plates four days after inoculation. **A1-A5)** 1x BP vs. *Pss* 26 on PDA media. **B1-B5)** Images after threshold adjustment in ImageJ. **C1-C5)** Image of measured area. A1, B1, C1: Replication 1; A2, B2, C2: Replication 2; A3, B3, C3: Replication 3; A4, B4, C4: Replication 4; A5, B5, C5: Replication 5.

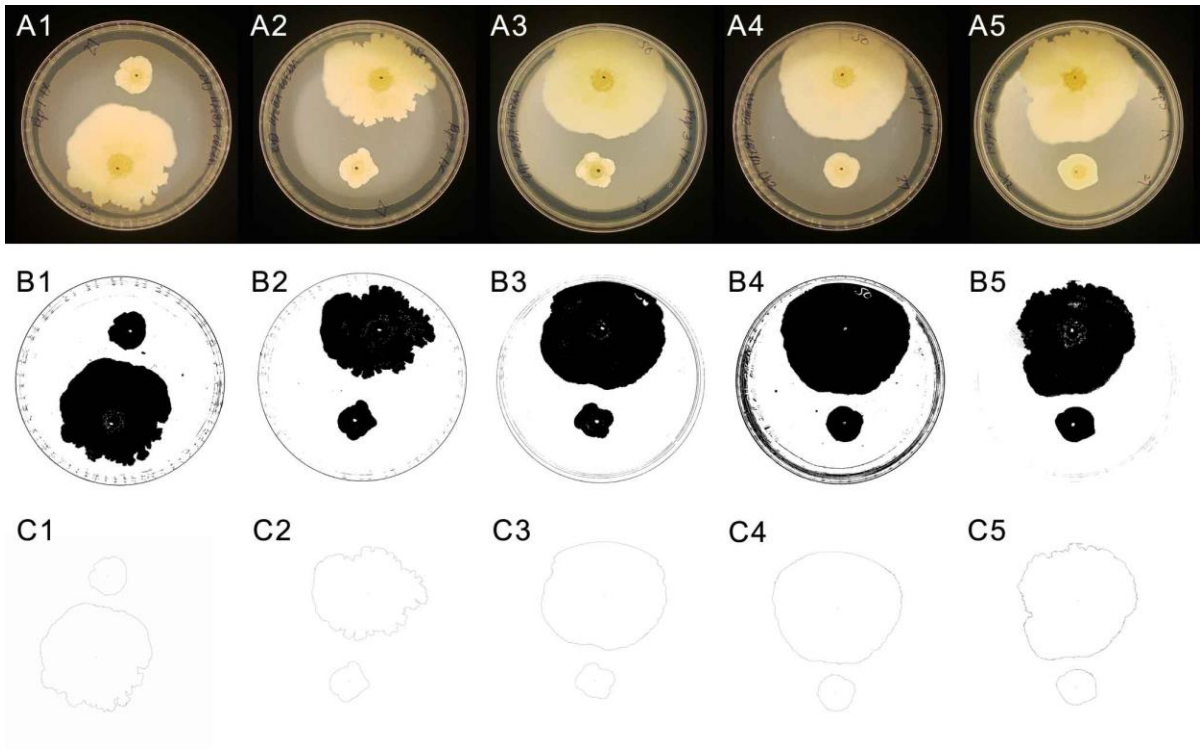


Figure C133. 2021 co-inoculated Petri plates four days after inoculation. **A1-A5)** 1x BP vs. *Pss* 27 on PDA media. **B1-B5)** Images after threshold adjustment in ImageJ. **C1-C5)** Image of measured area. A1, B1, C1: Replication 1; A2, B2, C2: Replication 2; A3, B3, C3: Replication 3; A4, B4, C4: Replication 4; A5, B5, C5: Replication 5.

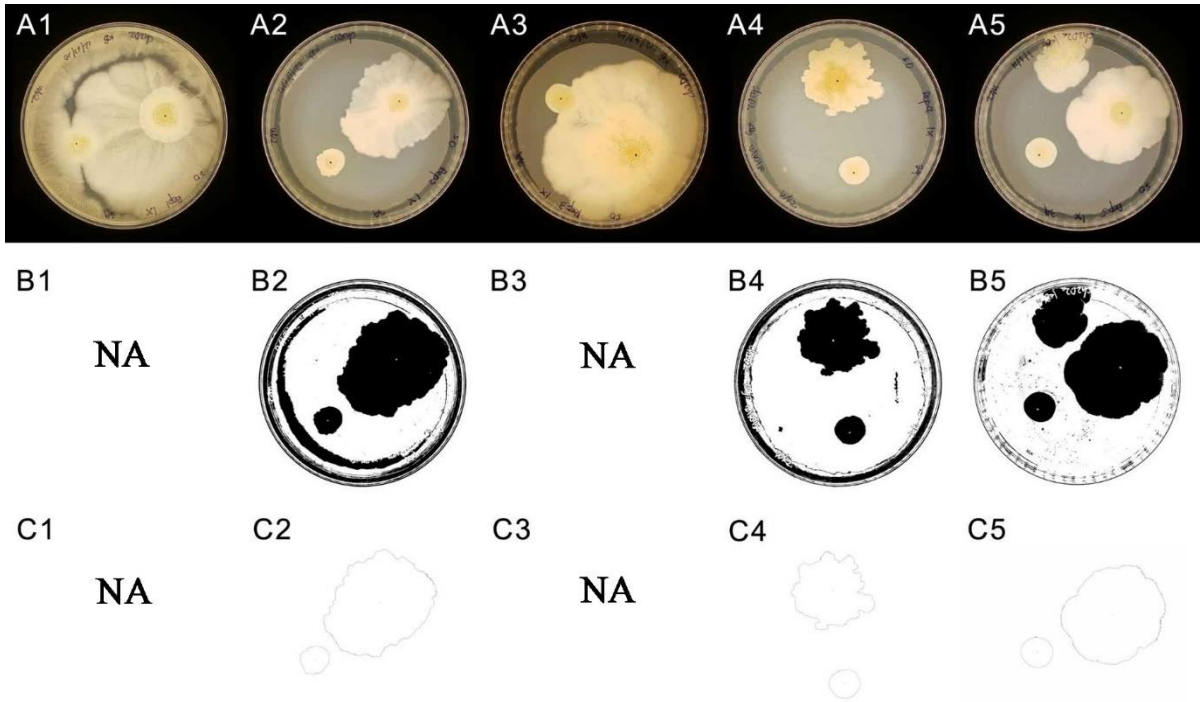


Figure C134. 2021 co-inoculated Petri plates four days after inoculation. **A1-A5)** 1x BP vs. *Pss* 34 on PDA media. **B1-B5)** Images after threshold adjustment in ImageJ. **C1-C5)** Image of measured area. A1, B1, C1: Replication 1; A2, B2, C2: Replication 2; A3, B3, C3: Replication 3; A4, B4, C4: Replication 4; A5, B5, C5: Replication 5. Images with NA are not available.

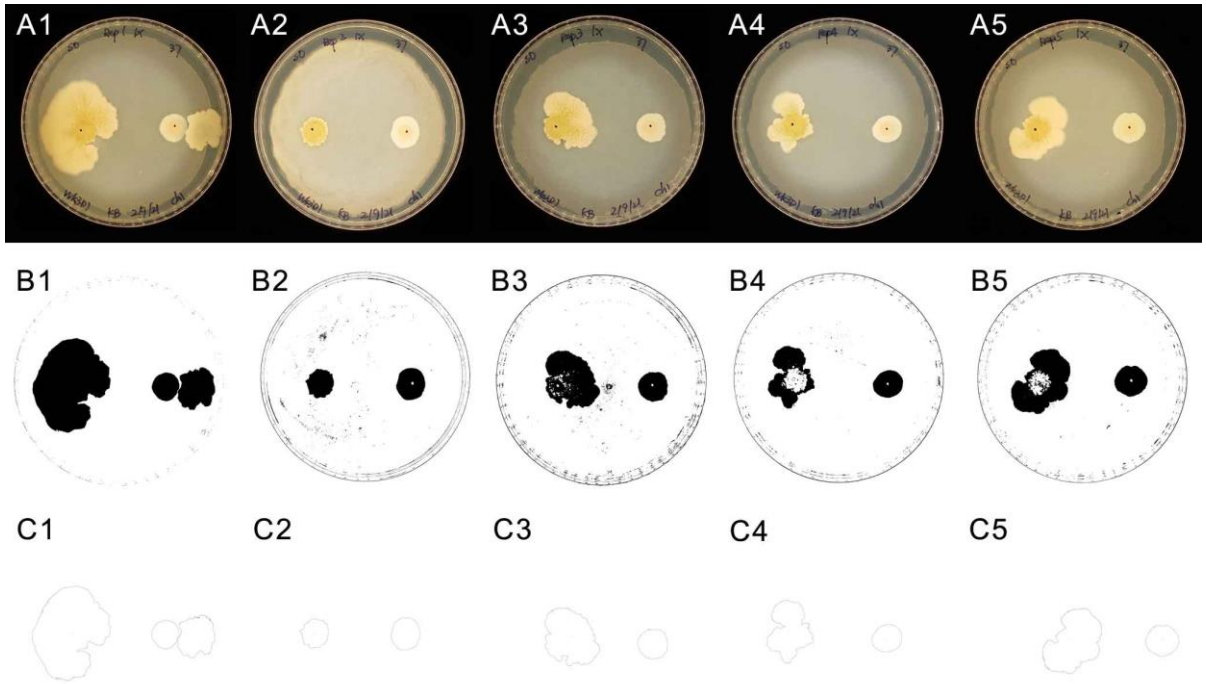


Figure C135. 2021 co-inoculated Petri plates four days after inoculation. **A1-A5)** 1x BP vs. *Pss* 37 on PDA media. **B1-B5)** Images after threshold adjustment in ImageJ. **C1-C5)** Image of measured area. A1, B1, C1: Replication 1; A2, B2, C2: Replication 2; A3, B3, C3: Replication 3; A4, B4, C4: Replication 4; A5, B5, C5: Replication 5.

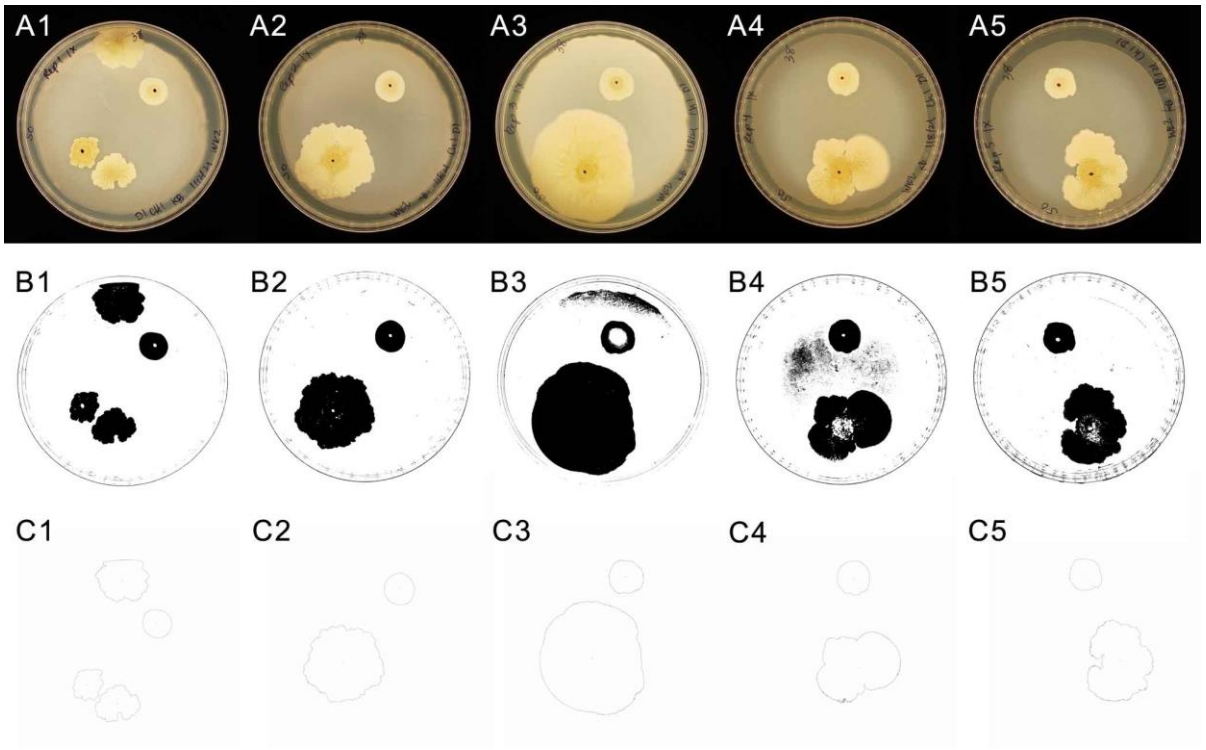


Figure C136. 2021 co-inoculated Petri plates four days after inoculation. **A1-A5)** 1x BP vs. *Pss* 38 on PDA media. **B1-B5)** Images after threshold adjustment in ImageJ. **C1-C5)** Image of measured area. A1, B1, C1: Replication 1; A2, B2, C2: Replication 2; A3, B3, C3: Replication 3; A4, B4,C4: Replication 4; A5, B5, C5: Replication 5.

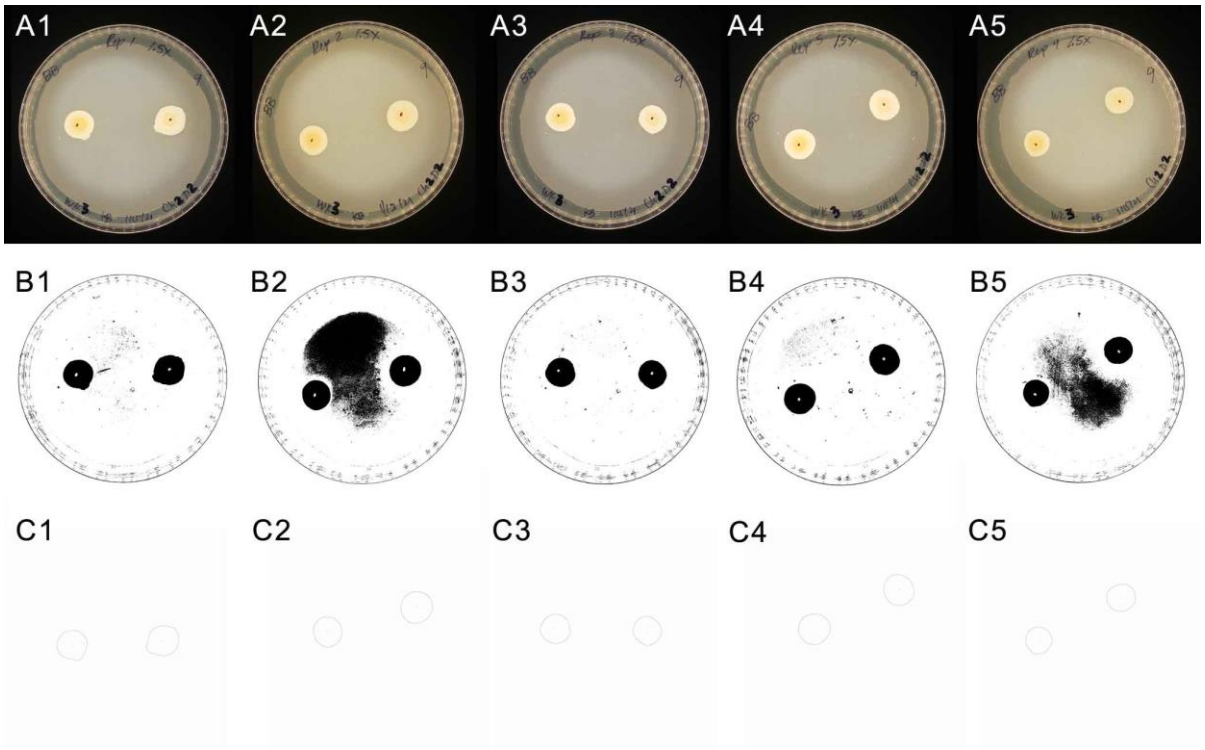


Figure C137. 2021 co-inoculated Petri plates four days after inoculation. **A1-A5)** 1.5x BB vs. *Pss* 9 on KB media. **B1-B5)** Images after threshold adjustment in ImageJ. **C1-C5)** Image of measured area. A1, B1, C1: Replication 1; A2, B2, C2: Replication 2; A3, B3, C3: Replication 3; A4, B4, C4: Replication 4; A5, B5, C5: Replication 5.

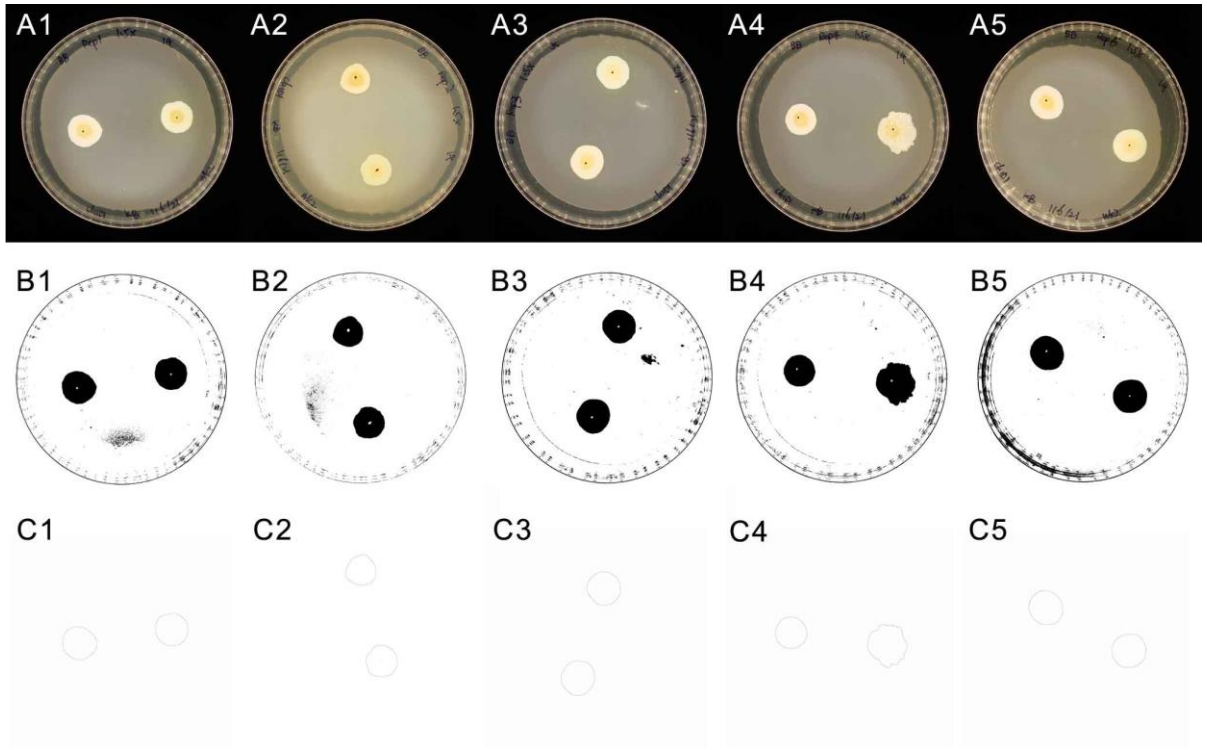


Figure C138. 2021 co-inoculated Petri plates four days after inoculation. **A1-A5)** 1.5x BB vs. *Pss* 14 on KB media. **B1-B5)** Images after threshold adjustment in ImageJ. **C1-C5)** Image of measured area. A1, B1, C1: Replication 1; A2, B2, C2: Replication 2; A3, B3, C3: Replication 3; A4, B4, C4: Replication 4; A5, B5, C5: Replication 5.

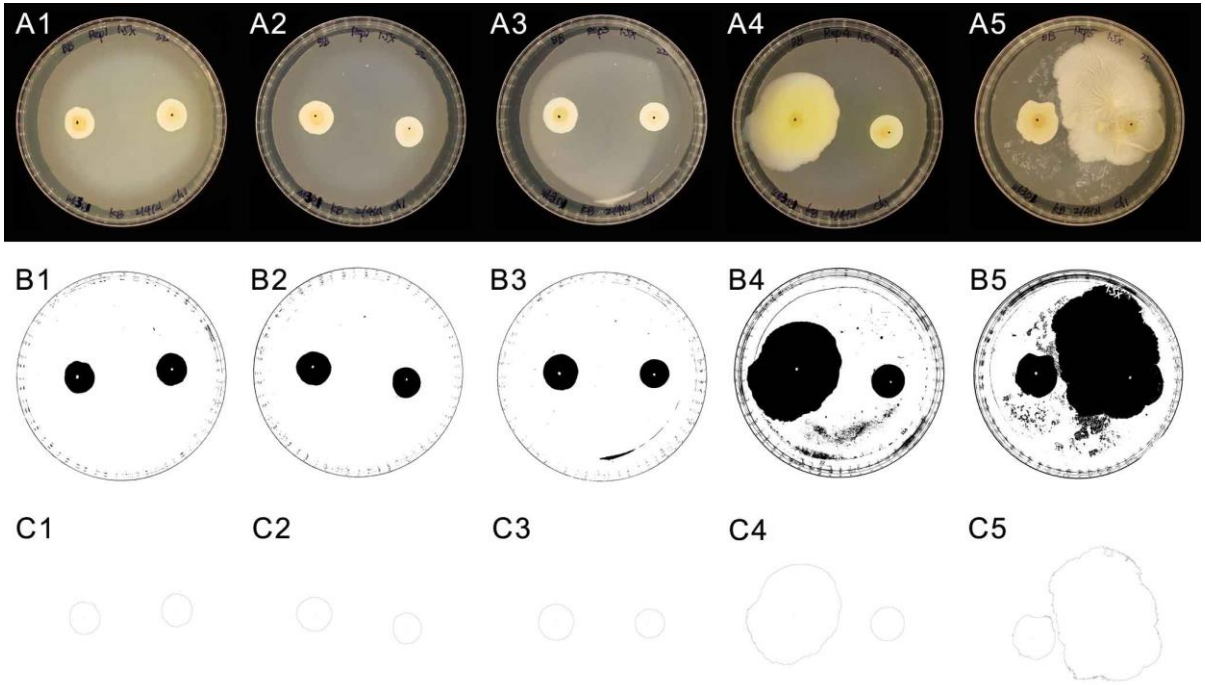


Figure C139. 2021 co-inoculated Petri plates four days after inoculation. **A1-A5)** 1.5x BB vs. *Pss* 22 on KB media. **B1-B5)** Images after threshold adjustment in ImageJ. **C1-C5)** Image of measured area. A1, B1, C1: Replication 1; A2, B2, C2: Replication 2; A3, B3, C3: Replication 3; A4, B4, C4: Replication 4; A5, B5, C5: Replication 5.

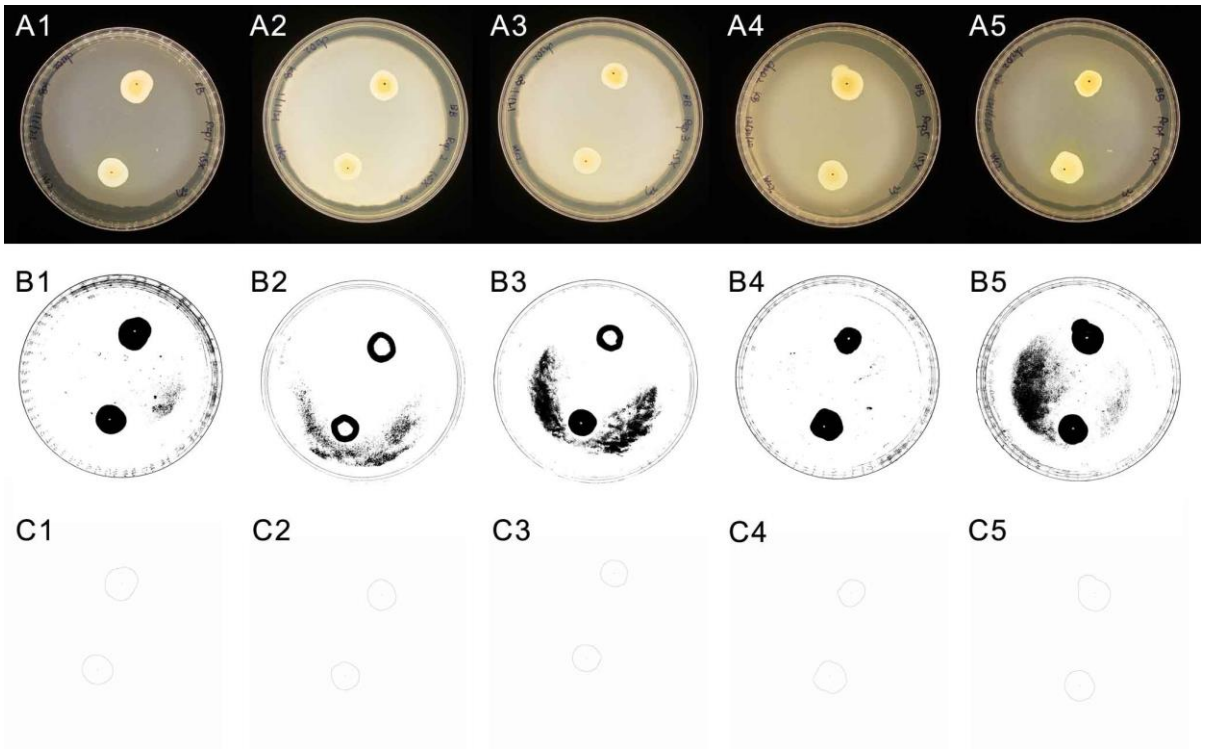


Figure C140. 2021 co-inoculated Petri plates four days after inoculation. **A1-A5)** 1.5x BB vs. *Pss* 23 on KB media. **B1-B5)** Images after threshold adjustment in ImageJ. **C1-C5)** Image of measured area. A1, B1, C1: Replication 1; A2, B2, C2: Replication 2; A3, B3, C3: Replication 3; A4, B4, C4: Replication 4; A5, B5, C5: Replication 5.

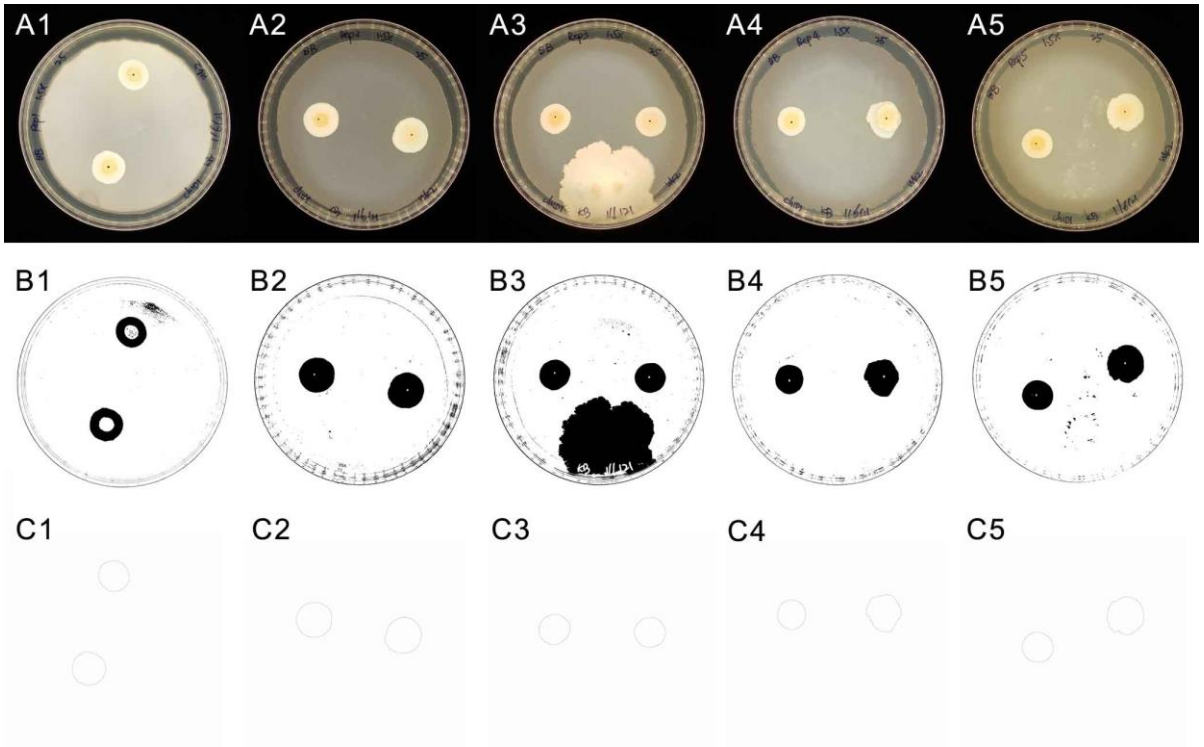


Figure C141. 2021 co-inoculated Petri plates four days after inoculation. **A1-A5)** 1.5x BB vs. *Pss* 25 on KB media. **B1-B5)** Images after threshold adjustment in ImageJ. **C1-C5)** Image of measured area. A1, B1, C1: Replication 1; A2, B2, C2: Replication 2; A3, B3, C3: Replication 3; A4, B4, C4: Replication 4; A5, B5, C5: Replication 5.

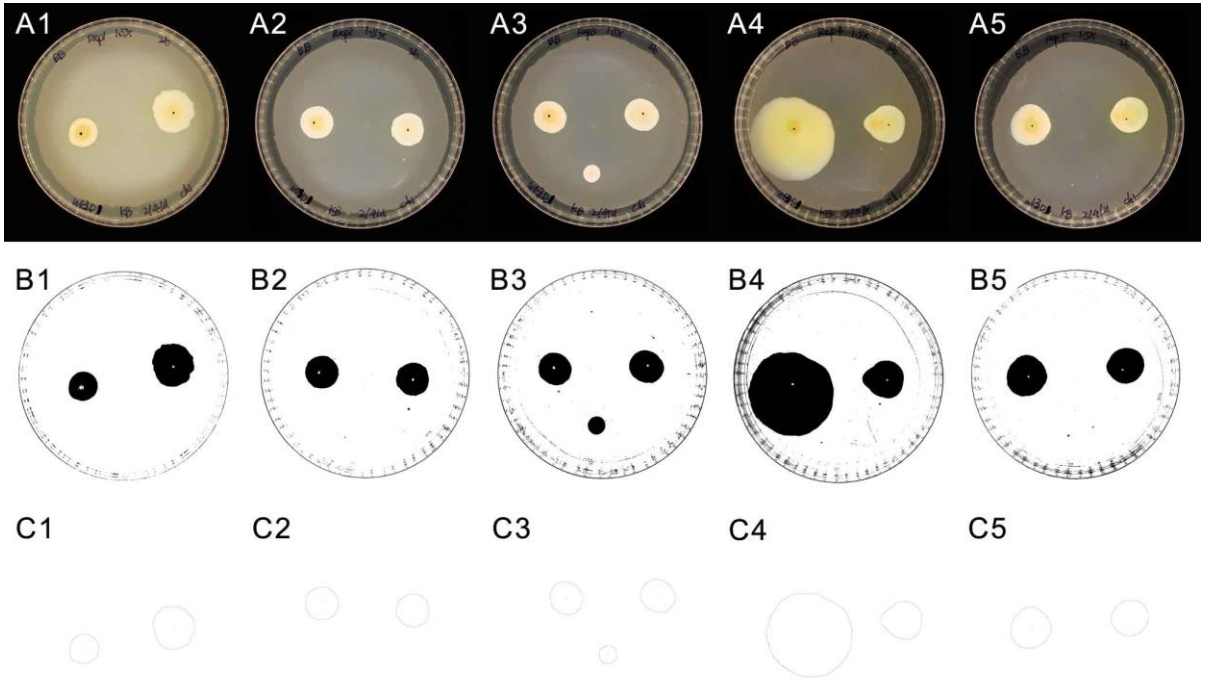


Figure C142. 2021 co-inoculated Petri plates four days after inoculation. **A1-A5)** 1.5x BB vs. *Pss* 26 on KB media. **B1-B5)** Images after threshold adjustment in ImageJ. **C1-C5)** Image of measured area. A1, B1, C1: Replication 1; A2, B2, C2: Replication 2; A3, B3, C3: Replication 3; A4, B4, C4: Replication 4; A5, B5, C5: Replication 5.

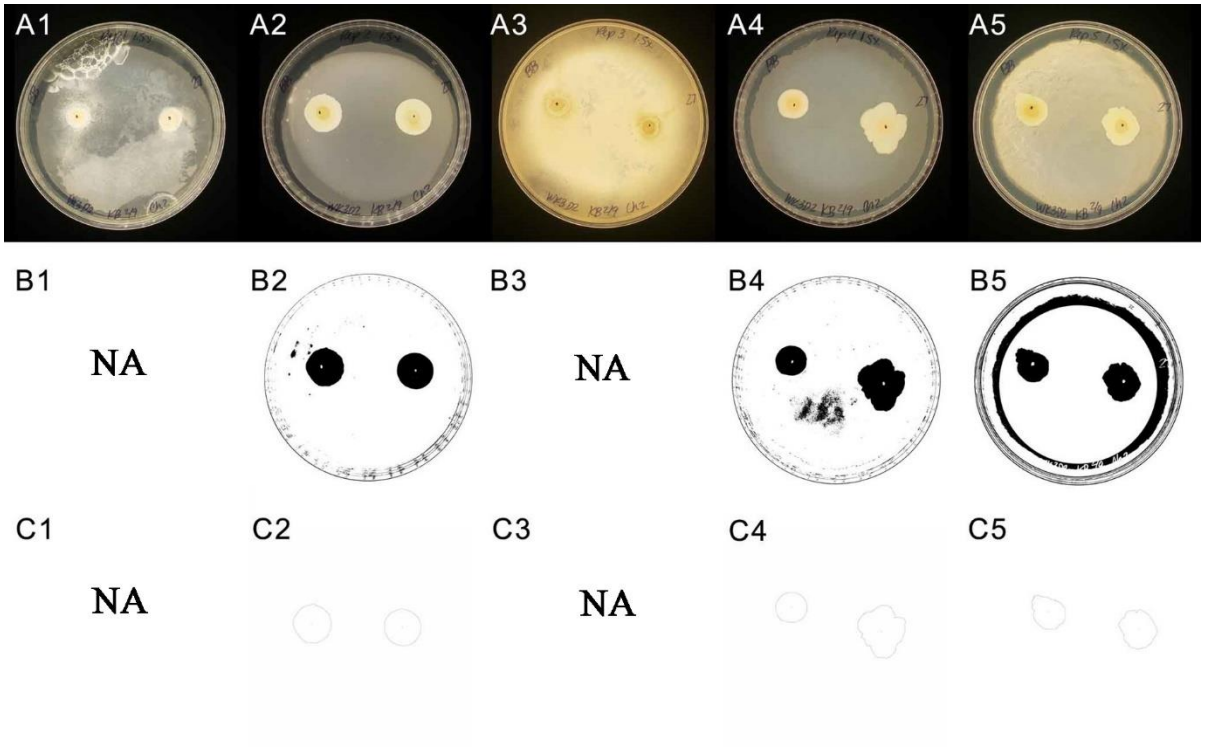


Figure C143. 2021 co-inoculated Petri plates four days after inoculation. **A1-A5)** 1.5x BB vs. *Pss* 27 on KB media. **B1-B5)** Images after threshold adjustment in ImageJ. **C1-C5)** Image of measured area. A1, B1, C1: Replication 1; A2, B2, C2: Replication 2; A3, B3, C3: Replication 3; A4, B4, C4: Replication 4; A5, B5, C5: Replication 5. Images with NA are not available.

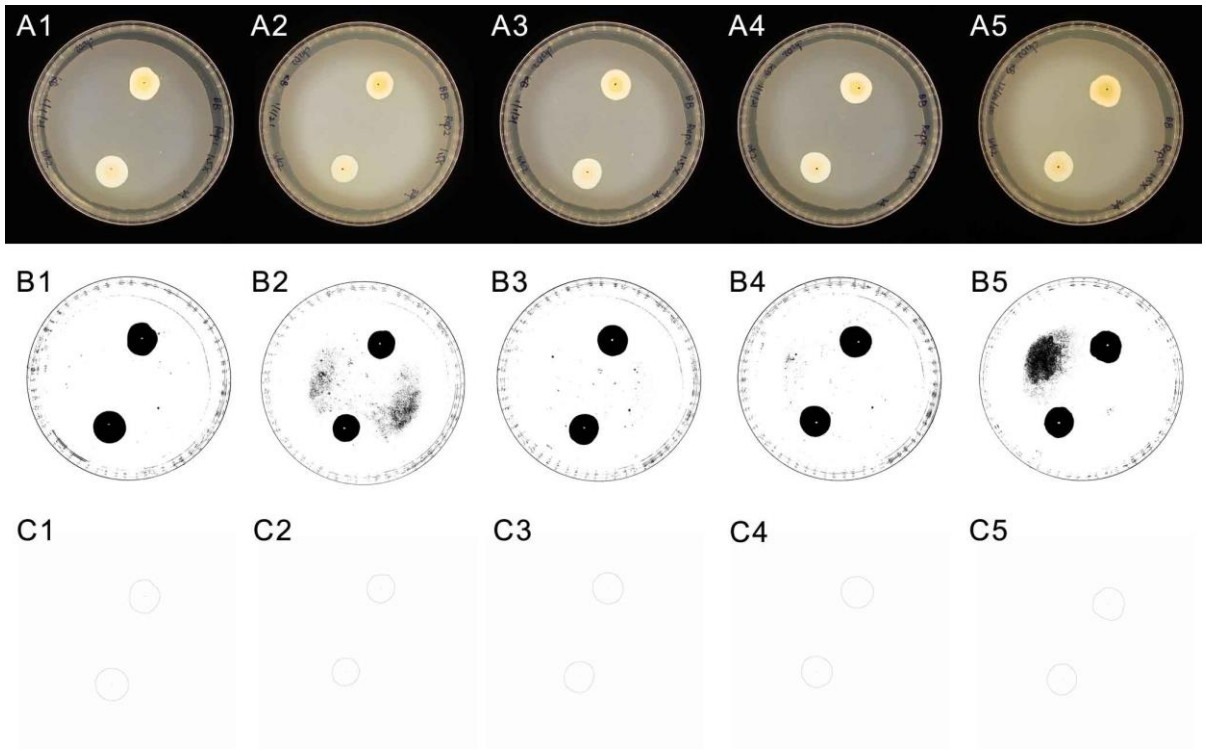


Figure C144. 52021 co-inoculated Petri plates four days after inoculation. **A1-A5)** 1.5x BB vs. *Pss* 34 on KB media. **B1-B5)** Images after threshold adjustment in ImageJ. **C1-C5)** Image of measured area. A1, B1, C1: Replication 1; A2, B2, C2: Replication 2; A3, B3, C3: Replication 3; A4, B4, C4: Replication 4; A5, B5, C5: Replication 5.

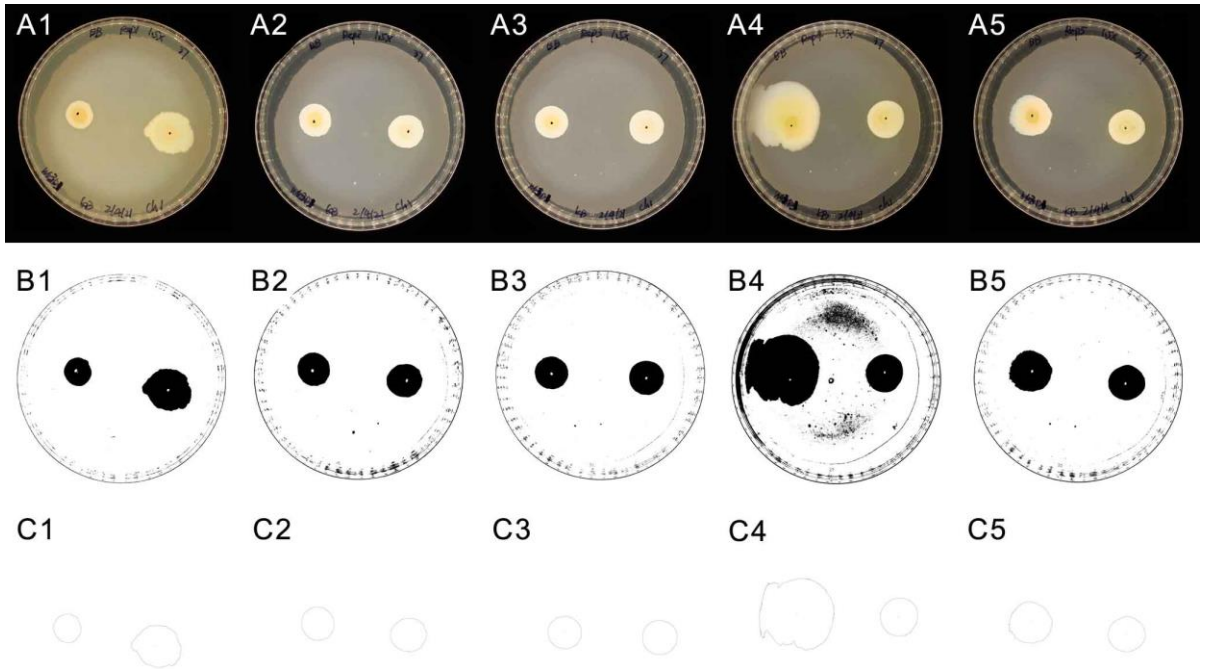


Figure C145. 2021 co-inoculated Petri plates four days after inoculation. **A1-A5)** 1.5x BB vs. *Pss* 37 on KB media. **B1-B5)** Images after threshold adjustment in ImageJ. **C1-C5)** Image of measured area. A1, B1, C1: Replication 1; A2, B2, C2: Replication 2; A3, B3, C3: Replication 3; A4, B4, C4: Replication 4; A5, B5, C5: Replication 5.

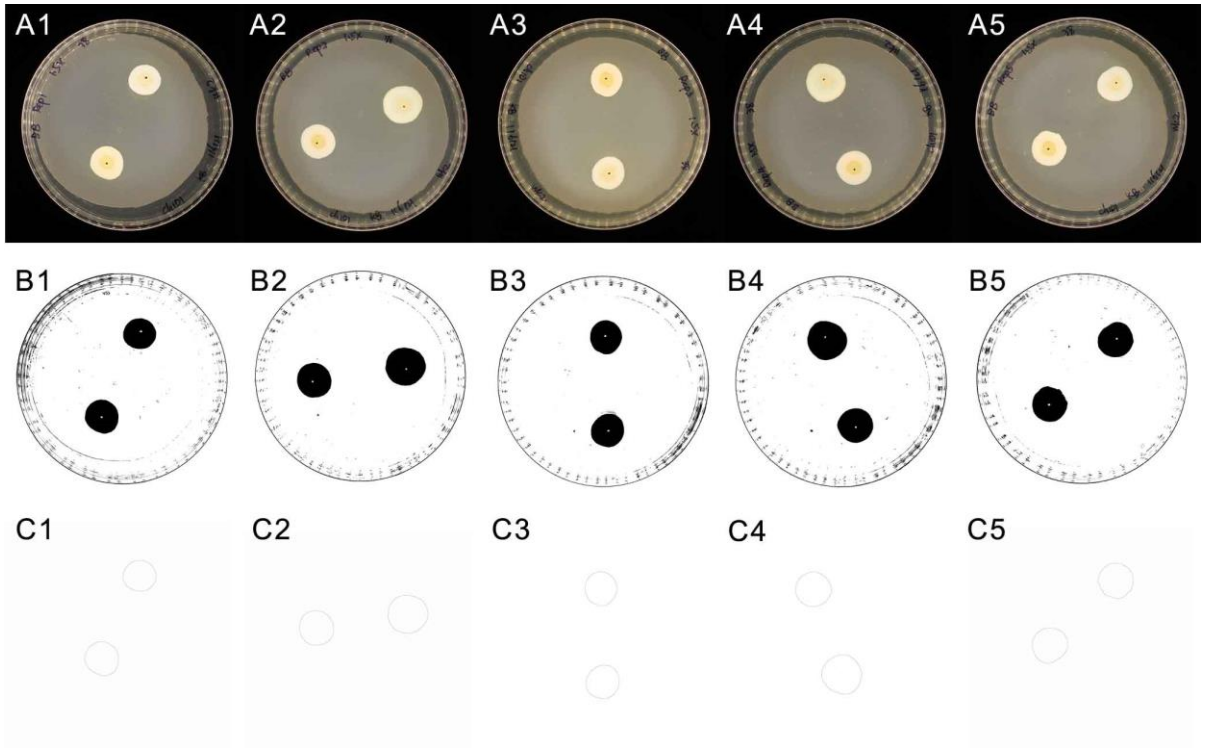


Figure C146. 2021 co-inoculated Petri plates four days after inoculation. **A1-A5)** 1.5x BB vs. *Pss* 38 on KB media. **B1-B5)** Images after threshold adjustment in ImageJ. **C1-C5)** Image of measured area. A1, B1, C1: Replication 1; A2, B2, C2: Replication 2; A3, B3, C3: Replication 3; A4, B4, C4: Replication 4; A5, B5, C5: Replication 5.

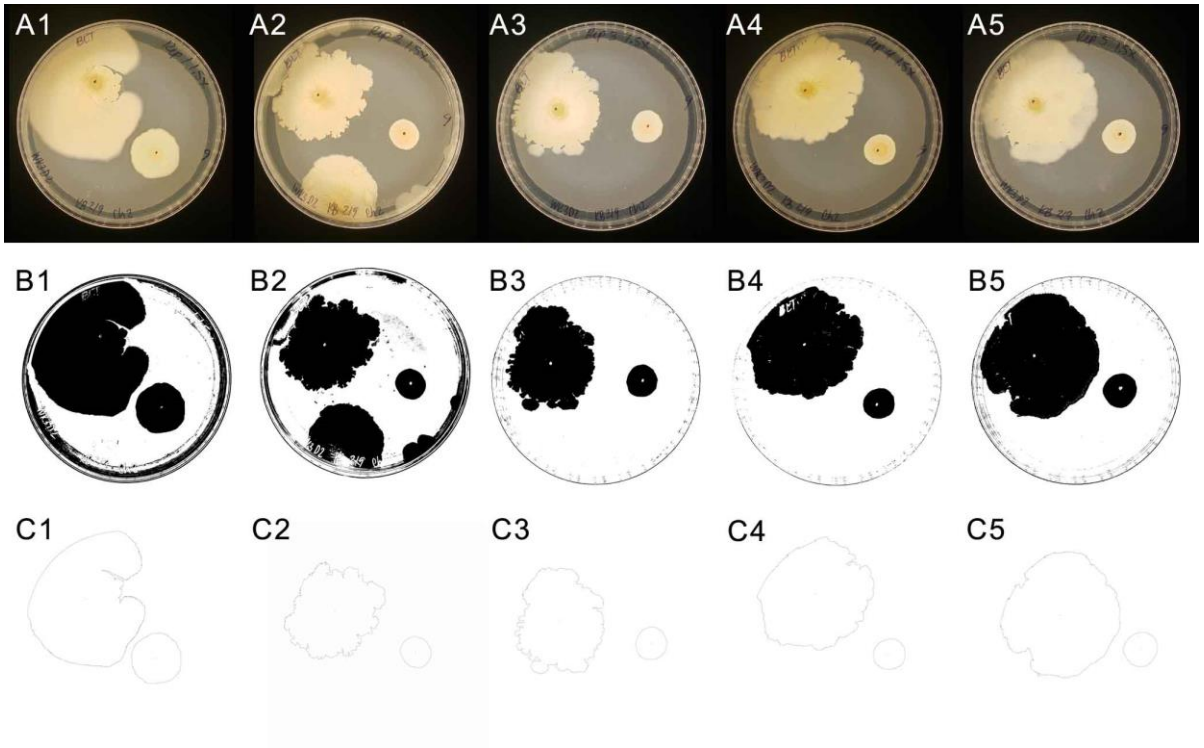


Figure C147. 2021 co-inoculated Petri plates four days after inoculation. **A1-A5)** 1.5x BLT vs. *Pss* 9 on KB media. **B1-B5)** Images after threshold adjustment in ImageJ. **C1-C5)** Image of measured area. A1, B1, C1: Replication 1; A2, B2, C2: Replication 2; A3, B3, C3: Replication 3; A4, B4, C4: Replication 4; A5, B5, C5: Replication 5.

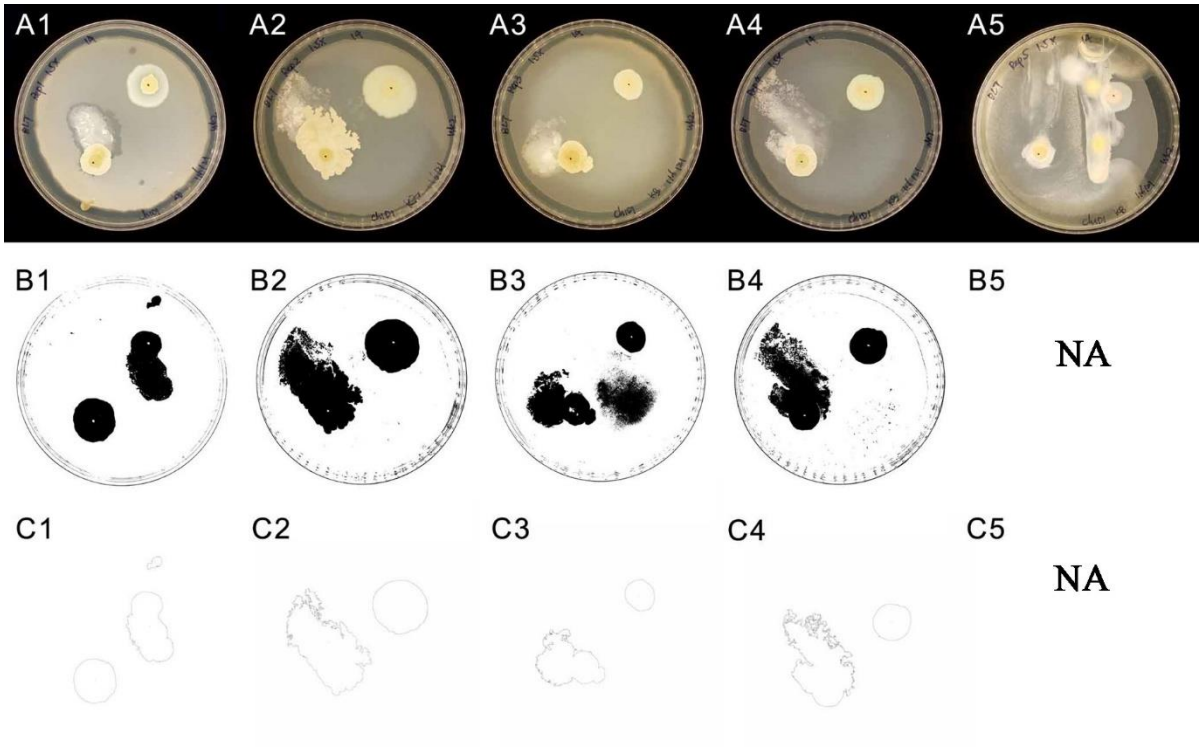


Figure C148. 2021 co-inoculated Petri plates four days after inoculation. **A1-A5)** 1.5x BLT vs. *Pss* 14 on KB media. **B1-B5)** Images after threshold adjustment in ImageJ. **C1-C5)** Image of measured area. A1, B1, C1: Replication 1; A2, B2, C2: Replication 2; A3, B3, C3: Replication 3; A4, B4, C4: Replication 4; A5, B5, C5: Replication 5. Images with NA are not available.

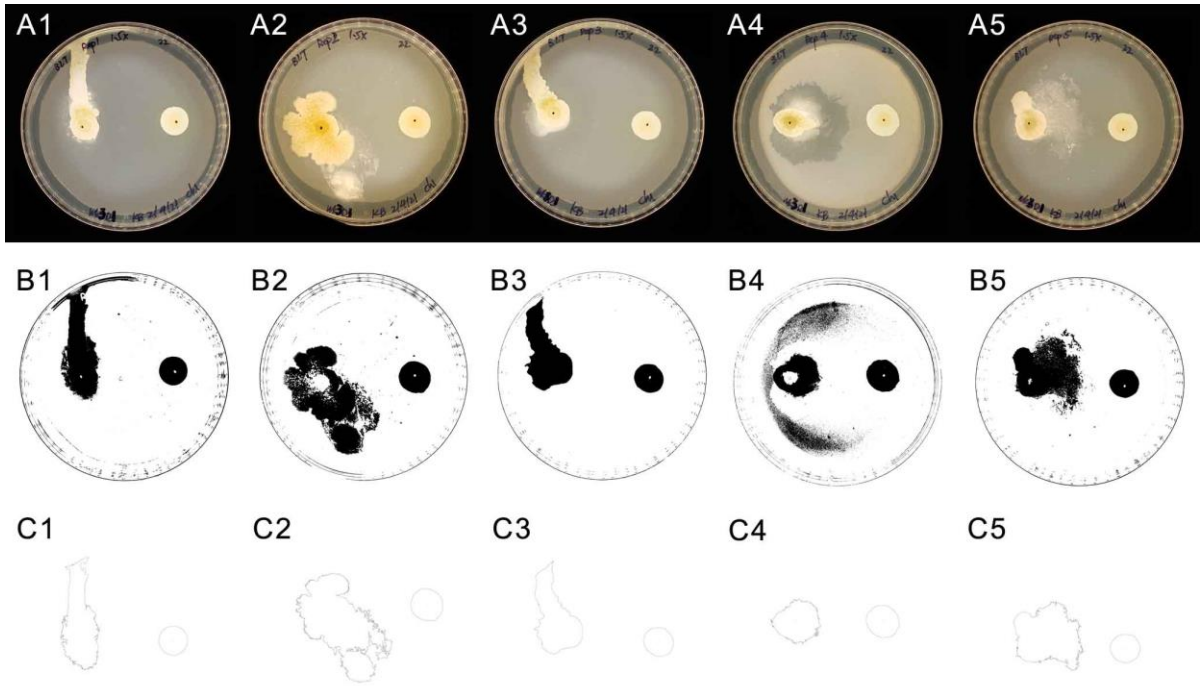


Figure C149. 2021 co-inoculated Petri plates four days after inoculation. **A1-A5)** 1.5x BLT vs. *Pss* 22 on KB media. **B1-B5)** Images after threshold adjustment in ImageJ. **C1-C5)** Image of measured area. A1, B1, C1: Replication 1; A2, B2, C2: Replication 2; A3, B3, C3: Replication 3; A4, B4, C4: Replication 4; A5, B5, C5: Replication 5.

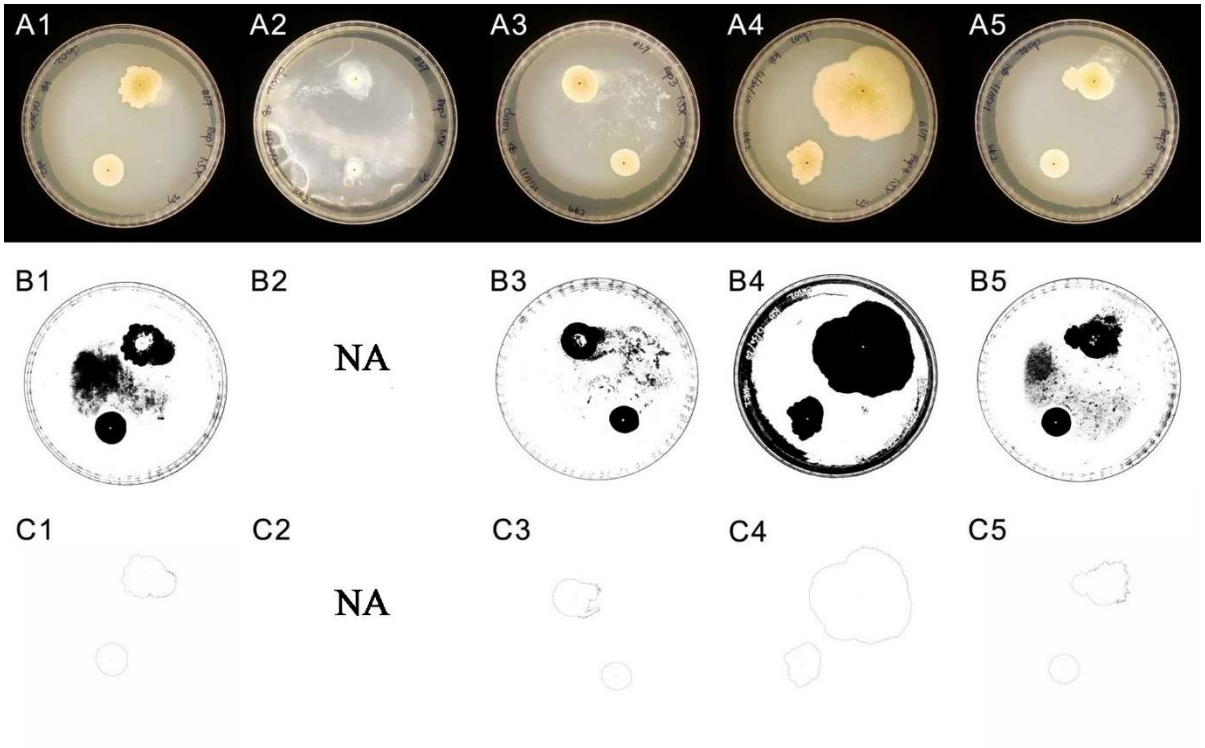


Figure C150. 2021 co-inoculated Petri plates four days after inoculation. **A1-A5)** 1.5x BLT vs. *Pss* 23 on KB media. **B1-B5)** Images after threshold adjustment in ImageJ. **C1-C5)** Image of measured area. A1, B1, C1: Replication 1; A2, B2, C2: Replication 2; A3, B3, C3: Replication 3; A4, B4, C4: Replication 4; A5, B5, C5: Replication 5. Images with NA are not available.

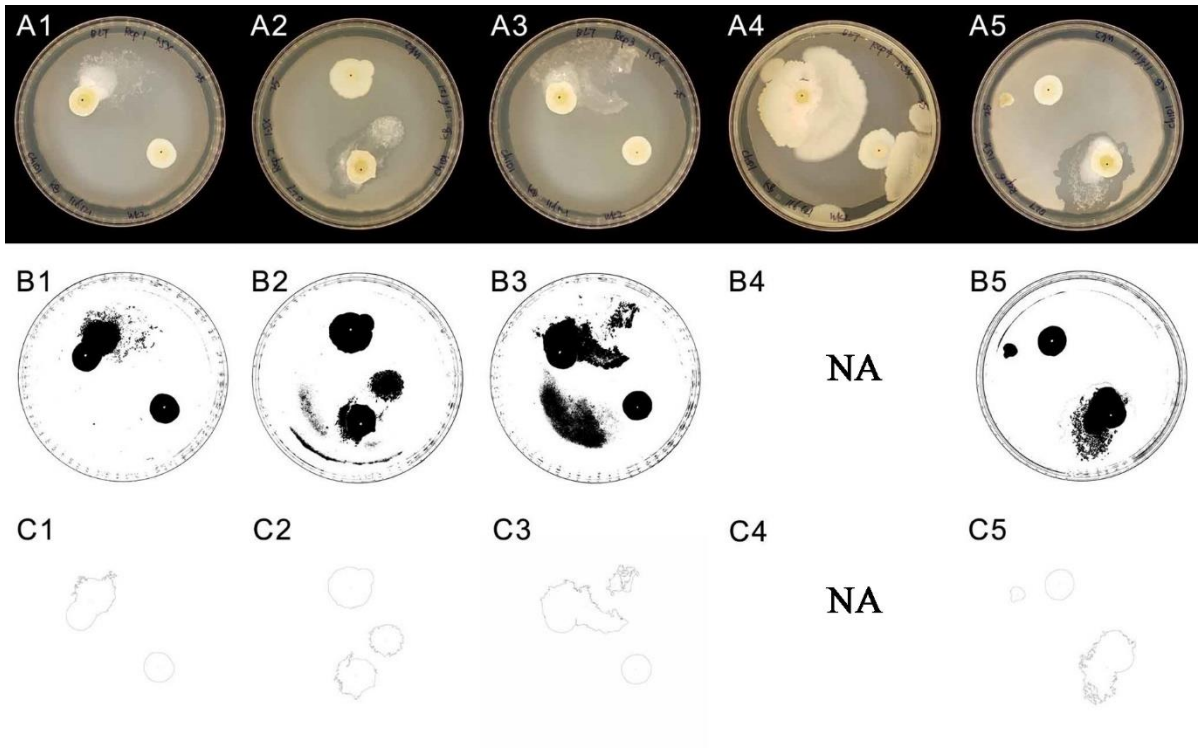


Figure C151. 2021 co-inoculated Petri plates four days after inoculation. **A1-A5)** 1.5x BLT vs. *Pss* 25 on KB media. **B1-B5)** Images after threshold adjustment in ImageJ. **C1-C5)** Image of measured area. A1, B1, C1: Replication 1; A2, B2, C2: Replication 2; A3, B3, C3: Replication 3; A4, B4, C4: Replication 4; A5, B5, C5: Replication 5. Images with NA are not available.

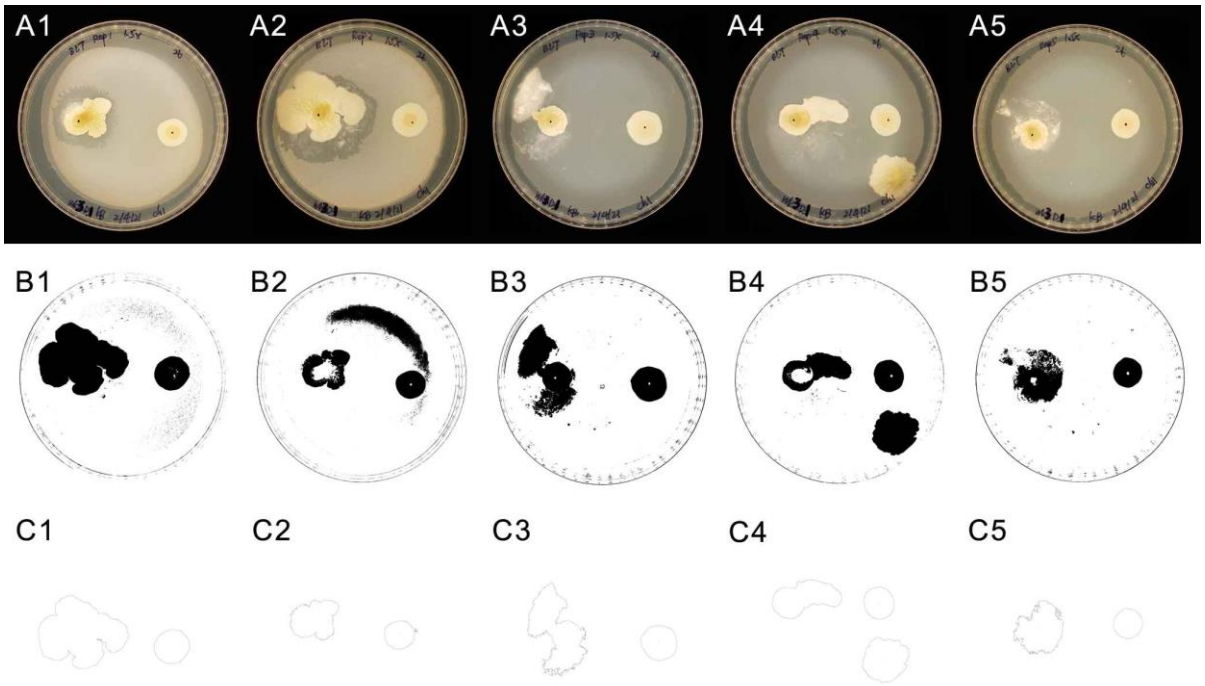


Figure C152. 2021 co-inoculated Petri plates four days after inoculation. **A1-A5)** 1.5x BLT vs. *Pss* 26 on KB media. **B1-B5)** Images after threshold adjustment in ImageJ. **C1-C5)** Image of measured area. A1, B1, C1: Replication 1; A2, B2, C2: Replication 2; A3, B3, C3: Replication 3; A4, B4, C4: Replication 4; A5, B5, C5: Replication 5.

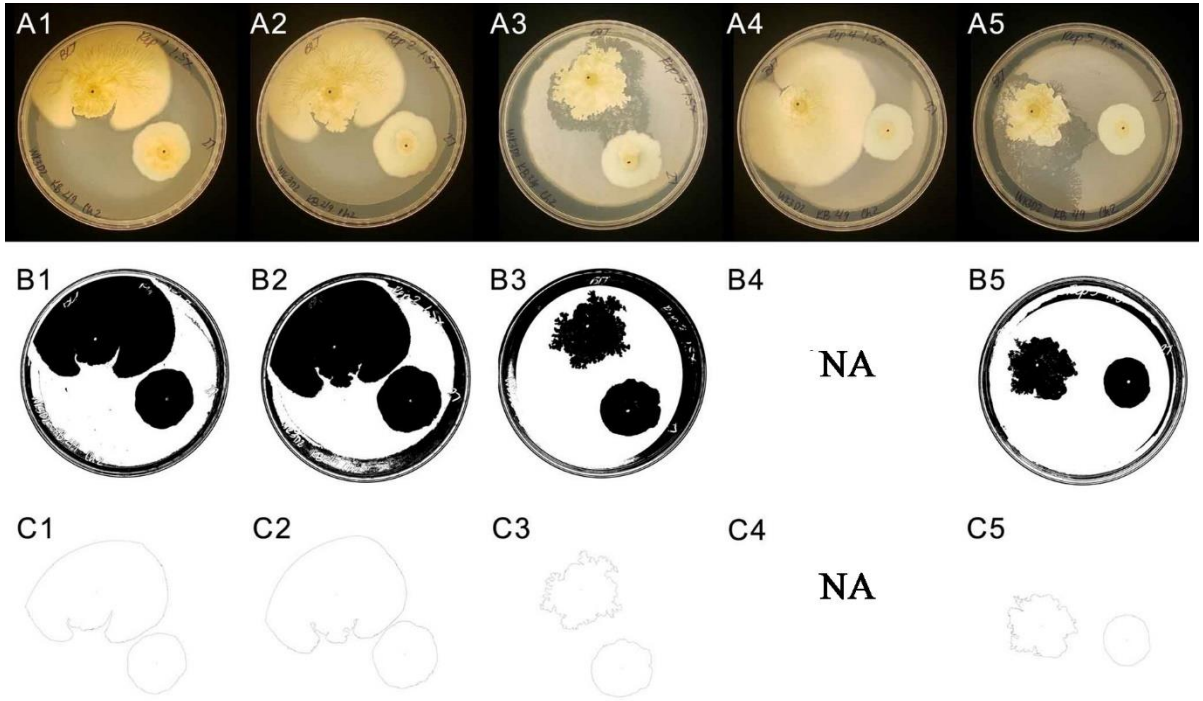


Figure C153. 2021 co-inoculated Petri plates four days after inoculation. **A1-A5)** 1.5x BLT vs. *Pss* 27 on KB media. **B1-B5)** Images after threshold adjustment in ImageJ. **C1-C5)** Image of measured area. A1, B1, C1: Replication 1; A2, B2, C2: Replication 2; A3, B3, C3: Replication 3; A4, B4, C4: Replication 4; A5, B5, C5: Replication 5. Images with NA are not available.

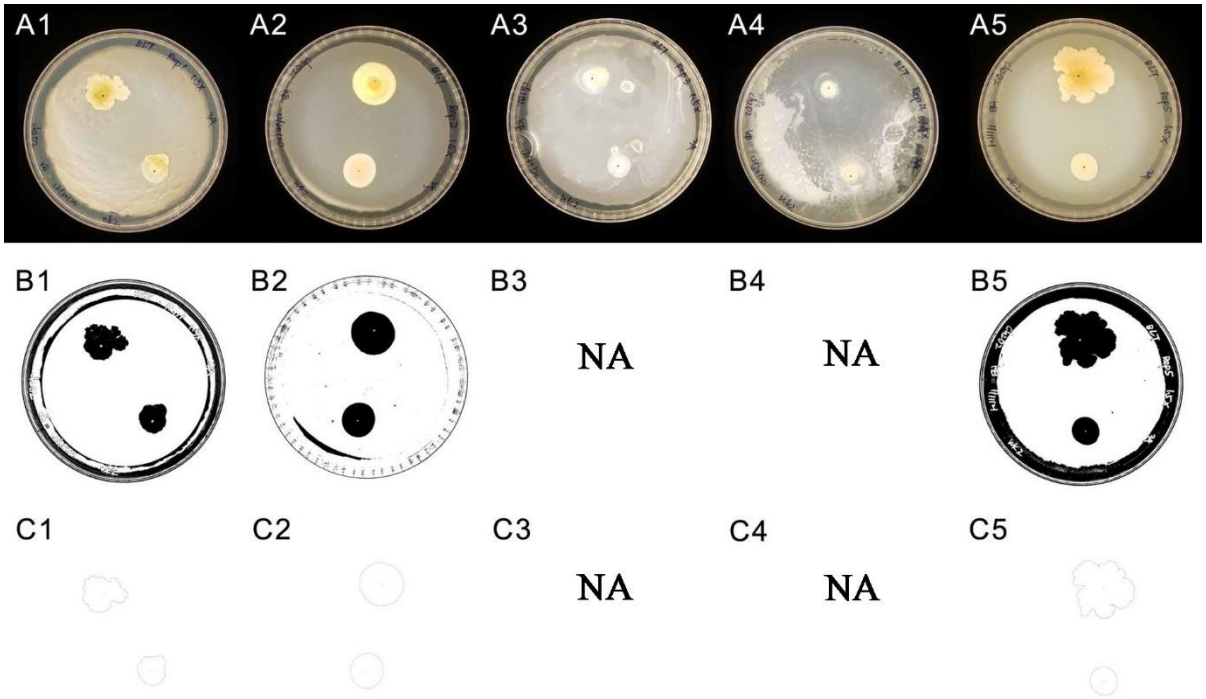


Figure C154. 2021 co-inoculated Petri plates four days after inoculation. **A1-A5)** 1.5x BLT vs. *Pss* 34 on KB media. **B1-B5)** Images after threshold adjustment in ImageJ. **C1-C5)** Image of measured area. A1, B1, C1: Replication 1; A2, B2, C2: Replication 2; A3, B3, C3: Replication 3; A4, B4, C4: Replication 4; A5, B5, C5: Replication 5. Images with NA are not available.

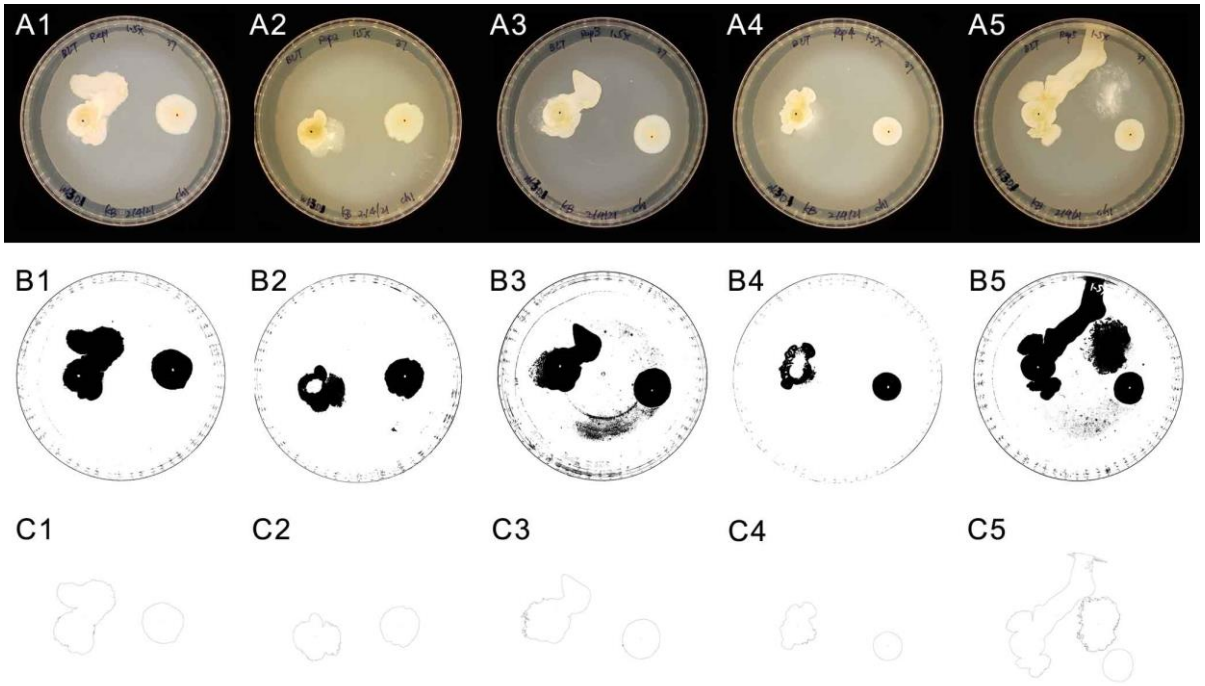


Figure C155. 2021 co-inoculated Petri plates four days after inoculation. **A1-A5)** 1.5x BLT vs. *Pss* 37 on KB media. **B1-B5)** Images after threshold adjustment in ImageJ. **C1-C5)** Image of measured area. A1, B1, C1: Replication 1; A2, B2, C2: Replication 2; A3, B3, C3: Replication 3; A4, B4, C4: Replication 4; A5, B5, C5: Replication 5.

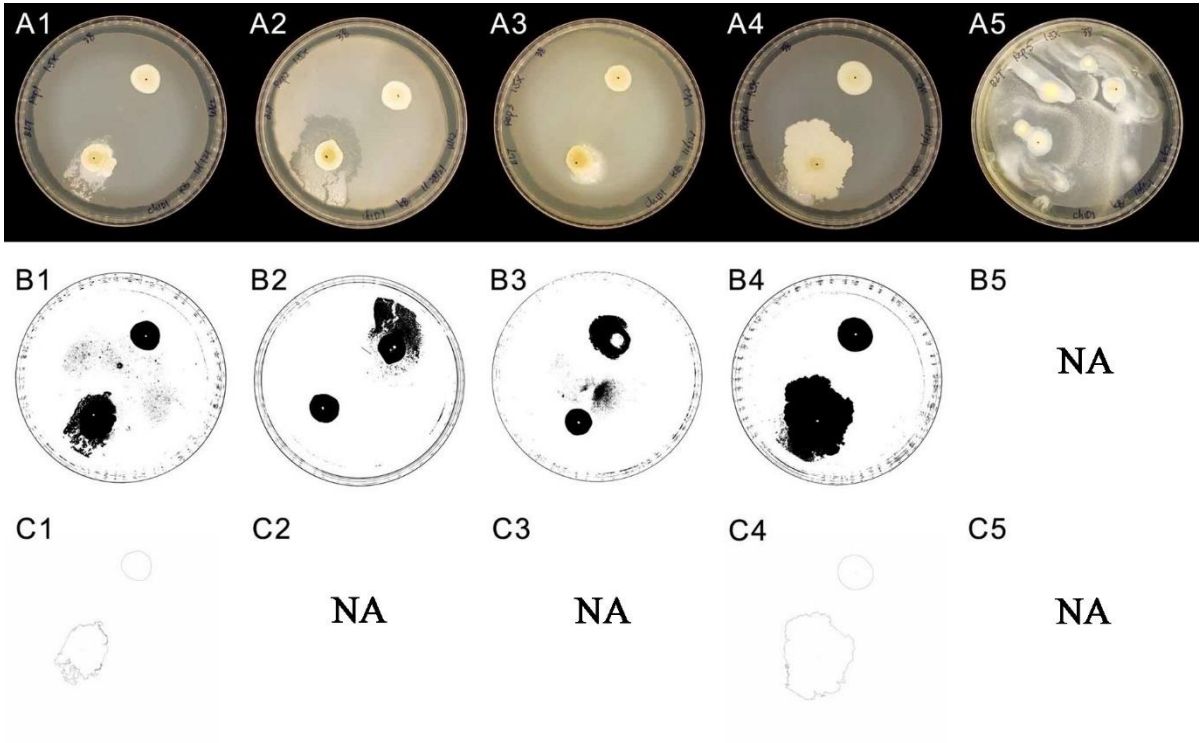


Figure C156. 2021 co-inoculated Petri plates four days after inoculation. **A1-A5)** 1.5x BLT vs. *Pss* 38 on KB media. **B1-B5)** Images after threshold adjustment in ImageJ. **C1-C5)** Image of measured area. A1, B1, C1: Replication 1; A2, B2, C2: Replication 2; A3, B3, C3: Replication 3; A4, B4, C4: Replication 4; A5, B5, C5: Replication 5. Images with NA are not available.

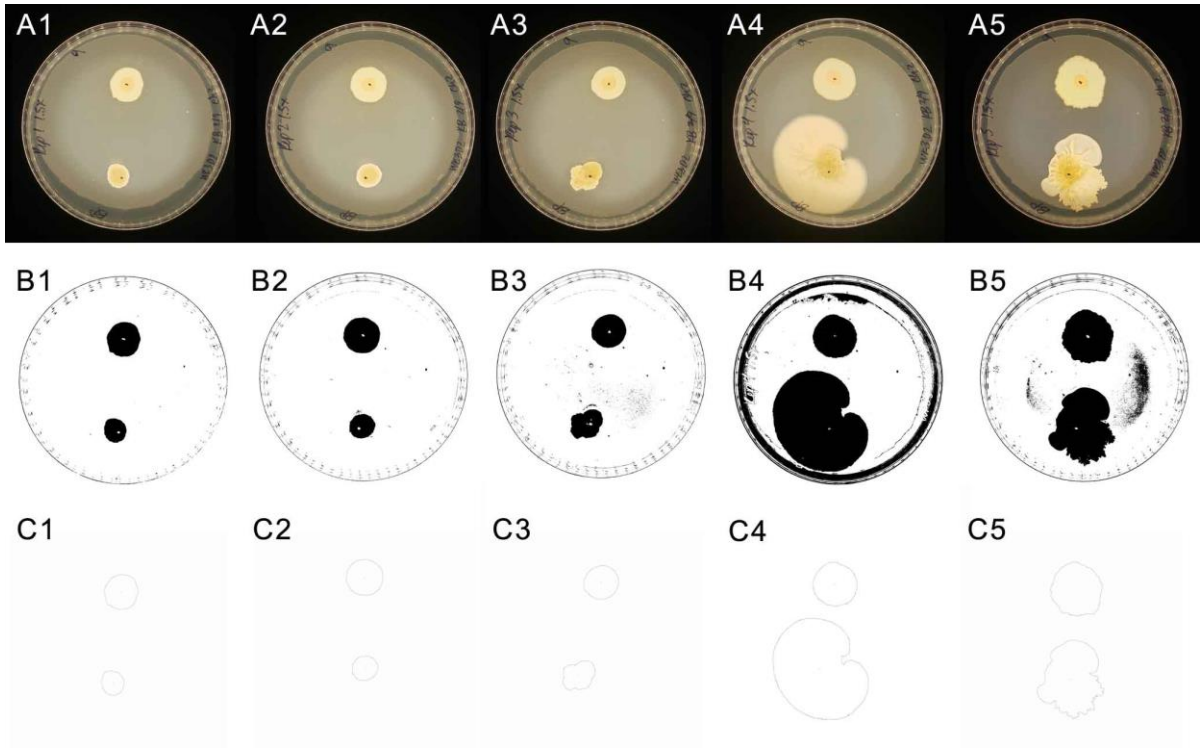


Figure C157. 2021 co-inoculated Petri plates four days after inoculation. **A1-A5)** 1.5x BP vs. *Pss* 9 on KB media. **B1-B5)** Images after threshold adjustment in ImageJ. **C1-C5)** Image of measured area. A1, B1, C1: Replication 1; A2, B2, C2: Replication 2; A3, B3, C3: Replication 3; A4, B4, C4: Replication 4; A5, B5, C5: Replication 5.

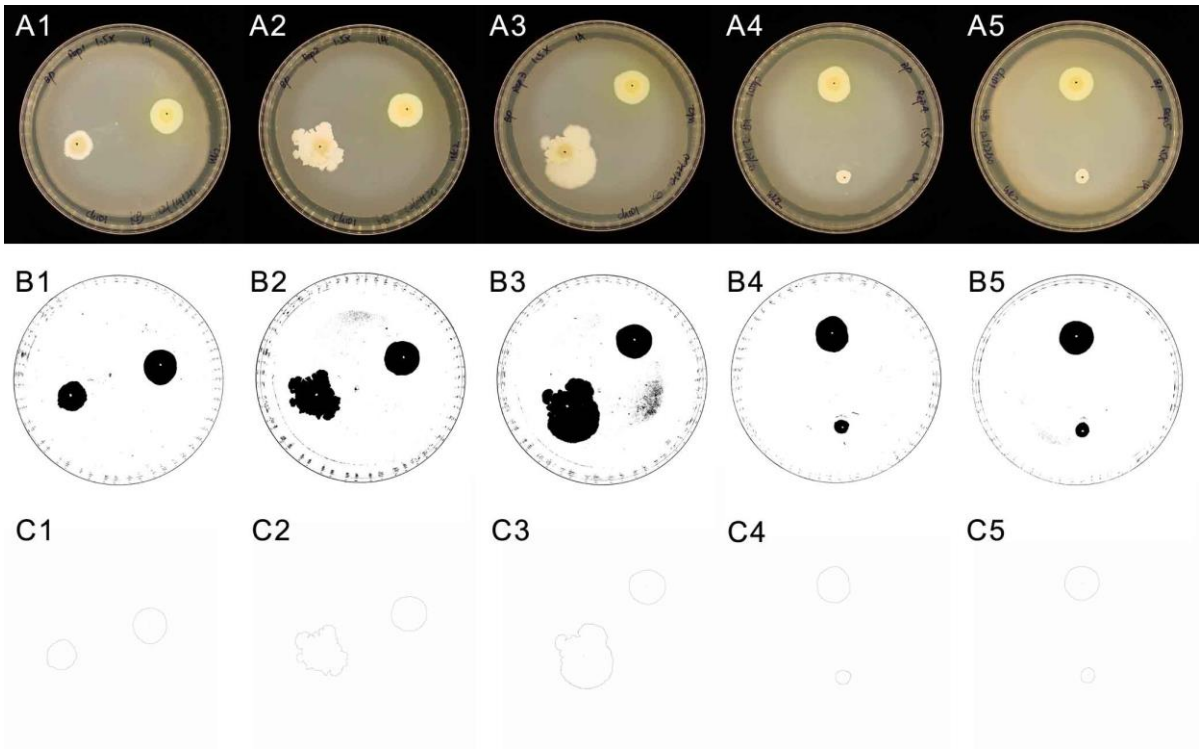


Figure C158. 2021 co-inoculated Petri plates four days after inoculation. **A1-A5)** 1.5x BP vs. *Pss* 14 on KB media. **B1-B5)** Images after threshold adjustment in ImageJ. **C1-C5)** Image of measured area. A1, B1, C1: Replication 1; A2, B2, C2: Replication 2; A3, B3, C3: Replication 3; A4, B4, C4: Replication 4; A5, B5, C5: Replication 5.

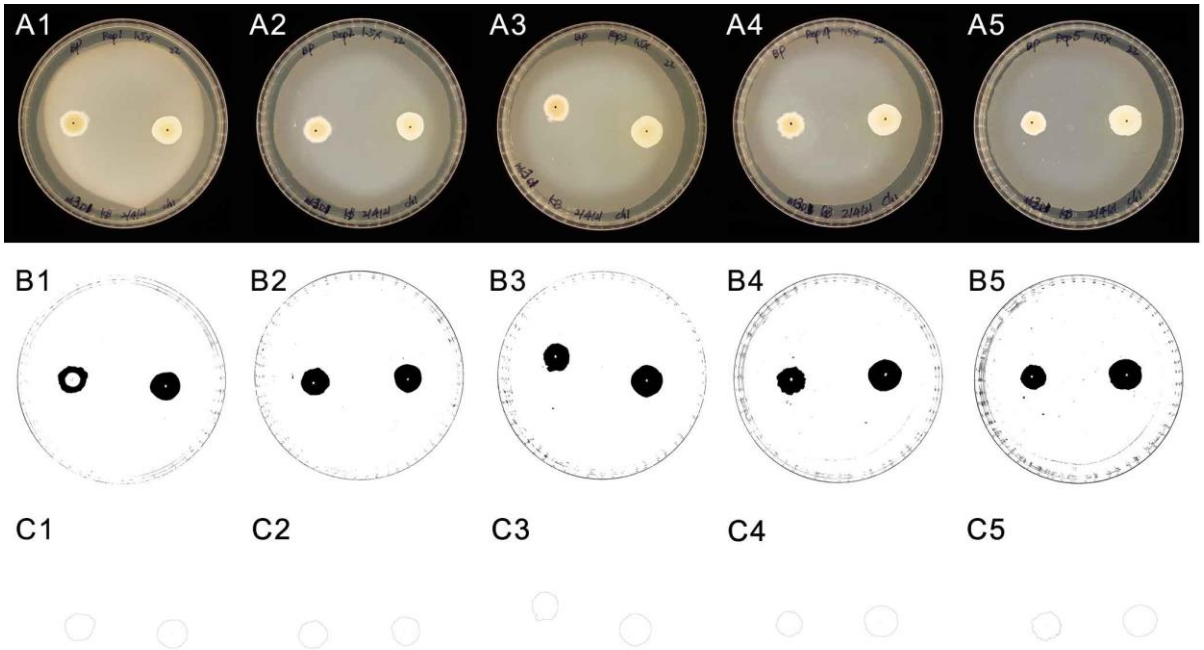


Figure C159. 2021 co-inoculated Petri plates four days after inoculation. **A1-A5)** 1.5x BP vs. *Pss* 22 on KB media. **B1-B5)** Images after threshold adjustment in ImageJ. **C1-C5)** Image of measured area. A1, B1, C1: Replication 1; A2, B2, C2: Replication 2; A3, B3, C3: Replication 3; A4, B4, C4: Replication 4; A5, B5, C5: Replication 5.

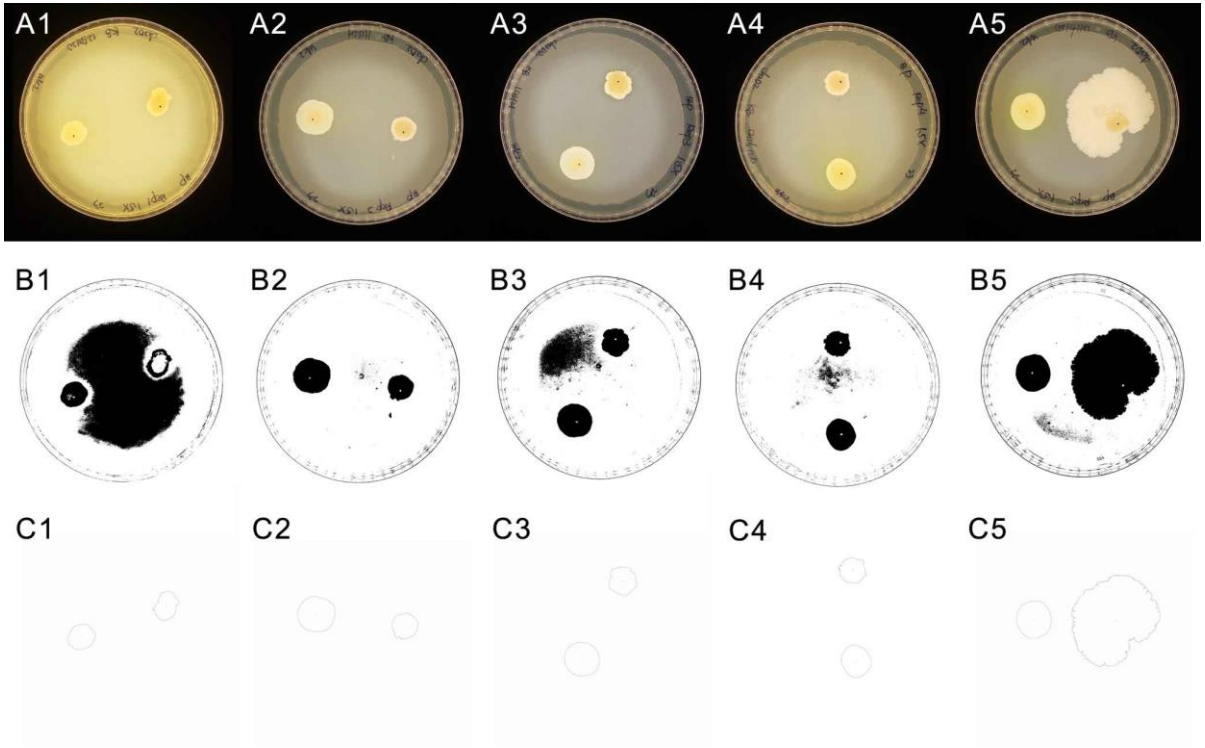


Figure C160. 2021 co-inoculated Petri plates four days after inoculation. **A1-A5)** 1.5x BP vs. *Pss* 23 on KB media. **B1-B5)** Images after threshold adjustment in ImageJ. **C1-C5)** Image of measured area. A1, B1, C1: Replication 1; A2, B2, C2: Replication 2; A3, B3, C3: Replication 3; A4, B4, C4: Replication 4; A5, B5, C5: Replication 5.

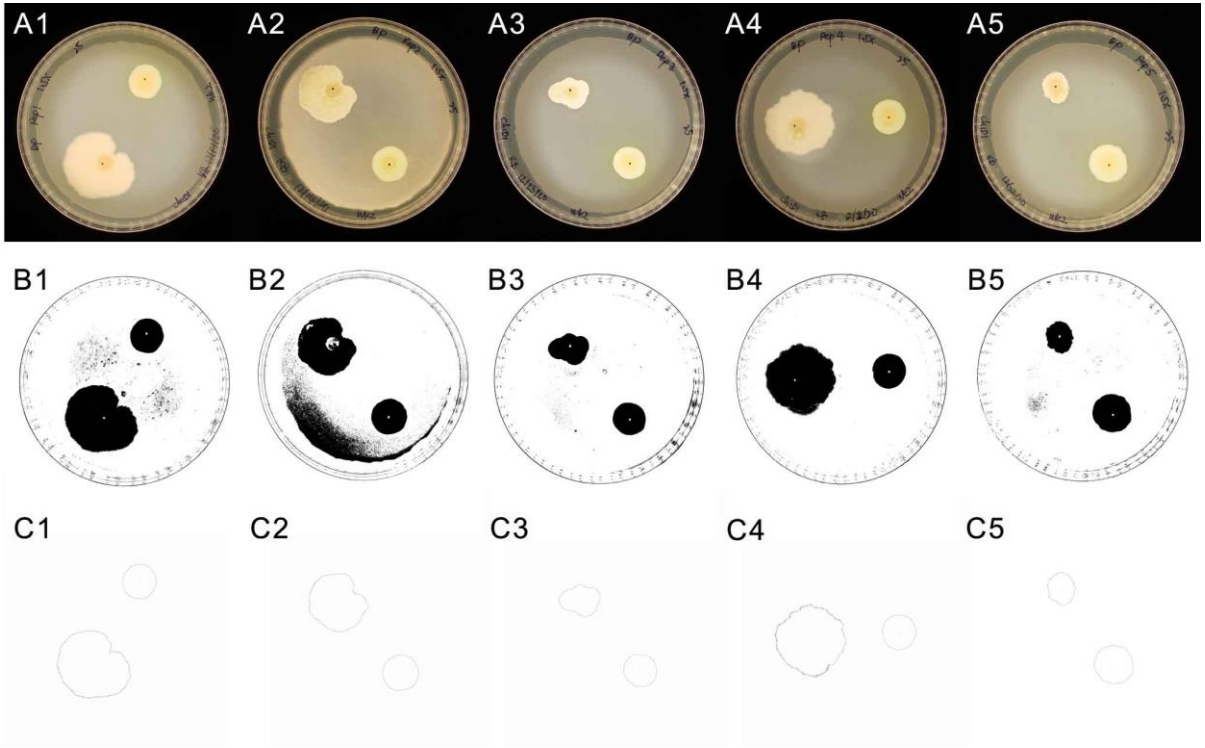


Figure C161. 2021 co-inoculated Petri plates four days after inoculation. **A1-A5)** 1.5x BP vs. *Pss* 25 on KB media. **B1-B5)** Images after threshold adjustment in ImageJ. **C1-C5)** Image of measured area. A1, B1, C1: Replication 1; A2, B2, C2: Replication 2; A3, B3, C3: Replication 3; A4, B4, C4: Replication 4; A5, B5, C5: Replication 5.

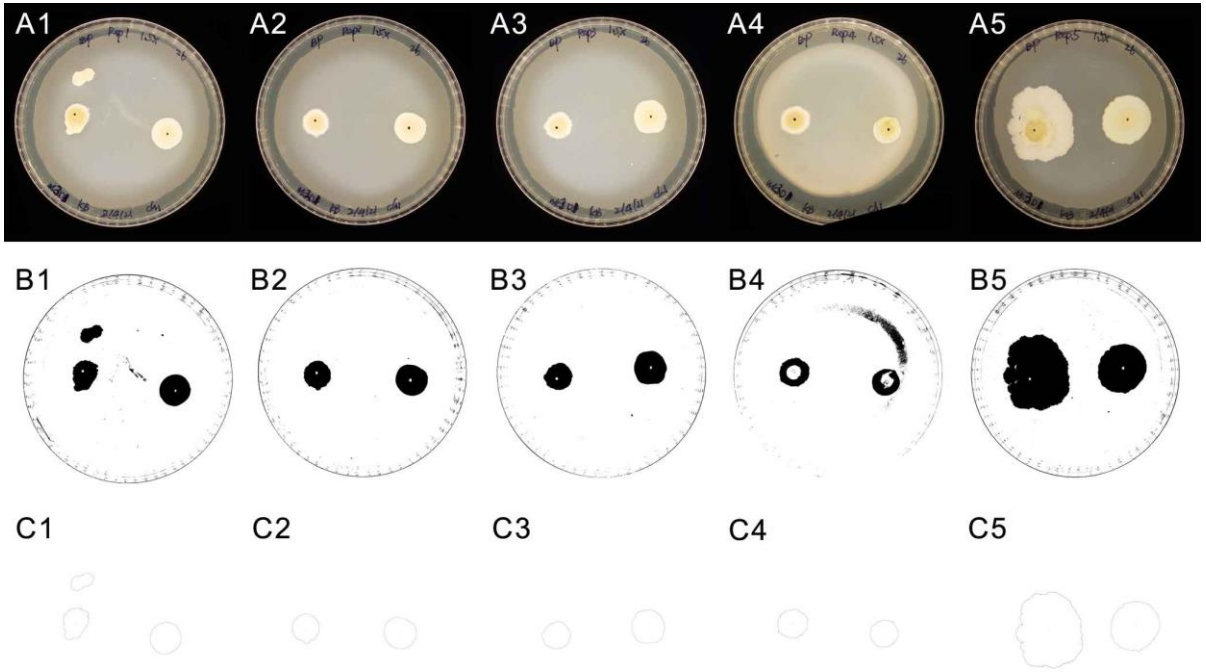


Figure C162. 2021 co-inoculated Petri plates four days after inoculation. **A1-A5)** 1.5x BP vs. *Pss* 26 on KB media. **B1-B5)** Images after threshold adjustment in ImageJ. **C1-C5)** Image of measured area. A1, B1, C1: Replication 1; A2, B2, C2: Replication 2; A3, B3, C3: Replication 3; A4, B4, C4: Replication 4; A5, B5, C5: Replication 5.

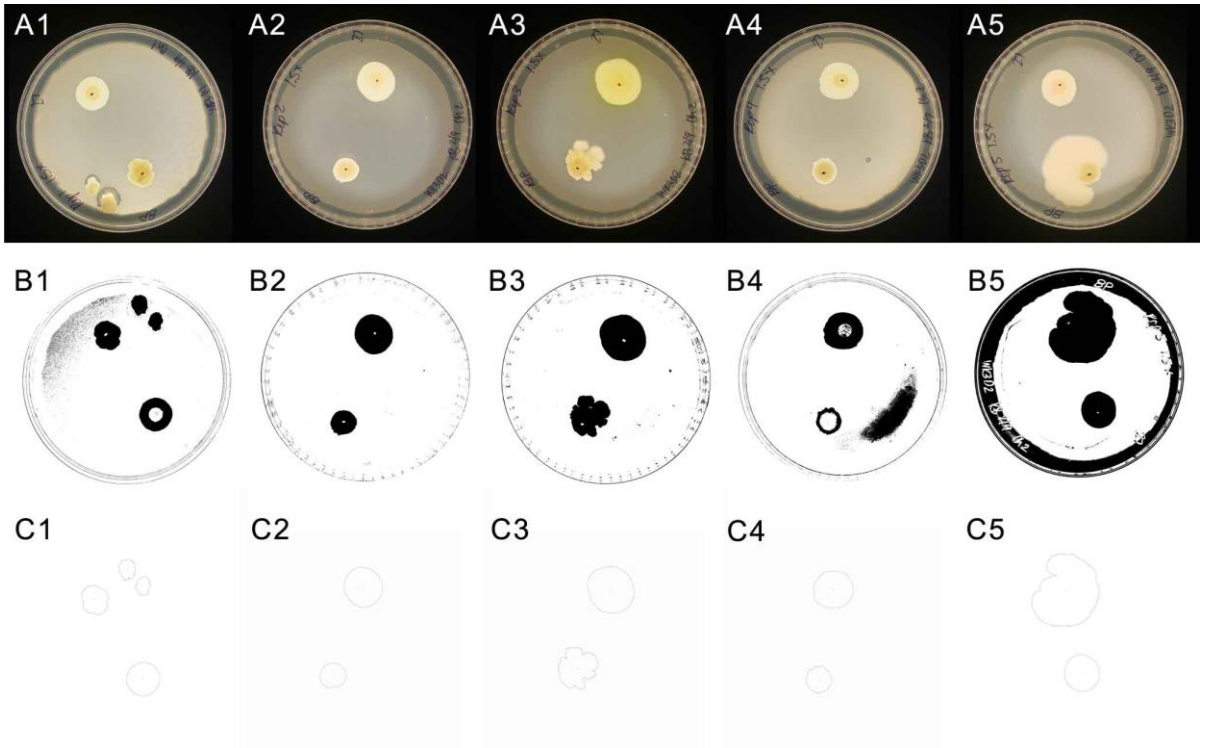


Figure C163. 2021 co-inoculated Petri plates four days after inoculation. **A1-A5)** 1.5x BP vs. *Pss* 27 on KB media. **B1-B5)** Images after threshold adjustment in ImageJ. **C1-C5)** Image of measured area. A1, B1, C1: Replication 1; A2, B2, C2: Replication 2; A3, B3, C3: Replication 3; A4, B4, C4: Replication 4; A5, B5, C5: Replication 5.

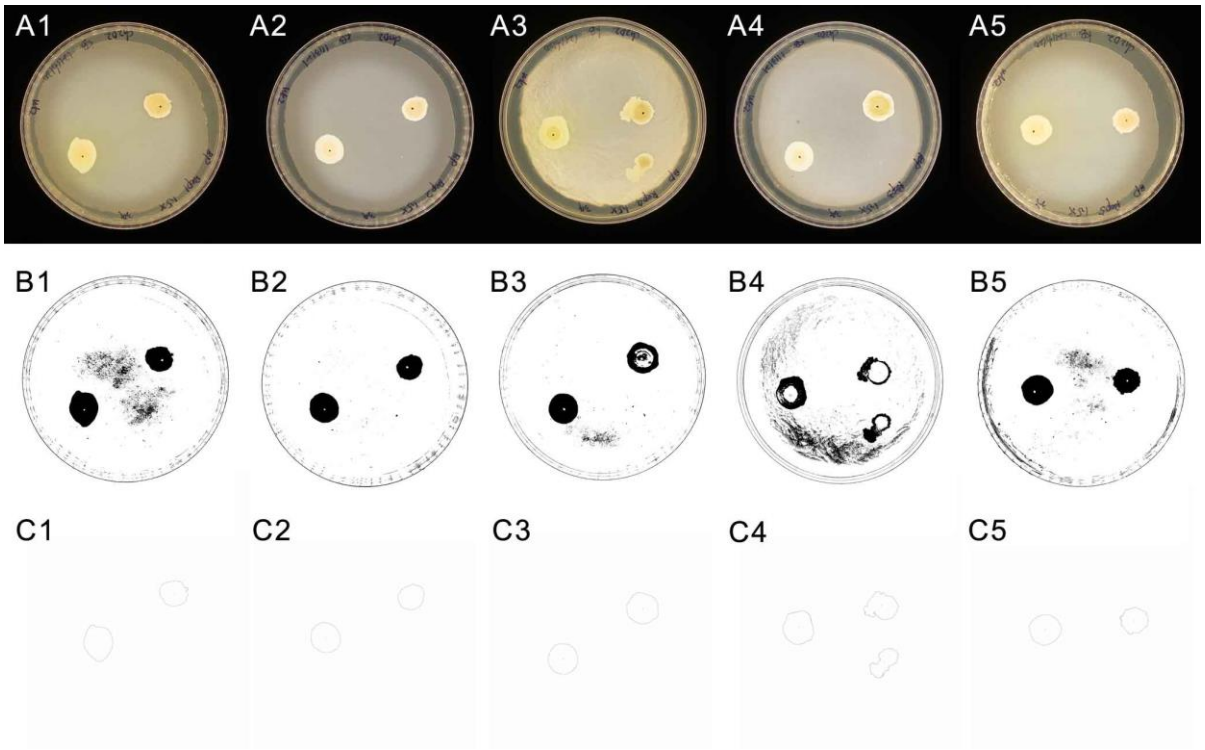


Figure C164. 2021 co-inoculated Petri plates four days after inoculation. **A1-A5)** 1.5x BP vs. *Pss* 34 on KB media. **B1-B5)** Images after threshold adjustment in ImageJ. **C1-C5)** Image of measured area. A1, B1, C1: Replication 1; A2, B2, C2: Replication 2; A3, B3, C3: Replication 3; A4, B4, C4: Replication 4; A5, B5, C5: Replication 5.

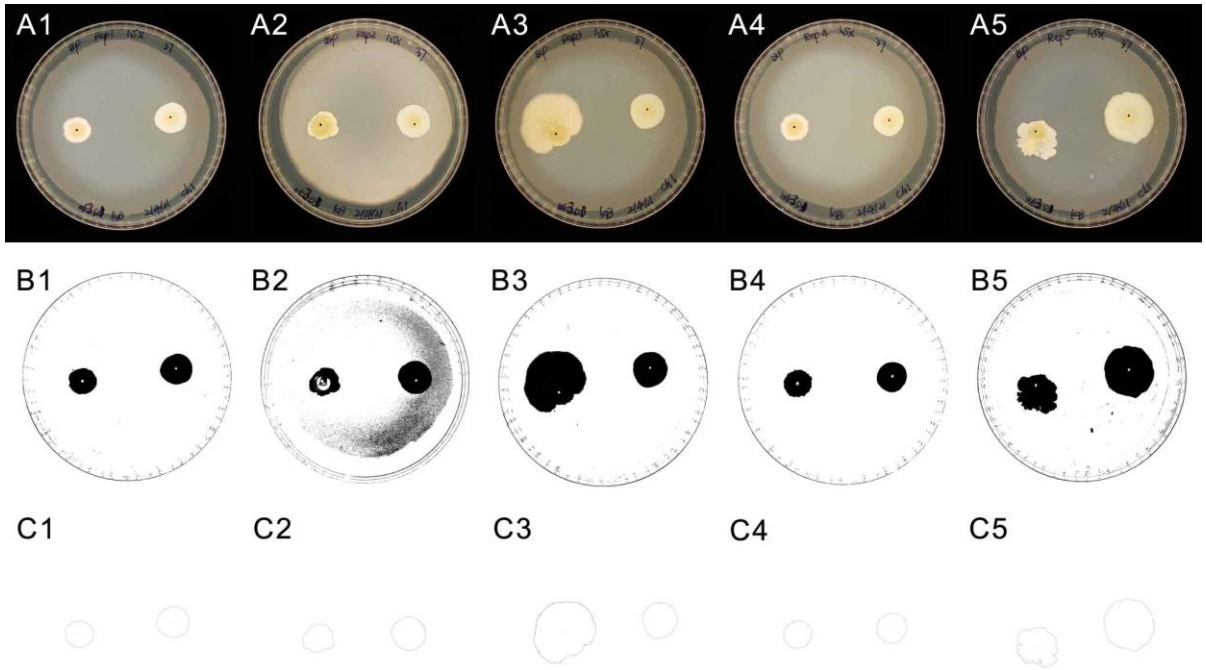


Figure C165. 2021 co-inoculated Petri plates four days after inoculation. **A1-A5)** 1.5x BP vs. *Pss* 37 on KB media. **B1-B5)** Images after threshold adjustment in ImageJ. **C1-C5)** Image of measured area. A1, B1, C1: Replication 1; A2, B2, C2: Replication 2; A3, B3, C3: Replication 3; A4, B4, C4: Replication 4; A5, B5, C5: Replication 5.

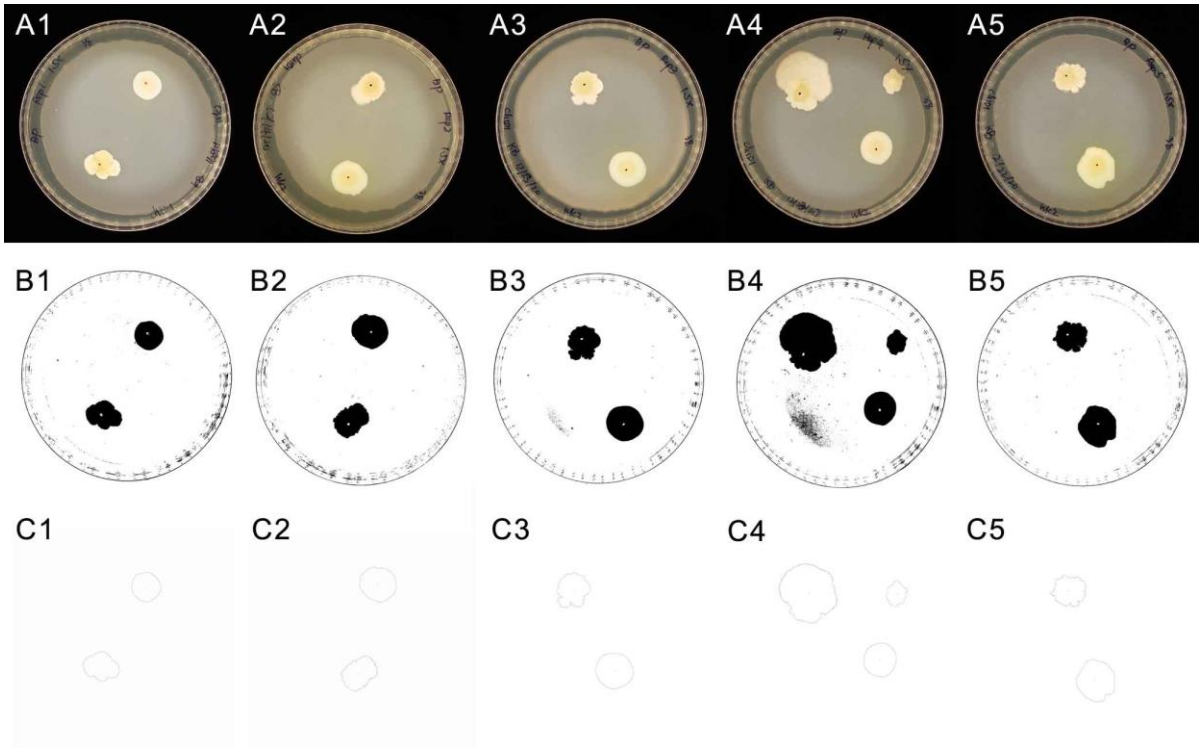


Figure C166. 2021 co-inoculated Petri plates four days after inoculation. **A1-A5)** 1.5x BP vs. *Pss* 38 on KB media. **B1-B5)** Images after threshold adjustment in ImageJ. **C1-C5)** Image of measured area. A1, B1, C1: Replication 1; A2, B2, C2: Replication 2; A3, B3, C3: Replication 3; A4, B4, C4: Replication 4; A5, B5, C5: Replication 5.

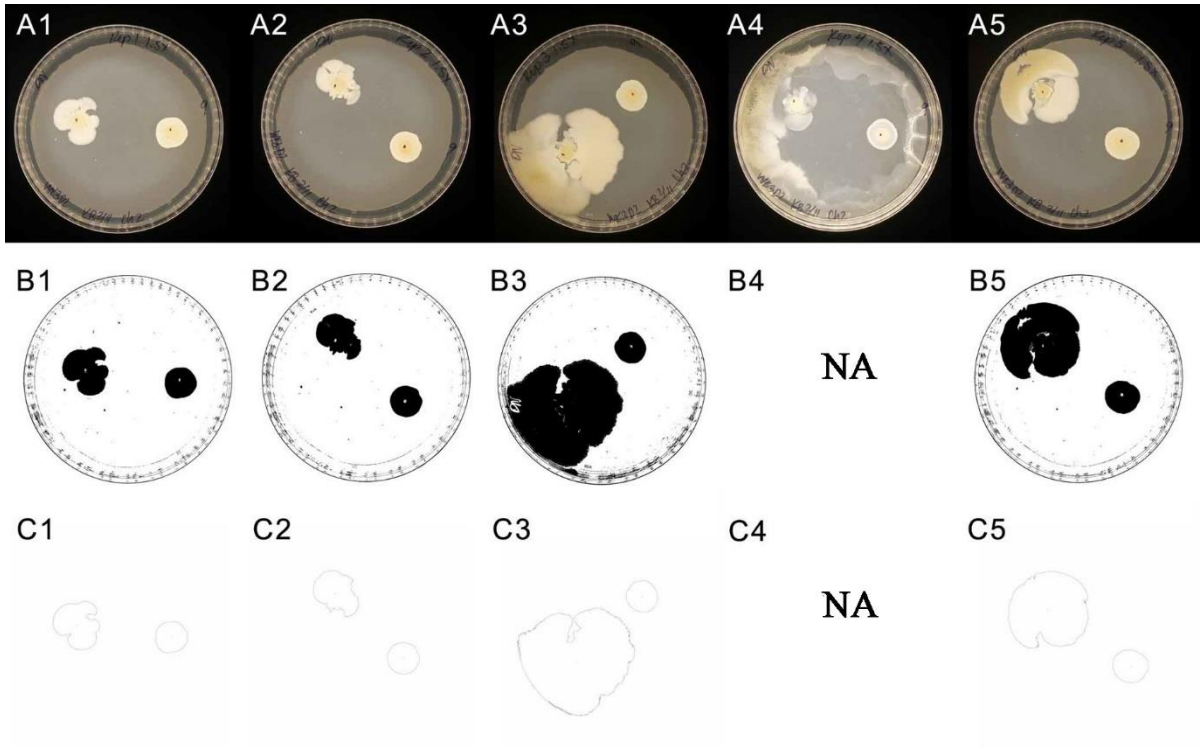


Figure C167. 2021 co-inoculated Petri plates four days after inoculation. **A1-A5)** 1.5x DN vs. *Pss* 9 on KB media. **B1-B5)** Images after threshold adjustment in ImageJ. **C1-C5)** Image of measured area. A1, B1, C1: Replication 1; A2, B2, C2: Replication 2; A3, B3, C3: Replication 3; A4, B4, C4: Replication 4; A5, B5, C5: Replication 5. Images with NA are not available.

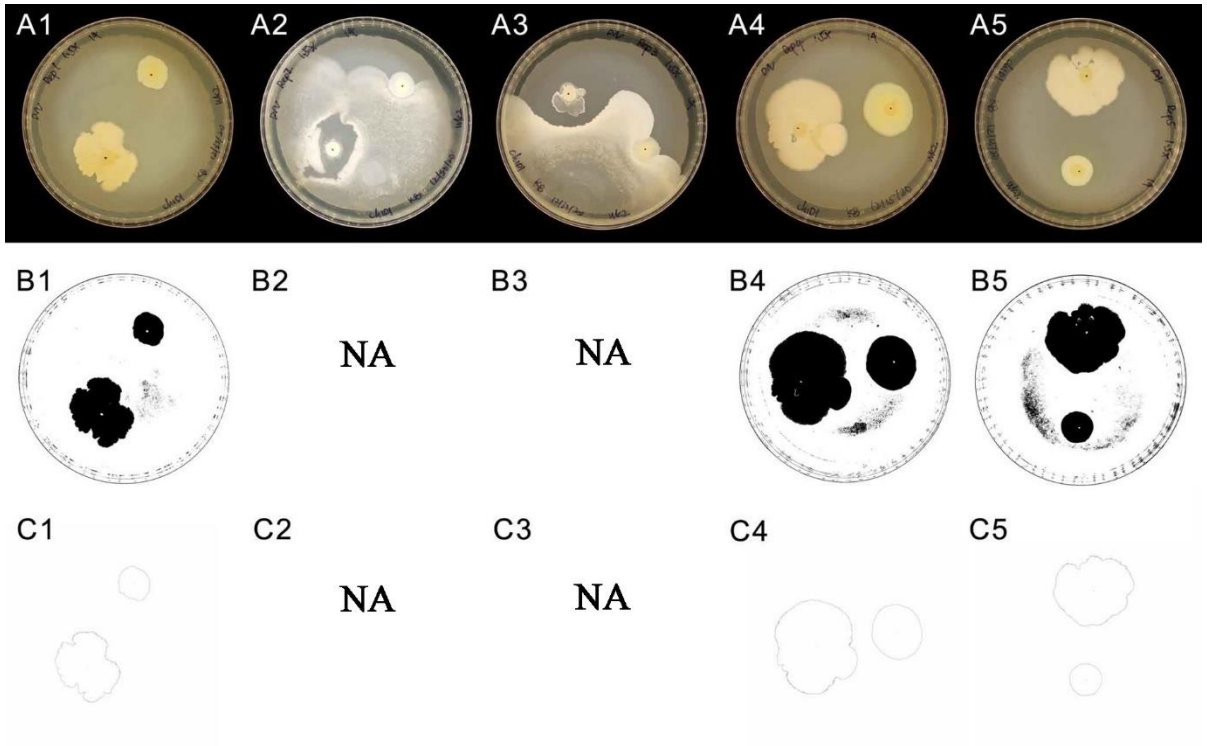


Figure C168. 2021 co-inoculated Petri plates four days after inoculation. **A1-A5)** 1.5x DN vs. *Pss* 14 on KB media. **B1-B5)** Images after threshold adjustment in ImageJ. **C1-C5)** Image of measured area. A1, B1, C1: Replication 1; A2, B2, C2: Replication 2; A3, B3, C3: Replication 3; A4, B4, C4: Replication 4; A5, B5, C5: Replication 5. Images with NA are not available.

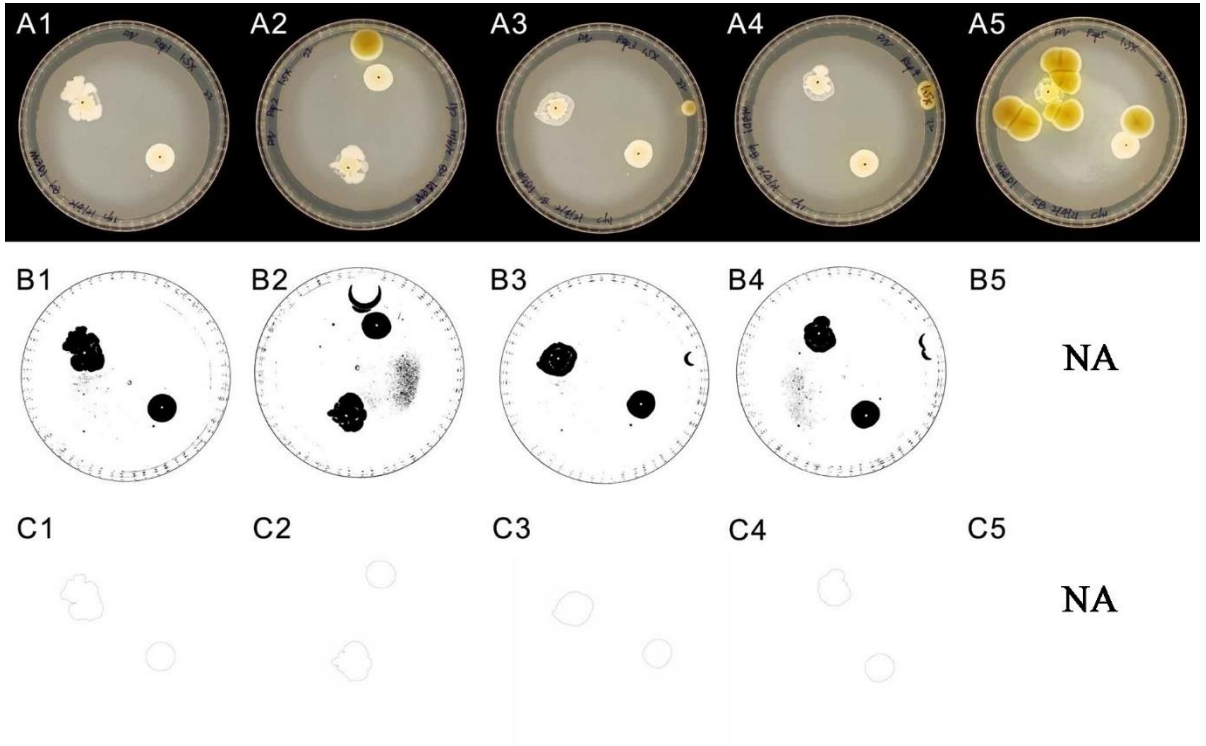


Figure C169. 2021 co-inoculated Petri plates four days after inoculation. **A1-A5)** 1.5x DN vs. *Pss* 22 on KB media. **B1-B5)** Images after threshold adjustment in ImageJ. **C1-C5)** Image of measured area. A1, B1, C1: Replication 1; A2, B2, C2: Replication 2; A3, B3, C3: Replication 3; A4, B4, C4: Replication 4; A5, B5, C5: Replication 5. Images with NA are not available.

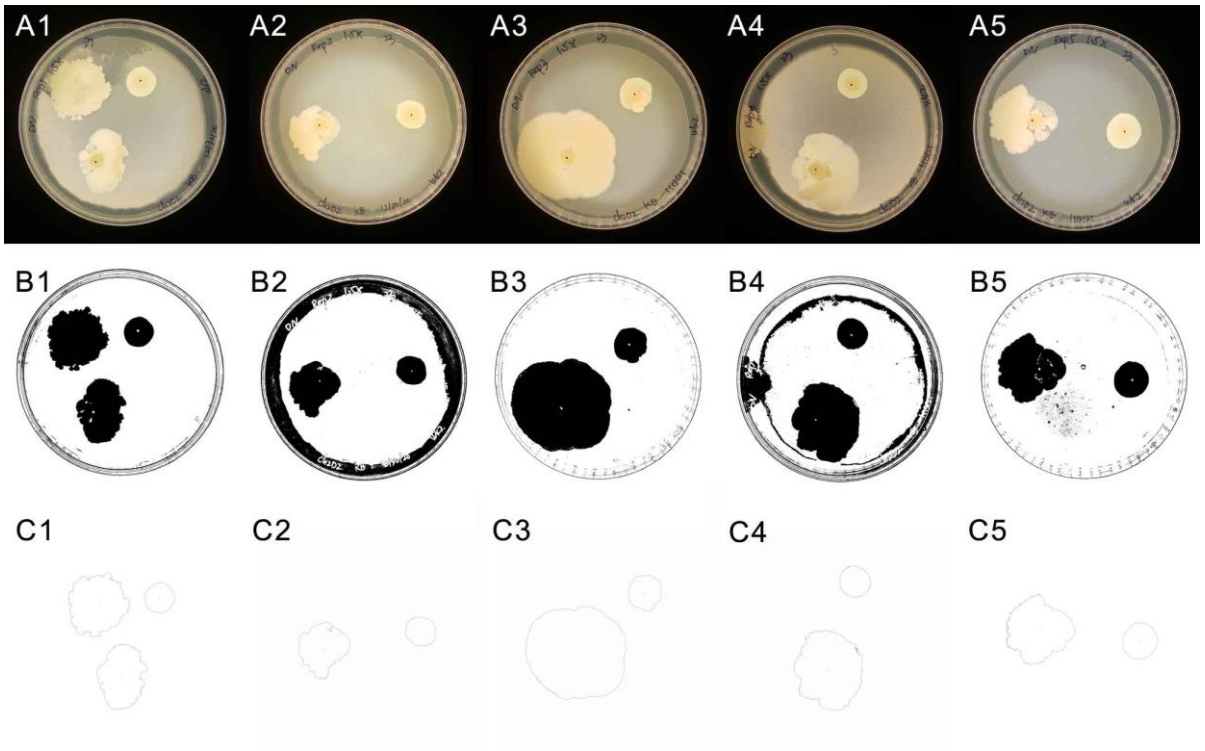


Figure C170. 2021 co-inoculated Petri plates four days after inoculation. **A1-A5)** 1.5x DN vs. *Pss* 23 on KB media. **B1-B5)** Images after threshold adjustment in ImageJ. **C1-C5)** Image of measured area. A1, B1, C1: Replication 1; A2, B2, C2: Replication 2; A3, B3, C3: Replication 3; A4, B4, C4: Replication 4; A5, B5, C5: Replication 5.

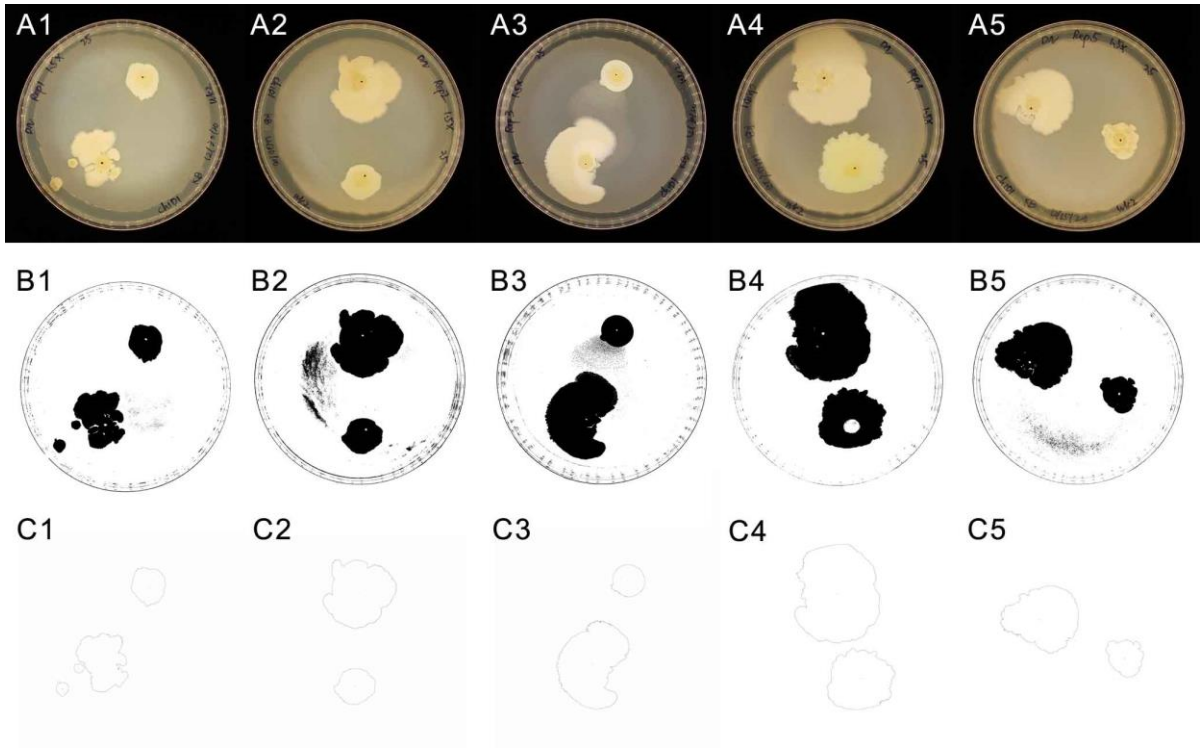


Figure C171. 2021 co-inoculated Petri plates four days after inoculation. **A1-A5)** 1.5x DN vs. *Pss* 25 on KB media. **B1-B5)** Images after threshold adjustment in ImageJ. **C1-C5)** Image of measured area. A1, B1, C1: Replication 1; A2, B2, C2: Replication 2; A3, B3, C3: Replication 3; A4, B4, C4: Replication 4; A5, B5, C5: Replication 5.

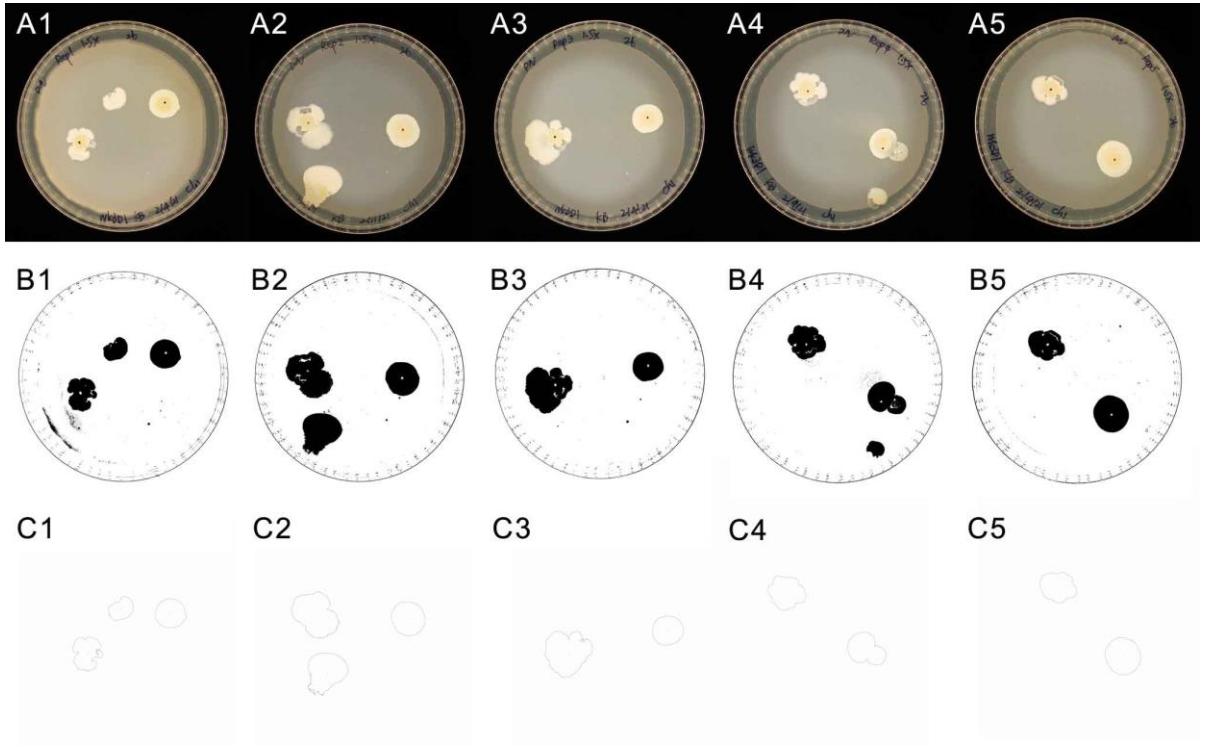


Figure C172. 2021 co-inoculated Petri plates four days after inoculation. **A1-A5)** 1.5x DN vs. *Pss* 26 on KB media. **B1-B5)** Images after threshold adjustment in ImageJ. **C1-C5)** Image of measured area. A1, B1, C1: Replication 1; A2, B2, C2: Replication 2; A3, B3, C3: Replication 3; A4, B4, C4: Replication 4; A5, B5, C5: Replication 5.

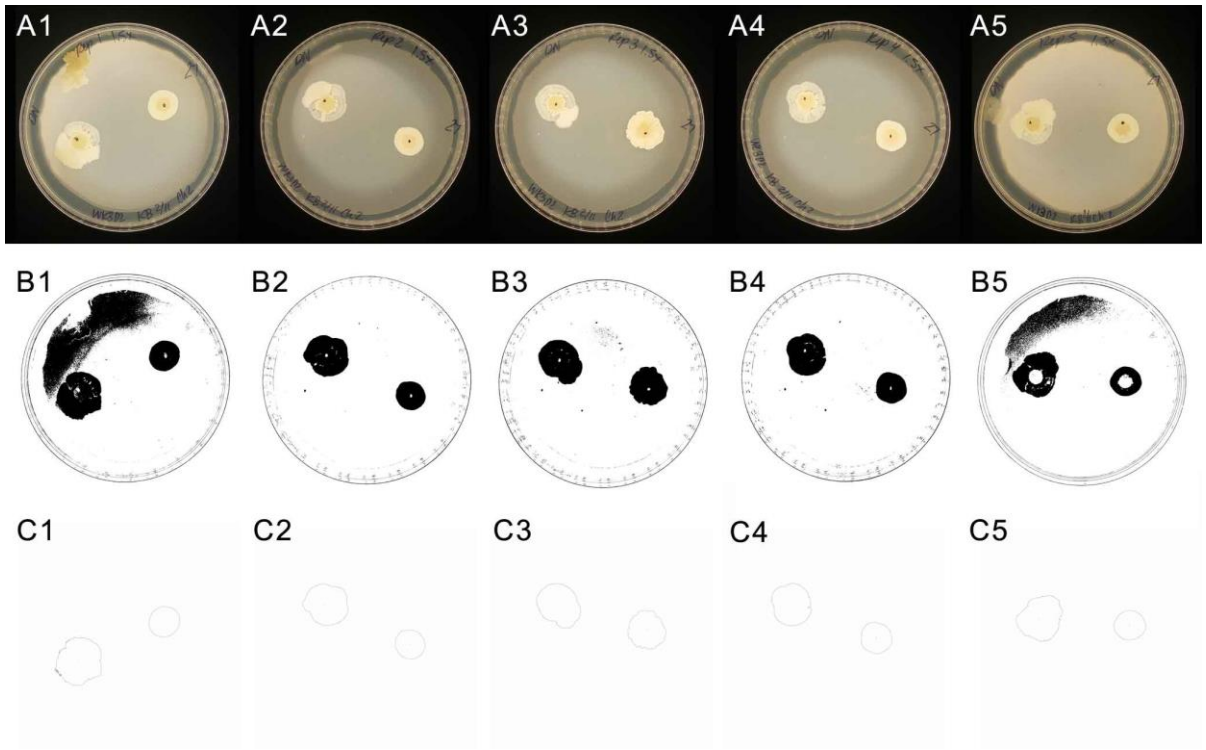


Figure C173. 2021 co-inoculated Petri plates four days after inoculation. **A1-A5)** 1.5x DN vs. *Pss* 27 on KB media. **B1-B5)** Images after threshold adjustment in ImageJ. **C1-C5)** Image of measured area. A1, B1, C1: Replication 1; A2, B2, C2: Replication 2; A3, B3, C3: Replication 3; A4, B4, C4: Replication 4; A5, B5, C5: Replication 5.

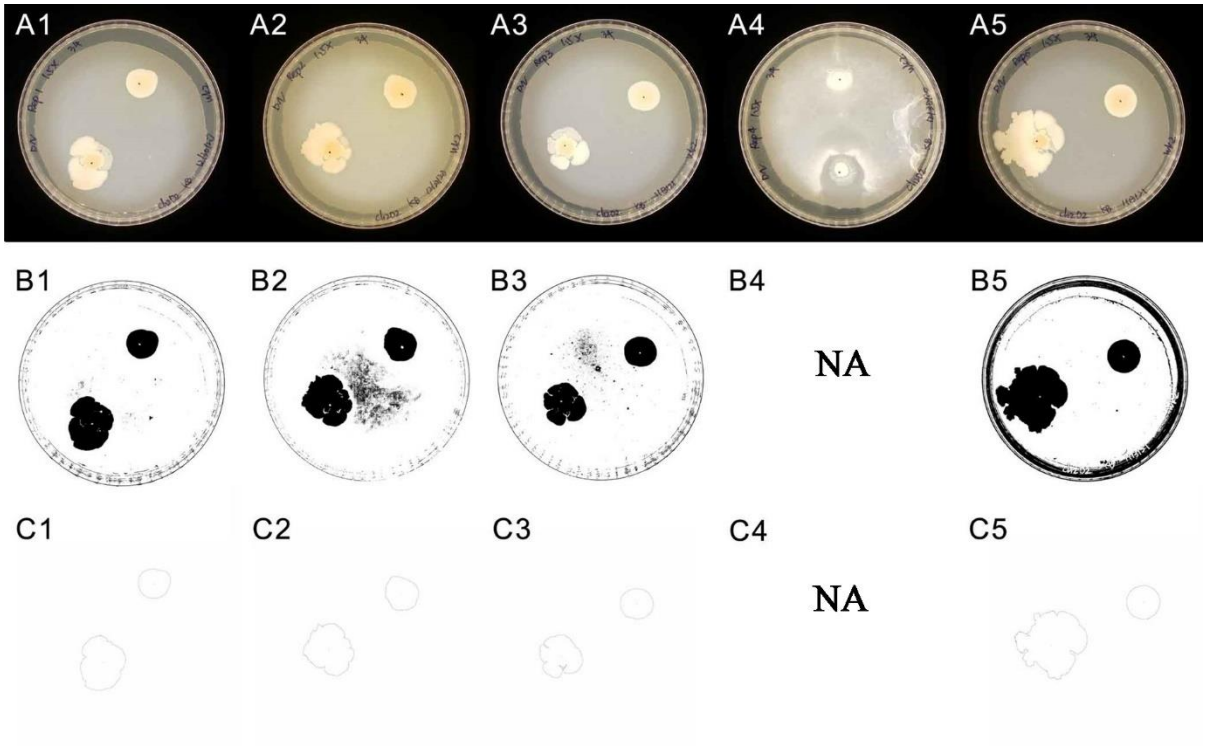


Figure C174. 2021 co-inoculated Petri plates four days after inoculation. **A1-A5)** 1.5x DN vs. *Pss* 34 on KB media. **B1-B5)** Images after threshold adjustment in ImageJ. **C1-C5)** Image of measured area. A1, B1, C1: Replication 1; A2, B2, C2: Replication 2; A3, B3, C3: Replication 3; A4, B4, C4: Replication 4; A5, B5, C5: Replication 5. Images with NA are not available.

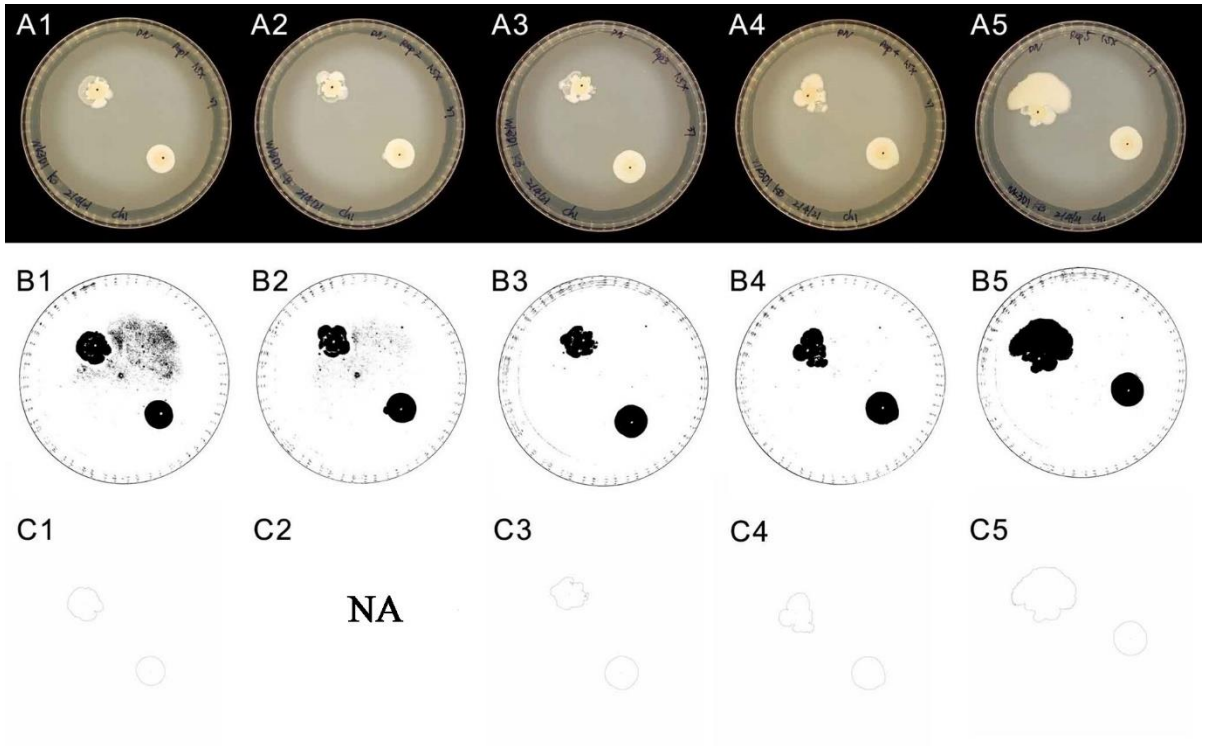


Figure C175. 2021 co-inoculated Petri plates four days after inoculation. **A1-A5)** 1.5x DN vs. *Pss* 37 on KB media. **B1-B5)** Images after threshold adjustment in ImageJ. **C1-C5)** Image of measured area. A1, B1, C1: Replication 1; A2, B2, C2: Replication 2; A3, B3, C3: Replication 3; A4, B4, C4: Replication 4; A5, B5, C5: Replication 5. Images with NA are not available.

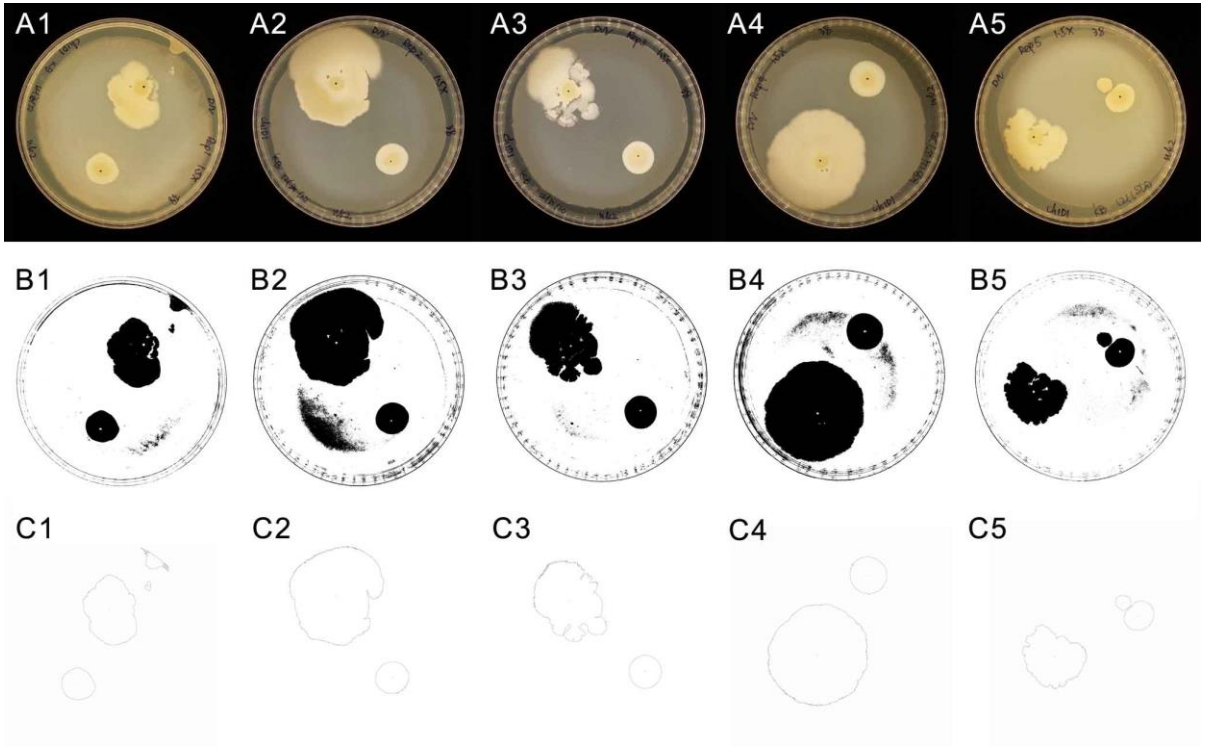


Figure C176. 2021 co-inoculated Petri plates four days after inoculation. **A1-A5)** 1.5x DN vs. *Pss* 38 on KB media. **B1-B5)** Images after threshold adjustment in ImageJ. **C1-C5)** Image of measured area. A1, B1, C1: Replication 1; A2, B2, C2: Replication 2; A3, B3, C3: Replication 3; A4, B4, C4: Replication 4; A5, B5, C5: Replication 5.

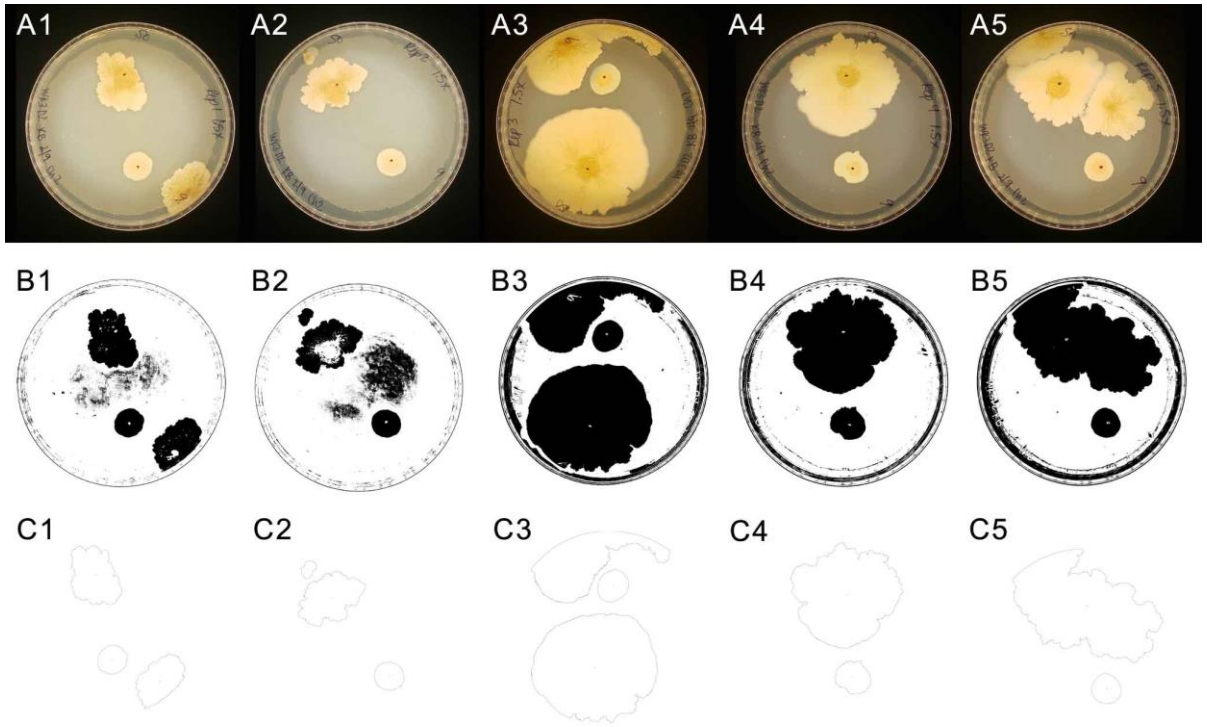


Figure C177. 2021 co-inoculated Petri plates four days after inoculation. **A1-A5)** 1.5x SO vs. *Pss* 9 on KB media. **B1-B5)** Images after threshold adjustment in ImageJ. **C1-C5)** Image of measured area. A1, B1, C1: Replication 1; A2, B2, C2: Replication 2; A3, B3, C3: Replication 3; A4, B4, C4: Replication 4; A5, B5, C5: Replication 5.

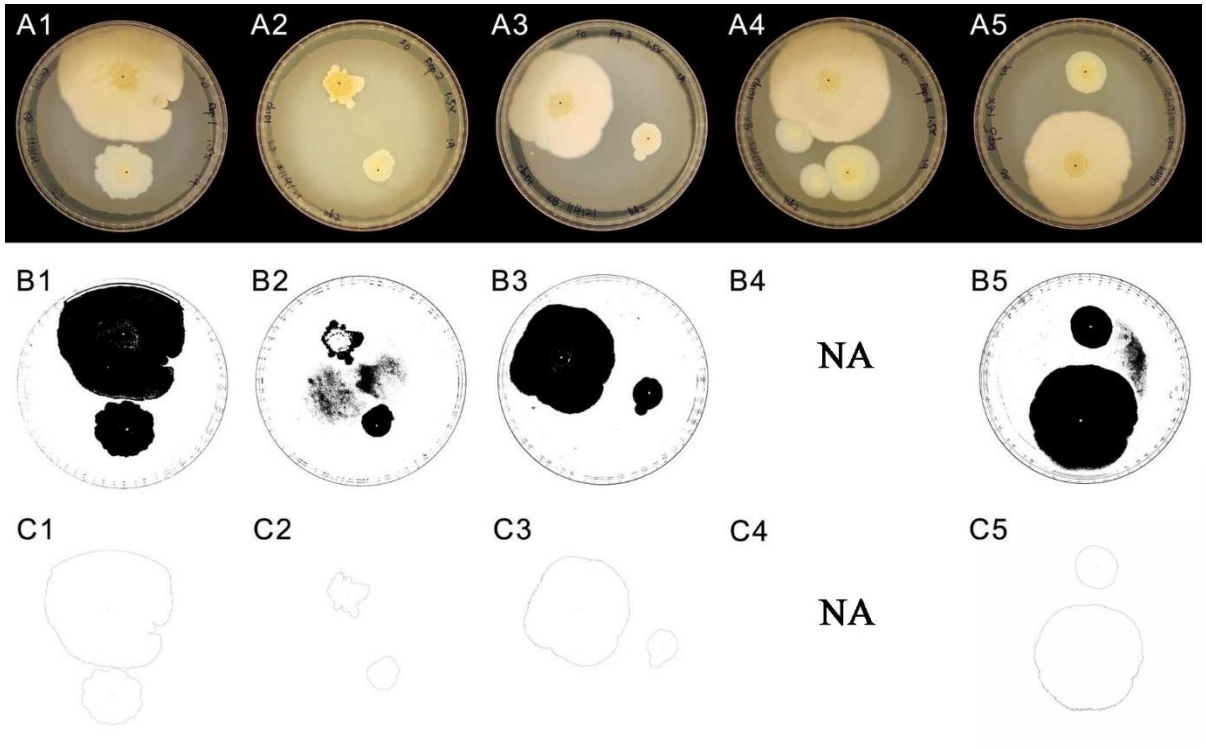


Figure C178. 2021 co-inoculated Petri plates four days after inoculation. **A1-A5)** 1.5x SO vs. *Pss* 14 on KB media. **B1-B5)** Images after threshold adjustment in ImageJ. **C1-C5)** Image of measured area. A1, B1, C1: Replication 1; A2, B2, C2: Replication 2; A3, B3, C3: Replication 3; A4, B4, C4: Replication 4; A5, B5, C5: Replication 5. Images with NA are not available.

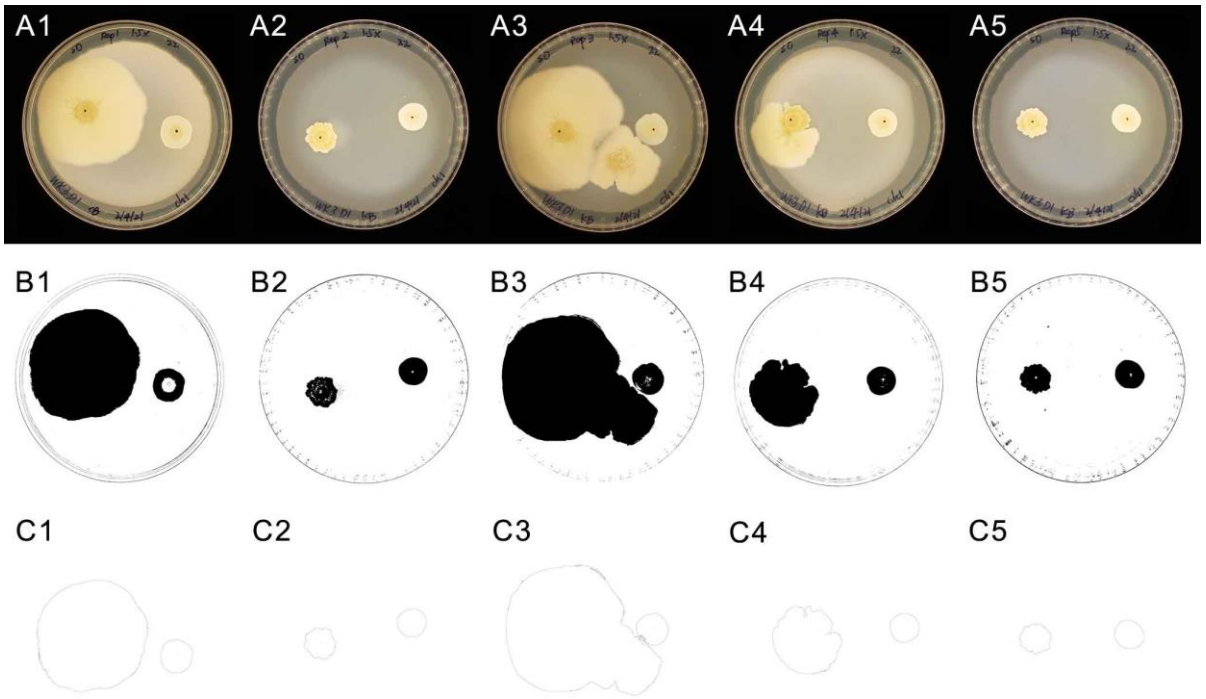


Figure C179. 2021 co-inoculated Petri plates four days after inoculation. **A1-A5)** 1.5x SO vs. *Pss* 22 on KB media. **B1-B5)** Images after threshold adjustment in ImageJ. **C1-C5)** Image of measured area. A1, B1, C1: Replication 1; A2, B2, C2: Replication 2; A3, B3, C3: Replication 3; A4, B4, C4: Replication 4; A5, B5, C5: Replication 5.

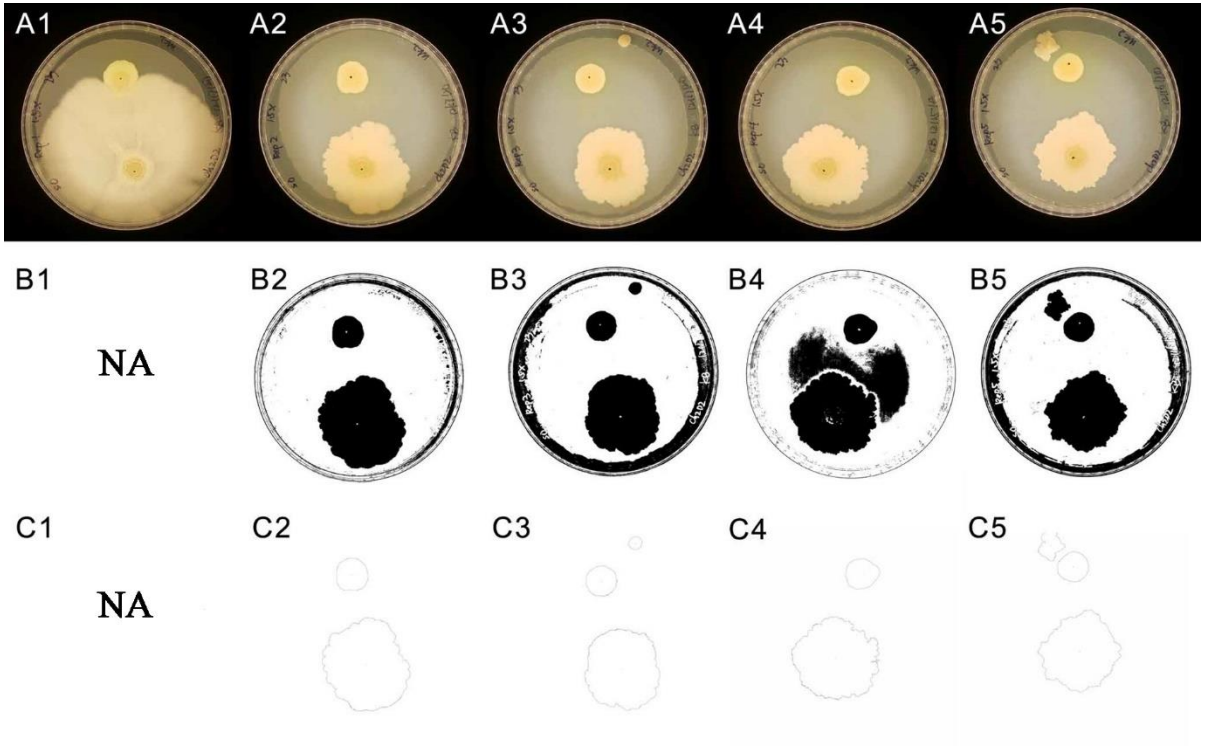


Figure C180. 2021 co-inoculated Petri plates four days after inoculation. **A1-A5)** 1.5x SO vs. *Pss* 23 on KB media. **B1-B5)** Images after threshold adjustment in ImageJ. **C1-C5)** Image of measured area. A1, B1, C1: Replication 1; A2, B2, C2: Replication 2; A3, B3, C3: Replication 3; A4, B4, C4: Replication 4; A5, B5, C5: Replication 5. Images with NA are not available.

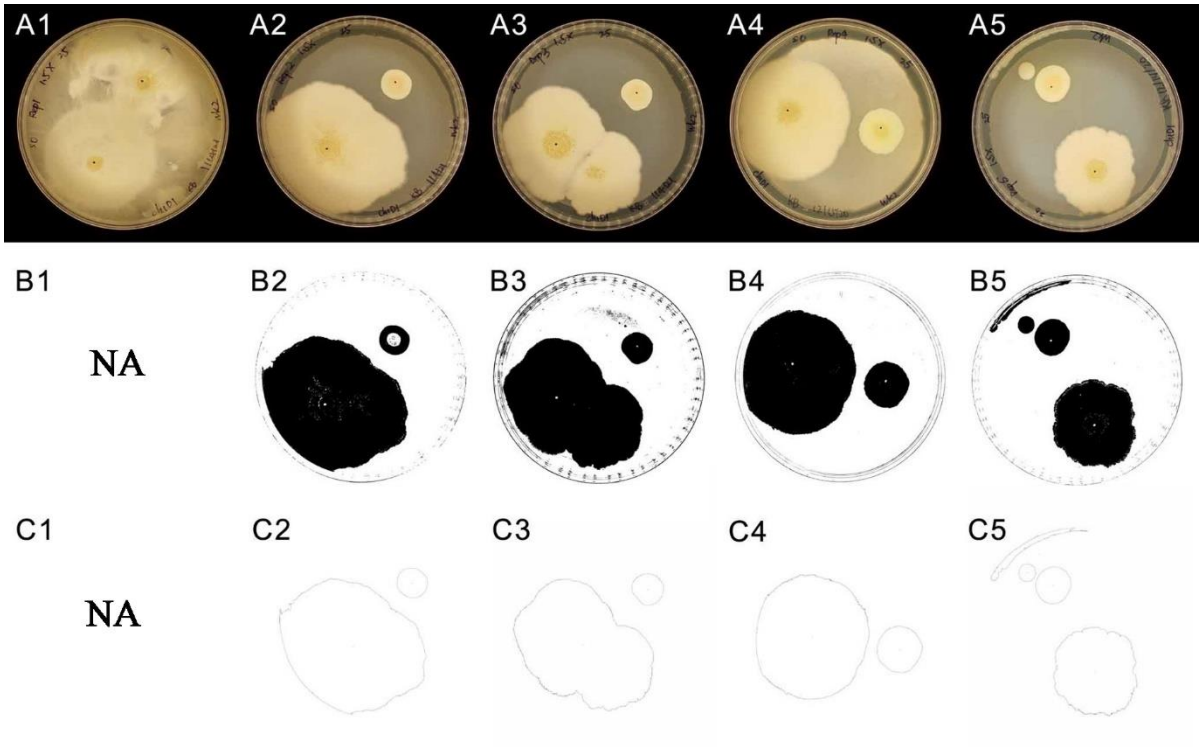


Figure C181. 2021 co-inoculated Petri plates four days after inoculation. **A1-A5)** 1.5x SO vs. *Pss* 25 on KB media. **B1-B5)** Images after threshold adjustment in ImageJ. **C1-C5)** Image of measured area. A1, B1, C1: Replication 1; A2, B2, C2: Replication 2; A3, B3, C3: Replication 3; A4, B4, C4: Replication 4; A5, B5, C5: Replication 5. Images with NA are not available.

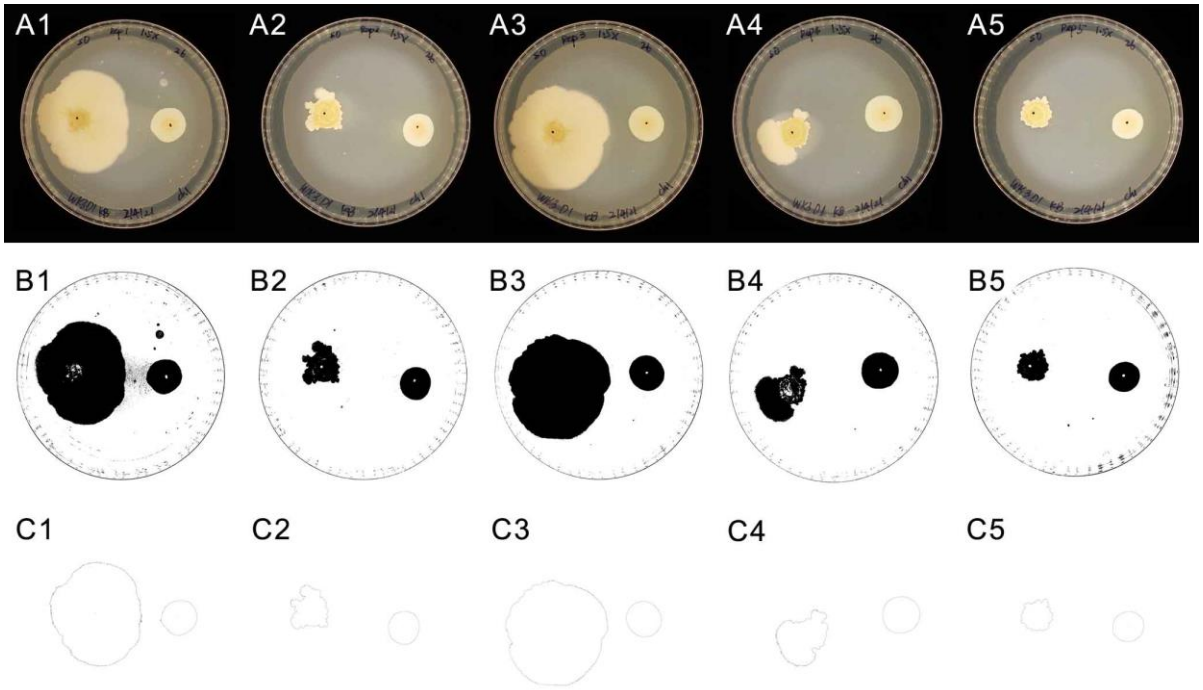


Figure C182. 2021 co-inoculated Petri plates four days after inoculation. **A1-A5)** 1.5x SO vs. *Pss* 26 on KB media. **B1-B5)** Images after threshold adjustment in ImageJ. **C1-C5)** Image of measured area. A1, B1, C1: Replication 1; A2, B2, C2: Replication 2; A3, B3, C3: Replication 3; A4, B4, C4: Replication 4; A5, B5, C5: Replication 5.

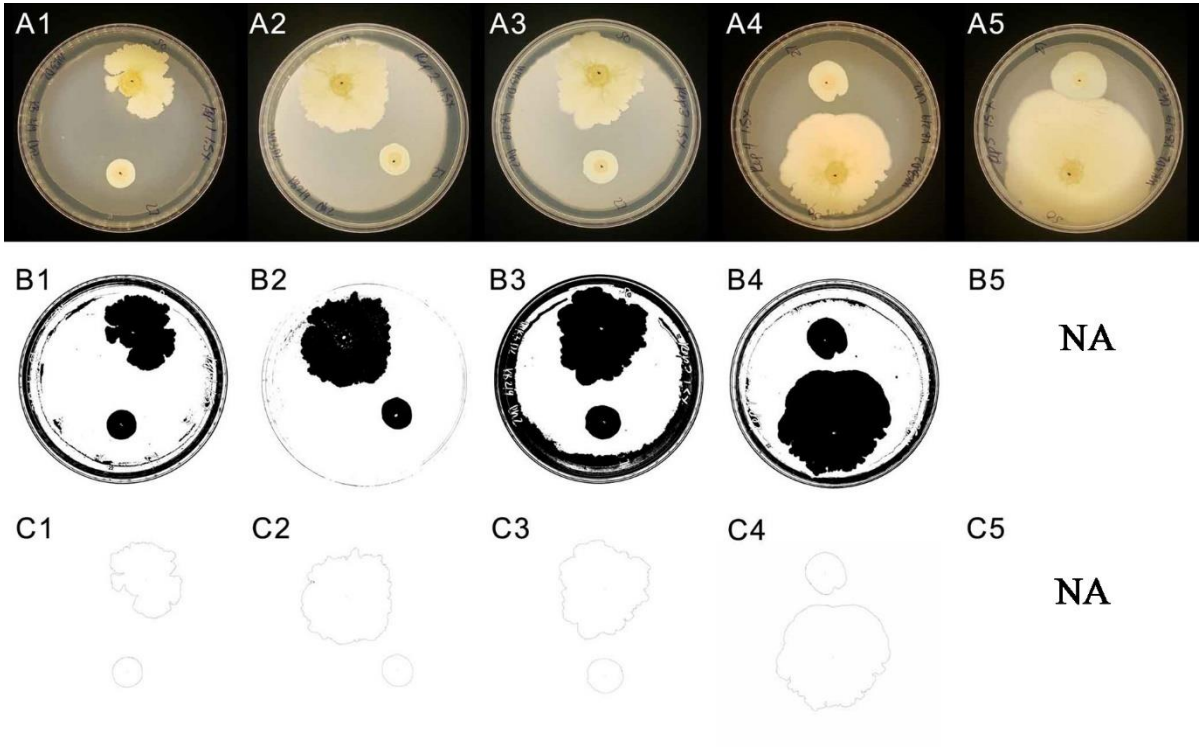


Figure C183. 2021 co-inoculated Petri plates four days after inoculation. **A1-A5)** 1.5x SO vs. *Pss* 27 on KB media. **B1-B5)** Images after threshold adjustment in ImageJ. **C1-C5)** Image of measured area. A1, B1, C1: Replication 1; A2, B2, C2: Replication 2; A3, B3, C3: Replication 3; A4, B4, C4: Replication 4; A5, B5, C5: Replication 5. Images with NA are not available.

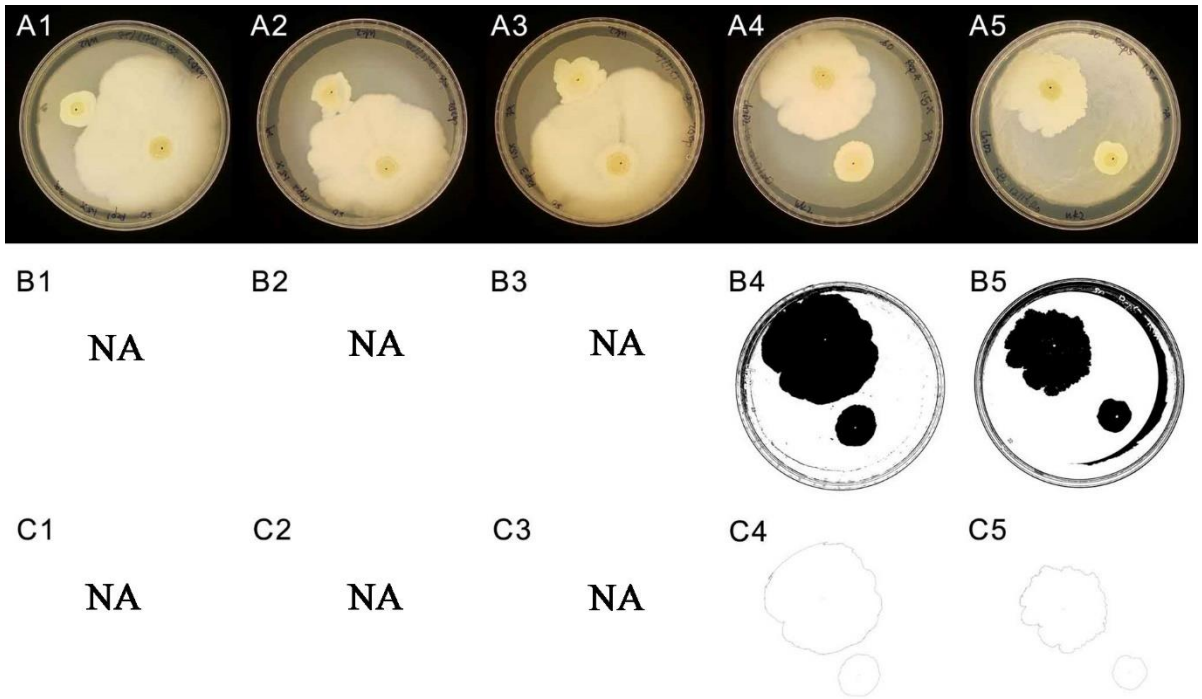


Figure C184. 2021 co-inoculated Petri plates four days after inoculation. **A1-A5)** 1.5x SO vs. *Pss* 34 on KB media. **B1-B5)** Images after threshold adjustment in ImageJ. **C1-C5)** Image of measured area. A1, B1, C1: Replication 1; A2, B2, C2: Replication 2; A3, B3, C3: Replication 3; A4, B4, C4: Replication 4; A5, B5, C5: Replication 5. Images with NA are not available.

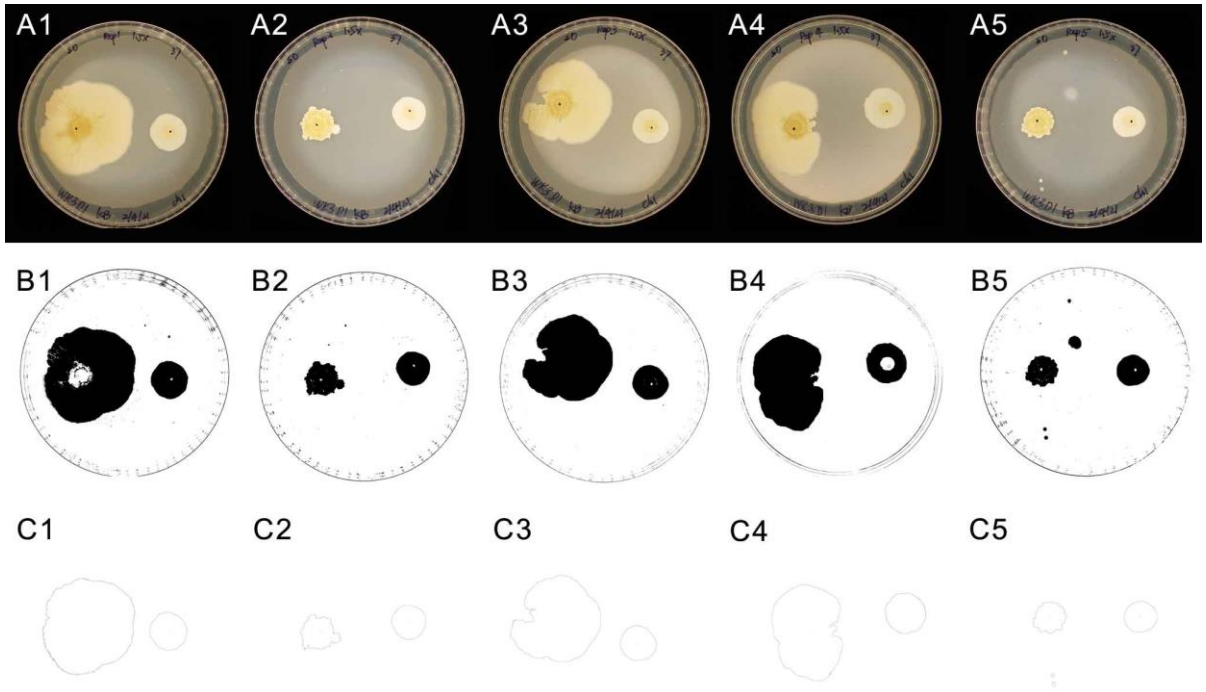


Figure C185. 2021 co-inoculated Petri plates four days after inoculation. **A1-A5)** 1.5x SO vs. *Pss* 37 on KB media. **B1-B5)** Images after threshold adjustment in ImageJ. **C1-C5)** Image of measured area. A1, B1, C1: Replication 1; A2, B2, C2: Replication 2; A3, B3, C3: Replication 3; A4, B4, C4: Replication 4; A5, B5, C5: Replication 5.

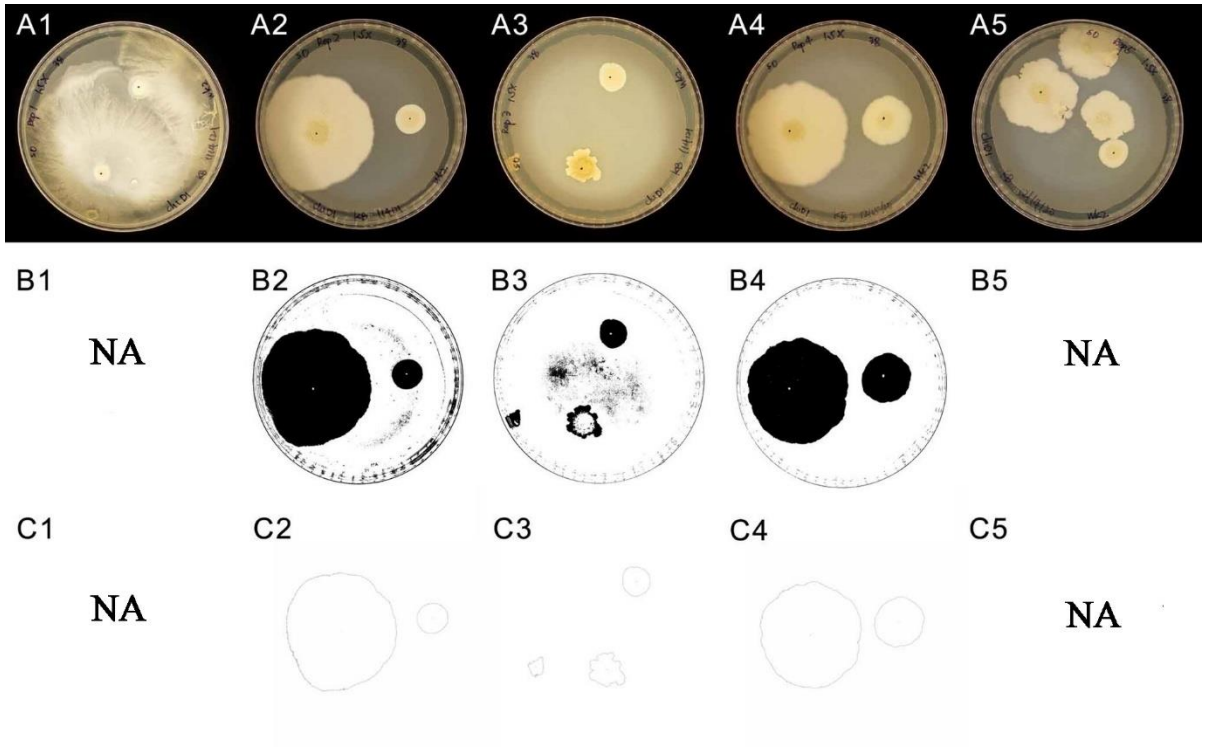


Figure C186. 2021 co-inoculated Petri plates four days after inoculation. **A1-A5)** 1.5x SO vs. *Pss* 38 on KB media. **B1-B5)** Images after threshold adjustment in ImageJ. **C1-C5)** Image of measured area. A1, B1, C1: Replication 1; A2, B2, C2: Replication 2; A3, B3, C3: Replication 3; A4, B4, C4: Replication 4; A5, B5, C5: Replication 5. Images with NA are not available.

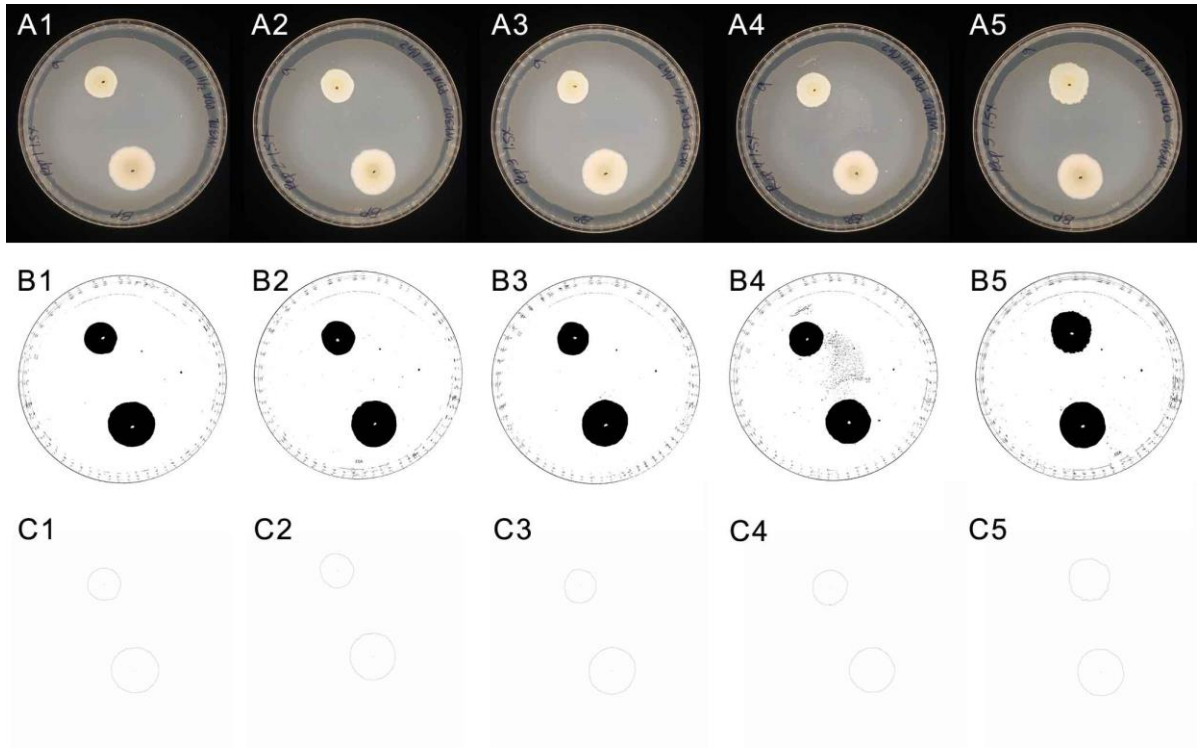


Figure C187. 2021 co-inoculated Petri plates four days after inoculation. **A1-A5)** 1.5x BP vs. *Pss* 9 on PDA media. **B1-B5)** Images after threshold adjustment in ImageJ. **C1-C5)** Image of measured area. A1, B1, C1: Replication 1; A2, B2, C2: Replication 2; A3, B3, C3: Replication 3; A4, B4, C4: Replication 4; A5, B5, C5: Replication 5.

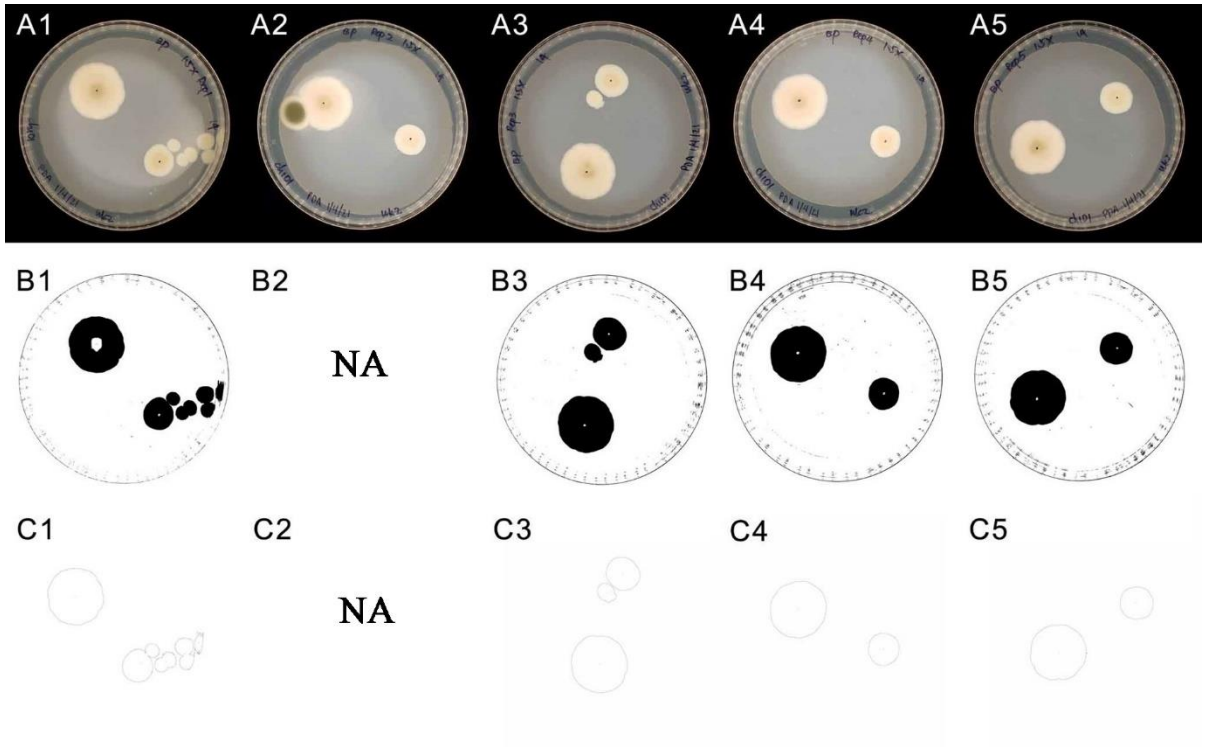


Figure C188. 2021 co-inoculated Petri plates four days after inoculation. **A1-A5)** 1.5x BP vs. *Pss* 14 on PDA media. **B1-B5)** Images after threshold adjustment in ImageJ. **C1-C5)** Image of measured area. A1, B1, C1: Replication 1; A2, B2, C2: Replication 2; A3, B3, C3: Replication 3; A4, B4, C4: Replication 4; A5, B5, C5: Replication 5. Images with NA are not available.

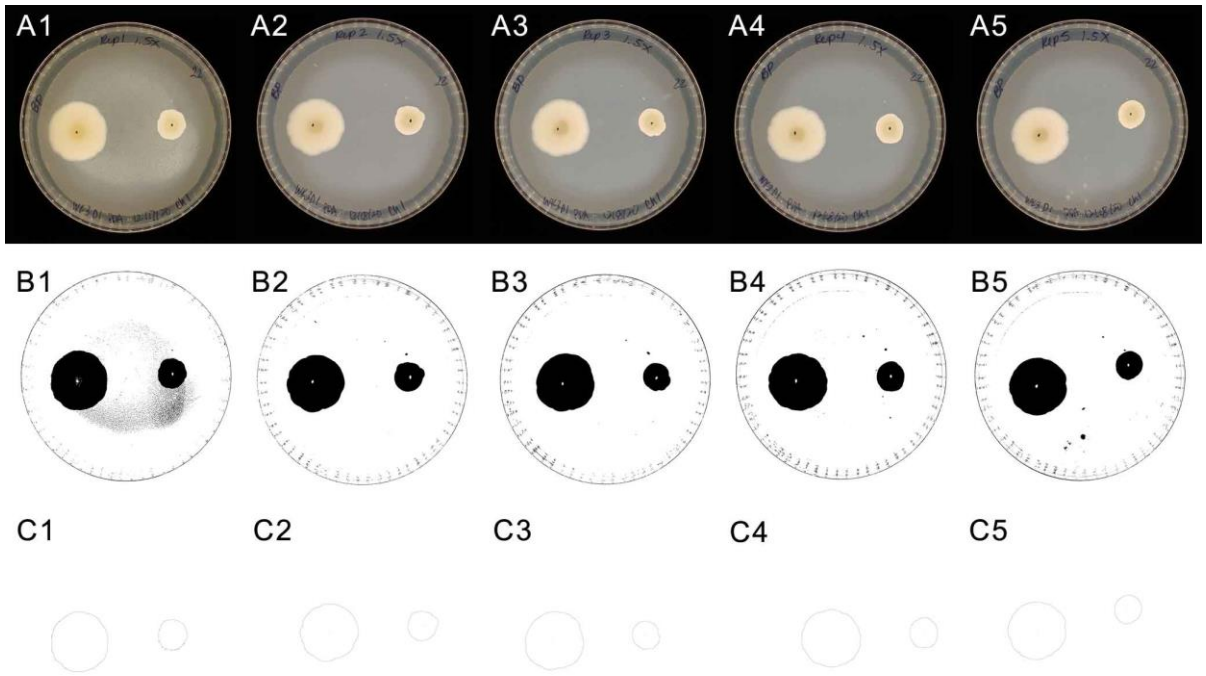


Figure C189. 2021 co-inoculated Petri plates four days after inoculation. **A1-A5)** 1.5x BP vs. *Pss* 22 on PDA media. **B1-B5)** Images after threshold adjustment in ImageJ. **C1-C5)** Image of measured area. A1, B1, C1: Replication 1; A2, B2, C2: Replication 2; A3, B3, C3: Replication 3; A4, B4, C4: Replication 4; A5, B5, C5: Replication 5.

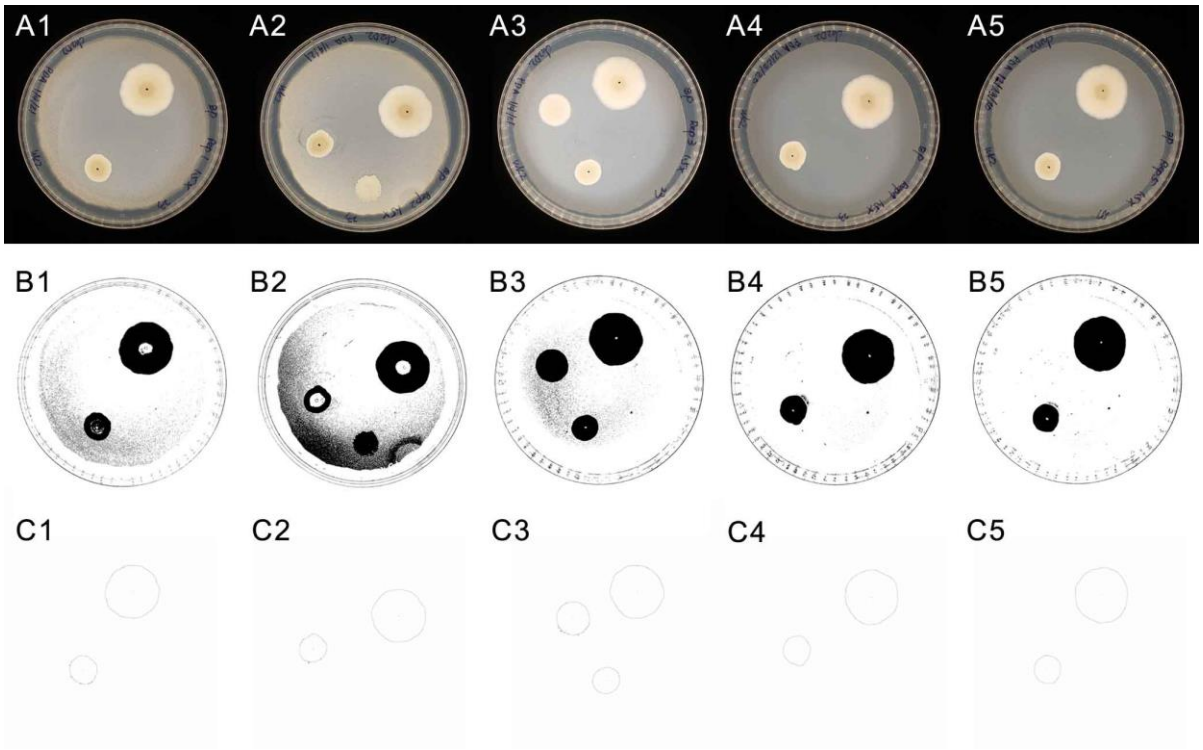


Figure C190. 2021 co-inoculated Petri plates four days after inoculation. **A1-A5)** 1.5x BP vs. *Pss* 23 on PDA media. **B1-B5)** Images after threshold adjustment in ImageJ. **C1-C5)** Image of measured area. A1, B1, C1: Replication 1; A2, B2, C2: Replication 2; A3, B3, C3: Replication 3; A4, B4, C4: Replication 4; A5, B5, C5: Replication 5.

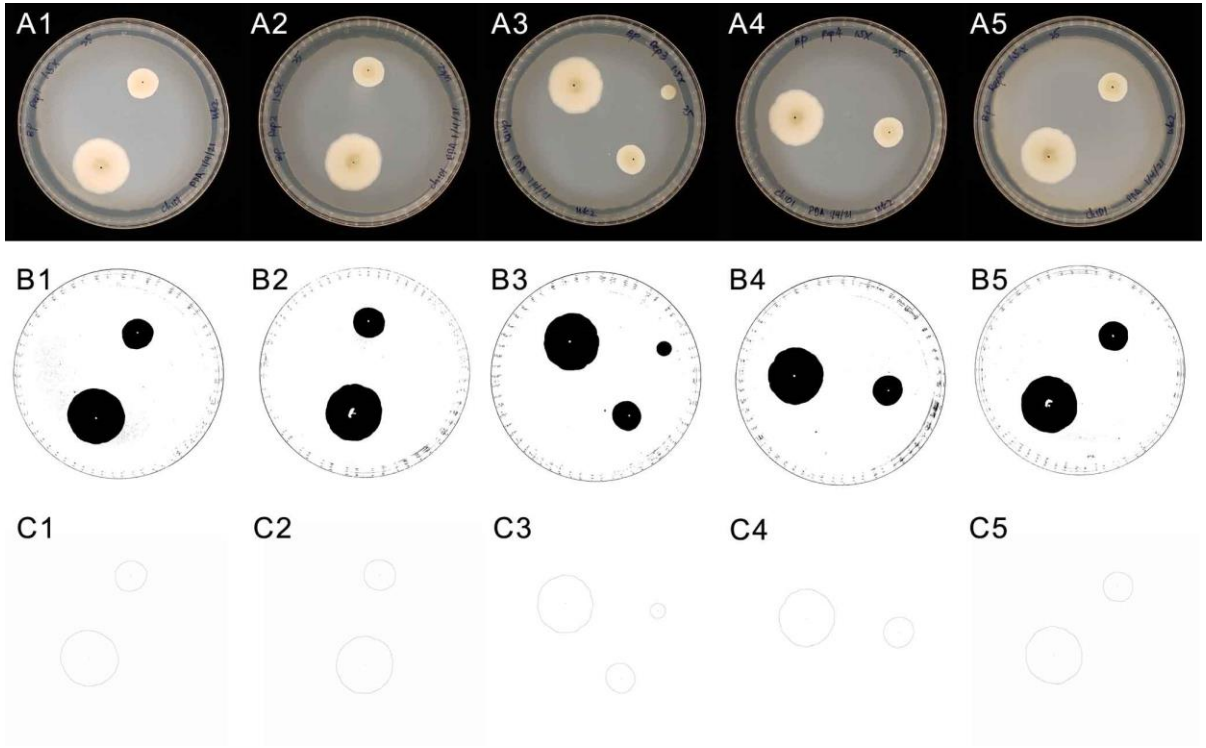


Figure C191. 2021 co-inoculated Petri plates four days after inoculation. **A1-A5)** 1.5x BP vs. *Pss* 25 on PDA media. **B1-B5)** Images after threshold adjustment in ImageJ. **C1-C5)** Image of measured area. A1, B1, C1: Replication 1; A2, B2, C2: Replication 2; A3, B3, C3: Replication 3; A4, B4, C4: Replication 4; A5, B5, C5: Replication 5.

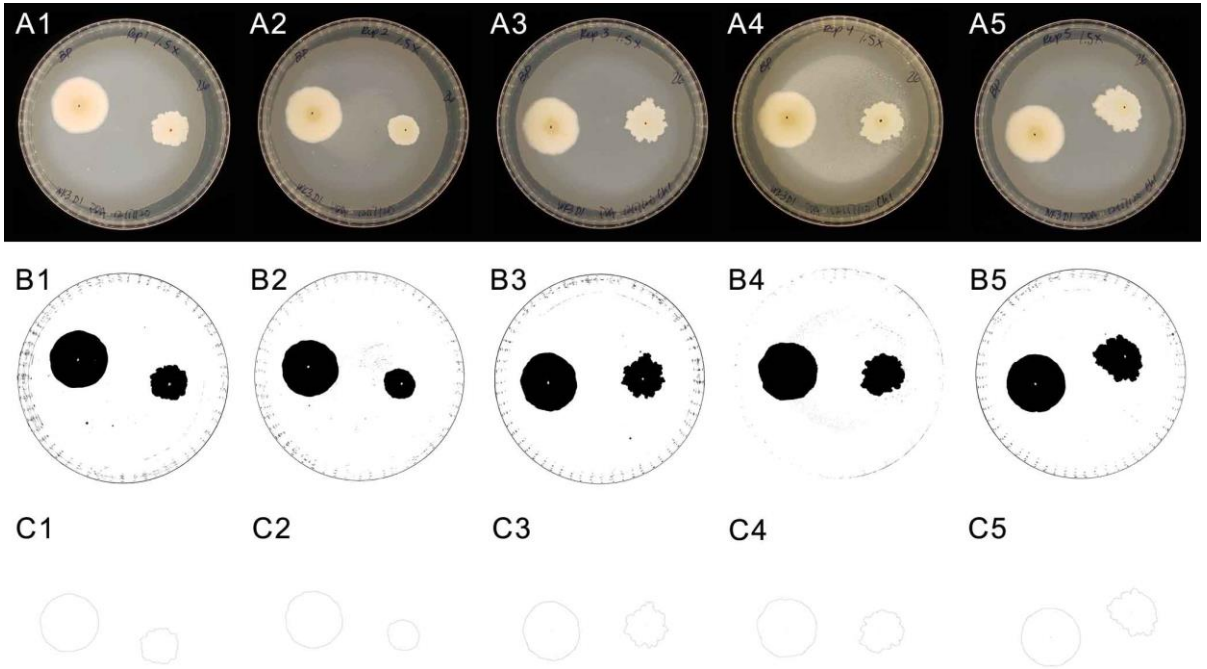


Figure C192. 2021 co-inoculated Petri plates four days after inoculation. **A1-A5)** 1.5x BP vs. *Pss* 26 on PDA media. **B1-B5)** Images after threshold adjustment in ImageJ. **C1-C5)** Image of measured area. A1, B1, C1: Replication 1; A2, B2, C2: Replication 2; A3, B3, C3: Replication 3; A4, B4, C4: Replication 4; A5, B5, C5: Replication 5.

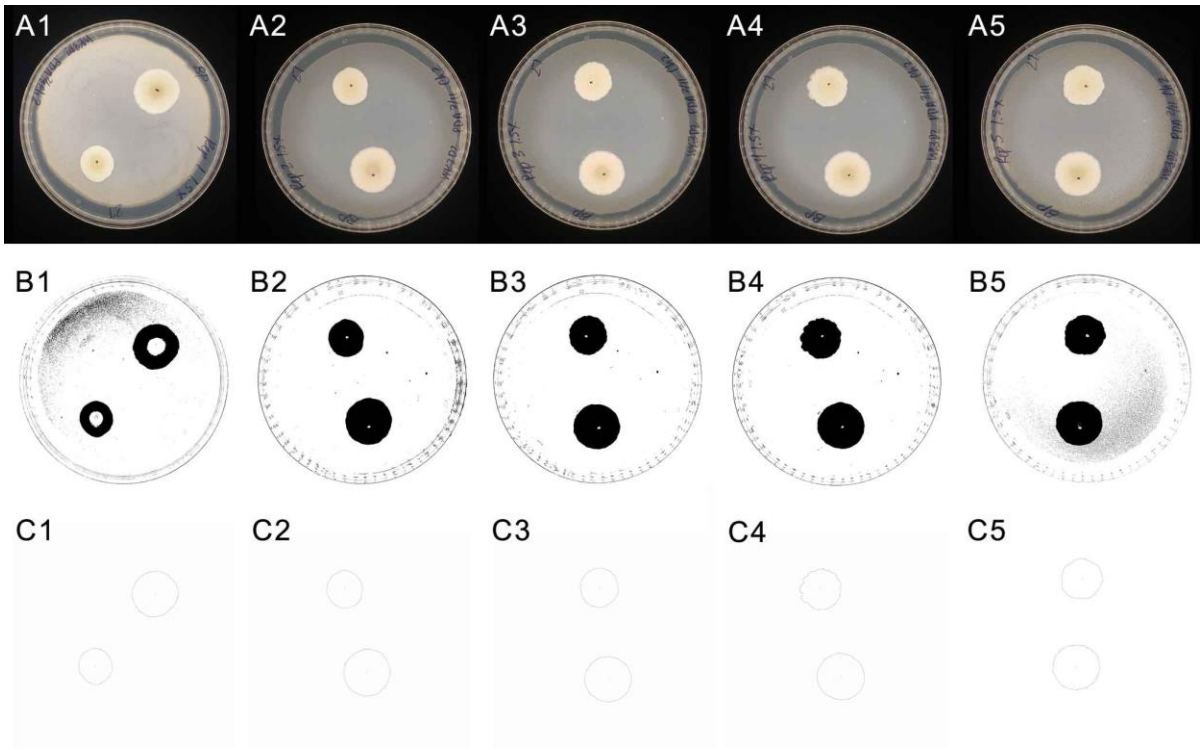


Figure C193. 2021 co-inoculated Petri plates four days after inoculation. **A1-A5)** 1.5x BP vs. *Pss* 27 on PDA media. **B1-B5)** Images after threshold adjustment in ImageJ. **C1-C5)** Image of measured area. A1, B1, C1: Replication 1; A2, B2, C2: Replication 2; A3, B3, C3: Replication 3; A4, B4, C4: Replication 4; A5, B5, C5: Replication 5.

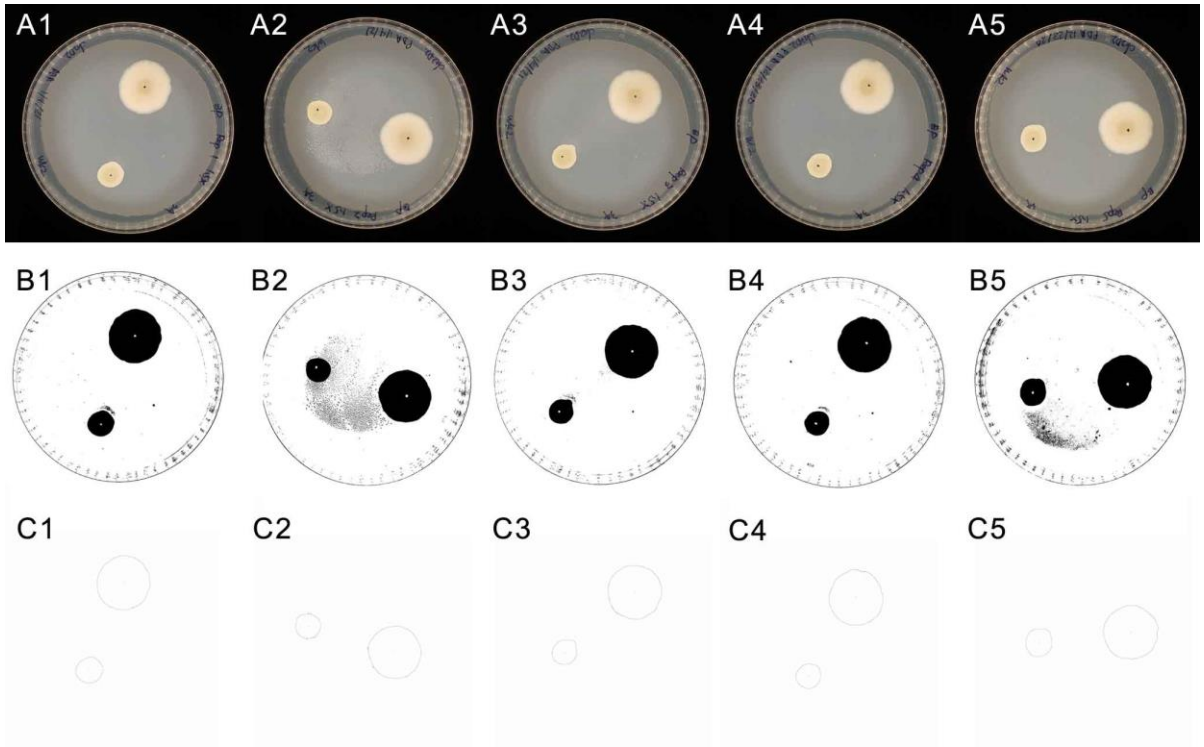


Figure C194. 2021 co-inoculated Petri plates four days after inoculation. **A1-A5)** 1.5x BP vs. *Pss* 34 on PDA media. **B1-B5)** Images after threshold adjustment in ImageJ. **C1-C5)** Image of measured area. A1, B1, C1: Replication 1; A2, B2, C2: Replication 2; A3, B3, C3: Replication 3; A4, B4, C4: Replication 4; A5, B5, C5: Replication 5.

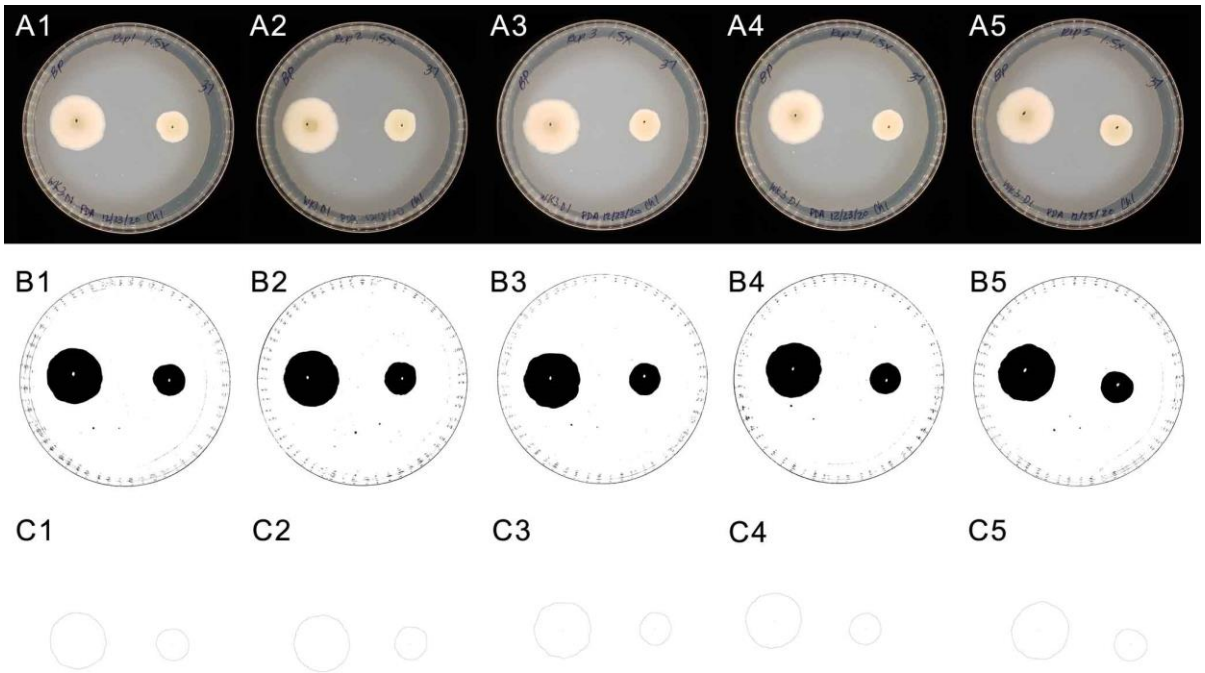


Figure C195. 2021 co-inoculated Petri plates four days after inoculation. **A1-A5)** 1.5x BP vs. *Pss* 37 on PDA media. **B1-B5)** Images after threshold adjustment in ImageJ. **C1-C5)** Image of measured area. A1, B1, C1: Replication 1; A2, B2, C2: Replication 2; A3, B3, C3: Replication 3; A4, B4, C4: Replication 4; A5, B5, C5: Replication 5.

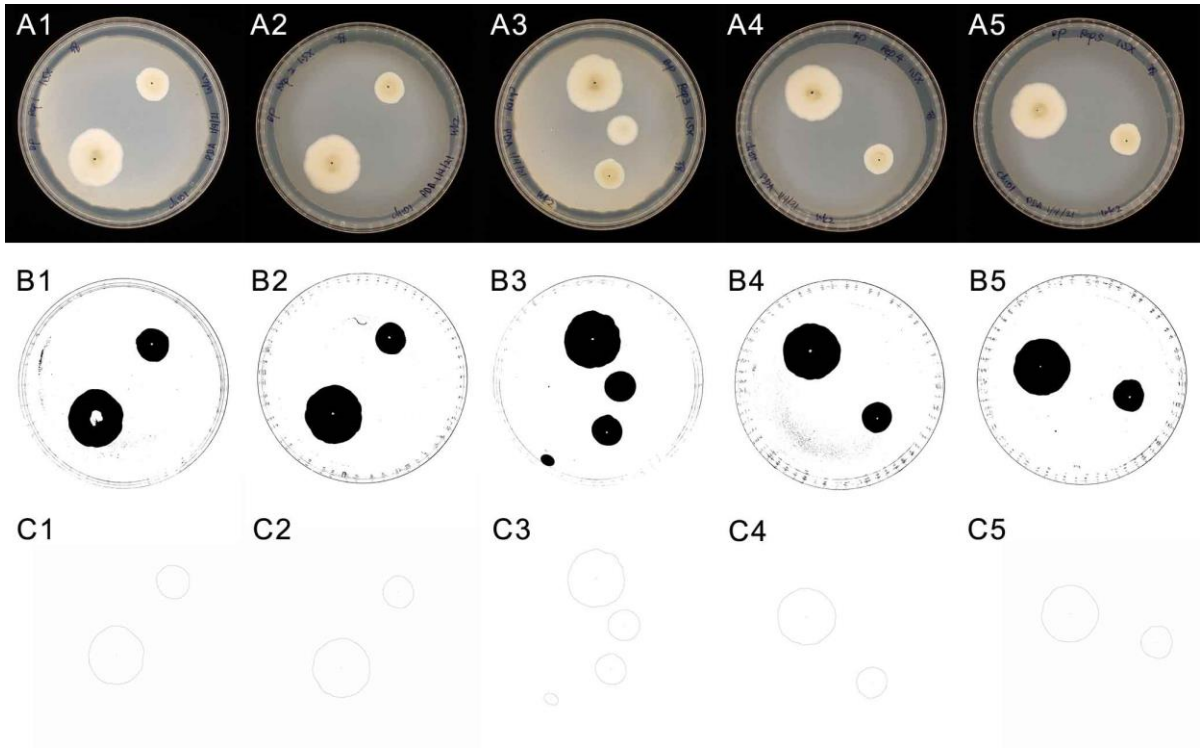


Figure C196. 2021 co-inoculated Petri plates four days after inoculation. **A1-A5)** 1.5x BP vs. *Pss* 38 on PDA media. **B1-B5)** Images after threshold adjustment in ImageJ. **C1-C5)** Image of measured area. A1, B1, C1: Replication 1; A2, B2, C2: Replication 2; A3, B3, C3: Replication 3; A4, B4, C4: Replication 4; A5, B5, C5: Replication 5.

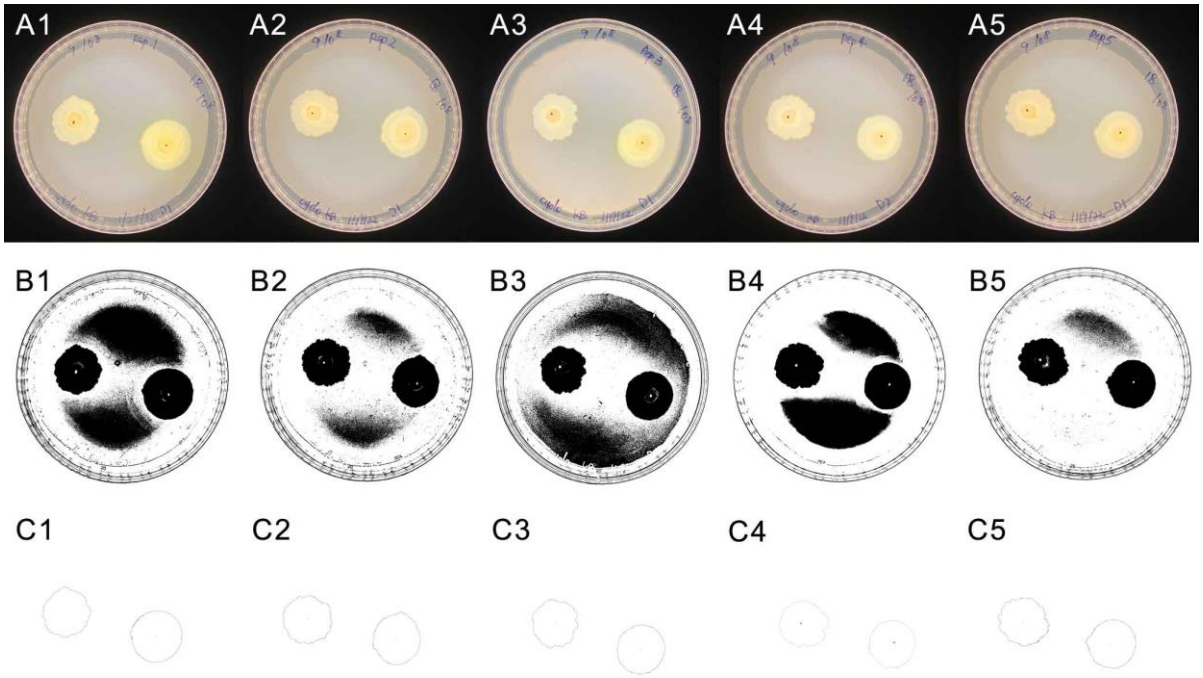


Figure C197. 2022 co-inoculated Petri plates four days after inoculation. **A1-A5)** *Pss* 9 at 10^8 cfu/ml vs. *Pss* 18 at 10^8 cfu/ml on KB media. **B1-B5)** Images after threshold adjustment in ImageJ. **C1-C5)** Image of measured area. A1, B1, C1: Replication 1; A2, B2, C2: Replication 2; A3, B3, C3: Replication 3; A4, B4, C4: Replication 4; A5, B5, C5: Replication 5.

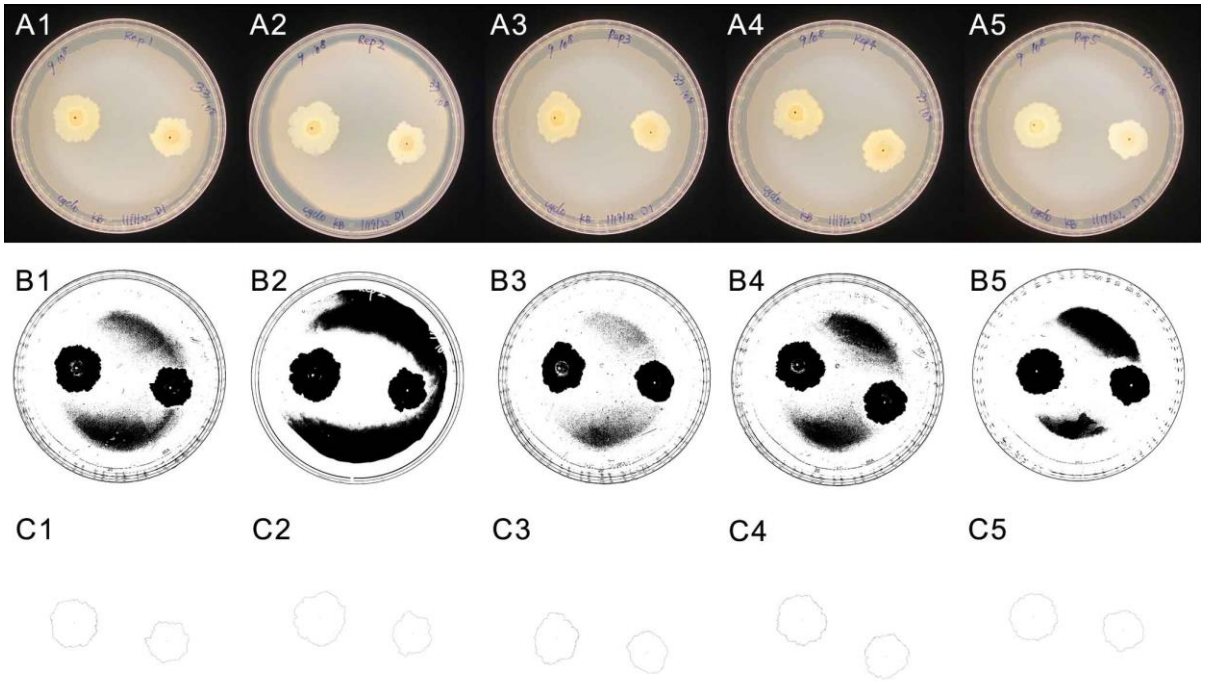


Figure C198. 2022 co-inoculated Petri plates four days after inoculation. **A1-A5)** *Pss* 9 at 10^8 cfu/ml vs. *Pss* 33 at 10^8 cfu/ml on KB media. **B1-B5)** Images after threshold adjustment in ImageJ. **C1-C5)** Image of measured area. A1, B1, C1: Replication 1; A2, B2, C2: Replication 2; A3, B3, C3: Replication 3; A4, B4, C4: Replication 4; A5, B5, C5: Replication 5.

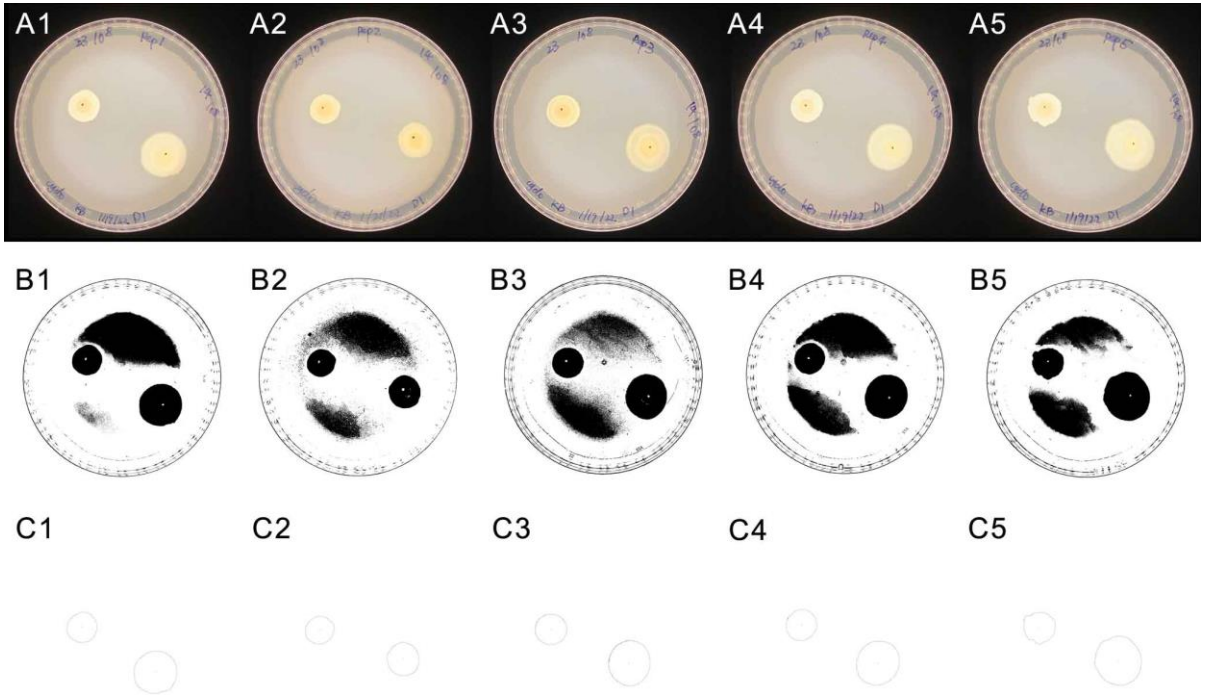


Figure C199. 2022 co-inoculated Petri plates four days after inoculation. **A1-A5)** *Pss* 23 at 10^8 cfu/ml vs. *Pss* 14 at 10^8 cfu/ml on KB media. **B1-B5)** Images after threshold adjustment in ImageJ. **C1-C5)** Image of measured area. A1, B1, C1: Replication 1; A2, B2, C2: Replication 2; A3, B3, C3: Replication 3; A4, B4, C4: Replication 4; A5, B5, C5: Replication 5.

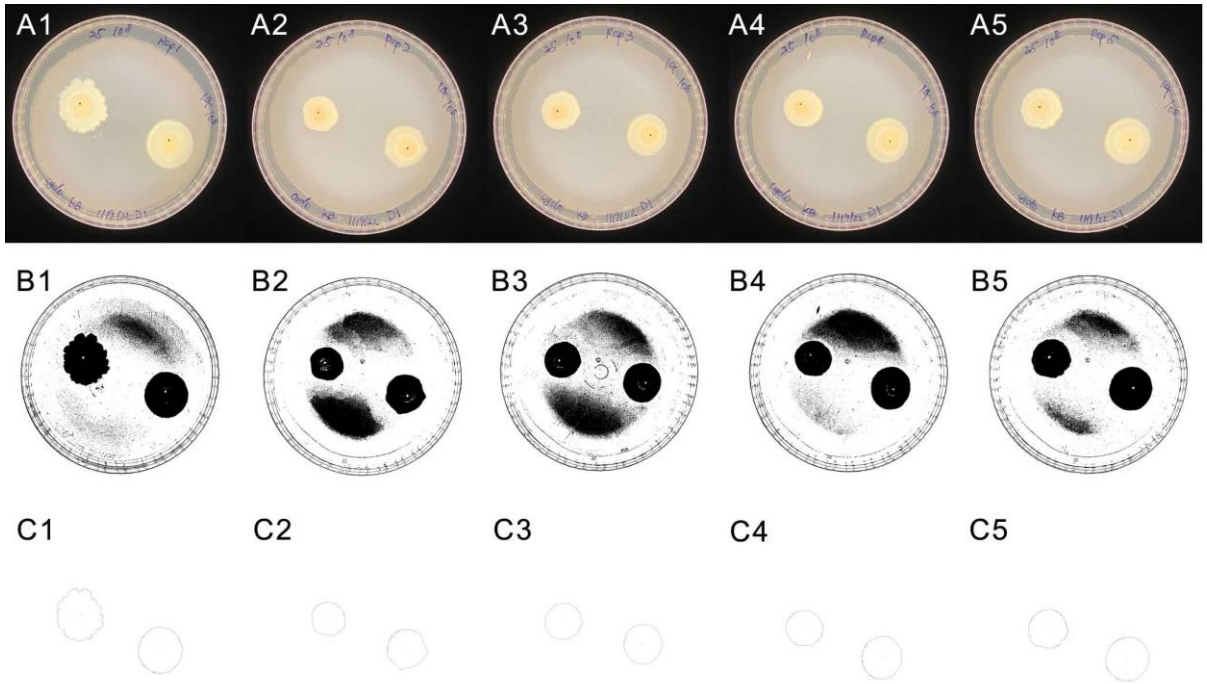


Figure C200. 2022 co-inoculated Petri plates four days after inoculation. **A1-A5)** *Pss* 25 at 10^8 cfu/ml vs. *Pss* 14 at 10^8 cfu/ml on KB media. **B1-B5)** Images after threshold adjustment in ImageJ. **C1-C5)** Image of measured area. A1, B1, C1: Replication 1; A2, B2, C2: Replication 2; A3, B3, C3: Replication 3; A4, B4, C4: Replication 4; A5, B5, C5: Replication 5.

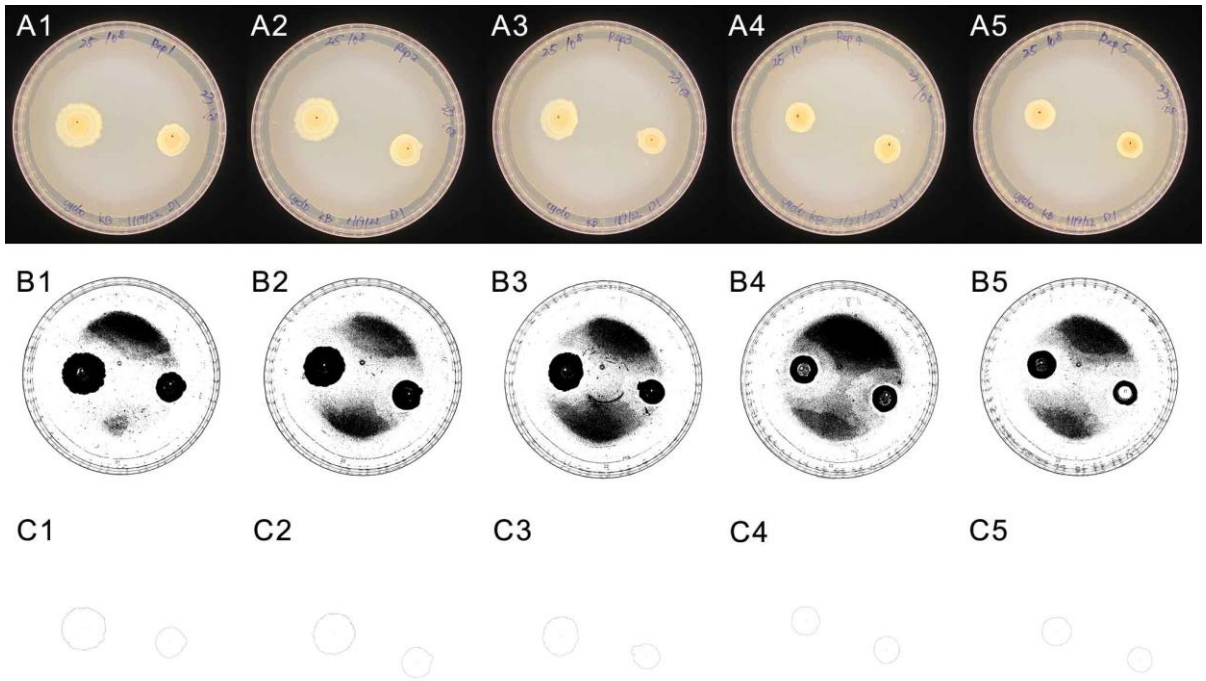


Figure C201. 2022 co-inoculated Petri plates four days after inoculation. **A1-A5)** *Pss* 25 at 10^8 cfu/ml vs. *Pss* 23 at 10^8 cfu/ml on KB media. **B1-B5)** Images after threshold adjustment in ImageJ. **C1-C5)** Image of measured area. A1, B1, C1: Replication 1; A2, B2, C2: Replication 2; A3, B3, C3: Replication 3; A4, B4, C4: Replication 4; A5, B5, C5: Replication 5.

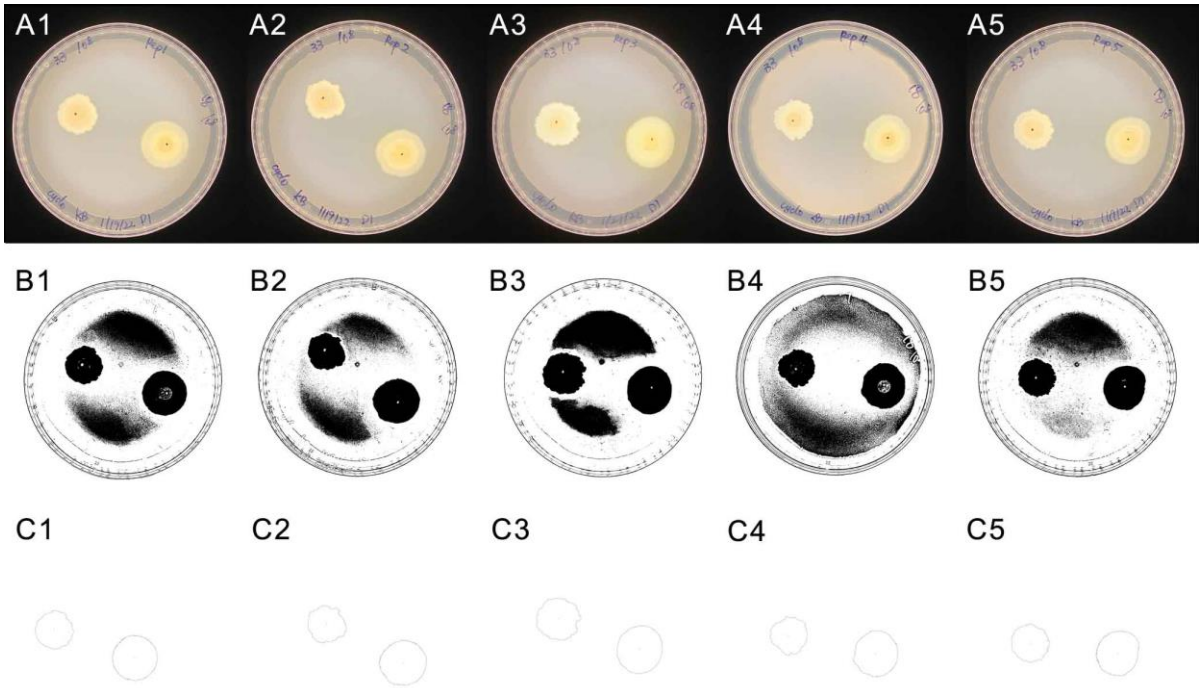


Figure C202. 2022 co-inoculated Petri plates four days after inoculation. **A1-A5)** *Pss* 33 at 10^8 cfu/ml vs. *Pss* 18 at 10^8 cfu/ml on KB media. **B1-B5)** Images after threshold adjustment in ImageJ. **C1-C5)** Image of measured area. A1, B1, C1: Replication 1; A2, B2, C2: Replication 2; A3, B3, C3: Replication 3; A4, B4, C4: Replication 4; A5, B5, C5: Replication 5.

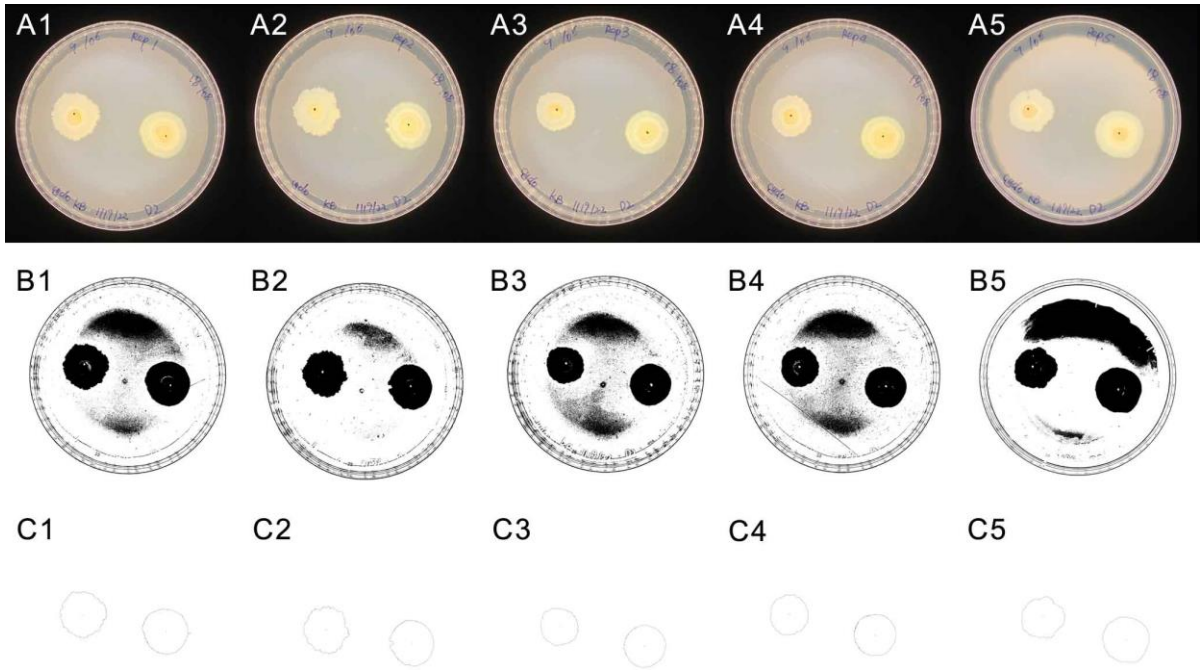


Figure C203. 2022 co-inoculated Petri plates four days after inoculation. **A1-A5)** *Pss* 9 at 10^6 cfu/ml vs. *Pss* 18 at 10^8 cfu/ml on KB media. **B1-B5)** Images after threshold adjustment in ImageJ. **C1-C5)** Image of measured area. A1, B1, C1: Replication 1; A2, B2, C2: Replication 2; A3, B3, C3: Replication 3; A4, B4, C4: Replication 4; A5, B5, C5: Replication 5.

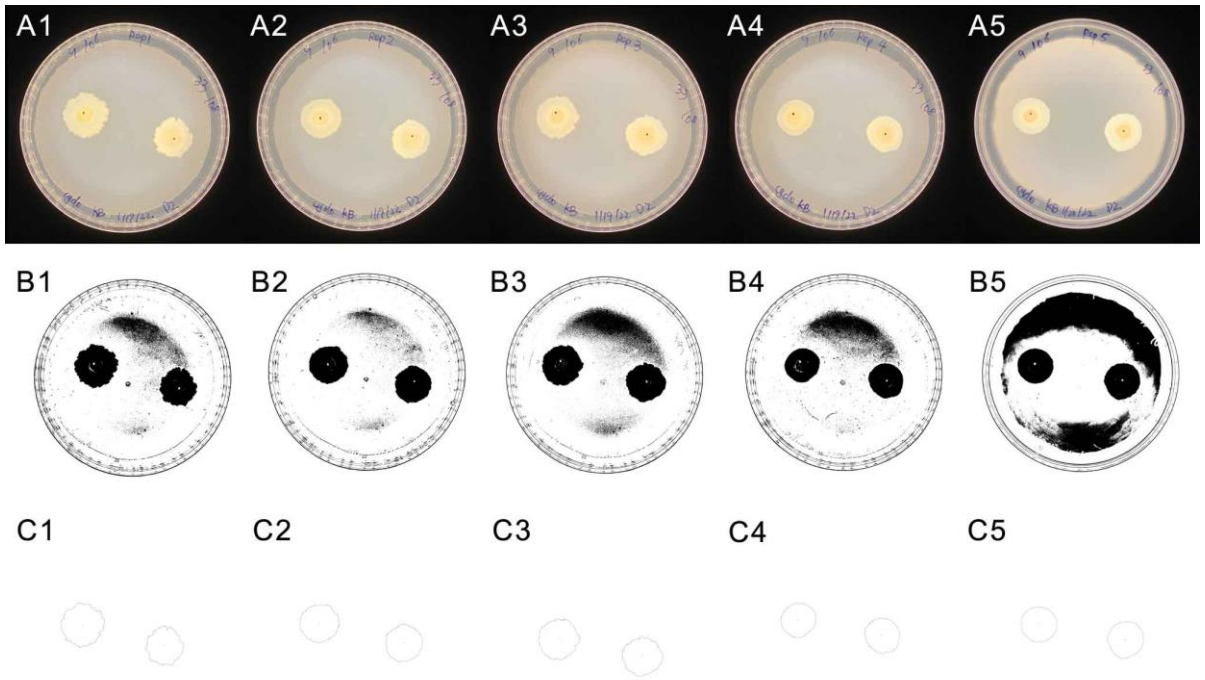


Figure C204. 2022 co-inoculated Petri plates four days after inoculation. **A1-A5)** *Pss* 9 at 10^6 cfu/ml vs. *Pss* 33 at 10^8 cfu/ml on KB media. **B1-B5)** Images after threshold adjustment in ImageJ. **C1-C5)** Image of measured area. A1, B1, C1: Replication 1; A2, B2, C2: Replication 2; A3, B3, C3: Replication 3; A4, B4, C4: Replication 4; A5, B5, C5: Replication 5.

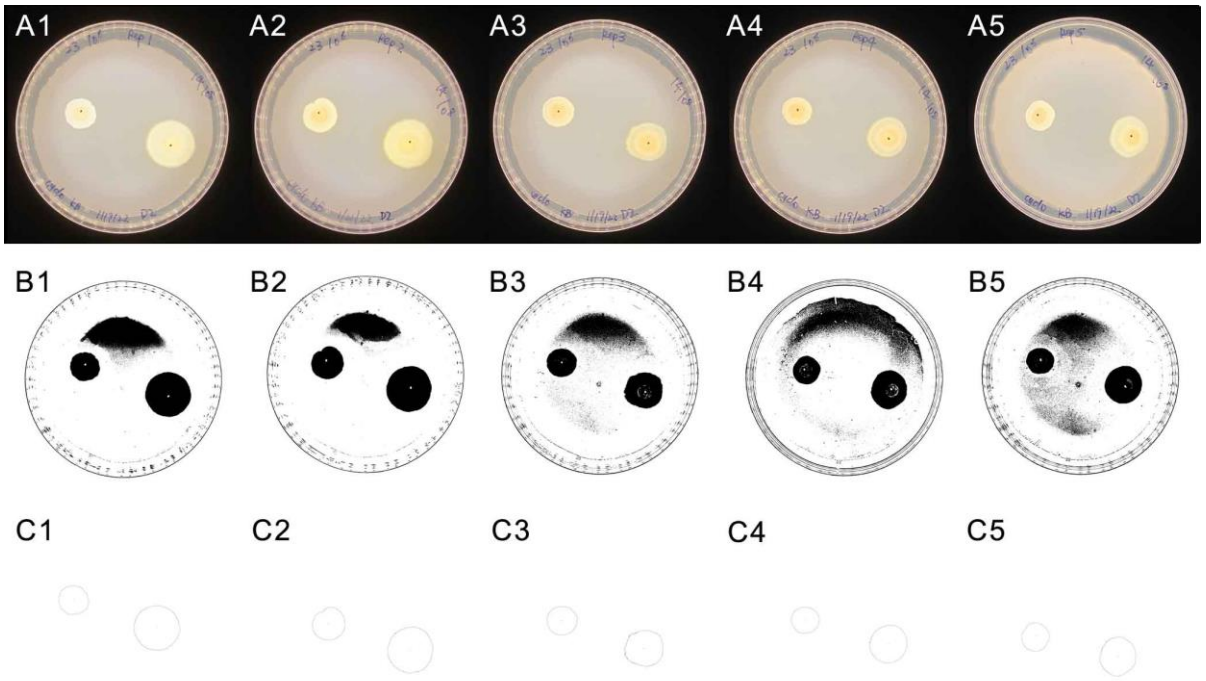


Figure C205. 2022 co-inoculated Petri plates four days after inoculation. **A1-A5)** *Pss* 23 at 10^6 cfu/ml vs. *Pss* 14 at 10^8 cfu/ml on KB media. **B1-B5)** Images after threshold adjustment in ImageJ. **C1-C5)** Image of measured area. A1, B1, C1: Replication 1; A2, B2, C2: Replication 2; A3, B3, C3: Replication 3; A4, B4, C4: Replication 4; A5, B5, C5: Replication 5.

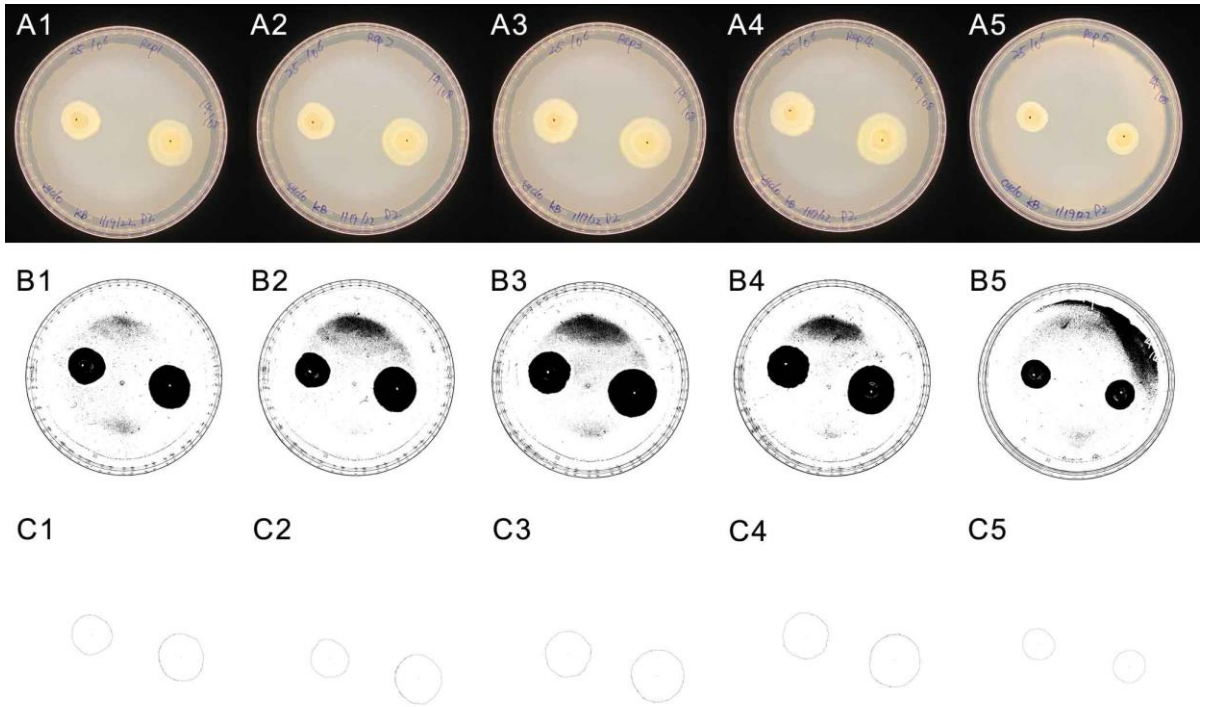


Figure C206. 62022 co-inoculated Petri plates four days after inoculation. **A1-A5)** *Pss* 25 at 10^6 cfu/ml vs. *Pss* 14 at 10^8 cfu/ml on KB media. **B1-B5)** Images after threshold adjustment in ImageJ. **C1-C5)** Image of measured area. A1, B1, C1: Replication 1; A2, B2, C2: Replication 2; A3, B3, C3: Replication 3; A4, B4, C4: Replication 4; A5, B5, C5: Replication 5.

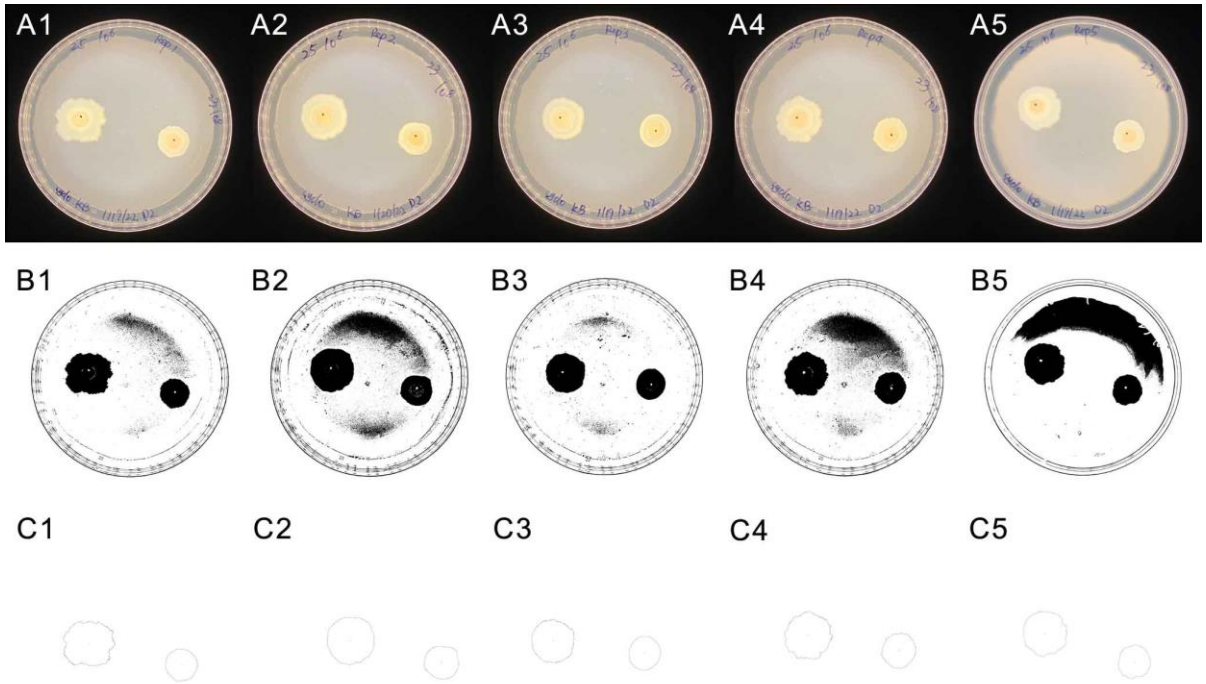


Figure C207. 2022 co-inoculated Petri plates four days after inoculation. **A1-A5)** *Pss* 25 at 10^6 cfu/ml vs. *Pss* 23 at 10^8 cfu/ml on KB media. **B1-B5)** Images after threshold adjustment in ImageJ. **C1-C5)** Image of measured area. A1, B1, C1: Replication 1; A2, B2, C2: Replication 2; A3, B3, C3: Replication 3; A4, B4, C4: Replication 4; A5, B5, C5: Replication 5.

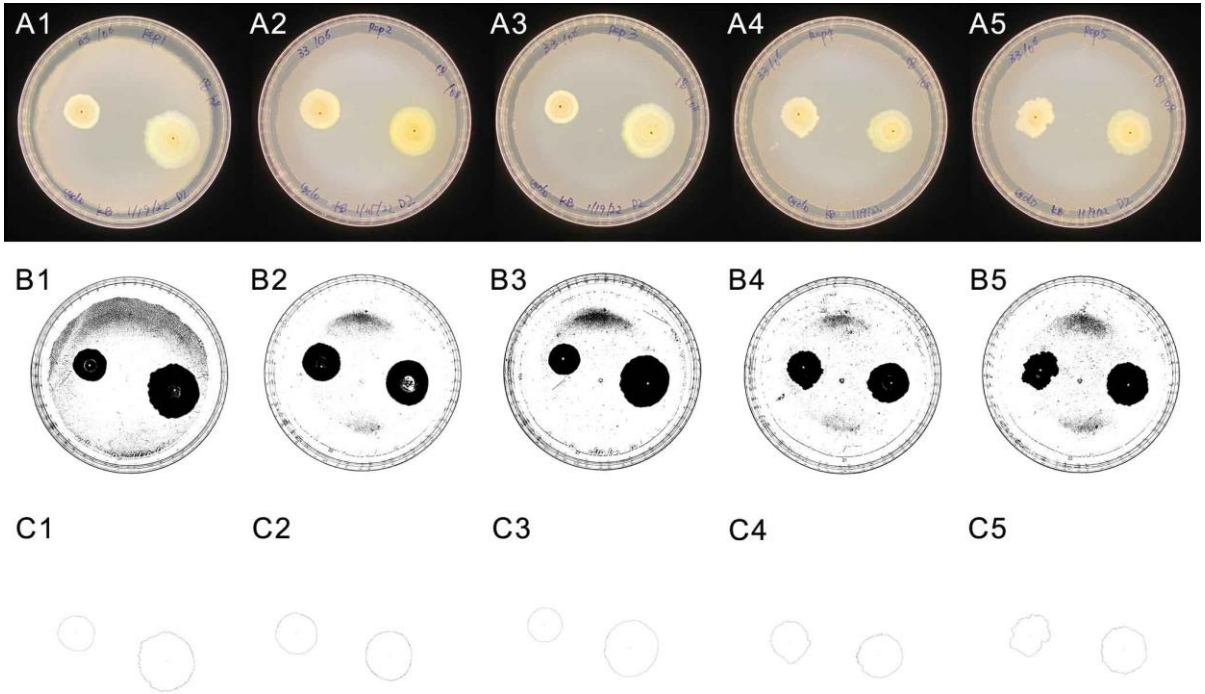


Figure C208. 2022 co-inoculated Petri plates four days after inoculation. **A1-A5)** *Pss* 33 at 10^6 cfu/ml vs. *Pss* 18 at 10^8 cfu/ml on KB media. **B1-B5)** Images after threshold adjustment in ImageJ. **C1-C5)** Image of measured area. A1, B1, C1: Replication 1; A2, B2, C2: Replication 2; A3, B3, C3: Replication 3; A4, B4, C4: Replication 4; A5, B5, C5: Replication 5.

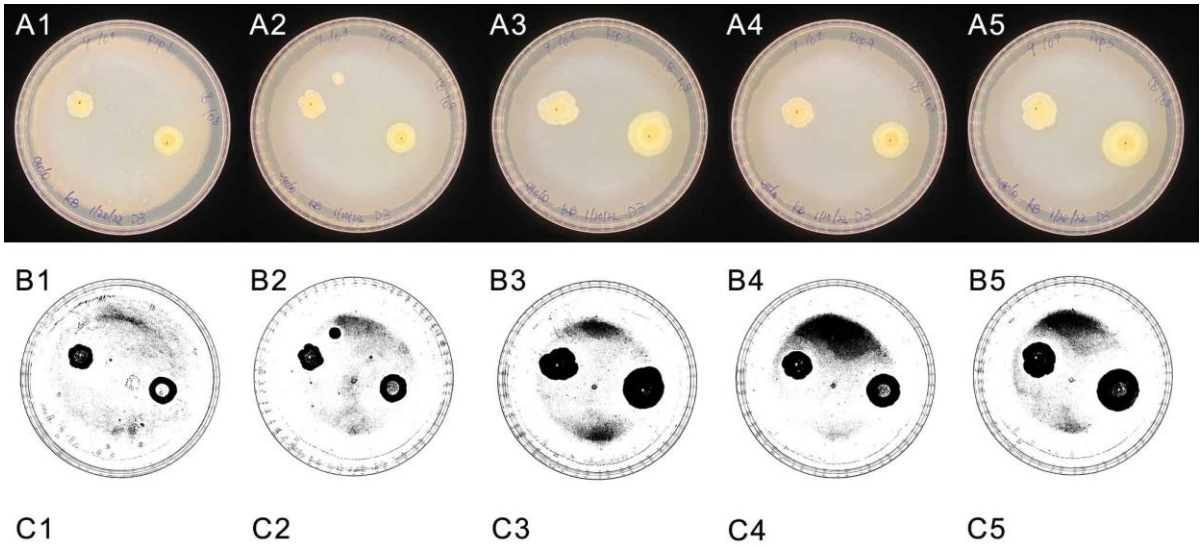


Figure C209. 2022 co-inoculated Petri plates four days after inoculation. **A1-A5)** *Pss* 9 at 10^4 cfu/ml vs. *Pss* 18 at 10^8 cfu/ml on KB media. **B1-B5)** Images after threshold adjustment in ImageJ. **C1-C5)** Image of measured area. A1, B1, C1: Replication 1; A2, B2, C2: Replication 2; A3, B3, C3: Replication 3; A4, B4, C4: Replication 4; A5, B5, C5: Replication 5.

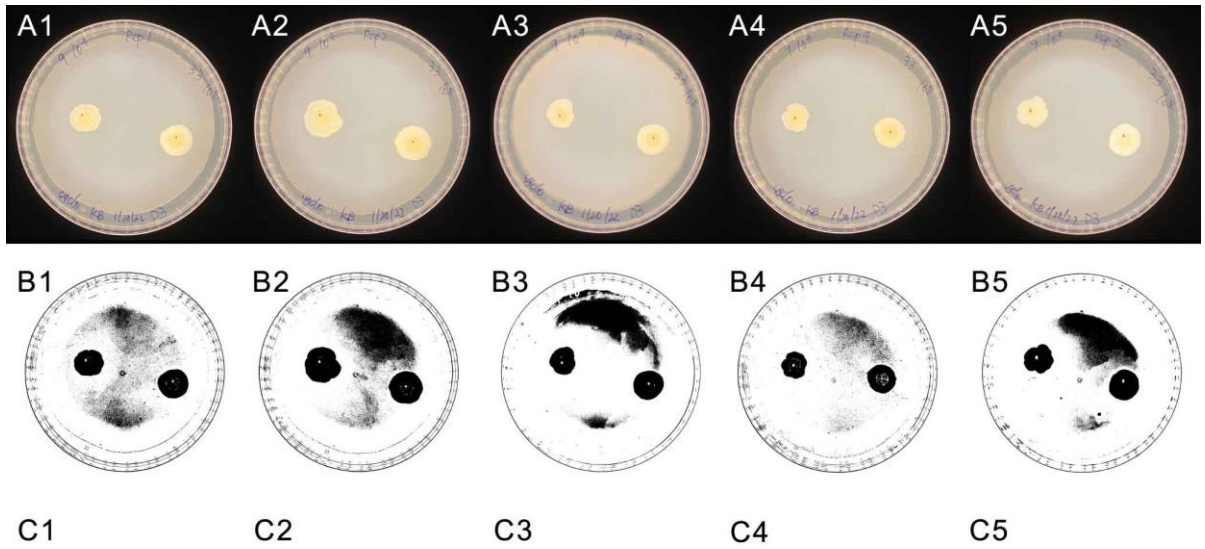


Figure C210. 2022 co-inoculated Petri plates four days after inoculation. **A1-A5)** *Pss* 9 at 10^4 cfu/ml vs. *Pss* 33 at 10^8 cfu/ml on KB media. **B1-B5)** Images after threshold adjustment in ImageJ. **C1-C5)** Image of measured area. A1, B1, C1: Replication 1; A2, B2, C2: Replication 2; A3, B3, C3: Replication 3; A4, B4, C4: Replication 4; A5, B5, C5: Replication 5.

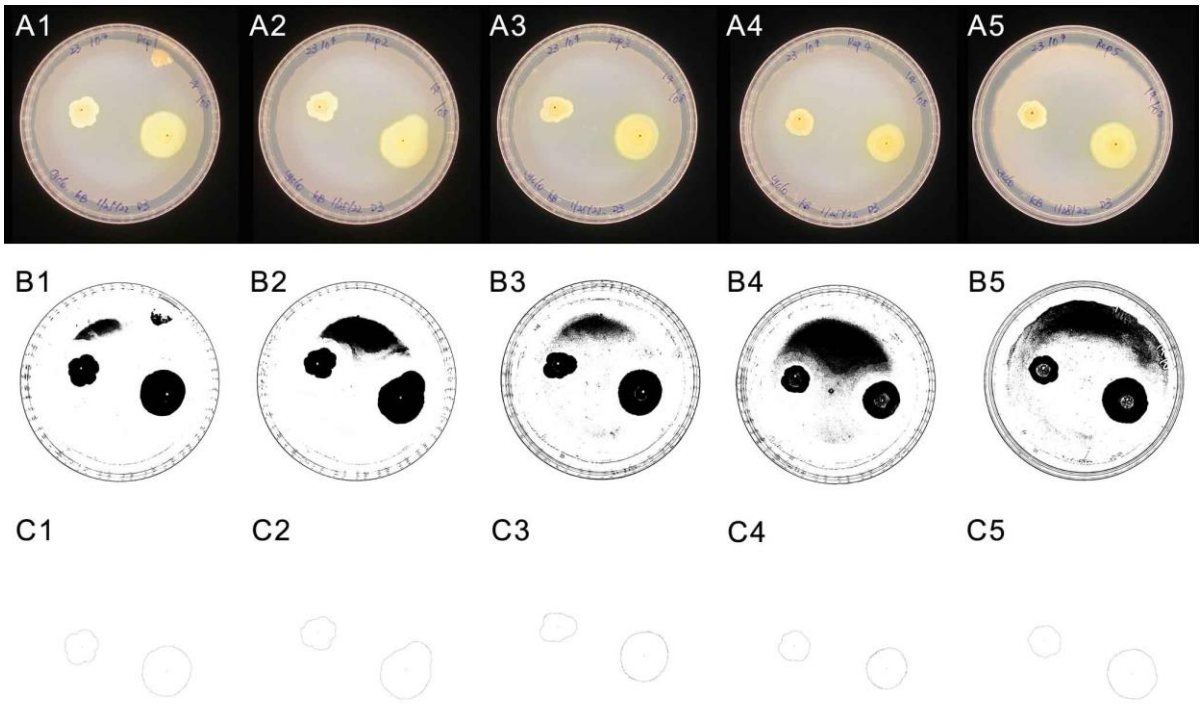


Figure C211. 2022 co-inoculated Petri plates four days after inoculation. **A1-A5)** *Pss* 23 at 10^4 cfu/ml vs. *Pss* 14 at 10^8 cfu/ml on KB media. **B1-B5)** Images after threshold adjustment in ImageJ. **C1-C5)** Image of measured area. A1, B1, C1: Replication 1; A2, B2, C2: Replication 2; A3, B3, C3: Replication 3; A4, B4, C4: Replication 4; A5, B5, C5: Replication 5.

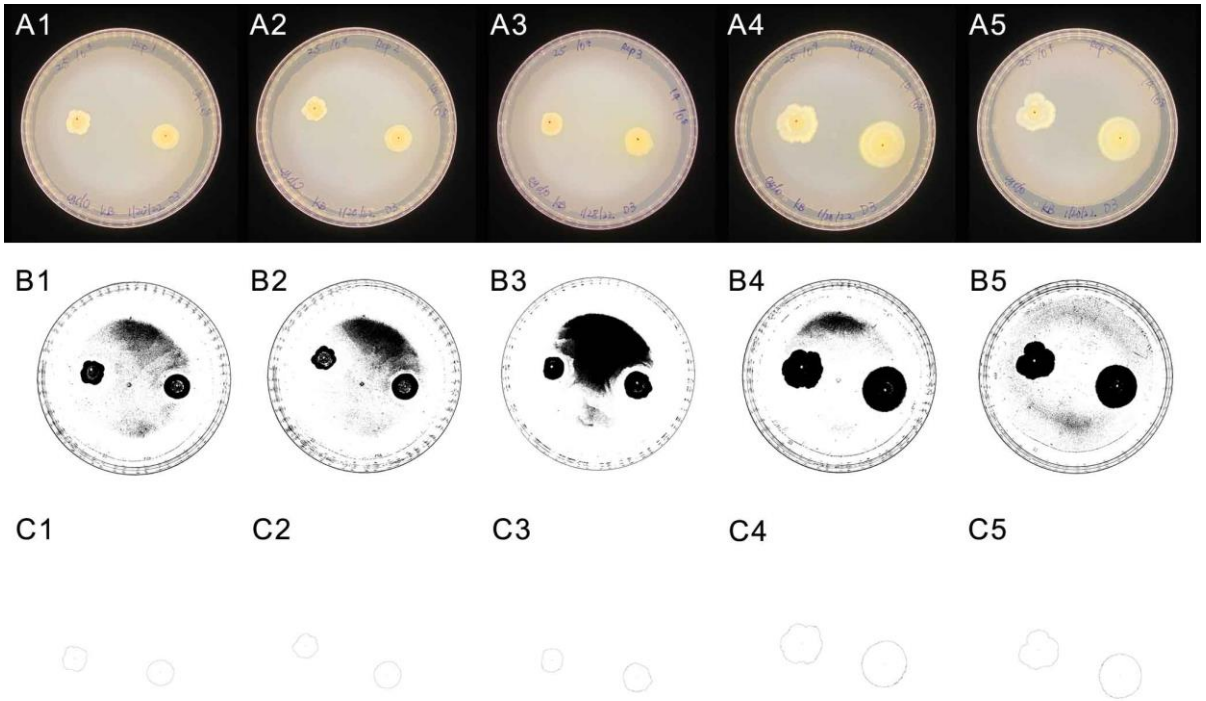


Figure C212. 2022 co-inoculated Petri plates four days after inoculation. **A1-A5)** *Pss* 25 at 10^4 cfu/ml vs. *Pss* 14 at 10^8 cfu/ml on KB media. **B1-B5)** Images after threshold adjustment in ImageJ. **C1-C5)** Image of measured area. A1, B1, C1: Replication 1; A2, B2, C2: Replication 2; A3, B3, C3: Replication 3; A4, B4, C4: Replication 4; A5, B5, C5: Replication 5.

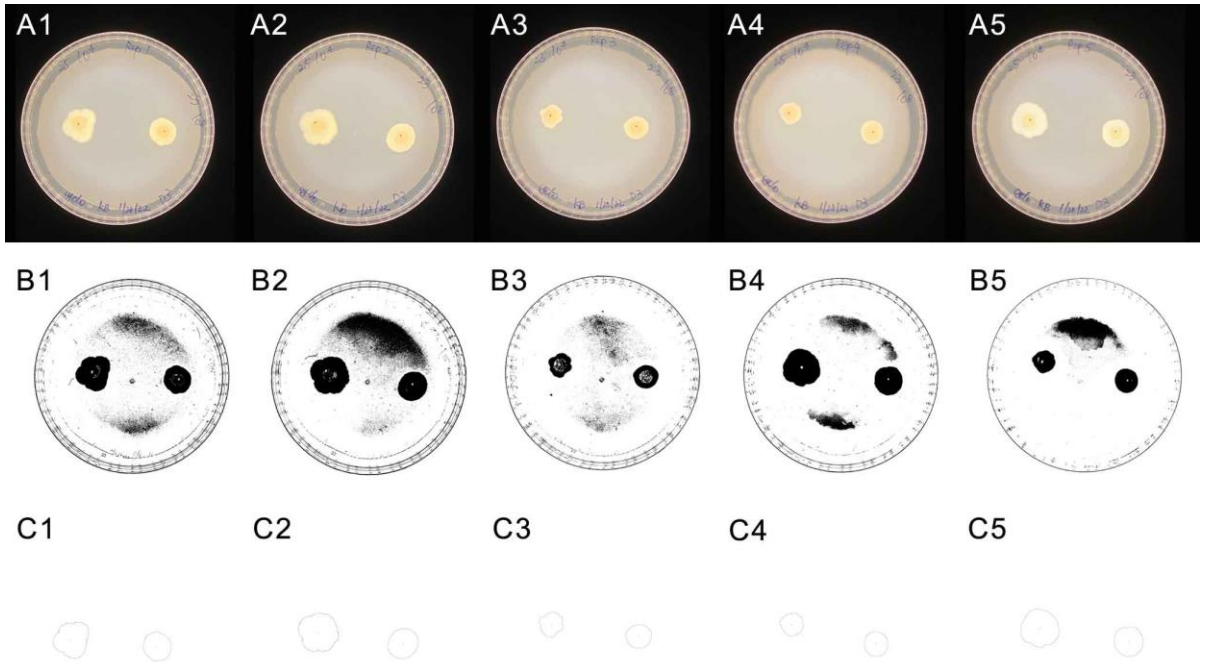


Figure C213. 2022 co-inoculated Petri plates four days after inoculation. **A1-A5)** *Pss* 25 at 10^4 cfu/ml vs. *Pss* 23 at 10^8 cfu/ml on KB media. **B1-B5)** Images after threshold adjustment in ImageJ. **C1-C5)** Image of measured area. A1, B1, C1: Replication 1; A2, B2, C2: Replication 2; A3, B3, C3: Replication 3; A4, B4, C4: Replication 4; A5, B5, C5: Replication 5.

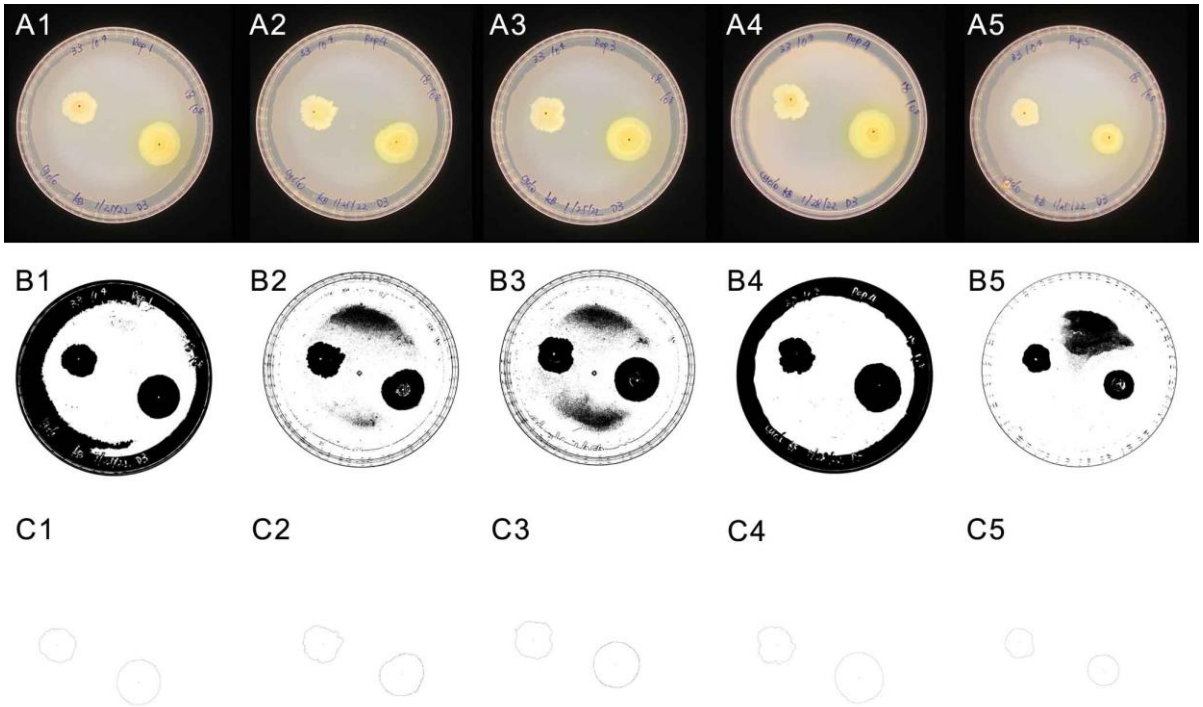


Figure C214. 2022 co-inoculated Petri plates four days after inoculation. **A1-A5)** *Pss* 33 at 10^4 cfu/ml vs. *Pss* 18 at 10^8 cfu/ml on KB media. **B1-B5)** Images after threshold adjustment in ImageJ. **C1-C5)** Image of measured area. A1, B1, C1: Replication 1; A2, B2, C2: Replication 2; A3, B3, C3: Replication 3; A4, B4, C4: Replication 4; A5, B5, C5: Replication 5.

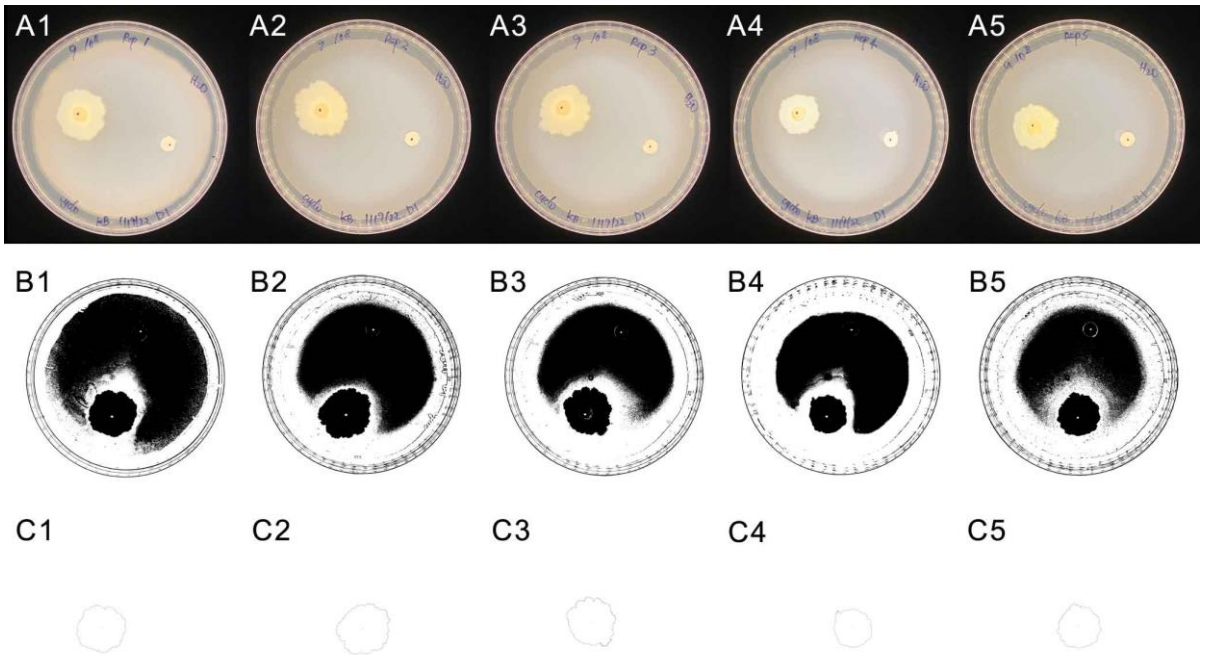


Figure C215. 2022 co-inoculated Petri plates four days after inoculation. **A1-A5)** *Pss* 9 at 10^8 cfu/ml vs. H_2O on KB media. **B1-B5)** Images after threshold adjustment in ImageJ. **C1-C5)** Image of measured area. A1, B1, C1: Replication 1; A2, B2, C2: Replication 2; A3, B3, C3: Replication 3; A4, B4, C4: Replication 4; A5, B5, C5: Replication 5.

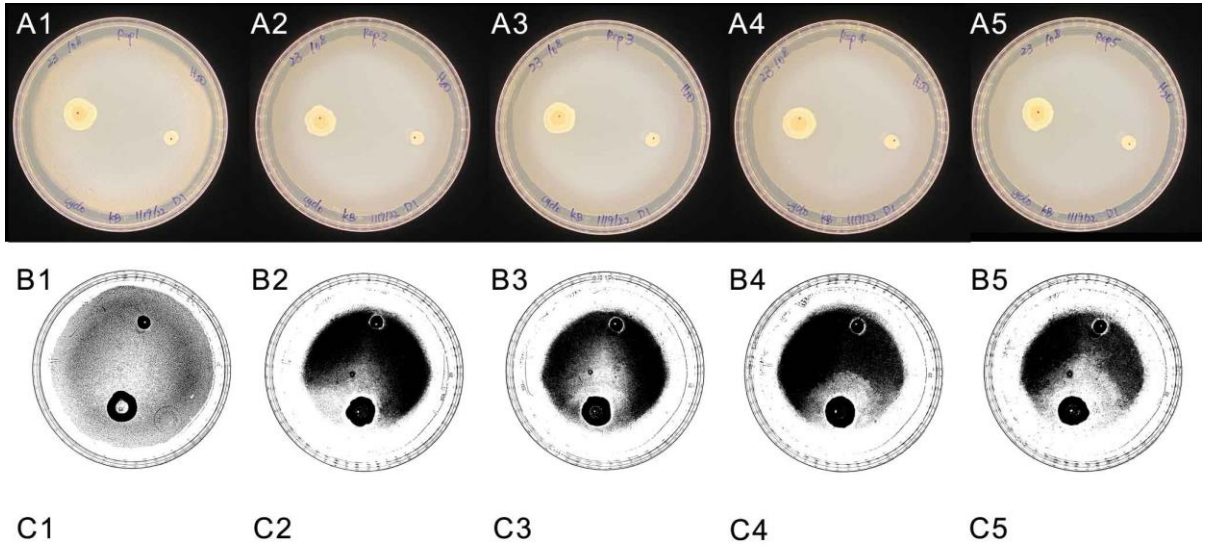


Figure C216. 2022 co-inoculated Petri plates four days after inoculation. **A1-A5)** *Pss* 23 at 10^8 cfu/ml vs. H_2O on KB media. **B1-B5)** Images after threshold adjustment in ImageJ. **C1-C5)** Image of measured area. A1, B1, C1: Replication 1; A2, B2, C2: Replication 2; A3, B3, C3: Replication 3; A4, B4, C4: Replication 4; A5, B5, C5: Replication 5.

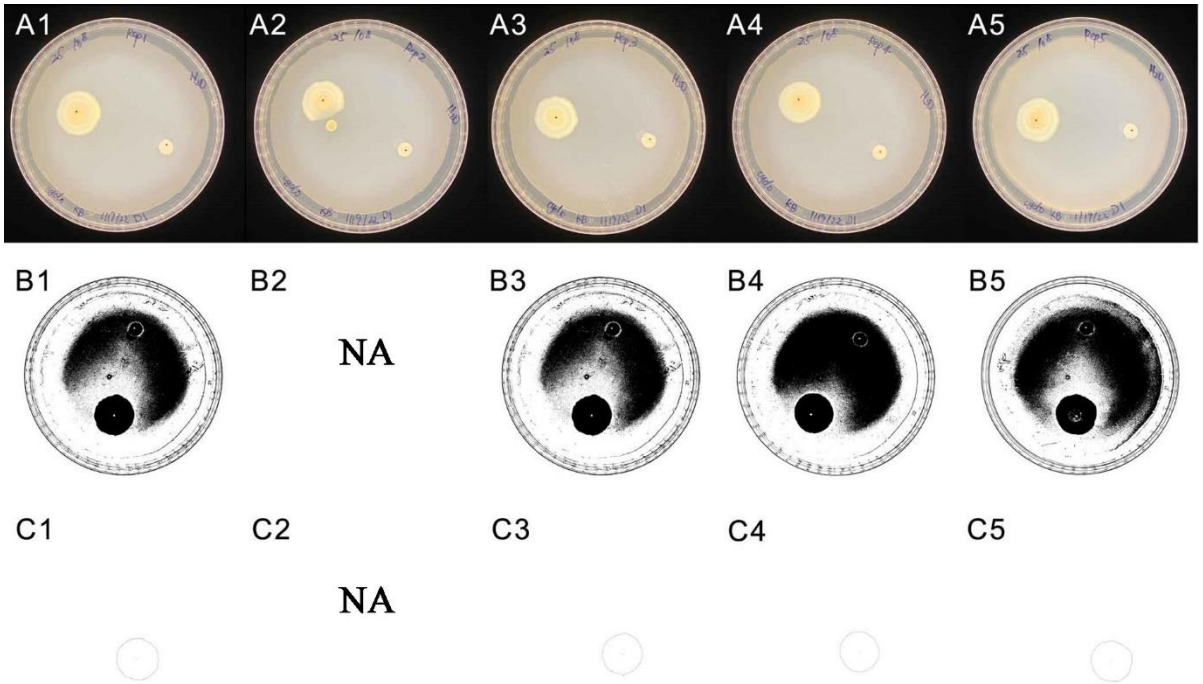


Figure C217. 2022 co-inoculated Petri plates four days after inoculation. **A1-A5)** *Pss* 25 at 10^8 cfu/ml vs. H_2O on KB media. **B1-B5)** Images after threshold adjustment in ImageJ. **C1-C5)** Image of measured area. A1, B1, C1: Replication 1; A2, B2, C2: Replication 2; A3, B3, C3: Replication 3; A4, B4, C4: Replication 4; A5, B5, C5: Replication 5. Images with NA are not available.

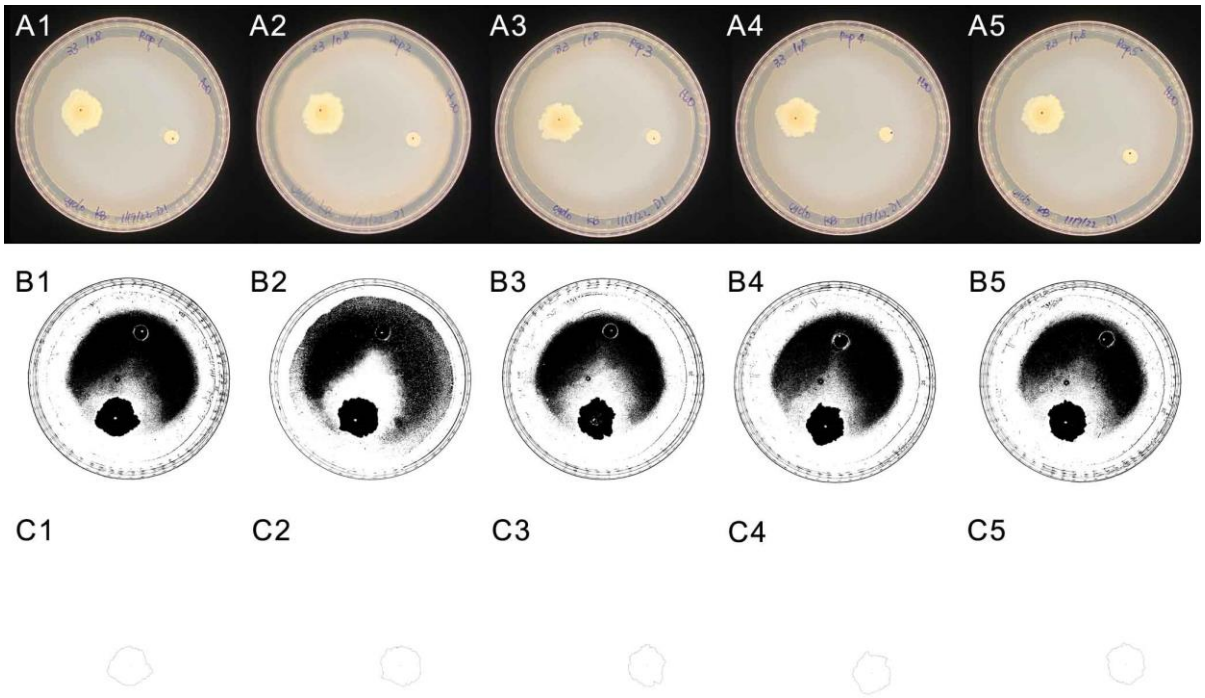


Figure C218. 2022 co-inoculated Petri plates four days after inoculation. **A1-A5)** *Pss* 33 at 10^8 cfu/ml vs. H_2O on KB media. **B1-B5)** Images after threshold adjustment in ImageJ. **C1-C5)** Image of measured area. A1, B1, C1: Replication 1; A2, B2, C2: Replication 2; A3, B3, C3: Replication 3; A4, B4, C4: Replication 4; A5, B5, C5: Replication 5.

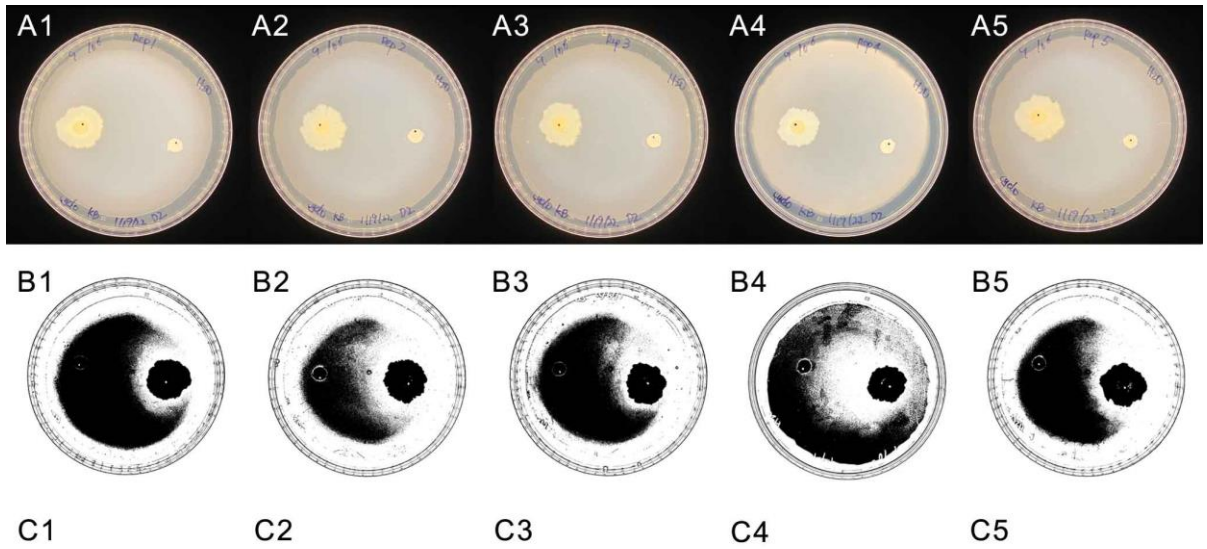


Figure C219. 2022 co-inoculated Petri plates four days after inoculation. **A1-A5)** *Pss* 9 at 10^6 cfu/ml vs. H_2O on KB media. **B1-B5)** Images after threshold adjustment in ImageJ. **C1-C5)** Image of measured area. A1, B1, C1: Replication 1; A2, B2, C2: Replication 2; A3, B3, C3: Replication 3; A4, B4, C4: Replication 4; A5, B5, C5: Replication 5.

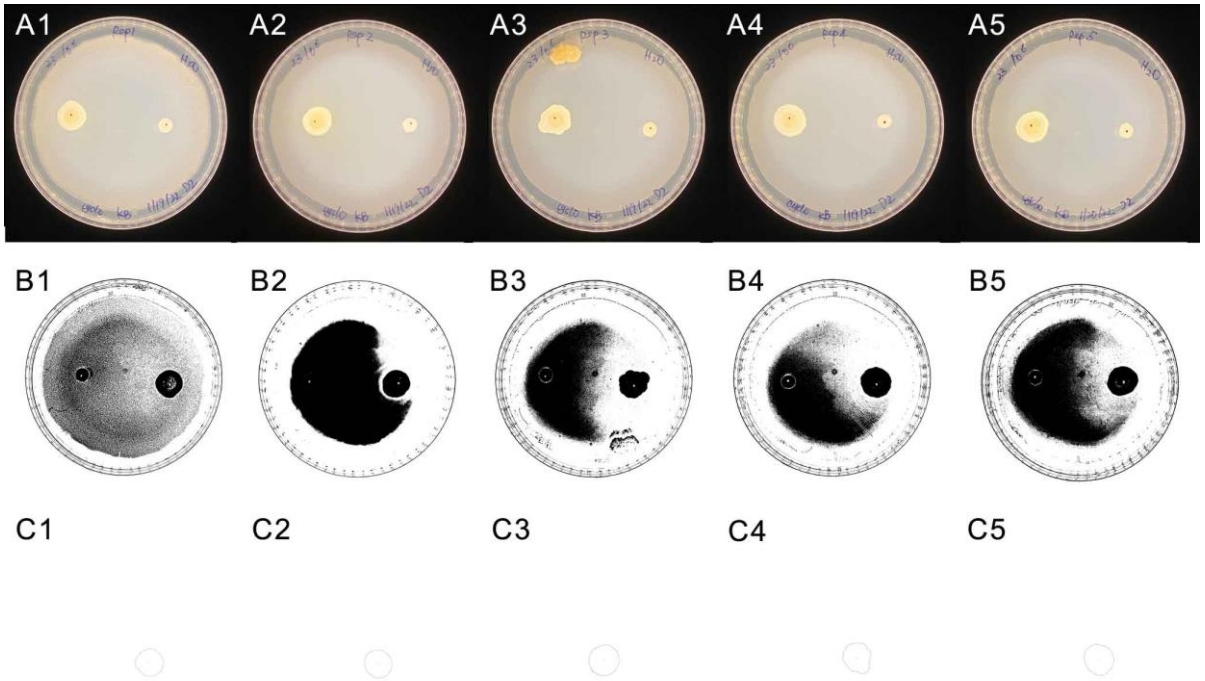


Figure C220. 2022 co-inoculated Petri plates four days after inoculation. **A1-A5)** *Pss* 23 at 10^6 cfu/ml vs. H_2O on KB media. **B1-B5)** Images after threshold adjustment in ImageJ. **C1-C5)** Image of measured area. A1, B1, C1: Replication 1; A2, B2, C2: Replication 2; A3, B3, C3: Replication 3; A4, B4, C4: Replication 4; A5, B5, C5: Replication 5.

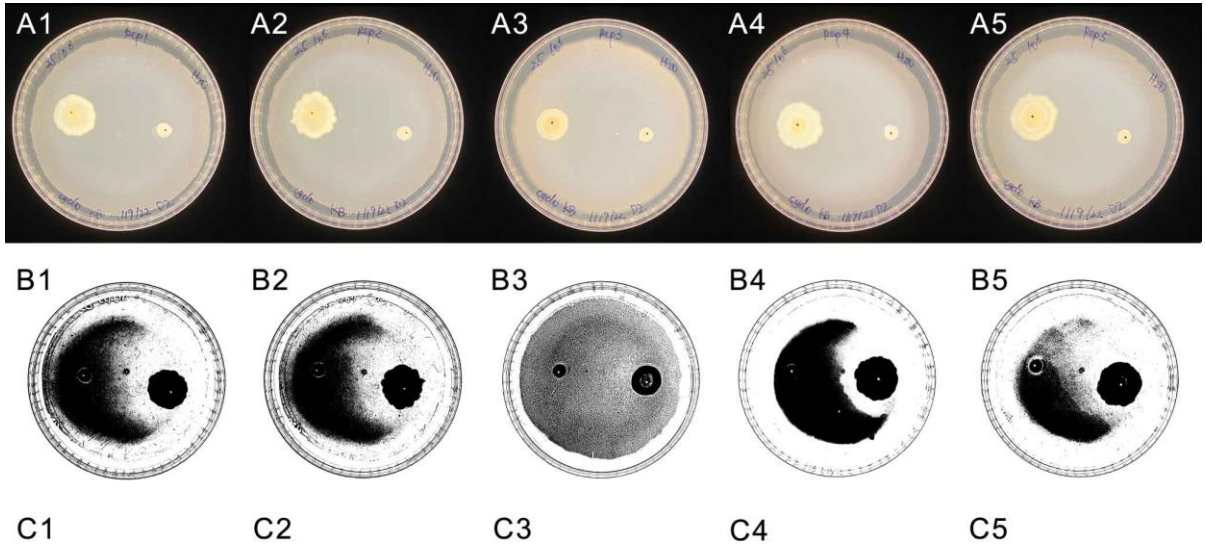


Figure C221. 2022 co-inoculated Petri plates four days after inoculation. **A1-A5)** *Pss* 25 at 10^6 cfu/ml vs. H_2O on KB media. **B1-B5)** Images after threshold adjustment in ImageJ. **C1-C5)** Image of measured area. A1, B1, C1: Replication 1; A2, B2, C2: Replication 2; A3, B3, C3: Replication 3; A4, B4, C4: Replication 4; A5, B5, C5: Replication 5.

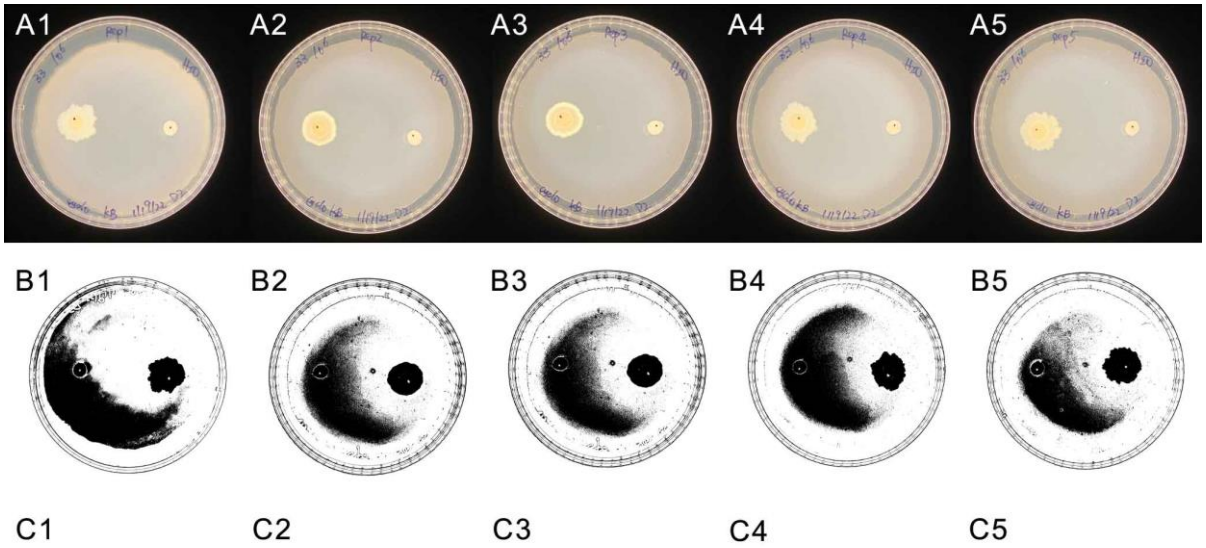


Figure C222. 2022 co-inoculated Petri plates four days after inoculation. **A1-A5)** *Pss* 33 at 10^6 cfu/ml vs. H_2O on KB media. **B1-B5)** Images after threshold adjustment in ImageJ. **C1-C5)** Image of measured area. A1, B1, C1: Replication 1; A2, B2, C2: Replication 2; A3, B3, C3: Replication 3; A4, B4, C4: Replication 4; A5, B5, C5: Replication 5.

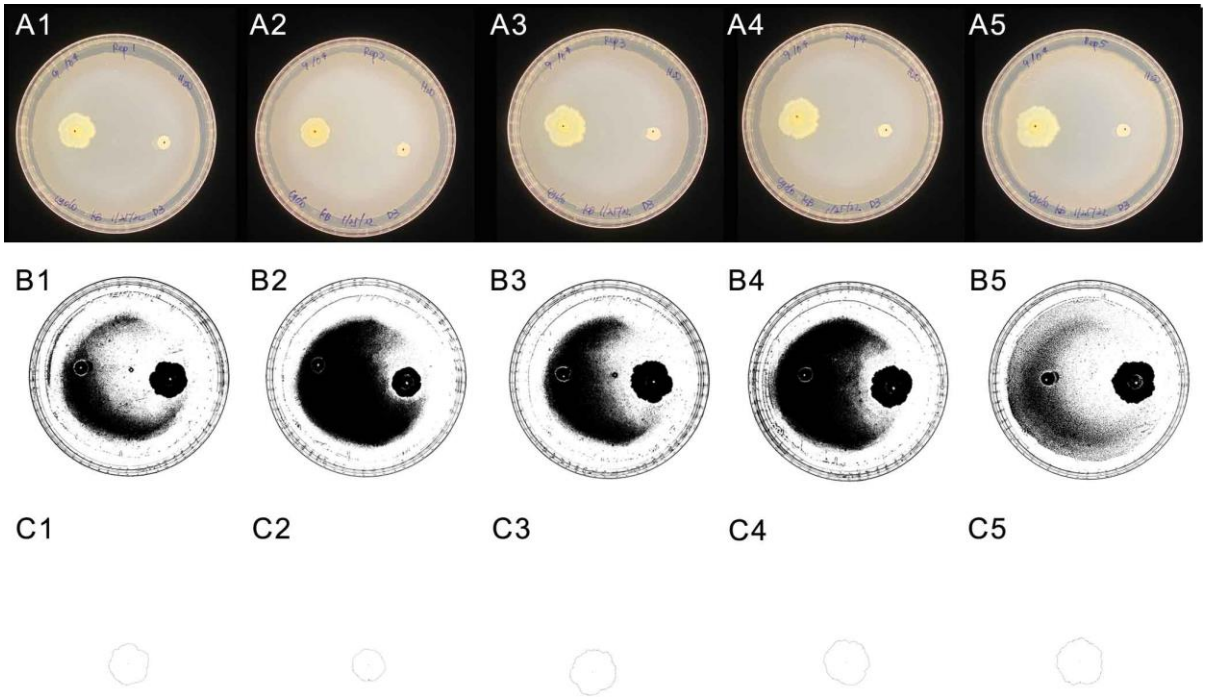


Figure C223. 2022 co-inoculated Petri plates four days after inoculation. **A1-A5)** *Pss* 9 at 10^4 cfu/ml vs. H_2O on KB media. **B1-B5)** Images after threshold adjustment in ImageJ. **C1-C5)** Image of measured area. A1, B1, C1: Replication 1; A2, B2, C2: Replication 2; A3, B3, C3: Replication 3; A4, B4, C4: Replication 4; A5, B5, C5: Replication 5.

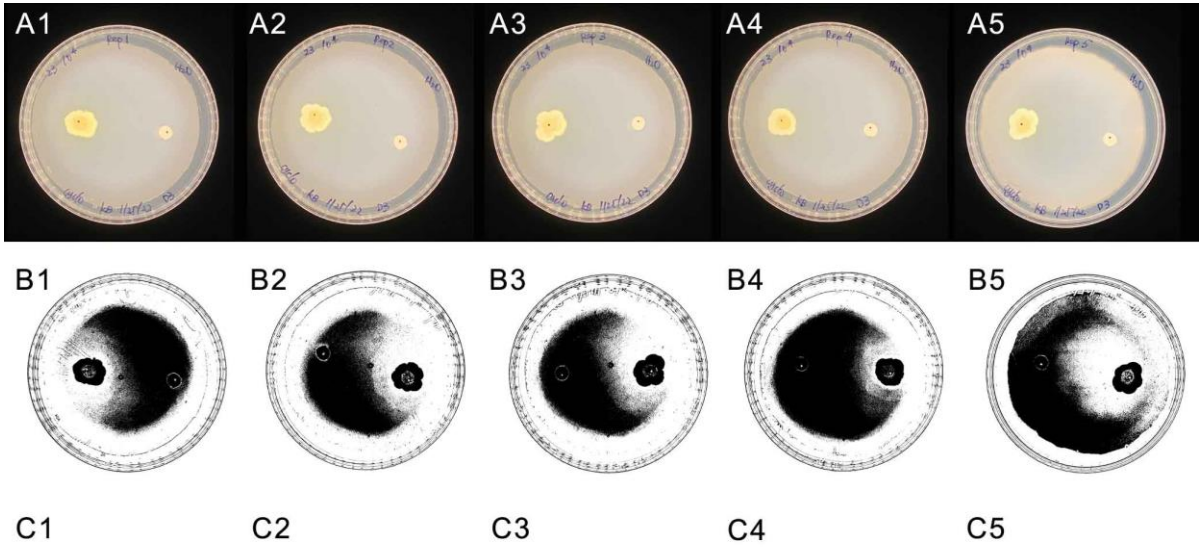


Figure C224. 2022 co-inoculated Petri plates four days after inoculation. **A1-A5)** *Pss* 23 at 10^4 cfu/ml vs. H_2O on KB media. **B1-B5)** Images after threshold adjustment in ImageJ. **C1-C5)** Image of measured area. A1, B1, C1: Replication 1; A2, B2, C2: Replication 2; A3, B3, C3: Replication 3; A4, B4, C4: Replication 4; A5, B5, C5: Replication 5.

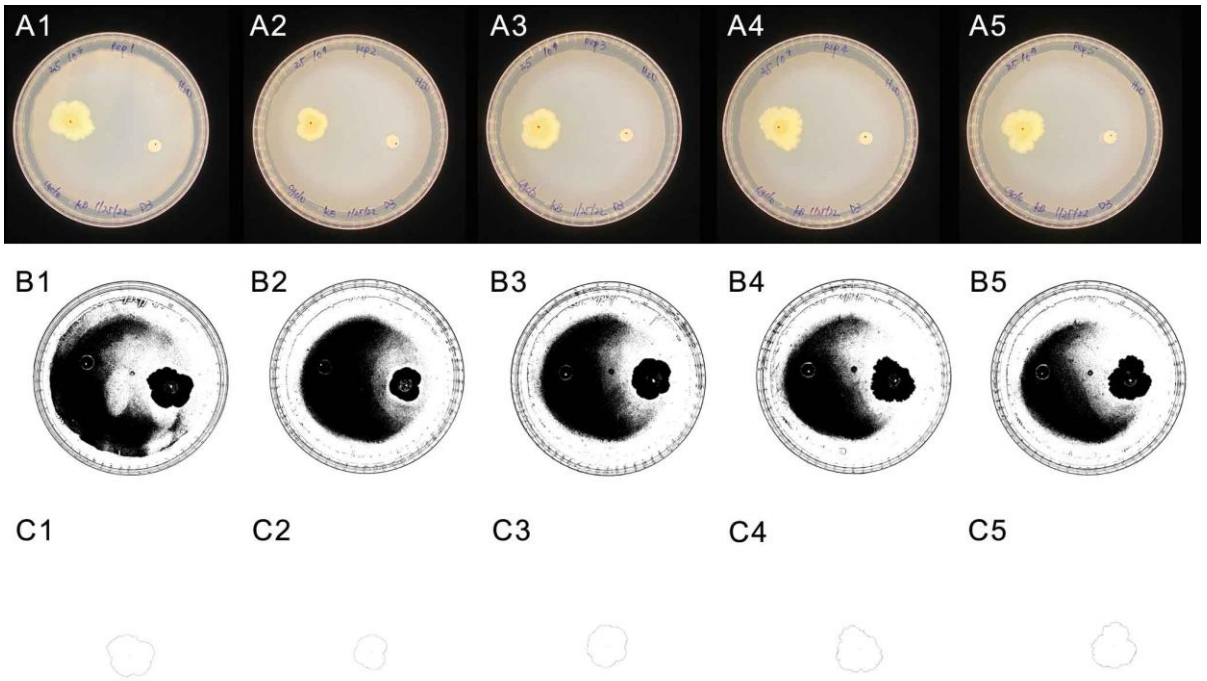


Figure C225. 2022 co-inoculated Petri plates four days after inoculation. **A1-A5)** *Pss* 25 at 10^4 cfu/ml vs. H_2O on KB media. **B1-B5)** Images after threshold adjustment in ImageJ. **C1-C5)** Image of measured area. A1, B1, C1: Replication 1; A2, B2, C2: Replication 2; A3, B3, C3: Replication 3; A4, B4, C4: Replication 4; A5, B5, C5: Replication 5.

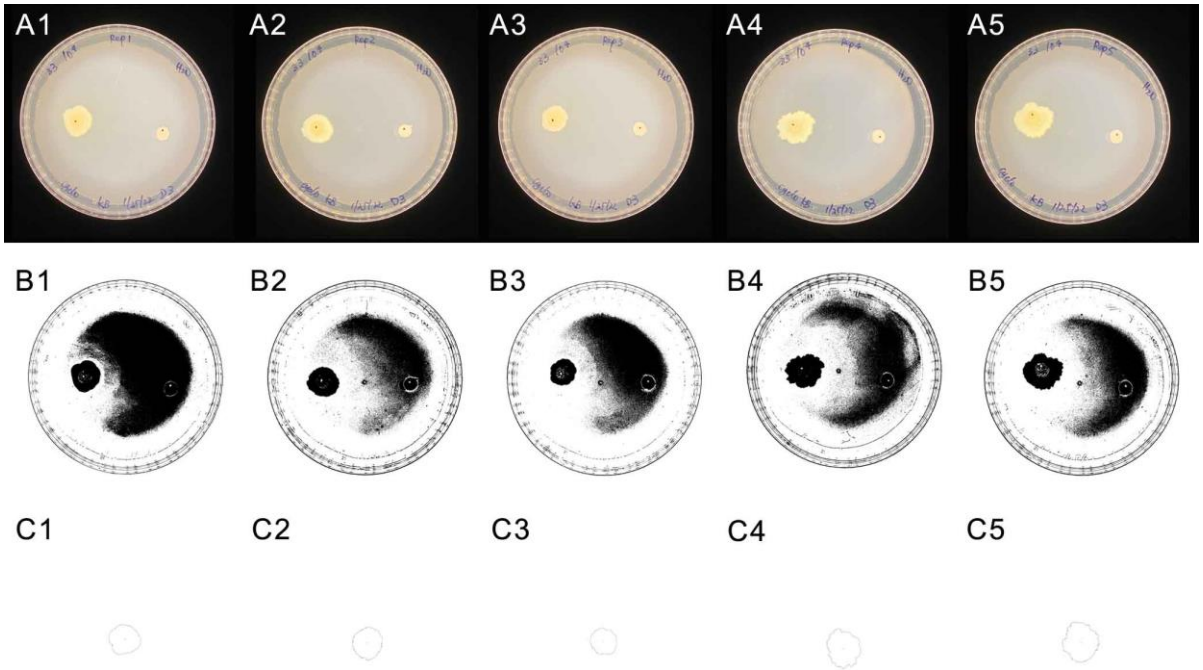


Figure C226. 2022 co-inoculated Petri plates four days after inoculation. **A1-A5)** *Pss* 33 at 10^4 cfu/ml vs. H_2O on KB media. **B1-B5)** Images after threshold adjustment in ImageJ. **C1-C5)** Image of measured area. A1, B1, C1: Replication 1; A2, B2, C2: Replication 2; A3, B3, C3: Replication 3; A4, B4, C4: Replication 4; A5, B5, C5: Replication 5.